Spin Models with Dissipation: Part II

Yury Holubeu *

August 28, 2025

This draft is not aimed for distribution.

Contents

Preface 7

VII Other Theories in a Nutshell 8

7 Other Formulas and Ideas 8
7.1 Old, Fundamental Articles . . . 8
7.2 Most Likely Useless Articles . . . 8
7.2.1 Iterative construction of conserved quantities in dissipative systems . . . 8

VIII Other My Theories 13

IX Other Special Theories, Models 14

8 Perturbative approach to weakly driven many-particle systems in the presence of approximate conservation laws by Lenarčič, Lange, Rosch 14
8.1 Model . . . 16
8.2 Zeroth order: generalized Gibbs ensemble . . . 16
8.2.1 Determination of λ_i . . . 17
8.2.2 Periodic driving . . . 18
8.2.3 Projection operators and effective forces . . . 19
8.2.4 Numerical construction of ρ_0 . . . 20
8.3 Perturbation theory . . . 21
8.3.1 Markovian perturbation . . . 21
8.3.2 Missing conservation laws . . . 23
8.3.3 Unitary driving, $\hat{P}\hat{\mathcal{L}}_1\hat{P} = 0$ . . . 25
8.4 Example: Interacting Fermions with particle-gain and loss . . . 26
8.4.1 Lindblad dynamics in a small system . . . 27
8.4.2 Boltzmann dynamics . . . 28
8.5 Conclusions . . . 34
8.6 Regularization of inverse . . . 35
8.7 Identities for super-operators . . . 35
8.8 Properties of projectors and inversion of projected Lindblad operators . . . 36
8.9 Correlation functions . . . 36
8.10 Unitary driving . . . 38
8.10.1 Projections of the inverse . . . 38
8.10.2 Zeroth order expansion point . . . 39
8.10.3 Monochromatic driving . . . 40

9 Pumping approximately integrable systems by Lange, Lenarčič, Rosch 40
9.0.1 Results . . . 41
9.0.2 Discussion . . . 46
9.0.3 Methods . . . 47

*https://yuriholubeu.github.io/, yuri.holubev@gmail.com

10 Engineering generalized Gibbs ensembles with trapped ions by Reiter, Lange, Jain et al. 51
10.1 Introduction . . . 51
10.2 Model . . . 54
10.3 Experimental signatures . . . 55
10.4 Dissipation engineering . . . 58
10.4.1 Setup . . . 59
10.4.2 Single-body dissipation . . . 60
10.4.3 Two-body dissipation . . . 61
10.5 Generalization of the couplings to the x-basis . . . 64
10.6 Scalable implementation . . . 66
10.7 Normal mode engineering in an array of micro traps . . . 67
10.7.1 Alternative realization in linear ion traps . . . 69
10.8 Conclusion and Outlook . . . 69
10.9 Theory of weakly driven nearly integrable systems . . . 70
10.9.1 Numerical results . . . 71
10.10Microscopic derivation of two-body decay . . . 72
10.11AC Stark shift of states . . . 74

11 From dissipationless to normal diffusion in easy-axis Heisenberg spin chain by Prelovšek, Nandy, Lenarčič et al. 76
11.1 Introduction . . . 76
11.2 Model and dissipationless diffusion . . . 77
11.3 Dynamical diffusion in closed systems . . . 78
11.4 Diffusion in open systems . . . 79
11.5 Finite wavevector and driving-field analysis . . . 80
11.6 Conclusions . . . 82
11.7 Perturbed XXZ spin chain: next-nearest-neighbor interaction . . . 82
11.8 Perturbed XXZ spin chain: staggered exchange . . . 83
11.9 Diffusion in the presence of finite driving field . . . 85

12 Critical behavior near the many-body localization transition in driven open systems by Zala Lenarčič, Alberton, Rosch, Altman 86
12.1 Theory . . . 86
12.2 Supplementary material . . . 92
12.2.1 Fractional diffusion . . . 92
12.2.2 Diffusive behavior in two dimensions . . . 92
12.2.3 Current dependence on the dynamical exponent . . . 93
12.2.4 Comparison to standard measures of dynamical scaling . . . 95
12.2.5 Convergence in system size, time and bond dimension . . . 95
12.2.6 Hydrodynamic equations as an expansion of Lindblad driving . . . 97

13 Transport in Stark Many Body Localized Systems by Zisling, Kennes, et al. 99
13.1 Supplementary Material: Transport in Stark Many Body Localized Systems . . . 106
13.1.1 Transition location . . . 106
13.1.2 Delocalization time extraction . . . 106
13.1.3 Finite-size subdiffusive behavior . . . 107
13.1.4 Sensitivity to boundary conditions . . . 107
13.1.5 Dynamical behavior of truncated effective Hamiltonians . . . 108
13.1.6 Convergence criteria of the Magnus expansion . . . 108
13.1.7 Density of states of the truncated effective Hamiltonians . . . 109
13.1.8 Finite-size analysis . . . 109

14 Iterative construction of conserved quantities in dissipative nearly integrable systems by Ulčakar, Lenarčič 113
14.1 Theory . . . 113
14.2 Supplemental Material . . . 119
14.3 Regularization of χ^{-1} in the non-local basis . . . 120
14.4 Conservation laws of transverse Ising model . . . 121
14.5 Example II: Heisenberg model. . . . 122
14.6 Iterative procedure for unitary perturbation . . . 123

15 From observations to complexity of quantum states via unsupervised learning by Schmitt, Lenarčič 123
15.1 Theory . . . 123
15.2 Supplemental material to From observations to complexity of quantum states via unsupervised learning by Schmitt, Lenarčič . . . 131
15.2.1 Conservation laws of transverse field Ising model . . . 131
15.2.2 From Lagrange parameters to latent representation . . . 131
15.2.3 Detecting the structure of noise . . . 134
15.2.4 Random unitary model . . . 135
15.2.5 Training of autoencoder networks . . . 136
15.2.6 Intrinsic dimension . . . 137
15.2.7 Hamiltonian reconstruction . . . 138

16 Reconstructing effective Hamiltonians from nonequilibrium (pre-)thermal steady states by Nandy, Schmitt et al. 140
16.1 Introduction . . . 141
16.2 Algorithm for Hamiltonian reconstruction using autoencoders . . . 143
16.3 Reconstructing short- and long-range interacting static Hamiltonians . . . 145
16.4 Reconstruction of effective Hamiltonians engineered by nonequilibrium drives . . . 146
16.4.1 Floquet driving . . . 147
16.4.2 Aperiodic random multipolar drives . . . 151
16.5 Conclusions and Future Outlook . . . 152
16.6 Details of the autoencoder . . . 153
16.7 Preparing the initial thermal state . . . 153
16.8 BCH Expansion . . . 154

X Another Explanations of a Typical Theories 156

XI Other, Not Used Theory 157

17 Quasiparticle cooling algorithms for quantum many-body state preparation by Lloyd, Michailidis et al. 157
17.1 Introduction . . . 157
17.2 Quasiparticle cooling protocol . . . 160
17.2.1 Setup and protocol . . . 160
17.2.2 Weak-coupling analysis . . . 162
17.2.3 Rate equation . . . 163
17.2.4 Choice of operators coupling to auxiliary qubits . . . 165
17.2.5 Choice of the filter function and two cooling protocols . . . 166
17.3 Theory of quasiparticle cooling in a spin chain . . . 169
17.3.1 Transverse-field Ising model . . . 169
17.3.2 A solvable model: cooling at the edge . . . 170
17.3.3 Finite density of auxiliaries . . . 171

17.4 Cooling non-integrable systems . . . 175
17.4.1 Longitudinal field TFIM . . . 175
17.4.2 Antiferromagnetic Heisenberg ladder . . . 177
17.5 Noise effects . . . 178
17.5.1 Rate equation in the presence of noise . . . 179
17.5.2 Application: cooling the transverse-field Ising model . . . 180
17.6 Discussion and outlook . . . 183
17.7 Details of modulated coupling pulse . . . 184
17.8 Detailed balance and thermal state preparation with MCP . . . 186
17.9 Quasiparticles in the TFIM . . . 187
17.10 Matrix elements for bulk cooling . . . 188
17.10.1 $Z_{j;\vec{\alpha};\vec{\beta}}$ matrix elements . . . 189
17.10.2 $\sigma^{\pm}_{j;\alpha;\beta}$ matrix elements . . . 189
17.11 Details of numerical simulations . . . 191
17.11.1 Free fermion simulations . . . 191
17.11.2 Tensor network simulations . . . 193
17.12 System-size dependence for Heisenberg ladder cooling . . . 195
17.13 Comparison of noisy kinetic equation and MPS simulations . . . 195

18 Correlations after Quantum Quenches in the *XXZ* Spin Chain: Failure of the Generalized Gibbs Ensemble by Pozsgay et al. 196
18.0.1 Introduction.— . . . 196
18.0.2 Quantum quench in the XXZ chain.— . . . 197
18.1 Supplementary Material for EPAPS Numerical methods . . . 201

19 Effects of atom losses on a one-dimensional lattice gas of hardcore bosons by Riggio, Rosso, Karevski, Dubail 204
19.1 Introduction . . . 204
19.2 The model . . . 205
19.2.1 Definition: lattice Tonks-Girardeau gas with K-body losses . . . 205
19.2.2 Adiabatic losses, effective description by slow motion of the charges . . . 206
19.2.3 Slow evolution of the rapidity distribution . . . 207
19.3 Deriving the loss functional . . . 209
19.3.1 One-body losses . . . 209
19.3.2 Two-body losses . . . 210
19.3.3 K-body losses with K even . . . 211
19.3.4 K-body losses with K odd . . . 212
19.4 Evolution of the rapidity distribution in a homogeneous gas . . . 213
19.4.1 Results for $K = 1$ . . . 214
19.4.2 Results for $K = 2$ . . . 215
19.4.3 Generic observations for arbitrary K . . . 219
19.5 Harmonically trapped gas . . . 221
19.5.1 Numerical method . . . 221
19.5.2 Results . . . 223
19.6 Conclusion . . . 225
19.7 Deriving solution (19.45) . . . 225
19.8 Derivation of Eq. (19.49) of the main text . . . 226
19.9 Additional data for the homogeneous $K = 2$ case . . . 228
19.10 Brief discussion on the spiral in figure Fig. 19.10 . . . 228
19.11 Convergence of numerical results . . . 229

20 Time evolution of local observables after quenching to an integrable model by Caux, Essler **230**
20.1 Main Theory . . . 230
20.2 Supplementary Material . . . 238
20.2.1 Calculation of the correlation matrix $\hat{\Gamma}$ (20.25) . . . 238
20.2.2 Order Parameter One-Point Function . . . 239

21 A note on symmetry reductions of the Lindblad equation **241**
21.1 Introduction . . . 241
21.2 Symmetric boundary driven open XXZ spin chains . . . 243
21.2.1 Numerical results and transport properties . . . 244
21.3 Discussion and conclusion . . . 247
21.4 Appendix: Symmetry reductions of quantum Liouvillian dynamics . . . 249

22 Quantum reaction-limited reaction-diffusion dynamics of noninteracting Bose gases by Rowlands et al. **251**
22.0.1 Introduction . . . 251
22.0.2 The system . . . 254
22.0.3 Diffusion and Reaction-limited Dynamics . . . 257
22.0.4 Results . . . 260
22.0.5 Annihilation reaction with interferences . . . 263
22.0.6 Discussion . . . 265
22.0.7 Coagulation . . . 268
22.0.8 Absorbing-state phase transition in quantum bosonic RD . . . 269
22.1 Continuum Limit of two-body annihilation with interferences . . . 274
22.2 Two-Body annihilation dynamics . . . 275
22.3 Coagulation dynamics . . . 277
22.4 Branching dynamics . . . 278

23 Quasilocal conserved operators in isotropic Heisenberg spin 1/2 chain by Ilievski et al. **279**
23.1 A: Explicit computation of the Hilbert-Schmidt kernel . . . 285
23.1.1 Reduction to the singlet subspace . . . 286
23.2 B: Finiteness of the gap for the auxiliary transfer matrix . . . 289
23.3 C: Fredholm-Gram-Schmidt orthogonalization for higher auxiliary spins . . . 290
23.4 D: Numerical example . . . 293

XII Articles about Potential Applications **294**

24 Collective Excitations and Nonequilibrium Phase Transition in Dissipative Fermionic Superfluids by Yamamoto, Nakagawa, et al **294**
24.1 Theory . . . 294
24.1.1 Introduction . . . 294
24.1.2 Dissipative BCS theory . . . 295
24.1.3 Collective excitations: phase and amplitude modes . . . 297
24.1.4 Collective excitations: Leggett mode . . . 298
24.1.5 Nonequilibrium phase transition . . . 300
24.1.6 Conclusions. . . . 300
24.2 Supplemental Material . . . 301
24.2.1 Detailed calculations of the time-dependent dissipative BCS theory . . . 301
24.2.2 Operator formalism of the BCS theory for a dissipative superfluid . . . 302
24.2.3 Generalization of the Bogoliubov-de Gennes analysis with a time-dependent BCS state . . . 303

24.2.4 Dynamics of pseudospins after switch-on of dissipation 305
24.2.5 Dynamics after sudden change of both the interaction and the dissipation . . . 306
24.2.6 A simplified model for understanding the nonequilibrium phase transition . . . 307

XIII Other Experiments **311**

XIV Localization: Other Articles **312**

XV Appendix **313**
.1 Appendix 313
.1.1 Literature 313

Bibliography **314**
.2 Bibliography from Most Useful Articles 314
.3 Bibliography from Old, Fundamental Articles 408
.4 Bibliography from Other Articles 438

Preface

Other My Theories

Other Special Theories, Models

Another Explanations of a Typical Theories

Articles about Potential Applications

Other Experiments

Amazing facts

(I'll reveal it later)

Puzzles for motivation

(I'll reveal it later)

Part VII
Other Theories in a Nutshell

7 Other Formulas and Ideas

7.1 Old, Fundamental Articles

7.2 Most Likely Useless Articles

7.2.1 Iterative construction of conserved quantities in dissipative nearly integrable systems

Setup.

$$\hat{\mathcal{L}}\rho = -i[H_0,\rho] + \hat{\mathcal{D}}\rho,\ \hat{\mathcal{D}}\rho = \epsilon\sum_i L_i\rho L_i^\dagger - \frac{1}{2}\{L_i^\dagger L_i,\rho\}, \tag{7.1}$$

$$\lim_{\epsilon\to 0}\lim_{t\to\infty}\rho = \sum_m a_m|m\rangle\langle m| \equiv \rho_D. \tag{7.2}$$

$\sum_n D_{mn}a_n = 0$, $D_{mn} = \langle m|(\hat{\mathcal{D}}|n\rangle\langle n|)|m\rangle$.

$$\lim_{\epsilon\to 0}\lim_{t\to\infty}\lim_{L\to\infty}\rho = \frac{e^{-\sum_m \lambda_m C_m}}{\mathrm{Tr}[e^{-\sum_m \lambda_m C_m}]} \equiv \rho_{\boldsymbol{\lambda}}, \tag{7.3}$$

$$\langle \dot{C}_{m'}\rangle = \mathrm{Tr}\left[C_{m'}\hat{\mathcal{D}}\frac{e^{-\sum_m \lambda_m C_m}}{\mathrm{Tr}[e^{-\sum_m \lambda_m C_m}]}\right] \stackrel{!}{=} 0 \quad \forall m'. \tag{7.4}$$

$$\hat{P}X = -\sum_{m,n}\frac{\partial\rho_{\boldsymbol{\lambda}}}{\partial\lambda_m}(\chi^{-1})_{m,n}\mathrm{Tr}[C_n X]. \tag{7.5}$$

$\chi_{m,n} = -\mathrm{Tr}[C_m\frac{\partial\rho_{\boldsymbol{\lambda}}}{\partial\lambda_n}] = \langle C_m C_n\rangle_{\rho_{\boldsymbol{\lambda}}} - \langle C_m\rangle_{\rho_{\boldsymbol{\lambda}}}\langle C_n\rangle_{\rho_{\boldsymbol{\lambda}}}$
$\langle O\rangle_{\rho_{\boldsymbol{\lambda}}} = \mathrm{Tr}[\rho_{\boldsymbol{\lambda}}O]$.

$$\hat{P}\dot{\rho}_{\boldsymbol{\lambda}} = -\sum_{m,n}\frac{\partial\rho_{\boldsymbol{\lambda}}}{\partial\lambda_m}(\chi^{-1})_{m,n}\mathrm{Tr}[C_n\hat{\mathcal{D}}\rho_{\boldsymbol{\lambda}}] = \sum_m\frac{\partial\rho_{\boldsymbol{\lambda}}}{\partial\lambda_m}\dot{\lambda}_m \tag{7.6}$$

$$\dot{\lambda}_m = -\sum_n(\chi^{-1})_{m,n}\mathrm{Tr}[C_n\hat{\mathcal{D}}\rho_{\boldsymbol{\lambda}}]. \tag{7.7}$$

Iteratively constructed truncated GGE.
Step 0: Start with a thermal state $\rho_{\tilde{\boldsymbol{\lambda}}}^{(0)} = e^{-\tilde{\lambda}_0^{(0)}H_0}/Z$ and find $\tilde{\lambda}_0^{(0)}$ from condition (14.4), $\mathrm{Tr}[H_0\hat{\mathcal{D}}e^{-\tilde{\lambda}_0^{(0)}H_0}] \stackrel{!}{=} 0$.
Step 1:

$$\tilde{C}_1 = \mathcal{N}_1^{-1}\sum_m w_m^{(1)}Q_m,$$
$$w_m^{(1)} = -\sum_n(\chi_{(0)}^{-1})_{mn}\mathrm{Tr}[Q_n\hat{\mathcal{D}}\rho_{\tilde{\boldsymbol{\lambda}}}^{(0)}], \tag{7.8}$$

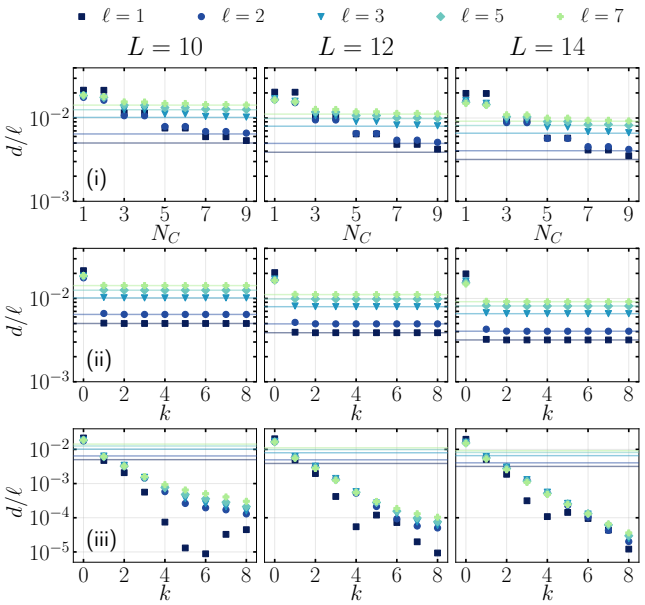


Figure 7.1: Scaled distances $d(\rho_{\boldsymbol{\lambda},\ell}, \rho_{D,\ell})/\ell$, Eq. (14.10), between the reduced density matrices of support ℓ for the diagonal steady state ensemble, Eq. (14.2), and different (truncated) generalized Gibbs ensembles. Solid lines correspond to the best GGEs with all $N_C^{\text{all}} = 2L - 2$ local conserved quantities on a given system size. From top to bottom, we consider tGGEs with: (i) N_C local conserved quantities $C_m, m = 0, ..., N_C - 1$, (ii) iterative scheme after the kth step for the basis $Q_m = C_m$, $m = 1, ..., N_C^{\text{all}} - 1$, (iii) iterative scheme after the kth step for basis $Q_m = |m\rangle\langle m|$. Parameters: Ising model with $h_x = 0.6$, $J = 1$, system sizes $L = 10, 12, 14$.

Step k:

$$\tilde{C}_k = \mathcal{N}_k^{-1} \sum_m w_m^{(k)} Q_m,$$
$$w_m^{(k)} = -\sum_n \left(\chi_{(k-1)}^{-1}\right)_{mn} \mathrm{Tr}[Q_n \hat{\mathcal{D}} \rho_{\tilde{\boldsymbol{\lambda}}}^{(k-1)}] \tag{7.9}$$

$\{\tilde{\lambda}_{k'}^{(k)}\}$
$\rho_{\tilde{\boldsymbol{\lambda}}}^{(k)} \propto e^{-\sum_{k'=0}^{k} \tilde{\lambda}_{k'}^{(k)} \tilde{C}_{k'}}$
$\tilde{C}_0 = H_0$.
$(\chi_{(k)})_{m,n} = \langle Q_m Q_n \rangle_{\rho_{\tilde{\boldsymbol{\lambda}}}^{(k)}} - \langle Q_m \rangle_{\rho_{\tilde{\boldsymbol{\lambda}}}^{(k)}} \langle Q_n \rangle_{\rho_{\tilde{\boldsymbol{\lambda}}}^{(k)}}$,
Results.

$$d(\rho_1, \rho_2) = \sqrt{\frac{\mathrm{Tr}[(\rho_1 - \rho_2)^2]}{\mathrm{Tr}[\rho_1^2] + \mathrm{Tr}[\rho_2^2]}} \tag{7.10}$$

$$H_0 = \sum_i J\sigma_i^z \sigma_{i+1}^z + h_x \sigma_i^x, \tag{7.11}$$

$$L_i = S_i^+ S_{i+1}^- + i S_{i+1}^- S_{i+2}^+ + a\sigma_i^x \sigma_{i+1}^z, \tag{7.12}$$

$$H_0 = \sum_i \sigma_i^x \sigma_{i+1}^x + \sigma_i^y \sigma_{i+1}^y + \sigma_i^z \sigma_{i+1}^z, \tag{7.13}$$

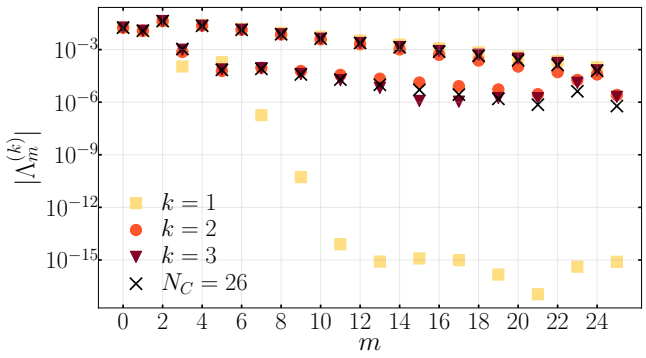


Figure 7.2: Interpreting the iterative procedure using the basis with all local conserved quantities $Q_m = C_m, m = 1, ..., 2L-3$. The weights $\Lambda_m^{(k)} = |\sum_{k'=1}^{k} \tilde{\lambda}_{k'}^{(k)} w_m^{(k')}/\mathcal{N}_{k'}|$ at each basis element Q_m after $k = 1, 2, 3$ iterative steps show which basis elements are more important. The exact weights are shown with crosses. Parameters: transverse field Ising model with $h_x = 0.6$ and $J = 1$ on $L = 14$ sites.

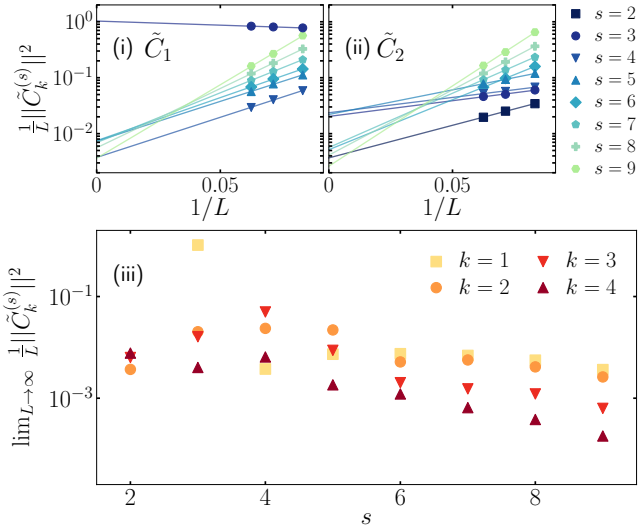


Figure 7.3: Nature of iterative conserved quantities, constructed in the basis of projectors on eigenstates, $Q_m = |m\rangle\langle m|$. (i,ii) Finite size scaling of norms $\frac{1}{L}||\tilde{C}_k^{(s)}||^2$ for the part $\tilde{C}_k^{(s)}$ of $k = 1, 2$ iterative conserved operator $\tilde{C}_k = \sum_s \tilde{C}_k^{(s)}$ that acts non-trivially only on support s. (iii) Thermodynamic norms $\lim_{L\to\infty} \frac{1}{L}||\tilde{C}_k^{(s)}||^2$ indicate that iterative conserved operators $\tilde{C}_k$ have a quasi-local nature. Parameters: Heisenberg model on $L = 12, 14, 16$.

Regularization of χ^{-1} in the non-local basis

$$\tilde{C}_k = \mathcal{N}_k^{-1} \sum_m w_m^{(k)} Q_m,$$
$$w_m^{(k)} = -\sum_n (\chi_{(k-1)}^{-1})_{mn} \mathrm{Tr}[Q_n \hat{\mathcal{D}} \rho_{\tilde{\boldsymbol{\lambda}}}^{(k-1)}] \tag{7.14}$$

$$\chi_{mn} = \mathrm{Tr}[Q_m Q_n \rho_{\tilde{\boldsymbol{\lambda}}}^{(k-1)}] - \mathrm{Tr}[Q_m \rho_{\tilde{\boldsymbol{\lambda}}}^{(k-1)}]\,\mathrm{Tr}[Q_n \rho_{\tilde{\boldsymbol{\lambda}}}^{(k-1)}].$$

$$|w\rangle = \chi^{-1}|q\rangle. \tag{7.15}$$

$a_m = \langle m|\rho_{\tilde{\boldsymbol{\lambda}}}^{(k-1)}|m\rangle,$
$\chi_{mn} = a_m(\delta_{mn} - a_n).$
$\mathrm{Tr}[\rho_{\tilde{\boldsymbol{\lambda}}}^{(k-1)}] = 1,$

$|v\rangle = \frac{1}{\sqrt{N_H}}|1,\ldots,1\rangle$,

$$\chi|1,\ldots,1\rangle = 0, \qquad \langle 1,\ldots,1|\chi = 0. \tag{7.16}$$

$\mathrm{Tr}[\hat{\mathcal{D}}\rho^{(k-1)}_{\tilde{\boldsymbol{\lambda}}}] = \sum_n q_n = 0$,

$$\langle 1,\ldots,1|q\rangle = 0 \tag{7.17}$$

$$\chi|w\rangle = |q\rangle, \quad |w\rangle = |w'\rangle + c|v\rangle \tag{7.18}$$

$\chi(|w'\rangle + c|v\rangle) = \chi|w'\rangle = |q\rangle$.

$$|w'\rangle = \tilde{\chi}^{-1}|q\rangle, \qquad \tilde{\chi} = \chi + |v\rangle\langle v| \tag{7.19}$$

$\mathrm{Tr}[\tilde{C}_k] = 0$

$$\chi_{\mathrm{b}} = \begin{pmatrix} \chi_{\tilde{P}_{N_H-1\times N_H-1}} & 0_{N_H-1\times 1} \\ 0_{1\times N_H-1} & 0 \end{pmatrix}_{\mathrm{b}}$$

$$|v\rangle_{\mathrm{b}} = \begin{pmatrix} 0_{N_H-1\times 1} \\ 1 \end{pmatrix}_{\mathrm{b}}, \quad |q\rangle_{\mathrm{b}} = \begin{pmatrix} q_{\tilde{P}_{N_H-1\times 1}} \\ 0 \end{pmatrix}_{\mathrm{b}}, \tag{7.20}$$

$$\tilde{\chi}_{\mathrm{b}} = \begin{pmatrix} \chi_{\tilde{P}} & 0 \\ 0 & 1 \end{pmatrix}_{\mathrm{b}} \quad \tilde{\chi}^{-1}_{\mathrm{b}} = \begin{pmatrix} \chi^{-1}_{\tilde{P}} & 0 \\ 0 & 1 \end{pmatrix}_{\mathrm{b}}. \tag{7.21}$$

$$\mathrm{Tr}[\tilde{C}_k] = \mathcal{N}_k^{-1}\sum_m w_m^{(k)} = \mathcal{N}_k^{-1}\langle v|w'\rangle = \\ = \mathcal{N}_k^{-1}\langle v|_{\mathrm{b}}\tilde{\chi}^{-1}_{\mathrm{b}}|q\rangle_{\mathrm{b}} = 0. \tag{7.22}$$

$$\rho^{(k)}_{\tilde{\boldsymbol{\lambda}}}(c) \equiv \frac{e^{-\sum_{k'=0}^{k}\tilde{\lambda}_{k'}\mathcal{N}_{k'}^{-1}\sum_m (w_m^{(k')}+c)Q_m}}{\mathrm{Tr}[e^{-\sum_{k'=0}^{k}\tilde{\lambda}_{k'}\mathcal{N}_{k'}^{-1}\sum_m (w_m^{(k')}+c)Q_m}]} \tag{7.23}$$

$$= \frac{\sum_m e^{-\sum_{k'=0}^{k}\tilde{\lambda}_{k'}\mathcal{N}_{k'}^{-1}(w_m^{(k')}+c)}Q_m}{\sum_m[e^{-\sum_{k'=0}^{k}\tilde{\lambda}_{k'}\mathcal{N}_{k'}^{-1}(w_m^{(k')}+c)}]}$$

$$= \frac{e^{-\sum_{k'=0}^{k}\tilde{\lambda}_{k'}\mathcal{N}_{k'}^{-1}c}\sum_m e^{-\sum_{k'=0}^{k}\tilde{\lambda}_{k'}\mathcal{N}_{k'}^{-1}w_m^{(k')}}Q_m}{e^{-\sum_{k'=0}^{k}\tilde{\lambda}_{k'}\mathcal{N}_{k'}^{-1}c}\sum_m[e^{-\sum_{k'=0}^{k}\tilde{\lambda}_{k'}\mathcal{N}_{k'}^{-1}w_m^{(k')}}]}$$

$$= \rho^{(k)}_{\tilde{\boldsymbol{\lambda}}}.$$

Conservation laws of transverse Ising model

$$H_0 = \sum_i J\sigma_i^z\sigma_{i+1}^z + h_x\sigma_i^x, \tag{7.24}$$

$$C_0 = H_0$$

$$C_2 = \sum_j JS^{zz}_{j,j+2} - h_x\sigma_j^y\sigma_{j+1}^y - h_x\hat{\sigma}_j^z\sigma_{j+1}^z - J\sigma_j^x$$

$$C_{2\ell>2} = \sum_j JS^{zz}_{j,j+\ell+1} - h_xS^{yy}_{j,j+\ell} - h_xS^{zz}_{j,j+\ell} + JS^{yy}_{j,j+\ell-1}$$

$$C_{2\ell-1} = J\sum_j S^{yz}_{j,j+\ell} - S^{zy}_{j,j+\ell}, \tag{7.25}$$

with $S^{\alpha\beta}_{i,j} = \sigma_i^\alpha\sigma_{i+1}^x\ldots\sigma_{j-1}^x\sigma_j^\beta$.

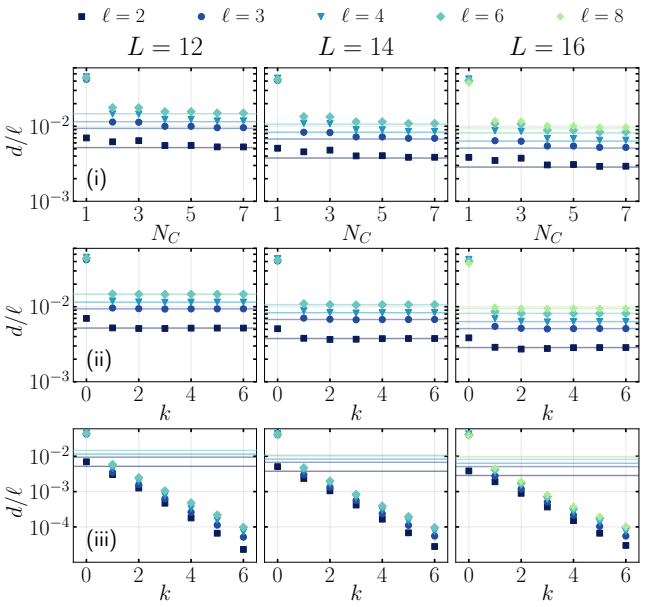


Figure 7.4: Scaled distances $d(\rho_{\boldsymbol{\lambda},\ell}, \rho_{D,\ell})/\ell$, Eq. (14.10), between the reduced density matrices of support ℓ of the diagonal steady state ensemble, Eq. (14.2), and different truncated generalized Gibbs ensembles. Solid lines correspond to the tGGEs including $N_C^{\max} = 8$ most local conserved quantities. From top to bottom we consider tGGEs with: (i) N_C local conserved quantities $C_m^{\text{loc}}, m = 0, ..., N_C - 1$, (ii) iterative scheme after the kth step for basis $Q_m = C_m^{\text{loc}}, m = 1, ..., N_C^{\max} - 1$, (iii) iterative scheme after the kth step for basis $Q_m = |m\rangle\langle m|$. Parameters: Heisenberg model, system sizes $L = 12, 14, 16$.

Example II: Heisenberg model.

$$H_0 = \sum_i \sigma_i^x \sigma_{i+1}^x + \sigma_i^y \sigma_{i+1}^y + \sigma_i^z \sigma_{i+1}^z, \tag{7.26}$$

$$L_i = S_i^+ S_{i+1}^- + i S_{i+1}^- S_{i+2}^+. \tag{7.27}$$

Iterative procedure for unitary perturbation

$$\tilde{C}_k = \mathcal{N}_k^{-1} \sum_m w_m^{(k)} Q_m, \tag{7.28}$$

$$w_m^{(k)} = -\sum_n \left(\chi_{(k-1)}^{-1}\right)_{mn} \text{Tr}[Q_n(\hat{\mathcal{D}} + \hat{\mathcal{L}}_1 \hat{Q} \hat{\mathcal{L}}_0^{-1} \hat{Q} \hat{\mathcal{L}}_1) \rho_{\tilde{\boldsymbol{\lambda}}}^{(k-1)}]$$

$\hat{\mathcal{L}}_j \rho = -i[H_j, \rho]$ for $j = 0, 1$,
$\hat{\mathcal{L}}_0^{-1} \rho = -\int_0^\infty dt e^{t\hat{\mathcal{L}}_0} \rho$
$\hat{Q}\rho = \mathbb{1} - \sum_m |m\rangle\langle m|\langle m|\rho|m\rangle$
$\text{Tr}[Q_n \hat{\mathcal{L}}_1 \rho_{\tilde{\boldsymbol{\lambda}}}^{(k-1)}] = 0$

Part VIII
Other My Theories

Part IX
Other Special Theories, Models

8 Perturbative approach to weakly driven many-particle systems in the presence of approximate conservation laws by Lenarčič, Lange, Rosch

This article is very hard to understand and I am not sure that it is really useful... Maybe it is not useful at all..

Abstract

We develop a Liouville perturbation theory for weakly driven and weakly open quantum systems in situations when the unperturbed system has a number of conservation laws. If the perturbation violates the conservation laws, it drives the system to a new steady state which can be approximately but efficiently described by a (generalized) Gibbs ensemble characterized by one Lagrange parameter for each conservation law. The value of those has to be determined from rate equations for conserved quantities. Remarkably, even weak perturbations can lead to large responses of conserved quantities. We present a perturbative expansion of the steady state density matrix; first we give the condition that fixes the zeroth order expression (Lagrange parameters) and then determine the higher order corrections via projections of the Liouvillian. The formalism can be applied to a wide range of problems including two-temperature models for electron-phonon systems, Bose condensates of excitons or photons or weakly perturbed integrable models. We test our formalism by studying interacting fermions coupled to non-thermal reservoirs, approximately described by a Boltzmann equation.

In equilibrium many particle systems can be efficiently described by Gibbs ensembles, characterized by one Lagrange parameter (inverse temperature, chemical potential) for each exactly conserved quantity (energy, particle number). Such a simple but powerful description is, in general, absent for driven non-equilibrium systems. As long as weak perturbations, which drive the system out of equilibrium, have small effects one can resort to perturbation theory. Kubo formulas, for example, describe the response to time-dependent Hamiltonian perturbations. Also for open systems described by Lindblad operators similar formulations of perturbation theory can be developed [1, 2, 3, 4, 5, 6, 7, 8, 9]. If the density matrix of the unperturbed system is not unique (as is the case for all Hamiltonian systems) one has to use degenerate Liouville perturbation theory [1, 7].

There are many situations where even weak perturbations of interacting many-particle systems can have large effects. A famous example is the Bose-Einstein condensation of excitons and polaritons [10, 11, 12]: irradiation by light creates more and more excitons which equilibrate approximately and form a Bose-Einstein condensate. Importantly, the exciton number is approximately conserved thus even weak pumping can compensate for exciton losses and leads to large densities of these excitations. Similarly, condensations of photons or magnons have been observed [13, 14, 15, 16, 17].

This is a general phenomenon: whenever approximate conservation laws exist, small perturbations which weakly break those conservation laws can drive the system out of equilibrium, to a steady state completely different from the initial one. In the example given above, the approximately conserved quantity is the exciton number. Other examples use the approximate conservation of spin to induce large nuclear spin polarization [18] for medical applications or use the weak coupling of electrons and phonons to induce vastly different temperatures in the two

subsystems [19, 20, 21, 22, 23]. In all cases, the long-time steady state – a Bose-Einstein condensate for the exciton example – is very different from any thermal state. Nevertheless, simple approximate theoretical descriptions can be found, e.g., by introducing an effective chemical potential for the excitons.

As we have argued recently in Ref. [26], this approach works quite generally: generalized Gibbs ensembles characterized by Lagrange parameters for approximately conserved quantities give an approximate description of the steady state of weakly perturbed driven systems. They describe situations where the driven system is completely different from the initial one, with Lagrange parameters determined by the perturbations. The nearly conserved quantities – e.g. the exciton number in the example discussed above – show a strong (non-linear) response to weak perturbations. In this paper we develop a perturbation theory around these generalized Gibbs ensembles and show that deviations remain small as long as the perturbations driving the system out of equilibrium are small. This is, however, only true if the correct zeroth order approximation, i.e. the correct generalized Gibbs ensemble, is chosen as the reference point of the perturbative expansion. The formalism is developed both for Lindblad and unitary time-periodic (Floquet) perturbations.

From this perspective our investigation is related to other Floquet studies in the presence of interactions and/or coupling to the environment [25, 26, 27, 28, 29, 30, 31, 32, 33]. For example, in Ref. [33] experiments of the Esslinger group on a Floquet-realization of the Haldane model [34] have been modeled based on the derivation of a Floquet-Boltzmann equation [33, 31]. The concept of a (time-dependent) temperature was used to describe the heating of interacting Floquet systems for situations where energy-conserving scattering processes dominate scattering events, where the energy changes. A related approach is taken when describing weakly-coupled electron-phonon systems out of equilibrium. Here one often associated two different temperatures to the two subsystems with energies that are separately approximately conserved [19, 20, 21, 22, 23, 35]. In Ref. [26] we used generalized Gibbs ensembles to describe the steady state of spin-chains coupled to phonons and driven by an external laser, modeled by a periodic driving. In these systems an infinite number of approximately conserved quantities exists due to the integrability of the underlying spin-1/2 Heisenberg model. As the heat current is also approximately conserved, one can realize large heat currents by weak driving.

From a more general point of view, our theoretical approach is based on the idea to project the dynamics of the density matrix on a few relevant degrees of freedom – in our case the approximate conservation laws. Such projection formalisms are widely used by many authors [36, 37, 38, 39, 40, 41, 42, 43] I'll look later at these articles. not sure, how useful are they, but some of them are cited a lot.... In contrast to these studies, we will use generalized Gibbs ensembles as a reference point and we focus our calculation on the computation of the steady state.

The article is organized in the following way: Sec. 8.1 prepares the perturbative setup, Sec. 8.2 gives the prescription on how to find the zeroth order approximation to the steady state via the introduction of a super-projector. The latter is used in Sec. 8.3 to determine corrections around the approximate description of the steady state both for Lindblad and unitary time-periodic (Floquet) perturbations. The applicability of our degenerate perturbation theory is tested in Sec. 23.93 on an example of interacting fermions coupled to non-thermal reservoirs which induce weak gain and loss of particles. We first perform an exact calculation on small system and then use approximate description by Boltzmann dynamics in the thermodynamic limit.

8.1 Model

We consider a many-particle quantum system described by the density operator ρ. Its dynamics is determined from the Liouville equation $\dot{\rho} = \hat{\mathcal{L}}\rho$, where $\hat{\mathcal{L}}$ is the Liouvillian superoperator. We consider situations where a Hamiltonian system is weakly perturbed. Therefore we split $\hat{\mathcal{L}} = \hat{\mathcal{L}}_0 + \hat{\mathcal{L}}_1$ into two parts, where $\hat{\mathcal{L}}_0$ describes the dominant unitary Hamiltonian evolution and $\hat{\mathcal{L}}_1$ a weak perturbation of strength ϵ which drives the system out of equilibrium,

$$\hat{\mathcal{L}}_0\rho = -i[H_0, \rho], \quad \hat{\mathcal{L}}_1\rho = \begin{cases} -i[\epsilon H_1, \rho], \\ \epsilon\hat{\mathcal{D}}\rho. \end{cases} \tag{8.1}$$

how to understand the {??? Most importantly, the unperturbed system described by H_0 has the property of having additional conserved quantities C_i, $[H_0, C_i] = 0$, $i = 1, .., N_c$. We are interested both in cases where N_c is small or when N_c is extensive as is the case when H_0 is integrable. The perturbation $\hat{\mathcal{L}}_1$ is of the unitary or/and of the Markovian Lindblad form. In H_1 we consider both static and time-dependent perturbations which are periodic in time. The Lindblad dynamics is described by

$$\hat{\mathcal{D}}\rho = \sum_\alpha \left(L_\alpha \rho L_\alpha^\dagger - \frac{1}{2}\{L_\alpha^\dagger L_\alpha, \rho\}\right) \tag{8.2}$$

with Lindblad operators L_α and how they look like?. We consider only translational invariant perturbations and situations where a unique (Floquet-) steady state is obtained. We assume that the perturbations break all conservation laws considered above. Remaining exactly conserved quantities are fixed by initial conditions and can easily be included in the theoretical description but are omitted in the following to simplify notations.

We are mainly interested in the nonequilibrium steady state. We split its density operator ρ_∞ into the zeroth order approximation ρ_0 and corrections $\delta\rho$,

$$\lim_{t\to\infty} \rho(t) = \rho_\infty = \rho_0 + \delta\rho. \tag{8.3}$$

with $\rho_0 = \lim_{\epsilon\to 0} \lim_{t\to\infty} \rho(t)$. Note that the limits $t \to \infty$ and $\epsilon \to 0$ do not commute: as we will show, small perturbations can completely change the density matrix in the long-time limit.

For perturbations periodic in time, the density matrix is periodically oscillating in the long time limit but one can still use the above formulas by interpreting them in Floquet space, see Section 8.2.2. The higher order corrections $\delta\rho$ are formally given by

$$\delta\rho = -\hat{\mathcal{L}}^{-1}\hat{\mathcal{L}}_1\rho_0, \quad \hat{\mathcal{L}}^{-1} \to \lim_{\eta\to 0}(\hat{\mathcal{L}} - \eta\hat{1})^{-1}. \tag{8.4}$$

where we used $\hat{\mathcal{L}}\rho_\infty = \hat{\mathcal{L}}_1\rho_0 + \hat{\mathcal{L}}\delta\rho = 0$ and $\hat{\mathcal{L}}_0\rho_0 = 0$. The inverse $\hat{\mathcal{L}}^{-1}$ should be interpreted using infinitesimal regularization η, see App. 8.6. Due to the conservation laws of H_0, $\hat{\mathcal{L}}_0\rho_0 = 0$ has no unique solution. While Eq. (8.4) is formally valid for arbitrary ρ_0 with $\hat{\mathcal{L}}_0\rho_0 = 0$, the correction $\delta\rho$ will only be small if ρ_0 is correctly chosen as discussed in the next section.

8.2 Zeroth order: generalized Gibbs ensemble

We have defined ρ_0 to fulfill the equation $\hat{\mathcal{L}}_0\rho_0 = 0$. In the thermodynamic limit, generic steady states of interacting many-particle system with (quasi-local) conservation laws C_i approach states which can be described by a (generalized) Gibbs ensemble (GGE)

$$\rho_0 = \frac{e^{-\sum_i \lambda_i C_i}}{\mathrm{Tr}[e^{-\sum_i \lambda_i C_i}]}, \tag{8.5}$$

More precisely, the system as a whole may be in a different ensemble (e.g. a canonical ensemble) but for the computation of local observables one expects that the different ensembles are generically equivalent in the thermodynamic limit. One manifestation of this is the eigenstate thermalization hypothesis [7, 45] which argues that a generic pure state becomes equivalent to a Gibbs state in the thermodynamic limit. Eq. (10.2) has also been extensively tested for integrable models [1, 47, 48, 49, 50, 51, 52, 37, 54, 55, 56, 57, 58, 59, 60, 61, 62, 63, 74, 64, 65, 66, 67, 68, 69, 52, 70, 71, 72, 48] which appear to approach a state described by ρ_0 after a quench. For certain local initial states (satisfying cluster decomposition property) this has been shown rigorously [74]. It has been argued recently that there exist a protocol based on truncated GGEs, convergent in number of included conservation laws [38].

Note that the parameters λ_i in Eq. (10.2) have not yet been determined. Most importantly, they are not fixed by initial conditions as the C_i are not conserved in the presence of the perturbations described by $\hat{\mathcal{L}}_1$. Instead the λ_i or, equivalently, the expectation values of the C_i have to be determined from rate equations governed by the weak perturbations. As we will show next, these will lead to changes of the λ_i of order $\mathcal{O}(1)$.

8.2.1 Determination of λ_i

All GGEs satisfy $\hat{\mathcal{L}}_0\rho_0 = 0$ by definition. Therefore the perturbation $\hat{\mathcal{L}}_1$ fixes the steady state parameters $\{\lambda_i\}$. Technically, we determine the $\{\lambda_i\}$ from the condition that the state is stationary in combination with the condition that $\delta\rho$ should be small in the limit $\epsilon \to 0$. The first condition ensures that $\langle \dot{C}_i \rangle = 0$, which is evaluated using straightforward perturbation theory

$$\begin{aligned} \langle \dot{C}_i \rangle &= \mathrm{Tr}[C_i \hat{\mathcal{L}} \rho_\infty] \\ &= \mathrm{Tr}[C_i \hat{\mathcal{L}}_1 \rho_0] + \mathrm{Tr}[C_i \hat{\mathcal{L}}_1 \delta\rho] \approx \mathrm{Tr}[C_i \hat{\mathcal{L}}_1 \rho_0] \end{aligned} \tag{8.6}$$

for $i = 1, ..., N_c$. Above we used that $\mathrm{Tr}[C_i \hat{\mathcal{L}}_0 \delta\rho] = 0$ due to $\hat{\mathcal{L}}_0^\dagger C_i = i[H_0, C_i] = 0$ and that $\delta\rho$ is small. Note that the adjoined of a Liouvillian is defined by the equation $\mathrm{Tr}[A\hat{\mathcal{L}}\rho] = \mathrm{Tr}[(\hat{\mathcal{L}}^\dagger A)\rho]$. We therefore obtain from $\langle \dot{C}_i \rangle = 0$ the condition fixing ρ_0

$$\mathrm{Tr}[C_i \hat{\mathcal{L}}_1 \rho_0] \stackrel{!}{=} 0 \tag{8.7}$$

If $\mathrm{Tr}[C_i \hat{\mathcal{L}}_1 \rho_0] = 0$ is trivially fulfilled for all ρ_0, one has to consider higher-order perturbation theory, see below.

Assuming for the moment that $\mathrm{Tr}[C_i \hat{\mathcal{L}}_1 \rho_0] \neq 0$ for all $i = 1, ..., N_c$ and generic ρ_0, then the N_c equations (8.7) can be used to fix the N_c Lagrange parameters λ_i. These equations can be viewed as *rate equations*, which describe how the perturbations change the approximately conserved C_i. Within the approximation used above, the size of the perturbation, i.e. the value of ϵ, completely drops out of the equation for the steady state. Therefore it fixes the Lagrange parameters (and, accordingly, also ρ_0) to order ϵ^0. While to this order the size of the perturbation is not important, its structure determines the Lagrange parameters and induces changes of order 1.

I need to see an example or use it myself to determine λ!

We now consider situations where $\mathrm{Tr}[C_i \hat{\mathcal{L}}_1 \rho_0] = 0$ for all ρ_0 are these exotic situations?. In this case one has to use perturbation theory at least to order ϵ^2 to fix ρ_0 to order ϵ^0. This is always the case for Hamiltonian perturbations where $\hat{\mathcal{L}}_1 \rho_0 = -i[\epsilon H_1, \rho_0]$ (this follows from $[C_i, \rho_0] = 0$ and the cyclic property of the trace). It corresponds to the well-known fact that transition rates, e.g., calculated from Fermi's golden rule, are always quadratic in the

perturbation. To calculate $\langle \dot{C}_i \rangle$ to order ϵ^2, $\delta\rho$ has to be expanded up to $\mathcal{O}(\epsilon)$ using Eq. (8.4) and the relation

$$(X+Y)^{-1} = X^{-1} - (X+Y)^{-1} Y X^{-1}, \tag{8.8}$$

with $X = \hat{\mathcal{L}}_0$ and $Y = \hat{\mathcal{L}}_1$. All inverses here and in the following are regularized as in Eq. (8.4). From this equation we find that $\delta\rho = -\hat{\mathcal{L}}_0^{-1}\hat{\mathcal{L}}_1\rho_0 + \hat{\mathcal{L}}^{-1}\hat{\mathcal{L}}_1\hat{\mathcal{L}}_0^{-1}\hat{\mathcal{L}}_1\rho_0$. A priori, it is not obvious that the first term linear in $\hat{\mathcal{L}}_1$ in this expression is large compared to the second one quadratic in $\hat{\mathcal{L}}_1$ due to possible singularities in $\hat{\mathcal{L}}^{-1}$ and we will indeed show that this is in general not the case. Nevertheless, using the machinery developed in Sec. 8.3, we can show that for the rate equation under discussion, one can make this approximation, see App. 8.10.2. Therefore we obtain from $\mathrm{Tr}[C_i\hat{\mathcal{L}}_1\delta\rho] = 0$ the condition

$$\mathrm{Tr}[C_i\hat{\mathcal{L}}_1\hat{\mathcal{L}}_0^{-1}\hat{\mathcal{L}}_1\rho_0] \stackrel{!}{=} 0. \tag{8.9}$$

As above, the size of ϵ drops out of this equation which therefore fixes ρ_0 to order ϵ^0 in situations where (8.7) is trivially fulfilled. For combined unitary and Markovian perturbations terms from Eq. (8.7) and Eq. (8.9) have to be considered simultaneously.

There can be situations where there is no contribution of order ϵ^2 to the decay rate of a conservation law such that the left-hand side of both Eq. (8.7) and Eq. (8.9) vanishes. This happens, for example, for an integrable Heisenberg chain perturbed by next-nearest neighbor interactions as discussed in Ref. [19] many years ago. Also in Refs. [77, 78] where perturbed L-site Ising model and Heisenberg model with strong magnetic field were studied, the boundary Lindblad operators fix the density matrix completely only after terms up to order L or $L-1$ were included, for odd and even system sizes, respectively. In such cases, one has to use Eq. (8.8) recursively to obtain higher-order corrections.

A non-trivial test of the order of perturbation that fixes ρ_0 can be obtained by exact (numerical) calculation of the Liouville gap, $\Lambda \equiv \min(|Re\ \lambda|; Re\ \lambda < 0)$, $\hat{\mathcal{L}}\rho = \lambda\rho$, on a system of smaller size. If scaling $\Lambda \sim \epsilon^k$ is obtained then ρ_0 is determined by the condition of order ϵ^k, which is for example $k = 1$ for Eq. (8.7) and $k = 2$ for Eq. (8.9).

8.2.2 Periodic driving

Above we have discussed stationary states obtained for $t \to \infty$ in systems with time-independent Liouvillians. The same approach can, however, also be used for systems with periodic driving. Here we focus on a case where $\hat{\mathcal{L}}_0$ and the associated conservation laws C_i are time-independent, while $\hat{\mathcal{L}}_1(t) = \hat{\mathcal{L}}_1(t+T)$ with period T. In this case only minor modifications of the formulation given above are necessary. In the long-time limit the density matrix always has oscillatory (Floquet) components,

$$\rho(t) = \sum_n e^{-in\omega t}\rho^{(n)},\ n \in \mathbb{Z}, \tag{8.10}$$

where $\rho^{(-n)} = \rho^{(n)\dagger}$, $\omega = 2\pi/T$. The analog of the unique stationary state of Eq. (8.3) is a state with time-independent Floquet components $\rho^{(n)}$. Due to the limit $\epsilon \to 0$ the zeroth order ρ_0 contains only time independent $\rho^{(n=0)}$ component. It is useful to organize the Floquet components into a vector $\boldsymbol{\rho} = \{\dots \rho^{(-1)}, \rho^{(0)}, \rho^{(1)}, \dots\}$ and promote the Liouvillian into a (static) matrix

$$\hat{\boldsymbol{\mathcal{L}}} = \hat{\boldsymbol{\mathcal{L}}}_0 + \hat{\boldsymbol{\mathcal{L}}}_1 \tag{8.11}$$

$$\hat{\boldsymbol{\mathcal{L}}}_1^{nm} = \hat{\mathcal{L}}_1^{n-m} = \frac{1}{T}\int_0^T \hat{\mathcal{L}}_1(t)e^{i\omega(n-m)t}dt \tag{8.12}$$

$$\hat{\boldsymbol{\mathcal{L}}}_0^{nm} = (in\omega + \hat{\mathcal{L}}_0)\delta_{nm} \tag{8.13}$$

Then the condition for ρ_0, Eq. (8.9), has to be reformulated in the above sense: with ρ_0 and C_i interpreted as vectors with non-zero $n = 0$ component and $\hat{\boldsymbol{\mathcal{L}}}_{\mathbf{1}}$, $\hat{\boldsymbol{\mathcal{L}}}_{\mathbf{0}}$ as matrices. $\hat{\boldsymbol{\mathcal{L}}}_{\mathbf{1}}$ contains off-diagonal terms due to periodic driving and diagonal terms in case of static perturbations. $\hat{\boldsymbol{\mathcal{L}}}_{\mathbf{0}}$ contains in addition to diagonal terms due to $\hat{\mathcal{L}}_0$ also $in\omega\delta_{nm}$ due to explicit time dependence of $\rho(t)$, $\dot{\rho} = \sum_n e^{-in\omega t}(-in\omega\rho^{(n)} + \dot{\rho}^{(n)})$. Stationarity of conserved quantities C_i, Eq. (8.9), in case of periodic driving applies to their time averages.

8.2.3 Projection operators and effective forces

When investigating corrections $\delta\rho$ of the steady state to the zeroth order approximation ρ_0 (or when investigating the time-dependence of $\rho(t)$), one has to distinguish corrections within the slow subspace with $\hat{\mathcal{L}}_0\delta\rho_\parallel = 0$ from those perpendicular to this subspace with $\hat{\mathcal{L}}_0\delta\rho_\perp \neq 0$. Therefore it is useful to introduce a super-projector $\hat{P}_{\rho_0}$ which projects on the (density-matrix) space tangential to the GGE manifold at the expansion point ρ_0. In the following, we will omit the argument ρ_0, using $\hat{P} = \hat{P}_{\rho_0}$ to avoid a cluttering of notations.

Small changes within the manifold around ρ_0 can be parametrized by $\delta\rho_\parallel = \sum_i \delta\lambda_i\, \partial\rho_0/\partial\lambda_i$ where $\delta\lambda_i$ are arbitrary infinitesimal changes of the Lagrange parameters. The super-operator $\hat{P}$, projecting on these density matrices, and its complement $\hat{Q}$ are uniquely given by [37]

$$\hat{P}X \equiv -\sum_{i,j} \frac{\partial\rho_0}{\partial\lambda_i}\, (\chi^{-1})_{ij} \mathrm{Tr}[C_j X] \tag{8.14}$$

$$\hat{Q}X \equiv (\hat{1} - \hat{P})X = X - \hat{P}X \tag{8.15}$$

where $\chi_{ij} = -\mathrm{Tr}[C_i\, \partial\rho_0/\partial\lambda_j] = \langle C_i C_j\rangle_{0,\mathrm{c}}$ is a matrix of generalized susceptibilities. We use the notation $\mathrm{Tr}[A\rho] = \langle A\rangle$ and $\mathrm{Tr}[A\rho_0] = \langle A\rangle_0$ for expectation values with respect to ρ_0. In addition, $\langle AB\rangle_{0,\mathrm{c}} = \langle AB\rangle_0 - \langle A\rangle_0\langle B\rangle_0$ stands for connected correlation function. $\hat{Q}$ and $\hat{P}$ have the property $\hat{Q}^2 = \hat{Q}$ and $\hat{P}^2 = \hat{P}$ with $\hat{P}\delta\rho_\parallel = \delta\rho_\parallel$ and are therefore projectors. By construction, $\hat{P}\delta\rho$ is for arbitrary $\delta\rho$ a linear combination of $\partial\rho_0/\partial\lambda_i$ and therefore an element of the tangential space. Note that $\hat{P}\rho_0 \neq \rho_0$ as $\hat{P}$ is a not a projector on the space of GGE density matrices but instead a projector on the tangential space at ρ_0. Note that Ref. [38] uses an alternative projector, which adds an extra term to guarantee $\hat{P}\rho_0 = \rho_0$.

The super-operator $\hat{P}^\dagger$, adjoint to $\hat{P}$, has also a direct physical interpretation. The natural scalar product within our approach is $\mathrm{Tr}[A\delta\rho]$, where A is an operator and $\delta\rho$ a density matrix, and therefore $\mathrm{Tr}[(\hat{P}^\dagger A)\delta\rho] = \mathrm{Tr}[A(\hat{P}\delta\rho)]$. We obtain

$$\hat{P}^\dagger A = -\sum_{ij} C_i\, (\chi^{-1})_{ji}\, \mathrm{Tr}\left[A\frac{\partial\rho_0}{\partial\lambda_j}\right]. \tag{8.16}$$

$P^\dagger$ acts on operators and maps each operator onto the space of conserved operators. It gives the part of an operator A which does not decay when the dynamics of the system is described by $\hat{\mathcal{L}}_0$ only. The super-operator $\hat{P}^\dagger$ naturally shows up when studying the dynamics of systems with conservation laws C_i. For example, the projection operator used in the memory matrix formalism [79, 80, 81, 19, 82] can (in this case) be identified with $\hat{P}^\dagger$. The operator can also be used to express the Drude weight of conductivities using the seminal results of Mazur [83] and Suzuki [84]. The Drude weight $D(T)$ is defined as the prefactor of a δ-function in the optical conductivity, $\mathrm{Re}[\sigma(\omega)] = \pi D(T)\delta(\omega) + \sigma_{\mathrm{reg}}(\omega)$. At finite temperatures T, the Drude weight is finite in situations where conservation laws C_i prohibit the decay of the current. Therefore the Drude weight in a thermal state [83, 84, 7] can simply be written in terms of the static cross susceptibility of J and $\hat{P}^\dagger J$, $D(T) = \frac{\beta}{L}\langle(\hat{P}^\dagger J)J\rangle_c$ where $\beta = 1/T$ and L is the system size.

Below, we will heavily rely on $\hat{P}$ when deriving perturbation theory for the stationary state. $\hat{P}$ can, however, also be used to define generalized forces allowing to track the changes of the Lagrange parameters during time evolution [36]. This allows to calculate, e.g., the heating of a driven system, and thus to obtain an intuitive picture on the dynamics. Assuming that a state $\rho_0(t)$ with time-dependent Lagrange parameters $\lambda_i(t)$ describes the system approximately, we can use

$$\begin{aligned}\hat{P}\dot{\rho} &\approx \sum_i \frac{\partial \rho_0}{\partial \lambda_i}\frac{\partial \lambda_i}{\partial t} = \sum_i \frac{\partial \rho_0}{\partial \lambda_i} F_i. \\ \dot{\lambda}_i = F_i &\approx -\sum_j (\chi^{-1})_{ij}\mathrm{Tr}[C_j\dot{\rho}] = -\sum_j (\chi^{-1})_{ij}\langle \dot{C}_j\rangle\end{aligned} \tag{8.17}$$

to obtain generalized forces F_i governing to leading order the dynamics of the Lagrange parameters. Depending on the studied case it is enough to include only the dominant contribution, e.g., $F_i = -\sum_j (\chi^{-1})_{ij}\mathrm{Tr}[C_j\hat{\mathcal{L}}_1\rho_0]$. In this paper, we will mainly focus on corrections to the stationary state, but we will discuss dynamics briefly in the context of the Boltzmann equation.

The stationarity condition (8.7) can be then rewritten as

$$\hat{P}(\hat{\mathcal{L}}_1\rho_0) = 0. \tag{8.18}$$

Geometrically it means that $\hat{\mathcal{L}}_1\rho_0$ must be perpendicular ($\perp$) to the slow manifold. Similarly the condition for unitary perturbation, Eq. (8.9), transcripts into

$$\hat{P}(\hat{\mathcal{L}}_1\hat{\mathcal{L}}_0^{-1}\hat{\mathcal{L}}_1\rho_0) = 0. \tag{8.19}$$

In both cases we require that the forces driving the system have effectively to be perpendicular to the GGE manifold.

Note also that in case of periodic driving $\hat{P}$ should be understood as a projector on the slow modes within $n = 0$ Floquet sector, Eq. (8.10). Therefore $\hat{P}\hat{\mathcal{L}}_1\rho_0 = 0$ and $\hat{P}\hat{\mathcal{L}}_1\hat{\mathcal{L}}_0^{-1}\hat{\mathcal{L}}_1\rho_0 = \hat{P}\hat{\mathcal{L}}_1\hat{Q}(\hat{Q}\hat{\mathcal{L}}_0\hat{Q})^{-1}\hat{Q}\hat{\mathcal{L}}_1\rho_0$.

8.2.4 Numerical construction of ρ_0

In cases where the relevant conservation laws are not known, one can construct for finite systems also the zeroth order result by brute force using exact diagonalization [26].

Using the exact eigenstates of H_0, $H_0|n\rangle = E_n^0|n\rangle$, the set of conservation laws is given by

$$\mathcal{Q} = \{|n\rangle\langle m| \text{ with } E_n^0 = E_m^0\}. \tag{8.20}$$

To use these conservation laws in Eq. (9.4) which is written for Hermitian conservation laws, one has to construct the corresponding Hermitian operators $|n\rangle\langle m| + |m\rangle\langle n|$ and $(|n\rangle\langle m| - |m\rangle\langle n|)/i$ for $n \neq m$. Denoting elements of $\mathcal{Q}$ by $\mathcal{Q}_i \in \mathcal{Q}$, one can write $\rho_0 = \sum \alpha_i \mathcal{Q}_i$ which fulfills by constuction the condition $\hat{\mathcal{L}}_0\rho_0 = 0$. In this case Eq. (8.7) is a linear equation for the parameters α_i which can be solved by finding the kernel of the matrix

$$\hat{\mathcal{L}}^{\mathcal{Q}}_{nm} = \mathrm{Tr}\,[\mathcal{Q}_n^\dagger \hat{\mathcal{L}}_1 \mathcal{Q}_m]. \tag{8.21}$$

Similarly, the exact solution of Eq. (8.9) is obtained by finding the eigenvector with eigenvalue 0 of

$$\hat{\mathcal{L}}^{\mathcal{Q}}_{nm} = -\mathrm{Tr}\,[\mathcal{Q}_n^\dagger \hat{\mathcal{L}}_1 \hat{\mathcal{L}}_0^{-1} \hat{\mathcal{L}}_1\ \mathcal{Q}_m]. \tag{8.22}$$

Note that the dimension of $\hat{\mathcal{L}}^{\mathcal{Q}}_{nm}$ is much smaller than the dimension of the full Liouvillian superoperators. For a spin-1/2 XXZ Heisenberg chain with L sites in the presence of an external

magnetic field, we found in Ref. [26] that the dimension of $\mathcal{Q}$ is approximately $2\cdot 2^L$ (the factor 2 arises from degeneracies in the spectrum), to be compared with $(2^L)^2 = 4^L$, the dimension of density matrices on which the Liouville super-operators act.

A tricky, unresolved question is under what condition the construction above converges in the thermodynamic limit. For example, there could in principle be situations where a conservation law exists only in the thermodynamics limit but not in the finite size system. A related question is whether the limits $\epsilon \to 0$ and $L \to \infty$ commute or not.

When using the set $\mathcal{Q}$ of conserved quantities, the projector $\hat{P}$ has to be replaced by $\tilde{P}$,

$$\tilde{P}X = \sum_{n,m} \langle n|X|m\rangle \delta_{E_n^0,E_m^0} \; |n\rangle\langle m| \tag{8.23}$$

projecting on the density operator subspace spanned by $|n\rangle\langle m|$, $E_n^0 = E_m^0$. This type of projector has been used also in other perturbative studies of Liouville dynamics [1, 7] implementing degenerate perturbation theory for super-operators in case of weak openness.

8.3 Perturbation theory

Projectors $\hat{P}, \hat{Q}$ are necessary to develop the perturbation theory of corrections to ρ_0, given to all orders by $\delta\rho$ in Eq. (8.4). Below we present a controlled expansion of the inverse $\hat{\mathcal{L}}^{-1}$, which removes possible singularities and separates different orders $\mathcal{O}(\epsilon^n)$ within the steady state. With $\|$ and $\perp$ we denote the density matrix subspaces, which are in the image of $\hat{P}$ and $\hat{Q}$, respectively, $\delta\rho = \hat{P}\delta\rho + \hat{Q}\delta\rho = \delta\rho_\| + \delta\rho_\perp$. Note that only the tangential component is relevant for the expectation values of conserved operators C_i,

$$\langle C_i\rangle = \mathrm{Tr}\big(C_i(\rho_0+\delta\rho)\big) = \mathrm{Tr}\big(C_i(\rho_0+\delta\rho_\|)\big) \tag{8.24}$$

as $\hat{Q}^\dagger C_i = 0$ for conserved quantities. $\delta\rho_\perp$ does, however, affect expectation values of other operators.

8.3.1 Markovian perturbation

not sure if I need it. Also, maybe it is easier to start with the example...

First we consider Liouvillians where the perturbations break all relevant conservation laws already to linear order in $\hat{\mathcal{L}}_1$ such that $\hat{P}\hat{\mathcal{L}}_1\hat{P}$ has no zero modes. Otherwise the procedure explained in Sec. 8.3.3 is needed.

Our goal is to expand $\delta\rho = -\hat{\mathcal{L}}^{-1}\hat{\mathcal{L}}_1\rho_0$, Eq. (8.4), using that we determined ρ_0 from the condition $\hat{P}\hat{\mathcal{L}}_1\rho_0 = 0$, Eq. (8.18). With this definition, we obtain

$$\delta\rho = -\hat{\mathcal{L}}^{-1}\hat{Q}\hat{\mathcal{L}}_1\rho_0. \tag{8.25}$$

where the Liouville inverse has to be interpreted using regulator as in Eq. (8.4), see also App. 8.6. Due to its conservation laws, $\hat{\mathcal{L}}_0^{-1}$, is singular. To avoid these singularities, we expand $\hat{\mathcal{L}}^{-1}$ around $\hat{\mathcal{L}}_0 + \hat{P}\hat{\mathcal{L}}_1\hat{P}$ using $\hat{\mathcal{L}}_1 = (\hat{P}+\hat{Q})\hat{\mathcal{L}}_1(\hat{P}+\hat{Q})$ and that $\hat{P}\hat{\mathcal{L}}_1\hat{P}$ is invertible in P subspace,

$$\begin{aligned}\hat{\mathcal{L}}^{-1}\hat{Q} &= (\hat{\mathcal{L}}_0+\hat{\mathcal{L}}_1)^{-1}\hat{Q} = (\hat{\mathcal{L}}_0+\hat{P}\hat{\mathcal{L}}_1\hat{P})^{-1} \\ &\times\sum_{n=0}^{\infty}\big[-(\hat{P}\hat{\mathcal{L}}_1\hat{Q}+\hat{Q}\hat{\mathcal{L}}_1\hat{P}+\hat{Q}\hat{\mathcal{L}}_1\hat{Q})(\hat{\mathcal{L}}_0+\hat{P}\hat{\mathcal{L}}_1\hat{P})^{-1}\big]^n\hat{Q}.\end{aligned} \tag{8.26}$$

For power counting in ϵ, it is important to realize that

$$\begin{aligned}(\hat{\mathcal{L}}_0+\hat{P}\hat{\mathcal{L}}_1\hat{P})^{-1}\hat{P} &= (\hat{P}\hat{\mathcal{L}}_1\hat{P})^{-1}\hat{P} \sim \mathcal{O}(1/\epsilon) \\ (\hat{\mathcal{L}}_0+\hat{P}\hat{\mathcal{L}}_1\hat{P})^{-1}\hat{Q} &= (\hat{Q}\hat{\mathcal{L}}_0\hat{Q})^{-1}\hat{Q} \sim \mathcal{O}(1)\end{aligned} \tag{8.27}$$

where we have used $\hat{P}\hat{\mathcal{L}}_0 = \hat{\mathcal{L}}_0\hat{P} = 0$. This reflects that the dynamics in the subspace of approximately conserved quantities is slow, while it is fast in the perpendicular space. Note that $(\hat{P}\hat{\mathcal{L}}_1\hat{P})^{-1}$ and $(\hat{Q}\hat{\mathcal{L}}_0\hat{Q})^{-1}$ in Eq. (8.27) should be interpreted as *inverses within the P and Q subspaces*, respectively, where $\hat{\mathcal{L}}_0$ and $\hat{\mathcal{L}}_1$ are invertible. One first performs projection and then the inversion within the subspace that dynamics was projected on. Moreover, Eq. (8.27) gives an alternative derivation of Eq. (8.18): the steady state ρ_0 has to fulfill $\hat{P}\hat{\mathcal{L}}_1\rho_0 = 0$, otherwise corrections $\delta\rho \sim \hat{\mathcal{L}}^{-1}\hat{P}\hat{\mathcal{L}}_1\rho_0 \sim 1$ which contradicts our perturbative approach in the limit $\epsilon \to 0$, see App. 8.10.2.

The combination of Eq. (8.25), (8.26) and (8.27) allows to obtain a straightforward expansion of $\delta\rho$ in powers of ϵ. The steady state density matrix has a distinct structure in the tangential ($\|$) and the perpendicular ($\perp$) subspace in all orders, therefore one has to consider the contributions from the two subspaces separately. To linear order in ϵ we obtain

$$\begin{aligned}
\delta\rho &\approx \delta\rho_{1,\|} + \delta\rho_{1,\perp} + \mathcal{O}(\epsilon^2), \\
\delta\rho_{1,\|} &= (\hat{P}\hat{\mathcal{L}}_1\hat{P})^{-1}\ \hat{P}\hat{\mathcal{L}}_1\hat{Q}\ \hat{\mathcal{L}}_0^{-1}\ \hat{Q}\hat{\mathcal{L}}_1\rho_0, && (8.28)\\
\delta\rho_{1,\perp} &= -\hat{\mathcal{L}}_0^{-1}\ \hat{Q}\hat{\mathcal{L}}_1\rho_0. && (8.29)
\end{aligned}$$

For brevity we use notation $\hat{Q}(\hat{Q}\hat{\mathcal{L}}_0\hat{Q})^{-1}\hat{Q} = \hat{Q}\hat{\mathcal{L}}_0^{-1}\hat{Q}$, where $\hat{\mathcal{L}}_0^{-1}$ should be understood as an inverse within Q subspace only. We would like to stress again, that ρ_0 already contains effects of order ϵ^0. But after ρ_0 has been correctly chosen, $\delta\rho$ does indeed vanishes for $\epsilon \to 0$, $\delta\rho \sim \epsilon$. In the $\|$ space, one has, however, to expand to second order in $\hat{\mathcal{L}}_1$ to obtain the correction of order ϵ due to the presence of the $(\hat{P}\hat{\mathcal{L}}_1\hat{P})^{-1}$ term. This contributes as $1/\epsilon$ factor, resulting in a term proportional to $\epsilon^2/\epsilon = \epsilon$. In the perpendicular space no such issue arises. The fact that perturbation theory for steady states has a different structure compared to perturbation theory in thermal equilibrium is well known, see, e.g. Ref. [86], and can simply be understood from the fact that rate equations determining the steady state have to be readjusted in the presence of perturbations.

Note that the change $\delta\rho_\|$ can in principle be absorbed in a redefinition of the Lagrange parameters, while $\delta\rho_\perp$ describes contributions which cannot be captured by a GGE ensemble.

For concrete calculations one needs to compute

$$(\hat{P}\hat{\mathcal{L}}_1\hat{P})^{-1}\hat{P}X = -\sum_{pr}\frac{\partial\rho_0}{\partial\lambda_p}(M^{-1})_{pr}\ \mathrm{Tr}[C_r X], \tag{8.30}$$

where M^{-1} is the inverse of matrix M with components $M_{pr} = -\mathrm{Tr}[C_p\,\hat{\mathcal{L}}_1(\partial\rho_0/\partial\lambda_r)]$, see App. 8.7. Then, for example, the change of the expectation value of a conserved operator C_i is given linearly in ϵ by, $\delta\langle C_i\rangle \approx \langle C_i\rangle_1$

$$\begin{aligned}
\langle C_i\rangle_1 &= \mathrm{Tr}\left[C_i(\hat{P}\hat{\mathcal{L}}_1\hat{P})^{-1}\hat{P}\hat{\mathcal{L}}_1\hat{Q}\hat{\mathcal{L}}_0^{-1}\hat{Q}\hat{\mathcal{L}}_1\rho_0\right] && (8.31)\\
&= \sum_{jk}\chi_{ij}\,(M^{-1})_{jk}\,\mathrm{Tr}\big[C_k\hat{\mathcal{L}}_1\hat{Q}\hat{\mathcal{L}}_0^{-1}\hat{Q}\hat{\mathcal{L}}_1\rho_0\big] && (8.32)
\end{aligned}$$

Higher order corrections can be obtained in a straightforward way from the Taylor expansion, Eq. (8.26), in combination with the rules of Eq. (8.27) which show how the inverse $(\hat{\mathcal{L}}_0 + \hat{P}\hat{\mathcal{L}}_1\hat{P})^{-1}$ has to be evaluated. Eq. (8.31) and its higher order generalization can be rewritten in terms of standard correlation functions as we discuss in App. 8.9 where concrete formulas for $\langle C_i\rangle_1$ and $\langle C_i\rangle_2 \sim \mathcal{O}(\epsilon^2)$ are given.

In Fig. 8.1 we give a graphical representation of the relevant terms in the tangential ($\|$) and the orthogonal ($\perp$) subspace. As written on the left of the figure, the two types of inverse Liouville super-operators in P and Q space are shown as white and black circles, respectively.

There are three types of links, $\hat{Q}\hat{\mathcal{L}}_1\hat{Q}$, $\hat{P}\hat{\mathcal{L}}_1\hat{Q}$ and $\hat{Q}\hat{\mathcal{L}}_1\hat{P}$, connecting black and black, white and black, and black and white circles, respectively. This simply follows from the rule that $\hat{P}\hat{Q} = 0 = \hat{Q}\hat{P}$.

Starting from $\hat{Q}\hat{\mathcal{L}}_1\rho_0$ (small square with thin line) to the right, one attaches circles and lines in all allowed combinations. The color of the last circle on the left, determines whether the density matrix operator is in P or Q space. The power in ϵ is determined by the number of lines minus the number of white circles as $(\hat{P}\hat{\mathcal{L}}_1\hat{P})^{-1} \sim 1/\epsilon$. The sign is simply given by $(-1)^{N_L}$ where N_L is the number of lines.

We have checked that the formulas discussed above can alternatively be derived starting from projection-operator based time-dependent perturbation theories in the version discussed by Breuer and Petruccione [43, 42].

As a remark we should point out that there is no need for any additional normalization since $\mathrm{Tr}\,\delta\rho = 0$ which is guaranteed by the regularization of the inverse operators, see Appendix 8.6.

8.3.2 Missing conservation laws

Above, we have assumed that all relevant conservation laws of the unperturbed system are known and have been included in the construction of the GGE (or that ρ_0 has been constructed numerically, see Sec. 8.2.4). It may, however, happen that either not all conservation laws are known or that it is just technically impossible to include them all. This might, for example, be the case in integrable systems where an infinite number of conservation laws exists.

In this case one may try to approximate system by a truncated GGE,

$$\rho_0^{[t]} = \frac{\exp\left[-\sum_i \lambda_i^{[t]} C_i^{[t]}\right]}{\mathrm{Tr}[e^{-\sum_i \lambda_i^{[t]} C_i^{[t]}}]} \tag{8.33}$$

considering only a finite subset of conserved operators. We denote by $\hat{P}_t$ the projector on the space tangential to the truncated GGE, and by $\chi^{[tt]}$ the matrix of susceptibilities, all defined as above.

A selection criterion for the truncated space could be, for example, to consider only the most local conservation laws, containing less than a certain number of derivatives in a continuum model or having a support of less than a certain number of sites for a lattice model. A truncated GGE was, for example, used in Ref. [26]. In the following we will consider two questions: (i)

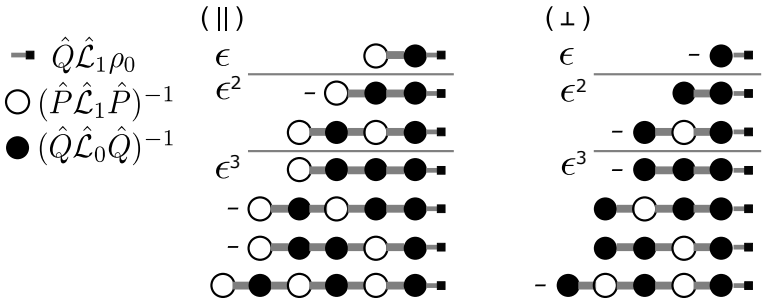


Figure 8.1: Diagrammatic depiction of the structure of corrections to the zeroth order density matrix ρ_0. One draws all possible combinations of open and filled circles starting to the right with a filled circle connected to a small square representing ρ_0. Then one eliminates all diagrams with a direct connection of two open circles. The order of the diagram is given by the number of filled circles, the sign by the total number of lines. The number of terms to order ϵ^n is given by 2^n. Note that the corrections to order n in the perpendicular and parallel sector are simply related by the relation $\delta\rho_{n,\parallel} = -(\hat{P}\hat{\mathcal{L}}_1\hat{P})^{-1}(\hat{P}\hat{\mathcal{L}}_1\hat{Q})\,\delta\rho_{n,\perp}$.

How can one compute perturbatively the effects of the 'other' conservation laws, and (ii) how does the perturbation theory developed above signal the presence of missing conservation laws.

In the following we denote the missing conservation laws not included in the truncated GGE by $C_i^{[m]}$. Similarly, we define susceptibility matrices $\chi_{ij}^{[mm]} = \langle C_i^{[m]} C_j^{[m]} \rangle_{0,c}$ and $\chi_{ij}^{[mt]} = \langle C_i^{[m]} C_j^{[t]} \rangle_{0,c}$, where $\langle \cdot \rangle_0$ stands for expectation values with respect to $\rho_0^{[t]}$. Without loss of generality, we assume that they are orthogonal to the $C_i^{[t]}$, $\chi_{ij}^{[mt]} = 0$ for all i, j (if this is not the case, one can simply replace them by $\hat{Q}_t^\dagger C_i^{[m]}$ where $\hat{Q}_t = \hat{1} - \hat{P}_t$). We define the projector on the tangential space corresponding to the missing conservation laws by

$$\hat{P}_m X = -\sum_{i,j} \frac{\partial \rho_0}{\partial \lambda_i^{[m]}}\Big|_{\rho_0^{[t]}} ((\chi^{[mm]})^{-1})_{ij} \ \mathrm{Tr}[C_j^{[m]} X] \tag{8.34}$$

with $(\partial \rho_0 / \partial \lambda_i^{[m]})\big|_{\rho_0^{[t]}} = -(C_i^{[m]} - \langle C_i^{[m]} \rangle_0)\rho_0$. The sum $\hat{P} = \hat{P}_t + \hat{P}_m$ is then the projector on the tangential space spanned by all conservation laws.

Assuming that the missing conservation laws give only a small correction to the Lagrange parameters λ_i, we can Taylor expand in $\delta\lambda_k = \lambda_k - \lambda_k^{[t]}$ using

$$\begin{aligned} \rho_0 &= \rho_0^{[t]} + \delta\rho_0, \\ \delta\rho_0 &= -\rho_0^{[t]} \sum_k \delta\lambda_k \bar{C}_k, \ \bar{C}_k = C_k - \langle C_k \rangle_0 \end{aligned} \tag{8.35}$$

where the k sum includes both the $C_i^{[t]}$ and $C_i^{[m]}$. From Eq. (8.7), we obtain directly a matrix equation $A\boldsymbol{\delta\lambda} = \boldsymbol{a}$ for $\delta\lambda_i$ solved by $\boldsymbol{\delta\lambda} = A^{-1}\boldsymbol{a}$ which is written in components as

$$\begin{aligned} \begin{pmatrix} \boldsymbol{\delta\lambda}^{[t]} \\ \boldsymbol{\delta\lambda}^{[m]} \end{pmatrix} &= \begin{pmatrix} A^{[tt]} & A^{[tm]} \\ A^{[mt]} & A^{[mm]} \end{pmatrix}^{-1} \begin{pmatrix} 0 \\ \boldsymbol{a}^{[m]} \end{pmatrix} \\ (\boldsymbol{a}^{[m]})_i &= \ \mathrm{Tr}[C_i^{[m]} \hat{\mathcal{L}}_1 \rho_0^{[t]}] = \langle \dot{C}_i^{[m]} \rangle_0 \\ A_{ij}^{[IJ]} &= \mathrm{Tr}[C_i^{[I]} \hat{\mathcal{L}}_1 (\bar{C}_j^{[J]} \rho_0^{[t]})] = \langle \dot{C}_i^{[I]} \bar{C}_j^{[J]} \rangle_{0,c} \end{aligned} \tag{8.36}$$

Note that $A^{[mm]}$ is equivalent to matrix M in Eq. (8.30).

From the change of the Lagrange parameters, one can also directly calculate the change of observables. We are mainly interested in the change of $\langle \delta C_i^{[t]} \rangle_0$

$$\begin{aligned} \langle \delta C_i^{[t]} \rangle_0 &= -\left(\chi^{[tt]} \left(A^{-1}\right)^{[tm]} \boldsymbol{a}^{[m]} \right)_i \\ &\approx \left(\chi^{[tt]} \left(A^{[tt]}\right)^{-1} A^{[tm]} \left(A^{[mm]}\right)^{-1} \boldsymbol{a}^{[m]} \right)_i \end{aligned} \tag{8.37}$$

In the last line we did an extra approximation, assuming that the relevant matrix elements between included and missing conservation laws, $C_i^{[t]}$ and $C_j^{[m]}$, are small, allowing to expand A^{-1} in $A^{[tm]}$. We conclude that the effect of the missing conservation laws is small if either $\langle \dot{C}_i^{[m]} \rangle_0$, the changes of missing conservation laws, are small and/or if the dynamical coupling $A_{ij}^{[tm]} = \langle \dot{C}_i^{[t]} \bar{C}_j^{[m]} \rangle_{0,c}$ is small. The latter susceptibility describes how a change of the Lagrange parameter $\lambda_j^{[m]}$ induces a finite $\langle \dot{C}_i^{[t]} \rangle_0$.

Fully equivalent to Eq. (8.37), one can write everything using projection super-operators $\hat{P}_t, \hat{P}_m$

$$\begin{aligned} \langle \delta C_i^{[t]} \rangle_0 &= -\mathrm{Tr}\left[C_i^{[t]} \hat{P}_t \left(\hat{P}\hat{\mathcal{L}}_1\hat{P}\right)^{-1} \hat{P}_m \hat{\mathcal{L}}_1 \rho_0^{[t]} \right] \\ &\approx \mathrm{Tr}\left[C_i^{[t]} (\hat{P}_t \hat{\mathcal{L}}_1 \hat{P}_t)^{-1} (\hat{P}_t \hat{\mathcal{L}}_1 \hat{P}_m)(\hat{P}_m \hat{\mathcal{L}}_1 \hat{P}_m)^{-1} \hat{P}_m \hat{\mathcal{L}}_1 \rho_0^{[t]} \right] \end{aligned} \tag{8.38}$$

Above, we have calculated effects which occur in cases when the problem was not solved accurately to order ϵ^0 because not all conservation laws of H_0 had been considered. If a theory is not treated correctly to order ϵ^0, any perturbative treatment in ϵ should signal this by the presence of divergencies. In the following, we will show that this is the case within our approach and we will identify directly the origin of these divergencies.

Technically, the divergence in the perturbative formula (8.31) arises from the inverse super-operator $\hat{Q}_t(\hat{Q}_t\hat{\mathcal{L}}_0\hat{Q}_t)^{-1}\hat{Q}_t$ when only a truncated set of conservation laws is used. As $\hat{P}_m$ is the projection operator on the missing conservation laws, we can calculate the divergent contribution from

$$\hat{Q}_t(\hat{Q}_t\hat{\mathcal{L}}_0\hat{Q}_t)^{-1}\hat{Q}_t = -\frac{\hat{P}_m}{\eta} + O(\eta^0) \tag{8.39}$$

where η is the regulator used to define $\hat{\mathcal{L}}_0^{-1}$, see appendix 8.6. We note that exactly the same divergences lead to the occurrence of infinities in the current response of, e.g., integrable systems. As already discussed in Sec. 8.2.3, the latter are described by Drude weights [83, 84, 7] obtained from $\langle(\hat{P}^\dagger J)J\rangle_c$.

The divergent contribution to $\langle\delta C_i^{[t]}\rangle$ within $O(\epsilon)$ perturbation theory around the truncated GGE is obtained from Eqs. (8.31) and (8.39) as

$$\begin{aligned}&\langle\delta C_i^{[t]}\rangle \approx \\ &-\mathrm{Tr}\left[C_i^{[t]}(\hat{P}_t\hat{\mathcal{L}}_1\hat{P}_t)^{-1}(\hat{P}_t\hat{\mathcal{L}}_1\hat{P}_m)\frac{1}{\eta}\hat{P}_m\hat{\mathcal{L}}_1\rho_0\right] + O(\eta^0)\end{aligned} \tag{8.40}$$

This contribution is of order ϵ/η. Comparing Eq. (8.40) and the second line of Eq. (8.38) one observes that the two terms are identical if one replaces $(-\eta)$ by $\hat{P}_m\hat{\mathcal{L}}_1\hat{P}_m$ which is linear in ϵ. Divergencies in perturbation theory can therefore be used to detect missing conservation laws. If, however, the weight of the divergent contribution is small, one can expect that adding the missing conservation laws will have little effect.

8.3.3 Unitary driving, $\hat{P}\hat{\mathcal{L}}_1\hat{P} = 0$

In the discussion given above, we assumed that $\hat{P}\hat{\mathcal{L}}_1\hat{P}$ is finite and invertible within P subspace. For an important class of perturbations, arising from a (Floquet) Hamiltonian H_1, this is not the case as $\mathrm{Tr}(C_i[H_1, \partial\rho_0/\partial\lambda_j]) = 0$ due to the cyclic property of the trace and one therefore finds $\hat{P}\hat{\mathcal{L}}_1\hat{P} = 0$. In this case, the rates with which the C_i change are second order in ϵ, as is well-known from Fermi's golden rule.

For $\hat{P}\hat{\mathcal{L}}_1\hat{P} = 0$ the exact inverse of the Liouvillian in the $\hat{P}$ sector is given by $\hat{P}\hat{\mathcal{L}}^{-1}\hat{P} = -\hat{P}(\hat{P}\hat{\mathcal{L}}_1\hat{Q}(\hat{Q}\hat{\mathcal{L}}\hat{Q})^{-1}\hat{Q}\hat{\mathcal{L}}_1\hat{P})^{-1}\hat{P}$, see appendix 8.10.1. In the limit of small ϵ, we therefore find

$$\hat{P}\hat{\mathcal{L}}^{-1}\hat{P} = \hat{P}(\hat{P}\hat{\mathcal{L}}_2\hat{P})^{-1}\hat{P} + \mathcal{O}(\epsilon^{-1}) \tag{8.41}$$

where

$$\hat{\mathcal{L}}_2 = -\hat{\mathcal{L}}_1\hat{Q}\,(\hat{Q}\hat{\mathcal{L}}_0\hat{Q})^{-1}\,\hat{Q}\hat{\mathcal{L}}_1. \tag{8.42}$$

$\hat{P}\hat{\mathcal{L}}_2\hat{P} \propto \epsilon^2$ is an effective Lindblad super-operator acting in the P space. With this notation the condition for ρ_0, Eq. (8.9), takes the form $\mathrm{Tr}[C_i\hat{\mathcal{L}}_2\rho_0] = 0$, or, equivalently, Eq. (8.19), is written as

$$\hat{P}\hat{\mathcal{L}}_2\rho_0 = 0. \tag{8.43}$$

where one should keep in mind that $\hat{P}$ project onto non-oscillatory density matrices only. Perturbation theory can now be derived in a straightforward way by a Taylor expansion of

$$(\hat{\mathcal{L}}_0 + \hat{\mathcal{L}}_1)^{-1} = \big((\hat{\mathcal{L}}_0 + \hat{P}\hat{\mathcal{L}}_2\hat{P}) + (\hat{\mathcal{L}}_1 - \hat{P}\hat{\mathcal{L}}_2\hat{P})\big)^{-1} \tag{8.44}$$

in the second term, with the inverse applied as in equation (8.4) for $\delta\rho$.

One can, again, derive diagrammatic rules to calculate corrections to order ϵ^n, see Fig. 8.2. Compared to the previous case, shown in Fig. 8.1, there are only two changes. First, $(\hat{P}\hat{\mathcal{L}}_1\hat{P})^{-1} \sim \mathcal{O}(\epsilon^{-1})$ (open circle) is replaced by $(\hat{P}\hat{\mathcal{L}}_2\hat{P})^{-1} \sim \mathcal{O}(\epsilon^{-2})$ and, second, two sets of diagrams do not contribute any more as they either cancel due to the $-\hat{P}\hat{\mathcal{L}}_2\hat{P}$ in Eq. (8.44) or are set to zero by the condition (8.43) for ρ_0. Explicitly, there are no diagrams with neighboring open circles, with the combination open-filled-open, and finally also the combination open-fillled-ρ_0 (small square). The cancellation of these diagrams is also a necessary condition for the series expansion in ϵ to be valid. In Fig. 8.2, we show all remaining diagrams up to $\mathcal{O}(\epsilon^3)$ and describe in the figure caption the corresponding diagramatic rules.

We would like to finish the section by pointing out that there can be more complex situations [19, 77] where perturbation theory to order ϵ^2 does not fix ρ_0 and where accordingly $\hat{P}\hat{\mathcal{L}}_2\hat{P}$ vanishes, see discussion at the end Sec. 8.2.1. Or even more general, there can be cases where Hamiltonian and Lindblad perturbations occur on equal footing or where some approximate conservation laws change by processes to order ϵ and others by order ϵ^2. We believe that in all these cases, one can generalize the approach described above: one defines projectors on subspaces governed by similar time-scales (same power of ϵ), identifies the leading-order dynamics ($\hat{P}\hat{\mathcal{L}}_2\hat{P}$ in the case discussed above) in each subsector perturbatively, uses this to fix ρ_0 in analogy to Eq. (8.43), and performs then a Taylor expansion using the analog of Eq. (8.44) as a starting point.

8.4 Example: Interacting Fermions with particle-gain and loss

In the following we will give two examples where the perturbation theory developed above applies. We consider interacting fermions driven out of equilibrium by a weak coupling to the environment. As perturbation we choose processes which lead to a particle loss with rate ϵl_n and a gain of particles with rate ϵg_n. In quantum optics experiments, the quasiparticles could be excitations of atoms (or cavities) and gain and loss is realized by emission and absorption of light. The same situation arises in experiments on exciton condensation, magnon condensation

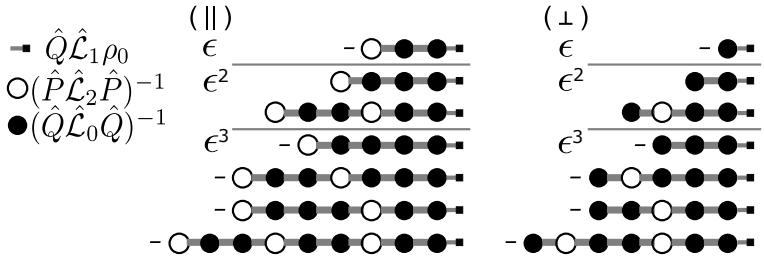


Figure 8.2: Diagrammatic depiction of the corrections $\delta\rho$ to the zeroth order density matrix ρ_0 for cases where $\hat{P}\hat{\mathcal{L}}_1\hat{P} = 0$ (unitary driving). One first draws all possible combinations of open and filled circles starting to the right with a filled circle connected to ρ_0 (small square). Then one eliminates all diagrams with neighboring open circles, all with the combination open-filled-open, and finally also the combination open-filled-ρ_0 (small square). The order is given by the number of filled minus the number of open circles, the sign by the total number of circles. The number of terms to order ϵ^n is 2^n. Some diagrams do, however, vanish for monochromatic perturbations, see appendix 8.10.3.

or in photon BECs [10, 11, 12, 13, 14, 15, 16, 17]. Also in experiments with ultracold atoms, loss processes arise when atoms absorb photons from external laser beams, kicking them out of their trap. However, most cold-atom experiments do not include processes where the lost atoms are replenished and therefore a true steady state, the main focus of our study, cannot be reached.

We first study in Sec. 8.4.1 a small finite-size system where we can compare directly perturbation theory and exact solution. Here it is important to realize that the applicability of perturbation theory for small systems (in the limit where perturbations are small compared to the level spacing) does not guarantee the validity of perturbation theory for systems close to the thermodynamic limit (perturbations large compared to the level spacing but small compared to internal equilibration rates). We therefore study in Sec. 8.4.2 the thermodynamic limit by considering a regime where the Boltzmann equation can be applied. A numerical investigation of the thermodynamic limit in a quantum approach is beyond the scope of the present paper and is left for future studies [87].

8.4.1 Lindblad dynamics in a small system

We consider a model where the Hamiltonian dynamics of the unperturbed system is given by

$$H_0 = \sum_{n=1}^{L} e_n c_n^\dagger c_n + U \sum_{n_1>n_2,n_3<n_4} c_{n_1}^\dagger c_{n_2}^\dagger c_{n_3} c_{n_4} \tag{8.45}$$

with $e_n = n/L$. Gain and loss processes are described by the Lindblad operators $L_n^g = c_n^\dagger$ and $L_n^l = c_n$ such that

$$\begin{aligned} \hat{\mathcal{L}}_1 &= \epsilon(\hat{D}_g + D_l) \\ \hat{D}_g &= \sum g_n \left(L_n^g \rho L_n^{g\,\dagger} - \frac{1}{2}\{L_n^{g\,\dagger} L_n^g, \rho\} \right) \\ \hat{D}_l &= \sum l_n \left(L_n^l \rho L_n^{l\,\dagger} - \frac{1}{2}\{L_n^{l\,\dagger} L_n^l, \rho\} \right) \end{aligned} \tag{8.46}$$

with

$$g_n = \frac{1}{4}, \quad l_n = e_n \tag{8.47}$$

The loss rate ϵl_n depends on energy. This mimics a situation where high-energy states have a higher probability to evaporate than low-energy states, thus implementing a cooling mechanism. Note that ϵ, the common prefactor of $\hat{D}_i$, controls the overall strength of both the heating and cooling terms.

The conservation laws of the small system are just projectors on the eigenstates of H_0, $|n\rangle\langle n|$ with $H_0|n\rangle = E_n^0|n\rangle$. Using the formulas of Secs. 8.2,8.3 we can easily solve for the 0th order steady state and determine the perturbations around it. In Fig. 8.3 we show the expectation values of particle and energy density as a function of perturbation strength ϵ, calculated from the exact steady state density matrix (solid line) or using our perturbation theory up to k-th order in ϵ on systems size $L = 4$, $k = 2, 4, 10$, and interaction strength $U = 0.3$.

so I need to try to reproduce these results, right???

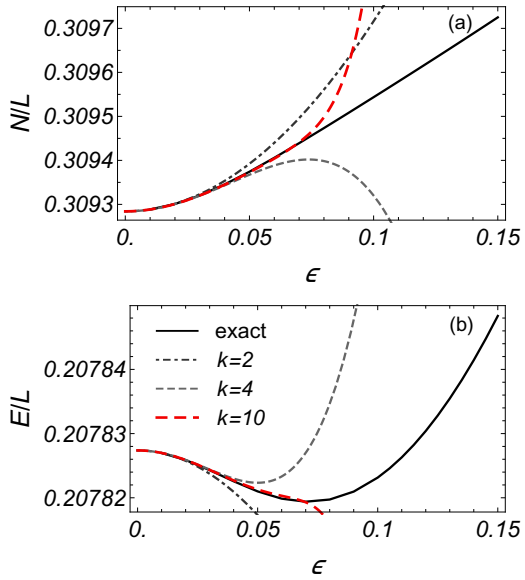


Figure 8.3: (Color online) Expectation values of (a) particle and (b) energy density as a function of perturbation strength ϵ, calculated from the exact steady state density matrix (solid line) or using our perturbation theory up to k-th order in ϵ on systems size $L = 4$, and interaction strength $U = 0.3$.

The figures show that for this small system with finite level spacing the perturbation theory works for small ϵ. For the chosen model we find both from the exact result and from the perturbation theory that the variations of particle number and energy are tiny. The perturbation theory breaks down for rather small ϵ of the order of the level spacing. This is a phenomenon well known from standard perturbation theory where perturbative corrections are inversely proportional to the level spacing. This is, however, dfferent when correlations functions are evaluated in the thermodynamics limit by taking first the limit $L \to \infty$ and then the limit $\eta \to 0$, where η is the regulator defined in Eq. (8.4), see also App. 8.9. While the perturbative correction linear in ϵ vanishes for the finite system (η smaller than level spacing), it is finite in the thermodynamics limit (η larger than level spacing).

8.4.2 Boltzmann dynamics

Now we consider a similar example in the thermodynamic limit where the unperturbed system H_0 has only two local conservation laws, energy and particle number. Interactions lead to an equilibration of all other conservation laws. We assume that the system can be described by weakly interacting quasiparticles with energies e_n, such that the collision term of a Boltzmann equation captures their equilibration dynamics. As above we consider fermions with a constant density of states, which we discretize using L single-particle states with energies e_n equally spaced between 0 and 1 with $e_n = n/L$, $n = 1, \ldots, L$. The Boltzmann equation takes

the form,

$$\frac{df_e}{dt} = M[f]_e + \epsilon\, D[f]_e \tag{8.48}$$

$$\begin{aligned} M[f]_e &= \int_0^1 de_1 de_2 de_3\, \delta(e + e_1 - e_2 - e_3) \\ &\qquad \times (\bar{f}_e \bar{f}_{e_1} f_{e_2} f_{e_3} - f_e f_{e_1} \bar{f}_{e_2} \bar{f}_{e_3}) \\ &= \frac{1}{L^2} \sum_{i,j,l} (\bar{f}_e \bar{f}_{e_i} f_{e_j} f_{e_l} - f_e f_{e_i} \bar{f}_{e_j} \bar{f}_{e_l})\; \delta_{e+e_i, e_j+e_l} \end{aligned}$$

$$D[f]_e = -l_e f_e + g_e \bar{f}_e \tag{8.49}$$

where f_{e_n} is the occupation function as function of the energy e_n and $\bar{f}_e = (1 - f_e)$. The Kronecker-δ guarantees energy conservation in each collision process of the discretized model. Note that we consider a model where momentum conservation does not play a role. For simplicity, we also set all transition rates due to collisions to unity. We keep the same type of perturbations as in the previous example, i.e. particle gain and loss. Instead of Lindblad operators these are now encoded directly in Boltzmann equation through $D[f]_e$, Eq. (8.49). Rates for particle gain and loss are the same as in Eq. (8.47), i.e., $g_e = 1/4, l_e = e$. Note that ϵ, the prefactor of $D[f]_e$, controls the overall strength of both the heating and cooling terms. Numerical calculations are performed for $L = 41$.

The perturbation theory derived in the main text can be with some straightforward modifications also applied to the open Boltzmann dynamics. Before we proceed we collect in Table

Table 1: Comparison of semi-classical open Boltzmann dynamics for level occupation function and quantum Liovillian formulation for density matrix

Boltzmann	Liouvillian
occupation function f_e	density matrix ρ
$\frac{df_e}{dt} = M[f]_e + \epsilon\, D[f]_e$	$\frac{d\rho}{dt} = \hat{\mathcal{L}}_0 \rho + \hat{\mathcal{L}}_1 \rho$
$f_e(t \to \infty) = f_e^0 + \delta f_e$	$\rho(t \to \infty) = \rho_0 + \delta\rho$
Fermi function: $f_e^0 = \frac{1}{1+e^{\beta(e-\mu)}}$	GGE: $\rho_0 = \frac{e^{-\lambda_i C_i}}{\mathrm{Tr}[e^{-\lambda_i C_i}]}$
conservation laws and scalar product	
$c_i(e)$ and $q_i^{\beta,\mu}$	C_i and $\partial\rho_0/\partial\lambda_i$
$\int de\, c_i(e) f_e$	$\mathrm{Tr}[C_i \rho] = \langle C_i \rangle$
$\chi_{ij}(\beta,\mu) = -\int de\, c_i(e)\, q_j^{\beta,\mu}(e)$	$\chi_{ij} = -\mathrm{Tr}[C_i \partial\rho_0/\partial\lambda_j]$
zeroth order perturbation theory	
$\int de\, c_i(e) \epsilon D[f^0]_e = 0$	$\mathrm{Tr}[C_i \hat{\mathcal{L}}_1 \rho_0] = 0$
$\hat{P}\big[D[f^0]\big] = 0$	$\hat{P}(\hat{\mathcal{L}}_1 \rho_0) = 0$
first order corrections	
$\boldsymbol{f}_\perp^1 = -(QM^{(0)}Q)^{-1} Q \boldsymbol{D}[\boldsymbol{f}^0]$	$\delta\rho_{1,\perp} = -(\hat{Q}\hat{\mathcal{L}}_0\hat{Q})^{-1}\; \hat{Q}\hat{\mathcal{L}}_1\rho_0$
$\boldsymbol{f}_\parallel^1 = (PD^{(1)}P)^{-1} PD^{(1)}Q \times$ $\times (QM^{(0)}Q)^{-1} Q \boldsymbol{D}[\boldsymbol{f}^0]$	$\delta\rho_{1,\parallel} = (\hat{P}\hat{\mathcal{L}}_1\hat{P})^{-1} \hat{P}\hat{\mathcal{L}}_1\hat{Q} \times$ $\times \hat{\mathcal{L}}_0^{-1} \hat{Q}\hat{\mathcal{L}}_1\rho_0$

1 all analogies with the formulation for the Liouvillian dynamics, developed in the main part of the article. Note that some objects are defined later within this section.

The collision integral M preserves the total energy $E = \sum_n e_n f_{e_n}$ and the particle number $N = \sum_n f_{e_n}$ and these are the only conserved quantities in the absence of loss/gain term. In the following we expand the level occupations f_e in orders of ϵ,

$$f_e(t \to \infty) = \sum_m \epsilon^m f_e^m. \tag{8.50}$$

In correspondence with $\hat{\mathcal{L}}_0 \rho_0 = 0$ now any Fermi-Dirac distribution f_e^0 satisfies $M[f^0] = 0$,

$$\begin{aligned} f_e^0(\beta,\mu) = \frac{1}{1+e^{\beta(e-\mu)}} \quad &\leftrightarrow \quad \rho_0, \\ M[f^0(\beta,\mu)]_e = 0 \quad &\leftrightarrow \quad \hat{\mathcal{L}}_0 \rho_0 = 0 \end{aligned} \tag{8.51}$$

and only the perturbation D fixes the parameters β and μ, where β is the Lagrange parameter of the energy and $-\beta\mu$ is the Lagrange parameter of the particle number.

Zeroth order— The parameters β and μ of the steady-state in the $\epsilon \to 0$ limit, $f_e^0(\beta,\mu)$, are determined by the stationarity of conserved quantities (total energy and particle number) from a set of coupled equations corresponding to Eq. (8.7),

$$\begin{aligned} \frac{1}{L}\frac{dE}{dt} &\approx \epsilon \int de\; e\big(-l_e f_e^0 + g_e(1-f_e^0)\big) \stackrel{!}{=} 0 \\ \frac{1}{L}\frac{dN}{dt} &\approx \epsilon \int de\; \big(-l_e f_e^0 + g_e(1-f_e^0)\big) \stackrel{!}{=} 0 \end{aligned} \tag{8.52}$$

For our model we find $\beta = 2.328$ and $\mu = 0.288$.

Projection operator — The two slow modes q_i, corresponding to $\partial\rho_0/\partial\lambda_i$ in the main text, are defined as

$$q_1^{\beta,\mu}(e) = \frac{\partial f_e^0}{\partial\beta}, \quad q_2^{\beta,\mu}(e) = \frac{\partial f_e^0}{\partial(-\beta\mu)} \tag{8.53}$$

where we identified $\lambda_2 = -\beta\mu$. Denoting the conserved quantities by

$$c_1(e) = e,\; c_2(e) = 1 \tag{8.54}$$

the analog of the projector super-operator defined by Eq. (9.4) is simply given by

$$\begin{aligned} \hat{P}[X] &= -\sum_{i,j=1}^{2} q_i^{\beta,\mu}(e)\; (\chi^{-1})_{ij} \int de\,(c_j(e)X(e)) \\ \chi_{ij}(\beta,\mu) &= -\int de\, c_i(e)\, q_j^{\beta,\mu}(e). \end{aligned} \tag{8.55}$$

With these notations, the steady state condition, Eq. (8.52), is the analog of Eq. (8.7)

$$\int de\, c_i(e) D[f^0]_e = 0 \quad \leftrightarrow \quad \mathrm{Tr}[C_i \hat{\mathcal{L}}_1 \rho_0] = 0$$

or, equivalently,

$$\hat{P}\big[D[f^0]\big] = 0 \quad \leftrightarrow \quad \hat{P}(\hat{\mathcal{L}}_1\rho_0) = 0.$$

Relaxation towards the steady state — While the main focus of this paper is the computation of the steady state, we briefly discuss the relaxation towards the steady state, which can easily be computed exactly by solving the Boltzmann equation.

Similarly as GGEs are expected to be a fairly good description shortly after the system has prethermalized [88, 89, 90, 8, 92, 40, 94, 95, 96, 97, 98, 41, 100, 101, 102, 103, 104, 105, 106, 107, 108] to the GGE manifold, also here the Fermi-Dirac distribution describes approximately not

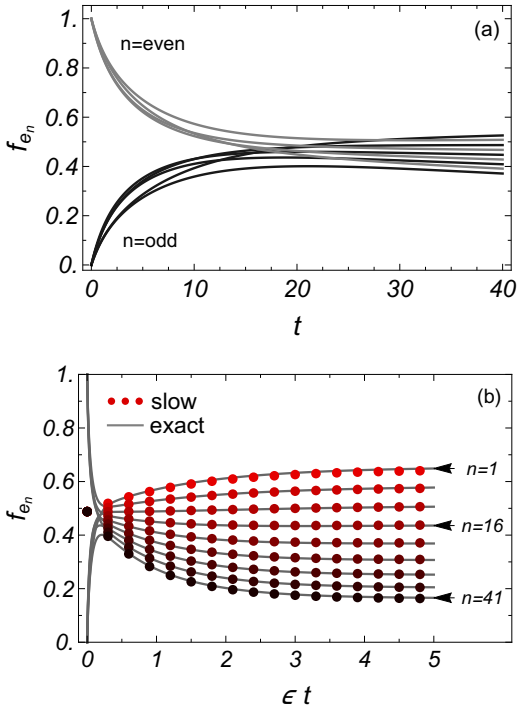


Figure 8.4: (Color online) Time evolution of the occupation function f_{e_n} shown for $n = 1, 6, 11, \ldots, 41$ ($L = 41$) and $\epsilon = 0.01$ starting from an initial state with $f_{e_n} = 1$ ($f_{e_n} = 0$) for states with even (odd) n, respectively. (a) On short time scales the system relaxes towards a state with $\beta \approx 0$ and equal occupation of all levels. (b) The time evolution toward the steady state occurs on a time scale set by $1/\epsilon$ and therefore the time axis has been rescaled by a factor ϵ. The points are obtained by solving the time evolution of the Lagrange parameters using Eq. (8.57) which then determine a Fermi distribution function. The comparison with the exact solution of the Boltzmann equation (lines) shows that this allows for a quantitative description of the slow dynamics for small ϵ.

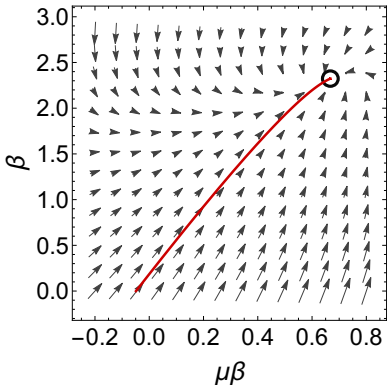


Figure 8.5: (Color online) Force fields calculated using Eq. (8.56) shown for $L = 41$. The force fields determine the time evolution of the Lagrange parameters according to Eq. (8.57). The red solid line shows the trajectory for the initial conditions used in Fig. 8.4, where a comparision to the exact solution of the Boltzmann equation is shown. The unique stationary state is indicated by a black circle.

only the steady state but also the approach to it. After a few collisions level occupations can be approximately described by a Fermi distribution with time-dependent parameters $\{\beta(t), \mu(t)\}$, whose evolution is determined by the forces introduced in Eq. (8.17).

In this case force field, see Eq. (8.17), has only two components,

$$F_i(\beta, \mu) = -\left(\chi^{-1}\right)_{ij} \int de\, c_j(e)\, \epsilon D[f^0]_e \tag{8.56}$$

and can be used to propagate parameters β and μ,

$$\frac{d\beta}{dt}(t) = F_1(t), \quad \frac{d(-\beta\mu)}{dt}(t) = F_2(t), \tag{8.57}$$

as soon as our system is approximately described by a Fermi-Dirac distribution. These equations are only valid to leading order in ϵ.

Fig. 8.4 shows the time-evolution obtained from a numerical solution of the Boltzmann equation for $\epsilon = 0.01$. We initialize our system with the non-equilibrium state $f_{e_n} = 1$ for states with even and $f_{e_n} = 0$ for states with odd n. Collisions lead to a rapid relaxation of this non-equilibrium state to a thermal state. We find that within our model this time scale is $\tau_0 \sim 5$, independent of ϵ for small ϵ. As the collision processes conserve energy and particle number, the approximate thermal state is determined by the initial values of energy and particle number, which leads to an initial relaxation towards a state with $\beta = 0$ and $\beta\mu = 0$ (in the thermodynamic limit). The subsequent dynamics is driven by the processes violating particle number and energy conservation (the gain and loss terms) and occurs on a time scale set by $1/\epsilon$. We find that these processes are quantitatively described by Eq. (8.57), as can be seen by comparing the dots and the solid line in the lower panel of Fig. 8.4.

Fig. 8.5 shows the force fields calculated according to Eq. (8.56) and the resulting dynamics in the space of Lagrange parameters.

Perturbation theory for the steady state — As a next step, we compare the exact steady-state solution of the Boltzmann equation for finite ϵ to the result of perturbation theory to linear order in ϵ. We expand around the Fermi functions $f^0_e(\beta, \mu)$ with parameters β and μ obtained from the 'zeroth order' described above. To linear order in ϵ, we obtain using $f_e = f^0_e + \epsilon f^1_e$ to $\mathcal{O}(\epsilon)$

$$\begin{aligned} 0 &= \epsilon(M^{(0)} + \epsilon D^{(1)})[f^1] + \epsilon D[f^0] \\ \Leftrightarrow f^1 &= -(M^{(0)} + \epsilon D^{(1)})^{-1} D[f^0] \end{aligned} \tag{8.58}$$

which has precisely the same form as Eq. (8.4) in the Liouville case. For the discrete case matrices $M^{(0)}, D^{(1)}$ are defined using a straightforward Taylor expansion

$$\begin{aligned} M[f]_{e_n} &\approx \epsilon \sum_{n'} M^{(0)}_{n,n'} f^1_{e_{n'}} \\ (-l_{e_n} f_{e_n} + g_{e_n} \bar{f}_{e_n}) &\approx D[f^0]_{e_n} + \epsilon \sum_{n'} D^{(1)}_{n,n'} f^1_{e'_n}. \end{aligned} \tag{8.59}$$

Note that $D^{(1)}$ is a diagonal matrix in our example. To obtain $\boldsymbol{f}^1 = \{f^1_{e_1}, f^1_{e_2}, \ldots, f^1_{e_L}\}$ corrections we can use the perturbation theory developed in Sec. 8.3.1. As before we need to treat the ($\|$) and ($\perp$) subspaces separately. Following Eqs. (8.28,8.29),

$$\begin{aligned} \boldsymbol{f}^1 &= \boldsymbol{f}^1_{\|} + \boldsymbol{f}^1_{\perp}, \\ \boldsymbol{f}^1_{\perp} &= -(QM^{(0)}Q)^{-1}\, \boldsymbol{D}[\boldsymbol{f}^0] \\ \boldsymbol{f}^1_{\|} &= (PD^{(1)}P)^{-1}\, PD^{(1)}Q\, (QM^{(0)}Q)^{-1}\, \boldsymbol{D}[\boldsymbol{f}^0], \end{aligned} \tag{8.60}$$

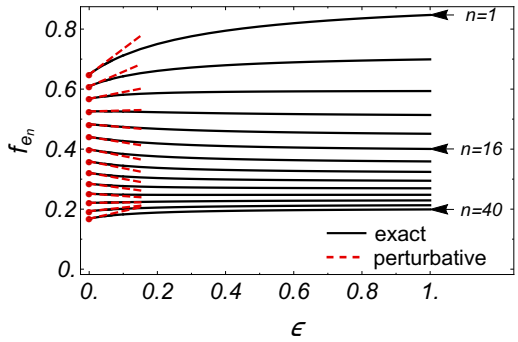


Figure 8.6: (Color online) Level occupation f_{e_n} as a function of perturbation strength ϵ. Solid lines are obtained from the exact calculation using Boltzmann equation, Eq. (8.48), while dashed lines are obtained from our perturbative approach, including zeroth and first order in ϵ. Only every third n is shown for system with $L = 41$ single-particle states.

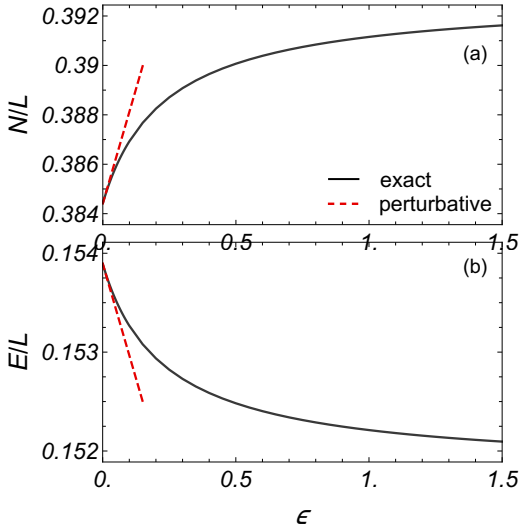


Figure 8.7: (Color online) (a) Particle and (b) energy density as a function of perturbation strength ϵ. The dashed line shows the result of perturbation theory, including zeroth and first order in ϵ.

where P, Q are written as matrices after evaluating Eq. (8.55) for discretized energies and $\hat{Q} = \hat{1} - \hat{P}$. Fig. 8.6 shows steady state level occupation f_{e_n} as a function of perturbation strength ϵ. In the limit $\epsilon \to 0$ Fermi functions obtained from condition Eq. (8.52) give the exact steady state occupation distributions. For finite $\epsilon \lesssim 0.05$ the corrections linear in ϵ describe well the exact result. In Fig. 8.7 we show similar results for the total energy and particle number of the system, which for the chosen model change only slightly.

It is also straightforward to calculate higher order corrections using perturbation theory applied to the Boltzmann equation. However, here one has to take into account that the Boltzmann equation is a non-linear equation in the occupation functions f_e while the Liouville equation is a linear equation in the density matrix ρ. Therefore the equations used to obtain higher order corrections differ in the two cases but the overall structure of perturbation theory (separation into parallel and perpendicular sector) remains the same.

8.5 Conclusions

The main observation, which is the basis of our study, is that many driven systems can be approximately but efficiently described by generalized Gibbs ensembles built from approximately conserved quantities. Such approximate conservation laws are important for many different systems. For example, in almost all solids, the coupling of electrons and phonons is weak due to the large mismatch of ionic and electronic masses. Therefore the difference of the electron and phonon Hamiltonians, $H_e - H_{\rm ph}$, is an approximate conservation law widely used in two-temperature models [19, 20, 21, 22, 23] which efficiently describe non-equilibrium states of solids. A more exotic example is the description of spin-chain materials using as the approximate conservation laws those of the underlying integrable Heisenberg model [26]. For such situations, we developed in this paper a perturbation theory for the steady state by perturbing around generalized Gibbs ensembles. Here it was essential to treat perturbations perpendicular and parallel to the manifold of generalized Gibbs states separately.

To show the validity of our concepts we studied a small finite size quantum system with Lindblad dynamics. For the future [87] we plan to test numerically our approach also for larger quantum systems close to the thermodynamic limit. In this paper we considered as an example for a large system only a model described by the Boltzmann equation. From a more general point of view, one can consider the Boltzmann equation also as a rate equation for approximately conserved quantities, the quasi-particle occupations $c_k^\dagger c_k$, thus fixing the parameters of the appropriate generalized Gibbs ensemble $e^{-\sum_k g_k c_k^\dagger c_k}$ (as in our paper, we assume a translationally invariant system here). Therefore it would be interesting to use our formalism to calculate corrections to the non-equilibrium steady state not captured by the Boltzmann approach. A comparison of the two formalisms and a systematic calculation of beyond-Boltzmann corrections for weakly interacting quantum systems is left for further studies. In the classical context such a formalism has been developed by Gurarie [109]. It would be in general interesting to test the validity of our approach in purely classical systems, for example, those described by the Fokker-Planck equation.

An obvious question is whether our perturbation theory in ϵ, where ϵ is the prefactor of driving terms breaking the conservation laws, has a finite radius of convergence and/or whether all expansion coefficients are finite. Similarly to many other (highly successful) perturbative expansions in physics, the radius of convergence is formally expected to be zero. This is obvious in the case when the perturbation arises from a Lindblad operator, where negative ϵ correspond to negative friction and therefore an unstable situation for arbitrarily small ϵ, which implies a vanishing radius of convergence. The expansion in ϵ should therefore be viewed as an asymptotic expansion similar to, e.g., the expansion in the fine-structure constant α in quantum-electrodynamics. A more difficult question is whether one can expect that all expansion coefficient in powers of ϵ are finite or not. This is an open question which requires further studies. There is, however, a possible mechanism which can induce non-analytic corrections: in the presence of exact symmetries, hydrodynamic modes exist which enforce long-ranged correlations and, for example, the presence of long-time tails after quenches [110, 111, 112]. These hydrodynamic modes obtain masses proportional to ϵ or ϵ^2 when the relevant conservation laws are weakly violated. A perturbative expansion in these masses can lead to non-analytic corrections even when perturbing around a GGE.

For the future it will be interesting to generalize our perturbative expansion for the steady state to dynamical questions. For example, we have already shown for a simple example based on the Boltzmann equation that time-dependent generalized Gibbs ensembles are a good starting point to investigate the approach of the steady state. It will be interesting to develop a perturbative expansion for such situations which will also allow to describe the dynamical response of driven systems and/or situations where instead of a unique steady state a limit cycle

(time crystal) is realized.

8.6 Regularization of inverse

Since $\hat{\mathcal{L}}$ has a zero mode, $\hat{\mathcal{L}}^{-1}$ is singular therefore formally one has to regularize it as in Eq. (8.4), which at the same time also avoids solution $\delta\rho = -\rho_0$ that satisfies $\hat{\mathcal{L}}(\rho_0 + \delta\rho)$ trivially. If we write $\rho_0 = \sum_\alpha c_\alpha \rho^\alpha$ in terms of $\hat{\mathcal{L}}$ (right) eigenstates ρ^α, $\hat{\mathcal{L}}\rho^\alpha = \lambda_\alpha \rho^\alpha$, then the regularization

$$\begin{aligned}\delta\rho &= -\lim_{\eta\to 0}(\hat{\mathcal{L}} - \eta\mathbb{1})^{-1}\hat{\mathcal{L}}_1\rho_0 = -\lim_{\eta\to 0}(\hat{\mathcal{L}} - \eta\mathbb{1})^{-1}\hat{\mathcal{L}}\rho_0, \\ &= -\lim_{\eta\to 0}(\hat{\mathcal{L}} - \eta\mathbb{1})^{-1}\sum_\alpha \lambda_\alpha c_\alpha \rho^\alpha \\ &= -\lim_{\eta\to 0}\sum_\alpha \frac{\lambda_\alpha}{\lambda_\alpha - \eta}\, c_\alpha\rho^\alpha = -\sum_{\alpha,\lambda_\alpha\neq 0} c_\alpha\rho^\alpha. \end{aligned} \tag{8.61}$$

gives the correct result, $\rho_0 + \delta\rho = \sum_{\alpha,\lambda_\alpha=0}\rho^\alpha$. The sign $\eta > 0$ is obtained from the property that $\mathrm{Re}\,\lambda_\alpha \leq 0$ guaranteeing the absence of exponentially growing solutions.

The regularization also guarantees that $\mathrm{Tr}\,\delta\rho = 0$. From $\mathrm{Tr}\,\dot{\rho} = \mathrm{Tr}[\hat{\mathcal{L}}\rho] = 0$, it follows that $\lambda_\alpha \mathrm{Tr}\,\rho^\alpha = 0$ and therefore $\mathrm{Tr}\,\rho^\alpha = 0$ for all α with $\lambda_\alpha \neq 0$. Using (8.61), we therefore find $\mathrm{Tr}\,\delta\rho = 0$.

8.7 Identities for super-operators

Below we check the properties of super-projector defined in Eq. (9.4).

Projection property

$$\begin{aligned}\hat{P}^2 X &= \sum_{i'j'ij}\frac{\partial\rho_0}{\partial\lambda_{i'}}(\chi^{-1})_{i'j'}\ \mathrm{Tr}\big[C_{j'}\frac{\partial\rho_0}{\partial\lambda_i}\big](\chi^{-1})_{ij}\ \mathrm{Tr}[C_j X] \\ &= -\sum_{i'j'ij}\frac{\partial\rho_0}{\partial\lambda_{i'}}(\chi^{-1})_{i'j'}\ \chi_{j'i}(\chi^{-1})_{ij}\ \mathrm{Tr}[C_j X] \\ &= -\sum_{i'j'j}\frac{\partial\rho_0}{\partial\lambda_{i'}}(\chi^{-1})_{i'j'}\ \delta_{j'j}\ \mathrm{Tr}[C_j X] = \hat{P}X \end{aligned} \tag{8.62}$$

Inverse within P subspace

Since $(\hat{P}\hat{\mathcal{L}}_1\hat{P})^{-1}$ is essential for building up the perturbation theory we confirm the validity of Eq. (8.30)

$$(\hat{P}\hat{\mathcal{L}}_1\hat{P})^{-1}\hat{P}X = -\sum_{pr}\frac{\partial\rho_0}{\partial\lambda_p}(M^{-1})_{pr}\ \mathrm{Tr}[C_r X], \tag{8.63}$$

with $M_{pr} = -\mathrm{Tr}[C_p\hat{\mathcal{L}}_1\frac{\partial\rho_0}{\partial\lambda_r}] = \langle \dot{C}_p C_r\rangle_{0,c}$ by calculating

$$\begin{aligned}&(\hat{P}\hat{\mathcal{L}}_1\hat{P})^{-1}(\hat{P}\hat{\mathcal{L}}_1\hat{P})X \\ &= -\sum_{pr,kl,ij}\frac{\partial\rho_0}{\partial\lambda_p}(M^{-1})_{pr}\ \chi_{rk}(\chi^{-1})_{kl}M_{li}\ (\chi^{-1})_{ij}\mathrm{Tr}[C_j X] \\ &= -\sum_{pr,kl,ij}\frac{\partial\rho_0}{\partial\lambda_p}(M^{-1})_{pr}\ \delta_{r,l}M_{li}\ (\chi^{-1})_{ij}\mathrm{Tr}[C_j X] = \hat{P}X. \end{aligned}$$

8.8 Properties of projectors and inversion of projected Lindblad operators

In this appendix we discuss the relation of the projectors $\hat{P}$ and $\tilde{P}$ and describe how projected Lindblad operators can be inverted.

We first note that any projected density matrix is traceless

$$\mathrm{Tr}[\hat{P}\rho] = 0 \tag{8.64}$$

which follows from $\mathrm{Tr}[\rho_0] = 1$ and therefore $\partial \mathrm{Tr}[\rho_0]/\partial\lambda_i = 0$.

If we consider all conservation laws from the set $\mathcal{Q} = \{|n\rangle\langle m|$ with $E_n^0 = E_m^0\}$, $H_0|n\rangle = E_n^0|n\rangle$, then we obtain

$$\hat{P}X = \tilde{P}X - \frac{\mathrm{Tr}[X]}{\mathrm{Tr}[\mathbb{1}]}\,\mathbb{1} \tag{8.65}$$

where $\tilde{P}X$ is part of X that can be written in terms of elements of $\mathcal{Q}$ (for non-degenerate case simply the diagonal part). Therefore $\hat{P}$ projects on conservation laws and subtracts the trace.

Assuming that $\hat{P}\hat{\mathcal{L}}_1\rho_0$, Eq. (8.18), has a unique solution with trace 1, then one can easily show that $\hat{P}\hat{\mathcal{L}}_1\hat{P}$ is invertible in $\hat{P}$ space. Assuming that $\hat{P}\hat{\mathcal{L}}_1\hat{P}\rho_1 = 0$, it follows immediately that $\hat{P}\hat{\mathcal{L}}_1(\rho_0 + \hat{P}\rho_1) = 0$. As ρ_0 is by assumption a unique solution, we find $\hat{P}\rho_1 = 0$. Therefore ρ_1 has no component in $\hat{P}$ space.

As $\hat{P}\mathbb{1} = 0$, the identity matrix is in the $\hat{Q}$ space, $\hat{Q}\mathbb{1} = \mathbb{1}$. This seems to be a problem as we have to invert $\hat{Q}\hat{\mathcal{L}}_0\hat{Q}$ and $\hat{\mathcal{L}}_0\mathbb{1} = 0$ for all $\hat{\mathcal{L}}_0$ describing unitary evolution . In all of our formulas, however, the inverse of $\hat{Q}\hat{\mathcal{L}}_0\hat{Q}$ is only applied to traceless density matrices, therefore no singularity arises from this zero mode. For numerical implementations one can simply add a 'mass term' m_0 to this zero mode by replacing $\hat{\mathcal{L}}_0 \to \hat{\mathcal{L}}_0 + m_0\hat{P}_{\mathbb{1}}$ where $\hat{P}_{\mathbb{1}}$ is the superoperator projecting onto the identity matrix defined by $\hat{P}_{\mathbb{1}}X = \mathbb{1}\,\mathrm{Tr}[X]/\mathrm{Tr}[\mathbb{1}]$.

8.9 Correlation functions

Higher order corrections $\delta\rho$ to ρ_0, as derived from our perturbation theory, can also be expressed in terms of multi-time correlation functions. In the main text we have already introduced

$$\begin{aligned} \chi_{ij} &= -\mathrm{Tr}[C_i\partial\rho_0/\partial\lambda_j] = \langle C_i C_j\rangle_{0,c} \\ M_{ij} &= -\mathrm{Tr}[C_i\hat{\mathcal{L}}_1(\rho_0/\partial\lambda_j)] = \langle \dot{C}_i C_j\rangle_{0,c} \end{aligned} \tag{8.66}$$

however, to express higher order $\mathcal{O}(\epsilon^n)$ contributions one needs also more complicated correlation functions

$$\begin{aligned} N_i^{(n)} &= \mathrm{Tr}[C_i\hat{\mathcal{L}}_1(\hat{\mathcal{L}}_0^{-1}\hat{\mathcal{L}}_1)^n\rho_0] = \mathrm{Tr}[\dot{C}_i(\hat{\mathcal{L}}_0^{-1}\hat{\mathcal{L}}_1)^n\rho_0] \\ M_{ij}^{(n)} &= -\mathrm{Tr}[\dot{C}_i(\hat{\mathcal{L}}_0^{-1}\hat{\mathcal{L}}_1)^n(\partial\rho_0/\partial\lambda_j)] \end{aligned} \tag{8.67}$$

In order to write them in a compact form with an explicit time ordering we introduce a general notation of *Lindblad super-operators in the interacting picture*,

$$\hat{\mathcal{L}}_1(t)\rho = L_\alpha(t)\rho L_\alpha^\dagger(t) - \frac{1}{2}\{L_\alpha^\dagger(t)L_\alpha(t),\rho\} \tag{8.68}$$

where Lindblad operators $L_\alpha(t) = e^{iH_0t}\,L_\alpha\,e^{-iH_0t}$ are evolved with respect to H_0.

Using this notation the lowest order correlation functions can be, according to Eq. (8.61), written as regularized time integrals

$$N_j^{(1)} = \mathrm{Tr}\big[C_j\hat{\mathcal{L}}_1(\hat{\mathcal{L}}_0^{-1}\hat{\mathcal{L}}_1)\rho_0\big] = -\int_{-\infty}^{\infty} dt_1\,\theta(t_1)e^{-\eta t_1}\,\mathrm{Tr}\big[\dot{C}_j(t_1)\hat{\mathcal{L}}_1(0)\rho_0\big] \tag{8.69}$$

$$N_j^{(2)} = \mathrm{Tr}\big[C_j\hat{\mathcal{L}}_1(\hat{\mathcal{L}}_0^{-1}\hat{\mathcal{L}}_1)^2\rho_0\big] = \int_{-\infty}^{\infty} dt_1dt_2\,\theta(t_1)\theta(t_2)e^{-\eta(t_1+t_2)}\mathrm{Tr}\big[\dot{C}_j(t_1+t_2)\hat{\mathcal{L}}_1(t_1)\hat{\mathcal{L}}_1(0)\rho_0\big] \tag{8.70}$$

$$M_{jk}^{(1)} = -\mathrm{Tr}\big[C_j\hat{\mathcal{L}}_1(\hat{\mathcal{L}}_0^{-1}\hat{\mathcal{L}}_1)\frac{\partial\rho_0}{\partial\lambda_k}\big] = \int_{-\infty}^{\infty} dt_1\,\theta(t_1)e^{-\eta t_1}\,\mathrm{Tr}\big[\dot{C}_j(t_1)\hat{\mathcal{L}}_1(0)\frac{\partial\rho_0}{\partial\lambda_k}\big] \tag{8.71}$$

$$M_{jk}^{(2)} = -\mathrm{Tr}\big[C_j\hat{\mathcal{L}}_1(\hat{\mathcal{L}}_0^{-1}\hat{\mathcal{L}}_1)^2\frac{\partial\rho_0}{\partial\lambda_k}\big] = -\int_{-\infty}^{\infty} dt_1dt_2\,\theta(t_1)\theta(t_2)e^{-\eta(t_1+t_2)}\mathrm{Tr}\big[\dot{C}_j(t_1+t_2)\hat{\mathcal{L}}_1(t_1)\hat{\mathcal{L}}_1(0)\frac{\partial\rho_0}{\partial\lambda_k}\big] \tag{8.72}$$

Note that the time ordering of (super-)operators is such that it is most naturally represented using Keldysh formalism.

First order

Using the correlation functions defined above and the equality $\mathrm{Tr}\big[C_k\hat{\mathcal{L}}_1\hat{Q}\hat{\mathcal{L}}_0^{-1}\hat{Q}\hat{\mathcal{L}}_1\rho_0\big] = \mathrm{Tr}\big[C_k\hat{\mathcal{L}}_1\hat{\mathcal{L}}_0^{-1}\hat{\mathcal{L}}_1\rho_0\big]$, following from $\hat{P}\hat{\mathcal{L}}_1\rho_0 = 0$ for properly chosen ρ_0, the linear contribution to the expectation values of conserved quantities, Eq. (8.32), gets the form

$$\langle C_i\rangle_1 = \sum_{jk}\chi_{ij}\,(M^{-1})_{jk}\,\mathrm{Tr}\big[C_k\hat{\mathcal{L}}_1\hat{Q}\hat{\mathcal{L}}_0^{-1}\hat{Q}\hat{\mathcal{L}}_1\rho_0\big] = \sum_{jk}\chi_{ij}\,(M^{-1})_{jk}N_k^{(1)} \tag{8.73}$$

Second order

Second order $\mathcal{O}(\epsilon^2)$ in the tangential part of $\delta\rho$ (relevant for expectation values of conserved quantities) has two contributions, $\delta\rho_{2,\parallel} = \delta\rho_{2,\parallel}^{(1)} + \delta\rho_{2,\parallel}^{(2)}$

$$\begin{aligned}\delta\rho_{2,\parallel}^{(1)}] &= -\,(\hat{P}\hat{\mathcal{L}}_1\hat{P})^{-1}\,\hat{P}\hat{\mathcal{L}}_1\hat{Q}\hat{\mathcal{L}}_0^{-1}\hat{Q}\hat{\mathcal{L}}_1\hat{Q}\hat{\mathcal{L}}_0^{-1}\hat{Q}\hat{\mathcal{L}}_1\rho_0\\ &= -\,(\hat{P}\hat{\mathcal{L}}_1\hat{P})^{-1}\,\hat{P}\hat{\mathcal{L}}_1\hat{\mathcal{L}}_0^{-1}\hat{\mathcal{L}}_1\hat{\mathcal{L}}_0^{-1}\hat{\mathcal{L}}_1\rho_0 + \hat{P}\hat{\mathcal{L}}_0^{-1}\hat{P}\hat{\mathcal{L}}_1\hat{\mathcal{L}}_0^{-1}\hat{\mathcal{L}}_1\rho_0 \qquad (8.74)\\ \delta\rho_{2,\parallel}^{(2)} &= (\hat{P}\hat{\mathcal{L}}_1\hat{P})^{-1}\,\hat{P}\hat{\mathcal{L}}_1\hat{Q}\,\hat{\mathcal{L}}_0^{-1}\,\hat{Q}\hat{\mathcal{L}}_1\hat{P}\,(\hat{P}\hat{\mathcal{L}}_1\hat{P})^{-1}\hat{P}\hat{\mathcal{L}}_1\hat{Q}\hat{\mathcal{L}}_0^{-1}\hat{Q}\hat{\mathcal{L}}_1\rho_0\\ &= (\hat{P}\hat{\mathcal{L}}_1\hat{P})^{-1}\,\hat{P}\hat{\mathcal{L}}_1\hat{\mathcal{L}}_0^{-1}\hat{\mathcal{L}}_1\hat{P}\,(\hat{P}\hat{\mathcal{L}}_1\hat{P})^{-1}\hat{P}\hat{\mathcal{L}}_1\hat{\mathcal{L}}_0^{-1}\hat{\mathcal{L}}_1\rho_0 - \hat{P}\hat{\mathcal{L}}_0^{-1}\hat{P}\hat{\mathcal{L}}_1\hat{\mathcal{L}}_0^{-1}\hat{\mathcal{L}}_1\rho_0 \qquad (8.75)\end{aligned}$$

which we obtain by inserting $\hat{Q} = \hat{1} - \hat{P}$ under condition $\hat{P}\hat{\mathcal{L}}_1\rho_0 = 0$ and using that $\hat{\mathcal{L}}_0^{-1}$ cannot change the subspace, i.e., $\hat{P}\hat{\mathcal{L}}_0^{-1} = \hat{\mathcal{L}}_0^{-1}\hat{P} = \hat{P}\hat{\mathcal{L}}_0^{-1}\hat{P}$. The two contributions then add up to

$$\delta\rho_{2,\parallel} = -\,(\hat{P}\hat{\mathcal{L}}_1\hat{P})^{-1}\,\hat{P}\hat{\mathcal{L}}_1\hat{\mathcal{L}}_0^{-1}\hat{\mathcal{L}}_1\hat{\mathcal{L}}_0^{-1}\hat{\mathcal{L}}_1\rho_0 + (\hat{P}\hat{\mathcal{L}}_1\hat{P})^{-1}\,\hat{P}\hat{\mathcal{L}}_1\hat{\mathcal{L}}_0^{-1}\hat{\mathcal{L}}_1\hat{P}\,(\hat{P}\hat{\mathcal{L}}_1\hat{P})^{-1}\hat{P}\hat{\mathcal{L}}_1\hat{\mathcal{L}}_0^{-1}\hat{\mathcal{L}}_1\rho_0 \tag{8.76}$$

Using this expression it is straightforward to write the $\mathcal{O}(\epsilon^2)$ contribution to the expectation value of conserved quantities in the steady state in terms of correlation functions. One should notice that each $\hat{P}$ 'cuts' the expression in the sense that content between to consequential $\hat{P}$ corresponds to one correlation function. The inverses $(\hat{P}\hat{\mathcal{L}}_1\hat{P})^{-1}$ are treated as in Eq. (8.63), contribute M^{-1} components to the final expression. Using the definition of projector $\hat{P}$, Eq. (9.4), the definition of the inverse $(\hat{P}\hat{\mathcal{L}}_1\hat{P})^{-1}$, Eq. (8.63), and definitions of multi-time correlation functions, Eq. (8.67), one obtains the following expression

$$\langle C_i\rangle_2 = \mathrm{Tr}[C_i\delta\rho_{2,\parallel}] = -\sum_{j,k}\chi_{ij}\,(M^{-1})_{jk}\,N_k^{(2)} + \sum_{j,k,l,m}\chi_{ij}\,(M^{-1})_{jk}\,M_{kl}^{(1)}\,(M^{-1})_{lm}\,N_m^{(1)}. \tag{8.77}$$

Lehmann representation
All expressions obtained from our perturbation theory can be calculated in a straightforward way using eigenstates and eigenenergies of H_0. As Lehmann representations are perhaps less common in the case of a Lindblad dynamics we show, for example, the Lehmann representation of $N_j^{(1)}$, Eq. (8.69), needed to calculate $\langle C_i \rangle_1$. By inserting the identity operator $\sum_m |m\rangle\langle m|$ between all operators and super-operators one obtains

$$N_j^{(1)} = \sum_{mnpr} \sum_{\alpha\beta} \frac{i}{(E_n^0 - E_p^0 - i\eta)} \left(C_r^{(j)} L_{rn}^{(\beta)} L_{pr}^{(\beta)\dagger} - \tfrac{1}{2}(C_p^{(j)} + C_n^{(j)}) L_{pr}^{(\beta)\dagger} L_{rn}^{(\beta)} \right) \left(L_{nm}^{(\alpha)} L_{mp}^{(\alpha)\dagger} \rho_m^0 - \tfrac{1}{2}(\rho_p^0 + \rho_n^0) L_{nm}^{(\alpha)\dagger} L_{mp}^{(\alpha)} \right), \tag{8.78}$$

where m, n, p, r run over the eigenstates $|m\rangle$, $H_0|m\rangle = E_m^0|m\rangle$, while α, β run over the Lindblad operators defined in Eq. (8.2). We use notation $\langle m|L_\alpha|n\rangle = L_{mn}^{(\alpha)}$ and $\langle m|\rho_0|m\rangle = \rho_m^0$, $\langle m|C_j|m\rangle = C_m^{(j)}$ where we assumed that the conserved quantities C_i are diagonal operators in the eigenbasis of H_0. As $\hat{\mathcal{L}}_0|n\rangle\langle m| = -i(E_n^0 - E_m^0)|n\rangle\langle m|$, the inverse is obtained as $\hat{\mathcal{L}}_0^{-1}|n\rangle\langle m| = \frac{i}{E_n^0 - E_m^0 - i\eta}|n\rangle\langle m|$ using the regularization of appendix 8.6. Note that η should always be chosen to be larger than the level spacing if one is interested in systems in the thermodynamic limit.

8.10 Unitary driving

In the case of unitary driving, the projection of the perturbation onto the P space vanishes, $\hat{P}\hat{\mathcal{L}}_1\hat{P} = 0$, and therefore also $\hat{P}(\hat{\mathcal{L}}_0 + \hat{\mathcal{L}}_1)\hat{P} = 0$. In this case, the formulas fixing the density matrix to zeroth order in the perturbations, Eq. (8.9), and the perturbation theory, presented in Sec. 8.3.3 have to be modified compared to the Lindblad dynamics where the inverse of $\hat{P}\hat{\mathcal{L}}_1\hat{P}$ within P space is well defined.

8.10.1 Projections of the inverse

Different projections of full inverse $(\hat{P}+\hat{Q})\hat{\mathcal{L}}^{-1}(\hat{P}+\hat{Q})$ can, for example, be obtained using the transformations

$$\begin{aligned} \hat{U} &= \hat{P} + \hat{Q} - (\hat{P}\hat{\mathcal{L}}_1\hat{Q})\,(\hat{Q}\hat{\mathcal{L}}\hat{Q})^{-1}\hat{Q} \\ \hat{V} &= \hat{P} + \hat{Q} - \hat{Q}(\hat{Q}\hat{\mathcal{L}}\hat{Q})^{-1}\,\hat{Q}\hat{\mathcal{L}}_1\hat{P} \end{aligned} \tag{8.79}$$

where $\hat{U}$ and $\hat{V}$ are chosen in such a way that they transform $\hat{\mathcal{L}}$ into a block-diagonal form (in $\hat{P}$ and $\hat{Q}$ space),

$$\hat{U}\hat{\mathcal{L}}\hat{V} = \hat{Q}\hat{\mathcal{L}}\hat{Q} - (\hat{P}\hat{\mathcal{L}}_1\hat{Q})(\hat{Q}\hat{\mathcal{L}}\hat{Q})^{-1}(\hat{Q}\hat{\mathcal{L}}_1\hat{P}). \tag{8.80}$$

The inverse $\hat{\mathcal{L}}^{-1}$ is then obtained from

$$\begin{aligned} \hat{\mathcal{L}}^{-1} &= \hat{V}\big(\hat{U}\hat{\mathcal{L}}\hat{V}\big)^{-1}\hat{U} \\ &= \hat{V}\big(\hat{P}(\hat{P}\hat{\mathfrak{L}}_2\hat{P})^{-1}\hat{P} + \hat{Q}(\hat{Q}\hat{\mathcal{L}}\hat{Q})^{-1}\hat{Q}\big)\hat{U} \end{aligned} \tag{8.81}$$

where

$$\hat{\mathfrak{L}}_2 = -\hat{\mathcal{L}}_1\hat{Q}\;(\hat{Q}\hat{\mathcal{L}}\hat{Q})^{-1}\;\hat{Q}\hat{\mathcal{L}}_1. \tag{8.82}$$

Using the definition of $\hat{U}$ and $\hat{V}$ we obtain for perturbations with $\hat{P}\hat{\mathcal{L}}_1\hat{P} = 0$ the following expressions for the projections

$$\begin{aligned}
\hat{P}\hat{\mathcal{L}}^{-1}\hat{P} &= \hat{P}(\hat{P}\hat{\mathfrak{L}}_2\hat{P})^{-1}\hat{P} \sim \frac{1}{\epsilon^2} \\
\hat{P}\hat{\mathcal{L}}^{-1}\hat{Q} &= -\hat{P}(\hat{P}\hat{\mathfrak{L}}_2\hat{P})^{-1}(\hat{P}\hat{\mathcal{L}}_1\hat{Q})\ (\hat{Q}\hat{\mathcal{L}}\hat{Q})^{-1}\hat{Q} \sim \frac{1}{\epsilon} \\
\hat{Q}\hat{\mathcal{L}}^{-1}\hat{P} &= -\hat{Q}(\hat{Q}\hat{\mathcal{L}}\hat{Q})^{-1}\ (\hat{Q}\hat{\mathcal{L}}_1\hat{P})(\hat{P}\mathfrak{L}_2\hat{P})^{-1}\hat{P} \sim \frac{1}{\epsilon} \\
\hat{Q}\hat{\mathcal{L}}^{-1}\hat{Q} &= 0
\end{aligned} \tag{8.83}$$

$(\hat{P}\hat{\mathfrak{L}}_2\hat{P})^{-1}$ and $(\hat{Q}\hat{\mathcal{L}}\hat{Q})^{-1}$ should be interpreted as inverses within P and Q subspace, respectively, while the left hand sides of Eqs. (8.83) correspond to the projections of the full (properly regularized) Liouville inverse onto P and Q subspace. Note that the last equation does not imply that $\hat{Q}(\hat{Q}\hat{\mathcal{L}}\hat{Q})^{-1}\hat{Q}$ vanishes (which is finite for $\epsilon \to 0$).

A direct consequence of the equations given above is that in the limit of small ϵ, the inverse in the P sector is given through $\hat{\mathcal{L}}_2$ defined in Eq. (8.42),

$$\hat{P}\hat{\mathcal{L}}^{-1}\hat{P} = \hat{P}(\hat{P}\hat{\mathfrak{L}}_2\hat{P})^{-1}\hat{P} \approx (\hat{P}\hat{\mathcal{L}}_2\hat{P})^{-1}\ (1 + \mathcal{O}(\epsilon)). \tag{8.84}$$

Note that $\hat{\mathcal{L}}_2$ is obtained from $\hat{\mathfrak{L}}_2$ just by replacing $\hat{Q}\hat{\mathcal{L}}\hat{Q}$ by $\hat{Q}\hat{\mathcal{L}}_0\hat{Q}$ in the inverse. $\hat{P}\hat{\mathcal{L}}_2\hat{P}$ takes over the role of an effective Lindblad super-operator in P space.

8.10.2 Zeroth order expansion point

Here we show that the condition (8.9),

$$\hat{P}(\hat{\mathcal{L}}_1\hat{\mathcal{L}}_0^{-1}\hat{\mathcal{L}}_1\rho_0) = 0, \tag{8.85}$$

does give the correct reference point ρ_0 for situations where $\hat{P}\hat{\mathcal{L}}_1\hat{P} = 0$. One way to show this is to use the perturbative analysis provided in Sec. 8.3.3 where the power counting of diagrams worked only if the correct reference point was chosen. Below we give a more direct argument.

As described in the main text, Eq. (8.85) is obtained from the requirement that the dominant contribution to the time-averaged expectation value of conserved quantities must vanish,

$$\langle\overline{\dot{C}_i}\rangle = \mathrm{Tr}[C_i\hat{P}\hat{\mathcal{L}}_1(\rho_0 + \delta\rho)] = \mathrm{Tr}[C_i\hat{P}\hat{\mathcal{L}}_1\delta\rho] \stackrel{!}{=} 0, \tag{8.86}$$

where $\hat{P}$ is used to extract the non-oscillatory component and $\mathrm{Tr}[C_i\hat{P}\hat{\mathcal{L}}_1\rho_0] = 0$ due to the cyclicity of trace. As discussed in the main text, the starting point is the exact formula for $\delta\rho$, Eq. (8.4) and the formula Eq. (8.8) which directly leads to

$$\begin{aligned}
\delta\rho &= \delta\rho^{(I)} + \delta\rho^{(II)} \\
&= -\hat{\mathcal{L}}_0^{-1}\hat{\mathcal{L}}_1\rho_0 + \hat{\mathcal{L}}^{-1}\hat{\mathcal{L}}_1\hat{\mathcal{L}}_0^{-1}\hat{\mathcal{L}}_1\rho_0.
\end{aligned} \tag{8.87}$$

If we use only $\delta\rho^{(I)}$ in Eq. (8.86), then Eq. (8.85) follows immediately. Equivalently, the condition Eq. (8.85) implies that the contribution from $\delta\rho^{(I)}$ vanishes in Eq. (8.86). In the following we will show that Eq. (8.85) also implies that the contribution from $\delta\rho^{(II)}$ to Eq. (8.86) vanishes, which is less obvious, and a useful consistency check.

Plugging $\delta\rho^{(II)}$ into Eq. (8.86) one finds

$$\begin{aligned}
&\mathrm{Tr}[C_i\hat{P}\hat{\mathcal{L}}_1\delta\rho^{(II)}] \\
&\quad = \mathrm{Tr}[C_i\hat{P}\hat{\mathcal{L}}_1\hat{\mathcal{L}}^{-1}\hat{\mathcal{L}}_1\hat{\mathcal{L}}_0^{-1}\hat{\mathcal{L}}_1\rho_0] \\
&\quad = \mathrm{Tr}[C_i\hat{P}\hat{\mathcal{L}}_1\hat{Q}\hat{\mathcal{L}}^{-1}\hat{Q}\hat{\mathcal{L}}_1\hat{\mathcal{L}}_0^{-1}\hat{\mathcal{L}}_1\rho_0] = 0
\end{aligned} \tag{8.88}$$

where the third line differs from the first one by two extra $\hat{Q}$ super-operators enclosing $\hat{\mathcal{L}}^{-1}$. The first one can be inserted because we consider the case $\hat{P}\hat{\mathcal{L}}_1\hat{P} = 0$ and therefore $\hat{P}\hat{\mathcal{L}}_1 = \hat{P}\hat{\mathcal{L}}_1\hat{Q}$. The second one can be used as a consequence of Eq. (8.85), which states that the $\hat{P}$ projection of the operator to the right of $\hat{\mathcal{L}}^{-1}$ vanishes. Finally, we can use that $\hat{Q}\hat{\mathcal{L}}^{-1}\hat{Q} = 0$, see Eq. (8.83), to prove that the whole expression vanishes.

To finish our argument, we still have to show that $\delta\rho$ is small for $\epsilon \to 0$ provided that Eq. (8.83) holds, which can be done using similar arguments as above. First, the combination $\hat{\mathcal{L}}_0^{-1}\hat{\mathcal{L}}_1\rho_0 = \hat{\mathcal{L}}_0^{-1}\hat{Q}\hat{\mathcal{L}}_1\rho_0$ is non-singular for $\hat{P}\hat{\mathcal{L}}_1\hat{P} = 0$ which implies that $\delta\rho^{(I)} \sim \mathcal{O}(\epsilon)$. Second, we used already above that $\delta\rho^{(II)} = \hat{\mathcal{L}}^{-1}\hat{\mathcal{L}}_1\hat{\mathcal{L}}_0^{-1}\hat{\mathcal{L}}_1\rho_0 = \hat{\mathcal{L}}^{-1}\hat{Q}\hat{\mathcal{L}}_1\hat{\mathcal{L}}_0^{-1}\hat{\mathcal{L}}_1\rho_0$. As $\hat{Q}\hat{\mathcal{L}}^{-1}\hat{Q} = 0$ and $\hat{P}\hat{\mathcal{L}}^{-1}\hat{Q} \sim \mathcal{O}(1/\epsilon)$ it follows immediately that also $\delta\rho^{(II)} \sim \mathcal{O}(\epsilon)$ which concludes the derivation of Eq. (8.85).

8.10.3 Monochromatic driving

Some of the diagrams depicted in Fig. 8.2 vanish when a perturbation which contains only oscillations with a single frequency ω is considered. In this case $\hat{P}(\hat{\mathcal{L}}_1)^3\hat{P} = 0$ since each application of $\hat{\mathcal{L}}_1$ changes the Floquet index n of $\rho^{(n)}$, Eq. (8.10), by ± 1. Consequently, for example, the $\mathcal{O}(\epsilon)$ diagram in the $(\|)$ sector vanishes and conservation laws are only changed by processes of order $\mathcal{O}(\epsilon^2)$, represented by the diagram in the second line of Fig. 8.2 (note that the third one vanishes as well). The situation is different in the presence of driving with higher harmonics, e.g. $\cos(\omega t)$ and $\cos(2\omega t)$, when $\hat{P}(\hat{\mathcal{L}}_1)^3\hat{P} \neq 0$. In this case the dominant stationary correction to the expectation value of C_i is of $\mathcal{O}(\epsilon)$, as shown by the diagram in the first line in the $(\|)$ sector.

8.11 Questions about Perturbative approach by Lernerchich et al.

8.11.1 Examples of Application (???)

(?????????? write if this is used or not????)

9 Pumping approximately integrable systems by Lange, Lenarčič, Rosch

Abstract

Weak perturbations can drive an interacting many-particle system far from its initial equilibrium state if one is able to pump into degrees of freedom approximately protected by conservation laws. This concept has for example been used to realize Bose-Einstein condensates of photons, magnons, and excitons. Integrable quantum systems, like the one-dimensional Heisenberg model, are characterized by an infinite set of conservation laws. Here we develop a theory of weakly driven integrable systems and show that pumping can induce large spin or heat currents even in the presence of integrability breaking perturbations, since it activates local and quasi-local approximate conserved quantities. The resulting steady state is qualitatively captured by a truncated generalized Gibbs ensemble with Lagrange parameters that depend on the structure but not on the overall amplitude of perturbations nor the initial state. We suggest to use spin-chain materials driven by terahertz radiation to realize integrability-based spin and heat pumps.

A simple classical example for a weakly driven system is a well-insulated greenhouse. Due to the approximate conservation of the energy within the greenhouse, even weak sunlight can lead to high temperatures in its interior, which can be computed from the simple rate equation

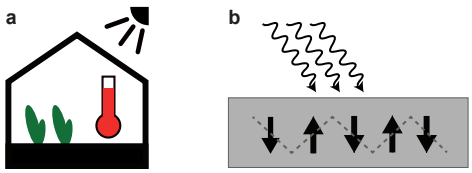


Figure 9.1: (a) A well-insulated greenhouse exposed to sunshine can heat up significantly since energy within it is approximately conserved. (b) As the heat current in spin chain materials is approximately conserved even weak terahertz radiation can induce large heat current. Material candidates must have appropriate crystal structure, schematically denoted by dashed lines indicating alternating chemical bonds.

for the energy transfer. Similarly, large spin accumulation can be achieved in systems with approximate spin conservation [1]. Using approximate conservation of the number of photons, magnons, or exciton polaritons, one can use pumping by light to reach densities which allow for the realization of Bose-Einstein condensates [13, 16, 11]. Number-conserving collisions induce a quasi-equilibrium state in these systems, which can be efficiently described by introducing a chemical potential whose value is determined by balancing pumping and decay processes. Related theoretical approaches that describe electron-phonon systems far from equilibrium are so-called two-temperature models [22]: here one uses that the energy of the electrons and phonons are approximately separately conserved to introduce two different temperatures for the subsystems.

Integrable many-particle systems, like the one-dimensional (1D) fermionic Hubbard model or the XXZ Heisenberg model, are described by an infinite number of (local or quasi-local) conservation laws [6, 50, 9, 22, 47, 48]. In closed integrable systems those prevent the equilibration into a simple thermal state, e.g., after a sudden change of parameters. Instead the system can be described by a generalized Gibbs ensemble (GGE) [1, 36, 25, 15, 16, 2, 3, 4, 20, 21]

$$\rho_0 \sim \exp\left(-\sum_i \lambda_i C_i\right) \tag{9.1}$$

where C_i are the conserved quantities and λ_i the corresponding Lagrange parameters. It has also been shown experimentally [19] that GGEs for a Lieb-Liniger model can provide highly accurate descriptions of interacting bosons in 1D.

Many materials are described with high accuracy by integrable models [23], however, weak integrability breaking terms and the coupling to thermal phonons imply that in equilibrium these systems are described by simple thermal states, $\rho_0 \sim e^{-\beta H}$, instead of GGEs. The proximity to the integrable point and the presence of approximate conservation laws leads to enhanced spin or heat conductivities (within linear-response theory) [19, 20, 82] and also to a slow relaxation after a quantum quench (via GGE-prethermalization) towards the equilibrium state [41].

We will show that – as in the greenhouse example, see Fig. 18.1 – such an approximately integrable system can be driven far from its thermal equilibrium by weak perturbations arising, e.g., from a driving periodic in time or from coupling to a non-thermal bath. In order to balance the constant heating due to driving the system has to be weakly open, e.g., by coupling to a phonon bath. As we will demonstrate this mechanism can be used for example to create large spin and heat currents. Besides the quasi 1D systems considered by us, also approximately many-body localized systems are characterized by infinitely many approximate conservation laws which may lead to a strong response to driving [28, 29].

9.0.1 Results

Weakly driven system.

We consider an interacting many-body system that is approximately described by Hamiltonian H_0 and characterized by a finite or infinite number of (quasi-)local conserved quantities C_i, $[H_0, C_i] = 0$, one of them being H_0. Energy and other conservations are weakly broken by coupling to thermal or non-thermal baths and/or perturbations periodic in time. For simplicity we assume periodic boundary conditions and a (discreet) translational invariance. We describe the system with density matrix ρ whose dynamics is governed by the Liouvillian super-operator $\hat{\mathcal{L}}$,

$$\dot{\rho} = \hat{\mathcal{L}}\rho, \quad \hat{\mathcal{L}} = \hat{\mathcal{L}}_0 + \epsilon\hat{\mathcal{L}}_1, \tag{9.2}$$

where $\hat{\mathcal{L}}$ can be split into the dominant unitary Hamiltonian evolution $\hat{\mathcal{L}}_0\rho = -i[H_0, \rho]$ and perturbation $\hat{\mathcal{L}}_1$ of strength ϵ. We are interested in the limit of small ϵ for $t \to \infty$ where a unique (Floquet) steady state ρ_∞ is obtained. The general structure of perturbation theory in this case has, e.g., been discussed in Refs. [30, 1, 2]. In this limit, ρ_∞ can be approximated by $\rho_0 = \lim_{\epsilon\to 0}\lim_{t\to\infty}\rho$ with $\hat{\mathcal{L}}_0\rho_0 = 0$ according to Eq. (9.2). We assume and later support numerically that ρ_0 is approximately described by a GGE, see Eq. (10.2).

Here it is essential to note that – as in the greenhouse example discussed above – the parameters λ_i are not determined by the initial state but by the form of the weak perturbations $\hat{\mathcal{L}}_1$. Our central goal is to compute the λ_i. We first discuss the case of Lindblad dynamics, where perturbation theory linear in ϵ can be used, and then focus on Hamiltonian dynamics where we have to consider ϵ^2 contributions.

Markovian perturbation.

Within the Markovian approximation one can use the Lindblad form for $\hat{\mathcal{L}}_1$ [33]. Note that Lindblad dynamics is considered here mainly for pedagogical purposes (formulas are simpler) while no Lindblad approximation is used for the models studied below. The coefficients λ_i that fix the GGE are determined from the condition that the change of the approximately conserved quantities has to vanish in the steady state

$$\langle \dot{C}_i \rangle = \mathrm{Tr}\,(C_i\hat{\mathcal{L}}\rho_0) = \mathrm{Tr}\,(C_i\epsilon\hat{\mathcal{L}}_1\rho_0) \stackrel{!}{=} 0, \tag{9.3}$$

where we used that $\hat{\mathcal{L}}_0\rho_0 = -i[H_0, \rho_0] = 0$. Relation (9.3) yields a set of coupled equations for λ_i, where the number of equations is equal to the number of conserved quantities. We define the super-projector $\hat{P}$ onto the tangential space of GGE density matrix,

$$\hat{P}X \equiv -\sum_{i,i'} \frac{\partial\rho_0}{\partial\lambda_i}\,(\chi^{-1})_{ii'}\mathrm{Tr}\,(C_{i'}X), \tag{9.4}$$

using $\chi_{ii'} = -\mathrm{Tr}\,(C_i\partial\rho_0/\partial\lambda_{i'})$. Then the conditions for ρ_0 can be compactly written as

$$\hat{\mathcal{L}}_0\rho_0 = 0, \quad \hat{P}(\hat{\mathcal{L}}_1\rho_0) = 0. \tag{9.5}$$

This equation can also be derived by considering higher order perturbations in ϵ, see Methods for details.

Hamiltonian perturbation.

For Hamiltonian dynamics $\epsilon\hat{\mathcal{L}}_1\rho = -i[H_1, \rho]$, where H_1 may be a sum of several integrability breaking perturbations. Perturbation theory linear in ϵ vanishes, $\mathrm{Tr}\,(C_i\epsilon\hat{\mathcal{L}}_1\rho_0) = 0$ for all λ_i.

Therefore one has to expand to order ϵ^2 and Eq. (9.5) is replaced by

$$\hat{\mathcal{L}}_0\rho_0 = 0, \quad \hat{P}(\hat{\mathcal{L}}_1\hat{\mathcal{L}}_0^{-1}\hat{\mathcal{L}}_1\rho_0) = 0. \tag{9.6}$$

Since $\hat{P}(\hat{\mathcal{L}}_1\rho_0) = 0$, $\hat{\mathcal{L}}_1\rho_0$ is not in the kernel of $\hat{\mathcal{L}}_0^{-1}$. For periodic driving this equation has to be interpreted within the Floquet formalism, see Methods.

Model.

As discussed in the introduction, our goal is to describe a situation which can be realized experimentally in spin-chain materials driven by lasers operating in the terahertz regime. We assume that spin chains are approximately described by a spin-1/2 XXZ Heisenberg model, possibly in the presence of an external magnetic field B,

$$H_0 = \sum_j \frac{J}{2}(S_j^+ S_{j+1}^- + S_j^- S_{j+1}^+) + \Delta S_j^z S_{j+1}^z - B S_j^z. \tag{9.7}$$

The system is driven out of equilibrium by a weak (integrability-breaking) time-dependent perturbation

$$H_{\rm d} = \epsilon_{\rm d} J \sum_j \Big((-1)^{j+1} \mathbf{S}_j \cdot \mathbf{S}_{j+1} \sin(\omega t) + (-1)^j S_j^z \cos(\omega t) \Big), \tag{9.8}$$

with driving frequency ω. This specific term has been chosen because it can induce heat and spin currents (as can be shown by a symmetry analysis), and because it can be realized experimentally. Such staggered exchange couplings and staggered magnetic fields arise naturally in certain compounds with (at least) two magnetic atoms per unit cell when coupled to uniform electric and magnetic fields, respectively [34, 35, 36, 21]. See Fig. 18.1 for a schematic drawing of such a compound and Methods for concrete experimental suggestions. Therefore $H_{\rm d}$ can be realized by shining a laser (typically at terahertz frequencies) onto the sample. In this case $\epsilon_{\rm d}^2$ is proportional to the laser power. Note that for $T = 0$ and $B = 0$ in the adiabatic limit, $\omega \to 0$, Eqs. (9.7,9.8) realize an adiabatic Thouless pump, where per pumping cycle one spin is transported by one unit cell [38]. We will be interested in the opposite regime of large ω and large (effective) temperatures.

Formally the periodic perturbation $H_{\rm d}$ would drive the system to infinite temperature [33, 40, 41, 42] (up to remaining conservation laws [43], possibly through a prethermal-like regime [106]). In a solid state experiment this is prohibited by the coupling to phonons and, ultimately, to the thermal environment of the experimental setup. We mimic this effect by coupling the spin system to a bath of Einstein phonons, $H_0^{\rm ph} = \omega_{\rm ph} \sum_j a_j^\dagger a_j + \ldots$, where dots stand for the couplings to further reservoirs which guarantee that the phonon system is kept at fixed temperature $T_{\rm ph}$, $\rho_{\rm ph} \sim e^{-H_0^{\rm ph}/T_{\rm ph}}$. See Methods for details on finite size calculation using a broadened distribution of phonon energies. The (weak) coupling to the spin system is described by

$$H_{\rm ph} = \epsilon_{\rm ph} J \sum_j \Big(\mathbf{S}_j \cdot \mathbf{S}_{j+1}(a_j + a_j^\dagger) + \gamma_{\rm m}(S_j^x S_{j+1}^z + S_j^z S_{j+1}^x)(a_j + a_j^\dagger) \Big). \tag{9.9}$$

To obtain a unique steady state it is essential to break all symmetries, including the S^z conservation. Relativistic effects which relax S^z are mimicked by $\gamma_{\rm m}$ in our approach. We expect $\gamma_{\rm m} \ll 1$ in materials without heavy elements. For simplicity we set $\gamma_{\rm m} = 1$ within our numerics

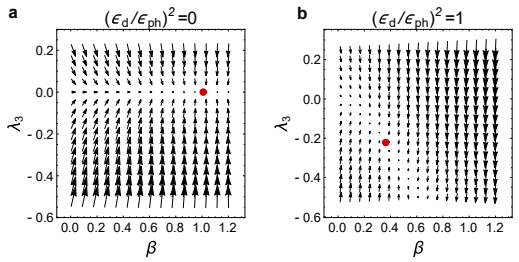


Figure 9.2: Effective force $\boldsymbol{F}$ in the space of Lagrange parameters (β, λ_3) using $e^{-\beta H_0 - \lambda_3 C_3}$ as an ansatz for the generalized Gibbs ensemble. Parameters: $J = \Delta = -B = \omega = \omega_{\rm ph} = T_{\rm ph}$. Lagrange parameters (β, λ_3) are plotted in units $1/J$ and $1/J^2$, respectively. (a) In the absence of an external driving, $\epsilon_{\rm d} = 0$, the stable fixed point (red dot) is given by the thermal ensemble, $\beta = 1/T_{\rm ph}$, $\lambda_3 = 0$. (b) When the system is driven by $H_{\rm d}$ ($\epsilon_{\rm d} = \epsilon_{\rm ph}$), it heats up and λ_3 becomes finite.

as this is found to minimize finite size effects, without a qualitative influence on the results. Besides phonons also other integrability breaking perturbations exist in real materials, including defects, which typically dominate at the lowest temperatures. For high temperatures of the order of J (relevant for the considered setup) it is realistic to assume that phonon coupling dominates.

In the presence of a periodic perturbation, Eq. (9.8), in the long-time limit the density matrix is changing periodically, $\rho(t \to \infty) = \sum_n e^{-i\omega n t} \rho^{(n)}$ with $\rho^{(n)\dagger} = \rho^{(-n)}$, $n \in \mathbb{Z}$. Within the Floquet formalism one therefore promotes the steady-state density matrix to a vector and Liouville operator to a matrix, see Methods. For weak driving, $\epsilon_{\rm d} \to 0$, only the $n = 0$ sector remains and the GGE ansatz, Eq. (10.2), simply reads $\rho_0^{(n)} = (\rho_0 \otimes \rho_{\rm ph})\, \delta_{n,0}$ where we included also the phonon density matrix, see above.

Steady state.

We will use two different approaches to determine an approximate solution for the steady state density matrix. First, we will parametrize ρ_0, Eq. (10.2), with a small number of (quasi-)local conserved quantities, C_i, $i = 1, \ldots, N_{\rm C}$. In an alternative approach, feasible for small systems, we take all conserved quantities into account: local and non-local, commuting and non-commuting. While the second approach is formally exact in the limit $\epsilon_{\rm d}, \epsilon_{\rm ph} \to 0$, the first one is, perhaps, more intuitive and can be computed for larger system sizes.

For the XXZ Heisenberg model an infinite set of mutually commuting local conserved quantities C_i is known, see Methods. C_1 is the total spin $C_1 = \sum_i S_i^z$ and $C_2 = H_{\rm XXZ}$. Importantly, C_3 is the heat current [7], $C_3 = J_{\rm H}(B = 0)$. In addition there also exist (infinite) sets of quasi-local commuting conserved quantities [9, 22, 47]. As shown in [8, 9] the spin-reversal parity-odd family has an overlap with the spin current $J_{\rm S}$ at $\Delta < J$. Therefore both heat and spin current could show a large response to a weak perturbation. For our analysis we choose three or five ($N_{\rm C} = 4, N_{\rm C} = 6$) most local conserved quantities C_i, $i = 1, ..., N_{\rm C} - 1$. From the quasi-local sets we include as a single (effective) operator the conserved part of spin current $J_{\rm S}^{\rm c}$, computed numerically [20, 47]. For details see Methods. In the presence of an external magnetic field, Eq. (9.7), the heat current also has, in addition to C_3, a spin current component, $J_{\rm H} = C_3 - B J_{\rm S}$.

For the visualization of our results it is useful to define generalized forces F_i in the space of Lagrange parameters by rewriting $\hat{P}\dot{\rho} = \sum_i \frac{\partial \rho_0}{\partial \lambda_i} F_i$ such that $\dot{\lambda}_i \approx F_i$,

$$F_i = \sum_{i'} (\chi^{-1})_{ii'} \mathrm{Tr}\left(C_{i'}\ \epsilon \hat{\mathcal{L}}_1 \hat{\mathcal{L}}_0^{-1} \epsilon \hat{\mathcal{L}}_1 \rho_0\right) \tag{9.10}$$

computed using exact diagonalization, see Methods. The vector $\mathbf{F}$ is a function of the Lagrange parameters λ_i which points into the direction of the steady state stable fixed point obtained from $F_i = 0$. In the absence of driving (Fig. 18.2a) one obtains the expected thermal state with $T = T_{\rm ph}$ while all other Lagrange parameters λ_i vanish. For finite driving the GGE is activated and the λ_i become finite (Fig. 18.2b). To obtain the steady state, we solve $\chi\mathbf{F} = 0$ using Newton's method.

For the second approach, performed on small N-site systems, we first numerically construct a basis in the set of all (local and non-local) conserved operators, $\mathcal{Q} = \{|n\rangle\langle m|$ with $E_m^0 = E_n^0\}$, where $H_0|n\rangle = E_n^0|n\rangle$. Due to degeneracies we find (for finite B and $\Delta \neq J$) about $2{\cdot}2^N$ elements $Q_i \in \mathcal{Q}$. In the limit $\epsilon_{\rm d}, \epsilon_{\rm ph} \to 0$ the steady state density matrix ρ_∞ has to fulfill $\hat{\mathcal{L}}_0\rho_\infty = 0$ and therefore can be exactly written as a linear combination of the Q_i, $\rho_\infty = \sum \alpha_i Q_i$. Using Eq. (9.6), we therefore find that the steady state density matrix for $\epsilon_{\rm d}, \epsilon_{\rm ph} \to 0$ is exactly given by the unique eigenvector with eigenvalue zero of the matrix

$$\mathcal{L}^{\mathcal{Q}}_{mn} = -\mathrm{Tr}\,(Q_m^\dagger\ \epsilon\hat{\mathcal{L}}_1\hat{\mathcal{L}}_0^{-1}\epsilon\hat{\mathcal{L}}_1 Q_n), \tag{9.11}$$

where $\hat{\mathcal{L}}_0, \hat{\mathcal{L}}_1$ are Floquet matrices, see Methods. Note that only the relative $\epsilon_{\rm d}/\epsilon_{\rm ph}$ and not the absolute strength of perturbations determine ρ_0, as can be seen by dividing the equations $\chi\boldsymbol{F} = 0$ or $\mathcal{L}^{\mathcal{Q}}\rho_0 = 0$ by $\epsilon_{\rm ph}^2$.

In Fig. 17.3 we show the expectation value of the energy and of the heat current densities

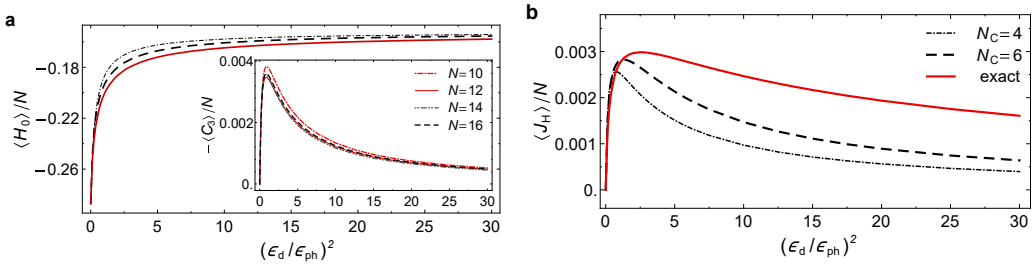


Figure 9.3: Expectation values of (a) energy and (b) heat current densities for a weakly driven spin chain, $\epsilon_{\rm d}, \epsilon_{\rm ph} \to 0$, as functions of the ratio of driving strength $\epsilon_{\rm d}$ and phonon coupling $\epsilon_{\rm ph}$. Red solid lines: exact result taking into account all 7969 conservation laws of a system of $N = 12$ sites. (a) For the energy accurate results are already obtained with a GGE ensemble based on $N_{\rm C} = 4$ (dot-dashed lines) or $N_{\rm C} = 6$ (dashed lines) conserved quantities. (b) Also the heat current $J_{\rm H} = C_3 - BJ_{\rm S}$ is qualitatively well described by the GGE ensemble but quantitative deviations are larger. Inset: Finite size analysis for (local) C_3 based on GGE ensemble with $N_{\rm C} = 6$ conserved quantities. Parameters: $J = 1, \Delta = 0.8, B = -1.0, \omega = 1.6\ \omega_{\rm ph}, \omega_{\rm ph} = T_{\rm ph} = 1$.

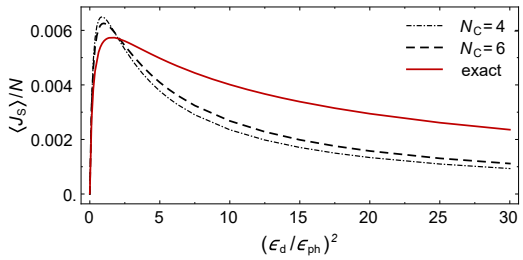


Figure 9.4: For vanishing magnetic field a spin current (but no heat current) is generated within our model for finite ratios of $\epsilon_{\rm d}/\epsilon_{\rm ph}$. The expectation value of spin current density is again maximal for $\epsilon_{\rm d}/\epsilon_{\rm ph} \approx 1$. Parameters: $J = 1, \Delta = 0.8, \omega = 1.6\,\omega_{\rm ph}, \omega_{\rm ph} = T_{\rm ph} = 1, N = 12$.

as functions of $\epsilon_{\rm d}/\epsilon_{\rm ph}$ taking into account $N_{\rm C} = 4$, $N_{\rm C} = 6$, and all conserved quantities. The energy density expectation value is already obtained with good accuracy for $N_{\rm C} = 4$ and even better for $N_{\rm C} = 6$. The heat current vanishes both in thermal equilibrium, $\epsilon_{\rm d} \to 0$, and for $\epsilon_{\rm ph} \to 0$, where the system is described by an infinite temperature state with finite magnetization, $\rho_0 \sim e^{-\lambda_1 S^z}$ and $\langle H_0 \rangle = -B\langle S_z \rangle$. It takes its largest value for $\epsilon_{\rm ph} \sim \epsilon_{\rm d}$. For the currents a description in terms of $N_{\rm C} = 4$ or 6 is qualitatively but not quantitatively accurate. Our study strongly suggests that further quasi-local conserved quantities contribute, as discussed in quench protocols [15, 16, 2], see also Ref. [20]. For the chosen parameters our results depend only weakly on the system size N, see inset of Fig. 17.3. System size analysis is performed for $N_{\rm C} = 6$ since the solution based on all conservations cannot be obtained for larger systems.

Our setup can also be used to create spin currents. Whilst, by symmetry (bond-centered rotation in real and spin space by π around y axis), a finite external field B is needed to obtain a finite heat current, this is not the case for the spin current. Fig. 17.4 displays the spin current density as a function of $\epsilon_{\rm d}/\epsilon_{\rm ph}$ for $B = 0$. Qualitatively one obtains a behavior rather similar to the results for the heat current shown in Fig. 17.3 with a maximum in the spin current for $\epsilon_{\rm ph} \sim \epsilon_{\rm d}$.

The external magnetic field B is a parameter which can easily be tuned experimentally. Fig. 17.7 shows heat and spin current densities as a function of external magnetic field B for $(\epsilon_{\rm d}/\epsilon_{\rm ph})^2 = 2.5$. Note that the sign of the magnetic field determines the sign of the heat current $\langle J_{\rm H} \rangle = \langle C_3 \rangle - B\langle J_{\rm S} \rangle$. All main features of the B-dependence are semi-quantitatively reproduced by the truncated GGE with $N_{\rm C} = 6$. For very large magnetic fields the convergence to the steady state fixed point becomes slow as transitions rates connecting sectors with different magnetization are strongly suppressed, see Methods for further details.

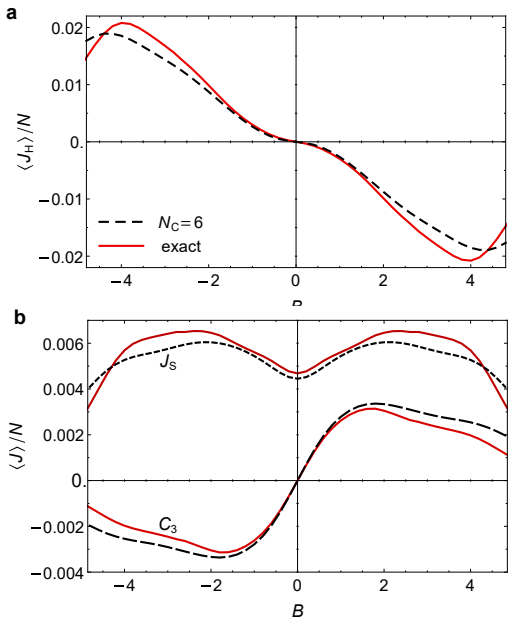


Figure 9.5: (a) Heat current $J_{\rm H}$, (b) spin current $J_{\rm S}$, and C_3 densities as a function of external magnetic field B obtained from a GGE ensemble with $N_{\rm C} = 6$ conserved quantities (dashed) or from an exact calculation (solid) including all conservations. Parameters: $(\epsilon_{\rm d}/\epsilon_{\rm ph})^2 = 2.5$, $J = 1, \Delta = 0.8, \omega = 1.6\ \omega_{\rm ph}, \omega_{\rm ph} = T_{\rm ph} = 1, N = 12$.

9.0.2 Discussion

We have demonstrated that driving approximately integrable systems activates and pumps into approximately conserved quantities. Perhaps the most simple experimental setup to measure the pumping effect predicted in this work, is to use a terahertz laser that excites a spin chain material like Cu-benzoate where by symmetry staggered terms of the form (9.8) are expected [34, 35]. As a consequence of the induced heat currents it is anticipated that the system cools down on one side while it heats up on the other. The direction of the effect can be controlled either by changing the direction of the laser beam or the sign of the external magnetic field B.

For the chosen parameters, the spin and heat currents expressed in dimensionless units appear to be rather small of the order of 10^{-3}. While these values can definitely be increased by tuning parameters, for example the external magnetic field, it is important to note that the currents are actually quite large compared to the typical heat or spin currents obtained in bulk materials. To create a heat current of similar size in a good heat conductor like Cu (assuming $J \sim k_{\mathrm{B}} \cdot 100\,\mathrm{K}$, $5\,\text{Å}$ for the distance of the spin chains, and $\kappa^{\mathrm{Cu}} \approx 400\,\mathrm{Wm^{-1}K^{-1}}$) one would need a temperature gradient of several $10^5\,\mathrm{Km^{-1}}$. Similarly, to create a (transversal) spin current of comparable size in a heavy element like Pt using the spin-Hall effect (assuming $\rho^{\mathrm{Pt}} \approx 10\,\mu\Omega\,\mathrm{cm}$ and $\alpha_{\mathrm{s}}^{\mathrm{Pt}} \approx 10\,\%$ for the spin Hall angle [48]) one needs electric fields of the order of $10^4\,\mathrm{Vm^{-1}}$ or sizable current densities of the order of $10^{11}\,\mathrm{Am^{-2}}$. These numbers are even more remarkable when one takes into account that the electron densities in Cu or Pt are at least an order of magnitude higher than the spin density for spin-chains with a distance of $5\,\text{Å}$.

While our study has focused on the steady state, it is instructive to discuss the relevant time scales for its buildup. For this argument we consider a quench where at time $t = 0$ an initial state is perturbed both by the integrable part of the Hamiltonian and by small non-integrable perturbations. At short times of the order of several $1/J$ the initial state will prethermalize [88, 40, 95, 52, 41] into a GGE where the values of the conserved quantities, $\langle C_i \rangle$, are set by the initial conditions (with small corrections from the perturbations [52, 53]). Further time evolution can be approximately described by a GGE with time-dependent Lagrange parameters. Their time-dependence is determined by perturbations which assert forces $F_i \sim \epsilon^2$, such that $d\lambda_i/dt \approx F_i$. Governed by the perturbations the system will loose the memory of its initial condition on a time scale of order $1/\epsilon^2$ and relax to the steady state (obtained from $F_i = 0$) which is, in general, completely unrelated to the prethermalized state. Note that the same approach predicts ordinary thermalization in the absence of external driving.

Our results suggest that the concept of generalized Gibbs ensembles has a much broader range of application than previously anticipated, now extended to open systems where symmetries are not exact and integrability is weakly broken. A truncated GGE proved to be useful for qualitative description, however, it showed quantitative discrepancies most probably due to disregarded quasi-local conserved quantities, as observed already in quench protocols [15, 16]. We are planning a future study tailored to address this issue systematically. It would be interesting to develop integrability-based methods similar to the quench-action approach [54, 5, 15, 16] to treat such situations.

Most important for applications is that the integrability is not required to be realized exactly but only approximately. Efficient pumping requires only that the pumping rates are of the same order of magnitude as the loss rates arising from integrability breaking terms. Especially the integrability based creation of large spin currents could find its application in future spintronics devices.

9.0.3 Methods

Perturbing around ρ_0.

The central equations (9.5) or (9.6), used to determine the density matrix ρ_0 in the limit $\epsilon \to 0$, have to be consistent and can also even be derived by considering perturbations around ρ_0, $\rho_\infty = \rho_0 + \delta\rho$.

First, the leading $\delta\rho$ correction to $\langle \dot{C}_i \rangle$, Eq. (9.3), arising from $\mathrm{Tr}\,(C_i \hat{\mathcal{L}}_0 \delta\rho)$ which is nominally of the same order as $\mathrm{Tr}\,(C_i \epsilon \hat{\mathcal{L}}_1 \rho_0)$ vanishes trivially as $\mathrm{Tr}\,(C_i[H_0, \delta\rho]) = \mathrm{Tr}\,(\delta\rho[C_i, H_0]) = 0$.

For arbitrary ρ_0, $\delta\rho$ is exactly given by $\delta\rho = -\hat{\mathcal{L}}^{-1}\epsilon\hat{\mathcal{L}}_1\rho_0$, where $\hat{\mathcal{L}}^{-1}$ is a short-hand notation for $\lim_{\eta\to 0}(\hat{\mathcal{L}} - \eta\hat{1})^{-1}$ with the infinitesimal regularizer η. The correct expansion point ρ_0 is found if $\lim_{\epsilon\to 0}\delta\rho = 0$. Below we show that for the projection operator $\hat{P}$, Eq. (9.4),

$$\hat{\mathcal{L}}^{-1}\hat{P} \sim \mathcal{O}(\epsilon^{-1}), \tag{9.12}$$

which would yield $\hat{\mathcal{L}}^{-1}\hat{P}\epsilon\hat{\mathcal{L}}_1\rho_0 \sim \mathcal{O}(1)$. This contradicts our perturbative approach unless $\hat{P}\hat{\mathcal{L}}_1\rho_0 = 0$, as set by our condition Eq. (9.5).

Eq. (9.12) is a consequence of the fact that $\hat{P}$ projects onto the tangential space to GGE density matrix. In this space $\hat{\mathcal{L}}_0$ vanishes by definition, $\hat{\mathcal{L}}_0(\partial\rho_0/\partial\lambda_i) = 0$, and $\hat{\mathcal{L}} = \hat{\mathcal{L}}_0 + \epsilon\hat{\mathcal{L}}_1$ is therefore of order ϵ. Technically, this can be seen by using the general relation

$$(\hat{X} + \hat{Y})^{-1} - \hat{X}^{-1} = -(\hat{X} + \hat{Y})^{-1}\hat{Y}\hat{X}^{-1} \tag{9.13}$$

for

$$\begin{aligned}\hat{X} &= \hat{P}\epsilon\hat{\mathcal{L}}_1\hat{P},\\ \hat{Y} &= \hat{\mathcal{L}}_0 + \hat{Q}\epsilon\hat{\mathcal{L}}_1\hat{Q} + \hat{P}\epsilon\hat{\mathcal{L}}_1\hat{Q} + \hat{Q}\epsilon\hat{\mathcal{L}}_1\hat{P},\end{aligned} \tag{9.14}$$

with $\hat{Q} = \hat{1} - \hat{P}$ and $\hat{X} + \hat{Y} = \hat{\mathcal{L}}$. Then

$$\begin{aligned}\hat{\mathcal{L}}^{-1}\hat{P} &= (\hat{X} + \hat{Y})^{-1}\hat{P}\\ &= \hat{X}^{-1}\hat{P} - (\hat{X} + \hat{Y})^{-1}\ \hat{Q}\ \hat{Y}\ \hat{P}\ \hat{X}^{-1}\hat{P}\\ &\sim \mathcal{O}(\epsilon^{-1}) + \mathcal{O}(1)\end{aligned} \tag{9.15}$$

The second term is $O(1)$ as $\hat{\mathcal{L}}_0\hat{P} = 0$ and therefore $\hat{Y}\hat{P} \sim O(\epsilon)$. The divergence of $\hat{\mathcal{L}}^{-1}\hat{P}$ for $\epsilon \to 0$ can be directly related to the fact that integrable systems are characterized by infinite conductivities (finite Drude weights) at finite temperatures [56] as can, e.g., be seen [19] within the memory matrix formalism [79].

All arguments given above can be generalized to situations where leading corrections arise from 2nd order perturbation theory in which case one obtains Eq. (9.6) instead of Eq. (9.5).

Staggered hopping and magnetic field modulation.

Sizable staggered g-tensors leading to staggered B-fields have been observed in a number of different compounds [34, 35, 36, 21]. Similarly an external electric field will distort the crystalline structure in these materials, leading to staggered exchange couplings linear in homogeneous electric fields. An example of such a material is Cu-benzoate [34] with the above modulations allowed by symmetry for electric (magnetic) fields applied in the 010 (001) crystallographic direction. In this system the staggered g-tensor has been measured to be approximately 0.08 [35], the size of the staggered exchange coupling is unknown. For simplicity, we assume in Eq. (9.8) that the two staggered terms are of the same size.

Conservation laws of the XXZ Heisenberg model.

An infinite set of local conserved quantities C_i of the Heisenberg model $H_{\rm XXZ} = H_0(B=0)$ can be obtained using the boost operator $O_{\rm b} = -i\sum_j j h_{j,j+1}$ (where $H_{\rm XXZ} = \sum_j h_{j,j+1}$) from the recursion relation $[O_{\rm b}, C_i] = C_{i+1}$ for $i > 1$ with $C_1 = \sum_j S^z_j$, $C_2 = H_{\rm XXZ}$ [50]. In general, C_i are operators involving maximally i neighboring sites. Importantly, C_3 in the absence of external magnetic field equals the heat current

$$J_{\rm H}(B=0) = C_3 = J^2 \sum_j (\boldsymbol{S}'_j \times \boldsymbol{S}''_{j+1}) \cdot \boldsymbol{S}'_{j+2} \tag{9.16}$$

with rescaled spin operators $S'^a_j = \sqrt{\lambda_a} S^a_j$, $S''^a_j = \sqrt{\lambda_z/\lambda_a} S^a_j$ for $\lambda_z = \Delta/J$, $\lambda_x = \lambda_y = 1$. In the presence of external magnetic field, Eq. (9.7), heat current has in addition to C_3 also a spin current component,

$$J_{\rm H} = J^2 \sum_j (\boldsymbol{S}'_j \times \boldsymbol{S}''_{j+1}) \cdot \boldsymbol{S}'_{j+2} - B J_{\rm S}. \tag{9.17}$$

As understood recently there also exist families of quasi-local conserved quantities [9, 22, 47], which are mostly disregarded in our study with the exception of a spin-reversal parity-odd operator, $J^{\rm c}_{\rm S}$. The latter is constructed as the conserved part of the spin current operator $J_{\rm S}$,

$$\begin{aligned} J_{\rm S} &= i\frac{J}{2}\sum_j (S^+_j S^-_{j+1} - S^-_j S^+_{j+1}) \\ J^c_{\rm S} &= \sum_{\tilde n} |\tilde n\rangle\langle\tilde n| J_S |\tilde n\rangle\langle\tilde n| \end{aligned} \tag{9.18}$$

where $|\tilde n\rangle$ are simultaneous eigenstates of the C_i. Since it is known that the spin current has an overlap with the quasi-local family [8] for $\Delta < J$, the conserved

$$J^{\rm c}_{\rm S}$$

contains quasi-local components (and, possibly, non-local components not contributing in the thermodynamic limit).

Floquet formulation.

For a periodically driven system described by $\dot\rho = \hat{\mathcal{L}}(t)\rho$ with $\hat{\mathcal{L}}(t+T) = \hat{\mathcal{L}}(t)$ the density matrix changes periodically in the long-time limit. Therefore it is useful to split it into Floquet components,

$$\rho = \sum_n e^{-in\omega t}\rho^{(n)}, n \in \mathbb{Z} \tag{9.19}$$

with $\rho^{(-n)} = \rho^{(n)\dagger}$ and $\omega = 2\pi/T$. The Floquet components are combined into the vector $\boldsymbol{\rho} = (\dots \rho^{(-1)}, \rho^{(0)}, \rho^{(1)}, \dots)$. The Liouvillian is promoted to a (static) matrix $\hat{\boldsymbol{\mathcal{L}}}_{nm} = in\omega\delta_{nm} + \hat{\mathcal{L}}_{n-m}$ with $\hat{\mathcal{L}}_{n-m} = \frac{1}{T}\int_0^T \hat{\mathcal{L}}(t) e^{i\omega(n-m)t} dt$. Using this notation, all results obtained for static Liouvillian super-operators directly translate to the time-periodic case. Within our setup, H_0, all approximate conservation laws C_i and the GGE density matrix ρ_0 are static and therefore the projection operator $\hat P$, Eq. (9.4), projects onto the $n = 0$ Floquet sector only. The steady state condition, Eq. (9.6), thus means that the approximately conserved quantities do not grow after averaging over an oscillation period. To second order in $\epsilon_{\rm d}$ only transitions from the $n = 0$ to the $n = \pm 1$ Floquet sector and back contribute to Eq. (9.6) or (9.10) as $\hat{\mathcal{L}}_n = 0$ for $|n| > 1$.

For the generalized force due to the periodic driving, we obtain from (9.10)

$$F_i^{(\mathrm{d})} = \frac{2\pi}{N}\epsilon_{\mathrm{d}}^2 \sum_{i'}(\chi^{-1})_{ii'} \sum_{m,k} \rho_m (C_{i',m} - C_{i',k}) \times$$
$$\times \Big\{ |\langle k|H_{\mathrm{d}}^{(+)}|m\rangle|^2 \delta(E_k^0 - E_m^0 - \omega)$$
$$+ |\langle k|H_{\mathrm{d}}^{(-)}|m\rangle|^2 \delta(E_k^0 - E_m^0 + \omega) \Big\} \tag{9.20}$$

where we used H_0 eigenstates $|m\rangle$ with $H_0|m\rangle = E_m^0|m\rangle$, matrix elements $\rho_m = \langle m|\rho_0|m\rangle$, $C_{i,m} = \langle m|C_i|m\rangle$, and the notation $H_{\mathrm{d}} = \epsilon_{\mathrm{d}} \left(e^{i\omega t} H_{\mathrm{d}}^{(-)} + e^{-i\omega t} H_{\mathrm{d}}^{(+)} \right)$. Note that Eq. (9.20) contains – as expected – transition rates well-known from Fermi's golden rule. Eq. (9.20) is evaluated for finite systems of size N by replacing the δ function by a Lorentzian $(1/\pi)\eta/(\omega^2+\eta^2)$ ($\eta = 0.1J$ for $N = 12$).

Eq. (9.20) is only valid for situations where all conservation laws commute with each other, with $C_i = \sum_m |m\rangle C_{i,m} \langle m|$, see below for a brief discussion of the non-commuting case.

Phonon coupling.

As written in the main text, we assume that the phonon system always remains at equilibrium, $\rho_{\mathrm{ph}} \sim e^{-H_0^{\mathrm{ph}}/T_{\mathrm{ph}}}$. Using Eq. (9.10), after tracing over phonons, we obtain for the generalized force

$$F_i^{(\mathrm{ph})} = 2\pi\epsilon_{\mathrm{ph}}^2 \sum_{i'}(\chi^{-1})_{ii'} \sum_{m,k} \rho_m (C_{i',m} - C_{i',k})$$
$$\times J^2 \left(|\langle k|\mathbf{S}_j \cdot \mathbf{S}_{j+1}|m\rangle|^2 + \gamma_{\mathrm{m}}^2 |\langle k|S_j^x S_{j+1}^z + S_j^z S_{j+1}^x|m\rangle|^2 \right)$$
$$\times \Big((n_{\mathrm{B}}(E_m^0 - E_k^0) + 1)\ A^{(\mathrm{ph})}(E_m^0 - E_k^0)$$
$$+ n_{\mathrm{B}}(E_k^0 - E_m^0)\ A^{(\mathrm{ph})}(E_k^0 - E_m^0) \Big) \tag{9.21}$$

where $n_{\mathrm{B}}(E) = 1/(e^{E/T_{\mathrm{ph}}} - 1)$ is the equilibrium Bose distribution evaluated at the temperature T_{ph} and $A^{(\mathrm{ph})}(\omega)$ is the phonon spectral function. For our finite size calculation we broaden the spectral function of the Einstein phonons using $A^{(\mathrm{ph})}(\omega) = \Theta(\omega) \frac{\omega}{\omega_{\mathrm{ph}}\eta\sqrt{\pi}} e^{-(\omega-\omega_{\mathrm{ph}})^2/\eta^2}$. This choice of broadening ensures detailed balance relations (necessary to obtain a thermal state in the absence of driving) and the positivity of phonon frequencies (necessary for stability).

For all plots we use $\eta = 0.4J$. However, we have checked that similar results are obtained, e.g., for $\eta = 0.1J$ for magnetic fields up to $|B| = 2J$. For larger fields $\eta = 0.1J$ does not provide a sufficient amount of relaxation between sectors with different magnetization and convergence becomes slow and unstable. For $\eta = 0.4J$ larger fields, $|B| \lesssim 5J$, can be reached.

Implementation of non-commuting conservation laws.

As discussed in the main text, a complete basis of all non-local commuting or non-commuting conserved quantities is given by $\mathcal{Q} = \{|n\rangle\langle m| \text{ with } E_m^0 = E_n^0\}$ which solve the equation $\hat{\mathcal{L}}_0 Q_i = 0$ for $Q_i \in \mathcal{Q}$. Using the exact eigenstates of H_0 it is straightforward to evaluate Eq. (9.11) where we use for our finite size calculations the broadening procedures described above. As a technical detail we note that, when one follows this procedure, one has to evaluate in the phonon sectors integrals of the type $\int \frac{A^{(\mathrm{ph})}(\omega')}{\omega - \omega'} n_{\mathrm{B}}(\omega') d\omega'$ numerically. For efficient evaluations we use interpolating functions for these integrals.

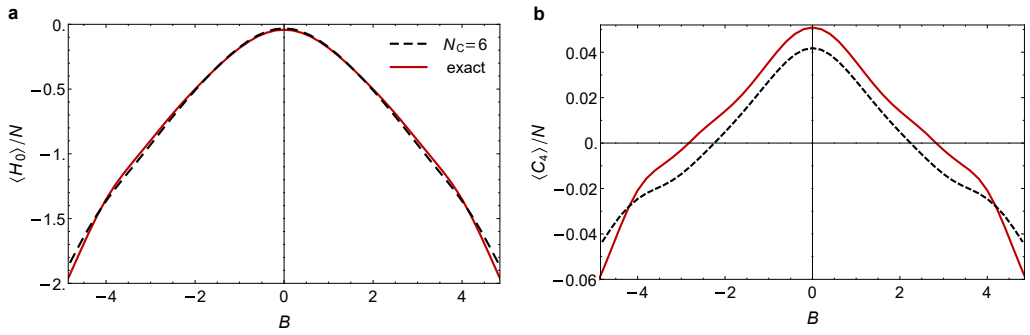


Figure 9.6: (a) The energy density and (b) the expectation value of another conserved quantity C_4 (4-spin operator) as a function of magnetic field B, obtained from calculation using all conserved quantities (solid) and a GGE with $N_C = 6$ (quasi-) local conserved quantities (dashed).

GGE estimation for other conserved quantities.

To provide further support for our claim that truncated GGEs give a semi-quantitative description of our weakly open system we show in Fig. 9.6 additional comparison of the $\langle H_0\rangle$ and $\langle C_4\rangle$ as a function of magnetic field B at $(\epsilon_d/\epsilon_{ph})^2 = 2.5$, comparing as in the main text the exact calculation including all conserved quantities and the truncated GGE with $N_C = 6$ (quasi-)local conserved quantities. The GGE ansatz captures the right magnitude and the correct behaviour in the dependence on B also for more complicated 4-spin operators like C_4. We use same parameters as for the Fig. 17.7 in the main text: $(\epsilon_d/\epsilon_{ph})^2 = 2.5, J = 1, \Delta = 0.8, \omega = 1.6\ \omega_{ph}, \omega_{ph} = T_{ph} = 1, N = 12$.

10 Engineering generalized Gibbs ensembles with trapped ions by Reiter, Lange, Jain et al.

Abstract

The concept of generalized Gibbs ensembles (GGEs) has been introduced to describe steady states of integrable models. Recent advances show that GGEs can also be stabilized in nearly integrable quantum systems when driven by external fields and open. Here, we present a weakly dissipative dynamics that drives towards a steady-state GGE and is realistic to implement in systems of trapped ions. We outline the engineering of the desired dissipation by a combination of couplings which can be realized with ion-trap setups and discuss the experimental observables needed to detect a deviation from a thermal state. We present a novel mixed-species motional mode engineering technique in an array of micro-traps and demonstrate the possibility to use sympathetic cooling to construct many-body dissipators. Our work provides a blueprint for experimental observation of GGEs in open systems and opens a new avenue for quantum simulation of driven-dissipative quantum many-body problems.

10.1 Introduction

Providing a compact description of complicated many-body systems is a challenging task. Studies of equilibration of interacting quantum many-body systems have revealed that one can borrow statistical descriptions, taking into account conservation laws of equilibrating systems, to achieve that [7, 2]. If we suddenly excite an ergodic system, for which energy is the only

conservation law, steady state expectation values will be given by a *Gibbs ensemble*

$$\rho_{\text{th}} = \frac{e^{-\beta H_0}}{\text{Tr}[e^{-\beta H_0}]} \tag{10.1}$$

with temperature $1/\beta$ determined by the amount of energy that has been injected into the system with the excitation process [7]. Such a description by the single parameter – temperature – is, therefore, an incredible simplification for an interacting model with a priori exponentially many degrees of freedom.

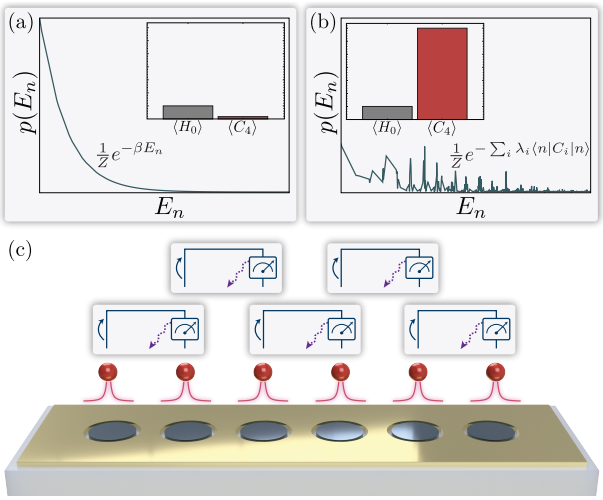


Figure 10.1: Activating integrability. (a) Following an excitation of a non-integrable or nearly integrable system, the steady state exhibits thermal behavior with small expectation values of operators other than the Hamiltonian. (b) A nearly integrable system with a weak dissipative drive will show highly non-thermal behavior with a distribution $p(E_n)$ approximately described by a generalized Gibbs ensemble (GGE) and large expectation values for conservation laws, e.g., $\langle C_4 \rangle$. (c) A one dimensional array of trapped-ions has interactions which decay as a power-law, and is thus nearly integrable for large exponents. We re-activate integrable effects by engineering the dissipation, which stabilizes a GGE as the steady state.

Similarly, *generalized Gibbs ensembles* (GGE) were proposed to describe local observables in steady states of systems with additional local conservation laws C_i. The existence of additional conservation laws highly restricts the dynamics and prevents the system from thermalizing. GGEs have a form related to that of a Gibbs ensemble [1],

$$\rho_{\text{GGE}} = \frac{e^{-\sum_i \lambda_i C_i}}{\text{Tr}[e^{-\sum_i \lambda_i C_i}]}. \tag{10.2}$$

but with additional Lagrange multipliers λ_i associated with additional conserved quantities C_i that all commute with the Hamiltonian, $[C_i, H_0] = 0$. Exemplary models with macroscopically many local conservation laws, where applicability of GGE has been widely studied theoretically, are Bethe-ansatz-solvable and non-interacting integrable systems [4, 3, 11, 5, 47, 48, 49, 50, 36, 37, 25, 15, 16, 58, 59, 60, 62, 63, 2, 64, 65, 66]. In this case, Lagrange parameters λ_i are fixed by the knowledge of the initial state $|\psi(0)\rangle$, as well as $\langle C_i \rangle = const$,

$$\langle \psi(0)|C_k|\psi(0)\rangle \stackrel{!}{=} \text{Tr}\left[C_k \frac{e^{-\sum_i \lambda_i C_i}}{\text{Tr}[e^{-\sum_i \lambda_i C_i}]}\right], \quad \forall k. \tag{10.3}$$

Since generically $\lambda_i \neq 0$, integrable systems remain non-thermal up to arbitrary times.

Applicability of GGEs was confirmed also experimentally in a cold atoms setup [19] where, up to some time, a closed and integrable system can be prepared. Ref. [19] showed that GGEs for a Lieb-Liniger model can provide an accurate description of an interacting trapped 1D Bose gas. However, it is very difficult to simulate integrable systems due to their fine-tuned nature: adding practically any other terms to an integrable model will break integrability and cause eventual thermalization [41, 11, 29, 30, 31, 32, 33, 34, 13, 36]. Therefore it was believed that in realistic systems traces of integrability can be seen only in the transient dynamics [40, 95, 103, 29, 97, 98, 52, 104, 100, 106] while the steady state is always thermal due to realistic integrability breaking terms.

In recent works [26, 25, 18], Lange and Lenarčič demonstrated that properties related to integrability are not as fragile as previously believed: if one weakly drives an only approximately integrable system and at the same time allows it to cool via a weak coupling to the environment, the system will nonetheless relax to a steady state approximated with a generalized Gibbs ensemble, supplemented with a small correction $\delta\rho$,

$$\rho_\infty \equiv \lim_{t\to\infty} \rho(t) = \rho_{\mathrm{GGE}} + \delta\rho. \tag{10.4}$$

The major difference to the closed strictly integrable setup, Eq. (10.3), is that here the Lagrange multipliers λ_i are determined by the integrability breaking perturbations themselves, through a stationarity condition [26, 25, 18]

$$\partial_t \langle C_k \rangle \approx \mathrm{Tr}\left[C_k \mathcal{L}_p \frac{e^{-\sum_i \lambda_i C_i}}{\mathrm{Tr}[e^{-\sum_i \lambda_i C_i}]} \right] \stackrel{!}{=} 0, \quad \forall k. \tag{10.5}$$

Here $\mathcal{L}_p$ denotes the Liouville operator corresponding to perturbations which weakly break the integrability, and as a consequence the conservation laws, while driving and cooling the system. Such a setup is much more versatile because it does not require the fine-tuned perfect integrability and at the same time allows for the engineering of GGEs through a particular choice of perturbations. A remarkable consequence is that one can stabilize steady states with large expectation values of nearly conserved operators $\langle C_i \rangle$, if a large corresponding λ_i is established. For example, in solid-state spin chain materials, approximately described by an XXZ model coupled to phonons, a weak laser driving could stabilize steady states with huge heat and spin currents, since these are (partial) conservation laws of the XXZ model [26]. Alternatively, driving and openness can be provided by Markovian dissipative processes [25]. As shown in Fig. 10.1, the latter could be experimentally realized with trapped-ion platforms where long-range interaction between ions inevitably breaks integrability. By adding engineered dissipative processes, a GGE ensemble would be stabilized. As a consequence, the distribution $p(E_n) = \exp(-\sum_i \lambda_i \langle n|C_i|n\rangle)/\mathrm{Tr}[e^{-\sum_i \lambda_i C_i}]$ over the eigenstates of $H_0|n\rangle = E_n|n\rangle$ would differ from a thermal one $p(E_n) = \exp(-\beta E_n)/\mathrm{Tr}[e^{-\beta H_0}]$. While $p(E_n)$ is essentially impossible to measure experimentally, the non-thermal nature of ρ_{GGE} is more easily detected through possible exceedingly large expectation values of conserved operators $\langle C_i \rangle$ of parent XY or transverse-Ising Hamiltonian.

In this work, we address the latter option and discuss an implementation based on ion-trap technology [25, 51, 52]. Controllable coherent couplings in ion-trap systems have been widely used for the realization of spin models [17, 54], and numerous milestone experiments have been conducted on a variety of systems [18, 56, 25, 6, 21, 60, 61, 47, 63]. State-of-the-art Paul traps [51, 21, 47], Penning traps [61, 64, 65], and micro-traps [66, 67, 68, 69, 70] offer a rich toolbox of couplings suitable to engineer coherent Hamiltonian, as well as dissipative interactions. Sympathetic cooling based on mixed-species ion chains is well-studied in Paul traps [71, 72, 73] where it is used to remove entropy from the motional modes of the ions. Here, we realize a driven-dissipative dynamics consisting of a spin Hamiltonian, in combination

with one- and two-body dissipation. The dissipators are engineered combining tunable carrier and sideband couplings with repumper drives or sympathetic cooling as sources of dissipation. To tightly confine the motional modes to the interacting particles, we propose a novel mixed-species mode engineering technique that can be realized in micro-trap arrays. The resulting dynamics stabilizes a steady state approximately described by a generalized Gibbs ensemble, despite different integrability breaking terms.

The paper is organized the following way: In Sec. 10.2 we introduce one choice of a Hamiltonian and Lindblad operators that could be realized in a trapped ion experiment. In Sec. 10.3 we present numerical results and discuss experimental signatures and means to measure that a GGE approximates the stabilized steady state. In Section 10.4–10.5 we present the engineering of the elementary dissipators. We then scale up the interactions in Sec. 10.6 and Sec. 10.7, where we discuss the mode engineering in arrays of micro-traps.

10.2 Model

The theory of activating integrability and engineering steady states described by generalized Gibbs ensembles in realistic systems is generic and applies to different systems approximately described by an integrable model, e.g., transverse field Ising or XXZ Heisenberg chain, Lieb-Liniger or Tonks-Girardeau Bose 1D gas. We choose an integrable model that is closest to the state-of-the art trapped ions setups. We consider the XY-Hamiltonian in the presence of a magnetic field h,

$$H_{\mathrm{XY}} = \sum_j J_x \sigma_j^x \sigma_{j+1}^x + J_y \sigma_j^y \sigma_{j+1}^y + h\sigma_j^z, \tag{10.6}$$

which belongs to the class of non-interacting integrable models. Such a Hamiltonian can be implemented by using standard techniques developed in the trapped-ion field. In contrast to Ref. [21], we rotate the spin axes by $\pi/2$ around the y-axis. The resulting YZ-model will allow us to facilitate an experimental implementation of Lindblad terms. We consider

$$H_0 = \sum_j J_z \sigma_j^z \sigma_{j+1}^z + J_y \sigma_j^y \sigma_{j+1}^y + h\sigma_j^x. \tag{10.7}$$

An alternative realization based on the XY-Hamiltonian in combination with sympathetic cooling is presented in Sec. 10.5.

In traditional setups with trapped ions, the coupling between spins that are d sites apart actually decays as $d^{-\alpha}\sigma_j^{z(y)}\sigma_{j+d}^{z(y)}$ with $\alpha \in [2,3]$. This is one inevitable source of integrability breaking since such Hamiltonian can no longer be diagonalized via a Jordan-Wigner transformation, neither is it Bethe-Ansatz solvable. However, if the decay is fast enough one can consider such a system as nearly integrable. In our analysis we will take into consideration only the leading contribution

$$H_1 = \epsilon_1 \sum_j J_z \sigma_j^z \sigma_{j+2}^z + J_y \sigma_j^y \sigma_{j+2}^y, \quad \epsilon_1 = \frac{1}{2^\alpha}. \tag{10.8}$$

H_1 alone would thermalize the system, however, non-thermal steady states approximated by GGE can be achieved when a weak coupling to Lindblad non-equilibrium baths is added. Here, we will consider the homogeneous bulk dissipators of two types, $a = 1, 2$,

$$\mathcal{D}^{(a)}\rho = \sum_j L_j^{(a)} \rho L_j^{(a)\dagger} - \frac{1}{2}\{L_j^{(a)\dagger} L_j^{(a)}, \rho\} \tag{10.9}$$

with Lindblad operators at site j

$$L_j^{(1)} = \sqrt{\epsilon(1-\gamma)}\, S_j^-, \quad \gamma \in [0,1] \tag{10.10}$$

$$L_j^{(2)} = \sqrt{\epsilon\gamma}\, S_j^+ P_{j+1}^{\downarrow}, \tag{10.11}$$

Here $P_j^{\downarrow} = \frac{1}{2}(\mathbb{1}_j - \sigma_j^z)$ is a projection on the spin-down state at site j.

The steady state density matrix ρ_∞ is determined by

$$\dot{\rho}_\infty = (\mathcal{L}_0 + \mathcal{L}_p)\rho_\infty = 0, \tag{10.12}$$

where $\mathcal{L}_0$ is a dominant term in the Liouvillian, while $\mathcal{L}_p = \mathcal{L}_u + \mathcal{L}_m$ captures unitary and Markovian perturbations,

$$\begin{aligned} \mathcal{L}_0\rho &= -i[H_0, \rho], \\ \mathcal{L}_u\rho &= -i\left[H_1, \rho\right], \\ \mathcal{L}_m\rho &= \left(\mathcal{D}^{(1)} + \mathcal{D}^{(2)}\right)\rho. \end{aligned} \tag{10.13}$$

Despite the fact that the underlying model H_0 in Eq. (10.6) is non-interacting, the next-nearest neighbor interaction H_1 and our choice of Lindblad operators hinders analytical solvability and requires a numerical solution. Since our Lindblad operators have local nature, we also cannot use recently proposed hydrodynamic description [24].

For a review of the theory of weakly driven nearly integrable systems, developed in [26, 25, 18] see App. 10.9. In the next section we go on to establish that this model does stabilize a steady state approximately described by a GGE ensemble, despite different sources of integrability breaking.

10.3 Experimental signatures

The experiment we are proposing would aim to show that a highly non-thermal steady state, described with a generalized Gibbs ensemble, can be stabilized in a nearly integrable model given by $H_0 + H_1$, Eqs. (10.7,10.8), if weakly driven ($\epsilon \ll 1$) with dissipation Eqs. (10.10,10.11).

To show that a GGE is stabilized by driving, we compare in Fig. 10.2 the steady state expectation values obtained with the exact density matrix, Eq. (10.12) or with a GGE, Eq. (10.14). A qualitative agreement confirms that a GGE is stabilized. The first notable conclusion from the numerical analysis is that in the limit of small driving, $\epsilon \ll 1$, a truncated generalized Gibbs ensemble

$$\rho_{\mathrm{tGGE}} = \frac{e^{-\sum_{i=1}^{N_c}\lambda_i C_i}}{\mathrm{Tr}[e^{-\sum_{i=1}^{N_c}\lambda_i C_i}]} \tag{10.14}$$

parametrized with only $N_c = 4$ Lagrange parameters can capture expectation values of local observables we are interested in, while other more complicated conservation laws can be neglected. In comparison, a full density matrix requires 4^N parameters in the system size N. This shows that a description in terms of truncated GGEs is extremely compact. For a more thorough comparison see App. 10.9.

Another interesting observation is that the next-nearest neighbors coupling H_1, Eq. (10.8), does not have a strong impact on the steady state. While in a closed setup H_1 is crucial as it dictates relaxation towards a thermal state, in our setup it is dominated by Lindblad terms, see App. 10.9 for details. Therefore, we neglect it in results presented in the main text.

A physically most interesting consequence of stabilizing a steady state approximately described with a GGE is that the expectation values of conservation laws,

$$\langle C_k \rangle = \mathrm{Tr}\left[C_k \frac{e^{-\sum_i \lambda_i C_i}}{\mathrm{Tr}[e^{-\sum_i \lambda_i C_i}]}\right], \tag{10.15}$$

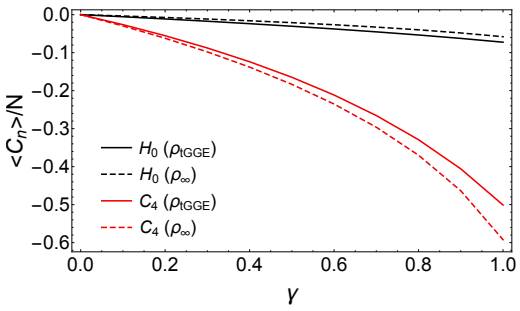


Figure 10.2: $\langle H_0\rangle$ and $\langle C_4\rangle$ as a function of relative driving strength γ, Eqs. (10.10,10.11). A qualitative agreement between the exact ρ_∞ and $\rho_{\rm tGGE}$ confirms that a generalized Gibbs ensemble is stabilized. A large $\langle C_4\rangle$, which could not be obtained from a nearly infinite temperature steady state consistent with a small $\langle H_0\rangle$, indicates that a highly non-thermal GGE is stabilized. Parameters: $J_y = h = 1$, $J_z = 0.1$; $N = 10, N_c = 4$ for $\rho_{\rm tGGE}$ and $N = 6, \epsilon = 0.01$ for ρ_∞.

can be much larger than in a thermal state, $\mathrm{Tr}[C_k e^{-\beta_0}/\mathrm{Tr}[e^{-\beta H_0}]]$. In this respect conservation laws are measurably distinct from other operators: a generic observable O will have a much smaller expectation value than a conservation law, $\mathrm{Tr}[O\rho_{\rm GGE}] \ll \mathrm{Tr}[C_k\rho_{\rm GGE}]$, given they have the same norm $\mathrm{Tr}[O^2] = \mathrm{Tr}[C_k^2]$. The conservation law C_k will show a particularly large expectation value if driving is such that it stabilizes a GGE with a large corresponding Lagrange parameter λ_k. Which $\lambda_k \neq 0$ depends on the symmetry of the driving, i.e., the Lindblad operators [26, 25, 75]. A strong response of conservation laws to weak driving could have practical implications, such as heat and spin pumping [26] in spin chain materials, but can also serve to detect that a GGE has been stabilized despite the integrability breaking terms. In the following we discuss ways to detect large expectation values of conserved (or partially conserved) operators, which could not be possible in a thermal state.

One possibility is to compare expectation values of observables which *do* or *do not* overlap with conservation laws. If driving stabilizes $\rho_{\rm GGE}$ with a large Langrange multiplier λ_i associated with the conservation law C_i, observable O that has a nonzero overlap with C_i, $\mathrm{Tr}[OC_i] \neq 0$, will show a large expectation value.

Let us, for example, consider $\langle\sigma^y_{j-1}\sigma^x_j\sigma^y_{j+1}\rangle \equiv \langle\mathrm{YXY}\rangle$ and $\langle\sigma^y_{j-1}\sigma^y_j\sigma^x_{j+1}\rangle \equiv \langle\mathrm{YYX}\rangle$. At least at small $J_z/J_y \ll 1$, where $H_0 \approx J_y\sigma^y_j\sigma^y_{j+1} + h\sigma^x_j$, it is easy to estimate thermal expectation values $\langle\mathrm{XYX}\rangle_{\rm th}, \langle\mathrm{XXY}\rangle_{\rm th}$ via expansion $\rho_{\rm th} = e^{-\beta H_0}/Z \approx (\mathbb{1} - \beta H_0 + \beta^2 H_0^2/2 + \dots)/Z$: a nonzero $\langle\mathrm{YYX}\rangle_{\rm th}$ is dominantly coming from the 2nd order in β, while $\langle\mathrm{YXY}\rangle_{\rm th}$ from the 3rd order. In a thermal state one would therefore expect $\langle\mathrm{YXY}\rangle_{\rm th} \ll \langle\mathrm{YYX}\rangle_{\rm th}$. However, our numerical result in Fig. 10.3 shows $\langle\mathrm{YXY}\rangle \gg \langle\mathrm{YYX}\rangle$. This observation is a clear sign that the steady state is not thermal. The large expectation value of $\langle\mathrm{YXY}\rangle$ is a direct consequence of the fact that this operator is part of C_4, Eq.(10.16), therefore its expectation value has also a linear contribution in λ_4 in the expansion, since driving stabilizes a GGE with $\lambda_4 \neq 0$.

In our setup, besides the Hamiltonian H_0 ($H_0 = C_2$ according to the notation we use, see App. 10.9), the next simplest local extensive conservation law $C_i = \sum_j c_j^{(i)}$ that shows a strong response to the dissipative driving is

$$C_4 = \sum_j \sum_{\mu=z,y} J_\mu\sigma^\mu_j\sigma^x_{j+1}\sigma^x_{j+2}\sigma^\mu_{j+3} - h\sigma^\mu_j\sigma^x_{j+1}\sigma^\mu_{j+2} + J_{\bar\mu}\sigma^\mu_j\sigma^\mu_{j+1}, \tag{10.16}$$

where $\bar z = y$ and $\bar y = z$. Fig. 10.2 shows the comparison of $\langle H_0\rangle = \langle C_2\rangle$ and $\langle C_4\rangle$ as a function of the relative strength γ, Eqs. (10.10,10.11), obtained from a GGE calculation on $N = 10$ sites or a full steady state density matrix on $N = 6$ sites. While $\langle H_0\rangle(\gamma)$ shows rather small

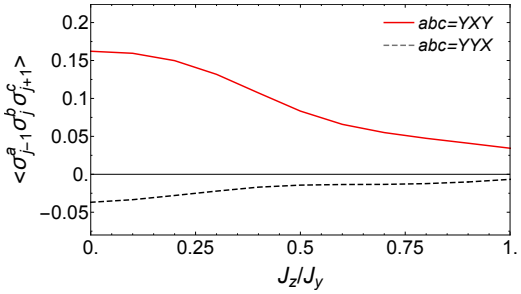


Figure 10.3: Expectation values $\langle\sigma^y_{j-1}\sigma^y_j\sigma^x_{j+1}\rangle$ and $\langle\sigma^y_{j-1}\sigma^x_j\sigma^y_{j+1}\rangle$ as a function of anisotropy J_z/J_y obtained from the exact steady state ρ_∞ at $N = 6, \epsilon = 0.01$, $J_y = 1$, $\gamma = 0.8$. $\langle\sigma^y_{j-1}\sigma^x_j\sigma^y_{j+1}\rangle$ shows a much larger value because it is part of a conservation law, C_4, Eq. (10.16).

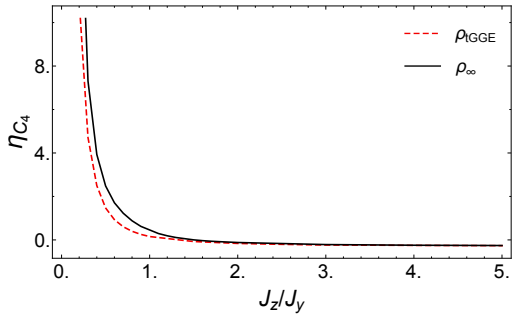


Figure 10.4: Ratio η_{C_4}, Eq. (10.17), measures how non-thermal the steady state is at different anisotropies J_z/J_y for $J_y = h = 1$, $\gamma = 0.5$. This result suggests that the experiment should optimally be performed at small J_z/J_y or $J_z = 0$. The calculation is based on the exact steady state ρ_∞ at $\epsilon = 0.01$ on $N = 6$ sites and on the truncated GGE ρ_{tGGE} on $N = 10$ sites using $N_C = 4$ conservation laws.

values, $\langle C_4\rangle(\gamma)$ is bigger. That would never be the case, if $\langle C_4\rangle(\gamma)$ was evaluated with respect to (an almost infinite temperature) thermal ensemble, which reproduces small $\langle H_0\rangle(\gamma)$. This observation alone suggests that a non-thermal steady state is stabilized.

In order to quantify how non-thermal the steady state is and to select optimal parameters, we introduce the ratio η_O

$$\eta_O = \frac{\text{Tr}[O\rho_x] - \text{Tr}[O\rho_{\text{th}}]}{\text{Tr}[O\rho_{\text{th}}]}, \tag{10.17}$$

calculated with respect to the exact steady state, $\rho_x = \rho_\infty$, or with the truncated GGE, $\rho_x = \rho_{\text{tGGE}}$. For calculations with $\rho_x = \rho_\infty$ we define ρ_{th} as a thermal state with respect to H_0, Eq. (10.6), with temperature determined from the condition $\text{Tr}[H_0\rho_\infty] = \text{Tr}[H_0 e^{-\beta H_0}/\text{Tr}[e^{-\beta H_0}]]$. For calculations based on $\rho_x = \rho_{\text{tGGE}}$ the temperature in ρ_{th} is calculated using a Gibbs ensemble ansatz with H_0 as the only conservation law.

In the following we focus on the operator $O = C_4$. In the absence of Lindblad driving $\mathcal{D}^{1(2)}$, the ratio equals $\eta_{C_4} = 0$ due to integrability breaking power-law decay of interactions in the Hamiltonian. In the presence of a weak Lindblad drive, on the other hand, the steady state can be highly non-thermal. Figure 10.4 shows η_{C_4} as a function of anisotropy J_z/J_y, obtained from the exact density matrix ρ_∞ on $N = 6$ sites at $\epsilon = 0.01$ and from a ρ_{tGGE} on $N = 10$. The dependence on J_z/J_y suggests that the experiment observing a highly non-thermal steady state ($\eta_{C_4} \gg 1$) achieved by a weak driving should operate at a small J_z/J_y or even at $J_z = 0$ (corresponding to the transverse-field Ising case).

Why η_{C_4} is so large for $J_z = 0$ (and small J_z) can be reasoned by looking directly at the

expectation values of $\langle H_0\rangle$ and $\langle C_4\rangle$, Fig. 10.5. $\langle H_0\rangle \approx 0$ is almost zero, suggesting an almost infinite temperature state ($\beta \approx 0$), which would imply $\langle C_4\rangle \approx 0$. On the other hand, the observed $\langle C_4\rangle \sim 1$ is actually large. This observation, together with a good agreement between ρ_∞ and ρ_{tGGE}, clearly shows that a GGE with a large λ_4 is stabilized, despite $\beta \approx 0$. Measuring $\langle H_0\rangle$ and $\langle C_4\rangle$ would thus serve as strong affirmation of our theory.

In Fig. 10.6, we show that at mild anisotropy, for example, $J_z/J_y = 0.9$, also a magnetic field h helps to prepare a more non-thermal state.

10.4 Dissipation engineering

Having shown that our dissipative driving can stabilize a steady state described by a GGE, we now discuss the implementation of the desired dynamics in a trapped-ion setup. To engineer suitable dissipative interactions, we combine coherent couplings with sources of dissipation such as induced spontaneous emission and sympathetic cooling. We use these tools to engineer the desired one- and two-body jump operators and verify their action numerically.

In this section, we assume that the YZ-Hamiltonian in Eq. (10.7) is implemented. This allows us to engineer the dissipation in Eqs. (10.10)–(10.11) between the levels $|\uparrow\rangle, |\downarrow\rangle$. As these are eigenstates of (stimulated) spontaneous emission, it is possible to use repumper beams as sources of dissipation. In Sec. 10.5, in turn, we assume that the XY-model in Eq. (10.6) is realized. This requires the dissipation to be engineered between the eigenstates of σ_x, as is demonstrated using sympathetic cooling.

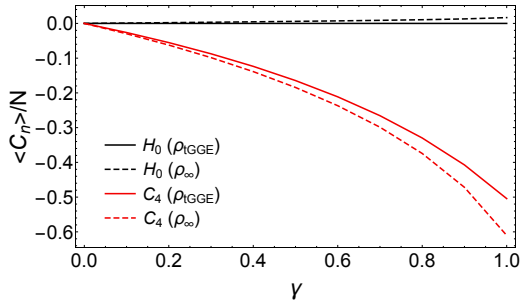


Figure 10.5: Expectation values $\langle H_0\rangle$ and $\langle C_4\rangle$ as a function of relative driving strength γ, Eqs. (10.10,10.11), for $J_z = 0$, corresponding to the transverse-field Ising case. Stabilized steady state is obviously highly non-thermal and described with a GGE with $\beta \approx 0$ and large λ_4, manifested via tiny $\langle H_0\rangle$ and large $\langle C_4\rangle$. Parameters: $J_y = h = 1$, $J_z = 0$; $N = 10, N_c = 4$ for ρ_{tGGE} and $N = 6, \epsilon = 0.01$ for ρ_∞.

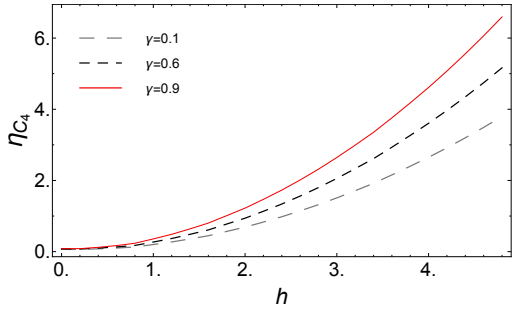
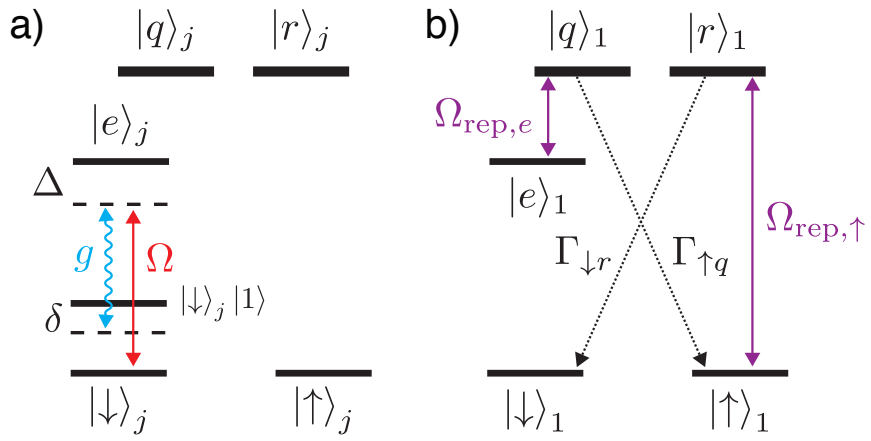


Figure 10.6: Ratio η_{C_4} as a function of magnetic field h for weak anisotropy $J_z/J_y = 0.9$ obtained from tGGE at $N = 10$, $J_y = 1$ and different ratios of Lindblad drivings $\gamma = 0.1, 0.6, 0.9$. Increasing the magnetic field assists in preparing a more non-thermal state.



ing

Figure 10.7: Setup for engineered single-body and two-body dissipation. We consider two trapped ions, $j = 1$ and $j = 2$, with two stable ground levels, $|\downarrow\rangle$ and $|\uparrow\rangle$, and three excited levels, $|e\rangle$, $|r\rangle$, and $|q\rangle$. The ions are subject to coherent couplings (solid lines) and dissipation (dotted lines). (a) A weak drive excites both ions from $|\downarrow\rangle$ to $|e\rangle$ (strength Ω, detuning Δ). The transition from $|e\rangle$ to $|\downarrow\rangle$ is coupled to the motional mode a (phonon detuning δ) by a red-sideband interaction (coupling constant g). The second ket denotes motional excitation and is dropped when in vacuum. (b) We realize single-body decay from $|\uparrow\rangle$ to $|\downarrow\rangle$ and from $|e\rangle$ to $|\uparrow\rangle$ on ion 1. This is done by optical pumping using tunable repumper beams (Rabi rates $\Omega_{\mathrm{rep},\uparrow}$ and $\Omega_{\mathrm{rep},e}$), via the unstable levels $|r\rangle$ and $|q\rangle$ (decay rates $\Gamma_{\downarrow r}$ and $\Gamma_{e\uparrow}$).

10.4.1 Setup

To implement the one- and two-body jump operators in Eqs. (10.10) and (10.11), we consider a system of trapped ions coupled through motional modes. To simplify the discussion, we start by considering a minimal instance consisting of two ions indexed 1 and 2, and a motional mode a, and generalize to more ions in Sec. 10.6–10.7. As is shown in Fig. 22.1, each of the ions is assumed to have two stable ground levels, $|\uparrow\rangle$ and $|\downarrow\rangle$, and three excited levels, $|e\rangle$, $|r\rangle$, and $|q\rangle$. The motional mode a is assumed to be cooled to the ground state, $|0\rangle$. The free Hamiltonian of this system is given by

$$H_{\mathrm{free}} = \delta a^\dagger a + \sum_{j=1}^{2} \Delta |e\rangle_j\langle e| + \Delta_r |r\rangle_j\langle r| + \Delta_q |q\rangle_j\langle q|. \tag{10.18}$$

Here we introduce a phonon detuning δ and an ionic detuning Δ, assuming that we work in a suitable rotating frame with respect to the fields to be introduced below. We will use level

$|r\rangle$ to realize the single-body decay in Eq. (10.10) and levels $|e\rangle$ and $|q\rangle$ in combination with mode a for the two-body dissipation in Eq. (10.11). Level $|q\rangle$ will be used to add a dissipation channel from level $|e\rangle$ to level $|\uparrow\rangle$. The ions are excited from $|\downarrow\rangle$ to $|e\rangle$ using a weak "carrier" drive

$$H_{\text{drive}} = \frac{\Omega}{2} \sum_{j=1}^{2} |e\rangle_j\langle\downarrow| + \text{H.c.}, \tag{10.19}$$

with a Rabi frequency Ω. In addition, levels $|\uparrow\rangle$ and $|e\rangle$ of ion 1 are excited to $|r\rangle$ and $|q\rangle$ by coherent "repumper" beams,

$$H_{\text{rep},\uparrow} = \frac{\Omega_{\text{rep},\uparrow}}{2} |r\rangle_1\langle\uparrow| + \text{H.c.} \tag{10.20}$$

$$H_{\text{rep},e} = \frac{\Omega_{\text{rep},e}}{2} |q\rangle_1\langle e| + \text{H.c.} \tag{10.21}$$

with Rabi rates $\Omega_{\text{rep},\uparrow/e}$. The coupling between ions 1 and 2, needed to engineer two-body dissipation, is mediated by a common motional mode, with creation (annihilation) operator $a^\dagger$ (a). This phonon mode is coupled to the transition from $|e\rangle$ to $|\downarrow\rangle$ by the red-sideband interaction

$$H_{\text{int}} = g \sum_{j=1}^{2} a^\dagger |\downarrow\rangle_j\langle e| + a|e\rangle_j\langle\downarrow| + \text{H.c.}, \tag{10.22}$$

with a coupling constant g.

In addition to the above coherent interactions, the excited level $|r\rangle$ is assumed to be inherently unstable and to decay to level $|\downarrow\rangle$ by spontaneous emission, which can be described using the jump operators,

$$L_{\downarrow r,j} = \sqrt{\Gamma_{\downarrow r}} |\downarrow\rangle_j\langle r|, \quad (j = 1, 2). \tag{10.23}$$

The excited level $|q\rangle$, in turn, is assumed to decay to $|\uparrow\rangle$,

$$L_{\uparrow q,j} = \sqrt{\Gamma_{\uparrow q}} |\uparrow\rangle_j\langle q|, \quad (j = 1, 2). \tag{10.24}$$

To describe the joint dynamics of the ions and the phonons, we use the following notation: the state of the system is described by two kets, where the first ket denotes the internal state of the ions, e.g., $|\downarrow\downarrow\rangle = |\downarrow\rangle_1|\downarrow\rangle_2$. Motional excitations are denoted by a second ket, e.g., $|\downarrow\downarrow\rangle|1\rangle$, which is dropped when the motion is in the ground state.

10.4.2 Single-body dissipation

To realize single-body dissipation, we employ standard optical pumping, combining excitation from $|\uparrow\rangle$ to $|r\rangle$ by $H_{\text{rep},\uparrow}$, Eq. (10.20), and decay from $|r\rangle$ to $|\downarrow\rangle$ by spontaneous emission $L_{\downarrow r,j}$. The effective jump operator [8] for the decay of level $|\uparrow\rangle$ to $|\downarrow\rangle$ through $|r\rangle$ is thus, after elimination of level $|r\rangle$, given by

$$L_{\text{eff}}^{(1)} = \sqrt{\gamma_1} |\downarrow\rangle_1\langle\uparrow| \equiv \sqrt{\frac{\Omega_{\text{rep},\uparrow}^2}{\Gamma_{\downarrow r}}} |\downarrow\rangle_1\langle\uparrow|, \tag{10.25}$$

We thereby realize the desired jump operator $L_1^{(1)} = \sqrt{\epsilon(1-\gamma)}\, S_1^-$ in Eq. (10.10). Using individual addressing techniques, this process can be made site-specific. The decay rate γ_1 can

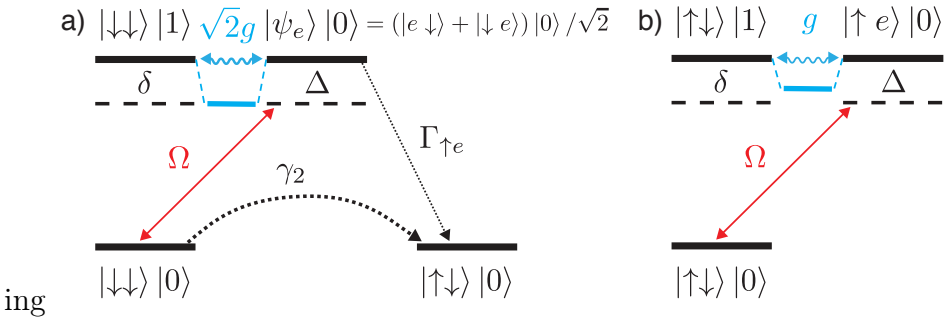
be tuned by varying $\Omega_{\mathrm{rep},\uparrow}$, assuming it to be much smaller than the natural linewidth of level $|r\rangle$, $\Gamma_{\downarrow r} \gg \Omega_{\mathrm{rep},\uparrow}$. Note that, while here we have only assumed the desired dissipation channel from $|r\rangle$ to $|\downarrow\rangle$, additional decay processes from these levels could be described by the same method.

To engineer the two-body dissipation in Eq. (10.11) in Sec. 10.4.3 below, we will also rely on an induced spontaneous emission process from $|e\rangle$ to $|\uparrow\rangle$. Here we assume that we can realize the YZ-Hamiltonian in Eq. (10.7). Alternatively, in the presence of the XY-Hamiltonian in Eq. (10.6), sympathetic cooling can be used as a source of dissipation, as is described in Sec. 10.5.

To realize optical pumping from $|e\rangle$ to $|\uparrow\rangle$, we couple $|e\rangle$ of ion 1 to the unstable level $|q\rangle$ (total decay rate Γ_q) using the repumper in Eq. (10.21). Together with the decay from $|q\rangle$ to $|\uparrow\rangle$ in Eq. (10.24), this realizes

$$L_{\uparrow e} = \sqrt{\Gamma}|\uparrow\rangle_1\langle e| \equiv \sqrt{\frac{\Omega_{\mathrm{rep},e}^2}{\Gamma_{\uparrow q}}}|\uparrow\rangle_1\langle e|. \tag{10.26}$$

Again, the decay rate Γ is tunable through the strength of the corresponding repumper beam $\Omega_{\mathrm{rep},e}$.



ing

Figure 10.8: Engineering of the two-body dissipation. (a) Desired effective decay process. State $|\downarrow\downarrow\rangle|0\rangle$ is coupled to the ion-excited state $|\psi_e\rangle|0\rangle = \frac{1}{\sqrt{2}}(|e\downarrow\rangle + |\downarrow e\rangle)|0\rangle$ by the drive Ω. $|\psi_e\rangle|0\rangle$ is strongly coupled to the motion-excited states $|\downarrow\downarrow\rangle|1\rangle$ by the sideband coupling g, which is enhanced by a factor $\sqrt{2}$ due to constructive interference. For $\Delta\delta = 2g^2$, the lower dressed state of $|\psi_e\rangle|0\rangle$ and $|\downarrow\downarrow\rangle|1\rangle$ (indicated in blue) is in resonance with the drive and hence rapidly excited from $|\downarrow\downarrow\rangle|0\rangle$. Through its contribution from $|\psi_e\rangle|0\rangle$, it decays to $|\uparrow\downarrow\rangle|0\rangle$ by spontaneous emission Γ. These resonant couplings form an effective decay process from $|\downarrow\downarrow\rangle|0\rangle$ to $|\uparrow\downarrow\rangle|0\rangle$, at an enhanced rate γ_2. (b) Undesired process. Also state $|\uparrow\downarrow\rangle|0\rangle$ is excited by the drive, to an ion-excited state $|e\uparrow\rangle|0\rangle$. The sideband coupling couples $|e\uparrow\rangle|0\rangle$ to $|\uparrow\downarrow\rangle|1\rangle$ at a coupling constant g. Their dressed states are thus out of resonance and only weakly populated by the drive.

10.4.3 Two-body dissipation

We now turn to the two-body dissipation in Eq. (10.11). Compared to the single-body dissipation in the previous section, the operator $L_j^{(2)}$ is more complicated to engineer, but itself sufficient to realize a highly non-thermal GGE (see Fig. 10.2 at $\gamma = 1$). For our minimal instance of two ions, the operator reads $L_1^{(2)} = \sqrt{\epsilon\gamma}\, S_1^+ P_2^\downarrow = \sqrt{\epsilon\gamma}\,|\uparrow\downarrow\rangle\langle\downarrow\downarrow|$. The action of this operator can be understood as a raising on spin 1, $S_1^+ = |\uparrow\rangle_1\langle\downarrow|$, conditioned on the state of spin 2.

We will now engineer the desired two-body dissipation based on the assumptions of weak driving, $\Omega^2 \ll \{\Gamma^2, g^2\}$, and strong coupling, $\Gamma^2 \ll g^2$. In this regime, the ground state $|\downarrow\downarrow\rangle|0\rangle$ is weakly excited by H_{drive} to the excited state $|\psi_e\rangle|0\rangle = \frac{1}{\sqrt{2}}(|e\downarrow\rangle + |\downarrow e\rangle)|0\rangle$, which comprises

of a superposition of excitations of both ions. Further excitation to the double-excited state $|ee\rangle$ can be neglected, as we will see further down. We engineer the desired mechanism using the couplings of $|\psi_e\rangle|0\rangle$:

The ion-excited state $|\psi_e\rangle|0\rangle$ is coupled to the motion-excited state $|\downarrow\downarrow\rangle|1\rangle$ by the red-sideband coupling H_{int}. Due to constructive interference between the excitation of the two ions, the corresponding rate is given by $\sqrt{2}g$. The Hamiltonian for the coupled subspace is

$$\begin{aligned} H_{\text{e},\downarrow\downarrow} = \Delta|\psi_e\rangle|0\rangle\langle 0|\langle\psi_e| + \delta|\downarrow\downarrow\rangle|1\rangle\langle 1|\langle\downarrow\downarrow| \\ + \sqrt{2}g(|\psi_e\rangle|0\rangle\langle 1|\langle\downarrow\downarrow| + |\downarrow\downarrow\rangle|1\rangle\langle 0|\langle\psi_e|), \end{aligned} \tag{10.27}$$

and illustrated in Fig. 10.8 a). Based on the assumption of a weak drive compared to the rapid dynamics of the excited subspace, we make a separation of timescales and first regard $H_{\text{e},\downarrow\downarrow}$ alone, without the drive:

Provided strong coupling, the excited states of the strongly coupled subspace hybridize and form dressed states $|\psi_\pm\rangle$ at detunings

$$\Delta_\pm = \frac{\Delta+\delta}{2} \pm \frac{1}{2}\sqrt{(\Delta+\delta)^2 + 4(\Delta\delta - 2g^2)}. \tag{10.28}$$

Setting the ionic and the motional detunings to $\Delta\delta = 2g^2$ (e.g., $\Delta = \delta = \sqrt{2}g$) brings the lower dressed state in resonance with the drive Ω, i.e., $\Delta_- = 0$. As a consequence, $|\downarrow\downarrow\rangle$ is resonantly excited to $|\psi_e\rangle$ which in turn decays to $|\uparrow\downarrow\rangle$ at a rate Γ. This results in the required effective decay from $|\downarrow\downarrow\rangle$ to $|\uparrow\downarrow\rangle$, mediated by the resonant lower dressed state, $|\psi_-\rangle$. In App. 10.10 we present a full microscopic derivation that yields the two-body Lindblad operator, Eq. (10.11),

$$L_{\text{eff}}^{(2)} = \sqrt{\gamma_2}|\uparrow\downarrow\rangle_{1,2}\langle\downarrow\downarrow|. \tag{10.29}$$

Using second-order perturbation theory in Ω/Γ the effective decay rate is given by,

$$\gamma_2 = \frac{4\Omega^2}{\Gamma}. \tag{10.30}$$

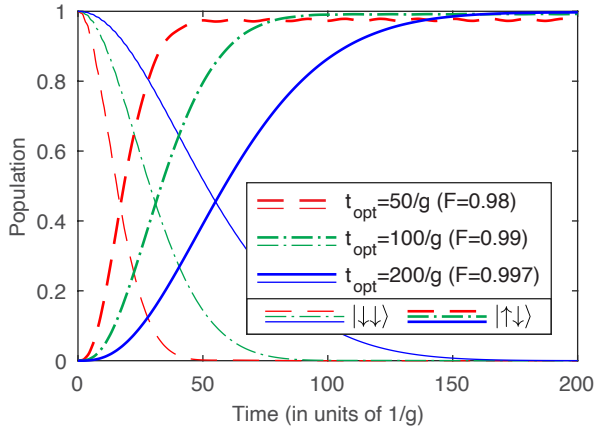
The decay rate γ_2, and hence the relative strength of the single- and two-body dissipation, can thus be adjusted by varying Ω and $\Gamma(\Omega_{\text{rep},e})$. γ_2 is ultimately limited by the linewidth Γ_q of level $|q\rangle$, which is involved in constructing the engineered single-body decay in Eq. (10.26).

Compared to γ_2, effective decay processes mediated by $|ee\rangle$ can be neglected: $|ee\rangle$ forms a coupled two-excitation subspace with $|\psi_e\rangle|1\rangle$ and $|\downarrow\downarrow\rangle|2\rangle$ (couplings $\sqrt{2}g$ and $2g$). While for the above parameter choice, the drive from $|\psi_e\rangle$ is in resonance with the two-excitation dressed states, the coupling rates of the so mediated effective process only enter to fourth order in perturbation theory and are thus negligibly small. Also AC Stark shifts arising from the weak off-resonant excitation of $|\uparrow\downarrow\rangle$ (cf. App. 10.11) can be safely ignored in the considered parameter regime.

Another imperfection inherent to the scheme is given by the population of the excited level $|\uparrow e\rangle$ which is off-resonantly excited from $|\uparrow\downarrow\rangle$ by the drive Ω, as illustrated in Fig. 10.8 b). For perfect individual addressing of the first ion by $H_{\text{rep},e}$, $|\uparrow e\rangle$ is steadily populated. Using adiabatic elimination, it is possible to estimate the steady-state population of an excited state such as $|\uparrow e\rangle$ [77, 78], which scales

$$P_{\uparrow e} \sim \frac{\Omega^2}{g^2}. \tag{10.31}$$

Population of the excited state $|\uparrow e\rangle$ is thus expected to be largely suppressed, as we numerically confirm in the following.



ing

Figure 10.9: Numerical simulation. We verify the engineering of the two-body dissipation by simulating the dynamics and plotting the population of the states $|\downarrow\downarrow\rangle$ (thin lines) and $|\uparrow\downarrow\rangle$ (thick lines) over time, starting from an initial state $|\downarrow\downarrow\rangle$. We present three different parameter choices, where we optimize the action of the scheme at different times $t_{\rm opt} = \{50, 100, 200\}/g$ (dashed lines, dash-dotted lines, solid lines). We obtain fidelities $F_{\rm opt} = \{0.98, 0.99, 0.997\}$ for the parameter choices $\Gamma_{\rm opt} = \{0.82, 0.48, 0.29\}g$ and $\Omega_{\rm opt} = \{0.15, 0.08, 0.05\}g \approx \Gamma_{\rm opt}/6$. Population in the excited states is negligible.

We verify the engineering of the two-body dissipation and assess its performance numerically by simulating the dynamics given by the master equation

$$\dot{\rho} = -i[H_{\rm free} + H_{\rm drive} + H_{\rm int}, \rho] + \mathcal{D}^{(\uparrow e)}\rho, \tag{10.32}$$
$$\mathcal{D}^{(\uparrow e)}\rho = L_{\uparrow e}\rho L_{\uparrow e}^\dagger - \frac{1}{2}\{L_{\uparrow e}^\dagger L_{\uparrow e}, \rho\}$$

We use this to obtain i) the optimal parameter choice, ii) the extent of unwanted population of the excited level $|\uparrow e\rangle$, and iii) the timescales of the dissipative compared to the unitary dynamics.

We assume that the system starts from $|\downarrow\downarrow\rangle|0\rangle$ and optimize the fidelity of the state $|\uparrow\downarrow\rangle|0\rangle$ after a chosen time, $t_{\rm opt} = \{50, 100, 200\}/g$ by the choice of the parameters Γ and Ω. The result is plotted in Fig. 10.9. From the initial state $|\downarrow\downarrow\rangle$, the system evolves to fidelities with $|\uparrow\downarrow\rangle$ of $F_{\rm opt} = \{0.98, 0.99, 0.997\}$ for the parameter choices $\Gamma_{\rm opt} = \{0.82, 0.48, 0.29\}g$ and $\Omega_{\rm opt} = \{0.15, 0.08, 0.05\}g \approx \Gamma_{\rm opt}/6$. After a short non-exponential transient ($t < 1/\gamma_{\rm eff}$) which builds up the excited state population, the curves attain the desired exponential form that is described by the effective jump operator in Eq. (10.29). This represents a close approximation to the desired dynamics.

The optimal parameters fulfill the conditions for weak driving and strong coupling, $\Omega^2 \ll \Gamma^2 \ll g^2$, which are the assumptions used in the above analysis. The residual population in $|\uparrow e\rangle$ is found to be $P_{\uparrow \rm e} \approx \{0.02, 0.008, 0.003\}$ and thus indeed negligible.

For the effective dissipation rate in Eq. (10.30) we obtain $\gamma_2 = \{0.054, 0.027, 0.014\}g$. For typical values of $g/(2\pi) \sim 10$ kHz, this yields $\gamma_2 = \{3.4, 1.7, 0.89\}$/ms. The convergence time $\tau = 1/\gamma_2$ (corresponding to the decay of the initial-state population to $1/{\rm e}$) is found to be $\tau = \{18, 37, 70\}/g = \{0.29, 0.59, 1.1\}$ ms, in good agreement with the results plotted in Fig. 10.9.

The achievable values for γ_2 should be compared with the typical coupling strength in realizations of the spin models of about $J_{x/y}/(2\pi) \sim 100$ Hz [21, 60], and the corresponding timescale of $\tau_{\rm spin} \sim 1$ ms. From the above numbers it can be seen that the effective dissipation rate can be tuned to values within the same order of magnitude as the coupling constants

of the spin model. Obtaining smaller values for γ_2 – and thus making the dissipation into a perturbation as assumed in Sec. 10.2–10.3 – is in turn achieved by choosing weaker repump and driving rates, Γ and Ω.

ing

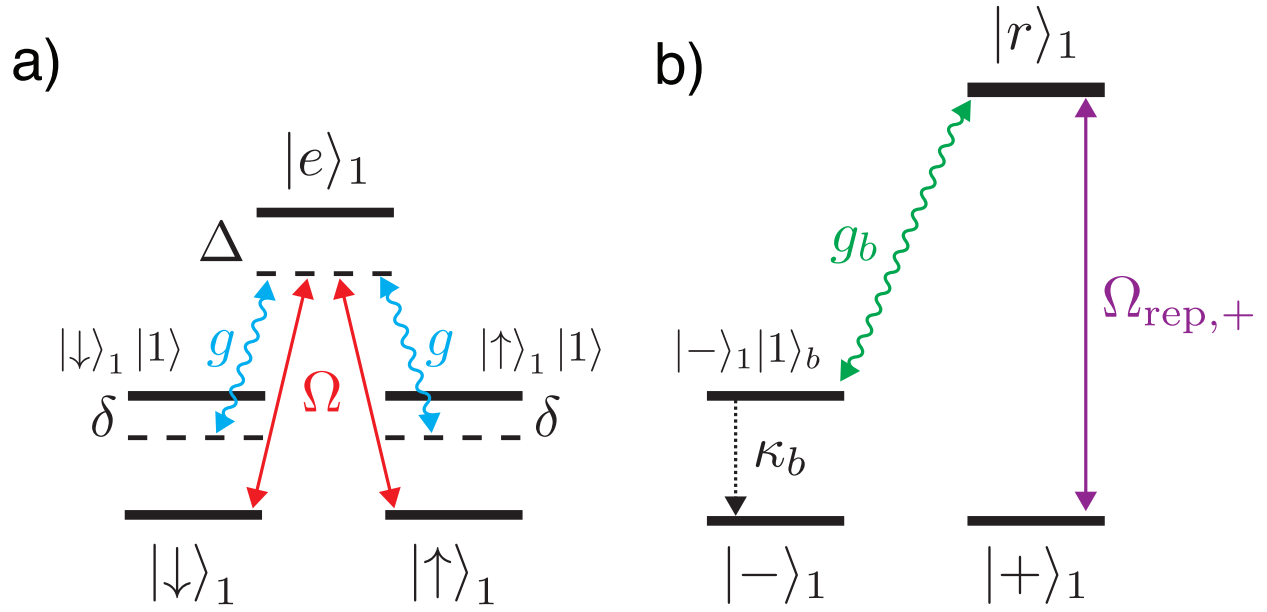


Figure 10.10: Generalization of the couplings to the x-basis. (a) To engineer two-body dissipation in the x-basis, we use couplings between the states $|\pm\rangle = (|\downarrow\rangle \pm |\uparrow\rangle)/\sqrt{2}$, and $|e\rangle$. This is achieved by coupling the levels $|\downarrow\rangle$ and $|\uparrow\rangle$ coherently to $|e\rangle$. (b) Dissipation in the x-basis is facilitated by sympathetic cooling of the motion. The single-body decay process from $|+\rangle$ to $|-\rangle$ is engineered by excitation from $|+\rangle$ by a weak drive ($\Omega_{\mathrm{rep},+}$) to an auxiliary level $|r\rangle$, a sideband coupling of the transition $|r\rangle \to |-\rangle$ to a motional mode b (g_b), and sympathetic cooling of b (κ_b). Decay from $|e\rangle$ to $|+\rangle$ (not shown) is engineered accordingly using a motional mode c, as is described in the text.

10.5 Generalization of the couplings to the x-basis

Spin models along arbitrary directions, with and without anisotropy, can be realized on trapped-ion platforms, such as Paul traps and Penning traps, and also in microtraps [17]. The majority of the available setups, however, support XY-Hamiltonians without anisotropy [21]. In the preceding section, we assumed the less common YZ spin Hamiltonian which enabled us to engineer the dissipation in the z-basis, the eigenbasis of decay by spontaneous emission. As an alternative to such implementation, we can utilize the more standard XY-Hamiltonian in Eq. (10.6). We should note, however, that in order to stabilize a non-trivial ($\rho_\infty \neq \mathbb{1}$) and distinguishingly non-thermal steady state, an engineered form of Lindblad operators with proper symmetries must be used. For example, the XY-Hamiltonian in combination with the dissipation in the z-basis would not result in a large $\langle C_4 \rangle$. This problem is resolved by using the XY-Hamiltonian in combination with dissipation in the rotated x-basis, the engineering of which is presented below.

We point out that a simpler alternative is given by using the XY-Hamiltonian in combination with *any* type of Lindblad dissipation. Such setting would yield a non-trivial dynamics towards a possibly trivial steady state, where *time evolution* is approximately captured with a time-dependent GGE [25]. However, the non-thermal features might not be very pronounced in a generic setup, therefore we focus here on a setup with non-trivial steady states with clearly

non-thermal nature.

We now engineer the dissipation in the x-direction which can stabilize a steady-state GGE,

$$L_j^{(1,x)} = \sqrt{\epsilon(1-\gamma)}S_{j,x}^{-}. \tag{10.33}$$

$$L_j^{(2,x)} = \sqrt{\epsilon\gamma}S_{j,x}^{+}P_{j+1,x}^{\downarrow}, \tag{10.34}$$

when combined with the XY Hamiltonian. Formally speaking, the change from the z- to the x-basis amounts to replacing the eigenstates of σ_z, $\{|\downarrow\rangle, |\uparrow\rangle\}$ with the eigenstates of σ_x, $|\pm\rangle = (|\downarrow\rangle \pm |\uparrow\rangle)/\sqrt{2}$, i.e., $|\downarrow\rangle \mapsto |-\rangle$, $|\uparrow\rangle \mapsto |+\rangle$, in all steps of our previous derivation performed for the dissipation in the z-direction. Physically, using $|\pm\rangle$ is realized by coupling to both transitions $|\downarrow\rangle \leftrightarrow |e\rangle$ and $|\uparrow\rangle \leftrightarrow |e\rangle$ coherently. The resulting interactions, illustrated in Fig. 10.10 a), read

$$H_{\mathrm{drive,x}} = \frac{\Omega}{2}\sum_{j=1}^{2}|e\rangle_j\langle -| + \mathrm{H.c.}, \tag{10.35}$$

$$H_{\mathrm{int,x}} = g\sum_{j=1}^{2}\left(a^\dagger|-\rangle_j\langle e| + a|e\rangle_j\langle -|\right). \tag{10.36}$$

On the other hand, decay by spontaneous emission, as utilized in the previous sections naturally occurs in the z-basis, $\{|\downarrow\rangle, |\uparrow\rangle\}$. In contrast to this, we now need to engineer sources of dissipation in the x-basis, which replaces Eqs. (10.23),(10.26) in the z-basis. In the following, we demonstrate how to achieve this using decay of excitations via the motional degree of freedom by sympathetic cooling.

As shown in Fig. 10.10 b), to implement the single-body decay in Eq. (10.33), we excite $|+\rangle$ to the auxiliary level $|r\rangle$ by a repumper

$$H_{\mathrm{rep},+} = \Omega_{\mathrm{rep},+}|r\rangle_1\langle +| + \mathrm{H.c.} \tag{10.37}$$

The excitation to level $|r\rangle$ is transferred coherently to an auxiliary motional mode b using a sideband interaction,

$$H_{\mathrm{b}} = g_{\mathrm{b}}b^\dagger|-\rangle_1\langle r| + \mathrm{H.c.}, \tag{10.38}$$

with a coupling constant g_{b}. Mode b is subject to sympathetic cooling which realizes the jump operator

$$L_{\mathrm{b}} = \sqrt{\kappa}b. \tag{10.39}$$

Adiabatic elimination of b leads, for $g_b \ll \kappa$, to the desired decay channel

$$L_{-r} = \sqrt{\Gamma_{-r}}|-\rangle_1\langle r|, \tag{10.40}$$

with a rate $\Gamma_{-r} = g_b^2/\kappa$, in analogy to Eq. (10.23). We realize the decay $L_{+e} = \sqrt{\Gamma_{+e}}|+\rangle_1\langle e|$ (cf. Eq. (10.26)) in a similar fashion, utilizing a motional mode c, which is subject to sympathetic cooling. Here, we couple $|e\rangle|0\rangle_c$ to $|+\rangle|1\rangle_c$ by a sideband drive (g_c), which then decays to $|+\rangle|0\rangle_c$ by sympathetic cooling (κ_c), resulting in an effective decay rate $\Gamma_{+e} = g_c^2/\kappa_c$. Involving level $|q\rangle$ is not necessary. Carrying out the same analysis as in Sec. 10.10, we obtain the effective operator

$$L_{\mathrm{eff}}^{(2,x)} = \sqrt{\gamma_{2,\mathrm{x}}}|+-\rangle_{1,2}\langle --|, \tag{10.41}$$

with a tunable decay rate $\gamma_{2,\mathrm{x}} = 4\Omega^2/\Gamma_{+e}^2$. We have thus realized the desired two-body dissipation in the x-basis in Eq. (10.34) by means of sympathetic cooling.

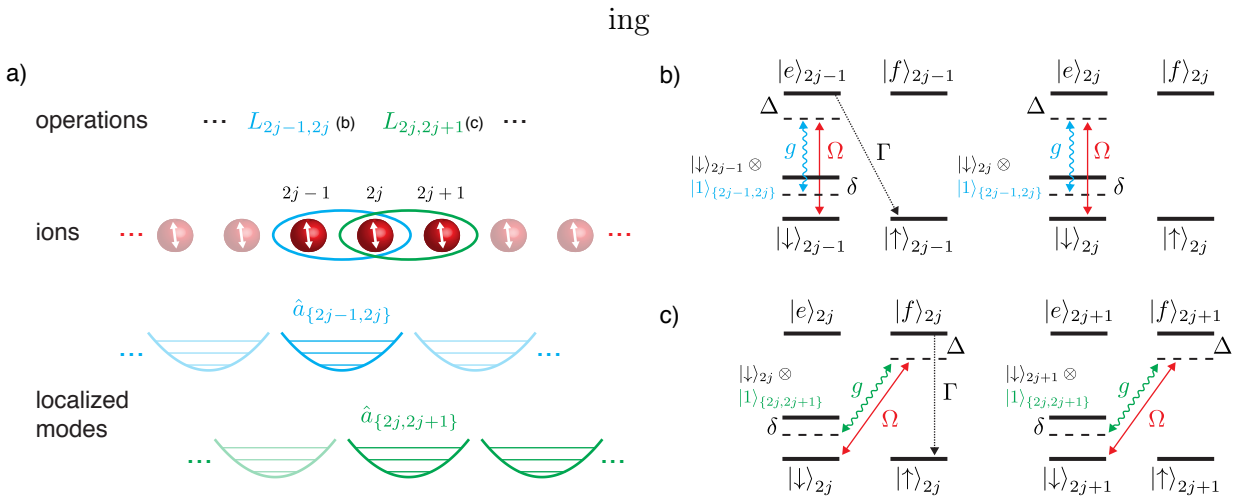


Figure 10.11: Scalable implementation in trapped ions. (a) Setup. We assume a string of N ions, denoted $2j\pm1$ for odd ions and $2j$ for even ions. Two-body dissipation represented by the jump operators $L_{2j-1,2j}$ and $L_{2j-1,2j}$ is realized by coupling pairs of ions to localized phonon modes. Two sets of motional modes, $a_{2j-1,2j}$ and $a_{2j,2j+1}$, couple to pairs of ions $\{2j-1,2j\}$ and $\{2j,2j+1\}$. This avoids interference on the overlap ion $2j$. (b)-(c) Coupling configurations for pairs of ions $\{2j-1,2j\}$ (b) and $\{2j,2j+1\}$ (c). We assume two addressable excited levels, $|e\rangle$ and $|f\rangle$, for each ion. For odd ions $2j-1$ (even ions $2j$), we facilitate a decay from level $|e\rangle$ ($|f\rangle$) to level $|\uparrow\rangle$ at a rate Γ, as is described in the text. The coherent drive Ω and the sideband couplings g act on the transition from $|e\rangle$ to $|\downarrow\rangle$ (from $|f\rangle$ to $|\downarrow\rangle$) on pairs of ions $\{2j-1,2j\}$ ($\{2j,2j+1\}$).

10.6 Scalable implementation

Next, we discuss how to scale the mechanisms discussed in Sec. 10.4-10.5 to larger numbers of ions. For a scalable implementation of our scheme, we assume a chain of N ions (with even N) and a level structure similar to Sec. 10.4.1. The physical system for the scalable implementation of two-body dissipation in Eq. (10.11) is shown in Fig. 10.11. The implementation of such system based on ion micro-traps is presented in Sec. 10.7. Here we seek to implement interactions on all pairs of ions, such as $\{2j-1,2j\}$ and $\{2j,2j+1\}$, as illustrated in Fig. 10.11 a). However, care has to be taken to avoid interference effects of the coherent couplings in the overlapping region, i.e., here ion $2j$. We achieve this by devising two independent coupling configurations to mediate the engineered decay on the two different groups of ions, $\{2j-1,2j\}$ and $\{2j,2j+1\}$, as can be seen from Fig. 10.11 b)-c). We assume each ion to have two (meta-) stable excited levels, $|e\rangle$ and $|f\rangle$, which are selectively addressable using, e.g., polarization selection rules.

For dissipation on pairs $\{2j-1,2j\}$, level $|e\rangle$ is used to mediate the two-body dissipation, whereas for pairs $\{2j,2j+1\}$ this is facilitated by level $|f\rangle$. Correspondingly, we employ two sets of localized phonon modes: Modes $a_{2j-1,2j}$ interact with ions $\{2j-1,2j\}$, and modes $a_{2j,2j+1}$, couple to pairs $\{2j,2j+1\}$. The engineering of the mode structure will be discussed in detail in Sec. 10.7.

To implement two-body dissipation, we again use tunable optical pumping of $|e\rangle$ and $|f\rangle$ to $|\uparrow\rangle$, in analogy to Sec. 10.4.3, Eq. (10.26). Utilizing different individually addressed repumper beams for "odd" ions $2j-1$ and "even" ions $2j$, we realize

$$L_{\uparrow e,2j-1} = \sqrt{\Gamma}|\uparrow\rangle_{2j-1}\langle e|, \tag{10.42}$$

$$L_{\uparrow f,2j} = \sqrt{\Gamma}|\uparrow\rangle_{2j}\langle f|. \tag{10.43}$$

Odd ions $2j-1$ thus decay from $|e\rangle$ to $|\uparrow\rangle$, whereas even ions $2j$ decay from $|f\rangle$ to $|\uparrow\rangle$, both at an equal rate Γ.

For the continuous and measurement-free interrogation of the system, we use two sets of coherent drives,

$$H_{\text{drive}} = H_{\text{drive},e} + H_{\text{drive},f} \tag{10.44}$$

$$H_{\text{drive},e} = \frac{\Omega}{2}\sum_{j=1}^{N/2}\left(|e\rangle_{2j-1}\langle\downarrow| + |e\rangle_{2j}\langle\downarrow|\right) + \text{H.c.}, \tag{10.45}$$

$$H_{\text{drive},f} = \frac{\Omega}{2}\sum_{j=1}^{N/2}\left(|f\rangle_{2j}\langle\downarrow| + |f\rangle_{2j+1}\langle\downarrow|\right) + \text{H.c.}, \tag{10.46}$$

coupling the ground level $|\downarrow\rangle$ to the excited level $|e\rangle$ or $|f\rangle$, as well as sideband interactions,

$$H_{\text{int}} = H_{\text{int},e} + H_{\text{int},f}, \tag{10.47}$$

$$H_{\text{int},e} = g\sum_{j=1}^{N/2} a^{\dagger}_{2j-1,2j}\left(|\downarrow\rangle_{2j-1}\langle e| + |\downarrow\rangle_{2j}\langle e|\right) + \text{H.c.}, \tag{10.48}$$

$$H_{\text{int},f} = g\sum_{j=1}^{N/2} a^{\dagger}_{2j,2j+1}\left(|\downarrow\rangle_{2j}\langle f| + |\downarrow\rangle_{2j+1}\langle f|\right) + \text{H.c.} \tag{10.49}$$

These realize coupling configurations, by which the transition $|e\rangle \leftrightarrow |\downarrow\rangle$ ($|f\rangle \leftrightarrow |\downarrow\rangle$) of any pair of ions $\{2j-1, 2j\}$ ($\{2j-1, 2j\}$) is coupled to a localized motional mode $a_{2j-1,2j}$ ($a_{2j,2j-1}$).

As a result, following the recipe in Sec. 10.4.3, we realize jump operators acting on pairs of ions over the whole chain,

$$L^{(2)}_{2j-1} = \sqrt{\gamma_2}|\uparrow\downarrow\rangle_{2j-1,2j}\langle\downarrow\downarrow| = \sqrt{\gamma_2}S^{+}_{2j-1}P^{\downarrow}_{2j}, \tag{10.50}$$

$$L^{(2)}_{2j} = \sqrt{\gamma_2}|\uparrow\downarrow\rangle_{2j,2j+1}\langle\downarrow\downarrow| = \sqrt{\gamma_2}S^{+}_{2j}P^{\downarrow}_{2j+1}. \tag{10.51}$$

In the second step, these operators are brought back into the form of Eq. (10.11). Making the association $\gamma_2 = \epsilon\gamma$, we have thereby engineered the desired two-body dissipation in a scalable manner.

Single-body dissipation in Eq. (10.10), is again realized – now for the whole chain – following the recipe in Sec. 10.4.2: Using locally addressed repumper beams to an unstable level $|r\rangle$ for each individual ion, we achieve local jump operators

$$L^{(1)}_{j} = \sqrt{\gamma_1}|\downarrow\rangle_j\langle\uparrow| \equiv \sqrt{\frac{\Gamma_{\downarrow r}\Omega^2_{\text{rep},\uparrow}}{\Gamma_r^2}}|\downarrow\rangle_j\langle\uparrow|. \tag{10.52}$$

Associating $\gamma_1 = \epsilon(1-\gamma)$, we have thus realized the desired single-body dissipation (Eq. (10.10)) for all ions in the chain.

The implementation of generalized dissipation in the x-basis, such as those in Eqs. (10.33)–(10.34) in Sec. 10.5 can be scaled up in an analogous manner.

10.7 Normal mode engineering in an array of micro traps

In the following, we discuss the physical implementation of the scalable setting detailed in Sec. 10.6 based on ion micro-traps [66, 67, 68, 69, 70]. To implement the desired mode structure, with localized modes subject to dissipation, we employ a novel approach to mixed-species normal mode engineering.

In an array of micro-traps individual control over the electric potential at each trap site allows us to engineer normal mode spectra suitable for implementing the desired operators. Previously the use of a special arrangement of the transverse frequencies of individual traps along a string has been proposed for encoding two-body bosonic gauge fields [68]. Here we consider similar ideas to construct phonon modes localized to triplets of neighboring ions (that is any ion together with both of its nearest-neighbors), and with the use of mixed species of ions effectively encode two-body as well as one-body operators. The use of two species of ions allows us to achieve this using mode engineering along only one axis of vibration instead of two transverse axes.

The calculation of the normal modes for a system of ions in an array of micro-traps [79, 70] involves first determining the equilibrium positions in the combined electric potential due to the trap electrodes and the Coulomb repulsion from the other ions. A Taylor series expansion about these positions up to second order then yields the effective harmonic potential experienced by each ion. The resulting Hamiltonian is then diagonalized to extract the eigenvalues, which give the frequencies of oscillation, and the eigenvectors, which give the relative amplitude of oscillation of each ion in any given normal mode. Since the trapping mechanism in Paul traps and Penning traps differs only in the radial directions, we focus here on the axial modes since the treatment would then be independent of the kind of trap for the discussion below.

To illustrate the idea we first consider a chain of a single species of trapped ions, each with mass m. The spatial separation between neighboring traps is given by d and the potentials are designed so that the trap frequencies $\omega_k = \omega_0 + (k-1)\Delta_{\mathrm{T}}$ increase linearly with the trap site k. If the frequency difference Δ_{T} is much larger than the two-ion exchange frequency, defined by $\Omega_{\mathrm{ex}} = e^2/(4\pi\epsilon_0 m\omega_0 d^3)$, we get for this system of coupled ions a spectrum of normal modes close to that of the non-interacting system. That is, the result is a set of modes with oscillation frequency near ω_k and participation mostly from the ion at that trap k (as well as ions at the nearest-neighboring traps, $k-1$ and $k+1$).

Now consider a chain of alternating ionic species of nearly equal mass in these traps. One of these species serves as a coolant ion while the other one is used to encode the spins through two suitable internal states, and is from here on called the 'spin ion'. The condition for nearly equal mass is useful for efficient sympathetic cooling of the spin species through the coolant species. As discussed above, the resulting normal mode structure consists of modes effectively localized to triplets of ions (except, of course, at the edges) but now there exist two kinds of modes – one where the central ion is the coolant ion with two neighboring spin ions, and the other where the central ion is a spin ion between two coolant ions. Fig. 10.12 a) shows this for a chain of alternating $^{40}Ca^{+}$and $^{43}Ca^{+}$ions arranged along the axial direction of the micro-trap array. The frequencies for the uncoupled arrangement of traps and for the coupled system are shown in figure 10.12 b). Here $\omega_0 = 2\pi \times 300$ kHz, $\Delta_{\mathrm{T}} = 2\pi \times 37.5$ kHz, and $d = 30$ µm. Since the participation of the ions drops roughly exponentially with the distance from the central trap we can assume almost no participation from other ions of the same species (since these lie two sites distant). This behavior can be seen from Fig. 10.12 c), where the amplitudes of motion of each ion in the axial modes is plotted. Note that each mode is assigned a color so that it is clear which ions dominate the oscillation in a particular mode, and at what frequency. Modes a which are localized to two spin-ions (and one coolant ion) allow us to engineer the two-body operators while modes b which are localized to one spin-ion (and two coolant ions) allow for implementing one-body operators. To match the notation of the Sec. 10.6, we associate the even-numbered trap sites with the spin ions by $2k \mapsto j$ (e.g. $a_{2,4} \mapsto a_{1,2}$), thereby excluding the odd-numbered trap sites containing the coolant ions. Employing sympathetic cooling of these modes, dissipation can be engineered in the σ_x-eigenbasis, following the recipes in Sec. 10.5.

Note that the laser-ion couplings in Sec. 10.6, Eqs. (10.44)–(10.49) require addressing of pairs of ions coherently with the same detuning Δ. As discussed in Sec. 10.4.3, Δ needs,

however, to be matched to the phonon detuning δ, which differs from ion to ion because to the trap frequency offset. The resulting mismatch can be compensated by local AC Stark shifts on $|e\rangle$ and $|f\rangle$, which can be generated by individually addressed lasers.

10.7.1 Alternative realization in linear ion traps

In conventional bulk ion traps, the desired dynamics can be implemented in a stepwise manner. Here we consider a sequential realization based on delocalized motional modes in combination with local addressing techniques [80, 21, 81, 82, 83]. We assume all ions to be detuned by a constant amount with respect to the coupling configurations in Sec. 10.6. For N ions, we now consider N timesteps. During each step, we direct a pair of individual addressing lasers on a pair of ions. This beam shifts the transitions of the ions into resonance with the carrier and sideband couplings in Eqs. (10.44)–(10.49). We thereby pairwise realize the desired dynamics on ions j and $j+1$, leaving the other ions uncoupled. In the next step, the individual addressing laser is shone onto another pair of ions, $j+1$ and $j+2$, and so forth. Provided short modulation times for the lasers, the timeframes for the ions may be reduced to stroboscopic length, resulting in a "Trotterized" realization of the desired dynamics.

10.8 Conclusion and Outlook

We have presented a scheme suitable to revive the effects of integrability in a controllably driven and open setup, where the underlying Hamiltonian dynamics is only approximately integrable. The scheme is based on weak couplings to Markovian baths in combination with nearly integrable quantum spin Hamiltonians, ingredients which are readily available in state-of-the-art trapped-ion setups. In addition, we present a novel technique for the engineering of motional modes in an array of mixed-species micro-traps, which support the realization of the desired dynamics.

Our numerical analysis shows that despite different sources of integrability breaking due to long-range interactions in the Hamiltonian and openness itself, a steady state is realized that cannot be modeled as a thermal ensemble. Instead, approximate expectation values of local observables can be obtained from a generalized Gibbs ensemble and we identify the experimental signatures which reveal that. We presented results for a rotated XY and transverse-field Ising Hamiltonian; however, the same Lindblad operators would activate a GGE in the interacting XXZ Heisenberg chain.

While our goal has been to engineer Lindblad dissipators which stabilize a non-trivial and highly non-thermal steady state by weak driving, a simpler task would be to consider a non-trivial dynamics towards a trivial (thermal, maximally mixed or empty) steady state. As has been shown in Ref. [25], the dynamics of a (nearly) integrable system weakly coupled to *arbitrary* Lindblad baths can be approximately described with a *time-dependent GGE*. An example of this is atom loss in cold-atom setups, whose effects have been observed [84] and theoretically addressed [30] very recently. The simplest combination of the strategy presented above would be to follow the dynamics of an XY-Hamiltonian, Eq. (10.6), in the presence of single-body decay, Eq. (10.10), alone.

Beyond this work, our dissipation engineering strategies open the door to experiments that will shed light on novel phenomena in open quantum systems. For example, the dissipators presented here have been used to study many-body localization through the perspective of open systems [35]. Our novel mixed-species mode engineering techniques based on arrays of ion micro-traps hold promise to become a powerful tool in quantum simulation. Here, sympathetic cooling is not only useful to reduce the entropy of the system, but also to realize complex dissipators. Generalizing these techniques may allow addressing open questions in non-equilibrium quantum

many-body physics.

10.9 Theory of weakly driven nearly integrable systems

Here we review the theory of weakly driven and open nearly integrable systems. We consider the setup discussed in the main text, where the dynamics of the system is given by a dominant integrable Hamiltonian H_0, in the presence of perturbations of unitary and Markovian nature, which weakly break the integrability. The corresponding Liouvillian terms are

$$\begin{aligned}\mathcal{L}_0\rho &= -i[H_0,\rho],\\ \mathcal{L}_u\rho &= -i\left[H_1(\epsilon_1),\rho\right],\\ \mathcal{L}_m\rho &= \left(\mathcal{D}^{(1)}(\epsilon)+\mathcal{D}^{(2)}(\epsilon)\right)\rho.\end{aligned}$$

The steady state density matrix is determined by

$$\dot{\rho}_\infty = (\mathcal{L}_0+\mathcal{L}_p)\rho_\infty = 0, \tag{10.53}$$

where $\mathcal{L}_p = \mathcal{L}_u + \mathcal{L}_m$. Because perturbations due to the Markovian dissipation $\mathcal{L}_m$ and the next-nearest neighbor interaction $\mathcal{L}_u$ are only weak, the exact steady state density matrix ρ_∞ can be split as

$$\rho_\infty = \rho_{\mathrm{BD}} + \delta\rho, \tag{10.54}$$

where a $\rho_{\mathrm{BD}} \sim \mathcal{O}(1)$, while $\delta\rho(\epsilon,\epsilon_1)$ is a small correction regulated by the strength of unitary and Markovian perturbations. ρ_{BD} must fulfill the zero-th order Liouville stationarity equation,

$$\mathcal{L}\rho_\infty \approx \mathcal{L}_0\rho_{\mathrm{BD}} = -i[H_0,\rho_{\mathrm{BD}}] = 0 \tag{10.55}$$

and therefore must have a block-diagonal form

$$\rho_{\mathrm{BD}} = \sum_{m,n} a_{mn}|m\rangle\langle n|\,\delta_{E_m^0,E_n^0}, \quad H_0|n\rangle = E_n^0|n\rangle \tag{10.56}$$

with respect to the eigenstates of H_0 and is parametrized with about 2^N parameters a_{mn}.

However, it turns out that description with ρ_{BD} is redundant and can be replaced with a generalized Gibbs ensemble, $\rho_{\mathrm{BD}} \to \rho_{\mathrm{GGE}}$, if H_0 is integrable [26, 25] and with a Gibbs ensemble $\rho_{\mathrm{BD}} \to \rho_{\mathrm{th}}$, if H_0 is ergodic [87].

While equivalence of ρ_{BD} and ρ_{GGE} is formally expected when calculating expectation values of local observables in the thermodynamic limit and with all conservation laws included, in most cases also a truncated GGE (tGGE) with a few conservation laws

$$\rho_{\mathrm{tGGE}} \equiv \frac{e^{-\sum_{i=1}^{N_C}\lambda_i C_i}}{\mathrm{Tr}[e^{-\sum_{i=1}^{N_C}\lambda_i C_i}]} \tag{10.57}$$

qualitatively well captures the expectation values of local observables, if their support is much smaller than the support of included conservation laws. Known exceptions are observables that are orthogonal to all included conservation laws [8].

In the following we will compare the expectation values evaluated with respect to ρ_∞, ρ_{BD} and ρ_{tGGE} in order to confirm that steady states can be approximately described with non-thermal generalized Gibbs ensembles. Note that since our choice of Lindblad operators breaks magnetization, as well as momentum conservation, the whole Hilbert space is of relevance.

The Lagrange parameters λ_i in Eq. (10.57) and parameters a_{mn} in Eq. (10.56) are determined from the stationarity conditions in the steady state [26, 18, 25],

$$\partial_t \mathrm{Tr}[C_i\, \rho_{\mathrm{tGGE}}] \stackrel{!}{=} 0, \tag{10.58}$$

$$\partial_t \mathrm{Tr}[|m\rangle\langle n|\rho_{\mathrm{BD}}] \stackrel{!}{=} 0, \quad E^0_m = E^0_n \tag{10.59}$$

for ρ_{tGGE} and ρ_{BD}, respectively. For our choice of perturbation the contributions to order ϵ and ϵ_1^2

$$\left\langle \dot{C}_i \right\rangle \approx \mathrm{Tr}[(\mathcal{L}_m + \mathcal{L}_{u,2})\rho_{\mathrm{tGGE}}] \stackrel{!}{=} 0, \tag{10.60}$$

$$\mathcal{L}_{u,2} \equiv -\mathcal{L}_u \mathcal{L}_0^{-1} \mathcal{L}_u \tag{10.61}$$

uniquely fix the λ_i (or equivalently a_{mn}) in the steady state. Note that $\mathcal{L}_0 \rho_{\mathrm{tGGE}} = 0$ because $[H_0, C_i] = 0$, and that unitary perturbation contributes to the decay of conservation laws only in the second order, since $\mathrm{Tr}[C_i \mathcal{L}_u \rho_{\mathrm{tGGE}}] = 0$ due to cyclicity of the trace. More details on the derivation of condition (10.60) and how to use $\mathcal{L}_0^{-1}$ in practice can be found in Ref. [18]. Here we give only the final result for $\left\langle \dot{C}_i \right\rangle$,

$$\begin{aligned} \left\langle \dot{C}_i \right\rangle = 2\pi \sum_{nm} (\langle m|C_i|m\rangle - \langle n|C_i|n\rangle)\langle n|\rho_{\mathrm{tGGE}}|n\rangle \\ \times \Big[|\langle n|H_1|m\rangle|^2 \frac{1}{\pi} \frac{\eta}{(E^0_n - E^0_m)^2 + \eta^2} \\ + \sum_j \left((1-\gamma) \left| \left\langle n|L_j^{(1)}|m \right\rangle \right|^2 + \gamma \left| \left\langle n|L_j^{(2)}|m \right\rangle \right|^2 \right) \Big] \end{aligned} \tag{10.62}$$

where finite broadening η has to be used for calculations at finite system sizes. Expressions relevant for ρ_{BD} are obtained by replacements $C_i \to |m\rangle\langle n|$ and $\rho_{\mathrm{tGGE}} \to \rho_{\mathrm{BD}}$.

10.9.1 Numerical results

We base our analysis on three approaches: (i) calculation of the exact steady state ρ_∞, Eq. (10.53), at finite but small ϵ, obtained from diagonalization of the full Liouvillian on small system sizes $N = 6$ where we exclude or include (NN) unitary integrability breaking H_1, (ii) exact calculation of ρ_{BD}, Eq. (10.56), on $N = 6, 8, 10$ and (iii) approximate calculation based on a truncated GGE, Eq. (10.57), including a finite number of $N_C = 4$ conservation laws C_i on $N = 10$. Note that each $C_i = \sum_i c_j^{(i)}$ is a translationally invariant sum of operators $c_j^{(i)}$ with support not larger than i. Due to finite size effects, only C_i with support smaller than $N/2$ can be included in the tGGE. C_i are obtained using the so-called boost operator, $B = -i \sum_j j h_j$, where $H_0 = \sum_j h_j$, from the recursive relation $C_{i+1} = [B, C_i]$ for $i \geq 2$ and $C_2 = H_0$. At the isotropic point, $J_y = J_z$ the magnetization $S^x = C_1$ is conserved as well.

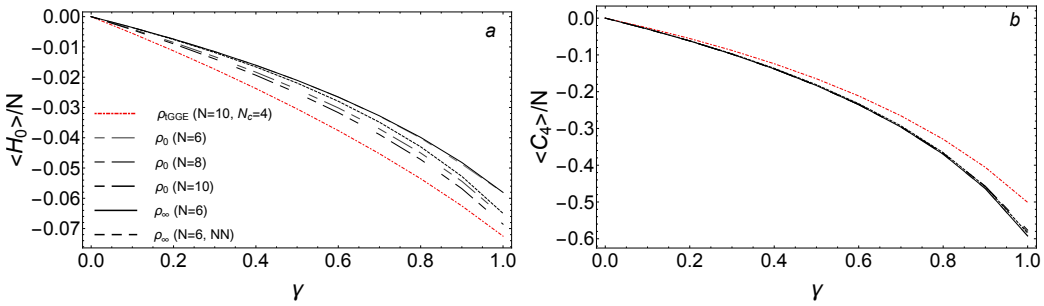


Figure 10.13: Expectation values of (a) energy and (b) C_4 densities as a function of relative driving strength γ, Eqs. (10.10,10.11). We compare results calculated i) with (NN) or without next nearest coupling H_1 from the exact steady state ρ_∞ at $\epsilon = 0.01$, ii) from ansatz $\rho_{\rm BD}$, and iii) from a truncated GGE $\rho_{\rm tGGE}$, using $N_C = 4$ conservation laws. System sizes $N = 6, 8, 10$ are used at $J_y = h = 1$, $J_z = 0.1$ and $\epsilon_1 = 0.05$ for (NN).

.

Fig. 10.13 shows $\langle H_0 \rangle$ and $\langle C_4 \rangle$ as a function of relative dissipator strength γ, Eqs. (10.10,10.11), obtained using different approximations described above at largest accessible system sizes. We observe a good agreement between the three approaches, also for other parameters not displayed. Results calculated from $\rho_{\rm BD}$ on $N = 6, 8, 10$ interpolate between the exact ($N = 6$) and tGGE ($N = 10$) results. While $\rho_{\rm BD}$ and ρ_∞ for small $\epsilon = 0.01$ agree very well on $N = 6$, increasing the system size shows a tendency of $\rho_{\rm BD}$ towards the $\rho_{\rm tGGE}$ result. A milder discrepancy of $\rho_{\rm tGGE}$ results is due to omitted conservation laws.

The important conclusion is two-fold: (i) The above analysis gives numerical support for the claim that the stabilized steady state can be approximated with a GGE despite different sources of integrability breaking. (ii) While $\rho_{\rm tGGE}$ is parametrized with $N_C = 4$ parameters, $\rho_{\rm BD}$ at $N = 10$ with about 10^3 and the full ρ_∞ would require about 10^6 parameters. Description in terms of a truncated GGE is therefore a highly compact parametrization of the steady state, which takes into account only the most relevant information.

We find that in the presence of Lindblad driving, the effect of next-nearest interaction, H_1, is rather weak. While in a closed setup H_1 is crucial as it dictates relaxation towards a thermal state, it is dominated with Lindblad terms in an open setup. Mathematically, this can be explained through Eq. (10.62) which shows that the unitary perturbation is constrained to act only between degenerate eigenstates, while the Markovian contribution has no such constraint. Fig. 10.13 shows that results obtained from the exact steady state ρ_∞ calculated with (NN) or without H_1 are very similar. While H_1 can be easily included into the calculation of the exact steady state ρ_∞, it brings certain ambiguity into the calculation of $\rho_{\rm BD}$ and $\rho_{\rm tGGE}$. Namely, on finite system sizes one has to introduce broadening η when calculating $\mathcal{L}_u \mathcal{L}_0^{-1} \mathcal{L}_u$, Eq. (10.62). As we showed in [25], broadening itself modifies the effective strength of the perturbation, meaning that different system sizes, requiring different broadening, cannot be directly compared. Since ρ_∞ shows that the effect of H_1 is small, we omit it in the calculation of $\rho_{\rm BD}$ and $\rho_{\rm tGGE}$.

10.10 Microscopic derivation of two-body decay

In the following, we verify that the mechanisms presented in Sec. 10.4.3 lead to the desired dissipative couplings in Eq. (10.11). To this end, we eliminate the excited degrees of freedom by means of the *effective operator formalism* [8]. This allows us to obtain the effective dynamics of the ground states.

To obtain the effective processes between the ground states, we need to evaluate the expres-

sions for the effective Hamiltonian and Lindblad operators [8],

$$H_{\text{eff}} = -\frac{1}{2}\left(V_- H_{\text{NH}}^{-1} V_+ + H.c.\right), \tag{10.63}$$

$$L_{\text{eff},k} = L_k H_{\text{NH}}^{-1} V_+, \tag{10.64}$$

with the relevant terms discussed below.

For the scheme at hand, V_+ is the weak excitation from the ground states to the excited states (de-excitation: $V_- = V_+^\dagger$), taken from Eq. (10.19),

$$V_+ = \frac{\Omega}{2}(\sqrt{2}|\psi_e\rangle\langle\downarrow\downarrow| + |\uparrow e\rangle\langle\uparrow\downarrow|). \tag{10.65}$$

While L_k can represent various sources of dissipation, the only relevant jump operator is given by Eq. (10.26), which can be written as

$$L_\Gamma = \sqrt{\frac{\Gamma}{2}}|\uparrow\downarrow\rangle\langle\psi_e|. \tag{10.66}$$

The evolution of the excited states is described by a non-Hermitian Hamiltonian,

$$H_{\text{NH}} = H_e - \frac{i}{2}\sum_k L_k^\dagger L_k = H_e - \frac{i}{2}L_\Gamma^\dagger L_\Gamma, \tag{10.67}$$

incorporating the excited-state Hamiltonian $H_{\text{e}} = H_{\text{e},\downarrow\downarrow} + H_{\text{e},\uparrow\downarrow}$, with $H_{\text{e},\downarrow\downarrow}$ as of Eq. (10.27) and

$$\begin{aligned} H_{\text{e},\uparrow\downarrow} = {} & \Delta|\uparrow e\rangle|0\rangle\langle 0|\langle\uparrow e| + \delta|\uparrow\downarrow\rangle|1\rangle\langle 1|\langle\uparrow\downarrow| \\ & + g(|\uparrow e\rangle|0\rangle\langle 1|\langle\uparrow\downarrow| + |\uparrow\downarrow\rangle|1\rangle\langle 0|\langle\uparrow e|). \end{aligned} \tag{10.68}$$

The jump operators relevant for Eq. (10.67) are given by induced spontaneous emission, as described by Eq. (10.66). The non-Hermitian terms in Eq. (10.67) can then be taken into account by generalizing the detunings from H_e to "complex" energies of the form $\tilde{\Delta} = \Delta - i(\Gamma/2)/2$. Here we assume no motional decoherence and hence, $\tilde{\delta} = \delta$. If necessary, processes like phonon decay, $L_\kappa = \sqrt{\kappa}a$, can be taken into by $\tilde{\delta} = \delta - i\kappa/2$. We obtain $H_{\text{NH}} = H_{\text{NH},\downarrow\downarrow} + H_{\text{NH},\uparrow\downarrow}$, with

$$\begin{aligned} H_{\text{NH},\downarrow\downarrow} = {} & \tilde{\Delta}_{\downarrow\downarrow}|\psi_e\rangle|0\rangle\langle 0|\langle\psi_e| + \tilde{\delta}|\downarrow\downarrow\rangle|1\rangle\langle 1|\langle\downarrow\downarrow| \\ & + \sqrt{2}g(|\psi_e\rangle|0\rangle\langle 1|\langle\downarrow\downarrow| + |\downarrow\downarrow\rangle|1\rangle\langle 0|\langle\psi_e|). \end{aligned} \tag{10.69}$$

$$\begin{aligned} H_{\text{NH},\uparrow\downarrow} = {} & \tilde{\Delta}_{\uparrow\downarrow}|\uparrow e\rangle|0\rangle\langle 0|\langle\uparrow e| + \tilde{\delta}|\uparrow\downarrow\rangle|1\rangle\langle 1|\langle\uparrow\downarrow| \\ & + g(|\uparrow e\rangle|0\rangle\langle 1|\langle\uparrow\downarrow| + |\uparrow\downarrow\rangle|1\rangle\langle 0|\langle\uparrow e|), \end{aligned} \tag{10.70}$$

having defined $\tilde{\Delta}_{\downarrow\downarrow} = \Delta - i(\Gamma/2)/2$, $\tilde{\Delta}_{\uparrow\downarrow} = \Delta$, $g_{\downarrow\downarrow} = g$, and $g_{\uparrow\downarrow} = \sqrt{2}g$. H_{NH} is block-diagonal and hence simple to invert,

$$\begin{aligned} H_{\text{NH}}^{-1} &= H_{\text{NH},\downarrow\downarrow}^{-1} + H_{\text{NH},\uparrow\downarrow}^{-1}, \\ H_{\text{NH},\downarrow\downarrow}^{-1} &= \tilde{\Delta}_{\downarrow\downarrow,\text{eff}}^{-1}|\psi_e\rangle|0\rangle\langle 0|\langle\psi_e| + \tilde{\delta}_{\downarrow\downarrow,\text{eff}}^{-1}|\downarrow\downarrow\rangle|1\rangle\langle 1|\langle\downarrow\downarrow| \\ &\quad + g_{\downarrow\downarrow,\text{eff}}^{-1}(|\psi_e\rangle|0\rangle\langle 1|\langle\downarrow\downarrow| + |\downarrow\downarrow\rangle|1\rangle\langle 0|\langle\psi_e|), \\ H_{\text{NH},\uparrow\downarrow}^{-1} &= \tilde{\Delta}_{\uparrow\downarrow,\text{eff}}^{-1}|\uparrow e\rangle|0\rangle\langle 0|\langle\uparrow e| + \tilde{\delta}_{\uparrow\downarrow,\text{eff}}^{-1}|\uparrow\downarrow\rangle|1\rangle\langle 1|\langle\uparrow\downarrow| \\ &\quad + g_{\uparrow\downarrow,\text{eff}}^{-1}(|\uparrow e\rangle|0\rangle\langle 1|\langle\uparrow e| + |\uparrow\downarrow\rangle|1\rangle\langle 0|\langle\uparrow e|). \end{aligned} \tag{10.71}$$

Here we have defined effective detunings and couplings,

$$\tilde{\Delta}_{ij,\text{eff}} = \tilde{\Delta}_{ij} - \frac{g_{ij}^2}{\tilde{\delta}}, \tag{10.72}$$

$$\tilde{\delta}_{ij,\text{eff}} = \tilde{\delta} - \frac{g_{ij}^2}{\tilde{\Delta}_{ij}}, \tag{10.73}$$

$$\tilde{g}_{ij,\text{eff}} = g_{ij} - \frac{\tilde{\Delta}_{ij}\tilde{\delta}}{g_{ij}}, \tag{10.74}$$

which mediate the effective processes. Using Eq. (10.64), we obtain for the effective jump operators for spontaneous emission

$$L_{\text{eff}}^{(2)} \equiv L_{\text{eff},\Gamma} = \sqrt{\gamma_2}|{\uparrow\downarrow}\rangle|0\rangle\langle 0|\langle{\downarrow\downarrow}|, \tag{10.75}$$

with the effective decay rate

$$\gamma_2 = \frac{(\Gamma/2)(\Omega/\sqrt{2})^2}{|\tilde{\Delta}_{\downarrow\downarrow,\text{eff}}|^2}. \tag{10.76}$$

For the parameter choice of Sec. 10.4.3 ($\Delta = \delta = \sqrt{2}g$), we find

$$\tilde{\Delta}_{\downarrow\downarrow,\text{eff}} = \tilde{\Delta}_{\downarrow\downarrow} - \frac{2g^2}{\tilde{\delta}} = -\frac{i\Gamma}{4}, \tag{10.77}$$

This yields an effective decay rate

$$\gamma_2 \approx \frac{4\Omega^2}{\Gamma}. \tag{10.78}$$

We can now associate the effective Lindblad operator in Eq. (10.75) with the desired one in Eq. (10.11),

10.11 AC Stark shift of states

We also derive the effective Hamiltonian using Eq. (10.63), and obtain

$$H_{\text{eff}} = -\frac{(\Omega/2)^2}{|\tilde{\Delta}_{\uparrow\downarrow,\text{eff}}|^2}\text{Re}(\tilde{\Delta}_{\uparrow\downarrow,\text{eff}})|{\uparrow\downarrow}\rangle|0\rangle\langle 0|\langle{\uparrow\downarrow}|, \tag{10.79}$$

where Re() denotes the real part. For our parameter choice $\Delta = \delta = \sqrt{2}g$, we have

$$\tilde{\Delta}_{\uparrow\downarrow,\text{eff}} = \tilde{\Delta}_{\uparrow\downarrow} - \frac{g^2}{\tilde{\delta}} = \frac{g}{\sqrt{2}}, \tag{10.80}$$

and, thus,

$$H_{\text{eff}} = -\frac{\Omega^2}{2\sqrt{2}g}|{\uparrow\downarrow}\rangle|0\rangle\langle 0|\langle{\uparrow\downarrow}|, \tag{10.81}$$

This term corresponds to an AC Stark shift of $|{\uparrow\downarrow}\rangle|0\rangle$, which can be safely neglected in the considered parameter regime $\Omega^2 \ll \{\Gamma^2, g^2\}$.

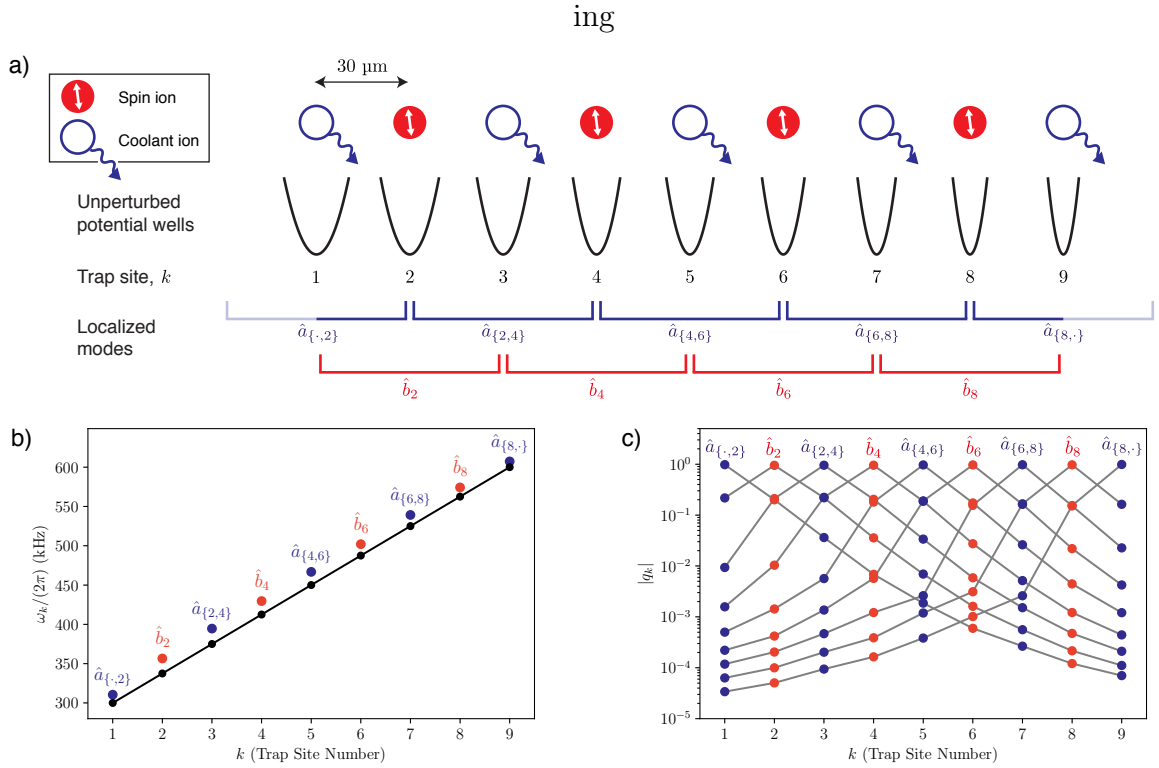


Figure 10.12: Mixed species implementation using micro-traps. (a). Ions in a linear chain of micro-traps are arranged along the axial direction (this corresponds to the axis with no radio frequency (r.f.) curvature in the case of Paul traps, and equivalently, the magnetic field axis in the case of Penning traps). The distance between neighboring traps here is 30 µm. Two kinds of ions are considered – one to encode the spins (the spin species, here $^{43}Ca^{+}$), and the other to facilitate cooling (the coolant species, here $^{40}Ca^{+}$). Each trap consists of a single ion with the species of the ion occupying the trap sites alternating between the spin and the coolant. By appropriately tuning the individual potential wells one can obtain motional modes localized to either one or two spin ions. (b). Frequency spectrum of the axial modes for an example configuration that leads to the localization of modes. In black are the axial frequencies of the individual micro-traps. These vary linearly with the trap site. The colored dots indicate the frequencies of the modes of collective motion for this system of ions. The motion in each mode is at a frequency close to the bare frequency of the trap and is dominated by the ion located at the trap (and its next-neighboring traps). (c). Eigenvectors of the axial modes showing the amplitudes of motion of each ion in the mode for this configuration. The participation of next-nearest (and further) neighboring ions drops off steeply in any given mode. Thus, as an approximation, each mode can be treated as being limited to triplets (or pairs in the case of ions at the edge) of ions.

11 From dissipationless to normal diffusion in easy-axis Heisenberg spin chain by Prelovšek, Nandy, Lenarčič et al.

Abstract

The anomalous spin diffusion of the integrable easy-axis Heisenberg chain originates in the ballistic transport of symmetry sectors with nonzero magnetization. Ballistic transport is replaced by normal dissipative transport in all magnetization sectors upon introducing the integrability-breaking perturbations, including external driving. Such behavior implies that the diffusion constant obtained for the integrable model is relevant for the spread of spin excitations but not for the spin conductivity. We present numerical results for closed systems and driven open systems, indicating that the diffusion constant shows a discontinuous variation as the function of perturbation strength.

11.1 Introduction

The transport in integrable quantum many-body models, the prominent example being the Heisenberg XXZ spin-1/2 chain, has attracted a lot of attention for a few decades and recently reached a high level of understanding via novel analytical and powerful numerical approaches [1]. However, there are still open fundamental questions, in particular, regarding the influence of integrability-breaking perturbations (IBP). While theoretical tools to deal with perturbations are well developed for the simpler but related problem of noninteracting fermions, perturbed integrable many-body systems still present a challenge [2, 3, 25].

The distinctive feature of integrable XXZ spin chain is the dissipationless ballistic transport at finite temperatures $T > 0$ [5, 6]. In the dynamical conductivity $\sigma(\omega) = 2\pi D\,\delta(\omega) + \sigma_{reg}(\omega)$ it is detected via finite Drude weight $D(T > 0) > 0$. While in general case the lower bound for D can be related to the local conserved quantities (CQ) of integrable models [7], for the most investigated case of easy-plane Heisenberg chain ($\Delta < 1$) one has to invoke also quasi-local CQ [8, 9, 48] to explain $D > 0$. A more general description of integrable transport is recently developed framework of generalized hydrodynamics (GHD) [11, 9, 13, 14, 15, 16, 17]. However, much less is understood about the role of IBP, which plausibly reduce the ballistic transport into a normal dissipative one [18, 6, 19, 20, 21], attributed to the decay of CQ in the perturbed system [22]. Transport in spin chains has been recently also realized and investigated experimentally in cold-atom systems [23, 24, 25]

A particular challenge is the easy-axis ($\Delta > 1$) XXZ model where $D = 0$ at zero magnetization $m = 0$, whereas the nonequilibrium steady state of open, boundary driven systems [26] and the Hamiltonian evolution of an inhomogeneous spin profile [27, 28, 29, 30] are consistent with a finite diffusion constant $\mathcal{D}_I > 0$. It has become increasingly evident that such transport is anomalous. Namely, integrable models do not exhibit internal dissipation [31]. The dc conductivity $\sigma_0 = \lim_{F\to 0} j_s/F$ is defined via the steady current, j_s, induced by a steady field, F, hence the conductivity is determined in the presence of nonzero driving. Such driving breaks integrability and restores normal transport (i.e., steady driving leads to a steady heating). More recently, the anomalous origin of spin diffusion within the integrable model has emerged also from GHD methodology, which explains diffusion constant $\mathcal{D}_I > 0$ as the grandcanonical (GC) superposition of ballistic (i.e. dissipationless) spreading of quasiparticles belonging to $m \neq 0$ sectors [32, 33, 17].

In this paper we investigate the effect of weak IBP of strength g on the high-T diffusion in the XXZ model, with the main conclusion that the dc diffusion constant $\mathcal{D}$, appearing at nonzero $g > 0$ is unrelated to the dissipationless diffusion $\mathcal{D}_I$ in the integrable system, as previously

hinted [34, 28] and recently also stated more explicitly [35]. As a consequence, the generalized Einstein relation $\mathcal{D} = \sigma_0/\chi_0$, which relates σ_0 and the spin susceptibility $\chi_0(T \to \infty) \sim 1/(4T)$ (taking $k_B = 1$) is not valid for integrable XXZ model, but restored in the presence of IBP. We establish this by studying different IBP and calculating dissipative/normal dc $\mathcal{D}(g)$ emerging from different methods: (a) the dynamical diffusion response in finite systems with $L \leq 32$ for different magnetization sectors $m \geq 0$, (b) the steady-state currents in open, boundary-driven systems allowing for much larger $L \leq 80$, (c) the time-dependent spin structure factor $S(q,t)$ at finite wavevectors $q = 2\pi/L$, (d) the variation of modulated spin profile under the influence of finite driving field $F > 0$.

In the large-L limit, results for $\mathcal{D}(g)$ of all methods are expected to converge (shown here for modest $g > 0$). Most important, results indicate that $\mathcal{D}_0 = \mathcal{D}(g \to 0) \ll \mathcal{D}_I$, i.e., diffusion reveals a jump upon introduction of IBP [36]. On contrary, the Einstein relation (based on the linearity of system's response to weak IBP) is not valid for the integrable system and different protocols, e.g., the sequence of limits $L \to \infty$ and $\omega \to 0$ ($t \to \infty$) may yield different results.

11.2 Model and dissipationless diffusion

We study $S = 1/2$ spin chain of length L with anisotropy $\Delta > 1$,

$$H = J \sum_i \left[\frac{1}{2} \left(S^+_{i+1} S^-_i + \text{H.c.} \right) + \Delta S^z_{i+1} S^z_i \right] + g H' \,. \tag{11.1}$$

We consider different IBP that conserve the translational symmetry of the model. In the main text we focus on the staggered field $g = \delta h$, $H' = \sum_i (-1)^i S^z_i$, while results for staggered exchange $g = \delta J$, $H' = (1/2) \sum_i (-1)^i (S^+_{i+1} S^-_i + \text{H.c.})$, and the next-nearest-neighbor (NNN) interaction $g = \Delta_2$, $H' = \sum_i S^z_{i+2} S^z_i$ are described in more detail in Appendix 11.7 and 11.8. Note that, considered H' conserve $S^z_{tot} = \sum_i S^z_i = mL$, where $|m| \leq 1/2$ is the magnetization of the system. We further use $J = 1$ and focus on the uniform spin current, which is for unperturbed H (also for $g = \delta h, \Delta_2$) given by $j_s = (J/2) \sum_l (i S^+_l S^-_{l+1} + \text{H.c.})$.

Before presenting results for perturbed XXZ chain, we provide a simple interpretation of the dissipationless diffusion emerging in the unperturbed system at $\Delta > 1$. We first notice that for latter system the Drude weight D for $m \ll 1$ is dominated by the overlap of j_s with the conserved energy current j_E [7],

$$TD \gtrsim \frac{1}{2L} \frac{\langle j_s j_E \rangle^2}{\langle (j_E)^2 \rangle} = \frac{\Delta^2 m^2}{1 + 2\Delta^2} \,. \tag{11.2}$$

In an infinite system, this leads to ballistic component in each $m \neq 0$ sector. However, in a finite system, the spin current acquires a finite relaxation time τ_L due to scatterings at the system boundaries. Introducing an effective velocity for the ballistic spin propagation, $\bar{v}$, one gets the corresponding scattering rate, $1/\tau_L = \bar{v}/L$. Consequently, the $\delta(\omega)$-contributions are broaden to Lorentzians with the widths $\Gamma_L = 1/\tau_L$. It leads to a finite (diffusive-like) response, $\sigma_m(\omega \to 0) = 2D(m)/\Gamma_L$, which is obviously only a finite-size effect in each sector $m \neq 0$. Nevertheless, the grand-canonical (GC) averaging over m effectively eliminates the size-dependence

$$\mathcal{D}_I = \frac{2L \langle D(m) \rangle_{GC}}{\bar{v} \chi_0} \sim \frac{4L}{\bar{v}} \langle m^2 \rangle_{GC} = \frac{1}{\bar{v}} \,, \tag{11.3}$$

where we take into account $\Delta \gg 1$ in Eq. (11.2) and high-T average $\langle m^2 \rangle_{GC} = 1/(4L)$. The underlying assumption is that the effective $\bar{v}$ weakly depends on m. We note that analogous GC analysis is also the basis of the lower bound [32] as well as the GHD result [33, 17] for $\mathcal{D}_I$.

This simple scenario introduces two crucial implications:

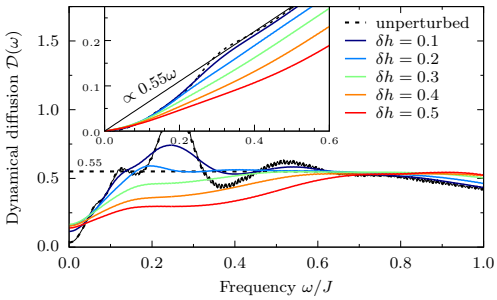


Figure 11.1: High-T dynamical diffusion $\mathcal{D}(\omega)$ evaluated for XXZ chain at magnetization $m = 0$ and fixed $\Delta = 1.5$, using MCLM on $L = 32$ system and various staggered fields δh. The inset shows the integrated quantity $I(\omega) = \int_0^\omega d\omega' \mathcal{D}(\omega')$, with the extrapolation to limit $L \to \infty$ for the unperturbed system.

- Since the diffusive spin propagation originates from the ballistic transport in $m \neq 0$ sectors, the diffusion is not related to any internal energy dissipation. It means that Eq. (11.3) is relevant for the propagation of spin excitations, but not for their dc response to a steady driving [34] since the latter is immanently connected with the internal energy dissipation (c.f. the Joule heating).

- The IBP introduces an L-independent mean free path, λ^*, which determines the scattering rate, $\tau_\lambda^{-1} = \bar{v}/\lambda^*$ and should be used instead of L in the numerator in Eq. (11.3). Then, Eq. (11.3) becomes just a finite-size contribution that vanishes as $\lambda^*/L \to 0$. In other words, even weak perturbation eliminates the contribution given by Eq. (11.3), leading to a discontinuous $\mathcal{D}$ in the thermodynamic limit.

11.3 Dynamical diffusion in closed systems

We calculate $T \gg 1$ dynamical conductivity $\tilde{\sigma}(\omega) = T\sigma(\omega)$ for systems with IBP with the linear-response (Kubo) relation

$$\tilde{\sigma}(\omega) = \frac{\pi}{LN_{st}} \sum_{n,m} |\langle n|j_s|m\rangle|^2 \delta(\omega - \epsilon_m + \epsilon_n)\,, \tag{11.4}$$

where $|n\rangle, |m\rangle$ are N_{st} many-body eigenstates with corresponding energies ϵ_n, ϵ_m. In L-site chains with PBC and fixed (canonical) magnetization m we evaluate $\tilde{\sigma}(\omega)$ using the micro-canonical Lanczos method (MCLM) [37, 38]. The method is upgraded [39] by performing large number of Lanczos steps, i.e. $M_L \sim 5000$. This allows for resolution $\delta\omega \sim 10^{-3}$ for systems up to $L = 32$ with $N_{st} \lesssim 10^7$. Dealing with perturbed/normal systems we adopt the Einstein relation, $\mathcal{D}(\omega) = \sigma(\omega)/\chi_0 = 4\tilde{\sigma}(\omega)$, as valid for $T \gg 1$ and $m \sim 0$.

We first comment on the canonical $m = 0$ results for $\mathcal{D}(\omega)$, as presented in Fig. 18.1, for particular anisotropy $\Delta = 1.5$ and calculated for maximum reachable $L = 32$ for various staggered field δh. Analogous results for $\Delta_2 > 0$ and $\delta J > 0$ are presented Appendices 11.7 and 11.8, respectively. For comparison, we include the unperturbed $\delta h = 0$ result obtained by the same protocol, with the inset showing the integrated spectra $I(\omega) = \int_0^\omega d\omega' \mathcal{D}(\omega')$. As already noticed [31], the integrable case exhibits vanishing dc value $\mathcal{D}(\omega \to 0) \sim 0$, but as well large $\omega \sim 1/L$ oscillations, which can still be made compatible (after $L \to \infty$ extrapolation) with the result $\mathcal{D}_I \sim 0.55$ (see the inset), obtained also by other numerical approaches [26, 40, 29, 1], being also in the range of the GHD result [17, 16].

On the other hand, results for finite $g = \delta h > 0$ reveal dc value $\mathcal{D}(\omega \to 0) = \mathcal{D}_0 > 0$, evidently smaller than the integrable one, $\mathcal{D}_0(g) \ll \mathcal{D}_I$. Such values are not finite-size effects,

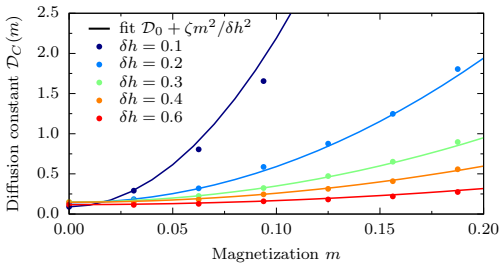


Figure 11.2: Canonical dc diffusion constant $\mathcal{D}_C(m)$ for $\Delta = 1.5$ as calculated for different magnetizations m with MCLM in a system of $L = 32$ sites for different staggered fields $\delta h > 0$. Results are fitted with parabolic dependence, Eq. (11.5) with fixed $\zeta = 2.1$.

which can be deduced also from the integrated spectra $I(\omega)$, which are for $g > 0$ systematically reduced, i.e., $I(\omega) < \mathcal{D}_I\omega$ in a wide range $\omega < 1$, requiring the reduction of $\mathcal{D}(\omega \sim 0)$. Some caution is appropriate for weakest perturbation, e.g., for $g \leq 0.1$, where $\mathcal{D}(\omega)$ in Fig. 18.1 still exhibits visible finite-size oscillations $\omega \sim 1/L$. This indicates that reachable systems might be too small for considered g, i.e., $L < \lambda^*$ where $\lambda^*(g)$ represents an effective mean-free path. Similar are conclusions for $g = \Delta_2, \delta J$ perturbations shown in Appendices 11.7 and 11.8, where L dependence of $\mathcal{D}(\omega)$ spectra is presented.

For given L, we employ MCLM to calculate canonical $\mathcal{D}_C(\omega, m)$ and extract dc $\mathcal{D}_C(\omega \to 0, m) = \mathcal{D}_C(m)$ corresponding to different m sectors. Results presented in Fig. 18.2 show parabolic dependence on m, at least for $g \ll 1$. This can be explained as follows. Considered IBP do not conserve j_E and lead to the normal (finite) dc energy/thermal conductivity κ_0, which scales (as expected from perturbation theory) as $\kappa_0 \propto 1/g^2$ [19, 20, 21, 41]. Taking into account the overlap of the spin current with j_E, Eq. (11.2), this leads to the dependence,

$$\mathcal{D}_C(m) = \mathcal{D}_0 + \zeta m^2/g^2. \tag{11.5}$$

Results in Fig. 18.2 are well represented with the above dependence, where ζ appears universal for all $g > 0$, plausibly still dependent on the type of perturbation, e.g., $\zeta = 2.1$ for $g = \delta h$, but $\zeta = 1.8, 9.0$ for $g = \Delta_2, \delta J$ cases, respectively (Appendices 11.7 and 11.8). The $\mathcal{D}_0 = \mathcal{D}_C(m = 0)$ represent weakly g dependent canonical $m = 0$ values, extracted from Fig. 18.1, and apparently determined by a mechanism unrelated to j_E.

It is straightforward to calculate the GC averaged value of $\mathcal{D}_{GC}$, corresponding to $\langle m \rangle_{GC} = 0$ at given size L. Namely, taking into account $\langle m^2 \rangle_{GC} = 1/(4L)$ we get

$$\mathcal{D}_{GC} = \mathcal{D}_0 + 4\zeta/(Lg^2)\,. \tag{11.6}$$

GC values are thus for weaker $g < 2\sqrt{\zeta/L}$ evidently $\mathcal{D}_{GC} \gg \mathcal{D}_0$, but should approach the latter value on increasing L. The results for $\delta h = 0.2, 0.4$ are presented in Fig. 17.3.

11.4 Diffusion in open systems

MCLM results above are based on the exact diagonalization, which restricts reachable sizes to $L \leq 32$. Larger L are therefore crucial to analyse regime of weaker perturbations $g \to 0$. For this purpose, we study open Heisenberg chains, where the spin current is driven via boundary Lindblad operators, $L_1 = \sqrt{1+\mu}S_1^-$, $L_2 = \sqrt{1-\mu}S_1^+$, $L_3 = \sqrt{1-\mu}S_L^-$, $L_4 = \sqrt{1+\mu}S_L^+$, simulating couplings to baths with a small difference μ in spin chemical potential [26]. We use time-evolving block-decimation (TEBD) technique for vectorized density matrices [46, 45], which evolves the density matrix ρ under the Liouvillian $\hat{\mathcal{L}}\rho = -i[H, \rho] + \hat{\mathcal{D}}\rho$, $\hat{\mathcal{D}}\rho = \sum_k L_k \rho L_k^\dagger - \frac{1}{2}\{L_k^\dagger L_k, \rho\}$, to reach the nonequilibrium steady-state ρ_{ss} for small $\mu \sim 0.01$ with bond dimension

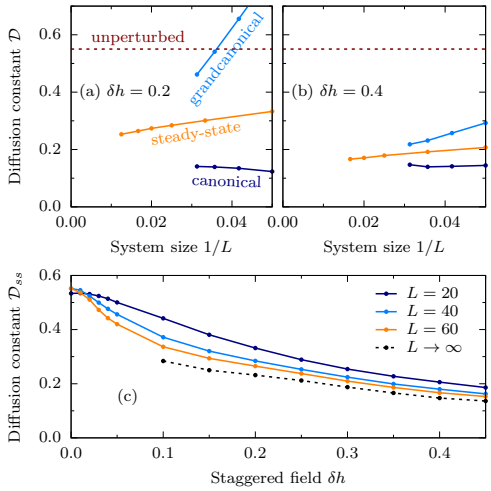


Figure 11.3: Diffusion constant $\mathcal{D}$ vs. $1/L$ obtained for fixed $\Delta = 1.5$ from finite-L results by three different approaches: canonical $m = 0$ sector MCLM results $\mathcal{D}_0$, GC average over m sectors $\mathcal{D}_{GC}$, and open-system steady-state $\mathcal{D}_{ss}$, for two staggered fields: (a) $\delta h = 0.2$, and (b) $\delta h = 0.4$. Displayed is also unperturbed value $\mathcal{D}_I = 0.55$. (c) Diffusion constant $\mathcal{D}_{ss}$ vs. δh, as obtained for sizes $L = 20, 40, 60$ within the steady-state open-system approach. Shown are also values obtained via linear $1/L \to 0$ scaling.

$\chi_{bd} = 128$. Finite bias μ yields a finite steady state spin currents $j_{ss} = \mathrm{Tr}[\rho_{ss} j_s]$ from which diffusion constant can be obtained as $\mathcal{D}_{ss} = -j_{ss}/\nabla s^z$, where the magnetization gradient for $L \gg 1$ is (nearly) homogeneous, $\nabla s^z = \mathrm{Tr}[(S^z_{i+1} - S^z_i)\rho_{ss}] \sim \mu/L$. Such approach allows to deal with substantially larger L, but is still limited to $L \leq 80$ due to very slow convergence towards the steady state as a consequence of small $\mathcal{D}_{ss} \ll 1$ for our parameters.

For open and closed systems, it is important to follow the L dependence of results. In Fig. 17.3(a,b) we summarize $\mathcal{D}$ from all methods, presented as scaling vs. $1/L$. It is evident that $\mathcal{D}_{ss}$ are for all cases between the canonical $m = 0$ values $\mathcal{D}_0$ and $\mathcal{D}_{GC}$. The latter can be considered as an upper bound to the desired thermodynamic $1/L \to 0$ result $\mathcal{D}(g)$. For larger $\delta h = 0.4$, $\mathcal{D}_{ss}$ as well as $\mathcal{D}_0$ and $\mathcal{D}_{GC}$ yield very consistent results allowing for a reliable extrapolation to $1/L \to 0$. Furthermore, for weak $\delta h = 0.2$, $\mathcal{D}_0$ are well below $\mathcal{D}_{GC}$ for reachable L, while $\mathcal{D}_{ss}$ still shows relevant variation with $1/L$, even with a visible change of slope indicating on possible crossover behavior with $1/L$.

In Fig. 17.3(c) we present the dependence of open-system $\mathcal{D}_{ss}$ on δh, as calculated for different sizes, $L = 20, 40, 60$. We notice that at weak $\delta h \to 0$ the open-system method reproduces unperturbed value, i.e., $\mathcal{D}_{ss} \sim \mathcal{D}_I$. The continuous decrease of $\mathcal{D}_{ss}$ with δh at fixed L can be interpreted as (partly) persisting ballistic component due to small size $L < \lambda^*(\delta h)$. Still, the results indicate on a crossover, i.e., with increasing L the decrease with δh becomes steeper and the region with $\mathcal{D}_{ss} \sim \mathcal{D}_I$ narrower. On the other hand, $\mathcal{D}_{ss}$ become quite L independent for larger $\delta h \geq 0.3$, as also evident from Fig. 17.3(b). In Fig. 17.3(c) we also present the result of a simple linear $1/L \to 0$ scaling (above the presumed crossover $\delta h \geq 0.1$ for reachable L), which can be regarded as an upper bound for the thermodynamic-limit value $\mathcal{D}_{ss}(\delta h)$. Resulting values reveal very modest variation with δh, consistent with $\mathcal{D}_{ss}(\delta h \to 0, L \to \infty) \ll \mathcal{D}_I$.

11.5 Finite wavevector and driving-field analysis

Transport can be also analysed by considering finite wavevector $q > 0$ correlations in closed systems with PBC. In particular, we evaluate the time-dependent spin structure factor $S(q,t)$ as correlations of the operator $S^z_q = (1/\sqrt{L}) \sum_j \exp(iqj) S^z_j$ for the smallest nonzero $q = 2\pi/L$.

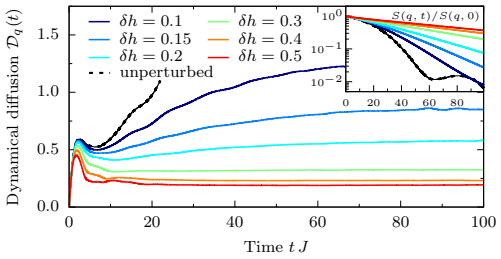


Figure 11.4: Time-dependent diffusion $\mathcal{D}_q(t)$ as extracted from corresponding spin-correlation functions $S(q,t)$ (shown in log scale as inset) evaluated for $L = 28$ and smallest finite $q = 2\pi/L$ for staggered fields $\delta h = 0 - 0.5$.

The numerical procedure is again MCLM in analogy to $\tilde{\sigma}(\omega)$, Eq. (11.4), now for $S(q,\omega)$. Large number $M_L \sim 10^4$ allows to follow the time evolution for $S(q,t)$ up to $t \gg 100$. Consequently, effective (time-dependent) diffusion can be extracted as $\mathcal{D}_q(t) = -\dot{S}(q,t)/[q^2 S(q,t)]$ [40]. It is evident that in normal systems such procedure yields constant $\mathcal{D}_q(t \to \infty) \sim \mathcal{D}$. We argue and confirm numerically that the stationary values $\mathcal{D}_q(t)$ can be interpreted as corresponding to the GC average for given system, since operator S^z_q creates an inhomogeneous magnetization S^z_i distribution, in contrast to j_s in Eq. (11.4) related to $q = 0$ and fixed S^z_{tot}. Results for normalized $S(q,t)$ (shown in log scale as inset) and extracted $\mathcal{D}_q(t)$, as calculated within MCLM for $L = 28$, are presented in Fig. 17.4. For the integrable system $\delta h = 0$ it has been already noticed [28] that $\mathcal{D}_q(t) \sim \mathcal{D}_I$ exhibit a plateau at intermediate $t < \tau_L$, corresponding to dissipationless diffusion. In contrast, for longer times, the $\mathcal{D}_q(t > \tau_L) \propto t$ reflects the relaxation of the Gaussian decay of $S(q,t)$ [28]. The same behavior persists (at least for reachable t) for weak perturbations δh.

On the other hand, $\delta h > 0$ leads to normal diffusion manifested by the saturated values $\mathcal{D}_q$ at longer times $t > \tau_\lambda$ and by the exponential decay of $S(q,t)$. The saturated values $\mathcal{D}_q$ agrees with the GC averages corresponding to Fig. 18.2 and Eq. (11.6). Here, the additional comments are in order: (a) the saturation of $\mathcal{D}_q(t)$ is unrelated to the mechanism of anomalous integrable diffusion restricted to short $t < \tau_L$. This is evident for all δh, in particular for weak δh where the saturation happens only at $t \gg \tau_L$. (b) Saturated $\mathcal{D}_q$ can be at weak $\delta h \leq 0.2$ (for presented L) even larger than $\mathcal{D}_I$. (c) Large $\mathcal{D}_q \sim \mathcal{O}(1)$ are finite-size results, decreasing as $1/L$. As already discussed for the GC case, the relevant results in the macroscopic limit $L \to \infty$ are again $\mathcal{D}_0$, Eq. (11.6).

Also weak external field $F > 0$ has highly nontrivial effect on an integrable chain at $\Delta > 1$. In the previous study [34], this has been investigated within a closed system with PBC at high, but finite T, by introducing time-dependent flux $\phi(t) = Ft$. The spin current j_s in a homogeneous canonical $m = 0$ was extracted from nearly steady-state at a weak F, with a corresponding dc spin conductivity $\tilde{\sigma}_0 = T(t) j_s(t)/F$ at the effective (time-dependent) temperature $T(t)$. Results clearly indicated that $\sigma_0 < \chi_0 \mathcal{D}_I$, i.e., the violation of the Einstein relation in an integrable system, in particular for $F \to 0$. Here, we present additional evidence that finite F breaks the integrability and consequently qualitatively changes the spin-transport response. Similarly as in Ref. [34], we introduce the $F > 0$ via flux $\phi(t)$ (Appendix 11.9). Extracted $\mathcal{D}_F(t)$ exhibits qualitatively the same features as results in Fig. 17.4. Again, saturated values $\mathcal{D}_F(t > \tau_L)$ at long-enough t emerge due to IBP $F > 0$ and are unrelated to intermediate-time $t \sim \tau_L$ saturation $\mathcal{D}_F(t \sim \tau_L) \sim \mathcal{D}_I$. Since the procedure simulates evolution of an inhomogeneous system, the stationary $\mathcal{D}_F$ corresponds to GC average, which can appear large, i.e., $\mathcal{D}_F > \mathcal{D}_I$ for weak F, but should decrease with L to $\mathcal{D}_F < \mathcal{D}_I$ for all $F > 0$.

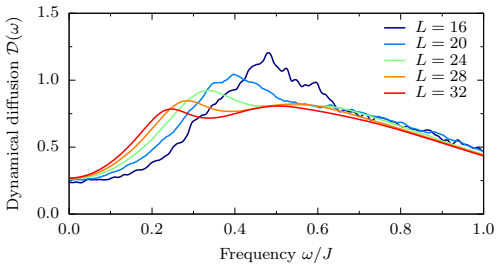


Figure 11.5: Dynamical diffusion $\mathcal{D}(\omega)$ for the XXZ spin chain perturbed with NNN interaction $\Delta_2 = 0.4$, as obtained with MCLM for canonical $m = 0$ system with different sizes $L = 16 - 32$.

11.6 Conclusions

By studying the high-T dynamical spin transport in perturbed anisotropic $S = 1/2$ XXZ Heisenberg chain at $\Delta > 1$, we establish consistent evidence that IBP lead to normal/dissipative transport, unrelated to the dissipationless diffusion $\mathcal{D}_I$ in the integrable system, which originates from ballistic transport in sectors with nonzero magnetization. We note that in contrast to theoretical results, the cold-atom experiments in this regime tend to support the subdiffusive transport [24], which might be due to short-time restrictions, due to presence of finite IBP, but as well due to importance of initial conditions in integrable systems. Our numerical evidence comes from the results of different approaches: canonical $m = 0$ sector results $\mathcal{D}_0$ and GC results $\mathcal{D}_{GC}$ for finite closed systems; steady-state analysis in open boundary-driven systems; finite-q correlations $S(q,t)$ for smallest finite $q = 2\pi/L$; and response to the finite driving field $F > 0$. Since this indicates the breakdown of the standard perturbation-theory approach to IBP, also the generalized Einstein relation is not valid for the integrable system.

Several additional comments are in order: (a) Despite expected normal transport, finite but small IBP remain challenge for all numerical approaches. Namely, thermodynamic $L \to \infty$ results are expected only in systems with $L > \lambda^*(g)$. With restriction of MCLM to $L = 32$ and steady-state of open systems up to $L = 80$, this still represents some restriction for weakest $g \leq 0.1$. (b) Clearly, the goal is to find first $\mathcal{D}(g)$, as extrapolated to the limit $L \to \infty$ and then $\mathcal{D}_0 = \mathcal{D}(g \to 0)$. While previous canonical $m = 0$ results with finite-field driving $F > 0$ [34] seem to indicate $\mathcal{D}(g \to 0) \to 0$ for vanishing F, present MCLM analysis and even more the open-system results for homogeneous Hamiltonian IBP are plausibly consistent with a jump [35], i.e., $\mathcal{D}_0 > 0$, but clearly $\mathcal{D}_0 < \mathcal{D}_I$. (c) In this work, we focused on results for a particular anisotropy parameter $\Delta = 1.5$, but the general conclusion should remain valid for the whole regime $\Delta > 1$. It is, however, expected that $\mathcal{D}(g)$ as well as desired $\mathcal{D}_0$ depend on Δ and possibly also on the actual form of IBP.

11.7 Perturbed XXZ spin chain: next-nearest-neighbor interaction

In this Appendix we discuss results for the NNN interaction $g = \Delta_2$ as IBP. The advantage of this perturbation for MCLM is that it does not break any translational symmetry, while it would require more effort to be encoded into the TEBD-based open-system analysis due to the long-range nature of exchange. It should be also recognized that at fixed g such perturbation is relatively weaker to considered $g = \delta h, \delta J$ examples, i.e., it makes sense to discuss cases up to $\Delta_2 \sim 0.8$. To illustrate the finite-size effects of MCLM canonical at $m = 0$, in Fig. 11.5 we present the evolution of $\mathcal{D}(\omega)$ at fixed $\Delta_2 = 0.4$ at various $L = 16 - 32$. While $L = 16$ is still dominated by large finite-size $\omega \sim 1/L$ peak (but also noise due to small Hilbert space), with increasing L the corresponding peak is shifted downwards as $1/L$ and, more importantly, loosing in intensity. At the same time there is only minor shift of the dc value $\mathcal{D}_0$.

In Fig. 11.6 we summarize the NNN results in analogy to Figs. 18.1,18.2,17.4. In Fig. 11.5(a)

we show high-T canonical $m = 0$ results for $\mathcal{D}(\omega)$ for $\Delta = 1.5$ for various $\Delta_2 = 0 - 0.8$, as calculated with MCLM on $L = 32$ sites. We note that smaller-L results for this case were presented already in Ref. [34]. Again, we conclude that unperturbed $\Delta_2 = 0$, but also weakest $\Delta_2 = 0.2$ result, show large finite-size $\omega \sim 1/L$ oscillations. This is not the case for larger $\Delta_2 \geq 0.4$. Evidently, for smaller Δ_2 it is important that we reach as large L as possible.

In Fig. 11.6(b) we display the canonical MCLM results for dc $\mathcal{D}_C(m)$ as function of magnetization m. Again, the variation can be captured with parabolic dependence with universal $\zeta = 9.0$, while values $\mathcal{D}_0$ in this case still significantly vary with Δ_2. Obtained $\mathcal{D}_0$ are below $\mathcal{D}_I$ for all considered $\Delta_2 > 0$. Finally, in Fig. 11.6(c) we present the $\mathcal{D}_q(t)$ as extracted from spin correlation $S(q = 2\pi/L, t)$. One can notice the intermediate saturation $\mathcal{D}_q(t) \sim \mathcal{D}_I$ in unperturbed and weak $\Delta_2 = 0.2$ case, with saturation at longer t indicating dissipative diffusion, even quantitatively consistent with the GC values following from Fig. 11.6(b).

11.8 Perturbed XXZ spin chain: staggered exchange

Results for the staggered-exchange IBP $g = \delta J$ are quite analogous and quantitatively similar to the case of staggered field $g = \delta h$. In Fig. 11.7 we display corresponding results $g = \delta J$. Canonical $m = 0$ MCLM results on $L = 32$ sites for $\mathcal{D}(\omega)$ in Fig. 11.7(a) for different $\delta J > 0$ reveal again the evolution from finite-size dominated oscillation $\omega \propto 1/L$ at weakest $\delta J \leq 0.1$, to nearly-L independent spectra $\mathcal{D}(\omega)$ for larger $\delta J \geq 0.2$. The reduction of integrated $I(\omega)$ (in the inset) in a wide range of ω is consistent with the clear reduction of dc $\mathcal{D}_0 \ll \mathcal{D}_I$ for

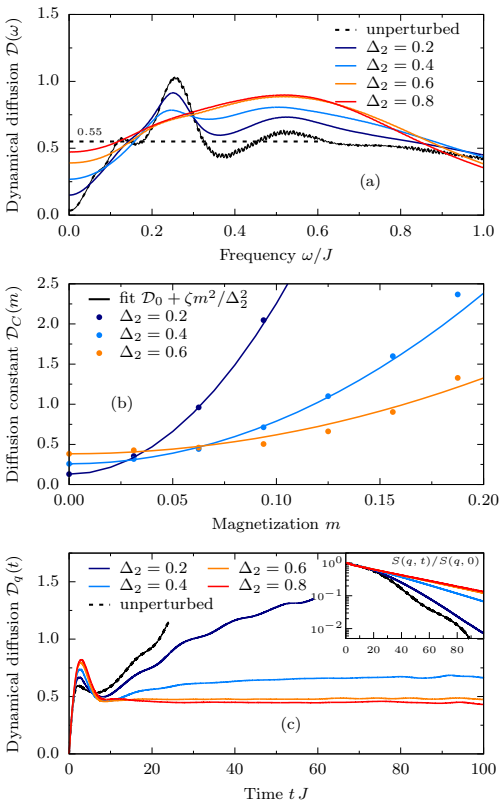


Figure 11.6: Results for diffusion at various strengths of NNN interactions $\Delta_2 = 0 - 0.8$ for XXZ chain with $\Delta = 1.5$. (a) High-T dynamical $\mathcal{D}(\omega)$, as calculated with MCLM on chain of $L = 32$. (b) Diffusion constant $\mathcal{D}_C(m)$ vs. magnetization m. Results are fitted with parabola with fixed $\zeta = 9.0$. (c) Time-dependent $\mathcal{D}_q(t)$, as extracted from spin correlations $S(q, t)$ with smallest finite $q = 2\pi/L$ evaluated for $L = 28$ system (inset shows the corresponding $S(q, t)$ in the log scale).

all $\delta J \geq 0.2$. Also similar to δh case are conclusions for the canonical diffusion $\mathcal{D}_C(m)$ presented in Fig. 11.7(b), fitted with parabola with universal $\zeta = 2.1$, as well as for the diffusion $\mathcal{D}_q(t)$ extracted from $S(q = 2\pi/L, t)$, presented in Fig. 11.7(c).

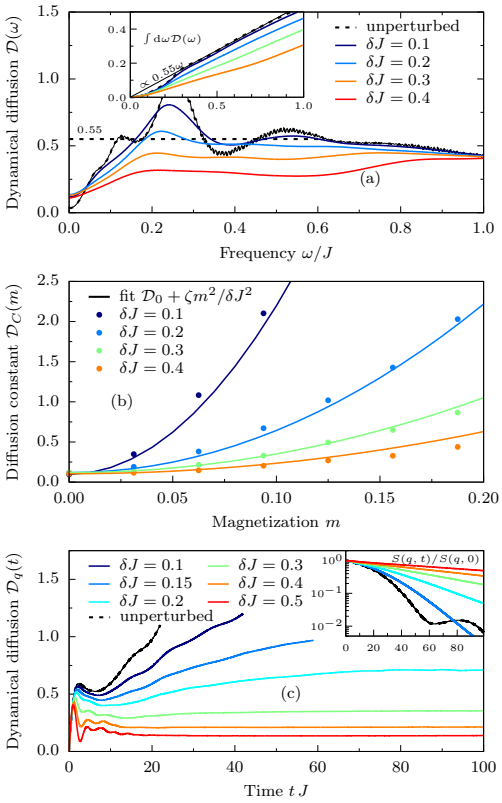


Figure 11.7: Results for diffusion for staggered-exchange perturbation $\delta J = 0 - 0.8$ for the XXZ chain with $\Delta = 1.5$. (a) High-T dynamical $\mathcal{D}(\omega)$, as calculated with MCLM on chain of $L = 32$. (b) Diffusion constant $\mathcal{D}_C(m)$ vs. magnetization m with results fitted to parabola with $\zeta = 2.1$. (c) Time-dependent $\mathcal{D}_q(t)$ as extracted from $S(q = 2\pi/L, t)$ evaluated for $L = 28$ system (the inset shows corresponding $S(q, t)$ in log scale).

Since δJ case allow for the same open-system treatment as the δh perturbation in the main text, we summarize $\mathcal{D}$ calculated by three different methods in Fig. 11.8 for two strengths $\delta J = 0.2, 0.4$, in analogy to Fig. 17.3 for δh perturbation. While for stronger $\delta J = 0.4$ all three methods yield quite converged results, for $\delta J = 0.2$ MCLM $\mathcal{D}_{GC} \gg \mathcal{D}_0$ are still quite apart for reachable L, whereas steady-state $\mathcal{D}_{ss}$ is for largest $L = 80$ apparently much closer to convergence.

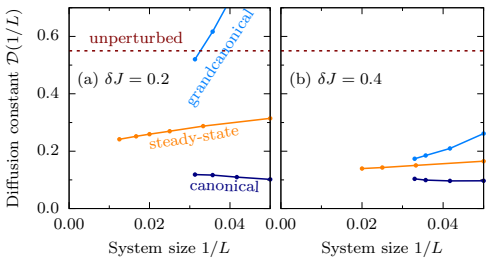


Figure 11.8: Diffusion constant $\mathcal{D}$ vs. $1/L$ obtained for fixed $\Delta = 1.5$ from finite-L results by three different approaches: canonical $m = 0$ sector MCLM results $\mathcal{D}_0$, GC average over m sectors $\mathcal{D}_{GC}$, and open-system steady-state $\mathcal{D}_{ss}$, for two staggered exchange: (a) $\delta J = 0.2$, and (b) $\delta J = 0.4$. Displayed is also unperturbed value $\mathcal{D}_I = 0.55$.

11.9 Diffusion in the presence of finite driving field

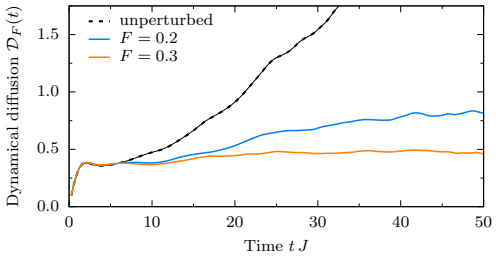


Figure 11.9: Time-dependent diffusion $\mathcal{D}_F(t)$ as extracted from the time evolution of the spin-density profile with the smallest finite $q = 2\pi/L$ for the system of $L = 28$ sites with $\Delta = 1.5$ for various driving fields $F = 0, 0.2, 0.3$.

The conductivity is defined as a ratio of the steady current j_s and the steady driving field F for vanishingly small driving, dc $\sigma_0 = \lim_{F\to 0} j_s/F$. As a consequence the system's response should be determined in the presence of small but nonzero driving. In generic nonintegrable systems, the current-current correlation functions do not exhibit any discontinuity upon introducing weak perturbations, so that dc σ_0 can be calculated strictly for $F = 0$. However, the correlation functions in the easy-axis XXZ model may change discontinuously upon introducing a perturbation, whereby the role of finite driving F might be different from Hamiltonian IBP discussed in the main text. To consider $F > 0$ we study the XXZ model with time dependent Hamiltonian

$$H(t \le 0) = J \sum_i \big[\frac{1}{2}(S^+_{i+1}S^-_i + \text{H.c.}) + \Delta S^z_{i+1}S^z_i\big] + \sum_i \frac{1}{2}\cos(qi)\, S^z_i, \tag{11.7}$$

$$H(t > 0) = J \sum_i \big[\frac{1}{2}(e^{iFt}S^+_{i+1}S^-_i + \text{H.c.}) + \Delta S^z_{i+1}S^z_i\big]. \tag{11.8}$$

Using MCLM, we generate the initial microcanonical state at time $t = 0$, $|\psi_0\rangle$, corresponding to high, but finite temperature, $T \simeq 5$. The last term in Eq. (11.7) is responsible for the spin-density wave, $\langle S^z_i\rangle_0 = \langle\psi_0|S^z_i|\psi_0\rangle \propto \cos(qi)$, where we choose the smallest finite $q = 2\pi/L$. Next, at $t > 0$ this term is switched off while the driving field $F > 0$ is switched on, and $|\psi_t\rangle$ evolves under the Hamiltonian (11.8). During time propagation we calculate the variance of the spatial spin profile, $(\delta S_t)^2 = (1/L)\sum_i \langle\psi_t|S^z_i|\psi_t\rangle^2$. For normal diffusive systems without driving the amplitude of the spin-density wave decays exponentially in time, $\delta S_t = \delta S_0 \exp(-\mathcal{D}_F q^2 t)$ hence the effective time-dependent diffusion constant can be obtained as $\mathcal{D}_F(t) = -\dot{\delta S}_t/[q^2 \delta S_t]$. It is evident that the present setup which is based on time propagation of the spin-density profile, is equivalent to the analysis based on the spin structure factor $S(q,t)$ of the main text. The disadvantage of the present approach is that the dynamics is evaluated at finite temperature ($T \gg 1$) and results may be affected by nonlinear contributions which are beyond the linear-response theory. However, the time-propagation method allows for time-dependent Hamiltonians and one may include the steady driving as in the Hamiltonian (11.8). The resulting $\mathcal{D}_F(t)$ is shown in Fig. 11.8 for the integrable case $F = 0$, as well as for driven systems with $F = 0.2$ and $F = 0.3$. It is clear that nonzero driving affects the spin dynamics in the same way, as IBP shown in Fig.17.4 as well as in Figs. 11.6(c) and Fig. 11.7(d).

12 Critical behavior near the many-body localization transition in driven open systems by Zala Lenarčič, Alberton, Rosch, Altman

12.1 Theory

Abstract

Coupling a many-body localized system to a thermal bath breaks local conservation laws and washes out signatures of localization. When the bath is non-thermal or when the system is also weakly driven, local conserved quantities acquire a highly non-thermal stationary value. We demonstrate how this property can be used to study the many-body localization phase transition in weakly open systems. Here, the strength of the coupling to the non-thermal baths plays a similar role as a finite temperature in a $T = 0$ quantum phase transition. By tuning this parameter, we can detect key features of the MBL transition: the divergence of the dynamical exponent due to Griffiths effects in one dimension and the critical disorder strength. We apply these ideas to study the MBL critical point numerically. The possibility to observe critical signatures of the MBL transition in an open system allows for new numerical approaches that overcome the limitations of exact diagonalization studies. Here we propose a scalable numerical scheme to study the MBL critical point using matrix-product operator solution to the Lindblad equation.

Many-body localization is a state of interacting quantum systems, which fail to thermalize subject to their intrinsic dynamics due to the effect of strong disorder [1, 2, 3]. A pertinent question, currently under intense theoretical study and debate, concerns the nature of the phase transition between the ergodic and localized phases. The transition represents a new class of dynamical quantum phase transitions, which involves a fundamental change of the entanglement structure in all, or at least many, of the eigenstates. The many-body localization transition is sharp only if the system is completely isolated, which imposes severe limitations on the ability to study it using standard theoretical, numerical, and experimental approaches. The requirement of a closed system appears to preclude experiments with solid state materials due to coupling to a phonon bath. Even in experiments with ultra-cold atoms and ion traps, which are usually considered to be exquisitely isolated, signatures of many-body localization are visibly polluted by extrinsic decay processes [4, 5, 6, 7]. Numerical experiments are also severely limited. Because of the need to address closed system dynamics, these have been mostly restricted to exact diagonalization (ED) of very small systems [8, 9, 10, 11, 12, 13, 14]. There is increasing evidence that such simulations are overwhelmed by transient finite-size effects that supersede the critical scaling behavior[15, 16, 17].

We propose to bypass the limitations posed by closed systems by studying signatures of the MBL transition in weakly open driven systems. In a previous work [18] some of us showed that in the limit of vanishing coupling ϵ to a bath and concomitantly weak drive strength $\epsilon\theta$, the MBL transition shows up as a singular change in the temperature variations across the sample. On the thermalizing side of the critical point the temperature fluctuations vanish in the limit $\epsilon \to 0$, while they remain finite on the MBL side. At non-vanishing coupling ϵ one expects this transition to broaden into a universal crossover governed by the critical point located at $\epsilon \to 0$. The dissipative coupling ϵ has a role similar to turning on a nonzero temperature above a $T = 0$ quantum phase transition. Studying the leading dependence of the spatial temperature fluctuations on ϵ in the vicinity of the critical point is analogous to studying the leading dependence of the order parameter on the temperature in a conventional quantum phase transition. Such a measurement allows to determine critical exponents as well as the critical disorder strength. Furthermore, the MBL transition in one dimensional systems

is thought to be preceded by a thermal Griffiths regime leading to sub-diffusive transport [19, 20, 21, 22, 23, 24, 25, 26, 27, 28, 29, 30, 31, 32, 33, 34, 35, 36, 37, 38]. We use an effective model of the Griffiths phase to show that the leading dependence of the temperature variations on the dissipative coupling ϵ reveals the continuously varying dynamical exponent z.

The open systems framework facilitates a new computational scheme to investigate the MBL transition, while overcoming the limitations of exact diagonalization. We use a truncated matrix-product operator to represent the density matrix of a disordered system described by a Lindblad equation with coupling ϵ to dissipators. We find a sharp signature of the Griffith regime with a continuously varying dynamical exponent that diverges at the critical point. We note the connection to Refs. [24, 35, 38], where Griffiths exponents have been computed numerically for a spin-chain coupled to Lindblad operators placed at the two ends of the chain to drive a steady state current. Because we study coupling to bulk Lindblad operators, the calculation can converge faster, allowing to access parameter regimes much closer to the MBL transition.

Hydrodynamic description– Consider a disordered ergodic system, weakly coupled to a thermal bath with temperature T_0 and a drive that heats the system; for example, a spin chain, coupled to phonons and driven by light [18]. Deep in the ergodic phase the system will reach a nearly thermal steady state, with smooth temperature variations determined by a heat flow equation supplemented by sink and source terms due to the coupling to the bath and drive, respectively,

$$\partial_t e(\boldsymbol{r}) - \nabla \cdot (\kappa(\boldsymbol{r}) \nabla T(\boldsymbol{r})) = -\epsilon\, g_1(\boldsymbol{r})(T(\boldsymbol{r}) - T_0) + \epsilon\, \theta g_2(\boldsymbol{r}) \tag{12.1}$$

We assumed, for simplicity, that energy is the only conserved quantity in the limit $\epsilon \to 0$. The disorder in the underlying model is translated to a weak modulation of the conductivity $\kappa(\boldsymbol{r}) = \bar{\kappa} + \delta\kappa(\boldsymbol{r})$ and of the couplings $g_{1(2)}(\boldsymbol{r}) = \bar{g} + \delta g_{1(2)}(\boldsymbol{r})$ to the thermal bath ($g_1(\boldsymbol{r})$) and the drive ($\theta g_2(\boldsymbol{r})$). The temperature profile varies around the mean value, $T(\boldsymbol{r}) = \bar{T} + \delta T(\boldsymbol{r})$, where the mean temperature $\bar{T} = T_0 + \theta$ is determined by the relative strength θ of the drive compared to the coupling to the bath.

Linearizing Eq. (12.27) in the disorder strength for the steady state gives $(-\bar{\kappa}\nabla^2 + \epsilon\bar{g})\delta T(\boldsymbol{r}) = \epsilon\, \theta\, \delta g(\boldsymbol{r})$, where $\delta g(\boldsymbol{r}) = \delta g_2(\boldsymbol{r}) - \delta g_1(\boldsymbol{r})$. This equation is solved for the local temperature variations using the Green's function, $\delta T(\boldsymbol{r}) = \epsilon\theta \int d\boldsymbol{r}' G(\boldsymbol{r} - \boldsymbol{r}')\delta g(\boldsymbol{r}')$, which is in momentum space given by $\tilde{G}(\boldsymbol{k}) = (\bar{\kappa}\, k^2 + \bar{g}\, \epsilon)^{-1}$. We can generalize to the sub-diffusive regime heuristically by using a renormalized Green's function, $G(\boldsymbol{k}) = (\bar{\gamma}|k|^z + \bar{g}\, \epsilon)^{-1}$, imposing dynamical scaling with exponent $z \geq 2$. Assuming Gaussian disorder with short range correlations, $\langle \delta g(\boldsymbol{r}) \delta g(\boldsymbol{r}') \rangle \equiv (\delta g)^2 \delta(\boldsymbol{r} - \boldsymbol{r}')$, we find in d dimensions,

$$\delta T \sim \theta\, |\delta g/\bar{g}|\, (\bar{g}/\bar{\gamma})^{d/2z}\ \ \epsilon^{d/2z}, \tag{12.2}$$

see Suppl. Mat. (SM), [39]. This approach, however, may not properly account for the effect of rare regions that dominate the transport in the Griffiths regime. Below we examine a minimal model that takes this physics into account.

Thermal resistor network – As a minimal model for the Griffiths regime we consider a chain of conducting islands, each characterized by its own temperature T_i, coupled by links representing insulating regions of size ℓ. Together with the energy sink and source terms, this leads to rate equations

$$\begin{aligned} \partial_t e_i - \Gamma_{i,i+1}(T_{i+1} - T_i) + \Gamma_{i-1,i}(T_i - T_{i-1}) \\ = -\epsilon g_{1,i}(T_i - T_0) + \epsilon\theta g_{2,i}. \end{aligned} \tag{12.3}$$

While this equation may look like a simple discretization of Eq. (12.27), there is a crucial difference coming from the probability distribution of the link conductances. An 'insulating' link of length ℓ has conductance $\Gamma_{\rm ins}(\ell) = \Gamma_0 e^{-\ell/a}$ with a being a microscopic scale. Close to

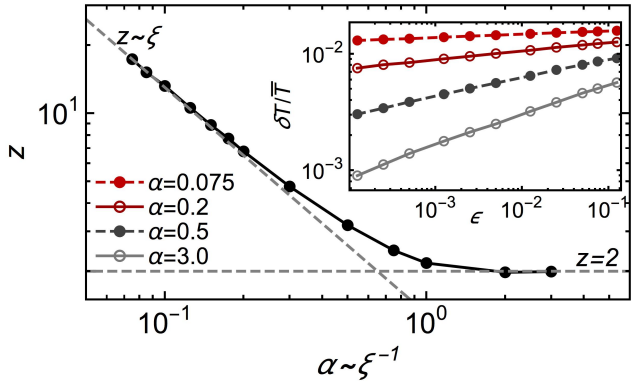


Figure 12.1: Fluctuations of the local temperatures, $\delta T/\bar{T}$, are computed from a resistor network model as function of the coupling strength ϵ to a thermal bath and driving. For small ϵ, temperature fluctuations are described by $\delta T/\bar{T} \sim \epsilon^{1/2z}$ with $z \sim \alpha^{-1} = \xi/a$ for $0 < \alpha < 1$, and $z = 2$ in the diffusive regime, $\alpha > 1$. Parameters: $\kappa_0 = 1$, $a\Gamma_0 = 5.0$, $T_0 = 1$, $\delta g_1 = 0.05$, $\delta g_2 = 0.05$, $\theta = T_0$, $N = 1000$, averaged over $M = 500$ configurations.

the critical point we expect the lengths distribution of insulating regions to be $p(\ell) = \frac{1}{\mathcal{N}} e^{-\ell/\xi}$ with ξ the diverging correlation length, leading to the distribution of link conductances $P(\Gamma) \sim (\Gamma/\Gamma_0)^{\alpha-1}$ with $\alpha = a/\xi \ll 1$. In this case the average resistivity of the chain $\langle \Gamma^{-1} \rangle$ diverges, indicating sub-diffusive transport [40, 21].

Coupling this system to a bath and to an energy source destroys the insulating behavior of the links, adding a channel of conductance through the link with conductivity $\epsilon\kappa_0$. Thus we take the heat conductance through a link to be $\Gamma = \epsilon\frac{\kappa_0}{\ell} + \Gamma_0 e^{-\ell/a}$, with an implicit cutoff $\ell \geq a$. Finally we take $g_{1(2),i} = \bar{g} + \delta g_{1(2),i}$ with $\delta g_{1(2),i}$ drawn from a uniform distribution in the range $[-\delta g_{1(2)}, \delta g_{1(2)}]$.

We solve for the steady state of Eq. (12.3) numerically to obtain temperature profiles and extract the normalized variation of local temperatures $\delta T/\bar{T} = \sqrt{\langle\langle \mathrm{Var}(T_i) \rangle\rangle}/\langle\langle \mathbb{E}(T_i) \rangle\rangle$. Here $\mathbb{E}$ and Var are the sample mean and variance, while $\langle\langle \cdot \rangle\rangle$ denotes averaging over disorder realizations. We assumed that the conducting islands are all of similar size.

The results for $\delta T/\bar{T}$ as a function of ϵ are shown in Fig. 12.1 for different values of $\alpha = a/\xi$. We get $\delta T \sim \epsilon^{1/2z}$ as anticipated in Eq. (12.2). We see that for $0 < \alpha < 1$ the dynamical exponent grows with the correlation length as $z \sim 1/\alpha = \xi/a$, whereas for $\alpha > 1$ it saturates to $z = 2$, as expected for a diffusive system. Thus we establish a direct relation between the leading dependence of the temperature fluctuations δT on ϵ and the dynamical exponent z, which governs the sub-diffusive behavior in a closed system [41, 42].

Before proceeding we comment on the behavior of the thermal resistor network in two dimensions. It is shown in the SM that in this case we have $\delta T \sim \epsilon^{d/4}$, implying $z = 2$ for all α. This is also the expected dynamical behavior in a two dimensional closed system because any rare region with large resistance can be short circuited by surrounding smaller resistors [43].

Charge transport – In solid state systems it is usually much easier to measure charge transport than the local temperature profile. It is therefore natural to seek signatures of MBL or the Griffiths regimes in the resistance of a weakly open system. In order to compute how the resistance scales with the external bath or drive coupling ϵ we consider a charge resistor network described by

$$\partial_t n_i - \left(\tilde{\Gamma}_{i,i+1}(\mu_{i+1} - \mu_i) - \tilde{\Gamma}_{i-1,i}(\mu_i - \mu_{i-1})\right) = 0. \tag{12.4}$$

Here μ_i is the electro-chemical potential on island i. $\tilde{\Gamma}_{i,j}$ are charge conductances on links, which are distributed exactly as the thermal conductances in Eq. (12.3). Unlike in Eq. (12.3),

there are no source or sink terms because the external coupling to the bath and the drive are assumed to conserve charge. In fact, we can consider a system with just a drive or just tunable coupling to phonons. Both give rise to a parallel channel of ohmic conductivity proportional to ϵ on the insulating links, $\tilde{\Gamma}(\ell) = \tilde{\Gamma}_0 e^{-\ell/a} + \epsilon\sigma_0/\ell$. Comparing the first and second term we see that the insulating behavior dominates for $\ell < \ell_* \approx a \ln \epsilon^{-1} + a \ln\ln \epsilon^{-1}$, while the bath or drive induced conductance dominates in longer links. To gain analytic insight we calculate the average resistivity of the chain, $\bar{\rho} = \bar{\ell}^{-1} \int d\ell P(\ell) \tilde{\Gamma}(\ell)^{-1}$,

$$\bar{\rho} \approx \frac{1}{\bar{\ell}\tilde{\Gamma}_0} \int_a^{\ell_*} d\ell \xi^{-1} e^{\ell(a^{-1}-\xi^{-1})} \approx \frac{\alpha}{\bar{\ell}\tilde{\Gamma}_0} \left(\frac{\epsilon}{\ln \epsilon^{-1}}\right)^{\alpha-1} \tag{12.5}$$

where $\alpha = a/\xi \sim 1/z$ and $\bar{\ell} = \int \mathrm{d}\ell P(\ell)\ell \sim \xi$. A numerical solution confirms this result, see SM. Thus it should be possible to measure the dynamical exponent z by varying the coupling ϵ via controlled cooling of the phonon bath or by varying the strength of an external drive.

Numerical solution of a spin model – Consideration of weakly open driven systems suggests a new approach for investigating the MBL transition numerically. Here we calculate how the local temperature variations in a spin-chain model change with the coupling to a weak drive that brings the system to a non-thermal steady state. The coherent part of the dynamics is governed by the Hamiltonian

$$H = \sum_i S_i \cdot S_{i+1} + h(\zeta_i^z S_i^z + \zeta_i^x S_i^x) \tag{12.6}$$

with open boundary conditions and disorder fields drawn uniformly from the range $\zeta_i^{x,z} \in [-1, 1]$. For simplicity we have chosen a model in which energy is the only conserved quantity. The MBL transition in the Hamiltonian (12.6) has been studied in Ref. [44] using exact diagonalization.

To obtain a non-equilibrium steady state we model weak coupling of the system to non-thermal baths within a Lindblad formalism:

$$\dot{\rho} = -i[H, \rho] + \epsilon \sum_{\nu,i} \left(L_i^\nu \rho L_i^{\nu\dagger} - \frac{1}{2}\{L_i^{\nu\dagger} L_i^\nu, \rho\} \right). \tag{12.7}$$

with the Lindblad operators

$$\begin{aligned} L_i^{\pm,1} &= \frac{S_i^\pm}{2\sqrt{2}} \left(\mathbb{1} - 2S_{i+1}^z\right), \; L_i^{\pm,2} = \left(\mathbb{1} - 2S_i^z\right) \frac{S_{i+1}^\pm}{2\sqrt{2}}, \\ L_i^z &= S_i^z. \end{aligned} \tag{12.8}$$

The precise choice is not important as long as some of the dissipators are non-Hermitian to ensure a non-trivial steady state, $\rho_\infty \neq \mathbb{1}$. In particular, we show in the SM. that a generic Lindblad equation leads to the hydrodynamic Eq. (12.27) for the smooth temperature variations.

The (unique) steady state ρ_∞ is obtained by solving the Lindblad time evolution using the time-evolving block decimation (TEBD) technique for a vectorized density matrix [45, 46]. The dephasing term L_i^z, Eq. (12.8), is used to ensure that the steady state is sufficiently close to the identity, so that a bond dimension of $\chi = 100$ is adequate to describe a system of $N = 20$ sites for $\epsilon \geq 0.01$. A larger bond dimensions and longer propagation times are needed for smaller ϵ, making computation in these cases more expensive, see SM. At fixed h, the same set of disorder configurations is used for different values of ϵ, while independent configurations are used at different values of h. This procedure helps to determine the exponent z as the ϵ dependence becomes less affected by the statistical ensemble. We average over 100 ($h = 1, 2$) or 300-500 ($h > 2$) disorder configurations.

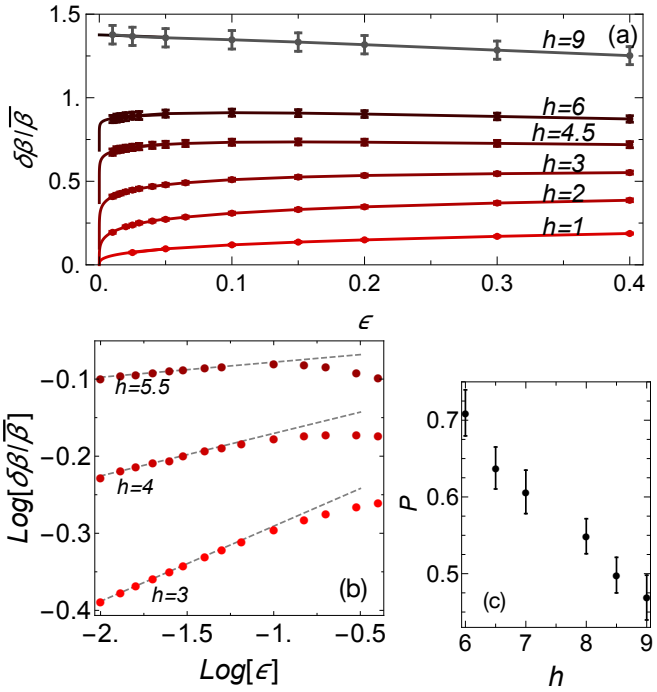


Figure 12.2: *Numerical Time Evolving Block Decimation results* – (a) The fluctuations of the inverse temperature, $\delta\beta/\bar{\beta}$, show two distinct dependences on ϵ: while they vanish proportionally to $\epsilon^{1/2z}$ on the ergodic side of the phase diagram, they obtain a finite value for $\epsilon \to 0$ with a linear correction in the MBL phase. Errorbars show (a correlated) statistical error, while line correspond to the fits. (b) Fits (dashed lines) to $\delta\beta/\bar{\beta}$ are used to obtain $z(h)$ shown in Fig. 12.3. (c) We estimate $h_c \approx 8.75 \pm 0.5$ from the condition that at h_c the probability P for $\delta\beta/\bar{\beta}$ to have a positive slope at smallest ϵ equals $P = 0.5$. That is, at h_c the sign of the slope is undetermined.

The goal of the calculation is to obtain the spatial variation of the local temperature for varying values of the dissipative coupling ϵ. To determine the local temperatures T_i we compare the two-site reduced density matrix of the steady state $\rho_\infty^{(i,i+1)}$ with a thermal state [47] by minimizing $F[T_i] = \mathrm{Tr}\left[\left(\rho_\infty^{(i,i+1)} - \rho_{\mathrm{th}}^{(i,i+1)}(T_i)\right)^2\right]$ with respect to T_i. We chose two sites as the minimal cluster that contains the non-local couplings in the Lindblad equation.

The inverse temperature variations $\delta\beta/\bar{\beta}$, obtained numerically as a function of ϵ, are shown in Fig. 12.2 for a range of disorder strengths. We observe different ϵ dependence in the MBL and ergodic phase, namely

$$\frac{\delta\beta}{\bar{\beta}}(\epsilon) \sim \begin{cases} \epsilon^{1/2z}, & h < h_c, \\ \frac{\delta\beta}{\bar{\beta}}\big|_{\epsilon\to 0} - b\,\epsilon + \mathcal{O}(\epsilon^2), & h \geq h_c \end{cases} . \tag{12.9}$$

In the MBL phase we see temperature variations of order one even in the limit $\epsilon \to 0$ as predicted in Ref. [[18]]. At finite ϵ we expect an analytic dependence on ϵ due to the local nature of the MBL phase. In the thermal regime, the temperature variations are expected to vanish in the limit $\epsilon \to 0$ [18]. We see an increase of the temperature variations with ϵ that fits well with the expected non-analytic behavior $\delta\beta/\bar{\beta} \sim \epsilon^{1/2z}$ at small values of ϵ, see Fig. 12.2(b). The fitted dynamical exponent z, shown in Fig. 12.3, changes continuously with disorder strength, growing rapidly as the MBL transition is approached. Error bars in Fig. 12.2c and Fig. 12.3 were obtained using bootstrap and jackknife resampling, respectively. The usage of a resampling methods for error estimates is necessary because statistical errors for different ϵ at fixed h are strongly correlated in our setup. As discussed above, the dynamical exponent is expected to diverge together with the correlation length ξ at the MBL critical point. The

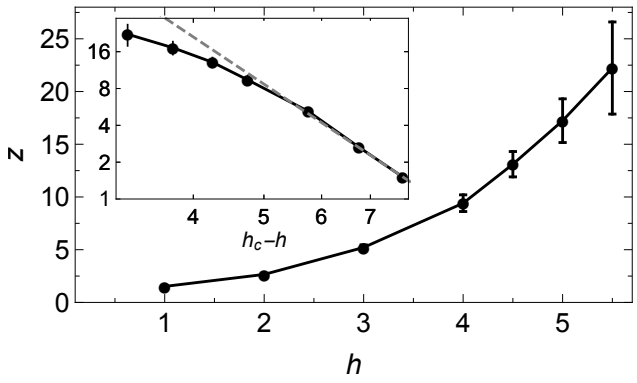


Figure 12.3: The dynamical exponent z increases sharply upon approaching the MBL phase transition. The apparent saturation is due to limitation to $\epsilon \geq 0.01$. Inset: z as function of $h_c - h$ on log-log scale assuming $h_c = 8.75$. Using $h_c = 8.75 \pm 0.5$, our results are consistent with $z \sim (h - h_c)^{-\nu}$ with critical exponent $\nu = 4 \pm 0.9$ (dashed line).

apparent saturation of z is an artifact of the fit procedure and not a finite-size effect; it is impossible to fit a small γ to the function ϵ^γ for realistic values of $\epsilon \gtrsim 0.01$. Thus the minimal value of ϵ limits the accuracy by which we can determine the critical disorder strength and the critical exponents. See SM for a systematic finite-size analysis and other numerical aspects.

We obtain a lower bound on the critical disorder strength h_c by recording the fraction P of disorder realizations showing $\delta\beta/\bar{\beta}$ increasing with ϵ near $\epsilon = 0.01$, Fig. 12.2(c). The estimation of h_c is also limited by the minimal $\epsilon = 0.01$ as h_c may increase somewhat if we use a smaller ϵ. From condition $P = 0.5$ we estimate $h_c \geq 8.75 \pm 0.5$ for $N = 20$, higher than the value $2 < h_c < 7$ estimated from an ED study of the same model [44]. This is consistent with recent analyses suggesting that ED results significantly underestimate h_c due to slow convergence of level spacing statistics [15, 16, 17]. Broadening of levels by the dissipative coupling appears to resolve these issues.

We extract a correlation length exponent ν from the divergence of $z \sim \xi \sim (h_c - h)^{-\nu}$. Using $h_c = 8.75 \pm 0.5$, we estimate $\nu \approx 4.0 \pm 0.9$, which is consistent with the Harris-Chayes bound, $\nu > 2/d$ [48, 49] and in agreement with single parameter scaling fits to renormalization group results [41, 42]. But we caution that when using $\epsilon \geq 0.01$ we can reliably fit an exponent only in the range $h \in [1, 4]$, not very close to the critical disorder strength. Based on our current data we cannot exclude Kosterlitz-Thouless like scaling with $z \sim \xi \sim e^{c/\sqrt{h_c - h}}$ as suggested by recent works [50, 51].

It is an interesting question how the "order parameter" $\delta\beta/\bar{\beta}$ behaves at the critical point itself $h = h_c$ in the limit $\epsilon \to 0$. Our results are consistent with a jump across the transition, but they also leave open the possibility of a logarithmic behavior as $-1/\log\epsilon$, which would allow a continuous change of $\delta\beta/\bar{\beta}$ across the transition.

Discussion – We have demonstrated the advantages of investigating the MBL transition as a function of the coupling strength ϵ to external non-equilibrium baths. In numerical computations, the finite coupling to baths limits the operator entanglement entropy allowing to use powerful matrix-product operator methods on both sides of the phase transition. We were able to obtain quantitative information on quantum critical properties, including the dynamical exponent z, the correlation length exponent ν and the critical disorder strength h_c. Moreover, having a weak coupling to the baths seems to regulate the calculation by broadening the many-body energy levels facilitating faster convergence to the asymptotic scaling limit. We also obtain a lower bound on h_c, which is much larger than h_c found by direct analysis of ED results [44]. This is consistent with recent analyses [15, 16, 17], which suggests that h_c is significantly

underestimated by ED studies.

Our numerical scheme is scalable in terms of the calculated spatial size. The limiting factor, instead, is the timescale imposed by the minimal value of the dissipative coupling ϵ. For the system size to dominate the critical scaling, the time $1/\epsilon$ would have to grow at least exponentially with L. This is a fundamental limitation stemming from the exponential dynamical scaling that characterizes the critical point.

Our approach to extract MBL from steady-state measurements in driven open systems is complementary to approaches studying the dynamics after a quench [4, 52] and opens the door to more experiments with solids in spite of the coupling to phonons. The non-equilibrium conditions discussed in the main text can be achieved by driving the system externally either with light, or with a bias voltage. Coupling strength to the environment would be tuned, e.g., by modulating the phonon temperature and the power of the light source. Local temperatures variations can be measured, for example by comparing the Stokes and Antistokes response in a local (tip-enhanced) Raman spectroscopy experiment [53, 54]. Another possibility would be a simpler resistivity measurement, where the dependence of the resistivity on the strength of coupling to phonons can also provide crucial information on the MBL transition.

12.2 Supplementary material

12.2.1 Fractional diffusion

In this section, we use the formalism of fractional calculus [56, 57] in order to generalize the hydrodynamic Eq. (1) to describe the sub- and super-diffusive case. The key idea is to modify the Green's function $G(\boldsymbol{r})$, describing the response of temperature fluctuations to a random pump and drive $\delta g(\boldsymbol{r})$ (recall that $\delta T(\boldsymbol{r}) = \epsilon\theta \int d\boldsymbol{r}' G(\boldsymbol{r}-\boldsymbol{r}')\delta g(\boldsymbol{r}')$), by replacing the Laplace operator ∇^2 with the Riesz fractional derivative ∇^z. The fractional derivative is defined via its Fourier transform $\mathcal{F}$,

$$\mathcal{F}\left(\boldsymbol{\nabla}^z y(\boldsymbol{r})\right) = -|k|^z \mathcal{F}(y(\boldsymbol{r})),\ z>0, \tag{12.10}$$

where $y(\boldsymbol{r})$ is an inifnitely differentiable function. Hence, the generalized continuity equation gives rise to the following Green's function in momentum space

$$G(\boldsymbol{k}) = \frac{1}{\bar{\gamma}|k|^z + \bar{g}\epsilon}. \tag{12.11}$$

Uncorrelated disorder $\langle \delta g(\boldsymbol{r})\delta g(\boldsymbol{r}')\rangle = (\delta g)^2\delta(\boldsymbol{r}-\boldsymbol{r}')$ gives the following scaling of temperature fluctuations with the dimension d and fractional power z

$$\begin{aligned}\langle \delta T^2\rangle &= \frac{\epsilon^2\theta^2}{L}\int G(\boldsymbol{r}-\boldsymbol{r}')G(\boldsymbol{r}-\boldsymbol{r}'')\langle \delta g(\boldsymbol{r}')\delta g(\boldsymbol{r}'')\rangle d\boldsymbol{r}d\boldsymbol{r}'d\boldsymbol{r}'' \\ &= \frac{\epsilon^2\theta^2\delta g^2}{(2\pi)^d}\int d\boldsymbol{k}\frac{1}{(\bar{\gamma}|k|^z+\epsilon\bar{g})^2} \\ &\sim \frac{\theta^2\delta g^2}{\bar{g}^2}\frac{\bar{g}^{d/z}}{\bar{\gamma}^{d/z}}\frac{(z-d)}{z^2\sin(d\pi/z)}\epsilon^{d/z},\end{aligned} \tag{12.12}$$

which is the result quoted in Eq. (2).

12.2.2 Diffusive behavior in two dimensions

In this section we generalize the random resistor model, used to describe the sub-diffusive behavior in the Griffiths regime of one dimensional systems, to the case of a two dimensional

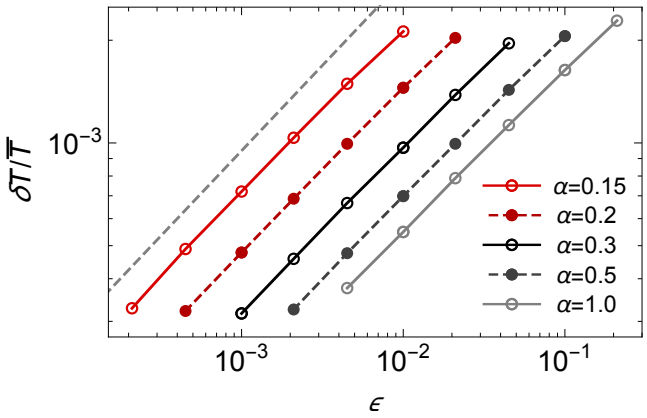


Figure 12.4: Fluctuations of the local temperatures, $\delta T/\bar{T}$ as function of the coupling strength ϵ to non-thermal baths, computed from a two-dimensional resistor network model with conductances (12.13) distributed as in Eq. (12.14). For $\epsilon \to 0$, a diffusive behavior with temperature fluctuations described by $\delta T/\bar{T} \sim \epsilon^{d/2z}$ with $z = 2$ is observed for all α. The gray dashed line shows $\delta T/\bar{T} \sim \epsilon^{1/2}$ for comparison. Parameters: $\kappa_0 = 1$, $a\Gamma_0 = 5.0$, $T_0 = 1$, $\delta g_1 = 0.05$, $\delta g_2 = 0.05$, $\theta = T_0$ $N \times N$ system with $N = 100$. Averaging over 500 configurations is performed.

system. We will show how diffusive behavior emerges in this model throughout the thermal phase as long as the correlation length associated with the transition remains finite.

Our two dimensional toy model consists of a square lattice of conducting islands connected by insulating links of linear length ℓ taken from a probability distribution $p(\ell) \sim e^{-(\ell/\xi)^2}$ (and generally in d dimensions $p(\ell) \sim e^{-(\ell/\xi)^d}$). This takes into account that in higher dimensions insulating regions are harder to construct than in one dimension because they can be short circuited by conducting paths. Conductances across the links are given by

$$\Gamma = \epsilon \frac{\kappa_0}{\ell^{2-d}} + \Gamma_0 e^{-\ell/a}, \quad \alpha = \frac{a}{\xi}. \tag{12.13}$$

This relation between the conductance and the link size implies a probability distribution of conductances that decays faster than any power law:

$$P(\Gamma) \sim \frac{1}{\Gamma} e^{-\alpha^d \left(\ln\left(\frac{\Gamma_0}{\Gamma}\right)\right)^d} \qquad \text{for} \quad \Gamma \gg \epsilon \frac{\kappa_0}{a^{2-d}}. \tag{12.14}$$

This contrasts with the power-law distribution obtained in one dimension $P(\Gamma) \sim (\Gamma_0/\Gamma)^{1-\alpha}$.

Fig. 12.4 shows temperature fluctuations as a function of coupling strength to the environment ϵ for $d = 2$. For all values of ξ we see a dependence $\delta\beta/\bar{\beta} \sim \epsilon^{1/2}$ consistent with diffusive behavior $z = 2$. This is in contrast to one dimension where we observed a continuously varying dynamical exponent $z \sim \xi/a$. This observation confirms the expectation [43] that Griffiths effect are absent in $d > 1$ where insulating regions cannot serve as bottlenecks, but are rather short-circuited by surrounding smaller resistivities.

12.2.3 Current dependence on the dynamical exponent

As an alternative to temperature fluctuations, we proposed in the main text, a setup that is driven via a small bias at the edges. In the bulk, the system is still coupled to phonons but not necessarily driven. The information about the dynamical exponent is in this case contained in the dependence of the current on the strength of coupling to the thermal phonon bath.

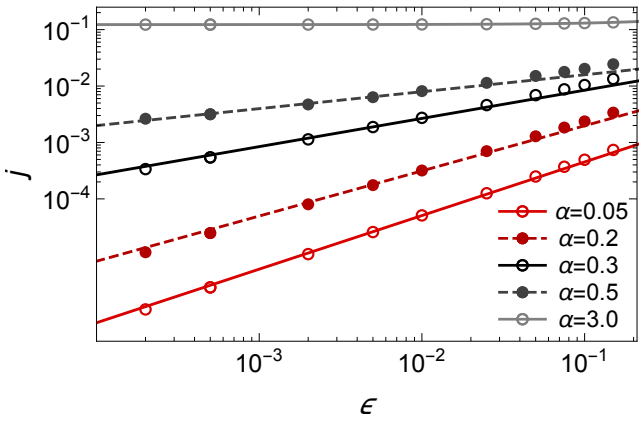


Figure 12.5: Dependence of particle current j on the strength of coupling to the baths ϵ in $d = 1$. For $\alpha < 1$, $j \sim \epsilon^{1-\alpha}$ is observed. For diffusive $\alpha > 1$, on the other hand, a finite $j(\epsilon \to 0)$ is observed. Parameters: $\sigma_0 = 1$, $a\tilde{\Gamma}_0 = 5.0$, $N = 2000$, $V = 0.1N$

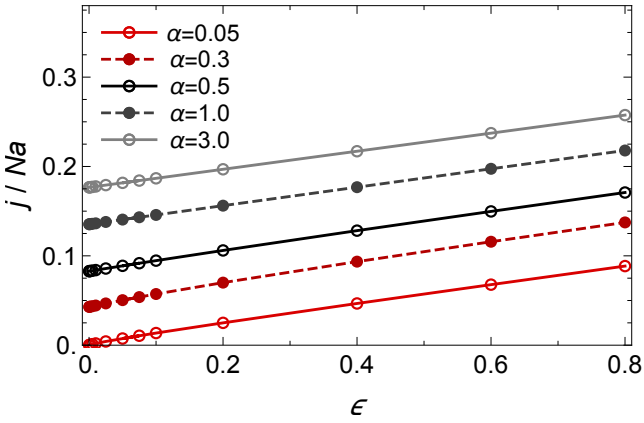


Figure 12.6: In $d = 2$ dimension, current density j/Na shows a similar behavior as the $d = 1$ diffusive case ($\alpha > 1$) and can be, to a good approximation, fitted with $c_1 + \epsilon c_2$. Parameters: $a\tilde{\Gamma}_0 = 5$, $\sigma_0 = 1$, system of $N \times N$ sites for $N = 100$, $V = 0.1N$.

The average resistivity, obtained by taking an ensemble average of the local conductances, was $\bar{\rho} \sim (\epsilon/\ln \epsilon^{-1})^{\alpha-1}$, where $\alpha = a/\xi \sim 1/z$.

In this section we compute the resistance of the network in one and two dimensions, obtained through numerical solution of the steady state rate equations. In the one dimensional case, for example, Kirchoff's law is

$$\left(\tilde{\Gamma}_{i,i+1}(\mu_{i+1} - \mu_i) - \tilde{\Gamma}_{i-1,i}(\mu_i - \mu_{i-1})\right) = 0. \tag{12.15}$$

In this case we set up a voltage bias across the chain $V = \mu_0 - \mu_N$, then solve for the island chemical potentials μ_i to get the current. As in the thermal case, we draw the link sizes along the chain from the distribution $p(\ell) \sim e^{-(\ell/\xi)^d}$, while the link conductances are:

$$\tilde{\Gamma} = \epsilon \frac{\sigma_0}{\ell^{2-d}} + \tilde{\Gamma}_0 e^{-\ell/a} \tag{12.16}$$

In the two dimensional case we set up a constant chemical potential $\mu = V$ on the left edge and a constant $\mu = 0$ on the right edge.

The result of the calculation of the current in a one dimensional chain for the case $\alpha < 1$ is shown in Fig. 12.5. The result agrees well with the analytic prediction for the resistance scaling

as $\epsilon^{\alpha-1}$, which was obtained in the main text up to logarithmic corrections. In the diffusive regime ($\alpha > 1$), the current has a non-zero $\epsilon \to 0$ limit, as we expect for a system with finite intrinsic resistivity. Also in two dimension we always find a finite resistivity in the $\epsilon \to 0$ as well as linear corrections, as shown in Fig. 12.6.

Remember that the dynamical exponent is related to α as $z \sim \alpha^{-1}$. Measuring the dependence $j(\epsilon, \alpha)$ in a disordered system would therefore provide information on z and it's divergence upon approaching the MBL transition even in disordered materials that are weakly coupling to phonons. The strength of coupling to phonons ϵ can be tuned by controlling the phonon temperature; see our previous work [18], where we showed that phonon temperature determines the effective coupling.

12.2.4 Comparison to standard measures of dynamical scaling

In this section we verify that the dynamical exponent z obtained from the temperature variations, through the relation $\delta T \sim \epsilon^{d/2z}$ is identical to the standard measure of dynamical scaling obtained from spreading of an energy fluctuation. To obtain the standard measure of z we consider an initially localized energy profile in the random resistor network $e_i = \delta_{i,x_0}$. We determine z by measuring the width of the energy packet $\sigma_E = \sqrt{\sum_i (i - x_0)^2 \tilde{e}_i(t)}$ and fitting it to a power law $\sigma_E \sim t^{1/z}$. Here $\tilde{e}_i(t) = \langle\langle e_i(t) \rangle\rangle$ is a disorder averaged energy distribution. For each realization of the disorder $e_i(t)$ is calculated using the continuity equation with $\epsilon = 0$:

$$\partial_t e_i - \Gamma_{i,i+1}(T_{i+1} - T_i) + \Gamma_{i-1,i}(T_i - T_{i-1}) = 0 \tag{12.17}$$

Note that here $\Gamma = \Gamma_0 e^{-\ell/a}$. Fig. 12.7 shows a qualitative agreement between the value of z obtained via these two different approaches.

12.2.5 Convergence in system size, time and bond dimension

In this section, we look more closely into what are the limiting factors of the calculation. We first investigate how our results on system size $N = 20$ depend on the bond dimension. Fig. 12.8 shows the relative change of the expectation value of $O = \delta\beta/\beta(\epsilon)$ with bond dimension χ at steady state. We set $\chi = 100$, used for the results in the main text, as a baseline. $O(\chi)$ is averaged over 60 disorder realizations, which are the same for different χ. We find that the error

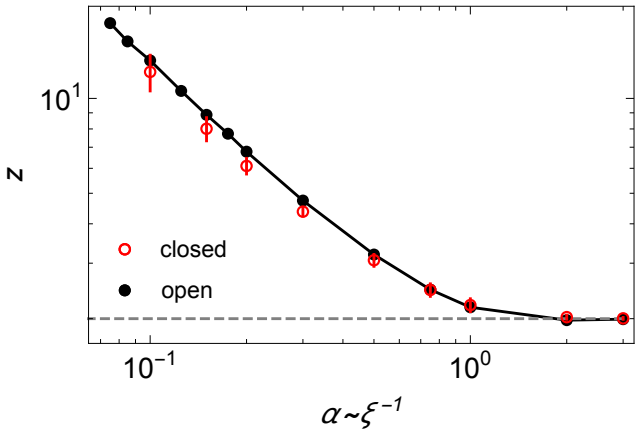


Figure 12.7: Comparison of the dynamical exponent z calculated from the fluctuations of the local temperatures (open) or from the from anomalous heat diffusion in a closed system (closed). Parameters: $\kappa_0 = 1$, $a\Gamma_0 = 5.0$, $T_0 = 1$, $\delta g_1 = 0.05$, $\delta g_2 = 0.05$, $\theta = T_0$, $N = 1000$, averaged over $M = 500$ configurations.

extrapolated to $\chi = \infty$ is small, e.g., for $h = 4$ below 0.1%. We also note that the extrapolated error estimate grows with decreasing ϵ, hence for smaller values of ϵ a larger bond dimension will be required, increasing the costs of computations at small ϵ.

In Fig. 12.9 we show the relaxation of temperature fluctuations $O(t) = \frac{\delta\beta}{\beta}(t)$ to steady state

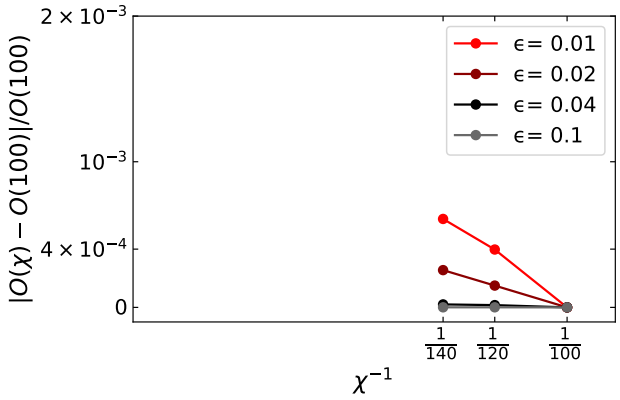


Figure 12.8: Relative error due to finite bond dimension $\chi = 100$ can be estimated from the ratio $|O(\chi) - O(\chi = 100)|/O(\chi = 100)$, $O(\chi) = \frac{\delta\beta}{\beta}(\chi)$. The error estimated from the $\chi \to \infty$ extrapolation is below 0.1% for smallest $\epsilon = 0.01$ used in our computations. Parameters: $N = 20$, $h = 4$, with averaging over 60 realizations.

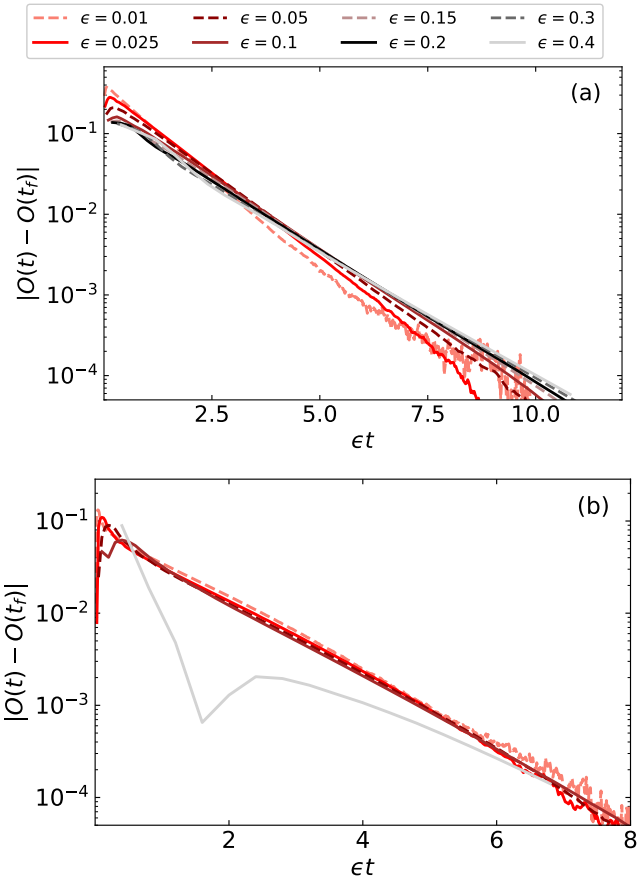


Figure 12.9: Evolution of $O(t) = \frac{\delta\beta}{\beta}(t)$ (with respect to $O(t_f)$ at maximal propagation time t_f) during the TEBD computation, for one disorder realization at $h = 4$, $\chi = 100$, for systems of size (a) $N = 20$ and (b) $N = 40$. Note that the time axis is rescaled by ϵ to reveal an exponential relaxation with a convergence rate proportional to ϵ.

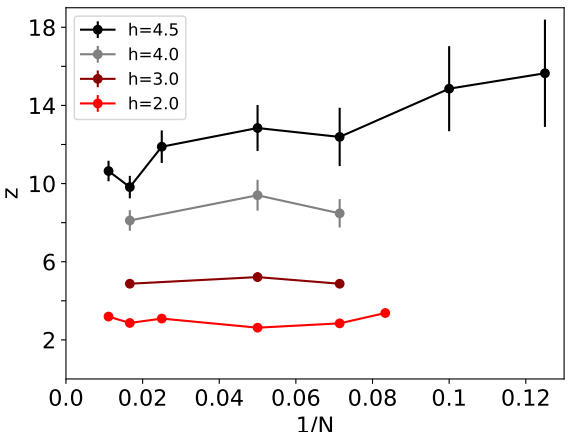


Figure 12.10: Finite-size analysis of the dynamical exponent z for $h = 2.0, 3.0, 4.0, 4.5$. Calculations are performed with bond dimension $\chi = 100$ and $\epsilon \geq 0.01$. A different number of realizations is used for different points, e.g., at $h = 2.0$ and $N \in [12, 90]$, $150 - 50$ realizations are used, for $h = 4.5$ and $N \in [8, 90]$, $790 - 190$ realizations are used. Fit error bars are obtained with the jackknife resampling of data with $\epsilon \geq 0.01$ and do not estimate systematic deviations from the z that would be obtained using $\epsilon < 0.01$, necessary for $h > 4$.

in the TEBD time evolution. Specifically, we plot $|O(t) - O(t_f)|$ with respect to the $O(t_f)$ at the maximal propagation time t_f. As expected, we see exponential relaxation to the steady-state value with a characteristic rate which scales as ϵ. Obtaining results for smaller ϵ is thus increasingly hard with TEBD.

Assuming that the necessary bond dimension χ is independent of system size, our approach should be scalable, with computational demands growing linearly with system size. Figs. 12.9(a,b) compare the convergence of $O(t) = \frac{\delta\beta}{\beta}(t)$ for a single realization at $N = 20, 40$ system sizes. While the computational time approximately doubles, the exponential convergence rate with TEBD evolution time t is comparable.

Finally, we present a finite size scaling analysis of the results. We show the dependence of the dynamical exponent z, obtained from our numerical scheme, on the system size. The exponent z is extracted by fitting a power law for the dependence of the temperature variance on ϵ with $\epsilon \geq 0.01$, Eq.(9) in the main text. The results are shown in Fig. 12.10.

In systems with disorder strengths $h = 2.0, 3.0, 4.0$ we do observe negligible finite size dependence. Recall that this is the range of h we used to extract the power law divergence of $z \sim (h_c - h)^{-\nu}$ on approaching the critical point. It is encouraging to see that this behavior is unaffected by finite size. We do see a non systematic finite size dependence for disorder strength $h = 4.5$, which we attribute to uncertainty in fitting the dynamical exponent z. Indeed, as noted in the main text, for $h > 4$ ($z > 8$) we can no longer extract a reliable power law fit to $\frac{\delta\beta}{\beta} \sim \epsilon^{\frac{1}{2z}}$ in the range $\epsilon \geq 0.01$. In order to reliably obtain larger values of z close to the critical point one would have to reduce the cutoff ϵ exponentially in z (equivalently, in ξ). Thus it is the finite time cutoff $(1/\epsilon)$ rather than the finite size, which limits the calculation.

As noted in the main text, calculations performed at smaller ϵ might yield somewhat larger h_c as well, which would, in turn, impact the value of ν obtained from $z \sim (h_c - h)^{-\nu}$ fit.

12.2.6 Hydrodynamic equations as an expansion of Lindblad driving

In the main text we introduced the hydrodynamic approach as an effective description of a

system that is coupled to a thermal (e.g. phonon) bath and to a drive (e.g. white light). Here we make the connection to the microscopic calculation, that was performed for a spin chain coupled to Markovian nonequilibrium baths described by Lindblad operators. We show that the hydrodynamic Eq. (1) can be derived using an expansion in small temperature variations around the thermal density matrix, determined from the Liouville equation $\dot{\rho} = (\hat{\mathcal{L}}_0 + \epsilon\hat{\mathcal{D}})\rho = 0$, where $\hat{\mathcal{L}}_0\rho = -i[H, \rho]$ and $\hat{\mathcal{D}}$ corresponds to the dissipator super-operator.

On the ergodic side, the system approaches a thermal state for $\epsilon \to 0$ [18]. For small epsilon, we can therefore expand the steady state density matrix in weak temperature variations around the thermal state

$$\rho \approx \rho_0(\bar{T}) + \sum_j \delta T_j \frac{\partial \rho}{\partial T_j}\Big|_{T_j=\bar{T}} + \cdots, \quad \rho_0(\bar{T}) \equiv \frac{e^{-H/\bar{T}}}{\mathrm{Tr}[e^{-H/\bar{T}}]} \tag{12.18}$$

We will now use the expansion (12.18) in order to show how the phenomenological terms in Eq. (1) can emerge from the microscopic Liouville equation.

First of all, the term $-\epsilon\bar{g}(T(\boldsymbol{r}) - \bar{T}))$ ensures the relaxation towards the correct mean temperature $\bar{T}$, which is determined from the stationarity condition applied to the total rate equation for the energy [18],

$$\langle \dot{H} \rangle = \mathrm{Tr}[H(\hat{\mathcal{L}}_0 + \epsilon\hat{\mathcal{D}})\rho_0(\bar{\beta})] = \mathrm{Tr}[H\,\epsilon\hat{\mathcal{D}}\,\rho_0(\bar{\beta})] \stackrel{!}{=} 0 \tag{12.19}$$

To see the emergence of the other terms in Eq. (1) we consider the behaviour of the local energy density $\langle h_i \rangle$, where $H = \sum_i h_i$,

$$\begin{aligned}
\frac{d}{dt}\langle h_i \rangle =& \mathrm{Tr}\left[h_i \hat{\mathcal{L}}_0 \rho\right] && (12.20)\\
&+ \mathrm{Tr}\left[h_i \epsilon\hat{\mathcal{D}}\rho_0(\bar{\beta})\right] && (12.21)\\
&+ \mathrm{Tr}\left[h_i \epsilon\hat{\mathcal{D}} \sum_j \frac{\partial\rho}{\partial T_j}\Big|_{T_j=\bar{T}} \delta T_j\right] && (12.22)\\
&+ \cdots
\end{aligned}$$

Using the definition for the energy currents, $j_{i,i+1} = i[h_i, h_{i+1}]$, we can see that the right hand side of expression (12.20) equals to the difference in expectation value of energy currents across neighboring links. On the other hand, in a system with spatially varying local temperatures, local current expectation values are proportional to local temperature gradients

$$\begin{aligned}
\mathrm{Tr}\left[h_i \hat{\mathcal{L}}_0 \rho\right] &= \mathrm{Tr}[(-j_{i,i+1} + j_{i-1,i})\rho] && (12.23)\\
&= \Gamma_{i,i+1}(T_{i+1} - T_i) - \Gamma_{i-1,i}(T_i - T_{i-1})\\
&\sim \nabla \cdot (\kappa(\boldsymbol{r})\nabla T(\boldsymbol{r})) && (12.24)
\end{aligned}$$

The term (12.21) corresponds to the gain and loss of local energy density due to the driving and dissipation, evaluated with respect to the homogeneous thermal state

$$\mathrm{Tr}\left[h_i \epsilon\hat{\mathcal{D}}\rho_0(\bar{\beta})\right] \sim \epsilon\,\theta g_2(\boldsymbol{r}). \tag{12.25}$$

Here $\langle g_2(\boldsymbol{r}_i)\rangle = \frac{1}{\theta N}\sum_i \mathrm{Tr}[h_i\hat{\mathcal{D}}\rho_0(\bar{\beta})] = 0$ due to Eq. (12.19).

Term (12.22) is of the same type, but comes from the next order expansion in the variation of local temperatures

$$\mathrm{Tr}\left[h_i \epsilon\hat{\mathcal{D}} \sum_j \frac{\partial\rho}{\partial T_j}\Big|_{T_j=\bar{T}} \delta T_j\right] \sim \epsilon g_1(\boldsymbol{r})\,\delta T(\boldsymbol{r}) \tag{12.26}$$

Collecting the dominant terms in the $(\delta T(\boldsymbol{r}))^n$ expansion, we get the hydrodynamic relation

$$\partial_t e - \nabla \cdot (\kappa(\boldsymbol{r})\, \nabla T(\boldsymbol{r})) = -\epsilon\, g_1(\boldsymbol{r})(T(\boldsymbol{r}) - \bar{T}) + \epsilon\, \theta g_2(\boldsymbol{r}) \tag{12.27}$$

which can be identified with Eq. (1), except that T_0 is replaced by $\bar{T}$ (set by Eq. 12.19) and that the last term contains only the random part with a zero mean, i.e., $g_2(\boldsymbol{r}) = \delta g_2(\boldsymbol{r})$.

13 Transport in Stark Many Body Localized Systems by Zisling, Kennes, et al.

Abstract

Using numerically exact methods we study transport in an interacting spin chain which for sufficiently strong spatially constant electric field is expected to experience Stark many-body localization. We show that starting from a generic initial state, a spin-excitation remains localized only up to a finite delocalization time, which depends exponentially on the size of the system and the strength of the electric field. This suggests that bona fide Stark many-body localization occurs only in the thermodynamic limit. We also demonstrate that the transient localization in a finite system and for electric fields stronger than the interaction strength can be well approximated by a Magnus expansion up-to times which grow with the electric field strength.

Introduction.—Statistical mechanics assumes that isolated, interacting systems with many degrees of freedom always approach the state of thermal equilibrium. More than a decade ago, it was argued that in the presence of a sufficiently strong disorder, this assumption can be defied, using a mechanism known as many-body localization (MBL) [357, 359, 3, 356, 5, 6, 7]. If such systems are isolated from the environment they will never thermalize. Perfect isolation from the environment is challenging in conventional condensed matter systems due to inevitable presence of phonons [8, 9], however evidence of MBL was obtained in numerous experiments in cold atoms in both one-dimensional [10, 11, 12] and two-dimensional systems [13]. While coupling to an external environment or a noise source is detrimental to MBL [14, 15], it was shown to be stable to periodic driving at sufficiently high frequencies. A phenomenon known as Floquet–MBL [16, 17, 18, 19].

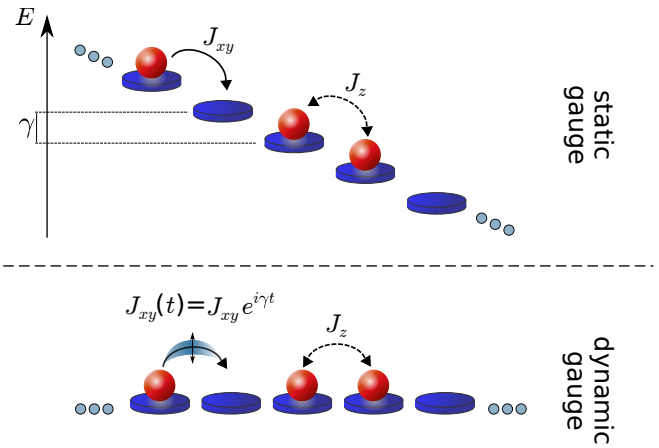


Figure 13.1: A schematic representation of the Stark localization problem in two gauges. The upper panel shows the static gauge, where particles are subject to a tilted potential. The bottom panel shows a dynamic gauge, where the scalar potential is written as a "vector potential," which produces time-dependent hopping.

Theoretical arguments in favor of MBL require the localization of all the single-particle states [357, 367]. For quenched disorder this requirement is naturally satisfied in one and two-dimensional systems due to Anderson localization [21]. Various attempts to relax this requirement were performed by considering models where some of the single-particle states are delocalized [22, 23, 24, 25, 26, 27, 28, 29], as also translationally invariant models where all of the states are delocalized in the absence of interactions [376, 31, 32, 33, 375, 35, 36, 37, 38, 28]. However, the observed localization is far from being convincing and typically suffers from severe finite-size effects [36]. Moreover, while some of these models show robust localization for special initial states, most initial states are apparently delocalized [376, 28].

Anderson localization is not the only mechanism which can be used to localize the single-particle states. Single-particle states can be localized by a periodic-in-time, spatially uniform electric field at certain drive frequencies [39, 40], and also by a static uniform electric field and any field strength [41]. The former is known as dynamic localization, and the later as Wannier-Stark localization. While it was shown that dynamic localization is not stable to the addition of interactions [42], Wannier-Stark localization was argued to be stable to interactions for sufficiently strong electric fields [43, 44], a phenomenon dubbed Stark-MBL. Via a gauge change, constant electric field can be replaced by a time-dependent vector potential (see Fig. 13.1). Therefore the Stark problem is equivalent to a periodically driven translationally invariant interacting model; see Eq. (13.3). The mechanism behind Stark-MBL is currently under debate, since many of the arguments of Refs. [357, 367] cannot be readily applied due to proliferation of resonances, which are known to induce asymptotic delocalization in certain cases [45]. It was proposed that Stark-MBL follows from an approximate "shattering" of the Hilbert space due to an almost-conservation of the dipole moment [44, 46, 47]. This argument is however applicable only for an infinite electric field, γ, where jumps between sites are prohibited due to energy conservation (see Fig. 13.1), and cannot be easily generalized for finite and modest electric fields where the Stark-MBL transition ostensibly occurs [43, 44, 48].

The dynamics in both localized and delocalized phases was studied theoretically [43, 44, 49, 50] and experimentally [51, 52, 53] starting from special initial states. Two-dimensional systems are delocalized and show subdiffusive transport [51, 49]. For one-dimensional systems and sufficiently strong electric fields both charge-density wave (CDW) [43, 44, 52, 53] and domain-walls initial states [50] do not appear to melt completely. In fact in Ref. [50] it was argued that the system is localized in the thermodynamic limit, for any nonzero electric field, though Ref. [54] suggested that this is a special property of domain-wall initial states.

In this Letter, we consider the nonequilibrium dynamics in a one-dimensional Stark-MBL system starting from a generic initial state, which corresponds to an average over all possible initial states. We demonstrate that in both presumably delocalized, and localized regions, a local spin excitation remains localized for increasingly long times when the system size is increased, suggesting that transport might be completely suppressed only in the thermodynamic limit.

Model.—The interacting Stark model is described by the following Hamiltonian,

$$\hat{H} = \sum_{j=1}^{L-1} \frac{J_{xy}}{2} \left(\hat{S}_j^+ \hat{S}_{j+1}^- + \text{h.c.} \right) + J_z \hat{S}_j^z \hat{S}_{j+1}^z + \sum_{j=1}^{L} W_j \hat{S}_j^z, \tag{13.1}$$

where L is the length of the spin-chain, "h.c." denotes the hermitian conjugate, $\hat{S}_j^{\pm}$, $\hat{S}_j^z$ are spin-1/2 operators, J_{xy} is the strength of the flip-flop term, J_z is the strength of the Ising term, and $W_j = (\gamma j + \alpha j^2/L^2)$ is a spatially varying potential, where γ corresponds to an electric field, α/L^2 is the magnitude of a shallow parabolic trap that we add in order to break some of the symmetries of the system, following Ref. [43]. The system conserves the total magnetization, $\hat{M} = \sum_j \hat{S}_j^z$ and in the thermodynamic limit is translationally invariant (for $\alpha = 0$). Through

this work we use open boundary conditions and set $J_{xy} = 2$, $J_z = 1$ and $\alpha = 0.5$, verifying that our results do not change qualitatively for other αs and J_zs, as also boundary conditions (see [48]). Via the Jordan-Wigner transformation [55], the model is equivalent to a system of spinless interacting fermions moving in a uniform electric field, however for the clarity of the presentation we proceed using the spin formalism.

A number of works show an apparent ergodicity breaking for $\gamma \gtrsim 1.5$ [43, 44] (see also [48]). In this Letter, using two numerically exact methods we study spin-transport in this model.

Methods.—

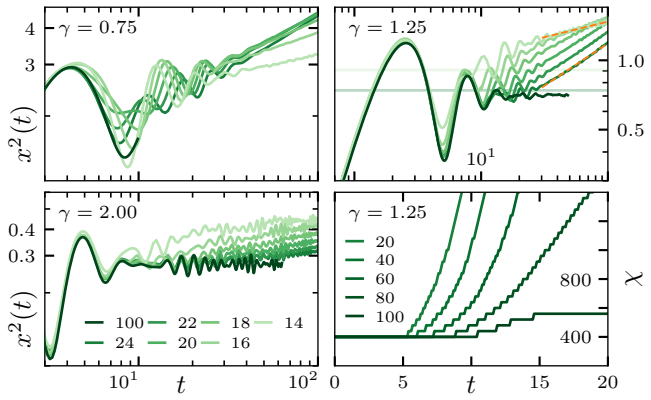


Figure 13.2: Mean-square displacement (MSD) as a function of time (top panels and bottom left) for $L \in [14, 24]$ (Krylov based method) and $L = 100$ (tDMRG). The orange dotted line correspond to power-law fits, while the horizontal lines indicate the plateau of the MSD calculated by taking the mean of the MSD between the 2nd and the 3rd peaks. The color of the plateau lines matches the coloring of the corresponding system size. Bottom right. Bond dimension, χ as a function of time obtained using tDMRG for $L \in [20, 100]$ and with a fixed discarded weight 10^{-7}. All plots were obtained for $J_{xy} = 2$, $J_z = 1$ and $\gamma = 1.25$.

To assess spin-transport in the system for various electric fields, γ, we calculate the infinite temperature spin-spin correlation function,

$$G_n(t) = \frac{1}{\mathcal{N}} \mathrm{Tr}\left[\hat{S}^z_n(t)\, \hat{S}^z_{L/2}\right], \tag{13.2}$$

where $\mathcal{N}$ is the Hilbert space dimension, and $\hat{S}^z_n(t)$ is the Heisenberg evolution of $\hat{S}^z_n$. This correlation function describes the spatial spreading of an initially local spin excitation on top of an infinite temperature state. The squared width of the excitation, is given by, $x^2(t) = \sum_n n^2 \left(G_n(t) - G_n(0)\right)$ and is analogous to the mean-square displacement (MSD). For diffusive transport, $x^2 \sim 2Dt$, with D coinciding with the diffusion coefficient calculated from the corresponding Kubo formula [56, 57, 58, 59].

We compute $G_n(t)$ using two complementary numerically exact methods. In the first method we work at a zero magnetization sector, with the Hilbert space dimension $\mathcal{N} = \binom{L}{L/2}$ and utilize dynamical typicality to reduce the trace in Eq. (13.2) to a unitary propagation of a random initial state taken from the Haar distribution [60, 58]. We then average over a small number of such samples. Our initial condition therefore corresponds to a generic initial state with volume law entanglement. We would like to stress that while the generation of such a highly entangled pure state is probably close to impossible experimentally, we could equally well take a random product state, which can be realized experimentally. Such a state would produce an equivalent result, though it would require more averaging over the initial states to to sample the correlation function in Eq. (13.2).

The unitary evolution is performed using a Krylov subspace method [61]. Given the exponential scaling of the Hilbert space dimension we are able access system sizes of $L \lesssim 24$, which correspond to $\mathcal{N} \leq 2\,704\,156$, though we can propagate the system for quite long times. As a complimentary method, which provides us access to large systems sizes, we use the time-dependent density matrix renormalization group (tDMRG) [62]. In this method the wavefunction is represented as a matrix product state (MPS), built of matrices with a maximal dimension χ, called the bond-dimension. The bond-dimension sets the maximum entanglement that the MPS can accommodate. If the bond dimension is set to be smaller than $\chi < d^{L/2}$, where d is the local Hilbert space dimension, the error in the MPS representation of the wavefunction is bounded by the truncation weight. In our simulations, we set the truncation weight to 10^{-7} allowing the bond dimension to grow dynamically during the propagation. Since for ergodic systems the entanglement is typically increasing linearly with time, the computational effort increases exponentially. We checked for converges of our results by decreasing the truncation weight to 10^{-8}. In tDMRG we use all magnetization sectors, and obtain $G_n(t)$ by the Heisenberg evolution of $\hat{S}^z_n(t)$, using the computational method detailed in Ref. [63]. Due to the equivalence between the ensembles of fixed and varying magnetization, in the thermodynamic limit, both Krylov based and tDMRG results are expected to agree up to some finite time when the finite size effects become important.

Results.—We calculate the MSD for a number of electric fields, $\gamma = 0.75 - 3$ and various system sizes $L = 14 - 24$ using the Krylov subspace method, and for sizes $L = 20 - 100$ using tDMRG. The results are presented in Fig. 13.2. For times $t \leq t^\star(\gamma, L)$ an initial growth of the MSD is followed by a localization plateau. This plateau is visible for $\gamma \gtrsim 1$, and becomes even more pronounced for larger system sizes. For all the studied γ's, including a regime where according to Refs. [43, 44] (see also [48]) the system is expected to be strongly localized, the late-time dynamics of a finite system is always delocalized, which allows us to identify the time $t^\star(\gamma, L)$, as the delocalization time. Note that our data suggests, that for $\gamma \gtrsim 1$ the system becomes localized only in the thermodynamic limit. The observed, apparently subdiffusive growth of the MSD for $t > t^\star(\gamma, L)$, which is consistent with previous experimental [51] and theoretical works [64, 65, 66, 54], is therefore a finite-size effect, and will not be considered further in this Letter (see however [48]). For $\gamma \leq 1$ our results are not conclusive, since the delocalization time, if it exists here, is very short, and the plateau in the MSD is not clearly visible. But, we do see that for $\gamma = 0.75$ the fast growth of the MSD is pushed to later times for larger system sizes, which hints that localization at the thermodynamic limit might occur for all $\gamma > 0$. A similar suggestion was recently raised in Ref. [50].

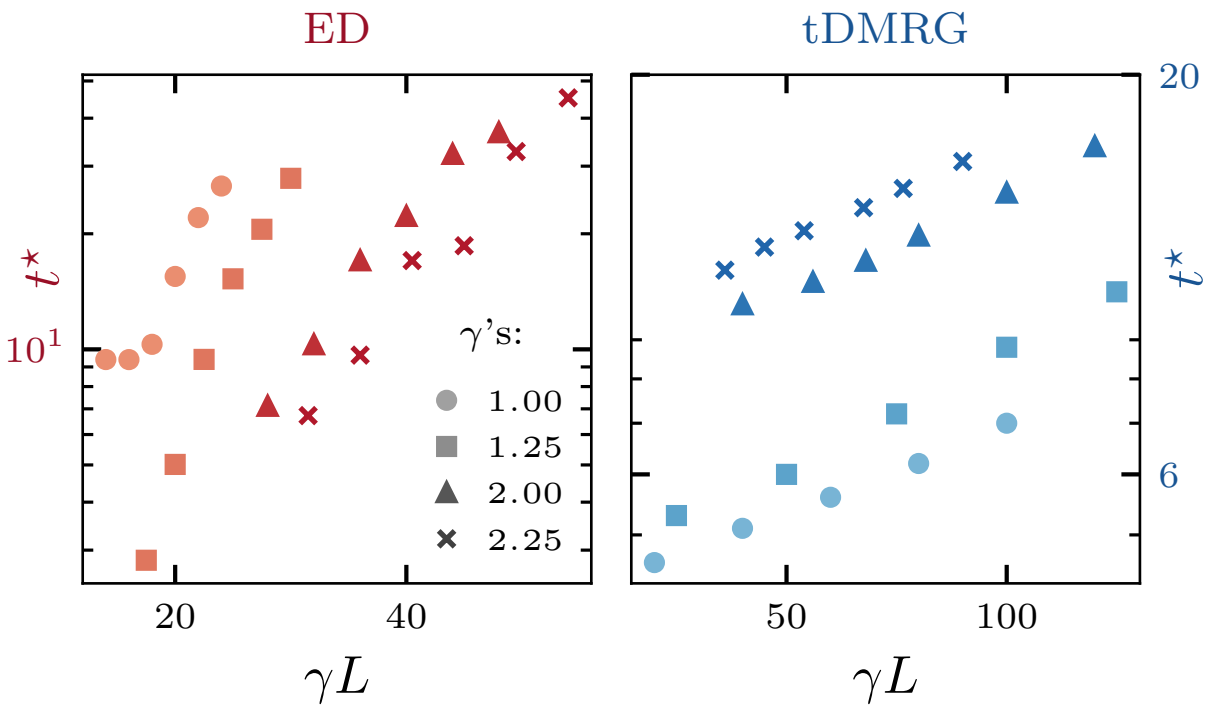


Figure 13.3: Delocalization time $t^\star$ as a function of γL for $\gamma = 1, 1.25, 2, 2.25$, as extracted from Krylov based method (left panel, $L \in [14, 24]$) and tDMRG (right panel, $L \in [20, 100]$). For all data points $J_z = 1$.

The localization–delocalization transition at a finite time, $t^\star(\gamma, L)$, can also be seen from the growth of the bond-dimension in tDMRG to maintain a chosen accuracy of the results (discarded weight). For $t \leq t^\star(\gamma, L)$ a modest bond-dimension is required, while for $t > t^\star(\gamma, L)$ to keep the same accuracy of the numerical evolution an increasingly larger bond-dimension is required. We stress that the bond-dimension is not a physical quantity and we only use it as an indicator of delocalization to obtain, $t^\star(\gamma, L)$[1].

To quantitatively study the dependence of $t^\star(\gamma, L)$ on γ and L, we extract it using two independent methods. For the Krylov subspace method it is extracted from the intersection point between two straight lines on a log-log scale: the plateau of the MSD (see caption in Fig. 13.2) and the apparent subdiffusive growth (dashed orange lines in Fig. 13.2). For tDMRG we define $t^\star(\gamma, L)$ as the time when the bond-dimension departs from its initial value (set to 400). While these definitions are of-course arbitrary, using different definitions did not result in a qualitative change. In Fig. 13.3 we show the delocalization time, $t^\star(\gamma, L)$ plotted vs γL on a semi-log scale for various tilts of the potential γ. We find that both Krylov subspace and tDMRG methods, suggest that the delocalization time increases exponentially both with γ and L, namely $t^\star \sim \exp[\gamma L]$, such that true localization is obtained only in the thermodynamic limit. Remarkably, the tDMRG simulation of this system becomes easier, namely with the same computational resources for larger system sizes one can go to longer times. This indicates a change in the bulk dynamics, when the size of the system is increased, even though the Hamiltonian is local.

[1]The entanglement entropy here would be an entanglement of an MPO, which is also not a measurable physical quantity

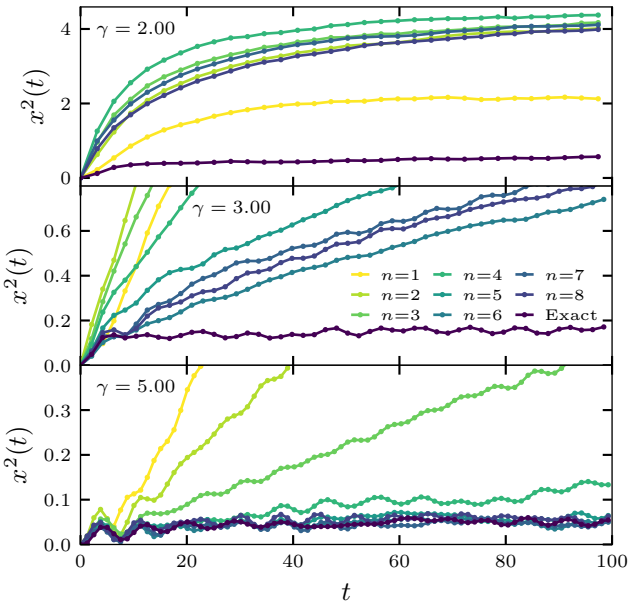


Figure 13.4: Mean-squared displacement as a function of time for various electric fields. The darkest lines correspond to numerically exact results obtained by using Eq. (13.3) for propagation. The colored lines with increasing brightness corresponds to evolution using effective Hamiltonians Eq. (13.4), obtained from a truncated Magnus expansion. For all panels, $J_{xy} = 2,\ J_z = 1,\ L = 14$.

Magnus expansion.—In order to better understand the dependence of $t^\star(\gamma, L)$ on γ we apply a time-dependent unitary transformation $\hat{U}(t) \equiv e^{-i\gamma t \sum_j j \hat{S}^z_j}$ to Eq. (13.1), which corresponds to a gauge change, replacing the potential term in Eq. (13.1) by a time-dependent "vector potential." This yields the following time-dependent Hamiltonian,

$$\hat{H}(t) = \sum_{j=1}^{L-1} \left[\frac{J_{xy}}{2} \left(e^{-i\gamma t} \hat{S}^+_j \hat{S}^-_{j+1} + \text{h.c.} \right) + J_z \hat{S}^z_j \hat{S}^z_{j+1} \right], \tag{13.3}$$

where the electric field, γ, takes the role of a frequency. The static part of the Hamiltonian is trivially localized and has a spectrum composed of highly degenerate energy bands, which differ by a number of domain walls. It takes an energy of $J_z/4$ to annihilate or create a domain wall, and therefore the bands are equally spaced. The time-dependent hopping facilitates transport in the system by two possible processes: either by connecting the various bands, or by higher order, virtual transitions from some state in a band to a different state in the same band. For $\gamma \gg J_z/4$ both processes are suppressed since multiple spin rearrangements are required to absorb the energy of the "photon" and the system is expected to be in a long-lived prethermal state described by the time-averaged Hamiltonian (which here coincides with the static part of $\hat{H}(t)$) up to times $t^\star \sim \exp[\gamma/J_z]$ [68, 69, 70]. A slightly different scaling was suggested in Ref. [47]. We have checked that for larger J_z, the apparent localization–delocalization transition shifted to larger γs [48].

The stroboscopic evolution of the system is determined by an effective Hamiltonian, which is defined from the one-period propagator,

$$\hat{U}(T) = \mathrm{e}^{-i\hat{H}_{\text{eff}}T} = \mathcal{T} \exp\left[-i \int_0^T \mathrm{d}\bar{t} \hat{H}(\bar{t}) \right], \tag{13.4}$$

where $\mathcal{T}$ corresponds to time-ordering, and $T = 2\pi/\gamma$ is the period. For $\gamma \gg J_z/4$ we can approximate $\hat{H}_{\text{eff}}$ by a Magnus expansion in γ^{-1} [71]. For γ smaller than the many-body bandwidth, this expansion is not guaranteed to converge, but it can approximate the dynamics of

the system up to some optimal order [72]. We use a recursive formula described in Ref. [71] to obtain $\hat{H}_{\text{eff}}$ up to order $n = 10$ for $L = 14$. Fig. 13.4 shows the stroboscopic evolution of the MSD computed numerically using $\hat{H}_{\text{eff}}^{(n)}$, which is $\hat{H}_{\text{eff}}$ truncated to an order n. We see that for $\gamma \leq 2$ the Magnus expansion fails to approximate the dynamics even for short times, while for $\gamma = 3, 5$ as the Magnus order n increases, the approximate solution approaches the exact solution for longer times (it is hard to reliably extract t_{magnus} from our data to obtain the functional dependence on n, but see Ref. [73]). There is little to no dependence of t_{magnus} on the system size (see [48]). Interestingly, the long times dynamics of $\hat{H}_{\text{eff}}^{(n)}$ is diffusive with a diffusion coefficient which decreases with n [48], even for $\gamma = 5$, where the system is expected to be strongly localized [43, 44].

Discussion.—In this Letter, using two complementary numerically exact methods, we have examined the dynamics of a spin-excitation starting from a generic initial condition in a spin-chain which is expected to exhibit Stark-MBL. For $\gamma > J_z$ we find strong evidence of a finite delocalization time, $t^\star(L, \gamma)$, which scales exponentially with both the size of the system and the electric field, namely $t^\star(L, \gamma) \sim \exp[\gamma L / J_z]$. For intermittent times $t < t^\star$ the spin-excitation is localized, while for $t > t^\star$ it delocalizes in a manner consistent with subdiffusion [51]. This strongly suggests that for $\gamma \gtrsim J_z$, Stark-MBL strictly occurs only in the thermodynamic limit, $L \to \infty$, while any finite system is ultimately delocalized for sufficiently long times. For $\gamma \leq J_z$ and system sizes and times accessible to us, the localization regime is not apparent. Nevertheless, we do see that the dynamics is delayed with increasing the system size, which can be consistent with a localization length larger than the system size $\xi(\gamma) \gg L$. It is therefore plausible to conjecture that that Stark-MBL in the thermodynamic limit occurs for all $\gamma > 0$, which is consistent with the conjecture in Ref. [50].

In the dynamic gauge, where the electric field is replaced by a periodically driven flip-flop term such that γ plays the role of the frequency, it is rigorously known that for $\gamma \gg J_z$ the heating time is exponential in γ / J_z [68, 69, 70]. We show that for sufficiently large electric fields, up to time t_{magnus}, the dynamics is well approximated by a static effective Hamiltonian obtained from a Magnus expansion truncated up to order n. This time increases with both γ / J_z and n (cf. Ref. [73]). The first order of the expansion is given by $\hat{H}_{\text{eff}}^{(1)} = J_z \sum_{j=1}^{L-1} \hat{S}_j^z \hat{S}_{j+1}^z + O(J_z / \gamma)$. The spectrum of $\hat{H}_{\text{eff}}^{(n)}$ is composed of equally space bands, $J_z/4$ distance apart, with a bandwidth of $O(J_z / \gamma)$ [48]. Therefore, for $\hat{H}_{\text{eff}}^{(n)}$ the situation is similar to models of quasi-MBL, which show asymptotic delocalization [33, 36, 45]. Indeed all $\hat{H}_{\text{eff}}^{(n>1)}$ show diffusion at long times, with a diffusion constant decreasing with n [48]. We would like to stress that the delocalization of $\hat{H}_{\text{eff}}^{(n)}$ occurs before the delocalization in Eq. (13.1) and Eq. (13.3) at time $t^\star$, and therefore Magnus expansion does not capture the delocalization regime of Eq. (13.1) and Eq. (13.3). It does suggest that the localization mechanism of Stark-MBL is probably different from Floquet-MBL, where the effective Hamiltonian is expected to be non-ergodic [16, 18].

While the analysis we provided explains the transient localization regime, it does not explain why the delocalization time increases with the size of the system, suggesting that Stark-MBL happens only in the thermodynamic limit. This conclusion remains qualitatively robust for both open and periodic boundary conditions, in the static and dynamic gauges, and with and without the parabolic potential in Eq. (13.1) [48]. A possible explanation could be that the measure of delocalized states is vanishing in the thermodynamic limit. This would also explain why localization appears to be robust for CDW and domain-wall initial states. We leave the exploration of this avenue to future studies.

13.1 Supplementary Material: Transport in Stark Many Body Localized Systems

13.1.1 Transition location

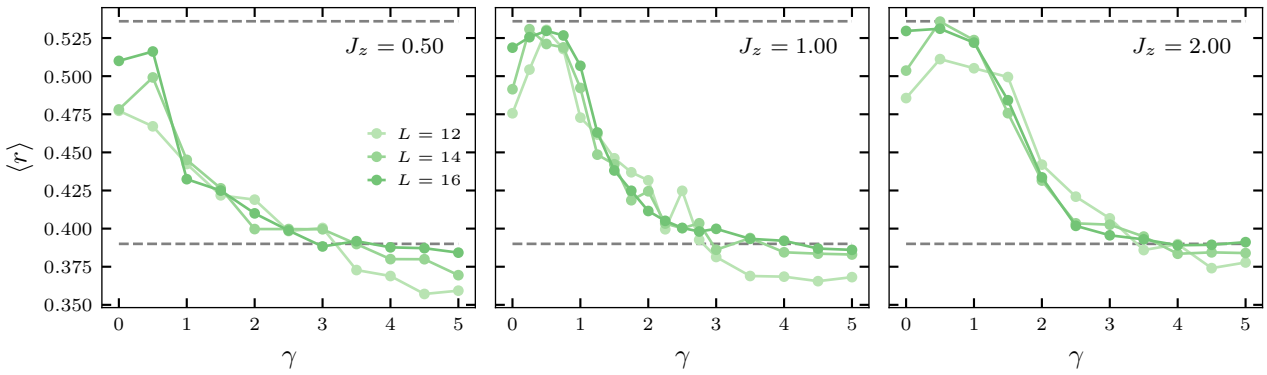


Figure 13.5: $\langle r \rangle$ as of a function of electric field strength for various interaction strengths (different panels), and system sizes. Larger system size corresponds to stronger color intensity. The black dashed lines correspond to WD statistics ($r \simeq 0.536$) and Poisson ($r \simeq 0.39$) statistics. The model parameters that were used are $J_{xy} = 2,\ J_z \in [0.5, 1, 2],\ \alpha = 0.5$.

To approximately assess the location of the Stark-MBL transition we use the standard metric,

$$r_\alpha = \min\left(\frac{s_\alpha}{s_{\alpha-1}}, \frac{s_{\alpha-1}}{s_\alpha}\right), \tag{13.5}$$

where $s_\alpha \equiv E_{\alpha+1} - E_\alpha$ are the spacing between adjacent eigenvalues of the Hamiltonian. For integrable systems the mean of this quantity ($\langle r \rangle$), is typically given by $\langle r \rangle \approx 0.39$, which corresponds to a Poissonian distribution, while for quantum chaotic systems it is $\langle r \rangle \approx 0.536$, which corresponds to Wigner Dyson distribution. In Fig. 13.5 we examine $\langle r \rangle$ as a function of the electric field strength γ for various couplings J_z. We observe a transition from a Wigner-Dyson distribution for low electric fields to a Poissonian distribution at high electric fields. The transition occurs approximately at $\gamma \approx J_z$. This analysis does not depend strongly on the size of the system, in contrast to the mean-square displacement results presented in the main text. The middle panel ($J_z = 1$) is in agreement with Ref. [44] although we have used a different mechanism to break the symmetries of the model.

13.1.2 Delocalization time extraction

In Fig. 13.6 we present the analysis used to obtain $t^\star(\gamma, L)$ in Fig. 13.3 in the main text. The mean-square displacement (MSD) shows severe finite size effects, with subdiffusive behavior delayed to later times for larger system sizes. The locations of the plateaus (green horizontal lines) are calculated by taking the mean of the MSD between the 2nd and the 3rd peaks of the MSD. We fit the late time behavior with a power-law fit, $x^2 \propto t^a$ (orange dashed lines), and estimate the delocalization time $t^\star(\gamma, L)$ by the intersection of the plateaus with the power-law fits (orange crosses).

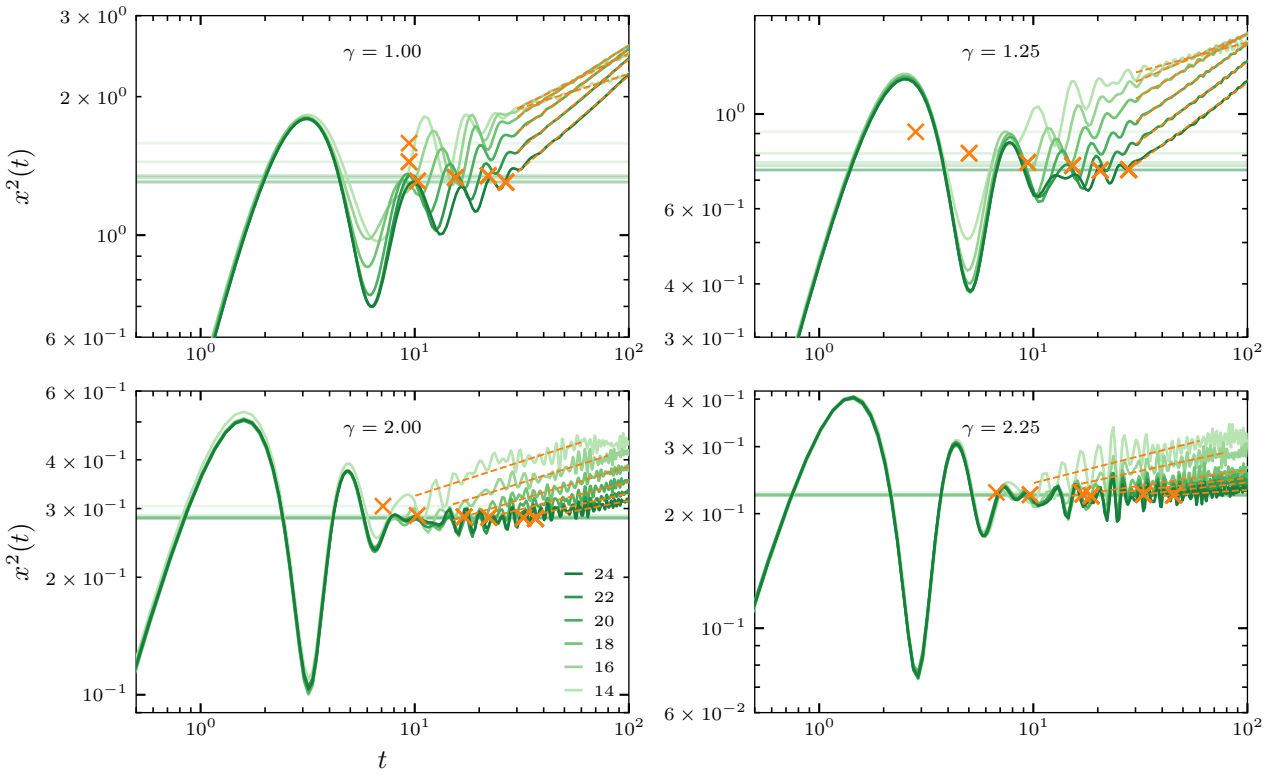


Figure 13.6: Mean-square displacement (MSD) as a function of time for $L \in [14, 24]$ (Krylov based method). The orange dashed line correspond to power-law fits ($x^2 \sim t^a$), while the horizontal lines indicate the plateau of the MSD calculated by taking the mean of the MSD between the 2nd and the 3rd peaks. The orange crosses are the estimated delocalization time $t^\star(\gamma, L)$ obtained from the intersection of the power-law fits with the plateau. The color of the plateau lines matches the coloring of the corresponding system size. All plots were obtained using $J_{xy} = 2,\ J_z = 1$.

13.1.3 Finite-size subdiffusive behavior

From the power law-fits in Fig. 13.6 we can obtain the dynamical exponent a, which corresponds to the late-time growth of the MSD, $x^2 \sim t^a$. We plot this exponent as a function of the electric field γ and for various system sizes in Fig. 13.7. One can see an apparent transition between a subdiffusive behavior ($a < 1$) to a localized behavior ($a \sim 0$), with very strong finite-size effects.While for $\gamma > J_z$ the exponent seems to converge with the size of the system, it is important to keep in mind that the onset of the subdiffusive transport is pushed to later times for larger system sizes, as one can see in the main text and in Fig. 13.6 indicating that the observed subdiffusive behavior is a finite-size effect.

13.1.4 Sensitivity to boundary conditions

In this Section we show that the conclusions of the main text are robust to changes in the gauge and the boundary conditions. In Fig. 13.8 we have calculated the MSD as a function of time, using the dynamical gauge, (13.3) in the main text for various electric fields γ (rows), various system sizes (color intensity), and two different boundary conditions (columns). We see that in the dynamic gauge the MSD shows less pronounced oscillations compared to the static gauge, allowing to spot the formation of the localization plateau already for $\gamma = 1$. The results remain qualitatively the same to the results in the static gauge (Fig.13.6), with severe finite size effects, and a delocalization time that is increasing with the system size. The quantitative

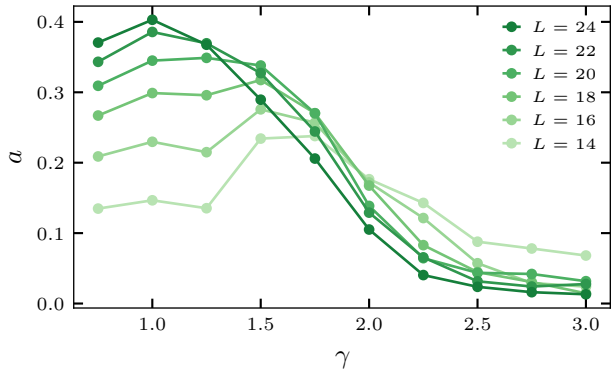


Figure 13.7: The dynamical exponent a as obtained from the fits to the MSD, $x^2 \propto t^a$ (see Fig. 13.6), as function of γ for various system sizes ($L \in [14, 24]$).

difference between open and periodic boundary conditions serves as another indication of finite-size effects, though the localization plateau for both boundary conditions appears at about the same MSD.

13.1.5 Dynamical behavior of truncated effective Hamiltonians

In this Section we study the late-times dynamical behavior of the effective Hamiltonians calculated using Magnus expansion in γ^{-1} up to some order n. In Fig. 13.9 (left column) we calculate the MSD for two electric fields (rows). We see that it develops a pronounced linear behavior, indicative of diffusion, $x^2 \sim 2Dt$, where D is the linear response diffusion coefficient. For even longer times the MSD saturates, since the system is finite. We extract the diffusion coefficient from the relevant time windows (black dashed lines in Fig. 13.9), and plot it as a function of the truncation order, n on the right column of Fig. 13.9.

The diffusion coefficient $D(\gamma, n)$ is monotonically decreasing with the order of the Magnus expansion and the strength of the electric field, approximately following $D \sim 1/n$. While this finding indicates that the truncated effective Hamiltonian is delocalized, it doesn't imply much on the original interacting Stark model, since the diffusive behavior of the effective Hamiltonian emerges for at times for which the dynamics under the effective Hamiltonian doesn't not well approximate the numerically exact dynamics. What is interesting, is that the infinite order Magnus expansion, if it is convergent, could correspond to localized dynamics.

13.1.6 Convergence criteria of the Magnus expansion

In this Section we examine the convergence of the Magnus expansion of the effective Hamiltonian,

$$\hat{H}_{\text{eff}}^{(n)} = \sum_{k=0}^{n} \hat{H}_k, \tag{13.6}$$

while each term $\hat{H}_k$ is of the order of γ^{-k}. The D'Alembert criterion of convergence is $\left\|\hat{H}_{k+1}\right\| / \left\|\hat{H}_k\right\| < 1$, where $\|.\|$ indicates the operator norm. In Fig. 13.10 we the D'Alembert criterion is presented for different electric fields, γ. We see that while for $\gamma \leq 2$ the series is divergent, for $\gamma \gtrsim 3$ is it convergent at least up to 10th order. We note that this doesn't necessarily mean that the series has a finite radius of convergence, since divergence can occur for relatively large expansions orders [73].

13.1.7 Density of states of the truncated effective Hamiltonians

The zero order truncated effective Hamiltonian, $\hat{H}^{(0)}_{\text{eff}}$ in (13.6) corresponds to the interaction term,

$$\hat{H}^{(0)}_{\text{eff}} = J_z \sum_{i=1}^{L} \hat{S}^z_i \hat{S}^z_{i+1}, \tag{13.7}$$

whose spectrum is composed of equally spaced degenerate bands, separated $J_z/4$ apart. The following terms of the expansion are of order J_z/γ, and they partially lift this degeneracy giving a width of J_z/γ to the bands. To demonstrate this in Fig. 13.11 we plot the density of states (DOS) of $\hat{H}^{(n)}_{\text{eff}}$ for a number of electric fields, γ. While the gaps are washed away for $J_z/4 < J_z/\gamma$, namely $\gamma < 4$, they become clearly visible as γ increases.

13.1.8 Finite-size analysis

In Fig. 13.12 we repeat the analysis of Fig. 13.4 from the main text for a number of system sizes, showing that there are no considerable system size dependence in the determination of t_{Magnus}, namely the time up to which there is a reasonable agreement between the MSD computed using $\hat{H}^{(n)}_{\text{eff}}$ and the MSD of the dynamical gauge Hamiltonian (13.3) in the main text.

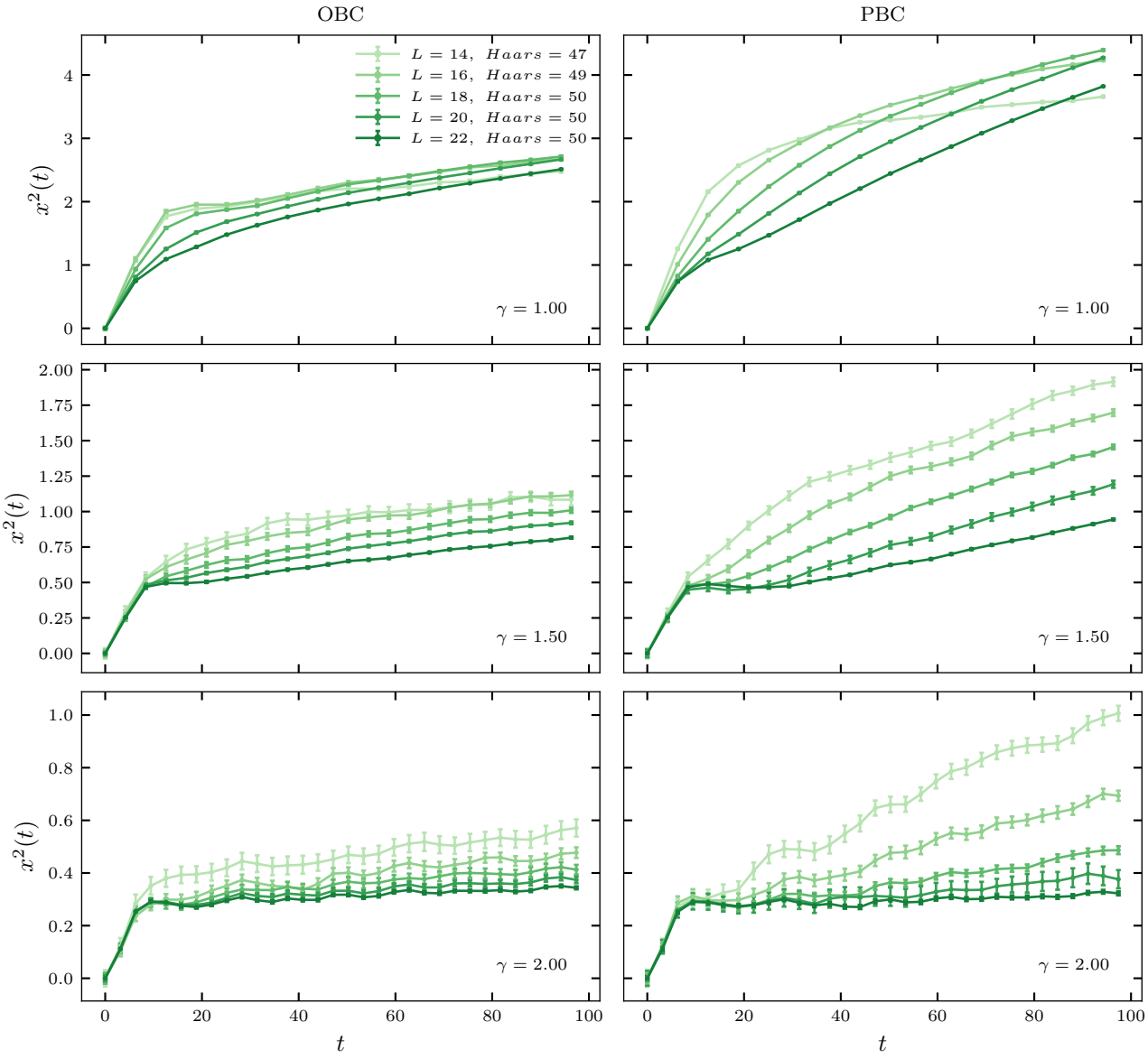


Figure 13.8: Mean-square displacement (MSD) as a function of time for $L \in [14, 24]$ (Krylov based method) calculated from the dynamic gauge (13.3) in the main text. Left column: open boundary conditions (OBC). Right column: periodic boundary conditions (PBC). Different rows have different electric fields $\gamma \in [1, 1.5, 2]$. All plots were obtained for $J_{xy} = 2,\ J_z = 1$.

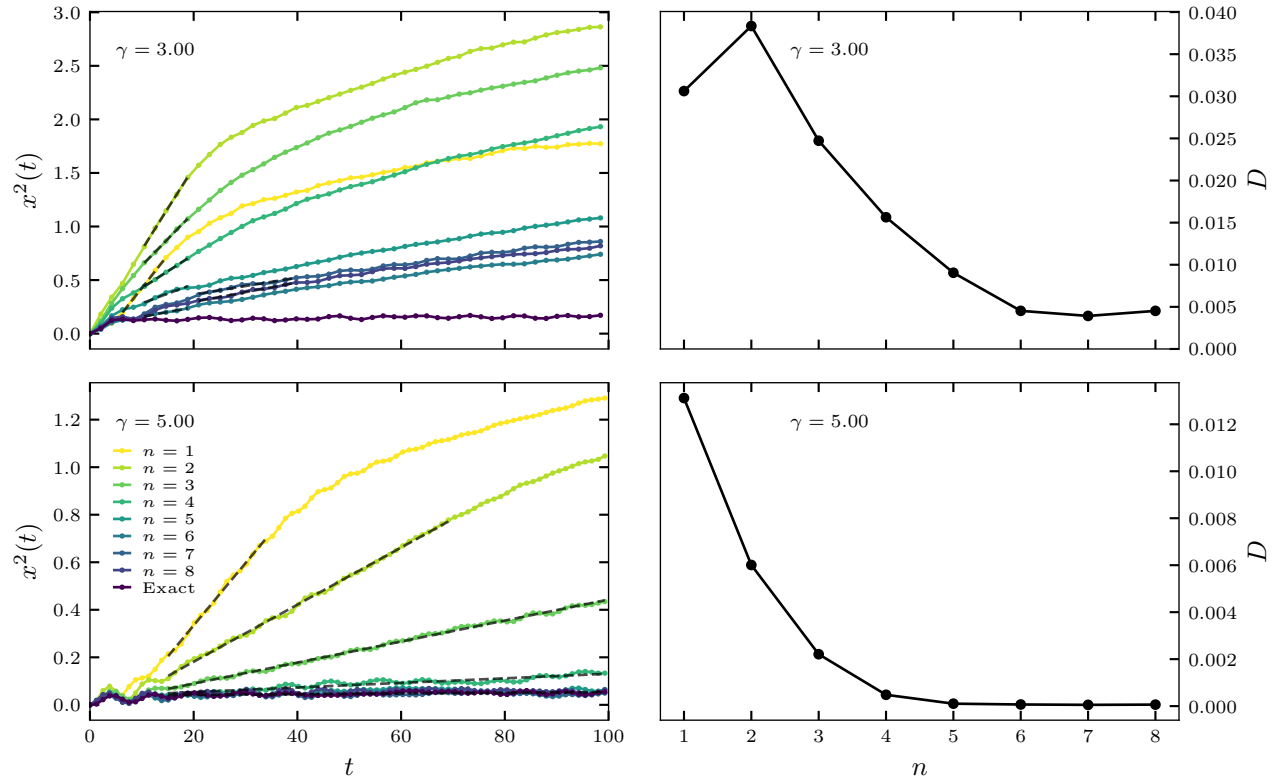


Figure 13.9: Mean-squared displacement as a function of time for two electric fields (left column). The darkest lines correspond to numerically exact results obtained using (Eq. 13.3 in the main text). The colored lines with increasing intensity corresponds to evolution using effective Hamiltonians (13.6), obtained from a truncated Magnus expansion. The black dashed lines corresponds to linear fits, $x^2 \sim 2D\,t$, and the diffusion coefficient D is plotted in the right column as function of the truncation order. For both $\gamma = 3, 5$ there is a visible trend of $D \propto 1/n$. The parameters used are, $J_{xy} = 2,\ J_z = 1,\ L = 14$.

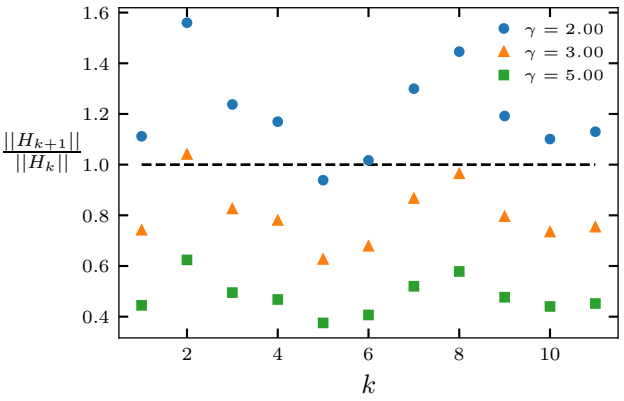


Figure 13.10: D'Alembert criterion of convergence as a function of the Magnus expansion order (k), $\left\|\hat{H}_{k+1}\right\| / \left\|\hat{H}_k\right\| < 1$ (see (13.6) for definition). Different colors (markers) represents different electric field strength $\gamma = 2, 3$ and 5. The dashed black line corresponds to a convergence requirement.. The parameters used are, $J_{xy} = 2,\ J_z = 1,\ L = 10$.

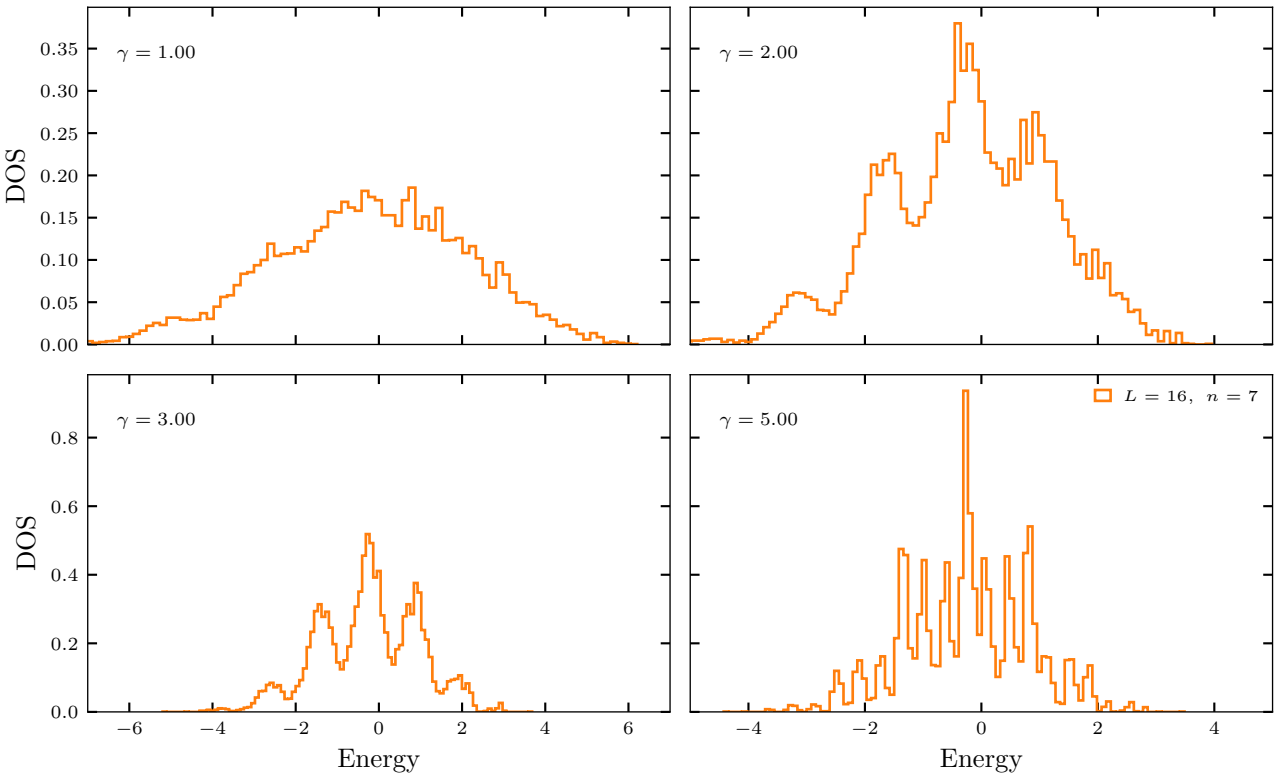


Figure 13.11: The density of states of the truncated effective Hamiltonian $\hat{H}_{\text{eff}}^{(n=7)}$ for $L = 16$ and $\gamma = 1, 2, 3$ and 5. .All plots were obtained for $J_{xy} = 2,\ J_z = 1$.

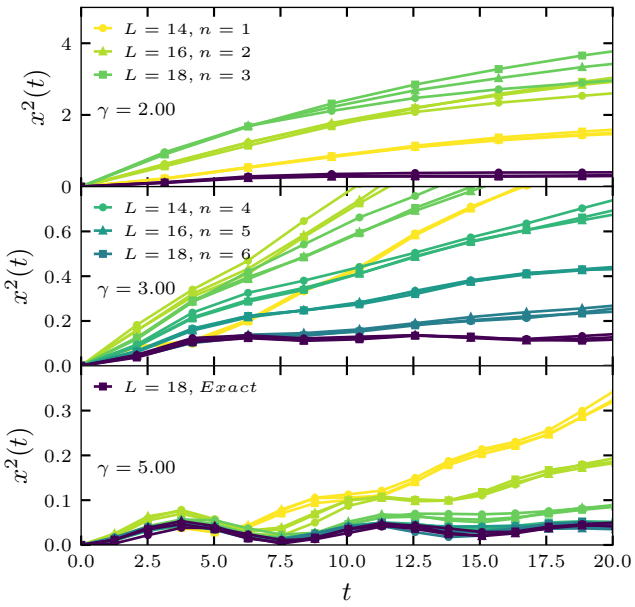


Figure 13.12: Finite size analysis of Fig. 13.4 in the main text. Mean-squared displacement as a function of time for various electric fields. The darkest lines correspond to numerically exact results obtained using (Eq. (13.3) in the main text). The colored lines corresponds to an evolution using the effective Hamiltonian (13.6), obtained from a truncated Magnus expansion. Different markers (○, ▲, ■) stand for different system sizes $L = 14, 16$ and 18, correspondingly. The used parameters are, $J_{xy} = 2,\ J_z = 1$.

14 Iterative construction of conserved quantities in dissipative nearly integrable systems by Ulčakar, Lenarčič

Abstract

Integrable systems offer rare examples of solvable many-body problems in the quantum world. Due to the fine-tuned structure, their realization in nature and experiment is never completely accurate, therefore effects of integrability are observed only transiently. One way to overcome this limitation is to weakly couple nearly integrable systems to baths and driving: these will stabilize integrable effects up to arbitrary time and encode them in the stationary state approximated by a generalized Gibbs ensemble. However, the description of such driven dissipative nearly integrable models is challenging and no exact analytical methods have been proposed so far. Here, we develop an iterative scheme in which integrability breaking perturbations (baths) determine the conserved quantities that play the leading role in a highly efficient truncated generalized Gibbs ensemble description. Our scheme paves the way for easier calculations in thermodynamically large systems and can be used to construct unknown conserved quantities.

14.1 Theory

Integrable models have played a paramount role in our understanding of nonequilibrium dynamics because, in some cases, their dynamics can be followed exactly. A modern milestones descriptions of integrable models has been the observation that the steady states reached after a sudden excitation are locally describable with a generalized Gibbs ensemble (GGE) [1, 2, 3, 4, 5]. This observation was a natural generalization of the equilibration of thermalizing generic models, where the steady state is locally described with a thermal Gibbs ensemble [6, 7]. The applicability of generalized Gibbs ensembles on a finite timescale was first established experimentally with cold atoms [8]. Recently, also spatially inhomogeneous dynamics of integrable systems was formulated using a local GGE description and generalized hydrodynamics [9, 10, 11], receiving experimental confirmations as well [12, 13, 14, 15, 16].

Due to their fine-tuned interactions, integrable models cannot be exactly realized in nature. On short to intermediate timescales, integrable models are realizable with quantum simulators [17, 18, 19] and can approximately describe some materials [20, 21, 22]. On longer timescales, additional Hamiltonian terms, such as longer range interaction in trapped ions experiment, coupling to phonons in solid state experiment, trapping potential, transverse couplings, and loss of atoms in cold atomic setups prevent integrable effects from persisting up to arbitrary times [23, 13, 12, 24]. The only way to sustain integrable effects in nearly integrable systems up to arbitrary times is to drive them out of equilibrium [25, 26, 18, 28, 29]. To prevent heating due to driving, such systems must also be weakly open. Numerical evidence shows that then the time evolution [25] as well as the steady state [26, 18, 28, 29] is again approximately described by a GGE. The equations of motion and the steady-state values for the Lagrange parameters associated with the conserved quantities entering the GGE are given deterministically by the integrability breaking perturbations, i.e., by the drive and coupling to the baths. This opens the possibility for GGE engineering [28] and stabilizing potentially technologically useful phenomena. For example, in spin chain materials, approximately described by the Heisenberg model, efficient spin and energy pumping could be realized [26]. So far, time-dependent GGE descriptions have also been used to describe the effect of particle loss in cold atoms [30, 31] and non-interacting systems coupled to baths [28, 32, 29, 33, 34, 35].

While the expanded role of GGE as a description of weakly open, nearly integrable systems is fundamentally important, in this case, concrete calculations of dynamics and steady states are

much more demanding than in isolated systems. Weak integrability breaking, which causes non-elastic scatterings and a slow reshuffling of quasiparticle content, makes the usual quasiparticle treatment of integrable models much harder; for interacting systems analytically (probably) impossible [30, 31]. One possible simplification is to approximate the GGE with macroscopically many Lagrange parameters with its truncated version. Such an approximation has been used in the context of isolated integrable systems [36, 37, 4, 38], as well as in driven dissipative, nearly integrable systems [26, 25, 28].

We propose a new iterative scheme, which adds the leading conserved quantities to the truncated GGE iteratively, as suggested by the driving and dissipation itself. Here, leading means having the main contribution to the GGE. We examine the convergence to the exact result and show that a good approximation is typically achieved within a few steps. Meaning, we have to find a solution of a few coupled equations for a few leading conserved quantities, instead of considering extensively many coupled equations for all conserved quantities. The only input for the method is the basis from which iterative conserved quantities are constructed.

Setup. We consider driven dissipative, nearly integrable setups with the dominant unitary dynamics given by an integrable Hamiltonian H_0. Weak driving and dissipation could be due to a Floquet unitary drive and coupling to a (thermal) bath; however, for simplicity, we will consider weak coupling to non-thermal Markovian baths, whose action is described by Lindblad operators L_i. As pointed out previously [26, 25, 18, 28, 29], non-static integrability breaking perturbations should stabilize a GGE generically, and the formalism described below can treat them all. The Liouville equation gives the dynamics of the density matrix operator,

$$\hat{\mathcal{L}}\rho = -i[H_0,\rho] + \hat{\mathcal{D}}\rho,\ \hat{\mathcal{D}}\rho = \epsilon \sum_i L_i \rho L_i^\dagger - \frac{1}{2}\{L_i^\dagger L_i, \rho\}, \tag{14.1}$$

where $\epsilon \ll 1$ is the strength of the coupling to baths. We will consider homogeneous coupling to baths, where Lindblad operators L_i of the same form act on every site i.

Perturbatively, the zeroth order approximation to the steady state is of a diagonal form in terms of eigenstates of H_0, $H_0|m\rangle = E_m|m\rangle$,

$$\lim_{\epsilon\to 0}\lim_{t\to\infty} \rho = \sum_m a_m |m\rangle\langle m| \equiv \rho_D. \tag{14.2}$$

Weights a_m are obtained from the kernel of the dissipator projected on the diagonal subspace [18, 39], $\sum_n D_{mn} a_n = 0$, $D_{mn} = \langle m|(\hat{\mathcal{D}}|n\rangle\langle n|)|m\rangle$. If the dissipator preserves a symmetry of the Hamiltonian, eigenstates can be taken within the symmetry sector with a unique steady state.

As suggested in our previous works [26, 25, 28, 18], for integrable H_0, the zeroth order diagonal ensemble ρ_D should be thermodynamically equivalent to a generalized Gibbs ensemble,

$$\lim_{\epsilon\to 0}\lim_{t\to\infty}\lim_{L\to\infty} \rho = \frac{e^{-\sum_m \lambda_m C_m}}{\mathrm{Tr}[e^{-\sum_m \lambda_m C_m}]} \equiv \rho_{\boldsymbol{\lambda}}, \tag{14.3}$$

where C_m are the (quasi-)local conserved quantities of the underlying integrable model, $[C_m, H_0] = 0$, and λ_m the associated Lagrange multipliers. In the steady state, the latter are determined by the stationarity conditions for all conserved quantities

$$\langle \dot{C}_{m'} \rangle = \mathrm{Tr}\left[C_{m'} \hat{\mathcal{D}} \frac{e^{-\sum_m \lambda_m C_m}}{\mathrm{Tr}[e^{-\sum_m \lambda_m C_m}]} \right] \stackrel{!}{=} 0 \quad \forall m'. \tag{14.4}$$

I.e., one must find the set of λ_m for which the flow of all conserved quantities is zero ($\stackrel{!}{=} 0$). This equation is very instructive: (i) it tells us that the form of integrability breaking

dissipators (Lindblad operators) will determine the λ_m values, and (ii) in order to find λ_m, one must solve a set of coupled non-linear equations. To reduce the complexity of step (ii), an approximate description in terms of a truncated GGE (tGGE) with a finite number of included conserved quantities has been used [26, 25, 28]. In that case, the expectation values of included conserved charges and of local operators constituting them were well captured. However, other local observables showed stronger deviations, particularly those overlapping with quasi-local conserved operators. To partially mend for that, the diagonal part of latter observables was included in the tGGE.

Also the dynamics towards the steady state can be approximated with a time-dependent GGE [25]. The equation of motion for $\lambda_m(t)$ is derived by the use of super-projector $\hat{P}$ onto slow modes, which are for the GGE Ansatz naturally given by the operators $\frac{\partial \rho_{\boldsymbol{\lambda}}}{\partial \lambda_m}$ tangential to the GGE manifold,

$$\hat{P}X = -\sum_{m,n} \frac{\partial \rho_{\boldsymbol{\lambda}}}{\partial \lambda_m} (\chi^{-1})_{m,n} \mathrm{Tr}[C_n X]. \tag{14.5}$$

Here, $\chi_{m,n} = -\mathrm{Tr}[C_m \frac{\partial \rho_{\boldsymbol{\lambda}}}{\partial \lambda_n}] = \langle C_m C_n \rangle_{\rho_{\boldsymbol{\lambda}}} - \langle C_m \rangle_{\rho_{\boldsymbol{\lambda}}} \langle C_n \rangle_{\rho_{\boldsymbol{\lambda}}}$ is the $\{m,n\}$ entry of matrix χ and $\langle O \rangle_{\rho_{\boldsymbol{\lambda}}} = \mathrm{Tr}[\rho_{\boldsymbol{\lambda}} O]$. Applying the super-projector to the slow dynamics on the GGE manifold,

$$\hat{P}\dot{\rho}_{\boldsymbol{\lambda}} = -\sum_{m,n} \frac{\partial \rho_{\boldsymbol{\lambda}}}{\partial \lambda_m} (\chi^{-1})_{m,n} \mathrm{Tr}[C_n \hat{\mathcal{D}} \rho_{\boldsymbol{\lambda}}] = \sum_m \frac{\partial \rho_{\boldsymbol{\lambda}}}{\partial \lambda_m} \dot{\lambda}_m \tag{14.6}$$

gives the rate of change for the Lagrange multiplier associated with C_m,

$$\dot{\lambda}_m = -\sum_n (\chi^{-1})_{m,n} \mathrm{Tr}[C_n \hat{\mathcal{D}} \rho_{\boldsymbol{\lambda}}]. \tag{14.7}$$

In the super-projector language it is given by the flow along the corresponding tangential direction. Here, the initial conditions $\lambda_m(0)$ are given by the initial state, as in the prethermal state [40, 41].

Iteratively constructed truncated GGE. We use the above super-projector technique to iteratively add the leading conserved quantities to a truncated description of the steady state for a given dissipator $\hat{\mathcal{D}}$. Given that the steady state Lagrange parameters are selected by the dissipator, Eq. (14.4), we will, in the first place, use $\hat{\mathcal{D}}$ to select the conserved quantities that we include in a truncated GGE Ansatz. If such an iterative truncated description converges to the exact one quickly, the procedure reduces the number of conditions (14.4) that need to be solved.

In the procedure, we iteratively construct conserved quantities $\tilde{C}_k$ from the user-defined operator basis Q_m. The latter should ideally be the set of all known (quasi)-local conserved quantities $Q_m = C_m$ of the integrable model H_0, but one can also restrict it to contain only some of them. If all conserved quantities are not known or are hard to work with, one can use the basis with projectors $Q_m = |m\rangle\langle m|$ onto all eigenstates of H_0 within the symmetry sector with a unique steady state. However, this introduces certain finite size effects that we discuss in the next section.

The iterative procedure has the following steps:

Step 0: Start with a thermal state $\rho^{(0)}_{\tilde{\boldsymbol{\lambda}}} = e^{-\tilde{\lambda}^{(0)}_0 H_0}/Z$ and find $\tilde{\lambda}^{(0)}_0$ from condition (14.4), $\mathrm{Tr}[H_0 \hat{\mathcal{D}} e^{-\tilde{\lambda}^{(0)}_0 H_0}] \stackrel{!}{=} 0$.

Step 1: Add the first iterative conserved quantity of the form

$$\tilde{C}_1 = \mathcal{N}_1^{-1} \sum_m w^{(1)}_m Q_m,$$
$$w^{(1)}_m = -\sum_n (\chi^{-1}_{(0)})_{mn} \mathrm{Tr}[Q_n \hat{\mathcal{D}} \rho^{(0)}_{\tilde{\boldsymbol{\lambda}}}], \tag{14.8}$$

where, according to Eq. (14.7), weights $w_m^{(1)}$ are given by the flows along additional directions $\frac{\partial \rho_{\boldsymbol{\lambda}}}{\partial \lambda_m}|_{\rho_{\tilde{\boldsymbol{\lambda}}}^{(0)}}$ when we allow for a GGE manifold that is not one dimensional (thermal) as in Step 0, but is spanned by additional basis Q_m conserved quantities. A new direction $\frac{\partial \rho_{\boldsymbol{\lambda}}}{\partial \lambda_m}|_{\rho_{\tilde{\boldsymbol{\lambda}}}^{(0)}}$ that causes a stronger correction to the existing solution is more important and should be weighted by a stronger bias $w_m^{(1)}$. In the end, we find $\{\tilde{\lambda}_0^{(1)}, \tilde{\lambda}_1^{(1)}\}$ for $\rho_{\tilde{\boldsymbol{\lambda}}}^{(1)} \propto e^{-\tilde{\lambda}_0^{(1)} H_0 - \tilde{\lambda}_1^{(1)} \tilde{C}_1}$ from the condition (14.4) for H_0 and $\tilde{C}_1$.

Step k: Add kth iterative conserved quantity

$$\begin{aligned} \tilde{C}_k &= \mathcal{N}_k^{-1} \sum_m w_m^{(k)} Q_m, \\ w_m^{(k)} &= -\sum_n \left(\chi_{(k-1)}^{-1}\right)_{mn} \mathrm{Tr}[Q_n \hat{\mathcal{D}} \rho_{\tilde{\boldsymbol{\lambda}}}^{(k-1)}] \end{aligned} \tag{14.9}$$

and find $\{\tilde{\lambda}_{k'}^{(k)}\}$ for $\rho_{\tilde{\boldsymbol{\lambda}}}^{(k)} \propto e^{-\sum_{k'=0}^{k} \tilde{\lambda}_{k'}^{(k)} \tilde{C}_{k'}}$ from the set of $k+1$ conditions (14.4) for $\{\tilde{C}_{k'}\}_{k'=0}^{k}$, where we denote the $\tilde{C}_0 = H_0$. Normalization $\mathcal{N}_k$ can be absorbed into the corresponding Lagrange parameter. However, it can also be chosen such that $\tilde{C}_k$ scales as an extensive operator. The susceptibility matrix, $(\chi_{(k)})_{m,n} = \langle Q_m Q_n \rangle_{\rho_{\tilde{\boldsymbol{\lambda}}}^{(k)}} - \langle Q_m \rangle_{\rho_{\tilde{\boldsymbol{\lambda}}}^{(k)}} \langle Q_n \rangle_{\rho_{\tilde{\boldsymbol{\lambda}}}^{(k)}}$, must be evaluated in each iterative step. Matrix $\chi_{(k)}$ is not invertible for the non-local basis with $Q_m = |m\rangle\langle m|$, however, one can regularize it as explained in the Supplementary material (SM), [42]. In case of (additional) unitary (Floquet) perturbations, the iterative procedure can be generalized to cover those as well [42].

Results. First, to quantify the (finite-size) error of different (truncated) GGE descriptions on length-scale ℓ, we use the distance between density matrices [37]

$$d(\rho_1, \rho_2) = \sqrt{\frac{\mathrm{Tr}[(\rho_1 - \rho_2)^2]}{\mathrm{Tr}[\rho_1^2] + \mathrm{Tr}[\rho_2^2]}} \tag{14.10}$$

and compare reduced density matrices on ℓ consecutive sites for different (truncated) GGE descriptions $\rho_{\boldsymbol{\lambda},\ell}$ and the diagonal solution $\rho_{D,\ell}$, Eq. (14.2). As noted in Ref. [37], the distance between two reduced space GGEs scales as $d(\rho_{\boldsymbol{\lambda},\ell}, \rho_{\boldsymbol{\lambda}',\ell}) \sim \ell \sum_i |\lambda_i - \lambda_i'|$ for large enough ℓ. Also for ρ_D close to a GGE, we expect $d(\rho_{\boldsymbol{\lambda},\ell}, \rho_{D,\ell})$ to scale with ℓ for large enough ℓ.

In Fig. 18.1, we show the scaled distances $d(\rho_{\boldsymbol{\lambda},\ell}, \rho_{D,\ell})/\ell$ for our first example, the transverse field Ising model

$$H_0 = \sum_i J\sigma_i^z \sigma_{i+1}^z + h_x \sigma_i^x, \tag{14.11}$$

which is a paradigmatic non-interacting integrable model. It preserves a series of local extensive operators C_m [43], see [42]. We choose the following Lindblad operators of a rather general form, with $a = 0.2$,

$$L_i = S_i^+ S_{i+1}^- + i S_{i+1}^- S_{i+2}^+ + a\sigma_i^x \sigma_{i+1}^z, \tag{14.12}$$

which stabilize a non-trivial steady state. Such structured dissipators could be realized with trapped ions simulators [44, 28] or superconducting circuits [45]. Moreover, we stress that our algorithm is generic and applicable to any non-hermitian Lindblad operators leading to (within the symmetry sector) a unique, non-trivial steady state.

Solid lines on all Fig. 18.1 panels denote the saturated distances $d_{s,\ell}$ for the best GGE solution on a given system size L, including all $N_C^{\mathrm{all}} = 2L - 2$ local conserved quantities on that system size. The solution is obtained by solving extensively many $N_C^{\mathrm{all}} \sim 2L$ coupled Eq. (14.4). As L is increased, saturated $d_{s,\ell}$ are decreased because in the thermodynamic limit, the complete GGE and the diagonal solution are equivalent, $\lim_{L\to\infty} d_{s,\ell} \to 0$. Finite $d_{s,\ell}$ are

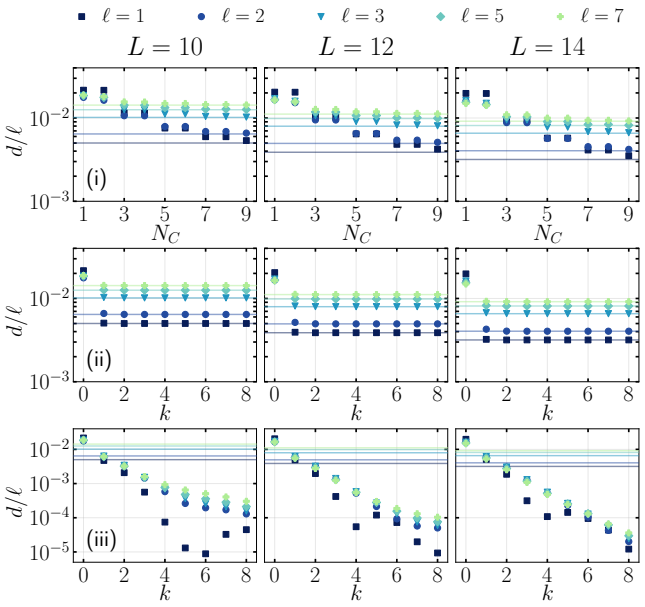


Figure 14.1: Scaled distances $d(\rho_{\boldsymbol{\lambda},\ell}, \rho_{D,\ell})/\ell$, Eq. (14.10), between the reduced density matrices of support ℓ for the diagonal steady state ensemble, Eq. (14.2), and different (truncated) generalized Gibbs ensembles. Solid lines correspond to the best GGEs with all $N_C^{\text{all}} = 2L - 2$ local conserved quantities on a given system size. From top to bottom, we consider tGGEs with: (i) N_C local conserved quantities $C_m, m = 0, ..., N_C - 1$, (ii) iterative scheme after the kth step for the basis $Q_m = C_m$, $m = 1, ..., N_C^{\text{all}} - 1$, (iii) iterative scheme after the kth step for basis $Q_m = |m\rangle\langle m|$. Parameters: Ising model with $h_x = 0.6$, $J = 1$, system sizes $L = 10, 12, 14$.

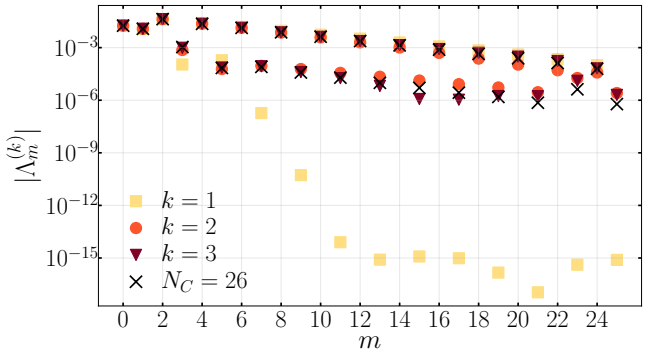


Figure 14.2: Interpreting the iterative procedure using the basis with all local conserved quantities $Q_m = C_m, m = 1, ..., 2L - 3$. The weights $\Lambda_m^{(k)} = |\sum_{k'=1}^{k} \tilde{\lambda}_{k'}^{(k)} w_m^{(k')} / \mathcal{N}_{k'}|$ at each basis element Q_m after $k = 1, 2, 3$ iterative steps show which basis elements are more important. The exact weights are shown with crosses. Parameters: transverse field Ising model with $h_x = 0.6$ and $J = 1$ on $L = 14$ sites.

just a finite-size effect. (i) Traditional tGGE: In the first row, we show the convergence to $d_{s,\ell}$ for a tGGE based on $N_C \leq N_C^{\text{all}}$ most local conserved quantities $C_m, m = 0, \dots N_C - 1$, where C_0 is the Hamiltonian. To find the solution, N_C coupled Eqs. (14.4) are solved. As N_C is increased, a better description with smaller distances d is obtained, but convergence is rather slow. (ii) Iterative tGGE with local basis: In the middle row, we show the convergence of $d(\rho_{\tilde{\boldsymbol{\lambda}},\ell}^{(k)}, \rho_{D,\ell})/\ell$ with respect to the number of iterative steps k for the iterative scheme using the basis of *all* local conserved quantities $Q_m = C_m$, excluding the Hamiltonian. The saturated distances $d_{s,\ell}$ (solid lines) are approached after only $k = 1$ iterative step. The advantage is that we now solve for $k + 1 = 2$ instead of extensively many $N_C^{\text{all}} \sim 2L$ conditions (14.4) in order to find the steady state. (iii) Iterative tGGE with non-local basis: In the last row, we present the

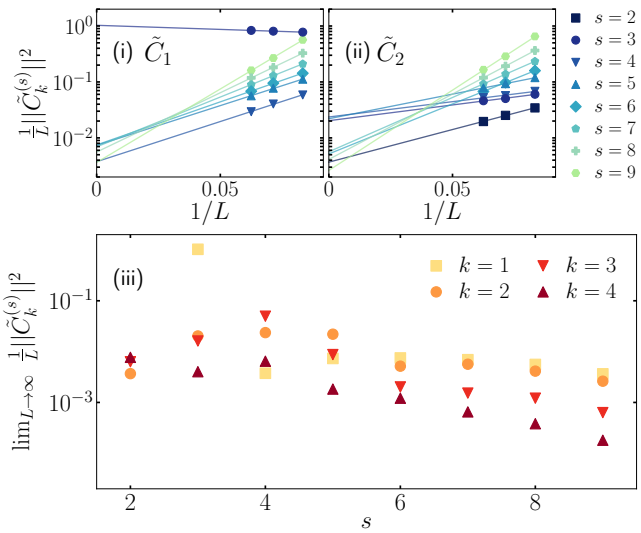


Figure 14.3: Nature of iterative conserved quantities, constructed in the basis of projectors on eigenstates, $Q_m = |m\rangle\langle m|$. (i,ii) Finite size scaling of norms $\frac{1}{L}||\tilde{C}_k^{(s)}||^2$ for the part $\tilde{C}_k^{(s)}$ of $k = 1, 2$ iterative conserved operator $\tilde{C}_k = \sum_s \tilde{C}_k^{(s)}$ that acts non-trivially only on support s. (iii) Thermodynamic norms $\lim_{L\to\infty} \frac{1}{L}||\tilde{C}_k^{(s)}||^2$ indicate that iterative conserved operators $\tilde{C}_k$ have a quasi-local nature. Parameters: Heisenberg model on $L = 12, 14, 16$.

convergence of the iterative scheme in the non-local basis $Q_m = |m\rangle\langle m|$ of projectors onto the eigenstates of H_0. The saturated distances $d_{s,\ell}$ (solid lines) are met after only $k = 1$ iterative step. Further reduction of d is largely due to non-local contributions in the non-local basis Q_m, which inherently share finite size effects of the diagonal solution ρ_D, Eq. (14.2). In that sense, ρ_D and the iterative solution in the diagonal basis, contain thermodynamically irrelevant information. We should note also that the iterative procedure in the non-local basis cannot be more efficient than finding ρ_D. However, its usefulness is in the interpretability, which is achieved by analyzing the structure of the leading conserved quantities. Below, we discuss the advantages of our iterative procedure in both bases.

When all (quasi-)local conserved quantities are known, the advantage of the iterative procedure performed in their basis is in efficiently interpreting the steady state by establishing the weights $\Lambda_m^{(k)}$ at different basis elements $Q_m = C_m$, in Fig. 18.2 shown for $k = 1, 2, 3$ iterative steps [46]. Weights $\Lambda_m^{(k)}$ reveal that conserved quantities C_{2n}, which are even under the parity transformation, are more important for our example and are well estimated after a single $k = 1$ iterative step. In the next iterative steps, smaller weights at less important odd conserved quantities C_{2n-1} are also captured. To further illustrate the fast convergence, we compare the iterative results to the asymptotic weights (absolute values of Lagrange parameters $|\lambda_m|$ denoted by crosses), obtained by solving extensively many conditions (14.4) for all local conserved quantities.

If conserved quantities are unknown or hard to work with, one should perform the iterative procedure in the non-local diagonal basis $Q_m = |m\rangle\langle m|$. The usefulness is again in the interpretability, obtained by analyzing the structure of leading iterative conserved quantities. Here, we perform it for the Heisenberg model,

$$H_0 = \sum_i \sigma_i^x \sigma_{i+1}^x + \sigma_i^y \sigma_{i+1}^y + \sigma_i^z \sigma_{i+1}^z, \tag{14.13}$$

known to have additional exotic quasi-local conserved quantities [47, 2, 48]. We again use Lindblad operators Eq. (14.12), now with $a = 0$ so that we can work in a single (largest) $S^z = 0$ magnetization sector. An analysis similar to Fig. 18.1 is performed in the SM, here we

focus on the interpretability. In order to assess the nature (i.e. locality) of iterative conserved quantities, we extract the norm $\lim_{L\to\infty} \frac{1}{L}||\tilde{C}_k^{(s)}||^2$ of the part of iterative conserved quantities that acts non-trivially on s consecutive sites, $\tilde{C}_k = \sum_s \tilde{C}_k^{(s)}$. Operator $\tilde{C}_k^{(s)}$ is obtained by summing the overlaps of $\tilde{C}_k$ with all Pauli strings acting non-trivially between s sites. In Fig. 17.3(i,ii), we plot the norms $\frac{1}{L}||\tilde{C}_k^{(s)}||^2$ for $k = 1, 2$ and different supports s on given system sizes $L = 12, 14, 16$ [49]. For small L, norms even increase with s. Only when we extrapolate the finite size result to the thermodynamic limit via $1/L$ scaling, Fig. 17.3(i,ii), for large enough s, norms are decaying exponentially with s, Fig. 17.3(iii), as expected for quasi-local conserved operators [47, 48]. Thus, only once we remove the finite-size non-local contributions, inherent to the non-local basis, we can conclude that our iterative conserved quantities are a quasi-local superposition of local [50] and quasi-local conserved quantities of the Heisenberg model [47, 48].

Conclusions and Outlook. In this Letter, we propose an iterative construction of conserved quantities of leading importance to describe nearly integrable, driven dissipative systems. Our approach is motivated by the fact that in such setups, the integrability breaking perturbations (couplings to baths and drives) determine the Lagrange parameters of a GGE approximation to the steady state. Here, we use the dissipator to select the combination of conserved quantities contributing significantly to the truncated GGE description. Such a physically motivated construction of truncated GGEs reduces the complexity of calculating steady state parameters, i.e., the Lagrange parameters. Namely, instead of solving extensively many coupled conditions (14.4) for all (quasi)local conserved quantities, we need to solve for just a few. A precise number is model and precision-dependent but is generally expected to be $\mathcal{O}(1)$ and low.

A clear usefulness of our approach that we already showcased here is in the interpretability: (i) If working in the basis of all local conserved operators, their weights reveal which of them are important for given Lindblads. (ii) If all (quasi-)local conserved quantities are not known or hard to work with, the iterative procedure can be performed in the non-local basis of projectors on eigenstates. The (quasi-)local structure of leading iterative conserved quantities can be analyzed a posteriori, giving the information about potentially unknown conserved quantities of the unperturbed model [51].

When evaluating the actual reduction of complexity, one should also consider the complexity of evaluating the rate equations (14.4) and building the conserved quantities, Eq. (14.9). Our current study used exact diagonalization, at a gain of thorough benchmarking against the diagonal ensemble, but at the loss of diagonalization itself representing the bottleneck of the procedure. At least for non-interacting many-body integrable systems, one can evaluate Eq. (14.4) and construct iterative conserved quantities (14.9) in the basis of mode occupation operators with polynomial complexity in system size, in which case our method reduces the exponent and simplifies thermodynamically large calculations; see comment [52] for scaling arguments. For interacting integrable models, Eqs.(14.4,14.9) could be evaluated using partition function approach [53, 54]. However, we leave exploring thermodynamic aspects for non-interacting and interacting models to a future study.

14.2 Supplemental Material

In the Supplemental Material, we (i) show how to regularize the inverse of susceptibility matrix χ^{-1} in the case of non-local basis of projectors $Q_m = |m\rangle\langle m|$, (ii) write the explicit form for the local conserved quantities of the transverse field Ising model, (iii) perform the analysis of different tGGE descriptions in the case of the Heisenberg model, and (iv) show how additional unitary perturbation can be included in the iterative procedure.

14.3 Regularization of χ^{-1} in the non-local basis

Here we address the invertibility of the susceptibility matrix χ, appearing in the calculation of weights $w_m^{(k)}$ at basis elements Q_m in the iterative conserved quantities $\tilde{C}_k$, Eq. (14.9),

$$\begin{aligned}\tilde{C}_k &= \mathcal{N}_k^{-1}\sum_m w_m^{(k)} Q_m,\\ w_m^{(k)} &= -\sum_n (\chi_{(k-1)}^{-1})_{mn}\,\mathrm{Tr}[Q_n \hat{\mathcal{D}}\rho_{\tilde{\boldsymbol{\lambda}}}^{(k-1)}]\end{aligned} \tag{14.14}$$

for different choices of operator basis Q_m. Let us first rewrite the equation for weights $w_m^{(k)}$, Eq. (14.14), in a vector form. To avoid the cluttering of notation, we omit the step index k in the vector representation. We denote the vector of weights with $|w\rangle = |w_1^{(k)}, \dots w_M^{(k)}\rangle$, with nth element being the weight at Q_n. The vector index runs from 1 up to the size of the Q_m basis M. Additionally we denote with $|q\rangle = |q_1^{(k-1)}, \dots q_M^{(k-1)}\rangle$ the vector with entries $q_n^{(k-1)} = \mathrm{Tr}[Q_n \hat{\mathcal{D}}\rho_{\tilde{\boldsymbol{\lambda}}}^{(k-1)}]$. Matrix χ has size $M\times M$ and it's elements are the connected correlation functions between the basis elements Q_m, $\chi_{mn} = \mathrm{Tr}[Q_m Q_n \rho_{\tilde{\boldsymbol{\lambda}}}^{(k-1)}] - \mathrm{Tr}[Q_m \rho_{\tilde{\boldsymbol{\lambda}}}^{(k-1)}]\,\mathrm{Tr}[Q_n \rho_{\tilde{\boldsymbol{\lambda}}}^{(k-1)}]$. The equation (14.14) for weights is then written as

$$|w\rangle = \chi^{-1}|q\rangle. \tag{14.15}$$

and can be solved if χ is invertible, which is the case for the basis of local conserved quantities $Q_m = C_m$. In the remaining part of this section, we show that for the non-local basis of projectors onto eigenstates of H_0, $Q_m = |m\rangle\langle m|$, matrix χ is non-invertible and we demonstrate how to calculate weights $|w\rangle$ by regularizing χ^{-1}.

For the non-local $Q_m = |m\rangle\langle m|$, matrix elements of χ can be expressed with coefficients of $\rho_{\tilde{\boldsymbol{\lambda}}}^{(k-1)}$ in the diagonal ensemble $a_m = \langle m|\rho_{\tilde{\boldsymbol{\lambda}}}^{(k-1)}|m\rangle$, such that $\chi_{mn} = a_m(\delta_{mn} - a_n)$. Due to the normalization of the density matrix $\mathrm{Tr}[\rho_{\tilde{\boldsymbol{\lambda}}}^{(k-1)}] = 1$, $N_H - 1$ coefficients a_m are free parameters, while one depends on the others. Here, N_H is the Hilbert space dimension and also the number of basis elements $M = N_H$. This implies that matrix χ has $N_H - 1$ linearly independent rows (or columns), and therefore rank $N_H - 1$. One vector is in the kernel of χ, meaning χ is non-invertible. The kernel vector $|v\rangle$ is in the eigenbasis of H_0 of form $|v\rangle = \frac{1}{\sqrt{N_H}}|1,\dots,1\rangle$, since the sum of any row (as well as column) in matrix χ in this basis equals zero,

$$\chi|1,\dots,1\rangle = 0, \qquad \langle 1,\dots,1|\chi = 0. \tag{14.16}$$

Note also that $\mathrm{Tr}[\hat{\mathcal{D}}\rho_{\tilde{\boldsymbol{\lambda}}}^{(k-1)}] = \sum_n q_n = 0$, or

$$\langle 1,\dots,1|q\rangle = 0 \tag{14.17}$$

due to the dissipator $\hat{\mathcal{D}}$ in Eq. (14.1) being of Lindblad form.

To avoid the issue of invertibility of χ, one can instead of Eq. (14.15) solve

$$\chi|w\rangle = |q\rangle, \quad |w\rangle = |w'\rangle + c|v\rangle \tag{14.18}$$

with a set of solutions parametrized by $c \in \mathbb{C}$, since $\chi(|w'\rangle + c|v\rangle) = \chi|w'\rangle = |q\rangle$. Below we show that

$$|w'\rangle = \tilde{\chi}^{-1}|q\rangle, \qquad \tilde{\chi} = \chi + |v\rangle\langle v| \tag{14.19}$$

is a solution giving rise to a traceless iterative conserved quantity $\mathrm{Tr}[\tilde{C}_k] = 0$ and that the choice of factor c does not affect the iterative steady state density matrix $\rho_{\tilde{\boldsymbol{\lambda}}}^{(k)}$.

In Eq. (14.19) we introduced a regularized inverse $\tilde{\chi}^{-1}$, motivated by the fact that we can choose an orthonormal basis, where one basis vector is the kernel vector $|v\rangle$ (subspace $\tilde{Q}$)

while others form a complementary subspace (subspace $\tilde{P}$) on which χ acts nontrivially. Using conditions in Eqs. (14.16, 14.17) and ordering the basis such that the kernel vector is the last one, χ, $|v\rangle$ and $|q\rangle$ have the following form in the new basis:

$$\chi_{\mathrm{b}} = \begin{pmatrix} \chi_{\tilde{P}_{N_H-1\times N_H-1}} & 0_{N_H-1\times 1} \\ 0_{1\times N_H-1} & 0 \end{pmatrix}_{\mathrm{b}}$$
$$|v\rangle_{\mathrm{b}} = \begin{pmatrix} 0_{N_H-1\times 1} \\ 1 \end{pmatrix}_{\mathrm{b}}, \quad |q\rangle_{\mathrm{b}} = \begin{pmatrix} q_{\tilde{P}_{N_H-1\times 1}} \\ 0 \end{pmatrix}_{\mathrm{b}}, \tag{14.20}$$

where $\chi_{\tilde{P}}$ and $q_{\tilde{P}}$ are the matrix χ and vector $|q\rangle$ projected onto subspace $\tilde{P}$. Subscript b labels the new basis. $\tilde{\chi}$ and its inverse are then

$$\tilde{\chi}_{\mathrm{b}} = \begin{pmatrix} \chi_{\tilde{P}} & 0 \\ 0 & 1 \end{pmatrix}_{\mathrm{b}} \quad \tilde{\chi}_{\mathrm{b}}^{-1} = \begin{pmatrix} \chi_{\tilde{P}}^{-1} & 0 \\ 0 & 1 \end{pmatrix}_{\mathrm{b}}. \tag{14.21}$$

Now one can easily see that the Ansatz in Eq. (14.19) is the solution to Eq. (14.18): $\chi_{\mathrm{b}}\tilde{\chi}_{\mathrm{b}}^{-1}|q\rangle_{\mathrm{b}} = |q\rangle_{\mathrm{b}}$. Moreover, it is also straightforward to show that the iterative conserved quantity, constructed from $|w'\rangle$, is traceless

$$\begin{aligned} \mathrm{Tr}[\tilde{C}_k] &= \mathcal{N}_k^{-1}\sum_m w_m^{(k)} = \mathcal{N}_k^{-1}\langle v|w'\rangle = \\ &= \mathcal{N}_k^{-1}\langle v|_{\mathrm{b}}\tilde{\chi}_{\mathrm{b}}^{-1}|q\rangle_{\mathrm{b}} = 0. \end{aligned} \tag{14.22}$$

Let us note that the transformation to a new basis is useful for analytical arguments, however, to work with $\tilde{\chi}$ in practice, the original basis can be used with $|v\rangle\langle v| = \frac{1}{N_H}|1,...,1\rangle\langle 1,...,1|$, as in Eq. (14.19), expressed in that basis.

Finally we show that shifting the solution $|w'\rangle$ by $c|v\rangle$, Eq. (14.18), does not affect the steady state density matrix $\rho_{\tilde{\boldsymbol{\lambda}}}^{(k)}$ at the corresponding iterative step. Adding $c|v\rangle$ in the language of the iterative tGGE means adding a constant weight c to each basis element Q_m, i.e.,

$$\begin{aligned} \rho_{\tilde{\boldsymbol{\lambda}}}^{(k)}(c) &\equiv \frac{e^{-\sum_{k'=0}^{k}\tilde{\lambda}_{k'}\mathcal{N}_{k'}^{-1}\sum_m (w_m^{(k')}+c)Q_m}}{\mathrm{Tr}[e^{-\sum_{k'=0}^{k}\tilde{\lambda}_{k'}\mathcal{N}_{k'}^{-1}\sum_m (w_m^{(k')}+c)Q_m}]} \\ &= \frac{\sum_m e^{-\sum_{k'=0}^{k}\tilde{\lambda}_{k'}\mathcal{N}_{k'}^{-1}(w_m^{(k')}+c)}Q_m}{\sum_m[e^{-\sum_{k'=0}^{k}\tilde{\lambda}_{k'}\mathcal{N}_{k'}^{-1}(w_m^{(k')}+c)}]} \\ &= \frac{e^{-\sum_{k'=0}^{k}\tilde{\lambda}_{k'}\mathcal{N}_{k'}^{-1}c}\sum_m e^{-\sum_{k'=0}^{k}\tilde{\lambda}_{k'}\mathcal{N}_{k'}^{-1}w_m^{(k')}}Q_m}{e^{-\sum_{k'=0}^{k}\tilde{\lambda}_{k'}\mathcal{N}_{k'}^{-1}c}\sum_m[e^{-\sum_{k'=0}^{k}\tilde{\lambda}_{k'}\mathcal{N}_{k'}^{-1}w_m^{(k')}}]} \\ &= \rho_{\tilde{\boldsymbol{\lambda}}}^{(k)}. \end{aligned} \tag{14.23}$$

We see that the contribution from $c|v\rangle$ cancels out, so we can skip it in the first place. Similarly we could take a different shift $c \to c_{k'}$ for every iterative conserved quantity $\tilde{C}_{k'}$ and get the same result as above.

14.4 Conservation laws of transverse Ising model

For transverse field Ising model,

$$H_0 = \sum_i J\sigma_i^z\sigma_{i+1}^z + h_x\sigma_i^x, \tag{14.24}$$

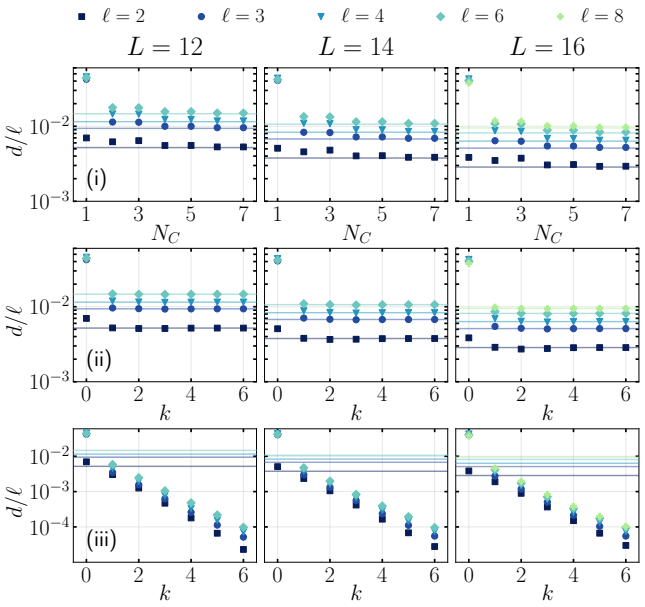


Figure 14.4: Scaled distances $d(\rho_{\boldsymbol{\lambda},\ell}, \rho_{D,\ell})/\ell$, Eq. (14.10), between the reduced density matrices of support ℓ of the diagonal steady state ensemble, Eq. (14.2), and different truncated generalized Gibbs ensembles. Solid lines correspond to the tGGEs including $N_C^{\max} = 8$ most local conserved quantities. From top to bottom we consider tGGEs with: (i) N_C local conserved quantities $C_m^{\text{loc}}, m = 0, ..., N_C - 1$, (ii) iterative scheme after the kth step for basis $Q_m = C_m^{\text{loc}}, m = 1, ..., N_C^{\max} - 1$, (iii) iterative scheme after the kth step for basis $Q_m = |m\rangle\langle m|$. Parameters: Heisenberg model, system sizes $L = 12, 14, 16$.

the conservation laws have the following form

$$\begin{aligned} C_0 &= H_0 \\ C_2 &= \sum_j J S^{zz}_{j,j+2} - h_x \sigma^y_j \sigma^y_{j+1} - h_x \hat{\sigma}^z_j \sigma^z_{j+1} - J\sigma^x_j \\ C_{2\ell>2} &= \sum_j J S^{zz}_{j,j+\ell+1} - h_x S^{yy}_{j,j+\ell} - h_x S^{zz}_{j,j+\ell} + J S^{yy}_{j,j+\ell-1} \\ C_{2\ell-1} &= J \sum_j S^{yz}_{j,j+\ell} - S^{zy}_{j,j+\ell}, \end{aligned} \tag{14.25}$$

with $S^{\alpha\beta}_{i,j} = \sigma^\alpha_i \sigma^x_{i+1} \dots \sigma^x_{j-1} \sigma^\beta_j$. In our analysis we use N_C most local ones from H_0 to C_{N_C-1}.

14.5 Example II: Heisenberg model.

Here, we perform a similar analysis to Fig. 1 in the main text for the paradigmatic interacting integrable model, the isotropic Heisenberg model,

$$H_0 = \sum_i \sigma^x_i \sigma^x_{i+1} + \sigma^y_i \sigma^y_{i+1} + \sigma^z_i \sigma^z_{i+1}, \tag{14.26}$$

and Lindblad operators

$$L_i = S^+_i S^-_{i+1} + i S^-_{i+1} S^+_{i+2}. \tag{14.27}$$

They preserve magnetization; therefore, each magnetization sector has its unique steady state, and we consider below the largest zero magnetization sector. Unlike the Ising model, the Heisenberg model has a few families of conserved operators: local extensive operators [50] and quasi-local extensive operators [2, 47, 48].

Fig. 14.4 shows the same analysis previously done for the Ising model. (i) Traditional tGGE: The first row shows the distances for tGGE based on the first N_C local conserved quantities, derived using the boost operator, $B = -i\sum_j jh_j$, $C^{\rm loc}_{m+1} = [B, C^{\rm loc}_m]$ and $C^{\rm loc}_0 = H_0$, where h_j are Hamiltonian densities $H_0 = \sum_j h_j$ [50]. In this notation, $C^{\rm loc}_1$ is the conserved energy current. For chosen Lindblads, approximate saturation in d happens for a rather small N_C number of local conserved quantities, therefore we perform our best calculation at $N_C^{\rm max} = 8$ local conserved quantities $C^{\rm loc}_m$ to obtain $d_{s,\ell}$ denoted by solid lines. (ii) Iterative tGGE with local basis: The second row shows the distances for the iterative approach, using the basis of first $N_C^{\rm max} = 8$ local conserved operators $Q_m = C^{\rm loc}_m, m = 1, ..., N_C^{\rm max} - 1$, excluding the Hamiltonian. The asymptotic distances $d_{s,\ell}$ (solid line) are approximately obtained after cca. $k = 1$ iterative step. (iii) Iterative tGGE with non-local basis: The third row shows the distances for the iterative approach using the non-local basis $Q_m = |m\rangle\langle m|$ of projectors onto the eigenstates of H_0. Already after the first iterative step, distances d are smaller then for the tGGE including local conserved quantities because the non-local basis Q_m captures also the impact of quasi-local conserved quantities of the Heisenberg model [47, 2, 48]. Partially, the reduction of d in the non-local basis is again due to non-local contributions on small systems considered. In the main text, we present a finite-size analysis of iterative conserved quantities created in this non-local basis, which removes the non-local contributions.

14.6 Iterative procedure for unitary perturbation

In case of (additional) unitary perturbation H_1, the dissipator $\hat{\mathcal{D}}$ in Eq. (14.9) should be replaced (or supplemented, if both types of perturbations occur simultaneously) by $\hat{\mathcal{L}}_1\hat{Q}\hat{\mathcal{L}}_0^{-1}\hat{Q}\hat{\mathcal{L}}_1$, i.e.,

$$\tilde{C}_k = \mathcal{N}_k^{-1}\sum_m w_m^{(k)} Q_m, \tag{14.28}$$
$$w_m^{(k)} = -\sum_n \left(\chi^{-1}_{(k-1)}\right)_{mn} \mathrm{Tr}[Q_n(\hat{\mathcal{D}} + \hat{\mathcal{L}}_1\hat{Q}\hat{\mathcal{L}}_0^{-1}\hat{Q}\hat{\mathcal{L}}_1)\rho^{(k-1)}_{\tilde{\boldsymbol{\lambda}}}]$$

where $\hat{\mathcal{L}}_j\rho = -i[H_j, \rho]$ for $j = 0, 1$, $\hat{\mathcal{L}}_0^{-1}\rho = -\int_0^\infty dt e^{t\hat{\mathcal{L}}_0}\rho$ and $\hat{Q}\rho = \mathbb{1} - \sum_m |m\rangle\langle m|\langle m|\rho|m\rangle$ is a super-projector orthogonal to the diagonal subspace, which ensures that the action of $\hat{\mathcal{L}}_0^{-1}$ is not singular. Unlike for the dissipator, where the contribution to the flow in the GGE manifold occurs already in the first order, for the unitary perturbation the first nontrivial contribution happens only in the second order as $\mathrm{Tr}[Q_n\hat{\mathcal{L}}_1\rho^{(k-1)}_{\tilde{\boldsymbol{\lambda}}}] = 0$ due to cyclicity of the trace [26, 18].

15 From observations to complexity of quantum states via unsupervised learning by Schmitt, Lenarčič

15.1 Theory

Abstract

The vast complexity is a daunting property of generic quantum states that poses a significant challenge for theoretical treatment, especially in non-equilibrium setups. Therefore, it is vital to recognize states which are locally less complex and thus describable with (classical) effective theories. We use unsupervised learning with autoencoder neural networks to detect the local complexity of time-evolved states by determining the minimal number of parameters needed to reproduce local observations. The latter can be used as a probe of thermalization, to assign the local complexity of density matrices in open setups

and for the reconstruction of underlying Hamiltonian operators. Our approach is an ideal diagnostics tool for data obtained from (noisy) quantum simulators because it requires only practically accessible local observations.

Finding a suited notion of the complexity of quantum many-body states is a key aspect of various lines of research on correlated quantum systems. Entanglement entropy has emerged as a highly relevant information-theoretic quantity in the case of pure states, that reveals universal features in exotic states of matter [1, 2, 3, 4, 5, 6], in quantum many-body dynamics far from equilibrium [7, 8], and it indicates the feasibility of classical computer simulations [9, 10, 11]. Recently, it has also been measured experimentally using cold atoms and trapped ions [12, 13]. Generalizations of entanglement entropy applicable to mixed states have been proposed [14] and entanglement witnesses can detect entanglement [15], e.g., in experiments where entanglement entropy is inaccessible. An alternative perspective is that of quantum circuit complexity, which corresponds to the minimal size of a circuit to prepare the state of interest from a fiducial state [16, 17, 18].

Entanglement and circuit complexity, however, do not universally align with the physically relevant degree of complexity of many-body states. For example, although ergodic many-body systems quickly become highly entangled under unitary non-equilibrium dynamics, the late time dynamics of physically relevant local observables is described by hydrodynamic equations of motion of a few quantities [19, 20, 112]. Moreover, their eventual thermalization implies that a few thermodynamic quantities fully characterize local properties, and entanglement entropy turns into thermodynamic entropy of subsystems. Since typical initial states are weakly entangled, it is expected that in terms of "local complexity" associated with local observables, the non-equilibrium dynamics typically passes an "information barrier" at intermediate times. Such a "barrier" has been identified by considering the operator entanglement entropy evolution in closed and open quantum systems [22, 23, 24, 25, 26] and the envisioned time-dependence of local quantum state complexity is depicted schematically in Fig. 15.1.

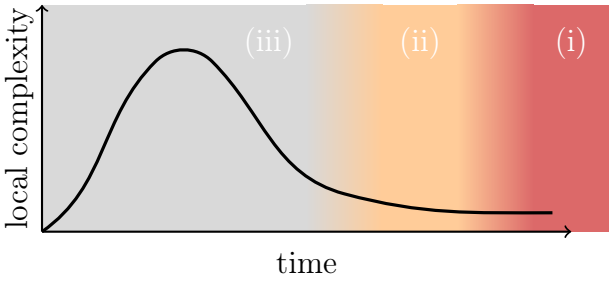


Figure 15.1: Schematic picture of the "information barrier" of quantum many-body dynamics. The different shaded areas illustrate the logical structure of this paper – we address (i) infinite time steady states, (ii) practically attainable states at late but finite times, and (iii) short to intermediate times, where the "information barrier" is crossed.

This Letter introduces a novel approach to analyze the local complexity of quantum many-body states based on recently developed machine learning techniques. At the core, we employ deep autoencoder networks [27], which we train in an unsupervised fashion with observable expectation values, in order to obtain a dimensional reduction enabling us to assess the effective complexity of the quantum state of interest. We address different regimes of non-equilibrium dynamics of open and closed quantum systems, which are indicated in Fig. 15.1 by the different background shadings. The paper is structured such that we progress from (i) the infinite time limit over (ii) practically attainable steady states at late finite times to (iii) the "information barrier" itself at intermediate and short times. Following this order, we can first test our approach in a controlled setting by assigning the local complexity of thermodynamic ensembles;

these are idealized local descriptions of steady states of chaotic or integrable models [28, 3, 4]. Then, we investigate the dynamical approach of a weakly dissipative system to such states in terms of our complexity measure. For nearly integrable systems, the absence of thermalization despite weak integrability breaking sources is a non-trivial effect [26, 25, 33, 18, 35], which can be detected with the unsupervised learning approach. Finally, we reveal an "information barrier" at intermediate times by analyzing the time-dependent local complexity in random unitary dynamics, which has in many recent works been proven to be a useful model to analyze typical features of non-equilibrium dynamics [36, 4, 5, 6, 7, 41, 42, 43, 44, 45, 46, 26]. Besides the assertion of complexity, we demonstrate how further information about effective descriptions can be extracted, e.g., to reconstruct Hamiltonians for thermal states.

Being based on local observations, this approach is suited to exploit highly resolved observations of many-body quantum systems that are possible in modern quantum simulators [47, 48, 12, 49, 50, 47, 48, 53].

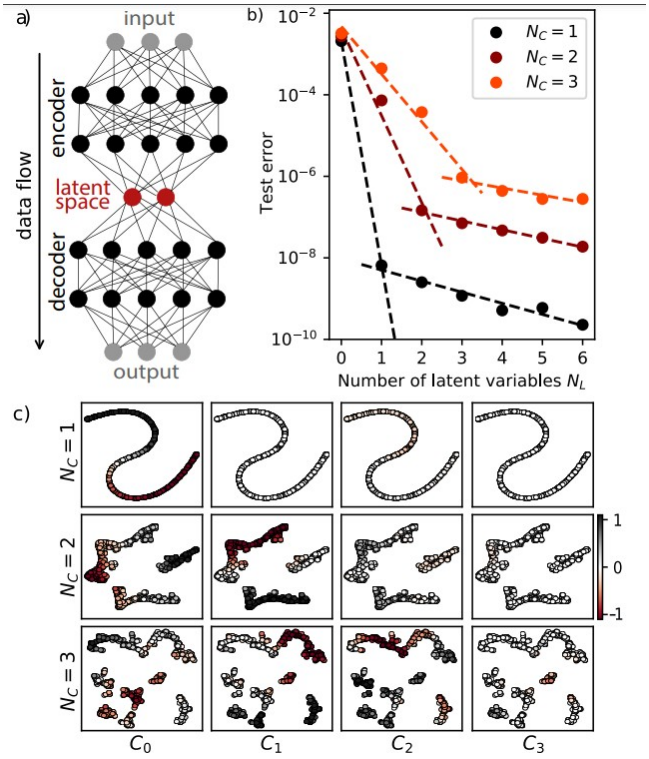


Figure 15.2: a) Schematic depiction of the neural autoencoder network. b) Test error as function of the number of latent variables obtained by training on the transverse-field Ising model data from (generalized) Gibbs ensembles with varying number of charges N_C. Dashed lines are linear fits included as a guide for the eye. c) t-SNE of the latent representation of (G)GEs with different number of charges N_C and $N_L = 4$. Color coding in each column is according to expectation values $\langle \hat{C}_i \rangle / N$ of charges, denoted in the bottom. Parameters: $N = 12, h_x = 0.6J, h_z = 0$.

Autoencoder.

The autoencoder [27] is an artificial neural network consisting of multiple layers. The input and output layers have the same dimension, and at least one of the additional layers between the two constitutes a "bottleneck" with a considerably smaller number of N_L neurons, spanning the N_L dimensional latent space. The part prior to the bottleneck is called *encoder*, the subsequent part is the *decoder*; see Fig. 15.2a. Deep learning with autoencoder neural networks has previously been explored as a tool to investigate a variety of physical problems. Examples are unsupervised discovery of physical concepts [54, 55], the identification of entangled

states [56], encoding of quantum many-body states [57], or the exploration of relations to non-equilibrium statistical mechanics [58].

Here, the objective of an autoencoder is to reconstruct the input data x given by local observations, despite the intermediate compression in the bottleneck. For this purpose, the reconstruction loss

$$\mathcal{L}_{\mathcal{D}_T}(\boldsymbol{\theta}) = \frac{1}{|\mathcal{D}_T|} \sum_{x\in\mathcal{D}_T} \big(f_{\boldsymbol{\theta}}(x) - x\big)^2 \tag{15.1}$$

over a training data set $\mathcal{D}_T$ is minimized by optimizing the variational parameters $\boldsymbol{\theta}$ of the neural network $f_{\boldsymbol{\theta}}$. Thereby, the encoder learns to map the input data to a suited low-dimensional *latent representation*, which holds the necessary information for the decoder to recover the original input x. Achieving a small reconstruction loss depends on the existence of such a low-dimensional representation, and too narrow bottlenecks lead to a larger loss $\mathcal{L}_{\mathcal{D}_T}$. Therefore, the effective dimensionality of a data set can be analyzed by varying the bottleneck width and comparing the corresponding reconstruction errors. This analysis should be conducted with validation data that was not used for training to exclude overfitting; we will call the reconstruction error (16.1) evaluated on the test data, the *test error*. Details about the network architecture and optimization are included in the Supplementary Material (SM) [39].

Training data.

In the exemplary applications below we consider quantum spin-$\frac{1}{2}$ chains, with composite Hilbert spaces $\mathcal{H} = \bigotimes_l h_l$, where $\dim(h_l) = 2$ and l is the lattice site index. As input for the encoder, we use data sets, where each element consists of the expectation values of all possible operator strings up to a fixed compact support $\mathcal{S}$, i.e., $O_\rho(\boldsymbol{\alpha}) = \mathrm{Tr}[\hat\rho\hat\sigma_1^{\alpha_1}\dots\hat\sigma_{|\mathcal{S}|}^{\alpha_{|\mathcal{S}|}}]$ with density matrix $\hat\rho$, $\boldsymbol{\alpha} = (\alpha_1,\dots,\alpha_{|\mathcal{S}|}) \in \{0,x,y,z\}^{|\mathcal{S}|}$ and $\hat\sigma_l^{0,x,y,z}$ denoting the identity and the Pauli matrices, respectively. Measuring these observables amounts to a full tomography of the reduced density matrix of the subsystem $\mathcal{S}$. While the corresponding cost grows exponentially with subsystem size $|\mathcal{S}|$, we show in our examples that already moderate supports $|\mathcal{S}| = 3, 4$ are informative of the local complexity; for larger supports it might be useful to employ the recently proposed classical shadow techniques [60, 13, 61].

In our analysis, we consider families of quantum states $\hat\rho_{\boldsymbol{\lambda}}$ parametrized by a potentially high-dimensional parameter $\boldsymbol{\lambda}$. Individual training data elements are given by observations $\{O_{\rho_{\boldsymbol{\lambda}}}(\boldsymbol{\alpha})|\boldsymbol{\alpha} \in \{0,x,y,z\}^{|\mathcal{S}|}\}$ for sampled parameters $\boldsymbol{\lambda}$. By optimizing the reconstruction objective (16.1) with autoencoder networks, we gain insights about the effective local complexity of $\hat\rho_{\boldsymbol{\lambda}}$ that is relevant for local observations. The complexity is quantified through the number of latent variables required for faithful reconstruction according to Eq. (16.1). For this procedure it is crucial to exhaustively sample the space of states $\hat\rho_{\boldsymbol{\lambda}}$ in order to avoid detecting spurious low-dimensional representations.

Idealized steady states of closed systems and Hamiltonian reconstruction.

As a first test bed, we consider (generalized) Gibbs ensembles ((G)GEs) of the spin-1/2 quantum Ising model (QIM)

$$\hat H = \sum_j \left(J\hat\sigma_j^z\hat\sigma_{j+1}^z + h_x\hat\sigma_j^x + h_z\hat\sigma_j^z \right) , \tag{15.2}$$

relevant for quantum simulators [43, 44, 45, 46, 47, 48]. For $h_z = 0$, the QIM (15.2) is integrable, featuring an extensive set of mutually commuting local charges $\hat C_i$ (see SM [39]), one of which is the Hamiltonian [43]. Conservation laws play a crucial role in the long-time description of excited integrable/chaotic systems, Fig. 15.1(i), when reduced density matrices become

indistinguishable from GGEs/GEs of the form [28, 3, 4]

$$\hat{\rho}_{\boldsymbol{\lambda}} = \frac{e^{\sum_i \lambda_i \hat{C}_i}}{\mathrm{Tr}[e^{\sum_i \lambda_i \hat{C}_i}]}. \tag{15.3}$$

Although long-time states show volume law entanglement entropy [7, 67], local observables are (for most practical purposes) determined by a few Lagrange parameters λ_i. Our goal is to detect these simple parametrizations.

To benchmark the utility of our approach to analyze such characteristics of long-time states, Fig. 15.1(i), we do not perform an actual time evolution but instead generate training data from GGEs with randomly drawn Lagrange multipliers $\lambda_i \in [-2, 2]$ using exact diagonalization techniques for the QIM (15.2) at $h_x = 0.6J$, $h_z = 0$ with system size $N = 12$. Each sampled $\boldsymbol{\lambda}$, yields a training data element with expectation values of all Pauli strings up to support $|\mathcal{S}| = 3$, and we separate these samples into training and test sets, see SM [39]. Fig. 15.2b displays the test errors, Eq. (16.1), achieved after training for different numbers of charges N_C included in the GGEs. We see that the error drops rapidly with an increasing number of latent variables N_L as long as $N_L < N_C$; for $N_L \geq N_C$ the curves level off in all cases. This behavior of the test error is expected because N_C is the minimal number of independent variables needed for encoding the GGE data. The change of slope becomes more distinct with larger training data sets [39].

In Fig. 15.2c we employ t-distributed stochastic neighbor embedding (t-SNE) [12] to visualize what the autoencoder learned to encode in its latent space. The t-SNE is a dimensional reduction technique, where the proximity of data points in the resulting low-dimensional representation is determined based on their Euclidian distance in the original space. The position of each point corresponds to the latent representation of one set of observations. The color code indicates the corresponding expectation value of the different charges. For $N_C = 1$, we find that also for a higher-dimensional latent space, $N_L > N_C$, the latent representation of observations lies on a one-dimensional manifold with energy density monotonously changing along it. When including more charges, we see that the dimensionality of the latent representation grows. For $N_C > 1$, the locations of extremal regions of the color code reveal that each charge can be associated with a different direction in the latent space. This indicates that the unsupervised learning procedure yielded an encoding directly related to the physical charges. In the SM [39], we show that the learned representation is connected to the charges through an invertible map, which is sufficient for an unambiguous encoding of the data.

Having demonstrated the possibility to identify and analyze ideal (G)GE states, we next turn to genuine late-time states, Fig. 15.1(ii). To add some additional structure to these states, we perform time evolution with respect to open quantum systems. As we show in the following, the local complexity of late-time states in closed and weakly open systems share many properties.

Steady states of open systems.

Here we characterize steady states of open systems described by the Liouville equation

$$\dot{\hat{\rho}} = i[\hat{\rho}, \hat{H}] + \epsilon \sum_{j,\gamma} \left(\hat{L}_j^{(\gamma)} \hat{\rho} \hat{L}_j^{(\gamma)\dagger} - \frac{1}{2} \{ \hat{L}_j^{(\gamma)\dagger} \hat{L}_j^{(\gamma)}, \hat{\rho} \} \right) \tag{15.4}$$

with couplings to non-equilibrium baths represented by Lindblad operators $\hat{L}_j^{(\gamma)}$. The strength of the Markovian part is parametrized by ϵ. In direct relation with the previous section, at a weak coupling to dissipators, $\epsilon \ll 1$, steady states for a chaotic (integrable) $\hat{H}$ can be approximated with (G)GEs, Eq. (15.3), which are corrected by a small $\delta\hat{\rho}(\epsilon)$, $\hat{\rho} \propto \hat{\rho}_{\boldsymbol{\lambda}} + \delta\hat{\rho}(\epsilon)$.

For an integrable $\hat{H}$, the absence of thermalization despite weak integrability breaking sources is a non-trivial effect observed in weakly open systems [26, 25, 33, 18, 35].

In this context, the unsupervised learning approach enables us to address several natural questions. For the integrable $\hat{H}$, we will utilize our approach to detect how many conservation laws must be considered to reproduce local observables – a question often raised in quench protocols in closed setups. For the chaotic $\hat{H}$, we will examine the effect of noise as of relevance for quantum simulators that are never completely isolated.

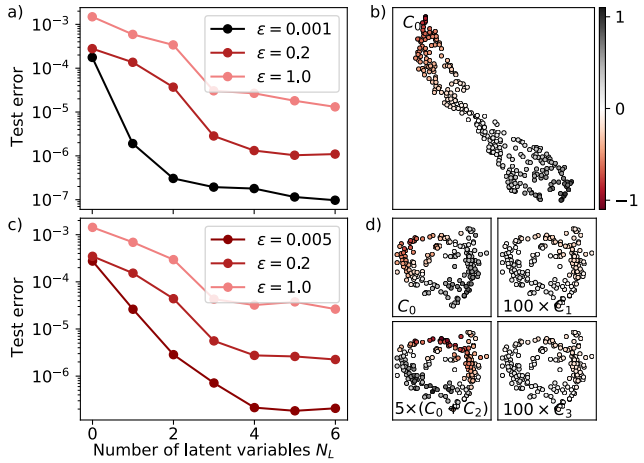


Figure 15.3: Results obtained by training on data from steady states for setups with different strength of openness ϵ, Eq. (15.4), for chaotic (top) and integrable (bottom) $\hat{H}$. a,c) Test error as function of the number of latent variables. b) t-SNE of the latent representation for chaotic $\hat{H}$ and $\epsilon = 0.001$, $N_L = 5$. Color coding is with respect to energy density. d) t-SNE of the latent representation for integrable $\hat{H}$ and $\epsilon = 0.005$, $N_L = 5$. Color coding is with respect to (rescaled) densities of charges written in the inset. The gradient in the coloring with respect to $(5/N)\langle \hat{C}_0 + \hat{C}_2 \rangle$ is roughly perpendicular to the gradient of $\langle \hat{C}_0 \rangle / N$. For our choice of Lindblads, inversion non-symmetric $\hat{C}_{1,3}$ show much smaller expectation values, i.e., not comparable to $\langle \hat{C}_0 \rangle / N$ even upon rescaling with 100 and are thus not so crucial for an approximate description. Parameters: $N = 40$, $h_x = 1.152J$, $h_z = 0.974J$ (top) and $h_x = 1.352J$ (bottom).

The Hamiltonian $\hat{H}$ is again the QIM, Eq. (15.2), while the Lindblad dissipators for different data elements are randomly rotated single and two-site operators, see SM [39]. The exact form of $\hat{L}_j^{(\gamma)}$ is not important, but sufficient randomness in either the form or the relative dissipation rates is needed to have a diverse enough training set. Fig. 15.3 shows results for steady states obtained using time-evolving block decimation technique [46, 45] for vectorized density matrices on systems of size $N = 40$, using bond dimension $\chi = 100$. For $|\mathcal{S}| = 4$, we plot the test error as a function of the number of latent variables for different strengths of coupling to Markovian baths ϵ and for Hamiltonians that are either integrable or non-integrable.

At a weak coupling to baths $\epsilon = 0.001$ and chaotic $\hat{H}$ the test error levels off at $N_L \approx 2$, Fig. 15.3a. In the SM [39], we show that the single latent variable, which already reaches high accuracy, again corresponds to the energy, confirming that Gibbs ensembles approximate density matrices. Further latent variables capture information about $\delta\hat{\rho}(\epsilon)$ corrections. We find that observables strongly and monotonously varying along the perpendicular direction of the tSNE representation are related to the features of the baths, i.e., the correlations that baths promote, see SM [39]. This could be used for the detection of noise type, as relevant for quantum error correction.

For integrable $\hat{H}$, Fig. 15.3c, more than one latent variable is needed even for an approximate description. The t-SNE in Fig. 15.3d reveals that the first two latent variables are related to linear combinations of the two most local inversion symmetric charges $\hat{C}_0 = \hat{H}$ and $\hat{C}_2$,

confirming that GGEs approximately describe steady states [26, 25, 33]. Furthermore, our approach exposes that of macroscopically many conservation laws, only two are particularly relevant for an approximate description of all local observables with support up to $|\mathcal{S}| = 4$. Further latent variables are for corrections $\delta\hat{\rho}(\epsilon)$. At stronger $\epsilon = 0.2, 1.0$, a larger number of latent variables is necessary. Hence, for our choice of Lindblad operators, there is no simple emergent description.

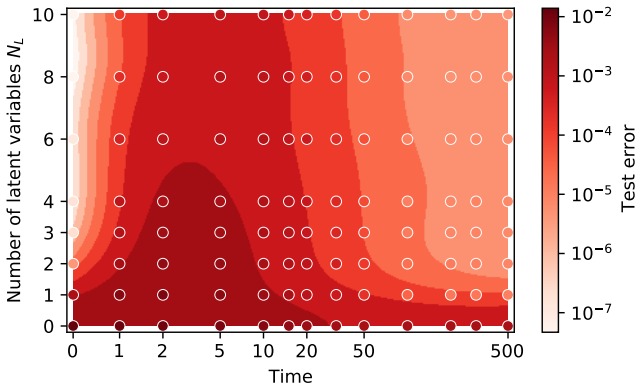


Figure 15.4: Complexity during random unitary evolution of $N = 20$ spins captured by the autoencoder network. Starting from a simple product state, an intermediate regime of high complexity is traversed before an effective one-dimensional description emerges at late times due to the presence of a conserved charge. For times $t > 1$ the scale is logarithmic. Data points (colored dots) are augmented by discretized heatmap based on a bivariate B-spline interpolation.

Random unitary evolution and information bottleneck.

Finally, we study the local complexity at intermediate times, Fig. 15.1(iii), by analyzing states evolved by random unitary dynamics. Random unitary circuits have recently received substantial interest because they allow the analysis of typical features of non-equilibrium dynamics [36, 4, 5, 6, 7, 41, 42, 43, 44, 45, 46, 26]. We will now show that in combination with our unsupervised learning of local complexity, they provide suited grounds to explore the information barrier, appearing at intermediate times in the time evolution from simple (product) states. To detect the information barrier, a detour away from Hamiltonian dynamics is necessary, in order to add a random component to the time evolution. From the perspective of the autoencoder, states that are obtained through deterministic dynamics starting from the few-parameter family of product states have a constant complexity: the fixed unitary map can be absorbed in the encoder/decoder of the network such that a few-parameter representation is possible at all times. On the other hand, the effective reduction of complexity at late times could also be studied under Hamiltonian dynamics when considering a higher-dimensional manifold of initial states.

Our model of random unitary evolution is based on alternating application of two-site gates on even and odd links of the spin chain. The unitary gates vary randomly from step to step, but they are homogeneous across the chain to preserve translational symmetry. Moreover, we choose the unitaries to be $U(1)$-symmetric to impose magnetization as a single conserved quantity. Building on the results of the previous sections, we anticipate that a single Lagrange multiplier associated with the magnetization conservation will locally characterize states at late times. The initial states are random translationally invariant product states. At each time step, we measure all operators with support $|\mathcal{S}| = 3$ and train the autoencoder with different N_L-dimensional bottlenecks. See SM [39] for details.

Fig. 15.4 displays the test errors that we find as a function of time and number of latent

variables. The full description of the initial product state by two Bloch angles is reflected in very small test errors when using two or more latent variables. At late times a single latent variable is sufficient for faithful reconstruction, consistent with convergence to a reduced density matrix corresponding to an ensemble fully characterized by a single Lagrange multiplier. At intermediate times, however, the reconstruction error becomes large even for rather wide bottlenecks because the generic dynamics modelled by random unitary circuits generates complex quantum states, for which no effective low-dimensional parametrization exists. In that sense, our unsupervised learning approach probes the information barrier of quantum many-body dynamics. This concept of local complexity should, on the other hand, not be mistaken for the circuit complexity, which generically grows as a function of the random circuit depth [18].

Hamiltonian reconstruction.

When our approach reveals that data has a (near) one-dimensional latent representation (like top Fig. 15.2c or Fig. 15.3b), presumably corresponding to thermal states ρ, this connection can be exploited to reconstruct $\hat{H}$, as we outline now for the translationally invariant case. We first single out operators $\hat{O}(\boldsymbol{\alpha}) \equiv \hat{O}_{j=1}(\boldsymbol{\alpha}) = \hat{\sigma}_1^{\alpha_1} \dots \hat{\sigma}_{|\mathcal{S}|}^{\alpha_{|\mathcal{S}|}}$ for which we measure a large average gradient of $O_\rho(\boldsymbol{\alpha}) = \mathrm{Tr}[\hat{\rho}\,\hat{O}(\boldsymbol{\alpha})]$ along the effective one-dimensional latent manifold, spanned by different temperatures. These are candidate Hamiltonian terms $\hat{H} = \sum_{j,\boldsymbol{\alpha}} a_{\boldsymbol{\alpha}} \hat{O}_j(\boldsymbol{\alpha})$. Using Newton's method or similar, we find coefficients $a_{\boldsymbol{\alpha}}$ up to a scaling factor from the conditions $\mathrm{Tr}[\hat{O}(\boldsymbol{\alpha})\, e^{\sum_{j,\boldsymbol{\alpha}} a_{\boldsymbol{\alpha}} \hat{O}_j(\boldsymbol{\alpha})}]/\mathrm{Tr}[e^{\sum_{j,\boldsymbol{\alpha}} a_{\boldsymbol{\alpha}} \hat{O}_j(\boldsymbol{\alpha})}] - O_\rho(\boldsymbol{\alpha}) = 0$. Testing this approach with the data presented in Fig. 15.2, h_x/J is reconstructed within the accuracy of the Newton's method. Using the data in Fig. 15.3b for $\epsilon = 0.001$, the relative strength of fields is obtained within 5% and 1% for h_x/J and h_z/J, respectively. See the SM [39] for more information on the algorithm. In contrast to other methods [71, 72, 73, 74], our approach is unsupervised and relies only on expectation values.

Discussion.

We have introduced an unsupervised learning approach that reveals information about the existence of effective low-dimensional descriptions of many-body quantum states. Although no domain knowledge is provided during optimization, we showed for some examples how physical information can be extracted from the trained autoencoders. In that sense, our results constitute a step towards interpretable machine learning of physics.

An alternative to our approach is the analysis of the intrinsic dimension of the data sets [9, 10, 11, 12, 13, 14, 15, 16, 17, 18, 84, 85]. In the SM [39] we include a corresponding analysis of our data as reference. While the results are consistent, the autoencoder method seems more robust, and it has the advantage to reveal further information beyond the minimal number of independent variables.

Autoencoders could be used, for example, to detect GGEs in weakly open trapped-ions setups [33]. Natural extensions of the present work could be the investigations of Floquet prethermal plateaus and of thermalization in strongly disordered many-body systems. Our method could complement the recent proposal to use supervised or confusion learning based on observations from cold atom experiments [86]. In the SM [39], we give first evidence that autoencoders can be used for noise-type recognition, relevant for quantum error correction, which opens another exciting direction. Finally, interesting questions to explore are the possibility of learning with incomplete or imperfect observations. In that regard, refinements of the deep learning model might be required, e.g., the utilization of variational autoencoders for resilience against noise [87].

15.2 Supplemental material to From observations to complexity of quantum states via unsupervised learning by Schmitt, Lenarčič

15.2.1 Conservation laws of transverse field Ising model

The transverse field Ising model, a special case of the quantum Ising model (QIM) used in the main text,

$$\hat{H} = \sum_j J\hat{\sigma}^z_j\hat{\sigma}^z_{j+1} + h_x\hat{\sigma}^x_j \tag{15.5}$$

is an example of non-interacting integrable model. If fermionized, the fermionic mode occupations are its non-local conservation laws. One can, alternatively, construct local conservation laws of the following form [43]

$$\begin{aligned}
\hat{C}_0 &= \hat{H} \\
\hat{C}_2 &= \sum_j J\hat{S}^{zz}_{j,j+2} - h_x\hat{\sigma}^y_j\hat{\sigma}^y_{j+1} - h_x\hat{\sigma}^z_j\hat{\sigma}^z_{j+1} - J\hat{\sigma}^x_j \\
\hat{C}_{2k>2} &= \sum_j J\hat{S}^{zz}_{j,j+k+1} - h_x\hat{S}^{yy}_{j,j+k} - h_x\hat{S}^{zz}_{j,j+k} + J\hat{S}^{yy}_{j,j+k-1} \\
\hat{C}_{2k-1} &= J\sum_j \hat{S}^{yz}_{j,j+k} - \hat{S}^{zy}_{j,j+k},
\end{aligned} \tag{15.6}$$

where $\hat{S}^{\alpha\beta}_{i,j} = \hat{\sigma}^\alpha_i\hat{\sigma}^x_{i+1}\ldots\hat{\sigma}^x_{j-1}\hat{\sigma}^\beta_j$. Such a formulation of conservation laws is useful, because there typically exists a hierarchy of importance in the description of equilibration in integrable systems: expectation values of local observables are typically reasonably well captured by truncated generalized Gibbs ensembles that include only the most local conservation laws [4].

Also in our study of QIM in the presence of weak openness and driving, t-SNE visualization of what was learned in the latent space pointed out that the two principal directions were spanned by a linear combination of $\hat{C}_0 = \hat{H}$ and $\hat{C}_2$, i.e., the expectation values of all operators with support up to 4 were given mainly by $\langle\hat{H}\rangle$ and $\langle\hat{C}_2\rangle$, while less local conservation laws were less crucial. While our choice of Lindblad driving, Eq. (15.16), was not parity symmetric, and thus $\langle\hat{C}_{2k-1}\rangle \neq 0$ and $\lambda_{2k-1} \neq 0$, the importance of $\hat{C}_1$ and $\hat{C}_3$ was clearly smaller. Coupling to baths that are by symmetry geared towards generation of currents would, on the other hand, promote the importance of $\langle\hat{C}_{2k-1}\rangle$ [25].

15.2.2 From Lagrange parameters to latent representation

An ideal test bed for the discussed methods are data sets of expectation values calculated from generalized Gibbs ensembles (GGEs). These are statistical density matrices of the form

$$\hat{\rho}_{\boldsymbol{\lambda}} = \frac{1}{Z(\boldsymbol{\lambda})}\exp\left(\sum_{i=0}^{N_C-1}\lambda_i\hat{C}_i\right), \tag{15.7}$$

defined by a set of N_C mutually commuting conserved charges $\hat{C}_i$, $[\hat{C}_i, \hat{C}_j] = 0$ and fully characterized by N_C parameters λ_i, which are called Lagrange multipliers. Lagrange multipliers of common charges have special names, for example the temperature or the chemical potential. Moreover, $Z(\boldsymbol{\lambda}) = \mathrm{Tr}[e^{\sum_i\lambda_i\hat{C}_i}]$ denotes the partition sum.

If the expectation values of the charges are known, the Lagrange multipliers are implicitly determined by

$$\langle\hat{C}_i\rangle = \mathrm{Tr}\big[\hat{C}_i\hat{\rho}_{\boldsymbol{\lambda}}\big] \equiv F_i(\boldsymbol{\lambda})\ . \tag{15.8}$$

In order to obtain the Lagrange multipliers one has to solve this system of non-linear equations, i.e., find F_i^{-1} such that

$$\lambda_i = F_i^{-1}(\boldsymbol{C}) \ , \tag{15.9}$$

where $\boldsymbol{C} = (\langle \hat{C}_1 \rangle, \ldots, \langle \hat{C}_{N_C} \rangle)$.

Generally, the charges can be written as linear combination of the local operator strings,

$$\hat{C}_i = \sum_{\boldsymbol{\alpha},j} c_{i\boldsymbol{\alpha}} \hat{O}_j(\boldsymbol{\alpha}) \tag{15.10}$$

We can expand the set of equations (15.8) to include all operator strings $\hat{O}(\boldsymbol{\alpha}) \equiv \hat{O}_1(\boldsymbol{\alpha}) = \hat{\sigma}_1^{\alpha_1} \ldots \hat{\sigma}_{|\mathcal{S}|}^{\alpha_{|\mathcal{S}|}}$ of a given support $|\mathcal{S}|$, characterized with $\boldsymbol{\alpha} = (\alpha_1, \ldots, \alpha_{|\mathcal{S}|}) \in \{0, x, y, z\}^{|\mathcal{S}|}$, yielding

$$\langle \hat{O}(\boldsymbol{\alpha}) \rangle = \mathrm{Tr}\big[\hat{O}(\boldsymbol{\alpha})\hat{\rho}_{\boldsymbol{\lambda}}\big] \equiv \tilde{F}_{\boldsymbol{\alpha}}(\boldsymbol{\lambda}) \tag{15.11}$$

Therefore, using Eq. (15.9), we can write the inverse of Eq. (15.11) as

$$\lambda_i = F_i^{-1}\Big(\sum_{\boldsymbol{\alpha}} c_{i\boldsymbol{\alpha}} \langle \hat{O}(\boldsymbol{\alpha}) \rangle \Big) \equiv \tilde{F}_i^{-1}(\boldsymbol{O}) \ . \tag{15.12}$$

Now $\boldsymbol{O}$ is a vector of all measured operators with different $\boldsymbol{\alpha}$ and corresponds to the type of data set introduced in the main text. Moreover, the self-consistency equation

$$\langle \hat{O}_i \rangle = \tilde{F}_i\big(\tilde{F}_1^{-1}(\boldsymbol{O}), \ldots, \tilde{F}_{N_C}^{-1}(\boldsymbol{O})\big) \tag{15.13}$$

resembles the structure of the bottleneck autoencoder: $\tilde{F}_i^{-1}$ is the non-linear encoder that reduces the input data to a low-dimensional latent representation $\boldsymbol{\lambda}$, and $\tilde{F}_i$ is the non-linear decoder that reproduces the input data from the given latent representation. In the main text, we showed that for data from GGEs the unsupervised training of bottleneck autoencoders indeed allows to identify meaningful low-dimensional representations related to the charges and Lagrange multipliers.

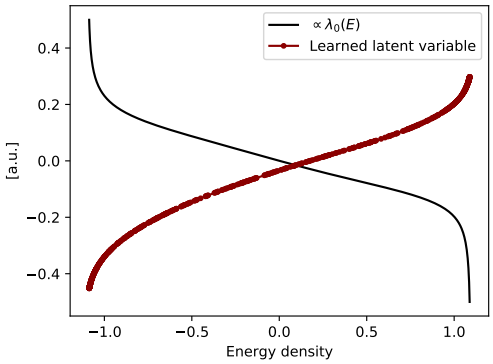


Figure 15.5: The learned latent representation of a network with a bottleneck of width one as function of energy density compared to the inverse temperature of the corresponding density matrix.

Here we give some additional information on this relation. First, we consider the thermal density matrices

$$\hat{\rho}_{\lambda_0} = \frac{1}{Z(\lambda_0)} \exp\left(\lambda_0 \hat{H}\right) \tag{15.14}$$

with $\hat{H}$ the QIM Hamiltonian (15.5) at $h_x/J = 0.6$. As shown in the main text, Fig. 1, we compute the expectation values (15.11) using exact diagonalization on $N = 12$ sites. For this purpose we exploit translational symmetry to reduce the dimension and work in the zero momentum sector. Considering all possible operators $\hat{O}(\boldsymbol{\alpha})$ supported on no more than $|\mathcal{S}| = 3$ lattice sites, we computed the expectation values for random temperatures, drawn from the uniform distribution on the interval $\lambda_0 \in [-2/J, 2/J]$.

Using a bottleneck network with a single latent variable, we achieve a test error $\mathcal{L}_{\text{test}} \approx 10^{-8}$. This indicates that a very accurate one-dimensional encoding is found, as we would expect, because the density matrix (15.14) is fully characterized by temperature as a single parameter. In Fig. 15.5 we show for our full data set the value attained by the latent variable as a function of energy. We include also the corresponding inverse temperatures. A naive expectation would be that during training the bottleneck networks learns to encode either the temperature or the energy density in the available latent variable. If temperature is encoded, the decoder would have to learn only the function $\tilde{F}(\lambda_0)$ as in Eq. (15.11). If energy is encoded, the decoder would also need to include the inversion as in Eq. (15.9), i.e., approximate $\tilde{F} \circ F^{-1}$. The result in Fig. 15.5, however, shows that the latent representation learned does not coincide with either of the two. And, in fact, it is sufficient to learn a latent representation $\boldsymbol{l}$ that is related to energy (or temperature) by an invertible function G, because with $E = G^{-1}(\boldsymbol{l})$ the decoder can learn $\tilde{F} \circ F^{-1} \circ G^{-1}$ in order to map the latent value $\boldsymbol{l}$ to the vector of observations $\boldsymbol{O}$. In Fig. 15.5 we see that $\boldsymbol{l} = G(E)$ is strictly monotonic and, hence, indeed invertible.

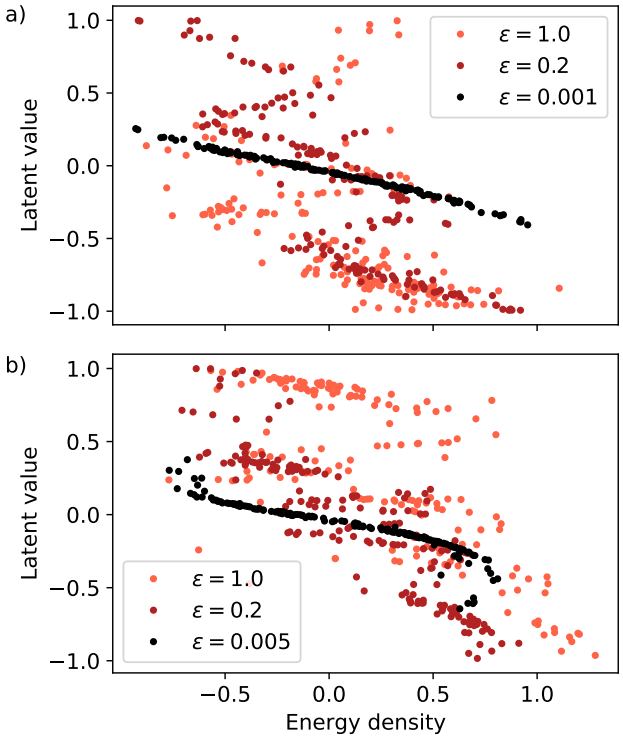


Figure 15.6: The learned latent representation as a function of energy density, obtained by a network with a single latent variable for different strength of coupling to the environment ϵ and (a) chaotic or (b) integrable $\hat{H}$. (a) Only for $\epsilon = 0.001$ and chaotic $\hat{H}$, energy and the first latent variable are related with an invertible function. (b) For $\epsilon = 0.005$ and integrable $\hat{H}$, the first latent variable and energy are strongly correlated, however, non-monotonicity indicates that further latent variables, associated with additional charges, are needed. At stronger couplings to baths $\epsilon = 0.2, 1.0$ the first latent variable is not related to energy at all.

In an open Markovian setup, such a relation exists in the limit of weak coupling to the

environment. In the main text, we consider steady states of combined unitary and Markovian dynamics

$$\dot{\hat{\rho}} = i[\hat{\rho}, \hat{H}] + \epsilon \sum_{j,\gamma} \left(\hat{L}_j^{(\gamma)} \hat{\rho} \hat{L}_j^{(\gamma)\dagger} - \frac{1}{2} \{ \hat{L}_j^{(\gamma)\dagger} \hat{L}_j^{(\gamma)}, \hat{\rho} \} \right). \tag{15.15}$$

The unitary part is given by the QIM, Eq. (15.5), potentially in an additional integrability breaking z-field, $h_z \sum_j \hat{\sigma}_j^z$. Bulk Lindblad operators $L_j^{(\gamma)}$ are rotated single ($\gamma = 1$) and two-site ($\gamma = 2$) operators,

$$\begin{aligned} \hat{L}_j^{(1)} &= R_z(\zeta') R_y(\phi') \frac{\hat{\sigma}_j^0 + \hat{\sigma}_j^z}{2} R_y^{-1}(\phi') R_z^{-1}(\zeta'), \\ \hat{L}_j^{(2)} &= \left(R_z(\zeta) R_y(\phi) \hat{S}_{j-1}^- R_y^{-1}(\phi) R_z^{-1}(\zeta) \right) \frac{\hat{\sigma}_j^0 - \hat{\sigma}_j^z}{2}. \end{aligned} \tag{15.16}$$

Here, $R_{z(y)}(\zeta)$ is a rotation for ζ around the $z(y)$ spin axis and $\zeta, \zeta', \phi, \phi' \in [-\pi, \pi]$ are chosen randomly.

At a weak coupling to the environment, $\epsilon \ll 1$ and a chaotic $\hat{H}$, the first latent value is still related to the energy $\mathrm{Tr}[\hat{H}\hat{\rho}]$ by an invertible function, as seen in Fig. 15.6a, showing results obtained with a single latent variable network. In our setup, the first latent variable turns out to be largely related to energy also for the integrable $\hat{H}$, Fig. 15.6b. The fact that further latent variables, related to other charges, are needed, is revealed only by extremal values of energy and latent values, which show that the relation is nonetheless non-invertible in this case. As we pointed out in the main text, for stronger couplings $\epsilon = 0.2, 1.0$ to baths, steady states are no longer approximately described by Gibbs ensembles of form (15.14), thus energy plays no unique role.

15.2.3 Detecting the structure of noise

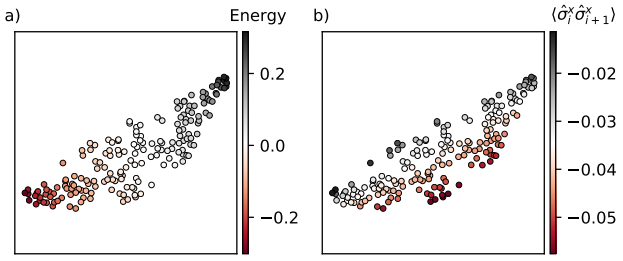


Figure 15.7: tSNE for the latent representation of steady state expectation values in setup with chaotic QIM and Eq.(15.18) Lindblad operators. The coloring is with respect to (a) the energy density and (b) correlations $\langle \hat{\sigma}_j^x \hat{\sigma}_{j+1}^x \rangle$. This reveals that the first latent variable is related to energy, while the second one detect the type of correlations that our structured noise is promoting. Parameters: $h_x/J = 0.709$, $h_z/J = 0.9042$, $\epsilon = 0.02$, $N = 40$, $\chi = 100$, $|\mathcal{S}| = 4$.

In the main text and above we showed that in the latent representation of steady states for weakly open system with chaotic H, the first latent variable is related to the energy density (or temperature). This is in agreement with the steady state $\hat{\rho}(\epsilon) \sim \hat{\rho}_{\lambda_0} + \delta\hat{\rho}(\epsilon)$ being approximated by a Gibbs ensemble $\hat{\rho}_{\lambda_0}$. However, further latent variables are needed to capture corrections $\delta\hat{\rho}(\epsilon)$. If baths have some structure, i.e., are promoting certain correlations, those correlations can be extracted from the additional latent variables.

To show this we consider chaotic QIM, weakly coupled to structured baths represented by dissipators

$$\hat{\mathcal{D}} = \epsilon\big(\gamma_1\hat{\mathcal{D}}^{(1)} + \gamma_2\hat{\mathcal{D}}^{(2)} + \gamma_3\hat{\mathcal{D}}^{(3)} + \gamma_4\hat{\mathcal{D}}^{(4)} + \hat{\mathcal{D}}^{(5)}\big) \tag{15.17}$$

with random rates $\gamma_1, \gamma_2, \gamma_3, \gamma_4 \in [0, 1]$ and of the form given by Lindblad operators

$$\begin{aligned} \hat{L}_j^{(1)} &= \hat{S}_j^{+,x}\hat{P}_{j+1}^{\downarrow,x}, \quad \hat{L}_j^{(2)} = \hat{P}_j^{\downarrow,x}\hat{S}_{j+1}^{+,x}, \\ \hat{L}_j^{(3)} &= \hat{S}_j^{-,x}\hat{P}_{j+1}^{\uparrow,x}, \quad \hat{L}_j^{(4)} = \hat{P}_j^{\uparrow,x}\hat{S}_{j+1}^{-,x}, \\ \hat{L}_j^{(5)} &= \hat{S}_j^z \end{aligned} \tag{15.18}$$

where $\hat{S}_j^{\pm,x} = \frac{1}{2}(-\hat{\sigma}_j^z \pm i\,\hat{\sigma}_j^y)$ and $\hat{P}_j^{\uparrow/\downarrow,x} = \frac{1}{2}(\hat{\sigma}_j^0 \pm \hat{\sigma}_j^x)$. It is clear that while $\hat{L}_j^{(5)}$ cause featureless dephasing, $\hat{L}_j^{(1-4)}$ enhance anti-ferromagnetic correlations in spin x-direction, $\langle\sigma_j^x\sigma_{j+1}^x\rangle < 0$.

Given that the latent representation provides compressed information on the steady state, we can use it to detect antiferromagnetic correlations in the data. Fig. 15.7 shows tSNE of the latent representation, colored by (a) the energy density and (b) correlation $\langle\sigma_j^x\sigma_{j+1}^x\rangle$. Like for the other choice of Lindblad operators, the first latent variable is related to energy, resulting in tSNE being primarily extended along this direction, Fig. 15.7a. As shown in Fig. 15.7b, the perpendicular direction is indeed spanned by the antiferromagnetic correlations $\langle\sigma_j^x\sigma_{j+1}^x\rangle < 0$, promoted by the bath. The second latent variable is thus capturing the most crucial information in $\delta\hat{\rho}(\epsilon)$, namely, the anti-ferromagnetic correlations.

As we demonstrated above, our approach has the potential do detect the form of structured noise that might be present in a quantum simulator or quantum computer, at each run with a different strength but of the same form. Knowing it could assist quantum error correction algorithms.

15.2.4 Random unitary model

We consider a model of random unitary dynamics of a spin-1/2 chain with $N = 20$ sites that preserves the total magnetization. In particular, we consider random two-site unitaries that are applied alternatingly on even and odd links of the chain. This approach preserves locality of dynamics despite the randomness and it was studied extensively in previous works [4, 5, 6, 7]. However, our model differs slightly from the conventional Haar random unitaries, because it is constructed with two constraints in mind, namely (i) the ability to work with a small number of distinct observations and (ii) the desire to resolve to some extent the short time dynamics.

In order to be able to work with a limited number of distinct observations (i) similar to the other applications in the present work, we consider translationally invariant random unitaries, which also obey lattice inversion symmetry. This restricts our choice to unitaries corresponding to Hamiltonians of the form

$$\hat{H} = a\big(\hat{S}_1^+\hat{S}_2^- + \hat{S}_1^-\hat{S}_2^+\big) + b\hat{\sigma}_1^z\hat{\sigma}_2^z + c\big(\hat{\sigma}_1^z + \hat{\sigma}_2^z\big)\ , \tag{15.19}$$

which is split into three blocks corresponding to the possible values of total magnetization of the two spins involved. For the zero magnetization block we sample random eigenvalues θ_1, θ_2 uniformly from $[-\pi, \pi]$, which translate into couplings $a = (\theta_2 - \theta_1)/2$ and $b = (\theta_1 + \theta_2)/2$. The diagonal components in the polarized sectors are $b \pm 2c$ and we sample uniformly distributed c from $[-\pi/2, \pi/2]$ as the third independent random variable.

Finally, to achieve (ii), we construct the random unitary as $\hat{U}(a, b, c) = e^{-i\Delta t\hat{H}}$ with $\Delta t = 0.1$. Thereby, all unitaries have a large admixture of the identity and do not fully scramble the two spin subspace within one step. In Fig. 3 the effect of this restriction is that for large numbers of latent variables the maximal test error is only reached after a few steps and not

immediately after the first step. We expect that considering larger support of observables would have a similar effect, because then locality of the random unitaries could be resolved.

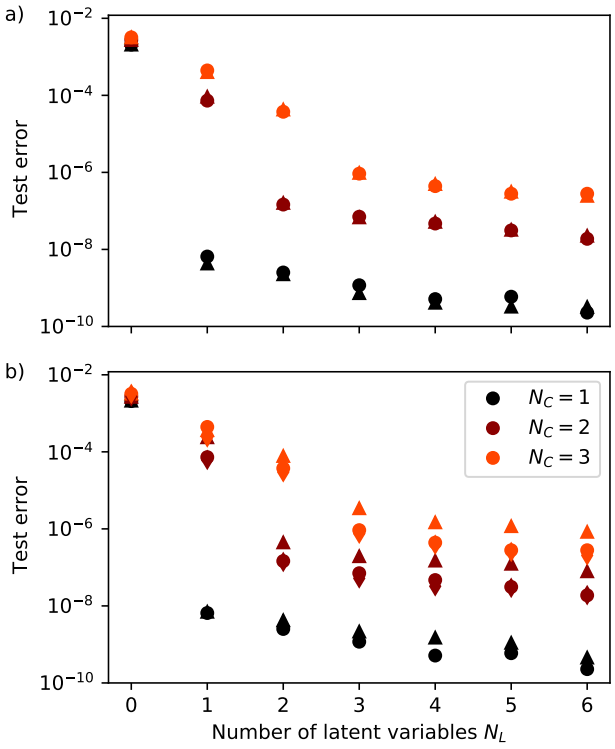


Figure 15.8: Dependence of the training outcome on varying network size and number of training data. The physical setting is the same as in Fig. 1 of the main text. a) Comparison of network widths 200 (triangles) and 400 (dots). b) Comparison of training data sizes 500 (triangles), 2000 (dots), and 8000 (diamonds).

15.2.5 Training of autoencoder networks

All results were obtained using basic feed-forward neural networks exhibiting the bottleneck structure discussed in the main text. A feed-forward neural network made up of layers corresponding to a sequence of alternating affine-linear and non-linear transformations. To obtain the activations $a_j^{(l)}$ of the l-th layer, the activatons of the previous layer, $a_j^{(l-1)}$, are transformed as

$$a_j^{(l)} = \sigma\Big(\sum_k W_{jk} a_k^{(l-1)} + b_j\Big) \,. \tag{15.20}$$

Here, W_{jk} and b_j are variational parameters and σ is a fixed non-linear activation function.

Throughout this work we used $\sigma \equiv \tanh$ and networks with two encoder layers between input and latent space, as well as two decoder layers between latent space and output, see Fig. 1 of the main text. Each of these layers had a size of 400 neurons; convergence in network size is demonstrated exemplarily in Fig. 15.8a. To train the network we used the Adam optimizer [8] with learning rate $r = 5 \times 10^{-4}$ and the standard parameters $\beta_1 = 0.9$, $\beta_2 = 0.999$, $\epsilon = 10^{-8}$. We chose training batch sizes and the total number of training steps depending on the size of the training data set and convergence behavior. These values are summarized in Tab. 2. The numbers of data given in this table are the total number of data used, of which 80% served as training data and 20% were used as test data. In Fig. 15.8b we show the effect of varying the size of the training data set exemplarily for the setting of Fig. 1 of the main text.

To avoid overfitting we adopted an "early stopping" procedure, in that we used the parameter sets that resulted in the minimal test error during optimization for our further analysis. While in many cases we observed the typical minimum in the test error at intermediate optimization steps (indicating later overfitting), we found that in cases where few variables fully describe the training data that perfect generalization is achieved and the test error is always reduced in the same way as the training error.

When comparing different sizes of the latent space, we include results obtained with zero latent variables as a reference. In that case the encoder and decoder are completely decoupled, meaning that the decoder receives no information about the input and the network can only learn the best constant to approximate the data, namely the mean.

15.2.6 Intrinsic dimension

Here we compare the autoencoder's dimensional reduction to an alternative way of computing the intrinsic dimension I_d of data [9, 10, 11, 12, 13, 14, 15, 16, 17, 18], using a nearest neighbor method introduced in Ref. [16], where one calculates the distribution $f(\mu)$ of the ratio of distances to the next-nearest and nearest neighbour, $\mu = r_2(\boldsymbol{x})/r_1(\boldsymbol{x})$, of the vector $\boldsymbol{x}$. In our case, the vector $\boldsymbol{x}$ contains as entries (i) expectation values of all N_O different measured operators or (ii) values of N_L different latent variables. For data points that are locally uniformly distributed on an I_d dimensional hypersphere, $f(\mu) = I_d \mu^{-I_d-1}$. We can determine I_d by fitting $f(\mu)$ to the input data for the encoder.

Following Ref. [16], the explicit algorithm for determining the intrinsic dimension I_d consists of the next steps:

1. For each vector $\boldsymbol{x}_j$, $j \in [1, N_{real}]$, containing as entries (i) expectation values of measured operators or (ii) values of latent neurons for j-th data element, find the Euclidean distance to the nearest and the next-nearest neighbour, $r_1(\boldsymbol{x}_j)$ and $r_2(\boldsymbol{x}_j)$, respectively.

2. Compute the ratio $\mu = \frac{r_2(\boldsymbol{x}_j)}{r_1(\boldsymbol{x}_j)}$ for each of N_{real} different data elements.

3. Get the distribution of μ, $f(\mu)$. For points that are drawn from an I_d dimensional hypersphere with constant density,
$$f(\mu) = I_d \, \mu^{-I_d-1} \tag{15.21}$$
For the algorithm to work, in our data, uniform distribution must be satisfied just locally, roughly on the level of nearest neighbors.

4. Calculate the cumulative distribution $P(\mu) = \sum_{\mu'<\mu} f(\mu')$ and fit I_d from the linear dependence
$$\ln(1 - P(\mu)) = -I_d \ln(\mu). \tag{15.22}$$

Setting	Num. data	Batch size	Num. steps
(G)GE	2000	128	250000
Lindblad evol.	~ 200	16	250000
Rnd. unitary	~ 1000	64	50000

Table 2: Training parameters for the different applications. Numbers of training data for Lindblad evolution and random unitary evolution varied slightly for the different physical parameter sets due to the compute time required for data generation.

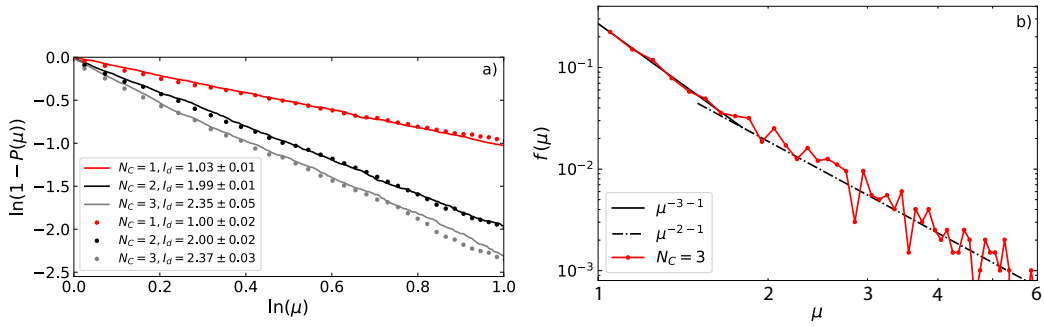


Figure 15.9: a) Dependence (15.22) for data set with QIM GGE expectation values that are parametrized with $N_C = 1, 2, 3$ Lagrange multipliers, implying $I_d = N_C$. I_d is fitted from the slope. Solid lines correspond to the analysis done directly on expectation values of operators (autoencoder input data) using $N_{real} = 2000$ different Lagrange multipliers. Points are obtained using data in the latent space, with a prior dimensional reduction performed by the encoder and $N_{real} = 1000$. b) Distribution (15.21) for $N_C = 3$ shows two distinct powers, corresponding to $I_d \approx 3$ at shorter scales ($\mu < 1.5$) and $I_d \approx 2$ at longer scales ($\mu > 2$).

Fig. 15.9a shows dependence (15.22) for sets of expectation values, calculated from GGEs, Eq. (15.7), with $N_C = 1, 2, 3$ charges of QIM ($\hat{C}_i, i = 0, 1, 2$, Eq. (15.6)) and random corresponding Lagrange multipliers. Here, we re-analyse the exact diagonalization results for $N = 12$ system size and $h_x/J = 0.6$, in the main text presented in Fig.1. The above procedure, where I_d is fitted from the linear slope in relation (15.22), is performed: (i) Directly on the GGE expectation values, i.e., the input data of encoder, for $N_{real} = 2000$ different choices of Lagrange parameters (solid lines). Each data element is presented as a $N_{\boldsymbol{O}}$ dimensional vector $\boldsymbol{x}_j$ with entries corresponding to measurements of operators $O(\boldsymbol{\alpha})$. Or (ii) on the data from the latent representation with $N_L = 4$ and $N_{real} = 1000$ training realizations. In this case, each data element is presented as a N_L dimensional vector $\boldsymbol{x}_j$ with entries corresponding to latent values. In the latter case, a prior dimension reduction is performed by the encoder.

Since the data is fully characterized by Lagrange parameters, we expect $I_d = N_C$, which is confirmed for $N_C = 1, 2$, Fig. 15.9a. Using Eq. (15.22) for $N_C = 3$, we get $I_d \approx 2.4 < 3$. The reason for this discrepancy is revealed when we look directly at the distribution $f(\mu)$, Eq. (15.21). Fig. 15.9b shows that for $N_C = 3$, $f(\mu)$ has two different slopes corresponding to $I_d \approx 3$ at shorter scales $\mu < 1.5$ and $I_d \approx 2$ at larger $\mu > 2$. In this case, Eq. (15.22) is not valid and should not be used. We do not have a physical interpretation of our observation, which nonetheless signals that method of Ref. [16] should be used with some caution when data has some extra structure. In these cases, analysing $f(\mu)$ is more appropriate compared to the cumulative distribution $P(\mu)$.

We conclude that I_d can give a good cross-check of the dimensional reduction by autoencoders; however, this approach can be subtle and it is restricted to detecting the effective dimensionality of the data without further insights into the characteristics of the encoded information.

15.2.7 Hamiltonian reconstruction

In this section we give more details on the algorithm for the reconstruction of translationally invariant Hamiltonians, which can be used under the condition that expectation values originate from (approximately) thermal states. A minimal knowledge on whether the energy is (at least approximately) conserved is thus required. The algorithm has the following steps:

1. Check that a single parameter (related to temperature or $\langle \hat{H} \rangle$ by an invertible function) to a good approximation describes all expectation values, i.e., the latent representation

must be (roughly) one dimensional. This can be done by calculating the test error as a function of number of latent variables or the intrinsic dimension I_d.

2. Calculate the t-SNE of the latent space of a trained autoencoder.

3. Find operators $\hat{O}(\boldsymbol{\alpha}) \equiv \hat{O}_{j=1}(\boldsymbol{\alpha}) = \hat{\sigma}_1^{\alpha_1} \dots \hat{\sigma}_{|\mathcal{S}|}^{\alpha_{|\mathcal{S}|}}$ with the largest gradient in measured expectation values $O_\rho(\boldsymbol{\alpha}) = \mathrm{Tr}[\hat{O}(\boldsymbol{\alpha})\hat{\rho}]$ with respect to their position in the t-SNE. Operators are labelled by $\boldsymbol{\alpha} = (\alpha_1, \dots, \alpha_{|\mathcal{S}|}) \in \{0, x, y, z\}^{|\mathcal{S}|}$ and $\hat{\sigma}_j^{0,x,y,z}$ denoting the identity and the Pauli matrices, respectively. Gradient in $O_\rho(\boldsymbol{\alpha})$ is calculated in two ways: (a) For exactly thermal states, along the local tangential direction of the one-dimensional t-SNE, see Fig.15.10a. (b) For approximately thermal states, along the first component according to the principal component analysis (PCA) of the t-SNE that is not strictly one-dimensional, see Fig.15.10b.

4. To get a scalar, average the gradient values over all points in the latent space. Operators with largest average gradients $\overline{\partial\langle O(\boldsymbol{\alpha})\rangle}$ are candidate terms in the Hamiltonian $H = \sum_{j,\boldsymbol{\alpha}} a_{\boldsymbol{\alpha}} \hat{O}_j(\boldsymbol{\alpha})$.

5. In order to find the prefactors $a_{\boldsymbol{\alpha}}$ and eliminate operators that are actually not in the Hamiltonian, run Newton's method (or some other method for calculation of roots) in order to find zeros of

$$\frac{\mathrm{Tr}[\hat{O}(\boldsymbol{\alpha}) e^{\lambda_0 \sum_{j,\boldsymbol{\alpha}} a_{\boldsymbol{\alpha}} \hat{O}_j(\boldsymbol{\alpha})}]}{\mathrm{Tr}[e^{\lambda_0 \sum_{j,\boldsymbol{\alpha}} a_{\boldsymbol{\alpha}} \hat{O}_j(\boldsymbol{\alpha})}]} - O_\rho(\boldsymbol{\alpha}) = 0, \, \forall \boldsymbol{\alpha}. \tag{15.23}$$

Here, $O_\rho(\boldsymbol{\alpha})$ are the measured expectation values. Thermal expectation values can be efficiently calculated using imaginary time evolution with tensor networks. We set $\lambda_0 \equiv 1$; this implies that we can determine only the relative values of coefficients in $\hat{H}$. To get the absolute values, we would need additional information, for example, from the dynamics under such a Hamiltonian.

An alternative way to fix $a_{\boldsymbol{\alpha}}$ would be to calculate the kernel of correlation matrix proposed in Ref. [19]. With a prior knowledge of a few Hamiltonian candidate terms, kernel calculation is very efficient because the correlation matrix is very small.

6. For approximately thermal states, average $a_{\boldsymbol{\alpha}}$ over different realizations to get a better estimate.

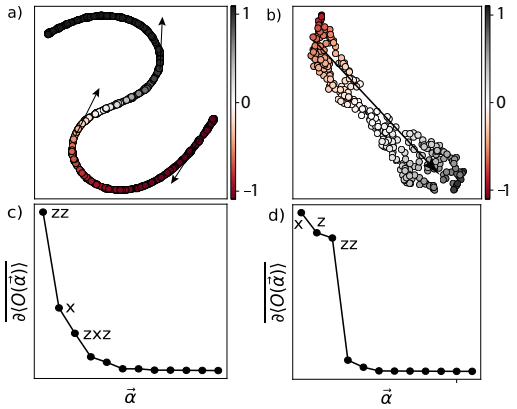


Figure 15.10: a) t-SNE for exactly thermal states of integrable QIM, Eq. (15.5). Gradients of measured expectation values $O_\rho(\boldsymbol{\alpha})$ are calculated along the tangential direction and then averaged along the curve. b) t-SNE for nearly thermal states of non-integrable QIM, $\hat{H} = \sum_j J\hat{\sigma}^z_j\hat{\sigma}^z_{j+1} + h_x\hat{\sigma}^x_j + h_z\hat{\sigma}^z_j$, obtained at a weak coupling to baths $\epsilon = 0.001$. Gradients of $O_\rho(\boldsymbol{\alpha})$ are calculated along the principal direction of PCA, shown with an arrow. c) and d) Averaged gradients $\overline{\partial\langle O(\boldsymbol{\alpha})\rangle}$ for different operators labelled with $\boldsymbol{\alpha}$ for a) and b) case, respectively. Terms from the Hamiltonian show that largest gradients, in particular if evaluated with respect to high temperature steady states as in b).

Now, we analyse the data presented in the main text (Fig.1c and Fig.2b) and previous sections. Fig. 15.10 shows (a,b) t-SNEs and (c,d) relative strengths of averaged gradients $\overline{\partial\langle O(\boldsymbol{\alpha})\rangle}$ for data obtained from Gibbs ensembles ($N_C = 1$) of integrable QIM (left) and from steady states of weakly open ($\epsilon = 0.001$) chaotic QIM (right). In the case of exactly thermal states with, $\hat{H} = \sum_j J\hat{\sigma}^z_j\hat{\sigma}^z_{j+1} + h_x\hat{\sigma}^x_j$, operators $O(\boldsymbol{\alpha})$ with $\boldsymbol{\alpha} = zz, x$ have largest $\overline{\partial\langle O(\boldsymbol{\alpha})\rangle}$, Fig. 15.10c. This confirms that our method detects the Hamiltonian terms. However, we also get significant contribution from operators that are products of terms in $\hat{H}$, i.e., $\boldsymbol{\alpha} = zxz$ and these are eliminated in the step 5. For weakly open case with $\hat{H} = \sum_j J\hat{\sigma}^z_j\hat{\sigma}^z_{j+1} + h_x\hat{\sigma}^x_j + h_z\hat{\sigma}^z_j$ and pretty high-temperature steady states, only the Hamiltonian terms $\boldsymbol{\alpha} = x, z, zz$ have significant values, Fig. 15.10d.

For exactly thermal states, the algorithm reconstructs the $\hat{H}$ up to very high precision, basically given by the quality of the Newton's method implementation. Also for nearly thermal expectation values, obtained with a chaotic $\hat{H}$ and a weak $\epsilon = 0.001$ coupling to Lindblad baths, the relative strength of fields is reconstructed up to 5% and 1% for h_x/J and h_z/J, respectively. This shows that Hamiltonian reconstruction would be possible also for results from slightly noisy quantum devices (NISQ) or from a condensed matter setup with inevitable coupling to phonons. At larger ϵ, errors grow since steady states are further away from thermal states.

16 Reconstructing effective Hamiltonians from nonequilibrium (pre-)thermal steady states by Nandy, Schmitt et al.

Abstract

Reconstructing Hamiltonians from local measurements is key to enabling reliable quantum simulation: both validating the implemented model, and identifying any left-over terms with sufficient precision is a problem of increasing importance. Here we propose a deep-learning-assisted variational algorithm for Hamiltonian reconstruction by preprocessing a dataset that is diagnosed to contain thermal measurements of local operators.

We demonstrate the efficient and precise reconstruction of local Hamiltonians, while long-range interacting Hamiltonians are reconstructed approximately. Away from equilibrium, for periodically and random multipolar driven systems, we reconstruct the effective Hamiltonian widely used for Floquet engineering of metastable steady states. Moreover, our approach allows us to reconstruct an effective quasilocal Hamiltonian even in the heating regime beyond the validity of the prethermal plateau, where perturbative expansions fail.

16.1 Introduction

A central idea at the core of modern quantum simulation is the utilization of highly controllable quantum degrees of freedom to emulate the behavior of complex quantum systems [1, 2, 3, 4, 5, 6, 7, 8, 9, 10, 11, 12, 13]. Besides developing the corresponding state preparation and stabilization techniques, this requires the implementation of the Hamiltonian that governs the physics of the system to be simulated, in the first place. To do this, different approaches have been developed, which leverage specific properties of the underlying quantum system. For instance, analog simulators, such as ultracold atoms [9, 14, 15, 16, 11] and trapped ions [3, 5, 4], are natural platforms of short- and long-range interacting Hubbard and Ising Hamiltonians. By contrast, the digital approach to quantum simulation [17, 18] implemented in superconducting qubits, Rydberg atom [19, 20, 21, 22, 23] or trapped ion [24, 23, 25] platforms, relies on constructing a time-evolution operator using consecutively applied discrete unitary gates.

Whenever the desired Hamiltonian cannot be implemented using the available building blocks in a straightforward way, nonequilibrium techniques, such as Floquet engineering [26, 27, 28] or dynamical decoupling [29, 30, 31, 32], become handy. Recently, periodic drives have enabled the realization of non-equilibrium phase transitions [33, 34], topologically non-trivial systems [35, 36, 37, 38, 39], artificial gauge fields [40, 41, 42] and discrete time crystals [43, 44, 45, 46, 47, 48, 49, 50]. Note that having an effective Hamiltonian is not guaranteed for generic nonequilibrium drives due to the lack of energy conservation; the necessary ingredients for the existence of effective Hamiltonians are currently the subject of intensive on-going research.

Whichever the implementation method may be, engineered effective Hamiltonians often come with additional, unwanted terms. These can be residual (longer-range) interactions, or leftover single-particle field terms; they can also arise due to coupling to existing higher-energy levels or additional cavity modes [51]. Moreover, nonequilibrium protocols used for Hamiltonian engineering rely on the existence of prethermal (meta-)stable steady states, in which heating (i.e., energy absorption and entanglement production) is suppressed up to controllably long times [52, 53, 54, 55, 56]. Nevertheless, residual terms in the effective Hamiltonian (e.g., higher-order corrections) eventually lead to accumulating detrimental heating. In parallel, verifying that a desired Hamiltonian is implemented to a given precision, is a crucial requirement for a reliable quantum simulation; moreover, certification of the realized Hamiltonians becomes indispensable for benchmarking the performance of present-day noisy intermediate scale quantum (NISQ) devices [57, 14, 58, 59, 60]. For all these reasons, developing a procedure, based on measurements of local observables, and capable of identifying and quantifying the Hamiltonian implemented in quantum simulators to a high precision, is a problem of ever-increasing importance.

During the last few years, several methods for Hamiltonian reconstruction have been put forward: from measurements on a single eigenstate [61, 62, 63, 64] using trusted quantum simulator [65, 66, 67]; or from eigenstate dynamics [68, 69, 70, 71, 72, 73, 74], via compressed sensing [75], using restricted Boltzmann machine tomography [76] and neural networks [77]. One common feature of these techniques is that they explicitly assume the underlying Hamiltonian to be both local and a translationally invariant sum of few-body terms. Furthermore, only a few of the above-mentioned methods are applicable to Floquet systems. Although reasonable

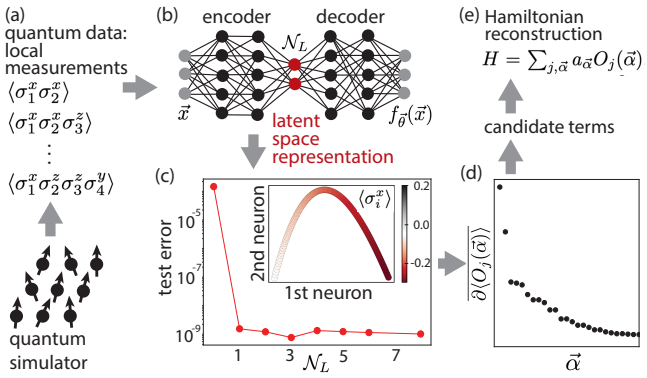


Figure 16.1: Schematic presentation of the Hamiltonian reconstruction algorithm proposed in this work. (a) The input for the Hamiltonian reconstruction are measurements of local operators performed in (locally) (pre-)thermal (steady) states at different temperatures, for example, obtained from a quantum simulator. (b) These serve as input data for the autoencoder, which (c) confirms that the data is indeed parametrized with a single parameter (temperature) by checking that the decoding 'test error' drops at a single neuron in the latent space, and (c, inset) to generate the latent representation of the dataset, which is one-dimensional for thermal data. (d) In the next step, the potential candidate terms $O_j(\vec{\alpha})$ in the Hamiltonian $H = \sum_{j,\vec{\alpha}} a_{\vec{\alpha}} O_j(\vec{\alpha})$ are pre-selected as the operators with the largest average gradient of expectation values $\overline{\partial\langle O_j(\vec{\alpha})\rangle}$ along the latent representation. (e) In the last step, the Hamiltonian coefficients $a_{\vec{\alpha}}$ are fixed. Here, we show actual data from effective Hamiltonian reconstruction in the prethermal plateau for our Floquet protocol, Eq. (16.9), presented in Fig. 16.3.

progress has been achieved recently in this direction [78, 79], the methods employed in these works demand an apriori intuition from the Floquet-Magnus expansion for the selection of candidate terms. However, a typical challenge in any Hamiltonian reconstruction algorithm often lies in developing a systematic method to select candidate terms. It is, therefore, highly desirable to propose an algorithm that relies on an unbiased approach to select the candidate terms of the target Hamiltonian.

In this work, we propose a machine learning-assisted algorithm for the reconstruction of Hamiltonians, which uses as the input the expectation values of local observables that are diagnosed to be thermal. We show that our algorithm can precisely reconstruct local Hamiltonians, while long-ranged Hamiltonians are approximately reproduced with certain limitations. It is worth mentioning that the presence of only few-body terms in the underlying Hamiltonian is advantageous for our method but it is not a necessary requirement. We apply our algorithm to Floquet and random multipolar driven systems with the purpose of reconstructing the effective Hamiltonian, responsible for the stroboscopic expectation values in the prethermal plateau and/or in the follow-up heating regime. For constructing the effective Hamiltonian in the prethermal plateau, our algorithm does not require any a priori intuition from the Floquet-Magnus expansion or any other similar perturbative technique when the selection of candidate terms is concerned. Furthermore, we go beyond prethermal steady states and analyze the heating regime, where perturbative expansions are known to fail. We extract an effective, quasistatic Hamiltonian, which reproduces the thermal measurements of local operators as the system approaches the infinite-temperature state. We directly observe that this effective Hamiltonian becomes less and less local as the system heats up, verifying a hypothesis laid out in previous work [52, 80].

The rest of the paper is organized as follows. In Sec. 16.2, we discuss in detail the algorithm of Hamiltonian reconstruction. Sec. 16.3 deals with illustrative examples where our method is used to reconstruct both short and long-range interacting static Hamiltonian. This is followed

by the central Sec. 16.4, which addresses Hamiltonian reconstruction in dynamical Floquet setups, starting with reconstruction in the prethermal regime. Thereafter, we discuss the insight our algorithm provides into the physics of unconstrained heating for both Floquet systems and non-Floquet systems that exhibit eventual thermal death. Finally, we conclude and present future perspectives in the Sec. 16.5.

16.2 Algorithm for Hamiltonian reconstruction using autoencoders

In our Hamiltonian reconstruction algorithm, we rely on a deep autoencoder neural network [81, 82], Fig. 16.1(b), which is used for the dimensional reduction of the data; in our algorithm this amounts to a preselection of the Hamiltonian candidate terms. In our case, each element of dataset contains measurements of different local operators in a given quantum state, see Fig. 16.1(a). Our approach is applicable if these states are (effectively) thermal. The autoencoder is used to generate a latent representation of the dataset and to verify that the dataset indeed contains measurements on thermal states; whenever this is the case, the latent representation is a one-dimensional manifold, Fig. 16.1(c). Such compressed representation of measurement helps us single out the candidates terms of the Hamiltonian, Fig. 16.1(d), significantly reducing the complexity of the Hamiltonian reconstruction, Fig. 16.1(e), performed in the subsequent step. Previously, some of us proposed part of the algorithm as a way to reconstruct spatially local Hamiltonians [83]. Here we extend the procedure to deal with long-range Hamiltonians as well. In the following, we explain the algorithm in more details.

The autoencoder is a deep neural network, where the input and output layers have the same dimension, while at least one of the middle layers has a considerably smaller number of neurons $\mathcal{N}_L$ and represents a bottleneck, Fig. 16.1(b). The part prior to the bottleneck is called the encoder, which maps the input data to a lower-dimensional latent representation. The decoder then maps the latent representation to the output. The network is set by minimizing the difference between the input $\vec{x}$ and the output $f_{\vec{\theta}}(\vec{x})$ with respect to the network parameters $\vec{\theta}$, averaged over a minibatch of data elements from the dataset $\mathcal{D}_T$,

$$\mathcal{L}_{\mathcal{D}_T}(\vec{\theta}) = \frac{1}{|\mathcal{D}_T|} \sum_{\vec{x}\in\mathcal{D}_T} \left(f_{\vec{\theta}}(\vec{x}) - \vec{x}\right)^2. \tag{16.1}$$

The latent representation's dimension, i.e., the intrinsic dimension of the data, is extracted from the same function (called 'test error'), evaluated for the optimized neural network parameters $\vec{\theta}$ on the rest of the unseen data elements. The intrinsic dimension of data is identified as the number of neurons in the bottleneck at which the 'test error' drops significantly and is flat upon further increasing $\mathcal{N}_L$, Fig. 16.1(c). Values at neurons in the bottleneck give the latent representation of data. In the inset of Fig. 16.1(c), an example of latent represetation is shown for a network with $\mathcal{N}_L = 2$ neurons in the bottleneck. Further technical details on our network are given in Appendix 16.6.

Our Hamiltonian reconstruction algorithm relies on precondition (0) and consists of Steps (1-5):

(0) Work under the assumption that we are given thermal expectation values of all local operators with support ℓ that is smaller than or equal to some pre-set number $\mathcal{S}$. These operators are measured in states of different temperatures: the set of all measurements for a given state represents one data element, while different states yield the dataset.

(1) Use autoencoder to check that the data elements indeed contain measurements with respect to (effectively) thermal states. In that case, the latent representation of the dataset is one-dimensional, with data elements within it ordered with respect to the temperature, or equivalently, the energy of the corresponding states.

(2) Since data elements in the latent representation are ordered with respect to the Hamiltonian expectation value, other operators that correspond to the individual terms in the Hamiltonian also show a pronounced variation along that one-dimensional manifold. Therefore, one can isolate candidate Hamiltonian terms $O_j(\vec{\alpha})$, $H = \sum_{j,\vec{\alpha}} a_{\vec{\alpha}} O_j(\vec{\alpha})$, via singling out those operators $O_j(\vec{\alpha}) = \sigma_j^{\alpha_j} ... \sigma_{j-1+|\ell|}^{\alpha_{j-1+|\ell|}}$ that have the largest average gradient $\overline{\partial \langle O_j(\vec{\alpha})\rangle}$ in the expectation value along the latent representation. We will assume periodic boundary conditions and a translationally invariant system with $O(\vec{\alpha}) \equiv O_{j=1}(\vec{\alpha})$, but the procedure can in principle be performed in the absence of that as well.

(3) Step (2) will, in addition to the actual terms, filter out also some spurious ones, which are not part of H but are, for example, products of actual Hamiltonian terms on neighboring sites. To fix the prefactors $a_{\vec{\alpha}}$, and to get rid of the spurious terms, we compare the 'trial' thermal expectation values (with respect to the trial Hamiltonian) to the actual measurements for one data element at a given (but unknown) temperature $1/\beta$, and find the solution of the following equation

$$\mathrm{Tr}\left[O(\vec{\alpha}')\frac{e^{-\beta\sum_{j,\vec{\alpha}} a_{\vec{\alpha}} O_j(\vec{\alpha})}}{Z}\right] - \langle O(\vec{\alpha}')\rangle_\beta = 0. \tag{16.2}$$

Since one does not know the temperature of the state, β remains undetermined; what is actually extracted is the product $\beta a_{\vec{\alpha}}$; β can be determined separately, e.g., from dynamical measurements.

For strictly local Hamiltonians and measurements that include all Hamiltonian terms (i.e., the maximal support of measured operators $\mathcal{S}$ is larger or equal to the support of H), Steps (1-3) will reconstruct H (up to a prefactor) with high precision (see examples below), as already proposed and tested in Ref. [83]. In the next steps, we extend the algorithm from Ref. [83] to be applicable to data from long-range Hamiltonians as well. For long-range interacting Hamiltonians, some error in the reconstruction is inevitable, stemming from the fact that we have measurements of only the most local terms in the Hamiltonian and that we can at most aim at reconstructing a local approximation of a long-range Hamiltonian. In that case, Steps (1-3) might still generate finite prefactors for "ghost" terms within the measured support. To remove those, we add here additional steps:

(4) Compare the solutions of Step (3) at a few different β, i.e., for different data elements. Ghost terms' coefficients will have a large relative variance across solutions for different states; hence, we drop terms with

$$\frac{\mathrm{Var}_\beta(a_{\vec{\alpha}}/a_{\vec{\alpha}_0})}{\mathbb{E}_\beta(a_{\vec{\alpha}}/a_{\vec{\alpha}_0})} > O(1). \tag{16.3}$$

where $a_{\vec{\alpha}_0}$ is the coefficient at the dominant term.

(5) Repeat Step (3) for the Hamiltonian ansatz without the ghost terms. This step just slightly corrects the result of Step (3).

The most expensive step of our reconstruction is Step (3); even after performing Step (2), potentially a large number of trial terms remain for Step (3). This can be particularly problematic for a Hamiltonian H with large support. In order to ameliorate this issue to a manageable extent, one can use an iterative scheme:

First, perform Steps (2-4), selecting contributing operators $O(\vec{\alpha})$ with maximal support $\mathcal{S}_k = \ell_k, k = 0$:

(k1) When increasing the maximal support to $\mathcal{S}_{k+1} = \ell_{k+1} = \ell_k + 1$, previously selected $\mathcal{S}_k$ support terms are retained by default, while Step (2) is performed only for operators with support ℓ_{k+1}.

(k2) Steps (3-4) are performed, including previously selected $\mathcal{S}_k = \ell_k$ and new ℓ_{k+1} support trial terms from (k1).

(k3) Terms surviving in (k2) are the new input for the next iteration.

In the end, Step (5) is performed.

16.3 Reconstructing short- and long-range interacting static Hamiltonians

We now benchmark our approach for two classes of H: local and long-range interacting Hamiltonians. The extent of applicability to the latter type of Hamiltonians has not been discussed in Ref. [83]. In any case, each data element consists of measurements in a thermal state (see appendix 16.7 for details of how we prepare the initial thermal states) with temperature $1/\beta$ for all local operators with support smaller than or equal to $\mathcal{S} = 4, 6$. We use inverse temperatures from the interval $\beta \in [0.05, 0.5]$.

First, we consider strictly local Hamiltonians with maximal support $\mathcal{R}$, for example,

$$H_L = \sum_i \left(h_z \sigma_i^z + \sum_{r=1}^{\mathcal{R}-1} (J_1\, \sigma_i^x \sigma_{i+r}^x + J_2\, \sigma_i^y \sigma_{i+r}^y) \right). \tag{16.4}$$

We find that the relative reconstruction error for coefficients h_z, J_1, J_2 highly depends on the maximal support of the measured operators $\mathcal{S}$:

$$\begin{aligned} \mathcal{S} \geq \mathcal{R} &: \text{relative error} \sim 10^{-6}, \\ \mathcal{S} < \mathcal{R} &: \text{relative error} \sim \mathcal{O}(1). \end{aligned} \tag{16.5}$$

Next, we consider long-range interacting Hamiltonians with power-law decaying interactions,

$$H_{LR} = \sum_i \left(h_z \sigma_i^z + \sum_{r=1}^{\frac{N}{2}-1} \frac{J}{r^\delta} (\sigma_i^x \sigma_{i+r}^x + \sigma_i^y \sigma_{i+r}^y) \right) \tag{16.6}$$

with periodic boundary conditions.

In this case, the reconstruction error highly depends on the maximal support of the measured operators $\mathcal{S}$ and the interaction strength decay exponent δ. Fig. 16.2(a) shows the relative error $|\delta a_\ell|/\bar{a}_\ell$, for compact representation averaged over all reconstructed Hamiltonian terms with support ℓ, i.e.,

$$\frac{|\delta a_\ell|}{\bar{a}_\ell} = \frac{|h_z - a_z|}{h_z}, \quad \ell = 1 \tag{16.7}$$

$$\frac{|\delta a_\ell|}{\bar{a}_\ell} = \frac{|2J/r^\delta - a_{xI\ldots Ix} + a_{yI\ldots Iy}|}{2J/r^\delta}, \quad \ell > 1 \tag{16.8}$$

We see that terms with larger support have larger relative error. In general, the latter increases for less local interactions (smaller δ). However, even if the Hamiltonian is not exactly reconstructed, its effect at the level of dynamics is captured in practice. To support that, we show in Fig. 16.2(b) time evolution from a domain wall initial state for the original and the reconstructed Hamiltonian for a few local observables. For the sake of comparison, we use the value of β that the data was measured at to divide the reconstructed coefficients $\beta a_{\vec{\alpha}}$ so as to obtain the actual Hamiltonian. In a temperature-agnostic protocol, β would be determined as the one at which the comparison is best, as we demonstrate in the next section.

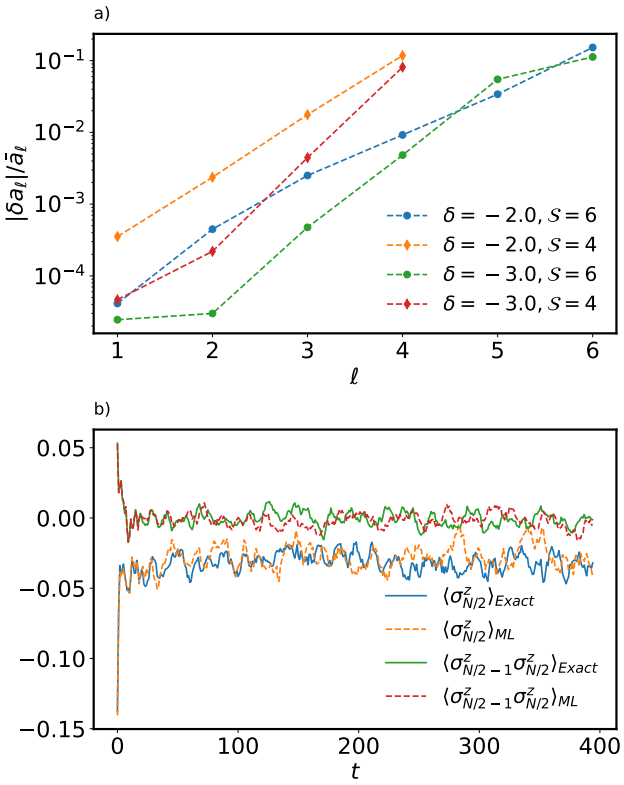


Figure 16.2: Evaluation of Hamiltonian reconstruction $H = \sum_{j,\vec{\alpha}} a_{\vec{\alpha}} O_j(\vec{\alpha})$ for the long-range interacting Hamiltonian from Eq. (16.6). (a) The relative error $|\delta a_\ell|/\bar{a}_\ell$ of all reconstructed coefficients at a given support ℓ. It is seen clearly that for a fixed δ (measure of long-rangedness of the Hamiltonian), terms with larger support have larger relative error. Also, for a given support ℓ, relative error decreases with increasing δ, i.e., considering more short-ranged underlying Hamiltonian. (b) Time evolution of two different observables with respect to (i) the original long-range H_{LR} with $\delta = 3$ from Eq (16.6), and (ii) its reconstruction H_{ML} using our method. This figure clearly shows that even though Hamiltonian reconstruction is not perfect for long-ranged systems, the reconstructed Hamiltonian nonetheless captures local dynamics quite well. Parameters: $N = 16, J = 1.0, h_z = 0.2, \delta = 3.0$.

16.4 Reconstruction of effective Hamiltonians engineered by nonequilibrium drives

Having benchmarked our approach, we now turn to our central example: effective Hamiltonian reconstruction in dynamical systems, which is of interest for verification of quantum simulators, where desired Hamiltonians are often engineered using periodic protocols. In these Floquet setups, the stroboscopic evolution is generated by the so-called Floquet Hamiltonian; while such closed systems are (in the absence of symmetries [84]) bound to eventually heat up to a featureless infinite temperature state [85, 86, 87], the heating process is delayed exponentially with increasing the frequency of the drive [52, 54]. When observed stroboscopically, at intermediate times, in the so-called prethermal plateau [88], the system is locally effectively described by a thermal state with respect to an effective Hamiltonian that can feature nontrivial transient states [52, 53, 54, 55]. Floquet protocols have thus been one of the central approaches in engineering non-equilibrium phenomena using quantum simulators and materials.

In the inverse frequency expansion or iterative rotating frame transformation, the effective Hamiltonian can be reconstructed up to some order [89]. However, this is generally a daunting task [89, 53] and the former cannot be computed in closed form for generic systems and

protocols. Here we propose an unbiased reconstruction, which does not rely on any expansion technique; instead, we reconstruct the effective Hamiltonian up to support $\mathcal{S}$, effectively resumming contributions from higher orders in the inverse frequency expansion within this support. As the inverse frequency series is formally divergent, the system eventually heats up; it is still not fully settled how this divergence is related to heating dynamics featured in the exact stroboscopic dynamics. Our approach reveals that stroboscopically, throughout the whole heating regime, the system locally appears as if in a thermal state with respect to an effective quasi-static Hamiltonian; moreover, we demonstrate directly how its support grows in time.

16.4.1 Floquet driving

Prethermal regime. In the following, we reconstruct the effective Hamiltonian, characterizing the stroboscopic pre-thermal state in the prethermal plateau, for the square pulse Floquet protocol

$$U = \exp\left(-iH_1 T/2\right) \exp\left(-iH_2 T/2\right) \tag{16.9}$$

$$H_1 = \sum_{j=1}^{N} J\sigma_j^z \sigma_{j+1}^z + h_x \sigma_j^x + h_z \sigma_j^z \tag{16.10}$$

$$H_2 = \gamma \sum_{j=1}^{N} \sigma_j^x \tag{16.11}$$

where U is the unitary matrix for one drive cycle which acts repeatedly on the system during the dynamics; T denotes the time period of the drive. Fig. 16.3(a) shows time-dependent expectation values $\langle \sigma^x \rangle$ for $J = 1.0, h_x = 0.9045, h_z = 0.809, \gamma = 0.4, \omega = 2\pi/T = 10.0$, for a time evolution from an initial thermal state with respect to H_1 and inverse temperature $\beta_0 = 0.1$.

For drive cycle numbers $n \gtrsim 5$, we observe an extended prethermal plateau. Visible oscillations are a consequence of finite size ($N = 12$) exact diagonalization propagation. In the large frequency regime $\omega \gg 1$ considered, the Floquet Hamiltonian can be perturbatively approximated using Baker-Campbell-Hausdorff (BCH) series expansion, as detailed in Appendix 16.8.

Our Hamiltonian reconstruction is performed on a dataset with elements containing measurement of local operators with maximal support $\mathcal{S} = 3$, in states that are evolved up to some fixed time within the prethermal plateau. As initial states for the time evolution we consider thermal states with respect to H_1, with inverse temperatures within the range $\beta_0 \in [0.05, 0.40]$. In principle, one could start from non-thermal states as well since these are expected to relax to thermal states in the plateau anyhow, due to the nonintegrability of the exact Floquet Hamiltonian. While Step (3) in the reconstruction algorithm [cf. Sec. 16.2] can in principle be performed for a single data element (a single state), we average the relative coefficients $a_{\vec{\alpha}}/a_x$ (a_x being the dominant one) for each $\vec{\alpha}$ over a few β_0 and a few measurement times in the prethermal plateau. As discussed in Sec. 16.2, our algorithm gives the coefficients up to an overall multiplicative factor β. This overall multiplicative constant β can be extracted from dynamics in the initial time window before the system reaches the prethermal plateau; as illustrated in the inset of Fig. 16.3(a). More precisely, we determine β by minimizing the difference $\sum_n |\mathrm{Tr}[OU^n \rho(0)(U^\dagger)^n] - \mathrm{Tr}[Oe^{-inTH_{\mathrm{ML}}(\beta)}\rho(0)e^{inTH_{\mathrm{ML}}(\beta)}]|$ between the exact and the reconstruction H_{ML} based time-dependent measurements of a dominant operator at early cycles.

In Fig. 16.3, our Hamiltonian reconstruction H_{ML} is compared to a second order (in T) BCH expansion, which contains terms with the same maximal support $\mathcal{S} = 3$. Fig. 16.3(a) compares the dynamics generated from (i) the exact unitary, Eq. (16.9), (ii) the Hamiltonian

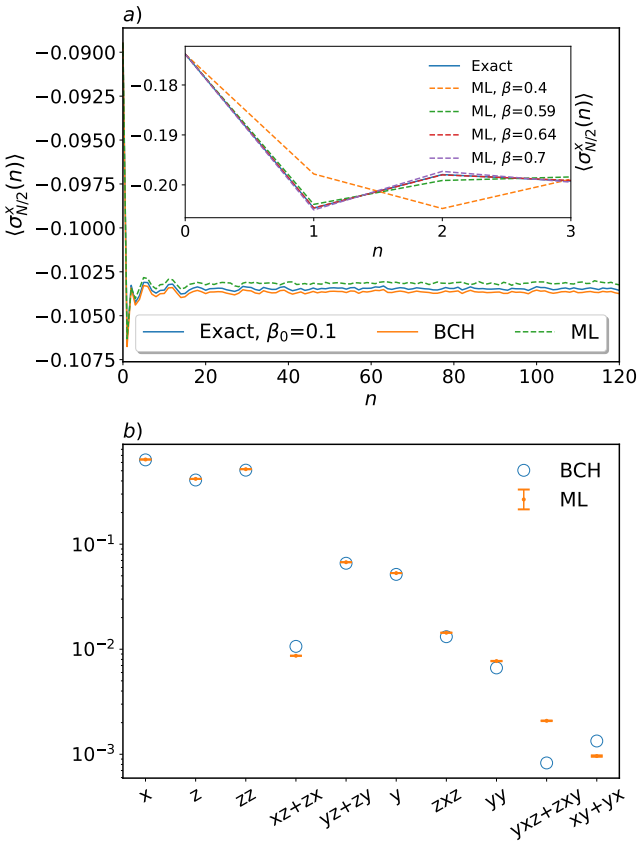


Figure 16.3: (a) Stroboscopic measurements of $\langle \sigma^x_{N/2} \rangle$ as a function of cycle number n, obtained from: (i) the exact Floquet protocol, (ii) time evolution with respect to the BCH Hamiltonian up to second order in T, and (iii) time evolution with respect to our reconstruction H_{ML}. Initial states are thermal w.r.t. H_1 at $\beta_0 = 0.1$. The inset demonstrates how we extract the overall multiplicative factor β of the coefficients obtained from our Hamiltonian reconstruction algorithm, as discussed in the main text. (b) Comparison of Hamiltonian coefficients computed from the BCH expansion and our Hamiltonian reconstruction algorithm. Clearly, our reconstruction algorithm predicts the coefficients (particularly the leading ones) quite accurately. Parameters: $J = 1.0, h_x = 0.9045, h_z = 0.809, \gamma = 0.4, \omega = 2\pi/T = 10.0, N = 12$.

constructed from the BCH approximation calculated up to second order in T, as discussed in the Appendix 16.8, and (iii) our reconstructed Hamiltonian H_{ML}, for an initial state with $\beta_0 = 0.1$. We emphasize that we have checked the cases also for other observables for a range of β_0-values ($\beta_0 \in [0.05, 0.3]$) and all such results show similar features as shown in Fig. 16.3(a).

Figure 16.3(b) compares the coefficients of different terms computed from the BCH expansion to that obtained via our machine learning-assisted Hamiltonian reconstruction algorithm. The matching is quite good for most (particularly for the leading) coefficients. The slightly worse performance of our reconstruction scheme in Fig. 16.3(a), compared to second-order BCH, is explained as a consequence of finite size ($N = 12$) effects, causing fluctuations on the prethermal plateau and other deviations from a strictly thermal state, affecting the reconstruction input data.

Heating regime. We now turn our attention to the post-prethermal heating regime; we use another Floquet protocol, where the length of the prethermal plateau and the rate at which the system heats up are more easily tunable. To this end, we follow Ref. [90] and consider the

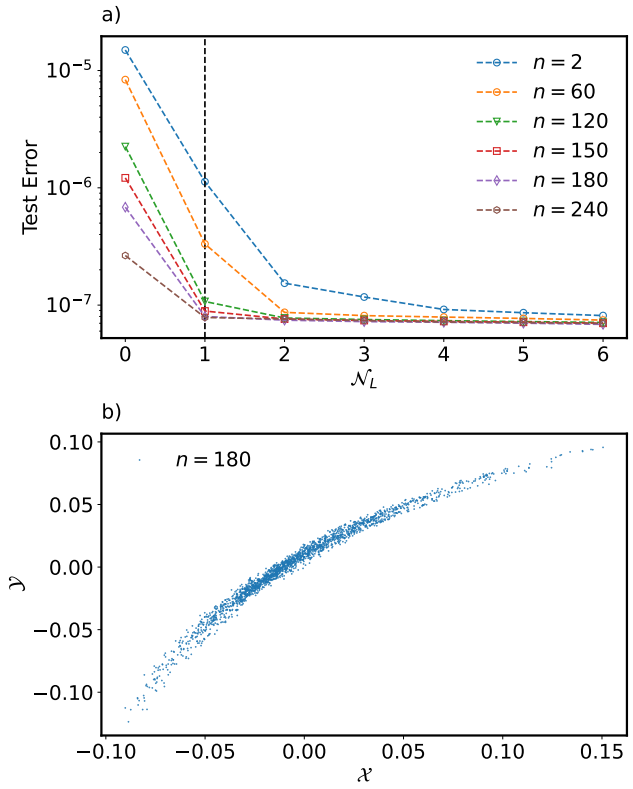


Figure 16.4: (a) Test error as a function of the latent space dimension $\mathcal{N}_L$ (number of bottleck neurons) at different cycle number n for Floquet driven systems, Eq. (16.12). At smaller cycle numbers e.g., $n = 2,\ 60$, the influence of initial states, prepared by applying random single-site rotations to thermal states, is still visible. For larger cycle numbers, the effectively one-dimensional latent representation signals that the system is in a thermal state throughout the entire heating regime. (b) Latent representation of dataset consisting of measurement at $n = 180$ in the heating regime. The x- and y-axis show values of the first and the second neuron in the bottleneck layer with $\mathcal{N}_L = 2$ neurons, giving a one-dimensional representation of data elements from different states. Parameters: $N = 18, \epsilon = 0.08, J = 1.0, h_x = 0.9045, h_z = 0.809, T = 12.7263, \beta_0 \in [0.05, 0.45]$.

following protocol

$$U = \exp\left(-i\tilde{H}_1 T/4\right) \exp\left(-i\tilde{H}_2\right) \exp\left(-i\tilde{H}_1 T/4\right),$$
$$\tilde{H}_1 = \sum_{i=1}^{N} J\sigma_i^z\sigma_{i+1}^z + h_z\sigma_i^z + h_x\sigma_i^x,\ \ \tilde{H}_2 = \epsilon\sum_{i=1}^{N}\sigma_i^x \tag{16.12}$$

where U is the unitary matrix for one drive cycle, which acts repeatedly on the system during the dynamics; T denotes the time period of the drive. As argued in Ref. [90], the heating rate is regulated by ϵ; the larger the ϵ, the faster the system heats up. Here we choose $\epsilon = 0.08$; Fig. 16.5(a), showing $\langle\tilde{H}_1/2\rangle$ at different cycle numbers n, confirms that heating towards the infinite temperature steady state is observed at easily accessible drive cycle numbers. We note that the period T is set to $T = 2(\pi k + \epsilon)$, with $k = 2$.

It has already been argued in Refs. [90, 91] that the system remains locally describable with a Gibbs ensemble in the whole heating regime. Here, we provide an independent check using the autoencoder analysis; it reveals that the latent representation is one-dimensional and thus is parametrized by a single parameter – the temperature – throughout the whole heating regime. To confirm this, we take as initial states the thermal states with respect to the zeroth

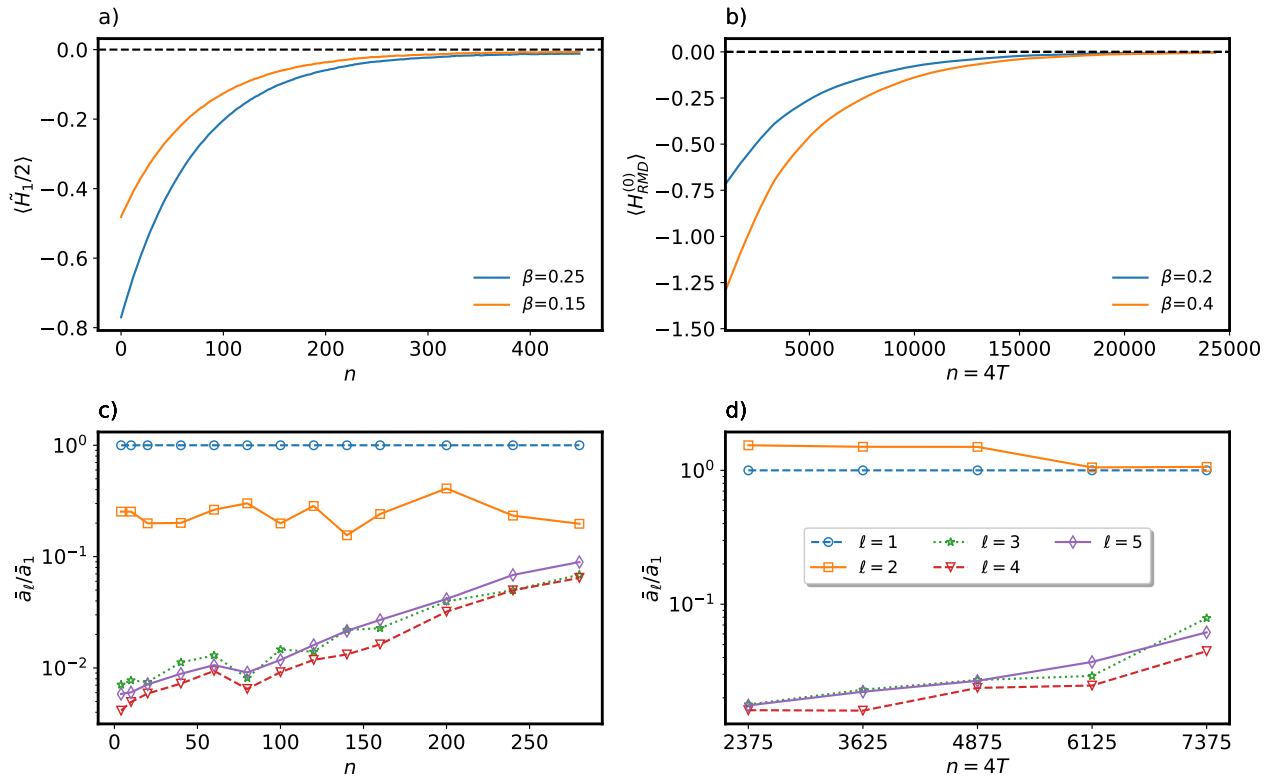


Figure 16.5: The considered (a) Floquet protocol, Eq. (16.12), with relevant parameters $N = 18, \epsilon = 0.08$ and (b) random multipolar driving with $N = 16, T = 1/25$, Eq. (16.13), exhibit heating to an infinite-temperature steady state at easily accessible times. Reconstruction of the instantaneous quasistatic effective Hamiltonian, $H_{\text{eff}}(n)$, responsible for locally thermal time-dependent measurements in the heating regime, reveals a growth of averaged normalized weight at less local terms with support $\ell = 3-5$ as a function of cycle number n, both, for (c) Floquet and (d) random multipolar driving.

order (in ϵ) Floquet Hamiltonian $\tilde{H}_1/2$ with $\beta_0 \in [0.05, 0.45]$; in addition, we perform weak, random, translationally invariant single-site rotations so that the initial states manifold is no longer one-dimensional. Then we evolve such states with Floquet time evolution and probe their intrinsic dimension at chosen times. Namely, if we considered initial states from the thermal manifold and mapped those with a time-evolution deterministic operator to states at a fixed time, from the perspective of an autoencoder, dataset remains on a one-dimensional manifold since mapping due to time propagation can be absorbed in the encoder/decoder part of the network. Therefore, to test the real, generic intrinsic dimension of measurement in the heating regime, we must start from a manifold of initial states with higher dimension that does not limit what we are probing. In Fig. 16.4(a) we show the 'test error', Eq.(16.1), as a function of the latent space dimension $\mathcal{N}_L$ (i.e., number of neurons in the bottleneck). After a few cycle numbers n, the 'test error' drops at one latent neuron and flattens upon adding any further latent neurons, signaling that the latent representation is one dimensional. This is confirmed also if we look directly at the latent space representation of the dataset at a fixed time, cf. Fig. 16.4(b).

Next, we attempt to reconstruct the effective quasistatic Hamiltonian $H_{\text{eff}}(n)$, responsible for thermal measurements in the heating regime at different cycle numbers n, $\langle O(\vec{\alpha}) \rangle_n = \langle \psi(nT)|O(\vec{\alpha})|\psi(nT)\rangle \equiv \text{Tr}[O(\vec{\alpha})e^{-H_{\text{eff}}(n)}/Z]$. This is challenging, yet interesting, because the inverse frequency expansions do not converge in the heating regime. Note that for the reconstruction of $H_{\text{eff}}(n)$, we resort to the iterative scheme described in Sec. 16.2, first selecting the

leading 60 contributing terms with maximal support $\mathcal{S}_0 = 4$ and then performing one iteration to increase the maximal support to $S_1 = 5$, including 160 terms in total. The average weight of all terms in the reconstructed $H_{\rm ML}(n)$ with support ℓ, $\bar{a}_\ell$, relative to $\bar{a}_1$, are shown in Fig. 16.5(c) plotted as a function of cycle number n. The relative growth of the weights of the less local terms with increasing n indicates that $H_{\rm eff}(n)$ becomes less and less local as the system absorbs energy from the drive. On the other hand, the Floquet Hamiltonian, defined from the unitary for one period evolution, is a time-independent object. Our interpretation is that $H_{\rm eff}(n)$ does not necessarily capture the stroboscopic dynamics in the system, but captures time-dependent thermal measurements. One way of motivating the growing support of $H_{\rm eff}(n)$ is in terms of operator growth [92]. Let us say we initialized the system in a thermal state with respect to $\tilde{H}_1$, $H_{\rm eff}(0) = \tilde{H}_1$. Time evolution of the corresponding thermal ensemble would be given by $U^n e^{-\tilde{H}_1}(U^\dagger)^n = e^{-U^n \tilde{H}_1 (U^\dagger)^n} = e^{-H_{\rm eff}(n)}$, with U defined in Eq. (16.12). For parametrically small ϵ, this should naturally lead to the parametrically regulated growth of the $H_{\rm eff}(n)$ operator. Our $H_{\rm ML}(n)$ reconstruction, shown in Fig. 16.5(c), is consistent with an exponential growth with n.

The growing support of $H_{\rm eff}(n)$ renders the reconstruction rather difficult, since one needs to take into consideration the contributions from terms with ever-growing support ℓ.

16.4.2 Aperiodic random multipolar drives

Periodically driven systems obey Floquet's theorem, which guarantees the existence of a static generator of stroboscopic dynamics. Away from the strictly periodic limit, this additional structure of the time-ordered propagator is lost, and the identification of an effective Hamiltonian becomes far less obvious.

It was recently found that *random multipolar driven* (RMD) systems, which are subject to an aperiodic energy-nonconserving drive, display similar prethermal properties [93]: such systems exhibit a prethermal regime (albeit with a weaker than exponential dependence of the duration of the prethermal plateau on drive frequency), followed by an eventual relaxation to an infinite temperature state. This behavior was proven mathematically by constructing an effective static Hamiltonian for the prethermal plateau using a generalization of the BCH expansion; like in Floquet systems, the expansion was shown to diverge in the heating regime [53, 94]. To the best of our knowledge, it is unclear whether an effective Hamiltonian exists, that describes the heating dynamics of RMD systems beyond the prethermal plateau, nor what its locality properties may be. This makes RMD systems an excellent candidate to test the capabilities of our algorithm in so far uncharted territory.

To investigate further the phenomenon of heating beyond Floquet, we consider many-body systems subject to a RMD drive. The protocol involves applying a random sequence of unitaries $U_\pm$, generated from two Hamiltonians $H_\pm$, each acting for a duration T. The level of multipolar correlation incorporated in the drive (via the structure of the random sequence of $U_\pm$) is characterised by an integer m. For instance, $m = 0$ corresponds to the case where random sequence of $U_\pm$ is considered, while $m = 1$ represents the case for a random sequence of *dipoles* having form U_+U_- or U_-U_+. Following the same logic, $m = 2$ describes a random sequence of *quadrupoles* having form $U_-U_+U_+U_-$ or $U_+U_-U_-U_+$. It was demonstrated in [93] that RMDs, characterized by a finite value of m, exhibit a prethermal regime with lifetime scaling as $(1/T)^{2m+1}$. For $m \to \infty$, the limit itself corresponds to the Thue-Morse sequence constructed out of $U_\pm$, leads to a sub-exponential (but faster than polynomial) in $1/T$ long-lived prethermal regime.

We focus on the following Hamiltonian generators

$$H_\pm = \sum_i J_x \sigma_i^x \sigma_{i+1}^x + J_z \sigma_i^z \sigma_{i+1}^z + B_\pm \sigma_i^x + B_z \sigma_i^z \tag{16.13}$$

where $B_\pm = B_0 \pm B_x$. We construct the basic unitary operators $U_\pm$ from $H_\pm$ as $U_\pm = \exp(-iH_\pm T)$.

Figure 16.5(b) shows the behaviour of the the mean energy $H^{(0)}_{\mathrm{RMD}} = (H_+ + H_-)/2$ for the system initialized in a thermal state with respect to $H^{(0)}_{\mathrm{RMD}}$. As we see, $\langle H^{(0)}_{\mathrm{RMD}} \rangle$ eventually reaches zero, indicating heating of the system to an infinite temperature state at late times. In much the same way as in the Floquet driving case, we can verify that the system remains locally thermal throughout the whole heating regime. To the best of our knowledge, this was not reported before.

In analogy to the Floquet case, we reconstruct the effective quasistatic $H_{\mathrm{eff}}(n)$ that captures the behavior of local stroboscopic thermal expectation values in the heating regime. We use the iterative scheme described in Sec. 16.2, first selecting the leading 40 contributing terms with maximal support $\mathcal{S}_0 = 4$ and then performing one further iteration to increase the maximal support to $\mathcal{S}_1 = 5$, including 120 terms in total. In Fig. 16.5(d) we show the average weights $\overline{a}_\ell$ (relative to $\overline{a}_1$) of terms with support ℓ for our reconstructed $H_{\mathrm{ML}}(n)$.

The above analysis shows that our algorithm is capable of identifying effective Hamiltonians in new setups where no analytical theory is yet available. Moreover, our results suggest the existence of simplified descriptions for the heating dynamics beyond prethermal times, where BCH-like expansions break down. Thus, the variational character of the Hamiltonian reconstruction method we propose can prove useful both in experimental nonequilibrium setups (e.g, to analyze dynamical decoupling sequences [29, 30, 31], or in the digital simulation of quantum dynamics [95, 96, 97]), and to facilitate the theoretical analysis of nonequilibrium drives beyond Floquet systems.

16.5 Conclusions and Future Outlook

We propose a new algorithm for the Hamiltonian reconstruction from the measurements of local operators. Reconstruction is possible under the assumption that we have access to the local measurements in different thermal states. We use autoencoder pre-processing of the data to (i) verify that the measurements are thermal and (ii) single out the Hamiltonian candidate terms in order to reduce the reconstruction complexity. The subsequent reconstruction is accurate for local Hamiltonians as long as the dataset contains measurement of all Hamiltonian terms (of course, without knowing, which of the measured operators are the Hamiltonian terms), while it is only approximate for long-range interacting Hamiltonians.

Beyond benchmarking, we apply Hamiltonian reconstruction to Floquet and random multipolar driven systems. For the former, we first reconstruct the effective Hamiltonian, responsible for the thermal local measurements in the prethermal plateau, and compare that to its BCH approximation. Using an autoencoder, we also confirm that the system remains locally thermal throughout the whole heating regime, and reconstruct the effective quasistatic Hamiltonian, corresponding to the Gibbs ensemble associated with the measurements at different times. We interpreted this effective quasistatic Hamiltonian's increasing support via operator growth that is parametrically regulated by the heating rate. Similar behaviour was observed also for the heating regime of the random multipolar driving. Despite the lack of an analytical theory, we confirmed that for the random multipolar driving, the heating process occurs via thermal states with growing temperature and increasingly non-local effective quasistatic Hamiltonian.

We envision our Hamiltonian reconstruction technique as a strong tool for the verification of quantum simulators that strive for the realization of exotic Hamiltonians. In our analysis, we focused on Floquet engineering, one of the most popular nonequilibrium techniques to achieve this goal, for which, however, Hamiltonians typically come with additional unwanted terms. Using autoencoder analysis to select the Hamiltonian candidate terms, we demonstrate how effective Hamiltonians can be reconstructed directly from the measurements in the prethermal

plateau or the heating regime, without relying on any assumption on the Hamiltonian terms or the high-frequency expansion. Our operator-based Hamiltonian reconstruction is directly suitable for the verification of Hamiltonians in Rydberg atoms or trapped ion setups. However, our approach would have to be extended to work with partial information stored in state snapshots in cold atoms experiments. Hamiltonian reconstruction is relevant also for condensed matter settings and quantum optics, where extracting the minimal model, responsible for the observed physics, is notoriously hard. Similarly, due to the limited types of measurement that are accessible in these systems, the envisioned desirable generalizations of our approach call for further studies.

Another non-trivial example where our scheme could be applied, includes entanglement Hamiltonian reconstruction, at least in the intermediate to late-time regime of excited systems, where entanglement Hamiltonian approaches the actual Hamiltonian [98]. In future studies, it would also be desirable to develop similar strategies to reconstruct other conservation laws of integrable models that generically relax to the states that are locally describable by the generalized Gibbs ensembles.

16.6 Details of the autoencoder

Our autoencoder consists of feed-forward neural network with the bottleneck structure. A feed-forward neural network is made up of layers, corresponding to a sequence of alternating affine-linear and non-linear transformations. The activation $a_j^{(l)}$ of the $l-$th layer is related to that of the previous layer $a_j^{(l-1)}$ as

$$a_j^l = \sigma\left(\sum_k W_{jk} a_k^{(l-1)} + b_j\right) \tag{16.14}$$

where W_{jk} and b_j are variational parameters and σ denotes the fixed non-linear activate function. For all the results produced in this paper, we fix $\sigma = \tanh$. Our network consists of two encoder layers between the input and the latent space, as well as two decoder layers between the latent space and the output. Each layer has 400 neurons. We used the Adam optimizer for training the network and learning rate $r = 0.0001$. 80% of the data serves as the training set, while rest are used as test set.

16.7 Preparing the initial thermal state

To prepare the initial thermal state for $N > 12$, we follow the prescription detailed in Ref. [90]. The procedure relies on the principle of quantum typicality [99, 100, 101, 102]. Typicality states that the expectation value of an operator $\mathcal{A}$, defined on a Hilbert space $\mathcal{H}$, can be approximated as

$$\frac{1}{\dim\mathcal{H}}\mathrm{Tr}[A] \approx \frac{1}{N}\sum_{n=1}^{N}\langle r_n|A|r_n\rangle \tag{16.15}$$

where $|r_n\rangle$ are Haar-random states. Note that the approximation becomes exact as $N \to \infty$. Therefore, thermal expectation value of observable A, with respect to some Hamiltonian H at inverse temperature β, is given as

$$\langle A\rangle_\beta \approx \frac{\frac{\dim(\mathcal{H})}{N}\sum_{n=1}^{N}\langle r_n|e^{-\beta H/2}Ae^{-\beta H/2}|r_n\rangle}{\frac{\dim(\mathcal{H})}{N}\sum_{n=1}^{N}\langle r_n|e^{-\beta H/2}e^{-\beta H/2}|r_n\rangle} \tag{16.16}$$

If we interpret the RHS of the above equation as an ensemble average, then the thermal density matrix can be approximated as

$$\rho_\beta \approx \frac{1}{Z_\beta}\frac{\dim(\mathcal{H})}{N}\sum_{n=1}^{N} e^{-\beta H/2}|r_n\rangle\langle r_n|e^{-\beta H/2} \tag{16.17}$$
$$Z_\beta \approx \frac{\dim(\mathcal{H})}{N}\sum_{n}^{N}\langle r_n|e^{-\beta H/2}e^{-\beta H/2}|r_n\rangle$$

To time evolve the thermal density matrix, we just need to evolve a set of pure states defined as $|\psi_n\rangle = e^{-\beta H/2}$ and then compute

$$\rho_\beta(t) \approx \frac{1}{Z_\beta}\frac{\dim(\mathcal{H})}{N}\sum_{n=1}^{N} U(t)|\psi_n\rangle\langle\psi_n|[U(t)]^\dagger \tag{16.18}$$

where $U(t)$ is the evolution operator.

16.8 BCH Expansion

First of all, we note that for that square pulse Floquet protocol used in the main text, Floquet-Magnus expansion is identical to the BCH expansion. Mathematically, BCH formula is the solution Z to the equation

$$e^X e^Y = e^Z \tag{16.19}$$

for possibly noncommutative X and Y in the Lie algebra of a Lie group. BCH formula essentially yields an expression for Z in terms of a formal series (not necessarily convergent) in X, Y, and iterated commutators thereof. The first few terms of the series are:

$$Z = X + Y + \frac{1}{2}[X,Y] + \frac{1}{12}([X,[X,Y]] - [Y,[X,Y]]) + ... \tag{16.20}$$

To make connection with our problem, we notice that the Floquet Hamiltonian H_F is defined via the relation

$$e^{-iH_1T/2}e^{-iH_2T/2} = e^{-iH_FT} \tag{16.21}$$

It is quite clear that Eq. (16.21) is same as Eq. (16.20) with $X = -iH_1T/2$ and $Y = -iH_2T/2$, where H_1 and H_2 are described by Eq. (16.10) and Eq.(16.11) respectively, in the main text. Now, resorting to Eq. (16.20), one can approximate the Floquet Hamiltonian H_F in different orders of T, such that $H_F = \sum_n H_F^{(n)}$, where $H_F^{(n)}$ is proportional to T^n. We perform such calculation up to order 2 and the results are charted down below:

$$H_F^{(0)} = \frac{1}{2}(H_1 + H_2) \tag{16.22}$$

$$H_F^{(1)} = \frac{\gamma T}{4} \sum_i \sigma_i^y \sigma_{i+1}^z + \sigma_i^z \sigma_{i+1}^y + h_z \sigma_i^y \tag{16.23}$$

$$\begin{aligned} H_F^{(2)} = &- \frac{T^2}{24}\gamma^2 h_z \sum_i \sigma_i^z - \frac{T^2}{24}\gamma h_z^2 \sum_i \sigma_i^x \\ &- \frac{T^2}{12}\gamma^2 \sum_i (\sigma_i^z \sigma_{i+1}^z - \sigma_i^y \sigma_{i+1}^y) \\ &- \frac{T^2}{24}\gamma h_z \sum_i (\sigma_i^x \sigma_{i+1}^z + \sigma_i^z \sigma_{i+1}^x) \\ &+ \frac{T^2}{12}\gamma h_x \sum_i (\sigma_i^z \sigma_{i+1}^z - \sigma_i^y \sigma_{i+1}^y) \\ &- \frac{T^2}{24}\gamma h_z \sum_i (\sigma_i^z \sigma_{i+1}^x + \sigma_i^x \sigma_{i+1}^z) \\ &- \frac{T^2}{12}\gamma \sum_i (\sigma_i^z \sigma_{i+1}^z \sigma_{i+2}^z + \sigma_i^x) \end{aligned} \tag{16.24}$$

Part X
Another Explanations of a Typical Theories

Part XI
Other, Not Used Theory

17 Quasiparticle cooling algorithms for quantum many-body state preparation by Lloyd, Michailidis et al.

Abstract

Probing correlated states of many-body systems is one of the central tasks for quantum simulators and processors. A promising approach to state preparation is to realize desired correlated states as steady states of engineered dissipative evolution. A recent experiment with a Google superconducting quantum processor [X. Mi *et al.*, Science 383, 1332 (2024)] demonstrated a cooling algorithm utilizing auxiliary degrees of freedom that are periodically reset to remove quasiparticles from the system, thereby driving it towards its ground state. In this work, we develop a kinetic theory framework to describe quasiparticle cooling dynamics, and employ it to compare the efficiency of different cooling algorithms. In particular, we introduce a protocol where coupling to auxiliaries is modulated in time to minimize heating processes, and demonstrate that it allows a high-fidelity preparation of ground states in different quantum phases. We verify the validity of the kinetic theory description by an extensive comparison with numerical simulations for the examples of a 1d transverse-field Ising model, the transverse-field Ising model with an additional integrability-breaking field, and a non-integrable antiferromagnetic Heisenberg spin ladder. In all cases we are able to efficiently cool into the many-body ground state. The effects of noise, which limits efficiency of variational quantum algorithms in near-term quantum processors, are investigated through the lens of the kinetic theory: we show how the steady state quasiparticle populations depend on the noise rate, and we establish maximum noise values for achieving high-fidelity ground states. This work establishes quasiparticle cooling algorithms as a practical, robust method for many-body state preparation on near-term quantum processors.

17.1 Introduction

One of the central challenges for quantum simulation is to find reliable algorithms to prepare desired entangled quantum many-body states. In particular, preparing low-energy states of a given many-body Hamiltonian is an essential task for probing quantum dynamics, modeling correlated quantum materials, and for quantum chemistry applications of quantum computers [1, 2, 3, 4]. Classical tasks such as high-dimensional optimization problems can also be formulated in terms of finding ground states of appropriate Hamiltonians [5, 6]. A number of quantum algorithms for preparing ground states of many-body Hamiltonians have been proposed [7, 8, 9, 10, 11, 12].

Two important classes of low-energy state-preparation protocols employed in experiments with noisy intermediate-scale quantum (NISQ) [13] devices are: (i) *adiabatic* protocols [9, 14], which rely on the adiabatic theorem and a slow variation of Hamiltonian parameters, and have been widely used in analogue quantum simulators such as ultracold atoms [15, 16] and Rydberg atom arrays [17, 18]; (ii) *variational* methods [19, 20, 21], suitable for digital quantum simulators, in which the target state is prepared by applying a variational quantum circuit to a simple initial state (e.g. a product state).

Unfortunately, unitary state-preparation protocols on NISQ processors are hindered by the presence of intrinsic decoherence. For example, superconducting qubits are subject to dephasing and decay processes, which introduce unwanted excitations to the system. Such protocols have

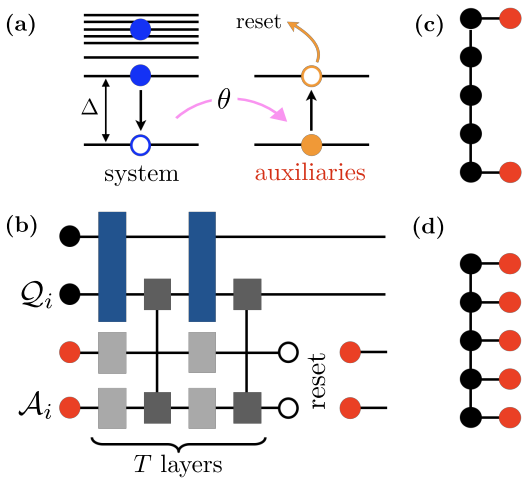


Figure 17.1: (a) Schematic mechanism of quasiparticle cooling: quasiparticles in the system, with energy above the system gap Δ, are resonantly transferred to auxiliary qubits, which are then reset to ground state, removing entropy and energy from the system. (b) Digital quantum circuit used in reset protocol: a system of N_S qubits $\mathcal{Q}_i$ is coupled to an auxiliary bath of N_A qubits $\mathcal{A}_i$. Unitary evolution under system, auxiliary, and interaction gates is applied, and repeated T times, followed by the reset of auxiliaries. This cooling cycle is repeated until the system converges to its steady state. (c) Edge cooling setup. (d) Bulk cooling setup, $N_A = N_S$.

no native mechanism to remove these excitations, so decoherence will eventually thermalize the system to a trivial state, e.g. a fully mixed state. This restricts the size of feasible circuits and limits the duration for which a quantum state can be stored on the device [22, 23]. Further, using variational circuits to prepare complex quantum states may be challenging due to flat optimization landscapes ('barren plateaus') [24, 25, 26].

A fundamentally different approach is to prepare many-body states as steady states of engineered dissipative evolution [27]. Because the dissipation directly competes with the decoherence effects, such state preparation methods can partially overcome the difficulties posed by noise. However, understanding which class of experimentally realisable dissipators can give rise to interesting quantum correlated steady states is a highly non-trivial question that has attracted much historic and recent interest [28, 29, 30, 31, 32, 33, 34]. In particular, specific protocols that involve *local* engineered dissipation for frustration-free Hamiltonians (a restricted but important class of models) have been proposed and implemented experimentally in few-qubit systems of trapped ions and superconducting qubits [25, 36, 37].

More recently, in an experiment [38] on the digital Google Quantum Processor, a physics-inspired cooling algorithm was demonstrated for cooling 1d and 2d quantum spin systems. In this experiment, the system evolved under a periodic (Floquet) quantum circuit specified by a unitary Floquet operator $\hat{U}_S$, constructed as a shallow quantum circuit of gates with finite, but small rotation angles. In this regime, the time evolution of local observables is well-approximated by a prethermal Hamiltonian H_{eff} [39]. The approximate conservation of H_{eff} stems from the suppression of heating processes, which are exponentially slow in the inverse rotation angles of gates in $\hat{U}_S$. The key idea of the implemented algorithm (displayed schematically in Fig. 18.1a,b — see also [40, 41, 42, 43, 44, 45] for related works) was to use a subset of qubits as auxiliaries, tuning their quasienergies and couplings to system qubits in order to resonantly transfer excitations from the system. The entropy of the system is removed by periodically resetting the auxiliary qubits. In the experiment, it was shown that the system reached a steady low-energy correlated state. Furthermore, the achieved steady states could be efficiently purified to yield high fidelities with respect to the true ground states, and it was argued that, asymptotically, the dissipative preparation is advantageous compared

to variational unitary protocols.

This progress calls for the development of practical, robust, dissipative many-body state preparation algorithms. In this work, we develop a theory of quasiparticle cooling on quantum processors, concentrating on efficient preparation of phases of matter with low-energy quasiparticle excitations, in realistic noisy environments. In such many-body systems, excited states at sufficiently low energy density can be described in terms of occupation numbers of non-interacting bosonic or fermionic degrees of freedom [46]. The quasiparticles generally have a finite lifetime, due to the decay to other states; however, provided this lifetime is sufficiently long, a quasiparticle description can be employed. A celebrated example is the Landau Fermi-liquid theory, which provides a description of interacting electrons in metals in terms of fermionic quasiparticles [46]. More broadly, quasiparticle descriptions apply to a variety of phases of matter including Fermi liquids, superconductors, and magnetically ordered states.

Focusing on 1d qubit – or, equivalently, spin-1/2 – systems, we consider generalised auxiliary-reset algorithms encompassing the one implemented in the experiment of Ref. [38]. We derive a dissipative kinetic equation describing the quasiparticle population dynamics under the action of the protocol, which allows for a transparent physical picture on how different parameters affect the state preparation fidelity. We show that, in particular, the success of the protocol relies on (i) the local cooling operators acting to remove quasiparticles from the system, (ii) the layout of auxiliary qubits, for example with auxiliaries only at the system boundaries or with a finite density of auxiliaries in the thermodynamic limit, as shown in Fig. 18.1c,d, and (iii) the time dependence of the system-auxiliary couplings. The first two factors ensure that the matrix elements of the cooling operators between low-lying excited states and the ground state remain finite in the thermodynamic limit; we argue that only in topologically trivial systems is it possible to reach the ground state in constant time, while requiring the cooling operators to be local, few-qubit operators. The time-dependence of the couplings meanwhile ensures that heating transitions are suppressed relative to cooling transitions, and is crucial in reaching high fidelities.

Below, we characterize the protocol performance by log-fidelity per qubit, $-\log \mathcal{F}/N_S$, where $\mathcal{F}$ is the fidelity of the steady state with respect to the true ground state, and N_S is the number of system qubits. Within our kinetic equation approach, we find $-\log \mathcal{F}/N_S \sim \exp(-\Omega(\Delta T))$ under the modulated coupling protocol, where Δ is the excitation gap and T is the number of unitary layers before the auxiliaries are reset (see Fig. 18.1b), which plays the role of an inverse temperature within the modulated coupling protocol. Thus, high fidelity can be achieved by increasing the unitary circuit depth.

We assess the validity of our theory first with the example of an integrable 1d transverse-field Ising model (TFIM) spin chain, where quasiparticles are infinitely long-lived and the relevant operators are known explicitly [47, 48]. This model exhibits two phases, a paramagnetic (PM) and an antiferromagnetic (AFM) phase. The distinct nature of the quasiparticle types in the two phases (magnons in the paramagnet and domain walls in the antiferromagnet), as well as spontaneous symmetry breaking in the AFM phase, lead to qualitative differences in the importance of different cooling processes. By performing extensive numerical simulations, we show that the kinetic equation correctly captures the system's evolution and its steady state even at a relatively strong auxiliary-system coupling — the regime relevant for current experiments. We compare the experimental protocol of Ref. [38] (where the couplings were kept constant) to our modulated coupling protocol, finding that the latter allows for much higher fidelities in the limit of large T.

As a further test for the applicability of our protocol, we study two non-integrable and strongly interacting models: the TFIM with an integrability-breaking longitudinal field [49], and a Heisenberg spin ladder in a strongly interacting regime [50]. Since many non-integrable systems have quasiparticle excitations which become weakly interacting at low energy densities,

we expect our analysis to apply, at least at low energies (the most relevant regime for ground state preparation). In both cases we observe that the system converges to an energy below the excitation gap, thus demonstrating that ground state preparation is not restricted to integrable models.

While our results for the different models demonstrate the theoretical applicability of our protocol, to be practically useful the algorithm must also be able to compete against the unwanted effects of noise. We modify the kinetic equation by incorporating noise-induced heating on top of the cooling protocol, and investigate how the non-equilibrium distribution of quasiparticle level occupations in the steady state is affected by noise, for the Floquet TFIM example. We observe that the density of quasiparticles in the steady state scales differently with the Markovian noise strength in the two phases, such that achieving low quasiparticle densities in the AFM phase requires significantly weaker noise. This scaling behaviour was predicted in Ref. [43], and can be understood within the kinetic framework from the nature of different quasiparticle types in the two phases. Nevertheless, we find that the modulated coupling protocol achieves high fidelities when the noise rate is small compared to the auxiliary-system coupling strength.

The rest of the paper is organized as follows: in Section 17.2 we describe the quasiparticle cooling protocol, and derive an equation for the evolution of the quasiparticle level populations, assuming weak auxiliary-system coupling. We discuss how the couplings can be tailored to remove quasiparticle excitations, and introduce the modulated coupling protocol (MCP) to suppress unwanted heating processes. In Section 17.3, we turn to cooling the integrable TFIM. We analyse cooling with boundary auxiliaries and with a finite density of auxiliaries, for different cooling protocols. We find that the MCP leads to effective cooling, which is accurately captured by the kinetic equation of Section 17.2. Non-integrable models are studied in Section 17.4, for the examples of the TFIM with an additional longitudinal field and a Heisenberg spin ladder. To check the protocol's robustness to decoherence, in Section 17.5 we generalise the kinetic theory to include noise, and examine how dephasing and decay processes affect the cooling of the TFIM. Finally, in Section 17.6, we provide concluding remarks and directions for future work.

17.2 Quasiparticle cooling protocol

17.2.1 Setup and protocol

We consider the following general setup for a system of qubits, or spins-1/2, a particular version of which was realized in the recent experiment with the Google quantum processor [38]. The central idea follows Ref. [27], and the main technical developments we present here are (i) the derivation of a simplified kinetic theory, based on the quasiparticle picture, and (ii) the introduction of time-dependent system-bath coupling, which, as we will see below, is crucial to reach high fidelities.

The qubits are divided into two groups, N_S qubits forming a system of interest, and N_A auxiliary qubits acting as a bath. One cycle of the protocol (cooling cycle), which effectively realizes a Floquet system coupled to an engineered bath, entails the following steps:

(i) Auxiliary (bath) qubits are initialized in a state described by a density matrix $\hat{\rho}_B^0$.

(ii) T layers of unitary evolution are applied. A unitary applied at time step $1 \leq \tau \leq T$ is a combination of the Floquet operator $\hat{U}_S$ acting on system qubits, a unitary $\hat{U}_B$ acting on the bath qubits, and an interaction term $\hat{U}_{\theta,\tau}$ which couples system and bath qubits. The interaction term is generally time-dependent, and θ is the coupling strength (see Eq. (17.8) below).

(iii) The bath qubits are reset into the initial state $\hat{\rho}_B^0$, which we will assume to be a stationary state of the bath unitary $\hat{U}_B$.

The main protocol control parameters are T, which we refer to as the reset time, and the system-auxiliary coupling. Resetting auxiliary qubits at the end of the cycle defines a quantum channel acting on the system,

$$\Phi(\hat{\rho}_S) = \mathrm{Tr}_B\ \hat{U}_T(\hat{\rho}_S \otimes \hat{\rho}_B^0)\hat{U}_T^\dagger, \tag{17.1}$$

where $\hat{U}_T$ is the combined cooling cycle unitary,

$$\hat{U}_T = \hat{U}_{\theta,T}\hat{U}_B\hat{U}_S \ldots \hat{U}_{\theta,1}\hat{U}_B\hat{U}_S, \tag{17.2}$$

the operator $\hat{\rho}_S$ is the system density matrix at the start of the cycle, and Tr_B is the trace over the bath degrees of freedom. The system density matrix after ν cooling cycles is given by

$$\hat{\rho}_S^\nu = \Phi^\nu(\hat{\rho}_S^0). \tag{17.3}$$

We will assume the steady state of the dynamics defined by this quantum channel is unique, and is reached independent of the initial state; we will not consider a scenario of initial states with anomalously slow relaxation to the steady state. In the analysis below we therefore take the initial state to be the maximally mixed state, $\hat{\rho}_S^0 \propto \hat{I}$, unless specified otherwise.

The system Floquet $\hat{U}_S$ can in particular correspond to an exact or prethermal effective Hamiltonian $\hat{H}_{\text{eff}}$,

$$\hat{U}_S \approx \exp\left(-\frac{i\pi}{2}\hat{H}_{\text{eff}}\right), \tag{17.4}$$

and our goal is to engineer dissipative evolution such that the steady state ($\nu \to \infty$) of the system is close to the ground state of $\hat{H}_{\text{eff}}$. In order to have a concrete model in mind, we will later study cooling in the case of the 1d Floquet transverse-field Ising model,

$$\hat{U}_S = \exp\left(-\frac{i\pi J}{2}\sum_{i=1}^{N_S-1}\hat{X}_i\hat{X}_{i+1}\right)\exp\left(\frac{i\pi g}{2}\sum_{i=1}^{N_S}\hat{Z}_i\right). \tag{17.5}$$

Here and below $\hat{X}_i, \hat{Y}_i, \hat{Z}_i$, denote the Pauli operators for qubit i, normalized as $\hat{X}_i^2 = \hat{Y}_i^2 = \hat{Z}_i^2 = 1$. The Floquet TFIM is exactly solvable via the Jordan-Wigner mapping to a model of non-interacting fermionic quasiparticles (see Appendix 17.9), and so provides a convenient setting to study quasiparticle cooling.

We keep the bath evolution simple, assuming for the initial bath state the product state with all spins up,

$$\hat{\rho}_B^0 = \otimes_{j=1}^{N_A}|0\rangle_{j\,j}\langle 0| \tag{17.6}$$

— note that in our convention the spin-up state is identified with the $|0\rangle$ state of the qubits — and for the bath unitary we choose

$$\hat{U}_B = \exp\left(\frac{i\pi h}{2}\sum_{j=1}^{N_A}\hat{Z}_j\right), \tag{17.7}$$

so that each auxiliary qubit simply acquires a phase in the eigenbasis of the $\hat{Z}$ operator. Parameter πh is referred to as the auxiliary quasienergy and does not depend on the unitary step τ.

In contrast, the system-bath coupling will in general vary in time:

$$\hat{U}_{\theta,\tau} = \exp(-i\theta f_\tau \hat{V}), \quad \hat{V} = \sum_{j=1}^{N_A} \hat{V}_j. \tag{17.8}$$

We have chosen to separate the time-dependence into the function f_τ, normalised according to $\sum_{\tau=1}^{T} f_\tau = 1$ [2], keeping θ as a small parameter which controls the coupling strength. Both f_τ and θ are dimensionless, and the interaction operator, which has dimension of energy, can in general be written in the form

$$\hat{V} = \sum_a \hat{A}^{a\dagger}\hat{B}^a + \hat{A}^a\hat{B}^{a\dagger}, \tag{17.9}$$

where operators $\hat{A}$ ($\hat{B}$) acts on system (bath). We refer to the $\hat{A}^a$ operators as the (system) cooling operators.

In the following we will assume that the bath operators $\hat{B}$ act simply as annihilation operators on the non-interacting bath set by Eq. (17.7):

$$\hat{U}_B^\dagger \hat{B}^a \hat{U}_B = e^{-i\pi h}\hat{B}^a. \tag{17.10}$$

This is simple to implement in the case of Eq. (17.7), by choosing $\hat{B}^a = \hat{\sigma}^+_{i_a}$, with i_a labelling the auxiliary qubit, where $\hat{\sigma}^\pm_i = (\hat{X}_i \pm \hat{Y}_i)/2$ are the spin raising/lowering operators. While our choice of the bath parameters may seem rather simple to simulate realistic cooling, we will see below that the complexity is shifted into the coupling choice, Eq. (17.8).

17.2.2 Weak-coupling analysis

In the remaining theoretical analysis, we assume that the excitations of the many-body system are well-defined, long-lived quasiparticles, and that we are in the limit of weak system-bath coupling, $\theta|V_j| \ll 1$. The quasiparticle assumption holds exactly in the example of the TFIM, Eq. (17.5); we note, however, that interacting systems away from criticality typically have quasiparticle excitations at low energies – examples include Fermi-liquids, superconductors, and symmetry-broken magnetic phases [46]. We expect the quasiparticle cooling algorithm to remain effective for such interacting systems, as we elaborate on in Subsection 17.2.4, and numerically demonstrate in Section 17.4. Our strategy will be to derive an equation describing evolution of the quasiparticle level occupations in the weak-coupling limit.

We define the quasiparticle occupation number operator $\hat{n}_k$, where index k labels fermionic quasiparticle levels (e.g. momentum in a system with periodic boundary conditions). The quasiparticles are sufficiently long-lived, such that $\hat{n}_k$ is an integral of motion of the system's evolution operator,

$$\hat{n}_k \hat{U}_S = \hat{U}_S \hat{n}_k. \tag{17.11}$$

In practice, it is sufficient to assume that the quasiparticle lifetime is much longer than the duration of one cooling cycle.

It is convenient to work in the interaction picture with respect to the evolution operator $\hat{U}_0 = \hat{U}_B\hat{U}_S$, such that an operator $\hat{O}_\tau$ (originally in the Schrödinger picture) is given by:

$$\hat{O}_{I\tau} = \hat{U}_0^{-\tau}\hat{O}_\tau\hat{U}_0^{\tau}, \quad 1 \le \tau \le T. \tag{17.12}$$

The evolution operator can be rewritten as follows,

$$\hat{U}_T = \hat{U}_0^T\hat{\mathcal{U}}_T, \quad \hat{\mathcal{U}}_T = \mathcal{T}\exp\Big(-i\theta\sum_{\tau=1}^{T} f_\tau \hat{V}_{I\tau}\Big), \tag{17.13}$$

[2] For protocols considered below, f_τ can be positive or negative, but for this choice the sum $\sum_{\tau=1}^{T}|f_\tau| \gtrsim 1$.

where $\mathcal{T}$ denotes time-ordering. Taking into account Eqs. (17.1,17.11), the quasiparticle occupation number after one cooling cycle reads:

$$n'_k = \mathrm{Tr}_S(\Phi(\hat{\rho}_S)\hat{n}_k) = \mathrm{Tr}_{SB}\Big(\hat{\rho}_S \otimes \hat{\rho}_B^0 \Big[\hat{\mathcal{U}}_T^\dagger \hat{n}_k \hat{\mathcal{U}}_T\Big]\Big). \tag{17.14}$$

At weak coupling, the occupation number change over one cycle, $\delta n_k = n'_k - n_k$, is small, and we compute it by expanding the r.-h.s. of the above equation to the second order in θ. Noting that the linear order in θ vanishes, and defining

$$\delta n_k = \mathrm{Tr}_S(\hat{\rho}_S \delta\hat{n}_k), \quad \delta\hat{n}_k = \mathrm{Tr}_B\Big(\hat{\rho}_B^0 \Big[\hat{\mathcal{U}}_T^\dagger \hat{n}_k \hat{\mathcal{U}}_T\Big]\Big) - \hat{n}_k, \tag{17.15}$$

this yields:

$$\delta\hat{n}_k = \theta^2 \sum_{ab} \sum_{\tau_1=1}^{T} \sum_{\tau_2=1}^{T} f_{\tau_1} f_{\tau_2} \Gamma_{ab}(\tau_1 - \tau_2) \Big(\hat{A}^{a\dagger}_{I\tau_1} \hat{n}_k \hat{A}^b_{I\tau_2} - \frac{1}{2}\{\hat{n}_k,\ \hat{A}^{a\dagger}_{I\tau_1} \hat{A}^b_{I\tau_2}\} \Big) + i\theta^2 [\hat{H}_{\mathrm{LS}}, \hat{n}_k]. \tag{17.16}$$

Here we defined the autocorrelators of the $\hat{B}$ operators,

$$\Gamma_{ab}(\tau) = \mathrm{Tr}_B\Big(\hat{\rho}_B^0 \hat{B}^a_{I\tau} \hat{B}^{b\dagger}_{I0}\Big), \tag{17.17}$$

and used relations $\Gamma_{ab}(\tau) = \Gamma^*_{ba}(-\tau)$. The fact that the autocorrelator depends on a single time variable is due to the assumption that $\hat{\rho}_B^0$ is a stationary state of $\hat{U}_B$. For simplicity, in the following we will also assume that Γ_{ab} is diagonal in the coupling operators, $\Gamma_{ab}(\tau) = \delta_{ab}\Gamma_{aa}(\tau)$; this will be the case in the examples we study. The second term in the r.-h.s. of Eq. (17.16) can be viewed as arising from the "Lamb shift" renormalization:

$$\hat{H}_{\mathrm{LS}} = \frac{i}{2} \sum_{ab} \sum_{\tau_1=1}^{T} \sum_{\tau_2=1}^{T} f_{\tau_1} f_{\tau_2} (\Theta(\tau_1 - \tau_2) - \Theta(\tau_2 - \tau_1)) \Gamma_{ab}(\tau_1 - \tau_2) \hat{A}^{a\dagger}_{I\tau_1} \hat{A}^b_{I\tau_2}. \tag{17.18}$$

where $\Theta(\tau)$ is the standard Heaviside step function, with the convention $\Theta(0) = 1/2$.

17.2.3 Rate equation

Note that the above derivation so far follows the steps of the textbook derivation of the Lindblad equation [52, 53], except here we focus on the Heisenberg-picture evolution of the occupation number operators, rather than on the system's density matrix. However, to derive the Lindblad equation one typically assumes a rapid decay of bath temporal correlations, compared to the system's dynamical timescales; in contrast, in our analysis the memory effects of the bath will play an essential role.

To simplify the analysis, we make an assumption that the system's density matrix at the beginning of a cooling cycle is diagonal in the quasiparticle basis, $[\hat{\rho}_S, \hat{n}_k] = 0$. We further assume that the correlations between occupations of different levels can be neglected. The former assumption can be justified in the limit $\theta \to 0$, by coarse-graining over sufficiently many cooling cycles (secular approximation). The latter assumption is more difficult to prove, but is closely related to the molecular chaos hypothesis in kinetic theory. In the context of integrable quantum systems it is often referred to as the time-dependent Generalized Gibbs ensemble (GGE) ansatz for $\hat{\rho}_S$ [54, 55, 56]. As we will show below, these assumptions lead to a theory of quasiparticle cooling which is in quantiative agreement with numerical simulations.

The diagonal assumption gives $\hat{\rho}_S = \sum_{\vec{\alpha}} \rho_{\vec{\alpha}\vec{\alpha}} |\vec{\alpha}\rangle\langle\vec{\alpha}|$, where $|\vec{\alpha}\rangle$ form a basis of states with occupation numbers $\{\alpha_k\}$, $\alpha_k = 0, 1$ and quasienergy

$$\varepsilon(\vec{\alpha}) = \sum_k \epsilon_k \alpha_k, \tag{17.19}$$

where ϵ_k is quasienergy of quasiparticle level k. The diagonal assumption still leaves us with 2^{N_S} coupled equations to solve. The second assumption, however, implies that the probabilities $\rho_{\vec{\alpha}\vec{\alpha}}$ can be expressed as a product over the single-quasiparticle distribution functions:

$$\rho_{\vec{\alpha}\vec{\alpha}} = \prod_q \frac{e^{-\alpha_q \lambda_q}}{1 + e^{-\lambda_q}}, \tag{17.20}$$

where the λ_q serve to parameterise the single-particle distribution. Eq. (17.20) is the familiar form for a gas of non-interacting fermionic particles. Equivalently, the probabilities can be written in terms of the average quasiparticle occupation numbers $n_q = \mathrm{Tr}(\hat{\rho}_S \hat{n}_q)$,

$$\rho_{\vec{\alpha}\vec{\alpha}} = \prod_q n_q^{\alpha_q} (1 - n_q)^{1-\alpha_q}, \tag{17.21}$$

by using the relation $n_q = e^{-\lambda_q}(1 + e^{-\lambda_q})^{-1}$.

Next, we compute the change in the occupation number over one cycle, δn_k, using the above form of the density matrix and Eq. (17.16). Since density $\hat{n}_k$ commutes with $\hat{\rho}_S$, the Lamb shift contribution plays no role. Denoting the Bohr frequencies by

$$\Delta(\vec{\alpha}, \vec{\beta}) = \varepsilon(\vec{\alpha}) - \varepsilon(\vec{\beta}), \tag{17.22}$$

we obtain

$$\delta n_k = \theta^2 \sum_{\vec{\alpha},\vec{\beta}} \sum_{a,\tau_1,\tau_2} \rho_{\vec{\alpha}\vec{\alpha}} (\beta_k - \alpha_k) f_{\tau_1} f_{\tau_2} \Gamma_{aa}(\tau_1 - \tau_2) e^{i(\tau_1 - \tau_2)\Delta(\vec{\alpha},\vec{\beta})} |\langle\vec{\beta}|\hat{A}^a|\vec{\alpha}\rangle|^2. \tag{17.23}$$

With our above choice of bath unitary (17.7) and of the $\hat{B}$ operators (17.10), the bath spectral function reads

$$\Gamma_{aa}(\tau) = e^{-i\pi h \tau}, \tag{17.24}$$

and Eq. (17.23) takes the following form:

$$\delta n_k = \theta^2 \sum_a \sum_{\vec{\alpha}\vec{\beta}} \rho_{\vec{\alpha}\vec{\alpha}} (\beta_k - \alpha_k) |F_{h,T}(\Delta(\vec{\alpha}, \vec{\beta}))|^2 |\langle\vec{\beta}|\hat{A}^a|\vec{\alpha}\rangle|^2. \tag{17.25}$$

Here, $\rho_{\vec{\alpha}\vec{\alpha}}$ is defined via Eq. (18.1) to yield a closed set of equations for the N_S quasiparticle occupations, and we defined

$$F_{h,T}(\epsilon) = \pi \sum_{\tau=1}^{T} f_\tau e^{i\tau(\epsilon - \pi h)}. \tag{17.26}$$

We refer to $F_{h,T}(\epsilon)$ as the filter function associated with f_τ. In short, it acts to filter out transitions occuring at unwanted frequencies, such as heating processes.

Eq. (17.25) is a general rate equation for quasiparticle level occupation numbers. It shows that the quasiparticle evolution is controlled by (i) the filter function, which encodes spectral features of the bath and time-dependent coupling, and (ii) the matrix elements of the operators $\hat{A}^a$ entering the system-auxiliary coupling. In order for the cooling protocol to remove quasiparticles from the system and drive into the many-body ground state, both of these features should be properly engineered, as we discuss next.

17.2.4 Choice of operators coupling to auxiliary qubits

First, we discuss the choice of the system cooling operators $\hat{A}^a$, entering the coupling Eq. (17.8). For simplicity, below we will consider 1d translationally invariant systems, with annihilation operator of a quasiparticle with quasimomentum k given by

$$\hat{Q}_k^- = \frac{1}{\sqrt{N_S}} \sum_{j=1}^{N_S} e^{ikj} \hat{Q}_j^-, \tag{17.27}$$

where $\hat{Q}_j^-$ is an operator centered at site j.

The auxiliary couplings $\hat{A}^a$ should be chosen such that the matrix elements for removing quasiparticle excitations in Eq. (17.25) are maximized. In principle, this can be accomplished by choosing the operators $\hat{A}^a$ to be quasiparticle annihilation operators $\hat{Q}_j^-$. Then, the matrix element appearing in Eq. (17.25) reads,

$$|\langle\vec{\beta}|\hat{Q}_j^-|\vec{\alpha}\rangle|^2 = \frac{1}{N_S} \sum_k (1-\beta_k)\alpha_k \prod_{q\neq k} \delta_{\alpha_q\beta_q}, \tag{17.28}$$

and the change of the quasiparticle occcupation numbers over one cooling period (assuming one auxiliary qubit per system site) is given by

$$\delta n_k = -\theta^2 |F_{h,T}(\epsilon_k)|^2 n_k, \tag{17.29}$$

i.e. the quasiparticle occupations decay exponentially with a rate set by the coupling strength and the filter function. The ground state is reached in time $O(\theta^{-2})$.

In practice, the precise form of the $\hat{Q}_j^-$ operators for a generic many-body system is often not known. These operators may have support on multiple sites, with size of the order of the correlation length. Furthermore, in phases with topological excitations, the operators may not even be local in the qubit basis. A clear example is the antiferromagnetic phase of the TFIM: while the excitations are local in a basis of non-interacting fermions, in the qubit basis, these excitations are domain walls, whose removal requires acting on a string of qubits (see Sec. 17.3).

This complicated structure of the $\hat{Q}_j^-$ operators poses an obstacle to choosing the cooling operators to coincide with annihilation operators – current hardware constraints dictate that the $\hat{A}^a$ operators should be relatively simple operators with support on at most a few neighbouring qubits. Despite this, the principle of adiabatic continuity [46, 57] implies that in gapped systems in which the quasiparticles are not topological, a choice of $\hat{A}^a$ operators can be made which is simultaneously hardware-efficient and which cools to the many-body ground state.

To illustrate this, suppose that the Hamiltonian of a gapped system in a topologically trivial phase can be written as (extension to Floquet systems in the prethermal regime is straightforward):

$$\hat{H}' = \hat{H}_0 + \lambda \hat{V}, \tag{17.30}$$

where H_0 is a simple solvable Hamiltonian where quasiparticles are created by local operators with support strictly on a few nearby sites, and $\hat{V}$ is a perturbation away from the simple point. Decomposing a Hamiltonian $\hat{H}'$ into above form is not unique, and we choose one such representation which minimizes the perturbation strength λ. For the TFIM example we have $H_0 = -g\sum_i \hat{Z}_i$ and $\hat{V} = \sum_i \hat{X}_i\hat{X}_{i+1}$, with $\lambda = J$; the quasiparticle annihilation operators of $\hat{H}_0$ are the single-spin operators $\hat{Q}_{0,j}^- = \hat{\sigma}_j^+$ in this case. According to Eq. (17.29), the non-interacting ground state at $\lambda = 0$ can be prepared exactly by choosing the cooling operators $\hat{A}^j = \hat{Q}_{0,j}^-$, and the operators are strictly local in the qubit basis.

When the interactions are switched on ($\lambda \neq 0$), then as long as $\hat{H}'$ and $\hat{H}_0$ remain in the same quantum phase, the principle of adiabatic continuity implies that the two Hamiltonians are

related by a quasi-local unitary transformation [57]. Both the ground state and the quasiparticle operators become 'dressed' by the transformation, while retaining their quantum numbers. This dressing of quasiparticles by the interactions can be characterised by the spectral function

$$S_{\hat{Q}_0^-}(k,\omega) = \sum_{\gamma'} |\langle\Omega'|\hat{Q}^-_{0,k}|\gamma'\rangle|^2 \delta(\omega - (\varepsilon_{\gamma'} - \varepsilon_0)), \tag{17.31}$$

where the sum runs over all excited states of the Hamiltonian $\hat{H}'$ and Ω' is now the interacting ground state with energy ε_0. In the $\lambda \to 0$ limit the spectral function exhibits a delta-function pole at the quasiparticle energy, $S(k,\omega) = \delta(\omega - \epsilon_k)$, while for finite λ, as long as the quasiparticle lifetime remains long, the spectral function retains a sharp feature centred around ϵ_k and with a width proportional to the inverse quasiparticle lifetime [3]. The weight (quasiparticle residue) Z_k of the pole is directly related to the matrix elements between the interacting ground state and single-quasiparticle excited states, $Z_k = |\langle\Omega'|\hat{Q}^-_{0,k}|k'\rangle|^2$ [46]. Thus, as long as the quasiparticle picture holds, Z_k remains non-zero and choosing the cooling operators according to $\hat{A}^j = \hat{Q}^-_{0,j}$ should lead to effective cooling of the low-energy excitations, albeit with cooling rate reduced by the factor of the quasiparticle residue.

This argument relies on the phase being adiabatically connected to a fixed-point Hamiltonian with simple, local quasiparticles, which is the case for gapped, topologically-trivial phases. In contrast, in systems where the underlying excitations are fractionalised, e.g. in the TFIM antiferromagnet or topologically ordered system, it is not possible to adiabatically connect the quasiparticle operators to local operators. Typically however, in such systems pairs or higher multiplets of quasiparticles may be annihilated locally. Similarly, as a system is tuned toward a critical point, the quasiparticle description may break down, leading to a vanishing quasiparticle residue, and a continuum of low-energy excitations emerges. In both of these cases we do not expect that the ground state can be prepared in constant time (scaling in the size of the system). We will see this explicitly in the case of the antiferromagnetic TFIM in Section 17.3.

To summarise our discussion, a possible strategy for choosing *local* cooling operators is to adiabatically connect the system's (effective) Hamiltonian to the nearest simple solvable Hamiltonian having local quasiparticle operators, and choose the coupling to auxiliary qubits to annihilate these quasiparticles. We note that, although above we viewed $\hat{V}$ as a perturbation, our argument is not restricted to weak-coupling: in Sec. 17.4, we will show that this method is effective in cooling an interacting spin ladder in the regime where the perturbation λ becomes of order one.

17.2.5 Choice of the filter function and two cooling protocols

We now turn to the second essential ingredient of efficient cooling, the engineering of the filter function in Eq. (17.26). When the cooling operators are chosen according to the argument in the previous Subsection, the operators will still generally have small matrix elements for transitions that increase the system energy, i.e. those corresponding to $\Delta(\vec{\alpha},\vec{\beta}) < 0$ in Eq. (17.25). As we now discuss, a proper choice of the filter function corrects for this deficiency by suppressing negative frequency (heating) transitions.

The filter function can be seen as a Fourier summation of the time-varying function f_τ, truncated to a finite number of terms, and so acts as a spectral filter on allowed transitions. Since in experiment the reset time is finite, spectral features of the filter function are broadened, with width of order $\delta\epsilon = 1/T$; however, assuming that T is sufficiently large compared to the inverse many-body gap, $T\Delta \gg 1$, it should be possible to choose the modulated function f_τ so

[3] In practice it is the spectral function that is measured in experiment and the validity of the quasiparticle description requires the existence of a sharp pole.

that the filter function strongly suppresses heating processes,

$$\left|\frac{F_{h,T}(+\epsilon)}{F_{h,T}(-\epsilon)}\right| \gg 1, \quad \epsilon \gtrsim \Delta. \tag{17.32}$$

For Floquet systems, the quasienergy is 2π-periodic and this statement needs clarification. It is natural to consider the prethermal limit where quasiparticle quasienergies are close to the energies of quasiparticles of the corresponding prethermal Hamiltonian [39]. For example, the transverse-field Ising model with arbitrary integrability-breaking local terms is in the prethermal regime as long as $|J|, |g| \ll 1$ and a similar condition is satisfied by the additional, integrability-breaking terms. In the prethermal regime, generally $|\epsilon_k| \ll \pi$, and heating processes due to Floquet evolution, and the associated energy non-conservation, are suppressed exponentially in $1/|g|, 1/|J|$. The prethermalization assumption then allows us to neglect processes in Eq. (17.25) where quasienergy changes by $\pm 2\pi, \pm 4\pi$ etc, since the corresponding matrix elements are strongly suppressed.

Next, we introduce two protocols which realise Eq. (17.32) to different degrees. In the first strategy, one aims to resonantly remove single quasiparticles from the system, by approximately matching auxiliary excitation quasienergy πh to a value ϵ within the quasiparticle band, $\Delta < \epsilon < \Delta + W$, where Δ is the single-particle quasienergy gap and W is the bandwidth. The function f_τ can be chosen to have a sufficiently broad profile, with width of order $1/W$, so that the filter function is centered at πh, with width of order W. A simple example is to use a constant pulse:

Step-wise cooling protocol (SCP)

The auxiliary quasienergy is matched to the quasiparticle band, $\Delta < \pi h < \Delta + W$, and the function

$$f_\tau = 1/T \tag{17.33}$$

is kept constant, therefore giving a 'step' pulse for $1 \leq \tau \leq T$. We will refer to this approach as the *step-wise cooling protocol (SCP)*.

The SCP was the strategy used in the experiment of Ref. [38]. The filter function corresponding to the SCP gives, up to a phase factor,

$$F^{\mathrm{SCP}}_{h,T}(\epsilon) = \frac{\pi}{T}\frac{\sin[(\epsilon - \pi h)T/2]}{\sin[(\epsilon - \pi h)/2]}, \tag{17.34}$$

which for $T \gg 1$ has a sharp peak at $\epsilon = \pi h$, with a width of order $\delta\epsilon = \frac{2\pi}{T}$. Thus, in the SCP, the processes of quasiparticle removal in Eq. (17.25) with quasienergies $\epsilon \approx \pi h$ are favored approximately according to

$$\left|\frac{F^{\mathrm{SCP}}_{h,T}(+\pi h)}{F^{\mathrm{SCP}}_{h,T}(-\pi h)}\right| \approx hT. \tag{17.35}$$

The SCP is efficient in systems with a sufficiently large quasiparticle gap and small bandwidth, as demonstrated in [38]; in this case the resonance peak of the filter function can be made broad enough to cover the entire quasiparticle band, while only having small weight at negative frequencies, suppressing heating processes. However, as the gap is decreased, in particular when a quantum critical point is approached, the heating processes become more important. Even in a gapped phase, the suppression of heating is only algebraic in quasiparticle energy, which leads to non-zero quasiparticle density in the steady state. Therefore, SCP does not allow for

high fidelity state preparation in most cases. A second disadvantage is the need to tune the auxiliary quasienergy πh to overlap with the possibly unknown quasiparticle band.

Instead of transitions occurring only at the natural resonant frequencies of the auxiliary qubits, transitions that lead to cooling may be engineered by strongly modulating the coupling f_τ in the time domain. In the task of cooling the system toward thermodynamic equilibrium (in particular the ground state), it is natural to consider those functions which satisfy the detailed balance condition [53]:

$$\left|\frac{F_{h,T}(+\epsilon)}{F_{h,T}(-\epsilon)}\right| = e^{\epsilon\beta/2}, \tag{17.36}$$

where β is the inverse temperature of the target equilibrium. The detailed balance condition ensures that heating processes are thermally suppressed, with the relative ratio of cooling to heating rates matching that in thermal equilibrium. Note that the SCP explicitly violates this condition, and thus drives the system into a non-equilibrium state with small quasiparticle density.

In order to construct a filter function which satisfies the detailed balance condition, we start by observing that the 'Fermi' function, $1+\tanh(\epsilon\beta/4)$, satisfies Eq. (17.36). However, the filter function must satisfy periodicity in the quasienergy argument, and so a correct choice is given by the 2π-periodic 'symmetrised' Fermi function

$$F_\beta(\epsilon) = \frac{\pi}{2A}\sum_{m=-\infty}^{\infty} e^{im\pi}\tanh([\epsilon - m\pi]\beta/4), \tag{17.37}$$

where A is a normalisation constant, and the function is symmetric about $\epsilon = \pi/2$. For $|\epsilon| \ll \pi$, this function looks like the Fermi function with 'thermal' broadening β, and satisfies the detailed balance condition. By decomposing Eq. (17.37) as a Fourier series (see Appendix 17.7), we are led to the following coupling time-dependence:

Modulated cooling protocol (MCP)

The coupling strength f_τ is modulated in time according to

$$f_\tau = \frac{2}{A\beta}\frac{\sin[\pi(\tau-\tau_0)/2]}{\sinh[2\pi(\tau-\tau_0)/\beta]}, \tag{17.38}$$

where $\tau_0 = T/2$, A is the normalization factor [a], and the auxiliary quasienergy is fixed at $\pi h = \pi/2$. We call this approach the *modulated cooling protocol (MCP)* .

[a] We note that the normalization factor is chosen according to the condition $\sum_{\tau=1}^{T} f_\tau = 1$. The modulated coupling in Eq. (17.38) is sign-changing, however, $\sum_{\tau=1}^{T}|f_\tau|$ is of order 1 for all cases considered below.

For finite T and $1 \ll \beta \ll T$, the filter function associated to the MCP gives a good approximation to Eq. (17.37), $F_{h,T}^{\mathrm{MCP}}(\epsilon) \approx F_\beta(\epsilon)$, with the Fourier series being effectively truncated at order T. Hence, the MCP satisfies detailed balance and leads to exponential suppression of heating processes in the limit given above. We have verified that $F_{h,T}^{\mathrm{MCP}}(\epsilon)$ in fact closely approximates $F^\beta(\epsilon)$ even when $\beta/T \approx 1$ (see Fig. 17.8, Appendix 17.7). Using the experimental values of Ref. [38], and setting $\gamma T/\theta^2 \approx 1$, where γ is the noise rate and θ the coupling strength, we find that the current practical regime in the presence of noise is around $T \approx 10$. Reduction of the noise levels in future quantum devices will allow the reset time to be further increased, which as we will see leads directly to higher state preparation fidelities.

In the rest of this paper, we focus on cooling gapped quasiparticle systems, where the many-body gap is $\Delta > 0$. Then for high-fidelity ground state preparation, it is sufficient to ensure $\beta\Delta \gg 1$ for the MCP. Due to the detailed balance condition, it is also possible to use the MCP to prepare finite-temperature thermal states, as we review in Appendix 17.8, simply by choosing β accordingly. We note that the strategy given above, of first writing down the filter function in the frequency domain and Fourier transforming to obtain the coupling modulation, is general and can be used to target other steady states which are not necessarily in thermal equilibrium.

17.3 Theory of quasiparticle cooling in a spin chain

In this Section, we study the performance of the cooling algorithms using the example of the TFIM, specified by the Floquet operator in Eq. (17.5). We assume the absence of noise (which we include in Section 17.5). We first consider the edge auxiliary setup (Fig. 18.1c). We will see that this leads to solvable dynamics in the sense that the density matrix of the system remains Gaussian. We show that the predictions of the rate equation derived above are in excellent agreement with the exact numerical solution. Then, we study the bulk auxiliary setup (Fig. 18.1d), where integrability is broken by the coupling to auxiliaries. In this case we compare the rate equation predictions to matrix-product states simulations of the dissipative evolution, finding again a good agreement. We investigate the dominant cooling and heating processes in the two phases, paramagnetic (PM) and antiferromagnetic (AFM), of the TFIM, finding qualitative differences due to the different nature of quasiparticles. By comparing the performance of the SCP and MCP, we find that the latter allows ground state preparation with high fidelity, in the noiseless case, by increasing the parameter β (T).

17.3.1 Transverse-field Ising model

We start by briefly summarizing the properties of the Floquet TFIM. This model can be mapped onto a p-wave superconducting chain by the Jordan-Wigner transformation:

$$\hat{\sigma}_j^- = \prod_{i=1}^{j-1} e^{i\pi \hat{c}_i^\dagger \hat{c}_i} \hat{c}_j^\dagger, \qquad \hat{Z}_j = 1 - 2\hat{c}_j^\dagger \hat{c}_j, \tag{17.39}$$

where $\hat{c}_j^\dagger, \hat{c}_j$ are fermionic creation/annihilation operators. The quasiparticle bands have quasienergies ϵ_k given by:

$$\cos\epsilon_k = \cos(\pi J)\cos(\pi g) - \sin(\pi J)\sin(\pi g)\cos k, \tag{17.40}$$

where $k \in [-\pi;\pi]$ is a quasimomentum. As a function of parameters J and g, the model has four phases, separated by phase transition lines at $J = g$, $J = 1-g$, where the quasiparticle gap Δ closes. The four phases are distinguished by the 0 and π Majorana edge modes [60, 61, 62]. Here we will be interested in the part of the phase diagram where $0 < (J, g) < 1/2$, and two phases exist: a paramagnetic (PM) phase at $g > J$, and an antiferromagnetic (AFM) phase at $g < J$. For $g, J \to 0$ these are the phases of the Hamiltonian TFIM; by analogy to this case, we define the Floquet vacuum projector

$$\Omega = \sum_g |\Omega_g\rangle\langle\Omega_g| \tag{17.41}$$

to project onto states where the valence quasiparticle band is filled, and the conduction band is empty i.e. $\hat{\eta}_k|\Omega_g\rangle = 0$, $\forall k$, with the quasiparticle annihilation operators $\hat{\eta}_k$ specified below.

The index g runs over the possible ground states: in the PM phase the vacuum state is unique, while in the AFM phase in the limit $N_S \to \infty$, the vacuum state is doubly degenerate, $g = \pm 1$, and the $\mathbb{Z}_2$ symmetry is spontaneously broken. In the fermionic counterpart of the TFIM, this degeneracy stems from the existence of zero-(quasi)energy Majorana edge modes, and the two vacuum states of the AFM differ by occupation of the Majorana level. The quasienergy gap between the ground and first excited state is given by $\Delta = 2\pi|J - g|$. In the rest of the paper, unless otherwise stated, results for the AFM (PM) phase correspond to the parameter points $J = 0.2$ (0.1), $g = 0.1$ (0.2).

For the open-boundary chain we consider, the allowed quasimomenta are quantized, $k_m \approx \pi(m-1)/N_S$, $m = 1, 2, .., N_S$, and the fermionic eigenmodes, defined by creation (annihilation) operators $\hat{\eta}_k^\dagger$ $(\hat{\eta}_k)$, are superpositions of plane waves with wave-vectors $\pm k$ (standing waves). The relation between on-site fermionic operators and eigenmodes is

$$c_j = \sum_k u_{jk}\eta_k + v_{jk}\eta_k^\dagger, \tag{17.42}$$

with the coefficients u, v referred to as the 'Bogolioubov coefficients'. We refer to Appendix 17.9 for a more detailed discussion and explicit relations.

In the paramagnetic limit $J = 0$, the quasiparticle annihilation operators are given by $\hat{\eta}_k = \frac{1}{\sqrt{N_S}} \sum_j e^{ijk} \hat{\sigma}_j^+$. Following the discussion in Subsection 17.2.4 regarding the optimal choice of system-auxiliary coupling in Eq. (17.8), for the rest of this section we set

$$\hat{V} = \pi \sum_j (\hat{\sigma}^+_{\mathcal{Q}_j} \hat{\sigma}^-_{\mathcal{A}_j} + \hat{\sigma}^-_{\mathcal{Q}_j} \hat{\sigma}^+_{\mathcal{A}_j}), \tag{17.43}$$

where $\mathcal{Q}_j$ $(\mathcal{A}_j)$ represent system (auxiliary) position associated with j-th coupling.

17.3.2 A solvable model: cooling at the edge

We now study a solvable example of cooling in the edge auxiliary setup of Fig 18.1c. In this case, the system cooling operator $\hat{\sigma}_1^+$ $(\hat{\sigma}_1^-)$ is free of the Jordan-Wigner string in the fermionic language, being proportional to $\hat{c}_1$ $(\hat{c}_1^\dagger)$ (see Eq. (17.39)). Therefore, in the rate equation (17.25), only processes where occupation of one of the quasiparticle levels changes by ± 1 are allowed. Due to reflection symmetry, the auxiliary at the other edge contributes equally to the cooling process, and Eq. (17.25) takes the form:

$$\delta n_k = -n_k W_k^- + (1 - n_k) W_k^+, \tag{17.44}$$

with the single-particle cooling and heating rates

$$W_k^- = 2\theta^2 |F_{h,T}(+\epsilon_k)|^2 |u_{1k}|^2, \tag{17.45}$$
$$W_k^+ = 2\theta^2 |F_{h,T}(-\epsilon_k)|^2 |v_{1k}|^2. \tag{17.46}$$

The coefficients $|u_{1k}|^2, |v_{1k}|^2$ naturally represent the probabilities for the quasiparticle (quasihole) to be found at the boundary. Assuming that the system is away from the critical point, the probabilities scale as $O(N_S^{-1})$ (from the normalization condition) away from the band edge, but are $O(k^2 N_S^{-1}) \approx O(N_S^{-3})$ near the band edge $k \approx 0, \pi$. This leads to a pronounced dependence of the cooling rates on the quasienergy ϵ_k, with the late time dynamics dominated by the cooling of modes near the band edges. Eq. (17.44) can be solved for the steady state populations

$$n_k^\infty = \frac{W_k^+}{W_k^+ + W_k^-}, \tag{17.47}$$

showing that a finite heating rate will inevitably lead to non-zero quasiparticle population.

As a first characterisation of the cooling performance, we study the dynamics of the quasiparticle density $n(t) = N_S^{-1}\sum_k n_k(t)$. We compare the rate equation predictions to exact numerical simulations, which can be performed efficiently in the case of edge cooling due to the problem's free-fermion nature (see Appendix 17.11). In Fig. 18.2a,b we plot $n(t)$ for both protocols, SCP and MCP, in the two phases, starting from the maximally mixed state $n(0) = 1/2$. We take $T = 4$, $h = 0.3$ in the SCP, and $T = 3\beta/2 = 28$, $h = 0.5$ in the MCP; the smaller reset time in the SCP case is approximately optimal (see Fig. 18.2c) while the MCP choice corresponds to $\Delta\beta \approx 4\pi$. In both cases $\theta = 0.02$ and $N_S = 20$. We observe a very good agreement between the rate equation theory (dashed lines) and the exact numerical simulation (solid lines). In the considered time window, for both PM and AFM phases under the MCP, the density decays predominantly exponentially in time, with a rate proportional to θ^2. In accordance with the arguments regarding heating rates in Section 17.2, the MCP exhibits a saturation of $n(t)$ at a much smaller value than the SCP (though in that case, the saturation is still to a relatively small value on account of the large quasiparticle gap). We also note the long time-scales associated with cooling to states of low quasiparticle density, with $\nu \approx 300\theta^{-2}$ for the PM phase under the MCP and even greater for the AFM. This is a consequence of the edge cooling setup, and the scaling of the Bogoliubov coefficients near the band edge discussed above.

As a second test, we examine the fidelity of the steady state distribution with respect to the Floquet vacuum, $\mathcal{F} = \mathrm{Tr}(\Omega\rho)$. In the case where Eq. (18.1) holds, the fidelity can be rewritten

$$\mathcal{F} = \prod_k (1 - n_k) \approx \exp(-\sum_k n_k). \tag{17.48}$$

The second line holds in the limit of sufficiently low total quasiparticle density. In this regime, the log-fidelity per qubit and quasiparticle density are approximately synonymous. In Fig. 18.2c we plot the steady state fidelity for the two pulses as the parameter β is increased, with $T = 3\beta/2$ fixed (for the SCP this is just a variation of parameter T). For parameters considered, the SCP allows to reach fidelity of order 0.99 per qubit while the MCP fidelity per qubit is better than one part in 10^6 by the point $\beta\Delta \approx 8\pi$. From Eq. (17.36), we see that the density of quasiparticles is bounded approximately as $n \sim e^{-\beta\Delta}$ for large β. The apparent saturation of MCP around $\beta\Delta = 8\pi$ is due to small ringing errors, which can be removed by increasing the ratio T/β — we refer the reader to Appendix 17.7 for more details. In practice, dominant heating processes arise due to noise and it pays to keep the ratio $T/\beta \gtrsim O(1)$.

From the above results, we conclude that the MCP is able to successfully prepare the ground state of the TFIM, with fidelity approaching 1 in the limit of large β. However, the associated time scale diverges with the system size, naturally a weakness of the edge cooling setup. The rate equation accurately captures the quasiparticle dynamics for the case of edge cooling. Next, we will consider the bulk cooling setup with a finite density of auxiliaries.

17.3.3 Finite density of auxiliaries

While providing an instructive example, the edge cooling setup is not practical for large systems. We argued above that the cooling timescale diverges with the system size in that case, which holds generally for models with local boundary dissipation [63]. Furthermore, the cooling rate remains constant while the heating rate due to noise scales with system size. Therefore, we now consider the setup in Fig. 18.1d, with a finite density of auxiliaries. For simplicity, we will assume that there is one auxiliary per system qubit.

In this setup, the dynamics is no longer integrable, and the system's density matrix develops non-Gaussian correlations due to the fact that the matrix elements for bulk $\hat{\sigma}_j^{\pm}$ operators carry

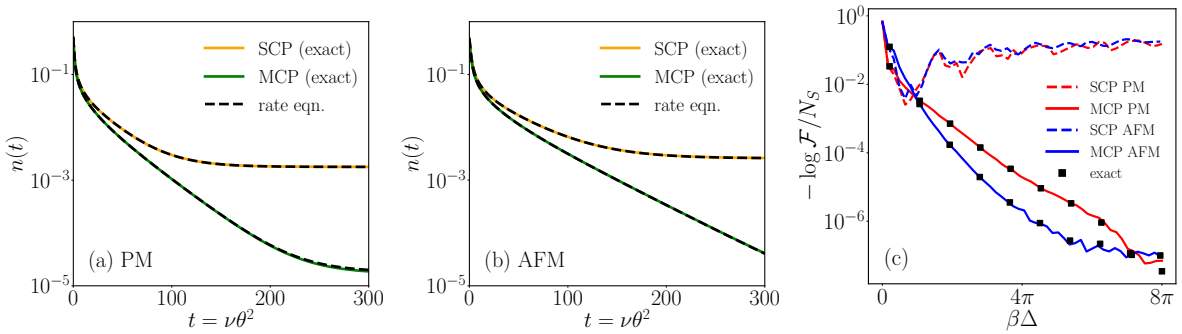


Figure 17.2: Performance of edge cooling protocol, for the parameter choice described in the main text. (a) Evolution of quasiparticle density $n(t)$ as a function of rescaled timescale $t = \nu\theta^2$, where ν is total number of cooling cycles, for the PM phase. We compare exact numerical results with $\theta = 0.02$ (solid lines) and the rate equation (dashed lines), for both SCP and MCP; (b) Same as in (a) but for AFM phase; (c) Log-fidelity per qubit of the steady state with quasiparticle vacuum, obtained from kinetic equation, as a function of the MCP parameter $T = 3\beta/2$. Black squares are exact numerical data, with $\theta = 0.001$, showing that kinetic theory accurately captures the steady state properties.

Jordan-Wigner strings in the fermionic formulation (see Eq. (17.39)). This allows for transitions between many-body eigenstates where the occupation numbers of several quasiparticle levels change at once.

To make progress, we therefore assume that the processes involving a small number quasiparticles are dominant. For cooling processes, this assumption is justified in the low-density limit $n_k \ll 1$, which describes the system's dynamics close to the ground state [4]. Restricting to processes involving at most two quasiparticles, we derive the following kinetic equation, containing cooling and heating terms, as well as terms that describe scattering between quasiparticles:

$$\delta n_k = -n_k W_k^- + (1-n_k)W_k^+ + \sum_q \Big[- n_k W_{k,q}^- n_q + (1-n_k)W_{k,q}^+(1-n_q) - n_k V_{k,q}^-(1-n_q) + (1-n_k)V_{k,q}^+ n_$$

(17.49)

We compute the rates in Eq. (17.49) assuming the system is near the vacuum state Ω, which yields:

$$W_k^{\mp} = \theta^2 \sum_{j=1}^{N_S} |F_{h,T}(\pm\epsilon_k)|^2 |\sigma^{\pm}_{j;0;k}|^2, \tag{17.50}$$

$$W_{k,q}^{\mp} = \theta^2 \sum_{j=1}^{N_S} |F_{h,T}(\pm(\epsilon_k+\epsilon_q))|^2 |\sigma^{\pm}_{j;0;k,q}|^2, \tag{17.51}$$

$$V_{k,q}^{\mp} = \theta^2 \sum_{j=1}^{N_S} |F_{h,T}(\pm(\epsilon_k-\epsilon_q))|^2 |\sigma^{\pm}_{j;q;k}|^2, \tag{17.52}$$

where we introduced the shorthand matrix-elements

$$\sigma^{\pm}_{j;k_1,\ldots,k_m;k'_1,\ldots,k'_n} = \langle k_1,\ldots,k_m|\hat{\sigma}_j^{\pm}|k'_1,\ldots,k'_n\rangle. \tag{17.53}$$

Above, the terms $W_k^{\mp}$ correspond to cooling/heating processes involving one quasiparticle, while the terms $W_{k,q}^{\mp}$ describe removing/adding a pair of quasiparticles, and $V_{k,q}^{\mp}$ describe quasiparticle

[4] Heating processes, in particular due to noise, may in principle involve a large number of particles; however, we will find that few-quasiparticle processes are dominant, and considering them gives an accurate approximation of heating rates.

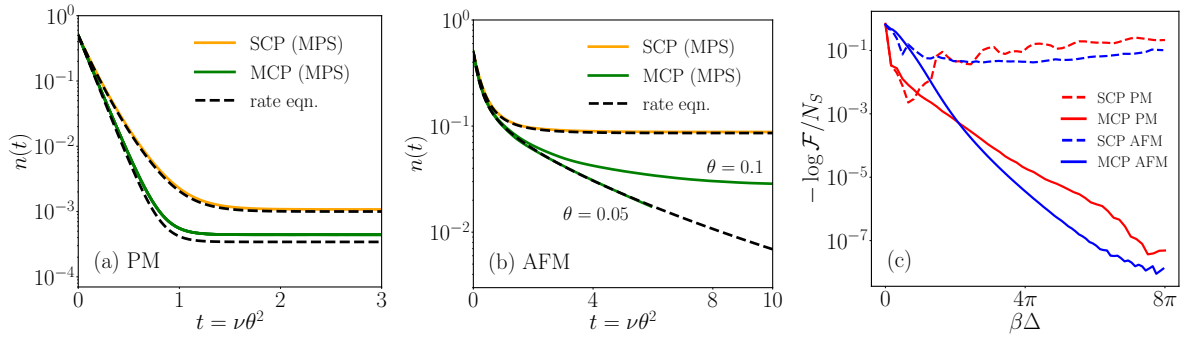


Figure 17.3: Performance of the bulk cooling protocol, with one auxiliary per system qubit and $N_S = 20$. The parameter choice is described in the main text. (a) Quasiparticle density $n(t)$ vs. rescaled timescale $t = \nu\theta^2$ in the PM phase. The MPS results (solid lines) are compared to the kinetic theory predictions (dashed lines), for both SCP and MCP. Parameter $\theta = 0.1$. (b) Same as in (a) but for the AFM phase. We show MPS results for two coupling strengths, $\theta = 0.1$ and 0.05, with the larger showing corrections to the rate equation. The AFM cools more slowly than the PM, as expected due to the topological nature of the quasiparticles. (c) Log-fidelity per qubit of the steady state with quasiparticle vacuum, calculated from the kinetic equation, as a function of the MCP parameter $T = 5\beta/2$.

scattering. Note that while the scattering does not directly change the total quasiparticle occupation number, it will tend to move quasiparticles toward lower quasienergies due to the presence of the filter function $F_{h,T}$. We expect that these rates will be weakly affected by a small finite background density of quasiparticles. The matrix elements can be evaluated using Wick's theorem (see Appendix 17.10 and a review [65]).

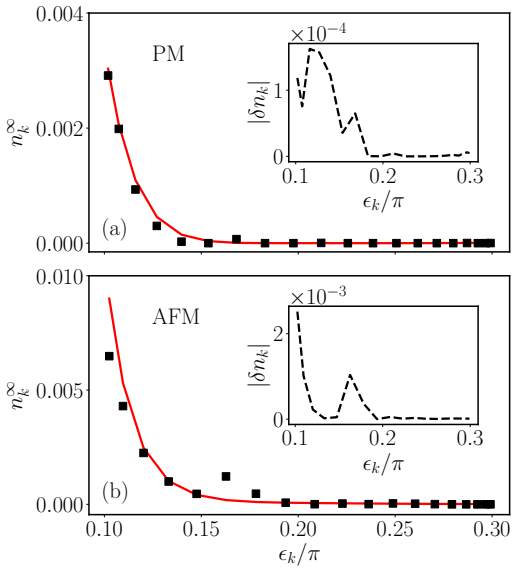


Figure 17.4: Quasiparticle occupation numbers n_k^∞ in the steady state, as a function of quasienergy ϵ_k. We compare MPS simulations (scatter points) and kinetic equation results (red line), for a system with $N_S = N_A = 20$ qubits in (a) PM and (b) AFM phases. The reset time is $T = \beta = 12$, and the coupling $\theta = 0.05$. The MPS simulations use a maximum bond dimension of $d = 100$. Inset: deviation $|\delta n_k|$ between rate equation and MPS values shown in main figure.

Crucially, the matrix elements entering in the above rates obey different selection rules in the PM and AFM phases. In the PM phase, there is a unique symmetric ground state.

Operators $\hat{\sigma}_j^{\pm}$ anticommute with the parity operator $\prod_j \hat{Z}_j$, so in the fermionic language they must change the fermion parity. Thus, two particle processes are forbidden in the PM phase, $W_{k,q}^{\mp} = V_{k,q}^{\mp} = 0$. In contrast, in the AFM phase, there are two vacuum states, $|\Omega_{\pm}\rangle$, which have parity ± 1. The cooling process can induce transitions between them by changing the occupation of the Majorana edge fermion. $W_{k,q}^{\mp}$ and $V_{k,q}^{\mp}$ matrix elements are non-vanishing in this case. The bra and ket states should be understood as quasiparticle states on top of different vacua. Note that the Majorana edge mode has a vanishing energy in the limit of large system size; hence, this mode cannot by cooled by our protocol and will remain effectively at an infinite temperature, corresponding to an equal weight mixture of the two vacuum states.

In the spin language, these selection rules follow from the phenomenological discussion in Subsection 17.2.4: since we chose the system-auxiliary couplings in Eq. (17.43) to match the local magnon excitations of the paramagnetic fixed point, we expect that also within the PM phase single excitations can be removed locally; in contrast, in the AFM phase, quasiparticles are dressed domain walls and can only be removed/created locally in pairs. This intuitive argument was pointed out in Ref. [43]. In Appendix 17.10, we study the distinct behavior of matrix elements in the two phases in detail. In particular, the two-particle matrix elements in the AFM phase are homogeneous in the bulk, but single-particle matrix elements decay exponentially with the distance of the auxiliary qubit from the boundary (since single domain walls can be removed at the edges of the chain), with a decay length set by the correlation length of the model. We will see below that this difference in quasiparticle nature leads to different efficiencies of the cooling in the two phases.

We now compare the predictions of the above kinetic theory to matrix product state (MPS) simulations of the system's density operator dynamics (more precisely, density matrix product operator simulations [66, 67]). The dynamics are performed using the standard time-evolving block decimation (TEBD) algorithm [68, 69], implemented via the ITensor library [70]. Implementation details and numerical verifications of asymptotic convergence are presented in Appendix 17.11.

As illustrated in Fig. 17.3a,b, the theory continues to be accurate for cooling with a finite density of auxiliaries, for both the SCP and MCP protocols. We fix system size $N_S = 20$ with one auxiliary per site. We use cooling parameters $T = 5$, $h = 0.3$ in the SCP and $T = \beta = 12$ in the MCP. The coupling is chosen to be $\theta = 0.1$ in the PM phase. In the AFM phase, this relatively large coupling leads to visible deviations between the MPS results and the kinetic equation prediction at late times; hence we include simulation results for a weaker coupling, $\theta = 0.05$, which leads to a good agreement. We use bond dimension $d = 100$ for both the SCP and MCP ($\theta = 0.05$) data, and $d = 150$ for the MCP ($\theta = 0.1$) data. These choices are converged in bond dimension (see Appendix 17.11). Our choice of larger θ and smaller MCP reset time (compared to the edge cooling case) helps to avoid high entanglement at intermediate times, which affects the accuracy of the MPS simulations. The MCP outperforms the SCP, and in Fig. 17.3c we provide further confirmation that the MCP can reach much higher fidelities, plotting the increase in the log-fidelity per qubit as the parameter $T = 5\beta/2$ is increased (we choose a large value of T/β to remove the ringing artifacts for the range of fidelities shown, see Appendix 17.7).

The difference in cooling distinct quasiparticle types in the PM and AFM phases is also evident in the timescales shown in Fig. 17.3a,b: the PM reaches a quasiparticle density below 10^{-3} after a small number of cooling cycles $O(\theta^{-2})$, with a clear exponential decay to the steady state value. In contrast, in the AFM phase, cooling slows down once quasiparticle density is below $n(t) \lesssim 10^{-1}$. This separation of timescales in the AFM is due to the fact that initial cooling proceeds quickly through pair annihilation processes, but this mechanism is suppressed $\propto n^2$ in the low density regime. Late-time cooling is therefore dominated by single-particle processes, which may only occur around the system edge.

As a final comparison between the kinetic equation and the MPS numerics, we look at the momentum-resolved quasiparticle occupations in the steady state, in Fig. 17.4, focusing on the MCP. To reach the steady state in our MPS simulations, we perform the simulations starting from the exact ground state. As we expect the (unique) steady state to be close to the true ground state, this allows for faster real-time simulations compared to starting from a high energy-density state. The figure illustrates that occupation numbers of all levels are below 10^{-2}, and the remaining population is mostly due to quasiparticles at the band edge. The finite weight on low energy modes stems from the relatively small value of the parameter $\beta\Delta \approx 2.4\pi$ chosen to aid the convergence of the MPS simulations.

To sum up, the analysis above demonstrates efficiency of MCP with a finite density of auxiliaries for removing quasiparticles after $O(\theta^{-2})$ cooling cycles, in the PM phase. In agreement with the arguments of Ref. [43], we also find that topological, domain-wall type quasiparticles are more challenging to remove. Nevertheless, in an idealized system without noise, our cooling protocol allows preparation of the ground state with very high fidelity, limited only by the choice of reset time T.

17.4 Cooling non-integrable systems

Having established the validity of our theory for the case of the TFIM, in this Section, we investigate the efficiency of the MCP for preparing ground states of non-integrable models. While these models are generally thermalizing, they typically have long-lived quasiparticles at low energy density. Therefore, the theory of dissipative cooling described in the previous sections for integrable systems, is expected to hold, once the system has been cooled to a state with sufficiently low energy density.

We study two examples of non-integrable systems using tensor network and quantum trajectory simulations: the TFIM in the paramagnetic regime with an additional longitudinal field [49], and an antiferromagnetic spin ladder with Heisenberg couplings between neighbouring sites [71]. In the longitudinal-field TFIM the physics is similar to the integrable case at low energies, except scattering now occurs between quasiparticles and multi-particle bound states emerge. Two-leg antiferromagnetic spin ladders model strongly-correlated low-dimensional magnetic systems [72, 73], with suggested connections to high-temperature superconductivity [50]. The low-energy spectrum features a band of spin-triplet excitations, as well as multi-particle bound states for intermediate coupling [71, 74]: thus, this relatively complex low-energy structure represents a good test for our cooling protocol.

17.4.1 Longitudinal field TFIM

The longitudinal field TFIM is defined by the Floquet unitary

$$\hat{U}'_S = e^{-i\hat{G}_0} e^{-i\hat{G}_1}, \tag{17.54}$$

$$\hat{G}_0 = \frac{\pi J}{2} \sum_{i=1}^{N_S-1} \hat{X}_i \hat{X}_{i+1}, \quad \hat{G}_1 = -\frac{\pi}{2} \sum_{i=1}^{N_S} g\hat{Z}_i + g_X \hat{X}_i.$$

We fix $J = 0.1$, $g = g_X = 0.15$, for which the model is in a paramagnetic phase [49]. As discussed above, since quasiparticles in the PM phase are simple magnons, we expect this to be the fastest regime to cool, and simulation accuracy is higher since the system reaches the low-density regime much faster.

Our parameter choice is in the Floquet regime, and not in the strict Trotter limit ($J, g_x, g_z \ll O(1)$). Thus, to characterize the cooling efficiency, we consider effective Hamiltonians obtained

in the first two orders of the Baker–Campbell–Hausdorff (BCH) expansion of Eq. (17.54), $\hat{U}'_S \approx e^{-i\hat{H}_l}$, $l = 0, 1$. The BCH formula gives

$$\hat{H}_0 = \hat{G}_0 + \hat{G}_1, \quad \hat{H}_1 = \hat{G}_0 + \hat{G}_1 - \frac{i}{2}[\hat{G}_0, \hat{G}_1]. \tag{17.55}$$

The cooling efficiency can then be characterized by measuring the energy and the fidelity of the system's density matrix with respect to the ground states of the above Hamiltonians:

$$E_l = \mathrm{tr}(\hat{H}_l\hat{\rho}), \qquad \mathcal{F}_l = \langle\Omega_l|\hat{\rho}|\Omega_l\rangle, \tag{17.56}$$

where $l \in \{0, 1\}$ denotes the BCH expansion order, and Ω is the corresponding ground state. The system is in the prethermal regime, due to the fact that $J, g, g_X \sim O(0.1)$, and is expected to cool towards the ground state of an effective Hamiltonian $\hat{H}_{l_*}$, with an optimal truncation order $l_* \geq 1$ of the BCH series. Thus, we expect the ground state of $\hat{H}_1$ to provide a better approximation than that of $\hat{H}_0$.

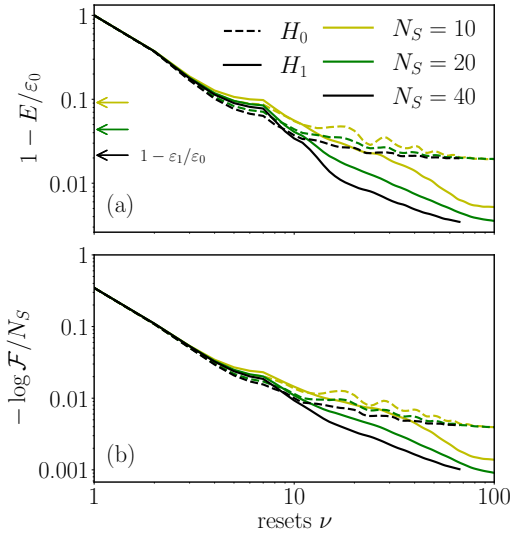


Figure 17.5: Cooling a non-integrable spin chain. (a) Evolution of energy, defined with respect to the ground state energy ε_0 of approximate effective Hamiltonian H_0 (dashed lines) and H_1 (full lines), as a function of the number of resets ν, for different system sizes. Corresponding energy values for the first excited states ε_1 of H_1 are indicated by arrows, showing convergence of energy to a value well below the excitation gap. (b) Log-fidelity per qubit vs. number of resets. Model parameters are $h_x = h_z = 0.15$, $J = 0.1$ (PM phase), reset time $T = \beta = 20$. The bond dimension of simulations is $d = 300$.

For the cooling protocol we focus on the MCP with finite density $N_A = N_S$. We take the coupling to auxiliaries to be the same as in Section 17.3. In contrast to the previous sections, where our aim was to develop a theory of cooling, here we generalise the protocol to cool more rapidly by using a large initial value of θ, later approaching the weak coupling limit $\theta \ll 1$ where the previous analysis is expected to hold. To this end, we initialize the coupling at $\theta(0) \approx 0.4$ and progressively reduce to a final value $\theta_\infty \approx 0.083$. The value of the coupling is reduced as $\theta(t+1) = 0.8\theta(t)$ whenever the energy of the system is reduced slower than a chosen rate, $0 < E_1(t) - E_1(t-1) < 0.01$. We found this choice to be efficient for the finite time simulations. Note that the function f_τ is still modulated within a cycle, see Eq. (17.38). We choose a reset time $T = \beta = 20$, for which $\Delta\beta \approx 5.2$, where Δ is the (many-body) energy gap of $\hat{H}_1$. The tensor-network simulations are performed similarly to the integrable case, see Appendix 17.11 for details.

In Fig. 17.5a, we show how the energies defined with respect to $\hat{H}_0$ and $\hat{H}_1$ evolve over the course of the cooling protocol, for three different system sizes $N_S = 10,\ 20,\ 40$. We observe that the system energy decays quickly toward the ground state energy of $\hat{H}_1$. (Note that due to the sweeping of θ the decay rate varies in time, as opposed to the clean exponential decay in the integrable case.) The expectation value of the zero-order Hamiltonian $\hat{H}_0$ saturates at a higher value than that of $\hat{H}_1$, indicating that the steady-state is well-approximated by the ground state of $\hat{H}_1$, as expected. Cooling efficiency appears to slightly increase with larger system sizes at later times, but larger system studies are required to provide a conclusive answer. In Fig. 17.5b, we observe similar behaviour in the decay of the log-fidelity per qubit, further corroborating the ability of MCP to cool the system to the ground state of an effective prethermal Hamiltonian.

17.4.2 Antiferromagnetic Heisenberg ladder

As a second example, we consider a two-leg ladder geometry of $N_S = 2 \times L$ sites, with antiferromagnetic Heisenberg couplings between neighbouring sites within each chain and across the rungs [71], of strength J and $J_\perp$ respectively. During the Floquet evolution, Heisenberg interactions are first applied to all odd-numbered bonds along the long (chain) axis of the ladder, followed by the even-numbered bonds, and finally across the rungs:

$$\hat{U}_S^{\text{lad}} = e^{-i\hat{G}_\perp} e^{-i\hat{G}_{\text{even}}} e^{-i\hat{G}_{\text{odd}}}, \tag{17.57}$$

$$\hat{G}_\perp = \frac{\pi J_\perp}{2} \sum_{\alpha,i=1}^{L} \hat{S}^\alpha_{1,i}\hat{S}^\alpha_{2,i}, \quad \hat{G}_{\text{even}} = \frac{\pi J}{2} \sum_{\sigma,\alpha,i=1}^{L/2-1} \hat{S}^\alpha_{\sigma,2i}\hat{S}^\alpha_{\sigma,2i+1},$$

$$\hat{G}_{\text{odd}} = \frac{\pi J}{2} \sum_{\sigma,\alpha,i=1}^{L/2} \hat{S}^\alpha_{\sigma,2i-1}\hat{S}^\alpha_{\sigma,2i},$$

where $\alpha = x, y, z$ labels the spin component, i runs along the long axis of the ladder, $\sigma = 1, 2$ labels the two sites belonging to each rung, and $\hat{S}^\alpha_{\sigma,i}$ are the spin-1/2 operators. Note the convention $\hat{S}^x = \hat{X}/2$ etc, and we have assumed that L is even.

The non-perturbative regime $J \approx J_\perp$ is relevant to experiments [50]. In this parameter regime, the system is gapped and adiabatically connected to the point $J/J_\perp \approx 0$. The physics can be easily understood in this limit, where the ladder decouples into isolated antiferromagnetic rungs, each hosting an $S = 0$ singlet-paired ground state with energy $-3J_\perp/4$, and a triplet of $S = 1$ excitations with energy $J_\perp/4$ [71]. The corresponding quasiparticle creation operators (with annihilation operators identical due to Hermiticity) are specified by $\hat{Q}^\alpha_k = \frac{1}{\sqrt{N_S}} \sum_j e^{ikj} \hat{Q}^\alpha_j$, where

$$\hat{Q}^\alpha_i = \hat{S}^\alpha_{1,i} - \hat{S}^\alpha_{2,i}, \tag{17.58}$$

and we have chosen the operators to anticommute with the parity operator exchanging the rung index σ. At lowest order in $J/J_\perp$, the quasiparticle band develops a finite dispersion as the excitations acquire a kinetic component along the ladder.

The adiabatic continuity argument suggests that the operators in Eq. (17.58) will continue to couple effectively to quasiparticles even in the regime $J/J_\perp \sim 1$. We therefore construct the cooling operators for the protocol to match the strong-coupling quasiparticle operators, taking the system-bath coupling as $\hat{V}^\alpha_j = \pi \hat{Q}^\alpha_{\mathcal{Q}_j} (\hat{\sigma}^-_{\mathcal{A}_j} + \sigma^+_{\mathcal{A}_j})$, with $\mathcal{Q}_j$ ($\mathcal{A}_j$) labelling the system (auxiliary) position associated with j-th coupling. Each auxiliary qubit couples with a single choice of α during each cooling cycle (in the numerics we randomly assign the couplings at the start of each cycle).

We test the effectiveness of the above cooling protocol, using the MCP with a finite density of auxiliary qubits. For the simulations we employ the quantum trajectory method, using

Google's qsim simulator [75]. Each trajectory represents an exact evolution of the system's wavefunction, conditioned on a stochastic sequence of events associated with the auxiliary reset. The initial state for each trajectory is a random computational basis state, uniformly sampled from an infinite-temperature ensemble. Similarly to the longitudinal-field TFIM, we measure the system energy with respect to the first two orders of the BCH expansion. We also track the system's average magnetization along the $\hat{z}$-axis, $\langle \hat{S}_i^z \rangle$, which is expected to be zero in the ground state due to the spin-symmetry of the Heisenberg terms.

The results are shown in Fig. 17.6, for a ladder of 2×10 qubits, coupled to 6 auxiliary qubits. The couplings $\mathcal{A}_j(\mathcal{Q}_j)$ are set randomly at the start of each cycle. We take $J = J_\perp = 0.2$, which is in the non-perturbative regime discussed above. The coupling strength is $\theta = 0.15$ and reset time $T = \beta = 30$. For these parameters the excitation gap of $\hat{H}_1$ is $\Delta = 0.19$ and $\Delta\beta \approx 5.8$. We observe the measured energies converging closely toward the ground state energy, with the final H_1 energy being slightly closer to the ground state than for H_0. At late times, the magnitude of the energy fluctuations falls below the excitation gap, indicative of a large overlap between the steady state and the system ground state. The measurements of the average magnetisation, displayed in the inset, show that the system approaches a magnetically disordered state on even faster timescales. We checked several other values of $J < J_\perp$ and found that the ground state convergence is robust. In Appendix 17.12, we provide additional data showing that the final energy density and time to reach the steady state is independent of system size, similarly to the TFIM paramagnet, assuming a finite density of auxiliary qubits. This agrees with our expectation that systems adiabatically connected to a fixed point with local excitations, can be cooled in constant time.

Together, the results for the longitudinal-field Ising model and Heisenberg spin ladder show that the MCP remains an effective tool for cooling non-integrable systems.

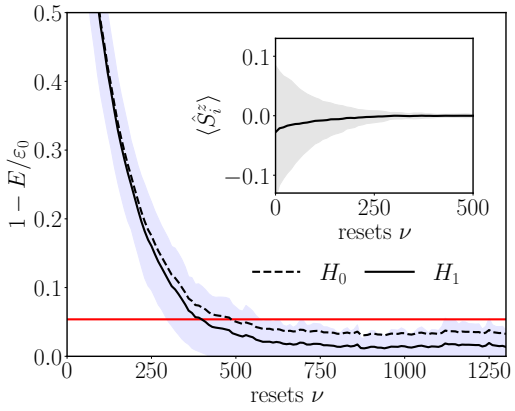


Figure 17.6: Cooling of a Heisenberg spin ladder. The mean energy for approximate effective Hamiltonians H_0 (dashed) and H_1 (solid) is shown, relative to the ground state energy, vs. the number of resets ν. The average is calculated over 100 trajectories, with the blue shaded area showing the standard deviation of the H_1 data. The excitation gap of H_1 is marked by the red line. Inset: Evolution of average magnetisation vs. number of resets. We use $J = J_\perp = 0.2$, $\theta = 0.15$, and the MCP with $T = \beta = 30$.

17.5 Noise effects

The results of the previous sections demonstrate the efficiency of our cooling protocol for preparing correlated ground states, assuming the reset time T can be made large, which is the case in the absence of noise. We now turn to the effects of unwanted decoherence. Each experimental platform comes with its own sources of noise, and our goal will be to understand the limitations it imposes on the cooling efficiency. We will focus on the single-qubit decay and

dephasing processes, relevant in systems of superconducting qubits. The kinetic equation can be generalized to include transitions mediated by weak noise. Using this modified kinetic theory, we study the 1d TFIM model and analyze the dependence of the steady state quasiparticle population on the noise strength.

17.5.1 Rate equation in the presence of noise

Considering continuous time evolution, single-qubit decoherence processes can be conveniently described within the Lindblad formalism [52]. The evolution of the system's density matrix $\hat{\rho}_S$ is given by (for the moment, we ignore the presence of auxiliary qubits):

$$\frac{d\hat{\rho}_S}{dt} = -i[\hat{H}, \hat{\rho}_S] + \delta\mathcal{D}(\hat{\rho}_S; \tilde{\gamma}), \tag{17.59}$$
$$\delta\mathcal{D}(\hat{\rho}_S; \tilde{\gamma}) = \sum_{j,\mu} \tilde{\gamma}_{j\mu} \left(\hat{L}_{j\mu} \hat{\rho}_S \hat{L}_{j\mu}^\dagger - \frac{1}{2}\{\hat{L}_{j\mu}^\dagger \hat{L}_{j\mu}, \hat{\rho}_S\} \right),$$

where index μ runs over possible decoherence processes, $\tilde{\gamma}_{j\mu}$ are their rates, and $\hat{L}_{j\mu}$ are the corresponding jump operators.

In the context of Floquet evolution, we will adopt the following simplified model: we assume that decoherence can be described by a quantum channel $\mathcal{D}$ acting on the system after one period of Floquet evolution. The quantum channel will be constructed by considering only the dissipative part $\delta\tilde{\mathcal{D}}$ of the Lindblad generator in Eq. (17.59), acting over the Floquet cycle duration Δt. Experimentally, quantum processors operate in the regime where $\tilde{\gamma}_{j\mu}\Delta t \ll 1$; then, this dissipative channel can be written as (to leading order in $\tilde{\gamma}$ coefficients):

$$\mathcal{D}(\hat{\rho}_S) \approx \hat{\rho}_S + \delta\mathcal{D}(\hat{\rho}_S; \gamma), \tag{17.60}$$

where we introduced dimensionless decoherence rates:

$$\gamma_{j\mu} = \tilde{\gamma}_{j\mu}\Delta t, \quad \gamma_{j\mu} \ll 1. \tag{17.61}$$

While this approximate model is only expected to be quantitatively accurate in the Trotter limit $g, J \ll 1$, we expect it to correctly capture the qualitative effects of noise on cooling even away from that limit. The main motivation for introducing this simplified model is that it decouples the unitary evolution of the cooling protocol from the decoherence effects, leading to a transparent and compact form of the noisy kinetic equation.

Within this model, the evolution of the system-bath density matrix over one cooling period is given by:

$$\Phi^\gamma(\rho_S) = \mathrm{Tr}_B\ \mathcal{D}\mathcal{M}_T ... \mathcal{D}\mathcal{M}_1(\hat{\rho}_S \otimes \hat{\rho}_B^0), \tag{17.62}$$

where

$$\mathcal{M}_\tau(\cdot) = \hat{U}_{\theta,\tau}\hat{U}_B\hat{U}_S(\cdot)\hat{U}_S^\dagger\hat{U}_B^\dagger\hat{U}_{\theta,\tau}^\dagger.$$

We follow the same steps that led to Eq. (17.25) above, now keeping first-order terms in θ^2 and $\gamma_{j\mu}$. The processes from cooling and noise contribute independently, since we discard next-order terms $O(\gamma\theta^2)$. The change in the quasiparticle occupations due to noise takes the standard Lindblad form

$$\delta\hat{n}_k = T\sum_{j,\mu} \gamma_{j\mu} \left(\hat{L}_{j\mu}^\dagger \hat{n}_k \hat{L}_{j\mu} - \frac{1}{2}\{\hat{L}_{j\mu}^\dagger \hat{L}_{j\mu}, \hat{n}_k\} \right), \tag{17.63}$$

and following Eqs. (17.16-17.25) we obtain the noisy rate equation, which includes cooling transitions $R_{\vec{\alpha}\vec{\beta}}$ and and an additional contribution $R^{\gamma}_{\vec{\alpha}\vec{\beta}}$ to transition rates from the noise terms:

$$\delta n_k = \sum_{\vec{\alpha},\vec{\beta}} \rho_{\vec{\alpha}\vec{\alpha}}(\beta_k - \alpha_k)[R_{\vec{\alpha}\vec{\beta}} + R^{\gamma}_{\vec{\alpha}\vec{\beta}}], \tag{17.64}$$

$$R_{\vec{\alpha}\vec{\beta}} = \theta^2 \sum_a |F_{h,T}(\Delta(\vec{\alpha},\vec{\beta}))|^2 |\langle\vec{\beta}|\hat{A}^a|\vec{\alpha}\rangle|^2, \tag{17.65}$$

$$R^{\gamma}_{\vec{\alpha}\vec{\beta}} = \sum_{j=1}^{N_S} \sum_{\mu} \gamma_{j\mu} T |\langle\vec{\beta}|\hat{L}_{j\mu}|\vec{\alpha}\rangle|^2. \tag{17.66}$$

17.5.2 Application: cooling the transverse-field Ising model

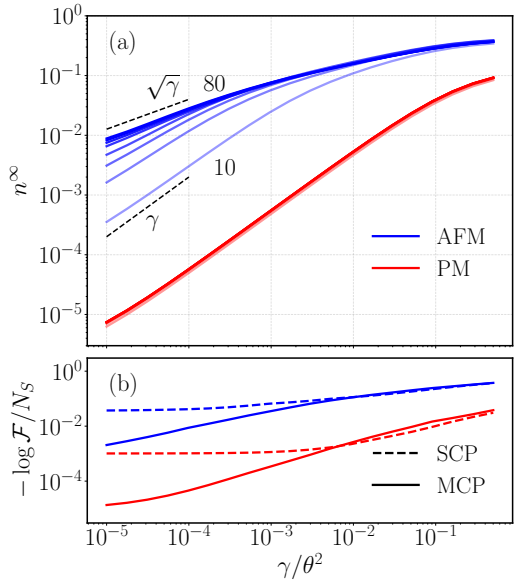


Figure 17.7: Performance of the cooling algorithm under decoherence. (a) Quasiparticle density in the steady state, as a function of noise ratio γ/θ^2, in PM (red) and AFM (blue) phases, for different system sizes N_S from 10 to 80. We use MCP with fixed $T = \beta = 6\pi/\Delta$. At weak noise, PM quasiparticle density scales linearly with γ, while AFM displays a crossover from $n \propto \gamma$ to $n \propto \sqrt{\gamma}$ behaviour as noise strength is reduced. (b) Log-fidelity between steady state and quasiparticle vacuum, for MCP (solid lines) and SCP (dashed lines). We fix $T = \beta$ and optimize over parameter β for each protocol.

Next, we apply the noisy kinetic equation to cooling of the transverse-field Ising model of Section 17.3 in the presence of decay to the qubit ground state, and dephasing noise. This corresponds to $\mu = d, \phi$, with jump operators

$$\hat{L}_{jd} = \hat{\sigma}^+_j, \qquad \hat{L}_{j\phi} = \hat{Z}_j. \tag{17.67}$$

We assume homogeneous decoherence rates for simplicity, $\gamma_{j\phi} = \gamma_\phi$, $\gamma_{jd} = \gamma_d$, and rescale the dephasing rate, $\gamma_\phi \to \gamma_\phi/2$, following standard conventions in the literature on open quantum system. Non-uniform decoherence rates can be further included in the rate equation without complication (we refer to [76] for a characterisation of site-dependent noise rates for the Google Quantum Processor).

Similar to our analysis in Sec. 17.3, we restrict to processes involving at most two quasiparticle levels. (Processes involving a higher number of quasiparticles can be systematically accounted for within our formalism.) This approximation yields the same kinetic equation derived in Sec. 17.3, Eq. (17.49), but with the rates modified by noise, $W \to \tilde{W}$, $V \to \tilde{V}$:

$$\tilde{W}_k^{\mp} = W_k^{\mp} + \sum_{j=1}^{N_S} \gamma_d T |\sigma^{\pm}_{j;0;k}|^2 + \frac{\gamma_\phi T}{2} |Z_{j;0;k}|^2, \tag{17.68}$$

$$\tilde{W}_{k,q}^{\mp} = W_{k,q}^{\mp} + \sum_{j=1}^{N_S} \gamma_d T |\sigma^{\pm}_{j;0;k,q}|^2 + \frac{\gamma_\phi T}{2} |Z_{j;0;k,q}|^2, \tag{17.69}$$

$$\tilde{V}_{k,q}^{\mp} = V_{k,q}^{\mp} + \sum_{j=1}^{N_S} \gamma_d T |\sigma^{\pm}_{j;q;k}|^2 + \frac{\gamma_\phi T}{2} |Z_{j;q;k}|^2. \tag{17.70}$$

The matrix elements satisfy the selection rules discussed in Sec. 17.3. Note that while the matrix elements for cooling and decay processes are identical here, the spectral filtering provided by the filter function distinguishes the two processes. We now summarise the main behaviour of the noisy rate equation in the paramagnetic and antiferromagnetic phases of the TFIM, with a more detailed discussion of matrix elements for $\hat{Z}_j$ and $\hat{\sigma}_j^{\pm}$ operators given in Appendix 17.10. In the PM phase, single particle loss and gain processes occur throughout the chain (cooling and decay contributions); quasiparticle pair creation/annihilation and number-conserving scattering events occur due to dephasing. In the AFM phase, on account of the domain-wall nature of excitations, only two-particle scattering and pair creation/annihilation processes can occur in the bulk, and they are induced by cooling, decay and dephasing. Single particle transitions require an interaction with the Majorana edge mode, and are localized to the chain edge.

We have compared the predictions of the noisy kinetic equation and MPS simulations in the presence of noise, finding again a good agreement in the parameter regimes accessible to MPS (moderate value of noise strength, or moderate times at a very weak noise). We refer the reader to Appendix 17.13 for a comparison of the steady state occupations, also for different coupling strengths. The rate equation, however, allows us to study system sizes and parameter regimes far beyond the reach of matrix product state simulations [5].

In Fig. 17.7a, we illustrate the quasiparticle density in the steady state, obtained from the kinetic equation, as a function of the noise strength. For simplicity, we choose $\gamma_d = \gamma_\phi = \gamma$ and fix auxiliary density $N_A = N_S$. We focus on the MCP with $T = \beta = 6\pi/\Delta$. We observe a qualitatively different behavior in the two phases, in line with above results on noiseless cooling. In the PM phase, the steady state quasiparticle density decays as a power-law function of noise, $n^{\infty}_{\mathrm{PM}} \propto \gamma^a$, $a \approx 1$, and is independent of the system size for $N_S \gtrsim 10$. In the AFM phase, in contrast, the density displays a power-law scaling which depends on system size, $n^{\infty}_{\mathrm{AFM}} \propto \gamma^{b(N_S)}$. For small systems and weak noise, we observe similar scaling to the PM, with $b \approx 1$; as either the system size or noise strength is increased, we find a crossover to a different power $b \approx 1/2$.

The utility of the kinetic theory is demonstrated with the following simplified versions of the kinetic equations, which capture the observed features in Fig. 17.7a: In the PM phase, where single-quasiparticle processes can occur throughout the system (bulk and edge), the evolution of the occupation number $n_k(t)$ is given by

$$\frac{dn_k(t)}{dt} \approx -C_1 \theta^2 n_k + C_\gamma \gamma T, \tag{17.71}$$

[5] The steady state can be efficiently found by root-finding algorithms, after the cooling and noise-induced rates have been calculated via Wick's theorem. In practice, the system reaches its steady state quickly and we evolve the rate equation in time until the quasiparticle occupations have effectively converged.

where C_1, C_γ are constants of order one. We assumed that MCP is in the regime where heating processes due to coupling to auxiliaries are strongly suppressed, and neglected the dependence of C_1, C_γ on k. For the noise we neglect terms $O(\gamma T n)$, since we are interested in the regime of weak noise and low density. Then, the expected steady state quasiparticle density is given by

$$n^\infty_{\rm PM} \approx \frac{C_\gamma \gamma T}{C_1 \theta^2}, \tag{17.72}$$

where we averaged over k, which gives the linear dependence on $\gamma T/\theta^2$ in Fig. 17.7a, for weak noise.

In the AFM phase, as discussed above, the single-quasiparticle cooling processes can only occur at the edge, and their rates are suppressed by

$$\theta^2 \Gamma_k = \theta^2 C_e |u_{1,k}|^2 \approx \theta^2 C_e \frac{k^2}{N_S} \tag{17.73}$$

(strictly speaking, this expression holds for small quasimomenta, $k \ll 1$, but we will see below that the steady state quasiparticle density is determined mostly by this quasimomentum range). The processes removing quasiparticle pairs can be modeled by a term $-C_2\theta^2 n_k n$, neglecting the k, q dependence of the rates $W^{\mp}_{k,q}$. The dominant heating mechanism is from pair creation in the bulk. Then, we arrive at

$$\begin{aligned}\frac{dn_k(t)}{dt} \approx & -\theta^2 \Gamma_k n_k - C_2 \theta^2 n_k n \\ & + C'_\gamma \gamma T (1-n_k)(1-n).\end{aligned} \tag{17.74}$$

The steady state occupation numbers are given by

$$n^\infty_k \approx \frac{C'_\gamma \gamma T}{\theta^2 \Gamma_k + C_2 \theta^2 n^\infty_{\rm AFM} + C'_\gamma \gamma T}, \tag{17.75}$$

supplemented by a self-consistency condition

$$n^\infty_{\rm AFM} = N_S^{-1} \sum_{m=1}^{N_S} n^\infty_{k_m}, \tag{17.76}$$

where we again neglected terms $O(\gamma T n)$ for the regime of interest. The solution $n^\infty_{\rm AFM}(\gamma)$ exhibits two regimes, depending on the noise strength. At stronger noise values, where $n^\infty N_S \gg 1$ (such that the total number of quasiparticles in the steady state of the system is much greater than 1), two-particle cooling processes dominate. Neglecting the sub-dominant single-particle cooling contribution Γ_k yields

$$n^\infty_{\rm AFM} \approx \left(\frac{C'_\gamma \gamma T}{C_2 \theta^2} \right)^{1/2}. \tag{17.77}$$

In the opposite limit, $n^\infty N_S \ll 1$, the single-particle cooling processes determine the steady state and we can neglect the C_2 term in Eq. (17.75). Then,

$$n^\infty_{\rm AFM} \approx \sum_{m=1}^{N_S} \frac{C'_\gamma \gamma T}{C_e \theta^2 m^2 N_S^{-2} + C'_\gamma \gamma T N_S} \approx C \frac{\gamma T N_S^2}{\theta^2}, \tag{17.78}$$

with $C = \pi^2 C'_\gamma/(6C_e)$. This expression holds in the weak-noise limit, $n^\infty N_S \sim \gamma T N_S^3/\theta^2 \ll 1$, and we made use of the approximate quantization condition $k_m \approx \pi(1-m)/N_S$, which holds for $k_m \ll \pi$. These approximate rate equations, Eqs. (17.77,17.78), capture the crossover behaviour displayed in Fig. 17.7a.

In Sec. 17.3 we argued that the fidelity of the steady state with the ground state approaches 1 as the MCP parameter $T \propto \beta$ is made large. In the presence of noise, there will be an optimal T_* and β_* that maximise the fidelity, since the noise strength also scales with T. We compare the log-fidelity per qubit for the MCP and the SCP vs. the noise ratio γ/θ^2, in Fig. 17.7b. For each point, we optimize the parameter β, fixing $T = \beta$ for simplicity (for the SCP this simply corresponds to optimizing T). We observe that, while at moderate noise values $\gamma/\theta^2 \gtrsim 10^{-2}$, the SCP marginally outperforms MCP, for weak noise the MCP reaches higher fidelities in both phases, approaching fidelity 1 as the noiseless limit is approached. We conclude that the MCP is able to prepare target states with high fidelity even in the presence of weak noise, but noise is more destructive in systems with topological excitations such as the 1d AFM example.

17.6 Discussion and outlook

In summary, in this work we investigated cooling protocols for preparing ground states of many-body systems on quantum processors. Our approach is reminiscent of cooling strategies in systems of ultracold atoms, including sympathetic cooling [78], but our protocol primarily aims to remove quasiparticles – emergent excitations above a many-body ground state. We developed a phenomenological kinetic theory framework, which accounts for competing cooling and heating processes induced by auxiliaries and by noise, discussed how to tailor the protocol parameters to remove quasiparticles from the system, and compared the efficiency of different cooling protocols.

Our results are directly applicable to studying correlated states with current digital quantum processors, as well as in analog processors with the fast reset capability: indeed, SCP was recently implemented on the Google Quantum Processor [38]. While reaching the ground state in that experiment was challenging due to the level of noise $\gamma \approx 0.01$, our work shows that, with e.g. $\theta = 0.1$, noise values of $\gamma \approx 10^{-3}$ will be sufficient for preparing steady states with quasiparticle density below $n \approx 10^{-2}$ in the paramagnetic phase (see Fig. 17.7b). In systems of $N_S = 100$ qubits, this translates to approximately one quasiparticle in the sample. Cooling the antiferromagnetic phase is more challenging, because the quasiparticles cannot be removed individually by local operators; nevertheless, noise level $\gamma \approx 10^{-6}$ allows to reach comparable densities. We expect that such low-energy states can be further efficiently purified to extract properties of the ground state and low-energy dynamics [38].

The quasiparticle cooling algorithm is a promising alternative to existing state-preparation methods, including variational unitary circuits [19, 20, 21], thanks to a degree of robustness with respect to noise it offers, as well as its generality. First, dissipation removes excitations created by noise, and the steady state is independent of the initial state and the history of errors. Second, our results for the non-integrable models studied here suggest that dissipative cooling should be suitable for preparing a broad class of correlated states, not restricted to integrable systems. Further, we note that the dissipative protocol can be adapted to complement existing state-preparation methods, for example by using the output of variational algorithms for the protocol initial state, or to aid in avoiding local minima in the variational landscape [79].

One area where we expect our cooling protocol to prove instrumental is in the study of 2d correlated systems: the ground states of such systems are challenging to probe numerically, but should be amenable to state preparation on quantum devices. The study of the Heisenberg ladder (a quasi-1d system) carried out in Section 17.4 suggests that the cooling protocol will remain effective also in 2d, in particular for the cases where the system's excitations can be adiabatically connected to local operators. It will be interesting to understand the advantages or limitations of dissipative cooling for these systems.

As pointed out in Ref. [43], and further highlighted by our analysis, systems with topological, non-local quasiparticles are more challenging to cool. On the fundamental level, this stems from

lower bounds [80, 81] on the preparation times of topologically ordered states (e.g., toric code). Exploring strategies of optimal cooling of such systems, for example by creating quasiparticle traps or making use of dynamical gauge fields [82], is a promising direction of future research.

The quasiparticle theory typically breaks down when crossing a quantum phase transition. It would be instructive to apply our analysis to quantum-critical points with gapless quasiparticles, and to study the possibility of cooling strongly interacting systems without long-lived quasiparticles. Although local operators are no longer expected to couple strongly to single-particle excitations, we expect that our cooling protocol should drive the system into a low energy steady state, as long as heating processes are efficiently suppressed (e.g. by the filter function). Generally, we may expect [83] that algorithms similar to ours will be able to efficiently prepare low energy states of thermalizing systems (which rules out examples such as spin glasses, where the cooling procedure will drive the system to one of the many metastable minima). We note that, despite the generality of this approach, we expect certain states will yet prove hard to prepare. One reason is that preparing ground states with high fidelity in general would allow one to solve QMA-complete problems [84], which would contradict a widely believed conjecture that QMA-complete problems cannot be solved efficiently on quantum computers. Still, we do not expect the extreme hard cases to arise in the absence of spin-glass order.

Our work suggests several other avenues for future research. First, we note that our protocol may be modified to prepare approximate finite-temperature Gibbs states [27, 83, 85, 34], by using the MCP filter function, Eq. (17.38), with effective temperature $T_{\text{eff}} = 1/\beta$. This is due to the fact that the MCP already satisfies the conditions for detailed balance, Eq. (17.36). We demonstrate cooling of finite temperature states in Appendix 17.8, leaving a more detailed investigation for future works. Weak noise processes in quantum processors generally violate detailed balance, and will make the steady state slightly non-thermal. In contrast, intrinsic thermalization mechanisms in interacting systems are expected to favor the thermal state. This competition, and the resulting steady state may be studied using digital [38] and analog quantum processors.

Finally, our protocol can be modified to engineer non-equilibrium quasiparticle distribution in the steady state [86]. The properties of the steady state, and evolution towards it can give useful insights into interactions between quasipaticles, their dynamics, and lifetimes – properties that play a central role in our understanding of correlated materials. We note that the accuracy of the kinetic theory we used to model the cooling protocol suggests that the dominant thermalization mechanisms are well approximated by few-particle processes. Applications of suitably modified protocols in quantum simulator experiments would unlock new avenues to study underlying dynamics and thermalization mechanisms.

17.7 Details of modulated coupling pulse

In this Appendix, we provide additional details regarding the modulated coupling protocol (MCP) defined in Eq. (17.38). As explained in Section 17.2, this pulse is advantageous in that the corresponding filter function, $F^{\text{MCP}}_{h,T}(\epsilon)$, approximately satisfies the thermal detailed balance condition, Eq. (17.36), with the inverse 'temperature' set by the parameter β. First we derive the form of the MCP, starting from the 2π-periodic function given by

$$F_\beta(\epsilon) = \frac{\pi}{2A} \sum_{m=-\infty}^{\infty} e^{im\pi} \tanh([\epsilon - m\pi]\beta/4). \tag{17.79}$$

The summation limit above should be taken as $\lim_{k\to\infty} \sum_{m=-2k}^{2k+1}$, although for $\beta \gtrsim 1$ is is sufficient to restrict to a small number of terms when considering the inverval $-\pi < \epsilon \leq \pi$. By

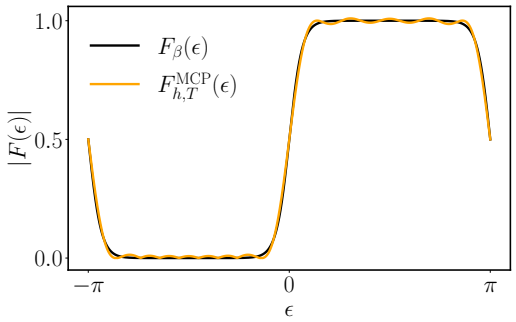


Figure 17.8: Comparison of $F_{h,T}^{\mathrm{MCP}}$ (Eq. (17.38), orange) and F_β (Eq. (17.79), black), for parameters $T = \beta = 20$.

inserting a resolution of the delta-function we arrive to the following Fourier series

$$F_\beta(\epsilon) = \sum_{m=-\infty}^{\infty} e^{im\epsilon} g(m), \tag{17.80}$$

$$g(m) = \frac{\pi}{2A} \int_{-\infty}^{\infty} \frac{d\epsilon'}{2\pi} e^{-im\epsilon'} [\tanh(\epsilon'\beta/4) - \tanh([\epsilon' - \pi]\beta/4)].$$

The components can be evaluated via residues,

$$g(m) = \frac{\pi}{iA\beta} \frac{(1 - e^{-i\pi m})}{\sinh(2\pi m/\beta)}, \tag{17.81}$$

and then, shifting the summation index to $\tau = m + \tau_0$ ($\tau_0 = T/2$) we have (up to an unimportant phase factor)

$$F_\beta(\epsilon) = \frac{2\pi}{A\beta} \sum_{\tau=-\infty}^{\infty} \frac{\sin[\pi(\tau - \tau_0)/2]}{\sinh[2\pi(\tau - \tau_0)/\beta]} e^{i\tau(\epsilon - \pi/2)}. \tag{17.82}$$

Truncating the series at a finite number of terms $1 \leq \tau \leq T$, we arrive at the MCP given in Eq. (17.38) of the main text. The truncation error is bounded by

$$|F_\beta - F_{h,T}^{\mathrm{MCP}}| \leq 2 \sum_{m=\tau_0+1}^{\infty} |g(m)| \lesssim A^{-1} e^{-2\pi T/\beta}, \tag{17.83}$$

so is small in the limit $\beta \ll T$. By design, in the prethermal regime $|\epsilon| \ll \pi$ we have

$$F_\beta(\epsilon) \approx \frac{\pi}{2A}(1 + \tanh(\epsilon\beta/4)), \tag{17.84}$$

which satisfies the detailed balance condition Eq. (17.36), and therefore so does the MCP filter function, up to the errors given above.

In Fig. 17.8 we compare $F_{h,T}^{\mathrm{MCP}}(\epsilon)$ as obtained from the MCP, with the Fermi function Eq. (17.79). (For the latter we truncate the series after a few terms with negligible error.) We take $\beta = 20$ and show the summation result for $T = \beta$. Even for this large value of β/T, the truncation ('ringing') error is small and $F_{h,T}^{\mathrm{MCP}}$ clearly captures the step-like form of the Fermi function. In realistic systems the errors due to noise will typically be larger than the above truncation errors, and we can obtain efficient cooling with values of T, β, considered in the main text.

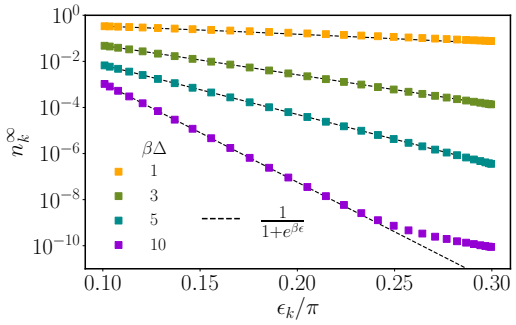


Figure 17.9: Steady state quasiparticle populations for cooling with thermal MCP, for effective temperature $T_{\text{eff}} = 1/\beta$. Results shown are for PM phase with one auxiliary per site, with system size $N_S = 30$ and reset time $T = 5\beta/2$. The dashed black lines are the expected thermal (Fermi) distributions.

17.8 Detailed balance and thermal state preparation with MCP

Above, we focused on preparation of ground states, which corresponds to the limit $\beta\Delta \to \infty$, where Δ is the excitation gap. However, our MCP protocol also provides a way to prepare thermal states (finite temperature Gibbs states) of the same effective Hamiltonian, a subject which has been the focus of several recent studies [27, 83, 87, 34]. The thermal Gibbs state at an effective temperature T_{eff} is defined by

$$\frac{\rho_{\vec{\alpha}\vec{\alpha}}}{\rho_{\vec{\beta}\vec{\beta}}} = \exp\left(-\frac{\varepsilon(\vec{\alpha}) - \varepsilon(\vec{\beta})}{T_{\text{eff}}}\right), \tag{17.85}$$

where $\rho_{\vec{\alpha}\vec{\alpha}}$ are the many-body populations in Eq. (18.1), ε is the total quasienergy of the many-body eigenstate.

This can be achieved by cooling the system using the MCP with the parameter $\beta = 1/T_{\text{eff}}$, and the additional constraint that the cooling operators $\hat{A}^a$ appearing in Eq. (17.9) are Hermitian. Then, the general rate equation, Eq. (17.25), with the Hermitian operators $\hat{A}^a$, can be written as

$$\delta n_k = \frac{1}{2}\sum_{\vec{\alpha}\vec{\beta}} (\beta_k - \alpha_k) w_{\vec{\alpha}\vec{\beta}} \left(\rho_{\vec{\alpha}\vec{\alpha}} - \rho_{\vec{\beta}\vec{\beta}} \frac{w_{\vec{\beta},\vec{\alpha}}}{w_{\vec{\alpha}\vec{\beta}}}\right) \tag{17.86}$$

where

$$w_{\vec{\alpha}\vec{\beta}} = \sum_a |F_{h,T}(\Delta(\vec{\alpha},\vec{\beta}))|^2 |\langle\vec{\beta}|\hat{A}^a|\vec{\alpha}\rangle|^2, \tag{17.87}$$

and $\Delta(\vec{\alpha},\vec{\beta}) = \varepsilon(\vec{\alpha}) - \varepsilon(\vec{\beta})$ are the Bohr frequencies. If the detailed balance condition holds, that is, when the terms inside the bracket above vanish identically,

$$\frac{\rho_{\vec{\alpha}\vec{\alpha}}}{\rho_{\vec{\beta}\vec{\beta}}} = \frac{|F_{h,T}(\Delta(\vec{\beta},\vec{\alpha}))|^2 \sum_a |\langle\vec{\alpha}|\hat{A}^a|\vec{\beta}\rangle|^2}{|F_{h,T}(\Delta(\vec{\alpha},\vec{\beta}))|^2 \sum_b |\langle\vec{\beta}|\hat{A}^b|\vec{\alpha}\rangle|^2}, \tag{17.88}$$

then this provides a solution to the steady state $\delta n_k = 0$. With the Hermitian constraint and choice $\beta = 1/T_{\text{eff}}$, using Eq. (17.36) for the MCP gives the required Gibbs state, Eq. (17.85).

As a demonstration, we calculate the steady state quasiparticle populations from the rate equation in the PM phase of the Floquet TFIM, with one auxiliary per site and keeping single-particle processes as in Section 17.3. We choose hermitian operators $\hat{A}^a = \hat{Z}_j$. The results are shown in Fig. 17.9, for several values of the inverse temperature β. We take system size $N_S = 30$ and $T = 5\beta/2$ to reduce ringing artifacts. The results are compared to the expected Fermi distributions which hold for fermionic quasiparticles when Eq. (17.85) is satisfied; the agreement

is generally excellent, suggesting that thermal Gibbs states can be efficiently prepared by the quasiparticle cooling algorithm (where, as in the ground state case, errors due to noise etc. will result in slightly non-equilibrium steady state populations).

17.9 Quasiparticles in the TFIM

The Floquet TFIM with open boundary conditions, considered as our cooling example throughout the main text, is defined by the Floquet unitary

$$\hat{U}_S = \exp\left(-\frac{i\pi J}{2}\sum_{i=1}^{N_S-1}\hat{X}_i\hat{X}_{i+1}\right)\exp\left(\frac{i\pi g}{2}\sum_{i=1}^{N_S}\hat{Z}_i\right). \tag{17.89}$$

This model can be mapped onto a quadratic fermionic chain by the Jordan-Wigner mapping, Eq. (17.39). For this purpose it is convenient to introduce a basis of Hermitian Majorana fermion operators, defined as

$$\hat{a}_{2i-1} = \hat{c}_i + \hat{c}_i^\dagger, \quad \hat{a}_{2i} = i(\hat{c}_i^\dagger - \hat{c}_i). \tag{17.90}$$

Then the unitary $\hat{U}_S$ acts on Majorana operators as a linear transformation:

$$\hat{U}_S^\dagger \hat{a}_i \hat{U}_S = \sum_{j=1}^{2N_S}(K_S)_{ij}\hat{a}_j. \tag{17.91}$$

From Eq. (17.89) we find the K_S matrix given by

$$K_S = \begin{pmatrix} 1 & 0 & 0 & \dots & 0 \\ 0 & \cos\pi J & -\sin\pi J & \dots & 0 \\ 0 & \sin\pi J & \cos\pi J & \dots & 0 \\ \vdots & \vdots & \vdots & \ddots & 0 \\ 0 & 0 & 0 & 0 & 1 \end{pmatrix} \begin{pmatrix} \cos\pi g & \sin\pi g & 0 & 0 & \dots \\ -\sin\pi g & \cos\pi g & 0 & 0 & \dots \\ 0 & 0 & \cos\pi g & \sin\pi g & \dots \\ 0 & 0 & -\sin\pi g & \cos\pi g & \dots \\ \vdots & \vdots & \vdots & \vdots & \ddots \end{pmatrix}. \tag{17.92}$$

The eigenmodes of $\hat{U}_S$ are Dirac fermions satisfying

$$\hat{U}_S^\dagger \hat{\eta}_k \hat{U}_S = e^{-i\epsilon_k}\hat{\eta}_k, \tag{17.93}$$

where k is a quantum number labeling the eigenmodes (the quasimomentum). Defining the eigenvectors of K_S (for $\epsilon_k \geq 0$) according to

$$K_S\psi_k = e^{-i\epsilon_k}\psi_k, \tag{17.94}$$

we have the expansion

$$\hat{\eta}_k = \frac{1}{\sqrt{2}}\sum_{j=1}^{N_S}\psi_{k,2j-1}^*\hat{a}_{2j-1} + \psi_{k,2j}^*\hat{a}_{2j}. \tag{17.95}$$

Due to particle-hole symmetry, the eigenvectors of K_S with negative quasienergy are related to those of positive quasienergy by the conjugation $\varphi_k = \psi_k^*$, $K_S\varphi_k = e^{i\epsilon_k}\varphi_k$. The eigenvectors ψ_k and quasienergies ϵ_k can be found by exact diagonalisation of the K_S matrix; see e.g. Ref. [88] or Appendix A of Ref. [38] for an analytical derivation. Note that the boundary condition defines the quantization condition for the N_S quasimomenta k_m, in terms of which the quasienergies are given by the exact formula

$$\cos\epsilon_k = \cos(\pi J)\cos(\pi g) - \sin(\pi J)\sin(\pi g)\cos k. \tag{17.96}$$

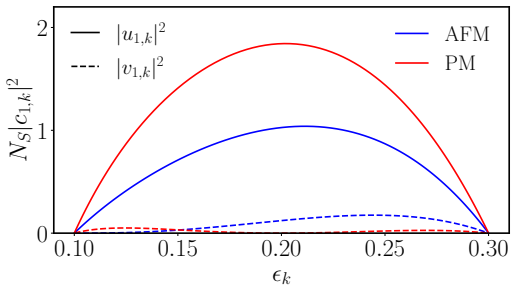


Figure 17.10: Profile of edge Bogoliubov coefficients $|u_{1k}|^2$, (solid) $|v_{1k}|^2$ (dashed), plotted vs quasienergy ϵ_k. We plot the coefficients rescaled by chain length N_S: squared coefficients are $O(1/N_S)$ in middle of quasiparticle band, but vanish as $O(1/N_S^3)$ at band edges.

Along with the definition of the Bogoliubov coefficients,

$$\hat{c}_j = \sum_k u_{jk}\hat{\eta}_k + v_{jk}\hat{\eta}_k^\dagger, \tag{17.97}$$

this gives the relations

$$u_{jk} = \frac{\psi_{k,2j-1} + i\psi_{k,2j}}{\sqrt{2}}, \tag{17.98}$$

$$v_{jk} = \frac{\psi^*_{k,2j-1} + i\psi^*_{k,2j}}{\sqrt{2}}, \tag{17.99}$$

specifying the standing-wave form of the eigenmodes.

Since the Bogoliubov coefficients at the boundary play a particularly important role in the cooling rates entering the kinetic equation for edge cooling, we plot the values of $|u_{1k}|^2$, $|v_{1k}^2|$ in Fig. 17.10, vs. the quasienergy ϵ_k. We observe that quasiparticle in the middle of the band typically have boundary overlap $|u_{1k}|^2 = O(N_S^{-1})$, while the overlap vanishes for quasiparticles with quasienergy near the two band edges. The overlap for these quasiparticles is expected to go as $O(N_S^{-3})$ [63].

17.10 Matrix elements for bulk cooling

In Sections 17.3, 17.5, we considered cooling in the example of the transverse-field Ising model, with two types of matrix elements appearing in the derivation of the rate equations: the $\hat{Z}_j$ matrix elements, which we denote as

$$Z_{j;\vec{\alpha};\vec{\beta}} = \langle\vec{\alpha}|\hat{Z}_j|\vec{\beta}\rangle, \tag{17.100}$$

and the $\hat{\sigma}_j^\pm$ matrix elements,

$$\sigma^\pm_{j;\vec{\alpha};\vec{\beta}} = \langle\vec{\alpha}|\hat{\sigma}_j^\pm|\vec{\beta}\rangle. \tag{17.101}$$

Here $|\vec{\alpha}\rangle$ are the many-body eigenstates of the TFIM, which are completely defined by their quasiparticle occupation numbers.

Although the TFIM defines an integrable model, calculation of spin matrix elements can be challenging [89], due to the fact that the Jordan-Wigner transformation between spin and fermion operators is non-local. We will see that this is the case for the $\hat{\sigma}_j^\pm$ matrix elements below. First, we focus on the simpler case of $\hat{Z}_j$:

17.10.1 $Z_{j;\vec{\alpha};\vec{\beta}}$ matrix elements

In the fermion basis $\hat{Z}$ is a quadratic operator, so only matrix elements between eigenstates differing in the occupation of at most two quasiparticle modes survive:

$$\begin{aligned} Z_{j;\vec{\alpha};\vec{\beta}} &= \langle\vec{\alpha}|(1-2\hat{c}_j^\dagger\hat{c}_j)|\vec{\beta}\rangle \\ &= \delta_{\vec{\alpha}\vec{\beta}} - 2\sum_{kq}\Big(u_{jk}^* u_{jq}[\hat{\eta}_k^\dagger\hat{\eta}_q]_{\vec{\alpha}\vec{\beta}} + u_{jk}^* v_{jq}[\hat{\eta}_k^\dagger\hat{\eta}_q^\dagger]_{\vec{\alpha}\vec{\beta}} + v_{jk}^* u_{jq}[\hat{\eta}_k\hat{\eta}_q]_{\vec{\alpha}\vec{\beta}} + v_{jk}^* v_{jq}[\hat{\eta}_k\hat{\eta}_q^\dagger]_{\vec{\alpha}\vec{\beta}}\Big) \end{aligned} \tag{17.102}$$

where e.g. $[\hat{\eta}_k^\dagger\hat{\eta}_q]_{\vec{\alpha}\vec{\beta}} \equiv \langle\vec{\alpha}|\hat{\eta}_k^\dagger\hat{\eta}_q|\vec{\beta}\rangle = 0, 1$ is only non-zero if $\vec{\alpha}$ and $\vec{\beta}$ differ only by the occupations of the k and q quasiparticle levels (including the case $k = q$). Since the Bogoliubov coefficients u_{jk}, v_{jk} can be obtained by diagonalisation of the single-particle Hamiltonian, the matrix elements are easily obtained.

In deriving the rate equation, we focused on the case of transitions to and from the ground state, and scattering between single quasiparticle levels. Thus we have

$$|Z_{j;0;k,q}|^2 = |\langle\Omega|\hat{Z}_j|k,q\rangle|^2 = 4|v_{jk}^* u_{jq}|^2 \tag{17.103}$$

as the probability for two quasiparticles with quasimomenta k, q, to annihilate, and

$$|Z_{j;k;q}|^2 = |\langle k|\hat{Z}_j|q\rangle|^2 = 4|u_{jk}^* u_{jq}|^2 \tag{17.104}$$

as the scattering probability $q \to k$. Since $\hat{Z}$ is hermitian, the pair-creation probability is equal to the pair-annihilation, i.e. $|Z_{j;0;k,q}|^2 = |Z_{j;k,q;0}|^2$. Note that, in the AFM phase there is also an amplitude for single-quasiparticle processes, due to the selection rules discusses in the main text i.e. one of k, q can be taken as the Majorana zero mode.

17.10.2 $\sigma^{\pm}_{j;\alpha;\beta}$ matrix elements

We now turn to quasiparticle processes mediated by the $\hat{\sigma}_j^\pm$ matrix elements. We focus on $\hat{\sigma}_j^+$ for illustration. In the fermion basis, $\hat{\sigma}_j^+$ comes attached with the Jordan-Wigner string operator,

$$\sigma^+_{j;\vec{\alpha};\vec{\beta}} = \langle\vec{\alpha}|\Big(\prod_{i=1}^{j-1} e^{i\pi\hat{c}_i^\dagger\hat{c}_i}\Big)\hat{c}_j|\vec{\beta}\rangle. \tag{17.105}$$

Due to this non-locality in the fermionic eigenbasis, multi-particle processes are allowed with $\hat{\sigma}_j^+$ changing the occupation numbers of up to $2j-1$ quasiparticle levels. Amazingly, the exact finite-volume matrix elements have been worked out for the case of the $\hat{X}_j$ operators in the TFIM with periodic boundary conditions [89]. Here, we focus on singe- and two-particle transitions near the ground state, which capture the dominant cooling processes at late times, as described in the main text. Our theory can be straightforwardly generalised to include higher-order processes.

Focusing on few-particle processes alows us to use Wick's theorem to evaluate the necessary matrix elements for systems up to several hundred sites: For free (more generally, Gaussian) theories, Wick's theorem states that

$$\langle\hat{a}_{i_1}\hat{a}_{i_2}\dots\hat{a}_{i_{2N}}\rangle_\Omega = \sum_P \zeta_P \prod_{k=1}^{N}\langle\hat{a}_{P(i_{2k-1})}\hat{a}_{P(i_{2k})}\rangle \tag{17.106}$$

$$= \mathrm{Pf}\begin{pmatrix} 0 & \langle\hat{a}_{i_1}\hat{a}_{i_2}\rangle & \langle\hat{a}_{i_1}\hat{a}_{i_3}\rangle & \dots & \langle\hat{a}_{i_1}\hat{a}_{i_{2N}}\rangle \\ & 0 & \langle\hat{a}_{i_2}\hat{a}_{i_3}\rangle & \dots & \langle\hat{a}_{i_2}\hat{a}_{i_{2N}}\rangle \\ & & 0 & \dots & \langle\hat{a}_{i_3}\hat{a}_{i_{2N}}\rangle \\ & & & \ddots & \vdots \\ & & & & 0 \end{pmatrix}. \tag{17.107}$$

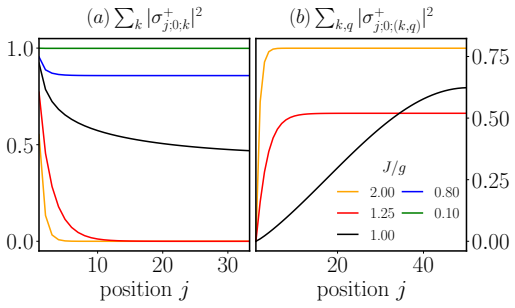


Figure 17.11: (a) Single-quasiparticle matrix elements $|\sigma^+_{j;0;k}|^2$ summed over quasimomenta k and plotted against operator position j, for different values of J/g. (b) Two-particle matrix elements $|\sigma^+_{j;0;(k,q)}|^2$ summed over k, q, and plotted against operator position j. Note that the two-particle matrix element is non-zero only in the AFM phase.

The sum runs over all possible permutations of the Majorana indices, and $\zeta_P = \pm 1$ is the sign of the permutation, carrying the fermion statistics. All expectation values are taken with respect to the ground state of the free theory, and for notational simplicity we introduced the Majorana fermion operators (Eq. (17.90)). In the second line we introduced the Pfaffian representation of Wick's theorem in terms of a skew-symmetric matrix Σ. In our case, since only the modulus squared of the correlation functions enters the rate equation, we may use

$$|\langle a_{i_1} a_{i_2} \dots a_{i_{2N}} \rangle_\Omega|^2 = |\mathrm{Pf}(\Sigma)|^2 = |\det(\Sigma)|. \tag{17.108}$$

which can be computed in time $O(N^3)$. For further reference, see e.g. [90, 65].

Single quasiparticle processes: We first consider single-quasiparticle transitions above the ground state,

$$\sigma^+_{j;0;k} = \langle \Omega | \hat{\sigma}^+_j | k \rangle \tag{17.109}$$

being the amplitude to directly annihilate a quasiparticle of quasimomentum k. We rewrite the single-particle element in fermion basis

$$|\sigma^+_{j;0;k}|^2 = |\langle \prod_{i=1}^{j-1} \hat{a}_{2i-1} \hat{a}_{2i} \; \hat{c}_j \hat{\eta}^\dagger_k \rangle_\Omega|^2. \tag{17.110}$$

The corresponding Wick's matrix Σ had dimension $2j \times 2j$. In Fig. 17.11a we show how the single-particle matrix elements in Eq. 17.110 (summed over k), depend on the TFIM phase parameter J/g and on the position of the operator j. The system size is $N_S = 100$. The matrix elements display a clear change in behaviour between the two phases: in the PM phase, single-particle transitions occur almost uniformly throughout the system bulk; in the AFM phase, transitions are localized within a few correlation lengths of the edge, with a correlation length $\xi_J \propto J/g$. This is as expected, based on the physical picture of domain-wall-like quasiparticles in the AFM (removing a single domain wall requires flipping a macroscopic number of spins).

Two-quasiparticle processes: Based on the physical picture, we expect that in the AFM phase, a pair of domain walls may collide in the bulk and annihilate, as this requires only local reconfigurations of spins. However, there is a subtlety, from the fact that $\hat{\sigma}^+_j$ has non-zero matrix elements only between eigenstates of different fermion parity. This rules out two-particle transitions in the PM phase, but as discussed in the main text, the issue is sidestepped in the AFM by interacting with the Majorana zero mode, whose action maps between the two nearly-

degenerate ground states. We therefore write

$$|\sigma^{+}_{j;0;k,q}|^2 = |\langle\Omega_+|\prod_{i=1}^{j-1}\hat{a}_{2i-1}\hat{a}_{2i}\ \hat{c}_j\hat{\eta}^\dagger_k\hat{\eta}^\dagger_q|\Omega_-\rangle|^2, \tag{17.111}$$

with $|\Omega_-\rangle = \hat{\eta}^\dagger_0|\Omega_-\rangle$, and $\hat{\eta}^\dagger_0$ the Majorana mode. These matrix elements may be evaluated with Wick's theorem on the $(2j+2)\times(2j+2)$ dimensional Σ-matrix. In Fig. 17.11b, we show how the summed matrix elements $\sum_{k,q}|\sigma^{+}_{j;0;k,q}|^2$ depend on the position j, for different values of J/g in the AFM phase. The pair matrix element is almost homogeneous in the bulk, vanishing in the edge region.

For completeness we also give the two-particle scattering elements, which are again non-zero only for the AFM phase:

$$|\sigma^{+}_{j;k;q}|^2 = |\langle\Omega_+|\hat{\eta}_k\prod_{i=1}^{j-1}\hat{a}_{2i-1}\hat{a}_{2i}\ \hat{c}_j\hat{\eta}^\dagger_q|\Omega_-\rangle|^2. \tag{17.112}$$

The scattering does not directly lead to cooling/heating of the system (the total number of quasiparticles is conserved by the scattering processes), however it can lead to a redistribution of quasiparticle density, which itself affects the cooling rate.

17.11 Details of numerical simulations

17.11.1 Free fermion simulations

For the edge cooling protocol analysed in Section 17.3 for the TFIM, the non-unitary dynamics described by Eq. (17.1) defines a Gaussian channel — a channel mapping Gaussian states to Gaussian states. A Gaussian state obeys Wick's theorem (see Eq. 17.107), meaning that the expectation values of all observables can be factorised purely in terms of 2-point fermionic correlation functions. Under the action of the cooling channel, Eq. (17.1), the matrix of 2-point functions can be efficiently updated, as we show below, and hence we have access to the arbitrary correlators of the time-dependent many-body state.

We introduce the antisymmetrised covariance matrix of Majorana correlators as

$$\Gamma_{ij} = \frac{i}{4}\langle[\hat{a}_i,\hat{a}_j]\rangle = \begin{cases} i\langle\hat{a}_i\hat{a}_j\rangle/2, & i\neq j \\ 0, & i=j \end{cases}, \tag{17.113}$$

where the Majorana fermions were defined in Eq. (17.90). The matrix includes both system and bath degrees of freedom, and has dimension $(2N_S+2)\times(2N_S+2)$ (we limit our discussion to the case of a single edge auxiliary for simplicity). We block the covariance matrix according to

$$\Gamma = \begin{pmatrix} \Gamma_{BB} & \Gamma_{SB} \\ \Gamma_{BS} & \Gamma_{SS} \end{pmatrix}. \tag{17.114}$$

where Γ_{SS} is the $2N_S\times 2N_S$ matrix containing system-system correlations, etc. For the initial condition, representing the system in the maximally mixed state and the auxiliary in the reset state, Eq. (17.6), we have

$$\Gamma_{SS} = 0 \tag{17.115}$$

$$\Gamma_{BB} = \frac{1}{2}\begin{pmatrix} 0 & -1 \\ 1 & 0 \end{pmatrix}, \quad \Gamma_{SB} = \Gamma_{BS} = 0. \tag{17.116}$$

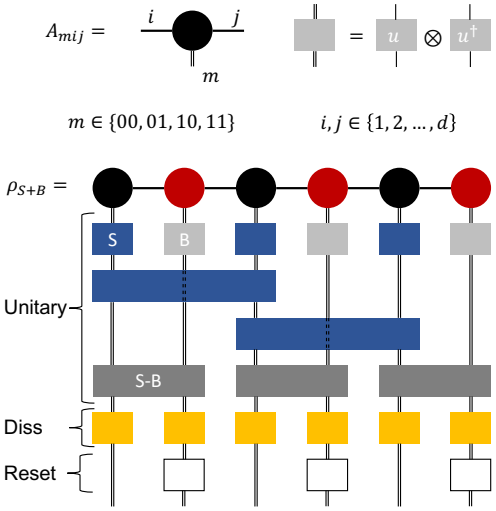


Figure 17.12: Tensor network implementation for one cooling cycle. System (auxiliary) qubits are denoted by black (red) tensors respectively. Different channels correspond to different blocks: bath evolution (light grey); system evolution (dark blue); system-bath coupling (dark grey); decoherence (yellow); auxiliary reset (white). The network is composed of rank-3 tensors A, has a bond dimension d and a 4-dimensional physical bond corresponding to the four (vectorised) states of the qubit's density matrix. The system is encoded in a one-dimensional geometry at the price of introducing next-nearest neighbor channels.

Due to the integrability of the TFIM, unitary evolution of the Majoranas in the Heisenberg picture acts as a linear map:

$$(\hat{U}_S^\dagger \hat{U}_B^\dagger \hat{U}_\theta^\dagger)\ \hat{a}_i\ (\hat{U}_\theta \hat{U}_B \hat{U}_S) = \sum_j (K_\theta K_B K_S)_{ij} \hat{a}_j, \tag{17.117}$$

where K_S is defined in (17.92), and $K_B = \exp(\pi h_B)$, $K_\theta = \exp(\pi h_\theta)$, with

$$h_B = \begin{pmatrix} 0 & h & 0 & \dots \\ -h & 0 & 0 & \dots \\ 0 & 0 & 0 & \dots \\ \vdots & \vdots & \vdots & \ddots \end{pmatrix}, \quad h_\theta = \begin{pmatrix} 0 & 0 & 0 & \theta & \dots \\ 0 & 0 & -\theta & 0 & \dots \\ 0 & \theta & 0 & 0 & \dots \\ -\theta & 0 & 0 & 0 & \dots \\ \vdots & \vdots & \vdots & \vdots & \ddots \end{pmatrix}, \tag{17.118}$$

all other elements being zero. Then, defining $\hat{U} = \hat{U}_\theta \hat{U}_B \hat{U}_S$ and $K = K_\theta K_B K_S$, the covariance matrix evolves under the unitary part of the cooling channel as,

$$\langle \hat{U}^\dagger \hat{\Gamma}_{ij} \hat{U} \rangle = K_{il} K_{jm} \langle [\hat{a}_l, \hat{a}_m] \rangle = (K \Gamma K^T)_{ij}. \tag{17.119}$$

The reset of the auxiliaries can be done by reinstating condition (17.116). If we denote the corresponding map by $\mathcal{R}$, then the cooling channel (17.1) acts on the covariance matrix according to:

$$[\Phi(\Gamma)]_{ij} = [\mathcal{R}(K \Gamma K^T)]_{ij}. \tag{17.120}$$

Thus the matrix Γ can be efficiently updated to obtain the dynamics, or (by vectorising the matrix Γ) the linear map Φ diagonalised to yield the steady state. Note that qubit dephasing can also be efficiently implemented in this scheme [91], but bulk auxiliaries or qubit decay break the necessary integrability.

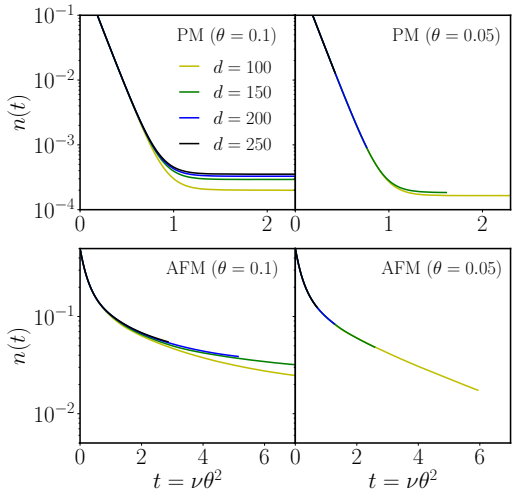


Figure 17.13: Convergence of ground state cooling simulations as a function of the MPS's bond dimension, for the integrable TFIM with the parameters used in Figure 17.3. We show data for both PM and AFM phases at two different bath couplings $\theta = 0.1$ (0.05), and for bond dimensions $d = 100, 150, 200, 250$.

17.11.2 Tensor network simulations

Here, we summarize the tensor network algorithm that was employed to simulate the dissipative dynamics in Sections 17.3-17.4. We give an overview of the relevant details, assuming the reader is familiar with the basics of matrix product algorithms; introductions can be found in e.g. [92, 93].

We assume a finite density of auxiliaries, one per system site. The total density matrix of the system plus auxiliaries is ρ_{SB}. We work with the vector unfolding of the density matrix product operator, which is written as a matrix product state (MPS),

$$\rho_{SB} = \sum_{\mathbf{m},\mathbf{s}} A^1_{m_1,s_1} A^2_{m_2,s_1,s_2} \dots A^N_{m_N,s_{N-1}} |m_1 \dots m_N\rangle, \tag{17.121}$$

where A^i is a rank-3 tensor graphically defined in Fig. 17.12. Virtual indices $\mathbf{s} = \{s_1, \dots, s_{N-1}\}$ are traced while physical indices $\mathbf{m} = \{m_1, \dots, m_N\}$ denote the different states of the system+bath, $N = 2N_S$. The system geometry in the presence of auxiliaries is quasi-1d, see Fig. 18.1d, and we adopt a 1-dimensional ordering that alternates between system and auxiliary qubits i.e. $\mathcal{Q}_1\mathcal{A}_1 \dots \mathcal{Q}_{N_S}\mathcal{A}_{N_S}$, as illustrated in Fig. 17.12. The dimension of the virtual indices of the MPS (bond dimension) is denoted d, and controls the amount of non-local correlations that can be represented by the state.

The time evolution is performed via the standard TEBD algorithm [68, 69], which updates the MPS in real time, followed by the reset channel acting on the bath, which can be efficiently implemented as discussed below. In Fig. 17.12 we illustrate the evolution for the example of the Floquet TFIM (17.5) with bath evolution and interaction, Eqs. (17.7-17.43). We first simultaneously perform the single-site unitary channels for the system and bath, then the two-body system channels, which correspond to next-nearest-neighbor gates, followed by the nearest-neighbor system-bath channel. Note that the next-nearest-neighbour gate arises from the quasi-1d geometry. This is the most expensive step of the algorithm as it requires two singular value decompositions and scales as $O(\dim(m)^4 d^3)$.

For the simulations with decoherence, following the unitary channel we apply the decoherence channel Eq. (17.62) with jump operators in Eq. (17.67). Finally the reset of auxiliaries is

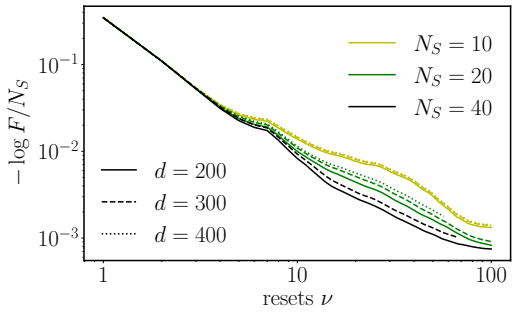


Figure 17.14: Convergence of ground state cooling simulations as a function of the MPS's bond dimension, for the non-integrable Ising model with the parameters used in Figure 17.5. Full/dashed/dotted bond dimensions $d = 200, 300, 400$ respectively. For increasing system sizes, there is a small drift with d at $\nu > 10$, but the monotonic increase of fidelity is observed for all bond dimensions.

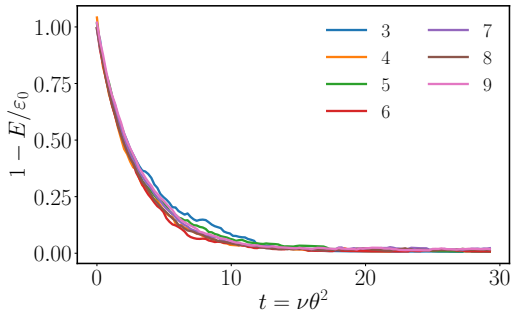


Figure 17.15: Energy of Heisenberg spin ladder vs. rescaled time $t = \nu\theta^2$, where ν is the number of resets and $\theta = 0.15$ is the coupling strength. Parameters are the same as in Fig. 17.6, except here we vary the system size, with ladders of $2 \times L$ qubits, with $3 \leq L \leq 9$. The data shows that cooling dynamics is independent of system size for the model considered.

performed by simply modifying the matrix elements of each auxiliary qubit tensor as,

$$\begin{aligned} A^i_{00 s_{i-1} s_i} &\to A^i_{00 s_{i-1} s_i} + A^i_{11 s_{i-1} s_i}, \\ A^i_{m \neq 00 s_{i-1} s_i} &\to 0. \end{aligned} \tag{17.122}$$

In the non-integrable TFIM in the presence of a longitudinal field, the local unitary operations are defined according to Eq. (17.54), and the rest of the algorithm is unaffected.

Next, we study the effects of truncation due to finite bond dimension during the cooling protocol in Figures 17.13 and 17.14. In Fig. 17.13 we consider the TFIM cooling for the parameters shown in Fig. 17.3 of the main text. We only show data for two values of the coupling, $\theta = 0.1, 0.05$ for the MCP, since the SCP protocol is well converged for all bond dimensions. We observe that the convergence is slower for the larger coupling, suggesting higher bond dimensions are needed to capture non-perturbative effects. Phenomenologically, such behavior is expected since higher-order in θ corrections are expected to lead processes that are less spatially local, thus requiring a larger bond dimension to be accurately captured.

The comparison of data obtained with different bond dimension $d = 200, 300, 400$ for the non-integrable model is shown in Fig. 17.14. We note that the bond dimension necessary for convergence depends on the correlation length of the ground state. For the parameters of the TFIM with longitudinal field used in the main text ($h_x = h_z = 0.15, J = 0.1$), the effects of truncation are almost negligible for bond dimension values considered.

17.12 System-size dependence for Heisenberg ladder cooling

Here we provide data for system-size dependence of cooling in the Heisenberg spin ladder, discussed in Section 17.4. We take the same parameters as in Section 17.4, i.e. $J = J_\perp = 0.2$, $\theta = 0.15$, and $T = \beta = 30$. Since the quasiparticle excitations are quasi-local (adiabatically connected to local operators), we expect that both the cooling time and the final energy density scale independently of system size. In Fig. 17.15 we show how the mean energy (averaged over 60 quantum trajectories) of the H_1 Floquet Hamiltonian decays, for systems with sizes of $2 \times L$ qubits, with $3 \leq L \leq 9$. We fix the number of auxiliary qubits at $N_A = \text{floor}(L/2) + 1$. The data clearly shows that the cooling behaviour is independent of system size, and cooling is achieved in time $O(\theta^{-2})$.

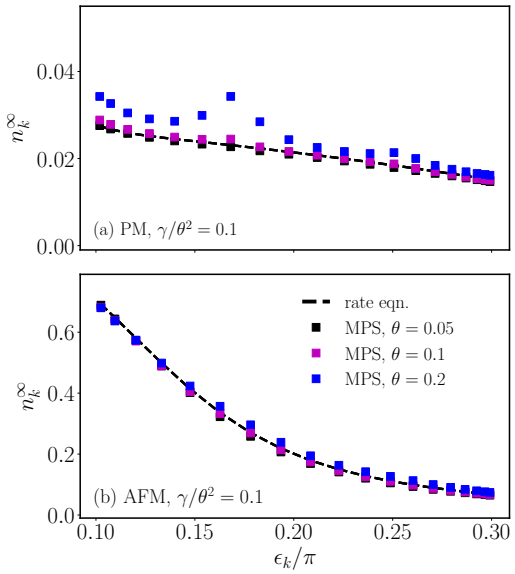


Figure 17.16: Quasiparticle occupation numbers n_k^∞ in steady state, as a function of quasienergy ϵ_k, for noise strength $\gamma_d = \gamma_\phi = 0.1\theta^2$. (a) PM and (b) AFM phases. Rate equation prediction (dashed line) vs. MPS simulations (points), for three values of the coupling θ. Protocol parameters are as in Fig. 17.4. The MPS simulations use a maximum bond dimension of $d = 100$.

17.13 Comparison of noisy kinetic equation and MPS simulations

In Section 17.5 we derived the kinetic equation in the presence of noise, Eq. (17.64), which includes transitions induced by qubit dephasing and decay. Here we compare the accuracy of the rate equation predictions against MPS simulations. We focus on the MCP with the same parameters as in Fig. 17.4, namely finite density of auxiliaries, $N_A = N_S = 20$, and $T = \beta = 12$. In Fig. 17.16 we plot the quasiparticle densities in the steady state, obtained from the kinetic equation prediction (black dashed line) and MPS simulations (scatter points). We use a maximum MPS bond dimension of $d = 100$ and run the simulations starting from the exact ground state, as described in Section 17.3. We fix the noise strength $\gamma_d = \gamma_\phi = 0.1\theta^2$, and show results for three different coupling strengths, $\theta = 0.2, 0.1, 0.05$, finding good qualitative agreement for the smaller coupling values $\theta = 0.1, 0.05$.

18 Correlations after Quantum Quenches in the *XXZ* Spin Chain: Failure of the Generalized Gibbs Ensemble by Pozsgay et al.

We study the nonequilibrium time evolution of the spin-1/2 anisotropic Heisenberg (XXZ) spin chain, with a choice of dimer product and Néel states as initial states. We investigate numerically various short-ranged spin correlators in the long-time limit and find that they deviate significantly from predictions based on the generalized Gibbs ensemble (GGE) hypotheses. By computing the asymptotic spin correlators within the recently proposed quench-action formalism [Phys. Rev. Lett. 110, 257203 (2013)], however, we find excellent agreement with the numerical data. We, therefore, conclude that the GGE cannot give a complete description even of local observables, while the quench-action formalism correctly captures the steady state in this case.

18.0.1 Introduction.—

Recent, spectacular advances in the field of ultracold atoms enabled experimentalists to investigate the coherent time evolution of almost perfectly isolated quantum many-body systems [1, 2, 4, 3]. These new developments triggered tremendous theoretical interest [5, 6, 7, 8, 10, 13, 11, 12, 14, 15, 9, 16, 17, 18] in a long-standing problem of fundamental physical importance: do isolated quantum systems reach an equilibrium in some sense, and if the answer is positive, what is the nature of the steady state reached?

In the absence of external driving forces, generic systems are expected to reach a steady state locally indistinguishable from thermal equilibrium [7, 5]. However, integrable systems behave differently because conservation of the expectation values of extra local charges prevents relaxation to a thermal state. It was suggested in Ref. [19] that in the integrable case the long-time asymptotic stationary state is described by a statistical ensemble involving all the local conserved charges $\{\hat{Q}_i\}$, the generalized Gibbs ensemble (GGE), defined by the density matrix

$$\hat{\rho}_{\mathrm{GGE}} = \frac{1}{Z} e^{-\sum_i \beta_i \hat{Q}_i}, \qquad Z = \mathrm{Tr}\; e^{-\sum_i \beta_i \hat{Q}_i}, \tag{18.1}$$

where the "chemical potentials" $\{\beta_i\}$ are determined by the expectation values of the charges in the ensemble and the initial quantum state.

The GGE idea has by now become widely accepted in the field and has been verified in several specific cases. Until recently, however, most investigations concerning GGE were carried out in theories equivalent to free fermions [20, 21, 22, 23, 24, 25, 27, 26, 28, 29] or by numerical studies of relatively small systems [30, 31]. It is only recently that it has become possible to examine genuinely interacting integrable systems such as the one-dimensional Bose gas [32, 33, 34], the XXZ Heisenberg spin chain [2, 36, 1] or field theories [38, 39, 40].

However, until now there have only been a few precision numerical tests for the predictions of the GGE against real-time dynamics [1]. In our Letter, we perform real-time numerical simulations on a genuinely interacting quantum system, the anisotropic Heisenberg model, and compare the relaxation of various local spin-spin correlation functions to the predictions of two competing theories: the overlap-incorporating thermodynamic Bethe ansatz (OTBA) approach, which implements the quench-action method [41], and the widely accepted GGE.

In agreement with some recent observations [42, 43] we find that these two approaches yield markedly different predictions. We arrive at a surprising conclusion: while the numerical results agree spectacularly with the OTBA, they differ significantly from the exact predictions of the GGE in a number of cases (see Fig. 18.2). These results lead to the inevitable conclusion

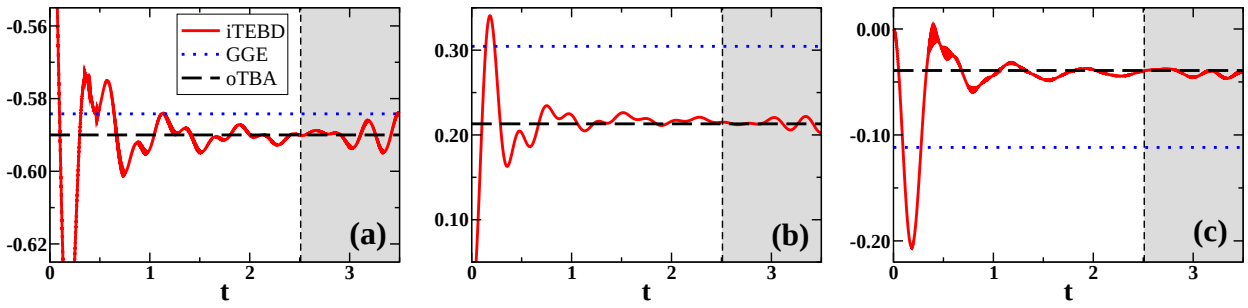


Figure 18.1: Numerical simulation of the time evolution of correlation functions (a) $\langle\sigma_1^z\sigma_2^z\rangle$, (b) $\langle\sigma_1^z\sigma_3^z\rangle$, (c) $\langle\sigma_1^z\sigma_4^z\rangle$ starting from the dimer initial state (18.4) for anisotropy $\Delta = 4$ as obtained by ITEBD (red lines). In the shaded region the results are not reliable. The horizontal lines show the GGE prediction [1] (blue dotted lines) and the prediction of the overlap TBA of the quench-action approach (black dashed lines).

that the GGE approach fails as a generic description of steady states in genuinely interacting integrable quantum systems.

18.0.2 Quantum quench in the XXZ chain.—

The XXZ Heisenberg chain is a chain of $s = 1/2$ spins interacting via the Hamiltonian

$$H = -\sum_{i=1}^{L} \left[\sigma_i^x\sigma_{i+1}^x + \sigma_i^y\sigma_{i+1}^y + \Delta(\sigma_i^z\sigma_{i+1}^z - 1)\right], \tag{18.2}$$

where $\sigma_i^{x,y,z}$ are the Pauli matrices at site i. This model describes magnetism in real compounds [44] and plays a fundamental role in the theory of strongly correlated condensed-matter systems [45]. Here we focus on the Ising regime $\Delta > 1$, which corresponds to a gapped antiferromagnetic phase in equilibrium.

We implement the nonequilibrium process via the paradigmatic setting of quantum quench [46, 47], whereby the time evolution of the system starts from the ground state of some Hamiltonian but then at time $t = 0$ some parameter of the system is abruptly changed. Quantum quenches of this kind can be implemented in a controlled fashion by realizing the XXZ chain in systems of cold atoms in optical lattices [52, 50, 51, 48, 49].

As initial states, we consider the translationally invariant projection of the Néel state

$$|\Psi_0^N\rangle = \frac{1+\hat{T}}{\sqrt{2}}|\uparrow\downarrow\uparrow\ldots\rangle = \frac{1}{\sqrt{2}}\big(|\uparrow\downarrow\uparrow\ldots\rangle + |\downarrow\uparrow\downarrow\ldots\rangle\big), \tag{18.3}$$

which is a ground state in the $\Delta \to \infty$ limit, and the similarly symmetrized dimer product state

$$|\Psi_0^D\rangle = \frac{1+\hat{T}}{\sqrt{2}}\left|\frac{(\uparrow\downarrow - \downarrow\uparrow)}{\sqrt{2}}\frac{(\uparrow\downarrow - \downarrow\uparrow)}{\sqrt{2}}\ldots\right\rangle, \tag{18.4}$$

which is one of the ground states of the Majumdar-Ghosh Hamiltonian [53]. Here, $\hat{T}$ is the one site translation operator on the lattice. It is expected that ground states of local Hamiltonians always relax to a steady state.

Failure of the GGE description of the steady state correlations.—

To demonstrate that the GGE cannot give an appropriate description of the steady state, we compare its predictions for correlation functions with the results of real-time

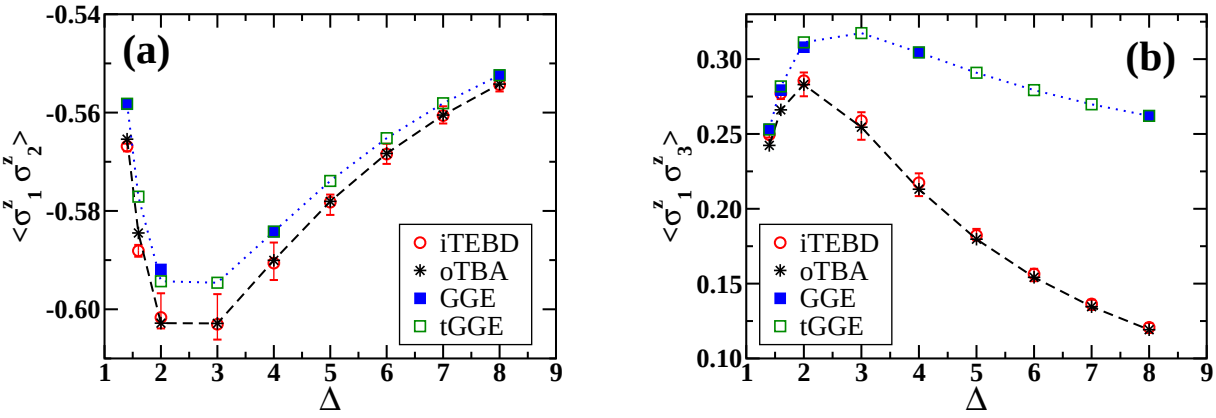


Figure 18.2: Δ dependence of the ITEBD (red circles with error bars), overlap TBA (black stars), full GGE [1] (full blue squares) and truncated GGE (empty green squares) results for the large time expectation values (a) $\langle\sigma_1^z\sigma_2^z\rangle$ and (b) $\langle\sigma_1^z\sigma_3^z\rangle$ after the quench from the dimer initial state (18.4).

out-of-equilibrium numerical simulations, performed using the infinite size time evolving block decimation (ITEBD) algorithm [54, 55]. In the simulations, translational invariance of the initial states in Eqs. (18.3) and (18.4) was implemented by averaging over the two components of the states [56]. The time evolution of three different correlators is shown in Fig. 18.1 for a quench starting from the dimer state for $\Delta = 4$ (red lines). The correlation functions quickly converge to stationary values before the simulations break down for large times (shaded regions) [57].

Strikingly, the exact GGE values of Ref. [1] (blue dotted lines in Fig. 18.1) deviate significantly from the ITEBD results. We report similar deviations for all $\Delta > 1$ in Fig. 18.2, where we display the long-time asymptotic values extracted from the ITEBD simulation (red circles) together with the GGE predictions (squares) for $\langle\sigma_1^z\sigma_2^z\rangle$ and $\langle\sigma_1^z\sigma_3^z\rangle$, as functions of Δ. We included truncated GGE (TGGE) results [2, 36] as well, obtained by keeping the first six nonzero charges in the density matrix (18.1). The discrepancy between the GGE and the ITEBD results is evident (for additional numerical data, see the Supplemental Material [39]).

The mismatch between real-time simulations and GGE results could be, in principle, the result of long relaxation times beyond the reach of the ITEBD simulations. We rule out this possibility by applying an alternative theoretical method, the overlap thermodynamic Bethe ansatz (OTBA) which implements the quench-action approach [34, 41] (see below), and predicts *exactly* the asymptotic values of the correlations. These values, shown as black dashed lines in Fig. 18.1 and black stars in Fig. 18.2, are clearly in excellent agreement with our ITEBD results. The state predicted by the OTBA is a steady state of maximal conditional entropy. Therefore, the excellent agreement proves that the ITEBD simulation has reached the true asymptotic steady state, and, thus makes the evidence for the breakdown of the GGE conclusive. Moreover, it also demonstrates that the quench-action-approach-based OTBA indeed correctly captures the steady state of the XXZ model.

The TGGE predictions evaluated in Ref. [2] and the OTBA results are also different in the Néel case, but for large Δ, where the TGGE is reliable, this difference is beyond our numerical resolution (Supplemental Material [39]). We obtained similar results for x-x correlators for both initial states, although for the latter ITEBD is not as accurate as for the z-z correlators (cf. Ref. [59]).

We remark that translational invariance would be broken for the dimer state without the symmetrization under $\hat{T}$ in Eqs. (18.3) and (18.4), and it is yet an open question whether it is

restored in the long-time limit after the quench [1, 27]. Nevertheless, the GGE was expected to describe the average over the two components of the states (18.3) and (18.4), and yet it fails to do so. Note that for the observable $\langle\sigma_1^z\sigma_3^z\rangle$ translational averaging is immaterial since it is identical on both sublattices.

Overlap thermodynamic Bethe ansatz (OTBA).—

The OTBA method is formulated in the framework of the Bethe ansatz (BA) [60], used to diagonalize the XXZ Hamiltonian (23.1). Eigenfunctions corresponding to spin waves of M flipped spins on a chain of length L are parametrized by a set of M complex numbers $\{\lambda_j\}$, called rapidities. Spin waves can form bound states described by specific configurations of rapidities, called strings [61]. In the thermodynamic limit (TDL), defined by $M\to\infty$, $L\to\infty$ with M/L fixed, it is convenient to introduce the densities $\rho_n(\lambda)$ of n strings in rapidity space, together with the densities $\rho_n^h(\lambda)$ of unoccupied levels (holes).

The quench-action approach of Ref. [41] has been developed to describe the steady state following a quantum quench in Bethe ansatz integrable systems and has been implemented before for the transverse field Ising chain [41] and the Lieb-Liniger model [34]. This variational approach selects the relevant states by minimizing the generalized free energy (quench action)

$$\mathcal{S}(\{\rho_n\}) = -\frac{2}{L}\mathrm{Re}\ln\langle\Psi_0|\{\rho_n(\lambda)\}\rangle - s(\{\rho_n(\lambda)\}). \tag{18.5}$$

The first term involves the overlap between the initial state $|\Psi_0\rangle$ and the steady state $|\{\rho_n(\lambda)\}\rangle$, characterized by the string densities $\{\rho_n(\lambda)\}$. The exact overlaps were computed for the Néel state (18.3) in Refs. [62, 63, 64, 65]. Here we also generalized the overlap formula for the dimer product state (18.4) along the lines of Ref. [63]. In the TDL, the logarithm of both overlaps can be written as

$$-\frac{2}{L}\mathrm{Re}\ \ln\langle\Psi_0|\{\rho_n(\lambda)\}\rangle = \sum_{n=1}^{\infty}\int_{-\pi/2}^{\pi/2} d\lambda\rho_n(\lambda)g_n(\lambda) \tag{18.6}$$

with the $g_n(\lambda)$ functions given by

$$g_1^N(\lambda) = -\ln\frac{\tan(\lambda+\frac{i\eta}{2})\tan(\lambda-\frac{i\eta}{2})}{4\sin^2(2\lambda)}, \tag{18.7a}$$

$$g_1^D(\lambda) = -\ln\frac{\sinh^4(\eta/2)\cot^2(\lambda)}{\sin(2\lambda+i\eta)\sin(2\lambda-i\eta)} \tag{18.7b}$$

for the Néel and dimer states, respectively. In both cases $g_n^{N,D}(\lambda) = \sum_{j=1}^n g_1^{N,D}[\lambda+(i\eta/2)(n+1-2j)]$ for higher strings ($n>1$).

The second term $s(\{\rho_n(\lambda)\})$ in Eq. (18.5) is the entropy density [66, 61] accounting for the number of microstates realizing the set of macroscopic $\{\rho_n(\lambda)\}$

$$s(\rho_n) = \sum_{n=1}^{\infty}\int d\lambda\,\frac{1}{2}\left[\rho_n\ln\frac{\rho_n+\rho_n^{\mathrm{h}}}{\rho_n} + \rho_n^{\mathrm{h}}\ln\frac{\rho_n+\rho_n^{\mathrm{h}}}{\rho_n^{\mathrm{h}}}\right]. \tag{18.8}$$

It is exactly half of the standard Yang-Yang entropy density [66, 61] due to the fact that only parity invariant microstates have nonzero overlap [34, 65].

The quench action (18.5) expresses the idea that the states relevant in the TDL are those with both large overlaps with the initial state and a large number of microscopic realizations. The steady state is captured by a saddle-point set of string densities, with the saddle-point approximation becoming exact in the TDL. The densities $\{\rho_n(\lambda)\}$ and $\{\rho_n^{\mathrm{h}}(\lambda)\}$ are, however, not independent; interactions couple the rapidities of all the spin excitations, as expressed by

the Bethe equations. As a consequence, the densities $\{\rho_n\}$ and $\{\rho_n^{\rm h}\}$ satisfy coupled integral equations (constraints) [61]

$$a_n(\lambda) = \rho_n(\lambda) + \rho_n^{\rm h}(\lambda) + \sum_{m=1}^{\infty} [T_{nm} \circ \rho_m](\lambda). \tag{18.9}$$

Here, $[a \circ b](\lambda) = \int_{-\pi/2}^{\pi/2} d\lambda' a(\lambda - \lambda') b(\lambda')$ denotes convolution, and the interaction kernel is expressed as $T_{nm} = (1 - \delta_{n,m}) a_{|n-m|} + a_{n+m} + 2 \sum_{j=1}^{\min\{n,m\}-1} a_{|n-m|+2j}$, with $\pi a_n(\lambda) = \sinh(n\eta)/[\cosh(n\eta) - \cos(2\lambda)]$ and $\cosh \eta = \Delta$. The constrained extremum of $\mathcal{S}(\{\rho_n(\lambda)\})$ is then found through the standard treatment [61] and leads to the following integral equations for the functions $\eta_n(\lambda) \equiv \rho_n^{\rm h}(\lambda)/\rho_n(\lambda)$:

$$\ln \eta_n(\lambda) = g_n(\lambda) + \mu n + \sum_{m=1}^{\infty} [T_{nm} \circ \ln(1 + \eta_m^{-1})](\lambda). \tag{18.10}$$

Here, μ is a Lagrange multiplier introduced to fix the overall magnetization to zero. By examining the $g_n(\lambda)$, we obtained for both initial states that $\ln \eta_n \sim \eta\, n^2$ for large n. This implies that the higher strings are suppressed as $\propto e^{-\eta n^2}$, so the infinite set of equations (18.10) can be safely truncated to relatively few equations, and solved numerically. Having the numerical solution for η_n at hand, we can replace them into Eq. (18.9) and determine the densities efficiently. (For further technical details see Ref. [59]).

OTBA consistency checks. —

There are several ways to check that the numerically obtained saddle-point string densities $\{\rho_n^*\}$ are, indeed, correct and correspond to the right initial states and to the right saddle point. A nontrivial check is provided by the computation of the norm of the initial state in the TDL, i.e.,

$$0 = -\frac{1}{L} \ln \langle \Psi_0 | \Psi_0 \rangle = \mathcal{S}(\{\rho_n^*(\lambda)\}), \tag{18.11}$$

with the quench action Eq. (18.5) evaluated via Eqs. (18.8) and (18.6) for the saddle-point solution. Equation (18.11) is, indeed, satisfied by our saddle-point solution within the accuracy of our numerical simulations $\mathcal{O}(10^{-8})$. Notice that if this integral sum rule was violated, then the spectral weight of the saddle-point solution would be zero in the TDL.

Another important consistency check is provided by the expectation values of the conserved charges. These can be expressed in terms of the saddle-point densities as [67]

$$\langle \hat{Q}_{2m} \rangle = \sum_{n=1}^{\infty} \int_{-\pi/2}^{\pi/2} d\lambda\, \rho_n^*(\lambda) q_n^{(2m)}(\lambda), \tag{18.12}$$

with $q_n^{(2m)}(\lambda) = 2\pi \sum_{j=1}^{n} [-(\partial/\partial\lambda)]^{2m} a_1[\lambda + (i\eta/2)(n+1-2j)]$, the energy, in particular, being given by $E = 2 \sinh \eta \langle \hat{Q}_2 \rangle$. The saddle-point values of these charges must equal their values in the initial states. These latter were computed for the symmetric Néel state in Refs. [2, 36]. Here we determined them using both these methods in the symmetrized dimer state, $|\Psi_0^D\rangle$. We evaluated the first six nonzero charges, $\{\langle \hat{Q}_{2m} \rangle\}_{m=1,\ldots,6}$ and compared them with the expectation values computed from Eq. (18.12). Excellent agreement up to more than 8 digits is found in all cases, providing a further stringent verification of the OTBA solution.

Steady state correlations.—

With the saddle-point string densities at hand, we then computed various short distance correlation functions in the steady state by making use of the recent results of two of the present authors, who provided exact formulas for the 2-point correlation functions in terms of the string densities [68]. We compared these values with the results of our ITEBD simulations. Excellent agreement is found between OTBA and ITEBD for both initial states and for all $\Delta > 1$ values (cf. Figs. 18.1 and 18.2 and the Supplemental Material [39] for detailed numerical data). This establishes the quench-action-approach-based OTBA as a correct description of the steady state and the failure of GGE at the same time.

Discussion.—

In this Letter, we studied various correlation functions in the asymptotic steady states for quantum quenches in the XXZ spin chain. We found that the predictions of the generalized Gibbs ensemble differ significantly from the results of real-time ITEBD simulations in the dimer case, thereby signaling the breakdown of the GGE. We also determined these asymptotic correlators by applying the quench-action-based overlap TBA description of the steady state, and obtained numerically accurate predictions. We found that while the quench-action-based OTBA correctly captures the asymptotic steady state, the GGE fails for the states considered here. Finding a macroscopic statistical ensemble description of the steady state and clarifying the conditions for the validity of the GGE in strongly interacting systems, therefore, remain intriguing open questions.

Note added.—

During the final stages of this work, a related paper appeared [43] that independently arrived at Eq. (18.7a) and in which the difference between the GGE and the OTBA predictions for nearest-neighbor correlators in the quench starting from the Néel state was observed as well.

18.1 Supplementary Material for EPAPS Numerical methods

In this section we present a collection of high precision numerical data as well as some details on the numerical simulations.

ITEBD simulation.—

We performed the simulations by an ITEBD-code, which made use of the $U(1)$ rotational symmetry of the XXZ model around the z-axis. Maximal bond dimensions of the $U(1)$ blocks were set to $\chi_{\text{block}} = 400$, resulting in a total bond dimension $\chi_{\text{tot}} > 1000$. We used a first order Trotter-expansion for the time evolution operator with a time step $dt = 0.001$, and verified that decreasing this time step does not modify our results.

To control the reliability of our data, we computed the truncated weight at each time-step, and requested that the one-step truncated weight be less than 10^{-8}. As an alternative method, we ran the code with different bond dimensions and determined the time, where the results deviated upon increasing bond dimension. The two methods resulted in approximately the same threshold time. The error bars in Fig. 2 of the main text and Tables 3 and 4 below were then estimated by extracting the minimal and maximal values of the correlators before the threshold time in the last time interval of length 1.0.

For $\Delta = 1.4$ and $\Delta = 1.6$ it is difficult to estimate the error because for the times the simulation can reach there is still a drift of the correlation functions; in these cases the errors

shown in the tables are computed from the fluctuations around this drifting average. The remaining drift of the average introduces a further systematical error, which is not included in our statistical estimate, and is hard to quantify reliably.

Precision of the OTBA solution.—

The precision of the solution of the OTBA system was improved by extrapolation in the discretization used in the numerical solutions of the integral equations.

Checking the sum rule (11) by plugging in our numerical solution for different values of Δ for both initial states we found that while both the overlap (6) and the entropy (8) are of order $\mathcal{O}(10^{-1})$, their difference, i.e. the quench action (5) is of order $\mathcal{O}(10^{-8})$ and shrinks while increasing the number of equations included, therefore it is interpreted as a numerical error of the truncated OTBA system. This provides very strong evidence that we indeed found the correct saddle point solution.

Results.—

The estimates of the asymptotic values of the correlations together with the OTBA predictions are listed for various Δ values in Table 3 for the zero momentum Néel state and in Table 4 for the dimer initial states. Based on the accuracy of the saturation of the sum rule and of the mean values of conserved charges, we can trust the results of the OTBA at least up to 7 digits. The tables also show the TGGE predictions and, when available from [1], the predictions of the full GGE as well.

In the Néel case the difference between the OTBA and TGGE results [2] is smaller than the accuracy of the ITEBD, except for $\Delta = 2$ where the TGGE seems to fail. However, in this case the TGGE with 6 charges has not yet converged in the truncation level. We expect that in the Néel case only the quenches to $\Delta < 1$ can conclusively decide between the OTBA and GGE predictions.

	$\langle\sigma_1^z\sigma_2^z\rangle$	$\langle\sigma_1^z\sigma_3^z\rangle$	$\langle\sigma_1^z\sigma_4^z\rangle$
$\Delta = 2$, ITEBD	-0.6623(37)	0.3963(68)	-0.2967(50)
OTBA	-0.6602541	0.3929011	-0.2921120
TGGE	-0.648906	0.386578	-0.280383
$\Delta = 3$, ITEBD	-0.8145(28)	0.6493(52)	-0.5763(45)
OTBA	-0.8151215	0.6480874	-0.5745134
TGGE	-0.8140907	0.6501061	-0.5757850
$\Delta = 4$, ITEBD	-0.8875(18)	0.7815(34)	-0.7321(33)
OTBA	-0.8875741	0.7812765	-0.7317703
TGGE	-0.8874100	0.7824718	-0.7328197
$\Delta = 5$, ITEBD	-0.9254(9)	0.8537(16)	-0.8193(16)
OTBA	-0.9253052	0.8532200	-0.8187737
TGGE	-0.9252648	0.8538195	-0.8193336

Table 3: Correlation functions in the steady state computed from the real time ITEBD simulation starting from the Néel state, compared with the OTBA and TGGE predictions.

	$\langle\sigma_1^z\sigma_2^z\rangle$	$\langle\sigma_1^z\sigma_3^z\rangle$	$\langle\sigma_1^z\sigma_4^z\rangle$
$\Delta = 1.4$, ITEBD	-0.5668(8)	0.2495(16)	-0.1468(8)
OTBA	-0.5654103	0.2423652	-0.1399874
GGE	-0.5583	0.2531	-0.1428
TGGE	-05582489	0.2530204	-0.1426594
$\Delta = 1.6$, ITEBD	-0.5881(14)	0.2771(35)	-0.1640(27)
OTBA	-0.5844820	0.2660954	-0.1523768
GGE	-0.5751	0.2793	-0.1575
TGGE	-0.5771005	0.2818048	-0.1607061
$\Delta = 2$, ITEBD	-0.6017(36)	0.2856(79)	-0.1493(61)
OTBA	-0.6028190	0.2830639	-0.1483621
GGE	-0.5919	0.3080	-0.1653
TGGE	-0.5943014	0.3112498	-0.1694210
$\Delta = 3$, ITEBD	-0.6030(46)	0.2588(92)	-0.0922(75)
OTBA	-0.6028720	0.2545210	-0.0896056
TGGE	-0.5945574	0.3173677	-0.1409851
$\Delta = 4$, ITEBD	-0.5906(38)	0.2174(76)	-0.0421(56)
OTBA	-0.5900476	0.2130988	-0.0391867
GGE	-0.5842	0.3045	-0.1118
TGGE	-0.5841759	0.3045031	-0.1117982
$\Delta = 5$, ITEBD	-0.5782(21)	0.1823(38)	-0.0062(30)
OTBA	-0.5780574	0.1796867	-0.0048808
TGGE	-0.5739028	0.2908932	-0.0900247
$\Delta = 6$, ITEBD	-0.5684(21)	0.1564(41)	0.0175(34)
OTBA	-0.5683073	0.1541999	0.0187079
TGGE	-0.5652571	0.2793170	-0.0740645
$\Delta = 7$, ITEBD	-0.5606(18)	0.1364(34)	0.0345(29)
OTBA	-0.5605040	0.1345920	0.0355613
TGGE	-0.5581836	0.2698481	-0.0621113
$\Delta = 8$, ITEBD	-0.5543(16)	0.1208(33)	0.0473(26)
OTBA	-0.5542031	0.1191975	0.0480651
GGE	-0.5524	0.2621	-0.05291
TGGE	-0.5523842	0.2621091	-0.0529131

Table 4: Correlation functions in the steady state computed from the real time ITEBD simulation starting from the dimer state, compared with the OTBA, TGGE and GGE predictions.

19 Effects of atom losses on a one-dimensional lattice gas of hardcore bosons by Riggio, Rosso, Karevski, Dubail

Abstract

Atom losses occur naturally during cold atoms experiments. Since this phenomenon is unavoidable, it is important to understand its effect on the remaining atoms. Here we investigate a toy model: a lattice gas of hard-core bosons subject to K-body losses (where $K = 1, 2, 3, \ldots$ is the number of atoms lost in each loss event) on K neighboring sites. In particular we investigate the effect of losses on the rapidity distribution $\rho(k)$ of the atoms. Under the assumption that losses are weak enough so that the system relaxes between two loss events, we are able to determine the loss functional $F[\rho](k)$ encoding the loss process for K-body losses. We derive closed expressions for the cases of one- and two-body losses, and show their effects on the evolution of the total number of particles. Then we add a harmonic trapping potential and study the evolution of the position-dependent rapidity distribution of this system by solving numerically the evolution equation for one-, two- and three-body losses.

19.1 Introduction

During the past two decades, cold atom experiments have become a key simulation platform to investigate the physics of low-dimensional quantum many-body systems [1]. While these experiments are typically well isolated and their dynamics at short times is well approximated by unitary dynamics, cold atom setups are always subject to atom losses. The effects of the latter on the dynamics of the gas can become important at longer times, and they are typically hard to describe theoretially. Cold atom experiments involve various loss processes, for instance one-body losses resulting from scattering with background thermal atoms [2], which can be significant. Inelastic two-body collisions can occur naturally or be intentionally engineered, leading to two-body losses [3, 4, 5, 6, 7, 8, 9, 10]. Three-body losses, where a highly bound diatomic molecule is formed, are invariably present and typically dominate the overall loss process [11, 12, 13]. In principle, loss processes involving more than three atoms also exist. In particular, losses involving four atoms have been reported in Refs. [14, 15]. Loss processes can sometimes be controlled and engineered [16] to bring out physical phenomena such as cooling [17, 18, 19, 20, 21, 22, 23, 24] and the quantum Zeno effect [25, 26, 27, 28, 29, 30, 31, 32, 33, 34, 35, 36, 37, 38, 39].

Despite the relevance of loss processes, a consistent general theory describing the effects of losses on the dynamics does not exist yet. One standard way to model atom losses is to use the Lindblad equation [26, 40, 25, 41, 42]. Several studies have inspected the interplay between the unitary dynamics and the lossy one in both bosonic [26, 25, 40, 43, 44] and fermionic gases [45, 46, 47, 48, 49, 50, 51, 44].

In one spatial dimension, several ultracold gases are integrable or nearly integrable, including continuous gases of bosons [52, 53, 54, 55, 56] or fermions [57, 58], sometimes with multiple components [59, 60], but also lattice gases like hard-core bosons [61, 62] or the Fermi-Hubbard model [63]. The question of losses in those integrable gases is particularly interesting. An integrable model admits a macroscopic number of conserved charges in comparison with non-integrable models where, typically, only the energy and the number of particle are conserved. Due to this large set of conserved quantities, an isolated integrable system has a singular property: the stationary states of the system are modeled by Generalized Gibbs Ensembles (GGE). A GGE is constructed by maximizing the entropy under the constraints imposed by all conservations laws [64]. However, under dissipative processes like atom losses, the conserved quantities of an integrable system are not conserved anymore, as the coupling between the

system and its environnement typically causes integrability breaking [65]. In principle, one then expects that integrability breaking leads to thermalization at very long times, possibly with a pre-thermalization phenomenon at intermediate time scales [66]. Some studies seem to confirm the thermalization but other works suggest otherwise [17].

Motivated by the outstanding challenge of developping a general theory of the effects of losses on the dynamics of integrable gases, here we introduce a toy model where we can theoretically investigate the effects of K-body losses ($K \geq 1$) on the dynamics of the simplest such gas. We propose to investigate hard-core bosons on a lattice —a famous model of integrable quantum gas dynamics that has been extensively studied theoretically [67, 68, 69, 70, 71, 72] and realized experimentally [61, 62]— subject to weak K-body atom losses: whenever K atoms occupy K neighboring sites, they can escape the system with some rate (Fig. 19.1).

We stress that experimentally realistic loss processes in optical lattices usually involve atoms on the same lattice site, so, strictly speaking, only the $K = 1$ version of our toy model is of experimental relevance. For $K \geq 2$, we are not aware of existing experimental setups that could engineer our K-site loss processes. However, from a theoretical perspective this model is very natural. Here our goal is to understand how integrability breaking caused by such loss events affects the dynamics of the gas. Of course, under atom losses, the stationary state at very long times is always the vacuum. However, what we want to investigate is how the vacuum is approached, and in particular whether or not to the gas is in a quasi-stationary thermal state. We investigate for instance the mean density $n(t) = \langle N(t) \rangle / L$ (where N is the number of atoms and L is the number of lattice sites) for different initial states and observe different non-trivial behaviors depending on the number K of atoms lost in each loss event. In particular, for two-body losses ($K = 2$), we analytically show that $n(t) \propto 1/t$ or $\propto 1/t^{1/2}$, depending on a specific property of the initial state (see below). More generally, for other values of $K \geq 2$ our numerical results are in agreement with a power-law decay $n(t) \propto t^{\alpha}$ where the exponent α typically depends on the initial state, and generically differs from the mean-field result $1/(K-1)$. This observation holds also if we add a harmonic potential; however in that case the exponent α changes and is different from the one found in the homogeneous case.

The paper is organized as follows. In Section 19.2 we define the model and discuss our assumptions. Our main hypothesis of slow losses, and fundamental concepts such as the rapidity distribution and the loss functional are introduced. In Section 19.3 we present our calculation of the loss functional for K-body losses, which crucially depends on the parity of K. In Section 19.4 we investigate the effect of atom losses on the rapidity distribution and on the mean density in the homogeneous gas, by combining analytical and numerical calculations. In Section 19.5, we add a harmonic trapping potential. We use a hydrodynamic-like approach similar to Generalized Hydrodynamics [73, 74] where we incorporate the loss functional (following similar proposals in Refs. [40, 43]), and design a numerical method for solving the resulting evolution equation for the rapidity distribution in the gas. We conclude in Section 19.6.

19.2 The model

19.2.1 Definition: lattice Tonks-Girardeau gas with K-body losses

We consider a lattice Tonks-Girardeau gas subject to atom losses. Each site $j \in \mathbb{Z}$ is occupied by either zero or one boson. We write σ_j^+ / σ_j^- for the operator that creates/annihilates a boson on site j. Because of the hard-core constraint, these operators do not satisfy the usual bosonic canonical commutation relations. Instead, they satisfy the algebra of Pauli matrices, $(\sigma_j^+)^2 = (\sigma_j^-)^2 = 0$, and $[\sigma_i^+, \sigma_j^-] = \delta_{i,j}\sigma_j^z$.

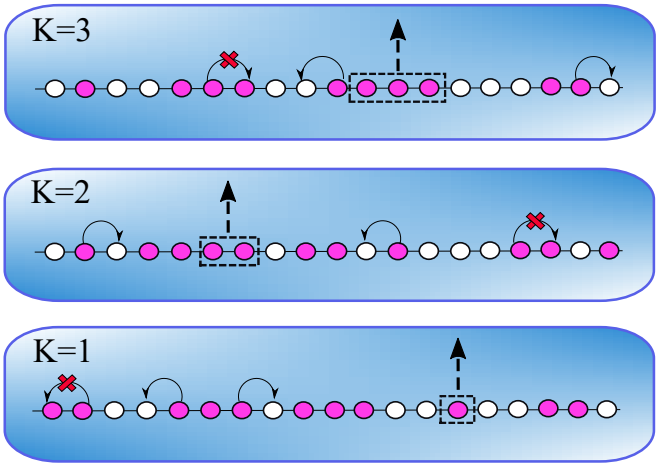


Figure 19.1: We consider a lattice gas of hardcore bosons (pink dots) that can jump from site to site. Two bosons cannot be on the same site. Losses are represented by the large black arrow which connects the bosons chain to its environment (blue background). Here we show the situation for one-body losses ($K = 1$), two-body losses ($K = 2$) and three-body losses ($K = 3$). For each cases, K consecutive atoms are removed and are lost in the 'environment'. In this paper losses are modeled by the Lindblad equation (19.2).

We consider the hard-core boson (HCB) Hamiltonian with nearest-neighbor hopping,

$$H_{\rm HCB} = -\frac{1}{2}\sum_{j\in\mathbb{Z}}(\sigma_j^+\sigma_{j+1}^- + \sigma_{j+1}^+\sigma_j^-). \tag{19.1}$$

This Hamiltonian generates the unitary part of the evolution of the gas. In addition, we assume that the gas is subject to incoherent K-body loss processes, with K a positive integer. To describe the losses, we assume that the dynamics is Markovian, and we consider the following Lindblad equation for the density matrix $\hat{\rho}$,

$$\begin{aligned}\dot{\hat{\rho}}(t) = &-i[H_{\rm HCB}, \hat{\rho}(t)] \\ &+\Gamma\sum_{j\in\mathbb{Z}}\left(L_j\,\hat{\rho}(t)\,L_j^\dagger - \frac{1}{2}\{L_j^\dagger L_j, \hat{\rho}(t)\}\right),\end{aligned} \tag{19.2}$$

Here Γ is a constant that sets the loss rate, while the Lindblad operators

$$L_j = \prod_{l=0}^{K-1}\sigma_{j+l}^- \tag{19.3}$$

remove K bosons from the K consecutive sites $j, j+1, \ldots, j+K-1$.

We stress that, with these loss terms, the model is not exactly solvable, so it is necessary to develop some effective approaches to tackle it.

19.2.2 Adiabatic losses, effective description by slow motion of the charges

To simplify the description of the system, we follow the approach of Ref. [40]. There the approach was developed for losses in a continuous gas, and it is based on the assumption that the losses are slow, so that the gas remains in a Generalized Gibbs Ensemble (GGE) with parameters that slowly drift in time (see e.g. [75] for a review). A similar description of slowly-evolving nearly integrable systems with weak integrability breaking had previously appeared

in Refs. [76, 77, 78]. Following these ideas, here we also assume that the loss processes occur on very long times compared to the relaxation time scale due to the unitary evolution of the gas. In that limit, the gas has time to reach a local stationary state after each loss event. To efficiently exploit that assumption, we look at the slow dynamics of the conserved charges.

For convenience, from now on we focus on a finite system of $L \gg 1$ sites, with periodic boundary conditions. The Hamiltonian $H_{\rm HCB}$ commutes with an infinite set of hermitian operators Q_a, $a = 0, 1, 2\ldots$ that can be constructed using the Jordan-Wigner mapping to non-interacting fermions (see Subsec. 19.2.3 for details). These operators also commute among themselves, $[Q_a, Q_b] = [H_{\rm HCB}, Q_a] = 0$. Moreover, they are local in the sense that $Q_a = \sum_{j=1}^{L} q_{a,j}$ where $q_{a,j}$ is a charge density operator that has compact support (i.e. it acts on a finite number of sites around j).

The time evolution of the expectation value $\langle Q_a \rangle(t) = {\rm tr}[\hat\rho(t) Q_a]$, is obtained from Eq. (19.2),

$$\langle \dot{Q}_a \rangle(t) = \frac{\Gamma}{2} \sum_{j=1}^{L} \left\langle L_j^\dagger \, [Q_a,\, L_j] + [L_j^\dagger,\, Q_a] L_j \right\rangle (t). \tag{19.4}$$

Moreover, the hermiticity of Q_a implies $\langle [L_j^\dagger, Q_a] L_j \rangle = \langle L_j^\dagger \, [Q_a,\, L_j] \rangle^*$. Thus,

$$\langle \dot{Q}_a \rangle(t) = \Gamma \sum_{j=1}^{L} {\rm Re} \left\langle L_j^\dagger [Q_a, L_j] \right\rangle (t). \tag{19.5}$$

This equation is exact and it is a direct consequence of Eq. (19.2). Notice that, in this form, it is not particularly useful, because to evaluate the r.h.s one needs to know the exact density matrix $\hat\rho(t)$.

Now comes the crucial step. Importantly, the operator $L_j^\dagger [Q_a, L_j]$ is local, because both the operator L_j and the charge density $q_{a,j}$ have compact support. This, together with the assumption of slow losses, allows us to use the idea of local relaxation in the system. Namely, we expect that, under unitary evolution, the density matrix of a small subsystem quickly relaxes to a Generalized Gibbs Ensemble (GGE). Expectation values of local observables can then be evaluated with respect to the GGE density matrix,

$$\hat\rho_{{\rm GGE},\{\langle Q_a \rangle\}} \propto e^{-\sum_a \beta_a Q_a}, \tag{19.6}$$

where the Lagrange multipliers β_a are fixed by the expectation values of the charges $\langle Q_a \rangle$, which must be equal to ${\rm tr}[\hat\rho_{{\rm GGE},\{\langle Q_b \rangle\}} Q_a]$. Evaluating the r.h.s of Eq. (19.4) in the GGE density matrix leads to a closed evolution equation for the slow motion of the charges induced by the losses,

$$\frac{d}{dt} \langle Q_a \rangle = \Gamma \sum_{j=1}^{L} {\rm Re} \left\langle L_j^\dagger [Q_a, L_j] \right\rangle_{{\rm GGE},\{\langle Q_b \rangle\}}. \tag{19.7}$$

It is this evolution equation that we study in great detail in this paper. For lattice HCB, the description is further simplified by specifying the form of the conserved charges Q_a. This is what we do next, by introducing the distribution of rapididites.

19.2.3 Slow evolution of the rapidity distribution

Hard-core bosons can be mapped to free fermions by a Jordan-Wigner transformation,

$$\sigma_j^+ = \prod_{i=1}^{j-1} (-1)^{c_i^\dagger c_i} \, c_j^\dagger, \qquad \sigma_j^- = \prod_{i=1}^{j-1} (-1)^{c_i^\dagger c_i} \, c_j. \tag{19.8}$$

Here the operators $c_j^\dagger/c_j$ create/annihilate a fermion on site j. They satisfy the canonical anticommutation relations $\{c_i, c_j^\dagger\} = \delta_{ij}$. Under the Jordan-Wigner mapping, the Hamiltonian (19.1) becomes

$$H_{\text{HCB}} = -\frac{1}{2}\sum_{j=1}^{L}(c_j^\dagger c_{j+1} + c_{j+1}^\dagger c_j). \tag{19.9}$$

Moreover, the fermions satisfy antiperiodic (resp. periodic) boundary conditions if the number of particles N in the system is even (resp. odd):

$$c_{L+1}^\dagger = (-1)^{N-1} c_1^\dagger. \tag{19.10}$$

The Fourier modes are

$$c^\dagger(k) = \frac{1}{\sqrt{L}}\sum_{j=1}^{L} e^{ikj} c_j^\dagger \tag{19.11}$$

with $k \in \frac{2\pi}{L}(\mathbb{Z} + \frac{1}{2})$ if N is even, and $k \in \frac{2\pi}{L}\mathbb{Z}$ if N is odd. Either way the Hamiltonian reads

$$H_{\text{HCB}} = \sum_k \varepsilon(k) c^\dagger(k) c(k), \tag{19.12}$$

with $\varepsilon(k) = -\cos k$.

It is clear from the form (19.12) that any operator of the form

$$Q[f] = \sum_k f(k) c^\dagger(k) c(k), \tag{19.13}$$

for any function $f(k)$, commutes with the Hamiltonian H_{HCB}. Moreover these conserved charges also commute among themselves. Convenient choices for $f(k)$ are $\cos(nk)$ or $\sin(nk)$ for $n \in \mathbb{N}$, which leads to a hermitian basis set of charges, where each charge has a charge density that is compactly supported.

However, for the purposes of this paper, rather than to work with a specific choice of basis for the space of conserved charges Q_a (or $Q[f]$), it is more convenient to work directly with the occupation number, or 'rapidity distribution',

$$\rho(k) \underset{L\to\infty}{=} \left\langle c^\dagger(k) c(k) \right\rangle, \quad \rho(k) \in [0,1]. \tag{19.14}$$

It is clear that if we know the rapidity distribution $\rho(k)$, then we also know the expectation values of any charge $Q[f]$, because $\langle Q[f] \rangle = \sum_k f(k)\rho(k)$.

Following Ref. [40], we can turn the evolution equation for the slow motion of the charges (19.4) into an equation for the slow evolution of the rapidity distribution itself,

$$\dot{\rho}(k) = -\Gamma F[\rho](k), \tag{19.15}$$

where the loss functional

$$F[\rho](k) = \sum_{j=1}^{L} \text{Re}\left\langle L_j^\dagger [L_j, c^\dagger(k)c(k)] \right\rangle_{\text{GGE},\rho}, \tag{19.16}$$

and the GGE density matrix itself is parameterized by the rapidity distribution $\rho(k)$. More precisely, the GGE density matrix is Gaussian for the fermions $c_j^\dagger, c_j$, and it is characterized by its two-point function $\left\langle c^\dagger(k)c(k') \right\rangle_{\text{GGE},\rho} = \rho(k)\delta_{k,k'}$. All higher-order correlations can be computed using Wick's theorem for fermionic operators.

The functional (19.16) is the central object of this paper. In the next section we compute it explicitly for K-body loss processes. For one- and two-boson loss processes we get simple closed expressions. For loss events involving larger numbers K of bosons, we will see that we can express the loss functional as a small determinant, which follows from applying Wick's theorem to Eq. (19.16).

19.3 Deriving the loss functional

In this section we compute the functional $F[\rho](k)$ explicitly. Importantly, in our calculation we uncover a different structure depending on the parity of the number K of bosons lost in each loss event, which can be traced back to the Jordan-Wigner string appearing in the mapping (19.8) to non-interacting fermions.

19.3.1 One-body losses

For $K = 1$ the Lindblad dissipators are $L_j = \sigma_j^-$. Using translational invariance, the loss functional (19.16) that we need to compute is

$$\begin{aligned} F[\rho](k) &= L \left\langle \sigma_1^+ [\sigma_1^-, c^\dagger(k)c(k)] \right\rangle_{\mathrm{GGE},\rho} \\ &= L \left\langle \sigma_1^+ \sigma_1^- c^\dagger(k)c(k) \right\rangle_{\mathrm{GGE},\rho} - L \left\langle \sigma_1^+ c^\dagger(k)c(k)\sigma_1^- \right\rangle_{\mathrm{GGE},\rho}, \end{aligned} \tag{19.17}$$

where L is the length of the system and the loss operator acts on the site $j = 1$. Both terms in the second line of (19.17) can be computed using the fact that the GGE is a gaussian state for the fermions, which allows us to use Wick's theorem. For the first term we have (using $c_1 = \frac{1}{\sqrt{L}} \sum_q e^{iq}\, c(q)$):

$$\begin{aligned} L \left\langle \sigma_1^+ \sigma_1^- c^\dagger(k)c(k) \right\rangle_{\mathrm{GGE},\rho} &= L \left\langle c_1^\dagger c_1 c^\dagger(k)c(k) \right\rangle_{\mathrm{GGE},\rho} \\ &= \sum_{qq'} e^{i(q-q')} \left\langle c^\dagger(q')c(q)c^\dagger(k)c(k) \right\rangle_{\mathrm{GGE},\rho} \\ &= \sum_{qq'} e^{i(q-q')} \big(\langle c^\dagger(q')c(q) \rangle \langle c^\dagger(k)c(k) \rangle + \\ &\qquad \langle c^\dagger(q')c(k) \rangle \langle c(q)c^\dagger(k) \rangle \big) \\ &= \langle N \rangle \rho(k) + \rho(k)(1-\rho(k)). \end{aligned} \tag{19.18}$$

The second term requires more care, because the operator $c^\dagger(k)c(k)$ is inserted between σ_1^+ and σ_1^-, and the latter change the parity of the number of particles in the system. The boundary conditions for the fermions are modified according to Eq. (22.23). Thus we need to relate the Fourier modes of the fermions with periodic boundary conditions to the ones with anti-periodic boundary conditions. For conciseness, let us introduce the two corresponding sets of momenta,

$$Q^{\mathrm{p}} = \frac{2\pi}{L} \times \{1, 2, \ldots, L\}, \tag{19.19}$$

$$Q^{\mathrm{ap}} = \frac{2\pi}{L} \times \{\frac{1}{2}, \frac{3}{2}, \ldots, L - \frac{1}{2}\}. \tag{19.20}$$

Then we have the following identities,

$$(k \in Q^{\mathrm{p}}) \qquad c(k) = \frac{i}{L} \sum_{q \in Q^{\mathrm{ap}}} \frac{e^{i(q-k)/2}}{\sin((q-k)/2)}\, c(q), \tag{19.21}$$

$$(k \in Q^{\mathrm{ap}}) \qquad c(k) = \frac{i}{L} \sum_{q \in Q^{\mathrm{p}}} \frac{e^{i(q-k)/2}}{\sin((q-k)/2)}\, c(q). \tag{19.22}$$

We can insert them into the second term of Eq. (19.17), which leads to

$$\left\langle \sigma_1^+ c^\dagger(k)c(k)\sigma_1^- \right\rangle = \frac{1}{L^2} \sum_{q,q'} \frac{e^{i(q-q')/2} \left\langle c_1^\dagger c^\dagger(q')\, c(q)c_1 \right\rangle}{\sin((q-k)/2) \sin((q'-k)/2)}. \tag{19.23}$$

This correctly implements the change of boundaries of the fermions. Next we can apply Wick's theorem to evaluate the four-fermion correlator $\left\langle c_1^\dagger c^\dagger(q')\, c(q) c_1 \right\rangle$. This leads to

$$L\left\langle \sigma_1^+ c^\dagger(k) c(k) \sigma_1^- \right\rangle = \\ \frac{\langle N\rangle}{L^2} \sum_q \frac{\rho(q)}{\sin^2(\frac{q-k}{2})} - \left(\frac{1}{L} \sum_q \cot(\frac{q-k}{2})\, \rho(q) \right)^2 - \frac{\langle N\rangle^2}{L^2}. \tag{19.24}$$

The first term in the above equation has a pole of order 2 at $q = k + 2\pi\mathbb{Z}$, and it is convenient to reduce its degree using the identity $\sum_q 1/\sin^2(\frac{q-k}{2}) = L^2$. This leads to the equivalent expression

$$L\left\langle \sigma_1^+ c^\dagger(k) c(k) \sigma_1^- \right\rangle = \frac{\langle N\rangle}{L^2} \sum_q \frac{\rho(q) - \rho(k)}{\sin^2(\frac{q-k}{2})} + \langle N\rangle\, \rho(k) \\ - \left(\frac{1}{L} \sum_p \cot(\frac{p-k}{2})\, \rho(p) \right)^2 - \frac{\langle N\rangle^2}{L^2}. \tag{19.25}$$

Putting the two terms (19.18)-(19.25) together and taking the thermodynamic limit $L \to \infty$, we arrive at the following form of the one-body loss functional

$$F[\rho](k) = \rho(k) - \rho^2(k) + \left(\fint_{-\pi}^{\pi} \frac{dp}{2\pi}\, \cot(\frac{k-p}{2})\, \rho(p) \right)^2 \\ + n \left(n + \fint_{-\pi}^{\pi} \frac{dq}{2\pi}\, \frac{\rho(k) - \rho(q)}{\sin^2(\frac{k-q}{2})} \right), \tag{19.26}$$

where $n = \langle N\rangle / L$ is the density of particle and $\fint$ means the Cauchy principal value of the integral. This is our main result for one-body losses. It is similar to (but different from) the formula given in Ref. [40] for the Tonks-Girardeau gas in the continuum. Notice that the functional is non-linear in $\rho(k)$, and also non-local in rapidity space.

19.3.2 Two-body losses

For $K = 2$, the dissipators are $L_j = \sigma_j^- \sigma_{j+1}^-$. Under the Jordan-Wigner mapping they become

$$L_j = \sigma_j^- \sigma_{j+1}^- = c_j (-1)^{c_j^\dagger c_j} c_{j+1} = -c_j c_{j+1}. \tag{19.27}$$

Then, to compute the functional F, we simply need to insert the dissipator (19.27) in the definition (19.16),

$$F[\rho](k) = \sum_j \left\langle \sigma_{j+1}^+ \sigma_j^+ [\sigma_j^- \sigma_{j+1}^-, c^\dagger(k) c(k)] \right\rangle \\ = \sum_{q,q',p,p'} \frac{e^{i(2p'+p-2q-q')}}{M} \left\langle c^\dagger(q) c^\dagger(q') [c(p) c(p'), c^\dagger(k) c(k)] \right\rangle. \tag{19.28}$$

Expanding the commutator in the braket leads to two terms

$$\left\langle c^\dagger(q) c^\dagger(q') [c(p) c(p'), c^\dagger(k) c(k)] \right\rangle \\ = \left\langle c^\dagger(q) c^\dagger(q') c(p) c(p') c^\dagger(k) c(k) \right\rangle \\ - \left\langle c^\dagger(q) c^\dagger(q') c^\dagger(k) c(k) c(p) c(p') \right\rangle. \tag{19.29}$$

The first term can be expressed as

$$\begin{aligned}&\left\langle c^\dagger(q)c^\dagger(q')c(p)c(p')c^\dagger(k)c(k)\right\rangle\\&=\left\langle c^\dagger(q)c^\dagger(q')c^\dagger(k)c(k)c(p)c(p')\right\rangle\\&+\delta_{p'k}\left\langle c^\dagger(q)c^\dagger(q')c(p)c(k)\right\rangle-\delta_{pk}\left\langle c^\dagger(q)c^\dagger(q')c(p')c(k)\right\rangle.\end{aligned}\tag{19.30}$$

The second term is the expectation value of $c^\dagger(k)c(k)$ in a state where two atoms have been removed, the parity of the initial number of particle is then unchanged. Hence, in contrast to the $K=1$ case treated in the previous subsection, here the parity of the number of atoms does not change.

One can then apply Wick's theorem, and take the thermodynamic limit to obtain the loss functional,

$$F[\rho](k)=\frac{2}{\pi}\int_{-\pi}^{\pi}dq\,\sin^2\left(\frac{k-q}{2}\right)\,\rho(q)\,\rho(k).\tag{19.31}$$

This is our main result for two-body losses. That functional presents some similarities with the loss functional found in the relation (5) of Ref. [25].

We now generalise this calculation to the case of K-body losses for K an arbitrary even integer.

19.3.3 K-body losses with K even

In this subsection we show that is possible to find a closed formula for the loss functional defined in (19.16) where the Lindblad operator is given by $L_j=\sigma_j\sigma_{j+1}\dots\sigma_{j+K-1}$. Taking the Fourier transform of L_j and $L_j^\dagger$ in (19.16), the loss functional reads

$$\begin{aligned}F^{\text{even}}[\rho](k)=&\frac{1}{L^{K-1}}\sum_{\substack{q_1,\dots,q_K\\q'_1,\dots,q'_K}}\exp i\sum_{l=1}^{K}(q_l-q'_l)l\times\\&\left\langle c^\dagger(q'_K)\dots c^\dagger(q'_1)[c(q_1)\dots c(q_K),c^\dagger(k)c(k)]\right\rangle.\end{aligned}\tag{19.32}$$

As mentionned in 19.3.2, in the case of even K-body losses the commutator in (19.32) reduces to K terms

$$\begin{aligned}&\left\langle c^\dagger(q'_K)\dots c^\dagger(q'_1)[c(q_1)\dots c(q_K),c^\dagger(k)c(k)]\right\rangle\\&=\delta_{kq_K}\left\langle c^\dagger(q'_K)\dots c^\dagger(q'_1)c(q_1)\dots c(q_{K-1})c(k)\right\rangle\\&-\delta_{kq_{(K-1)}}\left\langle c^\dagger(q'_K)\dots c^\dagger(q'_1)c(q_1)\dots c(q_{K-2})c(q_K)c(k)\right\rangle\\&+\dots\end{aligned}\tag{19.33}$$

and applying Wick's theorem on each terms leads to a product of K terms of the form $\left\langle c^\dagger(q')c(q)\right\rangle$. Using the property $\left\langle c^\dagger(q')c(q)\right\rangle=\delta_{qq'}\,\rho(q)$ and taking the thermodynamic limit, the loss functional in (19.32) can be expressed as a sum of K terms each consisting of a K by K matrix determinant. Let us introduce the $K\times K$ matrix $A^{(j)}_{[\rho]}$ with matrix elements

$$[A^{(j)}_{[\rho]}]_{ab}=\begin{cases}\frac{1}{2\pi}\int_{-\pi}^{\pi}dq\,e^{i(b-a)q}\,\rho(q) & \text{if } b\neq j\\ e^{i(b-a)k}\,\rho(k) & \text{if } b=j,\end{cases}\tag{19.34}$$

for indices $a,b=1,\dots,K$. The superscript j indicates which column depends on the rapidity k. Apart from the j^{th} column, the matrix essentially contains Fourier transforms of the rapidity

distribution $\rho(k)$. The loss functional then reduces to

$$F^{\text{even}}[\rho](k) = \sum_{j=1}^{K} \det(A^{(j)}_{[\rho]}). \tag{19.35}$$

The relation (19.35) is another fundamental result of this paper.

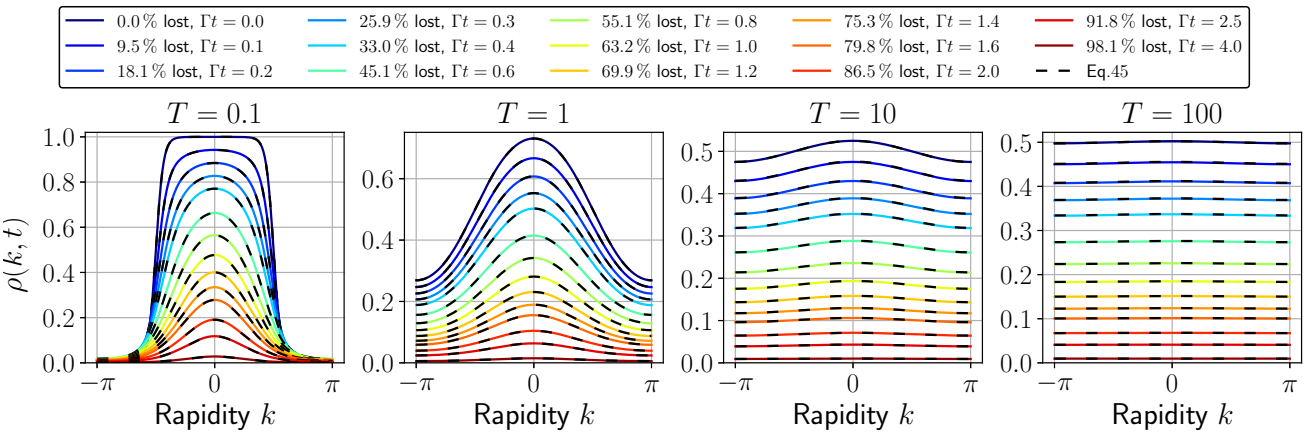


Figure 19.2: Effect of one-body losses on different rapidity distributions. The initial distribution is a thermal (Fermi-Dirac) distribution $\rho(k) = (1+\exp(-\cos(k)/T))^{-1}$, and we show the results for different initial temperatures $T = 0.1, 1.0, 10.0, 100.0$. The time evolution is obtained by solving Eq. (19.15) with the loss functional (19.26) with the Runge-Kutta method. Notice that the solution of Eq. (19.15) depends on the loss rate Γ only through the dimensionless time Γt. The black dashed lines correspond to formula (19.45) and show a perfect agreement with the numerical solution of the evolution equation.

19.3.4 K-body losses with K odd

In this last subsection we investigate the case of losses process with an odd number K of lost atoms. The reasoning is similar to the one we developped in the previous subsection, however like in the $K = 1$ case, we need to be careful about the change of boundary conditions for the fermions. We start by taking the Fourier transform of the Lindblad operators in the definition (19.16), which leads to the relation (19.32). The commutator in the loss functional gives two terms

$$\begin{aligned}
&\left\langle c^\dagger(q'_K)\dots c^\dagger(q'_1)[c(q_1)\dots c(q_K), c^\dagger(k)c(k)]\right\rangle \\
&= \left\langle c^\dagger(q'_K)\dots c^\dagger(q'_1)c(q_1)\dots c(q_K)c^\dagger(k)c(k)\right\rangle \\
&- \left\langle c^\dagger(q'_K)\dots c^\dagger(q'_1)c^\dagger(k)c(k)c(q_1)\dots c(q_K)\right\rangle .
\end{aligned} \tag{19.36}$$

As we have already discussed in the subsection 19.3.1, the first term is the expectation value of $c^\dagger(k)c(k)$ in a state where the initial number of particles is preserved. However the second term corresponds to the expectation value of $c^\dagger(k)c(k)$ in a state where K atoms have been removed. Since K is an odd number, the parity of the number of particle is changed and one needs to use the relations (19.21) to express $c^\dagger(k)c(k)$ in the appropriate parity sector. Inserting the relations (19.21) in the second term, one has

$$\begin{aligned}
&\left\langle c^\dagger(q'_K)\dots c^\dagger(q'_1)c^\dagger(k)c(k)c(q_1)\dots c(q_K)\right\rangle = \\
&\sum_{q,q'} \frac{e^{i(q-q')/2}\left\langle c^\dagger(q'_K)\dots c^\dagger(q'_1)c^\dagger(q')c(q)c(q_1)\dots c(q_K)\right\rangle}{L^2\sin((q-k)/2)\sin((q'-k)/2)}.
\end{aligned} \tag{19.37}$$

Before using Wick's theorem on the above formula, one can notice that the first term in the right-hand side of (19.36) can be written as

$$\begin{aligned}
&\left\langle c^\dagger(q'_K)\dots c^\dagger(q'_1)c(q_1)\dots c(q_K)c^\dagger(k)c(k)\right\rangle \\
&= \left\langle c^\dagger(q'_K)\dots c^\dagger(q'_1)c^\dagger(k)c(k)c(q_1)\dots c(q_K)\right\rangle \\
&+ \delta_{kq_K}\left\langle c^\dagger(q'_K)\dots c^\dagger(q'_1)c(q_1)\dots c(q_{K-1})c(k)\right\rangle \\
&- \delta_{kq_{(K-1)}}\left\langle c^\dagger(q'_K)\dots c^\dagger(q'_1)c(q_1)\dots c(q_{K-2})c(q_K)c(k)\right\rangle \\
&+ \dots,
\end{aligned} \tag{19.38}$$

where we used the anti-commutation relation for the fermionic operators. As we proceed in the previous subsection, the Wick's contractions of (19.37) and of the first term in the right-hand side of (19.38) can be written as two determinants of two matrices B and C. The matrices B and C are $(K+1)\times(K+1)$ hermitian matrices and their matrix elements depend on the Fourier and Hilbert transforms [79] of $\rho(k)$

$$[B_{[\rho]}]_{ab} = \begin{cases} \frac{1}{2\pi}\int_{-\pi}^{\pi} dq\, e^{i(b-a)q}\,\rho(q) \;\text{ if } a,\, b < K+1 \\ e^{-iak}\,\rho(k) \;\text{ if } b = K+1 \\ 0 \text{ if } a = b = K+1, \end{cases} \tag{19.39}$$

$$[C_{[\rho]}]_{ab} = \begin{cases} \frac{1}{2\pi}\int_{-\pi}^{\pi} dq\, e^{i(b-a)q}\,\rho(q) \text{ if } a,\, b < K+1 \\ \frac{1}{2\pi}\fint_{-\pi}^{\pi} dq\, e^{-i(a-1)q}\rho(q)(\cot(\frac{k-q}{2}) + i) \\ \text{if } b = K+1 \\ \frac{1}{2\pi}\fint_{-\pi}^{\pi} dq\, \dfrac{\rho(q)-\rho(k)}{\sin^2(\frac{k-q}{2})} \text{ if } a = b = K+1. \end{cases} \tag{19.40}$$

The loss functional for odd K takes the final form

$$\begin{aligned}
F_K^{\text{odd}}[\rho](k) = &\left(\sum_{j=1}^{K}\det(A^{(j)}_{[\rho]})\right) \\
&+ \left[\det(B_{[\rho]}) - \det(C_{[\rho]})\right].
\end{aligned} \tag{19.41}$$

It is possible to write a general expression valid both for even and odd K by introducing the factor $\dfrac{1-(-1)^K}{2}$ which vanishes for K even, so that our final result, valid in all cases, reads

$$\begin{aligned}
F_K[\rho](k) = &\left(\sum_{j=1}^{K}\det(A^{(j)}_{[\rho]})\right) \\
&+ \frac{1-(-1)^K}{2}\left[\det(B_{[\rho]}) - \det(C_{[\rho]})\right].
\end{aligned} \tag{19.42}$$

19.4 Evolution of the rapidity distribution in a homogeneous gas

Having established the general form of the loss functional $F[\rho]$ for K-body losses, Eqs. (19.26)-(19.31)-(19.35)-(19.41)-(19.42), we now turn to the time evolution of the rapidity distribution. We solve the evolution equation

$$\dot\rho(k) = -\Gamma F[\rho](k) \tag{19.43}$$

numerically (and analytically for the special case $K = 1$), and we focus in particular on the time evolution of the atom density $n = \int_{-\pi}^{\pi}\rho(k)\frac{dk}{2\pi}$.

19.4.1 Results for $K = 1$

For one-body losses the atom density always decays exponentially,

$$n(t) = n(0)e^{-\Gamma t}. \tag{19.44}$$

This simply follows from Eq. (19.4) applied to the total particle number $Q_a = N$ and to $L_j = \sigma_j^-$: it gives $\langle \dot{N} \rangle = -\Gamma \langle N \rangle$, which implies Eq. (19.44) for the atom density $n = N/L$.

It turns out the evolution equation (19.43) for the rapidity distribution can be solved exactly for the loss functional for $K = 1$ (see Eq. (19.26)). The solution is derived in Appendix 19.7; it reads

$$\rho(t,k) = n_0 e^{-\Gamma t} \Re \left(\frac{\tanh(n_0(e^{-\Gamma t}-1)) + \frac{i}{n_0} I(t,k)}{1 + \frac{i}{n_0} \tanh(n_0(e^{-\Gamma t}-1))\, I(t,k)} \right), \tag{19.45}$$

where $n_0 = n(0)$ is the initial atom density, $\rho_0(k) = \rho(t=0,k)$ is the initial rapidity distribution, and $I(t,k)$ is the integral

$$I(t,k) = \int_{-\pi}^{\pi} \frac{dq}{2\pi} \frac{\rho_0(q)}{\tan(\frac{k-q}{2} + i n_0(1-e^{-\Gamma t}))}. \tag{19.46}$$

A related expression for the continuous Tonks-Girardeau gas with one-body losses was obtained in Ref. [40].

In Fig. (19.2) we show the evolution of the rapidity distribution from thermal initial states at different temperatures. We display the analytical result (19.45), as well as the numerical solution of Eq. (19.43) obtained from the Runge-Kutta method; they are in perfect agreement, as they should.

We see that loss processes spread the distribution in rapidity space. In the limit of large temperature for the initial state, the rapidity distribution is flat, and remains flat at all times. For smaller initial temperatures, it evolves into a bell-shape distribution at late times, which is close to a Boltzmann distribution $\rho(k) \propto \exp[\cos(k)/T]$ with a density going to zero according to Eq. (19.44). This is further illustrated in Fig. 19.3.(a), where we plot the ratio $\rho(k,t)/n(t)$ in the limit $t \to \infty$, and fit the result with a Boltzmann distribution. The agreement is very good, even though it is clear from the exact formulas (19.45)-(19.46) that the distribution $\rho(k,t)$ never becomes exactly thermal, even at infinite time.

To find a more striking signature of the fact that the system never goes to a low-density thermal distribution, we consider the case of an oscillating initial rapidity distribution $\rho_0(k) = (1-\cos(sk))/2$, where s is an integer. In that case the long-time limit of the integral (19.46) can be evaluated analytically, $\lim_{t\to\infty} I(t,k) = (1 - e^{-2sn_0} e^{iks})/2$, and when injected in Eq. (19.45) it leads to a late-time rapidity distribution of the form

$$\frac{\rho(k,t)}{n(t)} \underset{t\to\infty}{=} \frac{\alpha + \beta\, \cos(sk)}{\gamma + \delta\, \cos(sk)}, \tag{19.47}$$

where the coefficients $\alpha, \beta, \gamma, \delta$ depend on the initial density n_0 and on the integer s. Thus, even at long time, the rescaled rapidity distribution is sensitive to the structure of the inital distribution (see also Fig.19.3.(b)). We conclude that in general the rapidity distribution does not go to a low-density thermal distribution at long times.

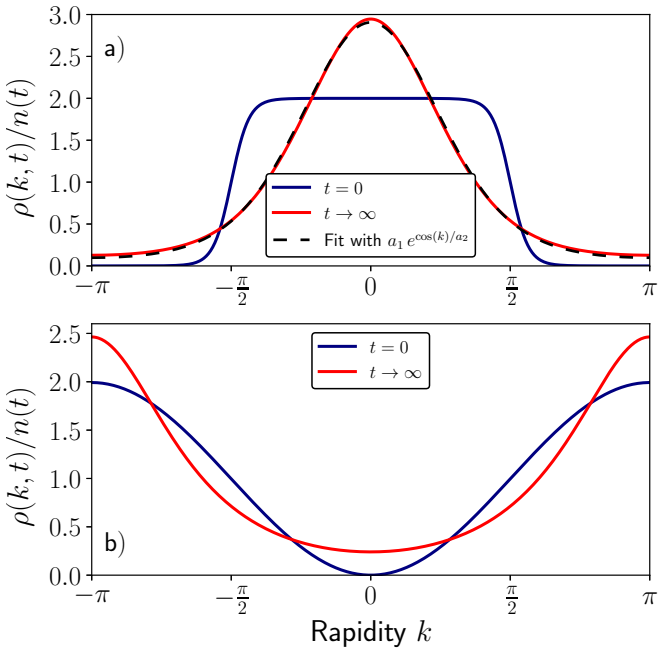


Figure 19.3: Long time behavior of different rapidity distributions rescaled by the corresponding density. a) The initial distribution (blue curve) is a Fermi-Dirac distributions $\rho_0(k) = (1 + \exp(-\cos(k)/T))^{-1}$ with T=0.1. The red curve is the distribution at long time according to Eq. (19.45). The black dashed line is a numerical fit with a Boltzmann distribution $a_1 \exp(\cos(k)/a_2)$. b) The initial distribution (blue curve) is a cosine function $\rho_0(k) = (1 - \cos(sk))/2$. The red curve is the distribution for $t \to \infty$. Here it is clear that the distribution does not become thermal.

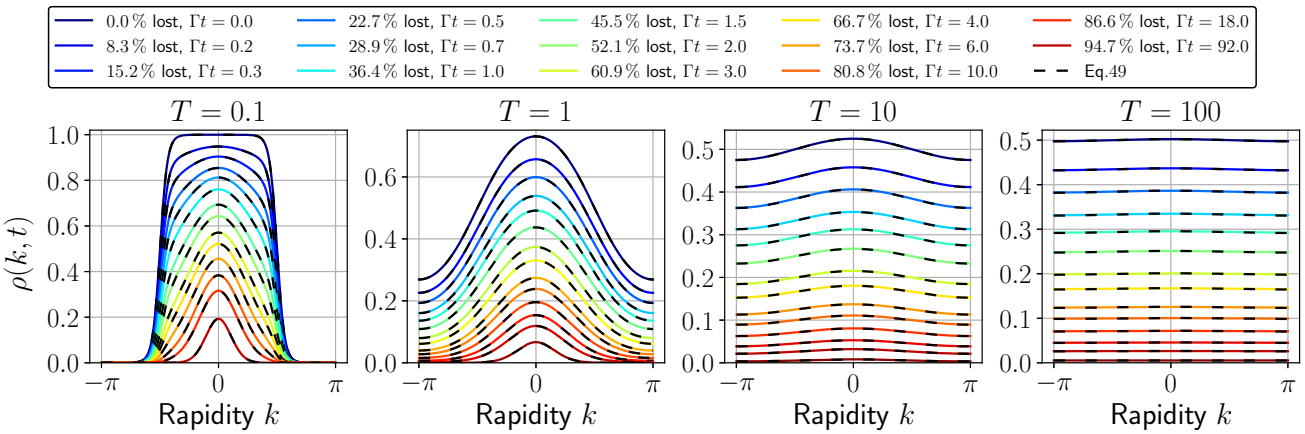


Figure 19.4: Effect of two-body losses on the rapidity distribution. The initial rapidity distribution $\rho(k,0) = 1/(1 + \exp(-\cos(k)/T))$ is chosen with $T = 0.1, 1, 10, 100$ from left to right. The black dashed curve is the analytic solution (see Eq. (19.49)). After several loss events the rapidity distribution takes the form of a gaussian centered at $k = 0$. As in the one-body case, if initially the rapidity distribution is flat then it remains flat under lossy evolution.

19.4.2 Results for $K = 2$

We now consider the time evolution equation for the rapidity distribution for the $K = 2$ case, which is characterized by the functional given by Eq. (19.31). For simplicity, here we focus on initial rapidity distributions $\rho_0(k)$ that are symmetric under reflection $k \to -k$. Since

the master equation is also invariant under $k \to -k$, this property is conserved throughout the entire evolution. Then Eq. (19.31) simplifies to the following expression,

$$F[\rho] = 2\,\rho(k)\,n(t) - \frac{1}{\pi}\cos(k)\rho(k)\int_{-\pi}^{\pi} dq\,\cos(q)\,\rho(q). \tag{19.48}$$

Eq. (19.48) highlights the two distinct contributions to the time evolution of $\rho(k,t)$: the first term in the right-hand side represents a mean-field contribution, as it does not introduce any structure in rapidity space, while the second term is responsible for generating quantum correlations and, consequently, introducing structure in $k-$space.

After some algebra presented in App. 19.8, one can derive an exact (implicit) expression for the rapidity distribution at all times:

$$\rho(k,t) = \rho_0(k) \times \exp -2\Gamma \int_0^t \left(1 - \sigma_0\cos(k)\sqrt{1+\frac{\partial_\tau n(\tau)}{2\Gamma\, n(\tau)^2}}\right) n(\tau)d\tau, \tag{19.49}$$

where $\sigma_0 = \mathrm{sgn}(\int_{-\pi}^{\pi}\cos(k)\rho_0(k)dk)$, with $\mathrm{sgn}(x) = \pm 1$ the sign function. Eq. (19.49) shows that $\rho(k,t)$ is entirely determined by $\rho_0(k)$ and $n(t)$. Notably, it reveals that rapidities are distributed according to a cosine law, with the $k = 0$ mode that has the longest lifetime.

In Fig. 19.4 we show the evolution of the rapidity distribution for initial thermal states at different temperatures, and in Fig. 19.5 we show the corresponding evolution of the mean atom density $n(t)$. It appears that, except for an initial infinite temperature state, the mean density always decays as $n(t) \propto 1/\sqrt{t}$ at very long times, while the density decreases as $1/t$ for an infinite temperature. These two behaviors follow from Eqs. (19.48)-(19.49), as we now explain.

Eq. (19.48) reveals that initial rapidity distributions that have a vanishing first Fourier mode $\int_{-\pi}^{\pi} dq\,\cos(q)\rho(q)$ always follow the exact same dynamics as the mean density, namely

$$n(t) = \frac{1}{1+2n(0)\Gamma t}, \tag{19.50}$$

characterized by a long-term decay as $\sim 1/t$. This power law is then always found for initial rapidity distributions with vanishing first Fourier mode, including infinite temperature states.

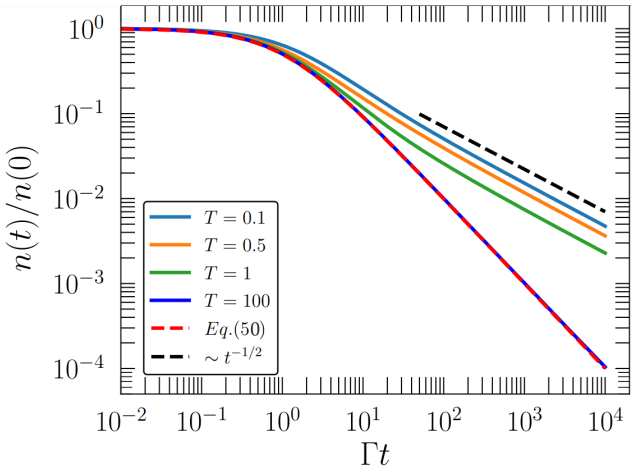


Figure 19.5: The mean density under two-body losses for different thermal initial rapidity distributions $\rho(k,0) = 1/(1+\exp(-\cos(k)/T))$. Colored curves are obtained by solving numerically the time evolution equation (19.15) for the loss functional (19.31) with the Runge-Kutta method. The red dashed line is the mean density associated to an initial rapidity distribution which is flat (i.e. infinite temperature), see Eq. (19.57). The dashed line is the expected long-time behavior $\sim t^{-1/2}$, see Eq.(19.55).

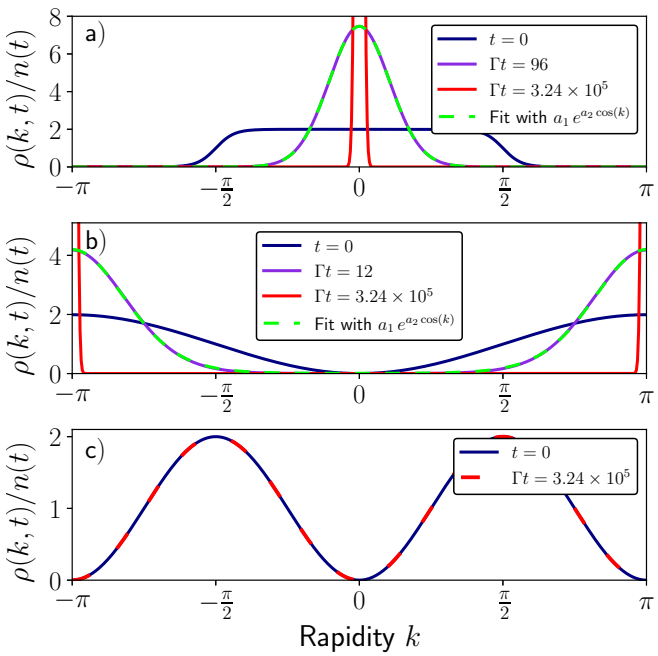


Figure 19.6: Long time behavior of different rapidity distributions rescaled by the corresponding density $n(t)$ under two-body losses. In a), b) and c), the blue curve represents the initial rapidity distribution while the red curve is the rapidity distribution at long time. The violet curve is the rescaled rapidity distribution at an intermediate time. a) The initial distribution is a Fermi-Dirac distributions $\rho_0(k) = (1 + \exp(-\cos(k)/T))^{-1}$ with T=0.1. The green dashed curve is a fit with a Boltzmann distribution $a_1 \exp(a_2 \cos(k))$ where a_2 is positive. b) The initial rapidity distribution is $(1 - \cos(k))/2$ which has a non-vanishing first Fourier mode. The green dashed curve is a fit with a Boltzmann distribution $a_1 \exp a_2 \cos(k)$ where a_2 is negative. c) The initial rapididty distribution is $(1 - \cos(2k))/2$ which has no first Fourier mode.

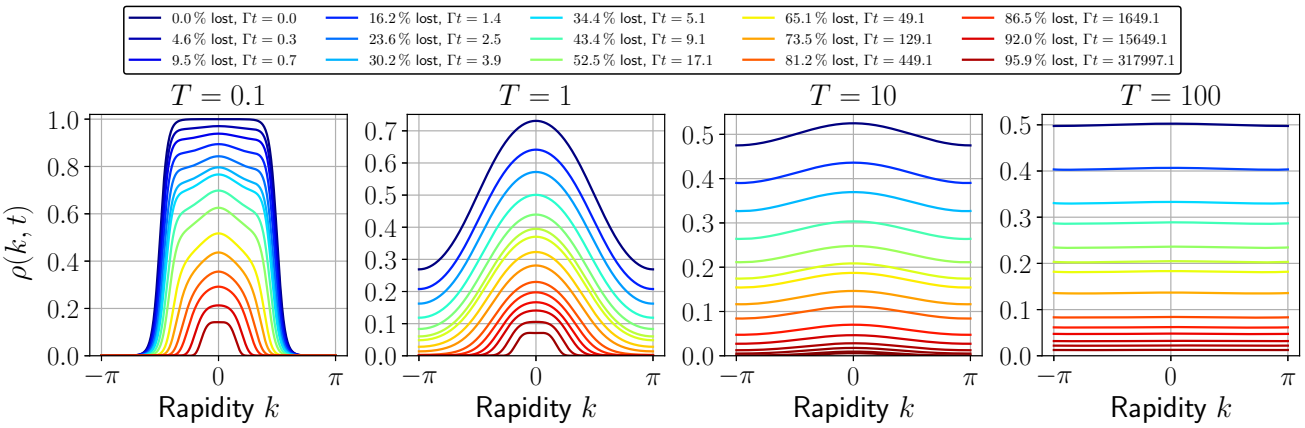


Figure 19.7: Evolution of the rapidity distribution under three-body losses. We numerically solve (19.15) for the loss functional $F[\rho](k)$ corresponding to $K = 3$, using the Runge-Kutta method. The initial rapidity distribution is the Fermi-Dirac distribution $\rho(k, 0) = 1/(1 + \exp(-\cos(k)/T))$ at half filling and for different temperatures $T = 0.10, 1.0, 100.0$ (from left to right).

In contrast, initial rapidity distributions that have a non-vanishing first Fourier mode decay as $\sim 1/\sqrt{t}$ at long times. This can be understood by looking at the long time limit of Eq. (19.49). Let us introduce the two time-dependent functions $g(t) = \int_0^t n(\tau)\, d\tau$ and $f(t) = \int_0^t \sqrt{1 + \frac{\partial_\tau n(\tau)}{2\Gamma\, n(\tau)^2}}\, n(\tau) d\tau$. Numerically we observe that $|\partial_\tau n(\tau)| \ll 2\Gamma n(\tau)^2$ at long times,

as soon as the initial rapidity distributions has a non-vaishing first Fourier mode. Then, expanding at first order in $|\partial_\tau n(\tau)|/(2\Gamma n(\tau)^2)$, $f(t)$ becomes

$$f(t) \simeq g(t) + \frac{1}{4\Gamma} \ln(\frac{n(t)}{n(0)}), \tag{19.51}$$

implying that, at large t, the difference between $f(t)$ and $g(t)$ grows as $\ln(t)$. Integrating Eq. (19.49) over k leads to the mean density

$$n(t) = \frac{e^{-2\Gamma g(t)}}{2\pi} \int_{-\pi}^{\pi} dk\, \rho_0(k)\, e^{2\Gamma\sigma_0 \cos(k) f(t)}. \tag{19.52}$$

Since the function $f(t)$ diverges at large t, the latter integral can be evaluated by the saddle-point approximation; we denote $k^*_{\sigma_0}$ the saddle point: $k^*_{\sigma_0} = 0$ if $\sigma_0 = +1$ and $k^*_{\sigma_0} = \pi$ if $\sigma_0 = -1$. We are thus left with:

$$\begin{aligned} \int_{-\pi}^{\pi} dk\, \rho_0(k)\, e^{2\Gamma\sigma_0 \cos(k) f(t)} & \\ & \underset{t\to\infty}{\simeq} e^{2\Gamma f(t)} \int_{-\infty}^{\infty} dk\, \rho_0(k)\, e^{-\Gamma k^2 f(t)} \\ & = \sqrt{\frac{\pi}{\Gamma f(t)}}\, \rho_0(k^*_{\sigma_0})\, e^{2\Gamma f(t)}. \end{aligned} \tag{19.53}$$

Using Eq. (19.51), we find

$$n(t) \underset{t\to\infty}{\simeq} \frac{1}{\Gamma f(t)} \frac{\rho_0(k^*_{\sigma_0})^2}{4\pi n(0)} \simeq \frac{1}{\Gamma g(t)} \frac{\rho_0(k^*_{\sigma_0})^2}{4\pi n(0)}, \tag{19.54}$$

where, in the second identity, we have used the fact that the logarithmic term in Eq. (19.51) is subleading. Since $n(t) = \partial_t g(t)$, we arrive at an ordinary differential equation of the form $\partial_t g(t) \propto 1/g(t)$. Consequently, $g(t) \propto \sqrt{t}$, and then

$$n(t) \propto t^{-1/2}, \tag{19.55}$$

as expected from our numerical results, see Fig. 19.5. We note that a similar result was found recently in a lattice gas with similar but different two-body loss term [25] as well as in its continuous analog [43], although we stress that the loss functionals and rate equations for these models are different from the ones of this paper.

We conclude this subsection with an investigation of the long time behavior of the rapidity distribution $\rho(k,t)$, which is determined by the mean density $n(t)$ according to Eq. (19.49). We have just we etablished that the first Fourier mode of the initial rapidity distribution strongly influences the long time behavior. In the case of a vanishing first Fourier mode, the rapidity density at time t is simply given (see Eqs. (19.50)-(19.49)) by $\rho(k,t) = \rho_0(k)\, n(t)/n(0)$. The ratio $\rho(k,t)/n(t)$ is then time-independent, as illustrated in Fig. 19.6(c). In contrast, when the first Fourier mode of the initial distribution $\rho_0(k)$ is non-zero, the ratio $\rho(k,t)/n(t)$ loses its dependence on the initial rapidity distribution at very long times. Indeed, in that case the rapidity distribution goes to a low-density, low-temperature, Boltzmann distribution of the form $\rho(k,t)/n(t) \simeq e^{\beta(t)\cos k}$ with the effective inverse temperature $\beta(t) = 2\sigma_0\Gamma f(t)$. This is illustrated for the case of an initial thermal rapidity distribution in Fig. 19.6(a), where we see that the ration $\rho(k,t)/n(t)$ gets concentrated around $k = 0$ and is very close to a Boltzmann distribution. Notice also that the effective temperature $\beta(t)$ is negative when the sign of the first Fourier mode of the initial rapidity distribution is negative. This is illustrated in

Fig. 19.6(b), where we display the ratio $\rho(k,t)/n(t)$ at late time for the far-from-thermal initial rapidity distribution $\rho_0(k) = (1-\cos(k))/2$. We observe that, at late times, the distribution gets concentrated around $k = \pi$ and corresponds to a Boltzmann distribution at negative temperature.

Remarkably, these observations are in stark contrast with our findings for the $K = 1$ case. While we found that, for $K = 1$, the rapidity distribution never goes to a thermal distribution at late time, here for $K = 2$ the distribution goes to a low-density, low-temperature (possibly negative), thermal distribution. This is always true, except in the special case where the first Fourier mode of the rapidity distribution vanishes; in that case the rapididity distribution is simply rescaled by a factor $n(t)/n(0)$ under lossy evolution.

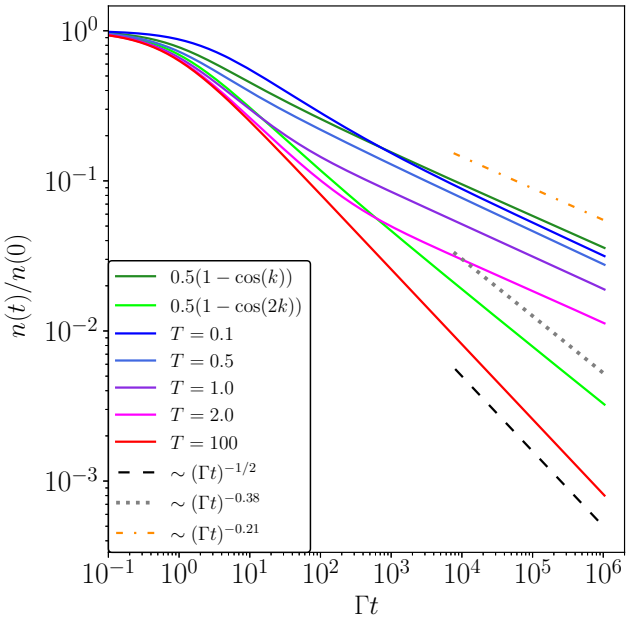


Figure 19.8: Time evolution of the boson density under three-body losses for different initial rapidity distributions at half filling. Colored curves are obtained by solving numerically the time evolution equation of $\rho(k)$ using the Runge-Kutta method with an non-regular time step. From blue to red, the simulation is performed with an initial distribution which is a Fermi-Dirac distribution $\rho(k,0) = (1+\exp(-\cos(k)/T))^{-1}$. The dark and light green curves are respectively obtained from initial rapidity distributions $\rho(k,0) = (1-\cos(k))/2$ and $\rho(k,0) = (1-\cos(2k))/2$. The three dashed lines are a guide to the eye showing power-law decay for three different exponents.

19.4.3 Generic observations for arbitrary K

We now turn to the case of higher K, and draw some general conclusions.

Numerically, we solve the time evolution equation of the rapidity distribution for three-body losses ($K = 3$), see Fig. 19.7 for the evolution of the rapidity distribution from an initial thermal state, and Fig. 19.8 for the atom density $n(t)$. In Fig. 19.7 we see that the effect of three-body losses is to spread the rapidity distribution in rapidity space, as already observed for one-body and two-body losses. We expect that this is a generic effect caused by K-body losses for any K. In Fig. 19.8, we observe that the mean density decays as $t^{-1/2}$ for an initial infinite temperature state, while for any non-zero initial temperature it crosses over to a $t^{-\alpha}$ decay at long times with an exponent $\alpha \simeq 0.21$. This exponent seems to be independent of the initial temperature as long as it is non-zero, see Fig. 19.8. However, for an initial rapidity distribution

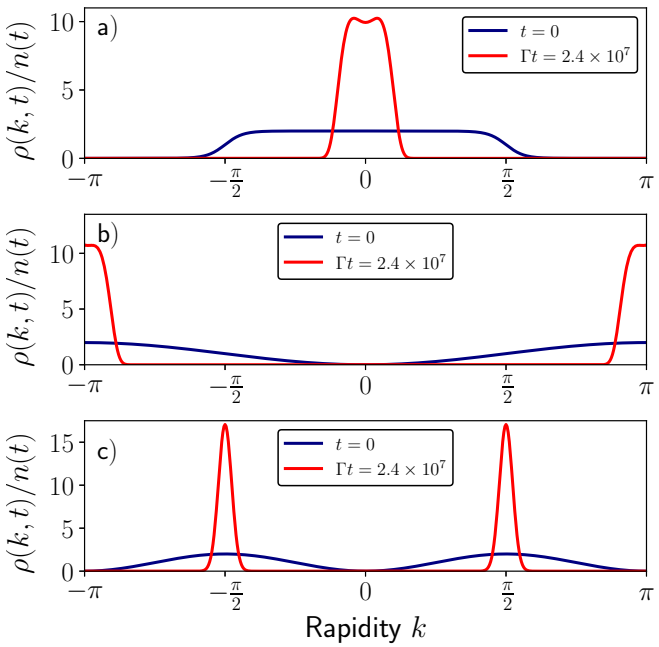


Figure 19.9: Long time behavior of different rapidity distributions rescaled by the corresponding density under three-body losses. For the subplots a, b and c, the blue curve represents the initial rapidity distribution while the red curve is the rapidity distribution at long time. a) The initial distribution is a Fermi-Dirac distributions $\rho_0(k) = 1/(1 + \exp(-\cos(k)/T))$ with T=0.1. b) Non-thermal initial rapidity distribution is $(1 - \cos(k))/2$. c) Non-thermal initial rapididty distribution is $(1 - \cos(2k))/2$.

that is far from thermal, such as for instance $\rho(k, t = 0) = (1 - \cos k)/2$ or $(1 - \cos(2k))/2$, we find that the density also decays as a power-law at late time, although with a different exponent α: the exponent is close to 0.21 for $\rho(k, t = 0) = (1 - \cos k)/2$, and close to 0.38 for $\rho(k, t = 0) = (1 - \cos(2k))/2$.

We have not been able to analytically derive the observed generic power-law decay for $K = 3$ or for higher K, beyond the special case of the initial infinite temperature state. The latter case is easily understood because, for an infinite temperature state the rapidity distribution is constant, $\rho(k) = n$, and the equation (19.15) can be solved analytically. Then the determinant of the matrix B is equal to the determinant of C, and the matrices A reduce to identical and diagonal matrices. Therefore the loss functional is simply given by

$$F_K[\rho](k) = Kn^K, \tag{19.56}$$

which is the result expected from the mean-field approach. Then the solution of the evolution equation (19.15) gives the mean density

$$n(t) = \frac{n(0)}{(1 + n(0)^{K-1} K(K-1)\,\Gamma t)^{1/(K-1)}}. \tag{19.57}$$

Beyond that simple case, we have not been able to express the loss functional in a simple form so as to derive the long-time decay of the mean density.

Similarly to the $K = 1$ and $K = 2$ cases, we have investigated the behavior of the rescaled rapidity distribution $\rho(k, t)/n(t)$ at late times. Recall that this ratio reveals that the gas generically (i.e. unless the first Fourier mode of $\rho(k)$ is tuned to zero) goes to a ‚low-density, low-temperature thermal state for $K = 2$, while for $K = 1$ it never does. In Fig. 19.9 we display this ratio at late time for $K = 3$. Fig. 19.9.(a) corresponds to a thermal initial rapidity distribution, and Figs. 19.9.(b)-(c) to non-thermal initial rapidity distributions $\rho(k, t = 0) = (1 - \cos k)/2$

and $(1-\cos(2k))/2$ respectively. We observe that the rescaled rapidity distribution concentrates around the maxima of the initial rapidity distribution at long times. Even for an initial thermal distribution (Fig. 19.9 (a)), the long time behavior of the density profile can not be described by a Boltzmann distribution, as it looks like a bell-shaped distribution that has a small dip at $k = 0$. A similar conclusion holds for Fig. 19.9.(b). Finally Fig. 19.9.(c) shows the emergence of peaks localised at $k = \pm\pi/2$. We conclude that, in contrast with the $K = 2$ case, the late-time rapidity distribution is generically non-thermal.

19.5 Harmonically trapped gas

In many cold atom experiments, the gas lies in a longitudinal trapping potential. This prompts us to study the influence of the trapping potential on the dynamics of our lossy lattice hard-core gas. For simplicity we restrict to a harmonic potential $V(x) = \omega^2 x^2/2$.

We adopt a coarse-grained perspective of the gas: we assume that the gas can be divided into fluid cells which contain a large number of bosons, and that the state of the gas within each fluid cell $[x, x+dx]$ is a certain macrostate represented by the local density of rapidities $\rho(x, k)$. Such coarse-grained descriptions have been very successful lately in describing the out-of-equilibrium quantum many-body dynamics of nearly integrable gases [74, 73, 64, 80, 81, 75, 82]. Here we investigate the effect of losses on our lattice hard-core gas within that coarse-grained description.

The equation satisfied by the position-dependent rapidity distribution is

$$\begin{aligned}&\partial_t\rho(x,k,t) + \sin(k)\,\partial_x\rho(x,k,t) - \omega^2 x\,\partial_k\rho(x,k,t)\\ &= -\Gamma F[\rho(x,.,t)](k).\end{aligned} \tag{19.58}$$

In the first line, the term $\partial_x \sin(k)\rho(x,k)$ corresponds to the gradient of the current of quasi-particles with rapidity k, $j(x,k) = \sin(k)\rho(x,k)$. Here $\sin(k)$ is the group velocity of quasi-particles with lattice dispersion relation $\varepsilon(k) = -\cos(k)$. The term $-\omega^2 x\,\partial_k\rho(x,k)$ in Eq. (19.58) corresponds to Newton's second law, and encodes the fact that the quasi-particles feel the harmonic potential and are accelerated according to $\dot{k} = -\partial_x V(x) = -\omega^2 x$. Finally, the r.h.s of Eq. (19.58) is the loss term at position x, which follows from the assumption that the gas is locally homogeneous so that we can apply the formalism developed in previous sections, this time within each fluid cell $[x, x + dx]$.

19.5.1 Numerical method

Our main goal in this section is to solve numerically the evolution equation (19.58). For this we use a split-step method. Assuming that we know the rapidity distribution $\rho_t(x,k)$, from time t to $t + \Delta t$ we first compute the new rapidity distribution $\rho'_{t+\Delta t}(x,k)$ generated by the transport of quasi-particles, and then compute $\rho_{t+\Delta t}(x,k)$ from $\rho'_{t+\Delta t}(x,k)$ by implementing localized lossy evolution during a time step Δt.

This gives the following scheme. For the transport part we rely on the fact that the underlying dynamics is the one of non-interacting quasi-particles. Each quasi-particle at position (x,k) in phase space evolves as

$$\begin{cases}\dfrac{dx}{dt} = \sin(k)\\[2ex] \dfrac{dk}{dt} = -\omega^2 x.\end{cases} \tag{19.59}$$

Let us call $X(x,k,t)$ and $K(x,k,t)$ the analytical solution of that equation. Then, the first step of our numerical scheme is

$$\rho'_{t+\Delta t}(X(x,k,t), K(x,k,t)) = \rho_t(x,k), \tag{19.60}$$

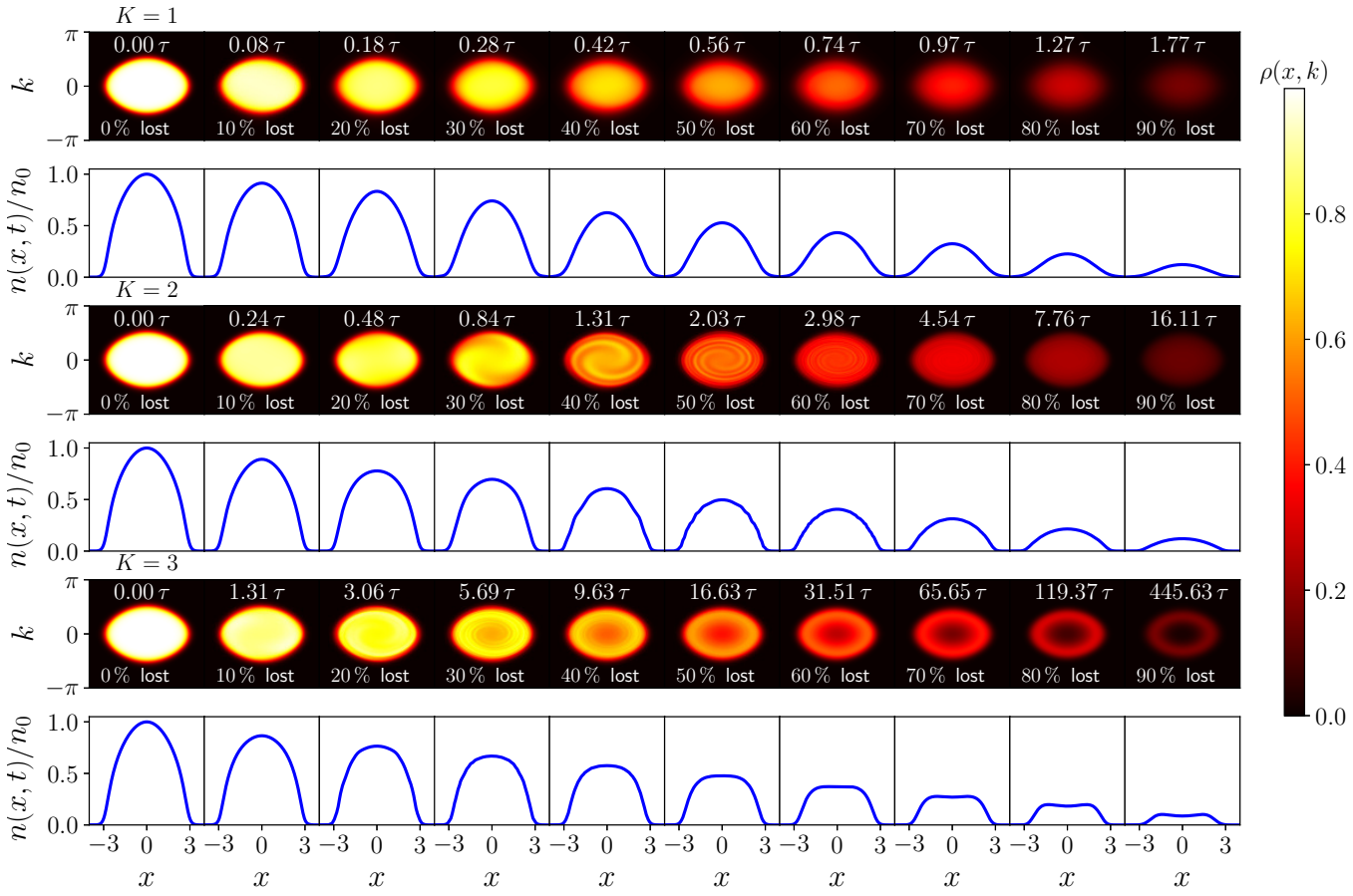


Figure 19.10: Evolution of the position-dependent distribution $\rho(x,k)$ in a harmonic trap and under K-body losses. The initial distribution is $\rho(x,k) = 1/(1+\exp((-\cos(k)+\omega^2x^2/2)/T))$ with harmonic trap frequency ω=1/2 and temperature T=0.1. The loss rate is Γ=0.1. The different snapshots show increasing times in units of $\tau = 2\pi/\omega$. Below each phase portrait we add the corresponding density profiles $n(x,t)$ obtained by integrating $\rho(x,k,t)$ over k. The density profiles are rescaled by the initial density at the trap center $n_0 = n(x=0,t=0) = 0.5$. The two first rows show the effects of one-body losses (K=1) on the distribution in phase-space and the corresponding density profiles. The two next rows show the effects of two-body losses (K=2) and the last two rows show the effect of three-body losses (K=3). Numerically, the x and k-axis are discretized with 300 points on each axis, and we use a time step of $\Delta t = 0.05$; we provide a check of convergence of the numerical method in Appendix 19.11.

and the second step is

$$\rho_{t+\Delta t}(x,k) = y(\Delta t, k), \tag{19.61}$$

where $y(\tau,k)$ is the solution of the differential equation

$$\partial_\tau y(\tau,k) = -\Gamma F[y(\tau,.)](k), \qquad y(0,k) = \rho'_{t+\Delta t,x}. \tag{19.62}$$

The rapidity distribution $\rho(x,k)$ is discretized on a regular grid in phase space, and the two steps in Eq. (19.60) and Eq. (19.61) are implemented as follows.

For the transport step in (19.60), we numerically integrate Eq. (19.59) for each point of the grid. Then, starting from the values $\rho_t(x,k)$ on the regular grid in phase space, we move each node of the grid according to $(x,k) \to (X(x,k,\Delta t), K(x,k,\Delta t))$. This gives us the rapidity distribution after transport over a time Δt, which however is defined on a new grid, different from the initial regular grid. To get the new rapidity distribution $\rho'_{t+\Delta t}(x,k)$ on the initial regular grid, we use linear interpolation. Notice that the whole procedure, including both the

numerical integration of (19.59) and the linear interpolation, needs to be performed only once. To benchmark this transport part, we have checked that this method gives excellent numerical precision for the simulated transport in the absence of losses.

The second step consists in solving numerically the differential equation (19.62) for each column of the grid in phase-space. The solution of each differential equation is obtained by the Runge-Kutta method with the initial condition $y(0,k) = \rho'_{t+\Delta t,x}$. We do this for each column of the grid, and we thus get the new space-dependent rapidity distribution $\rho_{t+\Delta t}(x,k)$ according to Eq. (19.61).

The combination of the two steps allows us to go from a rapidity distribution $\rho_t(x,k)$ to the new distribution $\rho_{t+\Delta t}(x,k)$, both defined on the same phase-space grid. We then repeat this procedure many times with a small time step Δt to simulate the lossy evolution of the gas in the trap.

19.5.2 Results

We have performed numerical simulations of the evolution of the position-dependent rapidity distribution $\rho(x,k)$ under K-body losses using the algorithm presented in the previous section, see Fig. 19.10. For the initial state, we use a thermal (Fermi-Dirac) rapidity distribution $\rho(x,k) = 1/(1+\exp(-\cos(k)+\omega^2x^2/2-\mu)/T)$, where μ is the chemical potential and T the temperature.

Our numerical study allows us to make the following general observations, illustrated in Fig. 19.10. For all K (we have simulated $K = 1,2,3$) the distribution typically spreads in phase-space, similarly to the homogeneous case. However, while the number of particles decays exponentially for $K = 1$, the loss dynamics is much slower for higher K, and this has visible effects on the distribution of rapidities after a given percentage of lost atoms.

For $K = 1$ we observe that the edges of the phase-space distribution get depopulated very fast and quickly results in a halo around the origin. The spreading is also clearly visible in real space in the particle density profile $n(x) = \int \rho(x,k)dk/(2\pi)$, see the second line of Fig. 19.10.

For $K = 2$, the situation is a little bit different, see Fig. 19.10. Until ∼20% of the atoms have been lost, the dynamics is similar to the one for $K = 1$, but after that we observe the formation of spirals in the bulk of the phase-space distribution. The spirals become more visible as the ratio Γ/ω is increased, see Appendix 19.10. Compared to $K = 1$, the bulk of the distribution also gets depopulated, leading to an approximately uniform circular droplet in phase-space, with a density that decays with time. This is visible in Fig. 19.10 after ∼50% of the atoms have been lost; we note that, compared to the case of one-body losses, the distribution spreads less significantly in phase-space.

For $K = 3$, we also observe a small spiral appearing at the center of the distribution after ∼30% of the atoms have been lost. This spiral remains localised at the center during the dynamics. Interestingly, as one can see from the fifth line in Fig. 19.10, this time it is the center of the phase-space distribution that decreases faster compared to the edges. After ∼60% of atoms lost, a hole starts developing at the center of the phase-space distribution, and the latter looks more and more like a ring. This is a clear signature of a strongly out-of-equilibrium gas in the trap, with a population inversion: the higher-energy single-particle orbitals get more populated than the low-energy ones. This effect is reflected in the corresponding real-space particle density $n(x)$ then acquires a doubly-peaked shape, with a local minimum at $x = 0$, similarly to what we observed also in the homogeneous case.

Finally, having simulated the dynamics of the position-dependent rapidity distribution $\rho(x,k)$, one can easily get the evolution of the total particle number $N(t)$ by integrating $\rho(x,k,t)$ over x and k at fixed time t. For one-body losses, one always finds an exponential decay $N(t) = e^{-\Gamma t}N(0)$. For two-body and three-body losses the result is more interesting.

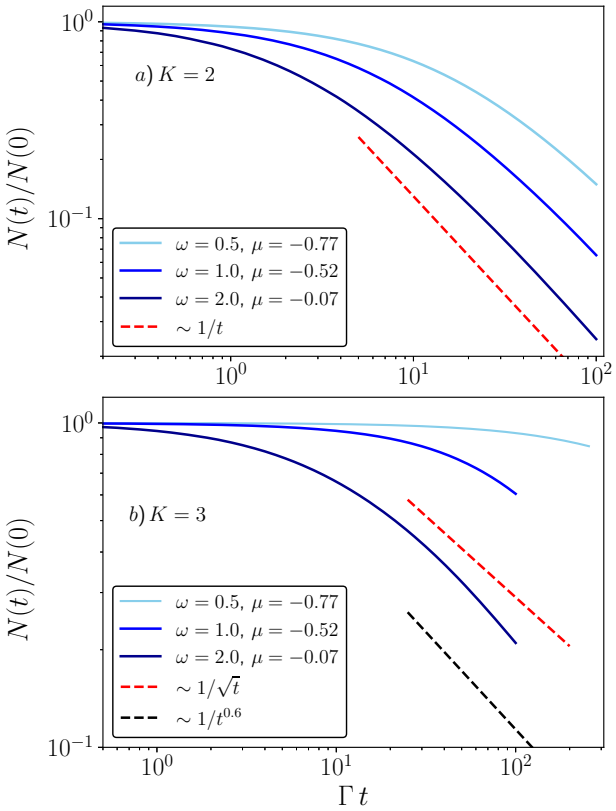


Figure 19.11: Time evolution of the total particle number under two-body losses. The initial distribution is $1/(1 + \exp((-\cos(k) + \omega^2 x^2/2 - \mu)/T)$, where $T = 0.1$ and μ, the chemical potential, is chosen to fix the initial mean particle density to 0.5 and $N(0)$ represents the initial number of particle. The loss rate is Γ=0.1. (a) Results for two-body losses. The red dashed line is the long time behavior of the total particle number for the homogeneous case with an initial rapidity distribution which has no first Fourier mode (see Fig.(19.4)). (b) Three-body losses. The black dashed line represents the asymptotic behavior of the mean density and the red dashed line is the mean-field prediction.

In Fig. 19.11.(a), we show the evolution of the mean density under two-body losses for different trap frequencies ω. Starting with a thermal distribution at temperature T and chemical potential μ, we observe that the mean density decreases at long times as $\sim 1/t$, a result that coincides with the mean-field (or infinite temperature) decay for the homogeneous gas. Moreover, we see that the higher the trap frequency the faster the decay of the total particle number. Indeed, as the trap frequency is increasing, the distribution concentrates around the center of the confinement potential. Since the density of particles is higher, the probability of finding two neighboring bosons increases and the depopulation is then accelerated.

For three-body losses, we see in Fig. 19.11.(b) that, like in the two-body case, a stronger confinement speeds up the decrease of total particle number. However, this time we do not observe a clear convergence towards the expectation from the mean-field (or infinite temperature) result for the homogeneous case, which would be $N(t) \sim t^{-1/2}$. We observe a number of particles that decreases approximately as a power-law $\sim t^{-\alpha}$ with an exponent $\alpha \simeq 0.6$. Our numerics does not allow us to draw a clear conclusion as to whether or not this would go to the mean-field exponent 1/2 at longer times. Nevertheless, let us stress that, qualitatively, the effect of three-body losses is the same as in the two-body case: compared to the homogeneous case, the trap dramatically speeds up the losses. This can be explained by the same mechanism as in the two-body case: since the density of particles is higher in the center, the probability of finding three neighboring bosons increases and the losses are enhanced.

19.6 Conclusion

We have studied the effects of K-body losses on a gas of lattice hardcore bosons, in particular their effect on the thermalisation of the gas at late time. For this, we have relied on the hypothesis of adiabatic losses used previously in Refs. [40, 76, 77, 78, 25]. We derived analytical results for the loss functional for any integer K in the form of a small finite determinant, and closed expressions in the cases $K = 1, 2$.

For $K = 1$ and $K = 2$, we solved analytically the time evolution equation of the rapidity distribution of the spatially homogeneous gas. In the case of one-body losses, our formula (19.45) shows that the loss functional is in general non-linear and non-local in rapidity space, as already observed for the continuous Lieb-Liniger gas in Ref. [40]. After investigating the long time behavior of the rapidity distribution, we concluded that one-body losses do not drive the gas to a low-density thermal equilibrium state at long times. In the case of two-body losses, our formula (19.49) gives an implicit expression for the rapidity distribution and using a similar method as in Ref. [25], we were able to investigate the long time behavior of the rapidity distribution and the mean particle density. In particular, we found that it decays generically as $\sim 1/\sqrt{t}$, except when the first Fourier mode of the initial distribution vanishes; in that case the particle density decays as $\sim 1/t$. A similar conclusion was drawn for a different loss process in Refs.[25, 43].

Finally, we considered the inhomogeneous system consisting in a lattice hardcore bosons gas in harmonic potential. We provided a numerical method to solve the dynamics combining the effects of the losses and of the trapping potential. We observed that for $K \geq 2$ the trap generically speeds up the decay of the total particle number. We also found that the gas typically evolves towards a highly non-thermal state; in particular for $K = 3$ we observe a striking ring-shaped distribution in phase space, which signals a inversion of population (i.e. higher energy single-particle orbitals get more populated than the lower energy ones), see Fig. 19.10. Further investigations are needed to draw more quantitative conclusions about the dynamics in the trap.

Note: while we were finishing this paper, a preprint by Perfetto, Carollo, Garrahan and Lesanovsky appeared [39], where a similar model of spinless fermions with $K = 2, 3, 4$-body losses is studied within the context of quantum reaction-diffusion dynamics of annihilation processes. Our hard-core model coincides with their model for K even, but not for K odd because of the Jordan-Wigner mapping, as we explained in detail in Sec. 19.3. Perfetto *et al.* do not focus on the effect of losses on the rapidity distributions of the gas, but rather on the evolution of the number of particles in the homogeneous setting. For the case of K even, where our models coincide, their findings about the evolution of the number of particles in the homogeneous setting are in agreement with ours.

19.7 Deriving solution (19.45)

For one-body losses, the time evolution of the rapidity distribution $\rho(t, k)$ is given by

$$\partial_t \rho = -\Gamma \left(\rho - (\rho^2 - \mathcal{H}(\rho)^2 - n^2(t)) + 2n(t)\mathcal{H}'(\rho) \right), \tag{19.63}$$

where Γ is the loss rate. We introduced the Hilbert transform $\mathcal{H}(f(x)) = \frac{1}{2\pi} \int_{-\pi}^{\pi} dy \frac{f(y)}{\tan(\frac{x-y}{2})}$ with $f(x)$ a periodic function. The mean density $n(t)$ is known: $n(t) = n_0 e^{-\Gamma t}$.

Here the rapidity distribution is a 2π-periodic real-valued function. From the rapidity distribution, we can construct a complex-valued function whose the imaginary part is the Hilbert transform of the real part: $Q = \rho(k) + i\mathcal{H}(\rho(k))$. Such a function is called an analytic signal

and can be analytically continued to the upper half-plane: the function $Q(z) = \frac{i}{2\pi}\int_{-\pi}^{\pi} \frac{dq\,\rho(q)}{\tan(\frac{z-q}{2})}$ is well-defined for $\Im(z) > 0$ and $\Re(z) \in [-\pi, \pi]$ and reduces to $\rho(k)$ on the real axis.

Taking the Hilbert transform of (19.63)

$$\partial_t \mathcal{H}(\rho) = -\Gamma\left(\mathcal{H}(\rho) - \mathcal{H}(\rho^2 - \mathcal{H}(\rho)^2) + 2n(t)\mathcal{H}(\mathcal{H}'(\rho))\right) \tag{19.64}$$

and adding (19.63) and i (19.64), one has

$$\partial_\tau Q(\tau, z) = -(Q(\tau, z) - i2n\partial_z Q(\tau, z) - Q^2(\tau, z) + n^2(\tau)). \tag{19.65}$$

We used some properties of the Hilbert transform: i) $\mathcal{H}(\mathcal{H}(f)) = -f$, ii) $\mathcal{H}'(f) = \mathcal{H}(f')$. Moreover, since $Q^2(z)$ is analytic for $\Im(z) > 0$, the function $\rho^2 - \mathcal{H}(\rho)^2 + i2\rho\mathcal{H}(\rho)$ is an analytic signal if and only if $\mathcal{H}(\rho^2 - \mathcal{H}(\rho)^2) = 2\rho\mathcal{H}(\rho)$.
Introducing the function $Y(\tau, z) = Q(\tau, z + i2n(\tau))$, one gets

$$\partial_\tau Y(\tau, z) = Y^2(\tau, z) - Y(\tau, z) - n^2(\tau) \tag{19.66}$$

This equation can be solved if one assumes $Y(\tau, z) = \alpha(\tau, z)\, e^{-\tau}$. Indeed, thanks to this trick the above equation reduces to

$$\partial_\tau \alpha(\tau, z) = (\alpha^2(\tau, z) - n_0^2)\, e^{-\tau} \tag{19.67}$$

Putting all terms depending on α in the left-hand side, one has

$$\int \frac{d\alpha}{\alpha^2 - n_0^2} = -e^{-\tau} + C_1, \tag{19.68}$$

which leads to

$$\alpha(\tau, z) = n_0 \tanh(n_0\, e^{-\tau} + C_2). \tag{19.69}$$

The initial condition $Y(0, z) = Y_0$ sets the constant: $C_2 = \tanh^{-1}(Y_0/n_0) - n_0$. Thus, one can write

$$\begin{aligned} Y(\tau, z) &= n(\tau) \tanh(n_0(e^{-\tau} - 1) + \tanh^{-1}(Y_0/n_0)) \\ &= n(\tau)\left(\frac{\tanh(n_0(e^{-\tau} - 1)) + Y_0/n_0}{1 + \tanh(n_0(e^{-\tau} - 1))Y_0/n_0}\right). \end{aligned} \tag{19.70}$$

Finally, the rapidity distribution reads

$$\rho(t, k) = n_0 e^{-\Gamma t}\Re\left(\frac{\tanh(n_0(e^{-\Gamma t} - 1)) + \frac{i}{2\pi n_0}\int_{-\pi}^{\pi} dq \frac{\rho_0(q)}{\tan(\frac{k-q}{2} + in_0(1 - e^{-\Gamma t}))}}{1 + \frac{i}{2\pi n_0}\tanh(n_0(e^{-\Gamma t} - 1))\int_{-\pi}^{\pi} dq \frac{\rho_0(q)}{\tan(\frac{k-q}{2} + in_0(1 - e^{-\Gamma t}))}}\right). \tag{19.71}$$

19.8 Derivation of Eq. (19.49) of the main text

In this section we present the main steps to derive the exact expression of the rapidity distribution in the homogeneous case for $K = 2$. We consider the time evolution of $n(t)$ written as:

$$\partial_t n(t) = \frac{1}{2\pi}\int_{-\pi}^{\pi} \partial_t \rho(k, t) dk. \tag{19.72}$$

We now insert the evolution equation (19.48) obtaining:

$$\begin{aligned}\partial_t n(t) =& -\frac{2\Gamma n(t)}{2\pi}\int_{-\pi}^{\pi}\rho(k,t)dk + \frac{\Gamma}{2\pi^2}\left(\int_{-\pi}^{\pi}\cos(k)\rho(k,t)dk\right)^2 \\ =& -2\Gamma n(t)^2 + \frac{\Gamma}{2\pi^2}\left(\int_{-\pi}^{\pi}\cos(k)\rho(k,t)dk\right)^2 \end{aligned} \tag{19.73}$$

By inverting the latter relation, one obtains:

$$\left|\int_{-\pi}^{\pi}\cos(k)\rho(k,t)dk\right| = \pi\sqrt{\frac{2}{\Gamma}\left(\partial_t n(t) + 2\Gamma n(t)^2\right)}, \tag{19.74}$$

where $|\bullet|$ denotes the absolute value. At this point of the derivation it is useful to introduce the following variable: $\sigma(t) = \mathrm{sgn}(\int_{-\pi}^{\pi}\cos(k)\rho(k,t)dk)$, with $\mathrm{sgn}(x)$ being the sign function. We now claim that the function $\sigma(t)$ is solely determined by its value at initial time, i.e. $\sigma(t) = \sigma(0) \doteqdot \sigma_0$, the argument goes as follows. (i) If the first Fourier mode vanishes at some time t, then it must vanish also at any later time. This follows from Eq. (19.48). (ii) This implies that the sign of the first Fourier mode is continuous in time. Since it can take only discrete values, it is in fact a constant.

By inserting the latter equation in Eq. (19.48) the time evolution of the rapidity distribution can be then recasted into the following form:

$$\dot{\rho}(k,t) = -2\Gamma\,\rho(k)\,n(t) + \Gamma\sigma_0\cos(k)\rho(k)\sqrt{\frac{2}{\Gamma}\left(\partial_t n(t) + 2\Gamma n(t)^2\right)}. \tag{19.75}$$

We now divide both sides by $\rho(k,t)$ and then integrate:

$$\ln\left(\frac{\rho(k,t)}{\rho_0(k)}\right) = -2\Gamma\int_0^t n(t')dt' + \Gamma\sigma_0\cos(k)\int_0^t\sqrt{\frac{2}{\Gamma}\left(\partial_{t'} n(t') + 2\Gamma n(t')^2\right)}dt'. \tag{19.76}$$

By exponentiating the latter equation we get:

$$\rho(k,t) = \rho_0(k)\exp -2\Gamma\int_0^t n(t')dt' + \sigma_0\cos(k)\int_0^t\sqrt{\frac{2\left(\partial_{t'} n(t') + 2\Gamma n(t')^2\right)}{\Gamma}}dt', \tag{19.77}$$

this concludes the derivation of Eq. (19.49).

19.9 Additional data for the homogeneous $K = 2$ case

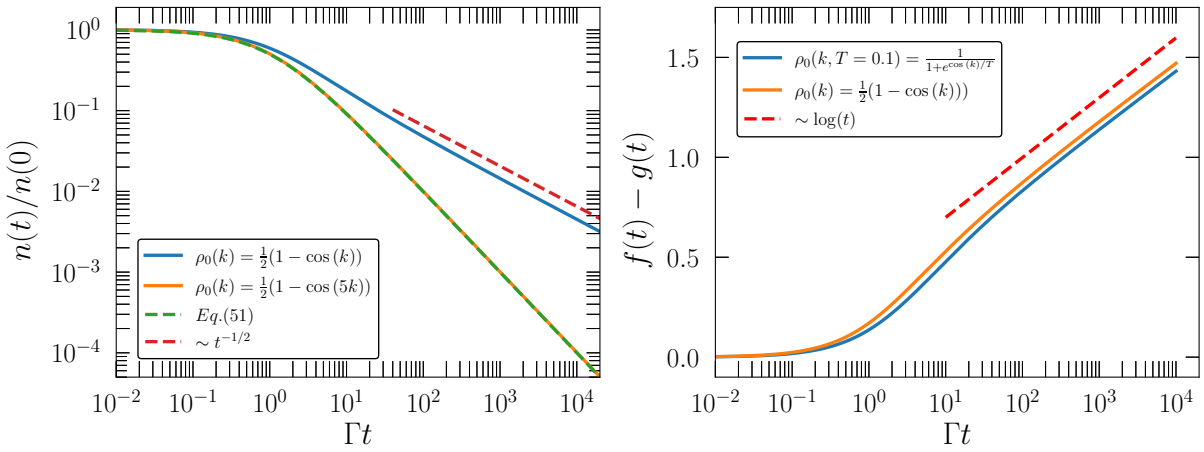


Figure 19.12: Left panel: the mean density under two-body losses for two different non-thermal rapidity distributions. Solid colored curves are obtained by solving numerically the time evolution equation of $\rho(k)$ for the loss functional (19.31) with a time step dt=0.05 and a loss rate Γ =0.1. The red dashed line is the long time limit of the mean density given by Eq. (19.50). The long time behavior for non vanishing first Fourier mode distributions is presented by the black dashed line (see Eq.(19.55)). Right panel: difference between the two function $f(t)$ and $g(t)$ defined in the main text for a thermal and non-thermal distributions.

In this section we present additional data concerning the homogeneous $K = 2$ case. In particular, we show in Fig. 19.12 (left panel) the dynamics of the mean density for two different initial rapidity distributions which are not thermal. Firstly, we consider an initial distribution given by $\rho_0(k) = \frac{1}{2}(1 - \cos(k))$, which has first Fourier mode different from zero. Secondly, we consider $\rho_0(k) = \frac{1}{2}(1 - \cos(5k))$, whose first Fourier mode vanishes. We see that the dynamics induced by the former distribution has a longtime behaviour guven by $\sim 1/\sqrt{t}$, whereas the latter, due to its vanishining first Fourier mode, is described by Eq. (19.50). This corroborates our findings for initial thermal distributions presented in the main text. Moreover, we show in Fig. 19.12 (right panel) the quantity $f(t) - g(t)$, where $g(t) = \int_0^t n(\tau)\, d\tau$ and $f(t) = \int_0^t \sqrt{1 + \frac{\partial_\tau n(\tau)}{2\Gamma n(\tau)^2}} n(\tau) d\tau$ for two different rapidity distributions. In the main text we took the first order expansion of $f(t)$ resulting in a logarthmic growth for the quantity $f(t) - g(t)$, which is thus corroborated by the numerical data here presented. As such, given an initial rapidity distribution whose first Fourier mode is non-vanishing, one has a longtime decay of the mean density given by $n(t) \sim 1/\sqrt{t}$.

19.10 Brief discussion on the spiral in figure Fig. 19.10

During the evolution of the position-dependent rapidity distribution in phase space (see Fig. 19.10) , the distribution exhibits a spiral, which is clearly visible after 40% of atoms lost for two-body losses. In principle, in a regime where the trap frequency ω is highly dominating the loss rate Γ, one expects that the distribution remains rotation invariant at all times. This implies that the spiral vanishes for $\omega \gg \Gamma$. To check this statement we compare the quantity $\rho(x, k)$ for two distincts values of ω (see the figure below). In figure Fig. 19.13 We can see that the spiral appearing for $\omega = 5\Gamma$ covers entirely the distribution, while for $\omega = 20\Gamma$ the spiral is localised at the distribution's center. Moreover, in the case $\omega = 20\Gamma$ we observe

small oscillations between the edges and the center of the distribution. The frequency of these oscillations is high compared to the center of the distribution.

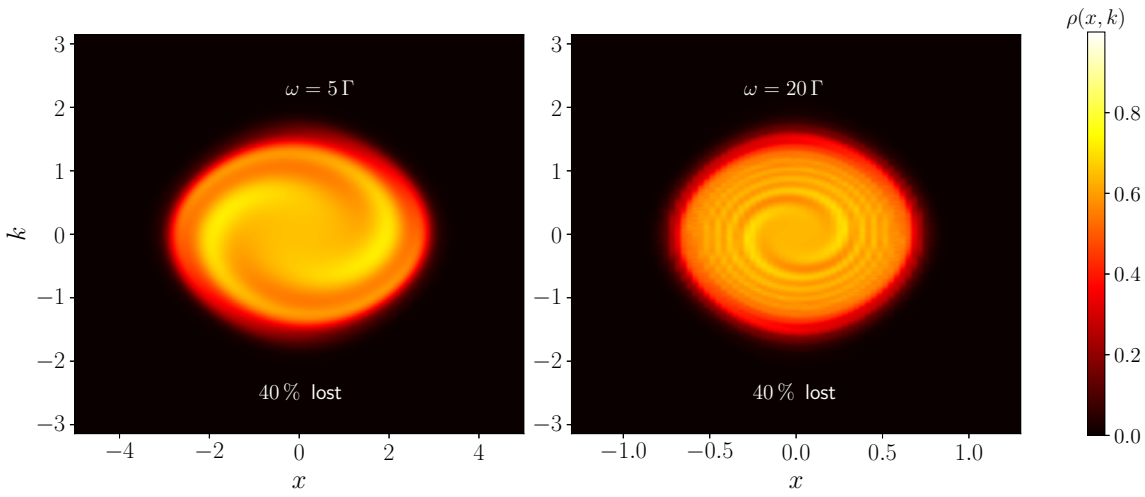


Figure 19.13: Phase portraits showing the spiral for two different values of ω. The initial distribution is identical to the one used in figure Fig. 19.10 and here we only consider the distribution after 40% of atoms lost.

19.11 Convergence of numerical results

In this Appendix we provide evidence for numerical convergence of the results displayed in Fig. 19.10. We have performed the same simulation as the one in Fig. 19.10 with a bigger numerical time step $\Delta = 0.25$ (instead of $\Delta = 0.05$). The physical parameters we use are (as in Fig. 19.10):

$$\rho(x, k, t = 0) = \frac{1}{1 + \exp\left(-\cos(k) + \omega^2 x^2/2\right)T}, \tag{19.78}$$

with $T = 0.1$ and $\omega = 1/2$. We show results for one-body losses ($K = 1$), with a loss rate Γ=0.1.

In Fig. 19.14, we compare the results obtained for two different time steps $\Delta t = 0.25$ (first row) and $\Delta t = 0.05$. We see that the results are converged.

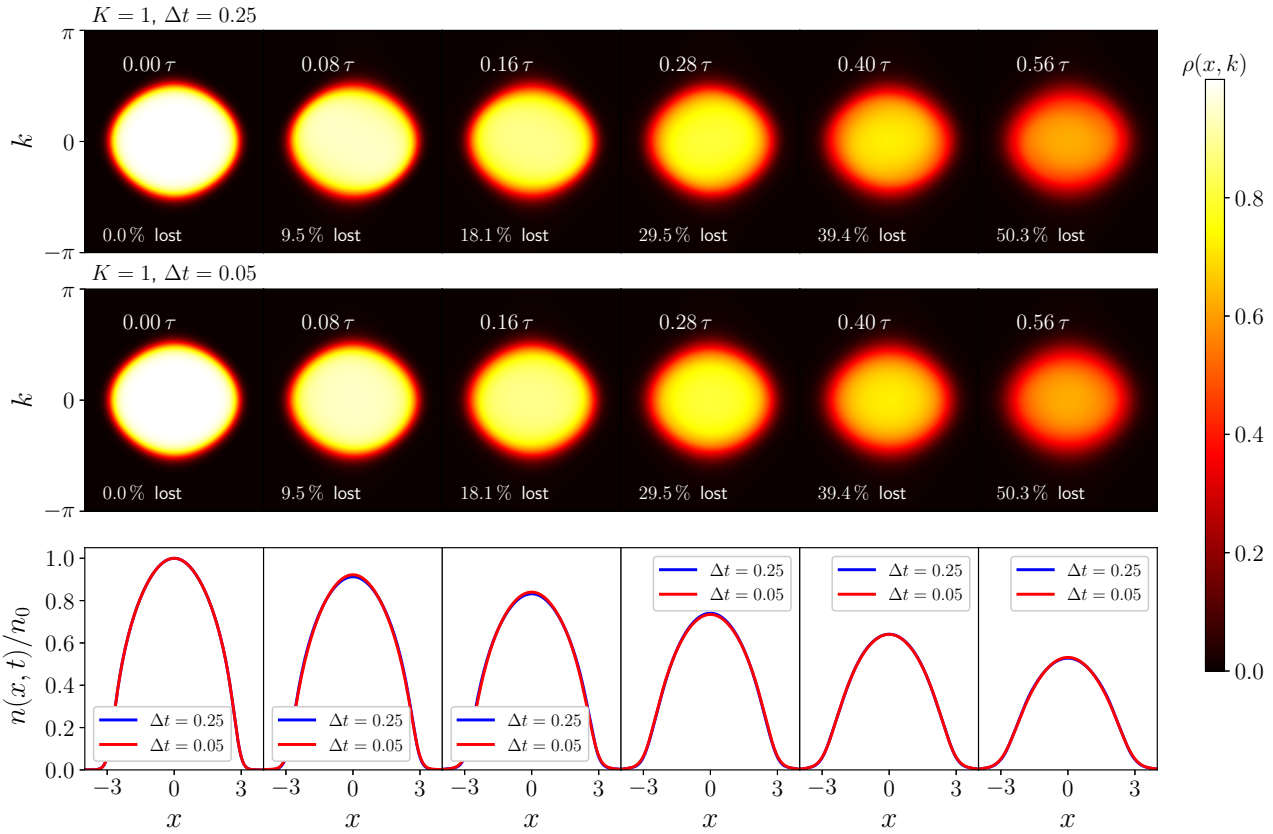


Figure 19.14: Dynamics of the local rapidity distribution $\rho(x,k)$ in phase space under one-body losses. The two first lines show the evolution of the distribution in phase space for two different time steps $\Delta t = 0.25$ and $\Delta t = 0.05$. The trap frequency is fixed to $\omega = 1/2$, $\Gamma = 0.1$ is the loss rate and τ is defined as $\tau = 2\pi/\omega$. The last line corresponds to the density profils obtained by integrating over k the local rapidity distribution. The numerical results are converged.

20 Time evolution of local observables after quenching to an integrable model by Caux, Essler

Abstract

We consider quantum quenches in integrable models. We argue that the behaviour of local observables at late times after the quench is given by their expectation values with respect to a single representative Hamiltonian eigenstate. This can be viewed as a generalization of the eigenstate thermalization hypothesis to quantum integrable models. We present a method for constructing this representative state by means of a generalized Thermodynamic Bethe Ansatz (GTBA). Going further, we introduce a framework for calculating the time dependence of local observables as they evolve towards their stationary values. As an explicit example we consider quantum quenches in the transverse-field Ising chain and show that previously derived results are recovered efficiently within our framework.

20.1 Main Theory

Introduction. Recent years have witnessed dramatic progress in the study of isolated quantum systems out of equilibrium, in particular in systems of optically trapped ultra-cold atomic gases. Key to these advances is the weak coupling to the environment, which allows the realization of essentially unitary time evolution on long time scales [1, 3, 3, 6, 9, 7]. The experimental

results have stimulated intense theoretical efforts aimed at answering fundamental questions such as: Do observables relax to time-independent values? What are the principles determining these values? How can one describe the relaxation towards stationary behaviour?

There is compelling evidence that nonequilibrium time evolution is strongly affected by dimensionality and the presence of conservation laws. The experiments of [3] on trapped ^{87}Rb atoms established that three-dimensional condensates rapidly relax to a stationary state characterized by an effective temperature, whereas constraining the motion of atoms to one dimension greatly reduces the relaxation rate of the momentum distribution function. These results spurred a flurry of theoretical activity aimed at shedding light on the precise effects of integrability on the nonequilibrium dynamics of many-body quantum systems (see [7, 8, 9, 80, 11, 12, 19, 13, 38, 26, 14, 27, 20, 23, 24, 28, 29, 30, 16, 21, 22, 17, 11, 15, 31, 32, 33, 34] and references therein).

So far two basic paradigms have emerged in translationally invariant models: at late times subsystems either thermalize, i.e. are characterized by a Gibbs distribution with an effective temperature, or they are described by a generalized Gibbs ensemble (GGE) [8]. When the time evolution occurs under the action of an integrable Hamiltonian, the GGE is applicable. Questions regarding the approach towards the steady state long after the quench remain difficult to tackle. Short and intermediate times can be efficiently studied by algorithms based on matrix-product states [13, 14, 15, 9], while numerical methods based on integrability have allowed to access arbitrary times in finite systems [16, 17, 11]. The only cases which have been largely understood are noninteracting theories such as the transverse field Ising chain [19, 20, 21, 22, 24, 23].

It is our purpose here to develop an efficient framework for the description of the out-of-equilibrium dynamics of a system evolving under an integrable Hamiltonian $H(h)$, where h is a system parameter such as an interaction strength or a magnetic field. Our approach applies equally to quantum spin chains and to continuum theories like the Lieb-Liniger model. The situation we have in mind is that of a quantum quench: a given system is prepared in the ground state $|\Psi\rangle$ of the short-ranged Hamiltonian $H(h_0)$, which itself may not be integrable. At time $t = 0$ the system parameter is suddenly changed from h_0 to h, and the system evolves unitarily under $H(h)$ for all $t > 0$, i.e. $|\Psi(t)\rangle = e^{-iH(h)t}|\Psi\rangle$. Our main focus is the calculation of the expectation values of generic, local (in space) operators $\mathcal{O}$

$$\langle \mathcal{O}(t)\rangle = \frac{\langle \Psi(t)|\mathcal{O}|\Psi(t)\rangle}{\langle \Psi(t)|\Psi(t)\rangle}. \tag{20.1}$$

Examples of $\mathcal{O}$ would be products of spin operators located in a finite segment of a spin chain, or density or field operators in quantum gases.

Our main result is to show that in the thermodynamic limit $L \to \infty$, at fixed particle density N/L and for a wide class of local observables, the expectation value (20.1) can be expressed in a simple way in terms of projections onto a *single* judiciously-chosen representative 'saddle point' eigenstate $|\Phi_s\rangle$ of $H(h)$:

$$\lim_{N\to\infty} \langle \mathcal{O}(t)\rangle = \lim_{N\to\infty} \left[\frac{\langle \Psi|\mathcal{O}(t)|\Phi_s\rangle}{2\langle \Psi|\Phi_s\rangle} + \Phi_s \leftrightarrow \Psi \right]. \tag{20.2}$$

In the stationary state, i.e. the limit $t \to \infty$, the averages of local observables are simply given by the expectation value in the eigenstate $|\Phi_s\rangle$

$$\lim_{t\to\infty} \lim_{N\to\infty} \langle \mathcal{O}(t)\rangle = \lim_{N\to\infty} \frac{\langle \Phi_s|\mathcal{O}|\Phi_s\rangle}{\langle \Phi_s|\Phi_s\rangle}. \tag{20.3}$$

We stress that no time averaging is involved in (20.3), which can be thought of as a generalization of the eigenstate thermalization hypothesis [1] to local observables in integrable models. We

wish to emphasize that the representation (20.2) offers a dramatic reduction in computational complexity as compared to earlier approaches.

GTBA approach to nonequilibrium evolution. Let us consider a quantum integrable model with Hamiltonian H solvable by Bethe Ansatz [28]. Let $\{|\Phi\rangle\}$ be a complete set of eigenstates, i.e. $H|\Phi\rangle = \omega_\Phi|\Phi\rangle$. The time evolution of an arbitrary initial state $|\Psi\rangle$ is then given by

$$|\Psi(t)\rangle = \sum_\Phi e^{-\mathcal{E}_\Phi} e^{-i\omega_\Phi t}|\Phi\rangle, \tag{20.4}$$

where $\mathcal{E}_\Phi$ are constant, complex-valued overlaps

$$\mathcal{E}_\Phi \equiv -\ln\langle\Phi|\Psi\rangle. \tag{20.5}$$

Substituting (20.4) into the numerator of (20.1) gives a spectral representation of the form

$$\langle\Psi|\mathcal{O}(t)|\Psi\rangle = \sum_{\Phi,\Phi'} e^{-\mathcal{E}^*_\Phi - \mathcal{E}_{\Phi'}} e^{i(\omega_\Phi - \omega_{\Phi'})t}\langle\Phi|\mathcal{O}|\Phi'\rangle. \tag{20.6}$$

This double sum over a full Hilbert space basis is a serious bottleneck. To proceed further, we look to the thermodynamic limit. In the Yang-Yang approach to equilibrium thermodynamics [37], a summation over states is recast as a functional integral over root densities ρ

$$|\Phi\rangle \to |\rho\rangle, \quad \sum_\Phi(...) \to \int \mathcal{D}[\rho] e^{S_\rho}(...). \tag{20.7}$$

Here S_ρ is the entropy of all states characterized by a given root density and (...) represents quantities with well-defined thermodynamic limits. Using (20.7) once, we can formally recast (20.6) in the form

$$\int \mathcal{D}[\rho] e^{S_\rho} \sum_\Phi \left[e^{-\mathcal{E}^*_\Phi - \mathcal{E}_\rho} e^{i(\omega_\Phi - \omega_\rho)t} \frac{\langle\Phi|\mathcal{O}|\rho\rangle}{2} + \Phi \leftrightarrow \rho \right]. \tag{20.8}$$

The reason for using (20.7) only once is that we are interested in local operators $\mathcal{O}$. These have the property that $\langle\Phi|\mathcal{O}|\Phi'\rangle \neq 0$ only if both $|\Phi\rangle$ and $|\Phi'\rangle$ scale to the same distribution ρ up to microscopic differences [6]. In the thermodynamic limit the denominator in (20.1) becomes

$$\langle\Psi|\Psi\rangle = \int \mathcal{D}[\rho] e^{-2\mathrm{Re}(\mathcal{E}_\rho) + \mathrm{S}_\rho}. \tag{20.9}$$

and can be evaluated by the method of steepest descent. The right-hand side of (20.9) can be viewed as the partition function of an integrable model with "generalized free energy"

$$\mathcal{F}_\rho \equiv 2\mathrm{Re}(\mathcal{E}_\rho) - \mathrm{S}_\rho. \tag{20.10}$$

Here S_ρ is the usual Yang-Yang entropy of the integrable Hamiltonian $H(h)$. In the simplest scalar case, realized e.g. in the Lieb-Liniger model, it takes the form $S_\rho = N\int d\lambda \left[(\rho+\rho^h)\ln(\rho+\rho^h) - \rho\ln\rho - \rho^h\ln\rho^h\right]$. The hole density ρ^h is related to the particle density ρ by the thermodynamic form of the Bethe equations

$$\rho(\lambda) + \rho^h(\lambda) = \frac{1}{2\pi} + \int d\lambda' K(\lambda-\lambda')\rho(\lambda'), \tag{20.11}$$

where $K(\lambda)$ is a known function for a given integrable model. The first term in (20.10) plays the role of an effective energy per temperature and hence acts as the "driving term" in a generalized

[6] In a large, finite system of size L, the changes to the root distribution would be of order L^{-1}.

Thermodynamic Bethe Ansatz (for details, see [37, 11]). Since the effective overlaps (20.5) are strictly bounded from below, there exists a saddle-point at ρ_s, i.e. $\frac{\delta \mathcal{F}_\rho}{\delta \rho}|_{\rho_s} = 0$ [7]. In the thermodynamic limit, fluctuations around the saddle point are negligible and thermodynamic averages can be calculated with respect to the energy eigenstate characterized by ρ_s. Given that the expectation values of all local integrals of motion in this state are by construction the same as those of the generalized Gibbs ensemble corresponding to $H(h)$ and $|\Psi(t=0)\rangle$, the saddle-point average of local observables precisely reproduces the GGE average in the sense of [21]. The functional integrals in (20.8) can be evaluated analogously: Given that $\langle \Phi|\mathcal{O}|\rho\rangle$ is non-zero only for states $\langle\Phi|$ such that $\omega_\Phi - \omega_\rho$ and $\mathcal{E}^*_\Phi + \mathcal{E}_\rho$ are intensive, the first term in (20.8) is dominated by the same saddle point ρ_s. The second term is treated analogously. Putting everything together we obtain the thermodynamic limit of (20.2). In practice we consider the theory in a large, finite volume L (at fixed density N/L) and a particular, representative eigenstate $|\Phi_s\rangle$ that reduces to $|\rho_s\rangle$ in the thermodynamic limit. The corresponding spectral representation is then

$$\langle \mathcal{O}(t)\rangle = \lim_{N\to\infty} \sum_\Phi \left\{ e^{\mathcal{E}^*_{\Phi_s} - \mathcal{E}^*_\Phi + i(\omega_\Phi - \omega_{\Phi_s})t} \frac{\langle \Phi|\mathcal{O}|\Phi_s\rangle}{2} \right.$$
$$\left. + e^{\mathcal{E}_{\Phi_s} - \mathcal{E}_\Phi - i(\omega_\Phi - \omega_{\Phi_s})t} \frac{\langle \Phi_s|\mathcal{O}|\Phi\rangle}{2} \right\}. \tag{20.12}$$

The gain in efficiency in (20.12) as compared to the "bare" spectral representation (20.6) is manifold: first of all, a single sum remains; moreover, this sum needs in practice to be carried out only over the subset of states with non-negligible matrix elements. We note that in our line of arguments we have not had to require t to be large. We conjecture that (20.12) describes the time evolution of local observables in the thermodynamic limit, at arbitrary times after the quench. Importantly, in the limit $t \to \infty$ the integrals over the summation over Φ can be carried out by a stationary phase approximation. This shows that in the stationary state only the expectation value in $|\Phi_s\rangle$ survives in (20.12), i.e.

$$\lim_{t\to\infty} \langle \mathcal{O}(t)\rangle = \lim_{N\to\infty} \langle \Phi_s|\mathcal{O}|\Phi_s\rangle. \tag{20.13}$$

The physical content of (20.12) is as follows. In the thermodynamic limit $\langle \mathcal{O}(t)\rangle$ is fully determined by states within a basin defined by the saddle point density ρ_s. The latter defines particular simultaneous eigenstates $|\Phi_s\rangle$ of all local conservation laws (including the Hamiltonian $H(h)$). At late, finite times $\langle \mathcal{O}(t)\rangle$ is determined by quantum interference effects due to "excitations" over the state $|\Phi_s\rangle$.

An explicit example: the Transverse Field Ising Chain. The Hamiltonian of the TFIC is given by

$$H(h) = -J \sum_{j=1}^{L} \left[\sigma^x_j \sigma^x_{j+1} + h\sigma^z_j \right], \tag{20.14}$$

where σ^α_j are Pauli matrices at site j of a one dimensional chain and we consider $J, h > 0$. At zero temperature and in the thermodynamic limit, the TFIC exhibits ferromagnetic long-range order along the x-direction for $h < 1$, while it is in a paramagnetic phase for $h > 1$ [39]. The two phases are separated by a quantum critical point in the Ising universality class. It is well known that $H(h)$ can be diagonalized by combined Jordan-Wigner and Bogoliubov transformations [39]

$$H(h) = \sum_p \varepsilon_h(p) \left(\alpha^\dagger_p \alpha_p - \frac{1}{2} \right), \tag{20.15}$$

[7] For simplicity, we assume the saddle-point to be unique, and to occur in the bulk rather than at a boundary of the Hilbert space. Generalizations are straightforward.

where the single-particle energy is given by $\varepsilon_h(k) = 2J\sqrt{1+h^2-2h\cos k}$. Our quench protocol is as follows: we prepare the system in the ground state $|\Psi\rangle$ for an initial value h_0 of the transverse magnetic field. At time $t = 0$ we instantaneously change the field from h_0 to h. The state of the system at times $t > 0$ is obtained by evolving with respect to the new Hamiltonian $H(h)$,

$$|\Psi(t)\rangle = e^{-iH(h)t}|\Psi\rangle. \tag{20.16}$$

The reduced density matrix of a subsystem A at time t after the quench is given by $\rho_A(t) = \mathrm{Tr}_{\bar{A}}\rho(t) = \mathrm{Tr}_{\bar{A}}|\Psi(t)\rangle\langle\Psi(t)|$, in which $\bar{A}$ is the complement of A. For quenches originating in the paramagnetic phase, i.e. $h_0 > 1$, the $\mathbb{Z}_2$ symmetry of rotations by π around the z-axis remains unbroken and it is possible to express $\rho_A(t)$ in the form [40]

$$\rho_A(t) = \frac{1}{2^\ell}\sum_{\mu_l=0,1}\left\langle\prod_{l=1}^{2\ell}a_l^{\mu_l}\right\rangle\left(\prod_{l=1}^{2\ell}a_l^{\mu_l}\right)^\dagger \propto e^{a_l W_{lm} a_m/4}\ . \tag{20.17}$$

Here the expectation value is with respect to the state $|\Psi(t)\rangle$ and a_{2n} and a_{2n-1} are Majorana fermion operators fulfilling anticommutation relations $\{a_j, a_k\} = 2\delta_{j,k}$, which are related to the lattice spins by a Jordan-Wigner transformation

$$a_{2n-1} = \Big[\prod_{m<n}\sigma_m^z\Big]\sigma_n^x\ , \quad a_{2n} = \Big[\prod_{m<n}\sigma_m^z\Big]\sigma_n^y\ . \tag{20.18}$$

The matrix W is given by $\tanh\frac{W}{2} = \Gamma$ [41], where

$$\Gamma_{jk} = \mathrm{Tr}\,[\rho(t)a_k a_j] - \delta_{j,k} = -\Gamma_{kj}. \tag{20.19}$$

In the thermodynamic limit, the correlation matrix is given by [22] $\Gamma_{2n-1,2j-1} = \Gamma_{2j,2n} = f_{j-n}$, $\Gamma_{2n-1,2j} = g_{n-j}$ with

$$\begin{aligned} g_l &= -i\int_{-\pi}^{\pi}\frac{\mathrm{d}k}{2\pi}e^{-ikl}\frac{h-e^{ik}}{\sqrt{1+h^2-2h\cos k}} \\ &\qquad\times\left[\cos\Delta_k - i\sin\Delta_k\cos(2\varepsilon_h(k)t)\right], \\ f_l &= \int_{-\pi}^{\pi}\frac{\mathrm{d}k}{2\pi}e^{-ikl}\sin\Delta_k\sin(2\varepsilon_h(k)t), \end{aligned} \tag{20.20}$$

where $\cos\Delta_k = \frac{4J^2(1+hh_0-(h+h_0)\cos k)}{\varepsilon_h(k)\varepsilon_{h_0}(k)}$. The reduced density matrix (20.17) is Gaussian, and hence multi-point correlation functions are obtained by Wick's theorem. Concomitantly all local correlation functions in the stationary state are fully specified by the two-point averages (20.19), (20.20) in the limit $t\to\infty$. So far we have considered only the case $h_0 > 1$. For quenches originating in the ferromagnetic phase, i.e. $h_0 < 1$, the reduced density matrix $\rho_A(t)$ is not Gaussian [40]. However, as shown in [22], $\rho_A(\infty)$ is again given by the $t\to\infty$ limit of (20.17).

Stationary Behaviour. We will now show how to recover these results in the GTBA framework. The simplest way to obtain the solution of the GTBA equations for the TFIC is to note that the mode occupation numbers constitute conserved quantities $[\alpha_k^\dagger\alpha_k, H(h)] = 0$. Hence the root density in the stationary state is simply given by

$$\rho(k) = \frac{\langle\Psi|\alpha_k^\dagger\alpha_k|\Psi\rangle}{2\pi} = \frac{1-\cos\Delta_k}{4\pi}, \tag{20.21}$$

and the particle density is $D = \int_{-\pi}^{\pi}dk\ \rho(k)$. The corresponding Hamiltonian eigenstate at density $D = 2N/L$ in a large, finite volume is then

$$|\Phi_s\rangle = \prod_{j=1}^{N}\alpha_{\kappa_j}^\dagger\alpha_{-\kappa_j}^\dagger|0;h\rangle\ , \tag{20.22}$$

where $|0;h\rangle$ is the fermionic vacuum state and the momenta $\kappa_j > 0$ are distributed according to the density (20.21), i.e. $\kappa_{j+1} = \kappa_j + 1/[L\rho(\kappa_j)]$. The density matrix corresponding to the state (20.22) is $\rho_s = |\Phi_s\rangle\langle\Phi_s|$ and by virtue of the product form (20.22) it is Gaussian. This means that it can be represented in the form (20.17) and is completely determined by its correlation matrix (20.19). The only non-vanishing matrix elements are

$$\big(\Gamma_s\big)_{2l-1,2l-2n} = -\frac{i}{L}\sum_k \frac{e^{-ink}(h-e^{ik})(1-2\delta_{k,\kappa_j})}{\sqrt{1+h^2-2h\cos k}}. \tag{20.23}$$

Turning the sum over momenta into an integral by means of the Euler-Maclaurin sum formula, we find that $\Gamma_s = \Gamma(\infty)$ and hence $\lim_{t\to\infty}\rho_A(t) = \rho_{s,A}$. This proves that the GTBA formalism reproduces the correct stationary state for the reduced density matrix for any finite subsystem in the thermodynamic limit, and hence for all local correlation functions.

Relaxation behaviour. Our general formalism suggests that the time evolution of local (in space) operators is given by (20.2), where the state $|\Phi_s\rangle$ is defined in the previous paragraph. We now demonstrate the validity of (20.2) for any local operator $\mathcal{O}$ in the case where the quench originates in the paramagnetic phase, such that the $\mathbb{Z}_2$ symmetry is unbroken. The proof is as follows: we start by defining two density matrices $\rho(t) = |\Psi(t)\rangle\langle\Psi(t)|$ and $\rho_s(t) = |\Phi_s(t)\rangle\langle\Phi_s(t)|$. Crucially, both of these density matrices are Gaussian as a Wick's theorem holds for averages calculated with respect to both of them. The right hand side of (20.2) can be written in the form

$$\left[\frac{\mathrm{Tr}\,[\rho_s(t)\rho(t)\mathcal{O}]}{2\,\mathrm{Tr}\,[\rho_s(t)\rho(t)]} + \rho \leftrightarrow \rho_s\right] \equiv \mathrm{Tr}\,[\hat{\rho}(t)\mathcal{O}]\,. \tag{20.24}$$

Because each term in $\hat{\rho}$ is a product of two Gaussian density matrices, it is Gaussian itself, and hence fully characterized by its correlation matrix

$$\hat{\Gamma}_{jk} = \mathrm{Tr}\,[\hat{\rho}(t)a_k a_j] - \delta_{j,k}. \tag{20.25}$$

The two-point functions in (20.25) are easily calculated, and as shown in the supplementary material we have $\lim_{N\to\infty}\hat{\Gamma}(t) = \Gamma(t)$. This proves that for any local observable $\mathcal{O}$ (such as products of spin operators contained in a finite subsystem) in the thermodynamic limit $\lim_{N\to\infty}\mathrm{Tr}\,[\hat{\rho}(t)\mathcal{O}] = \mathrm{Tr}\,[\rho(t)\mathcal{O}]$, and establishes eqn (20.2).

Our line of arguments breaks down for quenches originating in the ferromagnetic phase, because the density matrix $\rho(t)$ is no longer Gaussian [40]. In order to verify the validity of (20.2) in this case, we have analyzed the relaxation of the order parameter one-point function $\langle\Psi(t)|\sigma^x_\ell|\Psi(t)\rangle$ for quenches with $h_0, h < 1$ in the regime where the density of excitations of the post-quench Hamiltonian $H(h)$ in the initial state is small, i.e. $\langle\Psi|\alpha^\dagger_k\alpha_k|\Psi\rangle \ll 1$. The result for $Jt \gg 1$ in this case is [21]

$$\langle\Psi(t)|\sigma^x_\ell|\Psi(t)\rangle \approx (1-h^2)^{\frac{1}{8}}\exp\left[-2t\int_0^\pi \frac{dk}{\pi}\varepsilon'_h(k)K^2(k)\right]. \tag{20.26}$$

This result is recovered from (20.2) in a very efficient way as follows. Taking into account boundary conditions in a large, finite volume, the appropriate form of (20.2) for the order parameter expectation value is

$$\langle\Psi(t)|\sigma^x_\ell|\Psi(t)\rangle = \mathrm{Re}\left[\frac{{}_{\mathrm{R}}\langle\Psi(t)|\sigma^x_\ell|\Phi_s(t)\rangle_{\mathrm{NS}}}{{}_{\mathrm{NS}}\langle\Psi|\Phi_s\rangle_{\mathrm{NS}}}\right]. \tag{20.27}$$

Here R/NS correspond to periodic/antiperiodic boundary conditions on the fermions respectively, see e.g. [21]. As shown in [21], the state ${}_{\mathrm{R}}\langle\Psi(t)|$ can be written as a linear superposition

of energy eigenstates with n pairs of fermions ${}_{\rm R}\langle\Psi(t)| = \sum_{n=0}^{L/2} {}_{\rm R}\langle\Psi_n(t)|$. The late-time behaviour of (20.27) is determined by states with N pairs, i.e. the term with $n = N$. Retaining only this contribution, and using the known form of matrix elements of the order parameter [42], one readily obtains the result (20.26) by means of the techniques developed in [21]. More details are provided in the supplementary material.

Conclusions. We have argued that averages of local observables in the steady state reached long after a quantum quench to an integrable model can be described as expectation values with respect to a single eigenstate of the Hamiltonian (eqns (20.3) and (20.13)). This eigenstate can be constructed by means of a generalized Thermodynamic Bethe Ansatz and corresponds to a saddle point of an appropriately defined "free energy". Going further, we have shown that the time evolution of local observables is governed by states in the vicinity of this saddle-point through eqns (20.2) and (20.12). The spectral representation (20.12) allows to identify the physical mechanism underlying the relaxation for a given observable at late times. Our approach paves the way for analyzing quantum quenches in interacting integrable models and applications to the Lieb-Liniger and the sine-Gordon model are in progress. An interesting question concerns the range of initial states that can be analyzed within our framework. In quenches of the kind we have focussed on here, the initial state is translationally invariant and characterized by low entanglement. Whether these are necessary requirements and whether the regularity assumptions underlying our GTBA analysis hold for any such states are important points for further investigation.

This work was supported by the Foundation for Fundamental Research on Matter (FOM) and the Netherlands Organisation for Scientific Research (NWO) (JSC), the EPSRC under grants EP/I032487/1 and EP/J014885/1 (FHLE) and the National Science Foundation under grant NSF PHY11-25915 (JSC and FHLE). We thank the KITP in Santa Barbara for hospitality.

References

[1] M. Greiner, O. Mandel, T. W. Hänsch, and I. Bloch, Nature **419** 51 (2002).

[2] T. Kinoshita, T. Wenger, D. S. Weiss, Nature **440**, 900 (2006).

[3] S. Hofferberth, I. Lesanovsky, B. Fischer, T. Schumm, and J. Schmiedmayer, Nature **449**, 324 (2007).

[4] S. Trotzky Y.-A. Chen, A. Flesch, I. P. McCulloch, U. Schollwöck, J. Eisert, and I. Bloch, Nature Physics **8**, 325 (2012).

[5] M. Cheneau, P. Barmettler, D. Poletti, M. Endres, P. Schauss, T. Fukuhara, C. Gross, I. Bloch, C. Kollath, and S. Kuhr, Nature **481**, 484 (2012).

[6] M. Gring, M. Kuhnert, T. Langen, T. Kitagawa, B. Rauer, M. Schreitl, I. Mazets, D. Adu Smith, E. Demler, and J. Schmiedmayer, Science **337**, 1318 (2012).

[7] A. Polkovnikov, K. Sengupta, A. Silva, and M. Vengalattore, Rev. Mod. Phys. **83**, 863 (2011).

[8] M. Rigol, V. Dunjko, V. Yurovsky, and M. Olshanii, Phys. Rev. Lett. **98**, 050405 (2007).

[9] M. Rigol, V. Dunjko, and M. Olshanii, Nature **452**, 854 (2008).

[10] P. Calabrese and J. Cardy, J. Stat. Mech. P06008 (2007).

[11] A. Iucci and M. A. Cazalilla, Phys. Rev. A **80**, 063619 (2009).

[12] T. Barthel and U. Schollwöck, Phys. Rev. Lett. **100**, 100601 (2008).

[13] S. R. Manmana, S. Wessel, R. M. Noack, and A. Muramatsu, Phys. Rev. B **79**, 155104 (2009).

[14] M. C. Bañuls, J. I. Cirac, and M. B. Hastings, Phys. Rev. Lett. **106**, 050405 (2011).

[15] P. Barmettler, M. Punk, V. Gritsev, E. Demler, and E. Altman, New J. Phys. **12**, 055017 (2010).

[16] J. Mossel and J.-S. Caux, New J. Phys. **12**, 055028 (2010).

[17] J. Mossel and J.-S. Caux, New J. Phys. **14**, 075006 (2012).

[18] J.-S. Caux and R. M. Konik, Phys. Rev. Lett. **109**, 175301 (2012).

[19] D. Rossini, A. Silva, G. Mussardo, and G. Santoro, Phys. Rev. Lett. **102**, 127204 (2009); D. Rossini, S. Suzuki, G. Mussardo, G. E. Santoro, and A. Silva, Phys. Rev. B **82**, 144302 (2010).

[20] P. Calabrese, F.H.L. Essler, and M. Fagotti, Phys. Rev. Lett. **106**, 227203 (2011).

[21] P. Calabrese, F.H.L. Essler, and M. Fagotti, J. Stat. Mech. P07016 (2012).

[22] P. Calabrese, F.H.L. Essler, and M. Fagotti, J. Stat. Mech. P07022 (2012).

[23] A. Silva, Phys. Rev. Lett. **101**, 120603 (2008); H. Rieger and F. Iglói, Phys. Rev. B. **84**, 165117 (2011); F. Iglói and H. Rieger, Phys. Rev. Lett. **106**, 035701 (2011). M. Heyl, A. Polkovnikov and S. Kehrein, arXiv:1206.2505.

[24] F.H.L. Essler, S. Evangelisti and M. Fagotti, Phys. Rev. Lett. **109**, 247206 (2012).

[25] D. Fioretto and G. Mussardo, New J. Phys. **12**, 055015 (2010).

[26] G. Biroli, C. Kollath, and A.M. Läuchli, Phys. Rev. Lett. **105**, 250401 (2010).

[27] C. Gogolin, M. P. Müller, and J. Eisert, Phys. Rev. Lett. **106**, 040401 (2011).

[28] M. Rigol and M. Fitzpatrick, Phys. Rev. A **84**, 033640 (2011).

[29] S. Sotiriadis, D. Fioretto, and G. Mussardo, J. Stat. Mech. (2012) P02017.

[30] M. A. Cazalilla, A. Iucci, and M.-C. Chung, Phys. Rev. E **85**, 011133 (2012).

[31] L. Foini, L. F. Cugliandolo, and A. Gambassi, J. Stat. Mech.: Th. Exp. P09011 (2012).

[32] V. Gritsev, E. Demler, M. Lukin, and A. Polkovnikov, Phys. Rev. Lett. **99**, 200404 (2007).

[33] M. Moeckel and S. Kehrein, Ann. Phys. **324**, 2146 (2009).

[34] A. Mitra and T. Giamarchi, Phys. Rev. Lett. **107**, 150602 (2011).

[35] J. M. Deutsch, Phys. Rev. A **43**, 2046 (1991); M. Srednicki, Phys. Rev. E **50**, 888 (1994); M. Srednicki, J. Phys. A**29**, L75 (1996); M. Srednicki, J. Phys. A**32**, 1163 (1999).

[36] V. E. Korepin, N. M. Bogoliubov, and A. G. Izergin. Quantum Inverse Scattering Method and Correlation Functions. Cambridge Univ. Press, 1993.

[37] C. N. Yang and C. P. Yang, J. Math. Phys. **10**, 1115 (1969).

[38] J. Mossel and J.-S. Caux, J. Phys. A: Math. Theor. **45**, 255001 (2012).

[39] see e.g. S. Sachdev, Quantum phase transitions, Cambridge University Press.

[40] M. Fagotti and F.H.L. Essler, in preparation.

[41] G. Vidal, J. I. Latorre, E. Rico, and A. Kitaev, Phys. Rev. Lett. **90**, 227902 (2003); I. Peschel and V. Eisler, J. Phys. A **42**, 504003 (2009).

[42] G. von Gehlen, N. Iorgov, S. Pakuliak, V. Shadura and Y. Tykhyy, J. Phys. **A 41**, 095003 (2008); N. Iorgov, V. Shadura and Yu. Tykhyy, J. Stat. Mech. (2011) P02028.

20.2 Supplementary Material

20.2.1 Calculation of the correlation matrix $\hat{\Gamma}$ (20.25)

For quenches originating in the disordered phase the $\mathbb{Z}_2$ symmetry is unbroken and no subtleties emerge with regards to boundary conditions in a large, finite volume L. In particular all momenta in the formulas below can be taken in the NS sector, i.e. $p_n = \frac{2\pi}{L}(n+1/2)$, where $-L/2 \leq n < L/2$. The state $|\Psi(t)\rangle$ can be expressed in terms of eigenstates of $H(h)$ as [21]

$$|\Psi(t)\rangle = \prod_{k>0} \frac{1 + ie^{-2it\varepsilon_h(k)} K(k)\alpha^\dagger_{-k}\alpha^\dagger_k}{\sqrt{1+K^2(k)}}|0;h\rangle, \tag{20.28}$$

where $K(k) = \tan\big(\Delta_k/2\big)$, α_k and $\alpha^\dagger_k$ obey canonical anticommutation relations, and $\alpha_k|0;h\rangle = 0$. The time evolved state $|\Phi_s\rangle$ (20.22) is

$$|\Phi_s(t)\rangle = \prod_{j=1}^{N} e^{-2i\varepsilon_h(\kappa_j)t}\alpha^\dagger_{\kappa_j}\alpha^\dagger_{-\kappa_j}|0;h\rangle \ . \tag{20.29}$$

Our goal is to determine all two-point matrix elements of the form $\langle\Psi(t)|a_j a_k|\Phi_s(t)\rangle$, where a_j are the Majorana fermion operators defined in (20.18). The mode expansion of the a_j is

$$\begin{aligned} a_{2j-1} &= \frac{1}{\sqrt{L}}\sum_p e^{i\frac{\theta_p}{2}-ipj}\left[\alpha_p + \alpha^\dagger_{-p}\right], \\ a_{2j} &= -\frac{i}{\sqrt{L}}\sum_p e^{-i\frac{\theta_p}{2}-ipj}\left[\alpha_p - \alpha^\dagger_{-p}\right], \end{aligned} \tag{20.30}$$

where

$$e^{i\theta_k} = \frac{h - e^{ik}}{\sqrt{1+h^2-2h\cos k}}. \tag{20.31}$$

A straightforward calculation using the mode expansion and $\alpha_p|0;h\rangle = 0$ gives

$$\frac{\langle\Psi(t)|a_1 a_{2n+1}|\Phi_s(t)\rangle}{\langle\Psi|\Phi_s\rangle} = \delta_{n,0} - \frac{i}{L}\sum_p K(p)e^{ipn+2it\varepsilon_h(p)} + \frac{i}{L}\sum_{j=1}^{N}\left[e^{in\kappa_j} - e^{-in\kappa_j}\right]\left[K(\kappa_j)e^{2it\varepsilon_h(\kappa_j)} + \frac{e^{-2it_h(\kappa_j)}}{K(\kappa_j)}\right] \tag{20.32}$$

In the limit $N, L \to \infty$ with $D = 2N/L$ fixed we can turn sums into integrals using the Euler-Maclaurin sum formula

$$\frac{1}{L}\sum_{j=1}^{N} f(\kappa_j) = \int_0^\pi dk\ \rho(k)f(k) + \mathcal{O}\big(L^{-1}\big), \tag{20.33}$$

where $\rho(k)$ is the root density (20.21) characterizing the distribution of the momenta $\{\kappa_j\}$. Using that $K(k) = \tan(\Delta_k/2)$ we find

$$\lim_{N\to\infty} \frac{\langle\Psi(t)|a_1 a_{2n+1}|\Phi_s(t)\rangle}{\langle\Psi|\Phi_s\rangle} = \delta_{n,0} + f_{-n}, \tag{20.34}$$

where f_l is given in (20.20). By taking the complex conjugate of (20.34), we find

$$\lim_{N\to\infty} \frac{\langle\Phi_s(t)|a_1 a_{2n+1}|\Psi(t)\rangle}{\langle\Phi_s|\Psi\rangle} = \delta_{n,0} - f^*_{-n}, \tag{20.35}$$

Given that f_n is purely imaginary, we conclude that

$$\hat{\Gamma}_{2n+1,1} = \mathrm{Tr}\left[\hat{\rho}(t) a_1 a_{2n+1}\right] - \delta_{n,0} = f_{-n}. \tag{20.36}$$

By analogous calculations one finds that

$$\begin{aligned}
\lim_{N\to\infty} \frac{\langle\Psi(t)|a_2 a_{2n+2}|\Phi_s(t)\rangle}{\langle\Psi|\Phi_s\rangle} &= \delta_{n,0} + f_n, \\
\lim_{N\to\infty} \frac{\langle\Psi(t)|a_2 a_{2n+1}|\Phi_s(t)\rangle}{\langle\Psi|\Phi_s\rangle} &= g_n.
\end{aligned} \tag{20.37}$$

Taking the complex conjugates of eqns (20.37) and using that both f_n and g_n are purely imainary, we obtain

$$\begin{aligned}
\hat{\Gamma}_{2n+2,2} &= \mathrm{Tr}\left[\hat{\rho}(t) a_2 a_{2n+2}\right] - \delta_{n,0} = f_n \ , \\
\hat{\Gamma}_{2n+1,2} &= \mathrm{Tr}\left[\hat{\rho}(t) a_2 a_{2n+1}\right] = g_n.
\end{aligned} \tag{20.38}$$

Finally, using translational invariance we conclude that

$$\hat{\Gamma}_{ij} = \Gamma_{ij}, \tag{20.39}$$

where Γ_{ij} is given in (20.19), (20.20).

20.2.2 Order Parameter One-Point Function

As we are interested in the order parameter, we need to carefully keep track of boundary conditions. We follow the conventions summarized in the appendix of Ref. [21]. The state after the quench is given by [21]

$$\begin{aligned}
|\Psi(t)\rangle &= \frac{|\Psi(t)\rangle_{\mathrm{R}} + |\Psi(t)\rangle_{\mathrm{NS}}}{\sqrt{2}} \ , \\
|\Psi(t)\rangle_a &= \prod_{0<k\in a} \frac{1 + i e^{-2it\varepsilon_h(k)} K(k) \alpha^\dagger_{-k} \alpha^\dagger_k}{\sqrt{\left(1 + K^2(k)\right)}} |0; h\rangle_a,
\end{aligned} \tag{20.40}$$

where $a = \mathrm{R}, \mathrm{NS}$. The appropriate form of (20.2) reads

$$\langle\Psi(t)|\sigma^x_\ell|\Psi(t)\rangle = \lim_{N\to\infty} \mathrm{Re}\left[\frac{{}_{\mathrm{R}}\langle\Psi|\sigma^x_\ell(t)|\Phi_s\rangle_{\mathrm{NS}}}{{}_{\mathrm{NS}}\langle\Psi|\Phi_s\rangle_{\mathrm{NS}}}\right]. \tag{20.41}$$

The state ${}_{\mathrm{R}}\langle\Psi(t)|$ can be written as a linear superposition of energy eigenstates [21] with n pairs of fermions

$${}_{\mathrm{R}}\langle\Psi(t)| = \sum_{n=0}^{L/2} {}_{\mathrm{R}}\langle\Psi_n(t)| \ . \tag{20.42}$$

Inspection of the resulting matrix elements suggests that at late times the dominant contribution to (20.41) arises from terms with N pairs. The corresponding contribution is

$$\frac{{}_{\rm R}\langle\Psi_N(t)|\sigma^x_\ell|\Phi_s(t)\rangle_{\rm NS}}{{}_{\rm NS}\langle\Psi|\Phi_s\rangle_{\rm NS}} = \frac{(-1)^N}{N!}\sum_{0<p_1,\ldots,p_N} {}_{\rm R}\langle p_1,-p_1,\ldots p_N,-p_N|\sigma^x_\ell|\kappa_1,-\kappa_1,\ldots\kappa_N,-\kappa_N\rangle_{\rm NS}\prod_{j=1}^N \frac{K(p_j)}{K(\kappa_j)}e^{2it(\varepsilon_{p_j}-} \tag{20.43}$$

where $\varepsilon_p = \varepsilon_h(p)$. The matrix element of σ^x_ℓ in (20.43) is given by [21, 42]

$$\frac{(-1)^N 2^{2N}\sqrt{\xi}}{L^{2N}}\prod_{j,l}\epsilon^4_{\kappa_j,p_l}c^2_{\kappa_j,p_l}\prod_{j=1}^N\frac{\sin\kappa_j\sin p_j}{\varepsilon^2_{\kappa_j}\varepsilon^2_{p_j}} \times\prod_{j<j'}\frac{1}{\epsilon^4_{\kappa_j,\kappa_{j'}}\epsilon^4_{p_j,p_{j'}}c^2_{\kappa_j,\kappa_{j'}}c^2_{p_j,p_{j'}}}. \tag{20.44}$$

Here $\xi = |1-h^2|^{1/4}$, $\epsilon_{p,q} = (\varepsilon_p+\varepsilon_q)/2$ and $c_{p,q} = [\cos p - \cos q]^{-1}$. As a function of p_j it exhibits either simple or double poles when $p_j \to k_m$, and the leading contributions at late times arise from the vicinities of these singularities [21]. We proceed by rewriting the "pole-factor" as the square of a Cauchy determinant

$$\mathcal{P} = \prod_{j,l=1}^N c^2_{\kappa_j,p_l}\prod_{j<j'}\frac{1}{c^2_{p_j,p_{j'}}c^2_{\kappa_j,\kappa_{j'}}} = \big(\det C\big)^2\,,$$
$$C_{ij} = \frac{1}{\cos p_i - \cos\kappa_j}\,. \tag{20.45}$$

By expressing the determinant as a sum over permutations using the standard definition, we can recast $\mathcal{P}$ in the form $\mathcal{P} = \sum_{j=0}^{[N/2]}\mathcal{P}_{N-2j}$, where $\mathcal{P}_k$ has k double poles when viewed as a function of the $\cos p_r$. The most singular terms are ($x_r = \cos p_r$, $y_s = \cos k_s$)

$$\mathcal{P}_N = \sum_{P\in S_N}\prod_{j=1}^N\frac{1}{(x_j-y_{P_j})^2},$$
$$\mathcal{P}_{N-2} = -\frac{1}{2}\sum_{P\in S_N}\sum_{r\neq s}\prod_{j\neq r,s}^N\frac{1}{(x_j-y_{P_j})^2} \times\frac{1}{(x_r-y_{P_r})(x_r-y_{P_s})(x_s-y_{P_r})(x_s-y_{P_s})}. \tag{20.46}$$

The leading contribution to (20.43) at late times is obtained by retaining only the most singular part $\mathcal{P}_N$

$$\frac{{}_{\rm R}\langle\Psi_N(t)|\sigma^x_\ell|\Phi_s(t)\rangle_{\rm NS}}{{}_{\rm NS}\langle\Psi|\Phi_s\rangle_{\rm NS}} \approx \frac{2^{2N}\sqrt{\xi}}{L^{2N}N!}\sum_{0<p_1,\ldots,p_N}\mathcal{P}_N\prod_{j=1}^N\left[\frac{K(p_j)}{K(\kappa_j)}\frac{\sin\kappa_j\sin p_j}{\varepsilon^2_{\kappa_j}\varepsilon^2_{p_j}}e^{2it(\varepsilon_{p_j}-\varepsilon_{\kappa_j})}\right]\prod_{j,l}\epsilon^4_{\kappa_j,p_l}\prod_{j<j'}\frac{1}{\epsilon^4_{\kappa_j,\kappa_{j'}}\epsilon^4_{p_j,p_{j'}}}. \tag{20.47}$$

We can now carry out all sums over p_j using (D.1) of Ref. [[21]]. Retaining only the leading contributions at late times (and asymptotically large L) we find

$$\frac{{}_{\rm R}\langle\Psi_N(t)|\sigma^x_\ell|\Phi_s(t)\rangle_{\rm NS}}{{}_{\rm NS}\langle\Psi|\Phi_s\rangle_{\rm NS}} \approx \sqrt{\xi}\prod_{j=1}^N\left(1-\frac{4t}{L}\varepsilon'_{\kappa_j}\right) \simeq \sqrt{\xi}\exp\left[-\frac{4t}{L}\sum_{j=1}^N\varepsilon'_{\kappa_j}\right]. \tag{20.48}$$

Turning the sum over the κ_j into an integral this becomes

$$\frac{{}_{\rm R}\langle\Psi_N(t)|\sigma^x_\ell|\Phi_s(t)\rangle_{\rm NS}}{{}_{\rm NS}\langle\Psi|\Phi_s\rangle_{\rm NS}} \approx \sqrt{\xi}e^{-t\int_0^\pi \frac{dk}{\pi}\varepsilon'_k\left(1-\cos\Delta_k\right)}. \tag{20.49}$$

Observing that

$$1-\cos\Delta_k = \frac{2K^2(k)}{1+K^2(k)}, \tag{20.50}$$

and noting that the asymptotic result (20.49) is purely real, we recover the result obtained in [21] by summing the leading late-time divergences in the form factor expansion for the 1-point function to all orders. We stress that the current calculation is significantly simpler. Subleading contributions at late times can be obtained by taking into account $\mathcal{P}_{N-2j}$ with $j \geq 1$. These will be reported elsewhere.

21 A note on symmetry reductions of the Lindblad equation: transport in constrained open spin chains by Buč, Prosen

Abstract

We study quantum transport properties of an open Heisenberg XXZ spin 1/2 chain driven by a pair of Lindblad jump operators satisfying a global 'microcanonical' constraint, i.e. conserving the total magnetization. We will show that this system has an additional discrete symmetry which is particular to the Liouvillean description of the problem. Such symmetry reduces the dynamics even more than what would be expected in the standard Hilbert space formalism and establishes existence of multiple steady states. Interestingly, numerical simulations of the XXZ model suggest that a pair of distinct non-equilibrium steady states becomes indistinguishable in the thermodynamic limit, and exhibit sub-diffusive spin transport in the easy-axis regime of anisotropy $\Delta > 1$.

21.1 Introduction

Simulating interacting quantum many-body systems in-, and in particular, out-of- equilibrium is at the forefront of the current experimental and theoretical research (see e.g. [1], [2]). While it has been recognized that treating large isolated quantum-many body systems (with generic physical properties) poses a formidable task to any method of theoretical description or simulation, it has soon become apparent – first within the community of quantum optics [3] – that often a macroscopic number of observables can be treated as quantum noise, and that the behavior of a few essential physical observables can be extracted in terms of the formalism of open quantum systems [4, 5]. From mathematical-physics point of view most notable is perhaps the discovery of Lindblad, Gorini, Kossakowski and Sudarshan [6, 7], that within the Markovian approximation any time-development of an open system's (reduced) density operator $\rho(t)$, acting on a $N-$dimensional Hilbert space $\mathcal{H}$ describing the (slow) degrees of freedom of interest, can be described by the quantum Liouville equation in the form

$$\dot\rho(t) = \hat{\mathcal{L}}\rho(t) \equiv -\mathrm{i}[H,\rho(t)] + \sum_{m=1}^{N^2-1}\left(L_m\rho(t)L_m^\dagger - \frac{1}{2}\{L_m^\dagger L_m,\rho(t)\}\right) \tag{21.1}$$

where $[A,B] \equiv AB-BA$, $\{A,B\} \equiv AB+BA$, H is the Hermitian Hamiltonian operator, and L_m is a set of at most N^2-1 so-called Lindblad operators, all over $\mathcal{H}$. We use units in

which $\hbar = 1$. $\hat{\mathcal{L}}$ can be understood as a (super)operator acting on the space $\mathcal{B}(\mathcal{H})$ of bounded operators over Hilbert space $\mathcal{H}$. The space $\mathcal{B}(\mathcal{H})$ shall also be considered as a Hilbert space itself, equipped with the Hilbert-Schmidt inner product. The Liouvillian flow (21.1) is the most general one which is (i) local-in-time, (ii) respects the positivity $\rho(t) \geq 0$, and (iii) conserves the trace $\mathrm{tr}\,\rho(t) \equiv 1$, and forms the so-called quantum dynamical semi-group. However, the approach of open-quantum-system has only quite recently been applied to the non-equilibrium problems of condensed matter physics [8, 9, 10, 11, 12, 13, 14, 15], such as the controversial quantum transport problem in one-dimension [16, 17, 18].

The central object of concern in physics applications is the fixed point of dynamical semi-group, $\rho_\infty = \lim_{t\to\infty} \rho(t)$, or the null-vector of Liouvillian

$$\hat{\mathcal{L}}\rho_\infty = 0 \tag{21.2}$$

and which shall be termed non-equilibrium steady state (NESS). This state is relevant in the asymptotic long time limit of the evolution of the system, and does not decay despite the dissipative nature of the Lindblad equation. The interesting case, when the fixed point is a pure state $\rho_\infty = |\psi_\infty\rangle\langle\psi_\infty|$ is of particular appeal in quantum optics and quantum information theory [19], where such a state $|\psi_\infty\rangle$ is called a dark state. Sufficient condition for existence of a dark state is that $|\psi_\infty\rangle$ is an eigenstate of H and is annihilated by all jump operators, $L_m|\psi_\infty\rangle = 0$. Dark states are also known as examples of decoherence-free states, and are of importance in quantum computing [20].

We note that the Lindblad equation (21.1) can in general describe the system coupled to several thermal (or chemical, magnetic) baths at different values of the thermodynamic potentials, hence the resulting asymptotic states ρ_∞ can be considered as intrinsically nonequilibrium.

Of central importance is the understanding and control of uniqueness of NESS, for example for applications in quantum memories [21] which could be realized in terms of possibly degenerate (non-unique) NESSs. Another potentially very iteresting application of non-unique (multiple) steady states of Liouvillean quantum dynamics could be in detecting non-equilibrium quantum phase transitions, or regions of criticality [24]. Importantly, multiple fixed points of dynamical semigroups are also a crucial part of the concept of decoherence-free subspaces [20], one of the key ideas for fighting errors in quantum computation. Precise conditions for the uniqueness of NESS, i.e. independence of ρ_∞ of the initial condition $\rho(0)$, has been established a while ago [22, 23]. Essentially, it follows from the Evans theorem [22] that NESS is unique if and only if the set of operators $\{H, L_m, m = 1, 2, \ldots\}$ generates the entire multiplicative operator algebra $\mathcal{B}(\mathcal{H})$. One the other hand, the situations where NESS is not unique have been systematically much less explored. For example, in the case of existence of a discrete symmetry, of either (i) Liouvillian $\hat{\mathcal{L}}$ as a whole, or (ii) of all members of the set $\{H, L_m, m = 1, 2, \ldots\}$ one might expect non-unique NESSs classified by the eigenvalues of the symmetry operation.

In this paper we will analyze how the existence of symmetries can allow us to treat the transport problem in a boundary driven open anisotropic Heisenberg XXZ spin 1/2 chain with a micro-canonical constraint, i.e. enforcing the exact conservation of total spin (magnetization). Quite interestingly, our numerical results suggest that the two NESSs corresponding to the zero magnetization sector characterized by the eigenvalue of the parity-like symmetry become indistinguishable in the thermodynamic limit, and that in the easy-axis regime (of anisotropy $\Delta > 1$) the spin transport becomes sub-diffusive (insulating in the thermodynamic limit), quite different from the results [25, 26] for the un-constrained boundary-driven XXZ chain. This seems consistent with a recently claimed co-existence of diffusive and insulating transport in a gapped XXZ model [27]. In the Appendix we provide a general mathematical prescription how in both cases (i,ii) of the previous paragraph the symmetry can be facilitated to reduce the problem and block-diagonalize the matrix of the Liouvillian superoperator, whereas only in the second case (ii) the non-uniqueness of NESS is guaranteed by the existence of a symmetry

operator and distinct Liouvillian fixed points can be labelled by the eigenvalues of the symmetry operation.

21.2 Symmetric boundary driven open XXZ spin chains

In order to study a simple system which does not have a unique NESS and to provide some additional insight into the debate on quantum transport in one dimension [16, 27], we shall discuss a finite open anisotropic Heisenberg XXZ spin 1/2 chain on n sites, with the Hamiltonian

$$H = \sum_{i=1}^{n-1} \left[\sigma_i^{\mathrm{x}}\sigma_{i+1}^{\mathrm{x}} + \sigma_i^{\mathrm{y}}\sigma_{i+1}^{\mathrm{y}} + \Delta\sigma_i^{\mathrm{z}}\sigma_{i+1}^{z}\right]. \tag{21.3}$$

$\sigma_i^{\mathrm{x,y,z}}$ designate a set of standard Pauli matrices corresponding to physical sites $i = 1, 2, \ldots, n$ and acting on a Hilbert space $\mathcal{H} = (\mathbb{C}^2)^{\otimes n}$ of dimension $N = 2^n$. We couple the chain to magnetic reservoirs only through the boundary spins $i = 1$ and $i = n$.

Two cases can be considered:

1. Firstly, we take a set of four Lindblad operators

$$\begin{aligned} L_1^{\mathrm{w}} &= \sqrt{\Gamma(1-\mu)}\sigma_1^+, \qquad & L_3^{\mathrm{w}} &= \sqrt{\Gamma(1+\mu)}\sigma_n^+, \\ L_2^{\mathrm{w}} &= \sqrt{\Gamma(1+\mu)}\sigma_1^-, \qquad & L_4^{\mathrm{w}} &= \sqrt{\Gamma(1-\mu)}\sigma_n^-. \end{aligned} \tag{21.4}$$

   where two real parameters $\Gamma > 0$ and $\mu \in [0, 1]$ designate, respectively, the strength of coupling to a pair of magnetic reservoirs and strength of (non-equilibrium) driving. $\sigma_i^{\pm} = (\sigma_i^{\mathrm{x}} \pm \mathrm{i}\sigma_i^{\mathrm{y}})/2$ are the spin-flip operators.

2. Secondly, we consider a pair of Lindblad operators

$$L_1^{\mathrm{s}} = \Gamma(1-\mu)\sigma_1^+\sigma_n^-, \qquad L_2^{\mathrm{s}} = \Gamma(1+\mu)\sigma_1^-\sigma_n^+, \tag{21.5}$$

   again parametrized by two coupling parameters Γ, μ having the same interpretation as above. We note that the Liouvillian flow (21.1) equipped with (21.5) strictly conserves the total magnetization $M = \sum_{i=1}^{n} \sigma_i^{\mathrm{z}}$, at the expense of non-local coupling between the first and the last site. In fact, we can imagine Lindblad operators here as incoherent quantum jumps which transfer spin excitations between $i = 1$ and $i = n$ sites while conserving total number of spin-excitations (quasi-particles). Alternatively, such a model can be interpreted as a spin ring where hopping is fully coherent on bonds $(1, 2), (2, 3) \ldots, (n-1, n)$ while it is fully dissipative (and asymmetric for $\mu \neq 0$) on one bond $(n, 1)$, and is a particular case of quantum exclusion process complementing the one presented in Ref. [28] (see also [29, 30]).

We note that the quantum transport models described by the Hamiltonian (21.3) and (21.4), or (21.5), can be considered as out of equilibrium steady state models with minimal incoherent input, namely with incoherent processes taking place only on the boundary, or on the single bond.

Let P be a permutation operator which exchanges the site i with $n-i+1$ for all i. In fact, P can be written as a unitary operator over $\mathcal{H}$ with explicit representation in the computational basis (eigenbasis of σ_i^{z}, $\sigma_i^{\mathrm{z}}|a_1, a_2 \ldots a_n\rangle = (1-2a_i)|a_1, a_2 \ldots a_n\rangle$ for $a_i \in \{0, 1\}$) as

$$P = \sum_{(a_1, a_2, \ldots, a_n) \in \{0,1\}^n} |a_1, a_2, \ldots, a_n\rangle\langle a_n, a_{n-1}, \ldots, a_1| \tag{21.6}$$

and can be interpreted as a parity operator. Combining it with spin flips on all sites we define another unitary (parity-like) operator S as

$$S = P \prod_{i=1}^{n} \sigma_i^{\mathrm{x}}. \tag{21.7}$$

Clearly, S is a $\mathbb{Z}_2$ symmetry of the Hamiltonian, as $[H, S] = 0$ and $S^2 = 1$.

In case (i) with (21.4) one notes that $SL_1^{\mathrm{w}}S^\dagger \equiv \hat{S}L_1^{\mathrm{w}} = L_4^{\mathrm{w}}$ and $\hat{S}L_2^{\mathrm{w}} = L_3^{\mathrm{w}}$ hence the Liouvillian flow (21.1) exhibits a weak symmetry in the sense of Appendix, Eq. (21.11). Precisely the same case of symmetrically boundary driven XXZ chain (21.3,21.4) has been discussed in several recent papers [31, 32, 25, 33, 34, 35] and has been shown to exhibit interesting non-equilibrium trasport properties. In this case, one can use Evans theorem [22] in order to prove that NESS is unique. The number of invariant subspaces is $n_S = 2$, with symmetry S eigenvalues $s_1 = +1$ and $s_2 = -1$. Let the complete set of 4 symmetry adapted operator sub-spaces be now suggestively denoted as $\{s_\alpha, s_\beta\} \equiv \mathcal{B}_{\alpha,\beta}$. As pointed out in the Appendix (also explaining the notation), the symmetry $\hat{S}$ can still be used in order to reduce the Liouvillian to two blocks $\mathcal{B}_1 = \{+1,+1\} \oplus \{-1,-1\}$, and $\mathcal{B}_2 = \{+1,-1\} \oplus \{-1,+1\}$, which have roughly similar dimensions for large n.

Let us now focus on case (ii). S now becomes a strong symmetry (Appendix, Eq. (21.12)) of the flow (21.1,21.5) as $\hat{S}L_m^{\mathrm{s}} = L_m^{\mathrm{s}}$ for $m = 1, 2$. In this case, however, we have an additional strong (continuous, $U(1)$) symmetry, generated by magnetization operator $S_M = e^{\mathrm{i}\varphi M}$, as also $\hat{S}_M L_m^{\mathrm{s}} = L_m^{\mathrm{s}}$ and $\hat{S}_M H = H$. We shall say that the flow (21.1,21.5) obeys a micro-canonical constraint. Thus we can use the Theorem 21.1 of Appendix in order to prove the existence of a pair of distinct NESSs for each eigenvalue of total magnetization $s_{\mathrm{z}} \in \{-n, -n+2, \ldots, n-2, n\}$, i.e. we have a $2N+1$ dimensional convex set of fixed points of the Liouvillian flow.[8] As from the quantum transport point of view the most interesting is the zero magnetization sector, we will in the following fix $s_{\mathrm{z}} = 0$ and assume the size n to be even. There we have a line of degenerate NESS parametrized by a number from a unit interval $u \in [0, 1]$

$$\rho_\infty(u) = u\rho_\infty^1 + (1-u)\rho_\infty^2, \quad \rho_\infty^1 \in \{+1,+1\},\ \rho_\infty^2 \in \{-1,-1\}. \tag{21.8}$$

21.2.1 Numerical results and transport properties

Let us now turn to the physical properties of our microcanonically constrained open XXZ chain, in particular to the steady state spin current and magnetization profiles. The spin current operator corresponding to the bond $(i, i+1)$ is defined as,

$$j_i = \sigma_i^{\mathrm{x}}\sigma_{i+1}^{\mathrm{y}} - \sigma_i^{\mathrm{y}}\sigma_{i+1}^{\mathrm{x}} = 2\mathrm{i}(\sigma_i^-\sigma_{i+1}^+ - \sigma_i^+\sigma_{i+1}^-) \tag{21.9}$$

and obeys the operator continuity equation of the form $\frac{\mathrm{d}}{\mathrm{d}t}(\sigma_j^{\mathrm{z}}/2) = \mathrm{i}[H, \sigma^{\mathrm{z}}/2] = j_i - j_{i-1}$, for $i = 2, 3 \ldots, n-1$. Steady state expectation values shall be denoted as $J = \langle j_i \rangle$ (which does not depend on site index i due to continuity equation), and $M_i = \langle \sigma_i^{\mathrm{z}} \rangle$, where $\langle \bullet \rangle \equiv \mathrm{tr}\,(\bullet)\rho_\infty$. We have checked that the fixed point problem for Liouvillian flow (21.1,21.5) does not admit a closed form solution of a matrix product operator form of small finite rank as in the weakly-symmetric case [34], thus we had to resort to numerical simulations. Of course, we optimized our calculations by restricting the Liouvillean to diagonal blocks $\hat{\mathcal{L}}|_{\{+1,+1\}}$ (for ρ_∞^1) and $\hat{\mathcal{L}}|_{\{-1,-1\}}$ (for ρ_∞^2). For $n = 4, 6, 8$ and 10 sites we used exact numerical diagonalization, while for $n = 12, 14$ and 16 we used a wave-function Monte-Carlo approach called the method of quantum trajectories, as outlined in Appendix A of Ref. [32] (see also Ref. [14]). An efficient

[8] The dimension of the convex set of NESS is by one smaller than the number of distinct symmetry labelled fixed points $2(N-1)$ due to the trace constraint $\mathrm{tr}\,\rho = 1$.

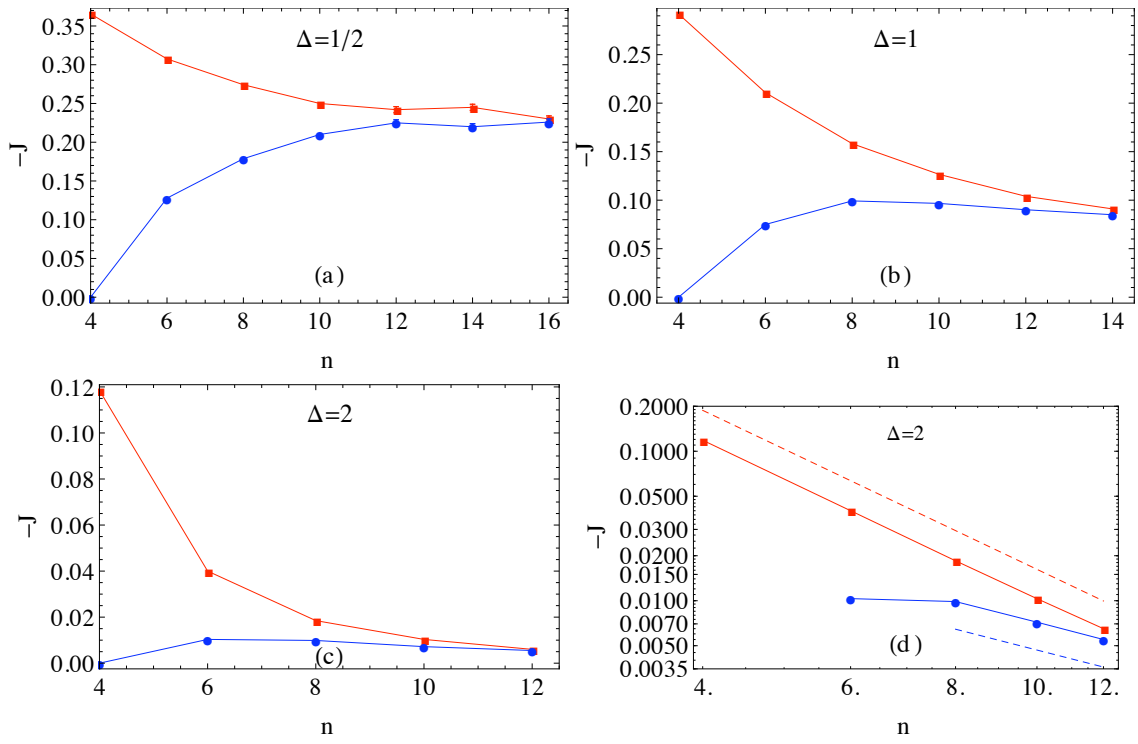


Figure 21.1: We plot negative current $-J$ against spin chain length n for $\Delta = 1/2$ (a), $\Delta = 1$ (b), and $\Delta = 2$ (c), and for NESSs from both symmetry subspaces, $\{+1, +1\}$ (red/squares) and $\{-1, -1\}$ (blue/circles). Data for $n \leq 10$ are numerically exact, while for $n \geq 12$ the statistical/Trotter error is always smaller than the size of the symbols. In panel (d) we plot the case $\Delta = 2$ in the log-log scale, suggesting the fast decay of $J(n)$. The two eye-guiding dashed lines have slopes -2.68 (red) and -1.44 (blue).

Trotter expansion of the propagator $e^{iH\delta_t}$ with complex coefficients [36] has been employed. The stochastic time-dependent Shrödinger equation has been simulated until the current was equal on all bonds, and the statistical error was small, both within the accuracy better than 1%.

We consider three characteristic values of the anisotropy parameter: $\Delta = 1/2$, $\Delta = 1$, and $\Delta = 2$, where the linear-response-transport in the grand-canonical ensemble (or in an open chain without the microcanonical constraint) has been found to be, respectively, ballistic [34], anomalous (super-diffusive/sub-ballistic) [35], and diffusive [18, 26]. On the other hand, linear-response transport in the micro-canonical ensemble in the latter case ($\Delta = 2$) has been suggested to be sub-diffusive (insulating) [2]. We chose the bath-coupling parameters as $\Gamma = 1$, $\mu = 0.2$, which put our setup in a near-linear-response regime, however, we also tried other values of bath parameters and the results did not change qualitatively. By considering a large driving parameter close to the maximum $\mu \approx 1$, we have found negative differential conductance for both symmetry subspaces (for $n = 8$), consistent with the behavior found in the unconstrained model [31, 32].

The spin chain with four sites is particularly interesting as the subspace $\{-1, -1\}$ is one-dimensional, i.e, the NESS in this subspace has to be pure state, i.e. a dark state. Being a pure state it cannot support current ($J = 0$) and has a vanishing magnetization on all 4 sites. Explicitly, the dark state then is of the form

$$|\psi_\infty\rangle = \frac{1}{\sqrt{2}} \left(|0110\rangle - |1001\rangle\right) \tag{21.10}$$

and does not depend on any system's parameters, Δ, Γ, μ. We did not find any dark states of

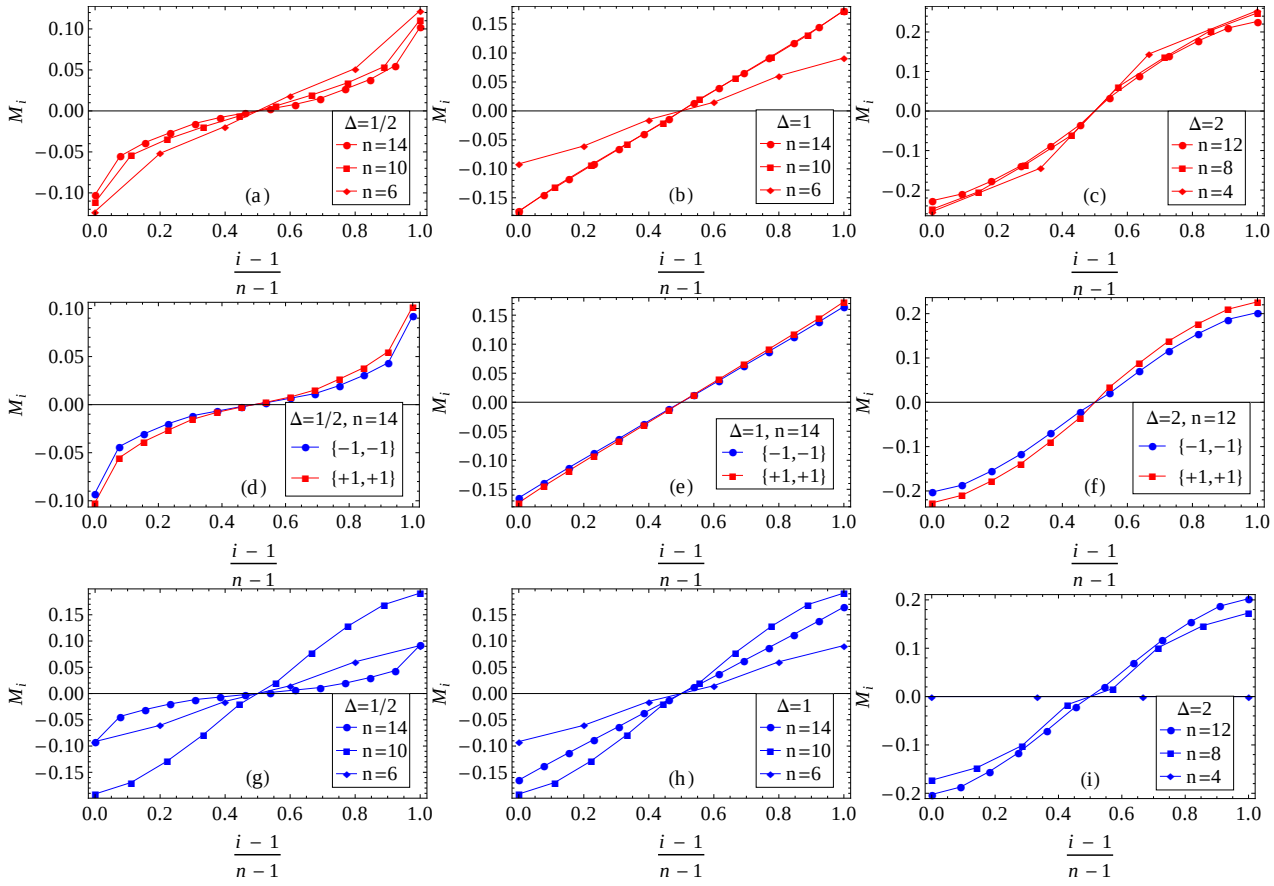


Figure 21.2: The magnetization profiles for various values of $\Delta = 1/2, 1, 2$ in the $\{+1,+1\}$ subspace, (a,b,c), respectively, and comparing different chain sizes (see the legends inside plots), and similar for the $\{-1,-1\}$ subspace in the lower row of plots (g,h,i). In the midle row of plots (d,e,f) we compare, again for $\Delta = 1/2, 1, 2$, and for the largest system size attainable, the magnetization profiles from the two symmetry sectors (red/blue).

our flow (21.1,21.5) for $n \geq 6$.

In Fig. 21.1 we display the behavior of the steady state current J versus the chain length n for the two distinct steady states $\rho_\infty^{(1)}$ and ρ_∞^2 in the spaces $\{+1,+1\}$ and $\{-1,-1\}$. We find a general trend of convergence of the two curves which suggest that the current might not depend on the symmetry sector in the thermodynamic limit and would therefore be unique. The same applies to magnetization profiles displayed in Fig. 21.2. This implies a kind of ergodicity and suggests physical irrelevance of the symmetry S in the thermodynamic limit. Furthermore, in the regime $\Delta = 1/2$ the current $J(n)$ tends to converge to a constant suggesting a ballistic behavior, for $\Delta = 1$ $J(n)$ seems to slowly (perhaps slightly super-diffusively) decrease with n, while for $\Delta = 2$, $J(n)$ decreases fast. As far as our numerics can suggest it seems that in the regime $\Delta = 2$, the decrease of $J(n)$ is definitely much faster than $1/n$ which is compatible with the suggested insulating behavior [2]. In Fig. 21.2 we make a detailed analysis of the magnetization profiles in both symmetry sectors, and for different system sizes. We find, consistently, that the profiles in the regimes $\Delta = 1/2$, $\Delta = 1$, and $\Delta = 2$, display ballistic, (slightly super-)diffusive, and sub-diffusive (insulating) behavior, respectively. In is perhaps interesting to remark that in the isotropic case $\Delta = 1$, for the largest system size that we could simulate, the profile seems to be almost perfectly linear which might also be compatible with

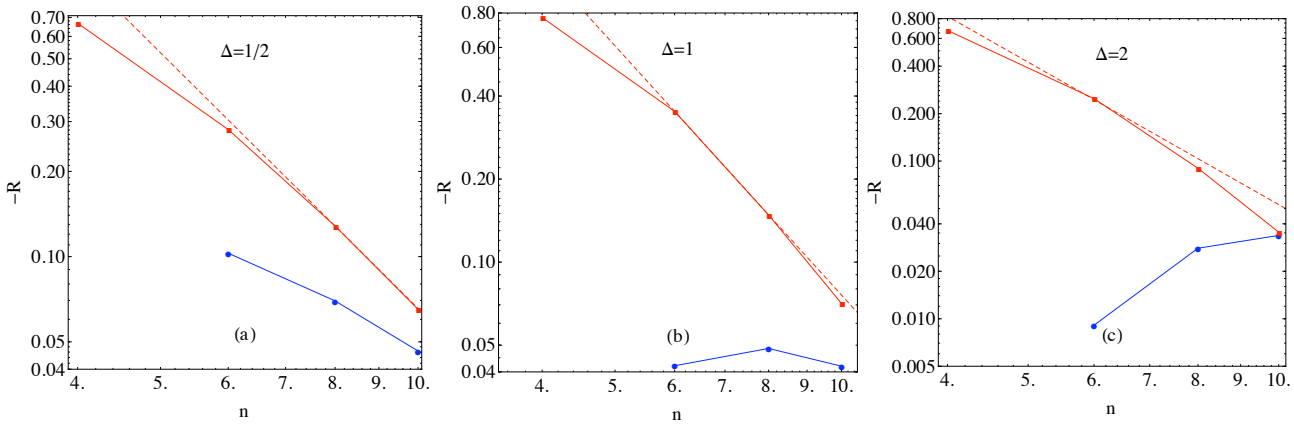


Figure 21.3: The scaling of the spectal gap R with the system size n in the log-log scale, for the three values of anisotropy $\Delta = 1/2$ (a), $\Delta = 1$ (b), and $\Delta = 2$ (c), and for the two symmetry subspaces, $\{+1, +1\}$ (red/squares) and $\{-1, -1\}$ (blue/circles). The dashed lines indicate the slope -3.

thermodynamically normal diffusive behavior in this regime (perhaps related to [38]).

In Fig. 21.3 we focus on the dependence of the relaxation rates of $\rho^\alpha(t)$ to the respective steady state ρ^α_∞ on the chain length n. The relaxation rate is determined as the Liouvillean spectral gap $R = \min_{\lambda_j \neq 0}(-\mathrm{Re}\,\lambda_j)$ where λ_j denote the eigenvalues of the Liouvillian superoperator $\hat{\mathcal{L}}$ in the respective symmetry subspace ($\{+1, +1\}$ or $\{-1, -1\}$). We find consistently that in the $\{+1, +1\}$ sector the spectral gap always quickly decays with n, perhaps faster than n^{-3}, which is the gap-scaling derived analytically or numerically suggested for some integrable spin chains with boundary driving [13, 35]. On the other hand, we are unable to conclude anything meaningful on the scaling of the gap in the $\{-1, -1\}$ symmetry sector, where the behavior of $R(n)$ may not even be monotonic. To complement the spectral information we plot in Fig. 21.4 the set of all Liouvillian eigenvalues λ_j which lie sufficiently close to the imaginary line (i.e. with sufficiently small damping rates $-\mathrm{Re}\lambda_j$). Further, we considered the density distribution of Liouvillian spectrum projected onto the real line, in fact a cumulative distribution $W(r) = \sum_{\lambda_j} \theta(r - \mathrm{Re}\,\lambda_j)/\sum_{\lambda_j} 1$ giving the probability that a randomly picked damping rate is larger than $-r$. Here $\theta(r)$ designates a Heaviside step function. The plot of $W(r)$ for the two symmetry sectors shown in Fig. 21.5 in the easy-axis regime $\Delta = 2$ suggests existence of two pseudo-gaps, particularly clearly for the $\{-1, -1\}$ symmetry sector.

21.3 Discussion and conclusion

We have presented a small but potentially very useful observation on the symmetry reduction of the Linbdblad master equations describing Markovian open quantum systems. We classified quantum Liouvillian symmetries as weak or strong, depending, respectively, on whether only the generator of master equation as a whole commutes with the symmetry operation, or whether each of the Lindblad (jump) operators, and the Hamiltonian, commute with the symmetry individually. We have shown that only existence of a strong symmetry implies nontrivial symmetry reductions inside the space of steady states (fixed points of the Markovian semi-group). We have also provided a non-trivial example of our construction in the context of quantum transport problem for the strongly interacting XXZ spin 1/2 chain. Namely defining an open XXZ chain with a micro-canonical constraint, we have shown that it exhibits a strong parity-type symmetry and outlined numerical computation of distinct steady states and the corresponding physical observables. Our numerical results seem to suggest that microcanonically constrained

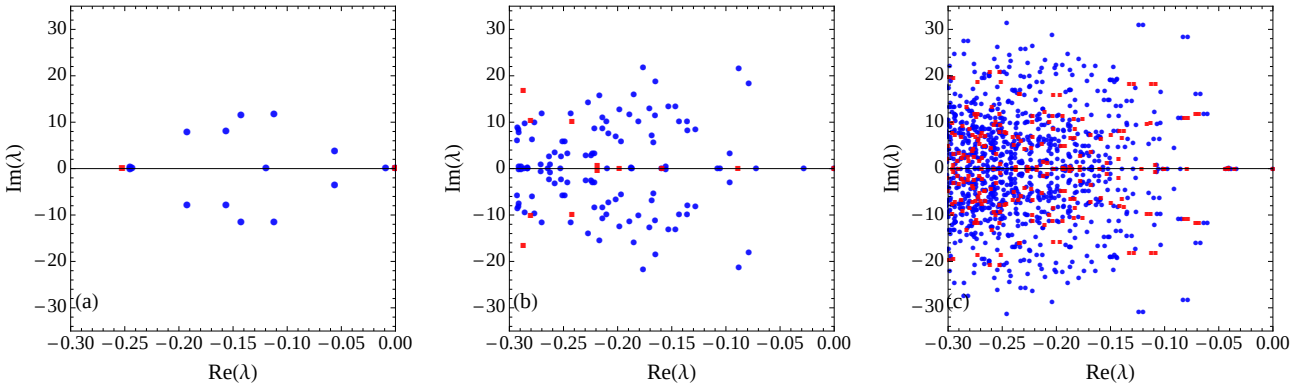


Figure 21.4: The full Liouvillian spectra $\{\lambda_j\}$ for the case of $\Delta = 2$ and for three different chain sizes $n = 6$ (a), $n = 8$ (b), and $n = 10$ (c), and for the two symmetry subspaces, $\{+1, +1\}$ (red/squares) and $\{-1, -1\}$ (blue/circles). We plot just a small part of the complex plane close to the imaginary line (i.e. plotting just the smallest rates corresponding to longest-lived modes).

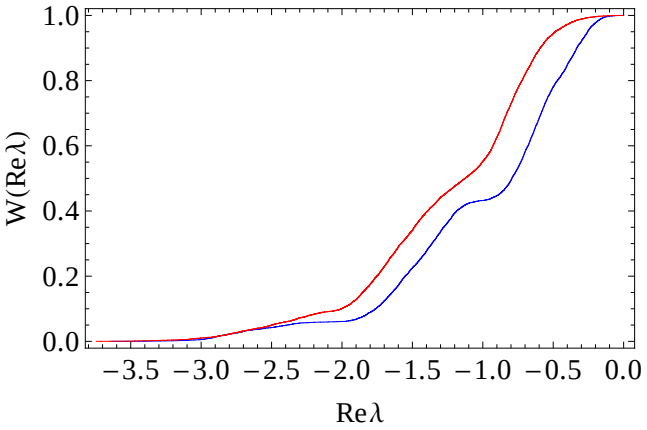


Figure 21.5: The cumulative distribution $W(r)$ of the the case $\Delta = 2$, $n = 10$, i.e. the probability that the randomly chosen decay rate $-\mathrm{Re}\,\lambda_j$ is larger than $-r$, for the two symmetry subspaces, $\{+1, +1\}$ (red) and $\{-1, -1\}$ (blue). Note the occurrence of two pseudo-gaps (strips in complex plane with very few – rarely distributed decay modes), particularly visible in the data for $\{-1, -1\}$.

open XXZ chain exhibits a sub-diffusive (thermodynamically insulating) behavior in the gapped Ising-like (easy axis) phase.

We note that both, weak and strong symmetries can provide practical advantage in description of quantum Liouvillian flows, as they both allow to block-diagonalize and hence reduce the dimension of the Liouvillian. One can also have a combination of both, namely independent generators of weak and strong symmetries, or non-abelian symmetries of either type. In particular, the study of non-abelian Liouvillian symmetries should be an important line of future research.

21.4 Appendix: Symmetry reductions of quantum Liouvillian dynamics

Let us consider two cases of symmetric Lindblad master equations with two different kinds of dissipators of the flow (21.1):

1. For the first kind, which we will call a weak symmetry, we assume that there exist a unitary operator S over $\mathcal{H}$, such that

$$\hat{\mathcal{L}}(SxS^\dagger) = S(\hat{\mathcal{L}}x)S^\dagger \tag{21.11}$$

for any $x \in \mathcal{B}(\mathcal{H})$.

2. For the second kind, which we will call a strong symmetry, we assume that a unitary operator S over $\mathcal{H}$ commutes with each member of the set $\{H, L_m, m = 1, 2, \ldots\}$ individually

$$[S, H] = 0, \quad [S, L_m] = 0, \ m = 1, 2, \ldots \tag{21.12}$$

Clearly (ii) implies (i), but not vice versa.

We continue by fixing some notation. Let $s_\alpha = e^{\mathrm{i}\theta_\alpha}$, $\alpha = 1, 2 \ldots n_S$ denote distinct eigenvalues of S, and let $\mathcal{H}_\alpha$ be the corresponding mutually orthogonal eigenspaces, so that we have a complete symmetry decomposition of the Hilbert space

$$\mathcal{H} = \bigoplus_{\alpha=1}^{n_S} \mathcal{H}_\alpha. \tag{21.13}$$

The adjoint representation of S on Hilbert space $\mathcal{B}(\mathcal{H})$ shall be denoted as $\hat{S}$,

$$\hat{S}(x) = SxS^\dagger. \tag{21.14}$$

The spectrum of a super-operator $\hat{S}$ is formed of all possible products $s_\alpha \bar{s}_\beta = e^{\mathrm{i}(\theta_\alpha - \theta_\beta)}$, since $\hat{S}(|\psi\rangle\langle\phi|) = s_\alpha \bar{s}_\beta |\psi\rangle\langle\phi|$ for any $|\psi\rangle \in \mathcal{H}_\alpha$, $|\phi\rangle \in \mathcal{H}_\beta$. Let s'_ν, $\nu = 1, 2, \ldots n_{\hat{S}}$ denote the distinct eigenvalues of $\hat{S}$, denoted such that $s'_1 = 1$, and $s'_\nu \neq 1$ for all $\nu \neq 1$. Note that the following bounds always hold

$$n_S \leq n_{\hat{S}} \leq n_S(n_S - 1). \tag{21.15}$$

The lower bound $n_{\hat{S}} = n_S$ is reached when $\{s_\alpha\}$ are roots of unity, i.e. in the case of $\mathbb{Z}_{n_S}$ symmetry obeying $S^{n_S} = 1$. The upper bound $n_{\hat{S}} = n_S(n_S - 1)$ is reached when there is no arithmetic structure in the spectrum $\{s_\alpha\}$ which may happen when S generates a continuous group of symmetry transformations. Let

$$\mathcal{B}(\mathcal{H}) = \bigoplus_{\nu=1}^{n_{\hat{S}}} \mathcal{B}_\nu \tag{21.16}$$

be the corresponding symmetry decomposition of the operator space $\mathcal{B}(\mathcal{H})$, where the $\hat{S}$-eigenspaces $\mathcal{B}_\nu$ are mutually orthogonal in the Hilbert-Schmidt sense.

Clearly, having a weak symmetry (21.11) is equivalent to having commuting superoperators

$$\hat{\mathcal{L}}\hat{S} = \hat{S}\hat{\mathcal{L}} \tag{21.17}$$

which means that the Liouvillian is block diagonalized with respect to the decomposition (21.16), namely

$$\hat{\mathcal{L}}\mathcal{B}_\nu \subseteq \mathcal{B}_\nu, \tag{21.18}$$

i.e. all spaces $\mathcal{B}_\nu$ are invariant w.r.t. the flow (21.1). Note that only $\mathcal{B}_1$ contains operators with non-vanishing trace, thus it should contain the fixed point $\rho_\infty \in \mathcal{B}_1$ due to the trace preservation. We remark that under the conditions of the Evans theorem [22] NESS can be unique despite the existence of a weak symmetry, as shall be the case in the example outlined in the next section.

Let us now assume the existence of a strong symmetry. In this case we can prove the following useful result:

Theorem 21.1. *Existence of a unitary operartor S with the property (21.12) implies:*

1. *Liouvillian $\hat{\mathcal{L}}$ can be block-decomposed into n_S^2 invariant subspaces*

$$\hat{\mathcal{L}}\mathcal{B}_{\alpha,\beta} \subseteq \mathcal{B}_{\alpha,\beta},$$

   where $\mathcal{B}_{\alpha,\beta} = \{|\psi\rangle\langle\phi|; |\psi\rangle \in \mathcal{H}_\alpha, |\phi\rangle \in \mathcal{H}_\beta\}$ for $\alpha, \beta = 1, 2, \ldots n_S$.

2. *We have at least n_S distinct fixed points (NESSs), which we can label by s_α, namely each diagonal operator space contains at least one fixed point,*

$$\rho_\infty^\alpha \in \mathcal{B}_{\alpha,\alpha}$$

   for $\alpha = 1, 2, \ldots n_S$.

Proof Let us write the super-operators of left and right multiplications with the symmetry operator $\hat{S}_{\mathrm{L}}(x) \equiv Sx$, $\hat{S}_{\mathrm{R}}(x) \equiv xS^\dagger$, for any $x \in \mathcal{B}(\mathcal{H})$. Since, clearly, $[\hat{S}_{\mathrm{L}}, \hat{S}_{\mathrm{R}}] = 0$, the spaces $\mathcal{B}_{\alpha,\beta}$ can be considered as the joint eigenspaces of both $\hat{S}_{\mathrm{L}}$ and $\hat{S}_{\mathrm{R}}$. Namely $\hat{S}_{\mathrm{L}}(|\psi\rangle\langle\phi|) = s_\alpha|\psi\rangle\langle\phi|$, $\hat{S}_{\mathrm{R}}(|\psi\rangle\langle\phi|) = \bar{s}_\beta|\psi\rangle\langle\phi|$, for any $|\psi\rangle \in \mathcal{H}_\alpha$, $|\phi\rangle \in \mathcal{H}_\beta$. Eq. (21.12) implies commutativity $[\hat{\mathcal{L}}, \hat{S}_{\mathrm{L}}] = 0$, $[\hat{\mathcal{L}}, \hat{S}_{\mathrm{R}}] = 0$, implying that any $\mathcal{B}_{\alpha,\beta}$ is also invariant subspace of $\hat{\mathcal{L}}$ proving point (i) of the theorem.

To prove (ii) we note again that operators with non-vanishing trace can only be contained in diagonal spaces $\mathcal{B}_{\alpha,\alpha}$, due to mutual orthogonality of $\mathcal{H}_\alpha$. Hence starting from some $\rho^\alpha(0) \in \mathcal{B}_{\alpha,\alpha}$ with $\operatorname{tr}\rho^\alpha(0) = 1$ (say $\rho(0) = P_\alpha/\operatorname{tr}P_\alpha$ where P_α is orthogonal projector to the subspace $\mathcal{H}_\alpha$), the flow (21.1) yields a fixed point ρ_∞^α in $\mathcal{B}_{\alpha,\alpha}$ for any $\alpha = 1, \ldots, n_S$. Again according to Evans theorem [22] this fixed point can be unique, or further degenerate. In any case, we have at least n_S distinct steady states, which may be labelled by the symmetry eigenvalue s_α. QED

Clearly, the direct sum of all invariant subspaces give the entire operator space

$$\mathcal{B}(\mathcal{H}) = \bigoplus_{\alpha=1}^{n_S}\bigoplus_{\beta=1}^{n_S}\mathcal{B}_{\alpha,\beta}, \tag{21.19}$$

and the quotient invariant spaces (21.16) are given by partial direct sums

$$\mathcal{B}_\nu = \bigoplus_{\alpha,\beta}^{s_\alpha\bar{s}_\beta=s'_\nu}\mathcal{B}_{\alpha,\beta}. \tag{21.20}$$

We remark that (non-positive) initial conditions $\rho(0)$ supported in the non-diagonal invariant spaces $\mathcal{B}_{\alpha,\beta}$, $\alpha \neq \beta$, which have vanishing trace, could in principle provide extra degeneracy of the null space of $\hat{\mathcal{L}}$, i.e. an extra dimension of the convex set of NESSs, or simply complete the description of the relaxation process for a general initial condition $\rho(0)$. In other words, we do not see any argument which would forbid the spectra of block-operators $\hat{\mathcal{L}}|_{\mathcal{B}_{\alpha,\beta}}$ to contain 0 even for $\alpha \neq \beta$, although this should be – if possible at all – an exceptional (non-generic) situation.

22 Quantum reaction-limited reaction-diffusion dynamics of noninteracting Bose gases by Rowlands et al.

Abstract

We investigate quantum reaction-diffusion systems in one-dimension with bosonic particles that coherently hop in a lattice, and when brought in range react dissipatively. Such reactions involve binary annihilation ($A+A \to \emptyset$) and coagulation ($A+A \to A$) of particles at distance d. We consider the reaction-limited regime, where dissipative reactions take place at a rate that is small compared to that of coherent hopping. In classical reaction-diffusion systems, this regime is correctly captured by the mean-field approximation. In quantum reaction-diffusion systems, for noninteracting fermionic systems, the reaction-limited regime recently attracted considerable attention because it has been shown to give universal power law decay beyond mean field for the density of particles as a function of time. Here, we address the question whether such universal behavior is present also in the case of the noninteracting Bose gas. We show that beyond mean-field density decay for bosons is possible only for reactions that allow for destructive interference of different decay channels. Furthermore, we study an absorbing-state phase transition induced by the competition between branching $A \to A+A$, decay $A \to \emptyset$ and coagulation $A+A \to A$. We find a stationary phase-diagram, where a first and a second-order transition line meet at a bicritical point which is described by tricritical directed percolation. These results show that quantum statistics significantly impact on both the stationary and the dynamical universal behavior of quantum reaction-diffusion systems.

22.0.1 Introduction

The systematic classification of universal properties in nonequilibrium many-body systems is a timely and challenging research direction in statistical mechanics. In this field, reaction-diffusion (RD) models are an important class of classical many-body nonequilibrium systems where dynamical critical behavior has been thoroughly studied [1, 2, 3, 4, 5, 6]. These systems describe particles which diffuse at rate Ω through random motion in space and, when brought in contact, can react with each other at rate Γ. The particle density $n(t)$ of RD systems at long times t decays as a power law. The latter is described in the "reaction-limited regime" of strong diffusion $\Gamma \ll \Omega$ by mean-field approximation [3, 1, 7, 8, 4, 9]. Fast diffusion, indeed, quickly erases spatial structures rendering the density profile homogeneous in space. Under these conditions, the dynamics is described by law of mass action rate equations, which for reactions as $mA \to lA$ ($l < m$) predict

$$n(t) \sim (\Gamma t)^{-1/(m-1)}. \tag{22.1}$$

In particular, annihilation $2A \to \emptyset$ at rate Γ_α ($m = 2$, $l = 1$) and coagulation $2A \to A$ ($m = 2$, $l = 1$) at rate Γ_γ within mean field behave as $n(t) \sim (\Gamma_{\alpha,\gamma} t)^{-1}$. In the opposite "diffusion-limited regime" $\Gamma/\Omega \sim 1$, instead, spatial fluctuations are relevant. Annihilation and coagulation, for

instance, belong the same universality class and in one dimension, $D = 1$, in both the cases one finds algebraic decay [10, 11, 12, 13, 14, 15, 16, 17, 18, 19, 5, 20, 21, 22, 23, 24] beyond mean field

$$n(t) \sim (\Omega t)^{-1/2}. \tag{22.2}$$

For $D > 1$, instead, the mean-field prediction (22.1) is retrieved as diffusion is effective in filling the whole available space thus eventually rendering the density homogeneous. Reaction-diffusion systems display also stationary-state universal properties. This happens when branching processes $A \to A+A$, at rate Γ_β, injecting particles into the system are considered. Namely, in the contact process (CP) [3, 2, 5, 6], the competition between branching and one-body decay $A \to \emptyset$, at rate Γ_δ, induces a stationary-state phase transition. In the thermodynamic limit and at long times, tuning the relative strength $\Gamma_\beta/\Gamma_\delta$ between the branching and the decay rate, one has either an active phase, where the stationary density is nonzero, or an inactive phase with zero density. In the latter phase, the stationary state is an absorbing-state void of particles and no fluctuations are possible. The absorbing-state phase transition of the contact process is of second-order and it belongs to the directed percolation universality class [3, 1, 7, 8, 4]. For restricted occupancy of the lattice, the stationary density in the active phase is finite, while in the unrestricted case one needs to include also annihilation and/or coagulation in order to have a finite stationary density [19, 6, 25].

Quantum RD systems have been only recently been addressed and studied in Refs. [26, 27, 28, 29, 30, 31, 32, 33, 34, 35, 36, 37, 38, 39, 40, 41]. The dynamics is formulated in terms of the Markovian quantum master equation [42, 43, 44], where coherent-Hamiltonian hopping replaces stochastic diffusion while reactions are dissipative. These quantum RD models attract significant attention since they connect the physics of Markovian open quantum systems [45, 46, 47, 48, 49, 50, 51, 52, 53] to that of systems with kinetic constraints [54, 55, 56, 57, 58, 59, 60, 61, 62, 63, 64, 65, 66, 67, 68]. From the experimental perspective, on the one hand, quantum RD systems naturally connect to cold-atomic experiments involving particle losses [69, 70, 71, 72, 73, 74, 75, 76]. From the theoretical perspective, on the other hand, quantum RD systems are interesting since they allow to investigate whether and how quantum effects alter the universal properties of the dynamics. However, a fair assessment of out-of-equilibrium universal properties necessarily requires considering simultaneously large system sizes and long times. This regime is hard to treat due to the exponential complexity of many-body quantum simulations. For this reason, quantum RD models provide a natural test-bed for quantum simulators [77, 78, 79, 80] and large-scale numerical simulations [26, 61, 62, 63, 81]. No analytical prediction for the quantum analogue of the diffusion-limited regime (22.2) is, indeed, currently available.

Quantum RD systems have been treated analytically, in the thermodynamic limit, only in the reaction-limited regime in Refs. [34, 35, 37, 36, 33, 38, 39, 41] for fermionic systems both in the lattice [34, 36, 38, 33, 39] and in the continuum [35, 37, 41]. Spin systems subject to m-body losses have been also considered in Ref. [40]. The studies [34, 35, 37, 36, 38, 39, 41, 40] are all based on the time-dependent generalized Gibbs ensemble (TGGE) method [82, 83, 84, 85, 86], while [41] employs Keldysh field-theory diagrammatics to show the emergence of the TGGE dynamical equation. It has been found in these references that universal decay beyond mean field is present for initial states displaying quantum coherences in real space. The law of mass action prediction (22.1) is, instead, recovered when the dynamics starts from incoherent initial states. This is specifically true for annihilation processes of m neighbouring particles $mA \to \emptyset$ [38, 39, 40] (on site multibody losses are not possible for fermions). For $2A \to \emptyset$, for coherent initial states, one specifically finds $n(t) \sim (\Gamma_\alpha t)^{-1/2}$. Coagulation reactions $2A \to A$, on the contrary, decay as $n(t) \sim (\Gamma_\gamma t)^{-1}$ with the mean-field exponent is found both for coherent and incoherent initial states. This, in particular, shows that for quantum systems binary annihilation and coagulation do not belong to the same universality class, in stark contrast to

the classical case. In Refs. [34, 38], annihilation reactions that create quantum superpositions between two nearest-neighbor decay channels were considered. Annihilation jump operators with this feature introduce inherent quantum interference effects and allows for a non-mean-field decay $n(t) \sim (\Gamma_\alpha t)^{-1/2}$ for both coherent and incoherent initial states. For the case where the CP is considered with branching and decay, the associated absorbing-state phase transition is of second order and it is found to belong to the mean-field directed percolation universality class.

The reaction-limited dynamics of the interacting Bose gas has been studied in Ref. [37]. In the limiting case of no interaction, it is therein found that the density for onsite losses $mA \to \emptyset$ decays according to the law of mass action (22.1). For other kinds of reactions additional analysis is, however, needed. In particular, it is interesting to understand whether reactions coupling bosons at different sites possibly creating superpositions between two, or more, decay channels induce beyond mean-field decay, as in the aforementioned fermionic cases. Furthermore, the quantum reaction-limited dynamics of the Bose gas in the presence of reactions, such as branching, creating particles has not been analyzed so far. In this perspective, for bosons, the universality class and the order of the absorbing-state phase transition taking place in the presence of branching is also not understood.

The goal of this manuscript is to address the impact of quantum bosonic statistics on the universal behavior of the quantum RD dynamics. In particular, we study the impact of the bosonic statistics both on the relaxation dynamics of the noninteracting Bose gas and on the universality class of its stationary phase diagram obtained in the presence of branching reactions. In both the relaxation and the stationary case, our goal is then to show that the universal properties of quantum RD dynamics of the Bose gas significantly differ both from the fermionic formulation and from their classical counterpart.

Our approach is based on analytically studying the quantum RD dynamics of the noninteracting Bose gas in the reaction-limited regime and in the thermodynamic limit. We employ the time-dependent generalised Gibbs ensemble (TGGE) method [82, 83, 84, 85, 86]. We first consider distance-selective binary losses, which amount to a loss of two bosons at a distance d. We further allow for the possibility of interference between two or three decay channels of the distance selective loss. We then move to the case of onsite coagulation reactions and eventually consider the absorbing-state phase transition induced by the competition between coagulation, branching and one-body decay.

We find that distance selective losses eventually always render, independently of the initial state, the law of mass action prediction

$$n(t) \sim (\Gamma_\alpha t)^{-1}, \quad \text{distance-selective } 2A \to \emptyset, \tag{22.3}$$

for any value of the distance d. This is in contrast to the case of fermionic systems, where non-mean-field behavior is found for nearest neighbor annihilation ($d = 1$). The case where interference between two annihilation decay channels is present is then discussed. When the channels are unequally weighted, we retrieve mean-field behaviour as in Eq. (22.3). For a fine-tuned equal balance between the two channels, instead, we find algebraic decay beyond mean-field for any value $d \geq 1$. Namely, we observe the same asymptotic decay as in Refs. [34, 38] for fermions,

$$n(t) \sim (\Gamma_\alpha t)^{-1/2}, \text{ two-channels interference, } 2A \to \emptyset. \tag{22.4}$$

The main difference with respect to the fermionic case is that in the latter case Eq. (22.4) does not require the two decay channels to be equally weighted. We eventually consider the case where the interference takes place between three neighbouring decay channels (rate $\Gamma_{\bar{\alpha}}$). In this case, we also find beyond mean-field decay

$$n(t) \sim (\Gamma_{\bar{\alpha}} t)^{-0.28}, \text{ three-channels interference, } 2A \to \emptyset. \tag{22.5}$$

for any $d \geq 1$. These results show that for bosons interference effects within the annihilation decay channels are necessary in order to get beyond mean-field algebraic decays. For onsite coagulation, we find mean-field decay

$$n(t) \sim (\Gamma_\gamma t)^{-1}, \tag{22.6}$$

when coagulation is considered alone. This decay is valid independently of the initial state considered. Equation (22.6) implies that for bosons annihilation (22.3) and coagulation share the same decay exponent and they belong, at least in the reaction-limited regime, to the same universality class. This again contrasts the fermionic case of Ref. [38], where the same reaction-limited decay exponent is observed only for incoherent initial states.

The competition between coagulation, one-body decay and branching in the CP reveals gives rise to an interesting phase diagram. It is of mean-field nature but considerably richer than the phase diagram obtained within the classical and fermionic reaction-limited cases. In particular, we find a change of the absorbing-state phase transition from first to second order as the relative strength $\Gamma_\beta/\Gamma_\delta$ between classical branching and decay is tuned. These first and second-order transition lines meet at a bicritical point, which is characterized by the mean-field exponents of tricritical directed percolation [87, 88, 89]. Mean-field exponents are here observed already in one dimensions since the reaction-limited regime with fast hopping mixing is considered. A similar phase diagram has been previously observed in Refs. [57, 58] for a different spin 1/2 model, where classical branching/coagulation competes with quantum branching/coagulation. Therein the order of the transition is changed as the relative strength between coherent and incoherent branching is tuned. The phase transitions observed in our work, however, solely rely on classical reactions, with the only quantum effect stemming from the hopping of the bosons.

This manuscript is structured as follows. In Sec. 22.0.2, we discuss the formulation of quantum RD dynamics in terms of the quantum master equation. We further present all the reactions processes analysed in the text. In Sec. 22.0.3, we briefly review known results of classical RD dynamics and then we discuss the quantum RD dynamics. In particular, we focus on the reaction-limited regime, which is the main subject of the text. We briefly introduce the TGGE method and we write the associated dynamical equation for the bosonic occupation function in momentum space. In Sec. 22.0.4, we specialize this equation to the various processes introduced in Sec. 22.0.2. In Sec. 22.0.6, we summarize and discuss our results. The Appendices 22.1-22.4 contain technical aspects and details regarding the calculations at the basis of the results presented in the main text.

22.0.2 The system

We consider bosonic particles on a quantum chain of length L with periodic boundary conditions. The j-th lattice site of the chain can therefore either be occupied, $\hat{n}_j|\cdots \mathrm{n}_j \cdots\rangle = \mathrm{n}_j|\cdots \mathrm{n}_j \cdots\rangle$, or empty, $\hat{n}_j|\cdots 0_j \cdots\rangle = 0$, with $\hat{n}_j = \hat{b}_j^\dagger \hat{b}_j$ the number operator at site j. Here, $\hat{b}_j$ and $\hat{b}_j^\dagger$ are bosonic destruction and creation operators, respectively, obeying the bosonic commutation rule $[\hat{b}_i, \hat{b}_j^\dagger] = \delta_{i,j}$. Each site can be occupied by n_j bosons with $\mathrm{n} \in \mathbb{N}$, so that the total number of particles at each lattice site is unrestricted. The quantum reaction-diffusion dynamics of the system is ruled by the Lindblad master equation [42, 43, 44] (we set $\hbar = 1$ in the whole manuscript)

$$\dot{\rho}(t) = -i\,[H, \rho(t)] + \mathcal{D}[\rho(t)], \tag{22.7}$$

where ρ is the density matrix. In the quantum formulation of the RD dynamics, classical-incoherent hopping (diffusion in the continuum limit) is replaced by coherent hopping of par-

ticles between neighbouring sites according to the Hamiltonian H:

$$H = -\Omega \sum_{j=1}^{L} \left(\hat{b}_j^\dagger \hat{b}_{j+1} + \hat{b}_{j+1}^\dagger \hat{b}_j \right), \tag{22.8}$$

with the hopping rate Ω. The Hamiltonian, thus, conserves the number of particles ($[H, N(t)] = 0$, with $\hat{N} = \sum_j \hat{n}_j$ the total particle number). We note that H describes the noninteracting Bose gas (vanishing interaction strength) on a optical lattice. The dissipator $\mathcal{D}[\rho]$ accounts for the irreversible reaction processes and it is of Lindblad form

$$\mathcal{D}(\rho) = \sum_{j,\nu} \left(L_j^\nu \rho L_j^{\nu\dagger} - \frac{1}{2} \left\{ L_j^{\nu\dagger} L_j^\nu, \rho \right\} \right), \tag{22.9}$$

where L_j^ν are dubbed jump operators. The superscript ν labels the different reaction types. We consider various reaction types, which are pictorially represented in Fig. 22.1. All these dissipative processes violate particle number conservation. Distance-selective binary annihilation $A + A \to \emptyset$ (rate Γ_α) destroys pairs of particles at a distance d and is represented by the jump operator

$$L_j^\alpha = \sqrt{\Gamma_\alpha} \hat{b}_j \left(\cos(\theta) \hat{b}_{j+d} - \sin(\theta) \hat{b}_{j-d} \right), \tag{22.10}$$

Here, the parameter $\theta \in [0, \pi)$ allows for interferences between two decay channels. At $\theta = 0$ or $\theta = \pi/2$, the annihilation operator reduces to the classical-incoherent binary annihilation of particles at distance d. Such incoherent distance-selective losses have been analyzed in Refs. [30, 31] for hard-core bosons, where they were implemented via laser-exciting highly excited electronic Rydberg states in the facilitation regime. For $\theta \neq 0, \pi/2$, on the other hand, the jump operators (22.10) effectuate transitions into quantum superposition states, thereby creating quantum coherence. Such setting, whose microscopic origin is the quantum interference of two annihilation channels, was previously studied in Refs. [34, 38] for fermions.

To further study the impact of interferences onto the quantum bosonic RD dynamics, we consider a binary annihilation process (rate $\Gamma_{\bar{\alpha}}$) which couple three decay channels

$$L_j^{\bar{\alpha}} = \sqrt{\Gamma_{\bar{\alpha}}} \hat{b}_j \left(\hat{b}_{j+d} + \hat{b}_{j-d} - 2\hat{b}_j \right), \tag{22.11}$$

between particles at fixed distance d. We refer to the jump operator (22.11) henceforth as second-order annihilation reaction as $L_j^{\bar{\alpha}}$ is constructed such that in the continuum space limit, the zeroth and the first order of the expansion the jump operator in the lattice spacing vanish (see Appendix 22.1 for the details). We anticipate (see the discussion in Subsecs. 22.0.5 for further details) that both the jump operator (22.10), with $\theta = \pi/4$, and (22.11) have a zero-momentum Bose-Einstein condensate state (BEC) as an exact dark state. Similar jump operators having the BEC as a many-body dark state, albeit still conserving the total particle number, have been studied, e.g., in Refs. [46, 49].

Other types of reactions we are considering is onsite coagulation $A + A \to A$ (rate Γ_γ)

$$L_j^\gamma = \sqrt{\Gamma_\gamma} \hat{n}_j \hat{b}_j. \tag{22.12}$$

and one-body decay $A \to \emptyset$ (rate Γ_δ)

$$L_j^\delta = \sqrt{\Gamma_\delta} \hat{b}_j. \tag{22.13}$$

In all the cases (22.10)-(22.13), the density of particles $n(t) = \langle \hat{N}(t) \rangle / L$ is a monotonically decreasing function of time t. The universal behavior of the dynamics lies in the asymptotic late-time approach of the system towards the steady state devoid of particles.

In order to have a nontrivial steady state, supporting a nonzero density of particles, we need to include reactions that increase the particle number (see Fig. 22.1). We do this by introducing onsite branching reactions $A \to A + A$ (rate Γ_β)

$$L_j^\beta = \sqrt{\Gamma_\beta}\hat{b}_j^\dagger \hat{n}_j, \tag{22.14}$$

which lead to the creation of an offspring from a lattice site already occupied by at least one particle. The form of the jump operators (22.12) and (22.14) is dictated by bosonic statistics, allowing reactions to take place at the same lattice site.

The competition between branching (22.14) and decay (22.13) in systems with restricted occupation of lattice sites (spin or fermionic systems) leads to a second-order (continuous) stationary-state phase transitions separating an active (nonzero density) phase from an inactive-aborbing one (with zero density) [25]. For bosons the maximum occupation number per site is unrestricted. Therefore, in order to have a finite density in the active phase also coagulation (22.12) (or annihilation (22.10)) has to be considered [19, 6, 25]. Here, universal behavior emerges near the critical point of the ensuing second-order phase transition, as we recall in the next Sec. 22.0.3.

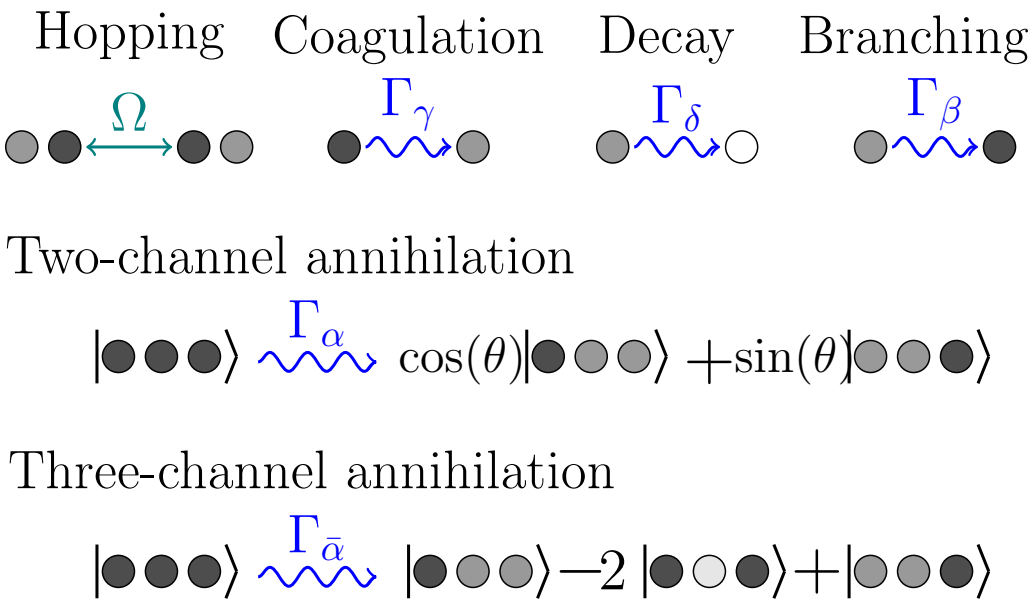


Figure 22.1: **Quantum RD dynamics.** Sketch of the fundamental processes of the quantum RD dynamics. We consider a quantum bosonic chain where each site (circles) can be occupied by an integer number $n \in \mathbb{N}$ of bosons. The grayscale filling of circles pictorially represents the higher (darker) or lower (brighter) occupancy of a lattice site. White circles represent empty lattice sites. In the top line, coherent hopping according to H in Eq. (22.8) at rate Ω is sketched. The latter replaces classical-incoherent hopping (diffusion in the continuum limit). The reactions are irreversible and are modelled by the jump operators Eqs. (22.10) - (22.14) of the Lindblad dynamics. Coagulation, branching and decay are sketched. Note that coagulation requires at least two particles on the lattice site (transition from darker-grey to brighter-grey circle), while decay can act also on single occupied site (transition from grey to white circle). In the middle line, the annihilation decay (22.10) at distance $d = 1$, for the sake of illustrative purposes, is shown. For $\theta \neq 0, \pi/2$ coherent superposition between different quantum mechanical states is introduced into the dynamics. In the bottom line, the action of the jump operator (22.11) is sketched ($d = 1$ again). In this case, superposition of three different states is introduced.

22.0.3 Diffusion and Reaction-limited Dynamics

The dynamics of the density $n(t)$ as a function time is the central quantity characterizing the emergent universal behavior of RD systems. Two different timescales rule the RD dynamics: the reaction time $\sim \Gamma^{-1}$ and the diffusion time $\sim \Omega^{-1}$. The former quantifies the time (on average) two nearby particles take to react, while the latter the time (on average) two particles take to get in contact. The dynamics changes qualitatively depending on the ratio Γ/Ω. The limit $\Gamma/\Omega \ll 1$ is named "reaction-limited regime", while the limit where Γ/Ω is at least $\Gamma/\Omega \sim 1$, is dubbed "diffusion-limited regime". The exponent δ of the asymptotic power-law decay $n(t) \sim t^{-\delta}$ is different in the two regimes. In Subsec. 22.0.3, we first briefly recall and discuss previous results concerning the bosonic RD dynamics for classical systems. In Subsec. 22.0.3, we then recall aspects of the quantum RD dynamics that are relevant for the treatment of the present manuscript. In particular, we focus on the quantum-reaction limited regime, which is the main focus of this manuscript.

Classical RD Dynamics

Within the classical RD realm, the reaction-limited regime is well-described by the so-called "law of mass action" rate equation [3, 1, 7, 8, 4]. This equation states that the rate of reactions equals the product of the concentrations of reactants. For the annihilation reaction, where m particles react to l particles (with $m > l \in \mathbb{N}$), the law of mass action equation yields,

$$\frac{\mathrm{d}}{\mathrm{d}t} n(t) = -(m-l)\Gamma n^m(t). \tag{22.15}$$

Equation (22.15) is valid whenever reactions occur everywhere in space with the same probability, i.e., it is valid in a well-stirred regime where the density $n(t)$ is homogeneous. This is precisely the reaction-limited regime $\Gamma/\Omega \ll 1$, where the fast hopping (diffusion in continuum space) mixing wipes out spatial patterns in the density profile coming from local depletion of the particle number. For $m \geq 2$, the long-time behaviour associated to (22.15) is

$$n(t) \quad \propto \quad (\Gamma t)^{-1/(m-1)}\,. \tag{22.16}$$

The exponent of the power-law decay depends on the number of reactants m involved in the reaction. Note that in this regime, the density is a function of the rescaled time $\tau = \Gamma t$ according to the reaction rate Γ. This further shows that in the reaction-limited regime the limiting factor for the asymptotic decay of the density is the reaction time (controlled by Γ^{-1}).

The diffusion-limited regime, $\Gamma/\Omega \sim 1$, is qualitatively different. In this regime the hopping mixing is finite and therefore spatial fluctuations in the density profile, due to local depletion of the particle number, are relevant in the kinetics. For classical systems with unrestricted occupation, this problem has been analytically tackled in Refs. [17, 18, 19, 5, 20, 22, 23, 24] by mapping the classical microscopic master equation into a bosonic second-quantization problem via the Doi-Peliti formalism [21, 20]. From the latter, a field-theory description can be eventually derived. The associated renormalization group scaling analysis yields for $2A \to \emptyset$ in one dimension $D = 1$:

$$n(t) \propto (\Omega t)^{-1/2}. \tag{22.17}$$

Here, the density depends on the rescaled time $\tau = \Omega t$ according to the diffusion rate. The decay (22.17) applies classically also for coagulation $2A \to A$, which belongs, indeed, to the same universality class of annihilation [90, 91, 92, 93, 94]. The result (22.17) shows that the limit factor for the decay of the density of particles is, in this case, the time needed for two far apart particles to meet. This is a universal property of the random walk, which is recurrent only for $D \leq 2$. This explain both the universal character of Eq. (22.17) and the emergence of the

upper critical dimension $D_c = 2$. For $D \geq D_c$, diffusion is effective in filling the whole space and one recover the mean-field prediction (22.16) (up to a logarithmic correction at $D = D_c = 2$).

Reaction-diffusion model can also host stationary state phase transitions between an active phase and an absorbing one. This happens when branching reactions $A \to A + A$ are included. The CP model, namely, describes the stationary phase transition ensuing from the competition between branching (22.14) and (22.13). In the case where site occupancy is unrestricted, the so-called bosonic contact process [6, 25], one further needs to include coagulation (22.12) (or annihilation (22.10) at $\theta = 0$ and $d = 0$) in order to have a finite stationary density. This can be heuristically understood by writing the law of mass action(22.15) in the presence of branching and decay

$$\frac{\mathrm{d}n(t)}{\mathrm{d}t} = (\Gamma_\beta - \Gamma_\delta)n(t) - \Gamma_\gamma n^2(t). \tag{22.18}$$

This equation trivially admits the stationary solution $n_{\mathrm{stat}} = 0$ corresponding to the absorbing phase. Furthermore, one has the additional solution

$$n_{\mathrm{stat}} = \frac{\Gamma_\beta - \Gamma_\delta}{\Gamma_\gamma}, \tag{22.19}$$

if $\Gamma_\beta > \Gamma_\delta$. In the case of restricted CP, one does not need coagulation to have a finite stationary density since a term proportional to n^2 is produced on the right hand side of (22.18) due to the restricted occupation constraint $[n(t)(1 - n(t))$ from the branching]. Equation (22.18) immediately locates the mean-field critical point $\Gamma_\beta^c = \Gamma_\delta$ of the phase transition. This transition is classically of second order and it belongs to the directed percolation universality class [1, 2, 3, 4, 5, 6]. Universal behavior lies in the algebraic behavior of the order parameter $n_{\mathrm{stat}} \sim (\Gamma_\beta - \Gamma_\beta^c)^\beta$ close to the transition point. The associated critical exponent is $\beta = 1$ within the reaction-limited regime. Away from this limit, the exponent $\beta \neq 1$ differs from the mean-field prediction and it depends on the space-dimensionality for $D \leq D_c$, and $D_c = 4$ [1, 2, 3, 4, 5, 6]. We do not report these values here as they are not central for the understanding of the results of this manuscript, which is focused on the quantum analogue of Eqs. (22.18) and (22.19). We introduce the quantum reaction-limited regime in the next Subsection. We will see in Sec. 22.0.4 that the ensuing quantum reaction-limited equation for the CP displays a much richer phase diagram than that of Eqs. (22.18) and (22.19).

Quantum RD Dynamics

For quantum RD systems little is currently known. The quantum master equation in Eqs. (22.7)-(22.14) cannot be solved analytically since it is not quadratic as a consequence of the structure of the jump operators. At the same time, large-scale numerics, involving large system sizes and long times, is severely hindered since the simulation of the quantum trajectories associated to Eq. (22.7) requires the knowledge of the whole many-body wavefunction. Due to the exponential scaling of the Hilbert space with the system size L such simulations become rapidly infeasible. For example, in Ref. [26], the quantum XX spin-chain Hamiltonian (which maps to free fermions via Jordan-Wigner transformation) subject to binary annihilation $2A \to \emptyset$ or coagulation $2A \to A$ has been studied. Therein the diffusion-limited regime $\Omega = \Gamma = 1$ is considered, the initial state is the fully filled product state $|\bullet\bullet\cdots\bullet\rangle$ and a maximal system size of $L = 22$ is taken. Under such conditions, a power-law decay $n(t) \sim t^{-b}$, with $1/2 < b < 1$ is obtained for annihilation. The dynamics is therefore slower than the mean-field prediction (22.15) but faster than the classical diffusion-limited analogue (22.17). This might be related to the faster ballistic spreading of quantum particles, compared to classical diffusion, albeit the extrapolation of these results to the thermodynamic limit is difficult to assess. No analytical prediction for the quantum-diffusion limited decay exponent is far present. A field-theory description for $2A \to \emptyset$ has been proposed in Ref. [41] using the Keldysh field-theory

representation of the quantum master equation. A systematic renormalization group scaling analysis of this action is, however, still missing.

The quantum reaction-limited regime ($\Gamma/\Omega \ll 1$) is in this perspective unique since it allows exact analytical calculations in the thermodynamic limit and at long times. This regime has been recently studied in a number of works for fermionic and spin systems [34, 35, 36, 38, 39, 40], where occupation restrictions are therefore present. It has been therein shown that for fermionic particles the binary annihilation ($2A \to \emptyset$) decays as $n(t) \sim t^{-1/2}$ for quantum coherent (in real space) initial states. The dynamics is therefore not always well-described by the mean-field approach despite the system being in the reaction-limited regime. Quantum effects due to coherences therefore allow for novel form of emergent behavior, which do not have a classical counterpart. The interacting Bose gas, modelled by the Lieb-Liniger Hamiltonian, subject to m-body annihilation, $mA \to \emptyset$, has been considered in Ref. [37]. In the noninteracting limit, mean-field decay (22.15) is found for every m. In the presence of nonzero interaction, the numerical evaluation of the differential equation for the density turns out to be cumbersome and therefore no estimate for the density decay exponent is therein made. The analysis of all the works [34, 35, 37, 36, 38, 39, 40] is based on the analytical approach of the time-dependent Gibbs ensemble (TGGE) method [82, 83, 84, 85]. We briefly recall here this method as it will be used for all the results presented in Sec. 22.0.4.

The reaction-limited regime $\Gamma/\Omega \ll 1$ corresponds to weak dissipation regime of the Lindblad dynamics. In this limit, the reaction time $\sim 1/\Gamma$ is much larger than the hopping time $\sim 1/\Omega$. Because of this separation of time scales, the state of the system $\rho(t)$ quickly relaxes to a stationary state $\rho_{SS}(t)$ of the Hamiltonian $[H, \rho_{SS}(t)] = 0$. The stable quasi-particles characterizing the integrable Hamiltonian H (22.8) (it is trivially integrable since it is quadratic) can still be defined but they acquire a finite lifetime $\sim 1/\Gamma$. This causes the stationary state of the system becoming time-dependent $\rho_{SS}(t)$ and changing over the long time scale $1/\Gamma$. The TGGE method makes an ansatz for $\rho_{SS}(t)$ in the form of a GGE [95, 96].This ansatz is motivated by the idea of local generalized thermalization of the Hamiltonian dynamics in the limit of slow reactions. In this limit, the density matrix quickly relaxes towards a maximal-entropy generalized Gibbs state, which keeps into account all the conserved charges of the Hamiltonian. In the case of the Hamiltonian (22.8), all the conserved charges are linear combination of the occupation number $\hat{n}_k$ in momentum space [95, 96]. For the Hamiltonian (22.8), the time-dependent GGE (TGGE) then reads as [82, 83, 84, 85]

$$\rho_{\mathrm{GGE}}(\tau) = \frac{1}{\mathcal{Z}(\tau)} \exp\left(- \sum_k \lambda_k(\tau) \hat{n}_k \right), \tag{22.20}$$

with $\mathcal{Z}(\tau) = \mathrm{Tr}[\exp(-\sum_k \lambda_k(\tau)\hat{n}_k)]$. Here $k \in (-\pi, \pi)$ is the quasi-momentum and $\hat{n}_k = \hat{b}_k^\dagger \hat{b}_k$ the number operator in Fourier space with $\hat{b}_k, \hat{b}_k^\dagger$ the bosonic Fourier-transformed operators (see Appendix 22.2). The GGE state describes averages $\langle \mathcal{O} \rangle_{\mathrm{GGE}}$ of local observables $\mathcal{O}$ in the thermodynamic limit. The time-dependence of the TGGE is contained in the Lagrange multipliers (or generalised inverse temperatures) $\lambda_k \to \lambda_k(\tau)$. This implies that conserved charges can still be defined, but they slowly (on a time scale $\sim 1/\Gamma$) drift in time as consequence of the dissipation. Since $[\hat{n}_k, H] = 0$ for all k, $[\rho_{\mathrm{GGE}}(t), H] = 0$ and the master equation (22.7) takes the form:

$$\frac{d}{dt}\rho_{\mathrm{GGE}}(t) = \mathcal{D}[\rho_{\mathrm{GGE}}(t)]. \tag{22.21}$$

The state in Eq. (22.20) is diagonal in momentum space (because of translation invariance) and Gaussian. The entire dynamics ensuing from (22.20) is consequently encoded in the bosonic occupation function in momentum space $B_q(t) \equiv \langle \hat{b}_q^\dagger \hat{b}_k \rangle_{\mathrm{GGE}}(t) = \delta_{q,k}/(\exp(\lambda_q(t)) - 1)$. The time evolution for the Lagrange parameters $\lambda_q(t)$ is therefore in one-to-one correspondence

with that of $B_q(t)$. The dynamical differential equation for the latter immediately follows from Eq. (22.21) exploiting that $[\rho_{\mathrm{GGE}}, \hat{n}_{\mathrm{q}}] = 0$ [38, 34, 35, 36]:

$$\frac{dB_q(t)}{dt} = \sum_{j,\nu} \langle L_j^{\nu\dagger} \left[\hat{n}_q, L_j^{\nu}\right] \rangle_{\mathrm{GGE}}, \quad \forall q. \tag{22.22}$$

In the Appendices 22.2-22.4, we report the expression of the jump operators L_j^{ν} in Fourier space and we detail all the calculations based on Eq. (22.22).

It is also clear from the previous equation that $B_q(t) = B_q(\tau = \Gamma t)$, i.e., the bosonic occupation function is a function of the rescaled time $\tau = \Gamma t$ according to the reaction rate only. This is consistent with the reaction-limited description of the classical RD dynamics (22.15) and (22.16) where time obeys the very same rescaling. As a matter of fact, the TGGE ansatz of Eqs. (22.20) and (22.22) is valid in the scaling limit $t \to \infty$, $\Gamma \to 0$ with $\tau = \Gamma t$ fixed, as shown in Refs. [82, 83, 84, 85] We also mention that in the present case $B_q(\tau)$ does not depend on the space coordinate x since we only deal in this manuscript with homogeneous Lindbladians evolving from homogeneous initial states. This is also the reason why the hopping rate Ω does not appear in the equation (22.22). In homogeneous systems, indeed, there is no transport of particles. Consequently, in the limit $\Gamma/\Omega \ll 1$, the Hamiltonian contribution is effectively integrated out assuming local relaxation to the GGE state (22.20). Whenever spatial inhomogeneities are included, the Hamiltonian additionally contributes to Eq. (22.21) via a convective term describing ballistic transport of particles. Equation (22.21) takes in this case the form of a Boltzmann equation [35, 37, 40, 41].

The right hand side of Eq. (22.22) can be exactly computed from the Wick's theorem since it amounts to computing higher-point bosonic correlation functions over the Gaussian state (22.20). This allows to derive exact rate equations for $B_q(\tau)$. Within this perspective, the TGGE method presented here bears similarities with the Hartree-Fock decoupling of four (and higher) body terms in the dynamical equation for the two-point function $\langle \hat{b}_n^\dagger \hat{b}_m \rangle$ (with m, n lattice-site indices). This decoupling is often used in dissipative many-body systems, see, e.g., Ref. [97], in order to truncate the infinite hierarchy of equations for the correlation functions to a closed and calculable form. We, however, remark that the Hartree-Fock decoupling is an uncontrolled approximation, while the validity of the TGGE ansatz is controlled by the parameter $\Gamma \to 0$ (reaction-limited regime) according to the scaling limit $\tau = \Gamma t$ fixed explained above. Furthermore, the similarity between the two methods applies only in the present case of the noninteracting Bose gas with quadratic Hamiltonian (22.8). As discussed in Ref. [37], for the interacting Bose gas described by the Lieb-Liniger Hamiltonian, the GGE is not Gaussian and higher point function in the GGE state cannot be reduced to the two-point function via Wick theorem. In the next Section, we specialize (22.22) for the various reaction processes introduced before in Eqs. (22.10)-(22.14).

22.0.4 Results

Results/results

In this Section, we present our results for the quantum reaction-limited RD dynamics of bosonic particles. In Subsec. 22.0.4, we first discuss the distance-selective annihilation process (22.10) ($\theta = 0$). In Subsec. 22.0.5, we move to the discussion of annihilation processes with interferences between two decay channels, (22.10) with $\theta \neq 0, \pi/2$. In Subsec. 22.0.6, we discuss the second-order annihilation process with three interfering decay channels (22.11). In Subsec. 22.0.7, coagulation decay (22.12) is studied. In Subsec. 22.0.8, we consider the branching process (22.14). We then study the corresponding absorbing-state phase transition arising from the competition between branching (22.14), coagulation (22.12) and one-body decay (22.13). The associated stationary phase diagram is reported and discussed.

For all the aforementioned cases, we solve the TGGE rate equation in Eq. (22.22) for the bosonic momentum occupation function $B_q(\tau)$. Namely, we consider three different initial conditions: the Bose Einstein condensate (BEC) , Eq. (22.23), the flat mode filling, Eq. (22.24), and the Gaussian distributed mode filling, Eq. (22.25). The implemented initial conditions are the following:

- Bose Condensate:
$$B_q(0) = B_{\mathrm{BEC},q} = N \cdot \delta_{q,0}, \tag{22.23}$$
- Flat Filling:
$$B_q(0) = B_{\mathrm{FF}} = n_0, \tag{22.24}$$
- Gaussian State:
$$B_q(0) = B_{\mathrm{GS},q} = 2\sqrt{\pi} \cdot e^{-q^2}. \tag{22.25}$$

In the BEC, the quasi-momentum $q = 0$ is macroscopically populated by the total number N of bosons initially in the system. In one spatial dimension, this state corresponds to a quasi-condensate pure state $|\mathrm{BEC}\rangle = (\hat{b}^\dagger_{q=0})^N|0\rangle/\sqrt{N!}$ [98, 99]. In the flat filling, every mode in momentum space is equally occupied by the same number n_0 of bosons. The parameter n_0 is therefore the initial density of particles. In the state (22.25), the occupation of the modes is Gaussian distributed. The density is computed from the occupation function $B_q(\tau)$ as

$$\langle n(\tau)\rangle_{\mathrm{GGE}} = \frac{1}{L}\sum_q B_q(\tau) = \int_{-\pi}^{\pi} \frac{\mathrm{d}q}{2\pi} B_q(\tau), \tag{22.26}$$

the latter equality being valid as $L \to \infty$. Henceforth, we set $N = L$ in Eq. (22.23), and $n_0 = 1$ in Eq. (22.24), so that for all the three initial conditions we have an initial density $n_0 = 1$ [9].

The BEC state (22.23) has quantum coherences in real space since the associated density matrix has non-zero off-diagonal matrix elements in the bosonic Fock-space basis. The latter being spanned by states of the form $|\{\mathrm{n}_j\}\rangle = \prod_{j\in\Lambda} \hat{b}_j^{\mathrm{n}_j}|0\rangle$, with Λ denoting an arbitrary set of lattice sites. Similarly, the Gaussian state (22.25) corresponds to an initial state of the GGE form (22.20) identified by the occupation function $B_{\mathrm{GS},q}$ inhomogeneous in momentum space. The latter is associated to a bosonic two-point correlation function in real space $\langle \hat{b}^\dagger_n \hat{b}_m\rangle_{\mathrm{GGE}}$ not diagonal. The latter fully characterizes the Gaussian initial state, which is therefore also in this case quantum coherent in the real space basis. On the contrary, for the flat initial occupation in momentum space (22.24), the two-point bosonic correlation function is diagonal. The associated initial density matrix $\rho_0 = \exp(-\lambda N)/\mathcal{Z}$ is diagonal in the classical basis of the Fock space introduced above. For these reasons, we will refer henceforth to initial states (22.23) and (22.25) as quantum coherent, in contrast with (22.24) which is incoherent.

The asymptotic decay exponent $\langle n\rangle_{\mathrm{GGE}}(\tau) \sim \tau^{-\delta}$ is evaluated by computing the effective exponent [3]:

$$\delta_{\mathrm{eff}}(\tau) = -\frac{\log\left(\langle n\rangle_{\mathrm{GGE}}(b\tau)/\langle n\rangle_{\mathrm{GGE}}(\tau)\right)}{\log(b)}. \tag{22.27}$$

Here, $b > 0$ is a scaling parameter. In all the calculations, we set $b = 1.5$. In the case of a power-law decay, the effective decay exponent $\delta_{\mathrm{eff}}(\tau)$ approaches asymptotically in time the exponent δ. We plot in the next Subsections δ_{eff} as a function of τ for the three different initial states (22.23)-(22.25) for the various reactions considered (22.10)-(22.12).

[9] For the state (22.25), the integral (22.26) is only approximately equal to 1 since the integral is restricted on the lattice to the Brillouin zone $k \in (-\pi, \pi)$.

Distance-selective loss

In this Subsection, we consider the binary annihilation jump operator in Eq. (22.10) without interferences (that is $\theta = 0$). We consider generic values of the distance d between the two bosons. The rate equation Eq. (22.22) then yields (see Appendix 22.2)

$$\frac{\mathrm{d}B_q}{\mathrm{d}\tau} = -\frac{2}{L} B_q \sum_k B_k \left(1 + \cos(d(k-q))\right), \tag{22.28}$$

with $\tau = \Gamma_\alpha t$ the re-scaled time. The results for different values of the distance d are shown in Fig. 22.2. In particular, we see that for $d = 0$ Eq. (22.28) does not couple q with other momenta $k \neq q$ and it therefore gives a closed equation for the density $\langle n \rangle_{\mathrm{GGE}}(t)$:

$$\frac{\mathrm{d}\langle n \rangle_{\mathrm{GGE}}(\tau)}{\mathrm{d}\tau} = -4\langle n \rangle^2_{\mathrm{GGE}}(\tau). \tag{22.29}$$

This equation coincides with the law of mass action (22.15) up to a factor 4 (instead of 2). This factor only affects the amplitude of the asymptotic decay, but not the exponent $\langle n \rangle_{\mathrm{GGE}}(\tau) \sim \tau^{-1}$. This result is consistent with that of Ref. [37] for onsite binary losses $mA \to \emptyset$ and $m = 2$. For $m > 2$, in Ref. [37], the asymptotic mean-field exponent $n(\tau) \sim \tau^{-1/(m-1)}$ is also recovered.

For $d \neq 0$, Eq. (22.29) still holds true for the BEC initial state (22.23). In this case, indeed, binary losses do not populate momenta $q \neq 0$, so that the momentum distribution is concentrated on $q = 0$ $B_q(\tau) = N(\tau)\delta_{q,0}$ at any time τ. In this case, Eq. (22.28) reduces to (22.29) for any d value. For the flat filling initial state Eq. (22.24), instead, the occupation function $B_q(\tau) = n(\tau)$ remains flat in q at any time τ and therefore (22.28) exactly reduces, at any time τ, for $d \neq 0$ to the law of mass action

$$\frac{\mathrm{d}\langle n \rangle_{\mathrm{GGE}}(\tau)}{\mathrm{d}\tau} = -2\langle n \rangle^2_{\mathrm{GGE}}(\tau). \tag{22.30}$$

This result is analogous to the one valid for fermions starting from incoherent initial states identified by a flat in q occupation function [38, 39, 40]. Also in those cases the fermionic quantum reaction-limited RD dynamics reduces to its classical counterpart. Meanwhile, for the initial Gaussian occupation function, studied in Refs. (22.25), Eq. (22.28) reduces to Eq. (22.30) only asymptotically for long τ values. The time needed to asymptotically approach (22.30) depends on the distance $d > 0$, the larger the latter, the faster the approach to the law of mass action dynamical behavior. This behavior holds generically for any initial state identified by an occupation function $B_q(0)$ inhomogeneous in momentum q.

a)
Results/Plots$_A$/distances$_f$f.tikz *Results/Plots$_A$/distances$_f$f$_e$xp.tikz*
b)
Results/Plots$_A$/distances$_g$auss.tikz *Results/Plots$_A$/distances$_g$auss$_e$xp.tikz*

Figure 22.2: **Distance-selective binary annihilation quantum RD dynamics.** (Left) Log-log plot of the density $\langle n \rangle_{\mathrm{GGE}}(\tau)$ as a function of $\tau = \Gamma_\alpha t$ from the solution of Eq. (22.28). (Right) Plot of the associated effective exponent $\delta_{\mathrm{eff}}(\tau)$ (22.27) as a function of τ (log scale on the horizontal axis only). **a)** Dynamics from the flat filling initial state (22.24) for three different values of the distance $d = 0, 1, 20$. For $d = 0$, the density follows Eq. (22.29), while for $d = 1, 20$ Eq. (22.30) is recovered. In all the cases, the asymptotic exponent (right plot) follows the mean-field prediction $\langle n \rangle_{\mathrm{GGE}}(\tau) \sim \tau^{-1}$. **b)** Dynamics from the initial Gaussian occupation function (22.25) for the same values of d as above. For $d = 0$, the density dynamics again follows (22.29), while for $d = 1, 20$, Eq. (22.30) is asymptotically obtained. Also in this case the asymptotic decay exponent follows from mean field, as the convergence of $\delta_{\mathrm{eff}}(\tau) \to 1$ shows (right plot).

Therefore, all the initial states considered show the same mean-field algebraic decay:

$$\langle n\rangle_{\rm GGE}(\tau)\sim\tau^{-1}. \tag{22.31}$$

This applies to both quantum coherent (22.23),(22.25) and incoherent (22.24) initial conditions. This is a fundamental difference from the RD dynamics of fermions. For fermionic systems, indeed, nearest neighbour binary annihilation ($d=1$ with the notation of this manuscript) and quantum coherent initial states give rise to the decay law $\langle n\rangle_{\rm GGE}(\tau)\sim\tau^{-1/2}$ [38], which deviates from the mean-field result. In the next Subsection, we study whether such bosonic mean-field decay is robust against the introduction of interference effects ($\theta\neq 0,\pi/2$) in the annihilation reaction channels.

22.0.5 Annihilation reaction with interferences

The TGGE rate equation (22.22) for the jump operators (22.10), i.e. generic values of θ, reads as (see Appendix 22.2 for the details of the calculations)

$$\frac{dB_q(\tau)}{d\tau}=-\frac{1}{L}\sum_k g_{\theta,d}(k,q)B_k(\tau)B_q(\tau), \tag{22.32}$$

with $\tau=t\Gamma_\alpha$ the re-scaled time and

$$\begin{aligned} g_{\theta,d}(k,q)=&2(1+\cos(d(k-q)))-\sin(2\theta)\\ &\left[2\cos(d(k+q))+\cos(2kd)+\cos(2qd)\right]. \end{aligned} \tag{22.33}$$

This differential equation is similar to the corresponding one for fermions of Ref. [38] (cf. Eq. (S10) therein), the only difference being in the opposite sign of the terms $\cos(d(k-q))$ and $\cos(d(k+q))$. In Fig. 22.3, we plot the solution of the differential Eq. (22.32) for the density $\langle n\rangle_{\rm GGE}(\tau)$ as a function of τ. We find that the long-time dynamics at $\theta=\frac{\pi}{4}$ is qualitatively different than that obtained for all other values, i.e., $\theta\neq\pi/4$. Namely, for all the considered initial states, we find that for $\theta\neq\pi/4$, the density decay exponent is gain the mean-field one $\langle n\rangle_{\rm GGE}(\tau)\sim\tau^{-1}$.

For $\theta=\pi/4$, however, the density is constant in time $\langle n\rangle_{\rm GGE}(\tau)=\langle n\rangle_{\rm GGE}(0)$. The BEC state is, indeed, a dark state of the jump operator in Eq. (22.10) at $\theta=\frac{\pi}{4}$, which amounts to saying that $|\text{BEC}\rangle$ is annihilated by all the annihilation (22.10) jump operators

$$L_j^\alpha|\text{BEC}\rangle=0,\quad\forall j,\quad\theta=\pi/4. \tag{22.34}$$

Moreover, the BEC is an eigenstate (the ground state in this case) of the Hamiltonian (22.8). This observation is consistent with the results of Refs. [46, 49], where the $|\text{BEC}\rangle$ state was similarly identified as an exact dark state of the quantum master equation of the noninteracting Bose gas. However, in Refs. [46, 49], the jump operators do not involve particle losses, but still they annihilate the antisymmetric part of the wavefunction due to terms $\hat{b}_i-\hat{b}_{i+d}$, thus rendering the BEC state dark. For the flat filling (22.24) and the Gaussian occupation states (22.25), instead, we find a slower decay $\langle n\rangle_{\rm GGE}(\tau)\sim\tau^{-1/2}$ compared to mean field, as shown in Fig. 22.3. The asymptotic 1/2 decay exponent (and the amplitude) can be exactly computed from the asymptotic of Eq. (22.32) (see again Appendix 22.2 for the details of the calculations). In particular, Eq. (22.32) admits the following implicit solution for the mode occupation function $B_q(\tau)$

$$B_q(\tau)=B_q(0)\sqrt{\frac{n(\tau)}{n(0)}}\exp\left[-2\sin^2(dq)\int_0^\tau {\rm d}t\, n(t)\right]. \tag{22.35}$$

Here, for the sake of brevity, we denoted $\langle n\rangle_{\rm GGE}(\tau) = n(\tau)$. The previous equation shows that $q = 0$ is the slowest decaying mode. Furthermore, for $B_q(0) = n(0)\delta(q)$ (the BEC occupation in the limit $L \to \infty$), Eq. (22.35) gives $n(\tau) = n(0)$ consistently with the previous discussion concerning the dark-state condition for the BEC. Using Eq. (22.35) into Eq. (22.26), the q integral for the density $n(\tau)$ can be asymptotically computed using the saddle-point approximation (which is justified since $\int_0^\tau {\rm d}t\, n(t) \to \infty$ as $\tau \to \infty$). The density asymptotic one obtains

$$n(\tau) \sim \left(\frac{B_\pi(0) + B_0(0) + 2\sum_{n=1}^{d-1} B_{q_n^*}(0)}{4d\sqrt{\pi n_0}} \right) \tau^{-1/2}, \tag{22.36}$$

with the saddle-points $q_n^* = n\pi/d$, $n = 1, 2 \ldots d-1$, determined by the $d-1$ zeros of the $\sin^2(dq)$ function in the interval $q \in (0, \pi)$. Therefore, when $\theta = \pi/4$ the decay exponent, $1/2$, does not depend on the distance d between the pair of bosons involved in the loss. The amplitude of the decay, instead, does generically depend on d. Only in the case of the flat-filling initial occupation (22.24), the amplitude of the decay takes the d-independent value $1/2\sqrt{n_0/\pi}$.

a)
Results/Plots$_B$/bc$_d$ensity.tikz *Results/Plots$_B$/bc$_d$ensity$_e$xp.tikz*
b)
Results/Plots$_B$/flat$_d$ensity.tikz *Results/Plots$_B$/flat$_d$ensity$_e$xp.tikz*
c)
Results/Plots$_B$/gauss$_d$ensity.tikz *Results/Plots$_B$/gauss$_d$ensity$_e$xp.tikz*

Figure 22.3: **Quantum RD dynamics of binary annihilation with interference between two decay channels** (Left) Log-log plot of the density $\langle n\rangle_{\rm GGE}(\tau)$ as a function of $\tau = \Gamma_\alpha t$ from Eqs. (22.32) and (22.33). (Right) Plot of the associated effective exponent $\delta_{\rm eff}(\tau)$ as a function of τ (log scale on the horizontal axis only). We set $d = 1$ in Eq. (22.10) for the two-body annihilation reaction and we show various values of $\theta = \pi/3, \pi/4, \pi/5$. **a)** Dynamics from the $|{\rm BEC}\rangle$ initial state (22.23). For $\theta = \pi/4$, the density is constant in time (top-red curve). For this reason, the effective exponent $\delta_{\rm eff}(\tau)$ is not shown on the right plot for $\theta = \pi/4$. For $\theta \neq \pi/4$, the density follows the mean-field decay $\langle n\rangle_{\rm GGE}(\tau) \sim \tau^{-1}$. **b)** Dynamics from the flat filling occupation function (22.24) for the same values of θ as in the previous panel. The density follows the mean-field decay for $\theta \neq 0, \pi/2$, while it obeys the slower non-mean-field decay $\langle n\rangle_{\rm GGE}(\tau) \sim \tau^{-1/2}$ for $\theta = \pi/4$. The right plot clearly shows the different asymptotic value of $\delta_{\rm eff}(\tau) \simeq 1/2$ for $\theta = \pi/4$ compared to the value $\delta_{\rm eff}(\tau) \simeq 1$ for $\theta \neq \pi/4$. **c)** Dynamics from the initial state (22.25) with Gaussian initial occupation function $B_q(0)$ for the same values of θ as in the previous panels. As in the case of panel (**b**), the non-mean-field decay is observed only for $\theta = \pi/4$.

To sum up, for the decay exponent of the particle density in the presence of binary annihilation with interference between two decay channels (22.10), we find

$$\langle n\rangle_{\rm GGE}(\tau) \sim \begin{cases} \tau^{-1/2} & \text{for} \quad \theta = \pi/4 \\ \tau^{-1} & \text{else.} \end{cases}, \tag{22.37}$$

both for incoherent initial states (22.24) and for coherent ones, e.g., with a Gaussian initial occupation function $B_q(0)$ (22.25). The same behavior (22.37) applies generically for initial quantum coherent states identified by a non-flat occupation function $B_q(0)$ of generic form. The $|{\rm BEC}\rangle$ state (22.23) for $\theta = \pi/4$ does not decay since it is dark with respect to the dissipation.

The result (22.37) significantly deviates from the one valid for fermions discussed in Ref. [38]. In the case of fermions, the decay $\langle n\rangle_{\rm GGE}(\tau) \sim \tau^{-1/2}$ is valid for any value of $\theta \neq 0, \pi/2$, not just $\theta = \pi/4$. The different behavior between fermions and bosons subject to binary annihilation with interference, and at the same time, the emergence of the beyond mean-field decay (22.37) can be understood by looking at the space continuum limit of Eq. (22.10). In the continuum limit, the lattice spacing a (so far set to 1) is reintroduced, so that lattice point are identified as $x_j = ja$ and $\ell = La$ is the dimensionful length of the system. The continuum limit is obtained by sending $a \to 0$, $L \to \infty$ with ℓ fixed, as we detail in Appendix 22.1. The jump operator (22.10) L^{α}_{ja} reduces, in this limit, to onsite pair annihilation $L^{\alpha}_{ja} \to L^{\alpha}(x) \sim \hat{b}^2(x)$ as long as $\theta \neq \pi/4$, with $\hat{b}(x) = \hat{b}_{ja}/\sqrt{a}$ being the continuum bosonic destruction field operator. This operator yields mean-field decay (22.31), following the same steps as those done in Sec. 22.0.4 for the lattice case. Only for $\theta = \pi/4$ (see again Appendix 22.1 for the details), the binary annihilation operator (22.10) in the continuum limit takes a different form $L^{\alpha}(x) \sim \hat{b}(x)\partial_x\hat{b}(x)$. The latter explicitly couples to spatial derivatives of the bosonic field. The operator $L^{\alpha}(x)$ for $\theta = \pi/4$ therefore introduces spatial fluctuations in the quantum trajectories unravelling of the dynamics since reactions can more likely take place in depletion regions, where the density experiences spatial variations. This effect eventually causes the decay law (22.37), which is beyond mean-field. In the fermionic case, the leading term $L^{\alpha}(x) \sim \hat{c}^2(x)$ of the continuum limit expansion, $\hat{c}(x)$ being the fermionic field destruction operator, is always zero because of the fermionic statistics. The continuum limit of fermionic nearest-neighbour annihilation is therefore always of the form $L^{\alpha}(x) \sim \hat{c}(x)\partial_x\hat{c}(x)$ and the decay $\langle n\rangle_{\rm GGE}(\tau) \sim \tau^{-1/2}$ applies for any $\theta \neq 0, \pi/2$.

In order to further understand the emergence of non-mean-field decay exponents due to interfering decay channels, we proceed by discussing in the following Subsection annihilation reactions (22.11) with interferences among three different decay channels.

22.0.6 Discussion

In this manuscript, we have studied the quantum reaction-limited reaction-diffusion dynamics of the noninteracting Bose gas. The main finding of the manuscript is that bosonic statistics considerably impacts on the universal properties of the quantum RD dynamics. In particular, we find that the combination of bosonic statistics with quantum effects, such as coherent hopping and quantum interferences, leads to universal nonequilibrium behavior different from both fermionic and classical RD systems.

The dynamics for QRD systems is formulated in terms of the quantum master equation (22.7)-(22.9). Within this formulation, we considered various types of reactions introduced in Sec. 22.0.2. Our analytical study is based on the time-dependent generalized Gibbs ensemble method, briefly recalled in Sec. 22.0.3. This method gives direct access to the quantum reaction-diffusion dynamics in the thermodynamic limit in the so-called reaction-limited regime $\Gamma/\Omega \ll 1$ of weak dissipation. Our results for the density algebraic decay $\langle n\rangle_{\rm GGE}(\tau) \sim \tau^{-\delta}$ in the presence of only reactions depleting the system are summarized in Table 5. We see that the law of mass action (22.16) decay exponent is generically recovered for all classical-incoherent reactions, such as distance selective losses (22.10) ($\theta \neq 0$) and coagulation. This result applies both to quantum coherent and incoherent initial states. Algebraic decay beyond mean field is possible for bosons only when interference between different decay channels is allowed, as shown in Figs. 22.3 and 22.4. In the case of first-order interference (22.10) with $\theta = \pi/4$, in Subsec. 22.0.5, we find, namely, a power-law decay with exponent 1/2 (cf. Eq. (22.36)). For all the other values $\theta \neq \pi/4$, mean-field decay is observed. For the second-order interference (22.11) in Subsec. 22.0.6, the decay exponent is, instead, approximately 0.28. Incoherent coagulation (22.12) decay also yields mean-field decay (22.42). These results show markedly different behavior between bosons and

L_j^ν	BEC	flat filling	Gaussian
$\sqrt{\Gamma_\alpha}\hat{b}_j\hat{b}_{j+d}$	1	1	1
$\sqrt{\Gamma_\alpha/2}\hat{b}_j\left(\hat{b}_{j+d}-\hat{b}_{j-d}\right)$	0	1/2	1/2
$\sqrt{\Gamma_{\bar{\alpha}}}\hat{b}_j\left(\hat{b}_{j+1}+\hat{b}_{j-1}-2\hat{b}_j\right)$	0	0.28	0.28
$\sqrt{\Gamma_\gamma}\hat{n}_j\hat{b}_j$	1	1	1

Table 5: **Summary of quantum reaction-limited density decay exponents for the noninteracting Bose gas.** In this table, we summarise our results from Eq. (22.20) for the different annihilation reaction types (22.10)-(22.12) treated in Subsecs. 22.0.4-22.0.7 in the reaction-limited regime $\Gamma/\Omega \ll 1$. In all the listed cases, the density decays as a power-law $\langle n\rangle_{\mathrm{GGE}}(\tau) = \tau^{-\delta}$ with the listed exponent δ. The exponent is given for each reaction and for the considered initial states. The flat filling (22.24) is incoherent, while the BEC (22.23) and the Gaussian state (22.25) are quantum coherent. In the case of the BEC, the value 0 of the exponent, on the second and third line, refers to the fact that the BEC is dark to these jump operators and therefore it does not decay.

fermions. In the latter case, power-law decay beyond mean field is, indeed, attained under broader conditions, such as also for classical annihilation reactions from incoherent initial states, and for generic interference decay $\theta \neq 0, \pi/2$ [38, 39, 40]. Furthermore, for bosons, coagulation and binary annihilation belong to the same universality class, at least as long as the reaction-limited regime is concerned. For fermions, instead, this is not true [38].

In table 6, we summarize the main critical exponents associated to the absorbing-state phase transition observed in bosonic systems in the presence of branching (22.14), coagulation and decay.

contact process (β, γ, δ)	2nd order transition $\beta = \delta/2$	bicritical point $(\beta/\gamma, \delta/\gamma) = (1/4, 1/2)$
$n_{\mathrm{SS}} \sim (\beta/\delta - 1/2)^\xi$	1	1/2
$n(t) \sim t^{-\chi}$	1	1/2

Table 6: **Summary of quantum reaction-limited exponents for the absorbing-state phase transition in the noninteracting Bose gas.** In this table, we summarise our results for the quantum RD model with absorbing-state phase transition in the reaction-limited regime (see Subsec. 22.0.8). This transition can be either of first or second order. In the table, we summarize the exponents (ξ, χ) associated to the latter. In the second column, the exponents associated to the second-order line $\beta = \delta/2$ are reported. These exponents are those of the mean-field directed percolation universality class. We further give (third column) the exponents associated with the bicritical point of Fig. 22.6. These exponents are those of the mean-field tricritical directed percolation universality class.

The corresponding stationary-state phase diagram in Fig. 22.6 is of mean-field nature. However, it is qualitatively different from both the classical mean-field (22.18) and the fermionic analogue [38]. In the bosonic case, we find that both a first-order and a second-order line are present.The first-order transition line has no classical counterpart. The second-order line is again characterized by the critical exponents of the mean-field directed percolation universality class (middle column of Table 6) as in the classical reaction-limited description (22.18). Inter-

estingly, the second-order line and the first-order one meet at a bicritical point. This point is identified by the mean-field exponents of the tricritical directed percolation universality class (rightmost column of Table 6). The universality class of the bicritical point is consequently different from directed percolation, which characterizes the classical dynamics. For bosons, the quantum mean-field description of the contact process phase diagram is therefore richer than the classical mean-field description in Eq. (22.18).

Our work paves the way for many future research directions concerning the Bose gas subject to dissipative loss processes. It would be interesting to study the quantum RD dynamics in the presence of reactions conserving the particle number as in Refs. [46, 49]. Therein, dissipation allows for the dynamical preparation of a pure $|\mathrm{BEC}\rangle$ state. This state is a many-body dark state of the dynamics and it is therefore attained at long times. It is important and experimentally relevant to study the stability of this dynamical preparation protocol of the BEC state against particle losses.

It is also interesting to look at different observables than the particle density. The two-point bosonic correlation function $\langle \hat{b}_n^\dagger \hat{b}_m \rangle_{\mathrm{GGE}}(\tau)$ can be readily computed within the TGGE method and its temporal decay would shed light on the decay of quantum coherences as the stationary state is approached. In addition, it is interesting to study Bose superfluids with weak dissipative losses. These models can be also addressed with the TGGE ansatz of this manuscript. We expect that for Bose superfluids the dynamics of the superfluid order parameter gives additional information on the decoherence in time of the system due to dissipation, as it has been shown in Ref. [33] for lossy fermionic superfluids.

Ultimately, it is desirable to go beyond the quantum reaction-limited regime $\Gamma/\Omega \ll 1$ discussed in this manuscript. The quantum analogue of the diffusion-limited decay (22.2) is, indeed, not known. Quantifying the anticipated quantum diffusion-limited algebraic decay might be possible by exploiting the field theory formulation of the quantum master equation via the Keldysh path integral method [102, 103]. In the diffusion-limited regime, the significance of spatial fluctuations due to the finite hopping is inherently increased. A systematic renormalization group scaling analysis is therefore needed in order to quantify the space dependence and the impact of spatial fluctuations on the decay exponents.

With respect to the absorbing-state phase transition, it is important to understand the reason behind the similarity between the phase diagram of Fig. 22.6 and the one found for the quantum contact process in Refs. [57, 58]. The model studied therein is different from the quantum RD model here proposed since coherent effects are introduced via a different Hamiltonian giving coherent branching/coagulation. In our case the Hamiltonian (22.8) simply gives free hopping. The field-theory scaling analysis of the quantum RD model of Subsec. 22.0.8 could, in this way, shed light on the, largely not understood, universality class of the quantum contact process away from the reaction-limited, mean-field, limit.

Second-order annihilation

The TGGE rate equation (22.22) can be specialized to the jump operator (22.11) following similar steps as those performed in Secs. 22.0.4 and 22.0.5. We report the main steps in Appendix 22.2, while here we give the final result:

$$\frac{\mathrm{d}B_q(\tau)}{\mathrm{d}\tau} = -\frac{4}{L} B_q \sum_k B_k \left[\cos(kd) + \cos(qd) - 2\right]^2 , \tag{22.38}$$

with the re-scaled time $\tau = \Gamma_{\bar{\alpha}} t$. The results of the numerical solution of the previous equation are reported in Fig. 22.4. The BEC initial state (22.23) is also dark, as in Eq. (22.34), with respect to the jump operator $L_j^{\bar{\alpha}}$ (for any j) and therefore it is a many-body dark state of the quantum master equation. The density $\langle n \rangle_{\mathrm{GGE}}(\tau) = \langle n \rangle_{\mathrm{GGE}}(0) = n_0$ consequently remains constant in time.

Results/Plots$_C$/density.tikz Results/Plots$_C$/exponent.tikz

Figure 22.4: **Quantum RD dynamics of second-order annihilation reaction.** Log-log plot (left) of the density $\langle n\rangle_{\rm GGE}(\tau)$ as a function of $\tau = \Gamma_{\bar\alpha} t$ from Eq. (22.38). In the right plot (log scale on the horizontal axis only), the effective exponent $\delta_{\rm eff}(\tau)$ as a function of τ (Eq. (22.27)) is shown. Both the initial state (22.24) with a flat in q occupation function, and (22.25) with an initial occupation function of Gaussian form are studied. In both cases, the same algebraic decay $\langle n\rangle_{\rm GGE}(\tau) \sim \tau^{-0.28}$ is observed. The exponent of the algebraic decay is quantified by plotting the effective exponent, which at long times converges to $\delta_{\rm eff}(\tau) \simeq 0.28$ for both initial states (22.24) and (22.25).

For both the flat filling (22.24) and the Gaussian occupation function (22.25) initial states, we, instead, observe algebraic decay asymptotically in time with a non-mean-field exponent

$$\langle n\rangle_{\rm GGE}(\tau) \sim \tau^{-0.28}. \tag{22.39}$$

This decay exponent is numerically computed by plotting the effective exponent $\delta_{\rm eff}(\tau)$ as a function of τ, as shown in the right panel of Fig. 22.4. The effective exponent (22.27) converges at long times to the value $\delta_{\rm eff}(\tau) \simeq 0.28$ for both the initial states considered. The choice of the initial state solely affects how fast the asymptotic value of $\delta_{\rm eff}$ is met, but not the value itself. We also verified that the result in Eq. (22.39) holds generically for initial states identified by a different q-dependent initial occupation function $B_q(0)$. In the case of Eq. (22.39), we remark, however, that it is not possible to derive analytically the asymptotic exponent, as we did in Eqs. (22.35) and (22.36) of Subsec. 22.0.5, due to the more complicated structure of Eq. (22.38).

The result (22.39) is a non-mean-field prediction for the algebraic decay. Following the same reasoning used at the end of the previous Subsec. 22.0.5, we can understand this behavior by looking at the continuum limit of the annihilation process (22.11) coupling three different decay channels. In this case, the continuum limit (see again Appendix 22.1 for the details) leads to a jump operator of the form $L^{\bar\alpha}(x) \sim \hat b(x)\partial_x^2 \hat b(x)$. The jump operator $L^{\bar\alpha}(x)$ couples now to second-order spatial derivatives (this is why we also name the process as "second-order annihilation") and it induces spatial fluctuations over larger regions and therefore deviations from the mean field are more sensible. In particular, the exponent decreases compared to Eq. (22.36) for the first-order interference drifting further from the mean-field value ($\delta = 1$).

Apparently, interference effects generally slow down the decay of the density compared to the classical reaction-limited case. In both cases analysed in Eqs. (22.36) and (22.39), we see that quantum interferences are necessary in order to observe beyond mean-field decay in the noninteracting Bose gas.

22.0.7 Coagulation

The onsite coagulation decay is modelled by the jump operator (22.12) introduced in Sec. 22.0.2. It describes the reaction $2A \to A$ where two (or more) bosons meet on the same site j leading to the destruction of one of the particles at the same lattice site. The resulting rate equation (cf. Appendix 22.3 for the details of the calculations) for the bosonic occupation function is

$$\frac{{\rm d}B_q(\tau)}{{\rm d}\tau} = -6B_q\langle n\rangle_{\rm GGE}^2 + 2\langle n\rangle_{\rm GGE}^2 - 4B_q\langle n\rangle_{\rm GGE}, \tag{22.40}$$

with $\tau = \Gamma_\gamma t$ the re-scaled time according to the coagulation rate. We note that for one-site coagulation, similarly to the case of onsite binary annihilation (22.29), the TGGE equation for the density is closed, and it reads

$$\frac{{\rm d}\langle n\rangle_{\rm GGE}}{{\rm d}\tau} = -\left(6\langle n\rangle_{\rm GGE}^3 + 2\langle n\rangle_{\rm GGE}^2\right). \tag{22.41}$$

This equation contains both a two-body term, $\langle n\rangle^2_{\rm GGE}$, as in the corresponding classical law of mass action (22.15), and a three-body term, $\langle n\rangle^3_{\rm GGE}$. The latter is notably absent in the classical law of mass action description. It is also absent in the fermionic quantum reaction-limited dynamics [38] and therefore a genuine property of the quantum bosonic reaction-limited dynamics. In the presence of coagulation only (and more generally in the presence of reactions depleting the system) this three-body term does not, however, impact the late time asymptotics. The density $\langle n\rangle_{\rm GGE}$, as a matter of fact, decays asymptotically in time to zero and therefore the three-body term $\langle n\rangle^3_{\rm GGE}$ can be neglected with respect to the two-body term $\langle n\rangle^2_{\rm GGE}$. The latter immediately gives the mean-field algebraic decay

$$\langle n\rangle_{\rm GGE}(\tau) \sim \tau^{-1}. \tag{22.42}$$

In Fig. 22.5, we report the numerical solution of Eq. (22.40) together with the plot of the associated effective exponent $\delta_{\rm eff}(\tau)$ versus the re-scaled time τ. The effective exponent converges to the mean-field exponent $\delta_{\rm eff}(\tau) \simeq 1$ at long times. This mean-field behaviour is, importantly, valid for any initial state (22.23)-(22.25), quantum coherent or not. A similar result has been derived in Ref. [38] for fermionic systems, where the coagulation decay similarly shows $\langle n\rangle_{\rm GGE}(\tau = \Gamma_\gamma t) = \tau^{-1}$ decay both for coherent and incoherent initial states. In the fermionic case, for a Fermi-sea initial state, quantum coherences are only observed in Ref. [38] to rescale time by a factor dependent on the initial density n_0, leaving the asymptotic decay exponent unchanged. In the bosonic case, instead, Eq. (22.41) gives the very same dynamics for all kind of initial conditions. We also note that the coefficient 2 in front of the two-body term on the right-hand side of Eq. (22.41) is half of the coefficient 4 of the onsite annihilation two-body term (22.29). This implies that the density $\langle n\rangle^{\rm coag/ann}_{\rm GGE}(\tau, n_0)$ (n_0 being the initial density) as a function of time in the annihilation and coagulation processes are asymptotically (as long as the $\langle n\rangle^3_{\rm GGE}$ term for coagulation can be neglected) related by

$$\langle n\rangle^{\rm coag}_{\rm GGE}(\tau, n_0) = 2\langle n\rangle^{\rm ann}_{\rm GGE}(\tau, n_0/2), \quad \text{for } \Gamma_\alpha = \Gamma_\gamma. \tag{22.43}$$

In the context of classical RD [90, 91, 92, 93, 94] this relation is taken as the hallmark that signals that both coagulation and annihilation dynamics belong to the same universality class. In particular, this implies that the two processes share the same asymptotic decay. Apparently in the bosonic quantum RD system the two processes still belong to the same universality class, at least in the reaction-limited regime. This statement applies to both quantum coherent and incoherent initial states, in contrast with the fermionic case of Ref. [38], where the equivalence (22.43) applies only for incoherent initial states.

Results/Plots$_D$/density.tikz *Results/Plots$_D$/exponent.tikz*

Figure 22.5: **Coagulation quantum RD dynamics.** Log-log plot (left) of the density $\langle n\rangle_{\rm GGE}(\tau)$ as a function of time τ. The initial condition in the given case is the flat filling state in Eq. (22.24), but the very same curve is obtained for the BEC (22.23) and the Gaussian occupation state (22.25). In all the cases, the density decays as in the mean-field approximation $\langle n\rangle_{\rm GGE} \sim \tau^{-1}$. In the right plot, the effective exponent $\delta_{\rm eff}(\tau)$ (22.27) is plotted (log scale on the horizontal axis only) and it converges to mean-field value 1 at long times.

22.0.8 Absorbing-state phase transition in quantum bosonic RD

In order to obtain a process with a stationary state featuring a non-zero density of particles, we need to include reactions increasing the particle number, thereby competing with the loss processes (22.10)-(22.12). Therefore, we consider onsite branching reactions $A \to A + A$ (22.14)

at rate Γ_β. For the branching reaction process, we found the following rate equation (see Appendix 22.4 for the calculation):

$$\frac{\mathrm{d}B_q(t)}{\mathrm{d}t} = \Gamma_\beta[2(2n - B_q) + 8n^2 + 6B_q n^2]. \tag{22.44}$$

In the following, we denote $\langle n\rangle_{\mathrm{GGE}}(t) = n$, dropping the time dependence for the sake of brevity. As in the case of onsite coagulation (22.41), the particle density obeys the closed equation

$$\frac{\mathrm{d}n(t)}{\mathrm{d}t} = \Gamma_\beta[2n + 8n^2 + 6n^3]. \tag{22.45}$$

We note that, as well as for coagulation, branching produces the three-body term, n^3, which is absent both in the classical and in the fermionic reaction-limited RD dynamics. The branching process leads to the creation of particles and therefore the density increases in time in Eq. (22.45).

This persistent growth can be countered by introducing annihilation reactions, and in the following we will study an absorbing-state phase transition that results from such competing processes. We consequently consider a model where (onsite) branching (22.14), at rate $\Gamma_\beta = \Gamma\beta$, is competing with (onsite) coagulation (22.12), at rate $\Gamma_\gamma = \Gamma\gamma$, and one-body decay (22.13), at rate $\Gamma_\delta = \Gamma\delta$. This parametrization of the rates allows to identify Γ as the overall dissipation (inverse) time scale, while β, γ, δ encode the relative strength of the three considered processes. Considering Eq. (22.45) together with (22.41) one then finds the rate equation

$$\frac{\mathrm{d}n}{\mathrm{d}\tau} = (2\beta - \delta)n + (8\beta - 2\gamma)n^2 + 6(\beta - \gamma)n^3, \tag{22.46}$$

where $\tau = \Gamma t$. Note, that the linear term, $-\delta n$, stems from the one-body decay process.

We already note that Eq. (22.46) is qualitatively different from the classical mean-field description (22.18) of the unrestricted contact process due to the presence of cubic and quartic terms in the density. However, Eq. (22.46) is still of mean-field type since it implies that the GGE is factorized also in real space: $\rho_{\mathrm{GGE}}(t) \sim \exp(-\beta(t)\hat{N})$. In this sense, for bosons, the quantum mean-field description is different and richer than the classical mean-field one. Eq. (22.46) can be equivalently written as

$$\frac{\mathrm{d}n(\tau)}{\mathrm{d}\tau} = -\frac{\partial W(n)}{\partial n}, \tag{22.47}$$

where

$$W(n) = (\delta - 2\beta)\frac{n^2}{2} + (2\gamma - 8\beta)\frac{n^3}{3} + 6(\gamma - \beta)\frac{n^4}{4}, \tag{22.48}$$

has the meaning of a potential. We remark that a similar fourth order potential $W(n)$ was found in Refs. [57, 58], which studied the so-called quantum contact process. Microscopically this process is, however, different to the one discussed here: it is formulated in terms of spin 1/2 particles (not bosons) and the Hamiltonian embodies coherent branching and coagulation, i.e., spin flips conditional on the excitation of a neighbouring spin. In our case, instead, the Hamiltonian (22.8) leads to free, unconstrained, hopping of particles. The dissipation is described by classical incoherent processes in both cases. Despite their apparent differences both models yield the same potential $W(n)$.

It is noteworthy that in Refs. [57, 58] the potential $W(n)$ describes the stationary phases of the quantum contact process only in the absence of spatial fluctuations, i.e., within the mean-field approximation. The latter is valid only in high spatial dimensions, while it fails in one dimension. In the present work, however, $W(n)$ emerges in one dimension in the reaction limited regime $\Gamma/\Omega \ll 1$ as an exact result.

The stationary-state phase diagram of the process (22.47) is reported in Fig. 22.6, where we plot the stationary state density $n_{\rm SS}$ (represent by the color code) as a function of the ratios β/γ and δ/γ. The stationary density $n_{\rm SS}$ is one of the (possibly multiple) minima of $W(n)$. The number of minima of $W(n)$ and their position depends on β/γ and δ/γ. For $\beta/\gamma > 1$, the potential $W(n)$ is unbounded from below and the active phase supports an infinite density. For this reason, we take $\beta/\gamma < 1$, in the following. In the Fig. 22.6, we also sketch the potential $W(n)$ so that the stationary state density $n_{\rm SS}$ value in the various regions of the phase diagram can be readily understood. We can identify three different phases a) – c):

a) If $\delta/\gamma < 2\beta/\gamma$, an active, i.e. finite density solution, $n_{\rm act} \neq 0$, of Eq. (22.46) is present:

$$n_{\rm act} = \frac{8\beta - 2\gamma + \sqrt{(8\beta - 2\gamma)^2 - 24(\gamma - \beta)(\delta - 2\beta)}}{12(\gamma - \beta)}. \tag{22.49}$$

The density $n_{\rm act}$ is the only minimum of $W(n)$, while $n_{\rm abs} = 0$ is a maximum. In this case, the system is therefore in the *active phase* $n_{\rm SS} = n_{\rm act}$.

b) For $\beta/\gamma > 1/4$ we define the curve $(\delta/\gamma)_c$ as

$$\left(\frac{\delta}{\gamma}\right)_c = \frac{2\beta}{\gamma} + \frac{1}{24}\frac{(2 - 8\beta/\gamma)^2}{1 - \beta/\gamma}. \tag{22.50}$$

For $\delta/\gamma < (\delta/\gamma)_c$ and $\delta/\gamma > 2\beta/\gamma$, the potential $W(n)$ has two minima $n_{\rm abs} = 0$ and $n_{\rm act}$ (22.49). For this choice of parameters the stationary state $n_{\rm SS}$ can be either $n_{\rm abs} = 0$ or $n_{\rm act}$ depending on the value of the initial density $n(\tau = 0) = n_0$. If n_0 is small enough so as it falls in the basin of attraction of $n_{\rm abs} = 0$, then $n_{\rm SS} = 0$. On the contrary, if n_0 is large enough so as to fall in the basin of attraction of $n_{\rm act}$, then the system is active $n_{\rm SS} = n_{\rm act}$. For this reason, we identify this region of the phase diagram as a *bistable phase*.

c) For $\beta/\gamma > 1/4$ and $\delta/\gamma > (\delta/\gamma)_c$, as well as for $\delta/\gamma > 2\beta/\gamma$ and $\beta/\gamma < 1/4$, the potential $W(n)$ has a single minimum $n_{\rm abs} = 0$. The system is therefore in the *absorbing phase* $n_{\rm SS} = 0$.

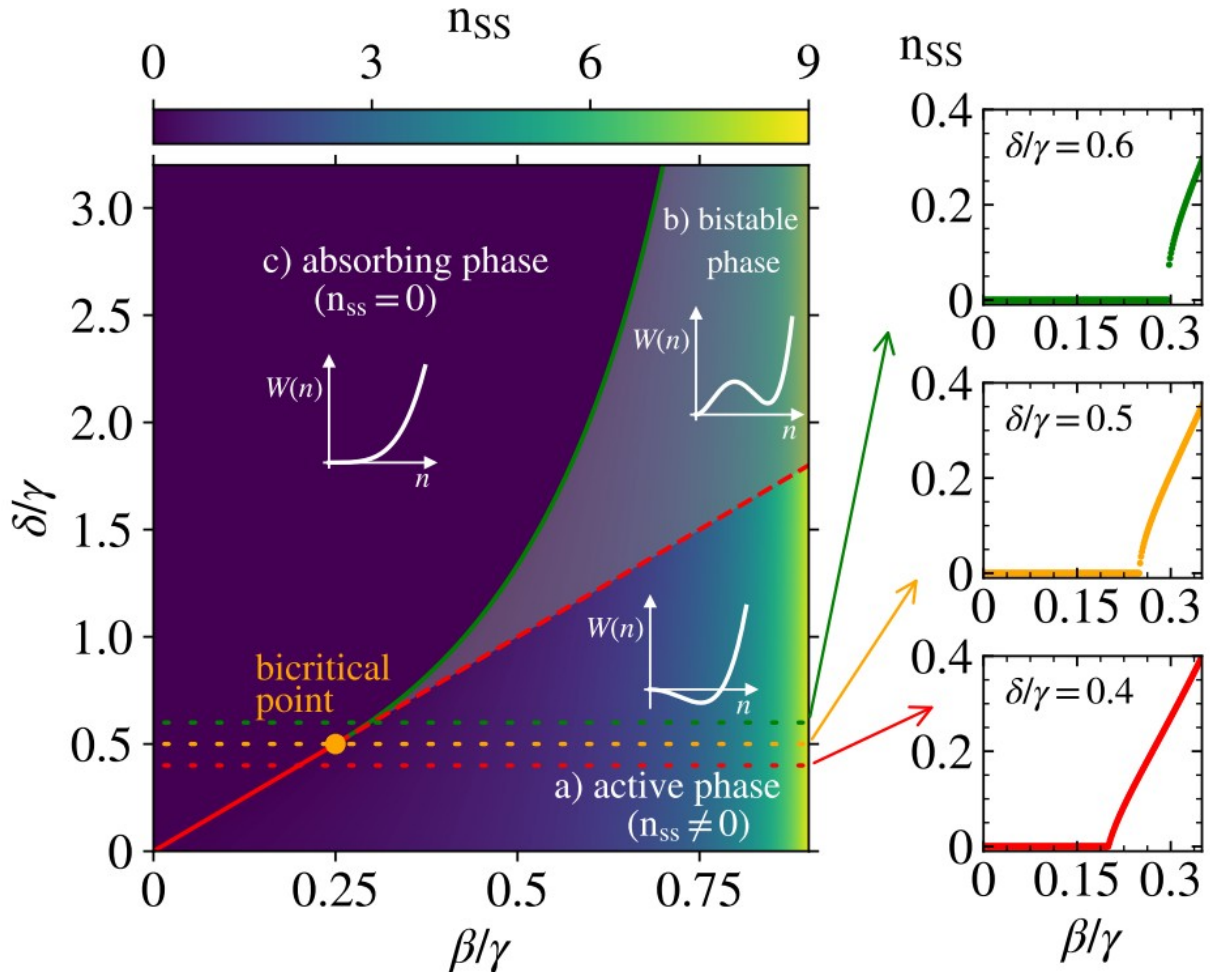


Figure 22.6: **Stationary phase diagram of quantum RD with incoherent branching and coagulation**. The stationary state density $n_{\rm SS}$, represented by the color code, is plotted as a function of the ratios β/γ, incoherent branching over incoherent coagulation, and δ/γ, incoherent decay over incoherent coagulation. We identify three different regions a) – c) in the phase diagram. In each region, we sketch the potential $W(n)$, Eq. (22.48). A second-order continuous phase transition separates the absorbing c) and the active a) phases and it is plotted with the red-solid line $\beta = \delta/2$. The stationary density $n_{\rm SS}$ vanishes continuously as a function of β/γ, as shown in the bottom-right panel for a fixed value of $\delta/\gamma = 0.4$. This transition belongs to the mean-field classical directed percolation universality class (22.51). A first-order discontinuous phase transition takes place across the green-solid line (22.50). This line separates the absorbing phase c) from a bistable phase b) (shown in grey-blurred scale). The bistable phase is delimited by the coexistence lines $(\delta/\gamma)_c$ (green solid) and $\delta = 2\beta$ (red dashed). Across the first-order line, the density discontinuously jumps from zero to the value $n_{\rm SS}$, as shown in the top-right panel for a fixed value of $\delta/\gamma = 0.6$ (green-dotted horizontal cut). The two coexistence lines meet at the bicritical point (orange dot) $(\beta/\gamma, \delta/\gamma) = (1/4, 1/2)$. At this point, the transition is still second order, as shown in the central-right panel, but it belongs to the mean-field tricritical directed percolation universality class (22.53) and (22.54).

For $\beta/\gamma < 1/4$, the boundary between a) and c) is given by the line $\beta/\delta = 1/2$, which is shown in red solid in Fig. 22.6. Along this line the order parameter $n_{\rm SS}$ of the transition varies continuously. This is shown in the bottom-right panel of Fig. 22.6, where the stationary density $n_{\rm SS}$ is displayed as a function β/γ for $\delta/\gamma = 0.4$ (horizontal red-dotted line in the density plot in Fig. 22.6). In particular, expanding Eq. (22.49) for $\beta - 2\delta \to 0$ and $\beta < \gamma/4$ one obtains

$$n_{\rm SS} \sim (\beta/\delta - 1/2)^1, \quad \beta/\gamma < 1/4. \tag{22.51}$$

At the same time, setting $\beta/\delta = 1/2$ and $\beta/\gamma < 1/4$, one finds that the density $n(t)$ decays asymptotically as

$$n(t) \sim t^{-1}, \quad \beta/\delta = 1/2, \quad \beta/\gamma < 1/4. \tag{22.52}$$

Equations (22.51) and (22.52) identify the critical exponents of the classical mean-field directed percolation universality class [1, 2, 3, 5, 6], as also recalled after Eq. (22.19). Along the second-order transition line, the cubic nonlinearity n^3 of (22.46) is therefore negligible and the transition is driven by the second-order n^2 nonlinearity. This renders (22.19) effectively analogous to the classical mean-field equation (22.19). The classical mean-field directed percolation exponents are therefore obtained. For $\beta/\gamma > 1/4$, the boundary between b) and c) is given by the curve $(\delta/\gamma)_c$ in Eq. (22.50) and it reveals, instead, a richer physics compared to the mean-field description (22.18) of the classical contact process. In particular, along the line $(\delta/\gamma)_c$ given by (22.50), plotted in solid green in Fig. 22.6, we find a first-order transition since the density jumps discontinuously from the value (22.49) to zero. This is shown in the middle panel in Fig. 22.6. Therein we plot the stationary density $n_{\rm SS}$ as a function of β/γ for fixed $\delta/\gamma = 0.6$ (horizontal green-dotted line).

Equation (22.50), for the first-order line, is obtained by calculating when the potential $W(n)$ has an inflection point $\mathrm{d}^2W(n)/\mathrm{d}n^2 = 0$. For $\delta/\gamma < (\delta/\gamma)_c$ and $\beta/\gamma > 1/4$, the inflection point morphs into a first minimum $n_{\rm act}$ (22.49), while a second minimum is given by $n_{\rm abs} = 0$. We emphasize that the relative height of the two minima $W(n_{\rm act})/W(n_{\rm abs})$ does not fix the stationary density since in this nonequilibrium case there is no principle of free-energy minimization as in equilibrium systems. In the latter case, indeed, $W(n)$ would be interpreted as a free energy and the equilibrium solution would necessarily be the absolute minimum of $W(n)$ in the thermodynamic limit. In the present nonequilibrium scenario, instead, the stationary density can take either the value $n_{\rm SS} = n_{\rm act}$ or the value $n_{\rm SS} = n_{\rm abs} = 0$ depending on the initial density n_0. This phenomenon is referred to as bistability and it happens in proximity of the first-order branch $(\delta/\gamma)_c$, where the absorbing and the active phase coexist due to the presence of two minima in $W(n)$. The bistable phase (plotted in grey blurred scale in Fig. 22.6) is delimited by the coexistence curves $(\delta/\gamma)_c$ (green-solid line) and $\delta = 2\beta$ (red-dashed line). Coexistence of difference phases in the presence of a first-order phase transition has been also observed in a different context, both in equilibrium and in nonequilibrium, for Dicke-Bose-Hubbard systems [100, 101].

The two coexistence lines meet the second-order line at the bicritical point $(\beta/\gamma, \delta/\gamma) = (1/4, 1/2)$ (represented in orange in Fig. 22.6). At this point, the transition is continuous, but it belongs to a different universality class than that of Eqs. (22.51) and (22.52). Namely, for $\beta/\gamma = 1/4$ and $2\beta - \delta \to 0$, we find from (22.49) the power law

$$n_{\rm SS} \sim (\beta/\delta - 1/2)^{1/2}, \quad \beta/\gamma = 1/4, \tag{22.53}$$

for the stationary density as a function of β/δ. This is shown in the central-right panel of Fig. 22.6, where $n_{\rm SS}$ is plotted as a function of β/γ for fixed $\delta/\gamma = 0.5$ (horizontal orange-dashed line in the density plot in Fig. 22.6). The jump discontinuity in $n_{\rm SS}$ across the first-order branch goes continuously to zero as the bicritical point is approached. Similarly, at $\beta/\delta = 1/2$ and $\beta = \gamma = 1/4$, one has that the density $n(t)$ decays algebraically in time as

$$n(t) \sim t^{-1/2}, \quad \beta/\delta = 1/2, \quad \beta/\gamma = 1/4. \tag{22.54}$$

The same critical exponents as in Eqs. (22.53) and (22.54) have been found also in Refs. [57, 58] for the mean-field regime of the quantum contact process involving both classical-incoherent and quantum-coherent branching/coagulation. Here, a similar bicritical point to that of Fig. 22.6 was found in the plane spanned by the classical and quantum branching rates (note the difference with Fig. 22.6, where both the axes β/γ and δ/γ are classical rates). The bicritical

point is argued in Refs. [57, 58] to be described by the tricritical directed percolation universality class [87, 88, 89]. For spatial dimension $D \geq 3$, the mean-field exponents (22.53) and (22.54) are found, while in $D < 3$ deviations from mean field are present. The results of the present manuscript suggest that the same universality class describes also the bicritical point of the model involving coherent hopping (22.8) and classical branching/coagulation. The mean-field values for the exponents (22.53) and (22.54) are then a consequence of considering the reaction-limited regime $\Gamma/\Omega \ll 1$, where spatial fluctuations can be neglected. Consequently, in the reaction-limited regime here considered, such exponents are exact already in one spatial dimension $D = 1$.

22.1 Continuum Limit of two-body annihilation with interferences

In this Appendix, we derive the space continuum limit of the annihilation operators (22.10) and (22.11). This continuum limit provides an argument for the emergence of non-mean-field algebraic decay exponents [see Eqs. (22.36) and (22.39)] in the noninteracting Bose gas subject to binary annihilation processes.

In order to perform the continuum limit, we reintroduce the lattice spacing a (formerly set to 1), which provides the shortest length scale of the problem. The dimensionful length of the chain is $\ell = La$, where L is the number of lattice sites. Lattice points are identified as $x_j = ja$ in units of the lattice spacing. The space continuum limit is achieved by taking the limit $a \to 0$, $L \to \infty$ with ℓ kept fixed. In this limit, the Lindblad equation (22.7)-(22.9) can be written as

$$\frac{\mathrm{d}\rho}{\mathrm{d}t} = -i[H,\rho] + \sum_{\nu} \int_0^{\ell} \mathrm{d}x \left[L^{\nu}(x)\rho L^{\nu\dagger}(x) - \frac{1}{2}\left\{ L^{\nu\dagger}(x)L^{\nu}(x), \rho \right\} \right]. \tag{22.55}$$

In the previous equation, the Hamiltonian H is obtained from the continuum limit of Eq. (22.8) as

$$H = -\Omega \sum_{j=1}^{L} \left(\hat{b}_{ja}^{\dagger} \hat{b}_{ja+a} + \hat{b}_{ja+a}^{\dagger} \hat{b}_{a} \right) \quad \to \quad H = \int_0^{\ell} \mathrm{d}x\, \hat{b}^{\dagger}(x)(-\overline{\Omega}\partial_x^2)\hat{b}(x), \tag{22.56}$$

with $\overline{\Omega} = \Omega a^2$. The continuum bosonic field operators $\hat{b}(x)$ and the jump operators $L^{\nu}(x)$ are defined as

$$\hat{b}(x) = \frac{\hat{b}_{ja}}{\sqrt{a}}, \quad \text{with} \quad [\hat{b}(x), \hat{b}^{\dagger}(x')] = \delta(x - x'), \quad \text{and} \quad L^{\nu}(x) = \frac{L^{\nu}_{ja}}{\sqrt{a}}. \tag{22.57}$$

The Hamiltonian (22.56) is the second-quantized Hamiltonian of free bosonic particles freely moving in free space, with the kinetic energy operator $\sim \partial_x^2$ proportional to the second partial derivative in the space coordinate x. The definition of the jump operators $L^{\nu}(x)$ includes a factor $\sqrt{a}$, which is needed in order to turn the sum over lattice sites in Eq. (22.9) into a space integral as in Eq. (22.55). In the remainder of this and the other Appendices, we denote bosonic operators $\hat{b}_j, \hat{b}_j^{\dagger}$ (and their continuum analogues $\hat{b}(x)$, $\hat{b}^{\dagger}(x)$) as $b_j, b_j^{\dagger}$, without the hat symbol for the sake of brevity. We use the same notation also for bosonic number operators $\hat{n}_j, \hat{n}_q$ in real and momentum space, respectively, which we denote as n_j, n_q.

The continuum limit $L^{\alpha}(x)$ of the binary annihilation jump operator can be obtained from the Taylor series of Eq. (22.10)

$$\begin{aligned} L^{\alpha}(x) = L^{\nu}_{ja}/\sqrt{a} &= \sqrt{\Gamma_{\alpha}/a}\, b_{ja} \left(\cos(\theta) b_{ja+da} - \sin(\theta) b_{ja+da} \right) \\ &= \sqrt{\Gamma_{\alpha}^{(1)}} b^2(x) + \sqrt{\Gamma_{\alpha}^{(2)}} b(x)\partial_x b(x) + \mathcal{O}(a^{5/2}), \end{aligned} \tag{22.58}$$

where the coefficients $\Gamma_\alpha^{(1/2)}$ are given by

$$\Gamma_\alpha^{(1)} = a\Gamma_\alpha(\cos(\theta)-\sin(\theta))^2, \quad \text{and} \quad \Gamma_\alpha^{(2)} = a^3 d^2 \Gamma_\alpha\,(\cos(\theta)+\sin(\theta))^2. \tag{22.59}$$

We can see that $\Gamma_\alpha^{(1)}$ is the leading term as $a \to 0$, implying that $L^\alpha(x) \sim b^2(x)$ reduces to a binary annihilation process. The point $\theta = \pi/4$ is, instead, special because in that case one has $\Gamma_\alpha^{(1)} = 0$ and the next term $\Gamma_\alpha^{(2)}$ becomes the leading one in the expansion. Such term produces the coupling $L^\alpha(x) \sim b(x)\partial_x b(x)$ between the annihilation process and spatial derivatives of the bosonic field. This property introduces spatial fluctuations in the dynamics, since the action of the jump operator is sensitive to spatial gradients of the density profile. This yields eventually yields the beyond mean-field decay law (22.36).

For the second-order annihilation process (22.11), it is immediate to verify that Eq. (22.11) in the continuum limit yields a second order derivative of the bosonic field $b(x)$. Namely, one has

$$\begin{aligned} L^{\bar\alpha}(x) = L^{\bar\alpha}_{ja}/\sqrt{a} &= \sqrt{\Gamma_{\bar\alpha}/a}\, b_{ja}(b_{ja+da} + b_{ja-da} - 2b_{ja}) \\ &= \sqrt{\Gamma^{(2)}_{\bar\alpha}}\, b(x)\partial_x^2 b(x), \end{aligned} \tag{22.60}$$

with the coefficient $\Gamma^{(2)}_{\bar\alpha} = a^5 d^4 \Gamma^{\bar\alpha}$. The jump operator (22.60) couples to second-order spatial derivatives of the bosonic field and therefore it accounts for spatial fluctuations of larger spatial extent. This causes the beyond mean-field decay of Eq. (22.39). In particular, the second space derivative probes larger space regions than the first one and therefore the decay exponent (22.39) decreases compared to that of Eq. (22.36). On the basis of this reasoning, we expect the decay exponent to become smaller the higher the order of the interference process (higher order spatial derivatives).

22.2 Two-Body annihilation dynamics

In this Appendix, we briefly report the main steps of the derivation of Eqs. (22.32) and (22.38) for the binary annihilation process ($2A \to \emptyset$) involving interferences of two (22.10) or three (22.11) decay channels, respectively. We consider throughout the case of periodic boundary conditions $b_{j+L} = b_j$ for the Hamiltonian in Eq. (22.8). As this derivation is based on the TGGE method we are taking the thermodynamic limit $L \to \infty$, the choice of the periodic boundary condition does not therefore change the final result. The Fourier transform of the bosonic operators $b_j, b_j^\dagger$ is defined as follows

$$b_{k_n} = \frac{1}{\sqrt{L}}\sum_{j=1}^{L} e^{-ik_n j} b_n, \quad \text{with inverse} \quad b_j = \frac{1}{\sqrt{L}}\sum_{k_n=\frac{2\pi}{L}}^{2\pi} e^{ik_n j} b_{k_n}, \tag{22.61}$$

where $k_n = 2\pi n/L$, with the integer number $n = 1, 2 \ldots, L$, are the quasi-momenta. The Fourier transformed operators satisfy the bosonic commutation relations $[b_k, b^\dagger_{k'}] = \delta_{k,k'}$. In the following, we write the quasi-momenta k_n as k for brevity. Sums $\sum_{k_n} = \sum_{n=1}^{L}$ over the integer $n = 1, 2 \ldots L$ will be denoted as $\sum_k$ for simplicity. When sum over multiple quasi-momenta $k_1, \ldots, k_L$ are present, e.g., $\sum_{k_1} \cdots \sum_{k_N}$, we use the shorter notation $\sum_{k_1,\ldots,k_N}$. In the thermodynamic limit $L \to \infty$, when the TGGE applies, the momenta become continuous variables $k \in (-\pi, \pi)$ and the summations over k_n turn to integrals as in Eq. (22.26).

The Fourier transform of the jump operator L_j^α [Eq. (22.10)] for the binary annihilation reaction gives,

$$L_j^\alpha = \frac{\sqrt{\Gamma_\alpha}}{L}\sum_{k,k'} b_k b_{k'} e^{ij(k+k')}\left(\cos(\theta)e^{idk'} - \sin(\theta)e^{-idk'}\right). \tag{22.62}$$

To explicitly write the right hand side of the rate equation in Eq. (22.22), we need to evaluate the commutator $[n_q, L_j^\alpha]$. For this purpose, the following commutation relations are useful

$$[n_q, b_k b_{k'}] = -b_k b_{k'} \left(\delta_{kq} + \delta_{k'q}\right), \quad \text{from} \quad [n_q, b_k] = -\delta_{kq} b_q. \tag{22.63}$$

Plugging the above relation (22.63) into the rate equation (22.22), we find

$$\frac{\mathrm{d}B_q}{\mathrm{d}t} = -\frac{\Gamma_\alpha}{L} \sum_{k_1,k_2,k,k'} \delta_{k+k',k_1+k_2} f^*_{\theta,d}(k_1) f_{\theta,d}(k') \left(\langle b^\dagger_{k_1} b^\dagger_{k_2} b_k b_q \rangle_{\mathrm{GGE}} \delta_{q,k'} + \langle b^\dagger_{k_1} b^\dagger_{k_2} b_{k'} b_q \rangle_{\mathrm{GGE}} \delta_{q,k} \right), \tag{22.64}$$

where we used the Fourier representation of the Kronecker delta

$$\delta_{k,k'} \equiv \delta_{k_n,k_m} = \frac{1}{L} \sum_{j=1}^{L} e^{ij2\pi(n-m)/L}. \tag{22.65}$$

In Eq. (22.64), we further defined the function

$$f_{\theta,d}(k) = \cos(\theta) e^{ikd} - \sin(\theta) e^{-ikd}. \tag{22.66}$$

The four-point bosonic correlation functions in Eq. (22.64) can be crucially decomposed in terms of the two-point bosonic occupation function $\langle b^\dagger_q b_k \rangle = B_q \delta_{q,k}$ since the GGE state (22.20) is Gaussian. This is achieved via application of Wick's theorem

$$\langle b^\dagger_{k_1} b^\dagger_{k_2} b_{k_1+k_2-q} b_q \rangle = B_{k_1} B_q \delta_{k_2,q} + B_{k_1} B_{k_2} \delta_{k_1,q}. \tag{22.67}$$

Using Eqs. (22.65)-(22.67) to evaluate Eq. (22.64) one obtains

$$\frac{\mathrm{d}B_q(\tau)}{\mathrm{d}\tau} = -\frac{1}{L} \sum_k g_{\theta,d}(k,q) B_k(\tau) B_q(\tau), \tag{22.68}$$

with $\tau = \Gamma_\alpha t$ the rescaled time. The function $g_{\theta,d}(k,q)$ is obtained from (22.66) as

$$\begin{aligned} g_{\theta,d}(k,q) &= 2\mathrm{Re}(f^*_{\theta,d}(k) f_{\theta,d}(q)) + |f_{\theta,d}(q)|^2 + |f_{\theta,d}(k)|^2 \\ &= 2(1 + \cos(d(k-q))) - \sin(2\theta) \left[2\cos(d(k+q)) + \cos(2kd) + \cos(2qd)\right]. \end{aligned} \tag{22.69}$$

Equations (22.68) and (22.69) coincide with Eqs. (22.32) and (22.33) of the main text. Upon setting $\theta = 0$, Eq. (22.69) immediately renders (22.28). For $\theta = \pi/4$, the expression in Eq. (22.69) simplifies to

$$g_{\pi/4,d}(k,q) = 2[\sin(kd) + \sin(qd)]^2 = 2[\sin^2(kd) + \sin^2(qd) + 2\sin(kd)\sin(qd)]. \tag{22.70}$$

This function is very similar to the one reported in Refs. [34, 38] for the case of fermions (setting $d = 1$ therein). The only difference with respect to the fermionic case lies in the sign change $[\sin(kd) - \sin(qd)]^2$, which in turn causes the last term on the right hand side of the second equality of Eq. (22.70) to have the opposite sign $-2\sin(kd)\sin(qd)$. This difference, however, is not important as long as one considers initial states whose distribution is even in q: $B_q(0) = B_{-q}(0)$. This is true for all the initial states (22.23)-(22.25) we considered in this work. If the initial state is, indeed, invariant under quasi-momenta reversal $q \to -q$, then this symmetry is kept at all times $B_q(\tau) = B_{-q}(\tau)$. This, in turn, implies that the last term on the right hand side the second equality of (22.70) is zero since $\sum_k \sin(kd) B_k(\tau) = 0$ (the $\sin(kd)$ function is odd in k). In this case, Eq. (22.32) reduces to the very same form discussed in Refs. [34, 38] for fermions:

$$\frac{dB_q(\tau)}{d\tau} = -\frac{1}{L} \sum_k g_{\pi/4,d}(k,q) B_k(\tau) B_q(\tau) = -\frac{1}{L} \sum_k [2\sin^2(kd) + 2\sin^2(qd)] B_k(\tau) B_q(\tau). \tag{22.71}$$

From this equation, we can derive the implicit solution (22.35) for $B_q(\tau)$, following similar derivations as those performed in Refs. [34, 35]. We report here this derivation for the sake of completeness. The equation for the density $\langle n\rangle_{\rm GGE}(\tau) \equiv n(t)$ from (22.68) reads as

$$\frac{\mathrm{d}n(\tau)}{\mathrm{d}\tau} = -4n(\tau)\frac{1}{L}\sum_k \sin^2(kd)B_k(\tau) \quad \rightarrow \quad \frac{1}{L}\sum_k \sin^2(kd)B_k(\tau) = -\frac{1}{4n(\tau)}\frac{\mathrm{d}n(\tau)}{\mathrm{d}\tau}. \tag{22.72}$$

We remark that (22.72) is not a closed equation for the density $n(t)$ since the occupation function $B_k(\tau)$ appears explicitly on the right hand side. The evolution for the occupation function B_q of the mode q is, indeed, coupled to that of all the other modes B_k through the function $g_{\pi/4,d}(k,q)$. This function arises from the structure of the jump operator (22.10) involving the superposition of two decay channels between nearest neighbouring sites. In the case of onsite processes, e.g., coagulation and branching discussed in Appendix 22.3 and 22.4 below, respectively, different Fourier modes are not coupled and one can write closed equations for the density of particles. Substituting Eq. (22.72) into (22.71) yields

$$\frac{dB_q(\tau)}{d\tau} = \frac{B_q\dot{n}(\tau)}{2n(\tau)} - 2\sin^2(dq)B_q(\tau)n(\tau), \tag{22.73}$$

with $\dot{n}(\tau) = \mathrm{d}n(\tau)/\mathrm{d}\tau$. The time integration of Eq. (22.73) gives

$$\ln\left(B_q(\tau)/B_q(0)\right) = \frac{1}{2}\ln\left(n(t)/n(0)\right) - 2\sin^2(qd)\int_0^\tau \mathrm{d}t\, n(t). \tag{22.74}$$

The exponentiation of (22.74) eventually yields Eq. (22.35) of the main text.

The derivation of Eq. (22.38) for the jump operator $L_j^{\bar{\alpha}}$ (22.11) describing second-order annihilation decay follows the very same steps as those leading to (22.68). In particular, Eq. (22.64) is still valid upon changing the definition of the function $f_{\theta,d}(k) \rightarrow f_d(k)$. For the jump operator (22.11) one has

$$f_d(k) = 2(\cos(kd) - 1). \tag{22.75}$$

Then, Eq. (22.68) is still valid with $g_{\theta,d}(k) \rightarrow g_d(k)$ and

$$g_d(k) = 2\mathrm{Re}(f_d^*(k)f_d(q)) + |f_d(q)|^2 + |f_d(k)|^2 = 4(\cos(kd) + \cos(qd) - 2)^2. \tag{22.76}$$

Eqs. (22.68) and (22.76) coincide with (22.38) of the main text. Both in the cases of Eq. (22.69) and in that of Eq. (22.76), we solve numerically the TGGE rate equation (22.68) by discretizing the momenta $k_n = 2\pi n/L$ in the interval $(-\pi,\pi)$. Here L parametrizes the resolution of the grid. We take the value $L = 10^4$. We have checked that the numerical data in Figs. 22.2-22.4 are stable upon further increasing L.

22.3 Coagulation dynamics

For the onsite coagulation dynamics in Eq. (22.12), the Fourier transform of the jump operator L_j^γ reads

$$L_j^\gamma = \sqrt{\frac{\Gamma_\gamma}{L^3}}\sum_{k_1,k_2,k_3} e^{ij(k_2+k_3-k_1)}b_{k_1}^\dagger b_{k_2}b_{k_3}. \tag{22.77}$$

The commutator $[n_q, L_j^\gamma]$ in Eq. (22.21) yields

$$[n_q, b_{k_1}^\dagger b_{k_2}b_{k_3}] = -b_{k_1}^\dagger b_{k_2}b_q\delta_{q,k_3} - b_{k_1}^\dagger b_{k_3}b_q\delta_{q,k_2} + b_q^\dagger b_{k_2}b_{k_3}\delta_{q,k_1}. \tag{22.78}$$

Inserting (22.77) (and the adjoint equation for $L_j^{\gamma\dagger}$) into (22.21) and using (22.78) to handle the commutator, one obtains

$$\frac{\mathrm{d}B_q(t)}{\mathrm{d}t} = \frac{\Gamma_\gamma}{L^2}\sum_{k,k',k_1,k_2} \langle b_k^\dagger b_{k'}^\dagger b_{k+k'-k_1-k_2+q} b_q^\dagger b_{k_1} b_{k_2}\rangle_{\mathrm{GGE}} - 2\langle b_k^\dagger b_{k'}^\dagger b_{k+k'+k_1-k_2-q} b_{k_1}^\dagger b_{k_2} b_q\rangle_{\mathrm{GGE}}. \tag{22.79}$$

The six-point bosonic correlation functions can be again computed exploiting the Gaussian structure of the GGE and therefore Wick's theorem. One has

$$\begin{aligned}\langle b_k^\dagger b_{k'}^\dagger b_{k+k'-k_1-k_2+q} b_q^\dagger b_{k_1} b_{k_2}\rangle_{\mathrm{GGE}} &= B_{k'}B_qB_k\delta_{k',k_2}\delta_{q,k_1} + B_{k'}B_qB_k\delta_{k',k_1}\delta_{q,k_2} + B_kB_qB_{k'}\delta_{k,k_1}\delta_{q,k_2} \\ &+ B_{k'}B_kB_q\delta_{k,k_2}\delta_{q,k_1} + B_kB_{k'}(1+B_q)\delta_{k,k_1}\delta_{k',k_2} + B_kB_{k'}(1+B_q)\delta_{k,k_2}\delta_{k',k_1}.\end{aligned} \tag{22.80}$$

and

$$\begin{aligned}\langle b_k^\dagger b_{k'}^\dagger b_{k+k'+k_1-k_2-q} b_{k_1}^\dagger b_{k_2} b_q\rangle_{\mathrm{GGE}} &= B_{k'}B_{k_1}B_k\delta_{k',k_2}\delta_{q,k_1} + B_{k'}B_{k_1}B_k\delta_{k',q}\delta_{k_1,k_2} + B_kB_{k_1}B_{k'}\delta_{k,k_2}\delta_{q,k_1} \\ &+ B_{k'}B_kB_{k_1}\delta_{k,q}\delta_{k_1,k_2} + B_kB_{k'}(1+B_{k_1})\delta_{k,k_2}\delta_{k',q} + B_kB_{k'}(1+B_{k_1})\delta_{k',k_2}\delta_{k,q}.\end{aligned} \tag{22.81}$$

Inserting (22.80) and (22.81) into (22.79), one eventually obtains

$$\frac{\mathrm{d}B_q(\tau)}{\mathrm{d}\tau} = -6B_q\langle n\rangle_{\mathrm{GGE}}^2 + 2\langle n\rangle_{\mathrm{GGE}}^2 - 4B_q\langle n\rangle_{\mathrm{GGE}}, \tag{22.82}$$

with $\tau = \Gamma_\gamma t$. This equation coincides with Eq. (22.40) of the main text. In this equation, crucially, the occupation B_q of the mode q is not coupled to that of the other modes $k \neq q$. This allows to write the closed equation (22.41) for the density. Therein three-body terms $\sim \langle n\rangle_{\mathrm{GGE}}^3$ are present. Note, that in the analogous calculation for the fermions [38] such terms cancel out, but here, for bosons, they do not. These cubic nonlinearities are the origin of the rich phase diagram emerging when coagulation competes with branching. We present the calculations for branching in the next Section of the Appendix.

22.4 Branching dynamics

We report here the main steps of derivation the rate equation Eq. (22.44). The steps are very similar to those of Appendix 22.3 and we therefore report only the main steps. The Fourier transform of the onsite branching jump operator L_j^β in Eq. (22.14) reads

$$L_j^\beta = \sqrt{\frac{\Gamma_\beta}{L^3}}\sum_{k_1,k_2,k_3} b_{k_1}^\dagger b_{k_2}^\dagger b_{k_3} e^{ij(k_3-k_1-k_2)}. \tag{22.83}$$

The commutator $[n_q, L_j^\beta]$ in Eq. (22.83) is readily computed from the knowledge of the following commutators

$$[n_q, b_{k_1}^\dagger b_{k_2}^\dagger b_{k_3}] = b_q^\dagger b_{k_2}^\dagger b_{k_3}\delta_{k_1,q} + b_q^\dagger b_{k_1}^\dagger b_{k_3}\delta_{k_2,q} - b_{k_1}^\dagger b_{k_2}^\dagger b_q\delta_{k_3,q}. \tag{22.84}$$

Inserting Eqs. (22.83) and (22.84) into (22.21) one obtains

$$\frac{\mathrm{d}B_q}{\mathrm{d}t} = \frac{\Gamma_\beta}{L^2}\sum_{k,k',k_1,k_2} 2\langle b_k^\dagger b_{k'} b_{k-k'-k_2+k_1+q} b_q^\dagger b_{k_1}^\dagger b_{k_2}\rangle_{\mathrm{GGE}} - \langle b_k^\dagger b_{k'} b_{k-k'-q+k_2+k_1} b_{k_1}^\dagger b_{k_2}^\dagger b_q\rangle_{\mathrm{GGE}}. \tag{22.85}$$

The calculation of the six-point functions follows to very same lines of the calculation of Eqs. (22.80) and (22.81) and we therefore do not report it here for the sake of brevity. The final result for the evolution equation for the occupation function B_q in momentum space reads

$$\frac{\mathrm{d}B_q(t)}{\mathrm{d}t} = \Gamma_\beta[2(2n - B_q) + 8n^2 + 6B_q n^2], \tag{22.86}$$

which coincides with Eq. (22.44) of the main text. As in the case of onsite coagulation, for onsite branching the evolution of a mode q is not coupled to the evolution of the other modes $k \neq q$. This allows to derive the closed equations (22.45) and (22.46) for the density of particles. These equations are akin to the classical law of mass action equation (22.18), but, at the same time, they are fundamentally different from those equations due to the three body terms. These terms generate the phase diagram discussed in Subsec. 22.0.8 of the main text, which shows a richer behavior than the classical mean-field contact process in Eq. (22.18).

23 Quasilocal conserved operators in isotropic Heisenberg spin 1/2 chain by Ilievski et al.

Abstract

Composing higher auxiliary–spin transfer matrices and their derivatives, we construct a family of quasilocal conserved operators of isotropic Heisenberg spin 1/2 chain and rigorously establish their linear independence from the well-known set of local conserved charges.

Introduction.– The Heisenberg chain of n spins $\frac{1}{2}$ with the Hamiltonian (known as the XXX model)

$$H = \sum_{x=0}^{n-1} (\vec{\sigma}_x \cdot \vec{\sigma}_{x+1} + \mathbb{1}), \tag{23.1}$$

where $\vec{\sigma}_x = (\sigma_x^{\mathrm{x}}, \sigma_x^{\mathrm{y}}, \sigma_x^{\mathrm{z}})$ are Pauli operators and periodic boundaries are assumed $\vec{\sigma}_n \equiv \vec{\sigma}_0$, is arguably the simplest nontrivial interacting quantum many-body model. The spectrum and eigenstates of H can be formulated in terms of the famous Bethe ansatz [1], which gave birth to the theory of quantum integrable systems [2, 3]. Eq. (23.1) has been originally proposed as the model of (anti)ferromagnetism in solids [4] and is indeed a very good description of the modern spin-chain materials [5]. It may also be considered as a fundamental paradigm of quantum statistical mechanics which is being used for developing theoretical mechanisms of non-equilibrium dynamics and thermalization or relaxation to the generalized Gibbs ensemble (GGE) [6, 7, 8].

The relaxation dynamics based on quantum quenches [9, 10, 11, 12] gave firm evidence that the full set of ($\sim n$) local conserved operators, the existence of which is granted for a quantum integrable system, is incomplete, in the sense that it cannot describe the steady state completely through a GGE. Similarly, a numerical experiment counting the number of linearly independent time-averaged local operators [13] indicated that the set of local conserved charges should be incomplete and numerical approximations of new quasilocal operators have been put forward.

In this Letter we explicitly construct new families of non-local but quasilocal operators by composition of a transfer matrix (TM) – in the sense of algebraic Bethe ansatz, but for higher integer or half-integer auxiliary spins $s > \frac{1}{2}$ – and its derivative, at a special combination of spectral parameters, which in the thermodynamic limit (TL) becomes equivalent to a logarithmic derivative of TM. Furthermore, we prove quasilocality (in full rigour for a finite set

of auxiliary spins s) as well as linear independence of these new operator families w.r.t. local conserved charges. Generally, we identify quasilocality with the condition of factorizability of the largest eigenvalue of an auxiliary TM that enters in the computation of the norm of the conserved operator, i.e. a product of higher-spin TM and its derivative. As we facilitate finite-dimensional unitary representations of quantum or Lie symmetries, the new quasilocal operators are always spin-reversal symmetric unlike in alternative recent constructions in the XXZ chain [14, 15, 16, 17] which only work at special, commensurate values of anisotropy. This features promise that our technique shall be applicable for generating new quasilocal charges in other generic integrable models with Lie or quantum group symmetries. Being able to construct a complete, or as large as possible set of independent quasilocal conserved charges is crucial for any application in quantum statistical mechanics, besides constructing GGE, e.g. in linear response theory at finite temperatures, studies of quantum ergodicity and many-body localization, etc. Quasilocal conservation laws are also closely related to boundary driven/dissipative quantum chains [14, 18].

Transfer matrices and conserved operators.– Let $\mathcal{V}_s$, $s \in \frac{1}{2}\mathbb{Z}^+$, denote a $2s+1$ dimensional spin-s module, $\mathcal{V}_s \equiv \mathbb{C}^{2s+1} = \mathrm{lsp}\{|m\rangle, m = -s, -s+1, \ldots, s\}$, lsp denoting a linear span of a set of vectors, carrying the unitary irreducible representation of $SU(2)$ with generators

$$\mathbf{s}^{\mathrm{z}}|m\rangle = m|m\rangle,\ \mathbf{s}^{\pm}|m\rangle = \sqrt{(s+1\pm m)(s\mp m)}|m\pm 1\rangle. \tag{23.2}$$

The physical Hilbert space is an $n-$fold tensor product of fundamental representations $\mathcal{H}_{\mathrm{p}} = \mathcal{V}_{1/2}^{\otimes n}$, with $\sigma^{\mathrm{z}} \equiv 2\mathbf{s}^{\mathrm{z}}$, $\sigma^{\pm} = \frac{1}{2}(\sigma^{\mathrm{x}} \pm \mathrm{i}\sigma^{\mathrm{y}}) \equiv \mathbf{s}^{\pm}$. Fixing arbitrary $s \in \frac{1}{2}\mathbb{Z}^+$ and considering another, auxiliary Hilbert space $\mathcal{H}_{\mathrm{a}} = \mathcal{V}_s$, we define Lax matrices as operators over $\mathcal{H}_{\mathrm{p}} \otimes \mathcal{H}_{\mathrm{a}}$

$$\mathbf{L}_{x,\mathrm{a}}(\lambda) = \lambda\mathbb{1} + \sigma_x^{\mathrm{z}}\mathbf{s}_{\mathrm{a}}^{\mathrm{z}} + \sigma_x^{+}\mathbf{s}_{\mathrm{a}}^{-} + \sigma_x^{-}\mathbf{s}_{\mathrm{a}}^{+} = \lambda\mathbb{1} + \vec{\sigma}_x \cdot \vec{\mathbf{s}}_{\mathrm{a}}, \tag{23.3}$$

where $\lambda \in \mathbb{C}$ is the spectral parameter. Throughout the Letter, operators acting nontrivially over the auxiliary Hilbert space are written in bold, or double strike font if acting over multiple (tensor product of) auxiliary spaces. As a simple consequence of Yang-Baxter equation, the (physical) TMs $T_s(\lambda) \in \mathrm{End}(\mathcal{H}_{\mathrm{p}})$

$$T_s(\lambda) = \mathrm{tr}_{\mathrm{a}}\mathbf{L}_{0,\mathrm{a}}(\lambda)\mathbf{L}_{1,\mathrm{a}}(\lambda)\cdots\mathbf{L}_{n-1,\mathrm{a}}(\lambda), \tag{23.4}$$

where s is the auxiliary spin, form a commuting family

$$[T_s(\lambda), T_{s'}(\lambda')] = 0, \quad \forall s, s', \lambda, \lambda'. \tag{23.5}$$

The fundamenal TM $T_{\frac{1}{2}}(\lambda)$ is generating the complete set of local conserved Hermitian operators

$$Q_k = -\mathrm{i}\partial_t^{k-1}\log T_{\frac{1}{2}}(\tfrac{1}{2}+\mathrm{i}t)|_{t=0} = \sum_{x=0}^{n-1}\hat{\mathcal{S}}^x\left(\mathbb{1}_{2^{n-k}}\otimes q_k\right), \tag{23.6}$$

$k \geq 2$, with $Q_2 = H$, where $q_k \in \mathrm{End}(\mathcal{V}_{1/2}^{\otimes k})$ is a $k-$point operator density, and $\hat{\mathcal{S}}$ is a cyclic lattice shift map over $\mathrm{End}(\mathcal{H}_{\mathrm{p}})$ defined by $\hat{\mathcal{S}}(\sigma_x^{\alpha}) = \sigma^{\alpha}_{\mathrm{mod}(x+1,n)}$.

Locality and quasilocality.– The 4^n-dimensional space of physical operators $\mathrm{End}(\mathcal{H}_{\mathrm{p}})$ is turned into a Hilbert space by defining a Hilbert-Schmidt (HS) inner product $(A,B) := \langle A^{\dagger}B\rangle$ w.r.t. the infinite-temperature state $\langle A\rangle := 2^{-n}\,\mathrm{tr}\,A$. Let $\{A\} := A - \langle A\rangle\mathbb{1}$ denote the traceless part of an operator. One of physically most important features of the local conservation laws Q_k is the extensivity of the HS norm $\|\{Q_k\}\|_{\mathrm{HS}}^2 := (\{Q_k\},\{Q_k\}) = \left(2^{-k}\,\mathrm{tr}\,(q_k^{\dagger}q_k) - |2^{-k}\,\mathrm{tr}\,q_k|^2\right) n \propto n$. We define (equivalently to [16]) a general traceless, translationally invariant operator $A = \hat{\mathcal{S}}(A) \in \mathrm{End}(\mathcal{H}_{\mathrm{p}})$ as quasilocal if two conditions are met: (i) $\|A\|_{\mathrm{HS}}^2 \propto n$, and (ii) for any

locally supported k-site operator $b = b_k \otimes \mathbb{1}_{2^{n-k}}$ the overlap (b, A) is asymptotically, as $n \to \infty$, independent of n.

One should stress that quasilocality only makes sense in TL $n \to \infty$ as it is the property of an infinite sequence of operators labelled by n, rather than operators for any fixed size n. More intuitively, a quasilocal operator Q can be thought of as a convergent sum of local operators $Q = \sum_{r=1}^{\infty} Q^{(r)}$, where $Q^{(r)}$ includes only terms supported on r contiguous sites and the sum $\|Q\|_{\rm HS}^2 = \sum_{r=1}^{\infty} \|Q^{(r)}\|_{\rm HS}^2$ is rapidly (typically exponentially) converging. Usually [14, 15, 16], quasilocality can be detected by inspecting the leading eigenvalue of a certain auxiliary transfer matrices, whose r-th power yields the partial norm of the $r-$site terms $\|Q^{(r)}\|_{\rm HS}^2$. The effect of quasilocal conserved operators to statistical mechanics is arguably *as important* as that of local operators. In particular, quasilocal charges can be understood as those conserved operators of one-dimensional systems which can influence equilibrated (steady-state) values, say after a quantum quench, of strictly local observables. Our central result is the following

Theorem:

Traceless operators $X_s(t)$, $s \in \frac{1}{2}\mathbb{Z}^+, t \in \mathbb{R}$, defined over the physical Hilbert space $\mathcal{H}_{\rm p}$ as

$$X_s(t) = [\tau_s(t)]^{-n} \left\{ T_s(-\tfrac{1}{2} + {\rm i}t) T_s'(\tfrac{1}{2} + {\rm i}t) \right\}, \tag{23.7}$$

$$\tau_s(t) = -t^2 - \left(s + \tfrac{1}{2}\right)^2, \tag{23.8}$$

where $T_s'(\lambda) \equiv \partial_\lambda T_s(\lambda)$, are quasilocal for all s, t and linearly independent from $\{Q_k; k \geq 2\}$ for $s > \frac{1}{2}$.

The fact that $X_s(t)$ are exactly conserved and $[X_s(t), X_{s'}(t')] = [X_s(t), Q_k] = 0$ follows directly from (23.5). The form of our ansatz (23.7) is inspired from an observation (see Eq. (23.6) or, e.g., Ref. [19]) that at $s = \frac{1}{2}$, TM becomes in TL $n \to \infty$ a unitary operator

$$T_{\frac{1}{2}}(\tfrac{1}{2} + {\rm i}t) \simeq \exp\left({\rm i} \sum_{k=1}^{\infty} \frac{t^k}{k!} Q_{k+1} \right), \tag{23.9}$$

and hence (23.7) can be associated with a logarithmic derivative via $T_s^\dagger(\lambda) \equiv T_s^T(\bar{\lambda}) = (-1)^n T_s(-\bar{\lambda})$ where the last equality is due to spin reversal symmetry $\mathbf{s}^{\rm z} \to -\mathbf{s}^{\rm z}$, $\mathbf{s}^{\pm} \to -\mathbf{s}^{\mp}$.

Proof of quasilocality.– First, we write a matrix product form of a general product of a pair of TMs [20]

$$T_s(\mu) T_s(\lambda) = {\rm tr}_{{\rm a}_1,{\rm a}_2} \prod_{x=0}^{n-1} \left(\sum_{\alpha \in \mathcal{J}} \mathbb{L}_s^\alpha(\mu, \lambda) \sigma_x^\alpha \right) \tag{23.10}$$

where the operators $\mathbb{L}_s^\alpha(\mu, \lambda)$, $\alpha \in \mathcal{J} := \{0, {\rm x}, {\rm y}, {\rm z}\}$ act over a pair of auxiliary spaces $\mathcal{H}_{{\rm a}_1} \otimes \mathcal{H}_{{\rm a}_2} \equiv \mathcal{V}_s \otimes \mathcal{V}_s$

$$\mathbb{L}_s^0(\mu, \lambda) = \lambda\mu \mathbb{1} + \vec{\mathbf{s}}_{{\rm a}_1} \cdot \vec{\mathbf{s}}_{{\rm a}_2}, \tag{23.11}$$

$$\vec{\mathbb{L}}_s(\mu, \lambda) = {\rm i}\, \vec{\mathbf{s}}_{{\rm a}_1} \times \vec{\mathbf{s}}_{{\rm a}_2} + \lambda \vec{\mathbf{s}}_{{\rm a}_1} + \mu \vec{\mathbf{s}}_{{\rm a}_2}. \tag{23.12}$$

Identity component can be written with the Casimir operator $\mathbf{C} = (\vec{\mathbf{s}}_{{\rm a}_1} + \vec{\mathbf{s}}_{{\rm a}_2})^2$ as $\mathbb{L}_s^0 = \mu\lambda\mathbb{1} + \frac{1}{2}(\mathbf{C} - \vec{\mathbf{s}}_{{\rm a}_1}^2 - \vec{\mathbf{s}}_{{\rm a}_2}^2)$, hence its spectrum reads $\tau_s^j(\mu, \lambda) = \frac{j(j+1)}{2} - s(s+1) + \mu\lambda$, $j = 0, 1, \ldots, 2s$. Placing the spectral parameters along one of the two lines

$$\mathcal{D}^\pm = \{(\mu_t^\pm, \lambda_t^\pm); t \in \mathbb{R}\} \subset \mathbb{C}^2,$$
$$\mu_t^\pm := \mp\tfrac{1}{2} + {\rm i}t, \quad \lambda_t^\pm := \pm\tfrac{1}{2} + {\rm i}t, \tag{23.13}$$

we define the restricted auxiliary operators as $\mathbb{L}_s^{\pm\alpha}(t) := \mathbb{L}_s^{\alpha}(\mu_t^{\pm}, \lambda_t^{\pm})$. The dominating eigenvalue of Hermitian operator $\mathbb{L}_s^{+0}(t) \equiv \mathbb{L}_s^{-0}(t)$ is $\tau_s(t) = \tau_s^0(\mu_t^{\pm}, \lambda_t^{\pm})$, Eq. (23.8), corresponding to the singlet eigenstate

$$|\psi_0\rangle = (2s+1)^{-1/2} \sum_{m=-s}^{s} (-1)^{s-m} |m\rangle \otimes |-m\rangle, \tag{23.14}$$

with a finite gap to the subleading eigenvalue $\tau_s'(t)$, $\delta = \log|\tau_s(t)/\tau_s'(t)| > 0$, for any t. The condition $(\vec{\mathbf{s}}_{\mathrm{a}_1} + \vec{\mathbf{s}}_{\mathrm{a}_2})|\psi_0\rangle = 0$ and the $SU(2)$ algebra $\vec{\mathbf{s}}_{\mathrm{a}_k} \times \vec{\mathbf{s}}_{\mathrm{a}_k} = \mathrm{i}\vec{\mathbf{s}}_{\mathrm{a}_k}$ imply the following useful identities

$$\begin{aligned} \vec{\mathbb{L}}_s^{+}(t)|\psi_0\rangle = 0, \quad \langle\psi_0|\vec{\mathbb{L}}_s^{+}(t) = -2\langle\psi_0|\vec{\mathbf{s}}_{\mathrm{a}_1}, \\ \langle\psi_0|\vec{\mathbb{L}}_s^{-}(t) = 0, \quad \vec{\mathbb{L}}_s^{-}(t)|\psi_0\rangle = -2\vec{\mathbf{s}}_{\mathrm{a}_1}|\psi_0\rangle. \end{aligned} \tag{23.15}$$

We proceed by constructing a TM over a 4-spin auxiliary space $\mathcal{H}_{\mathrm{a}} = \bigotimes_{k=1}^{4} \mathcal{H}_{\mathrm{a}_k}$, $\mathcal{H}_{\mathrm{a}_{1,2}} \equiv \mathcal{V}_s$, $\mathcal{H}_{\mathrm{a}_{3,4}} \equiv \mathcal{V}_{s'}$

$$\mathbb{T}_{s,s'}(\mu, \lambda, \mu', \lambda') = \sum_{\alpha \in \mathcal{J}} \mathbb{L}_s^{\alpha}(\mu, \lambda) \otimes \mathbb{L}_{s'}^{\alpha}(\mu', \lambda'), \tag{23.16}$$

which helps us to compute a general inner product of the form $K_{s,s'}(t,t') := (X_s(t), X_{s'}(t'))$. The Hilbert–Schmidt kernel (HSK) then immediately follows after differentiating traces of powers of suitable TMs

$$K_{s,s'}(t,t') = [\tau_s(t)\tau_{s'}(t')]^{-n} \partial_{\lambda_t^-} \partial_{\lambda_{t'}^+} \left(\mathrm{tr}\, \left[\mathbb{T}_{s,s'}(\mu_t^-, \lambda_t^-, \mu_{t'}^+, \lambda_{t'}^+)\right]^n - \mathrm{tr}\, \left[\mathbb{L}_s^0(\mu_t^-, \lambda_t^-)\right]^n \mathrm{tr}\, \left[\mathbb{L}_{s'}^0(\mu_{t'}^+, \lambda_{t'}^+)\right]^n \right). \tag{23.17}$$

As a consequence of boundary condition given by Eq. (23.15) we obtain that $\tau_{s,s'}(t,t') := \tau_s(t)\tau_{s'}(t)$ is always an eigenvalue of $\mathbb{T}_{s,s'}(t,t') := \mathbb{T}_{s,s'}(\mu_t^-, \lambda_t^-, \mu_{t'}^+, \lambda_{t'}^+)$ with a product-singlet eigenvector $|\Psi_0\rangle = |\psi_0\rangle \otimes |\psi_0\rangle$. One can further show that it is always a dominating and non-degenerate eigenvalue by demonstrating that $\mathbb{T}_{s,s'}(t,t') - \tau_s(t)\tau_{s'}(t)\mathbb{1}$ is a negative definite operator on $\mathcal{H}_{\mathrm{a}} \setminus \mathbb{C}|\Psi_0\rangle$ (see Sects. A,B of [21] for details. We note though that we managed to rigorously prove negativity only for $s \leq s_0 = 3/2$ and further succeeded to confirm it with exact numerical computations up to much larger maximal auxiliary spin s_0, while for any s it formally remains a conjecture). Denoting by $\tau_{s,s'}(\mu, \lambda, \mu', \lambda')$ the continuation of the dominating eigenvalue in the proximity of the domain $\mathcal{D}^- \times \mathcal{D}^+$, and using Hellmann-Feynman theorem to evaluate its first derivatives $\partial_{\lambda_t^-}\tau_{s,s'}(\mu_t^-, \lambda_t^-, \mu_{t'}^+, \lambda_{t'}^+) = \partial_{\lambda_t^-}\tau_s^0(\mu_t^-, \lambda_t^-)\tau_{s'}^0(\mu_{t'}^+, \lambda_{t'}^+)$, $\partial_{\lambda_{t'}^+}\tau_{s,s'}(\mu_t^-, \lambda_t^-, \mu_{t'}^+, \lambda_{t'}^+) = \tau_s^0(\mu_t^-, \lambda_t^-)\partial_{\lambda_{t'}^+}\tau_{s'}^0(\mu_{t'}^+, \lambda_{t'}^+)$, the HSK can be computed as

$$K_{s,s'}(t,t') = n[\tau_s(t)\tau_{s'}(t')]^{-1} \partial_{\lambda_t^-} \partial_{\lambda_{t'}^+} \left(\tau_{s,s'}(\mu_t^-, \lambda_t^-, \mu_{t'}^+, \lambda_{t'}^+) - \tau_s^0(\mu_t^-, \lambda_t^-)\tau_{s'}^0(\mu_{t'}^+, \lambda_{t'}^+) \right) + \mathcal{O}(e^{-\gamma n}). \tag{23.18}$$

Remarkably, n^2 term exactly cancels, while the finite-size corrections are exponentially small in the gap $\gamma = \log|\tau_{s,s'}(t,t')/\tau'| > 0$ to subleading eigenvalue of τ' of $\mathbb{T}_{s,s'}(t,t')$. We shall later derive an explicit expression for HSK.

What remains to be shown is that $X_s(t)$ have well defined expansions in terms of local operators in TL $n \to \infty$. For any k-local basis operator $\sigma_{1:k}^{\alpha} := \sigma_1^{\alpha_1}\sigma_2^{\alpha_2}\cdots\sigma_k^{\alpha_k}$, $\alpha_{1,k} \neq 0$, we write the component of (23.7) as $[\tau_s(t)]^{-n}\partial_{\lambda_t^+}(\sigma_{1:k}^{\alpha}, T_s(\mu_t^+)T_s(\lambda_t^+))$. For treating $n \to \infty$ asymptotics we substitute $[\mathbb{L}_s^{+0}(t)/\tau_s(t)]^{n-k} = |\psi_0\rangle\langle\psi_0| + \mathcal{O}(e^{-\delta n})$ and take into account the fact that the $\lambda-$derivative should always hit the last, $k-$th factor, producing $\partial_\lambda \vec{\mathbb{L}}_s = \vec{\mathbf{s}}_{\mathrm{a}_1}$, otherwise the whole term would vanish due to the Eqs. (23.15). Thus we find a compact matrix product formula for the components (with the $k = 1$ component vanishing)

$$(\sigma_{1:k}^{\alpha}, X_s(t)) = \langle\psi_{\alpha_1}|\mathbb{X}^{\alpha_2}\cdots\mathbb{X}^{\alpha_{k-1}}|\psi_{\alpha_k}\rangle + \mathcal{O}(e^{-\delta n}), \tag{23.19}$$

where $\mathbb{X}^\alpha := \mathbb{L}_s^{+\alpha}(t)/\tau_s(t)$, $|\psi_\alpha\rangle := \sqrt{2}\mathrm{i}\mathrm{s}_{\mathrm{a}_1}^\alpha|\psi_0\rangle/\tau_s(t)$. The HS norm of $X_s(t)$ projected onto ℓ sites, in the limit $n-\ell\to\infty$, can be written analogously to Eq. (23.17)

$$\lim_{n\to\infty}\sum_{k=2}^{\ell}(\ell-k+1)\sum_{\underline{\alpha}}|(\sigma^{\underline{\alpha}}_{1:k},X_s(t))|^2 = \tag{23.20}$$
$$\frac{1}{[\tau_s(t)]^{2\ell}}\partial_{\lambda_t^-}\partial_{\lambda_t^+}\Big(\langle\Psi_0|\left[\mathbb{T}_{s,s}(\mu_t^-,\lambda_t^-,\mu_t^+,\lambda_t^+)\right]^\ell|\Psi_0\rangle$$
$$-\langle\psi_0|\left[\mathbb{L}_s^0(\mu_t^-,\lambda_t^-)\right]^\ell|\psi_0\rangle\langle\psi_0|\left[\mathbb{L}_s^0(\mu_t^+,\lambda_t^+)\right]^\ell|\psi_0\rangle\Big).$$

thus resulting in expression $\propto\ell$, cf. Eq. (23.18), without any finite-size (ℓ-dependent) corrections as $|\Psi_0\rangle$ is an exact eigenstate. We have thus shown that the expansion

$$X_s(t)=\lim_{\ell\to\infty}\lim_{n\to\infty}\sum_{k=2}^{\ell}\sum_{\underline{\alpha}}(\sigma^{\underline{\alpha}}_{1:k},X_s(t))\sum_{x=0}^{n-1}\hat{\mathcal{S}}^x(\sigma^{\underline{\alpha}}_{1:k}), \tag{23.21}$$

is complete in the HS norm. Q.E.D.

Eqs. (23.20,23.21) have two useful implications: (i) As the state $|\Psi_0\rangle$ is a spin singlet (in 4−spin auxiliary space) the only relevant part of the $SU(2)$ invariant TM $\mathbb{T}_{s,s'}(t,t')=\sum_\alpha\mathbb{L}_s^{-\alpha}(t)\otimes\mathbb{L}_{s'}^{+\alpha}(t')$, is the $(2J+1)$-dimensional block, $J=\min\{s,s'\}$, constituting the spin singlet subspace of $\mathcal{H}_{\mathrm{a}}$, where it can be written explicitly as a tridiagonal matrix (see Sect A of [21]). (ii) The HSK can be compactly written in terms of the resolvent of the TM, similarly as in [16], namely $K_{s,s'}(t,t')=n\sum_{k=0}^\infty\langle\Psi|\left[\widetilde{\mathbb{T}}_{s,s'}(t,t')\right]^k|\Psi\rangle$, where $\widetilde{\mathbb{T}}_{s,s'}(t,t')=\mathbb{T}_{s,s'}(t,t')/[\tau_s(t)\tau_{s'}(t')]$ and $|\Psi\rangle=\sum_{\alpha\in\{\mathrm{x},\mathrm{y},\mathrm{z}\}}|\psi_\alpha\rangle\otimes|\psi_\alpha\rangle$, e.g. via solving a system of $2J$ linear equations

$$K_{s,s'}(t,t')=n\langle\Psi|\Phi\rangle,\quad(\mathbb{1}-\widetilde{\mathbb{T}}_{s,s'}(t,t'))|\Phi\rangle=|\Psi\rangle. \tag{23.22}$$

By deriving the explicit form of matrix elements of $\mathbb{T}_{s,s'}(t,t')$ and solving Eq. (23.22), we can encode the HSK explicitly in terms of a superposition of Cauchy-Lorentz distributions (assuming $s\le s'$) [see Sect. A of [21]]

$$K_{s,s'}(t,t')=n\frac{\kappa_{s,s'}(t-t')}{\tau_s(t)\tau_{s'}(t')}, \tag{23.23}$$
$$\kappa_{s,s'}=\sum_{l=1}^{2s}\frac{l(l+2(s'-s))(2s+1-l)(2s'+1+l)}{(2s+1)(2s'+1)}c_{s'-s+l},$$
$$\text{where}\quad c_s(\tau):=\frac{s}{s^2+\tau^2}.$$

Note that HSK is symmetric $K_{s,s'}(t,t')=K_{s',s}(t',t)$ and strictly positive $K_{s,s'}(t,t')>0$, $\forall s,s',t,t'$.

We would like to remind the reader that in TL $n\to\infty$ the $s=\frac{1}{2}$ family $X_{\frac{1}{2}}(t)$ is equivalent to the family of local charges Q_k, as follows from Eqs. (23.7,23.9)

$$X_{\frac{1}{2}}(t)=\sum_{k=0}^\infty\frac{t^k}{k!}Q_{k+2},\quad Q_{k+2}=\partial_t^kX_{\frac{1}{2}}(t)|_{t=0}. \tag{23.24}$$

Eq. (23.19) thus generates also a handy explicit matrix product representations of the standard local conservation laws Q_k or their densities q_k.

Proof of linear independence.– Let us first show that $X_1(t)$ are linearly independent from $X_{\frac{1}{2}}(t)$, i.e., from Q_k. We define an operator

$$\widetilde{X}_1(t) = X_1(t) - \int_{-\infty}^{\infty} \mathrm{d}t' f_t(t') X_{\frac{1}{2}}(t'), \tag{23.25}$$

where the function $f_t(t')$ is determined by minimizing the HS norm $\|\widetilde{X}_1(t)\|^2_{\mathrm{HS}}$, i.e. by the variation

$$\frac{\delta}{\delta f_t(t')}(\widetilde{X}_1(t), \widetilde{X}_1(t)) = 0, \tag{23.26}$$

resulting in the Fredholm equation of the first kind

$$\int_{-\infty}^{\infty} \mathrm{d}t'' K_{\frac{1}{2},\frac{1}{2}}(t',t'') f_t(t'') = K_{\frac{1}{2},1}(t',t). \tag{23.27}$$

Using the fact that the kernels (23.23) are related to Cauchy-Lorentz distributions $c_s(t)$ up to trivial rescalings, we make an ansatz $f_t(t') = (\tau_{\frac{1}{2}}(t')/\tau_1(t))\varphi(t-t')$ which maps (23.27) to a linear convolution equation $\frac{3}{4}c_1 * \varphi = \frac{4}{3}c_{\frac{3}{2}}$, which, using the well-known convolution identity $c_s * c_{s'} = \pi c_{s+s'}$, results in $\varphi = \frac{16}{9\pi}c_{\frac{1}{2}}$, or

$$f_t(t') = \frac{8}{9\pi} \frac{1+t'^2}{((3/2)^2+t^2)((1/2)^2+(t-t')^2)}. \tag{23.28}$$

The conclusion of this analysis is that a family $\widetilde{X}_1(t)$ is (a) quasilocal (see Sect. D of [21] for a numerical example) as its HSK, computed via Eqs. (23.23,23.25,23.28), is extensive $(\widetilde{X}_1(t), \widetilde{X}_1(t')) = \frac{n}{\tau_1(t)\tau_1(t')}(\frac{8}{9}c_1(t-t') - \frac{4}{27}c_2(t-t'))$ and (b) is orthogonal to (and hence linearly independent from) all known local operators contained in the $s = 1/2$ family $X_{1/2}(t)$, namely we have $(\widetilde{X}_1(t), Q_k) = (\widetilde{X}_1(t), X_{\frac{1}{2}}(t')) = 0$, for all t, t', k. More generally, one can orthogonalize $X_s(t)$ for higher s to all previous $X_{s'}(t')$ for $s' < s$, by making an ansatz $\widetilde{X}_s(t) = X_s(t) - \int_{-\infty}^{\infty} \mathrm{d}t' \left(f^t_{s,s-\frac{1}{2}}(t') X_{s-\frac{1}{2}}(t') + f^t_{s,s-1}(t') X_{s-1}(t') \right)$, with explicit expressions for bounded integrable functions $f^t_{s,s-1}(t'), f^t_{s,s-\frac{1}{2}}(t')$. These families are HS orthogonal for different auxiliary spins, namely $(\widetilde{X}_s(t), \widetilde{X}_{s'}(t')) = 0$ for $s \neq s'$, while $(\widetilde{X}_s(t), \widetilde{X}_s(t)) > 0$, i.e. $\widetilde{X}_s(t) \neq 0$, for all s, t (for details see Sect. C of [21]). This implies that $X_s(t)$ are linearly independent from all previous $X_{s'}(t')$, for $s' < s$, and in particular from $X_{\frac{1}{2}}(t')$ or Q_k. Q.E.D.

Discussion.– We have proposed a direct extension of local conserved operators derived from the logarithm of the fundamental TM [2, 3, 22] to higher spin auxiliary spaces. We have proved that in such a case, the resulting operators are quasilocal. An interesting side-result of our statement is an asymptotic (thermodynamic), $n \to \infty$, inversion formula [23] $T_s^{-1}(\frac{1}{2} + \mathrm{i}t) \simeq [\tau_s(t)]^{-1} T_s(-\frac{1}{2} + \mathrm{i}t)$, valid for any $s \in \frac{1}{2}\mathbb{Z}^+$, which can be proven by implementing our matrix product formula (23.19) together with the gap statements (Sect. B of [21]) to show that $T_s(\mu_t^{\pm}) T_s(\lambda_t^{\pm}) \simeq \tau_s(t)\mathbb{1}$. Our quasilocal operators $X_s(t)$ (23.7) can thus be understood as logarithmic derivatives of $T_s(\lambda_t^+)$. In TL $n \to \infty$ they become Hermitian operators for any $t \in \mathbb{R}$. For $s = \frac{1}{2}$, the Taylor expansion coefficients in t turn out to be local operators, while for $s > \frac{1}{2}$, they remain non-local but quasilocal. One could thus equivalently work with a discrete series of quasilocal operators $Q_{s,k+2} = (1/k!)\partial_t^k X_s(t)|_{t=0}$, $s \in \frac{1}{2}\mathbb{Z}^+, k \in \mathbb{Z}^+$, rather than with a series of continuous families $X_s(t)$. As a double index suggests, the number of relevant quasi-local charges in a large finite system may grow as n^2, rather than n as in the ultralocal case, although this question cannot be made precise with the results at hand.

Our results promise a number of timely applications and generalizations. The new quasilocal families should be included in order to correctly describe $k \to 0, \omega \to 0$ limit of dynamical

structure factors and general Drude weights at finite temperatures [24, 25, 26], or GGE in quantum quench protocols [8]. For computing stationary expectations of local observables after a quench from a non-thermal initial state, such as e.g. the Néel state $|\mathrm{N}\rangle$, one can readily demonstrate extensivity $\langle \mathrm{N}|X_s(t)|\mathrm{N}\rangle \propto n$ by extracting the leading eigenvalue of an associated transfer matrix, essentially proceeding along the lines of calculation done in Ref. [19] for the fundamental ($s = 1/2$) TM. Appropriate $q-$deformations of the concepts developed in this Letter should provide additional quasilocal operator families for the anisotropic Heisenberg model (XXZ chain). Extensions to $SU(N)$ symmetric integrable spin chains seem straightforward, whereas a generalization to continuous quantum integrable systems and field theories (such as Lieb-Liniger or sine-Gordon models) should be a challenge for the future. We close by stressing an important point of distinction with respect to spin-reversal symmetry breaking quasilocal conserved operators in XXZ model [14, 15, 16, 17]. Quasilocality, as abstractly formulated here, requires a finite-dimensional (but non-fundamental) representation of a quantum TM, and a factorizability condition for the leading eigenvalue of the associated auxiliary TM. This can happen, either for irreducible unitary representations of the symmetry group, but will result in operators which are always even under spin reversal, as is the case here; or due to the root-of-unity (commensurability) condition for the anisotropy, where highest-weight type non-unitary representations become reducible to finite dimensional ones, such as in the XXZ model.

E. I. thanks J. de Nardis and J.-S. Caux while T. P. thanks M. Mierzejewski and P. Prelovšek for valuable discussions on related topics. M. M. and T. P. acknowledge support by Slovenian Research Agency (grants P1-0044, J1-5439 and N1-0025).

23.1 A: Explicit computation of the Hilbert-Schmidt kernel

Let us define the following operator over the 4−spin auxiliary space $\mathcal{H}_{\mathrm{a}} = \bigotimes_{k=1}^{4} \mathcal{H}_{\mathrm{a}_k}$:

$$\mathbb{F}_{s,s'}(t,t') := \mathbb{T}_{s,s'}(t,t') - \tau_s(t)\tau_{s'}(t')\mathbb{1} \tag{23.29}$$

where $\mathbb{T}_{s,s'}(t,t')$ has been defined in the main text. For $s = s'$ and $t = t'$, the operator $\mathbb{T}_{s,s}(t,t)$ is the TM for computation of the HS norm, so its maximal eigenvalue has to be positive as the HS norm is always positive. To complete the proof of quasilocality, it amounts to show that $\mathbb{F}_{s,s}(t,t)$ is negative definite on $\mathcal{H}_{\mathrm{a}} \setminus \mathbb{C}|\Psi_0\rangle$ where $|\Psi_0\rangle = |\psi_0\rangle \otimes |\psi_0\rangle$ is the leading eigenvector, which implies that $[\tau_s(t)]^2$ is the maximal and non-degenerate eigenvalue with a finite gap to the sub-leading eigenvalue. This will be shown by explicitly constructing the operator (23.29) in a convenient basis (see section B for completing the proof of the gap), which in turn is needed for explicitly computing the HSK $K_{s,s'}(t,t') = (X_s(t), X_{s'}(t'))$ via Eq. (23.22) of the main text.

Using the expansion

$$\mathbb{F}_{s,s'}(t,t') = \sum_{a,b\in\{0,1,2\}}^{a+b\leq 2} t^a t'^b \, \mathbb{F}_{a,b}, \tag{23.30}$$

and suppressing dependence s, s' in $\mathbb{F}_{a,b}$ for compactness of notation, the non-vanishing matrix-components can be readily represented in terms of $SU(2)$ invariant tensors $\mathbb{F}_{a,b}$ by employing a shorthand notation for elementary $SU(2)$ symmetric operators over $\mathcal{H}_{\mathrm{a}}$: $[\![i,j]\!] := \vec{\mathbf{s}}_{\mathrm{a}_i} \cdot \vec{\mathbf{s}}_{\mathrm{a}_j}$ and

$[\![i,j,k]\!] := \mathrm{i}(\vec{\mathbf{s}}_{\mathrm{a}_i} \times \vec{\mathbf{s}}_{\mathrm{a}_j}) \cdot \vec{\mathbf{s}}_{\mathrm{a}_k}$, namely:

$$\mathbb{F}_{0,0} = -\tfrac{1}{4}s(s+1) - \tfrac{1}{4}s'(s'+1) - s(s+1)s'(s'+1) + [\![1,2]\!][\![3,4]\!] - [\![1,3]\!][\![2,4]\!] + [\![1,4]\!][\![2,3]\!] + \tfrac{1}{2}\left([\![1,2,3]\!] - [\![1,2,4]\!] - [\![1,3,4]\!] + [\![2,3,4]\!]\right) + \tfrac{1}{4}\left([\![1,4]\!] + [\![2,3]\!] - [\![1,2]\!] - [\![1,3]\!] - [\![2,4]\!] - [\![3,4]\!]\right), \tag{23.31}$$

$$\mathbb{F}_{1,0} = \tfrac{\mathrm{i}}{2}\left([\![1,3]\!] + [\![2,3]\!] - [\![1,4]\!] - [\![2,4]\!]\right) + \mathrm{i}\left([\![1,3,4]\!] + [\![2,3,4]\!]\right), \tag{23.32}$$

$$\mathbb{F}_{0,1} = \tfrac{\mathrm{i}}{2}\left([\![2,3]\!] + [\![2,4]\!] - [\![1,3]\!] - [\![1,4]\!]\right) + \mathrm{i}\left([\![1,2,3]\!] + [\![1,2,4]\!]\right), \tag{23.33}$$

$$\mathbb{F}_{1,1} = -[\![1,3]\!] - [\![1,4]\!] - [\![2,3]\!] - [\![2,4]\!], \tag{23.34}$$

$$\mathbb{F}_{0,2} = -s(s+1) - [\![1,2]\!], \tag{23.35}$$

$$\mathbb{F}_{2,0} = -s'(s'+1) - [\![3,4]\!]. \tag{23.36}$$

23.1.1 Reduction to the singlet subspace

By virtue of $SU(2)$ invariance of $\mathbb{T}_{s,s'}(t,t')$ the computation of HSK can be facilitated (assuming $s \leq s'$ throughout this section without loss of generality) in the invariant $2s+1$ dimensional subspace formed by singlet eigenstates, $\mathcal{H}_{\mathrm{a}} \supset \mathcal{V}_0 = \mathrm{lsp}\{|j\rangle; j = 0, 1, \ldots, 2s\}$, which can be expanded explicitly in terms of computational basis $|m_1 m_2 m_1' m_2'\rangle = |m_1\rangle_{\mathrm{a}_1}|m_2\rangle_{\mathrm{a}_2}|m_1'\rangle_{\mathrm{a}_3}|m_2'\rangle_{\mathrm{a}_4}$ with help of Wigner $3j$-symbols

$$|j\rangle = \sum_{M=-j}^{j} (-1)^{j-M}\sqrt{2j+1} \sum_{m_1,m_2=-s}^{s} \begin{pmatrix} s & s & j \\ m_1 & m_2 & -M \end{pmatrix} \sum_{m_1',m_2'=-s'}^{s'} \begin{pmatrix} s' & s' & j \\ m_1' & m_2' & M \end{pmatrix} |m_1 m_2 m_1' m_2'\rangle, \tag{23.37}$$

where only the extremal singlet state factorizes $|0\rangle \equiv |\Psi_0\rangle = |\psi_0\rangle_{\mathrm{a}_1\mathrm{a}_2}|\psi_0\rangle_{\mathrm{a}_3\mathrm{a}_4}$. Let us denote the restriction to the singlet subspace as $\mathbb{F}^{(0)}_{s,s'}(t,t') := \mathbb{F}_{s,s'}(t,t')|_{\mathcal{V}_0}$.

The proof is based on showing the following elementary statements: (i) $\mathbb{F}^{(0)}_{s,s'}(t,t')$ is a quadratic form in the difference variable $\tau := t - t'$, with identically vanishing linear terms $\mathbb{F}^{(0)}_{1,0} = \mathbb{F}^{(0)}_{0,1} \equiv 0$, i.e.

$$\mathbb{F}^{(0)}_{s,s'}(t,t') \equiv \mathbb{F}^{(0)}_{s,s'}(\tau) = \mathbb{D}\,\tau^2 + \mathbb{F}^{(0)}_{0,0}, \tag{23.38}$$

where $\mathbb{D} = \mathbb{F}^{(0)}_{0,2} = \mathbb{F}^{(0)}_{2,0} = -\frac{1}{2}\mathbb{F}^{(0)}_{1,1}$,

(ii) $\mathbb{F}^{(0)}_{s,s}(t,t')$ is a real symmetric tridiagonal matrix in orthonormal singlet basis $\{|j\rangle\}$.

Both statements follow from demonstrating, by employing certain elementary symmetry-based reductions, that all matrices $\mathbb{F}^{(0)}_{a,b}$ are expressible solely in terms of knowing only five types of matrix elements, namely

$$\langle j|[\![1,3]\!]|j\rangle, \tag{23.39}$$

$$\langle j|[\![1,3]\!]|j+1\rangle, \tag{23.40}$$

$$\langle j|[\![1,3]\!][\![2,4]\!]|j+1\rangle, \tag{23.41}$$

$$\langle j|[\![1,2,3]\!]|j+1\rangle, \quad \langle j|[\![2,3,4]\!]|j+1\rangle, \tag{23.42}$$

for all $|j\rangle \in \mathcal{V}_0$. The reductions of above expressions can be carried out after noticing simple transformation properties of $|j\rangle$ with respect to permutation operators P_{12} and P_{34} ($P_{ij} \in \mathrm{End}(\mathcal{H}_{\mathrm{a}})$ swaps $\mathcal{H}_{\mathrm{a}_i}$ and $\mathcal{H}_{\mathrm{a}_j}$)

$$P_{12}|j\rangle = (-1)^{j+2s}|j\rangle, \quad P_{34}|j\rangle = (-1)^{j+2s'}|j\rangle. \tag{23.43}$$

We find straightforward implications

$$\langle j|[\![1,4]\!]|j'\rangle = \langle j|[\![2,3]\!]|j'\rangle, \tag{23.44}$$

$$\langle j|[\![1,3]\!]|j'\rangle = \langle j|[\![2,4]\!]|j'\rangle \tag{23.45}$$

$$\langle j|[\![1,2,3]\!]|j'\rangle = -\langle j|[\![1,2,4]\!]|j'\rangle, \tag{23.46}$$

$$\langle j|[\![1,3,4]\!]|j'\rangle = -\langle j|[\![2,3,4]\!]|j'\rangle. \tag{23.47}$$

for any j, j', where, in addition, a sign reversal under odd permutation of factors has been used for the triple-product terms. Notably, these identification are enough to establish vanishing of linear terms, $\mathbb{F}^{(0)}_{1,0} = \mathbb{F}^{(0)}_{0,1} \equiv 0$. Furthermore, with an aid of Casimir invariants

$$[\![1,2]\!]|j\rangle = \left(-s(s+1) + \tfrac{1}{2}j(j+1)\right)|j\rangle, \tag{23.48}$$

$$[\![3,4]\!]|j\rangle = \left(-s'(s'+1) + \tfrac{1}{2}j(j+1)\right)|j\rangle, \tag{23.49}$$

we have $\langle j|\mathbb{F}^{(0)}_{0,2}|j\rangle = \langle j|\mathbb{F}^{(0)}_{2,0}|j\rangle = -\frac{1}{2}j(j+1)$. With assistance of symbolic algebra in Mathematica, using explicit form of singlet eigenstates (23.37) for general s, s' and j, we have been able to obtain $\langle j|\mathbb{F}^{(0)}_{1,1}|j\rangle = j(j+1)$, whereas vanishing of the upper-diagonal follows from Eqs. (23.44)-(23.47). The τ^2-dependence (i) is at the end given by elements $\langle j|\mathbb{F}^{(0)}_{0,2}|j\rangle = 2\langle j|[\![1,3]\!]|j\rangle = -\frac{1}{2}j(j+1)$.

Turning attention to the remaining (constant) term $\mathbb{F}^{(0)}_{0,0}$ we first note that all triple-product terms vanish on $\mathcal{V}_0$ after resorting to explicit evaluation of matrix elements from Eq. (23.42)

$$\langle j|[\![1,2,3]\!]|j{+}1\rangle = -\langle j|[\![2,3,4]\!]|j{+}1\rangle = \frac{(j+1)^2}{4}\sqrt{\frac{(2s-j)(2s'-j)(2(s+1)+j)(2(s'+1)+j)}{(2j+1)(2j+3)}}. \tag{23.50}$$

in conjunction with Eqs. (23.46,23.47). Notably, diagonal matrix elements of all triple-product terms vanish in accordance with their skew-symmetric nature. Furthermore, after repeating symmetry arguments based on Eq. (23.43) we arrive at the following explicit expressions: (a) for the diagonal matrix elements $a_j = \langle j|\mathbb{F}^{(0)}_{0,0}|j\rangle$

$$a_j = -\tfrac{1}{4}j(j+1) - s(s+1)s'(s'+1) + \left(\tfrac{1}{2}j(j+1) - s(s+1)\right)\left(\tfrac{1}{2}j(j+1) - s'(s'+1)\right), \tag{23.51}$$

and (b) for the first off-diagonal elements $b_j = \langle j|\mathbb{F}^{(0)}_{0,0}|j+1\rangle = \langle j+1|\mathbb{F}^{(0)}_{0,0}|j\rangle$

$$b_j = -\langle j|[\![1,3]\!]{+}2[\![1,3]\!][\![2,4]\!]|j{+}1\rangle = -\frac{j(j+1)(j+2)}{4}\sqrt{\frac{(2s-j)(2s'-j)(2(s+1)+j)(2(s'+1)+j)}{(2j+1)(2j+3)}} \tag{23.52}$$

We still owe the reader a brief remark in order to close (ii): by inspecting the structure of singlet eigenstates we can easily see that $SU(2)$ invariant appearing in the expansion of $\mathbb{T}_{s,s'}(t,t')$ can raise/lower any magnetic quantum numbers at most by two, thus $\mathbb{F}^{(0)}_{s,s'}(t,t')$ is a banded matrix which cannot have non-vanishing matrix elements beyond the second upper/lower diagonals. At last, due to symmetry cancellations of the second upper diagonal between $[\![1,3]\!][\![2,4]\!]$ and $[\![1,4]\!][\![2,3]\!]$ projected onto singlets $|j\rangle$, we finally remain with a strictly tridiagonal form. Finally, $\mathbb{F}^{0}_{s,s'}(t,t')$ is a symmetric matrix on $\mathcal{V}_0$, i.e. $\langle j|\mathbb{F}^{0}_{s,s'}(t,t')|j'\rangle = \langle j'|\mathbb{F}^{0}_{s,s'}(t,t')|j\rangle$, as consequence of mutual cancellation of skew-symmetric triple-product terms $[\![i,j,k]\!]$.

It is useful to note that the matrix of the linear system given by Eq. (23.22) in fact coincides with $\mathbb{F}^{(0)}_{s,s'}(\tau)$,

$$(\mathbb{1} - \widetilde{\mathbb{T}}_{s,s'}(t,t')) = -[\tau_s(t)\tau_{s'}(t')]^{-1}\mathbb{F}^{(0)}_{s,s'}(\tau). \tag{23.53}$$

Furthermore, note that the state $|0\rangle$ does not couple to the rest of $2s$-dimensional singlet space $\mathcal{V}_0' = \mathrm{lsp}\{|j\rangle, j = 1,\ldots,2s\}$, since $a_0 = b_0 = 0$. Thus, by solving the $2s$-dimensional tridiagonal linear system

$$\mathbb{F}^{(0)}_{s,s'}(\tau)|\Xi\rangle = |1\rangle, \tag{23.54}$$

we can readily obtain few explicit results for HSKs,

$$K_{s,s'}(t,t') = n[\tau_s(t)\tau_{s'}(t')]^{-1}\kappa_{s,s'}(t-t'), \quad \text{with} \quad \kappa_{s,s'}(\tau) = -\frac{4}{3}s(s+1)s'(s'+1)\langle 1|\Xi\rangle, \tag{23.55}$$

where the prefactor in front of $\kappa_{s,s'}(\tau)$ comes from expressing the state $|\Psi\rangle$ (see main text), expressed as $|\Psi\rangle = (2/\sqrt{3})\sqrt{s(s+1)s'(s'+1)}|1\rangle$. More explicitly, and using a suitable gauge transformation (redefinition of bra-ket basis in $\mathcal{V}_0'$ in order to remove the square-roots from off-diagonal matrix elements) and homogenizing the system (23.54), one can encode the HSK as

$$\kappa_{s,s'}(\tau) = -8s(s+1)s'(s'+1)\frac{\chi_1}{\chi_0}, \tag{23.56}$$

where χ_j satisfies a 3-point recurrence relation

$$(j+1)(2s+1+j)(2s'+1+j)\chi_{j-1}+j(2s-j)(2s'-j)\chi_{j+1}+(2j+1)(z-j(j+1))\chi_j = 0, \tag{23.57}$$

where $z \equiv 2(\tau^2+(s+\frac{1}{2})^2+(s'+\frac{1}{2})^2)$, which can be solved with a direct backward iteration by choosing the initial conditions $\chi_{2s+1}=0$, $\chi_{2s}=1$.

The solution, which is easily obtained explicitly for essentially arbitrary large s, s', can be neatly written in terms of a superposition of Cauchy distributions

$$c_s(t) = \frac{s}{s^2+t^2}, \tag{23.58}$$

and for few smallest auxiliary spins reads

$$\begin{aligned}
&\kappa_{\frac{1}{2},s} = \frac{2s(s+1)}{2s+1}c_{s+\frac{1}{2}},\\
&\kappa_{1,1} = \frac{8}{9}c_1+\frac{20}{9}c_2, \quad \kappa_{1,\frac{3}{2}} = \frac{5}{3}c_{\frac{3}{2}}+3c_{\frac{5}{2}}, \quad \kappa_{1,2} = \frac{12}{5}c_2+\frac{56}{15}c_3, \quad \kappa_{1,\frac{5}{2}} = \frac{28}{9}c_{\frac{5}{2}}+\frac{20}{9}c_{\frac{7}{2}}, \quad \kappa_{1,3} = \frac{80}{21}c_3+\frac{36}{7}c\\
&\kappa_{\frac{3}{2},\frac{3}{2}} = \frac{15}{16}c_1+3c_2+\frac{63}{16}c_3, \quad \kappa_{\frac{3}{2},2} = \frac{9}{5}c_{\frac{3}{2}}+\frac{21}{5}c_{\frac{5}{2}}+\frac{24}{5}c_{\frac{7}{2}}, \quad \kappa_{\frac{3}{2},\frac{5}{2}} = \frac{21}{8}c_2+\frac{16}{3}c_3+\frac{45}{8}c_4,\\
&\kappa_{2,2} = \frac{24}{25}c_1+\frac{84}{25}c_2+\frac{144}{25}c_3+\frac{144}{25}c_4, \quad \kappa_{2,\frac{5}{2}} = \frac{28}{15}c_{\frac{3}{2}}+\frac{24}{5}c_{\frac{5}{2}}+\frac{36}{5}c_{\frac{7}{2}}+\frac{20}{3}c_{\frac{9}{2}}. \qquad (23.5
\end{aligned}$$

Moreover, a simple form for the superposition coefficients for all small s, s' lead us to conjecture that they can be written as low-order rational expressions. Indeed we found a remarkably simple closed form expression

$$\kappa_{s,s'}(\tau) = \sum_{l=1}^{2s} \frac{l(l+2(s'-s))(2s+1-l)(2s'+1+l)}{(2s+1)(2s'+1)}c_{s'-s+l}(\tau), \tag{23.60}$$

which reproduces the solution of Eqs. (23.56,23.57) for any finite s, s', while we leave its rigorous derivation for the future.

For a curiosity, we may write another closed form expression of HSKs for general s, s' and τ, written in terms of a complex continuation of harmonic numbers known as the digamma function $\psi(z)$,

$$\psi(z) = \frac{\mathrm{d}}{\mathrm{d}z}\log\Gamma(z) = \sum_{k=1}^{\infty}\left(\frac{1}{k}-\frac{1}{k+z-1}\right)-\gamma_{\mathrm{EM}}, \tag{23.61}$$

where γ_{EM} is the Euler–Mascheroni constant, as

$$\kappa_{s,s'}(\tau) = \frac{s(s'(s'+1)+(s+1)^2+\tau^2)}{2s+1} - \frac{((s'-s)^2+\tau^2)((s+s'+1)^2+\tau^2)}{2(2s+1)(2s'+1)}\left(\psi^+_{s,s'}+\psi^-_{s,s'}\right), \tag{23.62}$$

making use of a compact notation $\psi^{\pm}_{s,s'} := \psi(s+s'+1\pm\mathrm{i}\tau)-\psi(s'-s+1\pm\mathrm{i}\tau)$. Remarkably, the second term gives rise to Cauchy distributions in (23.60) via recurrence formula

$$\psi(z+N)-\psi(z) = \sum_{k=0}^{N-1}\frac{1}{z+k}, \quad N\in\mathbb{N}, \tag{23.63}$$

yielding

$$\psi^{+}_{s,s'} + \psi^{-}_{s,s'} = \sum_{k=0}^{2s-1} \left(\frac{1}{k + (s' - s + 1 + \mathrm{i}\tau)} + \frac{1}{k + (s' - s + 1 - \mathrm{i}\tau)} \right) = 2 \sum_{k=1}^{2s} c_{s'-s+k}(\tau). \quad (23.64)$$

23.2 B: Finiteness of the gap for the auxiliary transfer matrix

Extensive $\sim n$ scaling of a general HSK can be attributed to the finite spectral gap with respect to the leading-modulus eigenvalue of $\mathbb{F}_{s,s'}(t,t')$ on the entire $\mathcal{H}_{\rm a}$. Thanks to Cauchy–Schwartz inequality

$$K_{s,s'}(t,t') \leq \sqrt{K_{s,s}(t,t) K_{s',s'}(t',t')}, \quad (23.65)$$

it is sufficient to focus on $s' = s$ and $t' = t$ case only (pertaining to HS norm of $X_s(t)$), where we expand

$$\mathbb{F}_{s,s}(t,t) = \mathbb{A} t^2 + \mathbb{B} t + \mathbb{C}, \quad (23.66)$$

with matrix-valued coefficients reading

$$\mathbb{A} = -2s(s+1) - (\llbracket 1,2 \rrbracket + \llbracket 1,3 \rrbracket + \llbracket 1,4 \rrbracket + \llbracket 2,3 \rrbracket + \llbracket 2,3 \rrbracket + \llbracket 3,4 \rrbracket) \equiv -\tfrac{1}{2} \mathbf{C}_s^{[4]}. \quad (23.67)$$

$$\mathbb{B} = -\mathrm{i}(\llbracket 1,4 \rrbracket - \llbracket 2,3 \rrbracket - \llbracket 1,2,3 \rrbracket - \llbracket 1,2,4 \rrbracket - \llbracket 1,3,4 \rrbracket - \llbracket 2,3,4 \rrbracket), \quad (23.68)$$

$$\mathbb{C} = -\tfrac{1}{2} s(s+1) - s^2(s+1)^2 + \llbracket 1,2 \rrbracket \llbracket 3,4 \rrbracket - \llbracket 1,3 \rrbracket \llbracket 2,4 \rrbracket + \llbracket 1,4 \rrbracket \llbracket 2,3 \rrbracket$$
$$+ \tfrac{1}{4}(\llbracket 1,4 \rrbracket + \llbracket 2,3 \rrbracket - \llbracket 1,2 \rrbracket - \llbracket 1,3 \rrbracket - \llbracket 2,4 \rrbracket - \llbracket 3,4 \rrbracket) + \tfrac{1}{2}(\llbracket 1,2,3 \rrbracket - \llbracket 1,2,4 \rrbracket - \llbracket 1,3,4 \rrbracket + \llbracket 2,3,4 \rrbracket) \quad (23.69)$$

These are just specialization of expressions given by Eqs.(23.29–23.36). The operator $\mathbf{C}_s^{[4]} := (\vec{\mathbf{S}}_{a_1} + \vec{\mathbf{S}}_{a_2} + \vec{\mathbf{S}}_{a_3} + \vec{\mathbf{S}}_{a_4})^2$ denotes the four-fold s-spin Casimir invariant with eigenvalues $s(s+1)$. Note that the auxiliary operator denoted by $\mathbb{C}$, such as in Eqs. (23.66,23.69), should not be confused with a set of complex numbers.

Denoting temporarily $\mathbb{T}_{s,s}(t,t) \to \mathbb{T}(t)$ we note a remarkable commutativity property,

$$[\mathbb{T}(t), \mathbb{T}(t')] = 0, \quad \forall t, t', \quad (23.70)$$

which is a direct consequence of Yang-Baxter equation. Specifically, considering a periodic chain of four spins s the auxiliary TM $\mathbb{T}(t)$ becomes the standard commuting quantum TM for the physical spin 1/2 now playing the role of auxiliary spin. This implies commutativity of all operator valued coefficients,

$$[\mathbb{A}, \mathbb{B}] = [\mathbb{A}, \mathbb{C}] = [\mathbb{B}, \mathbb{C}] = 0. \quad (23.71)$$

In order to prove strict negativity of $\mathbb{F}_{s,s}(t,t)$ on $\mathcal{H}_{\rm a} \backslash \mathbb{C}|\Psi_0\rangle$ it is enough to show that a quadratic (in t) equation $\langle \Phi | \mathbb{F}_{s,s}(t,t) | \Phi \rangle = 0$ does not have a solution, for any $|\Phi\rangle$ other than $|\Psi_0\rangle$. Due to (23.71) this amounts to demonstrate that a matrix-valued discriminant

$$\Delta := \mathbb{B}^2 - 4\mathbb{A}\mathbb{C}, \quad (23.72)$$

has only *non-positive* eigenvalues, while for any eigenvector $|\Phi_0\rangle$ of Δ corresponding to zero eigenvalue, it must hold that $\langle \Phi_0 | \mathbb{F}_{s,s}(t,t) | \Phi_0 \rangle < 0$.

Indeed, the entire singlet subspace $\mathcal{V}_0$ has the latter property, since we have $\Delta|_{\mathcal{V}_0} \equiv 0$ due to $\mathbb{A}|_{\mathcal{V}_0} = \mathbb{B}|_{\mathcal{V}_0} \equiv 0$. The negativity of $\mathbb{F}^{(0)}_{s,s}(\tau = 0) \equiv \mathbb{F}^{(0)}_{0,0}$ on $\mathcal{V}_0'$ follows from diagonal dominance of the tridiagonal matrix

$$-a_j > |b_j| + |b_{j-1}|, \quad j \geq 1, \quad (23.73)$$

based on explicit form of matrix elements (23.51,23.52).

Clearly, for large enough t (Casimir) coefficient $\mathbb{A}$ starts to dominate and therefore (non-singlet) eigenstates belonging to any higher spin multiplet necessarily become sub-leading and

the spectral gap $\gamma > 0$ is always due to the largest (smallest in modulus) (singlet) eigenvalue of $\mathbb{F}^{(0)}_{0,0}$. For a generic $t \in \mathbb{R}$ on the other hand it might happen that the gap γ is determined by eigenvectors outside of $\mathcal{V}_0$. At the moment we have only been able to rigorously confirm our statement for $s \in \{\frac{1}{2}, 1, \frac{3}{2}\}$ by analytically diagonalizing the operator Δ projected onto highest-weight total spin $S > 0$ subspaces of $\mathcal{H}_{\rm a}$ ($SU(2)$ descendants only contribute to degeneracies), or some larger s, by extensive numerical checks.

23.3 C: Fredholm-Gram-Schmidt orthogonalization for higher auxiliary spins

Using the appealing explicit form of HSK (23.23), derived in Sect. A, we here outline a general scheme of orthogonalization of $X_s(t)$ to $X_{s'}(t')$ for all $s' < s$, $t' \in \mathbb{R}$. We denote such orthogonalized quasilocal conserved operators as $\widetilde{X}_s(t)$. Picking a set of suitable functions $f^t_{s,s'}(t')$, for $s' \in \frac{1}{2}\mathbb{Z}^+ < s$, we seek for an operator

$$\widetilde{X}_s(t) = X_s(t) - \sum_{s'}^{s'<s} \int_{-\infty}^{\infty} \mathrm{d}t' f^t_{s,s'}(t') X_{s'}(t'), \tag{23.74}$$

which minimizes the HS norm $\|\widetilde{X}_s(t)\|^2_{\rm HS}$, i.e.,

$$\frac{\delta}{\delta f^t_{s,s'}(t')}(\widetilde{X}_s(t), \widetilde{X}_s(t)) = 0, \quad s' < s. \tag{23.75}$$

This yields a coupled linear system of $(2s-1) \times (2s-1)$ Fredholm equations of the first kind

$$\sum_{s''}^{s''<s} \int_{-\infty}^{\infty} \mathrm{d}t'' K_{s',s''}(t',t'') f^t_{s,s''}(t'') = K_{s',s}(t',t),$$
$$\forall t',\ s' < s. \tag{23.76}$$

If the unknown functions $f^t_{s,s'}(t')$ are sought for in terms of the following difference ansatz

$$\varphi_{s'',s}(t''-t) := \frac{\tau_s(t)}{\tau_{s''}(t'')} f^t_{s,s''}(t''), \tag{23.77}$$

then, noting that the HSK (23,23.55) also obeys a scaled difference form

$$\kappa_{s',s''}(t'-t'') = n^{-1}\tau_{s'}(t')\tau_{s''}(t'')K_{s',s''}(t',t''), \tag{23.78}$$

the Fredholm system (23.76) becomes equivalent to a linear convolution system

$$\sum_{s''}^{s''<s} \kappa_{s',s''} * \varphi_{s'',s} = \kappa_{s',s}, \quad s' < s, \tag{23.79}$$

where $(\varphi * \varphi')(t) := \int_{-\infty}^{\infty} \mathrm{d}t' \varphi(t')\varphi'(t-t')$.

For $s = 1$, this yields a single condition

$$\frac{3}{4} c_1 * \varphi_{\frac{1}{2},1} = \frac{4}{3} c_{\frac{3}{2}}, \tag{23.80}$$

with a unique solution, equivalent to (23.28),

$$\varphi_{\frac{1}{2},1} = \frac{16}{9\pi} c_{\frac{1}{2}}, \tag{23.81}$$

which follows directly from an elementary addition identity for the Cauchy distributions

$$c_s * c_{s'} = \pi c_{s+s'}. \tag{23.82}$$

For $s > 1$ the system (23.76) becomes nontrivial. Then, it turns advantageous to construct a linear isomorphism $\Lambda : \varphi \to g$ between the convolution ring of integrable functions (or distributions) $\varphi(t)$ with operations $(+, *)$ spanned by $\{c_s, s \in \frac{1}{2}\mathbb{Z}^+\}$, and the ring of functions $g(z)$ of a formal variable z with operations $(+, \cdot)$, where $\cdot$ is the usual pointwise multiplicaiton, analytic on the unit disc around the origin $z = 0$. The map Λ and its inverse Λ^{-1} are defined uniquely by:

$$\begin{aligned} &\Lambda(c_s) = \pi z^{2s}, \qquad \Lambda(\varphi * \varphi') = \Lambda(\varphi)\Lambda(\varphi'), \\ &\Lambda^{-1}(z^k) = \frac{1}{\pi} c_{\frac{k}{2}}, \quad \Lambda^{-1}(gg') = \Lambda^{-1}(g) * \Lambda^{-1}(g'), \end{aligned} \tag{23.83}$$

and the linearity. Note that a constant function in the image of Λ corresponds to a Dirac distribution $c_0(t) = \frac{1}{\pi}\delta(t)$, which, however, never appears in our calculation.

Using the following notation for the unknown functions $g_{s',s} := \Lambda(\varphi_{s',s})$, the Fredholm system (23.76) is Λ-mapped to $(2s-1) \times (2s-1)$ system of linear equations with coefficients that are polynomials in variable z

$$\sum_{s''}^{s''<s} G_{s',s''}(z) g_{s',s}(z) = G_{s',s}(z), \tag{23.84}$$

where (now assuming $s \le s'$ without loss of generality)

$$\begin{aligned} &G_{s,s'}(z) := \Lambda(\kappa_{s,s'})(z) = G_{s',s}(z) = \\ &\pi \sum_{l=1}^{2s} \frac{l(l+2(s'-s))(2s+1-l)(2s'+1+l)}{(2s+1)(2s'+1)} z^{2(s'-s+l)}. \end{aligned} \tag{23.85}$$

Elementary algebra yields a solution which is nonvanishing only for the last two components $s' = s-1$ and $s' = s - \frac{1}{2}$ (note that here $s > 1$):

$$g_{s',s}(z) = 0, \quad \text{for } s' < s-1, \tag{23.86}$$

$$\begin{aligned} g_{s-1,s}(z) &= \frac{1}{(s-1)^2}\left[\left(1-\frac{z^2}{\zeta_s}\right)^{-1} - 1\right] - \frac{s(2s-1)}{s(2s-1)-1} z^2, \\ g_{s-\frac{1}{2},s}(z) &= \frac{2(2s)^2}{(2s-1)(2s+1)} z \left[1 - \frac{1}{s(2s+1)}\left(1-\frac{z^2}{\zeta_s}\right)^{-1}\right] \end{aligned}$$

$$\text{where} \qquad \zeta_s = \frac{s(2s+1)}{(s-1)(2s-1)}. \tag{23.87}$$

Note that the convergence radius $\sqrt{\zeta_s}$ is always larger than 1, guaranteeing analyticity inside the unit disc. Expanding the geometric series and transforming back with Λ^{-1} (23.83), we

obtain explicit results for the two nonvanishing functions

$$f^t_{s,s-1}(t') = \frac{\tau_{s-1}(t')}{\pi\tau_s(t)}\left(-\frac{s(2s-1)}{s(2s-1)-1}c_1(t'-t) + \frac{1}{(s-1)^2}\sum_{l=1}^{\infty}\zeta_s^{-l}c_l(t'-t)\right),$$
$$f^t_{s,s-\frac{1}{2}}(t') = \frac{2(2s)^2\tau_{s-\frac{1}{2}}(t')}{\pi(2s-1)(2s+1)\tau_s(t)}\left(c_{\frac{1}{2}}(t'-t) - \frac{1}{s(2s+1)}\sum_{l=0}^{\infty}\zeta_s^{-l}c_{l+\frac{1}{2}}(t'-t)\right), \tag{23.88}$$

which complete the explicit construction of $\widetilde{X}_s(t)$ (23.74). We note that the exponentially convergent sums above, Eqs. (23.88), allow closed form expressions in terms of the Hypergeometric function ${}_2F_1$, or the incomplete Beta function, of argument $1/\zeta_s$ and with complex parameters.

It may be of interest also to consider HS-norms and HS-kernels defined with respect to orthogonalized quasilocal operators

$$\widetilde{K}_s(t,t') = (\widetilde{X}_s(t), \widetilde{X}_s(t')) = n\frac{\widetilde{\kappa}_s(t-t')}{\tau_s(t)\tau_{s'}(t')}. \tag{23.89}$$

For example, showing that $\widetilde{K}_s(t,t) = \|\widetilde{X}_s(t)\|^2_{\rm HS} > 0$ is a final step of the proof that the $X_s(t)$ are linearly independent for different s. In the opposite case, specifically if, for some s, $X_s(t)$ would be expressible as a linear combination of $X_{s'}(t')$, for $s' < s$, then one would have $\widetilde{X}_s(t) = 0$, and hence $\widetilde{K}_s(t,t) = 0$.

Clearly, designating $\widetilde{G}_s = \Lambda(\widetilde{\kappa}_s)$, we find

$$\begin{aligned}\widetilde{G}_s(z) &= G_{s,s}(z) - \sum_{s',s''}^{s',s''<s} g_{s',s}(z)G_{s',s''}(z)g_{s'',s}(z)\\ &= G_{s,s}(z) - \sum_{s'}^{s'<s} g_{s',s}(z)G_{s',s}(z)\\ &= \frac{(2s)^2\pi}{(s-1)^2(2s-1)(2s+1)}\\ &\quad\times\left[\frac{s(s-1)(2s-1)}{2s+1}z^2 + 1 - \left(1-\frac{z^2}{\zeta_s}\right)^{-1}\right],\end{aligned} \tag{23.90}$$

and transforming back

$$\begin{aligned}\widetilde{\kappa}_s(\tau) &= \frac{(2s)^2}{(s-1)^2(2s-1)(2s+1)}\\ &\times\left[\frac{s(s-1)(2s-1)}{2s+1}c_1(\tau) - \sum_{l=1}^{\infty}\zeta_s^{-l}c_l(\tau)\right].\end{aligned} \tag{23.91}$$

Specifically, noting that $c_{s'}(0) = 1/s'$:

$$\widetilde{\kappa}(0) = \frac{(2s)^2}{\pi(s-1)^2(2s-1)(2s+1)}\left[\frac{s(s-1)(2s-1)}{2s+1} + \log\frac{4s^3-2s+1}{s(2s-1)(2s+1)}\right], \tag{23.92}$$

which satisfies $\widetilde{\kappa}(0) > 0$ for any $s > 1$, and hence $\|\widetilde{X}_s(t)\|_{\rm HS}^2 = \widetilde{K}_s(t,t) = n\,\widetilde{\kappa}(0)/[\tau_s(t)]^2 > 0$. Note that the case $s = 1$ has been treated separately before.

23.4 D: Numerical example

Here we write out, explicitly, the leading terms of the simplest new quasilocal conserved operator that is orthogonal to all the local ones, namely $\widetilde{X}_{s=1}(t=0)$. Matrix product formula (23.19) inserted to Eq. (23.25) with (23.28) yields all the local terms in the infinite size limit $n \to \infty$, say up to support size $\ell \leq 4$

$$\begin{aligned}\widetilde{X}_1(0) = -\frac{7\cdot 2^5}{3^7}\sum_{x=0}^{n-1}\Big(&\vec{\sigma}_x\cdot\vec{\sigma}_{x+2} + \frac{155}{252}\vec{\sigma}_x\cdot\vec{\sigma}_{x+3}\\ &+\frac{16}{63}(\vec{\sigma}_x\cdot\vec{\sigma}_{x+1})(\vec{\sigma}_{x+2}\cdot\vec{\sigma}_{x+3}) - \frac{53}{84}(\vec{\sigma}_x\cdot\vec{\sigma}_{x+2})(\vec{\sigma}_{x+1}\cdot\vec{\sigma}_{x+3})\\ &-\frac{11}{84}(\vec{\sigma}_x\cdot\vec{\sigma}_{x+3})(\vec{\sigma}_{x+1}\cdot\vec{\sigma}_{x+2})\Big) + \text{h.o.t.}\end{aligned} \tag{23.93}$$

We note that this qualitatively agrees with the optimal quasilocal conserved operator Q' which has been constructed approximately by a systematic numerical procedure in Ref. [1]. Small quantitative deviations in the coefficients (note that [1] used spin-1/2 operators rather than Pauli matrices which attributes a relative factor of 4 in quartic/quadratic terms) can be explained by the fact that the operator (23.93), being just one member of the $s = 1$ family $\widetilde{X}_1(t)$, is not optimized with respect to a relative weight within a finite support ℓ, $\lambda_\ell(X) = \lim_{n\to\infty}\sum_{k=1}^{\ell}\sum_{\underline{\alpha}}|(\sigma^{\underline{\alpha}}_{1:k}, X)|^2/(X,X)$. On the other hand, the operator Q' of [1] is determined precisely by maximizing $\lambda_\ell(X)$ within a given set of conserved X. For $\widetilde{X}_1(0)$ we obtain $\lambda_\ell = 0.508, 0.682, 0.797$, for $\ell = 4, 5, 6$, respectively, while for the optimal numerical Q' one has [1] $\lambda_\ell = 0.605, 0.759, 0.840$. Moreover, numerical inspection of relative weights $\mu_\ell(X) = \lambda_\ell(X) - \lambda_{\ell-1}(X)$ of a sequence of higher quasilocal operators, $\widetilde{X}_s(0)$, $s = 1, \frac{3}{2}, 2$, indicates that for larger s the relative weights $\mu_\ell(\widetilde{X}_s(0))$ have clear maxima at larger supports $\ell \sim \ell^*(s)$, while after that they decay exponentially $\mu_\ell \sim e^{-\gamma\ell}, \ell > \ell^*(s)$.

[1] M. Mierzejewski, P. Prelovšek, and T. Prosen, Phys. Rev. Lett. **114**, 140601 (2015).

Part XII
Articles about Potential Applications

24 Collective Excitations and Nonequilibrium Phase Transition in Dissipative Fermionic Superfluids by Yamamoto, Nakagawa, et al

Abstract

We predict a new mechanism to induce collective excitations and a nonequilibrium phase transition of fermionic superfluids via a sudden switch-on of two-body loss, for which we extend the BCS theory to fully incorporate a change in particle number. We find that a sudden switch-on of dissipation induces an amplitude oscillation of the superfluid order parameter accompanied by a chirped phase rotation as a consequence of particle loss. We demonstrate that when dissipation is introduced to one of the two superfluids coupled via a Josephson junction, it gives rise to a nonequilibrium dynamical phase transition characterized by the vanishing dc Josephson current. The dissipation-induced collective modes and nonequilibrium phase transition can be realized with ultracold fermionic atoms subject to inelastic collisions.

24.1 Theory

24.1.1 Introduction

Collective excitations of superconductors and superfluids have been widely studied in condensed matter physics [1, 2, 3, 4, 5, 6, 7, 8, 9, 10, 11, 12, 13, 14, 15, 16, 17, 18, 19, 20]. Recent experimental progress in ultracold atoms has enabled studies of out-of-equilibrium dynamics of superfluids [21, 22, 23, 24]. For example, a periodic modulation of the amplitude of the order parameter excites the Higgs amplitude mode, which has been observed with ultracold fermions [23] and in solid-state systems by light illumination on BCS superconductors [25, 26, 27, 28, 29, 30, 31, 32, 33]. As for collective phase modes, the Nambu-Goldstone mode exists in neutral superfluids, and the relative-phase Leggett mode has been predicted for multiband superfluids [2, 34, 35, 36, 33, 37, 38]. In particular, ultracold atoms allow for a dynamical control of various system parameters, offering an ideal playground to investigate collective modes. However, they suffer from atom loss due to inelastic scattering, which has received little attention in literature.

In dissipative open quantum systems, the dynamics, after environmental degrees of freedom are traced out, is nonunitary and described by a completely positive and trace-preserving map [39, 40]. Such nonunitary dynamics is relevant for atomic, molecular, and optical systems, drastically changing various aspects of physics such as quantum critical phenomena [41, 42], quantum phase transitions [43, 44, 45], quantum transport [46, 47] and superfluidity [48, 49]. In particular, high controllability of parameters in ultracold atoms has enabled investigations of non-equilibrium quantum dynamics induced by dissipation [50, 51, 52, 53, 54, 55, 56, 57, 58, 59, 60, 61, 49, 62, 63], and studies of fermionic superfluidity in ultracold atoms undergoing inelastic collisions has achieved remarkable progress [48, 64, 65, 66, 67, 68, 69, 70, 71, 49]. The effect of particle loss in fermionic superfluids has been studied in the framework of the non-Hermitian BCS theory [49]; however, it ignores a significant change in particle number due to quantum jumps. It is crucially important to go beyond the non-Hermitian framework to describe the long-time dynamics of a superfluid and associated collective modes of order parameters.

In this Letter, we theoretically investigate collective excitations and a nonequilibrium phase transition of fermionic superfluids driven by a sudden switch-on of two-particle loss due to inelastic collisions between atoms. By formulating a dissipative BCS theory that fully incorporates a change in particle number, we find that dissipation fundamentally alters the superfluid order parameter and induces collective oscillations in its amplitude and phase. In particular, we elucidate that a coupling between the order parameter and dissipation leads to a chirped phase rotation, in sharp contrast to the case of an interaction quench in closed systems [see Fig. 24.1(a)].

To experimentally observe the collective phenomena induced by dissipation, we propose introducing a particle loss in one of two coupled superfluids to induce a relative-phase oscillation analogous to the Leggett mode [2, 34, 35, 36, 33, 37, 38] [see Fig. 24.1(b)]. The phase mode causes an oscillation of a Josephson current around a nonvanishing dc component. Remarkably, when dissipation becomes strong, the coupled system undergoes a nonequilibrium phase transition characterized by the vanishing dc Josephson current, which can be regarded as a generalization of a dynamical phase transition [11, 12, 72, 73] to dissipative quantum systems. Our findings can experimentally be tested with ultracold atoms through introduction of dissipation via a photoassociation process [50, 59].

24.1.2 Dissipative BCS theory

We consider ultracold fermionic atoms described by the three-dimensional attractive Hubbard model

$$H = \sum_{\boldsymbol{k}\sigma} \epsilon_{\boldsymbol{k}} c^\dagger_{\boldsymbol{k}\sigma} c_{\boldsymbol{k}\sigma} - U_{\rm R} \sum_i c^\dagger_{i\uparrow} c^\dagger_{i\downarrow} c_{i\downarrow} c_{i\uparrow}, \tag{24.1}$$

where $U_{\rm R} > 0$, $\epsilon_{\boldsymbol{k}}$ is the single-particle energy dispersion, and $c_{\boldsymbol{k}\sigma}$ ($c_{i\sigma}$) denotes the annihilation operator of a spin-σ fermion with momentum $\boldsymbol{k}$ (at site i). When the system is subject to inelastic collisions, scattered atoms are lost to a surrounding environment, resulting in dissipative dynamics as observed experimentally [50, 55, 56, 58]. Here, we study the time evolution of the density matrix ρ which is described by the Lindblad equation [39, 40]

$$\frac{d\rho}{dt} = \mathcal{L}\rho = -i[H,\rho] - \frac{\gamma}{2}\sum_i (\{L_i^\dagger L_i, \rho\} - 2L_i \rho L_i^\dagger), \tag{24.2}$$

where $L_i = c_{i\downarrow} c_{i\uparrow}$ is a Lindblad operator that describes two-body loss with loss rate $\gamma > 0$. We note that the kinetic energy of lost atoms is large because of large internal energy of atoms before inelastic collisions. Under such situations, atoms after inelastic collisions are quickly lost into the surrounding environment and the Born-Markov approximation is justified [74, 75, 76].

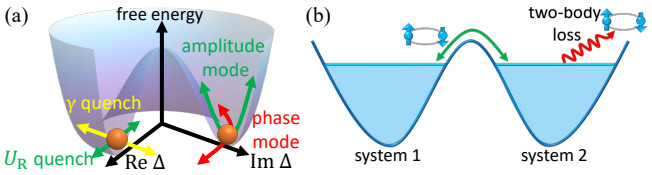


Figure 24.1: (a) Schematic illustration of the amplitude and phase modes in a Mexican-hat free-energy potential as a function of the complex order parameter Δ, when either the interaction $U_{\rm R}$ or the dissipation γ is suddenly switched on. A sudden quench of the interaction $U_{\rm R}$ and that of the dissipation γ kick Δ in a direction parallel and perpendicular to the radial direction, respectively. Note that a finite change of γ excites both the phase and amplitude modes. (b) Two superfluids coupled via a Josephson junction, where one superfluid (system 2) is subject to two-body loss.

We first study how the standard BCS theory is generalized in open dissipative systems by formulating a time-dependent mean-field theory in terms of a closed-time-contour path integral [77, 78]. We start with a generating functional defined as

$$Z = \mathrm{tr}\rho = \int \mathcal{D}[c_-, \bar{c}_-, c_+, \bar{c}_+] e^{iS} = 1, \tag{24.3}$$

with an action

$$\begin{aligned} S = \int_{-\infty}^{\infty} dt \Big[\sum_{\boldsymbol{k}\sigma} (\bar{c}_{\boldsymbol{k}\sigma+} i\partial_t c_{\boldsymbol{k}\sigma+} - \bar{c}_{\boldsymbol{k}\sigma-} i\partial_t c_{\boldsymbol{k}\sigma-}) - H_+ \\ + H_- + \frac{i\gamma}{2} \sum_i (\bar{L}_{i+} L_{i+} + \bar{L}_{i-} L_{i-} - 2L_{i+} \bar{L}_{i-}) \Big], \end{aligned} \tag{24.4}$$

where the subscripts + and - denote forward and backward paths, $H_\alpha = \sum_{\boldsymbol{k}\sigma} \epsilon_{\boldsymbol{k}} \bar{c}_{\boldsymbol{k}\sigma\alpha} c_{\boldsymbol{k}\sigma\alpha} - U_{\mathrm{R}} \sum_i \bar{c}_{i\uparrow\alpha} \bar{c}_{i\downarrow\alpha} c_{i\downarrow\alpha} c_{i\uparrow\alpha}$, $L_{i\alpha} = c_{i\downarrow\alpha} c_{i\uparrow\alpha}$, and $\bar{L}_{i\alpha} = \bar{c}_{i\uparrow\alpha} \bar{c}_{i\downarrow\alpha}$ $(\alpha = +, -)$. Note that the action has U(1) symmetry under $c_{i\sigma\alpha} \to e^{i\theta} c_{i\sigma\alpha}$ though the particle number is not conserved [79, 80]. By introducing auxiliary fields via the Hubbard-Stratonovich transformation, we rewrite the action in a quadratic form of fermionic Grassmann fields as [49, 81]

$$\begin{aligned} S = \int dt \Big\{ \sum_{\boldsymbol{k}} \Big[\bar{\psi}^t_{\boldsymbol{k}+} \begin{pmatrix} i\partial_t - \epsilon_{\boldsymbol{k}} & -\Delta \\ -\Delta^* & -i\partial_t + \epsilon_{\boldsymbol{k}} \end{pmatrix} \psi_{\boldsymbol{k}+} \\ - \bar{\psi}^t_{\boldsymbol{k}-} \begin{pmatrix} i\partial_t - \epsilon_{\boldsymbol{k}} & -\Delta \\ -\Delta^* & -i\partial_t + \epsilon_{\boldsymbol{k}} \end{pmatrix} \psi_{\boldsymbol{k}-} \Big] \Big\}, \end{aligned} \tag{24.5}$$

where $\bar{\psi}_{\boldsymbol{k}\alpha} = (\bar{c}_{\boldsymbol{k}\uparrow\alpha}, \ \ c_{-\boldsymbol{k}\downarrow\alpha})^t$ and $\psi_{\boldsymbol{k}\alpha} = (c_{\boldsymbol{k}\uparrow\alpha}, \ \ \bar{c}_{-\boldsymbol{k}\downarrow\alpha})^t$ $(\alpha = +, -)$. Here Δ is the superfluid order parameter which can be determined from the requirement that the action be extremal as [81]

$$\Delta = -\frac{U}{N_0} \sum_{\boldsymbol{k}} \mathrm{tr}(c_{-\boldsymbol{k}\downarrow} c_{\boldsymbol{k}\uparrow} \rho) \equiv -\frac{U}{N_0} \sum_{\boldsymbol{k}} \langle c_{-\boldsymbol{k}\downarrow} c_{\boldsymbol{k}\uparrow} \rangle, \tag{24.6}$$

where $U = U_R + i\gamma/2$ is an effective complex coupling constant including a contribution from the atom loss [49], and N_0 is the number of sites. Importantly, the order parameter includes the loss rate γ, which leads to dissipation-induced collective modes as discussed below. The action (24.5) describes the mean-field time-evolution equation of the density matrix as

$$\frac{d\rho}{dt} = -i[H_{\mathrm{eff}}, \rho], \tag{24.7}$$

$$H_{\mathrm{eff}} = \sum_{\boldsymbol{k}} \Psi^\dagger_{\boldsymbol{k}} \begin{pmatrix} \epsilon_{\boldsymbol{k}} & \Delta \\ \Delta^* & -\epsilon_{\boldsymbol{k}} \end{pmatrix} \Psi_{\boldsymbol{k}}, \tag{24.8}$$

where $\Psi_{\boldsymbol{k}} = (c_{\boldsymbol{k}\uparrow}, \ \ c^\dagger_{-\boldsymbol{k}\downarrow})^t$ is the Nambu spinor. In the Supplemental Material [81], we show that Eq. (24.7) can be derived from two different methods, i.e. the mean-field theory for the Lindblad equation and the time-dependent Bogoliubov-de Gennes analysis. While Eq. (24.7) appears to describe unitary evolution, it is consistent with the original Lindblad equation (24.2) as a consequence of the time-dependent BCS ansatz [81].

We use Anderson's pseudospin representation [1, 8, 32, 9, 10, 12, 14, 7, 11] defined by $\boldsymbol{\sigma}_{\boldsymbol{k}} = \frac{1}{2} \Psi^\dagger_{\boldsymbol{k}} \cdot \boldsymbol{\tau} \cdot \Psi_{\boldsymbol{k}}$ and $H_{\mathrm{eff}} = 2 \sum_{\boldsymbol{k}} \boldsymbol{b}_{\boldsymbol{k}} \cdot \boldsymbol{\sigma}_{\boldsymbol{k}}$, where $\boldsymbol{\tau} = (\tau_x, \ \ \tau_y, \ \ \tau_z)$ is the vector of the Pauli matrices. The pseudospins satisfy the commutation relations $[\sigma^j_{\boldsymbol{k}}, \sigma^k_{\boldsymbol{k}}] = i\epsilon_{jkl} \sigma^l_{\boldsymbol{k}}$. For simplicity of notation, we omit the bracket and regard $\boldsymbol{\sigma}_{\boldsymbol{k}}$ as the expectation value of the pseudospin

operator. By using the commutation relation of the pseudospins, Eq. (24.7) is mapped to the Bloch equation:

$$\frac{d\boldsymbol{\sigma}_{\boldsymbol{k}}}{dt} = 2\boldsymbol{b}_{\boldsymbol{k}} \times \boldsymbol{\sigma}_{\boldsymbol{k}}, \tag{24.9}$$

$$\boldsymbol{b}_{\boldsymbol{k}} = (\mathrm{Re}\Delta, \quad -\mathrm{Im}\Delta, \quad \epsilon_{\boldsymbol{k}}). \tag{24.10}$$

Equation (24.9) shows that the superfluid dynamics is characterized by precession of a pseudospin in an effective magnetic field $\boldsymbol{b}_k$. Here, the order parameter is determined self-consistently from the pseudospin expectation value as

$$\Delta = |\Delta| e^{i\theta} = -\frac{U}{N_0} \sum_{\boldsymbol{k}} (\sigma^x_{\boldsymbol{k}} - i\sigma^y_{\boldsymbol{k}}). \tag{24.11}$$

It is noteworthy that the norm of the pseudospin is conserved by the Bloch equation (24.9). The time evolution of the particle number due to particle loss is obtained from Eq. (24.7) as

$$\frac{1}{N_0}\frac{dN}{dt} = -\frac{2\gamma|\Delta|^2}{|U|^2}, \tag{24.12}$$

which reflects the dynamics of the order parameter.

24.1.3 Collective excitations: phase and amplitude modes

We numerically solve the Bloch equation (24.9) self-consistently under the condition (24.11). As an initial state, we prepare a BCS ground state with $\gamma = 0$, whose pseudospin representation is given by $\sigma^x_{\boldsymbol{k}}(0) = -\Delta_0/\sqrt{{\epsilon_{\boldsymbol{k}}}^2 + \Delta_0^2}$, $\sigma^y_{\boldsymbol{k}}(0) = 0$ and $\sigma^z_{\boldsymbol{k}}(0) = -\epsilon_{\boldsymbol{k}}/\sqrt{{\epsilon_{\boldsymbol{k}}}^2 + \Delta_0^2}$ with $\Delta_0 \in \mathbb{R}$. The single-particle energy $\epsilon_{\boldsymbol{k}}$ is measured from the Fermi energy of the initial state. The bandwidth W is defined by the energy difference between the upper and lower edges of the energy spectrum with a constant density of states. We then switch on the atom loss γ at $t = 0$. The results shown in Fig. 24.2 are obtained by the second-order Runge-Kutta method.

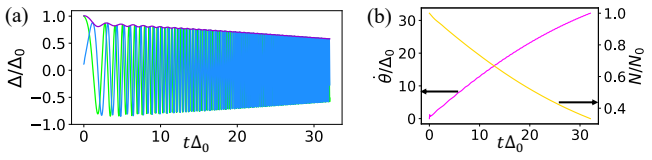


Figure 24.2: Dynamics of a superfluid after the atom loss with $\gamma = 2.81\Delta_0$ is switched on for the initial state with $U_{\mathrm{R}} = 12.2\Delta_0$ and bandwidth $W = 46.8\Delta_0$, where Δ_0 is the superfluid order parameter in the absence of the atom loss. (a) Real parts (light green), imaginary parts (blue), and the amplitude (violet) of the order parameter. (b) Angular velocity (pink) and particle number (yellow) plotted against time. The figures indicate a chirped phase rotation and an amplitude oscillation of Δ.

In the long-time limit, the amplitude of the superfluid order parameter Δ is suppressed due to dissipation, indicating a decay of superfluidity [see Fig. 24.2(a)]. We note that the order parameter decays in the long-time limit due to a decrease of the particle number [see Fig. 24.2(b)], and such behavior has no counterpart in the quench in isolated systems [11, 10]. Remarkably, after the dissipation γ is introduced, the U(1) phase of the order parameter rotates and shows chirping, i.e., its angular velocity increases with time [see Fig. 24.2(a), (b)] as a consequence of the dynamical shift of the Fermi level [81]. This property is unique to the dissipative superfluid and distinct from the usual dynamics in isolated systems where the U(1)

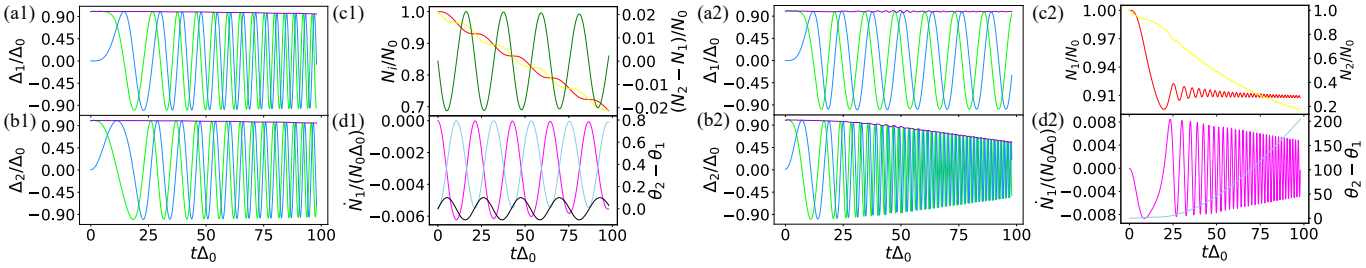


Figure 24.3: Dynamics of two fermionic superfluids after the switch-on of the atom loss γ and the tunnel coupling $V = 0.02\Delta_0$ with $U_\mathrm{R} = 3.06\Delta_0$ and bandwidth $W = 5.11\Delta_0$, where $\gamma = 0.03\Delta_0$ for (a1)-(d1) and $\gamma = 0.06\Delta_0$ for (a2)-(d2). (a), (b) Real parts (light green), imaginary parts (blue), and amplitudes (violet) of the order parameter for systems 1 and 2. (c) Particle numbers of system 1 (red) and system 2 (yellow), and their difference [green, in (c1)]. (d) Josephson current (pink) and phase difference (light blue) between the two systems. The black curve in (d1) shows an oscillation at frequency ω_L for comparison.

phase stays constant [10, 11, 12]. The phase rotation is understood from an initial-state free energy as a function of Δ [see Fig. 24.1(a)]. When dissipation is introduced, the sudden quench of the imaginary part of U in Eq. (24.11) pushes the order parameter towards the direction perpendicular to the radial direction irrespective of the initial choice of the gauge. Another way to understand the phase rotation is to introduce an effective chemical potential as $\Delta(t) = \exp(-2i\int_0^t \mu_\mathrm{eff}(t)dt)\Omega(t)$ ($\Omega \in \mathbb{R}$). By performing a global gauge transformation from Δ to Ω, the Bloch equation is written in the Larmor frame on which the energy dispersion is given by $\xi_{\boldsymbol{k}}(t) = \epsilon_{\boldsymbol{k}} - \mu_\mathrm{eff}(t)$. This gauge transformation indicates that the phase rotation corresponds to a decrease of the effective chemical potential, which is consistent with the behaviors of $\dot{\theta}$ and N in Fig. 24.2(b). This result can naturally be understood since the phase and the particle number are conjugate variables.

We also find amplitude oscillations in $|\Delta|$ as shown in Fig. 24.2(a). The amplitude oscillations are more pronounced when the interaction and the dissipation are simultaneously quenched [81]. The mechanism behind the oscillations is that the quench of the imaginary part of U changes the absolute value of Δ [see Fig. 24.1(a)]. The frequency of the amplitude oscillation is close to $2\Delta_0$ at an early stage, and increases as time evolves. This behavior is distinct from that of an isolated system, where the amplitude mode is characterized by the constant frequency. Such behavior can be observed from the measurement of the time-dependent particle number via Eq. (24.12).

24.1.4 Collective excitations: Leggett mode

To observe the chirped phase rotation of the superfluid order parameter that is a unique feature of dissipative superfluids, we propose that the phase rotation induced by dissipation can be detected when two superfluids are connected via a Josephson junction, which has been realized in ultracold atoms [82, 83, 84, 85, 86]. As the phase difference in the two superfluid order parameters is gauge-invariant, it leads to an observable Josephson current. We introduce dissipation to one of the two superfluids as schematically illustrated in Fig. 24.1(b) and assume that they are coupled via a tunneling Hamiltonian [38, 2]

$$H_\mathrm{tun} = -\frac{V}{N_0}\sum_{\boldsymbol{k}\boldsymbol{k}'}(c^\dagger_{1\boldsymbol{k}\uparrow}c^\dagger_{1-\boldsymbol{k}\downarrow}c_{2-\boldsymbol{k}'\downarrow}c_{2\boldsymbol{k}'\uparrow} + \mathrm{H.c.}), \tag{24.13}$$

where $V > 0$ is the amplitude of Cooper-pair tunneling between system 1 without dissipation and system 2 with two-particle loss. By performing a mean-field analysis, we can write the

system Hamiltonian as $H_{\rm sys} = H_1 + H_2 + H_{\rm tun} = H_1' + H_2'$, where $H_i \equiv \sum_{\boldsymbol{k}\sigma} \epsilon_{\boldsymbol{k}} c_{i\boldsymbol{k}\sigma}^\dagger c_{i\boldsymbol{k}\sigma} + \sum_{\boldsymbol{k}}(\Delta_i c_{i\boldsymbol{k}\uparrow}^\dagger c_{i-\boldsymbol{k}\downarrow}^\dagger + \text{H.c.})$ $(i = 1, 2)$ is the mean-field Hamiltonian of system i and $H_i' \equiv H_i - V/N_0 \sum_{\boldsymbol{k}\boldsymbol{k}'}(\langle c_{j-\boldsymbol{k}'\downarrow} c_{j\boldsymbol{k}'\uparrow}\rangle c_{i\boldsymbol{k}\uparrow}^\dagger c_{i-\boldsymbol{k}\downarrow}^\dagger + \text{H.c.})$ $[(i,j) = (1,2)$ or $(2,1)]$. In the pseudospin respresentation, the Hamiltonian is written as $H_i' = 2\sum_{\boldsymbol{k}} \boldsymbol{b}_{i\boldsymbol{k}} \cdot \boldsymbol{\sigma}_{i\boldsymbol{k}}$ with an effective magnetic field $\boldsymbol{b}_{i\boldsymbol{k}} = (\text{Re}\Delta_i', \ -\text{Im}\Delta_i', \ \epsilon_{i\boldsymbol{k}})$, which yields the Bloch equation $d\boldsymbol{\sigma}_{i\boldsymbol{k}}/dt = 2\boldsymbol{b}_{i\boldsymbol{k}} \times \boldsymbol{\sigma}_{i\boldsymbol{k}}$. The self-consistent conditions for the order parameters read $\Delta_1 = |\Delta_1| e^{i\theta_1} = -\frac{U_{\rm R}}{N_0}\sum_{\boldsymbol{k}}(\sigma_{1\boldsymbol{k}}^x - i\sigma_{1\boldsymbol{k}}^y)$ and $\Delta_2 = |\Delta_2| e^{i\theta_2} = -\frac{U}{N_0}\sum_{\boldsymbol{k}}(\sigma_{2\boldsymbol{k}}^x - i\sigma_{2\boldsymbol{k}}^y)$, where N_0 is the number of sites of each system. Here, the relations $\Delta_i' = \Delta_i - V/N_0 \sum_{\boldsymbol{k}}(\sigma_{j\boldsymbol{k}}^x - i\sigma_{j\boldsymbol{k}}^y)$ $[(i,j) = (1,2)$ or $(2,1)]$ are satisfied. Then, the Josephson current between the two superfluids is given by the rate of change in the particle number of system 1:

$$\frac{1}{N_0}\frac{dN_1}{dt} = -\frac{4V|\Delta_1||\Delta_2|}{U_{\rm R}|U|}\sin(\theta_2 - \theta_1 + \delta), \tag{24.14}$$

where $\delta = \tan^{-1}(-\gamma/2U_{\rm R})$ is the phase shift due to the sudden switch-on of the atom loss.

We numerically solve the coupled Bloch equations for $\boldsymbol{\sigma}_{i\boldsymbol{k}}$. We assume that dissipation γ and tunneling V are turned on at $t = 0$ for the BCS ground state. The numerical results for weak dissipation are shown in Fig. 24.3(a1)-(d1). In Figs. 24.3(a1) and (b1), the dynamics of two superfluids almost synchronize with each other because the time scale of particle loss is comparable with the inverse tunneling rate. In the pseudospin picture, the dynamics of particle numbers shown in Fig. 24.3(c1) can be interpreted as the nutation of pseudospins. Importantly, we see that, although the particle number of the system decreases in time, the corresponding amplitude of the order parameter stays almost constant. This implies that the condensate fraction against the total particle number becomes larger than that of the initial state. As inferred from Fig. 24.3(d1), the Josephson current oscillates around its dc component. Such behavior is reminiscent of Shapiro steps in a Josephson junction under irradiation of a microwave [87]; however, in the present case, the Josephson current oscillate spontaneously without any external field. Moreover, from Fig. 24.3(d1), the frequency of the oscillation of the phase difference between the two systems is close to that of the relative-phase mode known as the Leggett mode [2, 38] whose dispersion relation is given by $\omega_{\rm L} = 2\sqrt{(\lambda_{12} + \lambda_{21})|\Delta_1||\Delta_2|/\det\lambda}$, where $\lambda_{11} = \lambda_{22} = U_{\rm R}/W$, $\lambda_{12} = \lambda_{21} = V/W$ and $\det\lambda = \lambda_{11}\lambda_{22} - \lambda_{12}\lambda_{21}$. We note that ω_L includes the effect of loss through the order parameters. The Leggett mode with frequency $\omega_{\rm L}$ has been discussed in the context of a collective mode in a multiband superconductor irradiated by light [38]. The agreement between the frequencies of the relative-phase modes in very different situations can be understood as follows. When dissipation is weak, the time evolution of an order parameter is given by $\Delta_i(t) = \exp(-2i\int_0^t dt\mu_{i\rm eff}(t))|\Delta_i(t)|$ with an effective chemical potentials $\mu_{i\rm eff}$. Then, by performing a global gauge transformation from $c_{i\boldsymbol{k}\sigma}$ to $c_{i\boldsymbol{k}\sigma}\exp(i\int_0^t \sum_i \mu_{i\rm eff} dt/2)$, we can linearize the Bloch equation with respect to the relative phase difference between Δ_i's by following Ref. [38].

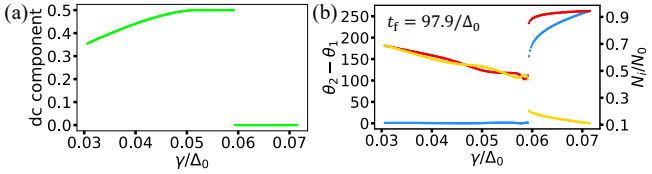


Figure 24.4: (a) DC component of the Josephson oscillation defined by $(\max_{0\le t\le t_{\rm f}}\{\sin(\theta_2(t) - \theta_1(t) + \delta)\} + \min_{0\le t\le t_{\rm f}}\{\sin(\theta_2(t) - \theta_1(t) + \delta)\})/2$ with $t_{\rm f} = 97.9/\Delta_0$. (b) Phase difference between the two systems (blue) and particle numbers of system 1 (red) and system 2 (yellow) after a sufficiently long time ($t_{\rm f} = 97.9/\Delta_0$). The parameters used are $U_{\rm R} = 3.06\Delta_0$, $V = 0.02\Delta_0$, and $W = 5.11\Delta_0$.

24.1.5 Nonequilibrium phase transition

In the presence of strong dissipation, the order parameter of system 2 oscillates faster than that of system 1 [see Fig. 24.3(a2), (b2)] and the phase difference monotonically increases in time [see Fig. 24.3(d2)]. This is because the dissipation rate larger than the tunneling rate makes system 1 fail to follow the decay of system 2, resulting in the dynamics similar to that of a single superfluid shown in Fig. 24.2. In particular, the chirped phase rotation of the superfluid order parameter of system 2 can be detected from the Josephson current [Fig. 24.3(d2)]. As the superfluidity of system 2 is suppressed, the Josephson current also decays, and the particle number of system 1 settles to a constant after some transient time [see Fig. 24.3(c2)]. The latter behavior is attributed to the continuous quantum Zeno effect [74, 75, 88, 89, 90, 49], which states that strong dissipation prevents tunneling and inhibits loss in system 1. In fact, an effective decay rate of system 1 is given by $\gamma_{\rm eff} \equiv |V_{\rm eff}|^2/\gamma$ with an effective tunneling rate $V_{\rm eff} = V\Delta_2/U_{\rm R}$ from Eq. (24.13), leading to suppression of decay $\gamma_{\rm eff} \to 0$ for $|\Delta_2|^2/\gamma \to 0$.

The two dynamically distinct regimes of superfluid behaviors suggest the existence of dynamical phases of matter [72, 73] in dissipative superfluids. The qualitative change in the superfluid behaviors with respect to the dissipation strength highlights a dynamical phase transition characterized by the vanishing dc Josephson current [Fig. 24.4(a)], where the dc component of the Josephson oscillation is defined by $(\max_{0\le t\le t_{\rm f}}\{\sin(\theta_2(t)-\theta_1(t)+\delta)\}+\min_{0\le t\le t_{\rm f}}\{\sin(\theta_2(t)-\theta_1(t)+\delta)\})/2$ [see Eq. (24.14)] after a sufficiently long time evolution with $t_{\rm f} = 97.9/\Delta_0$. We emphasize that the dynamical phase transition in dissipative superfluids is essentially distinct from the phase transition between ground states in a non-Hermitian BCS superfluid [49]. The former is caused by a change in particle number in the long-time dynamics, whereas the latter is caused by an exceptional point of a non-Hermitian BCS Hamiltonian, which is relevant to the short-time dynamics during which the number of particles does not change [91]. From Fig. 24.4(b), we see that the phase difference $\theta_2 - \theta_1$ starts to increase monotonically at the critical point and that the difference in particle number $(N_2 - N_1)/N_0$ becomes much larger. The behavior of the phase difference is reminiscent of the localization-diffusion transition of a quantum-mechanical particle moving in a washboard potential in the presence of frictional force [92, 93, 94]. However, the origin of the transition shown in Fig. 24.4 is essentially different from frictional force, since it cannot change the particle number. In fact, as shown in the Supplemental Material [81], the dynamical phase transition in Fig. 24.4 is triggered by the competition between the Josephson coupling and particle loss. Moreover, as the steady state is a vacuum due to the particle loss, the dynamical phase transition is observed only in the transient dynamics, and thus distinct from steady-state transitions.

24.1.6 Conclusions.

—We have investigated the loss-quench dynamics of fermionic superfluids, and have demonstrated that the dynamics exhibits amplitude and phase modes with chirped oscillations, the latter of which is a salient feature of a dissipative superfluid. To observe the chirped phase rotation, we have proposed a Josephson junction comprised of dissipative and nondissipative superfluids. We have shown that the relative-phase Leggett mode can be detected from the Josephson current for weak dissipation. Remarkably, when dissipation becomes strong, the superfluids exhibit the unique nonequilibrium phase transition triggered by particle loss. Our prediction can be tested with ultracold atomic systems of ^{6}Li [83, 84], for example, by introducing dissipation using photoassociation processes [50, 59]. It is of interest to explore how the dimensionality or confinement by a trap potential affects the dynamics and associated collective modes [15, 16, 17, 18].

24.2 Supplemental Material

24.2.1 Detailed calculations of the time-dependent dissipative BCS theory

We explain the details of the Hubbard-Stratonovich transformation that is used for the derivation of the time-dependent dissipative BCS theory in the path-integral formalism. The action (24.4) in the main text is rewritten as

$$S=\int_{-\infty}^{\infty}dt\Big[\sum_{\boldsymbol{k}\sigma}\Big(\bar{c}_{\boldsymbol{k}\sigma+}(i\partial_t-\epsilon_{\boldsymbol{k}})c_{\boldsymbol{k}\sigma+}-\bar{c}_{\boldsymbol{k}\sigma-}(i\partial_t-\epsilon_{\boldsymbol{k}})c_{\boldsymbol{k}\sigma-}\Big) +\sum_{\boldsymbol{k}\boldsymbol{k}'}(U\bar{c}_{\boldsymbol{k}\uparrow+}\bar{c}_{-\boldsymbol{k}\downarrow+}c_{-\boldsymbol{k}'\downarrow+}c_{\boldsymbol{k}'\uparrow+}-U^*\bar{c}_{\boldsymbol{k}\uparrow-}\bar{c}_{-\boldsymbol{k}\downarrow-}c_{-\boldsymbol{k}'\downarrow-}c_{\boldsymbol{k}'\uparrow-}-i\gamma c_{-\boldsymbol{k}\downarrow+}c_{\boldsymbol{k}\uparrow+}\bar{c}_{\boldsymbol{k}'\uparrow-}\bar{c}_{-\boldsymbol{k}'\downarrow-})\Big]. \tag{24.15}$$

We perform the Hubbard-Stratonovich transformation for each term in the second line of Eq. (24.15) with auxiliary fields Δ_α ($\alpha=+,-,\pm$) as

$$iU\bar{c}_{\boldsymbol{k}\uparrow+}\bar{c}_{-\boldsymbol{k}\downarrow+}c_{-\boldsymbol{k}'\downarrow+}c_{\boldsymbol{k}'\uparrow+}\to-i\Delta_+\bar{c}_{\boldsymbol{k}\uparrow+}\bar{c}_{-\boldsymbol{k}\downarrow+}-i\bar{\Delta}_+c_{-\boldsymbol{k}\downarrow+}c_{\boldsymbol{k}\uparrow+}+\frac{\bar{\Delta}_+\Delta_+}{iU}, \tag{24.16}$$

$$-iU^*\bar{c}_{\boldsymbol{k}\uparrow-}\bar{c}_{-\boldsymbol{k}\downarrow-}c_{-\boldsymbol{k}'\downarrow-}c_{\boldsymbol{k}'\uparrow-}\to i\Delta_-\bar{c}_{\boldsymbol{k}\uparrow-}\bar{c}_{-\boldsymbol{k}\downarrow-}+i\bar{\Delta}_-c_{-\boldsymbol{k}\downarrow-}c_{\boldsymbol{k}\uparrow-}-\frac{\bar{\Delta}_-\Delta_-}{iU^*}, \tag{24.17}$$

$$\gamma c_{-\boldsymbol{k}\downarrow+}c_{\boldsymbol{k}\uparrow+}\bar{c}_{\boldsymbol{k}'\uparrow-}\bar{c}_{-\boldsymbol{k}'\downarrow-}\to-\Delta_\pm\bar{c}_{\boldsymbol{k}\uparrow-}\bar{c}_{-\boldsymbol{k}\downarrow-}-\bar{\Delta}_\pm c_{-\boldsymbol{k}\downarrow+}c_{\boldsymbol{k}\uparrow+}-\frac{\bar{\Delta}_\pm\Delta_\pm}{\gamma}, \tag{24.18}$$

which yield

$$S=\int dt\Bigg\{\sum_{\boldsymbol{k}}\Bigg[\bar{\psi}^t_{\boldsymbol{k}+}\begin{pmatrix}i\partial_t-\epsilon_{\boldsymbol{k}} & -\Delta_+\\ -\bar{\Delta}_++i\bar{\Delta}_\pm & -i\partial_t+\epsilon_{\boldsymbol{k}}\end{pmatrix}\psi_{\boldsymbol{k}+}-\bar{\psi}^t_{\boldsymbol{k}-}\begin{pmatrix}i\partial_t-\epsilon_{\boldsymbol{k}} & -\Delta_--i\Delta_\pm\\ -\bar{\Delta}_- & -i\partial_t+\epsilon_{\boldsymbol{k}}\end{pmatrix}\psi_{\boldsymbol{k}-}\Bigg] +\frac{\bar{\Delta}_+\Delta_+}{iU}-\frac{\bar{\Delta}_-\Delta_-}{iU^*}-\frac{\bar{\Delta}_\pm\Delta_\pm}{\gamma}\Bigg\}, \tag{24.19}$$

where $\bar{\psi}_{\boldsymbol{k}\alpha}=\begin{pmatrix}\bar{c}_{\boldsymbol{k}\uparrow\alpha}, & c_{-\boldsymbol{k}\downarrow\alpha}\end{pmatrix}^t$ and $\psi_{\boldsymbol{k}\alpha}=\begin{pmatrix}c_{\boldsymbol{k}\uparrow\alpha}, & \bar{c}_{-\boldsymbol{k}\downarrow\alpha}\end{pmatrix}^t$ ($\alpha=+,-$). Then, from the saddle-point condition $\langle\partial S/\partial\Delta_\alpha\rangle=\langle\partial S/\partial\bar{\Delta}_\alpha\rangle=0$ ($\alpha=+,-,\pm$), we obtain

$$\Delta_+=-\frac{U}{N_0}\sum_{\boldsymbol{k}}\langle c_{-\boldsymbol{k}\downarrow+}c_{\boldsymbol{k}\uparrow+}\rangle,\quad \bar{\Delta}_+=-\frac{U}{N_0}\sum_{\boldsymbol{k}}\langle c^\dagger_{\boldsymbol{k}\uparrow+}c^\dagger_{-\boldsymbol{k}\downarrow+}\rangle, \tag{24.20}$$

$$\Delta_-=-\frac{U^*}{N_0}\sum_{\boldsymbol{k}}\langle c_{-\boldsymbol{k}\downarrow-}c_{\boldsymbol{k}\uparrow-}\rangle,\quad \bar{\Delta}_-=-\frac{U^*}{N_0}\sum_{\boldsymbol{k}}\langle c^\dagger_{\boldsymbol{k}\uparrow-}c^\dagger_{-\boldsymbol{k}\downarrow-}\rangle, \tag{24.21}$$

$$\Delta_\pm=\frac{\gamma\Delta_+}{U},\quad \bar{\Delta}_\pm=\frac{\gamma\bar{\Delta}_-}{U^*}, \tag{24.22}$$

where N_0 is the number of lattice sites and $\langle\cdots\rangle$ is the expectation value for fixed Δ_α and $\bar{\Delta}_\alpha$. Then, we can reduce the number of the auxiliary fields by using $\langle c_{-\boldsymbol{k}\downarrow\alpha}c_{\boldsymbol{k}\uparrow\alpha}\rangle=\mathrm{tr}(c_{-\boldsymbol{k}\downarrow}c_{\boldsymbol{k}\uparrow}\rho)$ ($\alpha=+,-$) and $\mathrm{tr}(A^\dagger\rho)=[\mathrm{tr}(A\rho)]^*$ [78], giving

$$\Delta_+=\bar{\Delta}^*_-, \tag{24.23}$$

$$\Delta_-=\bar{\Delta}^*_+. \tag{24.24}$$

Finally, the action (24.19) is rewritten as

$$S = \int dt \sum_{\boldsymbol{k}} \left\{ \bar{\psi}^t_{\boldsymbol{k}+} \begin{pmatrix} i\partial_t - \epsilon_{\boldsymbol{k}} & -\Delta \\ -\Delta^* & -i\partial_t + \epsilon_{\boldsymbol{k}} \end{pmatrix} \psi_{\boldsymbol{k}+} - \bar{\psi}^t_{\boldsymbol{k}-} \begin{pmatrix} i\partial_t - \epsilon_{\boldsymbol{k}} & -\Delta \\ -\Delta^* & -i\partial_t + \epsilon_{\boldsymbol{k}} \end{pmatrix} \psi_{\boldsymbol{k}-} \right\}, \quad (24.25)$$

where the superfluid order parameter of the system is given by

$$\Delta = -\frac{U}{N_0} \sum_{\boldsymbol{k}} \mathrm{tr}(c_{-\boldsymbol{k}\downarrow} c_{\boldsymbol{k}\uparrow} \rho) \equiv -\frac{U}{N_0} \sum_{\boldsymbol{k}} \langle c_{-\boldsymbol{k}\downarrow} c_{\boldsymbol{k}\uparrow} \rangle. \quad (24.26)$$

24.2.2 Operator formalism of the BCS theory for a dissipative superfluid

Here, we explain the operator formalism of the BCS theory for a dissipative superfluid that leads to Eq. (24.7) in the main text. First, we note that an operator $|\psi_+\rangle\langle\psi_-|$ acting on the Hilbert space of the system can be mapped to a tensor-product state $|\psi_+\rangle \otimes |\psi_-\rangle$ in the doubled Hilbert space $\mathbb{H}_+ \otimes \mathbb{H}_-$ [95, 96]. Using this mapping, we can rewrite the Liouvillian [see Eq. (24.2) in the main text for definition] as

$$\begin{aligned} i\mathcal{L} &= H_+ - H_- + i \sum_i \gamma_i (L_{i+} L^\dagger_{i-} - \frac{1}{2} L^\dagger_{i+} L_{i+} - \frac{1}{2} L^\dagger_{i-} L_{i-}) \\ &= \mathcal{H}_+ - \mathcal{H}^*_- + i\gamma \sum_{\boldsymbol{k}\boldsymbol{k}'} c_{-\boldsymbol{k}\downarrow+} c_{\boldsymbol{k}\uparrow+} c^\dagger_{\boldsymbol{k}'\uparrow-} c^\dagger_{-\boldsymbol{k}'\downarrow-}, \end{aligned} \quad (24.27)$$

where $L_{i\alpha} = c_{i\downarrow\alpha} c_{i\uparrow\alpha}$, and $c_{i\sigma\alpha}$ ($c_{\boldsymbol{k}\sigma\alpha}$) with $\alpha = +, -$ is the fermion annihilation operator in the real (momentum) space that acts on the Hilbert space $\mathbb{H}_\alpha$. The fermion operator with subscript $+$ ($-$) corresponds to the fermion field in the forward (backward) path in the path-integral formalism. The BCS Hamiltonian equivalent to Eq. (24.1) is given by

$$H_\alpha = \sum_{\boldsymbol{k}\sigma} \epsilon_{\boldsymbol{k}} c^\dagger_{\boldsymbol{k}\sigma\alpha} c_{\boldsymbol{k}\sigma\alpha} - U_{\mathrm{R}} \sum_{\boldsymbol{k}\boldsymbol{k}'} c^\dagger_{\boldsymbol{k}\uparrow\alpha} c^\dagger_{-\boldsymbol{k}\downarrow\alpha} c_{-\boldsymbol{k}'\downarrow\alpha} c_{\boldsymbol{k}'\uparrow\alpha}, \quad (24.28)$$

and $\mathcal{H}_\alpha$ is defined as

$$\begin{aligned} \mathcal{H}_\alpha &= H_\alpha - \frac{1}{2} i\gamma \sum_i L^\dagger_{i\alpha} L_{i\alpha} \\ &= \sum_{\boldsymbol{k}\sigma} \epsilon_{\boldsymbol{k}} c^\dagger_{\boldsymbol{k}\sigma\alpha} c_{\boldsymbol{k}\sigma\alpha} - U \sum_{\boldsymbol{k}\boldsymbol{k}'} c^\dagger_{\boldsymbol{k}\uparrow\alpha} c^\dagger_{-\boldsymbol{k}\downarrow\alpha} c_{-\boldsymbol{k}'\downarrow\alpha} c_{\boldsymbol{k}'\uparrow\alpha}. \end{aligned} \quad (24.29)$$

By applying the mean-field approximation to $\mathcal{L}$, we obtain the mean-field Liouvillian as

$$\begin{aligned} i\mathcal{L}_{\mathrm{MF}} =& \sum_{\boldsymbol{k}\sigma} \epsilon_{\boldsymbol{k}} c^\dagger_{\boldsymbol{k}\sigma+} c_{\boldsymbol{k}\sigma+} + \Delta_+ \sum_{\boldsymbol{k}} c^\dagger_{\boldsymbol{k}\uparrow+} c^\dagger_{-\boldsymbol{k}\downarrow+} + (\bar{\Delta}_+ - \frac{i\gamma}{U^*} \bar{\Delta}_-) \sum_{\boldsymbol{k}} c_{-\boldsymbol{k}\downarrow+} c_{\boldsymbol{k}\uparrow+} \\ & - \sum_{\boldsymbol{k}\sigma} \epsilon_{\boldsymbol{k}} c^\dagger_{\boldsymbol{k}\sigma-} c_{\boldsymbol{k}\sigma-} - (\Delta_- + \frac{i\gamma}{U} \Delta_+) \sum_{\boldsymbol{k}} c^\dagger_{\boldsymbol{k}\uparrow-} c^\dagger_{-\boldsymbol{k}\downarrow-} - \bar{\Delta}_- \sum_{\boldsymbol{k}} c_{-\boldsymbol{k}\downarrow-} c_{\boldsymbol{k}\uparrow-} \\ =& \sum_{\boldsymbol{k}} \Psi^\dagger_{\boldsymbol{k}+} \begin{pmatrix} \epsilon_{\boldsymbol{k}} & \Delta_+ \\ \bar{\Delta}_+ - \frac{i\gamma}{U^*} \bar{\Delta}_- & -\epsilon_{\boldsymbol{k}} \end{pmatrix} \Psi_{\boldsymbol{k}+} - \sum_{\boldsymbol{k}} \Psi^\dagger_{\boldsymbol{k}-} \begin{pmatrix} \epsilon_{\boldsymbol{k}} & \Delta_- + \frac{i\gamma}{U} \Delta_+ \\ \bar{\Delta}_- & -\epsilon_{\boldsymbol{k}} \end{pmatrix} \Psi_{\boldsymbol{k}-}, \end{aligned} \quad (24.30)$$

where $\Psi_{\boldsymbol{k}} = \begin{pmatrix} c_{\boldsymbol{k}\uparrow}, & c^\dagger_{-\boldsymbol{k}\downarrow} \end{pmatrix}^t$ is the Nambu spinor. As we can see from Eq. (24.27) and Eq. (24.29), the Liouvillian is invariant under the U(1) gauge transformations $c_{\boldsymbol{k}\sigma+} \to e^{i\theta} c_{\boldsymbol{k}\sigma+}$ and $c_{\boldsymbol{k}\sigma-} \to$

$e^{i\theta}c_{\boldsymbol{k}\sigma-}$. Moreover, under the exchange of forward and backward operators, $Pc_{\boldsymbol{k}\sigma+}P^{-1} = c_{\boldsymbol{k}\sigma-}$ and $Pc^\dagger_{\boldsymbol{k}\sigma+}P^{-1} = c^\dagger_{\boldsymbol{k}\sigma-}$ with $P^2 = 1$, the Liouvillian has the following symmetry

$$P(i\mathcal{L})^\dagger P^{-1} = -i\mathcal{L}. \tag{24.31}$$

By imposing the same symmetry on the mean-field Liouvillian as $P(i\mathcal{L}_{\rm MF})^\dagger P^{-1} = -i\mathcal{L}_{\rm MF}$, we obtain the relations for the order parameters as

$$\Delta^*_+ = \bar{\Delta}_-, \tag{24.32}$$
$$\Delta^*_- = \bar{\Delta}_+, \tag{24.33}$$

which coincide with those obtained in the path-integral formalism [see Eqs. (24.23) and (24.24)]. Finally, by rewriting the superfluid order parameter Δ_+ as

$$\Delta = -\frac{U}{N_0}\sum_{\boldsymbol{k}} \mathrm{tr}(c_{-\boldsymbol{k}\downarrow}c_{\boldsymbol{k}\uparrow}\rho) \equiv -\frac{U}{N_0}\sum_{\boldsymbol{k}}\langle c_{-\boldsymbol{k}\downarrow}c_{\boldsymbol{k}\uparrow}\rangle, \tag{24.34}$$

we obtain the equations for the density matrix as

$$\dot{\rho} = -i[H_{\rm eff}, \rho], \tag{24.35}$$
$$H_{\rm eff} = \sum_{\boldsymbol{k}} \Psi^\dagger_{\boldsymbol{k}} \begin{pmatrix} \epsilon_{\boldsymbol{k}} & \Delta \\ \Delta^* & -\epsilon_{\boldsymbol{k}} \end{pmatrix} \Psi_{\boldsymbol{k}}, \tag{24.36}$$

which are the same as Eqs. (24.7) and (24.8) in the main text.

24.2.3 Generalization of the Bogoliubov-de Gennes analysis with a time-dependent BCS state

We explain that Eq. (24.7) (Eq. (24.9) in the psedouspin representation) in the main text is equivalent to the Bogoliubov-de Gennes equation with a time-dependent BCS state [9, 3], which describes the unitary evolution of the density matrix.

We introduce the time-dependent BCS state of the effective Hamiltonian $H_{\rm eff} = \sum_{\boldsymbol{k}} \Psi^\dagger_{\boldsymbol{k}} \begin{pmatrix} \epsilon_{\boldsymbol{k}} & \Delta \\ \Delta^* & -\epsilon_{\boldsymbol{k}} \end{pmatrix} \Psi_{\boldsymbol{k}}$ as follows:

$$|\Psi_{\rm BCS}(t)\rangle = \prod_{\boldsymbol{k}} (u_{\boldsymbol{k}}(t) + v_{\boldsymbol{k}}(t)c^\dagger_{\boldsymbol{k}\uparrow}c^\dagger_{-\boldsymbol{k}\downarrow})|0\rangle, \tag{24.37}$$
$$|u_{\boldsymbol{k}}|^2 + |v_{\boldsymbol{k}}|^2 = 1, \tag{24.38}$$

where $|0\rangle$ is the vacuum of fermions. Here, the superfluid order parameter Δ is rewritten as

$$\Delta = -\frac{U}{N_0}\sum_{\boldsymbol{k}}\langle c_{-\boldsymbol{k}\downarrow}c_{\boldsymbol{k}\uparrow}\rangle = -\frac{U}{N_0}\sum_{\boldsymbol{k}} u^*_{\boldsymbol{k}}(t)v_{\boldsymbol{k}}(t). \tag{24.39}$$

Suppose that the density matrix is given by

$$\rho(t) = |\Psi_{\rm BCS}(t)\rangle\langle\Psi_{\rm BCS}(t)|. \tag{24.40}$$

Then, the time-evolution equation

$$\frac{d\rho(t)}{dt} = -i[H_{\rm eff}, \rho(t)] \tag{24.41}$$

[Eq. (24.7) in the main text] is equivalent to the Bogoliubov-de Gennes equation with the time-dependent BCS state

$$i\partial_t \begin{pmatrix} u_{\boldsymbol{k}} \\ v_{\boldsymbol{k}} \end{pmatrix} = \begin{pmatrix} -\epsilon_{\boldsymbol{k}} & \Delta^* \\ \Delta & \epsilon_{\boldsymbol{k}} \end{pmatrix} \begin{pmatrix} u_{\boldsymbol{k}} \\ v_{\boldsymbol{k}} \end{pmatrix}. \tag{24.42}$$

By defining $f_{\boldsymbol{k}}(t)$ and $g_{\boldsymbol{k}}(t)$ as

$$f_{\boldsymbol{k}} = u_{\boldsymbol{k}}^* v_{\boldsymbol{k}}, \tag{24.43}$$

$$g_{\boldsymbol{k}} = \frac{1}{2}(|u_{\boldsymbol{k}}|^2 - |v_{\boldsymbol{k}}|^2), \tag{24.44}$$

Eq. (24.42) is rewritten as

$$\frac{df_{\boldsymbol{k}}}{dt} = -2i\epsilon_{\boldsymbol{k}} f_{\boldsymbol{k}} - 2i\Delta g_{\boldsymbol{k}}, \tag{24.45}$$

$$\frac{dg_{\boldsymbol{k}}}{dt} = i\Delta f_{\boldsymbol{k}}^* - i\Delta^* f_{\boldsymbol{k}}. \tag{24.46}$$

These equations take the same forms as those for closed systems [9, 3]. Finally, by defining the psedouspins as

$$f_{\boldsymbol{k}} = \sigma_{\boldsymbol{k}}^x - i\sigma_{\boldsymbol{k}}^y, \tag{24.47}$$

$$g_{\boldsymbol{k}} = -\sigma_{\boldsymbol{k}}^z, \tag{24.48}$$

we obtain the same Bloch equation as discussed in the main text:

$$\frac{d\boldsymbol{\sigma}_{\boldsymbol{k}}}{dt} = 2\boldsymbol{b}_{\boldsymbol{k}} \times \boldsymbol{\sigma}_{\boldsymbol{k}}, \tag{24.49}$$

$$\boldsymbol{b}_{\boldsymbol{k}} = \left(\mathrm{Re}\Delta, \quad -\mathrm{Im}\Delta, \quad \epsilon_{\boldsymbol{k}}\right). \tag{24.50}$$

We note that the dynamics described by Eq. (24.41) conserves the purity $\mathrm{tr}[\rho^2]$ as

$$\frac{d\mathrm{tr}[\rho^2]}{dt} = 2\mathrm{tr}\left[\rho\frac{d\rho}{dt}\right] = -2i\mathrm{tr}(\rho[H_{\mathrm{eff}}, \rho]) = 0. \tag{24.51}$$

In general, the purity should decrease during the time evolution described by the quantum master equation [Eq. (24.2) in the main text]. This fact is consistent with the time-dependent BCS ansatz (24.37) as follows. Since $|\Psi_{\mathrm{BCS}}(t)\rangle$ can be expanded in terms of N-particle states

$$|\Psi_N\rangle = \sum_{\boldsymbol{k}_1 \cdots \boldsymbol{k}_{N/2}} a_{\boldsymbol{k}_1} \cdots a_{\boldsymbol{k}_{N/2}} c_{\boldsymbol{k}_1\uparrow}^\dagger c_{-\boldsymbol{k}_1\downarrow}^\dagger \cdots c_{\boldsymbol{k}_{N/2}\uparrow}^\dagger c_{-\boldsymbol{k}_{N/2}\downarrow}^\dagger |0\rangle \tag{24.52}$$

as

$$|\Psi_{\mathrm{BCS}}(t)\rangle = \sum_N c_N |\Psi_N\rangle, \tag{24.53}$$

the density matrix is written as

$$\begin{aligned} \rho &= |\Psi_{\mathrm{BCS}}(t)\rangle\langle\Psi_{\mathrm{BCS}}(t)| \\ &= \sum_N |c_N|^2 |\Psi_N\rangle\langle\Psi_N| + \sum_{N\neq N'} c_{N'}^* c_N |\Psi_N\rangle\langle\Psi_{N'}|. \end{aligned} \tag{24.54}$$

Then, for a gauge-invariant observable $\mathcal{O}$, its expectation value is given by

$$\langle \mathcal{O} \rangle \equiv \mathrm{tr}[\mathcal{O}\rho] = \sum_N |c_N|^2 \langle \Psi_N | \mathcal{O} | \Psi_N \rangle = \mathrm{tr}[\mathcal{O}\rho'], \tag{24.55}$$

where

$$\rho' = \sum_N |c_N|^2 |\Psi_N\rangle\langle\Psi_N| \tag{24.56}$$

is a mixed state of different particle numbers. Therefore, concerning gauge-invariant observables, the time-dependent BCS state (24.40) is indistinguishable from the mixed state (24.56) with $\mathrm{tr}[\rho'^2] < 1$. Since any physically observable quantity should be gauge invariant, the time-dependent BCS ansatz (24.37) can describe the time evolution of the density matrix consistently with the quantum master equation (24.2).

24.2.4 Dynamics of pseudospins after switch-on of dissipation

The physical origin of the chirping of the U(1) phase can be understood from the pseudospin picture. As shown in Fig. 24.5, when the sign of $\sigma^z_{\boldsymbol{k}}$ changes from positive to negative, the magnitudes of $\sigma^x_{\boldsymbol{k}}$ and $\sigma^y_{\boldsymbol{k}}$ increase due to the norm conservation of pseudospins. This indicates that the Cooper-pair amplitude at specific momenta rapidly changes when atoms at those momenta are lost from the system. Since Cooper pairs are formed near the Fermi surface, a loss of Cooper pairs leads to a downward shift of the Fermi level.

To see the effect of the dynamics of pseudospins on the collective phase mode, we calculate the angular velocity of the order parameter. From Eq. (11) in the main text, the real and imaginary parts of the order parameter are written as

$$|\Delta| \cos\theta = \mathrm{Re}\Delta = -U_1 \sum_{\boldsymbol{k}} \sigma^x_{\boldsymbol{k}} - \frac{\gamma}{2} \sum_{\boldsymbol{k}} \sigma^y_{\boldsymbol{k}}, \tag{24.57}$$

$$|\Delta| \sin\theta = \mathrm{Im}\Delta = -\frac{\gamma}{2} \sum_{\boldsymbol{k}} \sigma^x_{\boldsymbol{k}} + U_1 \sum_{\boldsymbol{k}} \sigma^y_{\boldsymbol{k}}. \tag{24.58}$$

By differentiating Eqs. (24.57) and (24.58) with respect to time, we obtain

$$|\Delta|^2 \frac{d\theta}{dt} = \left(U_1 \mathrm{Im}\Delta - \frac{\gamma}{2}\mathrm{Re}\Delta\right) \sum_{\boldsymbol{k}} \frac{d\sigma^x_{\boldsymbol{k}}}{dt} + \left(\frac{\gamma}{2}\mathrm{Im}\Delta + U_1 \mathrm{Re}\Delta\right) \sum_{\boldsymbol{k}} \frac{d\sigma^y_{\boldsymbol{k}}}{dt}. \tag{24.59}$$

Then, by substituting the Bloch equation (24.49) into Eq. (24.59), we arrive at

$$\frac{d\theta}{dt} = U_{\mathrm{R}}\left(1 - \frac{N}{N_0}\right) - \frac{2|U|^2}{|\Delta|^2 N_0^2} \sum_{\substack{\boldsymbol{k}\boldsymbol{k}' \\ \alpha = x,y}} \sigma^\alpha_{\boldsymbol{k}} \cdot \epsilon_{\boldsymbol{k}'} \sigma^\alpha_{\boldsymbol{k}'}, \tag{24.60}$$

in which the last term increases due to the shift of the Fermi level, leading to chirping of the U(1) phase. Here, we note that the first term on the right-hand side of Eq. (24.60) also increases as the particle number decreases; however, it is much smaller than the second term.

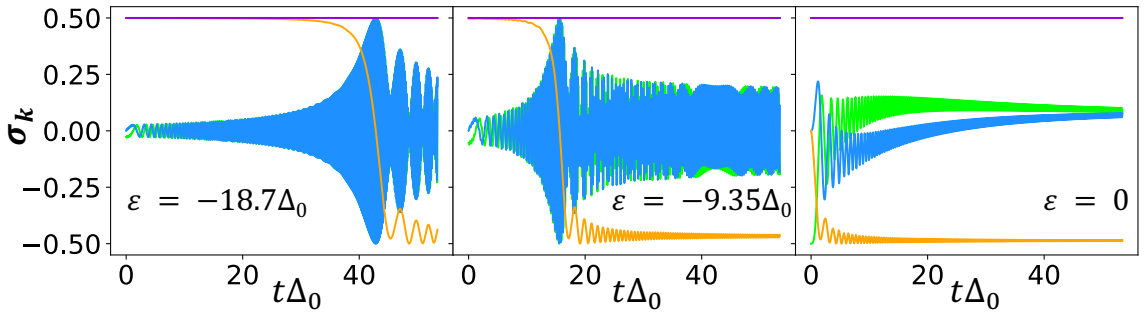


Figure 24.5: Dynamics of pseudospins [$\sigma_{\boldsymbol{k}}^x$ (light green), $\sigma_{\boldsymbol{k}}^y$ (blue), $\sigma_{\boldsymbol{k}}^z$ (orange), $|\boldsymbol{\sigma}_{\boldsymbol{k}}|$ (violet)] after the atom loss with $\gamma = 2.81\Delta_0$ is switched on for the initial state with $U_{\mathrm{R}} = 12.2\Delta_0$ and the Fermi energy $\epsilon_{\mathrm{F}} = 0$ for $\epsilon = -18.7\Delta_0$ (left), $-9.35\Delta_0$ (center), and 0 (right), where ϵ is the single-particle energy in the band $-23.4\Delta_0 \leq \epsilon \leq 23.4\Delta_0$.

24.2.5 Dynamics after sudden change of both the interaction and the dissipation

Figure 24.6 shows the dynamics after the dissipation γ is introduced at $t = 0$ and the interaction strength is simultaneously changed from $U_{\mathrm{R}} = 8.4\Delta_0$ to $U_{\mathrm{R}} = 16.8\Delta_0$. In Figs. 24.6(a) and (b), we see an amplitude oscillation larger than that in the loss quench dynamics shown in Figs. 24.2(a) and (b) in the main text. This behavior is due to the fact that a change in the real part of U causes a large initial shift of the amplitude of the order parameter [see Fig. 24.1(a) in the main text]. The U(1) phase rotates with an increasing angular velocity due to dissipation as in Figs. 24.6(a) and (b). The amplitude oscillation of the order parameter can be detected through monitoring of the particle number and from Eq. (24.12) in the main text. As shown in Figs. 24.6(c) and (d), the amplitude of the particle-number oscillation is a few percent of the initial particle number, which can be detected with current experimental techniques [83]. Since the oscillation in the particle number cannot appear in isolated systems, the dissipation-induced dynamics can be used as a unique signature for the amplitude mode of the superfluid order parameters.

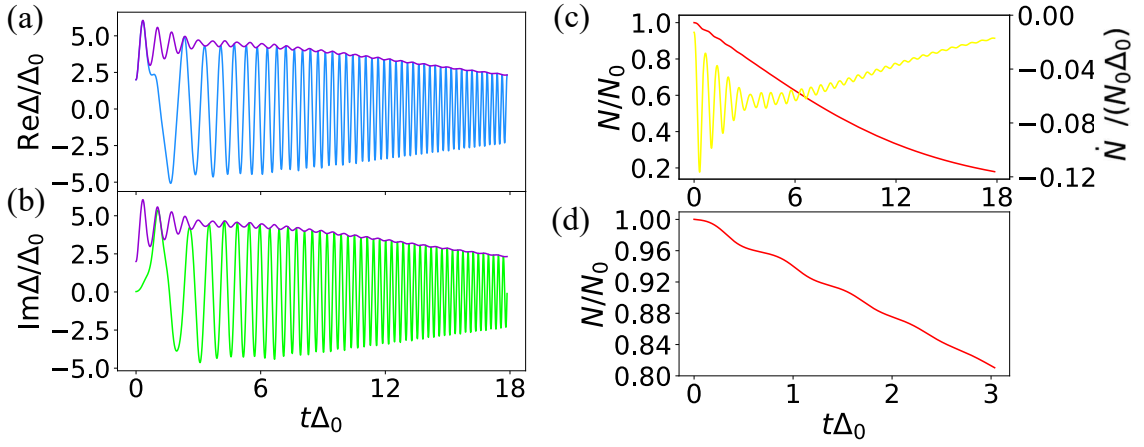


Figure 24.6: Dynamics of a superfluid after the interaction and the atom loss are suddenly changed. (a) Real parts (light green) there is a typo here, since on the plot it is vice versa and imaginary parts (blue) of the order parameter. The amplitudes of the order parameter are shown as violet curves in both figures. (c) The particle number of the system normalized by the initial particle number N_0 (red) and the rate of change in particle number (yellow). (d) An enlarged view of the particle number near $t = 0$. The parameters are suddenly changed from $U_{\mathrm{R}} = 8.4\Delta_0$ to $U = (16.8 + 0.45i)\Delta_0$ at $t = 0$ and the bandwidth is set to $W = 28\Delta_0$.

24.2.6 A simplified model for understanding the nonequilibrium phase transition

Here, we explain how the nonequilibrium phase transition associated with the vanishing dc Josephson current can be understood by considering a simplified model of the Josephson junction with particle loss. We consider two fermionic superfuids coupled via a Josephson junction, where two-body loss is introduced to one of them, as shown in Fig. 24.1(b) in the main text. The Josephson current flowing between the two systems is given by

$$I = \frac{1}{N_0}\frac{dN_1}{dt} = -I_0 \sin(\Delta\theta), \tag{24.61}$$

where, from Eq. (24.14) in the main text, $\Delta\theta = \theta_2 - \theta_1$, $I_0 = 4V|\Delta_1||\Delta_2|/U_{\rm R}|U|$, and we have neglected the phase shift δ because $\delta \ll \Delta\theta$. Taking into account the particle loss [see Eq. (24.12) in the main text], we obtain the rate of change in the particle number of system 1 and that of system 2 as

$$\frac{1}{N_0}\frac{dN_1}{dt} = -I_0 \sin(\Delta\theta), \tag{24.62}$$

$$\frac{1}{N_0}\frac{dN_2}{dt} = I_0 \sin(\Delta\theta) - \frac{2\gamma|\Delta_2|^2}{|U|^2}. \tag{24.63}$$

We assume that the time evolution of the phase difference $\Delta\theta$ is given by the effective chemical-potential difference $\Delta\mu_{\rm eff}$ between the two systems as

$$\frac{d\Delta\theta}{dt} = -2\Delta\mu_{\rm eff} = -\frac{W}{N_0}(N_2 - N_1), \tag{24.64}$$

where W is a bandwidth and we assume a constant density of states for simplicity (we can also understand this equation from the phenomenological time-dependent Ginzburg-Landau theory, which is explained in the last part of this section). We obtain the equation of motion for $\Delta\theta$ by using Eqs. (24.62), (24.63), and (24.64) as

$$\frac{d^2\Delta\theta}{dt^2} = -2WI_0 \sin(\Delta\theta) + \frac{2\gamma W|\Delta_2|^2}{|U|^2}. \tag{24.65}$$

This system is regarded as a Josephson junction with shunt resistance $R = +\infty$, capacitance $C = 1/2W$ and an external force $F = \gamma|\Delta_2|^2/|U|^2$, which is described as

$$C\frac{d^2\Delta\theta}{dt^2} + \frac{1}{R}\frac{d\Delta\theta}{dt} + I_0 \sin(\Delta\theta) = F. \tag{24.66}$$

That is, the time evolution of $\Delta\theta$ is equivalent to that of a particle moving in a washboard potential

$$V_{\rm wash} = -2WI_0 \cos(\Delta\theta) - \frac{2\gamma W|\Delta_2|^2\Delta\theta}{|U|^2}. \tag{24.67}$$

The condition for the extremum of $V_{\rm wash}$ is given by $dV_{\rm wash}/d\Delta\theta = 0$, giving

$$\sin(\Delta\theta) = \frac{\gamma|\Delta_2|^2}{I_0|U|^2}. \tag{24.68}$$

The solution to this equation does not exist for $\gamma|\Delta_2|^2/I_0|U|^2 > 1$ and the time evolution of $\Delta\theta$ becomes unstable. If we assume $|\Delta_1| \simeq |\Delta_2|$ when the time evolution is sufficiently slow, we obtain the critical strength of the atom loss as

$$\gamma_{\rm c} \simeq 4V, \tag{24.69}$$

which is of the same order of magnitude as that in the main text ($\gamma_c \simeq 3V$). Thus, the system exhibits a dynamical phase transition from the state in which $\Delta\theta$ oscillates around an extremum of $V_{\rm wash}$ for $\gamma < \gamma_c$ to the state in which $\Delta\theta$ slips down the washboard potential for $\gamma > \gamma_c$. Thus, the dynamical phase transition caused by the particle loss is the one between a trapped state and a running state. We note that the particle loss γ acts as an external force F rather than friction R in Eq. (24.66). The loss-induced dynamical phase transition occurs spontaneously without any external fields, and has an essentially different origin from the localization-delocalization transition induced by friction R [92, 93, 94].

These features are also obtained from a phenomenological introduction of two-body loss [74, 75], under which the rate of change in the particle number of system 1 and that of system 2 are given by

$$\frac{1}{N_0}\frac{dN_1}{dt} = -I_0 \sin(\Delta\theta), \tag{24.70}$$

$$\frac{1}{N_0}\frac{dN_2}{dt} = I_0 \sin(\Delta\theta) - \kappa_2 \left(\frac{N_2}{N_0}\right)^2, \tag{24.71}$$

where κ_2 is the two-body loss rate. By using Eqs. (24.64), (24.70), and (24.71), we obtain the equation of motion for $\Delta\theta$ as

$$\frac{d^2\Delta\theta}{dt^2} = -2WI_0 \sin(\Delta\theta) + W\kappa_2 \left(\frac{N_2}{N_0}\right)^2. \tag{24.72}$$

This system is regarded as a Josephson junction with resistance $R = +\infty$, capacitance $C = 1/2W$ and an external force $F = \frac{\kappa_2}{2}\left(\frac{N_2}{N_0}\right)^2$. As the system has the washboard potential

$$V_{\rm wash} = -2WI_0 \cos(\Delta\theta) - W\kappa_2 \left(\frac{N_2}{N_0}\right)^2 \Delta\theta, \tag{24.73}$$

the condition for the extremal of $V_{\rm wash}$ is given by

$$\sin(\Delta\theta) = \frac{\kappa_2}{2I_0}\left(\frac{N_2}{N_0}\right)^2. \tag{24.74}$$

If we assume that the variation of the parameters is sufficiently slow and approximate them as constant, the critical strength of the loss rate where the solution of $\Delta\theta$ becomes unstable is given by

$$\kappa_{2c} \simeq 2I_0. \tag{24.75}$$

We can numerically solve Eq. (24.70), (24.71), and (24.72), and the results are shown in Fig. 24.7. We see that the results shown in Fig. 24.7(a1) and (b1) [Fig. 24.7(a2) and (b2)] are qualitatively the same as those in Fig. 24.3(c1) and (d1) [Fig. 24.3(c2) and (d2)] in the main text, respectively.

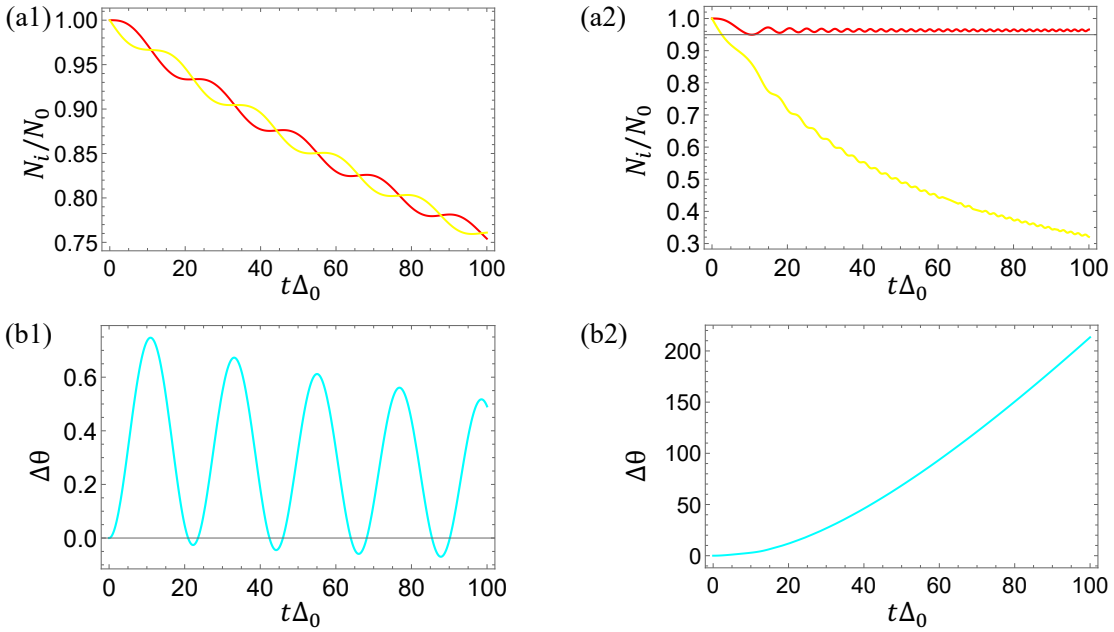


Figure 24.7: Numerical solution of N_1/N_0 (red), N_2/N_0 (yellow), and $\Delta\theta$ (light blue) in Eqs. (24.70), (24.71), and (24.72) with $W = 5.11\Delta_0$ and $I_0 = 0.009\Delta_0$. The loss rate κ_2 is set to $\kappa_2 = 0.006\Delta_0$ in (a1) and (b1), and $\kappa_2 = 0.02\Delta_0$ in (a2) and (b2).

The time-evolution equation of the phase [Eq. (24.64)] can be understood as a consequence of the gauge transformation ($\Delta_i(t) = \exp(-2i\int_0^t dt\mu_{i\mathrm{eff}}(t))|\Delta_i(t)|$), which reflects the conjugate nature of the particle number and the phase. From a more phenomenological point of view, Eq. (S47) can be understood using the time-dependent Ginzburg-Landau (GL) theory. Here we note that, strictly speaking, the GL theory cannot be applied to zero-temperature superfluids considered in our study, since the Taylor expansion of the free energy requires that the system should be close to the transition temperature. In nonequilibrium situations, the time-dependent GL theory cannot be applied to gapped superfluids and nonadiabatic regimes, since the time scale of the order-parameter dynamics becomes shorter than the lifetime of quasiparticles and quasiparticle contributions cannot be neglected [8, 32]. Moreover, for the application of the time-dependent GL theory, it is required that the deviation from equilibrium is sufficiently small, which cannot be satisfied in our dissipative superfluids which are driven far from equilibrium. However, we assume below that the GL theory could be phenomenologically used to investigate the dynamics of the dissipative superfluids. We start from the phenomenological GL equation of the superfluid condensate, which is expanded in a series of the order parameter

$$-\Gamma\left(\frac{\partial\Delta}{\partial t}+\frac{2ie\varphi}{\hbar}\Delta\right)=a\Delta+b|\Delta|^2\Delta, \tag{24.76}$$

where Γ is a positive constant, φ is the scalar potential, e is the charge, and we have assumed that the order parameter is spatially uniform. Here, we have introduced complex-valued coefficients a and b, which might describe the effect of the atom loss. However, we remark on the validity of this treatment below. In our study, the scalar potential does not exist. Instead, we introduce an effective chemical potential μ_{eff} that is determined from the total particle number of the system as follows:

$$-\Gamma\left(\frac{\partial\Delta}{\partial t}+2i\mu_{\mathrm{eff}}\Delta\right)=a\Delta+b|\Delta|^2\Delta. \tag{24.77}$$

By rewriting the equation in terms of the phase θ and the amplitude $|\Delta|$ of the order parameter (the latter is proportional to the square root of the superfluid density), we obtain the equation

of motion for the phase as

$$\frac{\partial\theta}{\partial t} = -2\mu_{\rm eff} - \frac{{\rm Im}(a) + {\rm Im}(b)|\Delta|^2}{\Gamma}. \tag{24.78}$$

For two superfluids connected via a Josephson junction, we similarly obtain

$$\frac{\partial(\theta_2 - \theta_1)}{\partial t} = -2(\mu_{2\rm eff} - \mu_{1\rm eff}) - \frac{{\rm Im}(a_2) + {\rm Im}(b_2)|\Delta_2|^2}{\Gamma_2}, \tag{24.79}$$

where the subscript 1 and 2 label the two superfluids, and we have introduced the effect of loss to superfluid 2. If the coefficients a and b are real, we arrive at Eq. (24.64):

$$\frac{\partial\Delta\theta}{\partial t} = -2\Delta\mu_{\rm eff}. \tag{24.80}$$

We note, however, that Eqs. (24.62) and (24.63) cannot be obtained from the GL theory, since N_1 and N_2 are the total particle numbers of the two superfluids, which are not directly related to the amplitude of the order parameter for dissipative superfluids. In the case of complex coefficients a and b, one might at first sight think that the effect of loss can be described by regarding the second term in Eq. (24.79) as an effective change in the chemical potential, which reads $\Delta\mu \simeq W(N - N_0)/N_0 \propto |\Delta|^2 - |\Delta_0|^2$. However, this result of the phenomenological treatment of the time-dependent GL theory has a serious problem. To see this, let us differentiate this equation with respect to time as $dN/dt \propto |\Delta|d|\Delta|/dt$. As the amplitude of the order parameter oscillates as shown in Fig. 2(a) in the main text, the equation $dN/dt \propto |\Delta|d|\Delta|/dt$ indicates that the total particle number of the system can increase since the oscillating part $d|\Delta|/dt$ can take a positive value. Such an increase of the particle number is unphysical since our system has no particle gain. As the correct equation obtained from the microscopic theory is $dN/dt \propto -|\Delta|^2$ [Eq. (24.12) in the main text], which indicates that the total particle number of the system monotonically decreases, Eq. (24.79) does not correctly describe the dynamics associated with the loss in the total particle number. Thus, it is highly nontrivial to consistently describe the dynamic evolution of the order parameter, collective excitations, and the dynamical phase transition caused by the particle loss in dissipative fermionic superfluids on the basis of the phenomenological GL theory.

If we wish to derive the time-dependent GL equation from the formalism based on the closed-time-contour path integral, we should start from a generating functional like Eq. (3) in the main text, and introduce the order parameter by performing the Hubbard-Stratonovich transformation. Then, by integrating out the fermionic degrees of freedom, we arrive at the action with respect to the order parameter. By expanding the exact action $S(\Delta, \Delta^*)$ around its extremal value $S(\Delta_0, \Delta_0^*)$, where Δ_0 is usually the equilibrium value that satisfies the BCS gap equation, the time-dependent GL equation is obtained from a saddle-point equation $\partial S(\Delta, \Delta^*)/\partial\Delta^*(r, t) = 0$ [97]. However, we have to pay careful attention to the condition that is assumed in the standard derivation: the deviation of the order parameter Δ around its extremal value Δ_0 should be small enough for the Taylor expansion to be justified. We also note that the standard derivation assumes that the total particle number of the system does not change. In contrast, as the particle number significantly changes in our system, the phase of the order parameter rotates and largely deviates from the stationary value as shown in Fig. 2 in the main text. Thus, a time-dependent GL theory that fully incorporates the change in particle number needs highly nontrivial consideration, which deserves further study.

Part XIII
Other Experiments

Part XIV
Localization: Other Articles

Part XV
Appendix

.1 Appendix

.1.1 Literature

Bibliography

References

.2 Bibliography from Most Useful Articles

From Generalized Gibbs ensemble in integrable lattice models by Vidmar

References

[1] E. Lieb, T. Schultz, and D. Mattis, Two soluble models of an antiferromagnetic chain, Annals of Physics **16**, 407 (1961).

[2] B. Sutherland, Beautiful Models (World Scientific, Singapore, 2004).

[3] T. Niemeijer, Some exact calculations on a chain of spins 1/2, Physica **36**, 377 (1967).

[4] P. Mazur, Non-ergodicity of phase functions in certain systems, Physica **43**, 533 (1969).

[5] E. Barouch and M. Dresden, Exact time-dependent analysis for the one-dimensional XY model, Phys. Rev. Lett. **23**, 114 (1969).

[6] E. Barouch, B. M. McCoy, and M. Dresden, Statistical mechanics of the XY model. I, Phys. Rev. A **2**, 1075 (1970).

[7] E. Barouch and B. M. McCoy, Statistical mechanics of the XY model. III, Phys. Rev. A **3**, 2137 (1971).

[8] H. Castella, X. Zotos, and P. Prelovšek, Integrability and ideal conductance at finite temperatures, Phys. Rev. Lett. **74**, 972 (1995).

[9] X. Zotos, F. Naef, and P. Prelovšek, Transport and conservation laws, Phys. Rev. B **55**, 11029 (1997).

[10] T. Prosen, Open XXZ spin chain: Nonequilibrium steady state and a strict bound on ballistic transport, Phys. Rev. Lett. **106**, 217206 (2011).

[11] X. Zotos and P. Prelovšek, Transport in one dimensional quantum systems, Strong interactions in low dimensions, edited by D. Baeriswyl and L. Degiorgi (Springer Netherlands, 2004).

[12] F. Heidrich-Meisner, A. Honecker, and W. Brenig, Transport in quasi one-dimensional spin-1/2 systems, Eur. Phys. J. Special Topics **151**, 135 (2007).

[13] R. Vasseur and J. E. Moore, Nonequilibrium quantum dynamics and transport: from integrability to many-body localization, J. Stat. Mech. 064010 (2016).

[14] I. Bloch, J. Dalibard, and W. Zwerger, Many-body physics with ultracold gases, Rev. Mod. Phys. **80**, 885 (2008).

[15] M. A. Cazalilla, R. Citro, T. Giamarchi, E. Orignac, and M. Rigol, One dimensional bosons: From condensed matter systems to ultracold gases, Rev. Mod. Phys. **83**, 1405 (2011).

[16] H. Moritz, T. Stöferle, M. Köhl, and T. Esslinger, Exciting collective oscillations in a trapped 1D gas, Phys. Rev. Lett. **91**, 250402 (2003).

[17] T. Kinoshita, T. Wenger, and D. S. Weiss, Observation of a one-dimensional Tonks-Girardeau gas, Science **305**, 1125 (2004).

[18] B. Paredes, A. Widera, V. Murg, O. Mandel, S. Fölling, I. Cirac, G. Shlyapnikov, T. H. Hänsch, and I. Bloch, Tonks-Girardeau gas of ultracold atoms in an optical lattice, Nature (London) **429**, 277 (2004).

[19] R. Folman, P. Krüger, D. Cassettari, B. Hessmo, T. Maier, and J. Schmiedmayer, Controlling cold atoms using nanofabricated surfaces: Atom chips, Phys. Rev. Lett. **84**, 4749 (2000).

[20] M. Greiner, O. Mandel, T. Hänsch, and I. Bloch, Collapse and revival of the matter wave field of a Bose-Einstein condensate, Nature (London) **419**, 51 (2002).

[21] S. Will, T. Best, U. Schneider, L. Hackermüller, D.-S. Lühmann, and I. Bloch, Time-resolved observation of coherent multi-body interactions in quantum phase revivals, Nature (London) **465**, 197 (2010).

[22] S. Will, D. Iyer, and M. Rigol, Observation of coherent quench dynamics in a metallic many-body state of fermionic atoms, Nature Communications **6**, 6009 (2015).

[23] T. Kinoshita, T. Wenger, and D. S. Weiss, A quantum Newton's cradle, Nature (London) **440**, 900 (2006).

[24] S. Hofferberth, I. Lesanovsky, B. Fisher, T. Schumm, and J. Schmiedmayer, Non-equilibrium coherence dynamics in one-dimensional Bose gases, Nature (London) **449**, 324 (2007).

[25] M. Gring, M. Kuhnert, T. Langen, T. Kitagawa, B. Rauer, M. Schreitl, I. Mazets, D. A. Smith, E. Demler, and J. Schmiedmayer, Relaxation and prethermalization in an isolated quantum system, Science **337**, 1318 (2012).

[26] T. Langen, S. Erne, R. Geiger, B. Rauer, T. Schweigler, M. Kuhnert, W. Rohringer, I. E. Mazets, T. Gasenzer, and J. Schmiedmayer, Experimental observation of a generalized Gibbs ensemble, Science **348**, 207 (2015).

[27] T. Langen, T. Gasenzer, and J. Schmiedmayer, Prethermalization and universal dynamics in near-integrable quantum systems, J. Stat. Mech. 064009 (2016).

[28] J. P. Ronzheimer, M. Schreiber, S. Braun, S. S. Hodgman, S. Langer, I. P. McCulloch, F. Heidrich-Meisner, I. Bloch, and U. Schneider, Expansion dynamics of interacting bosons in homogeneous lattices in one and two dimensions, Phys. Rev. Lett. **110**, 205301 (2013).

[29] L. Vidmar, J. P. Ronzheimer, M. Schreiber, S. Braun, S. S. Hodgman, S. Langer, F. Heidrich-Meisner, I. Bloch, and U. Schneider, Dynamical quasicondensation of hard-core bosons at finite momenta, Phys. Rev. Lett. **115**, 175301 (2015).

[30] J. Simon, W. S. Bakr, R. Ma, M. E. Tai, P. M. Preiss, and M. Greiner, Quantum simulation of antiferromagnetic spin chains in an optical lattice, Nature (London) **472**, 307 (2011).

[31] F. Meinert, M. J. Mark, E. Kirilov, K. Lauber, P. Weinmann, A. J. Daley, and H.-C. Nägerl, Quantum quench in an atomic one-dimensional Ising chain, Phys. Rev. Lett. **111**, 053003 (2013).

[32] T. Fukuhara, A. Kantian, M. Endres, M. Cheneau, P. Schauß, S. Hild, D. Bellem, U. Schollwöck, T. Giamarchi, C. Gross, I. Bloch, and S. Kuhr, Quantum dynamics of a mobile spin impurity, Nature Physics **9**, 235 (2013).

[33] T. Fukuhara, P. Schauß, M. Endres, S. Hild, M. Cheneau, I. Bloch, and C. Gross, Microscopic observation of magnon bound states and their dynamics, Nature (London) **502**, 76 (2013).

[34] S. Hild, T. Fukuhara, P. Schauß, J. Zeiher, M. Knap, E. Demler, I. Bloch, and C. Gross, Far-from-equilibrium spin transport in Heisenberg quantum magnets, Phys. Rev. Lett. **113**, 147205 (2014).

[35] M. Rigol, V. Dunjko, V. Yurovsky, and M. Olshanii, Relaxation in a completely integrable many-body quantum system: An ab initio study of the dynamics of the highly excited states of 1D lattice hard-core bosons, Phys. Rev. Lett. **98**, 050405 (2007).

[36] M. Rigol, A. Muramatsu, and M. Olshanii, Hard-core bosons on optical superlattices: Dynamics and relaxation in the superfluid and insulating regimes, Phys. Rev. A **74**, 053616 (2006).

[37] E. T. Jaynes, Information theory and statistical mechanics, Phys. Rev. **106**, 620 (1957).

[38] E. T. Jaynes, Information theory and statistical mechanics. II, Phys. Rev. **108**, 171 (1957).

[39] M. A. Cazalilla, Effect of suddenly turning on interactions in the Luttinger model, Phys. Rev. Lett. **97**, 156403 (2006).

[40] A. Iucci and M. A. Cazalilla, Quantum quench dynamics of the Luttinger model, Phys. Rev. A **80**, 063619 (2009).

[41] M. A. Cazalilla, A. Iucci, and M.-C. Chung, Thermalization and quantum correlations in exactly solvable models, Phys. Rev. E **85**, 011133 (2012).

[42] M. Kollar and M. Eckstein, Relaxation of a one-dimensional Mott insulator after an interaction quench, Phys. Rev. A **78**, 013626 (2008).

[43] A. Iucci and M. A. Cazalilla, Quantum quench dynamics of the sine-Gordon model in some solvable limits, New J. Phys. **12**, 055019 (2010).

[44] P. Calabrese, F. H. L. Essler, and M. Fagotti, Quantum quench in the transverse-field Ising chain, Phys. Rev. Lett. **106**, 227203 (2011).

[45] P. Calabrese, F. H. L. Essler, and M. Fagotti, Quantum quench in the transverse field Ising chain: I. time evolution of order parameter correlators, J. Stat. Mech. P07016 (2012).

[46] P. Calabrese, F. H. L. Essler, and M. Fagotti, Quantum quenches in the transverse field Ising chain: II. stationary state properties, J. Stat. Mech. P07022 (2012).

[47] F. H. L. Essler, S. Evangelisti, and M. Fagotti, Dynamical correlations after a quantum quench, Phys. Rev. Lett. **109**, 247206 (2012).

[48] M. Fagotti, Finite-size corrections versus relaxation after a sudden quench, Phys. Rev. B **87**, 165106 (2013).

[49] M. Fagotti and F. H. L. Essler, Reduced density matrix after a quantum quench, Phys. Rev. B **87**, 245107 (2013).

[50] L. Bucciantini, M. Kormos, and P. Calabrese, Quantum quenches from excited states in the Ising chain, J. Phys. A: Math. Theor. **47**, 175002 (2014).

[51] C. Gramsch and M. Rigol, Quenches in a quasidisordered integrable lattice system: Dynamics and statistical description of observables after relaxation, Phys. Rev. A **86**, 053615 (2012).

[52] T. M. Wright, M. Rigol, M. J. Davis, and K. V. Kheruntsyan, Nonequilibrium dynamics of one-dimensional hard-core anyons following a quench: Complete relaxation of one-body observables, Phys. Rev. Lett. **113**, 050601 (2014).

[53] J.-S. Caux and R. M. Konik, Constructing the generalized Gibbs ensemble after a quantum quench, Phys. Rev. Lett. **109**, 175301 (2012).

[54] J. Mossel and J.-S. Caux, Exact time evolution of space- and time-dependent correlation functions after an interaction quench in the one-dimensional Bose gas, New J. Phys. **14**, 075006 (2012).

[55] M. Collura, S. Sotiriadis, and P. Calabrese, Equilibration of a Tonks-Girardeau gas following a trap release, Phys. Rev. Lett. **110**, 245301 (2013).

[56] M. Collura, S. Sotiriadis, and P. Calabrese, Quench dynamics of a Tonks-Girardeau gas released from a harmonic trap, J. Stat. Mech. P09025 (2013).

[57] B. Pozsgay, Quantum quenches and generalized Gibbs ensemble in a Bethe Ansatz solvable lattice model of interacting bosons, J. Stat. Mech. P10045 (2014).

[58] S. Sotiriadis and P. Calabrese, Validity of the GGE for quantum quenches from interacting to noninteracting models, J. Stat. Mech. P07024 (2014).

[59] G. Goldstein and N. Andrei, Equilibration and generalized Gibbs ensemble for hard wall boundary conditions, Phys. Rev. B **92**, 155103 (2015).

[60] P. Calabrese and J. Cardy, Quantum quenches in extended systems, J. Stat. Mech. P06008 (2007).

[61] D. Fioretto and G. Mussardo, Quantum quenches in integrable field theories, New J. Phys. **12**, 055015 (2010).

[62] G. Mussardo, Infinite-time average of local fields in an integrable quantum field theory after a quantum quench, Phys. Rev. Lett. **111**, 100401 (2013).

[63] J. Cardy, Quantum quenches to a critical point in one dimension: some further results, J. Stat. Mech. 023103 (2016).

[64] B. Pozsgay, The generalized Gibbs ensemble for Heisenberg spin chains, J. Stat. Mech. P07003 (2013).

[65] M. Fagotti, M. Collura, F. H. L. Essler, and P. Calabrese, Relaxation after quantum quenches in the spin-$\frac{1}{2}$ Heisenberg XXZ chain, Phys. Rev. B **89**, 125101 (2014).

[66] M. Mierzejewski, P. Prelovšek, and T. Prosen, Breakdown of the generalized Gibbs ensemble for current-generating quenches, Phys. Rev. Lett. **113**, 020602 (2014).

[67] B. Wouters, J. De Nardis, M. Brockmann, D. Fioretto, M. Rigol, and J.-S. Caux, Quenching the anisotropic Heisenberg chain: Exact solution and generalized Gibbs ensemble predictions, Phys. Rev. Lett. **113**, 117202 (2014).

[68] B. Pozsgay, M. Mestyán, M. A. Werner, M. Kormos, G. Zaránd, and G. Takács, Correlations after quantum quenches in the XXZ spin chain: Failure of the generalized Gibbs ensemble, Phys. Rev. Lett. **113**, 117203 (2014).

[69] E. Ilievski, J. De Nardis, B. Wouters, J.-S. Caux, F. H. L. Essler, and T. Prosen, Complete generalized Gibbs ensembles in an interacting theory, Phys. Rev. Lett. **115**, 157201 (2015).

[70] F. H. L. Essler and M. Fagotti, Quench dynamics and relaxation in isolated integrable quantum spin chains, J. Stat. Mech. 064002 (2016).

[71] A. C. Cassidy, C. W. Clark, and M. Rigol, Generalized thermalization in an integrable lattice system, Phys. Rev. Lett. **106**, 140405 (2011).

[72] J. M. Deutsch, Quantum statistical mechanics in a closed system, Phys. Rev. A **43**, 2046 (1991).

[73] M. Srednicki, Chaos and quantum thermalization, Phys. Rev. E **50**, 888 (1994).

[74] M. Rigol, V. Dunjko, and M. Olshanii, Thermalization and its mechanism for generic isolated quantum systems, Nature (London) **452**, 854 (2008).

[75] T. Holstein and H. Primakoff, Field dependence of the intrinsic domain magnetization of a ferromagnet, Phys. Rev. **58**, 1098 (1940).

[76] M. Rigol, Finite-temperature properties of hard-core bosons confined on one-dimensional optical lattices, Phys. Rev. A **72**, 063607 (2005).

[77] P. Jordan and E. Wigner, Über das Paulische Aquivalenzverbot, Z. Phys. **47**, 631 (1928).

[78] M. Rigol and A. Muramatsu, Universal properties of hard-core bosons confined on one-dimensional lattices, Phys. Rev. A **70**, 031603 (2004).

[79] M. Rigol and A. Muramatsu, Ground-state properties of hard-core bosons confined on one-dimensional optical lattices, Phys. Rev. A **72**, 013604 (2005).

[80] M. Rigol and A. Muramatsu, Free expansion of impenetrable bosons on one-dimensional optical lattices, Mod. Phys. Lett. B **19**, 861 (2005).

[81] S. Katsura, Statistical mechanics of the anisotropic linear Heisenberg model, Phys. Rev. **127**, 1508 (1962).

[82] S. Sachdev, Quantum Phase Transitions (Cambridge University Press, New York, 2011).

[83] M. Mierzejewski, P. Prelovšek, and T. Prosen, Identifying local and quasilocal conserved quantities in integrable systems, Phys. Rev. Lett. **114**, 140601 (2015).

[84] E. Ilievski, M. Medenjak, and T. Prosen, Quasilocal conserved operators in the isotropic Heisenberg spin-1/2 chain, Phys. Rev. Lett. **115**, 120601 (2015).

[85] E. Ilievski, M. Medenjak, T. Prosen, and L. Zadnik, Quasilocal charges in integrable lattice systems, J. Stat. Mech. 064008 (2016).

[86] M. Rigol, Breakdown of thermalization in finite one-dimensional systems, Phys. Rev. Lett. **103**, 100403 (2009).

[87] M. Rigol, Quantum quenches and thermalization in one-dimensional fermionic systems, Phys. Rev. A **80**, 053607 (2009).

[88] S. Sorg, L. Vidmar, L. Pollet, and F. Heidrich-Meisner, Relaxation and thermalization in the one-dimensional Bose-Hubbard model: A case study for the interaction quantum quench from the atomic limit, Phys. Rev. A **90**, 033606 (2014).

[89] M. Rigol and M. Fitzpatrick, Initial-state dependence of the quench dynamics in integrable quantum systems, Phys. Rev. A **84**, 033640 (2011).

[90] L. C. Venuti and P. Zanardi, Gaussian equilibration, Phys. Rev. E **87**, 012106 (2013).

[91] S. Ziraldo, A. Silva, and G. E. Santoro, Relaxation dynamics of disordered spin chains: Localization and the existence of a stationary state, Phys. Rev. Lett. **109**, 247205 (2012).

[92] S. Ziraldo and G. E. Santoro, Relaxation and thermalization after a quantum quench: Why localization is important, Phys. Rev. B **87**, 064201 (2013).

[93] K. He, L. F. Santos, T. M. Wright, and M. Rigol, Single-particle and many-body analyses of a quasiperiodic integrable system after a quench, Phys. Rev. A **87**, 063637 (2013).

[94] J. Mossel, G. Palacios, and J.-S. Caux, Geometric quenches in quantum integrable systems, J. Stat. Mech. L09001 (2010).

[95] V. Alba and F. Heidrich-Meisner, Entanglement spreading after a geometric quench in quantum spin chains, Phys. Rev. B **90**, 075144 (2014).

[96] M. Fagotti, On conservation laws, relaxation and pre-relaxation after a quantum quench, J. Stat. Mech. P03016 (2014).

[97] S. Sachdev and A. P. Young, Low temperature relaxational dynamics of the Ising chain in a transverse field, Phys. Rev. Lett. **78**, 2220 (1997).

[98] F. Iglói and H. Rieger, Long-range correlations in the nonequilibrium quantum relaxation of a spin chain, Phys. Rev. Lett. **85**, 3233 (2000).

[99] K. Sengupta, S. Powell, and S. Sachdev, Quench dynamics across quantum critical points, Phys. Rev. A **69**, 053616 (2004).

[100] D. Rossini, A. Silva, G. Mussardo, and G. E. Santoro, Effective thermal dynamics following a quantum quench in a spin chain, Phys. Rev. Lett. **102**, 127204 (2009).

[101] D. Rossini, S. Suzuki, G. Mussardo, G. E. Santoro, and A. Silva, Long time dynamics following a quench in an integrable quantum spin chain: Local versus nonlocal operators and effective thermal behavior, Phys. Rev. B **82**, 144302 (2010).

[102] F. Iglói and H. Rieger, Quantum relaxation after a quench in systems with boundaries, Phys. Rev. Lett. **106**, 035701 (2011).

[103] H. Rieger and F. Iglói, Semiclassical theory for quantum quenches in finite transverse Ising chains, Phys. Rev. B **84**, 165117 (2011).

[104] A. Polkovnikov, Microscopic diagonal entropy and its connection to basic thermodynamic relations, Ann. Phys. **326**, 486 (2011).

[105] L. F. Santos, A. Polkovnikov, and M. Rigol, Entropy of isolated quantum systems after a quench, Phys. Rev. Lett. **107**, 040601 (2011).

[106] V. Gurarie, Global large time dynamics and the generalized Gibbs ensemble, J. Stat. Mech. P02014 (2013).

[107] M. Kormos, L. Bucciantini, and P. Calabrese, Stationary entropies after a quench from excited states in the Ising chain, EPL (Europhysics Letters) **107**, 40002 (2014).

[108] M. Collura, M. Kormos, and P. Calabrese, Stationary entanglement entropies following an interaction quench in 1D Bose gas, J. Stat. Mech. P01009 (2014).

[109] M. Rigol, Quantum quenches in the thermodynamic limit, Phys. Rev. Lett. **112**, 170601 (2014).

[110] M. Rigol, Fundamental asymmetry in quenches between integrable and nonintegrable systems, Phys. Rev. Lett. **116**, 100601 (2016).

[111] K. He and M. Rigol, Initial-state dependence of the quench dynamics in integrable quantum systems. II. Thermal states, Phys. Rev. A **85**, 063609 (2012).

[112] L. D'Alessio, Y. Kafri, A. Polkovnikov, and M. Rigol, From quantum chaos and eigenstate thermalization to statistical mechanics and thermodynamics, arXiv:1509.06411.

[113] J.-S. Caux and F. H. L. Essler, Time evolution of local observables after quenching to an integrable model, Phys. Rev. Lett. **110**, 257203 (2013).

[114] J. De Nardis, B. Wouters, M. Brockmann, and J.-S. Caux, Solution for an interaction quench in the Lieb-Liniger Bose gas, Phys. Rev. A **89**, 033601 (2014).

[115] J.-S. Caux, The quench action, J. Stat. Mech. 064006 (2016).

[116] E. A. Yuzbashyan, Generalized microcanonical and Gibbs ensembles in classical and quantum integrable dynamics, Annals of Physics **367**, 288 (2016).

[117] T. N. Ikeda, Y. Watanabe, and M. Ueda, Finite-size scaling analysis of the eigenstate thermalization hypothesis in a one-dimensional interacting Bose gas, Phys. Rev. E **87**, 012125 (2013).

[118] V. Alba, Eigenstate thermalization hypothesis and integrability in quantum spin chains, Phys. Rev. B **91**, 155123 (2015).

[119] R. Nandkishore and D. A. Huse, Many-body localization and thermalization in quantum statistical mechanics, Annual Review of Condensed Matter Physics **6**, 15 (2015).

[120] E. Altman and R. Vosk, Universal dynamics and renormalization in many-body-localized systems, Annual Review of Condensed Matter Physics **6**, 383 (2015).

From Stable Quantum-Correlated Many Body States through Engineered Dissipation

References

[1] I. Bloch, J. Dalibard, W. Zwerger, *Rev. Mod. Phys.* **80**, 885 (2008).

[2] R. Blatt, C. F. Roos, *Nat. Phys.* **8**, 277 (2012).

[3] E. Altman, *et al.*, *PRX Quantum* **2**, 017003 (2021).

[4] M. Cerezo, *et al.*, *Nat. Rev. Phys.* **3**, 625 (2021).

[5] J. R. McClean, S. Boixo, V. N. Smelyanskiy, R. Babbush, H. Neven, *Nat. Commun.* **9**, 4812 (2018).

[6] J. Q. You, Z. D. Wang, W. Zhang, F. Nori, *Sci. Rep.* **4**, 5535 (2014).

[7] A. Kitaev, *Ann. Phys.* **303**, 2 (2003).

[8] M. B. Plenio, S. F. Huelga, A. Beige, P. L. Knight, *Phys. Rev. A* **59**, 2468 (1999).

[9] B. Kraus, *et al.*, *Phys. Rev. A* **78**, 042307 (2008).

[10] S. Diehl, *et al.*, *Nat. Phys.* **4**, 878 (2008).

[11] F. Verstraete, M. M. Wolf, J. Ignacio Cirac, *Nat. Phys.* **5**, 633 (2009).

[12] C. Aron, M. Kulkarni, H. E. Türeci, *Phys. Rev. X* **6**, 011032 (2016).

[13] P. M. Harrington, E. J. Mueller, K. W. Murch, *Nat. Rev. Phys.* **4**, 660 (2022).

[14] M. Raghunandan, F. Wolf, C. Ospelkaus, P. O. Schmidt, H. Weimer, *Sci. Adv.* **6**, eaaw9268 (2020).

[15] S. Polla, Y. Herasymenko, T. E. O'Brien, *Phys. Rev. A* **104**, 012414 (2021).

[16] J. T. Barreiro, *et al.*, *Nature* **470**, 486 (2011).

[17] Y. Lin, *et al.*, *Nature* **504**, 415 (2013).

[18] S. Shankar, *et al.*, *Nature* **504**, 419 (2013).

[19] R. Ma, *et al.*, *Nature* **566**, 51 (2019).

[20] R. Acharya, *et al.*, *Nature* **614**, 676 (2023).

[21] M. McEwen, *et al.*, *Nat. Commun.* **12**, 1761 (2021).

[22] K. C. Miao, *et al.*, *Nat. Phys.* (2023).

[23] M. Ziman, P. Štelmachovič, V. Bužek, *Open Syst. Inf. Dyn.* **12**, 81 (2005).

[24] S. Boixo, *et al.*, *Nat. Phys.* **14**, 595 (2018).

[25] W. K. Wootters, *Phys. Rev. Lett.* **80**, 2245 (1998).

[26] F. Arute, *et al.*, *Science* **369**, 1084 (2020).

[27] D. J. Yates, F. H. L. Essler, A. Mitra, *Phys. Rev. B* **99**, 205419 (2019).

[28] X. Mi, *et al.*, *Science* **378**, 785 (2022).

[29] R. McWeeny, *Rev. Mod. Phys.* **32**, 335 (1960).

[30] R. Islam, *et al.*, *Nature* **528**, 77 (2015).

[31] A. Mazurenko, *et al.*, *Nature* **545**, 462 (2017).

[32] S. Ebadi, *et al.*, *Nature* **595**, 227 (2021).

[33] T. Brydges, *et al.*, *Science* **364**, 260 (2019).

[34] E. Lieb, T. Schultz, D. Mattis, *Ann. Phys.* **16**, 407 (1961).

[35] B. Bertini, *et al.*, *Rev. Mod. Phys.* **93**, 025003 (2021).

[36] A. Scheie, *et al.*, *Nat. Phys.* **17**, 726 (2021).

[37] D. Wei, *et al.*, *Science* **376**, 716 (2022).

[38] N. Keenan, N. F. Robertson, T. Murphy, S. Zhuk, J. Goold, *Npj Quantum Inf.* **9**, 72 (2023).

[39] V. Gritsev, A. Polkovnikov, *SciPost Phys.* **2**, 021 (2017).

[40] A. Morvan, *et al.*, *Nature* **612**, 240 (2022).

[41] X. Zotos, P. Prelovšek, *Phys. Rev. B* **53**, 983 (1996).

[42] M. Žnidarič, *Phys. Rev. Lett.* **106**, 220601 (2011).

[43] The current from Q_{26} to $Q_{\mathrm{a},2}$ should in principle be subtracted from $J(Q_1)$ to account for the particle loss into the drain. Since we are focusing on early time ($d < 15$) dynamics, this current is near or exactly 0 and does not affect the transport exponent. See SM for an explicit verification.

[44] B. Buča, C. Booker, M. Medenjak, D. Jaksch, *New J. Phys.* **22**, 123040 (2020).

[45] T. c. v. Prosen, *Phys. Rev. Lett.* **107**, 137201 (2011).

[46] E. Kapit, P. Roushan, C. Neill, S. Boixo, V. Smelyanskiy, *Phys. Rev. Res.* **2**, 043042 (2020).

[47] N. C. Harris, *et al.*, *Nat. Photonics* **11**, 447 (2017).

[48] S. Diehl, E. Rico, M. A. Baranov, P. Zoller, *Nat. Phys.* **7**, 971 (2011).

[49] C.-E. Bardyn, *et al.*, *New J. Phys.* **15**, 085001 (2013).

[50] E. Kapit, M. Hafezi, S. H. Simon, *Phys. Rev. X* **4**, 031039 (2014).

[51] X. Mi, *et al.*, *Nature* **601**, 531 (2022).

[52] X. Mi, *et al.*, *Science* **374**, 1479 (2021).

[53] P. V. Klimov, *et al.*, *Phys. Rev. Lett.* **121**, 090502 (2018).

[54] P. V. Klimov, J. Kelly, J. M. Martinis, H. Neven, *Preprint at https://arxiv.org/abs/2006.04594* (2020).

[55] F. Arute, *et al.*, *Nature* **574**, 505 (2019).

[56] C. Neill, *et al.*, *Nature* **594**, 508 (2021).

[57] K. W. Murch, *et al.*, *Phys. Rev. Lett.* **109**, 183602 (2012).

[58] Y. Lu, *et al.*, *Phys. Rev. Lett.* **119**, 150502 (2017).

[59] A. M. Kaufman, *et al.*, *Science* **353**, 794 (2016).

[60] J. C. Hoke, *et al.*, *Nature* **622**, 481 (2023).

[61] I. Peschel, *Journal of Physics A: Mathematical and General* **36**, L205 (2003).

[62] Z. Jiang, K. J. Sung, K. Kechedzhi, V. N. Smelyanskiy, S. Boixo, *Phys. Rev. Appl.* **9**, 044036 (2018).

[63] F. Verstraete, J. J. García-Ripoll, J. I. Cirac, *Phys. Rev. Lett.* **93**, 207204 (2004).

[64] G. Vidal, *Phys. Rev. Lett.* **93**, 040502 (2004).

[65] M. Fishman, S. R. White, E. M. Stoudenmire, *SciPost Phys. Codebases* p. 4 (2022).

[66] B. Li, J. Wang, *Phys. Rev. Lett.* **91**, 044301 (2003).

From Stark many-body localization

References

[350] P. W. Anderson, Phys. Rev. **109**, 1492 (1958).

[2] E. Abrahams, P. W. Anderson, D. C. Licciardello, and T. V. Ramakrishnan, Phys. Rev. Lett. **42**, 673 (1979).

[3] D. M. Basko, I. L. Aleiner, and B. L. Altshuler, Ann. Phys. (N. Y). **321**, 1126 (2006).

[359] I. V. Gornyi, A. D. Mirlin, and D. G. Polyakov, Phys. Rev. Lett. **95**, 206603 (2005).

[5] J. Z. Imbrie, J. Stat. Phys. **163**, 998 (2016).

[6] R. Nandkishore and D. A. Huse, Annu. Rev. Condens. Matter Phys. **6**, 15 (2014).

[7] D. A. Huse, R. Nandkishore, and V. Oganesyan, Phys. Rev. B **90**, 174202 (2014).

[8] M. Žnidarič, T. Prosen, and P. Prelovšek, Physical Review B **77**, 064426 (2008).

[9] J. H. Bardarson, F. Pollmann, and J. E. Moore, Phys. Rev. Lett. **109**, 017202 (2012).

[10] M. Serbyn, Z. Papić, and D. A. Abanin, Phys. Rev. Lett. **110**, 260601 (2013).

[11] R. Vosk, D. A. Huse, and E. Altman, Phys. Rev. X **5**, 031032 (2015).

[12] K. Agarwal, S. Gopalakrishnan, M. Knap, M. Müller, and E. Demler, Phys. Rev. Lett. **114**, 160401 (2015).

[13] M. Žnidarič, A. Scardicchio, and V. K. Varma, Phys. Rev. Lett. **117**, 040601 (2016).

[14] Y. Bar Lev, G. Cohen, and D. R. Reichman, Phys. Rev. Lett. **114**, 100601 (2015).

[15] M. Schreiber, S. S. Hodgman, P. Bordia, H. P. Lüschen, M. H. Fischer, R. Vosk, E. Altman, U. Schneider, and I. Bloch, Science **349**, 842 (2015).

[16] P. Bordia, H. Lüschen, S. Scherg, S. Gopalakrishnan, M. Knap, U. Schneider, and I. Bloch, Phys. Rev. X **7**, 041047 (2017).

[13] J.-Y. Choi, S. Hild, J. Zeiher, P. Schauß, A. Rubio-Abadal, T. Yefsah, V. Khemani, D. A. Huse, I. Bloch, and C. Gross, Science **352**, 1547 (2016).

[18] M. Rigol, V. Dunjko, V. Yurovsky, and M. Olshanii, Phys. Rev. Lett. **98**, 050405 (2007).

[13] T. Kinoshita, T. Wenger, and D. S. Weiss, Nature **440**, 900 (2006).

[37] M. Van Horssen, E. Levi, and J. P. Garrahan, Phys. Rev. B **92**, 100305(R) (2015).

[21] J. M. Hickey, S. Genway, and J. P. Garrahan, J. Stat. Mech. Theory Exp. **5**, 054047 (2016).

[22] W. De Roeck and F. Huveneers, Commun. Math. Phys. **332**, 1017 (2014).

[23] A. Smith, J. Knolle, R. Moessner, and D. L. Kovrizhin, Phys. Rev. Lett. **119**, 176601 (2017).

[24] N. Y. Yao, C. R. Laumann, J. I. Cirac, M. D. Lukin, and J. E. Moore, Phys. Rev. Lett. **117**, 240601 (2016).

[25] A. Bols and W. De Roeck, J. Math. Phys. **59**, 021901 (2018).

[2] G. Wannier, Rev. Mod. Phys. **34**, 645 (1962).

[27] For a treatment of a metal-insulator transition in a uniform electric field, see [34].

[28] C. Hooley and J. Quintanilla, Phys. Rev. Lett. **93**, 080404 (2004).

[29] See Supplemental Material below for further details.

[30] A. Polkovnikov, Ann. Phys. (N. Y). **326**, 486 (2011).

[9] V. Oganesyan and D. A. Huse, Phys. Rev. B **75**, 155111 (2007).

[32] D. J. Luitz, N. Laflorencie, and F. Alet, Phys. Rev. B **91**, 081103(R) (2015).

[33] E. P. L. van Nieuwenburg, Y. Baum, and G. Refael, arXiv:1808.00471 (2018).

[34] V. Prigodin and B. Altshuler, Phys. Lett. A **137**, 301 (1989).

From Transport in Stark MB Loca Syst

References

[357] D. Basko, I. L. Aleiner, and B. L. Altshuler, Metal-insulator transition in a weakly interacting many-electron system with localized single-particle states, Ann. Phys. **321**, 1126 (2006).

[359] I. V. Gornyi, A. Mirlin, and D. Polyakov, Interacting Electrons in Disordered Wires: Anderson Localization and Low-T Transport, Phys. Rev. Lett. **95**, 206603 (2005).

[3] E. Altman and R. Vosk, Universal Dynamics and Renormalization in Many-Body-Localized Systems, Annu. Rev. Condens. Matter Phys. **6**, 383 (2015).

[356] R. Nandkishore and D. A. Huse, Many-Body Localization and Thermalization in Quantum Statistical Mechanics, Annu. Rev. Condens. Matter Phys. **6**, 15 (2015).

[5] R. Vasseur and J. E. Moore, Nonequilibrium quantum dynamics and transport: From integrability to many-body localization, J. Stat. Mech. Theory Exp. **2016**, 064010 (2016).

[6] D. A. Abanin and Z. Papić, Recent progress in many-body localization, Ann. Phys. **529**, 1700169 (2017).

[7] D. A. Abanin, E. Altman, I. Bloch, and M. Serbyn, Colloquium: Many-body localization, thermalization, and entanglement, Rev. Mod. Phys. **91**, 021001 (2019).

[8] D. M. Basko, I. L. Aleiner, and B. L. Altshuler, Possible experimental manifestations of the many-body localization, Phys. Rev. B **76**, 052203 (2007).

[9] M. Ovadia, D. Kalok, I. Tamir, S. Mitra, B. Sacépé, and D. Shahar, Evidence for a Finite-Temperature Insulator, Sci. Rep. **5**, 13503 (2015).

[10] M. Schreiber, S. S. Hodgman, P. Bordia, H. P. Luschen, M. H. Fischer, R. Vosk, E. Altman, U. Schneider, and I. Bloch, Observation of many-body localization of interacting fermions in a quasirandom optical lattice, Science **349**, 842 (2015).

[11] P. Bordia, H. P. Lüschen, S. S. Hodgman, M. Schreiber, I. Bloch, and U. Schneider, Coupling Identical one-dimensional Many-Body Localized Systems, Phys. Rev. Lett. **116**, 140401 (2016).

[12] J. Smith, A. Lee, P. Richerme, B. Neyenhuis, P. W. Hess, P. Hauke, M. Heyl, D. A. Huse, and C. Monroe, Many-body localization in a quantum simulator with programmable random disorder, Nat. Phys. **12**, 907 (2016).

[13] J.-Y. Choi, S. Hild, J. Zeiher, P. Schauss, A. Rubio-Abadal, T. Yefsah, V. Khemani, D. A. Huse, I. Bloch, and C. Gross, Exploring the many-body localization transition in two dimensions, Science **352**, 1547 (2016).

[14] M. Žnidarič, Dephasing-induced diffusive transport in the anisotropic Heisenberg model, New J. Phys. **12**, 043001 (2010).

[15] S. Gopalakrishnan, K. R. Islam, and M. Knap, Noise-Induced Subdiffusion in Strongly Localized Quantum Systems, Phys. Rev. Lett. **119**, 046601 (2017).

[16] A. Lazarides, A. Das, and R. Moessner, Fate of Many-Body Localization Under Periodic Driving, Phys. Rev. Lett. **115**, 030402 (2015).

[17] P. Ponte, Z. Papić, F. Huveneers, and D. A. Abanin, Many-Body Localization in Periodically Driven Systems, Phys. Rev. Lett. **114**, 140401 (2015).

[18] D. A. Abanin, W. De Roeck, and F. Huveneers, Theory of many-body localization in periodically driven systems, Ann. Phys. **372**, 1 (2016).

[19] E. Bairey, G. Refael, and N. H. Lindner, Driving induced many-body localization, Phys. Rev. B **96**, 020201 (2017).

[367] J. Z. Imbrie, On Many-Body Localization for Quantum Spin Chains, J. Stat. Phys. **163**, 998 (2016).

[21] P. W. Anderson, Absence of Diffusion in Certain Random Lattices, Phys. Rev. **109**, 1492 (1958).

[22] R. Nandkishore and A. C. Potter, Marginal Anderson localization and many-body delocalization, Phys. Rev. B **90**, 195115 (2014).

[23] X. Li, S. Ganeshan, J. H. Pixley, and S. Das Sarma, Many-Body Localization and Quantum Nonergodicity in a Model with a Single-Particle Mobility Edge, Phys. Rev. Lett. **115**, 186601 (2015).

[24] X. Li, J. H. Pixley, D.-L. Deng, S. Ganeshan, and S. Das Sarma, Quantum nonergodicity and fermion localization in a system with a single-particle mobility edge, Phys. Rev. B **93**, 184204 (2016).

[25] R. Modak, S. Ghosh, and S. Mukerjee, Criterion for the occurrence of many-body localization in the presence of a single-particle mobility edge, Phys. Rev. B **97**, 104204 (2018).

[26] R. Modak and S. Mukerjee, Many-Body Localization in the Presence of a Single-Particle Mobility Edge, Phys. Rev. Lett. **115**, 230401 (2015).

[27] K. Hyatt, J. R. Garrison, A. C. Potter, and B. Bauer, Many-body localization in the presence of a small bath, Phys. Rev. B **95**, 035132 (2017).

[28] Y. Bar Lev, D. R. Reichman, and Y. Sagi, Many-body localization in system with a completely delocalized single-particle spectrum, Phys. Rev. B **94**, 201116 (2016).

[29] R. Vasseur, A. J. Friedman, S. A. Parameswaran, and A. C. Potter, Particle-hole symmetry, many-body localization, and topological edge modes, Phys. Rev. B **93**, 134207 (2016).

[376] G. Carleo, F. Becca, M. Schiró, and M. Fabrizio, Localization and glassy dynamics of many-body quantum systems, Sci. Rep. **2**, 243 (2012).

[31] M. Schiulaz and M. Müller, Ideal quantum glass transitions: Many-body localization without quenched disorder, in AIP Conf. Proc., Vol. 1610 (American Institute of Physics, 2014) p. 11.

[32] T. Grover and M. P. A. Fisher, Quantum Disentangled Liquids, J. Stat. Mech. Theory Exp. **2014**, P10010 (2013).

[33] M. Schiulaz, A. Silva, and M. Müller, Dynamics in many-body localized quantum systems without disorder, Phys. Rev. B **91**, 184202 (2015).

[375] N. Y. Yao, C. R. Laumann, J. I. Cirac, M. D. Lukin, and J. E. Moore, Quasi-Many-Body Localization in Translation-Invariant Systems, Phys. Rev. Lett. **117**, 240601 (2016).

[35] J. M. Hickey, S. Genway, and J. P. Garrahan, Signatures of many-body localisation in a system without disorder and the relation to a glass transition, J. Stat. Mech. Theory Exp. **2016**, 054047 (2016).

[36] Z. Papić, E. M. Stoudenmire, and D. A. Abanin, Many-body localization in disorder-free systems: The importance of finite-size constraints, Ann. Phys. **362**, 714 (2015).

[37] M. Van Horssen, E. Levi, and J. P. Garrahan, Dynamics of many-body localization in a translation-invariant quantum glass model, Phys. Rev. B **92**, 100305 (2015).

[38] M. Pino, L. B. Ioffe, and B. L. Altshuler, Nonergodic metallic and insulating phases of Josephson junction chains, Proc. Natl. Acad. Sci. **113**, 536 (2016).

[39] D. H. Dunlap and V. M. Kenkre, Dynamic localization of a charged particle moving under the influence of an electric field, Phys. Rev. B **34**, 3625 (1986).

[40] D. Dunlap and V. Kenkre, Dynamic localization of a particle in an electric field viewed in momentum space: Connection with Bloch oscillations, Phys. Lett. A **127**, 438 (1988).

[41] G. H. Wannier, Wave Functions and Effective Hamiltonian for Bloch Electrons in an Electric Field, Phys. Rev. **117**, 432 (1960).

[42] Y. Bar Lev, D. J. Luitz, A. Lazarides, Y. B. Lev, and A. Lazarides, Absence of dynamical localization in interacting driven systems, SciPost Phys. **3**, 029 (2017).

[43] M. Schulz, C. A. Hooley, R. Moessner, and F. Pollmann, Stark Many-Body Localization, Phys. Rev. Lett. **122**, 040606 (2019).

[44] E. van Nieuwenburg, Y. Baum, and G. Refael, From Bloch oscillations to many-body localization in clean interacting systems, Proc. Natl. Acad. Sci. **116**, 9269 (2019).

[45] A. A. Michailidis, M. Žnidarič, M. Medvedyeva, D. A. Abanin, T. Prosen, and Z. Papić, Slow dynamics in translation-invariant quantum lattice models, Phys. Rev. B **97**, 104307 (2018).

[46] S. Pai, M. Pretko, and R. M. Nandkishore, Localization in Fractonic Random Circuits, Phys. Rev. X **9**, 021003 (2019).

[47] V. Khemani, M. Hermele, and R. Nandkishore, Localization from Hilbert space shattering: From theory to physical realizations, Phys. Rev. B **101**, 174204 (2020).

[48] See supplemental material at [URL] for analysis of the spectral statistics, and additional analysis of the magnus expansion.

[49] P. Zhang, Subdiffusion in strongly tilted lattice systems, Phys. Rev. Res. **2**, 033129 (2020).

[50] E. V. H. Doggen, I. V. Gornyi, and D. G. Polyakov, Stark many-body localization: Evidence for Hilbert-space shattering, Phys. Rev. B **103**, L100202 (2021).

[51] E. Guardado-Sanchez, A. Morningstar, B. M. Spar, P. T. Brown, D. A. Huse, and W. S. Bakr, Subdiffusion and Heat Transport in a Tilted Two-Dimensional Fermi-Hubbard System, Phys. Rev. X **10**, 011042 (2020).

[52] W. Morong, F. Liu, P. Becker, K. S. Collins, L. Feng, A. Kyprianidis, G. Pagano, T. You, A. V. Gorshkov, and C. Monroe, Observation of Stark Many-Body Localization without Disorder, Tech. Rep. (2021).

[53] S. Scherg, T. Kohlert, P. Sala, F. Pollmann, B. Hebbe Madhusudhana, I. Bloch, and M. Aidelsburger, Observing non-ergodicity due to kinetic constraints in tilted Fermi-Hubbard chains, Nat. Commun. **12**, 4490 (2021).

[54] R. Yao, T. Chanda, and J. Zakrzewski, Nonergodic dynamics in disorder-free potentials, Ann. Phys. , 168540 (2021).

[55] P. Jordan and E. Wigner, über das Paulische Äuivalenzverbot, Z. Für Phys. **47**, 631 (1928).

[56] R. Steinigeweg, H. Wichterich, and J. Gemmer, Density dynamics from current auto-correlations at finite time- and length-scales, EPL Europhys. Lett. **88**, 10004 (2009).

[57] Y. Yan, F. Jiang, and H. Zhao, Energy spread and current-current correlation in quantum systems, Eur. Phys. J. B **88**, 11 (2015).

[58] D. J. Luitz and Y. Bar Lev, The ergodic side of the many-body localization transition, Ann. Phys. **529**, 1600350 (2017).

[59] R. Steinigeweg, F. Jin, D. Schmidtke, H. De Raedt, K. Michielsen, and J. Gemmer, Real-time broadening of nonequilibrium density profiles and the role of the specific initial-state realization, Phys. Rev. B **95**, 035155 (2017).

[60] S. Popescu, A. J. Short, and A. Winter, Entanglement and the foundations of statistical mechanics, Nat. Phys. **2**, 754 (2006).

[61] C. Moler and C. Van Loan, Nineteen dubious ways to compute the exponential of a matrix, twenty-five years later, SIAM Rev. **45**, 3 (2003).

[62] U. Schollwöck, The density-matrix renormalization group in the age of matrix product states, Ann. Phys. **326**, 96 (2011).

[63] D. Kennes and C. Karrasch, Extending the range of real time density matrix renormalization group simulations, Computer Physics Communications **200**, 37 (2016).

[64] P. Zhang, Subdiffusion in strongly tilted lattice systems, Phys. Rev. Res. **2**, 33129 (2020).

[65] A. Gromov, A. Lucas, and R. M. Nandkishore, Fracton hydrodynamics, Phys. Rev. Res. **2**, 033124 (2020).

[66] J. Feldmeier, P. Sala, G. De Tomasi, F. Pollmann, and M. Knap, Anomalous Diffusion in Dipole- and Higher-Moment-Conserving Systems, Phys. Rev. Lett. **125**, 245303 (2020).

[81] The entanglement entropy here would be an entanglement of an MPO, which is also not a measurable physical quantity.

[68] D. A. Abanin, W. De Roeck, and F. F. Huveneers, Exponentially Slow Heating in Periodically Driven Many-Body Systems, Phys. Rev. Lett. **115**, 256803 (2015).

[69] D. A. Abanin, W. De Roeck, W. W. Ho, and F. Huveneers, Effective Hamiltonians, prethermalization, and slow energy absorption in periodically driven many-body systems, Phys. Rev. B **95**, 014112 (2017).

[70] D. A. Abanin, W. De Roeck, W. W. Ho, F. Huveneers, W. D. Roeck, W. W. Ho, and F. Huveneers, A Rigorous Theory of Many-Body Prethermalization for Periodically Driven and Closed Quantum Systems, Commun Math Phys **354**, 809 (2017).

[71] S. Blanes, F. Casas, J. A. Oteo, and J. Ros, The Magnus expansion and some of its applications, Phys. Rep. **470**, 151 (2009).

[72] T. Mori, T. Kuwahara, and K. Saito, Rigorous Bound on Energy Absorption and Generic Relaxation in Periodically Driven Quantum Systems, Phys. Rev. Lett. **116**, 120401 (2016).

[73] T. Kuwahara, T. Mori, and K. Saito, Floquet-Magnus theory and generic transient dynamics in periodically driven many-body quantum systems, Ann. Phys. **367**, 96 (2016).

From An Open-System Quantum Simulator with Trapped Ions

References

[1] Ladd, T. D., Jelezko, F., Laflamme, R., Nakamura, Y., Monroe, C. et al. Quantum computers. Nature **464**, 45–53 (2010)

[2] Kimble, H. J. The quantum internet. Nature **453**, 1023–1030 (2008)

[3] Schoelkopf, R. J. & Girvin, S. M. Wiring up quantum systems. Nature **451**, 664–669 (2008)

[4] Neeley, M., Bialczak, R. C., Lenander, M., Lucero, E., Mariantoni, M. et al. Generation of three-qubit entangled states using superconducting phase qubits. Nature **467**, 570–573 (2010)

[5] Saffman, M., Walker, T. G. & Mølmer, K. Quantum information with Rydberg atoms. Rev. Mod. Phys. **82**, 2313–2363 (2010)

[6] Bloch, I., Dalibard, J. & Zwerger, W. Many-body physics with ultracold gases. Rev. Mod. Phys. **80**, 885–964 (2008)

[7] O'Brien, J. L. Optical quantum computing. Science **318**, 1567–1570 (2007)

[8] Clarke, J. & Wilhelm, F. K. Superconducting quantum bits. Nature **453**, 1031–1042 (2008)

[9] Hanson, R., Kouwenhoven, L. P., Petta, J. R., Tarucha, S. & Vandersypen, L. M. K. Spins in few-electron quantum dots. Rev. Mod. Phys. **79**, 1217–1265 (2007)

[10] Wrachtrup, J. & Jelezko, F. Processing quantum information in diamond. J. Phys.: Condens. Matter **18**, S807–S824 (2006)

[11] Feynman, R. Simulating physics with computers. Int. J. Theor. Phys. **21**, 467–488 (1982)

[12] Lloyd, S. Universal quantum simulators. Science **273**, 1073–1078 (1996)

[13] Buluta, I. & Nori, F. Quantum simulators. Science **326**, 108–111 (2009)

[14] Myatt, C. J. et al. Decoherence of quantum superpositions through coupling to engineered reservoirs. Nature **403**, 269–273 (2000)

[15] Deleglise, S., Dotsenko, I., Sayrin, C., Bernu, J., Brune, M. et al. Reconstruction of non-classical cavity field states with snapshots of their decoherence. Nature **455**, 510–514 (2008)

[16] Barreiro, J. T., Schindler, P., Gühne, O., Monz, T., Chwalla, M. et al. Experimental multiparticle entanglement dynamics induced by decoherence. Nature Phys. (2010). Advance Online Publication, doi:10.1038/nphys1781

[17] Krauter, H., Muschik, C. A., Jensen, K., Wasilewski, W., Petersen, J. M. et al. Entanglement generated by dissipation. arXiv:1006.4344 (2010)

[18] Diehl, S. et al. Quantum states and phases in driven open quantum systems with cold atoms. Nature Phys. **4**, 878–883 (2008)

[19] Cho, J., Bose, S. & Kim, M. S. Optical pumping into many-body entanglement. arXiv:1008.4088 (2010)

[20] Goldstein, G., Cappellaro, P., Maze, J. R., Hodges, J. S., Jiang, L. et al. Environment-assisted precision measurement. arXiv:1001.0089 (2010)

[21] Diehl, S., Yi, W., Daley, A. & Zoller, P. Driven dissipative d-wave pairing of atomic fermions. arXiv:1007.3420 (2010)

[22] Verstraete, F., Wolf, M. M. & Cirac, J. I. Quantum computation and quantum-state engineering driven by dissipation. Nature Phys. **5**, 633–636 (2009)

[23] Häffner, H., Roos, C. F. & Blatt, R. Quantum computing with trapped ions. Phys. Rep. **469**, 155–203 (2008)

[24] Home, J. P., Hanneke, D., Jost, J. D., Amini, J. M., Leibfried, D. et al. Complete methods set for scalable ion trap quantum information processing. Science **325**, 1227–1230 (2009)

[25] Kitaev, A. Y. Fault-tolerant quantum computation by anyons. Ann. Phys. **303**, 2 – 30 (2003)

[26] Nielsen, M. A. & Chuang, I. L. Quantum Computation and Quantum Information. Cambridge University Press (2000)

[27] Steane, A. M. Efficient fault-tolerant quantum computing. Nature **399**, 124–126 (1999)

[28] Lloyd, S. & Viola, L. Engineering quantum dynamics. Phys. Rev. A **65**, 010101 (2001)

[29] Dür, W., Bremner, M. J. & Briegel, H. J. Quantum simulation of interacting high-dimensional systems: The influence of noise. Phys. Rev. A **78**, 052325 (2008)

[30] Wiseman, H. M. & Milburn, G. J. Quantum Measurement and Control. Cambridge University Press (2009)

[31] Schmidt-Kaler, F. et al. How to realize a universal quantum gate with trapped ions. App. Phys. B **77**, 789–796 (2003)

[32] Mølmer, K. & Sørensen, A. Multiparticle entanglement of hot trapped ions. Phys. Rev. Lett. **82**, 1835–1838 (1999)

[33] Roos, C. F. Ion trap quantum gates with amplitude-modulated laser beams. New J. Phys. **10**, 013002 (2008)

[34] Monz, T. et al. Coherence of large-scale entanglement. arXiv:1009.6126 (2010)

[35] Schindler, P. et al. Experimental repetitive quantum error correction. In preparation (2010)

[36] Roos, C. F. et al. Control and measurement of three-qubit entangled states. Science **304**, 1478–1480 (2004)

[37] Gilchrist, A., Langford, N. K. & Nielsen, M. A. Distance measures to compare real and ideal quantum processes. Phys. Rev. A **71**, 062310 (2005)

[38] Jozsa, R. Fidelity for mixed quantum states. J. Mod. Opt. **41**, 2315–2353 (1994)

[39] Sackett, C. A. et al. Experimental entanglement of four particles. Nature **404**, 256–259 (2000)

[40] Gühne, O. & Seevinck, M. Separability criteria for genuine multiparticle entanglement. New J. Phys. **12**, 053002 (2010)

[41] Friedenauer, A., Schmitz, H., Glueckert, J., Porras, D. & Schaetz, T. Simulating a quantum magnet with trapped ions. Nature Phys. **4**, 757–761 (2008)

[42] Kim, K., Chang, M.-S., Korenblit, S., Islam, R., Edwards, E. E. et al. Quantum simulation of frustrated ising spins with trapped ions. Nature **465**, 590–593 (2010)

[43] Porras, D. & Cirac, J. I. Effective quantum spin systems with trapped ions. Phys. Rev. Lett. **92**, 207901 (2004)

[44] Müller, M., Hammerer, K., Zhou, Y., Roos, C. F. & Zoller, P. Open-system quantum simulation with trapped ions. In preparation (2010)

[45] Nayak, C., Simon, S. H., Stern, A., Freedman, M. & Das Sarma, S. Non-abelian anyons and topological quantum computation. Rev. Mod. Phys. **80**, 1083–1159 (2008)

[46] Moessner, R. & Sondhi, S. L. Resonating valence bond phase in the triangular lattice quantum dimer model. Phys. Rev. Lett. **86**, 1881–1884 (2001)

[47] Ralph, T. C., Bartlett, S. D., OBrien, J. L., Pryde, G. J. & Wiseman, H. M. Quantum nondemolition measurements for quantum information. Phys. Rev. A **73**, 012113 (2006)

[48] Fleming, G. R., Huelga, S. & Plenio, M., editors. Focus on Quantum Effects and Noise in Biomolecules, New J. Phys., volume 12. Institute of Physics (2010)

[49] R. Schmied, J. H. W. & Leibfried, D. Optimal surface-electrode trap lattices for quantum simulation with trapped ions. Phys. Rev. Lett. **102**, 233002 (2009)

[50] Weimer, H., Müller, M., Lesanovsky, I., Zoller, P. & Büchler, H. P. A Rydberg quantum simulator. Nature Phys. **6**, 382–388 (2010)

From Suppl-An Open-System Quantum Simulator with Trapped Ions

References

[1] Barrett, M. D., J. Chiaverini, T. Schaetz, J. Britton, W. M. Itano, J. D. Jost, E. Knill, C. Langer, D. Leibfried, R. Ozeri, and D. J. Wineland, 2004, Nature **429** (6993), 737

[2] Bouwmeester, D., et al., 1997, Nature **390**, 575

[3] Gilchrist, A., N. K. Langford, and M. A. Nielsen, 2005, Phys. Rev. A **71**, 062310

[4] Jezek, M., J. Fiurasek, and Z. Hradil, 2003, Phys. Rev. A **68** (1), 012305

[5] Jozsa, R., 1994, J. Mod. Opt. **41** (12), 2315

[6] Kitaev, A. Y., 2003, Ann. Phys. **303** (1), 2

[7] Lu, C.-Y., W.-B. Gao, O. Gühne, X.-Q. Zhou, Z.-B. Chen, and J.-W. Pan, 2009, Phys. Rev. Lett. **102** (3), 030502

[8] Monz, T., et al., 2010, arXiv:1009.6126

[9] Müller, M., K. Hammerer, Y. Zhou, C. F. Roos, and P. Zoller, 2010, In preparation

[10] Nebendahl, V., H. Häffner, and C. F. Roos, 2009, Phys. Rev. A **79** (1), 012312

[11] Pachos, J. K., W. Wieczorek, C. Schmid, N. Kiesel, R. Pohlner, and H. Weinfurter, 2009, New J. Phys. **11** (8), 083010

[12] Ralph, T. C., S. D. Bartlett, J. L. OBrien, G. J. Pryde, and H. M. Wiseman, 2006, Phys. Rev. A **73** (1), 012113

[13] Riebe, M., H. Häffner, C. F. Roos, W. Hänsel, J. Benhelm, G. P. T. Lancaster, T. W. Körber, C. Becher, F. Schmidt-Kaler, D. F. V. James, and R. Blatt, 2004, Nature **429** (6993), 734

From Collective Excitations and Nonequilibrium Phase Transition in Dissipative Fermionic Superfluids

References

[1] P. W. Anderson, "Random-Phase Approximation in the Theory of Superconductivity," Phys. Rev. **112**, 1900 (1958).

[2] A. Leggett, "Number-phase fluctuations in two-band superconductors," Prog. Theor. Phys. **36**, 901 (1966).

[3] A. Volkov and S. M. Kogan, "Collisionless relaxation of the energy gap in superconductors," Sov. Phys. JETP **38**, 1018 (1974).

[4] P. B. Littlewood and C. M. Varma, "Gauge-Invariant Theory of the Dynamical Interaction of Charge Density Waves and Superconductivity," Phys. Rev. Lett. **47**, 811 (1981).

[5] P. B. Littlewood and C. M. Varma, "Amplitude collective modes in superconductors and their coupling to charge-density waves," Phys. Rev. B **26**, 4883 (1982).

[6] C. M. Varma, "Higgs boson in superconductors," J. Low Temp. Phys. **126**, 901 (2002).

[7] A. V. Andreev, V. Gurarie, and L. Radzihovsky, "Nonequilibrium Dynamics and Thermodynamics of a Degenerate Fermi Gas Across a Feshbach Resonance," Phys. Rev. Lett. **93**, 130402 (2004).

[8] R. A. Barankov, L. S. Levitov, and B. Z. Spivak, "Collective Rabi Oscillations and Solitons in a Time-Dependent BCS Pairing Problem," Phys. Rev. Lett. **93**, 160401 (2004).

[9] R. A. Barankov and L. S. Levitov, "Dynamical selection in developing fermionic pairing," Phys. Rev. A **73**, 033614 (2006).

[10] E. A. Yuzbashyan and M. Dzero, "Dynamical Vanishing of the Order Parameter in a Fermionic Condensate," Phys. Rev. Lett. **96**, 230404 (2006).

[11] R. A. Barankov and L. S. Levitov, "Synchronization in the BCS Pairing Dynamics as a Critical Phenomenon," Phys. Rev. Lett. **96**, 230403 (2006).

[12] E. A. Yuzbashyan, O. Tsyplyatyev, and B. L. Altshuler, "Relaxation and Persistent Oscillations of the Order Parameter in Fermionic Condensates," Phys. Rev. Lett. **96**, 097005 (2006).

[13] V. Gurarie, "Nonequilibrium Dynamics of Weakly and Strongly Paired Superconductors," Phys. Rev. Lett. **103**, 075301 (2009).

[14] E. A. Yuzbashyan, M. Dzero, V. Gurarie, and M. S. Foster, "Quantum quench phase diagrams of an s-wave BCS-BEC condensate," Phys. Rev. A **91**, 033628 (2015).

[15] S. Hannibal, P. Kettmann, M. D. Croitoru, A. Vagov, V. M. Axt, and T. Kuhn, "Quench dynamics of an ultracold Fermi gas in the BCS regime: Spectral properties and confinement-induced breakdown of the Higgs mode," Phys. Rev. A **91**, 043630 (2015).

[16] P. Kettmann, S. Hannibal, M. D. Croitoru, V. M. Axt, and T. Kuhn, "Pure Goldstone mode in the quench dynamics of a confined ultracold Fermi gas in the BCS-BEC crossover regime," Phys. Rev. A **96**, 033618 (2017).

[17] S. Hannibal, P. Kettmann, M. D. Croitoru, V. M. Axt, and T. Kuhn, "Dynamical vanishing of the order parameter in a confined Bardeen-Cooper-Schrieffer Fermi gas after an interaction quench," Phys. Rev. A **97**, 013619 (2018).

[18] S. Hannibal, P. Kettmann, M. D. Croitoru, V. M. Axt, and T. Kuhn, "Persistent oscillations of the order parameter and interaction quench phase diagram for a confined Bardeen-Cooper-Schrieffer Fermi gas," Phys. Rev. A **98**, 053605 (2018).

[19] D. Pekker and C. Varma, "Amplitude/Higgs modes in condensed matter physics," Annu. Rev. Condens. Matter Phys. **6**, 269 (2015).

[20] R. Shimano and N. Tsuji, "Higgs Mode in Superconductors," Annu. Rev. Condens. Matter Phys. **11**, 103 (2020).

[21] U. Bissbort, S. Götze, Y. Li, J. Heinze, J. S. Krauser, M. Weinberg, C. Becker, K. Sengstock, and W. Hofstetter, "Detecting the Amplitude Mode of Strongly Interacting Lattice Bosons by Bragg Scattering," Phys. Rev. Lett. **106**, 205303 (2011).

[22] M. Endres, T. Fukuhara, D. Pekker, M. Cheneau, P. Schauβ, C. Gross, E. Demler, S. Kuhr, and I. Bloch, "The 'Higgs' amplitude mode at the two-dimensional superfluid/Mott insulator transition," Nature (London) **487**, 454 (2012).

[23] A. Behrle, T. Harrison, J. Kombe, K. Gao, M. Link, J.-S. Bernier, C. Kollath, and M. Köhl, "Higgs mode in a strongly interacting fermionic superfluid," Nat. Phys. **14**, 781 (2018).

[24] T. Harrison, M. Link, A. Behrle, K. Gao, A. Kell, J. Kombe, J.-S. Bernier, C. Kollath, and M. Köhl, "Decay and revival of a transient trapped Fermi condensate," arXiv:2007.11466 .

[25] R. Matsunaga, Y. I. Hamada, K. Makise, Y. Uzawa, H. Terai, Z. Wang, and R. Shimano, "Higgs Amplitude Mode in the BCS Superconductors $Nb_{1-x}Ti_xN$ Induced by Terahertz Pulse Excitation," Phys. Rev. Lett. **111**, 057002 (2013).

[26] R. Matsunaga, N. Tsuji, H. Fujita, A. Sugioka, K. Makise, Y. Uzawa, H. Terai, Z. Wang, H. Aoki, and R. Shimano, "Light-induced collective pseudospin precession resonating with Higgs mode in a superconductor," Science **345**, 1145 (2014).

[27] T. Papenkort, V. M. Axt, and T. Kuhn, "Coherent dynamics and pump-probe spectra of BCS superconductors," Phys. Rev. B **76**, 224522 (2007).

[28] T. Papenkort, T. Kuhn, and V. M. Axt, "Coherent control of the gap dynamics of BCS superconductors in the nonadiabatic regime," Phys. Rev. B **78**, 132505 (2008).

[29] A. P. Schnyder, D. Manske, and A. Avella, "Resonant generation of coherent phonons in a superconductor by ultrafast optical pump pulses," Phys. Rev. B **84**, 214513 (2011).

[30] M. Zachmann, M. D. Croitoru, A. Vagov, V. M. Axt, T. Papenkort, and T. Kuhn, "Ultrafast terahertz-field-induced dynamics of superconducting bulk and quasi-1D samples," New J. Phys. **15**, 055016 (2013).

[31] H. Krull, D. Manske, G. S. Uhrig, and A. P. Schnyder, "Signatures of nonadiabatic BCS state dynamics in pump-probe conductivity," Phys. Rev. B **90**, 014515 (2014).

[32] N. Tsuji and H. Aoki, "Theory of Anderson pseudospin resonance with Higgs mode in superconductors," Phys. Rev. B **92**, 064508 (2015).

[33] H. Krull, N. Bittner, G. Uhrig, D. Manske, and A. Schnyder, "Coupling of Higgs and Leggett modes in non-equilibrium superconductors," Nat. Commun. **7**, 11921 (2016).

[34] S. Sharapov, V. Gusynin, and H. Beck, "Effective action approach to the Leggett's mode in two-band superconductors," Eur. Phys. J. B **30**, 45 (2002).

[35] F. J. Burnell, J. Hu, M. M. Parish, and B. A. Bernevig, "Leggett mode in a strong-coupling model of iron arsenide superconductors," Phys. Rev. B **82**, 144506 (2010).

[36] N. Bittner, D. Einzel, L. Klam, and D. Manske, "Leggett Modes and the Anderson-Higgs Mechanism in Superconductors without Inversion Symmetry," Phys. Rev. Lett. **115**, 227002 (2015).

[37] T. Cea and L. Benfatto, "Signature of the Leggett mode in the A_{1g} Raman response: From MgB_2 to iron-based superconductors," Phys. Rev. B **94**, 064512 (2016).

[38] Y. Murotani, N. Tsuji, and H. Aoki, "Theory of light-induced resonances with collective Higgs and Leggett modes in multiband superconductors," Phys. Rev. B **95**, 104503 (2017).

[39] G. Lindblad, "On the generators of quantum dynamical semigroups," Commun. Math. Phys. **48**, 119 (1976).

[40] A. J. Daley, "Quantum trajectories and open many-body quantum systems," Adv. Phys. **63**, 77 (2014).

[41] Y. Ashida, S. Furukawa, and M. Ueda, "Parity-time-symmetric quantum critical phenomena," Nat. Commun. **8**, 15791 (2017).

[42] M. Nakagawa, N. Kawakami, and M. Ueda, "Non-Hermitian Kondo Effect in Ultracold Alkaline-Earth Atoms," Phys. Rev. Lett. **121**, 203001 (2018).

[43] S. Diehl, A. Tomadin, A. Micheli, R. Fazio, and P. Zoller, "Dynamical Phase Transitions and Instabilities in Open Atomic Many-Body Systems," Phys. Rev. Lett. **105**, 015702 (2010).

[44] M. Höning, M. Moos, and M. Fleischhauer, "Critical exponents of steady-state phase transitions in fermionic lattice models," Phys. Rev. A **86**, 013606 (2012).

[45] L. M. Sieberer, S. D. Huber, E. Altman, and S. Diehl, "Dynamical Critical Phenomena in Driven-Dissipative Systems," Phys. Rev. Lett. **110**, 195301 (2013).

[46] F. Damanet, E. Mascarenhas, D. Pekker, and A. J. Daley, "Controlling Quantum Transport via Dissipation Engineering," Phys. Rev. Lett. **123**, 180402 (2019).

[47] K. Yamamoto, Y. Ashida, and N. Kawakami, "Rectification in nonequilibrium steady states of open many-body systems," Phys. Rev. Research **2**, 043343 (2020).

[48] Y.-J. Han, Y.-H. Chan, W. Yi, A. J. Daley, S. Diehl, P. Zoller, and L.-M. Duan, "Stabilization of the p-wave superfluid state in an optical lattice," Phys. Rev. Lett. **103**, 070404 (2009).

[49] K. Yamamoto, M. Nakagawa, K. Adachi, K. Takasan, M. Ueda, and N. Kawakami, "Theory of Non-Hermitian Fermionic Superfluidity with a Complex-Valued Interaction," Phys. Rev. Lett. **123**, 123601 (2019).

[50] T. Tomita, S. Nakajima, I. Danshita, Y. Takasu, and Y. Takahashi, "Observation of the Mott insulator to superfluid crossover of a driven-dissipative Bose-Hubbard system," Sci. Adv. **3**, e1701513 (2017).

[51] G. Barontini, R. Labouvie, F. Stubenrauch, A. Vogler, V. Guarrera, and H. Ott, "Controlling the Dynamics of an Open Many-Body Quantum System with Localized Dissipation," Phys. Rev. Lett. **110**, 035302 (2013).

[52] R. Labouvie, B. Santra, S. Heun, S. Wimberger, and H. Ott, "Negative Differential Conductivity in an Interacting Quantum Gas," Phys. Rev. Lett. **115**, 050601 (2015).

[53] R. Labouvie, B. Santra, S. Heun, and H. Ott, "Bistability in a Driven-Dissipative Superfluid," Phys. Rev. Lett. **116**, 235302 (2016).

[54] H. P. Lüschen, P. Bordia, S. S. Hodgman, M. Schreiber, S. Sarkar, A. J. Daley, M. H. Fischer, E. Altman, I. Bloch, and U. Schneider, "Signatures of Many-Body Localization in a Controlled Open Quantum System," Phys. Rev. X **7**, 011034 (2017).

[55] M. J. Mark, E. Haller, K. Lauber, J. G. Danzl, A. Janisch, H. P. Büchler, A. J. Daley, and H.-C. Nägerl, "Preparation and Spectroscopy of a Metastable Mott-Insulator State with Attractive Interactions," Phys. Rev. Lett. **108**, 215302 (2012).

[56] K. Sponselee, L. Freystatzky, B. Abeln, M. Diem, B. Hundt, A. Kochanke, T. Ponath, B. Santra, L. Mathey, K. Sengstock, and C. Becker, "Dynamics of ultracold quantum gases in the dissipative Fermi–Hubbard model," Quantum Sci. Technol. **4**, 014002 (2018).

[57] R. Bouganne, M. B. Aguilera, A. Ghermaoui, J. Beugnon, and F. Gerbier, "Anomalous decay of coherence in a dissipative many-body system," Nat. Phys. **16**, 21 (2020).

[58] T. Tomita, S. Nakajima, Y. Takasu, and Y. Takahashi, "Dissipative Bose-Hubbard system with intrinsic two-body loss," Phys. Rev. A **99**, 031601(R) (2019).

[59] Y. Takasu, T. Yagami, Y. Ashida, R. Hamazaki, Y. Kuno, and Y. Takahashi, "PT-symmetric non-Hermitian quantum many-body system using ultracold atoms in an optical lattice with controlled dissipation," Prog. Theor. Exp. Phys. **2020**, 12A110 (2020).

[60] D. Witthaut, F. Trimborn, and S. Wimberger, "Dissipation Induced Coherence of a Two-Mode Bose-Einstein Condensate," Phys. Rev. Lett. **101**, 200402 (2008).

[61] I. Vidanović, D. Cocks, and W. Hofstetter, "Dissipation through localized loss in bosonic systems with long-range interactions," Phys. Rev. A **89**, 053614 (2014).

[62] M. Nakagawa, N. Tsuji, N. Kawakami, and M. Ueda, "Dynamical Sign Reversal of Magnetic Correlations in Dissipative Hubbard Models," Phys. Rev. Lett. **124**, 147203 (2020).

[63] M. Nakagawa, N. Kawakami, and M. Ueda, "Exact Liouvillian Spectrum of a One-Dimensional Dissipative Hubbard Model," Phys. Rev. Lett. **126**, 110404 (2021).

[64] R. Zhang, Y. Cheng, H. Zhai, and P. Zhang, "Orbital Feshbach Resonance in Alkali-Earth Atoms," Phys. Rev. Lett. **115**, 135301 (2015).

[65] M. Iskin, "Two-band superfluidity and intrinsic Josephson effect in alkaline-earth-metal Fermi gases across an orbital Feshbach resonance," Phys. Rev. A **94**, 011604(R) (2016).

[66] J. Xu, R. Zhang, Y. Cheng, P. Zhang, R. Qi, and H. Zhai, "Reaching a Fermi-superfluid state near an orbital Feshbach resonance," Phys. Rev. A **94**, 033609 (2016).

[67] L. He, J. Wang, S.-G. Peng, X.-J. Liu, and H. Hu, "Strongly correlated Fermi superfluid near an orbital Feshbach resonance: Stability, equation of state, and Leggett mode," Phys. Rev. A **94**, 043624 (2016).

[68] M. Höfer, L. Riegger, F. Scazza, C. Hofrichter, D. R. Fernandes, M. M. Parish, J. Levinsen, I. Bloch, and S. Fölling, "Observation of an Orbital Interaction-Induced Feshbach Resonance in ^{173}Yb," Phys. Rev. Lett. **115**, 265302 (2015).

[69] G. Pagano, M. Mancini, G. Cappellini, L. Livi, C. Sias, J. Catani, M. Inguscio, and L. Fallani, "Strongly Interacting Gas of Two-Electron Fermions at an Orbital Feshbach Resonance," Phys. Rev. Lett. **115**, 265301 (2015).

[70] G. Cappellini, L. F. Livi, L. Franchi, D. Tusi, D. Benedicto Orenes, M. Inguscio, J. Catani, and L. Fallani, "Coherent Manipulation of Orbital Feshbach Molecules of Two-Electron Atoms," Phys. Rev. X **9**, 011028 (2019).

[71] N. Darkwah Oppong, L. Riegger, O. Bettermann, M. Höfer, J. Levinsen, M. M. Parish, I. Bloch, and S. Fölling, "Observation of Coherent Multiorbital Polarons in a Two-Dimensional Fermi Gas," Phys. Rev. Lett. **122**, 193604 (2019).

[72] S. Smale, P. He, B. A. Olsen, K. G. Jackson, H. Sharum, S. Trotzky, J. Marino, A. M. Rey, and J. H. Thywissen, "Observation of a transition between dynamical phases in a quantum degenerate Fermi gas," Sci. Adv. **5**, eaax1568 (2019).

[73] J. A. Muniz, D. Barberena, R. J. Lewis-Swan, D. J. Young, J. R. Cline, A. M. Rey, and J. K. Thompson, "Exploring dynamical phase transitions with cold atoms in an optical cavity," Nature (London) **580**, 602 (2020).

[74] N. Syassen, D. M. Bauer, M. Lettner, T. Volz, D. Dietze, J. J. Garcia-Ripoll, J. I. Cirac, G. Rempe, and S. Dürr, "Strong dissipation inhibits losses and induces correlations in cold molecular gases," Science **320**, 1329 (2008).

[75] J. J. García-Ripoll, S. Dürr, N. Syassen, D. M. Bauer, M. Lettner, G. Rempe, and J. I. Cirac, "Dissipation-induced hard-core boson gas in an optical lattice," New J. Phys. **11**, 013053 (2009).

[76] S. Dürr, J. J. García-Ripoll, N. Syassen, D. M. Bauer, M. Lettner, J. I. Cirac, and G. Rempe, "Lieb-Liniger model of a dissipation-induced Tonks-Girardeau gas," Phys. Rev. A **79**, 023614 (2009).

[77] L. M. Sieberer, M. Buchhold, and S. Diehl, "Keldysh field theory for driven open quantum systems," Rep. Prog. Phys. **79**, 096001 (2016).

[78] A. Kamenev, Field theory of non-equilibrium systems (Cambridge University Press, Cambridge, England, 2011).

[79] B. Buča and T. Prosen, "A note on symmetry reductions of the Lindblad equation: transport in constrained open spin chains," New J. Phys. **14**, 073007 (2012).

[80] V. V. Albert and L. Jiang, "Symmetries and conserved quantities in Lindblad master equations," Phys. Rev. A **89**, 022118 (2014).

[81] See Supplemental Material, which includes Refs. [95, 96, 97], for detailed calculations of the time-dependent dissipative BCS theory, the operator formalism of the BCS theory for a dissipative superfluid, a generalization of the Bogoliubov-de Gennes analysis with a time-dependent BCS state, the dynamics of pseudospins after switch-on of dissipation, the dynamics after sudden change of both the interaction and the dissipation, and a simplified model for understanding the nonequilibrium phase transition. I am not sure, if it is true, since the articles look like they are on another topic.

[82] A. Spuntarelli, P. Pieri, and G. C. Strinati, "Josephson Effect throughout the BCS-BEC Crossover," Phys. Rev. Lett. **99**, 040401 (2007).

[83] G. Valtolina, A. Burchianti, A. Amico, E. Neri, K. Xhani, J. A. Seman, A. Trombettoni, A. Smerzi, M. Zaccanti, M. Inguscio, and G. Roati, "Josephson effect in fermionic superfluids across the BEC-BCS crossover," Science **350**, 1505 (2015).

[84] A. Burchianti, F. Scazza, A. Amico, G. Valtolina, J. A. Seman, C. Fort, M. Zaccanti, M. Inguscio, and G. Roati, "Connecting Dissipation and Phase Slips in a Josephson Junction between Fermionic Superfluids," Phys. Rev. Lett. **120**, 025302 (2018).

[85] N. Luick, L. Sobirey, M. Bohlen, V. P. Singh, L. Mathey, T. Lompe, and H. Moritz, "An ideal Josephson junction in an ultracold two-dimensional Fermi gas," Science **369**, 89 (2020).

[86] W. Kwon, G. Del Pace, R. Panza, M. Inguscio, W. Zwerger, M. Zaccanti, F. Scazza, and G. Roati, "Strongly correlated superfluid order parameters from dc Josephson supercurrents," Science **369**, 84 (2020).

[87] M. Tinkham, Introduction to superconductivity (Courier Corporation, 2004).

[88] B. Zhu, B. Gadway, M. Foss-Feig, J. Schachenmayer, M. L. Wall, K. R. A. Hazzard, B. Yan, S. A. Moses, J. P. Covey, D. S. Jin, J. Ye, M. Holland, and A. M. Rey, "Suppressing the Loss of Ultracold Molecules Via the Continuous Quantum Zeno Effect," Phys. Rev. Lett. **112**, 070404 (2014).

[89] A. J. Daley, J. M. Taylor, S. Diehl, M. Baranov, and P. Zoller, "Atomic Three-Body Loss as a Dynamical Three-Body Interaction," Phys. Rev. Lett. **102**, 040402 (2009).

[90] B. Yan, S. A. Moses, B. Gadway, J. P. Covey, K. R. Hazzard, A. M. Rey, D. S. Jin, and J. Ye, "Observation of dipolar spin-exchange interactions with lattice-confined polar molecules," Nature (London) **501**, 521 (2013).

[91] In Ref. [63], it is shown that exceptional points of a non-Hermitian Hamiltonian and a Liouvillian are the same when the system has either gain or loss. Thus, the Liouvillian under consideration exhibits the spectral singularity originating from the same exceptional points as those of the non-Hermitian BCS Hamiltonian [49].

[92] A. O. Caldeira and A. J. Leggett, "Influence of Dissipation on Quantum Tunneling in Macroscopic Systems," Phys. Rev. Lett. **46**, 211 (1981).

[93] A. Schmid, "Diffusion and Localization in a Dissipative Quantum System," Phys. Rev. Lett. **51**, 1506 (1983).

[94] F. Guinea, V. Hakim, and A. Muramatsu, "Diffusion and Localization of a Particle in a Periodic Potential Coupled to a Dissipative Environment," Phys. Rev. Lett. **54**, 263 (1985).

[95] N. Shibata and H. Katsura, "Dissipative spin chain as a non-Hermitian Kitaev ladder," Phys. Rev. B **99**, 174303 (2019).

[96] N. Shibata and H. Katsura, "Dissipative quantum Ising chain as a non-Hermitian Ashkin-Teller model," Phys. Rev. B **99**, 224432 (2019).

[97] H. T. C. Stoof, "Time-dependent Ginzburg-Landau theory for a weak-coupling superconductor," Phys. Rev. B **47**, 7979 (1993).

From Correlations after Quantum Quenches in the *XXZ* Spin Chain: Failure of the Generalized Gibbs Ensemble by Pozsgay et al.

References

[1] T. Kinoshita, T. Wenger, and D. S. Weiss, Nature (London) **440**, 900 (2006).

[2] M. Cheneau, P. Barmettler, D. Poletti, M. Endres, P. Schauss, T. Fukuhara, C. Gross, I. Bloch, C. Kollath, and S. Kuhr, Nature (London) **481**, 484 (2012).

[3] S. Trotzky, Y.-A. Chen, A. Flesch, I. P. McCulloch, U. Schollwöck, J. Eisert, and I. Bloch, Nat. Phys. **8**, 325 (2012).

[4] T. Fukuhara, P. Schauß, M. Endres, S. Hild, M. Cheneau, I. Bloch, and C. Gross, Nature (London) **502**, 76 (2013).

[5] A. Polkovnikov, K. Sengupta, A. Silva, and M. Vengalattore, Rev. Mod. Phys. **83**, 863 (2011).

[6] C. Kollath, A. M. Läuchli, and E. Altman, Phys. Rev. Lett. **98**, 180601 (2007).

[7] M. Rigol, V. Dunjko, and M. Olshanii, Nature (London) **452**, 854 (2008).

[8] T. Barthel and U. Schollwöck, Phys. Rev. Lett. **100**, 100601 (2008).

[9] M. Rigol, Phys. Rev. Lett. **103**, 100403 (2009).

[10] M. Cramer and J. Eisert, New J. Phys. **12**, 055020 (2010).

[11] L. F. Santos and M. Rigol, Phys. Rev. E **81**, 036206 (2010).

[12] P. Barmettler, M. Punk, V. Gritsev, E. Demler, and E. Altman, New J. Phys. **12**, 055017 (2010).

[13] M. C. Bañuls, J. I. Cirac, and M. B. Hastings, Phys. Rev. Lett. **106**, 050405 (2011).

[14] P. Calabrese, F. H. L. Essler, and M. Fagotti, Phys. Rev. Lett. **106**, 227203 (2011).

[15] P. Calabrese, F. H. L. Essler, and M. Fagotti, J. Stat. Mech. (2012) P07016.

[16] N. Sedlmayr, J. Ren, F. Gebhard, and J. Sirker, Phys. Rev. Lett. **110**, 100406 (2013).

[17] M. Marcuzzi, J. Marino, A. Gambassi, and A. Silva, Phys. Rev. Lett. **111**, 197203 (2013).

[18] D. Iyer, H. Guan, and N. Andrei, Phys. Rev. A **87**, 053628 (2013).

[19] M. Rigol, V. Dunjko, V. Yurovsky, and M. Olshanii, Phys. Rev. Lett. **98**, 050405 (2007).

[20] M. A. Cazalilla, Phys. Rev. Lett. **97**, 156403 (2006).

[21] D. Rossini, A. Silva, G. Mussardo, and G. E. Santoro, Phys. Rev. Lett. **102**, 127204 (2009).

[22] P. Calabrese, F. H. L. Essler, and M. Fagotti, J. Stat. Mech. (2012) P07022.

[23] M. A. Cazalilla, A. Iucci, and M.-C. Chung, Phys. Rev. E **85**, 011133 (2012).

[24] V. Gurarie, J. Stat. Mech. P02014 (2013).

[25] M. Fagotti and F. H. L. Essler, Phys. Rev. B **87**, 245107 (2013).

[26] M. Collura, S. Sotiriadis, and P. Calabrese, Phys. Rev. Lett. **110**, 245301 (2013).

[27] M. Fagotti, J. Stat. Mech. P03016 (2014).

[28] M. Kormos, M. Collura, and P. Calabrese, Phys. Rev. A **89**, 013609 (2014).

[29] S. Sotiriadis and P. Calabrese, J. Stat. Mech. (2014) P07024.

[30] A. C. Cassidy, C. W. Clark, and M. Rigol, Phys. Rev. Lett. **106**, 140405 (2011).

[31] T. M. Wright, M. Rigol, M. J. Davis, and K. V. Kheruntsyan, Phys. Rev. Lett. **113**, 050601 (2014).

[32] J.-S. Caux and R. M. Konik, Phys. Rev. Lett. **109**, 175301 (2012).

[33] M. Kormos, A. Shashi, Y.-Z. Chou, J.-S. Caux, and A. Imambekov, Phys. Rev. B **88**, 205131 (2013).

[34] J. De Nardis, B. Wouters, M. Brockmann, and J.-S. Caux, Phys. Rev. A **89**, 033601 (2014).

[35] B. Pozsgay, J. Stat. Mech. (2013) P07003.

[36] M. Fagotti and F. H. L. Essler, J. Stat. Mech. (2013) P07012.

[37] M. Fagotti, M. Collura, F. H. L. Essler, and P. Calabrese, Phys. Rev. B **89**, 125101 (2014).

[38] D. Fioretto and G. Mussardo, New J. Phys. **12**, 055015 (2010).

[39] G. Mussardo, Phys. Rev. Lett. **111**, 100401 (2013).

[40] S. Sotiriadis, G. Takács, and G. Mussardo, Phys. Lett. B **734**, 52 (2014).

[41] J.-S. Caux and F. H. L. Essler, Phys. Rev. Lett. **110**, 257203 (2013).

[42] J.-S Caux, in *Proceedings of the Workshop on Emergent Phenomena in the Dynamics of Quantum Matter, New York, 2014* (unpublished).

[43] B. Wouters, M. Brockmann, J. De Nardis, D. Fioretto, M. Rigol, and J.-S. Caux, Phys. Rev. Lett. **113**, 117202 (2014)

[44] A. Auerbach, Interacting Electrons and Quantum Magnetism (Springer, New York, 1994).

[45] F. H. L. Essler and R. M. Konik, in *From Fields to Strings: Circumnavigating Theoretical Physics*, edited by Misha Shifman, Arkady Vainshtein, and John Wheater, Ian Kogan Memorial Collection Vol. 3 (World Scientific, Singapore, 2004), p. 684.

[46] P. Calabrese and J. Cardy, J. Stat. Mech. (2005) P04010.

[47] P. Calabrese and J. Cardy, Phys. Rev. Lett. **96**, 136801 (2006).

[48] A. B. Kuklov and B. V. Svistunov, Phys. Rev. Lett. **90**, 100401 (2003).

[49] L.-M. Duan, E. Demler, and M. D. Lukin, Phys. Rev. Lett. **91**, 090402 (2003).

[50] T. Barthel, C. Kasztelan, I. P. McCulloch, and U. Schollwöck, Phys. Rev. A **79**, 053627 (2009).

[51] J. Simon, W. S. Bakr, R. Ma, M. E. Tai, P. M. Preiss, and M. Greiner, Nature (London) **472**, 307 (2011).

[52] Y.-A. Chen, S. Nascimbène, M. Aidelsburger, M. Atala, S. Trotzky, and I. Bloch, Phys. Rev. Lett. **107**, 210405 (2011).

[53] C. K. Majumdar and D. K. Ghosh, J. Math. Phys. **10**, 1388 (1969).

[54] G. Vidal, Phys. Rev. Lett. **93**, 040502 (2004).

[55] G. Vidal, Phys. Rev. Lett. **98**, 070201 (2007).

[56] This approach is justified in the TDL, where off-diagonal contributions vanish.

[57] The region of validity of the ITEBD simulations was determined by comparing results using different bond dimensions and the observed saturation of the entanglement. Our real-time simulation results are consistent with those obtained in Ref. [1].

[58] See the Supplemental Material below for details of the ITEBD simulation and numerical data.

[59] B. Pozsgay, M. Mestyán, M. A. Werner, M. Kormos, and G. Takács (to be published).

[60] H. Bethe, Zeitschrift fur Physik **71**, 205 (1931).

[61] M. Takahashi, Thermodynamics of One-Dimensional Solvable Models (Cambridge University Press, Cambridge, England, 1999).

[62] K. K. Kozlowski and B. Pozsgay, J. Stat. Mech. (2012) P05021.

[63] B. Pozsgay, J. Stat. Mech. (2014) P06011.

[64] M. Brockmann, J. De Nardis, B. Wouters, and J.-S. Caux, J. Phys. A **47**, 145003 (2014).

[65] M. Brockmann, J. De Nardis, B. Wouters, and J.-S. Caux, arXiv:1403.7469.

[66] C. N. Yang and C. P. Yang, J. Math. Phys. **10**, 1115 (1969).

[67] M. Lüscher, Nucl. Phys. B **117**, 475 (1976).

[68] M. Mestyán and B. Pozsgay, J. Stat. Mech. (2014) P09020.

References

[1] M. Fagotti, M. Collura, F. H. L. Essler, and P. Calabrese, Phys. Rev. B **89**, 125101 (2014).

[2] B. Pozsgay, J. Stat. Mech. P07003 (2013).

From "A note on symmetry reductions of the Lindblad equation: transport in constrained open spin chains" by Buč, Prosen

References

[1] I. Bloch, J. Dalibard, and W. Zwerger, Many-Body Physics with Ultracold Gases, Rev. Mod. Phys. 80, 885 (2008).

[2] A. Polkovnikov, K. Sengupta, A. Silva, and M. Vengalattore, Nonequilibrium dynamics of closed interacting quantum systems, Rev. Mod. Phys. **83**, 863 (2011) .

[3] C. W. Gardiner and P. Zoller, Quantum Noise, A Handbook of Markovian and Non-Markovian Quantum Stochastic Methods with Applications to Quantum Optics Springer, Berlin (2004).

[4] H.-P. Breuer and F. Petruccione, The Theory of Open Quantum Systems (Oxford University Press, Oxford 2002).

[5] R. Alicki and K. Lendi, Quantum Dynamical Semigroups and Applications, (Springer, Berlin Heidelberg 2007).

[6] G. Lindblad, On the generators of quantum dynamical semigroups, Comm. Math. Phys. **48**, 119 (1976).

[7] V. Gorini, A. Kossakowski and E. C. G. Sudarshan, Completely positive semigroups of N-level systems, J. Math. Phys. **17**, 821 (1976).

[8] K. Saito, Strong evidence of normal heat conduction in a one-dimensional quantum system, Europhys. Lett. **61**, 34 (2003).

[9] M. Michel, M. Hartmann, J. Gemmer and G. Mahler, Fourier's Law confirmed for a class of small quantum systems, Eur. Phys. J. B **34**, 325 (2003).

[10] C. Mejia-Monasterio, T. Prosen and G. Casati, Fourier's law in a quantum spin chain and the onset of quantum chaos, Europhys. Lett. **72**, 520 (2005).

[11] R. Steinigeweg, J. Gemmer and M. Michel, Normal-transport behavior in finite one-dimensional chaotic quantum systems, Europhys. Lett. **75**, 406 (2006).

[12] H. Wichterich, M. J. Henrich, H.-P. Breuer, J. Gemmer, and M. Michel, Modeling heat transport through completely positive maps, Phys. Rev. E **76**, 031115 (2007).

[13] T. Prosen, Third quantization: a general method to solve master equations for quadratic open Fermi systems, New J. Phys **10**, 043026 (2008).

[14] M. Michel, O. Hess, H. Wichterich and J. Gemmer, Transport in open spin chains: A Monte Carlo wave-function approach, Phys. Rev. B **77**, 104303 (2008).

[15] Y. Yan, C.-Q. Wu, G. Casati, T. Prosen, and B. Li, Nonballistic heat conduction in an integrable random-exchange Ising chain studied with quantum master equations, Phys. Rev. B **77**, 172411 (2008).

[16] X. Zotos and P. Prelovšek, Transport in one dimensional quantum systems, `http://arxiv.org/abs/cond-mat/0304630`.

[17] J. Sirker, R. G. Pereira, and I. Affleck, Conservation laws, integrability, and transport in one-dimensional quantum systems, Phys. Rev. B **83**, 035115 (2011).

[18] F. Heidrich-Meisner, A. Honecker, W. Brenig, Transport in quasi one-dimensional spin-1/2 systems, Eur. Phys. J. Special Topics **151**, 135 (2007).

[19] B. Kraus, H. P. Bchler, S. Diehl, A. Kantian, A. Micheli, P. Zoller, Preparation of Entangled States by Quantum Markov Processes, Phys. Rev. A **78**, 042307 (2008); S. Diehl, A. Micheli, A. Kantian, B. Kraus, H.P. Bchler, P. Zoller, Quantum States and Phases in Driven Open Quantum Systems with Cold Atoms, Nature Physics **4**, 878 (2008).

[20] D. A. Lidar and K. B. Whaley, Decoherence-Free Subspaces and Subsystems, in "Irreversible Quantum Dynamics", F. Benatti and R. Floreanini (Eds.), pp. 83-120 (Springer Lecture Notes in Physics vol. 622, Berlin, 2003); R. Blume-Kohout, Hui Khoon Ng, D. Poulin and L. Viola, The structure of preserved information in quantum processes, Phys. Rev. Lett. 100 030501 (2008).

[21] C. Simon et al., Quantum memories, Eur. Phys. J. D **58**, 1 (2010).

[22] D. E. Evans, Irreducible Quantum Dynamical Semigroups, Comm. Math. Phys. **54**, 293 (1977).

[23] H. Spohn, An algebraic condition for the approach to equilibrium of an open N-Level system, Lett. Math. Phys. **2**, 33 (1977).

[24] J. Eisert and T. Prosen, Noise-driven quantum criticality, `arXiv:1012.5013`; M. Hoening, M. Moos and M. Fleischhauer, Critical exponents of flux-equilibrium phase transitions in fermionic lattice models, `arXiv:1108.2263` .

[25] T. Prosen and M. Žnidarič, Matrix product simulations of non-equilibrium steady states of quantum spin chains, J. Stat. Mech, P02035 (2009).

[26] R. Steinigeweg, Decay of currents for strong interactions, Phys. Rev. E **84**, 011136 (2011).

[27] Mierzejewski, Bonca, Prelovsek, Integrable Mott Insulators Driven by a Finite Electric Field, Phys. Rev. Lett. **107**, 126601 (2011); R. Steinigeweg, J. Herbrych, P. Prelovšek and M. Mierzejewski, Coexistence of Anomalous and Normal Diffusion in Integrable Mott Insulators, `http://arxiv.org/abs/1201.2844`.

[28] V. Eisler, Crossover between ballistic and diffusive transport: the quantum exclusion process, J. Stat. Mech. (2011) P06007.

[29] K. Temme, M. M. Wolf and F. Verstraete, Stochastic exclusion processes versus coherent transport, `http://arxiv.org/abs/0912.0858`.

[30] M. Žnidarič, Solvable quantum nonequilibrium model exhibiting a phase transition and a matrix product representation, Phys. Rev. E 83, 011108 (2011); M. Žnidarič, Dephasing-induced diffusive transport in the anisotropic Heisenberg model, New J. Phys. **12**, 043001 (2010).

[31] G. Benenti, G. Casati, T. Prosen and D. Rossini, Negative differential conductivity in far-from-equilibrium quantum spin chains, Europhys. Lett. **85**, 37001 (2009)

[32] G. Benenti, G. Casati, T. Prosen, D. Rossini and M. Žnidarič, Charge and spin transport in strongly correlated one-dimensional quantum systems driven far from equilibrium, Phys. Rev. B **80**, 035110 (2009).

[33] T. Prosen and M. Žnidarič, Long-Range Order in Nonequilibrium Interacting Quantum Spin Chains, Phys. Rev. Lett. 105, 060603 (2010).

[34] T. Prosen, Open XXZ Spin Chain: Nonequilibrium Steady State and a Strict Bound on Ballistic Transport, Phys. Rev. Lett. **106**, 217206 (2011); T. Prosen, Exact Nonequilibrium Steady State of a Strongly Driven Open XXZ Chain, Phys. Rev. Lett. **107**, 137201 (2011).

[35] M. Žnidarič, Spin transport in a one-dimensional anisotropic Heisenberg model, Phys. Rev. Lett. **106**, 220601 (2011); M. Žnidarič, Transport in a one-dimensional isotropic Heisenberg model at high temperature, J. Stat. Mech. 2011, P12008 (2011).

[36] T. Prosen and I. Pižorn, High order non-unitary split-step decomposition of unitary operators, J. Phys. A: Math. Gen. 39, 5957 (2006).

[37] P. Prelovšek, S. El Shawish, X. Zotos, and M. Long, Anomalous scaling of conductivity in integrable fermion systems, Phys. Rev. B **70**, 205129 (2004).

[38] R. Steinigeweg and W. Brenig, Spin transport in the XXZ chain at finite temperature and momentum, Phys. Rev. Lett. **107**, 250602 (2011).

From Engineering GGE with trapped ions

References

[7] A. Polkovnikov, K. Sengupta, A. Silva, and M. Vengalattore, Rev. Mod. Phys. **83**, 863 (2011).

[2] C. Gogolin and J. Eisert, Rep. Prog. Phys. **79**, 056001 (2016).

[1] M. Rigol, V. Dunjko, V. Yurovsky, and M. Olshanii, Phys. Rev. Lett. **98**, 050405 (2007).

[4] F. H. L. Essler and M. Fagotti, J. Stat. Mech.: Theory Exp. P064002 (2016).

[3] L. Vidmar and M. Rigol, J. Stat. Mech.: Theory Exp. P064007 (2016).

[11] M. A. Cazalilla and M.-C. Chung, J. Stat. Mech.: Theory Exp. **2016**, 064004 (2016).

[5] J.-S. Caux, J. Stat. Mech.: Theory Exp. P064006 (2016).

[47] P. Calabrese and J. Cardy, J. Stat. Mech.: Theory Exp. **2007**, P06008 (2007).

[48] M. Cramer, C. M. Dawson, J. Eisert, and T. J. Osborne, Phys. Rev. Lett. **100**, 030602 (2008).

[49] T. Barthel and U. Schollwöck, Phys. Rev. Lett. **100**, 100601 (2008).

[50] F. H. L. Essler, S. Evangelisti, and M. Fagotti, Phys. Rev. Lett. **109**, 247206 (2012).

[36] B. Pozsgay, J. Stat. Mech.: Theory Exp. P07003 (2013).

[37] M. Fagotti and F. H. L. Essler, Phys. Rev. B **87**, 245107 (2013).

[25] M. Fagotti and F. H. Essler, J. Stat. Mech.: Theory Exp. P07012 (2013).

[15] B. Wouters, J. De Nardis, M. Brockmann, D. Fioretto, M. Rigol, and J.-S. Caux, Phys. Rev. Lett. **113**, 117202 (2014).

[16] B. Pozsgay, J. Stat. Mech.: Theory Exp. **2014**, P10045 (2014).

[58] S. Sotiriadis and P. Calabrese, J. Stat. Mech.: Theory Exp. **2014**, P07024 (2014).

[59] G. Goldstein and N. Andrei, Phys. Rev. A **90**, 043625 (2014).

[60] M. Brockmann, B. Wouters, D. Fioretto, J. De Nardis, R. Vlijm, and J.-S. Caux, J. Stat. Mech.: Theory Exp. **2014**, P12009 (2014).

[62] M. Rigol, Phys. Rev. E **90**, 031301(R) (2014).

[63] M. Mestyán, B. Pozsgay, G. Takács, and M. A. Werner, J. Stat. Mech.: Theory Exp. **2015**, P04001 (2015).

[2] E. Ilievski, J. De Nardis, B. Wouters, J.-S. Caux, F. H. L. Essler, and T. Prosen, Phys. Rev. Lett. **115**, 157201 (2015).

[64] J. Eisert, M. Friesdorf, and C. Gogolin, Nat. Phys. **11**, 124 (2015).

[65] E. Ilievski, E. Quinn, J. De Nardis, and M. Brockmann, J. Stat. Mech.: Theory Exp. **2016**, 063101 (2016).

[66] L. Piroli, E. Vernier, and P. Calabrese, Phys. Rev. B **94**, 054313 (2016).

[19] T. Langen, S. Erne, R. Geiger, B. Rauer, T. Schweigler, M. Kuhnert, W. Rohringer, I. E. Mazets, T. Gasenzer, and J. Schmiedmayer, Science **348**, 207 (2015).

[41] B. Bertini, F. H. L. Essler, S. Groha, and N. J. Robinson, Phys. Rev. Lett. **115**, 180601 (2015).

[11] B. Bertini, F. H. L. Essler, S. Groha, and N. J. Robinson, Phys. Rev. B **94**, 245117 (2016).

[29] K. Mallayya and M. Rigol, Phys. Rev. Lett. **120**, 070603 (2018).

[30] K. Mallayya, M. Rigol, and W. De Roeck, Phys. Rev. X **9**, 021027 (2019).

[31] J. Durnin, M. Bhaseen, and B. Doyon, arXiv preprint arXiv:2004.11030 (2020).

[32] Y. Tang, W. Kao, K.-Y. Li, S. Seo, K. Mallayya, M. Rigol, S. Gopalakrishnan, and B. L. Lev, Phys. Rev. X **8**, 021030 (2018).

[33] C. Li, T. Zhou, I. Mazets, H.-P. Stimming, Z. Zhu, Y. Zhai, W. Xiong, X. Zhou, X. Chen, and J. Schmiedmayer, arXiv preprint arXiv:1804.01969 (2018).

[34] J.-S. Caux, B. Doyon, J. Dubail, R. Konik, and T. Yoshimura, SciPost Phys. **6**, 70 (2019).

[13] M. Schemmer, I. Bouchoule, B. Doyon, and J. Dubail, Phys. Rev. Lett. **122**, 090601 (2019).

[36] F. Møller, C. Li, I. Mazets, H.-P. Stimming, T. Zhou, Z. Zhu, X. Chen, and J. Schmiedmayer, arXiv preprint arXiv:2006.08577 (2020).

[40] M. Moeckel and S. Kehrein, Phys. Rev. Lett. **100**, 175702 (2008).

[95] M. Kollar, F. A. Wolf, and M. Eckstein, Physical Review B **84**, 054304 (2011).

[103] R. Barnett, A. Polkovnikov, and M. Vengalattore, Phys. Rev. A **84**, 023606 (2011).

[29] M. Gring, M. Kuhnert, T. Langen, T. Kitagawa, B. Rauer, M. Schreitl, I. Mazets, D. A. Smith, E. Demler, and J. Schmiedmayer, Science **337**, 1318 (2012).

[97] A. Mitra, Phys. Rev. B **87**, 205109 (2013).

[98] M. Marcuzzi, J. Marino, A. Gambassi, and A. Silva, Phys. Rev. Lett. **111**, 197203 (2013).

[52] F. H. L. Essler, S. Kehrein, S. R. Manmana, and N. J. Robinson, Phys. Rev. B **89**, 165104 (2014).

[104] N. Nessi, A. Iucci, and M. A. Cazalilla, Phys. Rev. Lett. **113**, 210402 (2014).

[100] M. Babadi, E. Demler, and M. Knap, Phys. Rev. X **5**, 041005 (2015).

[106] E. Canovi, M. Kollar, and M. Eckstein, Phys. Rev. E **93**, 012130 (2016).

[26] F. Lange, Z. Lenarčič, and A. Rosch, Nat. Commun. **8**, 15767 (2017).

[25] F. Lange, Z. Lenarčič, and A. Rosch, Phys. Rev. B **97**, 165138 (2018).

[18] Z. Lenarčič, F. Lange, and A. Rosch, Phys. Rev. B **97**, 024302 (2018).

[25] J. T. Barreiro, M. Müller, P. Schindler, D. Nigg, T. Monz, M. Chwalla, M. Hennrich, C. F. Roos, P. Zoller, and R. Blatt, Nature **470**, 486 (2011).

[51] Y. Lin, J. Gaebler, F. Reiter, T. Tan, R. Bowler, A. Sørensen, D. Leibfried, and D. Wineland, Nature **504** (2013), 10.1038/nature12801.

[52] D. Leibfried, R. Blatt, C. Monroe, and D. Wineland, Rev. Mod. Phys. **75**, 281 (2003).

[17] D. Porras and J. I. Cirac, Phys. Rev. Lett. **92**, 207901 (2004).

[54] X.-L. Deng, D. Porras, and J. I. Cirac, Phys. Rev. A **72**, 063407 (2005).

[18] A. Friedenauer, H. Schmitz, J. T. Glueckert, D. Porras, and T. Schaetz, Nat. Phys. **4**, 757 (2008).

[56] K. Kim, M.-S. Chang, S. Korenblit, R. Islam, E. E. Edwards, J. K. Freericks, G.-D. Lin, L.-M. Duan, and C. Monroe, Nature **465**, 590 (2010).

[25] J. W. Britton, B. C. Sawyer, A. C. Keith, C.-C. J. Wang, J. K. Freericks, H. Uys, M. J. Biercuk, and J. J. Bollinger, Nature **484**, 489 (2012).

[6] R. Islam, C. Senko, W. C. Campbell, S. Korenblit, J. Smith, A. Lee, E. E. Edwards, C.-C. J. Wang, J. K. Freericks, and C. Monroe, Science **340**, 583 (2013).

[21] P. Jurcevic, B. P. Lanyon, P. Hauke, C. Hempel, P. Zoller, R. Blatt, and C. F. Roos, Nature **511**, 202 (2014).

[60] P. Richerme, Z.-X. Gong, A. Lee, C. Senko, J. Smith, M. Foss-Feig, S. Michalakis, A. V. Gorshkov, and C. Monroe, Nature **511**, 198 (2014).

[61] J. G. Bohnet, B. C. Sawyer, J. W. Britton, M. L. Wall, A. M. Rey, M. Foss-Feig, and J. J. Bollinger, Science **352**, 1297 (2016).

[47] J. Zhang, G. Pagano, P. W. Hess, A. Kyprianidis, P. Becker, H. Kaplan, A. V. Gorshkov, Z.-X. Gong, and C. Monroe, Nature **551**, 601 (2017).

[63] C. Kokail, C. Maier, R. van Bijnen, T. Brydges, M. K. Joshi, P. Jurcevic, C. A. Muschik, P. Silvi, R. Blatt, C. F. Roos, and P. Zoller, Nature **569**, 355 (2019).

[64] A. Safavi-Naini, R. J. Lewis-Swan, J. G. Bohnet, M. Gärttner, K. A. Gilmore, J. E. Jordan, J. Cohn, J. K. Freericks, A. M. Rey, and J. J. Bollinger, Phys. Rev. Lett. **121**, 040503 (2018).

[65] E. Jordan, K. A. Gilmore, A. Shankar, A. Safavi-Naini, J. G. Bohnet, M. J. Holland, and J. J. Bollinger, Phys. Rev. Lett. **122**, 053603 (2019).

[66] J. I. Cirac and P. Zoller, Nature **404**, 579 (2000).

[67] A. C. Wilson, Y. Colombe, K. R. Brown, E. Knill, D. Leibfried, and D. J. Wineland, Nature **512**, 57 (2014).

[68] D. Yang, G. S. Giri, M. Johanning, C. Wunderlich, P. Zoller, and P. Hauke, Phys. Rev. A **94**, 052321 (2016).

[69] M. Mielenz, H. Kalis, M. Wittemer, F. Hakelberg, U. Warring, R. Schmied, M. Blain, P. Maunz, D. L. Moehring, D. Leibfried, and T. Schaetz, Nat. Commun. **7**, 11839 (2016).

[70] S. Jain, J. Alonso, M. Grau, and J. P. Home, Phys. Rev. X **10**, 031027 (2020).

[71] M. D. Barrett, B. DeMarco, T. Schaetz, V. Meyer, D. Leibfried, J. Britton, J. Chiaverini, W. M. Itano, B. Jelenković, J. D. Jost, C. Langer, T. Rosenband, and D. J. Wineland, Phys. Rev. A **68**, 042302 (2003).

[72] M. Guggemos, D. Heinrich, O. A. Herrera-Sancho, R. Blatt, and C. F. Roos, New Journal of Physics **17**, 103001 (2015).

[73] V. Negnevitsky, M. Marinelli, K. K. Mehta, H.-Y. Lo, C. Flühmann, and J. P. Home, Nature **563**, 527 (2018).

[24] A. Bastianello, J. De Nardis, and A. De Luca, arXiv preprint arXiv:2003.01702 (2020).

[75] K. Yamamoto, Y. Ashida, and N. Kawakami, arXiv preprint arXiv:2009.00838 (2020).

[8] F. Reiter and A. S. Sørensen, Phys. Rev. A **85**, 032111 (2012).

[77] F. Reiter, D. Reeb, and A. S. Sørensen, Phys. Rev. Lett. **117**, 040501 (2016).

[78] F. Reiter, A. S. Sørensen, P. Zoller, and C. Muschik, Nat. Commun. **8**, 1822 (2017).

[79] D. V. F. James, Applied Physics B **66**, 181 (1998).

[80] P. Schindler, D. Nigg, T. Monz, J. T. Barreiro, E. Martinez, S. X. Wang, S. Quint, M. F. Brandl, V. Nebendahl, C. F. Roos, M. Chwalla, M. Hennrich, and R. Blatt, New Journal of Physics **15**, 123012 (2013).

[81] U. Warring, C. Ospelkaus, Y. Colombe, R. Jördens, D. Leibfried, and D. J. Wineland, Phys. Rev. Lett. **110**, 173002 (2013).

[82] S. Debnath, N. M. Linke, C. Figgatt, K. A. Landsman, K. Wright, and C. Monroe, Nature **536**, 63 (2016).

[83] K. A. Landsman, Y. Wu, P. H. Leung, D. Zhu, N. M. Linke, K. R. Brown, L. Duan, and C. Monroe, Phys. Rev. A **100**, 022332 (2019).

[84] A. Johnson, S. S. Szigeti, M. Schemmer, and I. Bouchoule, Phys. Rev. A **96**, 013623 (2017).

[30] I. Bouchoule, B. Doyon, and J. Dubail, arXiv preprint arXiv:2006.03583 (2020).

[35] Z. Lenarčič, O. Alberton, A. Rosch, and E. Altman, arXiv preprint arXiv:1910.01548 (2019).

[87] T. Shirai and T. Mori, Phys. Rev. E **101**, 042116 (2020).

[8] T. Prosen, Phys. Rev. Lett. **106**, 217206 (2011).

From Quasiparticle cooling algorithms for quantum many-body state preparation

References

[1] B. P. Lanyon, J. D. Whitfield, G. G. Gillett, M. E. Goggin, M. P. Almeida, I. Kassal, J. D. Biamonte, M. Mohseni, B. J. Powell, M. Barbieri, et al., Towards quantum chemistry on a quantum computer, Nature chemistry **2**, 106 (2010).

[2] A. Kandala, A. Mezzacapo, K. Temme, M. Takita, M. Brink, J. M. Chow, and J. M. Gambetta, Hardware-efficient variational quantum eigensolver for small molecules and quantum magnets, nature **549**, 242 (2017).

[3] B. Bauer, S. Bravyi, M. Motta, and G. K.-L. Chan, Quantum algorithms for quantum chemistry and quantum materials science, Chemical Reviews **120**, 12685 (2020).

[4] G. A. Quantum, Collaborators*†, F. Arute, K. Arya, R. Babbush, D. Bacon, J. C. Bardin, R. Barends, S. Boixo, M. Broughton, B. B. Buckley, et al., Hartree-fock on a superconducting qubit quantum computer, Science **369**, 1084 (2020).

[5] A. B. Finnila, M. A. Gomez, C. Sebenik, C. Stenson, and J. D. Doll, Quantum annealing: A new method for minimizing multidimensional functions, Chemical physics letters **219**, 343 (1994).

[6] E. Farhi, J. Goldstone, S. Gutmann, J. Lapan, A. Lundgren, and D. Preda, A quantum adiabatic evolution algorithm applied to random instances of an np-complete problem, Science **292**, 472 (2001).

[7] A. Y. Kitaev, Quantum measurements and the abelian stabilizer problem (1995), arXiv:quant-ph/9511026 [quant-ph] .

[8] D. S. Abrams and S. Lloyd, Quantum algorithm providing exponential speed increase for finding eigenvalues and eigenvectors, Phys. Rev. Lett. **83**, 5162 (1999).

[9] E. Farhi, J. Goldstone, S. Gutmann, and M. Sipser, Quantum computation by adiabatic evolution, arXiv preprint quant-ph/0001106 (2000).

[10] D. Poulin and P. Wocjan, Preparing ground states of quantum many-body systems on a quantum computer, Phys. Rev. Lett. **102**, 130503 (2009).

[11] S. Boixo, E. Knill, and R. D. Somma, Eigenpath traversal by phase randomization, Quantum Inf. Comput. **9**, 833 (2009).

[12] Y. Ge, J. Tura, and J. I. Cirac, Faster ground state preparation and high-precision ground energy estimation with fewer qubits, Journal of Mathematical Physics **60**, 022202 (2019).

[13] J. Preskill, Quantum computing in the nisq era and beyond, Quantum **2**, 79 (2018).

[14] T. Albash and D. A. Lidar, Adiabatic quantum computation, Reviews of Modern Physics **90**, 015002 (2018).

[15] M. Greiner, O. Mandel, T. Esslinger, T. W. Hänsch, and I. Bloch, Quantum phase transition from a superfluid to a mott insulator in a gas of ultracold atoms, Nature **415**, 39 (2002).

[16] J. Simon, W. S. Bakr, R. Ma, M. E. Tai, P. M. Preiss, and M. Greiner, Quantum simulation of antiferromagnetic spin chains in an optical lattice, Nature **472**, 307 (2011).

[17] G. Semeghini, H. Levine, A. Keesling, S. Ebadi, T. T. Wang, D. Bluvstein, R. Verresen, H. Pichler, M. Kalinowski, R. Samajdar, A. Omran, S. Sachdev, A. Vishwanath, M. Greiner, V. Vuletić, and M. D. Lukin, Probing topological spin liquids on a programmable quantum simulator, Science **374**, 1242 (2021), https://www.science.org/doi/pdf/10.1126/science.abi8794 .

[18] P. Scholl, M. Schuler, H. J. Williams, A. A. Eberharter, D. Barredo, K.-N. Schymik, V. Lienhard, L.-P. Henry, T. C. Lang, T. Lahaye, A. M. Läuchli, and A. Browaeys, Quantum simulation of 2d antiferromagnets with hundreds of rydberg atoms, Nature **595**, 233 (2021).

[19] M. Cerezo, A. Arrasmith, R. Babbush, S. C. Benjamin, S. Endo, K. Fujii, J. R. McClean, K. Mitarai, X. Yuan, L. Cincio, et al., Variational quantum algorithms, Nature Reviews Physics **3**, 625 (2021).

[20] J. Tilly, H. Chen, S. Cao, D. Picozzi, K. Setia, Y. Li, E. Grant, L. Wossnig, I. Rungger, G. H. Booth, and J. Tennyson, The variational quantum eigensolver: A review of methods and best practices, Physics Reports **986**, 1 (2022).

[21] D. A. Fedorov, B. Peng, N. Govind, and Y. Alexeev, Vqe method: a short survey and recent developments, Materials Theory **6**, 1 (2022).

[22] K. Bharti, A. Cervera-Lierta, T. H. Kyaw, T. Haug, S. Alperin-Lea, A. Anand, M. Degroote, H. Heimonen, J. S. Kottmann, T. Menke, W.-K. Mok, S. Sim, L.-C. Kwek, and A. Aspuru-Guzik, Noisy intermediate-scale quantum algorithms, Rev. Mod. Phys. **94**, 015004 (2022).

[23] T. Louvet, T. Ayral, and X. Waintal, Go-no go criteria for performing quantum chemistry calculations on quantum computers (2023), arXiv:2306.02620 [quant-ph] .

[24] J. R. McClean, S. Boixo, V. N. Smelyanskiy, R. Babbush, and H. Neven, Barren plateaus in quantum neural network training landscapes, Nature communications **9**, 4812 (2018).

[25] S. Wang, E. Fontana, M. Cerezo, K. Sharma, A. Sone, L. Cincio, and P. J. Coles, Noise-induced barren plateaus in variational quantum algorithms, Nature Communications **12**, 6961 (2021).

[26] S. H. Sack, R. A. Medina, A. A. Michailidis, R. Kueng, and M. Serbyn, Avoiding barren plateaus using classical shadows, PRX Quantum **3**, 020365 (2022).

[27] B. M. Terhal and D. P. DiVincenzo, Problem of equilibration and the computation of correlation functions on a quantum computer, Phys. Rev. A **61**, 022301 (2000).

[28] E. B. Davies, Markovian master equations, Communications in mathematical Physics **39**, 91 (1974).

[29] B. Kraus, H. P. Büchler, S. Diehl, A. Kantian, A. Micheli, and P. Zoller, Preparation of entangled states by quantum markov processes, Phys. Rev. A **78**, 042307 (2008).

[30] S. Diehl, A. Micheli, A. Kantian, B. Kraus, H. P. Büchler, and P. Zoller, Quantum states and phases in driven open quantum systems with cold atoms, Nat. Phys. **4**, 878 (2008).

[31] F. Verstraete, M. M. Wolf, and J. Ignacio Cirac, Quantum computation and quantum-state engineering driven by dissipation, Nat. Phys. **5**, 633 (2009).

[32] S. Roy, J. Chalker, I. Gornyi, and Y. Gefen, Measurement-induced steering of quantum systems, Physical Review Research **2**, 033347 (2020).

[33] M. J. Kastoryano and F. G. Brandao, Quantum gibbs samplers: The commuting case, Communications in Mathematical Physics **344**, 915 (2016).

[34] C.-F. Chen, M. J. Kastoryano, F. G. S. L. Brandão, and A. Gilyén, Quantum thermal state preparation (2023), arXiv:2303.18224 [quant-ph] .

[25] J. T. Barreiro, M. Müller, P. Schindler, D. Nigg, T. Monz, M. Chwalla, M. Hennrich, C. F. Roos, P. Zoller, and R. Blatt, An open-system quantum simulator with trapped ions, Nature **470**, 486 (2011).

[36] Y. Lin, J. P. Gaebler, F. Reiter, T. R. Tan, R. Bowler, A. S. Sørensen, D. Leibfried, and D. J. Wineland, Dissipative production of a maximally entangled steady state of two quantum bits, Nature **504**, 415 (2013).

[37] S. Shankar, M. Hatridge, Z. Leghtas, K. M. Sliwa, A. Narla, U. Vool, S. M. Girvin, L. Frunzio, M. Mirrahimi, and M. H. Devoret, Autonomously stabilized entanglement between two superconducting quantum bits, Nature **504**, 419 (2013).

[38] X. Mi, A. Michailidis, S. Shabani, K. Miao, P. Klimov, J. Lloyd, E. Rosenberg, R. Acharya, I. Aleiner, T. Andersen, et al., Stable quantum-correlated many-body states through engineered dissipation, Science **383**, 1332 (2024).

[39] D. A. Abanin, W. De Roeck, W. W. Ho, and F. Huveneers, Effective Hamiltonians, prethermalization, and slow energy absorption in periodically driven many-body systems, Physical Review B **95**, 014112 (2017).

[40] M. Metcalf, J. E. Moussa, W. A. de Jong, and M. Sarovar, Engineered thermalization and cooling of quantum many-body systems, Physical Review Research **2**, 023214 (2020).

[41] M. Raghunandan, F. Wolf, C. Ospelkaus, P. O. Schmidt, and H. Weimer, Initialization of quantum simulators by sympathetic cooling, Sci. Adv. **6**, eaaw9268 (2020).

[42] S. Polla, Y. Herasymenko, and T. E. O'Brien, Quantum digital cooling, Phys. Rev. A **104**, 012414 (2021).

[43] A. Matthies, M. Rudner, A. Rosch, and E. Berg, Programmable adiabatic demagnetization for systems with trivial and topological excitations (2023), arXiv:2210.17256 [quant-ph] .

[44] D. A. Puente, F. Motzoi, T. Calarco, G. Morigi, and M. Rizzi, Quantum state preparation via engineered ancilla resetting, arXiv preprint arXiv:2305.08641 (2023).

[45] L. Marti, R. Mansuroglu, and M. J. Hartmann, Efficient quantum cooling algorithm for fermionic systems (2024), arXiv:2403.14506 [quant-ph] .

[46] P. Coleman, Introduction to Many-Body Physics (Cambridge University Press, 2015).

[47] E. Lieb, T. Schultz, and D. Mattis, Two soluble models of an antiferromagnetic chain, Annals of Physics **16**, 407 (1961).

[48] S. Sachdev, Quantum phase transitions, Physics world **12**, 33 (1999).

[49] A. A. Ovchinnikov, D. V. Dmitriev, V. Y. Krivnov, and V. O. Cheranovskii, Antiferromagnetic ising chain in a mixed transverse and longitudinal magnetic field, Phys. Rev. B **68**, 214406 (2003).

[50] E. Dagotto and T. Rice, Surprises on the way from one-to two-dimensional quantum magnets: The ladder materials, Science **271**, 618 (1996).

[81] For protocols considered below, f_τ can be positive or negative, but for this choice the sum $\sum_{\tau=1}^{T} |f_\tau| \gtrsim 1$.

[52] H.-P. Breuer and F. Petruccione, The theory of open quantum systems (Oxford University Press, USA, 2002).

[53] D. A. Lidar, Lecture notes on the theory of open quantum systems (2020), arXiv:1902.00967 [quant-ph] .

[54] M. Rigol, V. Dunjko, V. Yurovsky, and M. Olshanii, Relaxation in a completely integrable many-body quantum system: An ab initio study of the dynamics of the highly excited states of 1d lattice hard-core bosons, Phys. Rev. Lett. **98**, 050405 (2007).

[55] F. Lange, Z. Lenarčič, and A. Rosch, Time-dependent generalized gibbs ensembles in open quantum systems, Physical Review B **97**, 165138 (2018).

[56] F. Gerbino, I. Lesanovsky, and G. Perfetto, Large-scale universality in quantum reaction-diffusion from keldysh field theory, Physical Review B **109**, L220304 (2024).

[57] M. B. Hastings and X.-G. Wen, Quasiadiabatic continuation of quantum states: The stability of topological ground-state degeneracy and emergent gauge invariance, Physical Review B—Condensed Matter and Materials Physics **72**, 045141 (2005).

[58] In practice it is the spectral function that is measured in experiment and the validity of the quasiparticle description requires the existence of a sharp pole.

[59] We note that the normalization factor is chosen according to the condition $\sum_{\tau=1}^{T} f_\tau = 1$. The modulated coupling in Eq. (17.38) is sign-changing, however, $\sum_{\tau=1}^{T} |f_\tau|$ is of order 1 for all cases considered below.

[60] M. Thakurathi, A. A. Patel, D. Sen, and A. Dutta, Floquet generation of majorana end modes and topological invariants, Phys. Rev. B **88**, 155133 (2013).

[61] B. Bauer, T. Pereg-Barnea, T. Karzig, M.-T. Rieder, G. Refael, E. Berg, and Y. Oreg, Topologically protected braiding in a single wire using floquet majorana modes, Phys. Rev. B **100**, 041102 (2019).

[62] A. Lerose, M. Sonner, and D. A. Abanin, Scaling of temporal entanglement in proximity to integrability, Phys. Rev. B **104**, 035137 (2021).

[63] M. Žnidarič, Relaxation times of dissipative many-body quantum systems, Physical Review E **92**, 042143 (2015).

[64] Heating processes, in particular due to noise, may in principle involve a large number of particles; however, we will find that few-quasiparticle processes are dominant, and considering them gives an accurate approximation of heating rates.

[65] G. B. Mbeng, A. Russomanno, and G. E. Santoro, The quantum ising chain for beginners (2020), arXiv:2009.09208 [quant-ph] .

[66] F. Verstraete, J. J. García-Ripoll, and J. I. Cirac, Matrix product density operators: Simulation of finite-temperature and dissipative systems, Phys. Rev. Lett. **93**, 207204 (2004).

[67] M. Zwolak and G. Vidal, Mixed-state dynamics in one-dimensional quantum lattice systems: A time-dependent superoperator renormalization algorithm, Phys. Rev. Lett. **93**, 207205 (2004).

[68] G. Vidal, Efficient classical simulation of slightly entangled quantum computations, Physical review letters **91**, 147902 (2003).

[69] G. Vidal, Efficient simulation of one-dimensional quantum many-body systems, Physical review letters **93**, 040502 (2004).

[70] M. Fishman, S. R. White, and E. M. Stoudenmire, The ITensor Software Library for Tensor Network Calculations, SciPost Phys. Codebases , 4 (2022).

[71] T. Barnes, E. Dagotto, J. Riera, and E. Swanson, Excitation spectrum of heisenberg spin ladders, Physical Review B **47**, 3196 (1993).

[72] M. Azuma, Z. Hiroi, M. Takano, K. Ishida, and Y. Kitaoka, Observation of a spin gap in sr cu 2 o 3 comprising spin-1/2 quasi-1d two-leg ladders, Physical review letters **73**, 3463 (1994).

[73] S. Notbohm, P. Ribeiro, B. Lake, D. Tennant, K. Schmidt, G. Uhrig, C. Hess, R. Klingeler, G. Behr, B. Büchner, et al., One-and two-triplon spectra of a cuprate ladder, Physical review letters **98**, 027403 (2007).

[74] L. Vanderstraeten, F. Verstraete, and J. Haegeman, Scattering particles in quantum spin chains, Physical Review B **92**, 125136 (2015).

[75] S. V. Isakov, D. Kafri, O. Martin, C. V. Heidweiller, W. Mruczkiewicz, M. P. Harrigan, N. C. Rubin, R. Thomson, M. Broughton, K. Kissell, et al., Simulations of quantum circuits with approximate noise using qsim and cirq, arXiv preprint arXiv:2111.02396 (2021).

[76] X. Mi, M. Sonner, M. Y. Niu, K. W. Lee, B. Foxen, R. Acharya, I. Aleiner, T. I. Andersen, F. Arute, K. Arya, et al., Noise-resilient edge modes on a chain of superconducting qubits, Science **378**, 785 (2022).

[77] The steady state can be efficiently found by root-finding algorithms, after the cooling and noise-induced rates have been calculated via Wick's theorem. In practice, the system reaches its steady state quickly and we evolve the rate equation in time until the quasiparticle occupations have effectively converged.

[78] G. Modugno, G. Ferrari, G. Roati, R. J. Brecha, A. Simoni, and M. Inguscio, Bose-einstein condensation of potassium atoms by sympathetic cooling, Science **294**, 1320 (2001), https://www.science.org/doi/pdf/10.1126/science.1066687 .

[79] C.-F. Chen, H.-Y. Huang, J. Preskill, and L. Zhou, Local minima in quantum systems, in Proceedings of the 56th Annual ACM Symposium on Theory of Computing (2024) pp. 1323–1330.

[80] S. Bravyi, M. B. Hastings, and F. Verstraete, Lieb-robinson bounds and the generation of correlations and topological quantum order, Physical review letters **97**, 050401 (2006).

[81] M. B. Hastings, Topological order at nonzero temperature, Physical review letters **107**, 210501 (2011).

[82] G. Kishony, M. S. Rudner, A. Rosch, and E. Berg, Gauged cooling of topological excitations and emergent fermions on quantum simulators, arXiv preprint arXiv:2310.16082 (2023).

[83] C.-F. Chen and F. G. Brandao, Fast thermalization from the eigenstate thermalization hypothesis, arXiv preprint arXiv:2112.07646 (2021).

[84] J. Kempe, A. Kitaev, and O. Regev, The complexity of the local hamiltonian problem, Siam journal on computing **35**, 1070 (2006).

[85] O. Shtanko and R. Movassagh, Preparing thermal states on noiseless and noisy programmable quantum processors (2023), arXiv:2112.14688 [quant-ph] .

[86] I. Ulčakar and Z. Lenarčič, Generalized gibbs ensembles in weakly interacting dissipative systems and digital quantum computers, arXiv preprint arXiv:2406.17033 (2024).

[87] P. Rall, C. Wang, and P. Wocjan, Thermal State Preparation via Rounding Promises, Quantum **7**, 1132 (2023).

[88] A. Lerose, M. Sonner, and D. A. Abanin, Scaling of temporal entanglement in proximity to integrability, Physical Review B **104**, 035137 (2021).

[89] N. Iorgov, V. Shadura, and Y. Tykhyy, Spin operator matrix elements in the quantum ising chain: fermion approach, Journal of Statistical Mechanics: Theory and Experiment **2011**, P02028 (2011).

[90] E. Barouch and B. M. McCoy, Statistical mechanics of the x y model. ii. spin-correlation functions, Physical Review A **3**, 786 (1971).

[91] T. Barthel and Y. Zhang, Solving quasi-free and quadratic lindblad master equations for open fermionic and bosonic systems, Journal of Statistical Mechanics: Theory and Experiment **2022**, 113101 (2022).

[92] R. Orús, A practical introduction to tensor networks: Matrix product states and projected entangled pair states, Annals of physics **349**, 117 (2014).

[93] J. C. Bridgeman and C. T. Chubb, Hand-waving and interpretive dance: an introductory course on tensor networks, Journal of physics A: Mathematical and theoretical **50**, 223001 (2017).

From Equilibration, thermalisation, and the emergence of statistical mechanics in closed quantum systems

References

[1] Gibbs J W 1902 Elementary principles in statistical mechanics (New York: C. Scribner)

[2] Uffink J 2006 Compendium of the foundations of classical statistical physics URL http://philsci-archive.pitt.edu/id/eprint/2691

[3] Neumann J 1929 Z. Phys. **57** 30

[4] Landau L D and Lifshitz E M 1980 Statistical physics 3rd ed (Course of Theoretical Physics vol 5) (Butterworth-Heinemann)

[5] Greiner M, Mandel O, Hänsch T W and Bloch I 2002 Nature **419** 51 doi: 10.1038/nature00968

[6] Greiner M, Mandel O, Esslinger T, Hänsch T W and Bloch I 2002 Nature **415** 39 doi: 10.1038/415039a

[7] Tuchman A, Orzel C, Polkovnikov A and Kasevich M 2006 Phys. Rev. A **74** 051601 doi: 10.1103/PhysRevA.74.051601

[8] Aidelsburger M, Atala M, Nascimbène S, Trotzky S, Chen Y A and Bloch I 2011 Phys. Rev. Lett. **107** 255301 doi: 10.1103/PhysRevLett.107.255301

[9] Bloch I 2005 Nature Phys. **1** 23 doi: 10.1038/nphys138

[10] Langen T, Geiger R and Schmiedmayer J 2015 Ann. Rev. Condens. Matter Phys. **6** 201 doi: 10.1146/annurev-conmatphys-031214-014548

[11] Sadler L E, Higbie J M, Leslie S R, Vengalattore M and Stamper-Kurn D M 2006 Nature **443** 312 doi: 10.1038/nature05094

[12] Regal C and Jin D S 2005 Experimental realization of BCS-BEC crossover physics with a Fermi gas Phd thesis University of Colorado preprint `arXiv:0601054`

[13] Kinoshita T, Wenger T and Weiss D S 2006 Nature **440** 900 doi: 10.1038/nature04693

[14] Hofferberth S, Lesanovsky I, Fischer B, Schumm T and Schmiedmayer J 2007 Nature **449** 324 doi: 10.1038/nature06149

[15] Weller A, Ronzheimer J P, Gross C, Esteve J, Oberthaler M K, Theocharis G and Kevrekidis P G 2008 Phys. Rev. Lett. **101** 130401 doi: 10.1103/PhysRevLett.101.130401

[16] Strohmaier N, Takasu Y, Günter K, Jördens R, Köhl M, Moritz H and Esslinger T 2007 Phys. Rev. Lett. **99** 220601 doi: 10.1103/PhysRevLett.99.220601

[17] Porras D and Cirac J I 2004 Phys. Rev. Lett. **92** 207901 doi: 10.1103/PhysRevLett.92.207901

[18] Friedenauer A, Schmitz H, Glückert J T, Porras D and Schätz T 2008 Nature Phys. **4** 757 doi: 10.1038/nphys1032

[19] Bissbort U, Cocks D, Negretti a, Idziaszek Z, Calarco T, Schmidt-Kaler F, Hofstetter W and Gerritsma R 2013 Phys. Rev. Lett. **111** 080501 doi: 10.1103/PhysRevLett.111.080501

[20] Häffner H, Hänsel W, Roos C F, Benhelm J, Chek-al Kar D, Chwalla M, Körber T, Rapol U D, Riebe M, Schmidt P O, Becher C, Gühne O, Dür W and Blatt R 2005 Nature **438** 643 doi: 10.1038/nature04279

[21] Jurcevic P, Lanyon B P, Hauke P, Hempel C, Zoller P, Blatt R and Roos C F 2014 Nature **511** 202 doi: 10.1038/nature13461

[22] Lanyon B P, Hempel C, Nigg D, Müller M, Gerritsma R, Zähringer F, Schindler P, Barreiro J T, Rambach M, Kirchmair G, Hennrich M, Zoller P, Blatt R and Roos C F 2011 Science **334** 57 doi: 10.1126/science.1208001

[23] Schindler P, Müller M, Nigg D, Barreiro J T, Martinez E A, Hennrich M, Monz T, Diehl S, Zoller P and Blatt R 2013 Nature Phys. **9** 361 doi: 10.1038/nphys2630

[24] Blatt R and Roos C F 2012 Nature Phys. **8** 277 doi: 10.1038/nphys2252

[25] Britton J W, Sawyer B C, Keith A C, Wang C C J, Freericks J K, Uys H, Biercuk M J and Bollinger J J 2012 Nature **484** 489 doi: 10.1038/nature10981

[26] Trotzky S, Chen Y A, Flesch A, McCulloch I P, Schollwöck U, Eisert J and Bloch I 2012 Nature Phys. **8** 325 doi: 10.1038/nphys2232

[27] Cheneau M, Barmettler P, Poletti D, Endres M, Schauss P, Fukuhara T, Gross C, Bloch I, Kollath C and Kuhr S 2012 Nature **481** 484 doi: 10.1038/nature10748

[28] Langen T, Geiger R, Kuhnert M, Rauer B and Schmiedmayer J 2013 Nature Phys. **9** 640 doi: 10.1038/nphys2739

[29] Gring M, Kuhnert M, Langen T, Kitagawa T, Rauer B, Schreitl M, Mazets I, Smith D A, Demler E and Schmiedmayer J 2012 Science **337** 1318 doi: 10.1126/science.1224953

[30] Ronzheimer J P, Schreiber M, Braun S, Hodgman S S, Langer S, McCulloch I P, Heidrich-Meisner F, Bloch I and Schneider U 2013 Phys. Rev. Lett. **110** 205301 doi: 10.1103/PhysRevLett.110.205301

[31] Orus R 2014 Ann. Phys. **349** 117 doi: 10.1016/j.aop.2014.06.013

[32] Schollwöck U 2011 Ann. Phys. **326** 96 doi: 10.1016/j.aop.2010.09.012

[33] Rigol M, Dunjko V and Olshanii M 2008 Nature **452** 854 doi: 10.1038/nature06838

[34] Rigol M 2009 Phys. Rev. Lett. **103** 100403 doi: 10.1103/PhysRevLett.103.100403

[35] Luitz D J, Laflorencie N and Alet F 2015 Phys. Rev. B **91** 081103(R) doi: 10.1103/PhysRevB.91.081103

[36] Troyer M, Alet F, Trebst S and Wessel S 2003 AIP Conf. Proc. **690** 156 doi: 10.1063/1.1632126

[37] Foulkes W, Mitas L, Needs R and Rajagopal G 2001 Rev. Mod. Phys. **73** 33 doi: 10.1103/RevModPhys.73.33

[38] Aoki H, Tsuji N, Eckstein M, Kollar M, Oka T and Werner P 2014 Rev. Mod. Phys. **86** 779 doi: 10.1103/RevModPhys.86.779

[39] Engel E, Dreizler R M, Rankings I, Algorithms S, Introduction A, Preferences M, Algorithms R S and Algorithms C S 2011 Density functional theory Theoretical and Mathematical Physics (Springer)

[40] Kohn W 1999 Rev. Mod. Phys. **71** 1253 doi: 10.1103/RevModPhys.71.1253

[41] Braun S, Friesdorf M, Hodgman S S, Schreiber M, Ronzheimer J P, Riera A, del Rey M, Bloch I, Eisert J and Schneider U 2015 Proc. Natl. Acad. Sc. **112** 3641 doi: 10.1073/pnas.1408861112

[42] Rigol M, Dunjko V, Yurovsky V and Olshanii M 2007 Phys. Rev. Lett. **98** 50405 doi: 10.1103/PhysRevLett.98.050405

[43] Lesanovsky I, Olmos B and Garrahan J P 2010 Phys. Rev. Lett. **105** 100603 doi: 10.1103/PhysRevLett.105.100603

[44] Dubey S, Silvestri L, Finn J, Vinjanampathy S and Jacobs K 2012 Phys. Rev. E **85** 011141 doi: 10.1103/PhysRevE.85.011141

[45] Beugeling W, Moessner R and Haque M 2014 Phys. Rev. E **89** 042112 doi: 10.1103/PhysRevE.89.042112

[46] Yukalov V 2011 Laser Phys. Lett. **8** 485 doi: 10.1002/lapl.201110002

[47] Ikeda T N, Watanabe Y and Ueda M 2013 Phys. Rev. E **87** 012125 doi: 10.1103/PhysRevE.87.012125

[48] Fine B V, Elsayed T A, Kropf C M and de Wijn A S 2014 Phys. Rev. E **89** 012923 doi: 10.1103/PhysRevE.89.012923

[49] Jensen R and Shankar R 1985 Phys. Rev. Lett. **54** 1879 doi: 10.1103/PhysRevLett.54.1879

[50] Moeckel M and Kehrein S 2008 Phys. Rev. Lett. **100** 175702 doi: 10.1103/PhysRevLett.100.175702

[51] Kollath C, Läuchli A and Altman E 2007 Phys. Rev. Lett. **98** 180601 doi: 10.1103/PhysRevLett.98.180601

[52] Deng S, Ortiz G and Viola L 2011 Phys. Rev. B **83** 094304 doi: 10.1103/PhysRevB.83.094304

[53] Campos Venuti L and Zanardi P 2010 Phys. Rev. A **81** 032113 doi: 10.1103/PhysRevA.81.032113

[54] Goth F and Assaad F F 2012 Phys. Rev. B **85** 085129 doi: 10.1103/PhysRevB.85.085129

[55] Rigol M and Fitzpatrick M 2011 Phys. Rev. A **84** 033640 doi: 10.1103/PhysRevA.84.033640

[56] Torres-Herrera E J and Santos L F 2014 Phys. Rev. A **89** 043620 doi: 10.1103/PhysRevA.89.043620

[57] Sengupta K, Powell S and Sachdev S 2004 Phys. Rev. A **69** 053616 doi: 10.1103/PhysRevA.69.053616

[58] Flesch A, Cramer M, McCulloch I, Schollwöck U and Eisert J 2008 Phys. Rev. A **78** 33608 doi: 10.1103/PhysRevA.78.033608

[59] Ates C, Garrahan J P and Lesanovsky I 2012 Phys. Rev. Lett. **108** 110603 doi: 10.1103/PhysRevLett.108.110603

[60] Fagotti M 2013 Phys. Rev. B **87** 165106 doi: 10.1103/PhysRevB.87.165106

[61] Calabrese P and Cardy J 2007 J. Stat. Mech. **2007** P06008 doi: 10.1088/1742-5468/2007/06/P06008

[62] Cazalilla M 2006 Phys. Rev. Lett. **97** 156403 doi: 10.1103/PhysRevLett.97.156403

[63] Fioretto D and Mussardo G 2010 New J. Phys. **12** 055015 doi: 10.1088/1367-2630/12/5/055015

[64] Calabrese P, Essler F H L and Fagotti M 2011 Phys. Rev. Lett. **106** 227203 doi: 10.1103/PhysRevLett.106.227203

[65] Eckstein M and Kollar M 2008 Phys. Rev. Lett. **100** 120404 doi: 10.1103/PhysRevLett.100.120404

[66] Campos Venuti L and Zanardi P 2010 Phys. Rev. A **81** 22113 doi: 10.1103/PhysRevA.81.022113

[67] Lloyd S 1988 Black holes, demons and the loss of coherence: How complex systems get information, Phd thesis Rockefeller University

[68] Popescu S, Short A J and Winter A 2005 preprint arXiv:quant-ph/0511225

[69] Gemmer J, Michel M and Mahler G 2009 Quantum thermodynamics (Lecture Notes in Physics vol 784) (Berlin, Heidelberg: Springer)

[70] Garnerone S 2013 Phys. Rev. B **88** 165140 doi: 10.1103/PhysRevB.88.165140

[71] Garnerone S and de Oliveira T R 2013 Phys. Rev. B **87** 214426 doi: 10.1103/PhysRevB.87.214426

[72] Hastings M B and Koma T 2006 Commun. Math. Phys. **265** 781 doi: 10.1007/s00220-006-0030-4

[73] Nachtergaele B and Sims R 2009 Locality estimates for quantum spin systems New trends in mathematical physics ed Sidoravičius V (Springer Netherlands) p 591

[74] Bravyi S, Hastings M and Verstraete F 2006 Phys. Rev. Lett. **97** 50401 doi: 10.1103/PhysRevLett.97.050401

[75] Kliesch M, Gogolin C and Eisert J 2014 Lieb-Robinson bounds and the simulation of time evolution of local observables in lattice systems Many-electron approaches in physics, chemistry and mathematics Mathematical Physics Studies ed Bach V and Delle Site L (Springer) p 301 preprint arXiv:1306.0716

[76] Calabrese P and Cardy J 2007 J. Stat. Mech. P10004 doi: 10.1088/1742-5468/2007/10/P10004

[77] Chiara G D, Montangero S, Calabrese P and Fazio R 2006 J. Stat. Mech. **2006** P03001 doi: 10.1088/1742-5468/2006/03/P03001

[78] Eisert J and Osborne T 2006 Phys. Rev. Lett. **97** 150404 doi: 10.1103/PhysRevLett.97.150404

[79] Läuchli A and Kollath C 2008 J. Stat. Mech. P05018 doi: 10.1088/1742-5468/2008/05/P05018

[80] Van Acoleyen K, Mariën M and Verstraete F 2013 Phys. Rev. Lett. **111** 5 doi: 10.1103/PhysRevLett.111.170501

[81] Lloyd S 2013 preprint arXiv:1307.0378

[82] Eisert J, Friesdorf M and Gogolin C 2015 Nature Phys. **11** 124 doi: 10.1038/nphys3215

[83] Cazalilla M A and Rigol M 2010 New J. Phys. **12** 55006 doi: 10.1088/1367-2630/12/5/055006

[84] Polkovnikov A, Sengupta K, Silva A and Vengalattore M 2011 Rev. Mod. Phys. **83** 863 doi: 10.1103/RevModPhys.83.863

[85] Seifert U 2012 Rep. Prog. Phys. **75** 126001 doi: 10.1088/0034-4885/75/12/126001

[86] Goold J, Huber M, Riera A, del Rio L and Skrzypzyk P 2016 J. Phys. A **49** 143001 doi: 10.1088/1751-8113/49/14/143001

[87] Nielsen M A and Chuang I L 2007 Quantum computation and quantum information (Cambridge University Press)

[88] Bhatia R 1997 Matrix analysis (New York: Springer)

[89] Short A J 2011 New J. Phys. **13** 053009 doi: 10.1088/1367-2630/13/5/053009

[90] Aubrun G and Lancien C 2013 Positivity preprint arXiv:1309.6003v1

[91] Short A J and Farrelly T C 2012 New J. Phys. **14** 013063 doi: 10.1088/1367-2630/14/1/013063

[92] Besicovitch A S 1926 Proc. Lond. Math. Soc. **s2-25** 495 doi: 10.1112/plms/s2-25.1.495

[93] Bañuls M C, Cirac J I and Wolf M M 2009 J. Phys. **171** 012032 doi: 10.1088/1742-6596/171/1/012032

[94] Friis N, Lee A and Bruschi D 2013 Phys. Rev. A **87** 022338 doi: 10.1103/PhysRevA.87.022338

[95] Kastoryano M J 2011 Quantum Markov chain mixing and dissipative engineering Phd thesis University of Copenhagen

[96] Kastoryano M J and Eisert J 2013 J. Math. Phys. **54** 102201 doi: 10.1063/1.4822481

[97] Plenio M B and Virmani S 2005 Quant. Inf. Comput. **7** 1 doi: 10.1007/978-3-319-04063-9-8

[98] Thirring W 2002 Quantum mathematical physics 2nd ed (Berlin Heidelberg: Springer)

[99] Bhattacharyya K and Mukherjee D 1986 J. Chem. Phys. **84** 3212 doi: 10.1063/1.450251

[100] Schulman L 1978 Phys. Rev. A **18** 2379 doi: 10.1103/PhysRevA.18.2379

[101] Peres A 1982 Phys. Rev. Lett. **49** 1118 doi: 10.1103/PhysRevLett.49.1118

[102] Bocchieri P and Loinger A 1957 Phys. Rev. **107** 337 doi: 10.1103/PhysRev.107.337

[103] Wallace D 2013 J. Math. Phys. **56** 022105 doi: 10.1063/1.4907384

[104] Haar D 1955 Rev. Mod. Phys. **27** 289 doi: 10.1103/RevModPhys.27.289

[105] Tasaki H 1998 Phys. Rev. Lett. **80** 1373 doi: 10.1103/PhysRevLett.80.1373

[106] Reimann P 2008 Phys. Rev. Lett. **101** 190403 doi: 10.1103/PhysRevLett.101.190403

[107] Linden N, Popescu S, Short A and Winter A 2009 Phys. Rev. E **79** 61103 doi: 10.1103/PhysRevE.79.061103

[108] Reimann P 2012 Phys. Scr. **86** 058512 doi: 10.1088/0031-8949/86/05/058512

[109] Reimann P and Kastner M 2012 New J. Phys. **14** 043020 doi: 10.1088/1367-2630/14/4/043020

[110] Hübener R, Sekino Y and Eisert J 2015 JHEP 166 doi: 10.1007/JHEP04(2015)166

[111] Cramer M and Eisert J 2009 New J. Phys. **12** 27 doi: 10.1088/1367-2630/12/5/055020

[112] Cramer M, Dawson C M, Eisert J and Osborne T J 2008 Phys. Rev. Lett. **100** 30602 doi: 10.1103/PhysRevLett.100.030602

[113] Neuenhahn C and Marquardt F 2012 Phys. Rev. E **85** 060101 doi: 10.1103/PhysRevE.85.060101

[114] Levstein P R, Usaj G and Pastawski H M 1998 J. Chem. Phys. **108** 2718 doi: 10.1063/1.475664

[115] Ledoux M 2001 The concentration of measure phenomenon (Mathematical Surveys and Monographs vol 89) (Americal Mathematical Society)

[116] Chatterjee S 2007 J. Func. Ana. **245** 379 doi: 10.1016/j.jfa.2007.01.003

[117] Popescu S, Short A J and Winter A 2006 Nature Phys. **2** 754 doi: 10.1038/nphys444

[118] Gogolin C 2010 Pure state quantum statistical mechanics Master's thesis Universität Würzburg preprint arXiv:1003.5058

[119] Bocchieri P and Loinger A 1959 Phys. Rev. **114** 948 doi: 10.1103/PhysRev.114.948

[120] Gogolin C 2014 Equilibration and thermalization in quantum systems Phd thesis Freie Universität Berlin URL http://www.cgogolin.de/downloads/Dissertation_Christian_Gogolin_Published.pdf

[121] Gong Z X and Duan L M 2011 preprint arXiv:1109.4696

[122] Cui S, Cao J P, Jing H, Fan H and Liu W M 2011 preprint arXiv:1110.4690

[123] Rigol M, Muramatsu A and Olshanii M 2006 Phys. Rev. A **74** 053616 doi: 10.1103/PhysRevA.74.053616

[124] Zhuang Q and Wu B 2013 Phys. Rev. E **88** 062147 doi: 10.1103/PhysRevE.88.062147

[125] Hutter A 2011 Understanding equipartition and thermalization from decoupling Master's thesis Institute for Theoretical Physics ETH Zürich

[126] Dupuis F, Berta M, Wullschleger J and Renner R 2014 Commun. Math. Phys. **328** 251 doi: 10.1007/s00220-014-1990-4

[127] Szehr O, Dupuis F, Tomamichel M and Renner R 2013 New J. Phys. **15** 053022 doi: 10.1088/1367-2630/15/5/053022

[128] Szehr O 2012 Decoupling theorems Master's thesis ETH Zurich preprint arXiv:1207.3927

[129] Konig R, Renner R and Schaffner C 2009 IEEE Trans. Inf. Th. **55** 4337 doi: 10.1109/TIT.2009.2025545

[130] Ciganović N, Beaudry N J and Renner R 2014 IEEE Trans. Inf. Th. **60** 1573 doi: 10.1109/TIT.2013.2295314

[131] Neumann J 2010 Europ. Phys. J. H **35** 201 doi: 10.1140/epjh/e2010-00008-5

[132] Goldstein S, Lebowitz J L, Mastrodonato C, Tumulka R and Zanghi N 2010 Proc. Roy. Soc. A **466** 3203 doi: 10.1098/rspa.2009.0635

[133] Brandão F G S L, Ćwikliński P, Horodecki M, Horodecki P, Korbicz J K and Mozrzymas M 2012 Phys. Rev. E **86** 031101 doi: 10.1103/PhysRevE.86.031101

[134] Masanes L, Roncaglia A J and Acín A 2013 Phys. Rev. E **87** 032137 doi: 10.1103/PhysRevE.87.032137

[135] Cramer M 2011 New J. Phys. **14** 053051 doi: 10.1088/1367-2630/14/5/053051

[136] Žnidarič M 2012 J. Phys. A **45** 125204 doi: 10.1088/1751-8113/45/12/125204

[137] Eisert J and Plenio M B 2003 Int. J. Quant. Inf. **1** 479 doi: 10.1142/S0219749903000371

[138] Braunstein S L 2005 Rev. Mod. Phys. **77** 513 doi: 10.1103/RevModPhys.77.513

[139] Adesso G and Illuminati F 2007 J. Phys. A **40** 7821 doi: 10.1088/1751-8113/40/28/S01

[140] Weedbrook C, Pirandola S, Garcia-Patron R, Cerf N J, Ralph T C, Shapiro J H and Lloyd S 2012 Rev. Mod. Phys. **84** 621 doi: 10.1103/RevModPhys.84.621

[141] Dudnikova T V, Komech a I and Spohn H 2003 J. Math. Phys. **44** 2596 doi: 10.1063/1.1571658

[142] Lanford O E and Robinson D W 1972 Commun. Math. Phys. **24** 193 doi: 10.1007/BF01877712

[143] Tegmark M and Yeh L 1994 Physica A **202** 342 doi: 10.1016/0378-4371(94)90181-3

[144] Barthel T and Schollwöck U 2008 Phys. Rev. Lett. **100** 100601 doi: 10.1103/PhysRevLett.100.100601

[145] Reed M and Simon B 1980 Methods of modern mathematical physics I: Functional Analysis (San Diego: Academic Press)

[146] Reed M and Simon B 1975 Methods of modern mathematical physics II: Fourier analysis, self-adjoint (San Diego: Academic Press)

[147] Goldstein S, Hara T and Tasaki H 2015 New J. Phys. **17** 045002 doi: 10.1088/1367-2630/17/4/045002

[148] Batu T, Fischer E, Fortnow L, Kumar R, Rubinfeld R and White P 2001 Testing random variables for independence and identity Proc. 2001 IEEE Int. Conf. Cluster Comp. (IEEE Comput. Soc) p 442 doi: 10.1109/SFCS.2001.959920

[149] Batu T, Fortnow L, Rubinfeld R, Smith W D and White P 2000 Testing that distributions are close Proceedings 41st Annual Symposium on Foundations of Computer Science (IEEE Comput. Soc) p 259 doi: 10.1109/SFCS.2000.892113

[150] Canonne C, Ron D and Servedio R A 2012 preprint arXiv:1211.2664

[151] Audenaert K M R, Mosonyi M and Verstraete F 2012 J. Math. Phys. **53** 122205 doi: 10.1063/1.4768252

[152] Audenaert K M R 2014 Quant. Inf. Comput. **14** 31

[153] Ududec C, Wiebe N and Emerson J 2013 Phys. Rev. Lett. **111** 080403 doi: 10.1103/PhysRevLett.111.080403

[154] Lieb E H and Robinson D W 1972 Commun. Math. Phys. **28** 251 doi: 10.1007/BF01645779

[155] Nachtergaele B and Sims R 2010 Contemp. Math. **529** 141

[156] Calabrese P and Cardy J 2006 Phys. Rev. Lett. **96** 136801 doi: 10.1103/PhysRevLett.96.136801

[157] Calabrese P and Cardy J 2005 J. Stat. Mech. P04010 doi: 10.1088/1742-5468/2005/04/P04010

[158] Geiger R, Langen T, Mazets I E and Schmiedmayer J 2014 New J. Phys. **16** 22 doi: 10.1088/1367-2630/16/5/053034

[159] Hauke P and Tagliacozzo L 2013 Phys. Rev. Lett. **111** 207202 doi: 10.1103/PhysRevLett.111.207202

[160] Mazza L, Rossini D, Endres M and Fazio R 2014 Phys. Rev. B **90** 020301(R) doi: 10.1103/PhysRevB.90.020301

[161] Richerme P, Gong Z X, Lee A, Senko C, Smith J, Foss-Feig M, Michalakis S, Gorshkov A V and Monroe C 2014 Nature **511** 198 doi: 10.1038/nature13450

[162] Nachtergaele B, Vershynina A and Zagrebnov V A 2011 AMS Contemp. Math. **552** 161

[163] Poulin D 2010 Phys. Rev. Lett. **104** 190401 doi: 10.1103/PhysRevLett.104.190401

[164] Eisert J, van den Worm M, Manmana S R and Kastner M 2013 Phys. Rev. Lett. **111** 260401 doi: 10.1103/PhysRevLett.111.260401

[165] Schuch N, Harrison S K, Osborne T J and Eisert J 2011 Phys. Rev. A **84** 032309 doi: 10.1103/PhysRevA.84.032309

[166] Nachtergaele B, Raz H, Schlein B and Sims R 2009 Commun. Math. Phys. **286** 1073 doi: 10.1007/s00220-008-0630-2

[167] Cramer M, Serafini A and Eisert J 2007 Locality of dynamics in general harmonic quantum systems Quantum information and many-body quantum systems preprint arXiv:0803.0890

[168] Burrell C K and Osborne T J 2007 Phys. Rev. Lett. **99** 167201 doi: 10.1103/PhysRevLett.99.167201

[169] Kim I H, Chandran A and Abanin D A 2014 preprint arXiv:1412.3073

[170] Hamza E and Sims Rand Stolz G 2012 Commun. Math. Phys. **315** 215 doi: 10.1007/s00220-012-1544-6

[171] Friesdorf M, Werner A H, Brown W, Scholz V B and Eisert J 2015 Phys. Rev. Lett. **14** 170505 doi: 10.1103/PhysRevLett.114.170505

[172] Malabarba A S L, García-Pintos L P, Linden N, Farrelly T C and Short A J 2014 Phys. Rev. E **90** 012121 doi: 10.1103/PhysRevE.90.012121

[173] Schiulaz M, Silva A and Markus M 2015 Phys. Rev. B **91** 184202 doi: 10.1103/PhysRevB.91.184202

[174] Sirker J, Konstantinidis N P, Andraschko F and Sedlmayr N 2014 Phys. Rev. A **89** 042104 doi: 10.1103/PhysRevA.89.042104

[175] Campos Venuti L, Jacobson N T, Santra S and Zanardi P 2011 Phys. Rev. Lett. **107** 010403 doi: 10.1103/PhysRevLett.107.010403

[176] Sorg S, Vidmar L, Pollet L and Heidrich-Meisner F 2014 Phys. Rev. A **90** 033606 doi: 10.1103/PhysRevA.90.033606

[177] Kim H, Bañuls M C, Cirac J I, Hastings M B and Huse D A 2015 Phys. Rev. E **92** 012128 doi: 10.1103/PhysRevE.92.012128

[178] Khatami E, Rigol M, Relaño A and García-García A M 2012 Phys. Rev. E **85** 050102 doi: 10.1103/PhysRevE.85.050102

[179] Brandino G P, De Luca A, Konik R M and Mussardo G 2012 Phys. Rev. B **85** 214435 doi: 10.1103/PhysRevB.85.214435

[180] Brandao F G S L, Harrow A W and Horodecki M 2012 preprint arXiv:1208.0692

[181] Kota V K B, Relaño A, Retamosa J and Vyas M 2011 J. Stat. Mech. **2011** P10028 doi: 10.1088/1742-5468/2011/10/P10028

[182] Fyodorov Y V 2005 Recent perspectives in random matrix theory and number theory, 31–78, London Math. Soc. Lecture Note Ser., 322

[183] Guhr T, Müller, Groeling A and Weidenmüller H A 1998 Phys. Rep. **299** 189 doi: 10.1016/S0370-1573(97)00088-4

[184] Canovi E, Rossini D, Fazio R, Santoro G E and Silva A 2011 Phys. Rev. B **83** 094431 doi: 10.1103/PhysRevB.83.094431

[185] Tabor M 1989 Chaos and integrability in nonlinear dynamics: An introduction (New York: Wiley)

[186] Bohigas O, Giannoni M and Schmit C 1984 Phys. Rev. Lett. **52** 1 doi: 10.1103/PhysRevLett.52.1

[187] Tao T 2012 Topics in random matrix theory (Graduate studies in mathematics vol 132) (Americal Mathematical Society)

[188] Mehta M L 1991 Random matrices Pure and Applied Mathematics (Academic Press)

[189] Srednicki M 1994 Phys. Rev. E **50** 888 doi: 10.1103/PhysRevE.50.888

[190] Hutter A and Wehner S 2013 Phys. Rev. A **87** 012121 doi: 10.1103/PhysRevA.87.012121

[191] Kastner M 2011 Phys. Rev. Lett. **106** 130601 doi: 10.1103/PhysRevLett.106.130601

[192] Bochner S and Chandrasekharan K 1949 Fourier transforms (Princeton University Press)

[193] Flambaum V V and Izrailev F M 2001 Phys. Rev. E **64** 026124 doi: 10.1103/PhysRevE.64.026124

[194] Torres-Herrera E J and Santos L F 2014 Phys. Rev. A **90** 033623 doi: 10.1103/PhysRevA.90.033623

[195] Torres-Herrera E J, Vyas M and Santos L F 2014 New J. Phys. **16** 063010 doi: 10.1088/1367-2630/16/6/063010

[196] Barouch E, McCoy B and Dresden M 1970 Phys. Rev. A **2** 1075 doi: 10.1103/PhysRevA.2.1075

[197] Krutitsky K V, Navez P, Queisser F and Schützhold R 2014 EPJ Quant. Tech. **1** doi: 10.1140/epjqt12

[198] Barmettler P, Punk M, Gritsev V, Demler E and Altman E 2009 Phys. Rev. Lett. **102** 130603 doi: 10.1103/PhysRevLett.102.130603

[199] Bañuls M C, Hastings M B, Verstraete F and Cirac J I 2009 Phys. Rev. Lett. **102** 240603 doi: 10.1103/PhysRevLett.102.240603

[200] Müller-Hermes A, Cirac J I and Bañuls M C 2012 New J. Phys. **14** 075003 doi: 10.1088/1367-2630/14/7/075003

[201] Hallberg K A 2006 Adv. Phys. **55** 477 doi: 10.1080/00018730600766432

[202] Cramer M, Flesch A, McCulloch I, Schollwöck U and Eisert J 2008 Phys. Rev. Lett. **101** 063001 doi: 10.1103/PhysRevLett.101.063001

[203] Karrasch C, Rentrop J, Schuricht D and Meden V 2012 Phys. Rev. Lett. **109** 126406 doi: 10.1103/PhysRevLett.109.126406

[204] Queisser F, Krutitsky K V, Navez P and Schützhold R 2014 Phys. Rev. A **89** 033616 doi: 10.1103/PhysRevA.89.033616

[205] Manmana S R, Wessel S, Noack R M and Muramatsu A 2009 Phys. Rev. B **79** 155104 doi: 10.1103/PhysRevB.79.155104

[206] del Campo A and Zurek W H 2014 Int. J. Mod. Phys. A **29** 1430018 doi: 10.1142/S0217751X1430018X

[207] Chandran A, Erez A, Gubser S S and Sondhi S L 2012 Phys. Rev. B **86** 064304 doi: 10.1103/PhysRevB.86.064304

[208] Stephan J M and Dubail J 2011 J. Stat. Mech. P08019 doi: 10.1088/1742-5468/2011/08/P08019

[209] Zangara P R, Dente A D, Torres-Herrera E J, Pastawski H M, Iucci A and Santos L F 2013 Phys. Rev. E **88** 032913 doi: 10.1103/PhysRevE.88.032913

[210] Ponomarev A V, Denisov S and Hänggi P 2011 Phys. Rev. Lett. **106** 010405 doi: 10.1103/PhysRevLett.106.010405

[211] Mossel J, Palacios G and Caux J S 2010 J. Stat. Mech. **2010** L09001 doi: 10.1088/1742-5468/2010/09/L09001

[212] Alba V and Heidrich-Meisner F 2014 Phys. Rev. B **90** 075144 doi: 10.1103/PhysRevB.90.075144

[213] Ponomarev A V, Denisov S, Gemmer J and Hänggi P 2012 Europhys. Lett. **98** 40011 doi: 10.1209/0295-5075/98/40011

[214] Bernard D and Doyon B 2015 Ann. Henri Poincaré **16** 113 doi: 10.1007/s00023-014-0314-8

[215] Bernard D and Doyon B 2012 J. Phys. A **45** 362001 doi: 10.1088/1751-8113/45/36/362001

[216] Bhaseen M J, Doyon B, Lucas A and Schalm K 2015 Nature Phys. **11** 509 doi: 10.1038/nphys3220

[217] Doyon B, Lucas A, Schalm K and Bhaseen M J 2015 J. Phys. A **48** 095002 doi: 10.1088/1751-8113/48/9/095002

[218] De Luca A, Viti J, Bernard D and Doyon B 2013 Phys. Rev. B **88** 134301 doi: 10.1103/PhysRevB.88.134301

[219] Bernard D, Doyon B and Viti J 2015 J. Phys. A **48** 05FT01 doi: 10.1088/1751-8113/48/5/05FT01

[220] Castro-Alvaredo O, Chen Y, Doyon B and Hoogeveen M 2014 J. Stat. Mech. P03011 doi: 10.1088/1742-5468/2014/03/P03011

[221] Gritsev V, Rostunov T and Demler E 2010 J. Stat. Mech. P05012 doi: 10.1088/1742-5468/2010/05/P05012

[222] Cramer M, Eisert J, Plenio M and Dreißig J 2006 Phys. Rev. A **73** 012309 doi: 10.1103/PhysRevA.73.012309

[223] Schuch N, Wolf M M, Verstraete F and Cirac J I 2008 Phys. Rev. Lett. **100** 030504 doi: 10.1103/PhysRevLett.100.030504

[224] Ge Y and Eisert J 2014 preprint `arXiv:1411.2995`

[225] Schuch N, Wolf M M, Vollbrecht K G H and Cirac J I 2008 New J. Phys. **10** 33032 doi: 10.1088/1367-2630/10/3/033032

[226] Eisert J, Cramer M and Plenio M B 2010 Rev. Mod. Phys. **82** 277 doi: 10.1103/RevModPhys.82.277

[227] Horodecki R, Horodecki P, Horodecki M and Horodecki K 2009 Rev. Mod. Phys. **81** 865 doi: 10.1103/RevModPhys.81.865

[228] Bennett C H, Bernstein H J, Popescu S and Schumacher B 1996 Phys. Rev. A **53** 2046

[229] Wootters W K 1998 Phys. Rev. Lett. **80** 2245 doi: 10.1103/PhysRevLett.80.2245

[230] Vidal G and Werner R F 2002 Phys. Rev. A **65** 032314 doi: 10.1103/PhysRevA.65.032314

[231] Eisert J 2001 Entanglement in quantum information theory Phd thesis University of Potsdam preprint `quant-ph/0610253`

[232] Eisert J and Plenio M B 1999 J. Mod. Opt. **46** 145 doi: 10.1080/09500349908231260

[233] Seevinck M P 2010 Quant. Inf. Proc. **9** 273 doi: 10.1007/s11128-009-0161-6

[234] Eisert J, Plenio M B, Bose S and Hartley J 2004 Phys. Rev. Lett. **93** 190402 doi: 10.1103/PhysRevLett.93.190402

[235] Sengupta K and Sen D 2009 Phys. Rev. A **80** 032304 doi: 10.1103/PhysRevA.80.032304

[236] Mazza L, Rossini D, Fazio R and Endres M 2015 New J. Phys. **17** 013015 doi: 10.1088/1367-2630/17/1/013015

[237] Ruutu V M H, Eltsov V B, Gill A J, Kibble T W B, Krusius M, Makhlin Y G, Placais B, Volovik G E and Xu W 1996 Nature **382** 334 doi: 10.1038/382334a0

[238] Ulm S, Roßnagel J, Jacob G, Degünther C, Dawkins S T, Poschinger U G, Nigmatullin R, Retzker A, Plenio M B, Schmidt-Kaler F and Singer K 2013 Nature communications **4** 2290 doi: 10.1038/ncomms3290

[239] Pyka K, Keller J, Partner H L, Nigmatullin R, Burgermeister T, Meier D M, Kuhlmann K, Retzker A, Plenio M B, Zurek W H, del Campo A and Mehlstдubler T E 2013 Nat. Comm. **4** 2291 doi: 10.1038/ncomms3291

[240] Polkovnikov A and Gritsev V 2008 Nature Phys. **4** 477 doi: 10.1038/nphys963

[241] Polkovnikov A 2005 Phys. Rev. B **72** 161201(R) doi: 10.1103/PhysRevB.72.161201

[242] Sen D, Sengupta K and Mondal S 2008 Phys. Rev. Lett. **101** 016806 doi: 10.1103/PhysRevLett.101.016806

[243] Barankov R and Polkovnikov A 2008 Phys. Rev. Lett. **101** 076801 doi: 10.1103/PhysRevLett.101.076801

[244] Schützhold R, Uhlmann M, Xu Y and Fischer U R 2006 Phys. Rev. Lett. **97** 200601 doi: 10.1103/PhysRevLett.97.200601

[245] Fischer U R, Schützhold R and Uhlmann M 2008 Phys. Rev. A **77** 043615 doi: 10.1103/PhysRevA.77.043615

[246] Chen D, White M, Borries C and DeMarco B 2011 Phys. Rev. Lett. **106** 235304 doi: 10.1103/PhysRevLett.106.235304

[247] Bernier J S, Poletti D, Barmettler P, Roux G and Kollath C 2012 Phys. Rev. A **85** 033641 doi: 10.1103/PhysRevA.85.033641

[248] Bernier J S, Roux G and Kollath C 2011 Phys. Rev. Lett. **106** 200601 doi: 10.1103/PhysRevLett.106.200601

[249] Dóra B, Haque M and Zaránd G 2011 Phys. Rev. Lett. **106** 156406 doi: 10.1103/PhysRevLett.106.156406

[250] Uhlmann M, Schützhold R and Fischer U R 2007 Phys. Rev. Lett. **99** 120407 doi: 10.1103/PhysRevLett.99.120407

[251] Uhlmann M, Schützhold R and Fischer U R 2010 New J. Phys. **12** 095020 doi: 10.1088/1367-2630/12/9/095020

[252] Uhlmann M, Schützhold R and Fischer U R 2010 Phys. Rev. D **81** 025017 doi: 10.1103/PhysRevD.81.025017

[253] Campo A and Sengupta K 2015 Eur. Phys. J. Special Topics **224** 189 doi: 10.1140/epjst/e2015-02350-4

[254] Gogolin C, Müller M P and Eisert J 2011 Phys. Rev. Lett. **106** 040401 doi: 10.1103/PhysRevLett.106.040401

[255] Boyd S and Vandenberghe L 2004 Convex optimization (Cambridge: Cambridge University Press)

[256] Brody D C, Hook D W and Hughston L P 2007 J. Phys. A **40** F503 doi: 10.1088/1751-8113/40/26/F01

[257] Perk J, Capel H and Siskens T 1977 Physica A **89** 304 doi: 10.1016/0378-4371(77)90106-6

[258] Girardeau M 1969 Phys. Lett. A **30** 442 doi: 10.1016/0375-9601(69)90232-1

[259] Caux J S and Essler F H L 2013 Phys. Rev. Lett. **110** 257203 doi: 10.1103/PhysRevLett.110.257203

[260] Brockmann M, Wouters B, Fioretto D, Nardis J D, Vlijm R and Caux J S 2014 J. Stat. Mech. **2014** P12009 doi: 10.1088/1742-5468/2014/12/P12009

[261] Cassidy A C, Clark C W and Rigol M 2011 Phys. Rev. Lett. **106** 140405 doi: 10.1103/PhysRevLett.106.140405

[262] Mussardo G 2013 Phys. Rev. Lett. **111** 100401 doi: 10.1103/PhysRevLett.111.100401

[263] Prosen T 2014 Nuclear Physics B **886** 1177 doi: 10.1016/j.nuclphysb.2014.07.024

[264] Wouters B, De Nardis J, Brockmann M, Fioretto D, Rigol M and Caux J S 2014 Phys. Rev. Lett. **113** 117202 doi: 10.1103/PhysRevLett.113.117202

[265] Mestyan M, Pozsgay B, Takacs G and Werner M A 2015 J. Stat. Mech. **2015** P04001 doi: 10.1088/1742-5468/2015/04/P04001

[266] Pozsgay B, Mestyán M, Werner M A, Kormos M, Zaránd G and Takács G 2014 Phys. Rev. Lett. **113** 117203 doi: 10.1103/PhysRevLett.113.117203

[267] Sels D and Wouters M 2015 Phys. Rev. E **92** 022123 doi: 10.1103/PhysRevE.92.022123

[268] Iucci A and Cazalilla M A 2009 Phys. Rev. A **80** 063619 doi: 10.1103/PhysRevA.80.063619

[269] Iucci A and Cazalilla M A 2010 New J. Phys. **12** 055019 doi: 10.1088/1367-2630/12/5/055019

[270] Fagotti M, Collura M, Essler F H L and Calabrese P 2014 Phys. Rev. B **89** 125101 doi: 10.1103/PhysRevB.89.125101

[271] Cazalilla M A, Iucci A and Chung M C 2012 Phys. Rev. E **85** 011133 doi: 10.1103/PhysRevE.85.011133

[272] Sotiriadis S and Calabrese P 2014 J. Stat. Mech. P07024 doi: 10.1088/1742-5468/2014/07/P07024

[273] Kormos M, Collura M and Calabrese P 2014 Phys. Rev. A **89** 013609 doi: 10.1103/PhysRevA.89.013609

[274] Mazza P P, Collura M, Kormos M and Calabrese P 2014 J. of Stat. Mech. **2014** P11016 doi: 10.1088/1742-5468/2014/01/P01009

[275] Kormos M, Shashi A, Chou Y Z, Caux J S and Imambekov A 2013 Phys. Rev. B **88** 205131 doi: 10.1103/PhysRevB.88.205131

[276] Nardis J D, Wouters B, Brockmann M and Caux J S 2014 Phys. Rev. A **89** 033601 doi: 10.1103/PhysRevA.89.033601

[277] Goldstein G and Andrei N 2012 preprint arXiv:1405.4224

[278] Prosen T and Ilievski E 2013 Phys. Rev. Lett. **111** 057203 doi: 10.1103/PhysRevLett.111.057203

[279] Zhang J M, Cui F C and Hu J 2012 Phys. Rev. E **85** 041138 doi: 10.1103/PhysRevE.85.041138

[280] Chen Y and Doyon B 2014 J. Stat. Mech. P09021 doi: 10.1088/1742-5468/2014/09/P09021

[281] Schrödinger E 1927 Ann. Phys. **388** 956 doi: 10.1002/andp.19273881504

[282] Kinchin A I 1949 Mathematical foundations for statistical mechanics (Mineola: Dover Publications, Inc.)

[283] Goldstein S, Lebowitz J, Tumulka R and Zanghì N 2006 Phys. Rev. Lett. **96** 50403 doi: 10.1103/PhysRevLett.96.050403

[284] Schrödinger E 1952 Statistical thermodynamics (Cambridge: Cambridge University Press)

[285] Halmos P R 1974 Measure theory Graduate Texts in Mathematics (New York: Springer)

[286] Haar A 1933 Ann. Math. **34** 147

[287] Zyczkowski K and Sommers H J 2001 J. Phys. A **34** 7111 doi: 10.1088/0305-4470/34/35/335

[288] Brody D C and Hughston L P 1998 J. Math. Phys. **39** 6502 doi: 10.1063/1.532661

[289] Bender C M, Brody D C and Hook D W 2005 J. Phys. A **38** L607 doi: 10.1088/0305-4470/38/38/L01

[290] Brody D C, Hook D W and Hughston L P 2007 Proc. Roy. Soc. A **463** 2021 doi: 10.1098/rspa.2007.1865

[291] Müller M P, Gross D and Eisert J 2011 Commun. Math. Phys. **303** 785 doi: 10.1007/s00220-011-1205-1

[292] Fresch B and Moro G J 2013 Eur. Phys. J. B **86** 233 doi: 10.1140/epjb/e2013-40023-6

[293] Ji K and Fine B V 2011 Phys. Rev. Lett. **107** 050401 doi: 10.1103/PhysRevLett.107.050401

[294] Reimann P 2007 Phys. Rev. Lett. **99** 160404 doi: 10.1103/PhysRevLett.99.160404

[295] Bartsch C and Gemmer J 2009 Phys. Rev. Lett. **102** 110403 doi: 10.1103/PhysRevLett.102.110403

[296] Sugiura S and Shimizu A 2012 Phys. Rev. Lett. **108** 240401 doi: 10.1103/PhysRevLett.108.240401

[297] White S 2009 Phys. Rev. Lett. **102** 190601 doi: 10.1103/PhysRevLett.102.190601

[298] Garnerone S, de Oliveira T R and Zanardi P 2010 Phys. Rev. A **81** 032336 doi: 10.1103/PhysRevA.81.032336

[299] Garnerone S, de Oliveira T R, Haas S and Zanardi P 2010 Phys. Rev. A **82** 052312 doi: 10.1103/PhysRevA.82.052312

[300] Steinigeweg R, Khodja A, Niemeyer H, Gogolin C and Gemmer J 2014 Phys. Rev. Lett. **112** 130403 doi: 10.1103/PhysRevLett.112.130403

[301] Bocchieri P and Loinger A 1958 Phys. Rev. **111** 668 doi: 10.1103/PhysRev.111.668

[302] Farquhar I E and Landsberg P T 1957 Proc. Roy. Soc. A **239** 134 doi: 10.1098/rspa.1957.0027

[303] Jaynes E T 1957 Phys. Rev. **106** 620 doi: 10.1103/PhysRev.106.620

[304] Jaynes E T 1957 Phys. Rev. **108** 171 doi: 10.1103/PhysRev.108.171

[305] Deutsch J 1991 Phys. Rev. A **43** 2046 doi: 10.1103/PhysRevA.43.2046

[306] Reimann P and Evstigneev M 2013 Phys. Rev. E **88** 052114 doi: 10.1103/PhysRevE.88.052114

[307] Berry M V 1977 J. Phys. A **10** 2083 doi: 10.1088/0305-4470/10/12/016

[308] Tasaki H 1997 preprint arXiv:9707255

[309] Mueller M P, Adlam E, Masanes L and Wiebe N 2015 Comm. Math. Phys. **340** 499 doi: 10.1007/s00220-015-2473-y

[310] Bañuls M C, Cirac J I and Hastings M B 2011 Phys. Rev. Lett. **106** 050405 doi: 10.1103/PhysRevLett.106.050405

[311] Riera A, Gogolin C and Eisert J 2012 Phys. Rev. Lett. **108** 080402 doi: 10.1103/PhysRevLett.108.080402

[312] Singh N 2011 preprint arXiv:1103.4003

[313] Larson J 2013 J. Phys. B **46** 224016 doi: 10.1088/0953-4075/46/22/224016

[314] Caux J S and Mossel J 2011 J. Stat. Mech. **2011** P02023 doi: 10.1088/1742-5468/2011/02/P02023

[315] Benet L, Leyvraz F and Seligman T 2003 Phys. Rev. E **68** 045201 doi: 10.1103/PhysRevE.68.045201

[316] Sakurai J J 1994 Modern quantum mechanics, revised edition (Reading: Addison Wesley Publishing Company)

[317] Hartmann M, Mahler G and Hess O 2005 J. Stat. Phys. **119** 1139 doi: 10.1007/s10955-004-4298-5

[318] Keating J P, Linden N and Wells H J 2015 Commun. Math. Phys. **338** 81 doi: 10.1007/s00220-015-2366-0

[319] Davis C and Kahan W M 1970 SIAM J. Num. Ana. **7** 1 doi: 10.1137/0707001

[320] Bhatia R, Davis C and McIntosh A 1983 Lin. Alg. App. **52-53** 45 doi: 10.1016/0024-3795(83)80007-X

[321] Kulkarni M, Tiwari K L and Segal D 2012 Phys. Rev. B **86** 155424 doi: 10.1103/PhysRevB.86.155424

[322] Brandao F G S L and Cramer M 2015 preprint arXiv:1502.03263

[323] Ikeda T N, Watanabe Y and Ueda M 2011 Phys. Rev. E **84** 021130 doi: 10.1103/PhysRevE.84.021130

[324] Foini L, Cugliandolo L F and Gambassi A 2011 Phys. Rev. B **84** 212404 doi: 10.1103/PhysRevB.84.212404

[325] Foini L, Cugliandolo L F and Gambassi A 2012 J. Stat. Mech. P09011 doi: 10.1088/1742-5468/2012/09/P09011

[326] del Rio L, Hutter A, Renner R and Wehner S 2014 preprint arXiv:1401.7997

[327] Santos L F and Rigol M 2010 Phys. Rev. E **82** 031130 doi: 10.1103/PhysRevE.82.031130

[328] Steinigeweg R, Herbrych J and Prelovšek P 2013 Phys. Rev. E **87** 012118 doi: 10.1103/PhysRevE.87.012118

[329] Rigol M and Srednicki M 2012 Phys. Rev. Lett. **108** 110601 doi: 10.1103/PhysRevLett.108.110601

[330] Rutkevich S B 2012 preprint arXiv:1201.0578

[331] Berges J, Borsányi S and Wetterich C 2004 Phys. Rev. Lett. **93** 142002 doi: 10.1103/PhysRevLett.93.142002

[332] Essler F H L, Kehrein S, Manmana S R and Robinson N J 2014 Phys. Rev. B **89** 165104 doi: 10.1103/PhysRevB.89.165104

[333] Marcuzzi M, Marino J, Gambassi A and Silva A 2013 Phys. Rev. Lett. **111** 197203 doi: 10.1103/PhysRevLett.111.197203

[334] Marino J and Silva A 2012 Phys. Rev. B **86** 060408 doi: 10.1103/PhysRevB.86.060408

[335] Marino J and Silva A 2014 Phys. Rev. B **89** 024303 doi: 10.1103/PhysRevB.89.024303

[336] Karzig T, Glazman L I and von Oppen F 2010 Phys. Rev. Lett. **105** 226407 doi: 10.1103/PhysRevLett.105.226407

[337] Pagel D, Alvermann A and Fehske H 2013 Phys. Rev. E **87** 012127 doi: 10.1103/PhysRevE.87.012127

[338] Santos L F, Borgonovi F and Izrailev F M 2012 Phys. Rev. E **85** 036209 doi: 10.1103/PhysRevE.85.036209

[339] Biroli G, Kollath C and Läuchli A M 2010 Phys. Rev. Lett. **105** 250401 doi: 10.1103/PhysRevLett.105.250401

[340] Žnidarič M, Prosen T, Benenti G, Casati G and Rossini D 2010 Phys. Rev. E **81** 051135 doi: 10.1103/PhysRevE.81.051135

[341] Yuzbashyan E A and Shastry B S 2013 J. Stat. Phys. **150** 704 doi: 10.1007/s10955-013-0689-9

[342] Braak D 2011 Phys. Rev. Lett. **107** 100401 doi: 10.1103/PhysRevLett.107.100401

[343] Pal A and Huse D A 2010 Phys. Rev. B **82** 174411 doi: 10.1103/PhysRevB.82.174411

[344] Oganesyan V and Huse D 2007 Phys. Rev. B **75** 155111 doi: 10.1103/PhysRevB.75.155111

[345] Huse D A, Nandkishore R and Oganesyan V 2014 Phys. Rev. B **90** 174202 doi: 10.1103/PhysRevB.90.174202

[346] Shimony A 1995 Annals of the New York Academy of Sciences **755** 675 doi: 10.1111/j.1749-6632.1995.tb39008.x

[347] Barnum H and Linden N 2001 J. Phys. A **34** 6787 doi: 10.1088/0305-4470/34/35/305

[348] Wei T C and Goldbart P 2003 Phys. Rev. A **68** 042307 doi: 10.1103/PhysRevA.68.042307

[349] Lychkovskiy O 2010 Phys. Rev. E **82** 11123 doi: 10.1103/PhysRevE.82.011123

[350] Anderson P W 1958 Phys. Rev. **109** 1492 doi: 10.1103/PhysRev.109.1492

[351] Sims R and Ueltschi D (eds) 2010 An introduction to the mathematics of Anderson localisation preprint arXiv:1104.2317

[352] Abrahams E (ed) 2010 50 years of Anderson localisation (World Scientific Publishing)

[353] 2008 A short introduction to Anderson localization (Bath: Oxford University Press)

[354] Lagendijk A, Van Tiggelen B and Wiersma D S 2009 Physics Today **62** 24 doi: 10.1063/1.3206091

[355] Fleishman L and Anderson P W 1980 Phys. Rev. B **21** 2366 doi: 10.1103/PhysRevB.21.2366

[356] Nandkishore R and Huse D A 2015 Ann. Rev. Condens. Matter Phys. **6** 15 doi: 10.1146/annurev-conmatphys-031214-014726

[357] Basko D M, Aleiner I L and Altshuler B L 2006 Ann. Phys. **321** 1126 doi: 10.1016/j.aop.2005.11.014

[358] Altshuler B, Gefen Y, Kamenev A and Levitov L 1997 Phys. Rev. Lett. **78** 2803 doi: 10.1103/PhysRevLett.78.2803

[359] Gornyi I V, Mirlin A D and Polyakov D G 2005 Phys. Rev. Lett. **95** 206603 doi: 10.1103/PhysRevLett.95.206603

[360] Bauer B and Nayak C 2013 J. Stat. Mech. **2013** P09005 doi: 10.1088/1742-5468/2013/09/P09005

[361] Abdul-Rahman H and Stolz G 2015 preprint 1505.02117v1

[362] Žnidarič M, Prosen T and Prelovšek P 2008 Phys. Rev. B **77** 064426 doi: 10.1103/PhysRevB.77.064426

[363] Bardarson H, Pollmann F and Moore J E 2012 Phys. Rev. Lett. **109** 017202 doi: 10.1103/PhysRevLett.109.017202

[364] Friesdorf M, Werner A H, Goihl M, Eisert J and Brown W 2015 New J. Phys. **17** 113054 doi: 10.1088/1367-2630/17/11/113054

[365] Chandran A, Kim I H, Vidal G and Abanin D a 2014 Phys. Rev. B **91** 085425 doi: 10.1103/PhysRevB.91.085425

[366] Chandran A, Carrasquilla J, Kim I H, Abanin D A and Vidal G 2015 Phys. Rev. B **92** 024201 doi: 10.1103/PhysRevB.92.024201

[367] Vosk R and Altman E 2013 Phys. Rev. Lett. **110** 067204 doi: 10.1103/PhysRevLett.110.067204

[368] Vosk R, Huse D A and Altman E 2015 Phys. Rev. X **5** 031032 doi: 10.1103/PhysRevX.5.031032

[369] Jacquod P and Shepelyansky D L 1997 Phys. Rev. Lett. **70** 1837 doi: 10.1103/PhysRevLett.79.1837

[370] Georgeot B and Shepelyansky D L 1998 Phys. Rev. Lett. **81** 5129 doi: 10.1103/PhysRevLett.81.5129

[371] Haake F 2010 Quantum signatures of chaos Springer Series in Synergetics (Berlin, Heidelberg: Springer)

[372] Serbyn M, Papić Z and Abanin D 2014 Phys. Rev. B **90** 174302 doi: 10.1103/PhysRevB.90.174302

[373] Torres-Herrera E J and Santos L F 2015 Phys. Rev. B **92** 014208 doi: 10.1103/PhysRevB.92.014208

[374] Hickey J M, Genway S and Garrahan J P 2014 preprint arXiv:1405.5780

[375] Yao N Y, Laumann C R, Cirac J I, Lukin M D and Moore J E 2014 7 preprint arXiv:1410.7407

[376] Carleo G, Becca F, Schiró M and Fabrizio M 2012 Sc. Rep. **2** 243 doi: 10.1038/srep00243

[377] Billy J, Josse V, Zuo Z, Bernard A, Hambrecht B, Lugan P, Clément D, Sanchez-Palencia L, Bouyer P and Aspect A 2008 Nature **453** 891 doi: 10.1038/nature07000

[378] Schreiber M, Hodgman S S, Bordia P, Lüschen H P, Fischer M H, Vosk R, Altman E, Schneider U and Bloch I 2015 Science **349** 842 doi: 10.1126/science.aaa7432

[379] Weigert S 1992 Physica D **56** 107 doi: 10.1016/0167-2789(92)90053-P

[380] Arnold V I 1989 Mathematical methods of classical mechanics (Springer)

[381] Moradi G, Napoli F and Ercolessi E 2001 Statistical mechanics: An intermediate course 2nd ed (Singapore: World Scientific)

[382] Pöschel J 2003 Proc. Symp. Pure Math. **69** 707

[383] Sutherland B 2004 Beautiful models (World Scientific)

[384] Hawkins M S 2008 Local conservation laws in quantum integrable systems Phd thesis University of Birmingham

[385] Castagnino M and Lombardi O 2006 Ch. Sol. Fract. **28** 879 doi: 10.1016/j.chaos.2005.08.149

[386] Casati G, Chirikov B and Guarneri I 1985 Phys. Rev. Lett. **54** 1350 doi: 10.1103/PhysRevLett.54.1350

[387] Prosen T and Žnidarič M 2013 Phys. Rev. Lett. **111** 124101 doi: 10.1103/PhysRevLett.111.124101

[388] Atas Y Y, Bogomolny E, Giraud O and Roux G 2013 Phys. Rev. Lett. **110** 084101 doi: 10.1103/PhysRevLett.110.084101

[389] Stepanov V V, Müller G and Stolze J 2008 Phys. Rev. E **77** 066202 doi: 10.1103/PhysRevE.77.066202

[390] Berry M V and Tabor M 1977 Proc. Roy. Soc. A **356** 375 doi: 10.1098/rspa.1977.0140

[391] Fendley P, Ludwig A and Saleur H 1995 Phys. Rev. Lett. **74** 3005 doi: 10.1103/PhysRevLett.74.3005

[392] Hartmann M, Mahler G and Hess O 2004 Lett. Math. Phys. **68** 103 doi: 10.1023/B:MATH.0000043321.00896.86

[393] Hartmann M, Mahler G and Hess O 2004 Phys. Rev. E **70** 066148 doi: 10.1103/PhysRevE.70.066148

[394] Hartmann M and Mahler G 2005 Europhys. Lett. **70** 579 doi: 10.1209/epl/i2004-10518-5

[395] Ferraro A, Aolita L, Cavalcanti D, Cucchietti F M and Acín A 2010 Phys. Rev. A **81** 052318 doi: 10.1103/PhysRevA.81.052318

[396] Kliesch M, Gogolin C, Kastoryano M J, Riera A and Eisert J 2014 Phys. Rev. X **4** 031019 doi: 10.1103/PhysRevX.4.031019

[397] Ruelle D 1999 Statistical mechanics: Rigorous results (World Scientific Publishing)

[398] Ruelle D 1964 Rev. Mod. Phys. **36** 580 doi: 10.1103/RevModPhys.36.580

[399] Ginibre J 1965 J. Math. Phys. **6** 252 doi: 10.1063/1.1704276

[400] Bratteli O and Robinson D W 1987 Operator algebras and quantum statisticaI mechanics 1 2nd ed (Springer Berlin Heidelberg)

[401] Greenberg W 1969 Commun. Math. Phys. **13** 335 doi: 10.1007/BF01645417

[402] Park Y M and Yoo H J 1995 J. Stat. Phys. **80** 223 doi: 10.1007/BF02178359

[403] Cardy J 1996 Scaling and renormalization in statistical physics Cambridge Lecture Notes in Physics (Cambridge University Press)

[404] Mejia Miranda Y and Slade G 2011 Elec. Comm. Prob. **16** 129 doi: 10.1214/ECP.v16-1612

[405] Penrose M D 1994 J. Stat. Phys. **77** 3 doi: 10.1007/BF02186829

[406] Bhattacharjee S M and Khare A 1995 Curr. Sc. **69** 816

[407] Hastings M 2006 Phys. Rev. B **73** 085115 doi: 10.1103/PhysRevB.73.085115

[408] Sklar L 1995 Physics and chance: Philosophical issues in the foundations of statistical mechanics (Cambridge University Press)

[409] Ehrenfest P and Ehrenfest T 2002 The conceptual foundations of the statistical approach in mechani Dover Phoenix editions (Cornell University Press)

[410] Penrose O 1979 Rep. Prog. Phys. **42** 1937 doi: 10.1088/0034-4885/42/12/002

[411] Clausius R 1857 Ann. Phys. Chem. **176** 353 doi: 10.1002/andp.18571760302

[412] Maxwell J 1860 Phil. Mag. **19** 19

[413] Maxwell J 1860 Phil. Mag. **20** 21

[414] Boltzmann L 1872 Wiener Ber. **66** 275 doi: 10.1017/CBO9781139381420.023

[415] Boltzmann L 1896 Vorlesungen über Gastheorie. Bd. 1. (Leipzig: Barth)

[416] Loschmidt J 1877 Wiener Ber. **76** 209

[417] Thomson W 1874 Nature **9** 441 doi: 10.1038/009441c0

[418] Zermelo E 1896 Ann. Phys. Chem. **293** 485 doi: 10.1002/andp.18962930314

[419] Boltzmann L 1896 Ann. Phys. Chem. **293** 773 doi: 10.1002/andp.18962930414

[420] Boltzmann L and Hasenöhrl F 1868 Wiener Ber. **58** 517 doi: 10.1017/CBO9781139381420.006

[421] Boltzmann L 1871 Wiener Ber. **63** 679 doi: 10.1017/CBO9781139381420.020

[422] Shannon C E and Weaver W 1949 The mathematical theory of communication (Univ of Illinois Press)

[423] Fuchs C A 2010 preprint arXiv:1003.5209

[424] Timpson C G 2008 Stud. Hist. Phil. Sc. B **39** 579 doi: 10.1016/j.shpsb.2008.03.006

[425] Ballentine L, Yang Y and Zibin J 1994 Phys. Rev. A **50** 2854 doi: 10.1103/PhysRevA.50.2854

[426] Bohr N 1972 The Doctor's Dissertation (Text and Translation) Niels Bohr collected works (Niels Bohr Collected Works vol 1) ed Rosenfeld L and Nielsen J R (Elsevier) chap Early Work, p 163

[427] Aharoni A 2000 Introduction to the theory of ferromagnetism International series of monographs on physics (Oxford University Press)

[428] Nolting W and Ramakanth A 2009 Quantum theory of magnetism (Springer)

[429] Greiner Neise S 1995 Thermodynamics and statistical mechanics (Springer)

From observ to complex of q states via unsupervised learning

References

[1] G. Vidal, J. I. Latorre, E. Rico, and A. Kitaev, Phys. Rev. Lett. **90**, 227902 (2003).

[2] P. Calabrese and J. Cardy, J. Stat. Mech.: Theory Exp. **2004**, P06002 (2004).

[3] A. Kitaev and J. Preskill, Phys. Rev. Lett. **96**, 110404 (2006).

[4] E. Fradkin and J. E. Moore, Phys. Rev. Lett. **97**, 050404 (2006).

[5] F. Pollmann, A. M. Turner, E. Berg, and M. Oshikawa, Phys. Rev. B **81**, 064439 (2010).

[6] A. Szasz, J. Motruk, M. P. Zaletel, and J. E. Moore, Phys. Rev. X **10**, 021042 (2020).

[7] P. Calabrese and J. Cardy, J. Stat. Mech.: Theory Exp. **2005**, P04010 (2005).

[8] J. H. Bardarson, F. Pollmann, and J. E. Moore, Phys. Rev. Lett. **109**, 017202 (2012).

[9] U. Schollwöck, Ann. Phys. **326**, 96 (2011), january 2011 Special Issue.

[10] R. Orús, Ann. Phys. **349**, 117 (2014).

[11] S. Paeckel, T. Köhler, A. Swoboda, S. R. Manmana, U. Schollwöck, and C. Hubig, Ann. Phys. **411**, 167998 (2019).

[12] R. Islam, R. Ma, P. M. Preiss, M. Eric Tai, A. Lukin, M. Rispoli, and M. Greiner, Nature **528**, 77 (2015).

[13] C. Kokail, R. van Bijnen, A. Elben, B. Vermersch, and P. Zoller, arXiv:2009.09000 (2020).

[14] M. B. Plbnio and S. Virmani, Quantum Info. Comput. **7**, 1–51 (2007).

[15] B. M. Terhal, Theor. Comput. Sci. **287**, 313 (2002), natural Computing.

[16] A. C.-C. Yao, in Proceedings of 1993 IEEE 34th Annual Foundations of Computer Science (IEEE, 1993) pp. 352–361.

[17] M. R. Dowling and M. A. Nielsen, Quantum Information & Computation **8**, 861 (2008).

[18] J. Haferkamp, P. Faist, N. B. Kothakonda, J. Eisert, and N. Y. Halpern, arXiv:2106.05305 (2021).

[19] J. Lux, J. Müller, A. Mitra, and A. Rosch, Phys. Rev. A **89**, 053608 (2014).

[20] A. Bohrdt, C. B. Mendl, M. Endres, and M. Knap, New J. Phys. **19**, 063001 (2017).

[112] E. Leviatan, F. Pollmann, J. H. Bardarson, D. A. Huse, and E. Altman, arXiv:1702.08894 (2017).

[22] J. Dubail, J. Phys. A: Math. Theor. **50**, 234001 (2017).

[23] H. Wang and T. Zhou, J. High Energy Phys. **2019**, 20 (2019).

[24] K. Noh, L. Jiang, and B. Fefferman, Quantum **4**, 318 (2020).

[25] T. Rakovszky, C. W. von Keyserlingk, and F. Pollmann, arXiv:2004.05177 (2020).

[26] I. Reid and B. Bertini, Phys. Rev. B **104**, 014301 (2021).

[27] G. E. Hinton and R. R. Salakhutdinov, Science **313**, 504 (2006).

[28] M. Rigol, V. Dunjko, V. Yurovsky, and M. Olshanii, Phys. Rev. Lett. **98**, 050405 (2007).

[3] L. Vidmar and M. Rigol, J. Stat. Mech.: Theory Exp. P064007 (2016).

[4] F. H. L. Essler and M. Fagotti, J. Stat. Mech.: Theory Exp. P064002 (2016).

[26] F. Lange, Z. Lenarčič, and A. Rosch, Nat. Comm. **8**, 1 (2017).

[25] F. Lange, Z. Lenarčič, and A. Rosch, Phys. Rev. B **97**, 165138 (2018).

[33] F. Reiter, F. Lange, S. Jain, M. Grau, J. P. Home, and Z. Lenarčič, arXiv:1910.01593 (2019).

[18] Z. Lenarčič, E. Altman, and A. Rosch, Phys. Rev. Lett. **121**, 267603 (2018).

[35] Z. Lenarčič, O. Alberton, A. Rosch, and E. Altman, Phys. Rev. Lett. **125**, 116601 (2020).

[36] W. G. Brown and L. Viola, Phys. Rev. Lett. **104**, 250501 (2010).

[4] A. Nahum, J. Ruhman, S. Vijay, and J. Haah, Phys. Rev. X **7**, 031016 (2017).

[5] A. Nahum, S. Vijay, and J. Haah, Phys. Rev. X **8**, 021014 (2018).

[6] C. W. von Keyserlingk, T. Rakovszky, F. Pollmann, and S. L. Sondhi, Phys. Rev. X **8**, 021013 (2018).

[7] T. Rakovszky, F. Pollmann, and C. W. von Keyserlingk, Phys. Rev. X **8**, 031058 (2018).

[41] V. Khemani, A. Vishwanath, and D. A. Huse, Phys. Rev. X **8**, 031057 (2018).

[42] A. Chan, A. De Luca, and J. T. Chalker, Phys. Rev. X **8**, 041019 (2018).

[43] C. Sünderhauf, D. Pérez-García, D. A. Huse, N. Schuch, and J. I. Cirac, Phys. Rev. B **98**, 134204 (2018).

[44] A. J. Friedman, A. Chan, A. De Luca, and J. T. Chalker, Phys. Rev. Lett. **123**, 210603 (2019).

[45] A. Chan, A. De Luca, and J. T. Chalker, Phys. Rev. Lett. **121**, 060601 (2018).

[46] B. Bertini and L. Piroli, Phys. Rev. B **102**, 064305 (2020).

[47] D. Leibfried, R. Blatt, C. Monroe, and D. Wineland, Reviews of Modern Physics **75**, 281 (2003).

[48] I. Bloch, J. Dalibard, and W. Zwerger, Rev. Mod. Phys. **80**, 885 (2008).

[49] C. Gross and I. Bloch, Science **357**, 995 (2017).

[50] J. Preskill, Quantum **2**, 79 (2018).

[47] S. Ebadi, T. T. Wang, H. Levine, A. Keesling, G. Semeghini, A. Omran, D. Bluvstein, R. Samajdar, H. Pichler, W. W. Ho, S. Choi, S. Sachdev, M. Greiner, V. Vuletic, and M. D. Lukin, arXiv:2012.12281 (2020).

[48] P. Scholl, M. Schuler, H. J. Williams, A. A. Eberharter, D. Barredo, K.-N. Schymik, V. Lienhard, L.-P. Henry, T. C. Lang, T. Lahaye, A. M. Läuchli, and A. Browaeys, arXiv:2012.12268 (2020).

[53] A. Blais, A. L. Grimsmo, S. Girvin, and A. Wallraff, arXiv:2005.12667 (2020).

[54] R. Iten, T. Metger, H. Wilming, L. del Rio, and R. Renner, Phys. Rev. Lett. **124**, 010508 (2020).

[55] K. Kottmann, P. Huembeli, M. Lewenstein, and A. Acín, Phys. Rev. Lett. **125**, 170603 (2020).

[56] N. Sá and I. Roditi, "Beta-variational autoencoder as an entanglement classifier," (2020), arXiv:2004.14420 [quant-ph] .

[57] I. A. Luchnikov, A. Ryzhov, P.-J. Stas, S. N. Filippov, and H. Ouerdane, Entropy **21** (2019), 10.3390/e21111091.

[58] W. Zhong, J. M. Gold, S. Marzen, J. L. England, and N. Y. Halpern, "Learning about learning by many-body systems," (2020), arXiv:2004.03604 [cond-mat.stat-mech] .

[39] "Supplemental material includes (i) expression for conservation laws of transverse field ising model and lindblad operators, (ii) relation between lagrange parameter and latent representation, (iii) possibility of noise type detection in case of coupling to structured baths, more information on the (iii) random unitary model, (iv) training procedure, (v) intrinsic dimension and (vi) hamiltonian reconstruction," .

[60] H.-Y. Huang, R. Kueng, and J. Preskill, Nat. Phys. **16**, 1050 (2020).

[61] A. Elben, R. Kueng, H.-Y. R. Huang, R. van Bijnen, C. Kokail, M. Dalmonte, P. Calabrese, B. Kraus, J. Preskill, P. Zoller, et al., Phys. Rev. Lett. **125**, 200501 (2020).

[43] K. Kim, S. Korenblit, R. Islam, E. Edwards, M. Chang, C. Noh, H. Carmichael, G. Lin, L. Duan, C. J. Wang, et al., New J. Phys. **13**, 105003 (2011).

[44] R. Islam, E. Edwards, K. Kim, S. Korenblit, C. Noh, H. Carmichael, G.-D. Lin, L.-M. Duan, C.-C. J. Wang, J. Freericks, et al., Nat. Comm. **2**, 1 (2011).

[45] H. Labuhn, D. Barredo, S. Ravets, S. De Léséleuc, T. Macrì, T. Lahaye, and A. Browaeys, Nature **534**, 667 (2016).

[46] J. Zhang, G. Pagano, P. W. Hess, A. Kyprianidis, P. Becker, H. Kaplan, A. V. Gorshkov, Z.-X. Gong, and C. Monroe, Nature **551**, 601 (2017).

[43] M. Grady, Phys. Rev.D **25**, 1103 (1982).

[67] V. Alba and P. Calabrese, SciPost Phys. **4**, 017 (2018).

[12] L. Van der Maaten and G. Hinton, J. Mach. Learn. Res. **9** (2008).

[46] M. Zwolak and G. Vidal, Phys. Rev. Lett. **93**, 207205 (2004).

[45] F. Verstraete, J. J. García-Ripoll, and J. I. Cirac, Phys. Rev. Lett. **93**, 207204 (2004).

[71] L. Che, C. Wei, Y. Huang, D. Zhao, S. Xue, X. Nie, J. Li, D. Lu, and T. Xin, arXiv:2012.12520 (2020).

[72] A. Valenti, E. van Nieuwenburg, S. Huber, and E. Greplova, Phys. Rev. Res. **1**, 033092 (2019).

[73] X. Ma, Z. Tu, and S.-J. Ran, arXiv:2012.03019 (2020).

[74] T. Xin, S. Lu, N. Cao, G. Anikeeva, D. Lu, J. Li, G. Long, and B. Zeng, npj Quantum Info. **5**, 1 (2019).

[9] S. Wold, K. Esbensen, and P. Geladi, Chemometr. Intell. Lab. Syst. **2**, 37 (1987).

[10] I. Borg and P. J. Groenen, Modern multidimensional scaling: Theory and applications (Springer Science & Business Media, 2005).

[11] M. Balasubramanian, E. L. Schwartz, J. B. Tenenbaum, V. de Silva, and J. C. Langford, Science **295**, 7 (2002).

[13] L. McInnes, J. Healy, and J. Melville, arXiv:1802.03426 (2018).

[14] E. Levina and P. Bickel, Advances in neural information processing systems **17**, 777 (2004).

[15] P. Campadelli, E. Casiraghi, C. Ceruti, and A. Rozza, Math. Probl. Eng. **2015** (2015).

[16] E. Facco, M. d'Errico, A. Rodriguez, and A. Laio, Sci. Rep. **7**, 1 (2017).

[17] T. Mendes-Santos, X. Turkeshi, M. Dalmonte, and A. Rodriguez, arXiv:2006.12953 (2020).

[18] E. Lopez Tomas, A. Scheuer, E. Abisset-Chavanne, and F. Chinesta, Mathematics and Mechanics of Complex Systems **6**, 251 (2018).

[84] X. Turkeshi, arXiv:2101.06245 (2021).

[85] A. Khan, D. Quigley, M. Marcus, E. Thyrhaug, and A. Datta, Phys. Rev. Lett. **126**, 150402 (2021).

[86] A. Bohrdt, S. Kim, A. Lukin, M. Rispoli, R. Schittko, M. Knap, M. Greiner, and J. Léonard, arXiv:2012.11586 (2020).

[87] D. P. Kingma and M. Welling, Found. Trends Mach. Learn. **12**, 307 (2019).

[55] J. Bezanson, A. Edelman, S. Karpinski, and V. B. Shah, SIAM review **59**, 65 (2017).

[89] P. Weinberg and M. Bukov, SciPost Phys. **2**, 003 (2017).

[90] P. Weinberg and M. Bukov, SciPost Phys. **7**, 20 (2019).

[91] Repository containing training data and code: `https://github.com/markusschmitt/learning_quantum_complexity`.

References

[43] M. Grady, Phys. Rev.D **25**, 1103 (1982).

[4] F. H. L. Essler and M. Fagotti, J. Stat. Mech.: Theory Exp. P064002 (2016).

[25] F. Lange, Z. Lenarčič, and A. Rosch, Phys. Rev. B **97**, 165138 (2018).

[4] A. Nahum, J. Ruhman, S. Vijay, and J. Haah, Phys. Rev. X **7**, 031016 (2017).

[5] A. Nahum, S. Vijay, and J. Haah, Phys. Rev. X **8**, 021014 (2018).

[6] C. W. von Keyserlingk, T. Rakovszky, F. Pollmann, and S. L. Sondhi, Phys. Rev. X **8**, 021013 (2018).

[7] T. Rakovszky, F. Pollmann, and C. W. von Keyserlingk, Phys. Rev. X **8**, 031058 (2018).

[8] D. P. Kingma and J. Ba, arXiv:1412.6980 (2014).

[9] S. Wold, K. Esbensen, and P. Geladi, Chemometr. Intell. Lab. Syst. **2**, 37 (1987).

[10] I. Borg and P. J. Groenen, Modern multidimensional scaling: Theory and applications (Springer Science & Business Media, 2005).

[11] M. Balasubramanian, E. L. Schwartz, J. B. Tenenbaum, V. de Silva, and J. C. Langford, Science **295**, 7 (2002).

[12] L. Van der Maaten and G. Hinton, J. Mach. Learn. Res. **9** (2008).

[13] L. McInnes, J. Healy, and J. Melville, arXiv:1802.03426 (2018).

[14] E. Levina and P. Bickel, Advances in neural information processing systems **17**, 777 (2004).

[15] P. Campadelli, E. Casiraghi, C. Ceruti, and A. Rozza, Math. Probl. Eng. **2015** (2015).

[16] E. Facco, M. d'Errico, A. Rodriguez, and A. Laio, Sci. Rep. **7**, 1 (2017).

[17] T. Mendes-Santos, X. Turkeshi, M. Dalmonte, and A. Rodriguez, arXiv:2006.12953 (2020).

[18] E. Lopez Tomas, A. Scheuer, E. Abisset-Chavanne, and F. Chinesta, Mathematics and Mechanics of Complex Systems **6**, 251 (2018).

[19] E. Bairey, I. Arad, and N. H. Lindner, Phys. Rev. Lett. **122**, 020504 (2019).

From quantum chaos and eigenstate thermalization to statistical mechanics and thermodynamics

References

[1] S.K. Ma, Statistical mechanics, World Scientific, Singapore, Philadelphia, 1985.

[2] R.P. Feynman, Statistical Mechanics: A Set of Lectures, Westview Press; 2 edition, 1998.

[3] L. Boltzmann, Ann. Phys. (Leipzig) 57 (1896), p. 773.

[4] L. Boltzmann, Ann. Phys. (Leipzig) 60 (1897), p. 392.

[5] J.W. Gibbs, Elementary Principles in Statistical Mechanics, Dover, New York, 1960.

[6] O. Penrose, Foundations of Statistical Mechanics, Pergamon, Oxford, 1970.

[7] J.L. Lebowitz and O. Penrose, Physics Today 2 (1973), p. 23.

[8] Y.G. Sinai, Sov. Math Dokl. 4 (1963), pp. 1818–1822.

[9] Y.G. Sinai, Russian Mathematical Surveys 25 (1970), pp. 137–191.

[10] L.A. Bunimovich, Commun. Math. Phys. 65 (1979), p. 295.

[11] N. Simanyi, Ann. Henri Poincaré 5 (2004), p. 203.

[12] H. Poincaré, Acta Math. 13 (1890), p. 1.

[13] L.D. Faddeev and L.A. Takhtajan, Hamiltonian Methods in the Theory of Solitons (Classics in Mathematics), Springer, 2007.

[14] E. Fermi, J. Pasta, and S. Ulam, Studies of nonlinear problems, Tech. Rep., 1955.

[15] T. Dauxois, Physics Today 61 (2008), pp. 55–57.

[16] G.P. Berman and F.M. Izrailev, Chaos 15 (2005), p. 015104.

[17] E. Kozik and B. Svistunov, J. of Low Temp. Phys. 156 (2009), p. 215.

[18] J.P. Bouchaud, J. Phys. I France 2 (1992), p. 1705.

[19] D. Levesque and L. Verlet, Journal of Statistical Physics 72, pp. 519–537.

[20] C. Jarzynski, Phys. Rev. Lett. 78 (1997), p. 2690.

[21] G.E. Crooks, Phys. Rev. E 60 (1999), p. 2721.

[22] D. Collin, F. Ritort, C. Jarzynski, S.B. Smith, I. Tinoco Jr, and C. Bustamante, Nature 437 (2005), p. 231.

[23] J. Kurchan, arXiv:cond-mat/0007360 (2000).

[24] H. Tasaki, arXiv:cond-mat/0009244 (2000).

[25] M. Campisi, P. Hänggi, and P. Talkner, Rev. Mod. Phys. 83 (2011), p. 771.

[26] J.M. Deutsch, Phys. Rev. A 43 (1991), pp. 2046–2049.

[27] M. Srednicki, Phys. Rev. E 50 (1994), pp. 888–901.

[28] M. Rigol, V. Dunjko, and M. Olshanii, Nature 452 (2008), p. 854.

[29] M. Srednicki, J. Phys. A 32 (1999), p. 1163.

[30] J. von Neumann, Zeitschrift für Physik 57 (1929), pp. 30–70, translated to English in European Phys. J. H **35**, 201 (2010).

[31] E. Wigner, Ann. of Math. 62 (1955), pp. 548–564.

[32] I. Bloch, J. Dalibard, and W. Zwerger, Rev. Mod. Phys. 80 (2008), pp. 885–964.

[33] M.A. Cazalilla, R. Citro, T. Giamarchi, E. Orignac, and M. Rigol, Rev. Mod. Phys. 83 (2011), pp. 1405–1466.

[34] M. Greiner, O. Mandel, T.W. Hänsch, and I. Bloch, Nature 419 (2002), pp. 51–54.

[35] S. Will, T. Best, U. Schneider, L. Hackermüller, D.S. Lühmann, and I. Bloch, Nature 465 (2010), pp. 197–201.

[36] S. Will, T. Best, S. Braun, U. Schneider, and I. Bloch, Phys. Rev. Lett. 106 (2011), p. 115305.

[37] S. Will, D. Iyer, and M. Rigol, Nat. Commun. 6 (2015), p. 6009.

[38] T. Kinoshita, T. Wenger, and D.S. Weiss, Nature 440 (2006), p. 900.

[39] M. Gring, M. Kuhnert, T. Langen, T. Kitagawa, B. Rauer, M. Schreitl, I. Mazets, D.A. Smith, E. Demler, and J. Schmiedmayer, Science 337 (2012), pp. 1318–1322.

[40] T. Langen, S. Erne, R. Geiger, B. Rauer, T. Schweigler, M. Kuhnert, W. Rohringer, I.E. Mazets, T. Gasenzer, and J. Schmiedmayer, Science 348 (2015), p. 207.

[41] S. Trotzky, Y.A. Chen, A. Flesch, I.P. McCulloch, U. Schollwöck, J. Eisert, and I. Bloch, Nature Phys. 8 (2012), p. 325.

[42] K. Winkler, G. Thalhammer, F. Lang, R. Grimm, J.H. Denschlag, A.J. Daley, A. Kantian, H.P. Büchler, and P. Zoller, Nature 441 (2006), p. 853.

[43] L. Xia, L. Zundel, J. Carrasquilla, J.M. Wilson, M. Rigol, and D.S. Weiss, Nature Phys. 11 (2015), p. 316.

[44] L. Childress, M.V.G. Dutt, J.M. Taylor, A.S. Zibrov, F. Jelezko, J. Wrachtrup, P.R. Hemmer, and M.D. Lukin, Science 314 (2006), p. 281.

[45] S. Wall, D. Brida, S.R. Clark, H.P. Ehrke, D. Jaksch, A. Ardavan, S. Bonora, H. Uemura, Y. Takahashi, T. Hasegawa, H. Okamoto, G. Cerullo, and A. Cavalleri, Nature Physics 7 (2011), p. 114.

[46] D.N. Basov, R.D. Averitt, D. van der Marel, M. Dressel, and K. Haule, Rev. Mod. Phys. 83 (2011), p. 471.

[47] J. Berges, K. Boguslavski, S. Schlichting, and R. Venugopalan, Phys. Rev. D 89 (2014), p. 074011.

[48] J. Dziarmaga, Adv. Phys. 59 (2010), pp. 1063–1189.

[49] A. Polkovnikov, K. Sengupta, A. Silva, and M. Vengalattore, Rev. Mod. Phys. 83 (2011), pp. 863–883.

[50] V.I. Yukalov, Laser Phys. Lett. 8 (2011), pp. 485–507.

[51] R. Nandkishore and D.A. Huse, Annual Review of Condensed Matter Physics 6 (2015), pp. 15–38.

[52] J. Eisert, M. Friesdorf, and C. Gogolin, Nature Physics 11 (2015), p. 124.

[53] C. Gogolin and J. Eisert, Reports on Progress in Physics 79 (2016), p. 056001.

[54] M.A. Cazalilla and M. Rigol, New J. Phys. 12 (2010), p. 055006.

[55] A.J. Daley, M. Rigol, and D.S. Weiss, New J. Phys. 16 (2014), p. 095006.

[56] A.J. Lichtenberg and M.A. Liebermann, Regular and chaotic dynamics (2nd ed), Springer, Berlin, New York, 1992.

[57] P. Cvitanovic, R. Artuso, R. Mainieri, G. Tanner, and G. Vattay, Chaos: Classical and Quantum, ChaosBook.org, Niels Bohr Institute, Copenhagen, 2012.

[58] V.I. Arnold, Mathematical Methods of Classical Mechanics, Springer-Verlag, New York, 1989.

[59] J.V. José and E.J. Saletan, Classical Dynamics: A Contemporary Approach, Cambridge Univ. Press, Cambridge, 1998.

[60] H.J. Stöckmann, Scholarpedia 5 (2010), p. 10243.

[61] L.D. Landau and E.M. Lifshitz, Mechanics, Third Edition (Volume 1), Butterworth-Heinemann, 1976.

[62] A.N. Kolmogorov, Dokl. Akad. Nauk. SSR 98 (1954), pp. 527–530.

[63] V.I. Arnold, Russian Math. Survey 18 (1963), pp. 13–40.

[64] J.K. Moser, Nach. Akad. Wiss. Göttingen, Math. Phys. Kl. II 1 (1962), pp. 1–20.

[65] A.J. Lichtenberg and M.A. Lieberman, Regular and Chaotic Dynamics, Applied Mathematical Sciences, Vol. 38, Springer-Verlag, New York, 1992.

[66] H.W. Broer, I. Hoveijn, M. van Noort, C. Simo, and G. Vegter, Journal of Dynamics and Differential Equations 16 (2004), p. 897.

[67] B.V. Chirikov, Physics Reports 52 (1979), pp. 263–379.

[68] G.Casati, B.V. Chirikov, F.M. Izrailev, and J. Ford, Stochastic behavior of a quantum pendulum under a periodic perturbation, in Stochastic Behavior in Classical and Quantum Hamiltonian Systems, G. Casati and J. Ford, eds., Lecture Notes in Physics, Vol. 93, Springer Berlin Heidelberg, 1979, pp. 334–352.

[69] L.F. Santos and M. Rigol, Phys. Rev. E 81 (2010), p. 036206.

[70] L.F. Santos and M. Rigol, Phys. Rev. E 82 (2010), p. 031130.

[71] T. Guhr, A. Müller, Groeling, and H.A. Weidenmüller, Physics Reports 299 (1998), pp. 189–425.

[72] Y. Alhassid, Rev. Mod. Phys. 72 (2000), p. 895.

[73] M.L. Mehta, Random Matrices, Amsterdam: Elsevier/Academic Press, 2004.

[74] V.E. Kravtsov, Random matrix theory: Wigner-Dyson statistics and beyond, arXiv:0911.0639.

[75] M. Hillery, R.F. O'Connell, M.O. Scully, and E.P. Wigner, Physics Reports 106 (1984), pp. 121–167.

[76] A. Polkovnikov, Annals of Phys. 325 (2010), p. 1790.

[77] L.D. Landau and E.M. Lifshitz, Quantum Mechanics, Third Edition: Non-Relativistic Theory (Volume 3), Butterworth-Heinemann, 1981.

[78] D. Stone, Physics Today 58 (2005), p. 37.

[79] M.C. Gutzwiller, J. Math. Phys. 12 (1971), p. 343.

[80] Z. Rudnick, Notices of the AMS 55 (2008), p. 32.

[81] E. Wigner, Ann. of Math. 65 (1957), pp. 203–207.

[82] E. Wigner, Ann. of Math. 67 (1958), pp. 325–326.

[83] F.J. Dyson, J. Math. Phys. 3 (1962), p. 140.

[84] L.E. Reichl, The transition to Chaos: Conservative Classical Sysstems and Quantum Manifestations, Springer, New York, 2004.

[85] O. Bohigas, M.J. Giannoni, and C. Schmit, Phys. Rev. Lett. 52 (1984), pp. 1–4.

[86] E.B. Bogomolny, B. Georgeot, M.J. Giannoni, and C. Schmit, Phys. Rev. Lett. 69 (1992), p. 1477.

[87] T.A. Brody, J. Flores, J.B. French, P.A. Mello, A. Pandey, and S.S.M. Wong, Rev. Mod. Phys. 53 (1981), p. 385.

[88] M.V. Berry and M. Tabor, Proc. Roy. Soc. A 356 (1977), pp. 375–394.

[89] A. Pandey and R. Ramaswamy, Phys. Rev. A 43 (1991), pp. 4237–4243.

[90] M.V. Berry, J. Phys. A 10 (1977), p. 2083.

[91] V.V. Flambaum and F.M. Izrailev, Phys. Rev. E 55 (1997), pp. R13–R16.

[92] V.V. Flambaum and F.M. Izrailev, Phys. Rev. E 56 (1997), pp. 5144–5159.

[93] V.K.B. Kota, Lecture Notes in Physics 884 (2014).

[94] K.H. Böchhoff, Nuclear Data for Science and Technology, Springer, Brussels and Luxemburg, 1983.

[95] D. Wintgen and H. Friedrich, Phys. Rev. A 35 (1987), pp. 1464–1466.

[96] O. Bohigas, R.U. Haq, and A. Pandey, Fluctuation Properties of Nuclear Energy Levels and Widths: Comparison of Theory with Experiment, in Nuclear Data for Science and Technology, Reidel, Dordrecht (1983), p. 809.

[97] M.V. Berry and M. Robnik, Journal of Physics A: Mathematical and General 17, p. 2413.

[98] M. Robnik, J. Phys. A: Math. Gen. 14, p. 3195.

[99] M. Rigol and L.F. Santos, Phys. Rev. A 82 (2010), p. 011604(R).

[100] C. Kollath, G. Roux, G. Biroli, and A. Laeuchli, J. Stat. Mech. (2010), p. P08011.

[101] L.F. Santos, F. Borgonovi, and F.M. Izrailev, Phys. Rev. Lett. 108 (2012), p. 094102.

[102] L.F. Santos, F. Borgonovi, and F.M. Izrailev, Phys. Rev. E 85 (2012), p. 036209.

[103] Y.Y. Atas, E. Bogomolny, O. Giraud, and G. Roux, Phys. Rev. Lett. 110 (2013), p. 084101.

[104] Y.Y. Atas, E. Bogomolny, O. Giraud, P. Vivo, and E. Vivo, Journal of Physics A: Mathematical and Theoretical 46 (2013), p. 355204.

[105] R. Modak, S. Mukerjee, and S. Ramaswamy, Phys. Rev. B 90 (2014), p. 075152.

[106] R. Modak and S. Mukerjee, New J. Phys. 16 (2014), p. 093016.

[107] V.K.B. Kota and R. Sahu, Physics Letters B 429 (1998), p. 1.

[108] L.D. Landau and E.M. Lifshitz, Statistical Physics, Third Edition, Part 1, Volume 5, Butterworth-Heinemann, 1980.

[109] L.F. Santos, A. Polkovnikov, and M. Rigol, Phys. Rev. E 86 (2012), p. 010102(R).

[110] J.M. Deutsch, H. Li, and A. Sharma, Phys. Rev. E 87 (2013), p. 042135.

[111] M. Mierzejewski, T. Prosen, D. Crivelli, and P. Prelovšek, Phys. Rev. Lett. 110 (2013), p. 200602.

[112] H. Kim and D.A. Huse, Phys. Rev. Lett. 111 (2013), p. 127205.

[113] S. Khlebnikov and M. Kruczenski, Phys. Rev. E 90 (2014), p. 050101.

[114] J.H. Bardarson, F. Pollmann, and J.E. Moore, Phys. Rev. Lett. 109 (2012), p. 017202.

[115] R. Vosk and E. Altman, Phys. Rev. Lett. 110 (2013), p. 067204.

[116] M. Serbyn, Z. Papić, and D.A. Abanin, Phys. Rev. Lett. 110 (2013), p. 260601.

[117] A. Nanduri, H. Kim, and D.A. Huse, Phys. Rev. B 90 (2013), p. 064201.

[118] P. Ponte, Z. Papić, F. Huveneers, and D.A. Abanin, Phys. Rev. Lett. 114 (2015), p. 140401.

[119] C. Neill, P. Roushan, M. Fang, Y. Chen, M. Kolodrubetz, Z. Chen, A. Megrant, R. Barends, B. Campbell, B. Chiaro, A. Dunsworth, E. Jeffrey, J. Kelly, J. Mutus, P.J.J. O'Malley, C. Quintana, D. Sank, A. Vainsencher, J. Wenner, T.C. White, A. Polkovnikov, and J.M. Martinis, arXiv:1601.00600 (2016).

[120] A.M. Kaufman, M.E. Tai, A. Lukin, M. Rispoli, R. Schittko, P.M. Preiss, and M. Greiner, arXiv:1603.04409 (2016).

[121] A.J. Daley, H. Pichler, J. Schachenmayer, and P. Zoller, Phys. Rev. Lett. 109 (2012), p. 020505.

[122] R. Islam, R. Ma, P.M. Preiss, M.E. Tai, A. Lukin, M. Rispoli, and M. Greiner, Nature 528.

[123] J.R. Garrison and T. Grover, arXiv:1503.00729 (2015).

[124] D.N. Page, Phys. Rev. Lett. 71 (1993), p. 1291.

[125] L.F. Santos, A. Polkovnikov, and M. Rigol, Phys. Rev. Lett. 107 (2011), p. 040601.

[126] C. Neuenhahn and F. Marquardt, Phys. Rev. E 85 (2012), p. 060101.

[127] G. Casati, B.V. Chirikov, I. Guarneri, and F.M. Izrailev, Phys. Rev. E 48 (1993), p. R1613(R).

[128] G. Casati, B. Chirikov, I. Guarneria, and F. Izrailev, Physics Letters A 223 (1996), p. 430.

[129] V.V. Flambaum and F.M. Izrailev, Phys. Rev. E 61 (2000), pp. 2539–2542.

[130] M. Rigol, Phys. Rev. Lett. 116 (2016), p. 100601.

[131] A.C. Cassidy, C.W. Clark, and M. Rigol, Phys. Rev. Lett. 106 (2011), p. 140405.

[132] K. He, L.F. Santos, T.M. Wright, and M. Rigol, Phys. Rev. A 87 (2013), p. 063637.

[133] L. Vidmar and M. Rigol, J. Stat. Phys. (2016), p. 064007.

[134] A. Polkovnikov, Annals of Phys. 326 (2011), p. 486.

[135] M. Rigol, Phys. Rev. Lett. 112 (2014), p. 170601.

[136] M. Rigol and M. Fitzpatrick, Phys. Rev. A 84 (2011), p. 033640.

[137] K. He and M. Rigol, Phys. Rev. A 85 (2012), p. 063609.

[138] V. Gurarie, J. Stat. Mech. (2013), p. P02014.

[139] M. Kormos, L. Bucciantini, and P. Calabrese, EPL (Europhysics Letters) 107 (2014), p. 40002.

[140] M. Collura, M. Kormos, and P. Calabrese, J. Stat. Mech. (2014), p. P01009.

[141] S. Goldstein, J.L. Lebowitz, R. Tumulka, and N. Zanghi, European Phys. J. H 35 (2010), pp. 173–200.

[142] H. Tasaki, Phys. Rev. Lett. 80 (1998), pp. 1373–1376.

[143] S. Goldstein, J.L. Lebowitz, R. Tumulka, and N. Zanghì, Phys. Rev. Lett. 96 (2006), p. 050403.

[144] S. Popescu, A.J. Short, and A. Winter, Nature Phys. 2 (2006), p. 754.

[145] M. Rigol and M. Srednicki, Phys. Rev. Lett. 108 (2012), p. 110601.

[146] M. Srednicki, J. Phys. A 29 (1996), p. L75.

[147] R.V. Jensen and R. Shankar, Phys. Rev. Lett. 54 (1985), pp. 1879–1882.

[148] M. Feingold and A. Peres, Phys. Rev. A 34 (1986), pp. 591–595.

[149] M. Wilkinson, Journal of Physics A: Mathematical and General 20 (1987), p. 2415.

[150] T. Prosen, Annals of Phys. 235 (1994), pp. 115–164.

[151] B. Eckhardt, S. Fishman, J. Keating, O. Agam, J. Main, and K. Müller, Phys. Rev. E 52 (1995), pp. 5893–5903.

[152] S. Hortikar and M. Srednicki, Phys. Rev. E 57 (1998), pp. 7313–7316.

[153] E. Akkermans and G. Montambaux, Mesoscopic Physics of Electrons and Photons, Cambridge University Press, 2007.

[154] E. Khatami, G. Pupillo, M. Srednicki, and M. Rigol, Phys. Rev. Lett. 111 (2013), p. 050403.

[155] J. Lux, J. Müller, A. Mitra, and A. Rosch, Phys. Rev. A 89 (2014), p. 053608.

[156] P. Reimann, Phys. Rev. Lett. 115 (2015), p. 010403.

[157] M. Rigol, Phys. Rev. Lett. 103 (2009), p. 100403.

[158] M. Rigol, Phys. Rev. A 80 (2009), p. 053607.

[159] R. Steinigeweg, J. Herbrych, and P. Prelovšek, Phys. Rev. E 87 (2013), p. 012118.

[160] W. Beugeling, R. Moessner, and M. Haque, Phys. Rev. E 89 (2014), p. 042112.

[161] H. Kim, T.N. Ikeda, and D.A. Huse, Phys. Rev. E 90 (2014), p. 052105.

[162] R. Steinigeweg, A. Khodja, H. Niemeyer, C. Gogolin, and J. Gemmer, Phys. Rev. Lett. 112 (2014), p. 130403.

[163] A. Khodja, R. Steinigeweg, and J. Gemmer, Phys. Rev. E 91 (2015), p. 012120.

[164] W. Beugeling, R. Moessner, and M. Haque, Phys. Rev. E 91 (2015), p. 012144.

[165] E. Khatami, M. Rigol, A. Relaño, and A.M. Garcia-Garcia, Phys. Rev. E 85 (2012), p. 050102(R).

[166] S. Genway, A.F. Ho, and D.K.K. Lee, Phys. Rev. A 86 (2012), p. 023609.

[167] G. Biroli, C. Kollath, and A.M. Läuchli, Phys. Rev. Lett. 105 (2010), p. 250401.

[168] G. Roux, Phys. Rev. A 81 (2010), p. 053604.

[169] S. Sorg, L. Vidmar, L. Pollet, and F. Heidrich-Meisner, Phys. Rev. A 90 (2014), p. 033606.

[170] R. Mondaini, K.R. Fratus, M. Srednicki, and M. Rigol, Phys. Rev. E 93 (2016), p. 032104.

[171] T.N. Ikeda, Y. Watanabe, and M. Ueda, Phys. Rev. E 87 (2013), p. 012125.

[172] V. Alba, Phys. Rev. B 91 (2015), p. 155123.

[173] S. Mukerjee, V. Oganesyan, and D. Huse, Phys. Rev. B 73 (2006), p. 035113.

[174] H. Ott, E. de Mirandes, F. Ferlaino, G. Roati, G. Modugno, and M. Inguscio, Phys. Rev. Lett. 92 (2004), p. 160601.

[175] C.D. Fertig, K.M. O'Hara, J.H. Huckans, S.L. Rolston, W.D. Phillips, and J.V. Porto, Phys. Rev. Lett. 94 (2005), p. 120403.

[176] N. Strohmaier, Y. Takasu, K. Günter, R. Jördens, M. Köhl, H. Moritz, and T. Esslinger, Phys. Rev. Lett. 99 (2007), p. 220601.

[177] U. Schneider, L. Hackermüller, J.P. Ronzheimer, S. Will, S. Braun, T. Best, I. Bloch, E. Demler, S. Mandt, D. Rasch, and A. Rosch, Nature Phys 8 (2012), pp. 213–218.

[178] J.P. Ronzheimer, M. Schreiber, S. Braun, S.S. Hodgman, S. Langer, I.P. McCulloch, F. Heidrich-Meisner, I. Bloch, and U. Schneider, Phys. Rev. Lett. 110 (2013), p. 205301.

[179] C. Kollath, A.M. Läuchli, and E. Altman, Phys. Rev. Lett. 98 (2007), p. 180601.

[180] S.R. Manmana, S. Wessel, R.M. Noack, and A. Muramatsu, Phys. Rev. Lett. 98 (2007), p. 210405.

[181] M. Cramer, A. Flesch, I.P. McCulloch, U. Schollwöck, and J. Eisert, Phys. Rev. Lett. 101 (2008), p. 063001.

[182] A. Flesch, M. Cramer, I.P. McCulloch, U. Schollwöck, and J. Eisert, Phys. Rev. A 78 (2008), p. 033608.

[183] M. Eckstein, M. Kollar, and P. Werner, Phys. Rev. Lett. 103 (2009), p. 056403.

[184] M.C. Bañuls, J.I. Cirac, and M.B. Hastings, Phys. Rev. Lett. 106 (2011), p. 050405.

[185] P.R. Zangara, A.D. Dente, E.J. Torres-Herrera, H.M. Pastawski, A. Iucci, and L.F. Santos, Phys. Rev. E 88 (2013), p. 032913.

[186] G.E. Crooks, Journal of Statistical Physics 90 (1998), pp. 1481–1487.

[187] U. Seifert, Rep. Prog. Phys. 75 (2012), p. 126001.

[188] W. Thirring, Quantum Mathematical Physics. Second Ed., Springer-Verlag. Berlin, Heidelberg, 2002.

[189] E.M. Lifshitz and L.P. Pitaevskii, Physical Kinetics, Landau Lifshitz Course of Theoretical Physics, Vol. 10, Elsevier, 2006.

[190] N.G.V. Kampen, Stochastic Processes in Physics and Chemistry, Elsevier. Amsterdam, The Netherlands, 2003.

[191] A.W. Marshall and I. Olkin, Inequalities: Theory of Majorization, AcademicPress, NewYork, 1979.

[192] A. Polkovnikov, Phys. Rev. Lett. 101 (2008), p. 220402.

[193] G. Bunin, L. D'Alessio, Y. Kafri, and A. Polkovnikov, Nature Phys. 7 (2011), p. 913.

[194] A.E. Allahverdyan and K.V. Hovhannisyan, EPL (Europhysics Letters) 95 (2011), p. 60004.

[195] T.N. Ikeda, N. Sakumichi, A. Polkovnikov, and M. Ueda, Annals of Physics 354 (2015), p. 338.

[196] K. Ji and B.V. Fine, Phys. Rev. Lett. 107 (2011), p. 050401.

[197] M. Bukov, L. D'Alessio, and A. Polkovnikov, Advances in Physics 64 (2015), pp. 139–226.

[198] S. Kullback and R.A. Leibler, Annals of Mathematical Statistics 22 (1951), p. 79.

[199] A. Lenard, Journal of Statistical Physics 19 (1978), pp. 575–586.

[200] R. Balian, From microphysics to macrophysics. 2nd Ed., Springer, 2006.

[201] L. D'Alessio and A. Polkovnikov, Annals of Physics 345 (2014), p. 141.

[202] M. Kolodrubetz, B.K. Clark, and D.A. Huse, Phys. Rev. Lett. 109 (2012), p. 015701.

[203] L. Bonnes, F.H. Essler, and A.M. Läuchli, Phys. Rev. Lett. 113 (2014), p. 187203.

[204] A.E. Allahverdyan and T.M. Nieuwenhuizen, Phys. Rev. E 71 (2005), p. 046107.

[205] G.N. Bochkov and Y.E. Kuzovlev, JETP 45 (1977), p. 125.

[206] G.N. Bochkov and Y.E. Kuzovlev, Physica A 106 (1981), p. 443.

[207] C. Jarzynski, Annual Review Condensed Matter Physics 2 (2011), pp. 329–351.

[208] D. Andrieux and P. Gaspard, J. Stat. Mech. (2007), p. P02006.

[209] D.J. Evans and D.J. Searles, Phys. Rev. E 50 (1994), p. 1645.

[210] P. Pradhan, Y. Kafri, and D. Levine, Phys. Rev. E 77 (2008), p. 041129.

[211] P.L. Krapivsky, S. Redner, and E. Ben-Naim, A Kinetic View of Statistical Physics, Cambridge University Press, 2010.

[212] C. Jarzynski, Phys. Rev. A 46 (1992), p. 7498.

[213] C. Jarzynski, Phys. Rev. E 48 (1993), p. 4340.

[214] G. Bunin and Y. Kafri, Journal of Physics A: Mathematical and Theoretical 46 (2013), p. 095002.

[215] E. Ott, Phys. Rev. Lett. 42 (1979), p. 1628.

[216] D. Cohen, Ann. Phys. (NY) 283 (2000), p. 175.

[217] B. Cleuren, C.V. den Broeck, and R. Kawai, Phys. Rev. E 74 (2006), p. 021117.

[218] P. Gaspard and D. Andrieux, J. Stat. Mech. (2011), p. P03024.

[219] G.D. Mahan, Many-Particle Physics (Physics of Solids and Liquids), Third edition, Springer, 2000.

[220] C. Jarzynski and W.J. Świątecki, Nucl. Phys. A 552 (1993), p. 1.

[221] J. Blocki, F. Brut, and W.J. Swiatecki, Nuclear Physics A 554 (1993), pp. 107 – 117.

[222] J. Blocki, J. Skalski, and W.J. Swiatecki, Nuclear Physics A 594 (1995), pp. 137 – 155.

[223] A.V. Kargovsky, E.I. Anashkina, O.A. Chichigina, and A.K. Krasnova, Phys. Rev. E 87 (2013), p. 042133.

[224] J. Demers and C. Jarzynski, Phys. Rev. E 92 (2015), p. 042911.

[225] P. Mehta and A. Polkovnikov, Annals of Phys. 332 (2013), p. 110.

[226] L. D'Alessio and P.L. Krapivsky, Phys. Rev. E 83 (2011), p. 011107.

[227] M.P. Allen and D.J. Tildesley, Computer simulation of liquids, Oxford University Press, 1989.

[228] B. Sutherland, Beautiful Models, World Scientific, Singapore, 2004.

[229] J.S. Caux and J. Mossel, J. Stat. Mech. (2011), p. P02023.

[230] E.A. Yuzbashyan and B.S. Shastry, J. Stat. Phys. 150 (2013), p. 704.

[231] E.A. Yuzbashyan, Annals of Physics 367 (2016), pp. 288 – 296.

[232] M. Rigol, V. Dunjko, V. Yurovsky, and M. Olshanii, Phys. Rev. Lett. 98 (2007), p. 050405.

[233] E.T. Jaynes, Phys. Rev. 106 (1957), pp. 620–630.

[234] E.T. Jaynes, Phys. Rev. 108 (1957), pp. 171–190.

[235] M.A. Cazalilla, Phys. Rev. Lett. 97 (2006), p. 156403.

[236] M. Rigol, A. Muramatsu, and M. Olshanii, Phys. Rev. A 74 (2006), p. 053616.

[237] M. Kollar and M. Eckstein, Phys. Rev. A 78 (2008), p. 013626.

[238] T. Barthel and U. Schollwöck, Phys. Rev. Lett. 100 (2008), p. 100601.

[239] A. Iucci and M.A. Cazalilla, Phys. Rev. A 80 (2009), p. 063619.

[240] A. Iucci and M.A. Cazalilla, New J. Phys. 12 (2010), p. 055019.

[241] P. Calabrese, F.H.L. Essler, and M. Fagotti, Phys. Rev. Lett. 106 (2011), p. 227203.

[242] P. Calabrese, F.H.L. Essler, and M. Fagotti, J. Stat. Mech. (2012), p. P07022.

[243] M.A. Cazalilla, A. Iucci, and M.C. Chung, Phys. Rev. E 85 (2012), p. 011133.

[244] J.S. Caux and R.M. Konik, Phys. Rev. Lett. 109 (2012), p. 175301.

[245] C. Gramsch and M. Rigol, Phys. Rev. A 86 (2012), p. 053615.

[246] F.H.L. Essler, S. Evangelisti, and M. Fagotti, Phys. Rev. Lett. 109 (2012), p. 247206.

[247] M. Collura, S. Sotiriadis, and P. Calabrese, Phys. Rev. Lett. 110 (2013), p. 245301.

[248] M. Collura, S. Sotiriadis, and P. Calabrese, J. Stat. Mech. (2013), p. P09025.

[249] J.S. Caux and F.H.L. Essler, Phys. Rev. Lett. 110 (2013), p. 257203.

[250] G. Mussardo, Phys. Rev. Lett. 111 (2013), p. 100401.

[251] M. Fagotti, Phys. Rev. B 87 (2013), p. 165106.

[252] M. Fagotti and F.H.L. Essler, Phys. Rev. B 87 (2013), p. 245107.

[253] M. Fagotti, M. Collura, F.H.L. Essler, and P. Calabrese, Phys. Rev. B 89 (2014), p. 125101.

[254] B. Pozsgay, J. Stat. Mech. (2014), p. P10045.

[255] T.M. Wright, M. Rigol, M.J. Davis, and K.V. Kheruntsyan, Phys. Rev. Lett. 113 (2014), p. 050601.

[256] M. Cramer, C.M. Dawson, J. Eisert, and T.J. Osborne, Phys. Rev. Lett. 100 (2008), p. 030602.

[257] K. He and M. Rigol, Phys. Rev. A 87 (2013), p. 043615.

[258] M.C. Chung, A. Iucci, and M.A. Cazalilla, New J. Phys. 14 (2012), p. 075013.

[259] E.J. Torres-Herrera and L.F. Santos, Phys. Rev. E 88 (2013), p. 042121.

[260] S. Ziraldo and G.E. Santoro, Phys. Rev. B 87 (2013), p. 064201.

[261] T. Holstein and H. Primakoff, Phys. Rev. 58 (1940), pp. 1098–1113.

[262] P. Jordan and E. Wigner, Z. Phys. 47 (1928), p. 631.

[263] M. Rigol and A. Muramatsu, Phys. Rev. A 72 (2005), p. 013604.

[264] M. Rigol and A. Muramatsu, Mod. Phys. Lett. 19 (2005), p. 861.

[265] M. Rigol, Phys. Rev. A 72 (2005), p. 063607.

[266] S. Ziraldo, A. Silva, and G.E. Santoro, Phys. Rev. Lett. 109 (2012), p. 247205.

[267] L. Campos Venuti and P. Zanardi, Phys. Rev. E 87 (2013), p. 012106.

[268] S. Sachdev, Quantum Phase Transitions. 2nd Ed., Cambridge University Press, 2011.

[269] M. Kormos, A. Shashi, Y.Z. Chou, J.S. Caux, and A. Imambekov, Phys. Rev. B 88 (2013), p. 205131.

[270] J. De Nardis, B. Wouters, M. Brockmann, and J.S. Caux, Phys. Rev. A 89 (2014), p. 033601.

[271] F.H.L. Essler, G. Mussardo, and M. Panfil, Phys. Rev. A 91 (2015), p. 051602.

[272] B. Wouters, J. De Nardis, M. Brockmann, D. Fioretto, M. Rigol, and J.S. Caux, Phys. Rev. Lett. 113 (2014), p. 117202.

[273] B. Pozsgay, M. Mestyán, M.A. Werner, M. Kormos, G. Zaránd, and G. Takács, Phys. Rev. Lett. 113 (2014), p. 117203.

[274] M. Mierzejewski, P. Prelovšek, and T. Prosen, Phys. Rev. Lett. 113 (2014), p. 020602.

[275] G. Goldstein and N. Andrei, Phys. Rev. A 90 (2014), p. 043625.

[276] M. Rigol, Phys. Rev. E 90 (2014), p. 031301(R).

[277] B. Pozsgay, J. Stat. Mech. (2014), p. P09026.

[278] E. Ilievski, M. Medenjak, and T. Prosen, Phys. Rev. Lett. 115 (2015), p. 120601.

[279] E. Ilievski, J. De Nardis, B. Wouters, J.S. Caux, F.H.L. Essler, and T. Prosen, Phys. Rev. Lett. 115 (2015), p. 157201.

[280] J.S. Russel, Rep. Br. Assoc. Adv. Sci. (1844), pp. 311–390.

[281] D. Korteweg and G. de Vries, Philos. Mag. 39 (1895), pp. 422–443.

[282] I. Mazets, Eur. Phys. J. D 65 (2011), p. 43.

[283] J. Berges, S. Borsányi, and C. Wetterich, Phys. Rev. Lett. 93 (2004), p. 142002.

[284] M. Moeckel and S. Kehrein, Phys. Rev. Lett. 100 (2008), p. 175702.

[285] M. Moeckel and S. Kehrein, Ann. Phys. 324 (2009), p. 2146.

[286] M. Eckstein, A. Hackl, S. Kehrein, M. Kollar, M. Moeckel, P. Werner, and F.A. Wolf, Eur. Phys. J. Special Topics 180 (2010), p. 217.

[287] M. Kollar, F.A. Wolf, and M. Eckstein, Phys. Rev. B 84 (2011), p. 054304.

[288] T. Kitagawa, A. Imambekov, J. Schmiedmayer, and E. Demler, New J. Phys. 13 (2011), p. 073018.

[289] A. Mitra, Phys. Rev. B 87 (2013), p. 205109.

[290] E. Kaminishi, T. Mori, T.N. Ikeda, and M. Ueda, Nat. Phys. 11.

[291] M. Tavora, A. Rosch, and A. Mitra, Phys. Rev. Lett. 113 (2014), p. 010601.

[292] F.H.L. Essler, S. Kehrein, S.R. Manmana, and N.J. Robinson, Phys. Rev. B 89 (2014), p. 165104.

[293] M. Fagotti and M. Collura, arXiv:1507.02678 (2015).

[294] M. Babadi, E. Demler, and M. Knap, Phys. Rev. X 5 (2015), p. 041005.

[295] L. Mathey and A. Polkovnikov, Phys. Rev. A 81 (2010), p. 033605.

[296] R. Barnett, A. Polkovnikov, and M. Vengalattore, Phys. Rev. A 84 (2011), p. 023606.

[297] D.M. Stamper-Kurn and M. Ueda, Rev. Mod. Phys. 85 (2013), p. 1191.

[298] N. Nessi, A. Iucci, and M.A. Cazalilla, Phys. Rev. Lett. 113 (2014), p. 210402.

[299] V. Gurarie, Nucl.Phys. B 441 (1995), p. 569.

[300] C. Scheppach, J. Berges, and T. Gasenzer, Phys.Rev.A 81 (2010), p. 033611.

[301] B. Nowak, J. Schole, D. Sexty, and T. Gasenzer, Phys. Rev. A 85 (2012), p. 043627.

[302] E. Shimshoni, N. Andrei, and A. Rosch, Phys. Rev. B 68 (2003), p. 104401.

[303] E. Boulat, P. Mehta, N. Andrei, E. Shimshoni, and A. Rosch, Phys. Rev. B 76 (2007), p. 214411.

[304] M. Serbyn, Z. Papić, and D.A. Abanin, Phys. Rev. Lett. 111 (2013), p. 127201.

[305] D. Huse and V. Oganesyan, Phys. Rev. B 90 (2014), p. 174202.

[306] M. Stark and M. Kollar, arXiv:1308.1610 (2013).

[307] P.L. Kapitza, Soviet Phys. JETP 21 (1951), p. 588.

[308] B. Chirikov and D. Shepelyansky, Scholarpedia 3 (2008), p. 3550.

[309] J.M. Greene, J. Math. Phys. 20 (1979), p. 1183.

[310] R.S. MacKay, Physica D 7 (1983), p. 283.

[311] R.S. MacKay and I. Percival, Comm. Math. Phys. 94 (1985), p. 469.

[312] M.E. Fisher, The Nature of Critical Points, in Boulder Lectures in Theoretical Physics, Vol. 7, University of Colorado, Boulder (1965).

[313] C.N. Yang and T.D. Lee, Phys. Rev. 87 (1952), p. 404.

[314] M. Heyl and M. Vojta, Phys. Rev. B 92 (2015), p. 104401.

[315] M. Heyl, A. Polkovnikov, and S. Kehrein, Phys. Rev. Lett. 110 (2013), p. 135704.

[316] A.M. Odlyzko, The 10^{22}-nd zero of the Riemann zeta function, in Dynamical, spectral, and arithmetic zeta functions (San Antonio, TX, 1999), Contemp. Math., Vol. 290, Amer. Math. Soc., Providence, RI, 2001, pp. 139–144.

[317] D.A. Sivak and G.E. Crooks, Phys. Rev. Lett. 108 (2012), p. 190602.

From "Quench dynamics and relaxation in isolated integrable quantum spin chains" by Essler, Fagotti

References

[1] J. M. Deutsch, Quantum statistical mechanics in a closed system, Phys. Rev. A **43**, 2046 (1991); M. Srednicki, Chaos and quantum thermalization, Phys. Rev. E **50**, 888 (1994).

[2] M. Greiner, O. Mandel, T.W. Hänsch, and I. Bloch, Collapse and revival of the matter wave field of a Bose?Einstein condensate, Nature **419**, 51-54 (2002).

[3] T. Kinoshita, T. Wenger, D. S. Weiss, A quantum Newton's cradle, Nature **440**, 900 (2006).

[4] S. Hofferberth, I. Lesanovsky, B. Fischer, T. Schumm, and J. Schmiedmayer, Non-equilibrium coherence dynamics in one-dimensional Bose gases, Nature **449**, 324-327 (2007).

[5] L. Hackermuller, U. Schneider, M. Moreno-Cardoner, T. Kitagawa, S. Will, T. Best, E. Demler, E. Altman, I. Bloch and B. Paredes, Anomalous Expansion of Attractively Interacting Fermionic Atoms in an Optical Lattice, Science **327**, 1621 (2010).

[6] S. Trotzky Y.-A. Chen, A. Flesch, I. P. McCulloch, U. Schollwöck, J. Eisert, and I. Bloch, Probing the relaxation towards equilibrium in an isolated strongly correlated 1D Bose gas, Nature Phys. **8**, 325 (2012).

[7] M. Gring, M. Kuhnert, T. Langen, T. Kitagawa, B. Rauer, M. Schreitl, I. Mazets, D. A. Smith, E. Demler, and J. Schmiedmayer, Relaxation Dynamics and Pre-thermalization in an Isolated Quantum System, Science **337**, 1318 (2012).

[8] U. Schneider, L. Hackermüller, J. P. Ronzheimer, S. Will, S. Braun, T. Best, I. Bloch, E. Demler, S. Mandt, D. Rasch, and A. Rosch, Fermionic transport and out-of-equilibrium dynamics in a homogeneous Hubbard model with ultracold atoms, Nature Phys. **8**, 213 (2012).

[9] M. Cheneau, P. Barmettler, D. Poletti, M. Endres, P. Schauss, T. Fukuhara, C. Gross, I. Bloch, C. Kollath, and S. Kuhr, Light-cone-like spreading of correlations in a quantum many-body system, Nature **481**, 484 (2012).

[10] T. Langen, R. Geiger, M. Kuhnert, B. Rauer, and J. Schmiedmayer, Local emergence of thermal correlations in an isolated quantum many-body system, Nature Physics **9**, 640 (2013).

[11] F. Meinert, M.J. Mark, E. Kirilov, K. Lauber, P. Weinmann, A.J. Daley, and H.-C. Nägerl, Quantum Quench in an Atomic One-Dimensional Ising Chain, Phys. Rev. Lett. **111**, 053003 (2013).

[12] T. Fukuhara, A. Kantian, M. Endres, M. Cheneau, P. Schauß, S. Hild, D. Bellem, U. Schollwöck, T. Giamarchi, C. Gross, I. Bloch, and S. Kuhr, Quantum dynamics of a mobile spin impurity, Nature Physics **9**, 235 (2013).

[13] T. Fukuhara, P. Schauß, M. Endres, S. Hild, M. Cheneau, I. Bloch, and C. Gross, Microscopic observation of magnon bound states and their dynamics, Nature **502**, 76 (2013).

[14] J.P. Ronzheimer, M. Schreiber, S. Braun, S.S. Hodgman, S. Langer, I.P. McCulloch, F. Heidrich-Meisner, I. Bloch and U. Schneider, Expansion dynamics of interacting bosons in homogeneous lattices in one and two dimensions, Phys. Rev. Lett. **110**, 205301 (2013).

[15] N. Navon, A.L. Gaunt, R.P. Smith and Z. Hadzibabic, Critical Dynamics of Spontaneous Symmetry Breaking in a Homogeneous Bose gas, Science **347**, 167 (2015).

[16] P. Jurcevic, B. P. Lanyon, P. Hauke, C. Hempel, P. Zoller, R. Blatt, and C. F. Roos, Quasiparticle engineering and entanglement propagation in a quantum many-body system, Nature **511**, 202 (2014).

[17] P. Richerme, Z.-X. Gong, A. Lee, C. Senko, J. Smith, M. Moss-Feig, S. Michalakis, A. V. Gorshkov, and C. Monroe, Non-local propagation of correlations in quantum systems with long-range interactions, Nature **511**, 198 (2014).

[18] T. Langen, T. Gasenzer and J. Schmiedmayer, Prethermalization and universal dynamics in near-integrable quantum systems, arXiv:1603.09385 (2016).

[19] E. H. Lieb and W. Liniger, Exact Analysis of an Interacting Bose Gas. I. The General Solution and the Ground State Phys. Rev. **130**, 1605 (1963); E. H. Lieb, Exact Analysis of an Interacting Bose Gas. II. The Excitation Spectrum, Phys. Rev. **130**, 1616 (1963).

[20] V.E. Korepin, A.G. Izergin, and N.M. Bogoliubov, Quantum Inverse Scattering Method, Correlation Functions and Algebraic Bethe Ansatz (Cambridge University Press, 1993).

[21] B. Davies and V.E. Korepin, Higher conservation laws for the quantum non-linear Schroedinger equation, arXiv:1109.6604 (2011).

[22] A. C. Cassidy, C. W. Clark, and M. Rigol, Generalized Thermalization in an Integrable Lattice System, Phys. Rev. Lett. **106**, 140405 (2011).

[23] C. Gramsch and M. Rigol, Quenches in a quasidisordered integrable lattice system: Dynamics and statistical description of observables after relaxation, Phys. Rev. A **86**, 053615 (2012).

[24] T.M. Wright, M. Rigol, M.J. Davis, and K.V. Kheruntsyan, Nonequilibrium Dynamics of One-Dimensional Hard-Core Anyons Following a Quench: Complete Relaxation of One-Body Observables, Phys. Rev. Lett. **113**, 050601 (2014).

[25] P. Calabrese, F.H.L. Essler, and M. Fagotti, Quantum Quench in the Transverse-Field Ising Chain, Phys. Rev. Lett. **106**, 227203 (2011).

[26] P. Calabrese, F.H.L. Essler, and M. Fagotti, Quantum quench in the transverse field Ising chain: I. Time evolution of order parameter correlators. J. Stat. Mech. (2012) P07016.

[27] P. Calabrese, F.H.L. Essler, and M. Fagotti, Quantum Quench in the Transverse Field Ising Chain II: Stationary State Properties, J. Stat. Mech. (2012) P07022.

[28] M. Fagotti and F.H.L. Essler, Reduced density matrix after a quantum quench, Phys. Rev. B **87**, 245107 (2013).

[29] F.H.L. Essler, S. Evangelisti and M. Fagotti, Dynamical Correlations After a Quantum Quench, Phys. Rev. Lett. **109**, 247206 (2012).

[30] M. Fagotti, Finite-size corrections versus relaxation after a sudden quench, Phys. Rev. B **87**, 165106 (2013).

[31] M. Kormos, L. Bucciantini, and P. Calabrese, Stationary entropies after a quench from excited states in the Ising chain, EPL **107** 40002 (2014).

[32] L. Bucciantini, M. Kormos, P. Calabrese, Quantum quenches from excited states in the Ising chain, J. Phys. A: Math. Theor. **47** 175002 (2014).

[33] D. Rossini, A. Silva, G. Mussardo, and G.E. Santoro, Effective Thermal Dynamics Following a Quantum Quench in a Spin Chain, Phys. Rev. Lett. **102**, 127204 (2009); D. Rossini, S. Suzuki, G. Mussardo, G.E. Santoro, and A. Silva, Long time dynamics following a quench in an integrable quantum spin chain: Local versus nonlocal operators and effective thermal behavior, Phys. Rev. B **82**, 144302 (2010).

[34] F. Igói and H. Rieger, Long-Range Correlations in the Nonequilibrium Quantum Relaxation of a Spin Chain, Phys. Rev. Lett. **85**, 3233 (2000).

[35] K. Sengupta, S. Powell, and S. Sachdev, Quench dynamics across quantum critical points, Phys. Rev. A **69**, 053616 (2004).

[36] A. Silva, Statistics of the Work Done on a Quantum Critical System by Quenching a Control Parameter, Phys. Rev. Lett. **101**, 120603 (2008).

[37] F. Iglói and H. Rieger, Quantum Relaxation after a Quench in Systems with Boundaries, Phys. Rev. Lett. **106**, 035701 (2011).

[38] L. Foini, L.F. Cugliandolo, and A. Gambassi, Fluctuation-dissipation relations and critical quenches in the transverse field Ising chain, Phys. Rev. B **84**, 212404 (2011).

[39] H. Rieger and F. Iglói, Semiclassical theory for quantum quenches in finite transverse Ising chains, Phys. Rev. B **84**, 165117 (2011).

[40] D. Schuricht and F.H.L. Essler, Dynamics in the Ising field theory after a quantum quench, J. Stat. Mech. (2012) P04017.

[41] L. Foini, L.F. Cugliandolo, and A. Gambassi, Dynamic correlations, fluctuation-dissipation relations, and effective temperatures after a quantum quench of the transverse field Ising chain, J. Stat. Mech. (2012) P09011.

[42] M. Heyl, A. Polkovnikov, and S. Kehrein, Dynamical Quantum Phase Transitions in the Transverse-Field Ising Model, Phys. Rev. Lett. **110**, 135704 (2013).

[43] T. Caneva, E. Canovi, D. Rossini, G.E. Santoro, and A. Silva, Applicability of the generalized Gibbs ensemble after a quench in the quantum Ising chain, J. Stat. Mech. (2011) P07015.

[44] T. Antal, Z. Racz, A. Rakos, and G. M. Schutz, Transport in the XX chain at zero temperature: Emergence of flat magnetization profiles, Phys. Rev. E **59**, 4912 (1999).

[45] E. Barouch, B. McCoy, and M. Dresden, Statistical Mechanics of the XY Model. I, Phys. Rev. A **2**, 1075 (1970).

[46] E. Barouch and B. McCoy, Statistical Mechanics of the XY Model. II, Phys. Rev. A **3**, 786 (1971).

[47] E. Barouch and B. McCoy, Statistical Mechanics of the XY Model. III, Phys. Rev. A **3**, 2137 (1971).

[48] M. Fagotti and P. Calabrese, Evolution of entanglement entropy following a quantum quench: Analytic results for the XY chain in a transverse magnetic field, Phys. Rev. A **78**, 010306(R) (2008).

[49] M. A. Cazalilla, A. Iucci, and M.-C. Chung, Thermalization and quantum correlations in exactly solvable models, Phys. Rev. E **85**, 011133 (2012).

[50] B. Blass, H. Rieger, and F. Iglói, Quantum relaxation and finite-size effects in the XY chain in a transverse field after global quenches, EPL **99** 30004 (2012).

[51] M. Fagotti, On conservation laws, relaxation and pre-relaxation after a quantum quench, J. Stat. Mech. (2014) P03016.

[52] M. Fagotti, Local conservation laws in spin-1/2 XY chains with open boundary conditions, J. Stat. Mech. (2016) 063105 (doi:10.1088/1742-5468/2016/06/063105).

[53] M. Collura, P. Calabrese, and F.H.L. Essler, Quantum quench within the gapless phase of the spin-1/2 Heisenberg XXZ spin chain, Phys. Rev. B **92**, 125131 (2015).

[54] J. Lancaster and A. Mitra, Quantum quenches in an XXZ spin chain from a spatially inhomogeneous initial state, Phys. Rev. E **81**, 061134 (2010).

[55] T. Sabetta and G. Misguich, Nonequilibrium steady states in the quantum XXZ spin chain, Phys. Rev. B **88**, 245114 (2013).

[56] L. Bonnes, F.H.L. Essler and A. Läuchli, "Light-Cone" Dynamics After Quantum Quenches in Spin Chains, Phys. Rev. Lett. **113**, 187203 (2014).

[57] E. Canovi, D. Rossini, R. Fazio, G. Santoro, and A. Silva, Many-body localization and thermalization in the full probability distribution function of observables, New J. Phys. **14**, 095020 (2012).

[58] M. Fagotti and F.H.L. Essler, Stationary behaviour of observables after a quantum quench in the spin-1/2 Heisenberg XXZ chain, J. Stat. Mech. (2013) P07012.

[59] B. Pozsgay, The generalized Gibbs ensemble for Heisenberg spin chains, J. Stat. Mech. (2013) P07003.

[60] M. Fagotti, Dynamical Phase Transitions as Properties of the Stationary State: Analytic Results after Quantum Quenches in the Spin-1/2 XXZ Chain, arXiv:1308.0277; B. Pozsgay, Dynamical free energy and the Loschmidt-echo for a class of quantum quenches in the Heisenberg spin chain, Stat. Mech. (2013) P10028.

[61] W. Liu and N. Andrei, Quench Dynamics of the Anisotropic Heisenberg Model, Phys. Rev. Lett. **112**, 257204 (2014).

[62] P. Barmettler, M. Punk, V. Gritsev, E. Demler, and E. Altman, Relaxation of antiferromagnetic order in spin-1/2 chains following a quantum quench, Phys. Rev. Lett. **102**, 130603 (2009); P. Barmettler, M. Punk, V. Gritsev, E. Demler, and E. Altman, Quantum quenches in the anisotropic spin-1/2 Heisenberg chain: different approaches to many-body dynamics far from equilibrium, New J. Phys. **12**, 055017 (2010).

[63] M, Fagotti, M, Collura, F.H.L. Essler, and P. Calabrese, Relaxation after quantum quenches in the spin-1/2 Heisenberg XXZ chain, Phys. Rev. B **89**, 125101 (2014).

[64] E. Ilievski, J. De Nardis, B. Wouters, J.-S. Caux, F.H.L. Essler, T. Prosen, Complete Generalized Gibbs Ensemble in an interacting Theory, Phys. Rev. Lett. **115**, 157201 (2015).

[65] M. Brockmann, B. Wouters, D. Fioretto, J. De Nardis, R. Vlijm and J.-S. Caux, Quench action approach for releasing the Néel state into the spin-1/2 XXZ chain, Stat. Mech. (2014) P12009.

[66] B. Wouters, J. De Nardis, M. Brockmann, D. Fioretto, M. Rigol, and J.-S. Caux, Quenching the Anisotropic Heisenberg Chain: Exact Solution and Generalized Gibbs Ensemble Predictions, Phys. Rev. Lett. **113**, 117202 (2014).

[67] B. Pozsgay, Overlaps between eigenstates of the XXZ spin-1/2 chain and a class of simple product states, J. Stat. Mech. (2014) P06011.

[68] B. Pozsgay, M. Mestyán, M.A. Werner, M. Kormos, G. Zaránd, and G. Takács, Correlations after Quantum Quenches in the XXZ Spin Chain: Failure of the Generalized Gibbs Ensemble, Phys. Rev. Lett. **113**, 117203 (2014).

[69] M. Mestyán, B. Pozsgay, G. Takács, and M.A. Werner, Quenching the XXZ spin chain: quench action approach versus generalized Gibbs ensemble, J. Stat. Mech. (2015) P04001.

[70] M. Rigol, Quantum quenches in the thermodynamic limit. II. Initial ground states, Phys. Rev. E **90**, 031301(R) (2014).

[71] J. Mossel and J.-S. Caux, Relaxation dynamics in the gapped XXZ spin-1/2 chain, New J. Phys. **12** 055028 (2010).

[72] V. Alba and P. Calabrese, The quench action approach in finite integrable spin chains, arXiv:1512.02213 (2015).

[73] M. Kollar and M. Eckstein, Relaxation of a one-dimensional Mott insulator after an interaction quench, Phys. Rev. A **78**, 013626 (2008).

[74] T. Enss and J. Sirker, Lightcone renormalization and quantum quenches in one-dimensional Hubbard models, New J. Phys. **14**, 023008 (2012).

[75] D. Iyer, R. Mondaini, S. Will, and M. Rigol, Coherent quench dynamics in the one-dimensional Fermi-Hubbard model, Phys. Rev. A **90**, 031602(R) (2014).

[76] L. Riegger, G. Orso and F. Heidrich-Meisner, Interaction quantum quenches in the one-dimensional Fermi-Hubbard model with spin imbalance Phys. Rev. A **91**, 043623 (2015).

[77] A. Bauer, F. Dorfner and F. Heidrich-Meisner, Temporal decay of Néel order in the one-dimensional Fermi-Hubbard model, Phys. Rev. A **91**, 053628 (2015).

[78] S. Sotiriadis, P. Calabrese, and J. Cardy, Quantum quench from a thermal initial state, EPL **87** 20002 (2009).

[79] S. Sotiriadis, G. Martelloni, Equilibration and GGE in interacting-to-free Quantum Quenches in dimensions $d > 1$, J. Phys. A: Math. Theor. **49** 095002 (2016).

[80] P. Calabrese and J. Cardy, Quantum quenches in extended systems, J. Stat. Mech. (2007) P06008.

[81] M.A. Cazalilla, Effect of Suddenly Turning on Interactions in the Luttinger Model, Phys. Rev. Lett. **97**, 156403 (2006).

[82] A. Iucci and M. A. Cazalilla, Quantum quench dynamics of the Luttinger model, Phys. Rev. A **80**, 063619 (2009).

[83] J. Rentrop, D. Schuricht and V. Meden, Quench dynamics of the Tomonaga-Luttinger model with momentum-dependent interaction, New J. Phys. **14** 075001 (2012).

[84] C. Karrasch, J. Rentrop, D. Schuricht, and V. Meden, Luttinger-liquid universality in the time evolution after an interaction quench, Phys. Rev. Lett. **109**, 126406 (2012).

[85] B. Dóra, Á. Bácsi, and G. Zaránd, Generalized Gibbs ensemble and work statistics of a quenched Luttinger liquid, Phys. Rev. B **86**, 161109(R) (2012).

[86] N. Nessi and A. Iucci, Quantum quench dynamics of the Coulomb Luttinger model, Phys. Rev. B **87**, 085137 (2013).

[87] M. A. Cazalilla, M.-C. Chung, Quantum Quenches in the Luttinger model and its close relatives, arXiv:1603.04252 (2016).

[88] P. Calabrese and J. Cardy, Quantum quenches in 1+1 dimensional conformal field theories, arXiv:1603.02889 (2016)

[89] P. Calabrese and J. Cardy, Evolution of entanglement entropy in one-dimensional systems, J. Stat. Mech. (2005) P04010.

[90] P. Calabrese and J. Cardy, Time Dependence of Correlation Functions Following a Quantum Quench, Phys. Rev. Lett. **96**, 136801 (2006).

[91] J. Cardy, Thermalization and Revivals after a Quantum Quench in Conformal Field Theory, Phys. Rev. Lett. **112**, 220401 (2014).

[92] S. Sotiriadis, Memory-preserving equilibration after a quantum quench in a 1d critical model, arXiv:1507.07915 (2015).

[93] J. Cardy, Quantum quenches to a critical point in one dimension: some further results, J. Stat. Mech. (2016) 023103.

[94] V. Gritsev, E. Demler, M. Lukin, and A. Polkovnikov, Spectroscopy of Collective Excitations in Interacting Low-Dimensional Many-Body Systems Using Quench Dynamics, Phys. Rev. Lett. **99**, 200404 (2007).

[95] B. Bertini, D. Schuricht, and F.H.L. Essler, Quantum quench in the sine-Gordon model, J. Stat. Mech. (2014) P10035.

[96] M. Kormos and G. Zaránd, Quantum quenches in the sine-Gordon model: a semiclassical approach, arXiv:1507.02708 (2015).

[97] D. Fioretto and G. Mussardo, Quantum quenches in integrable field theories, New J. Phys. **12**, 055015 (2010).

[98] B. Bertini, L. Piroli, P. Calabrese, Quantum quenches in the sinh-Gordon model: steady state and one point correlation functions, arXiv:1602.08269 (2016).

[99] B. Pozsgay, Mean values of local operators in highly excited Bethe states, J. Stat. Mech. (2011) P01011.

[100] G. Mussardo, Infinite-Time Average of Local Fields in an Integrable Quantum Field Theory After a Quantum Quench, Phys. Rev. Lett. **111**, 100401 (2013).

[101] S. Evangelisti, Semi-classical theory for quantum quenches in the O(3) non-linear sigma model, J. Stat. Mech. (2013) P04003.

[102] A. Lamacraft, Noise correlations in the expansion of an interacting one-dimensional Bose gas from a regular array, Phys. Rev. A **84**, 043632 (2011).

[103] J. Mossel and J.-S. Caux, Exact time evolution of space- and time-dependent correlation functions after an interaction quench in the one-dimensional Bose gas, New J. Phys. **14**, 075006 (2012).

[104] M. Collura, S. Sotiriadis and P. Calabrese, Equilibration of a Tonks-Girardeau Gas Following a Trap Release, Phys. Rev. Lett. **110**, 245301 (2013); Quench dynamics of a Tonks-Girardeau gas released from a harmonic trap, J. Stat. Mech. (2013) P09025.

[105] M. Kormos, A. Shashi, Y.-Z. Chou, J.-S. Caux and A. Imambekov, Interaction quenches in the one-dimensional Bose gas, Phys. Rev. B **88**, 205131(2013)

[106] M. Collura, S. Sotiriadis, and P. Calabrese, Quench dynamics of a Tonks-Girardeau gas released from a harmonic trap, J. Stat. Mech. (2013) P09025.

[107] J. De Nardis, B. Wouters, M. Brockmann, and J.-S. Caux, Solution for an interaction quench in the Lieb-Liniger Bose gas, Phys. Rev. A **89**, 033601 (2014).

[108] P.P. Mazza, M. Collura, M. Kormos, and P. Calabrese, Interaction quench in a trapped 1D Bose gas, J. Stat. Mech. (2014) P11016.

[109] M. Collura, M. Kormos, and P. Calabrese, Stationary entanglement entropies following an interaction quench in 1D Bose gas, J. Stat. Mech. (2014) P01009.

[110] M. Kormos, M. Collura and P. Calabrese, Analytic results for a quantum quench from free to hard-core one-dimensional bosons, Phys. Rev. A **89**, 013609 (2014).

[111] J. De Nardis and J.-S. Caux, Analytical expression for a post-quench time evolution of the one-body density matrix of one-dimensional hard-core bosons, J. Stat. Mech. (2014) P12012.

[112] F.H.L. Essler, G. Mussardo, and M. Panfil, Generalized Gibbs ensembles for quantum field theories, Phys. Rev. A **91**, 051602(R) (2015).

[113] J. De Nardis, L. Piroli and J.-S. Caux, Relaxation dynamics of local observables in integrable systems, Phys. A: Math. Theor. **48** 43FT01 (2015).

[114] L. Piroli, P. Calabrese, and F.H.L. Essler, Multiparticle Bound-State Formation following a Quantum Quench to the One-Dimensional Bose Gas with Attractive Interactions, Phys. Rev. Lett. **116**, 070408 (2016).

[115] M. Collura and D. Karevski, Critical Quench Dynamics in Confined Systems, Phys. Rev. Lett. **104**, 200601 (2010).

[116] J. Dziarmaga, Dynamics of a Quantum Phase Transition and Relaxation to a Steady State, Adv. Phys. **59**, 1063 (2010); C. De Grandi, V. Gritsev and A. Polkovnikov, Quench dynamics near a quantum critical point: application to the sine-Gordon model, Phys. Rev. B **81**, 224301 (2010); A. Dutta, G. Aeppli, B.K. Chakrabarti, U. Divakaran, T.F. Rosenbaum and D. Sen, Quantum phase transitions in transverse field spin models: from statistical physics to quantum information, Cambridge University Press, Cambridge 2015.

[117] W.H. Zurek, Cosmological experiments in condensed matter systems, Phys. Rep. **276**, 177 (1996).

[118] A. Polkovnikov, K. Sengupta, A. Silva, and M. Vengalattore, Colloquium: Nonequilibrium dynamics of closed interacting quantum systems, Rev. Mod. Phys. **83**, 863 (2011).

[119] C. Gogolin and J. Eisert, Equilibration, thermalisation, and the emergence of statistical mechanics in closed quantum systems - a review, arXiv:1503.07538 (2015).

[120] A. Lamacraft and J.E. Moore, Potential insights into non-equilibrium behavior from atomic physics, in Ultracold Bosonic and Fermionic Gases, eds A. Fetter, K. Levin and D. Stamper-Kurn, Elseview 2012; arXiv:1106.3567 (2011).

[121] L. D'Alessio, Y. Kafri, A. Polkovnikov and M. Rigol, From Quantum Chaos and Eigenstate Thermalization to Statistical Mechanics and Thermodynamics, arXiv:1509.06411 (2015).

[122] R. A. Barankov, L. S. Levitov, Synchronization in the BCS Pairing Dynamics as a Critical Phenomenon, Phys. Rev. Lett. **96**, 230403 (2006); E.A. Yuzbashyan and M. Dzero, Dynamical vanishing of the order parameter in a fermionic condensate, Phys. Rev. Lett. **96**, 230404 (2006).

[123] G. Vidal, J.I. Latorre, E. Rico, and A. Kitaev, Entanglement in Quantum Critical Phenomena, Phys. Rev. Lett. **90**, 227902 (2003).

[124] I. Peschel and V. Eisler, Reduced density matrices and entanglement entropy in free lattice models, J. Phys. A: Math. Theor. **42** 504003 (2009).

[125] F. Verstraete, M.M. Wolf, D. Perez-Garcia, and J.I. Cirac, Criticality, the Area Law, and the Computational Power of Projected Entangled Pair States, Phys. Rev. Lett. **96** 220601 (2006); M. B. Hastings, Entropy and entanglement in quantum ground states, Phys. Rev.

B **76**, 035114 (2007); N. de Beaudrap, T.J. Osborne, and J. Eisert, Ground states of unfrustrated spin Hamiltonians satisfy an area law, New J. Phys. **12** 095007 (2010).

[126] T. Barthel and U. Schollwöck, Dephasing and the Steady State in Quantum Many-Particle Systems, Phys. Rev. Lett. **100**, 100601 (2008).

[127] M. Fagotti and M. Collura, Universal prethermalization dynamics of entanglement entropies after a global quench, arXiv:1507.02678 (2015).

[128] S. Sotiriadis and P. Calabrese, Validity of the GGE for quantum quenches from interacting to noninteracting models, J. Stat. Mech. (2014) P07024.

[129] E. Bettelheim, A.G. Abanov and P. Wiegmann, Quantum Shock Waves - the case for non-linear effects in dynamics of electronic liquids, Phys. Rev. Lett. **97**, 246401 (2006).

[130] E. Bettelheim, A.G. Abanov and P. Wiegmann, Orthogonality catastrophe and shock waves in a non-equilibrium Fermi gas, Phys.Rev.Lett. **97**, 246402 (2006).

[131] S. Sotiriadis and J. Cardy, Inhomogeneous Quantum Quenches, J. Stat. Mech. P11003 (2008).

[132] P. Calabrese, C. Hagendorf, and P. Le Doussal, Time evolution of 1D gapless models from a domain-wall initial state: SLE continued?, J. Stat. Mech. P07013 (2008).

[133] E. Bettelheim and P. Wiegmann, Fermi distribution of semicalssical non-eqilibrium Fermi states, Phys. Rev. B **84**, 085102 (2011).

[134] L. Vidmar, S. Langer, I.P. McCulloch, U. Schneider, U. Schollwoeck and F. Heidrich-Meisner, Sudden expansion of Mott insulators in one dimension Phys. Rev. B **88**, 235117 (2013).

[135] V. Eisler and Z. Racz, Full Counting Statistics in a Propagating Quantum Front and Random Matrix Spectra, Phys. Rev. Lett. **110**, 060602 (2013).

[136] M.A. Rajabpour and S. Sotiriadis, Quantum quench of the trap frequency in the harmonic Calogero model, Phys. Rev. A **89**, 033620 (2014).

[137] Z. Mei, L. Vidmar, F. Heidrich-Meisner and C. J. Bolech, Unveiling hidden structure of many-body wavefunctions of integrable systems via sudden expansion experiments, Phys. Rev. A **93**, 021607 (2016).

[138] W.H. Aschbacher and C.-A. Pillet, Non-Equilibrium Steady States of the XY Chain, J. Stat. Phys. **112**, 1153 (2003).

[139] W.H. Aschbacher and J.-M. Barbaroux, Out of Equilibrium Correlations in the XY Chain, Lett. Math. Phys. **77**, 11 (2006).

[140] D. Bernard and B. Doyon, Energy flow in non-equilibrium conformal field theory, J. Phys. A: Math. Theor. **45**, 362001 (2012).

[141] J.-S. Caux and R. M. Konik, Constructing the Generalized Gibbs Ensemble after a Quantum Quench, Phys. Rev. Lett. **109**, 175301 (2012).

[142] D. Bernard and B. Doyon, Non-Equilibrium Steady States in Conformal Field Theory, Ann. H. Poincaré **16**, 113 (2015).

[143] M. Mintchev and P. Sorba, Luttinger liquid in a non-equilibrium steady state, J. Phys. A: Math. Theor. **49**, 095006 (2013).

[144] A. De Luca, J. Viti, D. Bernard, and B. Doyon, Nonequilibrium thermal transport in the quantum Ising chain, Phys. Rev. B **88**, 134301 (2013).

[145] T. Sabetta and G. Misguich, Nonequilibrium steady states in the quantum XXZ spin chain, Phys. Rev. B **88**, 245114 (2013).

[146] B. Doyon, M. Hoogeveen, and D. Bernard, Energy flow and fluctuations in non-equilibrium conformal field theory on star graphs, Stat. Mech. (2014) P03002.

[147] O. Castro-Alvaredo, Y. Chen, B. Doyon, and M. Hoogeveen, Thermodynamic Bethe ansatz for non-equilibrium steady states: exact energy current and fluctuations in integrable QFT, J. Stat. Mech. (2014) P03011.

[148] A. De Luca, G. Martelloni, and J. Viti, Stationary states in a free fermionic chain from the quench action method, Phys. Rev. A **91**, 021603(R) (2014).

[149] B. Doyon, A. Lucas, K. Schalm, and M.J Bhaseen, Non-equilibrium steady states in the Klein-Gordon theory, J. Phys. A: Math. Theor. 48 095002 (2015).

[150] B. Doyon, Lower bounds for ballistic current and noise in non-equilibrium quantum steady states, Nucl. Phys. B **892**, 190 (2015).

[151] J. Viti; J.-M. Stéphan; J. Dubail; M. Haque, Inhomogeneous quenches in a fermionic chain: exact results, arXiv:1507.08132 (2015).

[152] T. Platini and D. Karevski, Relaxation in the XX quantum chain, J. Phys. A: Math. Theor. **40** 1711 (2007).

[153] V. Eisler, D. Karevski, T. Platini, and I. Peschel, Entanglement evolution after connecting finite to infinite quantum chains, J. Stat. Mech. (2008) **P01023**.

[154] D. Bernard and B. Doyon, Conformal field theory out of equilibrium: a review, arXiv:1603.07765 (2016).

[155] R. Vasseur and J.E. Moore, Nonequilibrium quantum dynamics and transport: from integrability to many-body localization, arXiv:1603.06618 (2016).

[156] M. Cramer, C.M. Dawson, J. Eisert, and T.J. Osborne, Exact Relaxation in a Class of Nonequilibrium Quantum Lattice Systems, Phys. Rev. Lett. **100**, 030602 (2008).

[157] M. Cramer and J. Eisert, A quantum central limit theorem for non-equilibrium systems: exact local relaxation of correlated states, New J. Phys. **12**, 055020 (2010).

[158] J. Sirker, N.P. Konstantinidis, F. Andraschko, and N. Sedlmayr, Locality and thermalization in closed quantum systems, Phys. Rev. A **89**, 042104 (2014).

[159] J.R. Garrison and T. Grover, Does a single eigenstate encode the full Hamiltonian?, arXiv:1503.00729.

[160] M. Rigol and M. Srednicki, Alternatives to Eigenstate Thermalization, Phys. Rev. Lett. **108**, 110601 (2012).

[161] M. Rigol, V. Dunjko, and M. Olshanii, Thermalization and its mechanism for generic isolated quantum systems, Nature **452**, 854 (2008).

[162] S. Braun, J.P. Ronzheimer, M. Schreiber, S.S. Hodgman, T. Rom, I. Bloch, U. Schneider, Negative Absolute Temperature for Motional Degrees of Freedom, Science **339**, 52 (2013).

[163] T. Prosen, A new class of completely integrable quantum spin chains, J. Phys. A: Math. Gen. **31** L397 (1998); M. Grady, Infinite set of conserved charges in the Ising model, Phys. Rev. D **25**, 1103 (1981).

[164] E.T. Jaynes, Information Theory and Statistical Mechanics, Phys. Rev. **106**, 620 (1957).

[165] M. Rigol, V. Dunjko, V. Yurovsky, and M. Olshanii, Relaxation in a Completely Integrable Many-Body Quantum System: An Ab Initio Study of the Dynamics of the Highly Excited States of 1D Lattice Hard-Core Bosons, Phys. Rev. Lett. **98**, 50405 (2007).

[166] B. Doyon, Thermalization and pseudolocality in extended quantum systems, arXiv:1512.03713 (2015).

[167] M. Rigol, Breakdown of thermalization in finite one-dimensional systems, Phys. Rev. Lett. **103**, 100403 (2009).

[168] M. Rigol, Quantum quenches and thermalization in one-dimensional fermionic systems, Phys. Rev. A **80**, 053607 (2009).

[169] G. Biroli, C. Kollath, and A.M. Läuchli, Effect of Rare Fluctuations on the Thermalization of Isolated Quantum Systems, Phys. Rev. Lett. **105**, 250401 (2010).

[170] L.F. Santos and M. Rigol, Localization and the effects of symmetries in the thermalization properties of one-dimensional quantum systems, Phys. Rev. E **82**, 031130 (2010).

[171] M. Rigol and L.F. Santos, Quantum chaos and thermalization in gapped systems, Phys. Rev. A **82**, 011604(R) (2010).

[172] C. Neuenhahn and F. Marquardt, Thermalization of interacting fermions and delocalization in Fock space, Phys. Rev. E **85** 060101 (2012).

[173] R. Steinigeweg, J. Herbrych, and P. Prelovsek, Eigenstate thermalization within isolated spin-chain systems, Phys. Rev. E **87**, 012118 (2013).

[174] W. Beugeling, R. Moessner, and M. Haque, Finite-size scaling of eigenstate thermalization, Phys. Rev. E **89** 042112 (2014).

[175] H. Kim, T.N. Ikeda, and D.A. Huse, Testing whether all eigenstates obey the Eigenstate Thermalization Hypothesis, Phys. Rev. E **90**, 052105 (2014).

[176] W. Beugeling, R. Moessner, and M. Haque, Off-diagonal matrix elements of local operators in many-body quantum systems, Phys. Rev. E **91**, 012144 (2015).

[177] J.-S. Caux and F.H.L. Essler, Time Evolution of Local Observables After Quenching to an Integrable Model, Phys. Rev. Lett. **110**, 257203 (2013).

[178] E. Lieb, T. Schultz, D. Mattis, Two soluble models of an antiferromagnetic chain, Ann. Phys. **16**, 407 (1961).

[179] V. Alba, Simulating the Generalized Gibbs Ensemble (GGE): a Hilbert space Monte Carlo approach, arXiv:1507.06994 (2015).

[180] B. Fröhlich, M. Feld, E. Vogt, M. Koschorreck, W. Zwerger, and M. Köhl Radio-Frequency Spectroscopy of a Strongly Interacting Two-Dimensional Fermi Gas, Phys. Rev. Lett. **106**, 105301 (2011).

[181] S. Bravyi, M. B. Hastings, and F. Verstraete, Lieb-Robinson Bounds and the Generation of Correlations and Topological Quantum Order, Phys. Rev. Lett. **97**, 050401 (2006).

[182] E. Khatami, G. Pupillo, M. Srednicki, and M. Rigol, Fluctuation-Dissipation Theorem in an Isolated System of Quantum Dipolar Bosons after a Quench, Phys. Rev. Lett. **111**, 050403 (2013).

[183] G. De Chiara, S. Montangero, P. Calabrese, and R. Fazio, Entanglement entropy dynamics of Heisenberg chains, J. Stat. Mech. (2006) P03001.

[184] A. Läuchli and C. Kollath, Spreading of correlations and entanglement after a quench in the one-dimensional Bose-Hubbard model, J. Stat. Mech. (2008) P05018.

[185] S. R. Manmana, S. Wessel, R. M. Noack, and A. Muramatsu, Time evolution of correlations in strongly interacting fermions after a quantum quench, Phys. Rev. B **79**, 155104 (2009).

[186] G. Carleo, F. Becca, L. Sanchez-Palencia, S. Sorella, and M. Fabrizio, Light-cone effect and supersonic correlations in one- and two-dimensional bosonic superfluids. Phys. Rev. A **89**, 031602 (2014).

[187] P. Hauke and L. Tagliacozzo, Spread of Correlations in Long-Range Interacting Quantum Systems, Phys. Rev. Lett. **111**, 207202 (2013).

[188] J. Schachenmayer, B. P. Lanyon, C. F. Roos, and A. J. Daley, Entanglement Growth in Quench Dynamics with Variable Range Interactions, Phys. Rev. X **3**, 031015 (2013).

[189] J. Eisert, M. van den Worm, S. R. Manmana, and M. Kastner, Breakdown of Quasilocality in Long-Range Quantum Lattice Models, Phys. Rev. Lett. **111**, 260401 (2013).

[190] D. Vodola, L. Lepori, E. Ercolessi, and G. Pupillo, Long-range Ising and Kitaev models: phases, correlations and edge modes, 2016 New J. Phys. **18** 015001.

[191] M. V. Regemortel, D. Sels, and M. Wouters, Information propagation and equilibration in long-range Kitaev chains, arXiv:1511.05459 (2015).

[192] A.S. Buyskikh, M. Fagotti, J. Schachenmayer, F.H.L. Essler, A. J. Daley, Entanglement growth and correlation spreading with variable-range interactions in spin and fermionic tunnelling models, Phys. Rev. A 93, 053620 (2016) [http://dx.doi.org/10.1103/PhysRevA.93.053620].

[193] D.B. Abraham, E. Barouch, G. Gallavotti and A. Martin-Löf, Thermalization of a Magnetic Impurity in the Isotropic XY Model, Phys. Rev. Lett. **25**, 1449 (1970); D.B. Abraham, E. Barouch, G. Gallavotti and A. Martin-Löf, Dynamics of a Local Perturbation in the XY Model. I-Approach to Equilibrium, Stud. Appl. Math. **50**, 121 (1971); C. Kollath, U. Schollwöck and W. Zwerger, Spin-charge separation in cold Fermi-gases: a real time analysis Phys. Rev. Lett. **95**, 176401 (2005); P. Calabrese and J. Cardy, Entanglement and correlation functions following a local quench: a conformal field theory approach, J. Stat. Mech. (2007) P10004; J.-M. Stéphan and Jérôme Dubail, Local quantum quenches in critical one-dimensional systems: entanglement, the

Loschmidt echo, and light-cone effects, J. Stat. Mech. (2011) P08019; M. Ganahl, E. Rabel, F.H.L. Essler and H.-G. Evertz, Observation of Complex Bound States in the Spin-1/2 Heisenberg XXZ Chain Using Local Quantum Quenches, Phys. Rev. Lett. **108**, 077206 (2012).

[194] E. H. Lieb and D. W. Robinson, The finite group velocity of quantum spin systems, Commun. Math. Phys. **28**, 251 (1972).

[195] R. Sims and B. Nachtergaele, Lieb-Robinson bounds in quantum many-body physics, edited by R. Sims and D. Ueltschi, Entropy and the Quantum, Vol. 529 (American Mathematical Society, 2010).

[196] J. Jünemann, A. Cadarso, D. Perez-Garcia, A. Bermudez, and J. J. García-Ripoll, Lieb-Robinson Bounds for Spin-Boson Lattice Models and Trapped Ions, Phys. Rev. Lett. **111**, 230404 (2013).

[197] M. Kliesch, C. Gogolin, and J. Eisert, Lieb-Robinson bounds and the simulation of time evolution of local observables in lattice systems, edited by L. D. Site and Bach, Many-Electron Approaches in Physics, Chemistry and Mathematics: A Multidisciplinary View (Springer, 2013).

[198] D. Poulin, Lieb-Robinson Bound and Locality for General Markovian Quantum Dynamics, Phys. Rev. Lett. **104**, 190401 (2010).

[199] P. Bocchieri and A. Loinger, Quantum Recurrence Theorem, Phys. Rev. **107**, 337 (1957).

[200] S. Sachdev, Quantum Phase Transitions, Cambridge University Press, 2001.

[201] O. Viehmann, J. von Delft, and F. Marquardt, Observing the Nonequilibrium Dynamics of the Quantum Transverse-Field Ising Chain in Circuit QED, Phys. Rev. Lett. **110**, 030601 (2013); O. Viehmann, J. von Delft, and F. Marquardt, The quantum transverse-field Ising chain in circuit quantum electrodynamics: effects of disorder on the nonequilibrium dynamics, New J. Phys. **15** 035013 (2013).

[202] E. Lieb, T. Schultz and D. Mattis, Two soluble models of an antiferromagnetic chain, **16**, 407 (1961).

[203] B.M. McCoy, E. Barouch and D.B. Abraham, Statistical Mechanics of the XY Model. IV. Time-Dependent Spin-Correlation Functions, **4**, 2331 (1971); O. Derzhko and T. Krokhmalskii, Dynamic structure factor of the spin-1/2 transverse Ising chain, **56**, 11659 (1997); O. Derzhko and T. Krokhmalskii, Numerical approach for the study of the spin-1/2 xy chains dynamic properties, Physica **B 208**, 221 (1999).

[204] A. Bugrij, Correlation function of the two-dimensional Ising model on the finite lattice. I, Theor. Math. Phys. **127**, 528 (2001); A. Bugrij and O. Lisovyy, Spin matrix elements in 2D Ising model on the finite lattice, Phys. Lett. **A 319**, 390 (2003); G. von Gehlen, N. Iorgov, S. Pakuliak, V. Shadura and Y. Tykhyy, Form-factors in the Baxter-Bazhanov-Stroganov model II: Ising model on the finite lattice, J. Phys. **A 41**, 095003 (2008); N. Iorgov, V. Shadura and Yu. Tykhyy, Spin operator matrix elements in the quantum Ising chain: fermion approach, J. Stat. Mech. (2011) P02028.

[205] I. Peschel, Calculation of reduced density matrices from correlation functions, J. Phys. A **36**, L205 (2003).

[206] M. C. Bañuls, J. I. Cirac, and M. B. Hastings, Strong and Weak Thermalization of Infinite Nonintegrable Quantum Systems, Phys. Rev. Lett. **106**, 050405 (2011).

[207] F. Iglói, Z. Szatmári, and Y.-C. Lin, Entanglement entropy dynamics of disordered quantum spin chains, Phys. Rev. B **85**, 094417 (2012).

[208] G. Torlai, L. Tagliacozzo, and G. De Chiara, Dynamics of the entanglement spectrum in spin chains, J. Stat. Mech. (2014) P06001.

[209] A. Coser, E. Tonni and P. Calabrese, Entanglement negativity after a global quantum quench, J. Stat. Mech. (2014) P12017.

[210] M.G. Nezhadhaghighi and M.A. Rajabpour, Entanglement dynamics in short- and long-range harmonic oscillators, Phys. Rev. B **90**, 205438 (2014).

[211] S. R. White and A. E. Feiguin, Real-Time Evolution Using the Density Matrix Renormalization Group, Phys. Rev. Lett. **93**, 076401 (2004); A. J. Daley, C. Kollath, U. Schollwöck, and G. Vidal, Time-dependent density-matrix renormalization-group using adaptive effective Hilbert spaces, J. Stat. Mech. (2004) P04005.

[212] G. Vidal, Classical Simulation of Infinite-Size Quantum Lattice Systems in One Spatial Dimension, Phys. Rev. Lett. **98**, 070201 (2007).

[213] V. Gurarie, Global large time dynamics and the generalized Gibbs ensemble, J. Stat. Mech. (2013) P02014.

[214] F. H. L. Essler, H. Frahm, F. Göhmann, A. Klümper, and V. E. Korepin, *The One-Dimensional Hubbard Model*, Cambridge University Press, Cambridge (2005).

[215] M. Gaudin, La fonction d'onde de Bethe, Masson, Paris 1983, English translation by J.-S. Caux, Cambridge University Press, Cambridge 2014.

[216] S. Sotiriadis, D. Fioretto, and G. Mussardo, Zamolodchikov-Faddeev algebra and quantum quenches in integrable field theories, J. Stat. Mech. (2012) P02017.

[217] D.X. Horváth, b, , S. Sotiriadis, and G. Takács, Initial states in integrable quantum field theory quenches from an integral equation hierarchy, Nucl. Phys. B **902**, 508 (2016).

[218] J.-S. Caux, The Quench Action, arXiv:1603.04689 (2016).

[219] B. Pozsgay, Quantum quenches and generalized Gibbs ensemble in a Bethe Ansatz solvable lattice model of interacting bosons, J. Stat. Mech. (2014) P10045.

[220] G. Goldstein and N. Andrei, Failure of the GGE hypothesis for integrable models with bound states, arXiv:1405.4224 (2014).

[221] A.B. Zamolodchikov and Al.B. Zamolodchikov, Factorized S-matrices in Two Dimensions as the Exact Solutions of Certain Relativistic Quantum Field Theory Models, Ann. Phys. **120**, 253 (1979).

[222] L. D. Faddeev, Quantum completely integral models of field theory, Sov. Sci. Rev. Math. Phys. C **1**, 107 (1980).

[223] F.H.L. Essler and R.M. Konik, Finite Temperature Dynamical Correlations in Massive Integrable Quantum Field Theories, J. Stat. Mech. (2009) P09018.

[224] E.H. Lieb, Exact Solution of the Problem of the Entropy of Two-Dimensional Ice, Exact Solution of the Problem of the Entropy of Two-Dimensional Ice, Phys. Rev. Lett. **18**, 692 (1967); E.H. Lieb, Exact Solution of the Two-Dimensional Slater KDP Model of a Ferroelectric, Phys. Rev. Lett. 19, **108** (1967); B. Sutherland, Exact Solution of a Two-Dimensional Model for Hydrogen-Bonded Crystals, Phys. Rev. Lett. **19**, 103 (1967).

[225] L.D. Faddeev and L. Takhtadzhyan, Spectrum and scattering of excitations in the one-dimensional isotropic Heisenberg model, J. Sov. Math. **24**, 241 (1984).

[226] M. Takahashi and M. Suzuki, One-Dimensional Anisotropic Heisenberg Model at Finite Temperatures, Prog. Theor. Phys. **48**, 2187 (1972); M. Takahashi, Thermodynamics of one dimensional solvable models, Cambridge University Press, Cambridge 1999.

[227] A.M. Tsvelik, Incommensurate phases of quantum one-dimensional magnetics, Phys. Rev. B **42**, 779 (1990); H. Frahm, Integrable spin-1/2 XXZ Heisenberg chain with competing interactions, J. Phys. A: Math. Gen. **25**, 1417 (1992); A.A. Zvyagin and A. Klümper, Quantum phase transitions and thermodynamics of quantum antiferromagnets with next-nearest-neighbor couplings, Phys. Rev. B **68**, 144426 (2003).

[228] N. Muramoto and M. Takahashi, Integrable Magnetic Model of Two Chains Coupled by Four-Body Interactions, J. Phys. Soc. Jpn **68**, 2098 (1999).

[229] M.P. Grabowski, P. Mathieu, Structure of the Conservation Laws in Quantum Integrable Spin Chains with Short Range Interactions, Ann. Phys. **243**, 299 (1995).

[230] A. Klümper and K. Sakai, The thermal conductivity of the spin-1/2 XXZ chain at arbitrary temperature, J. Phys. A **35**, 2173 (2002); K. Sakai and A. Klümper, Non-dissipative thermal transport in the massive regimes of the XXZ chain, J. Phys. A: Math. Gen. **36** 11617 (2003).

[231] A. Klümper, Thermodynamics of the anisotropic spin-1/2 Heisenberg chain and related quantum chains, Z. Phys. B **91**, 507 (1993); C. Destri and H.J. de Vega, Unified approach to Thermodynamic Bethe Ansatz and finite size corrections for lattice models and field theories, Nucl. Phys. B **438**, 314 (1995).

[232] M. Bortz and F. Göhmann, Exact thermodynamic limit of short-range correlation functions of the antiferromagnetic XXZ-chain at finite temperatures, Eur. Phys. J. B **46**, 399 (2005); H. E. Boos, F. Göhmann, A. Klümper, and J. Suzuki, Factorization of the finite temperature correlation functions of the XXZ chain in a magnetic field, J. Phys. A: Math. Theor. **40**, 10699 (2007); H.E. Boos, J. Damerau, F. Göhmann, A. Klümper, J. Suzuki, and A. Weiße, Short-distance thermal correlations in the XXZ chain, J. Stat. Mech. (2008) P08010; C. Trippe, F. Göhmann, and A. Klümper, Short-distance thermal correlations in the massive XXZ chain, Eur. Phys. J. B **73**, 253 (2010).

[233] F. Göhmann, A. Klümper, and A. Seel, Integral representation of the density matrix of the XXZ chain at finite temperatures, J. Phys. A: Math Gen. **37**, 7625 (2004).

[234] H.E. Boos, M. Jimbo, T. Miwa, F. Smirnov, and Y. Takeyama, Algebraic Representation of Correlation Functions in Integrable Spin Chains, Annales Henri Poincare **7**, 1395 (2006); H.E. Boos, M. Jimbo, T. Miwa, F. Smirnov, and Y. Takeyama, Hidden Grassmann Structure in the XXZ Model, Commun. Math. Phys **272**, 263 (2007); H.E. Boos, M. Jimbo, T. Miwa, F. Smirnov, and Y. Takeyama,Hidden Grassmann Structure in the XXZ Model II: Creation Operators, Commun. Math. Phys **286**, 875 (2009); M. Jimbo, T.

Miwa, and F. Smirnov, Hidden Grassmann structure in the XXZ model III: introducing the Matsubara direction, J. Phys. A: Math. Theor. **42**, 304018.

[235] E. Ilievski, M. Medenjak, and T. Prosen, Quasilocal Conserved Operators in the Isotropic Heisenberg Spin-1/2 Chain, Phys. Rev. Lett. **115**, 120601 (2015).

[236] E. Ilievski, M. Medenjak, T. Prosen, and L. Zadnik, arXiv:1603.00440 (2016).

[237] T. Prosen, Open XXZ Spin Chain: Nonequilibrium Steady State and a Strict Bound on Ballistic Transport, Phys. Rev. Lett. **106**, 217206 (2011); T. Prosen and E. Ilievski, Families of Quasilocal Conservation Laws and Quantum Spin Transport, Phys. Rev. Lett. **111**, 057203 (2013); T. Prosen, Quasilocal conservation laws in XXZ spin-1/2 chains: Open, periodic and twisted boundary conditions, Nucl. Phys. B **886**, 1177 (2014); R.G. Pereira, V. Pasquier, J. Sirker, and I. Affleck, Exactly conserved quasilocal operators for the XXZ spin chain, J. Stat. Mech. (2014); P09037; L. Piroli and E. Vernier, Quasi-local conserved charges and spin transport in spin-1 integrable chains, arXiv:1601.07289 (2016).

[238] J. Sirker, R.G. Pereira, I. Affleck Conservation laws, integrability and transport in one-dimensional quantum systems Phys. Rev. B **83**, 035115 (2011).

[239] L.A. Takhtajan, The picture of low-lying excitations in the isotropic Heisenberg chain of arbitrary spins, Phys. Lett. A **87**, 479 (1982); H.M. Babujian, Exact solution of the isotropic Heisenberg chain with arbitrary spins: Thermodynamics of the model, Nucl. Phys. **B215**, 317 (1983); A.N. Kirillov and N.Yu. Reshetikhin, Exact solution of the integrable XXZ Heisenberg models with arbitrary spin. I. The ground state and the excitation spectrum J. Phys. **A20**, 1565 (1987); A.N Kirillov and N.Yu. Reshetikhin Exact solution of the integrable XXZ Heisenberg model with arbitrary spin. II. Thermodynamics of the system J. Phys. **A20**, 1587 (1987).

[240] E. Ilievski, E. Quinn, J. De Nardis and M. Brockmann, String-charge duality in integrable lattice models, arXiv:1512.04454 (2015).

[241] B. Sutherland, Model for a multicomponent quantum system, Phys. Rev. B **12**, 3795 (1975); P.P. Kulish, E.K. Sklyanin, Solutions of the Yang-Baxter equation, J. Sov. Math. **19**, 1596 (1982); N. Andrei and H. Johannesson, Higher dimensional representations of the SU(N) Heisenberg model, Phys. Lett. A**104**, 370 (1984); P.P.Kulish, Integrable graded magnets, J. Soviet Math. **35**, 2648 (1985); F.H.L. Essler and V.E. Korepin, Algebraic Bethe Ansatz and Higher Conservation Laws for the Supersymmetric t-J Model, Phys. Rev. B **46**, 9147 (1992); A. Foerster and M. Karowski, Algebraic properties of the Bethe ansatz for an $spl(2,1)$ supersymmetric t-J model, Nucl.Phys. B **396**, 611 (1993); F.H.L. Essler, V.E. Korepin and K. Schoutens, Exact Solution of an Electronic Model of Superconductivity I, Int. J. Mod. Phys. B **8**, 3205 (1994); F. Göhmann, Algebraic Bethe ansatz for the gl(1|2) generalized model and Lieb-Wu equations, Nucl. Phys. B **620**, 5-1, (2002). S. Belliard and E. Ragoucy, Nested Bethe ansatz for 'all' closed spin chains, J. Phys. **A41**, 295202 (2008).

[242] B. Pozsgay and V. Eisler, Real-time dynamics in a strongly interacting bosonic hopping model: Global quenches and mapping to the XX chain, arXiv:1602.03065 (2016).

[243] P.P. Mazza, J.-M. Stéphan, E. Canovi, V. Alba, M. Brockmann, and M. Haque, Overlap distributions for quantum quenches in the anisotropic Heisenberg chain, J. Stat. Mech. (2016) 013104.

[244] C. Kollath, A. M. Läuchli, and E. Altman, Quench Dynamics and Nonequilibrium Phase Diagram of the Bose-Hubbard Model, Phys. Rev. Lett. **98**, 180601 (2007).

[245] M. Moeckel and S. Kehrein, Interaction Quench in the Hubbard Model, Phys. Rev. Lett. **100**, 175702 (2008).

[246] M. Moeckel and S. Kehrein, Real-time evolution for weak interaction quenches in quantum systems, Ann. of Phys. **324**, 2146 (2009).

[247] S. Sotiriadis and J. Cardy, Quantum quench in interacting field theory: A self-consistent approximation, Phys. Rev. B **81**, 134305 (2010).

[248] M. Kollar, F.A. Wolf, and M. Eckstein, Generalized Gibbs ensemble prediction of prethermalization plateaus and their relation to nonthermal steady states in integrable systems, Phys. Rev. B **84**, 054304 (2011).

[249] A. Mitra and T. Giamarchi, Mode-Coupling-Induced Dissipative and Thermal Effects at Long Times after a Quantum Quench, Phys. Rev. Lett. **107**, 150602 (2011).

[250] G. Carleo, F. Becca, M. Schiró, and M. Fabrizio, Localization and Glassy Dynamics Of Many-Body Quantum Systems, Scientific Reports **2** (2012).

[251] J. Marino and A. Silva, Relaxation, prethermalization, and diffusion in a noisy quantum Ising chain, Phys. Rev. B **86**, 060408(R) (2012).

[252] M. Stark and M. Kollar, Kinetic description of thermalization dynamics in weakly interacting quantum systems, arXiv:1308.1610 (2013).

[253] M. Marcuzzi, J. Marino, A. Gambassi, and A. Silva, Prethermalization in a Nonintegrable Quantum Spin Chain after a Quench, Phys. Rev. Lett. **111**, 197203 (2013).

[254] A. Mitra, Correlation functions in the prethermalized regime after a quantum quench of a spin-chain, Phys. Rev. B **87**, 205109 (2013)

[255] F.H.L. Essler, S. Kehrein, S.R. Manmana, and N.J. Robinson, Quench Dynamics in a Model with Tuneable Integrability Breaking, Phys. Rev. B **89**, 165104 (2014).

[256] B. Nowak, J. Schole, T. Gasenzer, Universal dynamics on the way to thermalisation, New J. Phys. **16**, 093052 (2014).

[257] G. Delfino, Quantum quenches with integrable pre-quench dynamics, J. Phys. A: Math. Theor. **47** 402001 (2014).

[258] B. Bertini and M. Fagotti, Pre-relaxation in weakly interacting models, J. Stat. Mech. (2015) P07012.

[259] B. Bertini, F.H.L. Essler, S. Groha, N.J. Robinson, Prethermalization and thermalization in models with weak integrability breaking, Phys. Rev. Lett. **115**, 180601 (2015).

[260] G.P. Brandino, J.-S. Caux, and R.M. Konik, Glimmers of a Quantum KAM Theorem: Insights from Quantum Quenches in One-Dimensional Bose Gases, Phys. Rev. X **5**, 041043 (2015).

[261] M. Babadi, E. Demler, and M. Knap, Far-from-Equilibrium Field Theory of Many-Body Quantum Spin Systems: Prethermalization and Relaxation of Spin Spiral States in Three Dimensions, Phys. Rev. X **5**, 041005 (2015).

[262] M. Olshanii, Geometry of Quantum Observables and Thermodynamics of Small Systems, Phys. Rev. Lett. **114**, 060401 (2015).

[263] M. Fagotti, Control of global properties in a closed many-body quantum system by means of a local switch, arXiv:1508.04401 (2015).

[264] N. Nessi and A. Iucci, Glass-like Behavior in a System of One Dimensional Fermions after a Quantum Quench, arXiv:1503.02507 (2015).

[265] T. Kitagawa, A. Imambekov, J. Schmiedmayer and E. Demler, The dynamics and prethermalization of one-dimensional quantum systems probed through the full distributions of quantum noise, New J. Phys. **13** 073018 (2011).

[266] T. Langen, S. Erne, R. Geiger, B. Rauer, T. Schweigler, M. Kuhnert, W. Rohringer, I.E. Mazets, T. Gasenzer and J. Schmiedmayer, Experimental Observation of a Generalized Gibbs Ensemble, Science **348**, 207 (2015).

[267] G. Goldstein and N. Andrei, Equilibration and Generalized GGE in the Lieb Liniger gas, arXiv:1309.3471 (2013).

[268] M. Kliesch, C. Gogolin, M.J. Kastoryano, A. Riera, and J. Eisert, Locality of Temperature, Phys. Rev. X **4**, 031019 (2014).

[269] A.M. Tsvelick and P.B. Wiegmann, Exact results in the theory of magnetic alloys, Adv. Phys. **32**, 453 (1983).

.3 Bibliography from Old, Fundamental Articles

From Time-dependent generalized Gibbs ensembles in open quantum systems by Lange, Lenarčič, Rosch

References

[7] A. Polkovnikov, K. Sengupta, A. Silva, and M. Vengalattore, Rev. Mod. Phys. **83**, 863 (2011).

[2] C. Gogolin and J. Eisert, Reports on Progress in Physics **79**, 056001 (2016).

[19] L. D'Alessio, Y. Kafri, A. Polkovnikov, and M. Rigol, Advances in Physics **65**, 239 (2016).

[6] M. Rigol, V. Dunjko, and M. Olshanii, Nature **452**, 854 (2008).

[110] J. Lux, J. Müller, A. Mitra, and A. Rosch, Phys. Rev. A **89**, 053608 (2014).

[111] A. Bohrdt, C. Mendl, M. Endres, and M. Knap, New Journal of Physics (2017).

[112] E. Leviatan, F. Pollmann, J. H. Bardarson, and E. Altman, arXiv:1702.08894 (2017).

[4] F. H. L. Essler and M. Fagotti, Journal of Statistical Mechanics: Theory and Experiment P064002 (2016).

[3] L. Vidmar and M. Rigol, Journal of Statistical Mechanics: Theory and Experiment P064007 (2016).

[10] P. Calabrese and J. Cardy, Journal of Statistical Mechanics: Theory and Experiment **2016**, 064003 (2016).

[11] M. A. Cazalilla and M.-C. Chung, Journal of Statistical Mechanics: Theory and Experiment **2016**, 064004 (2016).

[1] M. Rigol, V. Dunjko, V. Yurovsky, and M. Olshanii, Phys. Rev. Lett. **98**, 050405 (2007).

[37] M. Fagotti and F. H. L. Essler, Phys. Rev. B **87**, 245107 (2013).

[36] B. Pozsgay, Journal of Statistical Mechanics: Theory and Experiment P07003 (2013).

[25] M. Fagotti and F. H. Essler, Journal of Statistical Mechanics: Theory and Experiment P07012 (2013).

[2] E. Ilievski, J. De Nardis, B. Wouters, J.-S. Caux, F. H. L. Essler, and T. Prosen, Phys. Rev. Lett. **115**, 157201 (2015).

[47] E. Ilievski, M. Medenjak, and T. Prosen, Phys. Rev. Lett. **115**, 120601 (2015).

[22] M. Mierzejewski, P. Prelovšek, and T. Prosen, Phys. Rev. Lett. **114**, 140601 (2015).

[48] E. Ilievski, M. Medenjak, T. Prosen, and L. Zadnik, Journal of Statistical Mechanics: Theory and Experiment P064008 (2016).

[5] J.-S. Caux, Journal of Statistical Mechanics: Theory and Experiment P064006 (2016).

[54] J.-S. Caux and F. H. L. Essler, Phys. Rev. Lett. **110**, 257203 (2013).

[60] M. Brockmann, B. Wouters, D. Fioretto, J. De Nardis, R. Vlijm, and J.-S. Caux, Journal of Statistical Mechanics: Theory and Experiment **2014**, P12009 (2014).

[15] B. Wouters, J. De Nardis, M. Brockmann, D. Fioretto, M. Rigol, and J.-S. Caux, Phys. Rev. Lett. **113**, 117202 (2014).

[16] B. Pozsgay, M. Mestyán, M. A. Werner, M. Kormos, G. Zaránd, and G. Takács, Phys. Rev. Lett. **113**, 117203 (2014).

[63] M. Mestyán, B. Pozsgay, G. Takács, and M. A. Werner, Journal of Statistical Mechanics: Theory and Experiment **2015**, P04001 (2015).

[66] L. Piroli, E. Vernier, and P. Calabrese, Phys. Rev. B **94**, 054313 (2016).

[38] B. Pozsgay, E. Vernier, and M. Werner, arXiv preprint arXiv:1703.09516 (2017).

[17] T. Kinoshita, T. Wenger, and D. S. Weiss, Nature **440**, 900 (2006).

[29] M. Gring, M. Kuhnert, T. Langen, T. Kitagawa, B. Rauer, M. Schreitl, I. Mazets, D. A. Smith, E. Demler, and J. Schmiedmayer, Science **337**, 1318 (2012).

[30] D. A. Smith, M. Gring, T. Langen, M. Kuhnert, B. Rauer, R. Geiger, T. Kitagawa, I. Mazets, E. Demler, and J. Schmiedmayer, New Journal of Physics **15**, 075011 (2013).

[92] T. Langen, T. Gasenzer, and J. Schmiedmayer, J. Stat. Mech. **2016**, 064009 (2016).

[19] T. Langen, S. Erne, R. Geiger, B. Rauer, T. Schweigler, M. Kuhnert, W. Rohringer, I. E. Mazets, T. Gasenzer, and J. Schmiedmayer, Science **348**, 207 (2015).

[23] Y. Tang, W. Kao, K.-Y. Li, S. Seo, K. Mallayya, M. Rigol, S. Gopalakrishnan, and B. L. Lev, arXiv preprint arXiv:1707.07031 (2017).

[19] P. Jung, R. W. Helmes, and A. Rosch, Phys. Rev. Lett. **96**, 067202 (2006).

[20] P. Jung and A. Rosch, Phys. Rev. B **76**, 245108 (2007).

[41] B. Bertini, F. H. L. Essler, S. Groha, and N. J. Robinson, Phys. Rev. Lett. **115**, 180601 (2015).

[37] M. Eckstein, M. Kollar, and P. Werner, Phys. Rev. Lett. **103**, 056403 (2009).

[38] M. Stark and M. Kollar, arXiv:1308.1610 (2013).

[96] J. Marino and A. Silva, Phys. Rev. B **86**, 060408 (2012).

[98] M. Marcuzzi, J. Marino, A. Gambassi, and A. Silva, Phys. Rev. Lett. **111**, 197203 (2013).

[11] B. Bertini, F. H. L. Essler, S. Groha, and N. J. Robinson, Phys. Rev. B **94**, 245117 (2016).

[42] M. Buchhold, M. Heyl, and S. Diehl, Phys. Rev. A **94**, 013601 (2016).

[43] F. R. A. Biebl and S. Kehrein, Phys. Rev. B **95**, 104304 (2017).

[40] M. Moeckel and S. Kehrein, Phys. Rev. Lett. **100**, 175702 (2008).

[95] M. Kollar, F. A. Wolf, and M. Eckstein, Physical Review B **84**, 054304 (2011).

[52] F. H. L. Essler, S. Kehrein, S. R. Manmana, and N. J. Robinson, Phys. Rev. B **89**, 165104 (2014).

[26] F. Lange, Z. Lenarčič, and A. Rosch, Nature communications **8**, 15767 (2017).

[48] M. Fagotti, Journal of Statistical Mechanics: Theory and Experiment **2014**, P03016 (2014).

[49] B. Bertini and M. Fagotti, Journal of Statistical Mechanics: Theory and Experiment **2015**, P07012 (2015).

[33] M. Genske and A. Rosch, Phys. Rev. A **92**, 062108 (2015).

[18] Z. Lenarčič, F. Lange, and A. Rosch, Phys. Rev. B **97**, 024302 (2018).

[52] M. P. Grabowski and P. Mathieu, Journal of Physics A: Mathematical and General **29**, 7635 (1996).

[36] B. Robertson, Phys. Rev. **144**, 151 (1966).

[37] B. Robertson, Phys. Rev. **160**, 206 (1968).

[38] K. Kawasaki and J. D. Gunton, Phys. Rev. A **8**, 2048 (1973).

[42] T. Koide, Prog. Theor. Phys. **107**, 525 (2002).

[43] H. P. Breuer and F. Petruccione, The theory of open quantum systems (Oxford University Press, New York, 2002).

[44] J. T. Barreiro, M. Müller, P. Schindler, D. Nigg, T. Monz, M. Chwalla, M. Hennrich, C. F. Roos, P. Zoller, and R. Blatt, Nature **470**, 486 (2011).

[8] F. Reiter and A. S. Sørensen, Phys. Rev. A **85**, 032111 (2012).

[60] N. Friis, O. Marty, C. Maier, C. Hempel, P. Jurcevic, M. Plenio, M. Huber, C. Roos, R. Blatt, B. Lanyon, et al., arXiv preprint arXiv:1711.11092 (2017).

[10] B. Bertini, M. Collura, J. De Nardis, and M. Fagotti, Phys. Rev. Lett. **117**, 207201 (2016).

[9] O. A. Castro-Alvaredo, B. Doyon, and T. Yoshimura, Phys. Rev. X **6**, 041065 (2016).

[63] V. B. Bulchandani, R. Vasseur, C. Karrasch, and J. E. Moore, Phys. Rev. Lett. **119**, 220604 (2017).

From Complete Generalized Gibbs Ensemble in an interacting Theory

References

[1] M. Rigol, V. Dunjko, V. Yurovsky, and M. Olshanii, Phys. Rev. Lett. **98**, 050405 (2007).

[2] M. Rigol, A. Muramatsu, and M. Olshanii, Phys. Rev. A **74**, 053616 (2006).

[3] M. A. Cazalilla, Phys. Rev. Lett. **97**, 156403 (2006).

[4] P. Calabrese and J. Cardy, J. Stat. Mech.: Th. Exp. **2007**, P06008 (2007).

[5] M. Cramer, C. M. Dawson, J. Eisert, and T. J. Osborne, Phys. Rev. Lett. **100**, 030602 (2008).

[6] T. Barthel and U. Schollwöck, Phys. Rev. Lett. **100**, 100601 (2008).

[7] D. Fioretto and G. Mussardo, New J. Phys. **12**, 055015 (2010).

[8] P. Calabrese, F. H. L. Essler, and M. Fagotti, Phys. Rev. Lett. **106**, 227203 (2011).

[9] P. Calabrese, F. H. L. Essler, and M. Fagotti, J. Stat. Mech.: Th. Exp. **2012**, P07016 (2012).

[10] M. Fagotti and F. H. L. Essler, Phys. Rev. B **87**, 245107 (2013).

[11] J.-S. Caux and R. M. Konik, Phys. Rev. Lett. **109**, 175301 (2012).

[12] F. H. L. Essler, S. Evangelisti, and M. Fagotti, Phys. Rev. Lett. **109**, 247206 (2012).

[13] A. C. Cassidy, C. W. Clark, and M. Rigol, Phys. Rev. Lett. **106**, 140405 (2011).

[14] J.-S. Caux and F. H. L. Essler, Phys. Rev. Lett. **110**, 257203 (2013).

[15] M. Collura, S. Sotiriadis, and P. Calabrese, Phys. Rev. Lett. **110**, 245301 (2013).

[16] G. Mussardo, Phys. Rev. Lett. **111**, 100401 (2013).

[17] B. Pozsgay, J. Stat. Mech.: Th. Exp. **2013**, P07003 (2013).

[18] M. Fagotti and F. H. L. Essler, J. Stat. Mech.: Th. Exp. **2013**, P07012 (2013).

[19] M. Kormos, A. Shashi, Y.-Z. Chou, J.-S. Caux, and A. Imambekov, Phys. Rev. B **88**, 205131 (2013).

[20] M. Fagotti, M. Collura, F. H. L. Essler, and P. Calabrese, Phys. Rev. B **89**, 125101 (2014).

[21] B. Wouters, J. De Nardis, M. Brockmann, D. Fioretto, M. Rigol, and J.-S. Caux, Phys. Rev. Lett. **113**, 117202 (2014).

[22] B. Pozsgay, M. Mestyán, M. A. Werner, M. Kormos, G. Zaránd, and G. Takács, Phys. Rev. Lett. **113**, 117203 (2014).

[23] M. Kormos, M. Collura, and P. Calabrese, Phys. Rev. A **89**, 013609 (2014).

[24] J. De Nardis, B. Wouters, M. Brockmann, and J.-S. Caux, Phys. Rev. A **89**, 033601 (2014).

[25] S. Sotiriadis and P. Calabrese, J. Stat. Mech.: Th. Exp. **2014**, P07024 (2014).

[26] F. H. L. Essler, G. Mussardo, and M. Panfil, Phys. Rev. A **91**, 051602 (2015).

[27] M. Mestyán, B. Pozsgay, G. Takács, and M. A. Werner, J. Stat. Mech.: Th. Exp. **2015**, P04001 (2015).

[28] V. E. Korepin, N. M. Bogoliubov, and A. G. Izergin, Quantum Inverse Scattering Method and Correlation Functions (Cambridge Univsity Press, Cambridge, 1993).

[29] B. Pozsgay, J. Stat. Mech.: Th. Exp. **2014**, P09026 (2014).

[30] G. Goldstein and N. Andrei, arXiv:1405.4224 .

[31] E. Ilievski, M. Medenjak, and T. Prosen, arXiv:1506.05049 .

[32] M. Brockmann, B. Wouters, D. Fioretto, J. D. Nardis, R. Vlijm, and J.-S. Caux, J. Stat. Mech.: Th. Exp. **2014**, P12009 (2014).

[33] H. Bethe, Zeit. für Physik **71**, 205 (1931).

[34] R. Orbach, Phys. Rev. **112**, 309 (1958).

[35] M. Gaudin, La fonction d'onde de Bethe (Masson, Paris, 1983) (English translation by J-S Caux, Cambridge University Press 2014).

[36] M. Takahashi, Thermodynamics of one-dimensional solvable models (Cambridge University Press, Cambridge, 1999).

[37] J. Mossel and J.-S. Caux, J. Phys. A: Math. Theor. **45**, 255001 (2012).

[38] M. Brockmann, J. D. Nardis, B. Wouters, and J.-S. Caux, J. Phys. A: Math. Theor. **47**, 145003 (2014).

[39] T. Prosen, Phys. Rev. Lett. **106**, 217206 (2011).

[40] T. Prosen and E. Ilievski, Phys. Rev. Lett. **111**, 057203 (2013).

[41] E. Ilievski and T. Prosen, Commun. Math. Phys. **318**, 809 (2013).

[42] T. Prosen, Nucl. Phys. B **886**, 1177 (2014).

[43] R. G. Pereira, V. Pasquier, J. Sirker, and I. Affleck, J. Stat. Mech.: Th. Exp. **2014**, P09037 (2014).

[44] M. Mierzejewski, P. Prelovšek, and T. Prosen, Phys. Rev. Lett. **114**, 140601 (2015).

[81] M. Medenjak, E. Ilievski and T. Prosen, to be published.

[46] V. V. Bazhanov, T. Łukowski, C. Meneghelli, and M. Staudacher, J. Stat. Mech.: Th. Exp. **2010**, P11002 (2010).

[47] V. V. Bazhanov and V. V. Mangazeev, Nucl. Phys. B **775**, 225 (2007).

[48] J. Suzuki, J. Phys. A: Math. Gen. **32**, 2341 (1999).

[49] A. Klümper and P. A. Pearce, Physica A **183**, 304 (1992).

[50] M. Mestyán and B. Pozsgay, J. Stat. Mech.: Th. Exp. **2014**, P09020 (2014).

From Pumping approximately integrable systems by Lange, Lenarčič, Rosch

References

[1] Kikkawa, J. M. & Awschalom, D. D. Resonant spin amplification in n-type GaAs. Phys. Rev. Lett. **80**, 4313–4316 (1998).

[2] Klaers, J., Schmitt, J., Vewinger, F. & Weitz, M. Bose-Einstein condensation of photons in an optical microcavity. Nature **468**, 545–548 (2010).

[3] Demokritov, S. et al. Bose–Einstein condensation of quasi-equilibrium magnons at room temperature under pumping. Nature **443**, 430–433 (2006).

[4] Kasprzak, J. et al. Bose–Einstein condensation of exciton polaritons. Nature **443**, 409–414 (2006).

[5] Allen, P. B. Theory of thermal relaxation of electrons in metals. Phys. Rev. Lett. **59**, 1460–1463 (1987).

[6] Faddeev, L. Algebraic aspects of the Bethe ansatz. International Journal of Modern Physics A **10**, 1845–1878 (1995).

[7] Grabowski, M. P. & Mathieu, P. Structure of the conservation laws in integrable spin chains with short range interactions. Ann. Phys. **243**, 299–371 (1995).

[8] Prosen, T. & Ilievski, E. Families of quasilocal conservation laws and quantum spin transport. Phys. Rev. Lett. **111**, 057203 (2013).

[9] Mierzejewski, M., Prelovšek, P. & Prosen, T. Identifying local and quasilocal conserved quantities in integrable systems. Phys. Rev. Lett. **114**, 140601 (2015).

[10] Ilievski, E., Medenjak, M. & Prosen, T. Quasilocal conserved operators in the isotropic Heisenberg spin-1/2 chain. Phys. Rev. Lett. **115**, 120601 (2015).

[11] Ilievski, E., Medenjak, M., Prosen, T. & Zadnik, L. Quasilocal charges in integrable lattice systems. Journal of Statistical Mechanics: Theory and Experiment **2016**, 064008.

[12] Rigol, M., Dunjko, V., Yurovsky, V. & Olshanii, M. Relaxation in a completely integrable many-body quantum system: An *Ab Initio* study of the dynamics of the highly excited states of 1d lattice hard-core bosons. Phys. Rev. Lett. **98**, 050405 (2007).

[13] Pozsgay, B. The generalized Gibbs ensemble for Heisenberg spin chains. Journal of Statistical Mechanics: Theory and Experiment **2013**, P07003.

[14] Fagotti, M. & Essler, F. H. Stationary behaviour of observables after a quantum quench in the spin-1/2 Heisenberg XXZ chain. Journal of Statistical Mechanics: Theory and Experiment **2013**, P07012.

[15] Wouters, B. et al. Quenching the anisotropic Heisenberg chain: Exact solution and generalized Gibbs ensemble predictions. Phys. Rev. Lett. **113**, 117202 (2014).

[16] Pozsgay, B. et al. Correlations after quantum quenches in the XXZ spin chain: Failure of the generalized Gibbs ensemble. Phys. Rev. Lett. **113**, 117203 (2014).

[17] Ilievski, E. et al. Complete generalized Gibbs ensembles in an interacting theory. Phys. Rev. Lett. **115**, 157201 (2015).

[18] Vidmar, L. & Rigol, M. Generalized Gibbs ensemble in integrable lattice models. Journal of Statistical Mechanics: Theory and Experiment **2016**, 064007.

[19] Essler, F. H. L. & Fagotti, M. Quench dynamics and relaxation in isolated integrable quantum spin chains. Journal of Statistical Mechanics: Theory and Experiment **2016**, 064002.

[20] Ilievski, E., Quinn, E. & Caux, J.-S. From interacting particles to equilibrium statistical ensembles. Phys. Rev. B **95**, 115128 (2017).

[21] De Luca, A., Collura, M. & De Nardis, J. Non-equilibrium spin transport in the XXZ chain: steady spin currents and emergence of magnetic domains. https://arxiv.org/abs/1612.07265 (2016).

[22] Langen, T. et al. Experimental observation of a generalized Gibbs ensemble. Science **348**, 207–211 (2015).

[23] Mourigal, M. et al. Fractional spinon excitations in the quantum Heisenberg antiferromagnetic chain. Nature Physics **9**, 435–441 (2013).

[24] Jung, P., Helmes, R. W. & Rosch, A. Transport in almost integrable models: Perturbed Heisenberg chains. Phys. Rev. Lett. **96**, 067202 (2006).

[25] Jung, P. & Rosch, A. Spin conductivity in almost integrable spin chains. Phys. Rev. B **76**, 245108 (2007).

[26] Jung, P. & Rosch, A. Lower bounds for the conductivities of correlated quantum systems. Phys. Rev. B **75**, 245104 (2007).

[27] Bertini, B., Essler, F. H. L., Groha, S. & Robinson, N. J. Prethermalization and thermalization in models with weak integrability breaking. Phys. Rev. Lett. **115**, 180601 (2015).

[28] De Luca, A. & Rosso, A. Dynamic nuclear polarization and the paradox of quantum thermalization. Phys. Rev. Lett. **115**, 080401 (2015).

[29] De Luca, A., Rodríguez-Arias, I., Müller, M. & Rosso, A. Thermalization and many-body localization in systems under dynamic nuclear polarization. Phys. Rev. B **94**, 014203 (2016).

[30] Cirac, J. I., Blatt, R., Zoller, P. & Phillips, W. D. Laser cooling of trapped ions in a standing wave. Phys. Rev. A **46**, 2668–2681 (1992).

[31] Benatti, F., Nagy, A. & Narnhofer, H. Asymptotic entanglement and Lindblad dynamics: a perturbative approach. Journal of Physics A: Mathematical and Theoretical **44**, 155303 (2011).

[32] Li, A. C. Y., Petruccione, F. & Koch, J. Perturbative approach to Markovian open quantum systems. Scientific Reports **4**, 4887 (2014).

[33] Petruccione, F. & Breuer, H.-P. The theory of open quantum systems (Oxford Univ. Press, 2002).

[34] Affleck, I. & Oshikawa, M. Field-induced gap in Cu benzoate and other $s = \frac{1}{2}$ antiferromagnetic chains. Phys. Rev. B **60**, 1038–1056 (1999).

[35] Nojiri, H., Ajiro, Y., Asano, T. & Boucher, J. Magnetic excitation of $s = 1/2$ antiferromagnetic spin chain Cu benzoate in high magnetic fields. New Journal of Physics **8**, 218 (2006).

[36] Kimura, S. et al. Collapse of magnetic order of the quasi one-dimensional ising-like antiferromagnet $BaCo_2V_2O_8$ in transverse fields. Journal of the Physical Society of Japan **82**, 033706 (2013).

[37] Niesen, S. K. et al. Substitution effects on the temperature versus magnetic field phase diagrams of the quasi-one-dimensional effective Ising spin-$\frac{1}{2}$ chain system $baco_2v_2o_8$. Phys. Rev. B **90**, 104419 (2014).

[38] Shindou, R. Quantum spin pump in $s = 1/2$ antiferromagnetic chains–holonomy of phase operators in sine-Gordon theory–. Journal of the Physical Society of Japan **74**, 1214–1223 (2005).

[39] Genske, M. & Rosch, A. Floquet-Boltzmann equation for periodically driven Fermi systems. Phys. Rev. A **92**, 062108 (2015).

[40] D'Alessio, L. & Rigol, M. Long-time behavior of isolated periodically driven interacting lattice systems. Phys. Rev. X **4**, 041048 (2014).

[41] Lazarides, A., Das, A. & Moessner, R. Equilibrium states of generic quantum systems subject to periodic driving. Phys. Rev. E **90**, 012110 (2014).

[42] Ponte, P., Chandran, A., Papić, Z. & Abanin, D. A. Periodically driven ergodic and many-body localized quantum systems. Annals of Physics **353**, 196–204 (2015).

[43] Lazarides, A., Das, A. & Moessner, R. Periodic Thermodynamics of Isolated Quantum Systems. Phys. Rev. Lett. **112**, 150401 (2014).

[44] Canovi, E., Kollar, M. & Eckstein, M. Stroboscopic prethermalization in weakly interacting periodically driven systems. Phys. Rev. E **93**, 012130 (2016).

[45] Zotos, X., Naef, F. & Prelovšek, P. Transport and conservation laws. Phys. Rev. B **55**, 11029–11032 (1997).

[46] Prosen, T. Open XXZ spin chain: Nonequilibrium steady state and a strict bound on ballistic transport. Phys. Rev. Lett. **106**, 217206 (2011).

[47] Mierzejewski, M., Prelovšek, P. & Prosen, T. Breakdown of the generalized Gibbs ensemble for current-generating quenches. Phys. Rev. Lett. **113**, 020602 (2014).

[48] Sinova, J., Valenzuela, S. O., Wunderlich, J., Back, C. H. & Jungwirth, T. Spin hall effects. Rev. Mod. Phys. **87**, 1213–1260 (2015).

[49] Berges, J., Borsányi, S. & Wetterich, C. Prethermalization. Phys. Rev. Lett. **93**, 142002 (2004).

[50] Moeckel, M. & Kehrein, S. Interaction quench in the hubbard model. Phys. Rev. Lett. **100**, 175702 (2008).

[51] Kollar, M., Wolf, F. A. & Eckstein, M. Generalized Gibbs ensemble prediction of prethermalization plateaus and their relation to nonthermal steady states in integrable systems. Physical Review B **84**, 054304 (2011).

[52] Essler, F. H. L., Kehrein, S., Manmana, S. R. & Robinson, N. J. Quench dynamics in a model with tuneable integrability breaking. Phys. Rev. B **89**, 165104 (2014).

[53] Mierzejewski, M., Prosen, T. & Prelovšek, P. Approximate conservation laws in perturbed integrable lattice models. Phys. Rev. B **92**, 195121 (2015).

[54] Caux, J.-S. & Essler, F. H. L. Time evolution of local observables after quenching to an integrable model. Phys. Rev. Lett. **110**, 257203 (2013).

[55] Caux, J.-S. The quench action. Journal of Statistical Mechanics: Theory and Experiment **2016**, 064006.

[56] Zotos, X. Finite temperature Drude weight of the one-dimensional spin- 1/2 Heisenberg model. Phys. Rev. Lett. **82**, 1764–1767 (1999).

[57] Forster, D. Hydrodynamic fluctuations, broken symmetry, and correlation functions, (Benjamin, Massachusetts, 1975).

From Generalized Gibbs ensembles in weakly interacting dissipative systems and digital quantum computers by Ulčakar, Lenarčič

References

[45] X. Mi, A. A. Michailidis, S. Shabani, K. C. Miao, P. V. Klimov, J. Lloyd, E. Rosenberg, R. Acharya, I. Aleiner, T. I. Andersen, et al., Stable quantum-correlated many-body states through engineered dissipation, Science **383**, 1332 (2024).

[44] J. T. Barreiro, M. Müller, P. Schindler, D. Nigg, T. Monz, M. Chwalla, M. Hennrich, C. F. Roos, P. Zoller, and R. Blatt, An open-system quantum simulator with trapped ions, Nature **470**, 486 (2011).

[3] F. Verstraete, M. M. Wolf, and J. Ignacio Cirac, Quantum computation and quantum-state engineering driven by dissipation, Nature physics **5**, 633 (2009).

[4] P. M. Harrington, E. J. Mueller, and K. W. Murch, Engineered dissipation for quantum information science, Nature Reviews Physics **4**, 660 (2022).

[5] B. Kraus, H. P. Büchler, S. Diehl, A. Kantian, A. Micheli, and P. Zoller, Preparation of entangled states by quantum Markov processes, Phys. Rev. A **78**, 042307 (2008).

[6] C.-F. Chen, H.-Y. Huang, J. Preskill, and L. Zhao, Local minima in quantum systems, arXiv:2309.16596 (2023).

[7] F. e. a. Fang, Probing critical phenomena in open quantum systems using atom arrays, arXiv:2402.15376 (2024).

[8] A. Matthies, M. Rudner, A. Rosch, and E. Berg, Programmable adiabatic demagnetization for systems with trivial and topological excitations, arXiv:2210.17256 .

[9] D. B. Kaplan, N. Klco, and A. Roggero, Ground states via spectral combing on a quantum computer, arXiv:1709.08250 (2017).

[10] H. Wang, Quantum algorithm for preparing the ground state of a system via resonance transition, Scientific Reports **7**, 16342 (2017).

[11] J.-J. Feng, B. Wu, F. Wilczek, et al., Quantum computing by coherent cooling, Physical Review A **105**, 052601 (2022).

[12] S. Polla, Y. Herasymenko, and T. E. O'Brien, Quantum digital cooling, Phys. Rev. A **104**, 012414 (2021).

[13] M. P. Zaletel, A. Kaufman, D. M. Stamper-Kurn, and N. Y. Yao, Preparation of low entropy correlated many-body states via conformal cooling quenches, Phys. Rev. Lett. **126**, 103401 (2021).

[14] M. Metcalf, J. E. Moussa, W. A. de Jong, and M. Sarovar, Engineered thermalization and cooling of quantum many-body systems, Phys. Rev. Res. **2**, 023214 (2020).

[15] G. Kishony, M. S. Rudner, A. Rosch, and E. Berg, Gauged cooling of topological excitations and emergent fermions on quantum simulators, arXiv:2310.16082 (2023).

[16] J. Lloyd, A. Michailidis, X. Mi, V. Smelyanskiy, and D. A. Abanin, Quasiparticle cooling algorithms for quantum many-body state preparation, arXiv:2404.12175 (2024).

[4] F. H. L. Essler and M. Fagotti, Quench dynamics and relaxation in isolated integrable quantum spin chains, J. Stat. Mech. Theory Exp. **2016**, 064002 (2016).

[3] L. Vidmar and M. Rigol, Generalized Gibbs ensemble in integrable lattice models, J. Stat. Mech. Theory Exp. **2016**, 064007 (2016).

[19] L. D'Alessio, Y. Kafri, A. Polkovnikov, and M. Rigol, From quantum chaos and eigenstate thermalization to statistical mechanics and thermodynamics, Advances in Physics **65**, 239 (2016).

[1] M. Rigol, V. Dunjko, V. Yurovsky, and M. Olshanii, Relaxation in a Completely Integrable Many-Body Quantum System: An Ab Initio Study of the Dynamics of the Highly Excited States of 1D Lattice Hard-Core Bosons, Phys. Rev. Lett. **98**, 050405 (2007).

[67] P. Calabrese, F. H. L. Essler, and M. Fagotti, Quantum quench in the transverse-field ising chain, Phys. Rev. Lett. **106**, 227203 (2011).

[69] P. Calabrese, F. H. L. Essler, and M. Fagotti, Quantum quenches in the transverse field ising chain: Ii. stationary state properties, Journal of Statistical Mechanics: Theory and Experiment **2012**, P07022 (2012).

[68] P. Calabrese, F. H. L. Essler, and M. Fagotti, Quantum quench in the transverse field ising chain: I. time evolution of order parameter correlators, Journal of Statistical Mechanics: Theory and Experiment **2012**, P07016 (2012).

[24] F. H. L. Essler, S. Evangelisti, and M. Fagotti, Dynamical correlations after a quantum quench, Phys. Rev. Lett. **109**, 247206 (2012).

[25] M. Fagotti, Finite-size corrections versus relaxation after a sudden quench, Phys. Rev. B **87**, 165106 (2013).

[37] M. Fagotti and F. H. L. Essler, Reduced density matrix after a quantum quench, Phys. Rev. B **87**, 245107 (2013).

[27] L. Bucciantini, M. Kormos, and P. Calabrese, Quantum quenches from excited states in the ising chain, Journal of Physics A: Mathematical and Theoretical **47**, 175002 (2014).

[26] F. Lange, Z. Lenarčič, and A. Rosch, Pumping approximately integrable systems, Nat. Commun. **8**, 1 (2017).

[18] Z. Lenarčič, F. Lange, and A. Rosch, Perturbative approach to weakly driven many-particle systems in the presence of approximate conservation laws, Phys. Rev. B **97**, 024302 (2018).

[25] F. Lange, Z. Lenarčič, and A. Rosch, Time-dependent generalized Gibbs ensembles in open quantum systems, Phys. Rev. B **97**, 165138 (2018).

[28] F. Reiter, F. Lange, S. Jain, M. Grau, J. P. Home, and Z. Lenarčič, Engineering generalized Gibbs ensembles with trapped ions, Phys. Rev. Res. **3**, 033142 (2021).

[29] M. Schmitt and Z. Lenarčič, From observations to complexity of quantum states via unsupervised learning, Phys. Rev. B **106**, L041110 (2022).

[33] I. Ulčakar and Z. Lenarčič, Iterative construction of conserved quantities in dissipative nearly integrable systems, Phys. Rev. Lett. **132**, 230402 (2024).

[30] I. Bouchoule, B. Doyon, and J. Dubail, The effect of atom losses on the distribution of rapidities in the one-dimensional Bose gas, SciPost Phys. **9**, 044 (2020).

[32] D. Rossini, A. Ghermaoui, M. B. Aguilera, R. Vatré, R. Bouganne, J. Beugnon, F. Gerbier, and L. Mazza, Strong correlations in lossy one-dimensional quantum gases: From the quantum Zeno effect to the generalized Gibbs ensemble, Phys. Rev. A **103**, L060201 (2021).

[33] F. Gerbino, I. Lesanovsky, and G. Perfetto, Large-scale universality in Quantum Reaction-Diffusion from Keldysh field theory, arXiv:2307.14945 (2023).

[34] G. Perfetto, F. Carollo, J. P. Garrahan, and I. Lesanovsky, Reaction-Limited Quantum Reaction-Diffusion Dynamics, Phys. Rev. Lett. **130**, 210402 (2023).

[35] S. Rowlands, I. Lesanovsky, and G. Perfetto, Quantum reaction-limited reaction–diffusion dynamics of noninteracting bose gases, New Journal of Physics **26**, 043010 (2024).

[39] F. Riggio, L. Rosso, D. Karevski, and J. Dubail, Effects of atom losses on a one-dimensional lattice gas of hard-core bosons, Phys. Rev. A **109**, 023311 (2024).

[40] M. Ringbauer, M. Meth, L. Postler, R. Stricker, R. Blatt, P. Schindler, and T. Monz, A universal qudit quantum processor with trapped ions, Nature Physics **18**, 1053 (2022).

[22] A. Scheie, N. E. Sherman, M. Dupont, S. E. Nagler, M. B. Stone, G. E. Granroth, J. E. Moore, and D. A. Tennant, Detection of Kardar–Parisi–Zhang hydrodynamics in a quantum Heisenberg spin-1/2 chain, Nat. Phys. **17**, 726 (2021).

[42] A. Scheie, P. Laurell, B. Lake, S. E. Nagler, M. B. Stone, J.-S. Caux, and D. A. Tennant, Quantum wake dynamics in Heisenberg antiferromagnetic chains, Nature Communications **13**, 5796 (2022).

[43] K. Kim, S. Korenblit, R. Islam, E. Edwards, M. Chang, C. Noh, H. Carmichael, G. Lin, L. Duan, C. J. Wang, et al., Quantum simulation of the transverse ising model with trapped ions, New J. Phys. **13**, 105003 (2011).

[44] R. Islam, E. Edwards, K. Kim, S. Korenblit, C. Noh, H. Carmichael, G.-D. Lin, L.-M. Duan, C.-C. J. Wang, J. Freericks, et al., Onset of a quantum phase transition with a trapped ion quantum simulator, Nat. Comm. **2**, 1 (2011).

[45] H. Labuhn, D. Barredo, S. Ravets, S. De Léséleuc, T. Macrì, T. Lahaye, and A. Browaeys, Tunable two-dimensional arrays of single rydberg atoms for realizing quantum ising models, Nature **534**, 667 (2016).

[46] J. Zhang, G. Pagano, P. W. Hess, A. Kyprianidis, P. Becker, H. Kaplan, A. V. Gorshkov, Z.-X. Gong, and C. Monroe, Observation of a many-body dynamical phase transition with a 53-qubit quantum simulator, Nature **551**, 601 (2017).

[47] S. Ebadi, T. T. Wang, H. Levine, A. Keesling, G. Semeghini, A. Omran, D. Bluvstein, R. Samajdar, H. Pichler, W. W. Ho, et al., Quantum phases of matter on a 256-atom programmable quantum simulator, Nature **595**, 227 (2021).

[48] P. Scholl, M. Schuler, H. J. Williams, A. A. Eberharter, D. Barredo, K.-N. Schymik, V. Lienhard, L.-P. Henry, T. C. Lang, T. Lahaye, A. M. Läuchli, and A. Browaeys, Programmable quantum simulation of 2D antiferromagnets with hundreds of Rydberg atoms, arXiv:2012.12268 (2020).

[49] K. J. Satzinger et al., Realizing topologically ordered states on a quantum processor, Science **374**, 1237 (2021).

[50] D. A. Lidar, Lecture notes on the theory of open quantum systems, arXiv:1902.00967 (2019).

[43] M. Grady, Infinite set of conserved charges in the ising model, Phys. Rev. D **25**, 1103 (1982).

[55] W. H. Press, Numerical recipes 3rd edition: The art of scientific computing (Cambridge university press, 2007).

[36] B. Pozsgay, The generalized gibbs ensemble for heisenberg spin chains, J. Stat. Mech. Theory Exp. **2013**, P07003 (2013).

[38] B. Pozsgay, E. Vernier, and M. A. Werner, On generalized gibbs ensembles with an infinite set of conserved charges, J. Stat. Mech. Theory Exp. **2017**, 093103 (2017).

From "From Bloch Oscillations to Many Body Localization in Clean Interacting Systems" by van Nieuwenburg, Baum, Refael

References

[1] P. W. Anderson, "Absence of diffusion in certain random lattices," Phys. Rev. **109**, 1492–1505 (1958).

[2] D.M. Basko, I.L. Aleiner, and B.L. Altshuler, "Metal–insulator transition in a weakly interacting many-electron system with localized single-particle states," Annals of Physics **321**, 1126 – 1205 (2006).

[3] I. V. Gornyi, A. D. Mirlin, and D. G. Polyakov, "Interacting electrons in disordered wires: Anderson localization and low-t transport," Phys. Rev. Lett. **95**, 206603 (2005).

[4] Rahul Nandkishore and David A. Huse, "Many-body localization and thermalization in quantum statistical mechanics," Annual Review of Condensed Matter Physics **6**, 15–38 (2015).

[5] Dmitry A. Abanin and Zlatko Papić, "Recent progress in many-body localization," Annalen der Physik **529**, 1700169–n/a (2017), 1700169.

[6] John Z. Imbrie, "Diagonalization and many-body localization for a disordered quantum spin chain," Phys. Rev. Lett. **117**, 027201 (2016).

[7] David A. Huse, Rahul Nandkishore, and Vadim Oganesyan, "Phenomenology of fully many-body-localized systems," Phys. Rev. B **90**, 174202 (2014).

[8] Vadim Oganesyan and David A. Huse, "Localization of interacting fermions at high temperature," Phys. Rev. B **75**, 155111 (2007).

[9] Arijeet Pal and David A. Huse, "Many-body localization phase transition," Phys. Rev. B **82**, 174411 (2010).

[10] Ronen Vosk, David A. Huse, and Ehud Altman, "Theory of the many-body localization transition in one-dimensional systems," Phys. Rev. X **5**, 031032 (2015).

[11] Yevgeny Bar Lev and David R. Reichman, "Dynamics of many-body localization," Phys. Rev. B **89**, 220201 (2014).

[12] Christopher David White, Michael Zaletel, Roger S. K. Mong, and Gil Refael, "Quantum dynamics of thermalizing systems," Phys. Rev. B **97**, 035127 (2018).

[13] E. van Nieuwenburg, E. Bairey, and G. Refael, "Learning phase transitions from dynamics," ArXiv e-prints (2017), arXiv:1712.00450 [cond-mat.dis-nn] .

[14] Bela Bauer and Chetan Nayak, "Area laws in a many-body localized state and its implications for topological order," Journal of Statistical Mechanics: Theory and Experiment **2013**, P09005 (2013).

[15] Marko Žnidarič, Tomaž Prosen, and Peter Prelovšek, "Many-body localization in the heisenberg XXZ magnet in a random field," Phys. Rev. B **77**, 064426 (2008).

[16] Jens H. Bardarson, Frank Pollmann, and Joel E. Moore, "Unbounded growth of entanglement in models of many-body localization," Phys. Rev. Lett. **109**, 017202 (2012).

[17] Vedika Khemani, S. P. Lim, D. N. Sheng, and David A. Huse, "Critical properties of the many-body localization transition," Phys. Rev. X **7**, 021013 (2017).

[18] Sarang Gopalakrishnan, Markus Müller, Vedika Khemani, Michael Knap, Eugene Demler, and David A. Huse, "Low-frequency conductivity in many-body localized systems," Phys. Rev. B **92**, 104202 (2015).

[19] Timothy C. Berkelbach and David R. Reichman, "Conductivity of disordered quantum lattice models at infinite temperature: Many-body localization," Phys. Rev. B **81**, 224429 (2010).

[20] Achilleas Lazarides, Arnab Das, and Roderich Moessner, "Fate of many-body localization under periodic driving," Phys. Rev. Lett. **115**, 030402 (2015).

[21] Luca D'Alessio and Anatoli Polkovnikov, "Many-body energy localization transition in periodically driven systems," Annals of Physics **333**, 19 – 33 (2013).

[22] Vedika Khemani, Achilleas Lazarides, Roderich Moessner, and S. L. Sondhi, "Phase structure of driven quantum systems," Phys. Rev. Lett. **116**, 250401 (2016).

[23] J. Smith, A. Lee, P. Richerme, B. Neyenhuis, P. W. Hess, P. Hauke, M. Heyl, D. A. Huse, and C. Monroe, "Many-body localization in a quantum simulator with programmable random disorder," Nature Phys. **12** (2016), 10.1038/nphys3783.

[24] Jae-yoon Choi, Sebastian Hild, Johannes Zeiher, Peter Schauß, Antonio Rubio-Abadal, Tarik Yefsah, Vedika Khemani, David A. Huse, Immanuel Bloch, and Christian Gross, "Exploring the many-body localization transition in two dimensions," Science **352**, 1547–1552 (2016).

[25] Michael Schreiber, Sean S. Hodgman, Pranjal Bordia, Henrik P. Lüschen, Mark H. Fischer, Ronen Vosk, Ehud Altman, Ulrich Schneider, and Immanuel Bloch, "Observation of many-body localization of interacting fermions in a quasirandom optical lattice," Science **349**, 842–845 (2015).

[26] S. S. Kondov, W. R. McGehee, W. Xu, and B. DeMarco, "Disorder-induced localization in a strongly correlated atomic hubbard gas," Phys. Rev. Lett. **114**, 083002 (2015).

[27] Pranjal Bordia, Henrik Lüschen, Sebastian Scherg, Sarang Gopalakrishnan, Michael Knap, Ulrich Schneider, and Immanuel Bloch, "Probing slow relaxation and many-body localization in two-dimensional quasiperiodic systems," Phys. Rev. X **7**, 041047 (2017).

[28] Wojciech De Roeck, Francois Huveneers, Markus Müller, and Mauro Schiulaz, "Absence of many-body mobility edges," Phys. Rev. B **93**, 014203 (2016).

[29] A. Smith, J. Knolle, D. L. Kovrizhin, and R. Moessner, "Disorder-free localization," Phys. Rev. Lett. **118**, 266601 (2017).

[30] A. Smith, J. Knolle, R. Moessner, and D. L. Kovrizhin, "Absence of ergodicity without quenched disorder: From quantum disentangled liquids to many-body localization," Phys. Rev. Lett. **119**, 176601 (2017).

[31] Adam Smith, Johannes Knolle, Roderich Moessner, and Dmitry L. Kovrizhin, "Dynamical localization in F_2 lattice gauge theories," Phys. Rev. B **97**, 245137 (2018).

[32] Tarun Grover and Matthew P A Fisher, "Quantum disentangled liquids," Journal of Statistical Mechanics: Theory and Experiment **2014**, P10010 (2014).

[33] Yu. Kagan and L.A. Maksimov, "Localization in a system of interacting particles diffusing in a regular crystal," JETP **60**, 201 (1984).

[34] Wojciech De Roeck and Francois Huveneers, "Scenario for delocalization in translation-invariant systems," Phys. Rev. B **90**, 165137 (2014).

[35] Mauro Schiulaz, Alessandro Silva, and Markus Müller, "Dynamics in many-body localized quantum systems without disorder," Phys. Rev. B **91**, 184202 (2015).

[36] N. Y. Yao, C. R. Laumann, J. I. Cirac, M. D. Lukin, and J. E. Moore, "Quasi-many-body localization in translation-invariant systems," Phys. Rev. Lett. **117**, 240601 (2016).

[37] Shankar Iyer, Vadim Oganesyan, Gil Refael, and David A. Huse, "Many-body localization in a quasiperiodic system," Phys. Rev. B **87**, 134202 (2013).

[38] Henrik P. Lüschen, Pranjal Bordia, Sebastian Scherg, Fabien Alet, Ehud Altman, Ulrich Schneider, and Immanuel Bloch, "Observation of slow dynamics near the many-body localization transition in one-dimensional quasiperiodic systems," Phys. Rev. Lett. **119**, 260401 (2017).

[39] Vedika Khemani, D. N. Sheng, and David A. Huse, "Two universality classes for the many-body localization transition," Phys. Rev. Lett. **119**, 075702 (2017).

[40] Isaac H. Kim and Jeongwan Haah, "Localization from superselection rules in translationally invariant systems," Phys. Rev. Lett. **116**, 027202 (2016).

[41] Gregory H. Wannier, "Wave functions and effective hamiltonian for bloch electrons in an electric field," Phys. Rev. **117**, 432–439 (1960).

[42] Casati G., Chirikov B.V., Izraelev, and F.M. Ford J., "Stochastic behavior of a quantum pendulum under a periodic perturbation," Casati G., Ford J. (eds) Stochastic Behavior in Classical and Quantum Hamiltonian Systems. Lecture Notes in Physics, vol 93. Springer, Berlin, Heidelberg **93** (1979).

[43] Yuval Baum, Evert P. L. van Nieuwenburg, and Gil Refael, "From dynamical localization to bunching in interacting floquet systems," SciPost Phys. **5**, 17 (2018).

[44] David J. Luitz, Yevgeny Bar Lev, and Achilleas Lazarides, "Absence of dynamical localization in interacting driven systems," SciPost Phys. **3**, 029 (2017).

[45] Martin Eckstein and Philipp Werner, "Damping of bloch oscillations in the hubbard model," Phys. Rev. Lett. **107**, 186406 (2011).

[46] Dmitry O. Krimer, Ramaz Khomeriki, and Sergej Flach, "Delocalization and spreading in a nonlinear stark ladder," Phys. Rev. E **80**, 036201 (2009).

[47] P. Pieri and G. C. Strinati, "Derivation of the gross-pitaevskii equation for condensed bosons from the bogoliubov–de gennes equations for superfluid fermions," Phys. Rev. Lett. **91**, 030401 (2003).

[48] Jean-Claude Garreau, "Quantum simulation of disordered systems with cold atoms," Comptes Rendus Physique **18**, 31 – 46 (2017), prizes of the French Academy of Sciences 2015 / Prix de l'Académie des sciences 2015.

[49] L. Sanchez-Palencia, D. Clément, P. Lugan, P. Bouyer, G. V. Shlyapnikov, and A. Aspect, "Anderson localization of expanding bose-einstein condensates in random potentials," Phys. Rev. Lett. **98**, 210401 (2007).

[50] Thomas Guhr, Axel Müller–Groeling, and Hans A. Weidenmüller, "Random-matrix theories in quantum physics: common concepts," Physics Reports **299**, 189 – 425 (1998).

[51] Maxim Olshanii, Kurt Jacobs, Marcos Rigol, Vanja Dunjko, Harry Kennard, and Vladimir A. Yurovsky, "An exactly solvable model for the integrability and chaos transition in rough quantum billiards," Nature Communications **3** (2012), 10.1038/ncomms1653.

[52] David J. Luitz, Nicolas Laflorencie, and Fabien Alet, "Many-body localization edge in the random-field heisenberg chain," Phys. Rev. B **91**, 081103 (2015).

[53] Corentin L. Bertrand and Antonio M. García-García, "Anomalous thouless energy and critical statistics on the metallic side of the many-body localization transition," Phys. Rev. B **94**, 144201 (2016).

[54] Kazue Kudo and Tetsuo Deguchi, "Finite-size scaling with respect to interaction and disorder strength at the many-body localization transition," Phys. Rev. B **97**, 220201 (2018).

[55] A. Chandran, A. Pal, C. R. Laumann, and A. Scardicchio, "Many-body localization beyond eigenstates in all dimensions," Phys. Rev. B **94**, 144203 (2016).

[56] Wojciech De Roeck and Francois Huveneers, "Stability and instability towards delocalization in many-body localization systems," Phys. Rev. B **95**, 155129 (2017).

[57] Wojciech De Roeck and John Z. Imbrie, "Many-body localization: stability and instability," Philosophical Transactions of the Royal Society of London A: Mathematical, Physical and Engineering Sciences **375** (2017), 10.1098/rsta.2016.0422.

[58] Shriya Pai, Michael Pretko, and Rahul M. Nandkishore, "Localization in fractonic random circuits," arXiv e-prints , arXiv:1807.09776 (2018), arXiv:1807.09776 [cond-mat.stat-mech] .

[59] M. Schulz, C. A. Hooley, R. Moessner, and F. Pollmann, "Stark many-body localization," ArXiv e-prints (2018), arXiv:1808.01250 [cond-mat.dis-nn] .

[60] D.P. Kingma and J. Ba, "Adam: A Method for Stochastic Optimization," ArXiv e-prints (2014), arXiv:1412.6980 .

[61] C. Moler and C. Van Loan, "Nineteen dubious ways to compute the exponential of a matrix, twenty-five years later," SIAM Review **45**, 3–49 (2003), https://doi.org/10.1137/S00361445024180 .

[62] Luc Giraud, Julien Langou, Miroslav Rozložník, and Jasper van den Eshof, "Rounding error analysis of the classical gram-schmidt orthogonalization process," Numerische Mathematik **101**, 87–100 (2005).

From "A quantum Newton's cradle" by Kinoshita, Wenger, Weiss

1. Coleman, S. Quantum sine-Gordon equation as the massiveThipring model. Phys. Rev. D 11, 2088-2097(1975).
2. Tabor, M. Chaos and Integrability in Nonlinear Dynamics(Wiley, New York, 1989).
3. Bemman, G. P. & Izrailev, F. M. The Fermi-Pastalam problem: fifty years of progress. Chaos 15 , 015104 (2005).
4. Benman, G. P. , Borgonoxi, F. , Izrailev, F. M. & Smenzi, A. Irregular dynamics in a one-dimensional Bose system. Phys. Rev. Lett. 92, 030404 (2004). I
5. Minguzzi, A. & Gangardt, D. M. Exact coherent states of a harmonically confined Tonks-Ginardeau gas. Phys. Rev. Lett. 94, 240404 (2005). I
6. Proukakis, N. P., Schmiedmayer, J. & && Stopf, H. T. C. Quasi-condensate growth on an atom chip. Preprint at http://anxix. org/ cond-mat/0509154 (2005). II 7. Hercmann, F. & Schmalzle, P. Simple explanation of a well-known collision experiment. Am. J. Phys. 49, 761-764(1981).
8. Ginardeau, M. Relationship between systems of impenetrable bosons and fermions in one dimension. J. Math. Phys. 1, 516-523(1960). II
9. Girardeau, M. D. & Wright, E. M. Measurement of one-particle correlations and momentum distributions for trapped 1D gases. Phys. Rev. Lett. 87, 050403 (2001). II
10 ParedesBet alTonksGirardeau gas of ultracold atoms in an optical lattice Nature 4292772812004
11 KinoshitaTWengerT & WeissDSObservation of a onedimensional TonksGirardeau gasScience 305112511282004
12 RigolM & MuramatsuAFermionization in an expanding 1D gas of hardcore bosonsPhysRevLett94 240403 2005
13 PedriPSantosLhbergP & StringariSViolation of selfsimilarity in the expansion of a onedimensional Bose gasPhysRevA 68 043601 2003
14 DunjkoVLorentV & OlshaniiMBosons in cigarshaped trapsThomas Fermi regimeTonksGirardeau regimeand in betweenPhysRevLett86 541354162001
15 KinoshitaTWengerT & WeissDSLocal pair correlations in one dimensional Bose gasesPhysRevLett95 190406 2005
16 GangardtDM & ShlyapnikovGVStability and phase coherence of trapped 1D Bose gasesPhysRevLett90 010401 2003
17 TolraBLet alObservation of reduced threebody recombination in a correlated 1D degenerate Bose gasPhysRevLett92 190401 2004
18 LiebEH & LinigerWExact analysis of an interacting Bose gasThe general solution and the ground statePhysRev130160516161963
19 WuSWangYJDiotQ & PrentissMSplitting matter waves using an optimized standingwave lightpulse sequencePhysRevA 71 043602 2005
20 WangYJet alAtom Michelson interferometer on a chip using a Bose Einstein condensatePhysRevLett94 090405 2005
21 MooreMGBergemanT & OlshaniiMScattering in tight atom waveguidesJPhysIV 11669862004
22 OlshaniiMAtomic scattering in the presence of an external confinement and a gas of impenetrable bosonsPhysRevLett819389411998
23 WuH & FootCJDirect simulation of evaporative coolingJPhysB 29 L321L3281996
24 RamanCet alEvidence for a critical velocity in a BoseEinstein condensed gasPhysRevLett83250225051999
25 CarusottoIet alSensitive measurement of forces at the micron scale using Bloch oscillations of ultracold atomsPhysRevLett95 093202 2005
26 FallaniLet alObservation of dynamical instability for a BoseEinstein condensate in a

moving 1D optical latticePhysRevLett93 140406 2004
27 GustavsonTLLandraginA & KasevichMARotation sensing with a dual atominterferometer Sagnac gyroscopeClassQuantum Grav1723852398 2000
28 OlshaniiM & DunjkoVInterferometry in dense nonlinear media and interactioninduced loss of contrast in microfabricated atom interferometers Preprint at httparxivorgcondmat05053582005
29 MiesnerHJet alBosonic stimulation in the formation of a BoseEinstein condensateScience 279100510071998
30 KinoshitaTWengerT & WeissDSAlloptical BoseEinstein condensation using a compressible crossed dipole trapPhysRevA 7111602R2005

From Chaos and Quantum Thermalization by Srednicki

[1] Ya. G. Sinai, Ups. Mat. Nauk 25, 137 (1970) [Russ. Math. Surv. 25, 137 (1970)].
[2] M. V. Berry, in Topics in Nonlinear Dynamics, S. Jorna, ed. (AIP, New York, 1978).
[3] G. M. Zaslavsky, Chaos in Dynamic Systems (Harwood, Chur, 1985).
[4] M. C. Gutzwiller, Chaos in Classical and Quantum Mechanics (Springer-Verlag, New York, 1990).
[5] L. E. Reichl, A Modern Course in Statistical Physics (Univ. of Texas, Austin, 1980).
[6] A. N. Kolmogorov, Dokl. Acad. Nauk SSSR 98, 527 (1954); V. I. Arnol'd, Usp. Mat. Nauk 18, 13 (1963) [Russ. Math. Surv. 18, 9 (1963)]; J. Moser, Nachr. Akad. Wiss. Göttingen 1 (1962).
[7] N. S. Krylov, Works on the Foundations of Statistical Mechanics (Princeton Univ., Princeton, 1979).
[8] M. V. Berry, J. Phys. A 10, 2083 (1977).
[9] M. V. Berry, in Les Houches XXXVI, Chaotic Behavior of Deterministic Systems, G. Iooss, R. H. G. Helleman, and R. Stora, eds. (North-Holland, Amsterdam, 1983).
[10] M. V. Berry, in Les Houches LII, Chaos and Quantum Physics, M.-J. Giannoni, A. Voros, and J. Zinn-Justin, eds. (North-Holland, Amsterdam, 1991).
[11] A. Voros, Ann. Inst. H. Poincaré A 24, 31 (1976); 26, 343 (1977); in Stochastic Behavior in Classical and Quantum Hamiltonian Systems, G. Casati and J. Ford, eds. (SpringerVerlag, Berlin, 1979).
[12] A. I. Shnirelman, Ups. Mat. Nauk 29, 181 (1974); Y. Colin de Verdière, Comm. Math. Phys. 102, 497 (1985); S. Zelditch, Duke Math J. 55, 919 (1987).
[13] M. V. Berry, Phil. Trans. R. Soc. Lond. A 287, 237 (1977).
[14] S. W. McDonald and A. N. Kaufman, Phys. Rev. Lett. 42, 1189 (1979).
[15] E. J. Heller, Phys. Rev. Lett. 53, 1515 (1984).
[16] S. W. McDonald and A. N. Kaufman, Phys. Rev. A 37, 3067 (1988).
[17] M. Shapiro, J. Ronkin, and P. Brumer, Chem. Phys. Lett. 148, 177 (1988).
[18] E. J. Heller, in Les Houches LII, Chaos and Quantum Physics, M.-J. Giannoni, A. Voros, and J. Zinn-Justin, eds. (North-Holland, Amsterdam, 1991).
[19] R. Aurich and F. Steiner, Physica D 48, 445 (1991).
[20] R. Aurich and F. Steiner, Physica D 64, 185 (1993).
[21] F. Steiner, in Festschrift Universität Hamburg 1994: Schlaglichter der Forschung zum 75. Jahrestag, R. Ansorge, ed. (Dietrich Reimer Verlag, Hamburg, 1994).
[22] L. D. Landau and E. M. Lifshitz, Statistical Physics (Permagon, Oxford, 1980).
[23] R. Jancel, Foundations of Classical and Quantum Statistical Mechanics (Permagon, Oxford, 1969).
[24] E. B. Bogomolny, Physica D 31, 169 (1988).
[25] M. V. Berry, Proc. R. Soc. Lond. A 423, 219 (1989).
[26] P. Gaspard, in Quantum Chaos - Quantum Measurement, P. Cvitanović, I. Percival, and

A. Wirzba, eds. (Kluwer, Dordrecht, 1992).
[27] M. V. Berry and J. P. Keating, Proc. R. Soc. Lond. A 437, 151 (1992); O. Agam and S. Fishman, J. Phys. A 26, 2113 (1993).
[28] S. Tomsovic and E. J. Heller, Phys. Rev. Lett. 67, 664 (1991); Phys. Rev. E 47, 282 (1993); M. A. Sepúlveda, S. Tomsovic and E. J. Heller, Phys. Rev. Lett. 69, 402 (1992).
[29] G. H. Wannier, Statistical Physics (Wiley, New York, 1966).
[30] A. L. Fetter and J. D. Walecka, Quantum Theory of Many-Particle Systems (McGrawHill, San Francisco, 1971).
[31] J. S. Langer, private communication.
[32] N. G. van Kampen, in Chaotic Behavior in Quantum Systems, G. Casati, ed. (Plenum, New York, 1985).
[33] O. Bohigas, in Les Houches LII, Chaos and Quantum Physics, M.-J. Giannoni, A. Voros, and J. Zinn-Justin, eds. (North-Holland, Amsterdam, 1991).

From Subdiffusion and heat transport in a tilted 2D Fermi-Hubbard system by Guardado-Sanchez, Morningstar et al.

References

[1] F. Bloch, Z. Phys. **52**, 555 (1929).

[2] G. H. Wannier, Rev. Mod. Phys. **34**, 645 (1962).

[3] E. E. Mendez, F. Agulló-Rueda, and J. M. Hong, Phys. Rev. Lett. **60**, 2426 (1988).

[4] P. Voisin, J. Bleuse, C. Bouche, S. Gaillard, C. Alibert, and A. Regreny, Phys. Rev. Lett. **61**, 1639 (1988).

[5] A. Nahum, J. Ruhman, S. Vijay, and J. Haah, Phys. Rev. X **7**, 031016 (2017).

[6] A. Nahum, S. Vijay, and J. Haah, Phys. Rev. X **8**, 021014 (2018).

[7] C. W. von Keyserlingk, T. Rakovszky, F. Pollmann, and S. L. Sondhi, Phys. Rev. X **8**, 021013 (2018).

[8] V. Khemani, A. Vishwanath, and D. A. Huse, Phys. Rev. X **8**, 031057 (2018).

[9] T. Rakovszky, F. Pollmann, and C. W. von Keyserlingk, Phys. Rev. X **8**, 031058 (2018).

[10] S. Gopalakrishnan, D. A. Huse, V. Khemani, and R. Vasseur, Phys. Rev. B **98**, 220303 (2018).

[11] T. Banks and A. Lucas, Phys. Rev. E **99**, 022105 (2019).

[12] F. Meinert, M. J. Mark, E. Kirilov, K. Lauber, P. Weinmann, M. Gröbner, and H.-C. Nägerl, Phys. Rev. Lett. **112**, 193003 (2014).

[13] J.-y. Choi, S. Hild, J. Zeiher, P. Schauß, A. Rubio-Abadal, T. Yefsah, V. Khemani, D. A. Huse, I. Bloch, and C. Gross, Science **352**, 1547 (2016).

[14] H. Bernien, S. Schwartz, A. Keesling, H. Levine, A. Omran, H. Pichler, S. Choi, A. S. Zibrov, M. Endres, M. Greiner, V. Vuletić, and M. D. Lukin, Nature **551**, 579 (2017).

[15] S. Scherg, T. Kohlert, J. Herbrych, J. Stolpp, P. Bordia, U. Schneider, F. Heidrich-Meisner, I. Bloch, and M. Aidelsburger, Phys. Rev. Lett. **121**, 130402 (2018).

[16] M. Rispoli, A. Lukin, R. Schittko, S. Kim, M. E. Tai, J. Léonard, and M. Greiner, Nature , 579 (2019).

[17] E. Guardado-Sanchez, P. T. Brown, D. Mitra, T. Devakul, D. A. Huse, P. Schauß, and W. S. Bakr, Phys. Rev. X **8**, 021069 (2018).

[18] P. T. Brown, D. Mitra, E. Guardado-Sanchez, R. Nourafkan, A. Reymbaut, C.-D. Hébert, S. Bergeron, A.-M. S. Tremblay, J. Kokalj, D. A. Huse, P. Schauß, and W. S. Bakr, Science **363**, 379 (2019).

[19] S. Mandt, A. Rapp, and A. Rosch, Phys. Rev. Lett. **106**, 250602 (2011).

[20] A. Rapp, S. Mandt, and A. Rosch, Phys. Rev. Lett. **105**, 220405 (2010).

[21] S. Braun, J. P. Ronzheimer, M. Schreiber, S. S. Hodgman, T. Rom, I. Bloch, and U. Schneider, Science **339**, 52 (2013).

[22] E. van Nieuwenburg, Y. Baum, and G. Refael, Proc. Natl. Acad. Sci. U.S.A. **116**, 9269 (2019).

[23] M. Schulz, C. A. Hooley, R. Moessner, and F. Pollmann, Phys. Rev. Lett. **122**, 040606 (2019).

[24] P. Sala, T. Rakovszky, R. Verresen, M. Knap, and F. Pollmann, arXiv:1904.04266 (2019).

[25] V. Khemani and R. Nandkishore, arXiv:1904.04815 (2019).

[26] P. T. Brown, D. Mitra, E. Guardado-Sanchez, P. Schauß, S. S. Kondov, E. Khatami, T. Paiva, N. Trivedi, D. A. Huse, and W. S. Bakr, Science **357**, 1385 (2017).

[27] See the Supplemental Material.

[28] S. Pai, M. Pretko, and R. M. Nandkishore, Phys. Rev. X **9**, 021003 (2019).

[29] S. Pai and M. Pretko, arXiv:1903.06173 (2019).

[30] R. M. Nandkishore and M. Hermele, Annu. Rev. Condens. Matter Phys. **10**, 295 (2019).

[31] P. T. Brown, E. Guardado-Sanchez, B. M. Spar, E. W. Huang, T. P. Devereaux, and W. S. Bakr, arXiv:1903.05678 (2019).

[32] P. M. Preiss, R. Ma, M. E. Tai, A. Lukin, M. Rispoli, P. Zupancic, Y. Lahini, R. Islam, and M. Greiner, Science **347**, 1229 (2015).

[33] R. Ma, M. E. Tai, P. M. Preiss, W. S. Bakr, J. Simon, and M. Greiner, Phys. Rev. Lett. **107**, 095301 (2011).

From Perturbative approach to weakly driven many-particle systems in the presence of approximate conservation laws by Lenarčič, Lange, Rosch

References

[1] F. Benatti, A. Nagy and H. Narnhofer, Journal of Physics A: Mathematical and Theoretical **44**, 155303 (2011).

[2] A. C. Y. Li, F. Petruccione and J. Koch, Scientific Reports **4**, 4887 (2014).

[3] A. C. Y. Li, F. Petruccione and J. Koch, Phys. Rev. X **6**, 021037 (2016).

[4] Z. Maizelis, M. Rudner and M. I. Dykman, Phys. Rev. B **89**, 155439 (2014).

[5] J. J. García-Ripoll, S. Dürr, N. Syassen, D. M. Bauer, M. Lettner, G. Rempe, and J. I. Cirac, New Journal of Physics **11**, 013053 (2009).

[6] E. M. Kessler, Phys. Rev. A **86**, 012126 (2012).

[7] M. Žnidarič, Phys. Rev. E **92**, 042143 (2015).

[8] F. Reiter and A. S. Sørensen, Phys. Rev. A **85**, 032111 (2012).

[9] H. C. F. Lemos and T. Prosen, Phys. Rev. E **95**, 042137 (2017).

[10] L. V. Butov, A. L. Ivanov, A. Imamoglu, P. B. Littlewood, A. A. Shashkin, V. T. Dolgopolov, K. L. Campman, A. C. Gossard, Phys. Rev. Lett. **86**, 5608 (2001).

[11] J. Kasprzak, M. Richard, S. Kundermann, A. Baas, P. Jeambrun, J. M. J. Keeling, F. M. Marchetti, M. H. Szymańska, R. Andre, J. L. Staehli, V. Savona, P. B. Littlewood, B. Deveaud, Le Si Dang, Nature **443**, 409 (2006).

[12] R. Balili, V. Hartwell, D. Snoke, L. Pfeiffer and K. West, Science **316**, 1007 (2007).

[13] J. Klaers, J. Schmitt, F. Vewinger and M. Weitz, Nature **468**, 545 (2010).

[14] J. Klaers, J. Schmitt, T. Damm, F. Vewinger and M. Weitz, Phys. Rev. Lett. **108**, 160403 (2012).

[15] J. Schmitt, T. Damm, D. Dung, F. Vewinger, J. Klaers, M. Weitz, Phys. Rev. Lett. **112**, 030401 (2014).

[16] S. O. Demokritov, V. E. Demidov, O. Dzyapko, G. A. Melkov, A. A. Serga, B. Hillebrands, A. N. Slavin, Nature **443**, 430 (2006).

[17] A. V. Chumak, G. A. Melkov, V. E. Demidov, O. Dzyapko, V. L. Safonov, S. O. Demokritov, Phys. Rev. Lett. **102**, 187205 (2009).

[18] T. G. Walker and W. Happer, Reviews of Modern Physics **69**, 629 (1997).

[19] S. Anisimov, B. Kapeliovich and T. Perelman, Zh. Eksp. Teor. Fiz **66**, 375 (1974).

[20] B. H. Armstrong, Phys. Rev. B **23**, 883 (1981).

[21] G. L. Eesley, Phys. Rev. B **33**, 2144 (1986).

[22] P. B. Allen, Phys. Rev. Lett. **59**, 1460 (1987).

[23] N. Singh, International Journal of Modern Physics B **24**, 1141 (2010).

[24] F. Lange, Z. Lenarčič and A. Rosch, Nature communications **8**, 15767 (2017).

[25] H. Dehghani, T. Oka and A. Mitra, Phys. Rev. B **90**, 195429 (2014).

[26] T. Shirai, T. Mori and S. Miyashita, Phys. Rev. E **91**, 030101 (2015).

[27] T. Iadecola, T. Neupert and C. Chamon, Phys. Rev. B **91**, 235133 (2015).

[28] D. E. Liu, Phys. Rev. B **91**, 144301 (2015).

[29] K. Iwahori and N. Kawakami, Phys. Rev. B **94**, 184304 (2016).

[30] T. Shirai, J. Thingna, T. Mori, S. Denisov, P. Hänggi and S. Miyashita, New Journal of Physics **18**, 053008 (2016).

[31] K. I. Seetharam, C.-E. Bardyn, N. H. Lindner, M. S. Rudner and G. Refael, Phys. Rev. X **5**, 041050 (2015).

[32] K. Iwahori and N. Kawakami, arXiv:1702.03506 (2017).

[33] M. Genske and A. Rosch, Phys. Rev. A **92**, 062108 (2015).

[34] G. Jotzu, M. Messer, R. Desbuquois, M. Lebrat, T. Uehlinger, D. Greif, T. Esslinger, Nature **515**, 237 (2014).

[35] M. Sentef, A. F. Kemper, B. Moritz, J. K. Freericks, Z. X. Shen, T. P. Devereaux, Phys. Rev. X **3**, 041033 (2013).

[36] B. Robertson, Phys. Rev. **144**, 151 (1966).

[37] B. Robertson, Phys. Rev. **160**, 206 (1968).

[38] K. Kawasaki and J. D. Gunton, Phys. Rev. A **8**, 063604 (1973).

[39] M. Ochiai, Phys. Rev. A **44**, 145 (1973).

[40] C. R. Willis and R. H. Picard, Phys. Rev. A **9**, 1343 (1974).

[41] H. Grabert and W. Weidlich, Z. Phys. **268**, 139 (1974).

[42] T. Koide, Prog. Theor. Phys. **107**, 525 (2002).

[43] H. P. Breuer and F. Petruccione, The theory of open quantum systems (Oxford University Press, New York, 2002).

[44] A. Polkovnikov, K. Sengupta, A. Silva and M. Vengalattore, Rev. Mod. Phys. **83**, 863 (2011).

[45] R. Nandkishore and D. A. Huse, Annu. Rev. Condens. Matter Phys. **6**, 15 (2015).

[46] M. Rigol, V. Dunjko, V. Yurovsky and M. Olshanii, Phys. Rev. Lett. **98**, 050405 (2007).

[47] P. Calabrese and J. Cardy, Journal of Statistical Mechanics: Theory and Experiment **2007**, P06008 (2007).

[48] M. Cramer, C. M. Dawson, J. Eisert and T. J. Osborne, Phys. Rev. Lett. **100**, 030602 (2008).

[49] T. Barthel and U. Schollwöck, Phys. Rev. Lett. **100**, 100601 (2008).

[50] F. H. L. Essler, S. Evangelisti and M. Fagotti, Phys. Rev. Lett. **109**, 247206 (2012).

[51] B. Pozsgay, Journal of Statistical Mechanics: Theory and Experiment **2013**, P07003 (2013).

[52] M. Fagotti and F. H. L. Essler, Journal of Statistical Mechanics: Theory and Experiment **2013**, P07012 (2013).

[53] M. Fagotti and F. H. L. Essler, Phys. Rev. B **87**, 245107 (2013).

[54] M. Fagotti, Journal of Statistical Mechanics: Theory and Experiment **2014**, P03016 (2014).

[55] M. Fagotti, M. Collura, F. H. L. Essler and P. Calabrese, Phys. Rev. B **89**, 125101 (2014).

[56] B. Wouters, J. DeNardis, M. Brockmann, D. Fioretto, M. Rigol, J.-S. Caux, Phys. Rev. Lett. **113**, 117202 (2014).

[57] B. Pozsgay, M. Mestyan, M. A. Werner, M. Kormos, G. Zarand, G. Takács, Phys. Rev. Lett. **113**, 117203 (2014).

[58] S. Sotiriadis and P. Calabrese, Journal of Statistical Mechanics: Theory and Experiment **2014**, P07024 (2014).

[59] G. Goldstein and N. Andrei, Phys. Rev. A **90**, 043625 (2014).

[60] M. Brockmann, B. Wouters, D. Fioretto, J. De Nardis, R. Vlijm and J.-S. Caux, Journal of Statistical Mechanics: Theory and Experiment **2014**, P12009 (2014).

[61] B. Pozsgay, Journal of Statistical Mechanics: Theory and Experiment **2014**, P10045 (2014).

[62] M. Rigol, Phys. Rev. E **90**, 031301 (2014).

[63] M. Mestyán, B. Pozsgay, G. Takács and M. A. Werner, Journal of Statistical Mechanics: Theory and Experiment **2015**, P04001 (2015).

[64] J. Eisert, M. Friesdorf and C. Gogolin, Nature Physics **11**, 124 (2015).

[65] E. Ilievski, E. Quinn, J. De Nardis and M. Brockmann, Journal of Statistical Mechanics: Theory and Experiment **2016**, 063101 (2016).

[66] L. Piroli, E. Vernier and P. Calabrese, Phys. Rev. B **94**, 054313 (2016).

[67] P. Calabrese, F. H. L. Essler and M. Fagotti, Phys. Rev. Lett. **106**, 227203 (2011).

[68] P. Calabrese, F. H. L. Essler and M. Fagotti, Journal of Statistical Mechanics: Theory and Experiment **2012**, P07016 (2012).

[69] P. Calabrese, F. H. L. Essler and M. Fagotti, Journal of Statistical Mechanics: Theory and Experiment **2012**, P07022 (2012).

[70] J.-S. Caux and F. H. L. Essler, Phys. Rev. Lett. **110**, 257203 (2013).

[71] F. H. L. Essler and M. Fagotti, Journal of Statistical Mechanics: Theory and Experiment **2016**, 064002 (2016).

[72] F. H. L. Essler, G. Mussardo and M. Panfil, Journal of Statistical Mechanics: Theory and Experiment **2017**, 013103 (2017).

[73] E. Ilievski, M. Medenjak, T. Prosen and L. Zadnik, Journal of Statistical Mechanics: Theory and Experiment P064008 (2016).

[74] E. Ilievski, J. DeNardis, B. Wouters, J. S. Caux, F. H. L. Essler, T. Prosen, Phys. Rev. Lett. **115**, 157201 (2015).

[75] B. Pozsgay, E. Vernier and M. Werner, arXiv preprint arXiv:1703.09516 (2017).

[76] P. Jung, R. W. Helmes and A. Rosch, Phys. Rev. Lett. **96**, 067202 (2006).

[77] Z. Lenarčič and T. Prosen, Phys. Rev. E **91**, 030103 (2015).

[78] G. Benenti, G. Casati, T. c. v. Prosen, D. Rossini and M. Žnidarič, Phys. Rev. B **80**, 035110 (2009).

[79] D. ForsterHydrodynamic fluctuations, broken symmetry, and correlation functions Vol. 47 (Reading, Mass., WA Benjamin, Inc.(Frontiers in Physics), 1975).

[80] H. Mori, Progress of theoretical physics **33**, 423 (1965).

[81] R. Zwanzig and R. Balescu, J. Chem. Phys **33**, 1338 (1960).

[82] P. Jung and A. Rosch, Phys. Rev. B **75**, 245104 (2007).

[83] P. Mazur, Physica **43**, 533 (1969).

[84] M. Suzuki, Physica **51**, 277 (1971).

[85] X. Zotos, F. Naef and P. Prelovsek, Phys. Rev. B **55**, 11029 (1997).

[86] A. Rosch, J. Paaske, J. Kroha and P. Wölfle, Phys. Rev. Lett. **90**, 076804 (2003).

[87] Article in preparation.

[88] J. Berges, S. Borsányi and C. Wetterich, Phys. Rev. Lett. **93**, 142002 (2004).

[89] G. Aarts, G. F. Bonini and C. Wetterich, Phys. Rev. D **63**, 025012 (2000).

[90] M. Gring, M. Kuhnert, T. Langen, T. Kitagawa, B. Rauer, M. Schreitl, I. Mazets, D. Adu Smith, E. Demler and J. Schmiedmayer, Science **337**, 1318 (2012).

[91] T. Langen, S. Erne, R. Geiger, B. Rauer, T. Schweigler, M. Kuhnert, W. Rohringer, I. Mazets, T. Gasenzer, J. Schmiedmayer, Science **348** (2015).

[92] T. Langen, T. Gasenzer and J. Schmiedmayer, J. Stat. Mech. **2016**, 064009 (2016).

[93] M. Moeckel and S. Kehrein, Phys. Rev. Lett. **100**, 175702 (2008).

[94] C. Kollath, A. M. Läuchli and E. Altman, Phys. Rev. Lett. **98**, 180601 (2007).

[95] M. Kollar, F. A. Wolf and M. Eckstein, Physical Review B **84**, 054304 (2011).

[96] J. Marino and A. Silva, Phys. Rev. B **86**, 060408 (2012).

[97] A. Mitra, Phys. Rev. B **87**, 205109 (2013).

[98] M. Marcuzzi, J. Marino, A. Gambassi and A. Silva, Phys. Rev. Lett. **111**, 197203 (2013).

[99] B. Bertini, F. H. L. Essler, S. Groha and N. J. Robinson, Phys. Rev. Lett. **115**, 180601 (2015).

[100] M. Babadi, E. Demler and M. Knap, Phys. Rev. X **5**, 041005 (2015).

[101] M. Buchhold and S. Diehl, Phys. Rev. A **92**, 013603 (2015).

[102] M. Marcuzzi, J. Marino, A. Gambassi and A. Silva, Phys. Rev. B **94**, 214304 (2016).

[103] R. Barnett, A. Polkovnikov and M. Vengalattore, Phys. Rev. A **84**, 023606 (2011).

[104] N. Nessi, A. Iucci and M. A. Cazalilla, Phys. Rev. Lett. **113**, 210402 (2014).

[105] B. Nowak, J. Schole and T. Gasenzer, New J. Phys. **16**, 093052 (2014).

[106] E. Canovi, M. Kollar and M. Eckstein, Phys. Rev. E **93**, 012130 (2016).

[107] D. Golež, P. Werner and M. Eckstein, Phys. Rev. B **94**, 035121 (2016).

[108] A. Chiocchetta, A. Gambassi, S. Diehl and J. Marino, Phys. Rev. Lett. **118**, 135701 (2017).

[109] V. Gurarie, Nuclear Physics B **441**, 569 (1995).

[110] J. Lux, J. Müller, A. Mitra and A. Rosch, Phys. Rev. A **89**, 053608 (2014).

[111] A. Bohrdt, C. Mendl, M. Endres and M. Knap, New Journal of Physics (2017).

[112] E. Leviatan, F. Pollmann, J. H. Bardarson, D. A. Huse, and E. Altman, arXiv:1702.08894 (2017).

From "Observing non-ergodicity due to kinetic constraints in tilted Fermi-Hubbard chains" by Scherg, Kohlert, et al.

References

[1] C. Gogolin and J. Eisert, Equilibration, thermalisation, and the emergence of statistical mechanics in closed quantum systems, Rep. Prog. Phys. **79**, 056001 (2016).

[2] L. D'Alessio, Y. Kafri, A. Polkovnikov, and M. Rigol, From quantum chaos and eigenstate thermalization to statistical mechanics and thermodynamics, Advances in Physics **65**, 239 (2016).

[3] T. Mori, T. N. Ikeda, E. Kaminishi, and M. Ueda, Thermalization and prethermalization in isolated quantum systems: a theoretical overview, Journal of Physics B: Atomic, Molecular and Optical Physics **51**, 112001 (2018).

[4] P. Calabrese, F. H. L. Essler, and M. Fagotti, Quantum Quench in the Transverse-Field Ising Chain, Phys. Rev. Lett. **106**, 227203 (2011).

[5] R. Nandkishore and D. A. Huse, Many-Body Localization and Thermalization in Quantum Statistical Mechanics, Annu. Rev. Condens. Matter Phys. **6**, 15 (2015).

[6] E. Altman and R. Vosk, Universal Dynamics and Renormalization in Many-Body-Localized Systems, Annu. Rev. Condens. Matter Phys. **6**, 383 (2015).

[7] D. A. Abanin, E. Altman, I. Bloch, and M. Serbyn, Colloquium: Many-body localization, thermalization, and entanglement, Rev. Mod. Phys. **91**, 021001 (2019).

[8] J. M. Deutsch, Quantum statistical mechanics in a closed system, Phys. Rev. A **43**, 2046 (1991).

[9] M. Srednicki, Chaos and quantum thermalization, Phys. Rev. E **50**, 888 (1994).

[10] M. Rigol, V. Dunjko, and M. Olshanii, Thermalization and its mechanism for generic isolated quantum systems, Nature **452**, 854 (2008).

[11] See Supplemental Material, which includes Refs. [69, 70, 71, 72, 73, 74, 75, 77, 78, 79, 76, 80, 82, 83, 84, 85, 86, 87, 88, 89, 90, 91, 92, 93, 94, 95, 96, 97], not cited in the main text, for details on: the interaction picture, the dynamical symmetry between attractive and repulsive interactions, the effective Hamiltonians for different regimes, fragmentation in the resonant regime, constrained dynamics in the presence of higher order terms and on-site interactions, the scaling analysis of the steady-state imbalance and the entanglement entropy, details on the experimental sequence, creating a homogeneous potential, creating a linear potential, interaction averaging, calibration of parameters, extraction of the interaction energy U_{res} and the numerical implementation of the exact diagonalization technique.

[12] N. Shiraishi and T. Mori, Systematic Construction of Counterexamples to the Eigenstate Thermalization Hypothesis, Phys. Rev. Lett. **119**, 030601 (2017).

[13] R. Mondaini, K. Mallayya, L. F. Santos, and M. Rigol, Comment on "Systematic Construction of Counterexamples to the Eigenstate Thermalization Hypothesis", Phys. Rev. Lett. **121**, 038901 (2018).

[14] S. Moudgalya, S. Rachel, B. A. Bernevig, and N. Regnault, Exact excited states of nonintegrable models, Phys. Rev. B **98**, 235155 (2018).

[15] C. J. Turner, A. A. Michailidis, D. A. Abanin, M. Serbyn, and Z. Papić, Weak ergodicity breaking from quantum many-body scars, Nature Physics **14**, 745 (2018).

[16] T. Iadecola and M. Schecter, Quantum many-body scar states with emergent kinetic constraints and finite-entanglement revivals, Phys. Rev. B **101**, 024306 (2020).

[17] S. Chattopadhyay, H. Pichler, M. D. Lukin, and W. W. Ho, Quantum many-body scars from virtual entangled pairs, Phys. Rev. B **101**, 174308 (2020).

[18] H. Bernien, S. Schwartz, A. Keesling, H. Levine, A. Omran, H. Pichler, S. Choi, A. S. Zibrov, M. Endres, M. Greiner, V. Vuletić, and M. D. Lukin, Probing many-body dynamics on a 51-atom quantum simulator, Nature **551**, 579 (2017).

[19] C. J. Turner, A. A. Michailidis, D. A. Abanin, M. Serbyn, and Z. Papić, Quantum scarred eigenstates in a Rydberg atom chain: Entanglement, breakdown of thermalization, and stability to perturbations, Phys. Rev. B **98**, 155134 (2018).

[20] P. Sala, T. Rakovszky, R. Verresen, M. Knap, and F. Pollmann, Ergodicity Breaking Arising from Hilbert Space Fragmentation in Dipole-Conserving Hamiltonians, Phys. Rev. X **10**, 011047 (2020).

[21] V. Khemani, M. Hermele, and R. Nandkishore, Localization from Hilbert space shattering: From theory to physical realizations, Phys. Rev. B **101**, 174204 (2020).

[22] T. Rakovszky, P. Sala, R. Verresen, M. Knap, and F. Pollmann, Statistical localization: From strong fragmentation to strong edge modes, Phys. Rev. B **101**, 125126 (2020).

[23] S. Moudgalya, A. Prem, R. Nandkishore, N. Regnault, and B. A. Bernevig, Thermalization and its absence within Krylov subspaces of a constrained Hamiltonian, arXiv:1910.14048 (2019).

[24] M. van Horssen, E. Levi, and J. P. Garrahan, Dynamics of many-body localization in a translation-invariant quantum glass model, Phys. Rev. B **92**, 100305 (2015).

[25] M. Schiulaz, A. Silva, and M. Müller, Dynamics in many-body localized quantum systems without disorder, Phys. Rev. B **91**, 184202 (2015).

[26] N. Y. Yao, C. R. Laumann, J. I. Cirac, M. D. Lukin, and J. E. Moore, Quasi-Many-Body Localization in Translation-Invariant Systems, Phys. Rev. Lett. **117**, 240601 (2016).

[27] Z. Papić, E. M. Stoudenmire, and D. A. Abanin, Many-body localization in disorder-free systems: The importance of finite-size constraints, Annals of Physics **362**, 714 (2015).

[28] A. Smith, J. Knolle, D. L. Kovrizhin, and R. Moessner, Disorder-Free Localization, Phys. Rev. Lett. **118**, 266601 (2017).

[29] A. Smith, J. Knolle, R. Moessner, and D. L. Kovrizhin, Absence of Ergodicity without Quenched Disorder: From Quantum Disentangled Liquids to Many-Body Localization, Phys. Rev. Lett. **119**, 176601 (2017).

[30] M. Brenes, M. Dalmonte, M. Heyl, and A. Scardicchio, Many-Body Localization Dynamics from Gauge Invariance, Phys. Rev. Lett. **120**, 030601 (2018).

[31] M. Schulz, C. A. Hooley, R. Moessner, and F. Pollmann, Stark Many-Body Localization, Phys. Rev. Lett. **122**, 040606 (2019).

[32] E. v. Nieuwenburg, Y. Baum, and G. Refael, From Bloch oscillations to many-body localization in clean interacting systems, PNAS **116**, 9269 (2019).

[33] L.-N. Wu and A. Eckardt, Bath-Induced Decay of Stark Many-Body Localization, Phys. Rev. Lett. **123**, 030602 (2019).

[34] S. R. Taylor, M. Schulz, F. Pollmann, and R. Moessner, Experimental probes of Stark many-body localization, Phys. Rev. B **102**, 054206 (2020).

[35] R. Yao and J. Zakrzewski, Many-body localization of bosons in an optical lattice: Dynamics in disorder-free potentials, Phys. Rev. B **102**, 104203 (2020).

[36] H. Ott, E. de Mirandes, F. Ferlaino, G. Roati, G. Modugno, and M. Inguscio, Collisionally Induced Transport in Periodic Potentials, Phys. Rev. Lett. **92**, 160601 (2004).

[37] N. Strohmaier, Y. Takasu, K. Günter, R. Jördens, M. Köhl, H. Moritz, and T. Esslinger, Interaction-Controlled Transport of an Ultracold Fermi Gas, Phys. Rev. Lett. **99**, 220601 (2007).

[38] J. H. Bardarson, F. Pollmann, and J. E. Moore, Unbounded Growth of Entanglement in Models of Many-Body Localization, Phys. Rev. Lett. **109**, 017202 (2012).

[39] A. D. Luca and A. Scardicchio, Ergodicity breaking in a model showing many-body localization, EPL **101**, 37003 (2013).

[40] Note, imbalance is defined as a charge imbalance between even and odd lattice sites in our system and does not probe spin imbalances. The magnetization of systems is conserved during the evolution and it is equal to zero at all times.

[41] Note, that in the clean translationally-invariant Fermi-Hubbard model the initial CDW corresponds to an infinite temperature state and a finite imbalance value is a hallmark signature of localization. In the tilted model, the spectrum is superextensive complicating a meaningful definition of temperature. This is overcome by transforming into the interaction picture with respect to the tilt potential, which leaves all density observables invariant and allows us to establish the imbalance as a good probe for ergodicity breaking [11].

[42] M. Ben Dahan, E. Peik, J. Reichel, Y. Castin, and C. Salomon, Bloch Oscillations of Atoms in an Optical Potential, Phys. Rev. Lett. **76**, 4508 (1996).

[43] A. Buchleitner and A. R. Kolovsky, Interaction-Induced Decoherence of Atomic Bloch Oscillations, Phys. Rev. Lett. **91**, 253002 (2003).

[44] A. R. Kolovsky and A. Buchleitner, Floquet-Bloch operator for the Bose-Hubbard model with static field, Phys. Rev. E **68**, 056213 (2003).

[45] A. Tomadin, R. Mannella, and S. Wimberger, Many-Body Interband Tunneling as a Witness of Complex Dynamics in the Bose-Hubbard Model, Phys. Rev. Lett. **98**, 130402 (2007).

[46] A. Tomadin, R. Mannella, and S. Wimberger, Many-body Landau-Zener tunneling in the Bose-Hubbard model, Phys. Rev. A **77**, 013606 (2008).

[47] M. Gustavsson, E. Haller, M. J. Mark, J. G. Danzl, G. Rojas-Kopeinig, and H.-C. Nägerl, Control of Interaction-Induced Dephasing of Bloch Oscillations, Phys. Rev. Lett. **100**, 080404 (2008).

[48] P. M. Preiss, R. Ma, M. E. Tai, A. Lukin, M. Rispoli, P. Zupancic, Y. Lahini, R. Islam, and M. Greiner, Strongly correlated quantum walks in optical lattices, Science **347**, 1229 (2015).

[49] U. Schollwöck, The density-matrix renormalization group in the age of matrix product states, Annals of Physics **326**, 96 (2011).

[50] S. Paeckel, T. Köhler, A. Swoboda, S. R. Manmana, U. Schollwöck, and C. Hubig, Time-evolution methods for matrix-product states, Annals of Physics **411**, 167998 (2019).

[51] J. Hauschild and F. Pollmann, Efficient numerical simulations with Tensor Networks: Tensor Network Python (TeNPy), SciPost Phys. Lect. Notes , 5 (2018).

[52] P. Bordia, H. P. Lüschen, S. S. Hodgman, M. Schreiber, I. Bloch, and U. Schneider, Coupling Identical one-dimensional Many-Body Localized Systems, Phys. Rev. Lett. **116**, 140401 (2016).

[53] U. Schneider, L. Hackermüller, J. P. Ronzheimer, S. Will, S. Braun, T. Best, I. Bloch, E. Demler, S. Mandt, D. Rasch, and A. Rosch, Fermionic transport and out-of-equilibrium dynamics in a homogeneous Hubbard model with ultracold atoms, Nature Physics **8**, 213–218 (2012).

[54] M. Schreiber, S. S. Hodgman, P. Bordia, H. P. Lüschen, M. H. Fischer, R. Vosk, E. Altman, U. Schneider, and I. Bloch, Observation of many-body localization of interacting fermions in a quasirandom optical lattice, Science **349**, 842 (2015).

[55] S. Pai and M. Pretko, Dynamical Scar States in Driven Fracton Systems, Phys. Rev. Lett. **123**, 136401 (2019).

[56] H. Zhao, J. Vovrosh, F. Mintert, and J. Knolle, Quantum Many-Body Scars in Optical Lattices, Phys. Rev. Lett. **124**, 160604 (2020).

[57] A. Kshetrimayum, J. Eisert, and D. M. Kennes, Stark time crystals: Symmetry breaking in space and time, arXiv:2007.13820 (2020).

[58] E. Bairey, G. Refael, and N. H. Lindner, Driving induced many-body localization, Phys. Rev. B **96**, 020201 (2017).

[59] D. S. Bhakuni, R. Nehra, and A. Sharma, Drive-induced many-body localization and coherent destruction of Stark many-body localization, Phys. Rev. B **102**, 024201 (2020).

[60] J. Feldmeier, P. Sala, G. de Tomasi, F. Pollmann, and M. Knap, Anomalous Diffusion in Dipole- and Higher-Moment Conserving Systems, arXiv:2004.00635 (2020).

[61] E. Guardado-Sanchez, A. Morningstar, B. M. Spar, P. T. Brown, D. A. Huse, and W. S. Bakr, Subdiffusion and Heat Transport in a Tilted Two-Dimensional Fermi-Hubbard System, Phys. Rev. X **10**, 011042 (2020).

[62] S. Pai and M. Pretko, Fractons from confinement in one dimension, Phys. Rev. Research **2**, 013094 (2020).

[63] R. Verdel, F. Liu, S. Whitsitt, A. V. Gorshkov, and M. Heyl, Real-time dynamics of string breaking in quantum spin chains, Phys. Rev. B **102**, 014308 (2020).

[64] Z.-C. Yang, F. Liu, A. V. Gorshkov, and T. Iadecola, Hilbert-Space Fragmentation from Strict Confinement, Phys. Rev. Lett. **124**, 207602 (2020).

[65] B. Yang, H. Sun, R. Ott, H.-Y. Wang, T. V. Zache, J. C. Halimeh, Z.-S. Yuan, P. Hauke, and J.-W. Pan, Observation of gauge invariance in a 71-site Bose-Hubbard quantum simulator, arXiv:2003.08945 (2020).

[66] J. Sebby-Strabley, M. Anderlini, P. S. Jessen, and J. V. Porto, Lattice of double wells for manipulating pairs of cold atoms, Phys. Rev. A **73**, 033605 (2006).

[67] S. Fölling, S. Trotzky, P. Cheinet, M. Feld, R. Saers, A. Widera, T. Müller, and I. Bloch, Direct observation of second-order atom tunnelling, Nature **448** (2007).

[68] S. Scherg, T. Kohlert, J. Herbrych, J. Stolpp, P. Bordia, U. Schneider, F. Heidrich-Meisner, I. Bloch, and M. Aidelsburger, Nonequilibrium Mass Transport in the 1D Fermi-Hubbard Model, Phys. Rev. Lett. **121**, 130402 (2018).

[69] C. Parra-Murillo and S. Wimberger, Manifold Approach for a Many-Body Wannier-Stark System: Localization and Chaos in Energy Space, Acta Physica Polonica A **124** (2014).

[70] C. A. Parra-Murillo, J. Madroñero, and S. Wimberger, Two-band Bose-Hubbard model for many-body resonant tunneling in the Wannier-Stark system, Phys. Rev. A **88**, 032119 (2013).

[71] D. V. Else, W. W. Ho, and P. T. Dumitrescu, Long-Lived Interacting Phases of Matter Protected by Multiple Time-Translation Symmetries in Quasiperiodically Driven Systems, Phys. Rev. X **10**, 021032 (2020).

[72] N. Goldman and J. Dalibard, Periodically Driven Quantum Systems: Effective Hamiltonians and Engineered Gauge Fields, Phys. Rev. X **4**, 031027 (2014).

[73] A. Eckardt and E. Anisimovas, High-frequency approximation for periodically driven quantum systems from a Floquet-space perspective, New Journal of Physics **17**, 093039 (2015).

[74] M. Bukov, L. D'Alessio, and A. Polkovnikov, Universal high-frequency behavior of periodically driven systems: from dynamical stabilization to Floquet engineering, Adv. Phys. **64**, 139 (2015).

[75] D. A. Abanin, W. De Roeck, and F. Huveneers, Exponentially Slow Heating in Periodically Driven Many-Body Systems, Phys. Rev. Lett. **115**, 256803 (2015).

[76] L. D'Alessio and M. Rigol, Long-time Behavior of Isolated Periodically Driven Interacting Lattice Systems, Physical Review X **4** (2014).

[77] D. A. Abanin, W. De Roeck, W. W. Ho, and F. Huveneers, Effective Hamiltonians, prethermalization, and slow energy absorption in periodically driven many-body systems, Phys. Rev. B **95**, 014112 (2017).

[78] W. De Roeck and V. Verreet, Very slow heating for weakly driven quantum many-body systems, arXiv:1911.01998 (2019).

[79] D. V. Else, B. Bauer, and C. Nayak, Prethermal Phases of Matter Protected by Time-Translation Symmetry, Phys. Rev. X **7**, 011026 (2017).

[80] T. Kuwahara, T. Mori, and K. Saito, Floquet–Magnus theory and generic transient dynamics in periodically driven many-body quantum systems, Annals of Physics **367**, 96–124 (2016).

[81] This discussion would also apply in the limit of incommensurate Δ_σ and U when going to the frame with respect to the interacting term.

[82] S. Bravyi, D. P. DiVincenzo, and D. Loss, Schrieffer–Wolff transformation for quantum many-body systems, Annals of Physics **326**, 2793–2826 (2011).

[83] E. S. Mananga and T. Charpentier, Introduction of the Floquet-Magnus expansion in solid-state nuclear magnetic resonance spectroscopy, The Journal of Chemical Physics **135**, 044109 (2011).

[84] T. Mikami, S. Kitamura, K. Yasuda, N. Tsuji, T. Oka, and H. Aoki, Brillouin-Wigner theory for high-frequency expansion in periodically driven systems: Application to Floquet topological insulators, Phys. Rev. B **93**, 144307 (2016).

[85] D. Abanin, W. De Roeck, W. W. Ho, and F. Huveneers, A Rigorous Theory of Many-Body Prethermalization for Periodically Driven and Closed Quantum Systems, Commun. Math. Phys. **354**, 809 (2017).

[86] R. Sensarma, D. Pekker, E. Altman, E. Demler, N. Strohmaier, D. Greif, R. Jördens, L. Tarruell, H. Moritz, and T. Esslinger, Lifetime of double occupancies in the Fermi-Hubbard model, Phys. Rev. B **82**, 224302 (2010).

[87] N. M. R. Peres, R. G. Dias, P. D. Sacramento, and J. M. P. Carmelo, Finite-temperature transport in finite-size Hubbard rings in the strong-coupling limit, Phys. Rev. B **61**, 5169 (2000).

[88] C.-J. Lin and O. I. Motrunich, Explicit construction of quasiconserved local operator of translationally invariant nonintegrable quantum spin chain in prethermalization, Phys. Rev. B **96**, 214301 (2017).

[89] C. E. Soliverez, An effective Hamiltonian and time-independent perturbation theory, Journal of Physics C: Solid State Physics **2**, 2161 (1969).

[90] T. Kato, On the Convergence of the Perturbation Method. I, Progress of Theoretical Physics **4**, 514 (1949).

[91] D. Prato and P. W. Lamberti, A note on Magnus formula, The Journal of Chemical Physics **106**, 4640 (1997).

[92] D. N. Page, Average entropy of a subsystem, Phys. Rev. Lett. **71**, 1291 (1993).

[93] L. Vidmar and M. Rigol, Entanglement Entropy of Eigenstates of Quantum Chaotic Hamiltonians, Phys. Rev. Lett. **119** (2017).

[94] G. De Tomasi and I. M. Khaymovich, Multifractality meets entanglement: Relation for nonergodic extended states, Phys. Rev. Lett. **124** (2020).

[95] C. A. Regal, M. Greiner, and D. S. Jin, Observation of Resonance Condensation of Fermionic Atom Pairs, Phys. Rev. Lett. **92**, 040403 (2004).

[96] C. A. Regal and D. S. Jin, Measurement of Positive and Negative Scattering Lengths in a Fermi Gas of Atoms, Phys. Rev. Lett. **90**, 230404 (2003).

[97] R. Jördens, Metallic and Mott-Insulating Phases in Fermionic Quantum Gases, Ph.D. thesis, ETH Zurich, Zürich (2010).

.4 Bibliography from Other Articles

From "A new class of completely integrable quantum spin chains" by Prosen

References

[1] see e.g. V.E.Korepin, N.M.Bogoliubov, and A.G.Izergin, Quantum Inverse scattering Method and Correlation Functions, Cambridge University Press (Cambridge, 1993); also [5] and references therein.

[2] X.Zotos and P.Prelovšek, Phys.Rev.B **53**, 983 (1996); H.Castella, X.Zotos and P.Prelovšek, Phys.Rev.Lett. **74**, 972 (1995); X.Zotos, F.Naef and P.Prelovšek, Phys. Rev. B **55**, 11029 (1997).

[3] In the forthcoming publication we discuss an 'exponentially large' invariant dynamical Lie subalgebra of $\mathfrak{U}$, corresponding to non-integrable kicked Heisenberg XXZ chain, whose power grows as $\sim 1.7^p$ and in which we find a unique nontrivial conservation law that explains deviations from quantum ergodicity and normal transport as observed numerically in (T. Prosen, cond-mat/9707180).

[4] M.Grady, Phys.Rev.D **25**, 1103 (1982).

[5] M.P.Grabowski and P.Mathieu, Ann.Phys.(NY) **243**, 299 (1995).

From Understanding many-body physics in one dimension from the Lieb-Liniger model by Jiang, Chen, Guan

References

[1] Bethe H 1931 *Z. Physik* **71** 205

[2] Lieb E H and Liniger W 1963 *Phys. Rev.* **130** 1605

[3] Yang C N and Yang C P 1969 *J. Math. Phys.* **10** 1115

[4] Yang C N 1967 *Phys. Rev. Lett.* **19** 1312

[5] Baxter R J 1972 *Ann. Phys.* **70** 193

[6] Baxter R J 1972 *Ann. Phys.* **70** 323

[7] Gaudin M 1967 *Phys. Lett. A* **24** 55

[8] Baxter R J 1982 Exactly Solved Models in Statistical Mechanics (London: Academic Press)

[9] Yang C N 1983 Selected Papers 1945–1980 W. H. Freeman and Company

[10] Yang C N 2013 Selected Papers II World Scientific

[11] Korepin V E, Izergin A G and Bogoliubov N M 1993 Quantum Inverse Scattering Method and Correlation Functions (Cambridge: Cambridge University Press)

[12] Takahashi M 1999 Thermodynamics of One-Dimensional Solvable Models (Cambridge: Cambridge University Press)

[13] Essler F H L, Frahm H, Ghmann F, Klmper A and Korepin V E 2005 The One-Dimensional Hubbard Model (Cambridge: Cambridge University Press)

[14] Sutherland B 2004 Beautiful Models (Singapore: World Scientific)

[15] Gaudin M 2014 The Bethe Wavefunction (Cambridge: Cambridge University Press)

[16] Olshanii M 1998 Phys. Rev. Lett. **81** 938

[17] Olshanii M and Dunjko V 2003 Phys. Rev. Lett. **91** 090401

[18] Dunjko V, Lorent V and Olshanii M 2001 *Phys. Rev. Lett.* **86** 5413

[19] Girardeau M, Nguyen H and Olshanii M 2004 *Opt. Commun.* **243** 3

[20] Gaudin M 1971 *Phys. Rev. A* **4** 386

[21] Iida T and Wadati M 2005 *J. Phys. Soc. Jpn.* **74** 1724

[22] Batchelor M T, Guan X W and Mcguire J B 2004 *J. Phys. A* **37** L497

[23] Bortz M private communications

[24] Paredes P 2004 *Nature* **429** 277

[25] Kinoshita T, Wenger T and Weiss D S 2004 *Science* **305** 1125

[26] Guan X W and Batchelor M T 2011 *J. Phys. A: Math. Theor.* **44** 102001

[27] Guan L M private communications

[28] Panfil M and Caux J S 2014 *Phys. Rev. A* **89** 033605

[29] Ristivojevic Z 2014 *Phys. Rev. Lett.* **113** 015301

[30] Astrakharchik G E, Boronat J, Casulleras and Giorgini S 2005 *Phys. Rev. Lett.* **95** 190407

[31] Batchelor M T, Bortz M, Guan X W and Oelkers N 2005 *J. Stat. Mech.: Theory Exp.* L10001

[32] Chen S, Guan L, Yin X, Hao Y and Guan X W 2010 *Phys. Rev. A* **81** 031609

[33] Panfil M, Nardis J D and Caux J S 2013 *Phys. Rev. Lett.* **110** 125302

[34] Kormos M, Mussardo G and Trombettoni A 2011 *Phys. Rev. A* **83** 013617

[35] Girardeau M D and Astrakharchik G E 2009 *Phys. Rev. A* **81** 061601(R)

[36] Giamarchi T 2004 Quantum Physics in One Dimension (Cambridge: Cambridge University Press)

[37] Cazalilla M A, Citro R, Giamarchi T, Orignac E and Rigol M 2011 *Rev. Mod. Phys.* **83** 1405

[38] Caux J S and Calabrese P 2006 *Phys. Rev. A* **74** 031605

[39] Panfil M and Caux J S 2014 *Phys. Rev. A* **89** 033605

[40] Belavin A A, Polyakov A M and Zamolodchikov A B 1984 *Nucl. Phys. B* **241** 333

[41] Guan X W, Batchelor M T and Lee C 2013 *Rev. Mod. Phys.* **85** 1633

[42] Gangardt D M and Shlyapnikov G V 2003 *Phys. Rev. Lett.* **90** 010401

[43] Kheruntsyan K V, Gangardt D M, Drummond P D and Shlyapnikov G V 2003 *Phys. Rev. Lett.* **91** 040403

[44] Batchelor M T and Guan X W 2007 *Laser Phys. Lett.* **4** 77

[45] Klumper A and Patu O I 2014 *Phys. Rev. A* **90** 053626

[46] Gangardt D M and Shlyapnikov G V 2003 *Phys. Rev. Lett.* **90** 010401

[47] Kheruntsyan K V, Gangardt D M, Drummond P D and Shlyapnikov G V 2003 *Phys. Rev. Lett.* **91** 040403

[48] Kheruntsyan K V, Gangardt D M, Drummond P D and Shlyapnikov G V 2005 *Phys. Rev. A* **71** 053615

[49] Tan S 2008 *Ann. Phys.* **323** 2952

[50] Tan S 2008 *Ann. Phys.* **323** 2971

[51] Tan S 2008 *Ann. Phys.* **323** 2987

[52] Chen Y Y, Jiang Y Z, Guan X W and Zhou Q 2014 *Nat. Commun.* **5** 51040

[53] Cazalilla M A 2003 *Phys. Rev. A* **67** 053606

[54] Guan X W, Batchelor M T and Takahashi M 2007 *Phys. Rev. A* **76** 043617

[55] Batchelor M T 2014 *Int. J. Mod. Phys. B* **28** 1430010

[56] Kinoshita T, Wenger T and Weiss D S 2005 *Phys. Rev. Lett.* **95** 190406

[57] Guarrera V, Muth D, Labouvle R, Vogler A, Barontlnl G, Flelschhauer M and Ott H 2012 *Phys. Rev. A* **86** 021601

[58] Armijo J, Jacqmin T, Kheruntsyan and Bouchoule 2010 *Phys. Rev. Lett.* **105** 230402

[59] Tolra B L, O'Hara K M, Huckans J H, Phillips W D, Rolston S L and Porto J V 2004 *Phys. Rev. Lett.* **92** 190401

[60] Haller E, Rabie M, Mark M J, Danzl J G, Hart R, Lauber K, Pupillo G and Ngerl H C 2011 *Phys. Rev. Lett.* **107** 230404

[61] Kuhnert M, Geiger R, Langen T, Gring M, Rauer B, Kitagawa T, Demler E, Smith D A and Schmiedmayer J 2013 *Phys. Rev. Lett.* **110** 090405

[62] van Amerongen A H, van Es J J P, Wicke P, Kheruntsyan K V and van Druten N J 2008 *Phys. Rev. Lett.* **100** 090402

[63] Vogler A, Labouvie R, Stubenrauch F, Barontini G, Guarrera V and Ott H 2013 *Phys. Rev. A* **88** 031603

[64] Haller E, Gustavss M, Mark M J, Danzl J G, Hart R, Pupillo G and Ngerl H C 2009 *Science* **325** 1224

[65] Jacqmin T, Armijo J, Berrada T, Kheruntsyan K V and Bouchoule I 2011 *Phys. Rev. Lett.* **106** 230405

[66] Esteve J, Trebbia J B, Schumm T, Aspect A, Westbrook C I and Bouchoule I 2006 *Phys. Rev. Lett.* **96** 130403

[67] Armijo J 2012 *Phys. Rev. Lett.* **108** 225306

[68] Karpiuk T, Deuar P, Bienias P, Witkowska E, Pawlowski K, Gajda M, Rzazewski K and Brewczyk M 2012 *Phys. Rev. Lett.* **109** 205302

[69] Fabbri N, Panfil M, Clment D, Fallani L, Inguscio M, Fort C and Caux J S 2014 arXiv:1406.2176v2 [cond-mat.quant-gas]

[70] Kinoshita T, Wenger T and Weiss D S 2006 *Nature* **440** 900

[71] Hofferberth S, Lesanovsky I, Fischer B, Schumm T and Schmiedmayer J 2007 *Nature* **449** 324

[72] Ronzheimer J P 2013 *Phys. Rev. Lett.* **110** 205301

[73] The experiments are chosen for the most relative to the Lieb–Liniger model, and by no means exhaustive.

[74] Langen T, Geiger R, Kuhnert M, Rauer B and Schmiedmayer J 2013 *Nat. Phys.* **9** 640

[75] Stimming H P, Mauser N J, Schmiedmayer J and Mazets I E 2010 *Phys. Rev. Lett.* **105** 015301

[76] Langen T, Erne S, Geiger R, Rauer B, Schweigler T, Kuhnert M, Rohringer W, Mazets I E, Gasenzer T and Schmiedmayer J 2014 arXiv:1411.7185v1 [cond-mat.quant-gas])

[77] Witkowska E, Deuar P, Gajda M and Rzaewski K 2011 *Phys. Rev. Lett.* **106** 135301

[78] Jacqmin T, Fang B, Berrada T, Rosclde T and Bouchoule I 2012 *Phys. Rev. A* **86** 043626

[79] Haller E, Hart R, Mark M J, Danzl J G, Reichsllner L, Gustavsson M, Dalmonte M, Pupillo G and Ngerl H C 2010 *Nature* **466** 597

[80] Guan X W 2014 *Int. J. Mod. Phys. B* **28** 1430015

[81] Guan X W, Batchelor M T and Takahashi M 2007 *Phys. Rev. A* **76** 043617

[82] Rigol M, Dunjko V, Yurovsky V and Olshanii M 2007 *Phys. Rev. Lett.* **98** 050405

[83] Rigol M, Dunjko V and Olshanii M 2008 *Nature* **452** 854

[84] Kormos M, Chou Y Z and Imambekov A 2011 *Phys. Rev. Lett.* **107** 230405

[85] Cheianov V V, Smith H and Zvonarev M B 2006 J. Stat. Mech.: Theory Exp. P08015

[86] Kormos M, Mussardo G and Trombettoni A 2009 *Phys. Rev. Lett.* **103** 210404

[87] Kormos M, Mussardo G and Trombettoni A 2010 *Phys. Rev. A* **81** 043606

[88] Kormos M, Mussardo G and Pozsgay B 2010 *J. Stat. Mech.: Theory Exp.* P05014

[89] Caux J S and Essler F H L 2013 *Phys. Rev. Lett.* **110** 257203

[90] Nardis J, Wouters B, Brockmann M and Caux J S 2014 *Phys. Rev. A.* **89** 033601

[91] Goldstein G and Andrei N 2014 arXiv:1405.6365v1 [cond-mat.quant-gas]

[92] Goldstein G and Andrei N 2013 arXiv:1309.3471v1 [cond-mat.quant-gas]

[93] Lyer D and Andrei N 2012 *Phys. Rev. Lett.* **109** 115304

[94] Pozsgay B 2014 arXiv:1406.4613v2 [cond-mat.stat-mech]

[95] Wouters B, Nardis J D, Brockmann M, Fioretto D, Rigol M and Caux J S 2014 *Phys. Rev. Lett.* **113** 117202

[96] Brockmann M, Wouters B, Fioretto D, Nardis J D, Vlijm R and C J S 2014 *J. Stat. Mech.* P12009

[97] Pozsgay B, Mestyn M, Werner M A, Kormos M, Zarnd G and Takcs G 2014 *Phys. Rev. Lett.* **113** 117203

[98] Goldstein G and Andrei N 2014 arXiv:1405.4224v2 [cond-mat.quant-gas]

From "From dissip-less to norm diffus in easy-axis Heisen sp ch"

References

[1] B. Bertini, F. Heidrich-Meisner, C. Karrasch, T. Prosen, R. Steinigeweg, and M. Žnidarič, "Finite-temperature transport in one-dimensional quantum lattice models," Rev. Mod. Phys. **93**, 025003 (2021).

[2] A. Bastianello, A. De Luca, and R. Vasseur, "Hydrodynamics of weak integrability breaking," J. Stat. Mech. **2021**, 114003 (2021).

[3] K. Mallayya, M. Rigol, and W. De Roeck, "Prethermalization and thermalization in isolated quantum systems," Phys. Rev. X **9**, 021027 (2019).

[25] F. Lange, Z. Lenarčič, and A. Rosch, "Time-dependent generalized gibbs ensembles in open quantum systems," Phys. Rev. B **97**, 165138 (2018).

[5] H. Castella, X. Zotos, and P. Prelovšek, "Integrability and ideal conductance at finite temperatures," Phys. Rev. Lett. **74**, 972 (1995).

[6] X Zotos and P Prelovšek, "Evidence for ideal insulating or conducting state in a one-dimensional integrable system." Phys. Rev. B **53**, 983 (1996).

[7] X. Zotos, F. Naef, and P. Prelovšek, "Transport and conservation laws," Phys. Rev. B **55**, 11029 (1997).

[8] T. Prosen, "Open XXZ spin chain: Nonequilibrium steady state and a strict bound on ballistic transport," Phys. Rev. Lett. **106**, 217206 (2011).

[9] T. Prosen and E. Ilievski, "Families of quasilocal conservation laws and quantum spin transport," Phys. Rev. Lett. **111**, 057203 (2013).

[48] E. Ilievski, M. Medenjak, T. Prosen, and L. Zadnik, "Quasilocal charges in integrable lattice systems," J. Stat. Mech. **2016**, 064008.

[11] B. Bertini, M. Collura, J. De Nardis, and M. Fagotti, "Transport in out-of-equilibrium xxz chains: Exact profiles of charges and currents," Phys. Rev. Lett. **117**, 207201 (2016).

[9] O. A. Castro-Alvaredo, B. Doyon, and T. Yoshimura, "Emergent hydrodynamics in integrable quantum systems out of equilibrium," Phys. Rev. X **6**, 041065 (2016).

[13] E. Ilievski and J. De Nardis, "Microscopic Origin of Ideal Conductivity in Integrable Quantum Models," Phys. Rev. Lett. **119**, 020602 (2017).

[14] V. B. Bulchandani, R. Vasseur, C. Karrasch, and J. E. Moore, "Bethe-Boltzmann hydrodynamics and spin transport in the XXZ chain," Phys. Rev. B **97**, 045407 (2018).

[15] J. De Nardis, D. Bernard, and B. Doyon, "Hydrodynamic diffusion in integrable systems," Phys. Rev. Lett. **121**, 160603 (2018).

[16] J. de Nardis, D. Bernard, and B. Doyon, "Diffusion in generalized hydrodynamics and quasiparticle scattering," SciPost Phys. **6**, 049 (2019).

[17] S. Gopalakrishnan and R. Vasseur, "Kinetic Theory of Spin Diffusion and Superdiffusion in XXZ Spin Chains," Physical Review Letters **122**, 127202 (2019).

[18] H. Castella and X. Zotos, "Finite-temperature mobility of a particle coupled to a fermionic environment," Phys. Rev. B **54**, 4375 (1996).

[19] P. Jung, R. W. Helmes, and A. Rosch, "Transport in almost integrable models: Perturbed Heisenberg chains," Phys. Rev. Lett. **96**, 067202 (2006).

[20] P. Jung and A. Rosch, "Spin conductivity in almost integrable spin chains," Phys. Rev. B **76**, 245108 (2007).

[21] M. Žnidarič, "Weak integrability breaking: Chaos with integrability signature in coherent diffusion," Phys. Rev. Lett. **125**, 180605 (2020).

[22] M. Mierzejewski, T. Prosen, and P. Prelovšek, "Approximate conservation laws in perturbed integrable lattice models," Phys. Rev. B **92**, 195121 (2015).

[23] S. Hild, T. Fukuhara, P. Schauß, J. Zeiher, M. Knap, E. Demler, I. Bloch, and C. Gross, "Far-from-equilibrium spin transport in heisenberg quantum magnets," Phys. Rev. Lett. **113**, 147205 (2014).

[24] P. N. Jepsen, J. Amato-Grill, I. Dimitrova, W. W. Ho, E. Demler, and W. Ketterle, "Spin transport in a tunable Heisenberg model realized with ultracold atoms," Nature **588**, 403 (2020).

[25] D. Wei, A. Rubio-Abadal, B. Ye, F. Machado, J. Kemp, K. Srakaew, S. Hollerith, J. Rui, S. Gopalakrishnan, N. Y. Yao, I. Bloch, and J. Zeiher, "Quantum gas microscopy of Kardar-Parisi-Zhang superdiffusion," Science **376**, 716 (2022).

[26] M. Žnidarič, "Spin transport in a one-dimensional anisotropic Heisenberg model," Phys. Rev. Lett. **106**, 220601 (2011).

[27] R. Steinigeweg and J. Gemmer, "Density dynamics in translationally invariant spin-$\frac{1}{2}$ chains at high temperatures: A current-autocorrelation approach to finite time and length scales," Phys. Rev. B **80**, 184402 (2009).

[28] R. Steinigeweg, J. Herbrych, P. Prelovšek, and M. Mierzejewski, "Coexistence of anomalous and normal diffusion in integrable mott insulators," Phys. Rev. B **85**, 214409 (2012).

[29] C. Karrasch, J. E. Moore, and F. Heidrich-Meisner, "Real-time and real-space spin and energy dynamics in one-dimensional spin- 1 2 systems induced by local quantum quenches at finite temperatures," Phys. Rev. B **89**, 075139 (2014).

[30] R. Steinigeweg, J. Gemmer, and W. Brenig, "Spin and energy currents in integrable and nonintegrable spin-$\frac{1}{2}$ chains: A typicality approach to real-time autocorrelations," Phys. Rev. B **91**, 104404 (2015).

[31] P. Prelovšek, S. El Shawish, X. Zotos, and M. Long, "Anomalous scaling of conductivity in integrable fermion systems," Phys. Rev. B **70**, 205129 (2004).

[32] M. Medenjak, C. Karrasch, and T. Prosen, "Lower bounding diffusion constant by the curvature of drude weight," Phys. Rev. Lett. **119**, 080602 (2017).

[33] E. Ilievski, J. De Nardis, M. Medenjak, and T. Prosen, "Superdiffusion in one-dimensional quantum lattice models," Phys. Rev. Lett. **121**, 230602 (2018).

[34] M. Mierzejewski, J. Bonča, and P. Prelovšek, "Integrable mott insulators driven by a finite electric field," Phys. Rev. Lett. **107**, 126601 (2011).

[35] J. De Nardis, S. Gopalakrishnan, R. Vasseur, and B. Ware, "Subdiffusive hydrodynamics of nearly-integrable anisotropic spin chains," arXiv:2109.13251 .

[36] J. De Nardis, S. Gopalakrishnan, R. Vasseur, and B. Ware, "Stability of superdiffusion in nearly integrable spin chains," Phys. Rev. Lett. **127**, 057201 (2021).

[37] M. W. Long, P. Prelovšek, S. El Shawish, J. Karadamoglou, and X. Zotos, "Finite-temperature dynamical correlations using the microcanonical ensemble and the lanczos algorithm," Phys. Rev. B **68**, 235106 (2003).

[38] P. Prelovšek and J. Bonča, "Ground state and finite temperature lanczos methods," Strongly Correlated Systems - Numerical Methods, (2013), 10.1007/978-3-642-35106-8.

[39] P. Prelovšek, M. Mierzejewski, and J. Herbrych, "Coexistence of diffusive and ballistic transport in integrable quantum lattice models," Phys. Rev. B **104**, 115163 (2021).

[40] R. Steinigeweg and W. Brenig, "Spin Transport in the XXZ Chain at Finite Temperature and Momentum," Phys. Rev. Lett. **107**, 250602 (2011).

[41] M. Mierzejewski, J. Pawłowski, P. Prelovšek, and J. Herbrych, "Multiple relaxation times in perturbed XXZ chain," arXiv:2112.08158 .

[46] M. Zwolak and G. Vidal, "Mixed-state dynamics in one-dimensional quantum lattice systems: A time-dependent superoperator renormalization algorithm," Phys. Rev. Lett. **93**, 207205 (2004).

[45] F. Verstraete, J. J. García-Ripoll, and J. I. Cirac, "Matrix product density operators: Simulation of finite-temperature and dissipative systems," Phys. Rev. Lett. **93**, 207204 (2004).

[55] J. Bezanson, A. Edelman, S. Karpinski, and V. B. Shah, "Julia: A fresh approach to numerical computing," SIAM Review **59**, 65 (2017).

From Effects of atom losses on a one-dimensional lattice gas of hardcore bosons

References

[1] I. Bloch, J. Dalibard, and W. Zwerger, "Many-body physics with ultracold gases," Rev. Mod. Phys., vol. 80, pp. 885–964, Jul 2008. http://dx.doi.org/10.1103/RevModPhys.80.885.

[2] S. Knoop, J. S. Borbely, R. van Rooij, and W. Vassen, "Nonexponential one-body loss in a bose-einstein condensate," Phys. Rev. A, vol. 85, p. 025602, Feb 2012. http://dx.doi.org/10.1103/PhysRevA.85.025602.

[3] Browaeys, A., Poupard, J., Robert, A., Nowak, S., Rooijakkers, W., Arimondo, E., Marcassa, L., Boiron, D., Westbrook, C. I., and Aspect, A., "Two body loss rate in a magneto-optical trap of metastable he," Eur. Phys. J. D, vol. **8**, no. 2, pp. 199–203, (2000). http://dx.doi.org/10.1007/s100530050027.

[4] L. Franchi, L. F. Livi, G. Cappellini, G. Binella, M. Inguscio, J. Catani, and L. Fallani, "State-dependent interactions in ultracold 174yb probed by optical clock spectroscopy," New Journal of Physics, vol. 19, p. 103037, nov 2017. http://dx.doi.org/10.1088/1367-2630/aa8fb4.

[5] T. Tomita, S. Nakajima, I. Danshita, Y. Takasu, and Y. Takahashi, "Observation of the mott insulator to superfluid crossover of a driven-dissipative bose-hubbard system," Science Advances, vol. 3, no. 12, p. e1701513, 2017. http://dx.doi.org/10.1126/sciadv.1701513.

[6] N. Syassen, D. M. Bauer, M. Lettner, T. Volz, D. Dietze, J. J. García-Ripoll, J. I. Cirac, G. Rempe, and S. Dürr, "Strong dissipation inhibits losses and induces correlations in cold molecular gases," Science, vol. 320, no. 5881, pp. 1329–1331, 2008. http://dx.doi.org/10.1126/science.1155309.

[7] T. Tomita, S. Nakajima, Y. Takasu, and Y. Takahashi, "Dissipative bose-hubbard system with intrinsic two-body loss," Phys. Rev. A, vol. 99, p. 031601, Mar 2019. http://dx.doi.org/10.1103/PhysRevA.99.031601.

[8] B. Yan, S. A. Moses, B. Gadway, J. P. Covey, K. R. A. Hazzard, A. M. Rey, D. S. Jin, and J. Ye, "Observation of dipolar spin-exchange interactions with lattice-confined polar molecules," Nature, vol. 501, pp. 521–525, Sep 2013. http://dx.doi.org/10.1038/nature12483.

[9] K. Sponselee, L. Freystatzky, B. Abeln, M. Diem, B. Hundt, A. Kochanke, T. Ponath, B. Santra, L. Mathey, K. Sengstock, and C. Becker, "Dynamics of ultracold quantum gases in the dissipative fermi–hubbard model," Quantum Science and Technology, vol. 4, p. 014002, sep 2018. http://dx.doi.org/10.1088/2058-9565/aadccd.

[10] K. Honda, S. Taie, Y. Takasu, N. Nishizawa, M. Nakagawa, and Y. Takahashi, "Observation of the sign reversal of the magnetic correlation in a driven-dissipative fermi gas in double wells," Phys. Rev. Lett., vol. 130, p. 063001, Feb 2023. http://dx.doi.org/10.1103/PhysRevLett.130.063001.

[11] J. Söding, D. Guéry-Odelin, P. Desbiolles, F. Chevy, H. Inamori, and J. Dalibard, "Three-body decay of a rubidium bose–einstein condensate," Applied Physics B, vol. 69, pp. 257–261, Oct 1999. http://dx.doi.org/10.1007/s003400050805.

[12] T. Weber, J. Herbig, M. Mark, H.-C. Nägerl, and R. Grimm, "Three-body recombination at large scattering lengths in an ultracold atomic gas," Phys. Rev. Lett., vol. 91, p. 123201, Sep 2003. http://dx.doi.org/10.1103/PhysRevLett.91.123201.

[13] B. L. Tolra, K. M. O'Hara, J. H. Huckans, W. D. Phillips, S. L. Rolston, and J. V. Porto, "Observation of reduced three-body recombination in a correlated 1d degenerate bose gas," Phys. Rev. Lett., vol. 92, p. 190401, May 2004. http://dx.doi.org/10.1103/PhysRevLett.92.190401.

[14] F. Ferlaino, S. Knoop, M. Berninger, W. Harm, J. P. D'Incao, H.-C. Nägerl, and R. Grimm, "Evidence for universal four-body states tied to an efimov trimer," Phys. Rev. Lett., vol. 102, p. 140401, Apr 2009. http://dx.doi.org/10.1103/PhysRevLett.102.140401.

[15] J. H. Gurian, P. Cheinet, P. Huillery, A. Fioretti, J. Zhao, P. L. Gould, D. Comparat, and P. Pillet, "Observation of a resonant four-body interaction in cold cesium rydberg atoms," Phys. Rev. Lett., vol. 108, p. 023005, Jan 2012. http://dx.doi.org/10.1103/PhysRevLett.108.023005.

[16] D. M. Harber, J. M. McGuirk, J. M. Obrecht, and E. A. Cornell, "Thermally Induced Losses in Ultra-Cold Atoms Magnetically Trapped Near Room-Temperature Surfaces," Journal of Low Temperature Physics, vol. **133**, pp. 229–238, Nov. (2003). http://dx.doi.org/10.1023/A:1026084606385.

[17] A. Johnson, S. S. Szigeti, M. Schemmer, and I. Bouchoule, "Long-lived nonthermal states realized by atom losses in one-dimensional quasicondensates," Physical Review A, vol. **96**, p. 013623, July (2017). http://dx.doi.org/10.1103/PhysRevA.96.013623.

[18] I. Bouchoule, M. Schemmer, and C. Henkel, "Cooling phonon modes of a Bose condensate with uniform few body losses," SciPost Phys., vol. 5, p. 043, 2018. http://dx.doi.org/10.21468/SciPostPhys.5.5.043.

[19] L. H. Dogra, J. A. P. Glidden, T. A. Hilker, C. Eigen, E. A. Cornell, R. P. Smith, and Z. Hadzibabic, "Can three-body recombination purify a quantum gas?," Phys. Rev. Lett., vol. 123, p. 020405, Jul 2019. http://dx.doi.org/10.1103/PhysRevLett.123.020405.

[20] P. Grišins, B. Rauer, T. Langen, J. Schmiedmayer, and I. E. Mazets, "Degenerate bose gases with uniform loss," Phys. Rev. A, vol. 93, p. 033634, Mar 2016. http://dx.doi.org/10.1103/PhysRevA.93.033634.

[21] B. Rauer, P. Grišins, I. E. Mazets, T. Schweigler, W. Rohringer, R. Geiger, T. Langen, and J. Schmiedmayer, "Cooling of a one-dimensional bose gas," Phys. Rev. Lett., vol. 116, p. 030402, Jan 2016. http://dx.doi.org/10.1103/PhysRevLett.116.030402.

[22] M. Schemmer, A. Johnson, R. Photopoulos, and I. Bouchoule, "Monte carlo wavefunction description of losses in a one-dimensional bose gas and cooling to the ground state by quantum feedback," Phys. Rev. A, vol. 95, p. 043641, Apr 2017. http://dx.doi.org/10.1103/PhysRevA.95.043641.

[23] M. Schemmer and I. Bouchoule, "Cooling a bose gas by three-body losses," Phys. Rev. Lett., vol. 121, p. 200401, Nov 2018. http://dx.doi.org/10.1103/PhysRevLett.121.200401.

[24] I. Bouchoule and M. Schemmer, "Asymptotic temperature of a lossy condensate," SciPost Phys., vol. 8, p. 060, 2020. http://dx.doi.org/10.21468/SciPostPhys.8.4.060.

[25] D. Rossini, A. Ghermaoui, M. B. Aguilera, R. Vatré, R. Bouganne, J. Beugnon, F. Gerbier, and L. Mazza, "Strong correlations in lossy one-dimensional quantum gases: from the quantum Zeno effect to the generalized Gibbs ensemble," Physical Review A, vol. 103, p. L060201, June (2021). http://dx.doi.org/10.1103/PhysRevA.103.L060201.

[26] J. J. García-Ripoll, S. Dürr, N. Syassen, D. M. Bauer, M. Lettner, G. Rempe, and J. I. Cirac, "Dissipation-induced hard-core boson gas in an optical lattice," New Journal of Physics, vol. **11**, p. 013053, Jan. (2009). http://dx.doi.org/10.1088/1367-2630/11/1/013053.

[27] E. Misra and C. Sudarshan, "The zeno's paradox in quantum theory," J. Math. Phys., vol. 18, p. 756, 1977.

[28] W. M. Itano, D. J. Heinzen, J. J. Bollinger, and D. J. Wineland, "Quantum zeno effect," Phys. Rev. A, vol. 41, pp. 2295–2300, 1990. http://dx.doi.org/10.1103/PhysRevA.41.2295.

[29] A. Beige, D. Braun, and P. L. Knight, "Driving atoms into decoherence-free states," New J. Phys., vol. 2, pp. 22–22, sep 2000. http://dx.doi.org/10.1088/1367-2630/2/1/322.

[30] A. Beige, D. Braun, B. Tregenna, and P. L. Knight, "Quantum computing using dissipation to remain in a decoherence-free subspace," Phys. Rev. Lett., vol. 85, pp. 1762–1765, Aug 2000. http://dx.doi.org/10.1103/PhysRevLett.85.1762.

[31] J. Kempe, D. Bacon, D. A. Lidar, and K. B. Whaley, "Theory of decoherence-free fault-tolerant universal quantum computation," Phys. Rev. A, vol. 63, p. 042307, Mar 2001. http://dx.doi.org/10.1103/PhysRevA.63.042307.

[32] P. Facchi, H. Nakazato, and S. Pascazio, "From the quantum zeno to the inverse quantum zeno effect," Phys. Rev. Lett., vol. 86, pp. 2699–2703, Mar 2001. http://dx.doi.org/10.1103/PhysRevLett.86.2699.

[33] P. Facchi and S. Pascazio, "Quantum zeno subspaces," Phys. Rev. Lett., vol. 89, p. 080401, Aug 2002. http://dx.doi.org/10.1103/PhysRevLett.89.080401.

[34] R. Schützhold and G. Gnanapragasam, "Quantum zeno suppression of three-body losses in bose-einstein condensates," Phys. Rev. A, vol. 82, p. 022120, Aug 2010. http://dx.doi.org/10.1103/PhysRevA.82.022120.

[35] K. Stannigel, P. Hauke, D. Marcos, M. Hafezi, S. Diehl, M. Dalmonte, and P. Zoller, "Constrained dynamics via the zeno effect in quantum simulation: Implementing non-abelian lattice gauge theories with cold atoms," Phys. Rev. Lett., vol. 112, p. 120406, Mar 2014. http://dx.doi.org/10.1103/PhysRevLett.112.120406.

[36] Z. Gong, S. Higashikawa, and M. Ueda, "Zeno hall effect," Phys. Rev. Lett., vol. 118, p. 200401, May 2017. http://dx.doi.org/10.1103/PhysRevLett.118.200401.

[37] H. Fröml, C. Muckel, C. Kollath, A. Chiocchetta, and S. Diehl, "Ultracold quantum wires with localized losses: Many-body quantum zeno effect," Phys. Rev. B, vol. 101, p. 144301, Apr 2020. http://dx.doi.org/10.1103/PhysRevB.101.144301.

[38] K. Snizhko, P. Kumar, and A. Romito, "Quantum zeno effect appears in stages," Phys. Rev. Research, vol. 2, p. 033512, Sep 2020. http://dx.doi.org/10.1103/PhysRevResearch.2.033512.

[39] A. Biella and M. Schiró, "Many-Body Quantum Zeno Effect and Measurement-Induced Subradiance Transition," Quantum, vol. 5, p. 528, Aug. 2021. http://dx.doi.org/10.22331/q-2021-08-19-528.

[40] I. Bouchoule, B. Doyon, and J. Dubail, "The effect of atom losses on the distribution of rapidities in the one-dimensional Bose gas," SciPost Phys. 9, 044, June (2020). http://dx.doi.org/10.21468/SciPostPhys.9.4.044.

[41] I. Bouchoule, L. Dubois, and L.-P. Barbier, "Losses in interacting quantum gases: Ultraviolet divergence and its regularization," Phys. Rev. A, vol. 104, p. L031304, Sep 2021. http://dx.doi.org/10.1103/PhysRevA.104.L031304.

[42] F. Minganti, V. Savona, and A. Biella, "Dissipative phase transitions in n-photon driven quantum nonlinear resonators," 2023. http://dx.doi.org/10.48550/arXiv.2303.03355.

[43] L. Rosso, A. Biella, and L. Mazza, "The one-dimensional Bose gas with strong two-body losses: the effect of the harmonic confinement," SciPost Physics, vol. **12**, p. 044, Jan. (2022). http://dx.doi.org/10.21468/SciPostPhys.12.1.044.

[44] C.-H. Huang, T. Giamarchi, and M. A. Cazalilla, "Modeling particle loss in open systems using keldysh path integral and second order cumulant expansion," 2023. http://dx.doi.org/10.48550/arXiv.2305.13090.

[45] B. Zhu, B. Gadway, M. Foss-Feig, J. Schachenmayer, M. L. Wall, K. R. A. Hazzard, B. Yan, S. A. Moses, J. P. Covey, D. S. Jin, J. Ye, M. Holland, and A. M. Rey, "Suppressing the loss of ultracold molecules via the continuous quantum zeno effect," Phys. Rev. Lett., vol. 112, p. 070404, Feb 2014. http://dx.doi.org/10.1103/PhysRevLett.112.070404.

[46] L. Rosso, D. Rossini, A. Biella, and L. Mazza, "One-dimensional spin-1/2 fermionic gases with two-body losses: Weak dissipation and spin conservation," Phys. Rev. A, vol. 104, p. 053305, Nov 2021. http://dx.doi.org/10.1103/PhysRevA.104.053305.

[47] L. Rosso, L. Mazza, and A. Biella, "Eightfold way to dark states in su(3) cold gases with two-body losses," Phys. Rev. A, vol. 105, p. L051302, May 2022. http://dx.doi.org/10.1103/PhysRevA.105.L051302.

[48] L. Rosso, A. Biella, J. De Nardis, and L. Mazza, "Dynamical theory for one-dimensional fermions with strong two-body losses: Universal non-hermitian zeno physics and spin-charge separation," Phys. Rev. A, vol. 107, p. 013303, Jan 2023. http://dx.doi.org/10.1103/PhysRevA.107.013303.

[49] M. Nakagawa, N. Tsuji, N. Kawakami, and M. Ueda, "Dynamical sign reversal of magnetic correlations in dissipative hubbard models," Phys. Rev. Lett., vol. 124, p. 147203, Apr 2020. http://dx.doi.org/10.1103/PhysRevLett.124.147203.

[50] M. Nakagawa, N. Kawakami, and M. Ueda, "Exact liouvillian spectrum of a one-dimensional dissipative hubbard model," Phys. Rev. Lett., vol. 126, p. 110404, Mar 2021. http://dx.doi.org/10.1103/PhysRevLett.126.110404.

[51] G. Perfetto, F. Carollo, J. P. Garrahan, and I. Lesanovsky, "Reaction-limited quantum reaction-diffusion dynamics," Phys. Rev. Lett., vol. 130, p. 210402, May 2023. http://dx.doi.org/10.1103/PhysRevLett.130.210402.

[52] B. Paredes, A. Widera, V. Murg, O. Mandel, S. Fölling, I. Cirac, G. V. Shlyapnikov, T. W. Hänsch, and I. Bloch, "Tonks–girardeau gas of ultracold atoms in an optical lattice," Nature, vol. 429, no. 6989, pp. 277–281, 2004.

[53] T. Kinoshita, T. Wenger, and D. S. Weiss, "Observation of a one-dimensional tonks-girardeau gas," Science, vol. 305, no. 5687, pp. 1125–1128, 2004.

[54] E. Haller, M. Gustavsson, M. J. Mark, J. G. Danzl, R. Hart, G. Pupillo, and H.-C. Nägerl, "Realization of an excited, strongly correlated quantum gas phase," Science, vol. 325, no. 5945, pp. 1224–1227, 2009.

[55] A. Van Amerongen, J. Van Es, P. Wicke, K. Kheruntsyan, and N. Van Druten, "Yang-yang thermodynamics on an atom chip," Physical review letters, vol. 100, no. 9, p. 090402, 2008.

[56] T. Jacqmin, J. Armijo, T. Berrada, K. V. Kheruntsyan, and I. Bouchoule, "Sub-poissonian fluctuations in a 1d bose gas: from the quantum quasicondensate to the strongly interacting regime," Physical review letters, vol. 106, no. 23, p. 230405, 2011.

[57] H. Moritz, T. Stöferle, K. Günter, M. Köhl, and T. Esslinger, "Confinement induced molecules in a 1d fermi gas," Physical review letters, vol. 94, no. 21, p. 210401, 2005.

[58] Y.-a. Liao, A. S. C. Rittner, T. Paprotta, W. Li, G. B. Partridge, R. G. Hulet, S. K. Baur, and E. J. Mueller, "Spin-imbalance in a one-dimensional fermi gas," Nature, vol. 467, no. 7315, pp. 567–569, 2010.

[59] G. Pagano, M. Mancini, G. Cappellini, P. Lombardi, F. Schäfer, H. Hu, X.-J. Liu, J. Catani, C. Sias, M. Inguscio, et al., "A one-dimensional liquid of fermions with tunable spin," Nature Physics, vol. 10, no. 3, pp. 198–201, 2014.

[60] P. Wicke, S. Whitlock, and N. Van Druten, "Controlling spin motion and interactions in a one-dimensional bose gas," arXiv preprint arXiv:1010.4545, 2010.

[61] J. P. Ronzheimer, M. Schreiber, S. Braun, S. S. Hodgman, S. Langer, I. P. McCulloch, F. Heidrich-Meisner, I. Bloch, and U. Schneider, "Expansion dynamics of interacting bosons in homogeneous lattices in one and two dimensions," Physical review letters, vol. 110, no. 20, p. 205301, 2013.

[62] L. Vidmar, J. P. Ronzheimer, M. Schreiber, S. Braun, S. S. Hodgman, S. Langer, F. Heidrich-Meisner, I. Bloch, and U. Schneider, "Dynamical quasicondensation of hard-core bosons at finite momenta," Physical review letters, vol. 115, no. 17, p. 175301, 2015.

[63] F. H. Essler, H. Frahm, F. Göhmann, A. Klümper, and V. E. Korepin, The one-dimensional Hubbard model. Cambridge University Press, 2005.

[64] B. Doyon, "Lecture notes on Generalised Hydrodynamics," SciPost Physics Lecture Notes, p. 18, Aug. (2020). http://dx.doi.org/10.21468/SciPostPhysLectNotes.18.

[65] A. Hutsalyuk and B. Pozsgay, "Integrability breaking in the one dimensional Bose gas: Atomic losses and energy loss," Physical Review E, vol. **103**, p. 042121, Apr. (2021). http://dx.doi.org/10.1103/PhysRevE.103.042121.

[66] B. Bertini, F. H. Essler, S. Groha, and N. J. Robinson, "Prethermalization and Thermalization in Models with Weak Integrability Breaking," Physical Review Letters, vol. **115**, p. 180601, Oct. (2015). http://dx.doi.org/10.1103/PhysRevLett.115.180601.

[67] M. Rigol and A. Muramatsu, "Fermionization in an expanding 1d gas of hard-core bosons," Physical review letters, vol. 94, no. 24, p. 240403, 2005.

[68] M. Rigol, A. Muramatsu, and M. Olshanii, "Hard-core bosons on optical superlattices: Dynamics and relaxation in the superfluid and insulating regimes," Physical Review A, vol. 74, no. 5, p. 053616, 2006.

[69] M. Rigol, V. Dunjko, V. Yurovsky, and M. Olshanii, "Relaxation in a completely integrable many-body quantum system: an ab initio study of the dynamics of the highly excited states of 1d lattice hard-core bosons," Physical review letters, vol. 98, no. 5, p. 050405, 2007.

[70] L. Vidmar, S. Langer, I. McCulloch, U. Schneider, U. Schollwöck, and F. Heidrich-Meisner, "Sudden expansion of mott insulators in one dimension," Physical Review B, vol. 88, no. 23, p. 235117, 2013.

[71] L. Vidmar, W. Xu, and M. Rigol, "Emergent eigenstate solution and emergent gibbs ensemble for expansion dynamics in optical lattices," Physical Review A, vol. 96, no. 1, p. 013608, 2017.

[72] W. Xu and M. Rigol, "Expansion of one-dimensional lattice hard-core bosons at finite temperature," Physical Review A, vol. 95, no. 3, p. 033617, 2017.

[73] O. A. Castro-Alvaredo, B. Doyon, and T. Yoshimura, "Emergent Hydrodynamics in Integrable Quantum Systems Out of Equilibrium," Physical Review X, vol. **6**, p. 041065, Dec. (2016). http://dx.doi.org/10.1103/PhysRevX.6.041065.

[74] B. Bertini, M. Collura, J. De Nardis, and M. Fagotti, "Transport in Out-of-Equilibrium X X Z Chains: Exact Profiles of Charges and Currents," Physical Review Letters, vol. **117**, p. 207201, Nov. (2016). http://dx.doi.org/10.1103/PhysRevLett.117.207201.

[75] I. Bouchoule and J. Dubail, "Generalized hydrodynamics in the one-dimensional bose gas: theory and experiments," Journal of Statistical Mechanics: Theory and Experiment, vol. 2022, p. 014003, jan 2022. http://dx.doi.org/10.1088/1742-5468/ac3659.

[76] F. Lange, Z. Lenarčič, and A. Rosch, "Time-dependent generalized Gibbs ensembles in open quantum systems," Physical Review B, vol. **97**, p. 165138, Apr. (2018). http://dx.doi.org/10.1103/PhysRevB.97.165138.

[77] F. Lange, Z. Lenarčič, and A. Rosch, "Pumping approximately integrable systems," Nature Communications, vol. 8, p. 15767, Jun 2017. http://dx.doi.org/10.1038/ncomms15767.

[78] Z. Lenarčič, F. Lange, and A. Rosch, "Perturbative approach to weakly driven many-particle systems in the presence of approximate conservation laws," Phys. Rev. B, vol. 97, p. 024302, Jan 2018. http://dx.doi.org/10.1103/PhysRevB.97.024302.

[79] P. L. Butzer and R. J. Nessel, Fourier analysis and approximation. Lehrbücher und Monographien aus dem Gebiete der exakten Wissenschaften. Mathematische Reihe, Bd. 40, Basel, Stuttgart: Birkhäuser, 1971.

[80] M. Schemmer, I. Bouchoule, B. Doyon, and J. Dubail, "Generalized hydrodynamics on an atom chip," Phys. Rev. Lett., vol. 122, p. 090601, Mar 2019. http://dx.doi.org/10.1103/PhysRevLett.122.090601.

[81] N. Malvania, Y. Zhang, Y. Le, J. Dubail, M. Rigol, and D. S. Weiss, "Generalized hydrodynamics in strongly interacting 1d bose gases," Science, vol. 373, no. 6559, pp. 1129–1133, 2021. http://dx.doi.org/10.1126/science.abf0147.

[82] M. Coppola and D. Karevski, "Some speculations about local thermalization of nonequilibrium extended quantum systems," Condensed Matter Physics, vol. **26**, no. 1, p. 13502, (2023). http://dx.doi.org/10.5488/CMP.26.13502.

[83] G. Perfetto, F. Carollo, J. P. Garrahan, and I. Lesanovsky, "Quantum reaction-limited reaction-diffusion dynamics of annihilation processes," arXiv preprint arXiv:2305.06944, 2023. http://dx.doi.org/10.48550/arXiv.2305.06944.

From Quantum reaction-limited reaction-diffusion dynamics of noninteracting Bose gases

References

[1] V. Privman, Nonequilibrium statistical mechanics in one dimension (Cambridge University Press, 1997).

[2] M. Henkel, H. Hinrichsen, S. Lübeck, and M. Pleimling, Non-equilibrium phase transitions, Vol. 1 (Springer, 2008).

[3] H. Hinrichsen, Non-equilibrium critical phenomena and phase transitions into absorbing states, Adv. Phys. **49**, 815 (2000).

[4] P. L. Krapivsky, S. Redner, and E. Ben-Naim, A kinetic view of statistical physics (Cambridge University Press, 2010).

[5] U. C. Täuber, Critical dynamics: a field theory approach to equilibrium and non-equilibrium scaling (Cambridge University Press, 2014).

[6] M. Henkel and H. Hinrichsen, The non-equilibrium phase transition of the pair-contact process with diffusion, J. Phys. A: Math. Gen. **37**, R117 (2004).

[7] K. Kang and S. Redner, Fluctuation-dominated kinetics in diffusion-controlled reactions, Phys. Rev. A **32**, 435 (1985).

[8] V. Privman and M. D. Grynberg, Fast-diffusion mean-field theory for k-body reactions in one dimension, J. Phys. A. Math. Gen. **25**, 6567 (1992).

[9] S. J. V. Urbano, D. L. González, and G. Téllez, Steady state of a two-species annihilation process with separated reactants, Phys. Rev. E **108**, 024118 (2023).

[10] D. Toussaint and F. Wilczek, Particle–antiparticle annihilation in diffusive motion, J. Chem. Phys. **78**, 2642 (1983).

[11] J. L. Spouge, Exact solutions for a diffusion-reaction process in one dimension, Phys. Rev. Lett. **60**, 871 (1988).

[12] V. Privman, Exact results for diffusion-limited reactions with synchronous dynamics, Phys. Rev. E **50**, 50 (1994).

[13] D. C. Torney and H. M. McConnell, Diffusion-limited reactions in one dimension, J. Phys. Chem. **87**, 1941 (1983).

[14] K. Kang and S. Redner, Fluctuation effects in Smoluchowski reaction kinetics, Phys. Rev. A **30**, 2833 (1984).

[15] K. Kang and S. Redner, Scaling approach for the kinetics of recombination processes, Phys. Rev. Lett. **52**, 955 (1984).

[16] K. Kang, P. Meakin, J. Oh, and S. Redner, Universal behaviour of n-body decay processes, J. Phys. A: Math. Gen. **17**, L665 (1984).

[17] Z. Rácz, Diffusion-controlled annihilation in the presence of particle sources: Exact results in one dimension, Phys. Rev. Lett. **55**, 1707 (1985).

[18] U. C. Tauber, Dynamic phase transitions in diffusion-limited reactions, arXiv:cond-mat/0205327 (2002) .

[19] U. C. Täuber, M. Howard, and B. P. Vollmayr-Lee, Applications of field-theoretic renormalization group methods to reaction–diffusion problems, J. Phys. A: Math. Gen. **38**, R79 (2005).

[20] M. Doi, Stochastic theory of diffusion-controlled reaction, J. Phys. A: Math. Gen. **9**, 1479 (1976).

[21] M. Doi, Second quantization representation for classical many-particle system, J. Phys. A: Math. Gen. **9**, 1465 (1976).

[22] L. Peliti, Path integral approach to birth-death processes on a lattice, J. Phys. France **46**, 1469 (1985).

[23] L. Peliti, Renormalisation of fluctuation effects in the a+ a to a reaction, J. Phys. A: Math. Gen. **19**, L365 (1986).

[24] D. C. Mattis and M. L. Glasser, The uses of quantum field theory in diffusion-limited reactions, Rev. Mod. Phys. **70**, 979 (1998).

[25] M. Paessens and G. M. Schütz, Phase transitions and correlations in the bosonic pair contact process with diffusion: exact results, J. Phys. A. Math. Gen. **37**, 4709 (2004).

[26] M. van Horssen and J. P. Garrahan, Open quantum reaction-diffusion dynamics: Absorbing states and relaxation, Phys. Rev. E **91**, 032132 (2015).

[27] I. Bouchoule and J. Dubail, Breakdown of tan's relation in lossy one-dimensional bose gases, Phys. Rev. Lett. **126**, 160603 (2021).

[28] I. Bouchoule and J. Dubail, Generalized hydrodynamics in the one-dimensional bose gas: theory and experiments, J. Stat. Mech.: Theory Exp. **2022** (1), 014003.

[29] J. J. García-Ripoll, S. Dürr, N. Syassen, D. M. Bauer, M. Lettner, G. Rempe, and J. I. Cirac, Dissipation-induced hard-core boson gas in an optical lattice, New J. Phys. **11**, 013053 (2009).

[30] C. Ates, B. Olmos, W. Li, and I. Lesanovsky, Dissipative binding of lattice bosons through distance-selective pair loss, Phys. Rev. Lett. **109**, 233003 (2012).

[31] B. Everest, M. R. Hush, and I. Lesanovsky, Many-body out-of-equilibrium dynamics of hard-core lattice bosons with nonlocal loss, Phys. Rev. B **90**, 134306 (2014).

[32] I. Bouchoule, L. Dubois, and L.-P. Barbier, Losses in interacting quantum gases: Ultraviolet divergence and its regularization, Phys. Rev. A **104**, L031304 (2021).

[33] G. Mazza and M. Schirò, Dissipative dynamics of a fermionic superfluid with two-body losses, Phys. Rev. A **107**, L051301 (2023).

[34] D. Rossini, A. Ghermaoui, M. B. Aguilera, R. Vatré, R. Bouganne, J. Beugnon, F. Gerbier, and L. Mazza, Strong correlations in lossy one-dimensional quantum gases: From the quantum zeno effect to the generalized gibbs ensemble, Phys. Rev. A **103**, L060201 (2021).

[35] L. Rosso, A. Biella, and L. Mazza, The one-dimensional Bose gas with strong two-body losses: the effect of the harmonic confinement, SciPost Phys. **12**, 44 (2022).

[36] L. Rosso, A. Biella, J. De Nardis, and L. Mazza, Dynamical theory for one-dimensional fermions with strong two-body losses: Universal non-hermitian zeno physics and spin-charge separation, Phys. Rev. A **107**, 013303 (2023).

[37] I. Bouchoule, B. Doyon, and J. Dubail, The effect of atom losses on the distribution of rapidities in the one-dimensional Bose gas, SciPost Phys. **9**, 44 (2020).

[38] G. Perfetto, F. Carollo, J. P. Garrahan, and I. Lesanovsky, Reaction-limited quantum reaction-diffusion dynamics, Phys. Rev. Lett. **130**, 210402 (2023).

[39] G. Perfetto, F. Carollo, J. P. Garrahan, and I. Lesanovsky, Quantum reaction-limited reaction-diffusion dynamics of annihilation processes, arXiv:2305.06944 (2023) .

[40] F. Riggio, L. Rosso, D. Karevski, and J. Dubail, Effects of atom losses on a one-dimensional lattice gas of hardcore bosons, arXiv:2307.02298 (2023) .

[41] F. Gerbino, I. Lesanovsky, and G. Perfetto, Large-scale universality in quantum reaction-diffusion from keldysh field theory, arXiv:2307.14945 (2023) .

[42] G. Lindblad, On the generators of quantum dynamical semigroups, Comm. Math. Phys. **48**, 119 (1976).

[43] V. Gorini, A. Kossakowski, and E. C. G. Sudarshan, Completely positive dynamical semigroups of n-level systems, J. Math. Phys. **17**, 821 (1976).

[44] H.-P. Breuer and F. Petruccione, The theory of open quantum systems (Oxford University Press on Demand, 2002).

[45] A. Griessner, A. J. Daley, S. R. Clark, D. Jaksch, and P. Zoller, Dark-state cooling of atoms by superfluid immersion, Phys. Rev. Lett. **97**, 220403 (2006).

[46] S. Diehl, A. Micheli, A. Kantian, B. Kraus, H. P. Büchler, and P. Zoller, Quantum states and phases in driven open quantum systems with cold atoms, Nat. Phys. **4**, 878 (2008).

[47] B. Kraus, H. P. Büchler, S. Diehl, A. Kantian, A. Micheli, and P. Zoller, Preparation of entangled states by quantum markov processes, Phys. Rev. A **78**, 042307 (2008).

[48] S. Diehl, E. Rico, M. A. Baranov, and P. Zoller, Topology by dissipation in atomic quantum wires, Nat. Phys. **7**, 971 (2011).

[49] A. Tomadin, S. Diehl, and P. Zoller, Nonequilibrium phase diagram of a driven and dissipative many-body system, Phys. Rev. A **83**, 013611 (2011).

[50] C.-E. Bardyn, M. A. Baranov, C. V. Kraus, E. Rico, A. İmamoğlu, P. Zoller, and S. Diehl, Topology by dissipation, New J. Phys. **15**, 085001 (2013).

[51] C. Pérez-Espigares, M. Marcuzzi, R. Gutiérrez, and I. Lesanovsky, Epidemic dynamics in open quantum spin systems, Phys. Rev. Lett. **119**, 140401 (2017).

[52] B. Buča, C. Booker, M. Medenjak, and D. Jaksch, Bethe ansatz approach for dissipation: exact solutions of quantum many-body dynamics under loss, New J. Phys. **22**, 123040 (2020).

[53] F. Carollo and I. Lesanovsky, Nonequilibrium dark space phase transition, Phys. Rev. Lett. **128**, 040603 (2022).

[54] I. Lesanovsky and J. P. Garrahan, Kinetic Constraints, Hierarchical Relaxation, and Onset of Glassiness in Strongly Interacting and Dissipative Rydberg Gases, Phys. Rev. Lett. **111**, 215305 (2013).

[55] B. Olmos, I. Lesanovsky, and J. P. Garrahan, Out-of-equilibrium evolution of kinetically constrained many-body quantum systems under purely dissipative dynamics, Phys. Rev. E **90**, 042147 (2014).

[56] B. Everest, M. Marcuzzi, J. P. Garrahan, and I. Lesanovsky, Emergent kinetic constraints, ergodicity breaking, and cooperative dynamics in noisy quantum systems, Phys. Rev. E **94**, 052108 (2016).

[57] M. Marcuzzi, M. Buchhold, S. Diehl, and I. Lesanovsky, Absorbing state phase transition with competing quantum and classical fluctuations, Phys. Rev. Lett. **116**, 245701 (2016).

[58] M. Buchhold, B. Everest, M. Marcuzzi, I. Lesanovsky, and S. Diehl, Nonequilibrium effective field theory for absorbing state phase transitions in driven open quantum spin systems, Phys. Rev. B **95**, 014308 (2017).

[59] R. Gutiérrez, C. Simonelli, M. Archimi, F. Castellucci, E. Arimondo, D. Ciampini, M. Marcuzzi, I. Lesanovsky, and O. Morsch, Experimental signatures of an absorbing-state phase transition in an open driven many-body quantum system, Phys. Rev. A **96**, 041602 (2017).

[60] D. Roscher, S. Diehl, and M. Buchhold, Phenomenology of first-order dark-state phase transitions, Phys. Rev. A **98**, 062117 (2018).

[61] F. Carollo, E. Gillman, H. Weimer, and I. Lesanovsky, Critical behavior of the quantum contact process in one dimension, Phys. Rev. Lett. **123**, 100604 (2019).

[62] E. Gillman, F. Carollo, and I. Lesanovsky, Numerical simulation of critical dissipative non-equilibrium quantum systems with an absorbing state, New J. Phys. **21**, 093064 (2019).

[63] E. Gillman, F. Carollo, and I. Lesanovsky, Nonequilibrium phase transitions in $(1+1)$-dimensional quantum cellular automata with controllable quantum correlations, Phys. Rev. Lett. **125**, 100403 (2020).

[64] T. M. Wintermantel, Y. Wang, G. Lochead, S. Shevate, G. K. Brennen, and S. Whitlock, Unitary and nonunitary quantum cellular automata with Rydberg arrays, Phys. Rev. Lett. **124**, 070503 (2020).

[65] S. Helmrich, A. Arias, G. Lochead, T. M. Wintermantel, M. Buchhold, S. Diehl, and S. Whitlock, Signatures of self-organized criticality in an ultracold atomic gas, Nature **577**, 481 (2020).

[66] R. Nigmatullin, E. Wagner, and G. K. Brennen, Directed percolation in nonunitary quantum cellular automata, Phys. Rev. Research **3**, 043167 (2021).

[67] J. Kazemi and H. Weimer, Genuine bistability in open quantum many-body systems, arXiv:211.05352 (2021).

[68] F. Carollo, M. Gnann, G. Perfetto, and I. Lesanovsky, Signatures of a quantum stabilized fluctuating phase and critical dynamics in a kinetically constrained open many-body system with two absorbing states, Phys. Rev. B **106**, 094315 (2022).

[69] N. Syassen, D. M. Bauer, M. Lettner, T. Volz, D. Dietze, J. J. García-Ripoll, J. I. Cirac, G. Rempe, and S. Dürr, Strong dissipation inhibits losses and induces correlations in cold molecular gases, Science **320**, 1329 (2008).

[70] A. Traverso, R. Chakraborty, Y. N. Martinez de Escobar, P. G. Mickelson, S. B. Nagel, M. Yan, and T. C. Killian, Inelastic and elastic collision rates for triplet states of ultracold strontium, Phys. Rev. A **79**, 060702 (2009).

[71] A. Yamaguchi, S. Uetake, D. Hashimoto, J. M. Doyle, and Y. Takahashi, Inelastic collisions in optically trapped ultracold metastable ytterbium, Phys. Rev. Lett. **101**, 233002 (2008).

[72] B. Yan, S. A. Moses, B. Gadway, J. P. Covey, K. R. Hazzard, A. M. Rey, D. S. Jin, and J. Ye, Observation of dipolar spin-exchange interactions with lattice-confined polar molecules, Nature **501**, 521 (2013).

[73] B. Zhu, B. Gadway, M. Foss-Feig, J. Schachenmayer, M. L. Wall, K. R. A. Hazzard, B. Yan, S. A. Moses, J. P. Covey, D. S. Jin, J. Ye, M. Holland, and A. M. Rey, Suppressing the loss of ultracold molecules via the continuous quantum zeno effect, Phys. Rev. Lett. **112**, 070404 (2014).

[74] K. Sponselee, L. Freystatzky, B. Abeln, M. Diem, B. Hundt, A. Kochanke, T. Ponath, B. Santra, L. Mathey, K. Sengstock, et al., Dynamics of ultracold quantum gases in the dissipative fermi–hubbard model, Quantum Sci. Technol. **4**, 014002 (2018).

[75] T. Kinoshita, T. Wenger, and D. S. Weiss, Local pair correlations in one-dimensional bose gases, Phys. Rev. Lett. **95**, 190406 (2005).

[76] T. Tomita, S. Nakajima, I. Danshita, Y. Takasu, and Y. Takahashi, Observation of the mott insulator to superfluid crossover of a driven-dissipative bose-hubbard system, Sci. Adv. **3**, e1701513 (2017).

[77] J. Zeiher, R. Van Bijnen, P. Schauß, S. Hild, J.-y. Choi, T. Pohl, I. Bloch, and C. Gross, Many-body interferometry of a Rydberg-dressed spin lattice, Nat. Phys. **12**, 1095 (2016).

[78] H. Kim, Y. Park, K. Kim, H.-S. Sim, and J. Ahn, Detailed balance of thermalization dynamics in Rydberg-atom quantum simulators, Phys. Rev. Lett. **120**, 180502 (2018).

[79] S. Ebadi, T. T. Wang, H. Levine, A. Keesling, G. Semeghini, A. Omran, D. Bluvstein, R. Samajdar, H. Pichler, W. W. Ho, et al., Quantum phases of matter on a 256-atom programmable quantum simulator, Nature **595**, 227 (2021).

[80] M. Jo and M. Kim, Simulating open quantum many-body systems using optimised circuits in digital quantum simulation, arXiv:2203.14295 (2022).

[81] M. Jo, J. Lee, K. Choi, and B. Kahng, Absorbing phase transition with a continuously varying exponent in a quantum contact process: A neural network approach, Phys. Rev. Research **3**, 013238 (2021).

[82] F. Lange, Z. Lenarčič, and A. Rosch, Time-dependent generalized gibbs ensembles in open quantum systems, Phys. Rev. B **97**, 165138 (2018).

[83] K. Mallayya, M. Rigol, and W. De Roeck, Prethermalization and thermalization in isolated quantum systems, Phys. Rev. X **9**, 021027 (2019).

[84] F. Lange, Z. Lenarčič, and A. Rosch, Pumping approximately integrable systems, Nat. Commun. **8**, 1 (2017).

[85] Z. Lenarčič, F. Lange, and A. Rosch, Perturbative approach to weakly driven many-particle systems in the presence of approximate conservation laws, Phys. Rev. B **97**, 024302 (2018).

[86] I. Ulčakar and Z. Lenarčič, Iterative construction of conserved quantities in dissipative nearly integrable systems, arXiv:2310.03809 (2023) .

[87] P. Grassberger, On phase transitions in schlögl's second model, Z. Phys. B **47**, 365 (1982).

[88] S. Lübeck, Tricritical directed percolation, J. Stat. Phys. **123**, 193 (2006).

[89] P. Grassberger, Tricritical directed percolation in 2+ 1 dimensions, J. Stat. Mech.: Theory Exp. **2006** (01), P01004.

[90] M. Henkel, E. Orlandini, and G. Schutz, Equivalences between stochastic systems, J. Phys. A: Math. Gen. **28**, 6335 (1995).

[91] M. Henkel, E. Orlandini, and J. Santos, Reaction–diffusion processes from equivalent integrable quantum chains, Ann. Phys. **259**, 163 (1997).

[92] K. Krebs, M. P. Pfannmüller, B. Wehefritz, and H. Hinrichsen, Finite-size scaling studies of one-dimensional reaction-diffusion systems. part i. analytical results, J. Stat. Phys. **78**, 1429 (1995).

[93] H. Simon, Concentration for one and two-species one-dimensional reaction-diffusion systems, J. Phys. A: Math. Gen. **28**, 6585 (1995).

[94] D. Ben-Avraham and É. Brunet, On the relation between one-species diffusion-limited coalescence and annihilation in one dimension, J. Phys. A: Math. Gen. **38**, 3247 (2005).

[95] F. H. Essler and M. Fagotti, Quench dynamics and relaxation in isolated integrable quantum spin chains, J. Stat. Mech.: Theory Exp. **2016** (6), 064002.

[96] L. Vidmar and M. Rigol, Generalized gibbs ensemble in integrable lattice models, J. Stat. Mech.: Theory Exp. **2016** (6), 064007.

[97] M. Kiefer-Emmanouilidis and J. Sirker, Current reversals and metastable states in the infinite bose-hubbard chain with local particle loss, Phys. Rev. A **96**, 063625 (2017).

[98] C. J. Pethick and H. Smith, Bose–Einstein condensation in dilute gases (Cambridge university press, 2008).

[99] M. A. Cazalilla, R. Citro, T. Giamarchi, E. Orignac, and M. Rigol, One dimensional bosons: From condensed matter systems to ultracold gases, Rev. Mod. Phys. **83**, 1405 (2011).

[100] R. Landig, L. Hruby, N. Dogra, M. Landini, R. Mottl, T. Donner, and T. Esslinger, Quantum phases from competing short-and long-range interactions in an optical lattice, Nature **532**, 476 (2016).

[101] T. Wu, S. Ray, and J. Kroha, Temporal bistability in the dissipative dicke-bose-hubbard system, arXiv:2311.13301 (2023) .

[102] A. Kamenev, Field theory of non-equilibrium systems (Cambridge University Press, 2023).

[103] L. M. Sieberer, M. Buchhold, and S. Diehl, Keldysh field theory for driven open quantum systems, Rep. Prog. Phys. **79**, 096001 (2016).

From "Reconstructing effective Hamiltonians from nonequilibrium (pre-)thermal steady states" by Nandy, Schmitt et al

References

[1] M. Lewenstein, A. Sanpera, V. Ahufinger, B. Damski, A. Sen(De), and U. Sen, Ultracold atomic gases in optical lattices: mimicking condensed matter physics and beyond, Advances in Physics **56**, 243 (2007), https://doi.org/10.1080/00018730701223200 .

[2] D. Jaksch and P. Zoller, The cold atom hubbard toolbox, Annals of Physics **315**, 52 (2005), special Issue.

[3] R. Blatt and C. F. Roos, Quantum simulations with trapped ions, Nature Physics **8**, 277 (2012).

[4] C. Schneider, D. Porras, and T. Schaetz, Experimental quantum simulations of many-body physics with trapped ions, Reports on Progress in Physics **75**, 10.1088/0034-4885/75/2/024401 (2012).

[5] S. Korenblit, D. Kafri, W. C. Campbell, R. Islam, E. E. Edwards, Z. X. Gong, G. D. Lin, L. M. Duan, J. Kim, K. Kim, and C. Monroe, Quantum simulation of spin models on an arbitrary lattice with trapped ions, New Journal of Physics **14**, 10.1088/1367-2630/14/9/095024 (2012), arXiv:1201.0776 .

[6] R. Islam, C. Senko, W. C. Campbell, S. Korenblit, J. Smith, A. Lee, E. E. Edwards, C. C. Wang, J. K. Freericks, and C. Monroe, Emergence and frustration of magnetism with variable-range interactions in a quantum simulator, Science **340**, 583 (2013).

[7] J. Simon, W. S. Bakr, R. Ma, M. E. Tai, P. M. Preiss, and M. Greiner, Quantum simulation of antiferromagnetic spin chains in an optical lattice, Nature **472**, 307 (2011), arXiv:1103.1372 .

[8] J. M. Gambetta, J. M. Chow, and M. Steffen, Building logical qubits in a superconducting quantum computing system, npj Quantum Information **3**, 0 (2017), arXiv:1510.04375 .

[9] I. Bloch, J. Dalibard, and W. Zwerger, Many-body physics with ultracold gases, Rev. Mod. Phys. **80**, 885 (2008).

[10] R. Jördens, N. Strohmaier, K. Günter, H. Moritz, and T. Esslinger, A Mott insulator of fermionic atoms in an optical lattice, Nature **455**, 204 (2008), arXiv:0804.4009 .

[11] C. Gross and I. Bloch, Quantum simulations with ultracold atoms in optical lattices, Science **357**, 995 (2017).

[12] A. Mazurenko, C. S. Chiu, G. Ji, M. F. Parsons, M. Kanász-Nagy, R. Schmidt, F. Grusdt, E. Demler, D. Greif, and M. Greiner, A cold-atom Fermi-Hubbard antiferromagnet, Nature **545**, 462 (2017).

[13] E. Zohar, J. I. Cirac, and B. Reznik, Quantum simulations of lattice gauge theories using ultracold atoms in optical lattices, Reports on Progress in Physics **79**, 014401 (2015).

[14] I. Bloch, J. Dalibard, and S. Nascimbène, Quantum simulations with ultracold quantum gases, Nature Physics **8**, 267 (2012).

[15] M. Aidelsburger, M. Atala, M. Lohse, J. T. Barreiro, B. Paredes, and I. Bloch, Realization of the hofstadter hamiltonian with ultracold atoms in optical lattices, Phys. Rev. Lett. **111**, 185301 (2013).

[16] I. Bloch and M. Greiner, Exploring quantum matter with ultracold atoms in optical lattices (Academic Press, 2005) pp. 1–47.

[17] R. P. Feynman, Simulating physics with computers, International Journal of Theoretical Physics **21**, 467 (1982).

[18] S. Lloyd, Universal quantum simulators, Science **273**, 1073 (1996), https://www.science.org/doi/pdf/10.1126/science.273.5278.1073 .

[19] U. L. Heras, A. Mezzacapo, L. Lamata, S. Filipp, A. Wallraff, and E. Solano, Digital quantum simulation of spin systems in superconducting circuits, Phys. Rev. Lett. **112**, 200501 (2014).

[20] R. Barends, L. Lamata, J. Kelly, L. García-Álvarez, A. G. Fowler, A. Megrant, E. Jeffrey, T. C. White, D. Sank, J. Y. Mutus, B. Campbell, Y. Chen, Z. Chen, B. Chiaro, A. Dunsworth, I. C. Hoi, C. Neill, P. J. O'Malley, C. Quintana, P. Roushan, A. Vainsencher, J. Wenner, E. Solano, and J. M. Martinis, Digital quantum simulation of fermionic models with a superconducting circuit, Nature Communications **6**, 1 (2015), arXiv:1501.07703 .

[21] L. Lamata, A. Parra-Rodriguez, M. Sanz, and E. Solano, Digital-analog quantum simulations with superconducting circuits, Advances in Physics: X **3**, 519 (2018), arXiv:1711.09810 .

[22] H. Weimer, M. Müller, H. P. Büchler, and I. Lesanovsky, Digital quantum simulation with Rydberg atoms, Quantum Information Processing **10**, 885 (2011), arXiv:1104.3081 .

[23] M. Müller, S. Diehl, G. Pupillo, and P. Zoller, Engineered Open Systems and Quantum Simulations with Atoms and Ions, Advances in Atomic, Molecular and Optical Physics **61**, 1 (2012), arXiv:1203.6595 .

[24] B. P. Lanyon, C. Hempel, D. Nigg, M. Müller, R. Gerritsma, F. Zähringer, P. Schindler, J. T. Barreiro, M. Rambach, G. Kirchmair, M. Hennrich, P. Zoller, R. Blatt, and C. F. Roos, Universal digital quantum simulation with trapped ions, Science **334**, 57 (2011), https://www.science.org/doi/pdf/10.1126/science.1208001 .

[25] J. T. Barreiro, M. Müller, P. Schindler, D. Nigg, T. Monz, M. Chwalla, M. Hennrich, C. F. Roos, P. Zoller, and R. Blatt, An open-system quantum simulator with trapped ions, Nature **470**, 486 (2011), arXiv:1104.1146 .

[26] N. Goldman and J. Dalibard, Periodically driven quantum systems: Effective hamiltonians and engineered gauge fields, Phys. Rev. X **4**, 031027 (2014).

[27] M. Bukov, L. D'Alessio, and A. Polkovnikov, Universal high-frequency behavior of periodically driven systems: from dynamical stabilization to floquet engineering, Advances in Physics **64**, 139 (2015).

[28] A. Eckardt, Colloquium: Atomic quantum gases in periodically driven optical lattices, Rev. Mod. Phys. **89**, 011004 (2017).

[29] L. Viola and S. Lloyd, Dynamical suppression of decoherence in two-state quantum systems, Phys. Rev. A **58**, 2733 (1998).

[30] L. Viola, E. Knill, and S. Lloyd, Dynamical decoupling of open quantum systems, Phys. Rev. Lett. **82**, 2417 (1999).

[31] J. Bylander, S. Gustavsson, F. Yan, F. Yoshihara, K. Harrabi, G. Fitch, D. G. Cory, Y. Nakamura, J.-S. Tsai, and W. D. Oliver, Noise spectroscopy through dynamical decoupling with a superconducting flux qubit, Nature Physics **7**, 565 (2011).

[32] J. Choi, H. Zhou, H. S. Knowles, R. Landig, S. Choi, and M. D. Lukin, Robust dynamic hamiltonian engineering of many-body spin systems, Phys. Rev. X **10**, 031002 (2020).

[33] A. Eckardt, C. Weiss, and M. Holthaus, Superfluid-insulator transition in a periodically driven optical lattice, Phys. Rev. Lett. **95**, 260404 (2005).

[34] A. Zenesini, H. Lignier, D. Ciampini, O. Morsch, and E. Arimondo, Coherent control of dressed matter waves, Phys. Rev. Lett. **102**, 100403 (2009).

[35] T. Oka and H. Aoki, Photovoltaic hall effect in graphene, Phys. Rev. B **79**, 081406 (2009).

[36] T. Kitagawa, E. Berg, M. Rudner, and E. Demler, Topological characterization of periodically driven quantum systems, Phys. Rev. B **82**, 235114 (2010).

[37] G. Jotzu, M. Messer, R. Desbuquois, M. Lebrat, T. Uehlinger, D. Greif, and T. Esslinger, Experimental realization of the topological Haldane model with ultracold fermions, Nature **515**, 237 (2014).

[38] N. H. Lindner, G. Refael, and V. Galitski, Floquet topological insulator in semiconductor quantum wells, Nature Physics **7**, 490 (2011), arXiv:1008.1792 .

[39] B.-Y. Sun, N. Goldman, M. Aidelsburger, and M. Bukov, Engineering and probing non-abelian chiral spin liquids using periodically driven ultracold atoms, PRX Quantum **4**, 020329 (2023).

[40] M. Aidelsburger, M. Atala, S. Nascimbène, S. Trotzky, Y.-A. Chen, and I. Bloch, Experimental realization of strong effective magnetic fields in an optical lattice, Phys. Rev. Lett. **107**, 255301 (2011).

[41] J. Struck, C. Ölschläger, M. Weinberg, P. Hauke, J. Simonet, A. Eckardt, M. Lewenstein, K. Sengstock, and P. Windpassinger, Tunable gauge potential for neutral and spinless particles in driven optical lattices, Phys. Rev. Lett. **108**, 225304 (2012).

[42] A. Bermudez, T. Schaetz, and D. Porras, Synthetic gauge fields for vibrational excitations of trapped ions, Phys. Rev. Lett. **107**, 150501 (2011).

[43] D. V. Else, C. Monroe, C. Nayak, and N. Y. Yao, Discrete time crystals, Annual Review of Condensed Matter Physics **11**, 467 (2020), https://doi.org/10.1146/annurev-conmatphys-031119-050658 .

[44] V. Khemani, R. Moessner, and S. L. Sondhi, A Brief History of Time Crystals, (2019), arXiv:1910.10745 .

[45] K. Sacha and J. Zakrzewski, Time crystals: a review, Reports on Progress in Physics **81**, 016401 (2017).

[46] X. Mi, M. Ippoliti, C. Quintana, A. Greene, Z. Chen, J. Gross, F. Arute, K. Arya, J. Atalaya, R. Babbush, J. C. Bardin, J. Basso, A. Bengtsson, A. Bilmes, A. Bourassa, L. Brill, M. Broughton, B. B. Buckley, D. A. Buell, B. Burkett, N. Bushnell, B. Chiaro, R. Collins, W. Courtney, D. Debroy, S. Demura, A. R. Derk, A. Dunsworth, D. Eppens, C. Erickson, E. Farhi, A. G. Fowler, B. Foxen, C. Gidney, M. Giustina, M. P. Harrigan, S. D. Harrington, J. Hilton, A. Ho, S. Hong, T. Huang, A. Huff, W. J. Huggins, L. B. Ioffe, S. V. Isakov, J. Iveland, E. Jeffrey, Z. Jiang, C. Jones, D. Kafri, T. Khattar, S. Kim, A. Kitaev, P. V. Klimov, A. N. Korotkov, F. Kostritsa, D. Landhuis, P. Laptev, J. Lee, K. Lee, A. Locharla, E. Lucero, O. Martin, J. R. McClean, T. McCourt, M. McEwen, K. C. Miao, M. Mohseni, S. Montazeri, W. Mruczkiewicz, O. Naaman, M. Neeley, C. Neill, M. Newman, M. Y. Niu, T. E. O'Brien, A. Opremcak, E. Ostby, B. Pato, A. Petukhov, N. C. Rubin, D. Sank, K. J. Satzinger, V. Shvarts, Y. Su, D. Strain, M. Szalay, M. D. Trevithick, B. Villalonga, T. White, Z. J. Yao, P. Yeh, J. Yoo, A. Zalcman, H. Neven, S. Boixo, V. Smelyanskiy, A. Megrant, J. Kelly, Y. Chen, S. L. Sondhi, R. Moessner, K. Kechedzhi, V. Khemani, and P. Roushan, Time-crystalline eigenstate order on a quantum processor, Nature **601**, 531 (2022).

[47] J. Zhang, P. W. Hess, A. Kyprianidis, P. Becker, A. Lee, J. Smith, G. Pagano, I. D. Potirniche, A. C. Potter, A. Vishwanath, N. Y. Yao, and C. Monroe, Observation of a discrete time crystal, Nature **543**, 217 (2017), arXiv:1609.08684 .

[48] S. Choi, J. Choi, R. Landig, G. Kucsko, H. Zhou, J. Isoya, F. Jelezko, S. Onoda, H. Sumiya, V. Khemani, C. Von Keyserlingk, N. Y. Yao, E. Demler, and M. D. Lukin, Observation of discrete time-crystalline order in a disordered dipolar many-body system, Nature **543**, 221 (2017), arXiv:1610.08057 .

[49] F. M. Gambetta, F. Carollo, M. Marcuzzi, J. P. Garrahan, and I. Lesanovsky, Discrete time crystals in the absence of manifest symmetries or disorder in open quantum systems, Phys. Rev. Lett. **122**, 015701 (2019).

[50] W. Beatrez, C. Fleckenstein, A. Pillai, E. de Leon Sanchez, A. Akkiraju, J. Diaz Alcala, S. Conti, P. Reshetikhin, E. Druga, M. Bukov, et al., Critical prethermal discrete time crystal created by two-frequency driving, Nature Physics **19**, 407 (2023).

[51] C. H. Johansen, J. Lang, A. Morales, A. Baumgärtner, T. Donner, and F. Piazza, Multimode-polariton superradiance via floquet engineering, SciPost Physics **12**, 094 (2022).

[52] T. Mori, T. Kuwahara, and K. Saito, Rigorous bound on energy absorption and generic relaxation in periodically driven quantum systems, Phys. Rev. Lett. **116**, 120401 (2016).

[53] T. Kuwahara, T. Mori, and K. Saito, Floquet–magnus theory and generic transient dynamics in periodically driven many-body quantum systems, Annals of Physics **367**, 96 (2016).

[54] D. A. Abanin, W. De Roeck, W. W. Ho, and F. m. c. Huveneers, Effective hamiltonians, prethermalization, and slow energy absorption in periodically driven many-body systems, Phys. Rev. B **95**, 014112 (2017).

[55] M. Bukov, S. Gopalakrishnan, M. Knap, and E. Demler, Prethermal floquet steady states and instabilities in the periodically driven, weakly interacting bose-hubbard model, Phys. Rev. Lett. **115**, 205301 (2015).

[56] A. Morningstar, D. A. Huse, and V. Khemani, Universality classes of thermalization for mesoscopic floquet systems, arXiv preprint arXiv:2210.13444 (2022).

[57] E. Altman, K. R. Brown, G. Carleo, L. D. Carr, E. Demler, C. Chin, B. DeMarco, S. E. Economou, M. A. Eriksson, K.-M. C. Fu, M. Greiner, K. R. Hazzard, R. G. Hulet, A. J. Kollár, B. L. Lev, M. D. Lukin, R. Ma, X. Mi, S. Misra, C. Monroe, K. Murch, Z. Nazario, K.-K. Ni, A. C. Potter, P. Roushan, M. Saffman, M. Schleier-Smith, I. Siddiqi, R. Simmonds, M. Singh, I. Spielman, K. Temme, D. S. Weiss, J. Vučković, V. Vuletić, J. Ye, and M. Zwierlein, Quantum simulators: Architectures and opportunities, PRX Quantum **2**, 017003 (2021).

[58] A. J. Daley, I. Bloch, C. Kokail, S. Flannigan, N. Pearson, M. Troyer, and P. Zoller, Practical quantum advantage in quantum simulation, Nature **607**, 667 (2022).

[59] W. Dür, M. J. Bremner, and H. J. Briegel, Quantum simulation of interacting high-dimensional systems: The influence of noise, Phys. Rev. A **78**, 052325 (2008).

[60] G. G. Guerreschi, J. Hogaboam, F. Baruffa, and N. P. D. Sawaya, Intel quantum simulator: a cloud-ready high-performance simulator of quantum circuits, Quantum Science and Technology **5**, 034007 (2020).

[61] X. L. Qi and D. Ranard, Determining a local Hamiltonian from a single eigenstate, Quantum **3**, 1 (2019), arXiv:1712.01850 .

[62] E. Chertkov and B. K. Clark, Computational inverse method for constructing spaces of quantum models from wave functions, Phys. Rev. X **8**, 031029 (2018).

[63] M. Greiter, V. Schnells, and R. Thomale, Method to identify parent hamiltonians for trial states, Phys. Rev. B **98**, 081113 (2018).

[64] E. Bairey, I. Arad, and N. H. Lindner, Learning a local hamiltonian from local measurements, Phys. Rev. Lett. **122**, 020504 (2019).

[65] C. E. Granade, C. Ferrie, N. Wiebe, and D. G. Cory, Robust online hamiltonian learning, New Journal of Physics **14**, 103013 (2012).

[66] N. Wiebe, C. Granade, C. Ferrie, and D. G. Cory, Hamiltonian learning and certification using quantum resources, Phys. Rev. Lett. **112**, 190501 (2014).

[67] J. Wang, S. Paesani, R. Santagati, S. Knauer, A. A. Gentile, N. Wiebe, M. Petruzzella, J. L. O'brien, J. G. Rarity, A. Laing, and M. G. Thompson, Experimental quantum Hamiltonian learning, Nature Physics **13**, 551 (2017), arXiv:1703.05402 .

[68] D. Burgarth, K. Maruyama, and F. Nori, Coupling strength estimation for spin chains despite restricted access, Phys. Rev. A **79**, 020305 (2009).

[69] C. Di Franco, M. Paternostro, and M. S. Kim, Hamiltonian tomography in an access-limited setting without state initialization, Phys. Rev. Lett. **102**, 187203 (2009).

[70] J. Zhang and M. Sarovar, Quantum hamiltonian identification from measurement time traces, Phys. Rev. Lett. **113**, 080401 (2014).

[71] J. Kim, J. Kwon, M. Kim, J. Do, D. Lee, and H. Han, Low-dielectric-constant polyimide aerogel composite films with low water uptake, Polymer Journal **48**, 829 (2016).

[72] A. Sone and P. Cappellaro, Hamiltonian identifiability assisted by a single-probe measurement, Phys. Rev. A **95**, 022335 (2017).

[73] Y. Wang, D. Dong, B. Qi, J. Zhang, I. R. Petersen, and H. Yonezawa, A quantum hamiltonian identification algorithm: Computational complexity and error analysis, IEEE Transactions on Automatic Control **63**, 1388 (2018).

[74] Z. Li, L. Zou, and T. H. Hsieh, Hamiltonian Tomography via Quantum Quench, Physical Review Letters **124**, 160502 (2020), arXiv:1912.09492 .

[75] K. Rudinger and R. Joynt, Compressed sensing for hamiltonian reconstruction, Phys. Rev. A **92**, 052322 (2015).

[76] M. Kieferová and N. Wiebe, Tomography and generative training with quantum boltzmann machines, Phys. Rev. A **96**, 062327 (2017).

[77] A. Valenti, E. Van Nieuwenburg, S. Huber, and E. Greplova, Hamiltonian learning for quantum error correction, Physical Review Research **1**, 1 (2019), arXiv:1907.02540 .

[78] L. Pastori, T. Olsacher, C. Kokail, and P. Zoller, Characterization and verification of trotterized digital quantum simulation via hamiltonian and liouvillian learning, PRX Quantum **3**, 030324 (2022).

[79] T. Olsacher, L. Pastori, C. Kokail, L. M. Sieberer, and P. Zoller, Digital quantum simulation, learning of the floquet hamiltonian, and quantum chaos of the kicked top, Journal of Physics A: Mathematical and Theoretical **55**, 334003 (2022).

[80] M. Bukov, M. Heyl, D. A. Huse, and A. Polkovnikov, Heating and many-body resonances in a periodically driven two-band system, Phys. Rev. B **93**, 155132 (2016).

[81] H. Bourlard and Y. Kamp, Auto-association by multilayer perceptrons and singular value decomposjournaition, Biological Cybernetics **59**, 291 (2004).

[82] M. Tschannen, O. Bachem, and M. Lucic, Recent Advances in Autoencoder-Based Representation Learning, , 1 (2018), arXiv:1812.05069 .

[83] M. Schmitt and Z. Lenarčič, From observations to complexity of quantum states via unsupervised learning, Phys. Rev. B **106**, L041110 (2022) .

[84] A. Lazarides, A. Das, and R. Moessner, Equilibrium states of generic quantum systems subject to periodic driving, Phys. Rev. E **90**, 012110 (2014).

[85] A. Lazarides, A. Das, and R. Moessner, Equilibrium states of generic quantum systems subject to periodic driving, Phys. Rev. E **90**, 012110 (2014).

[86] L. D'Alessio and M. Rigol, Long-time behavior of isolated periodically driven interacting lattice systems, Phys. Rev. X **4**, 041048 (2014).

[87] S. A. Weidinger and M. Knap, Floquet prethermalization and regimes of heating in a periodically driven, interacting quantum system, Scientific Reports **7**, 1 (2017), arXiv:1609.09089 .

[88] W. W. Ho, T. Mori, D. A. Abanin, and E. G. Dalla Torre, Quantum and classical floquet prethermalization, Annals of Physics , 169297 (2023).

[89] M. Bukov, L. D'Alessio, and A. Polkovnikov, Universal high-frequency behavior of periodically driven systems: from dynamical stabilization to floquet engineering, Advances in Physics **64**, 139 (2015), https://doi.org/10.1080/00018732.2015.1055918 .

[90] C. Fleckenstein and M. Bukov, Thermalization and prethermalization in periodically kicked quantum spin chains, Phys. Rev. B **103**, 144307 (2021).

[91] T. N. Ikeda and A. Polkovnikov, Fermi's golden rule for heating in strongly driven floquet systems, Phys. Rev. B **104**, 134308 (2021).

[92] D. E. Parker, X. Cao, A. Avdoshkin, T. Scaffidi, and E. Altman, A universal operator growth hypothesis, Phys. Rev. X **9**, 041017 (2019).

[93] H. Zhao, F. Mintert, R. Moessner, and J. Knolle, Random multipolar driving: Tunably slow heating through spectral engineering, Phys. Rev. Lett. **126**, 040601 (2021).

[94] T. Mori, H. Zhao, F. Mintert, J. Knolle, and R. Moessner, Rigorous bounds on the heating rate in thue-morse quasiperiodically and randomly driven quantum many-body systems, Phys. Rev. Lett. **127**, 050602 (2021).

[95] M. Heyl, P. Hauke, and P. Zoller, Quantum localization bounds trotter errors in digital quantum simulation, Science advances **5**, eaau8342 (2019).

[96] H. Zhao, M. Bukov, M. Heyl, and R. Moessner, Making trotterization adaptive for nisq devices and beyond, arXiv preprint arXiv:2209.12653 (2022).

[97] H. Zhao, M. Bukov, M. Heyl, and R. Moessner, Adaptive trotterization for time-dependent hamiltonian quantum dynamics using instantaneous conservation laws, arXiv preprint arXiv:2307.10327 (2023).

[98] M. Dalmonte, V. Eisler, M. Falconi, and B. Vermersch, Entanglement Hamiltonians: From Field Theory to Lattice Models and Experiments, Annalen der Physik **534**, 1 (2022), arXiv:2202.05045 .

[99] C. Bartsch and J. Gemmer, Dynamical typicality of quantum expectation values, Phys. Rev. Lett. **102**, 110403 (2009).

[100] P. Reimann, Dynamical typicality of isolated many-body quantum systems, Phys. Rev. E **97**, 062129 (2018).

[101] P. Reimann and L. Dabelow, Typicality of prethermalization, Phys. Rev. Lett. **122**, 080603 (2019).

[102] J. Richter and R. Steinigeweg, Combining dynamical quantum typicality and numerical linked cluster expansions, Phys. Rev. B **99**, 094419 (2019).

From Iterative construction of conserved quantities in dissipative nearly integrable systems

References

[1] M. Rigol, V. Dunjko, V. Yurovsky, and M. Olshanii, Relaxation in a Completely Integrable Many-Body Quantum System: An Ab Initio Study of the Dynamics of the Highly Excited States of 1D Lattice Hard-Core Bosons, Phys. Rev. Lett. **98**, 050405 (2007).

[2] E. Ilievski, J. De Nardis, B. Wouters, J.-S. Caux, F. H. L. Essler, and T. Prosen, Complete Generalized Gibbs Ensembles in an Interacting Theory, Phys. Rev. Lett. **115**, 157201 (2015).

[3] L. Vidmar and M. Rigol, Generalized Gibbs ensemble in integrable lattice models, J. Stat. Mech. Theory Exp. **2016**, 064007 (2016).

[4] F. H. L. Essler and M. Fagotti, Quench dynamics and relaxation in isolated integrable quantum spin chains, J. Stat. Mech. Theory Exp. **2016**, 064002 (2016).

[5] J.-S. Caux, The Quench Action, J. Stat. Mech. Theory Exp. **2016**, 064006 (2016).

[6] M. Rigol, V. Dunjko, and M. Olshanii, Thermalization and its mechanism for generic isolated quantum systems, Nature **452**, 854 (2008).

[7] A. Polkovnikov, K. Sengupta, A. Silva, and M. Vengalattore, Colloquium: Nonequilibrium dynamics of closed interacting quantum systems, Rev. Mod. Phys. **83**, 863 (2011).

[8] T. Langen, S. Erne, R. Geiger, B. Rauer, T. Schweigler, M. Kuhnert, W. Rohringer, I. E. Mazets, T. Gasenzer, and J. Schmiedmayer, Experimental observation of a generalized Gibbs ensemble, Science **348**, 207 (2015).

[9] O. A. Castro-Alvaredo, B. Doyon, and T. Yoshimura, Emergent Hydrodynamics in Integrable Quantum Systems Out of Equilibrium, Phys. Rev. X **6**, 041065 (2016).

[10] B. Bertini, M. Collura, J. De Nardis, and M. Fagotti, Transport in Out-of-Equilibrium XXZ Chains: Exact Profiles of Charges and Currents, Phys. Rev. Lett. **117**, 207201 (2016).

[11] B. Doyon, Lecture notes on Generalised Hydrodynamics, SciPost Phys. Lect. Notes , 18 (2020).

[12] N. Malvania, Y. Zhang, Y. Le, J. Dubail, M. Rigol, and D. S. Weiss, Generalized hydrodynamics in strongly interacting 1D Bose gases, Science **373**, 1129 (2021).

[13] M. Schemmer, I. Bouchoule, B. Doyon, and J. Dubail, Generalized Hydrodynamics on an Atom Chip, Phys. Rev. Lett. **122**, 090601 (2019).

[14] F. Cataldini, F. Møller, M. Tajik, J. a. Sabino, S.-C. Ji, I. Mazets, T. Schweigler, B. Rauer, and J. Schmiedmayer, Emergent Pauli Blocking in a Weakly Interacting Bose Gas, Phys. Rev. X **12**, 041032 (2022).

[15] F. Møller, C. Li, I. Mazets, H.-P. Stimming, T. Zhou, Z. Zhu, X. Chen, and J. Schmiedmayer, Extension of the Generalized Hydrodynamics to the Dimensional Crossover Regime, Phys. Rev. Lett. **126**, 090602 (2021).

[16] K. Yang, Y. Zhang, K.-Y. Li, K.-Y. Lin, S. Gopalakrishnan, M. Rigol, and B. L. Lev, Phantom energy in the nonlinear response of a quantum many-body scar state, arXiv:2308.11615 (2023).

[17] T. Kinoshita, T. Wenger, and D. S. Weiss, A quantum Newton's cradle, Nature **440**, 900 (2006).

[18] F. Meinert, M. Panfil, M. J. Mark, K. Lauber, J.-S. Caux, and H.-C. Nägerl, Probing the Excitations of a Lieb-Liniger Gas from Weak to Strong Coupling, Phys. Rev. Lett. **115**, 085301 (2015).

[19] T. Langen, S. Erne, R. Geiger, B. Rauer, T. Schweigler, M. Kuhnert, W. Rohringer, I. E. Mazets, T. Gasenzer, and J. Schmiedmayer, Experimental observation of a generalized Gibbs ensemble, Science **348**, 207 (2015).

[20] C. Hess, Heat conduction in low-dimensional quantum magnets, Eur. Phys. J. Spec. Top. **151**, 73 (2007).

[21] S. K. Niesen, O. Breunig, S. Salm, M. Seher, M. Valldor, P. Warzanowski, and T. Lorenz, Substitution effects on the temperature versus magnetic field phase diagrams of the quasi-one-dimensional effective Ising spin-$\frac{1}{2}$ chain system $BaCo_2V_2O_8$, Phys. Rev. B **90**, 104419 (2014).

[22] A. Scheie, N. E. Sherman, M. Dupont, S. E. Nagler, M. B. Stone, G. E. Granroth, J. E. Moore, and D. A. Tennant, Detection of Kardar–Parisi–Zhang hydrodynamics in a quantum Heisenberg spin-1/2 chain, Nat. Phys. **17**, 726 (2021).

[23] Y. Tang, W. Kao, K.-Y. Li, S. Seo, K. Mallayya, M. Rigol, S. Gopalakrishnan, and B. L. Lev, Thermalization near Integrability in a Dipolar Quantum Newton's Cradle, Phys. Rev. X **8**, 021030 (2018).

[24] A. Bastianello, A. De Luca, B. Doyon, and J. De Nardis, Thermalization of a Trapped One-Dimensional Bose Gas via Diffusion, Phys. Rev. Lett. **125**, 240604 (2020).

[25] F. Lange, Z. Lenarčič, and A. Rosch, Time-dependent generalized Gibbs ensembles in open quantum systems, Phys. Rev. B **97**, 165138 (2018).

[26] F. Lange, Z. Lenarčič, and A. Rosch, Pumping approximately integrable systems, Nat. Commun. **8**, 1 (2017).

[18] Z. Lenarčič, F. Lange, and A. Rosch, Perturbative approach to weakly driven many-particle systems in the presence of approximate conservation laws, Phys. Rev. B **97**, 024302 (2018).

[28] F. Reiter, F. Lange, S. Jain, M. Grau, J. P. Home, and Z. Lenarčič, Engineering generalized Gibbs ensembles with trapped ions, Phys. Rev. Res. **3**, 033142 (2021).

[29] M. Schmitt and Z. Lenarčič, From observations to complexity of quantum states via unsupervised learning, Phys. Rev. B **106**, L041110 (2022).

[30] I. Bouchoule, B. Doyon, and J. Dubail, The effect of atom losses on the distribution of rapidities in the one-dimensional Bose gas, SciPost Phys. **9**, 044 (2020).

[31] A. Hutsalyuk and B. Pozsgay, Integrability breaking in the one-dimensional Bose gas: Atomic losses and energy loss, Phys. Rev. E **103**, 042121 (2021).

[32] D. Rossini, A. Ghermaoui, M. B. Aguilera, R. Vatré, R. Bouganne, J. Beugnon, F. Gerbier, and L. Mazza, Strong correlations in lossy one-dimensional quantum gases: From the quantum Zeno effect to the generalized Gibbs ensemble, Phys. Rev. A **103**, L060201 (2021).

[33] F. Gerbino, I. Lesanovsky, and G. Perfetto, Large-scale universality in Quantum Reaction-Diffusion from Keldysh field theory, arXiv:2307.14945 (2023).

[34] G. Perfetto, F. Carollo, J. P. Garrahan, and I. Lesanovsky, Reaction-Limited Quantum Reaction-Diffusion Dynamics, Phys. Rev. Lett. **130**, 210402 (2023).

[35] S. Rowlands, I. Lesanovsky, and G. Perfetto, Quantum reaction-limited reaction–diffusion dynamics of noninteracting bose gases, New Journal of Physics **26**, 043010 (2024).

[36] B. Pozsgay, The generalized gibbs ensemble for heisenberg spin chains, J. Stat. Mech. Theory Exp. **2013**, P07003 (2013).

[37] M. Fagotti and F. H. L. Essler, Reduced density matrix after a quantum quench, Phys. Rev. B **87**, 245107 (2013).

[38] B. Pozsgay, E. Vernier, and M. A. Werner, On generalized gibbs ensembles with an infinite set of conserved charges, J. Stat. Mech. Theory Exp. **2017**, 093103 (2017).

[39] In the case of degeneracies of H_0, Eq. (14.2) should be extended to a block-diagonal form; however, we expect that thermodynamically, both descriptions are equivalent, and we will work with diagonal ensemble here.

[40] M. Moeckel and S. Kehrein, Interaction Quench in the Hubbard Model, Phys. Rev. Lett. **100**, 175702 (2008).

[41] B. Bertini, F. H. L. Essler, S. Groha, and N. J. Robinson, Prethermalization and Thermalization in Models with Weak Integrability Breaking, Phys. Rev. Lett. **115**, 180601 (2015).

[42] See Supplemental Material for information on (i) regularization of χ^{-1} in the case of non-local basis of projectors $Q_m = |m\rangle\langle m|$, (ii) explicit form for the local conserved quantities of the transverse field Ising model, (iii) analysis of different tGGE descriptions in the case of the Heisenberg model, and (iv) additional unitary perturbation. All citation are included in the main text.

[43] M. Grady, Infinite set of conserved charges in the ising model, Phys. Rev. D **25**, 1103 (1982).

[44] J. T. Barreiro, M. Müller, P. Schindler, D. Nigg, T. Monz, M. Chwalla, M. Hennrich, C. F. Roos, P. Zoller, and R. Blatt, An open-system quantum simulator with trapped ions, Nature **470**, 486 (2011).

[45] X. Mi, A. A. Michailidis, S. Shabani, K. C. Miao, P. V. Klimov, J. Lloyd, E. Rosenberg, R. Acharya, I. Aleiner, T. I. Andersen, et al., Stable quantum-correlated many-body states through engineered dissipation, Science **383**, 1332 (2024).

[46] Here, we used the natural normalization $||\tilde{C}_k||^2 = L$ with $||A||^2 = \frac{\mathrm{tr}[AA^\dagger]}{N_H} - \frac{\mathrm{tr}[A]\mathrm{tr}[A^\dagger]}{N_H^2}$ and N_H the Hamiltonian Hilbert space dimension. The Hamiltonian has it's own Lagrange multiplier, so $\Lambda_0^{(k)} = |\tilde{\lambda}_0^{(k)}|$.

[47] E. Ilievski, M. Medenjak, and T. Prosen, Quasilocal Conserved Operators in the Isotropic Heisenberg Spin-1/2 Chain, Phys. Rev. Lett. **115**, 120601 (2015).

[48] E. Ilievski, M. Medenjak, T. Prosen, and L. Zadnik, Quasilocal charges in integrable lattice systems, J. Stat. Mech. Theory Exp. **2016**, 064008 (2016).

[49] Here, we use the normalization $\mathcal{N}_k = \sqrt{\frac{1}{LN_H}\sum_m |w_m^{(k)}|^2}$, where N_H is the Hamiltonian Hilbert space dimension. Therefore $\tilde{C}_k$ are scaling extensively, $||\tilde{C}_k||^2 \sim L$, where $||A||^2 = \frac{\mathrm{tr}[AA^\dagger]}{N_H} - \frac{\mathrm{tr}[A]\mathrm{tr}[A^\dagger]}{N_H^2}$.

[50] M. Grabowski and P. Mathieu, Structure of the Conservation Laws in Quantum Integrable Spin Chains with Short Range Interactions, Annals of Physics **243**, 299 (1995).

[51] G. Bentsen, I.-D. Potirniche, V. B. Bulchandani, T. Scaffidi, X. Cao, X.-L. Qi, M. Schleier-Smith, and E. Altman, Integrable and chaotic dynamics of spins coupled to an optical cavity, Phys. Rev. X **9**, 041011 (2019).

[52] Our current study used exact diagonalization on Hilbert space of dimension N_H with its own complexity $\mathcal{O}(N_H^3)$. Then the reduction of complexity from $\mathcal{O}(L^2\,N_H)$ to $\mathcal{O}(k^3\,N_H)$ for solving equations (14.4) does not remove the bottleneck. Here, we used that k is the number of necessary iterative steps and that finding roots for n variables scales as $\mathcal{O}(n^a)$, with $a = 2$ for the Powell method employed [55]. Scaling $\mathcal{O}(k^3 N_H)$ is obtained by taking into account that in each (intermediate) iterative step $k' \leq k$, $\mathcal{O}(k'^2)$ root findings are performed, summing up to $\mathcal{O}(k^3)$ in total. However, at least for non-interacting many-body integrable systems, one can evaluate Eq. (14.4) and construct iterative conserved quantities (14.9) in the basis of mode occupation operators in $\mathcal{O}(L^b)$ steps. Then our iterative method diminishes the complexity from $O(L^{b+2})$ for finding Lagrange multipliers of all conserved quantities to $O(k^3\,L^b)$ for k iterative conserved quantities.

[53] E. Ilievski, E. Quinn, J. D. Nardis, and M. Brockmann, String-charge duality in integrable lattice models, J. Stat. Mech. Theory Exp. **2016**, 063101 (2016).

[54] E. Ilievski and E. Quinn, The equilibrium landscape of the Heisenberg spin chain, SciPost Phys. **7**, 033 (2019).

[55] W. H. Press, Numerical recipes 3rd edition: The art of scientific computing (Cambridge university press, 2007).

From Quasilocal conserved operators in isotropic Heisenberg spin 1/2 chain by Ilievski et al.

References

[1] H. Bethe, Z. Phys. **71**, 205 (1931).

[2] L. D. Faddeev, How Algebraic Bethe Ansatz works for integrable model, Les-Houches lectures, `arXiv:hep-th/9605187`.

[3] V. E. Korepin, N. M. Bogoliubov and A. G. Izergin, Quantum Inverse Scattering Method and Correlation Functions, (Cambridge University Press, Cambridge, 1993).

[4] W. Heisenberg, Z. Phys. **49**, 619 (1928).

[5] A. V. Sologubenko et al., J. Low Temp. Phys. **147**, 387 (2007); F. Heidrich-Meisner et al., Eur. Phys. J. Special Topics **151**, 135 (2007).

[6] A. Polkovnikov et al., Rev.Mod.Phys. **83**, 863 (2011).

[7] E. T. Jaynes, Phys. Rev. **108**, 171 (1957); J. M. Deutsch, Phys. Rev. A **43**, 2046 (1991); M. Srednicki, Phys. Rev. E **50**, 888 (1994).

[8] M. Rigol et al., Phys. Rev. Lett., **98**, 050405 (2007); M. A. Cazalilla, Phys. Rev. Lett. **97**, 156403 (2006); P. Calabrese and J. Cardy, Phys. Rev. Lett., **96**, 136801 (2006); T. Barthel and U. Schollwöck, Phys. Rev. Lett. **100**, 100601 (2008); D. Fioretto and G. Mussardo, New J. of Phys. **12**, 055015 (2010); J.-S. Caux and F. H. L. Essler, Phys. Rev. Lett. **110**, 257203 (2013).

[9] B. Wouters et al., Phys. Rev. Lett. **113**, 117202 (2014); M. Brockmann et al., J. Stat. Mech. P12009 **(2014)**.

[10] M. Mierzejewski, P. Prelovšek, and T. Prosen, Phys. Rev. Lett. **113**, 020602 (2014).

[11] B. Pozsgay et al., Phys. Rev. Lett. **113**, 117203 (2014); M. Mestyan et al., J. Stat. Mech. P04001 **(2015)**.

[12] G. Goldstein and N. Andrei, `arXiv:1405.4224`.

[13] M. Mierzejewski, P. Prelovšek, and T. Prosen, Phys. Rev. Lett. **114**, 140601 (2015).

[14] T. Prosen, Open XXZ Spin Chain: Nonequilibrium Steady State and a Strict Bound on Ballistic Transport Phys. Rev. Lett. **106**, 217206 (2011).

[15] T. Prosen and E. Ilievski, Phys. Rev. Lett. **111**, 057203 (2013).

[16] T. Prosen, Nucl. Phys. B **886**, 1177 (2014).

[17] R. G. Pereira, V. Pasquier, J. Sirker, I. Affleck, J. Stat. Mech. P09037 (**2014**).

[18] T. Prosen, `arXiv:1504.0078` to appear as a Topical Review in J. Phys. A.

[19] M. Fagotti and F. H. L. Essler, J. Stat. Mech. P07012 **(2013)**.

[20] Similarly as has been discussed for the $s = 1/2$ case in: H. Katsura, J. Stat. Mech. P01006 **(2015)**.

[21] Supplemental material associated with this manuscript.

[22] M. P. Grabowski and P. Mathieu, Ann. Phys. **243** 299 (1995).

[23] Similar inversion relations in fundamental representations, corresponding $s = 1/2$ in our case, are discussed in: J. M. Maillard, J. Physique **46**, 329 (1985); P. A. Pearce, Phys. Rev. Lett. **58**, 1502 (1987); A. Klümper, A. Schadschneider, and J. Zittartz, Z. Phys. B **76**, 247 (1989).

[24] X. Zotos, F. Naef, and P. Prelovšek. Phys. Rev. B **55**, 11029 (1997).

[25] R. Steinigeweg, J. Herbrych, and P. Prelovšek, Phys. Rev. E **87**, 012118 (2013).

[26] E. Ilievski and T. Prosen, Commun. Math. Phys. **318**, 809 (2013).

From Critical behavior near the many-body localization transition in driven open systems by Zala Lenarčič, Alberton, Rosch, Altman

References

[1] D. Basko, I. Aleiner and B. Altshuler, Annals of Physics **321**, 1126 (2006).

[2] I. V. Gornyi, A. D. Mirlin and D. G. Polyakov, Phys. Rev. Lett. **95**, 206603 (2005).

[3] D. A. Abanin, E. Altman, I. Bloch and M. Serbyn, Rev. Mod. Phys. **91**, 021001 (2019).

[4] M. Schreiber et al., Science **349**, 842 (2015).

[5] H. P. Lüschen, P. Bordia, S. Scherg, F. Alet, E. Altman, U. Schneider, and I. Bloch, Phys. Rev. Lett. **119**, 260401 (2017).

[6] A. Lukin et al., Science **364**, 256 (2019).

[7] J. Smith et al., Nat. Phys. **12**, 907 (2016).

[8] D. J. Luitz, N. Laflorencie and F. Alet, Phys. Rev. B **91**, 081103(R) (2015).

[9] V. Oganesyan and D. A. Huse, Phys. Rev. B **75**, 155111 (2007).

[10] A. Pal and D. A. Huse, Phys. Rev. B **82**, 174411 (2010).

[11] J. A. Kjäll, J. H. Bardarson and F. Pollmann, Phys. Rev. Lett. **113**, 107204 (2014).

[12] V. Khemani, S. P. Lim, D. N. Sheng and D. A. Huse, Phys. Rev. X **7**, 021013 (2017).

[13] M. Serbyn and J. E. Moore, Phys. Rev. B **93**, 041424(R) (2016).

[14] R. Vasseur, S. A. Parameswaran and J. E. Moore, Phys. Rev. B **91**, 140202(R) (2015).

[15] J. Šuntajs, J. Bonča, T. Prosen and L. Vidmar, arXiv:1905.06345 (2019).

[16] D. A. Abanin et al, arXiv:1911.04501 (2019).

[17] R. .K. Panda, A. Scardicchio, M. Schulz, S. R. Taylor, and M. Žnidarič, EPL 128 (2019) 67003.

[18] Z. Lenarčič, E. Altman and A. Rosch, Phys. Rev. Lett. **121**, 267603 (2018).

[19] M. Žnidarič, New Journal of Physics **12**, 043001 (2010).

[20] R. Nandkishore, S. Gopalakrishnan and D. A. Huse, Phys. Rev. B **90**, 064203 (2014).

[21] K. Agarwal, S. Gopalakrishnan, M. Knap, M. Müller and E. Demler, Phys. Rev. Lett. **114**, 160401 (2015).

[22] S. Johri, R. Nandkishore and R. N. Bhatt, Phys. Rev. Lett. **114**, 117401 (2015).

[23] M. H. Fischer, M. Maksymenko and E. Altman, Phys. Rev. Lett. **116**, 160401 (2016).

[24] M. Žnidarič, A. Scardicchio and V. K. Varma, Phys. Rev. Lett. **117**, 040601 (2016).

[25] M. V. Medvedyeva, T. Prosen and M. Žnidarič, Phys. Rev. B **93**, 094205 (2016).

[26] P. Bordia, H. P. Luschen, S. S. Hodgman, M. Schreiber, I. Bloch,U. Schneider, Phys. Rev. Lett. **116**, 140401 (2016).

[27] P. Prelovšek, Phys. Rev. B **94**, 144204 (2016).

[28] E. Levi, M. Heyl, I. Lesanovsky and J. P. Garrahan, Phys. Rev. Lett. **116**, 237203 (2016).

[29] H. P. Lüschen et al., Phys. Rev. X **7**, 011034 (2017).

[30] D. J. Luitz, F. Huveneers and W. De Roeck, Phys. Rev. Lett. **119**, 150602 (2017).

[31] R. Nandkishore and S. Gopalakrishnan, Annalen der Physik **529** (2017).

[32] B. Everest, I. Lesanovsky, J. P. Garrahan and E. Levi, Phys. Rev. B **95**, 024310 (2017).

[33] J. Marino and R. M. Nandkishore, Phys. Rev. B **97**, 054201 (2018).

[34] A. Rubio-Abadal et al., Phys. Rev. X 9, 041014 (2019).

[35] M. Schulz, S. R. Taylor, C. A. Hooley and A. Scardicchio, Phys. Rev. B **98**, 180201(R) (2018).

[36] F. Weiner, F. Evers and S. Bera, Phys. Rev. B **100**, 104204 (2019).

[37] M. Schulz, S. Taylor, A. Scardicchio and M. Žnidarič, J. Stat. Mech. (2020) 023107.

[38] J. J. Mendoza-Arenas, M. Žnidaric, V. K. Varma, J. Goold, S. R. Clark, A. Scardicchio, Phys. Rev. B **99**, 094435 (2019).

[39] See Supplementary Material for (i) a derivation of relation between temperature fluctuations and transport properties of disordered systems, (ii) a comparison to a more standard measure of subdiffusivity, (iii) resistor network results in two dimensions, (iv) the discussion on an alternative experimental realization involving current measurement, (v) numerical aspects of our TEBD calculation, (vi) a derivation on how the phenomenological terms in hydrodynamic description can emerge from the microscopic Liouville equation. Supplementary Material includes Refs. [56, 57, 43, 18].

[40] J. Hulin, J. Bouchaud and A. Georges, Journal of Physics A: Mathematical and General **23**, 1085 (1990).

[41] R. Vosk, D. A. Huse and E. Altman, Phys. Rev. X **5**, 031032 (2015).

[42] A. C. Potter, R. Vasseur and S. A. Parameswaran, Phys. Rev. X **5**, 031033 (2015).

[43] S. Gopalakrishnan, K. Agarwal, E. A. Demler, D. A. Huse and M. Knap, Phys. Rev. B **93**, 134206 (2016).

[44] S. D. Geraedts, N. Regnault and R. M. Nandkishore, New Journal of Physics **19**, 113021 (2017).

[45] F. Verstraete, J. J. García-Ripoll and J. I. Cirac, Phys. Rev. Lett. **93**, 207204 (2004).

[46] M. Zwolak and G. Vidal, Phys. Rev. Lett. **93** 207205, (2004).

[47] M. C. Bañuls, J. I. Cirac and M. B. Hastings, Phys. Rev. Lett. **106**, 050405 (2011).

[48] A. B. Harris, Journal of Physics C: Solid State Physics **7**, 3082 (1974).

[49] J. T. Chayes, L. Chayes, D. S. Fisher and T. Spencer, Phys. Rev. Lett. **57**, 2999 (1986).

[50] A. Goremykina, R. Vasseur and M. Serbyn, Phys. Rev. Lett. **122**, 040601 (2019).

[51] P. T. Dumitrescu, A. Goremykina, S. A. Parameswaran, M. Serbyn and R. Vasseur, Phys. Rev. B **99**, 094205 (2019).

[52] K. X. Wei, C. Ramanathan and P. Cappellaro, Phys. Rev. Lett. **120**, 070501 (2018).

[53] M. S. Anderson, Applied Physics Letters **76**, 3130 (2000).

[54] A. Sternbach et al., arXiv:1706.08478 (2017).

[55] J. Bezanson, A. Edelman, S. Karpinski and V. B. Shah, SIAM review **59**, 65 (2017).

[56] S. Ş. Bayın, Journal of Mathematical Physics **57**, 123501 (2016).

[57] A. A. A. Kilbas, H. M. Srivastava and J. J. Trujillo, Theory and applications of fractional differential equations Vol. 204 (Elsevier Science Limited, 2006).